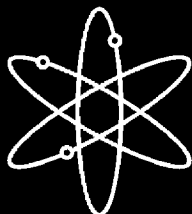


Overpressurization Test of a 1:4-Scale Prestressed Concrete Containment Vessel Model



Sandia National Laboratories



**U.S. Nuclear Regulatory Commission
Office of Nuclear Regulatory Research
Washington, DC 20555-0001**



**Nuclear Power Engineering Corporation
Tokyo 105, Japan**



AVAILABILITY OF REFERENCE MATERIALS IN NRC PUBLICATIONS

NRC Reference Material

As of November 1999, you may electronically access NUREG-series publications and other NRC records at NRC's Public Electronic Reading Room at <http://www.nrc.gov/reading-rm.html>. Publicly released records include, to name a few, NUREG-series publications; *Federal Register* notices; applicant, licensee, and vendor documents and correspondence; NRC correspondence and internal memoranda; bulletins and information notices; inspection and investigative reports; licensee event reports; and Commission papers and their attachments.

NRC publications in the NUREG series, NRC regulations, and *Title 10, Energy*, in the Code of *Federal Regulations* may also be purchased from one of these two sources.

1. The Superintendent of Documents
U.S. Government Printing Office
Mail Stop SSOP
Washington, DC 20402-0001
Internet: bookstore.gpo.gov
Telephone: 202-512-1800
Fax: 202-512-2250
2. The National Technical Information Service
Springfield, VA 22161-0002
www.ntis.gov
1-800-553-6847 or, locally, 703-605-6000

A single copy of each NRC draft report for comment is available free, to the extent of supply, upon written request as follows:

Address: Office of the Chief Information Officer,
Reproduction and Distribution
Services Section
U.S. Nuclear Regulatory Commission
Washington, DC 20555-0001
E-mail: DISTRIBUTION@nrc.gov
Facsimile: 301-415-2289

Some publications in the NUREG series that are posted at NRC's Web site address <http://www.nrc.gov/reading-rm/doc-collections/nuregs> are updated periodically and may differ from the last printed version. Although references to material found on a Web site bear the date the material was accessed, the material available on the date cited may subsequently be removed from the site.

Non-NRC Reference Material

Documents available from public and special technical libraries include all open literature items, such as books, journal articles, and transactions, *Federal Register* notices, Federal and State legislation, and congressional reports. Such documents as theses, dissertations, foreign reports and translations, and non-NRC conference proceedings may be purchased from their sponsoring organization.

Copies of industry codes and standards used in a substantive manner in the NRC regulatory process are maintained at—

The NRC Technical Library
Two White Flint North
11545 Rockville Pike
Rockville, MD 20852-2738

These standards are available in the library for reference use by the public. Codes and standards are usually copyrighted and may be purchased from the originating organization or, if they are American National Standards, from—

American National Standards Institute
11 West 42nd Street
New York, NY 10036-8002
www.ansi.org
212-642-4900

Legally binding regulatory requirements are stated only in laws; NRC regulations; licenses, including technical specifications; or orders, not in NUREG-series publications. The views expressed in contractor-prepared publications in this series are not necessarily those of the NRC.

The NUREG series comprises (1) technical and administrative reports and books prepared by the staff (NUREG-XXXX) or agency contractors (NUREG/CR-XXXX), (2) proceedings of conferences (NUREG/CP-XXXX), (3) reports resulting from international agreements (NUREG/IA-XXXX), (4) brochures (NUREG/BR-XXXX), and (5) compilations of legal decisions and orders of the Commission and Atomic and Safety Licensing Boards and of Directors' decisions under Section 2.206 of NRC's regulations (NUREG-0750).

DISCLAIMER: This report was prepared as an account of work sponsored by an agency of the U.S. Government. Neither the U.S. Government nor any agency thereof, nor any employee, makes any warranty, expressed or implied, or assumes any legal liability or responsibility for any third party's use, or the results of such use, of any information, apparatus, product, or process disclosed in this publication, or represents that its use by such third party would not infringe privately owned rights.

Overpressurization Test of a 1:4-Scale Prestressed Concrete Containment Vessel Model

Manuscript Completed: March 2003
Date Published: March 2003

Prepared by
M.F. Hessheimer, E.W. Klamerus,
L.D. Lambert, G.S. Rightley,
R.A. Dameron*

Sandia National Laboratories
Operated by Sandia Corporation for the
U.S. Department of Energy
Albuquerque, NM 87185

*ANATECH Corporation
5435 Oberlin Drive
San Diego, CA 92121

Prepared for

Nuclear Power Engineering Corporation
Systems Safety Department
Tokyo 105, Japan
under Fia DE-F104-91-AL73734

Division of Engineering Technology
Office of Nuclear Regulatory Research
U.S. Nuclear Regulatory Commission
Washington, DC 20555-0001
NRC Job Code Y6131

NUPEC Project Manager: S. Shibata

NRC Project Manager: J.F. Costello



ABSTRACT

The Nuclear Power Engineering Corporation (NUPEC) of Japan and the U.S. Nuclear Regulatory Commission (NRC), Office of Nuclear Regulatory Research, cosponsored and jointly funded a Cooperative Containment Research Program at Sandia National Laboratories (SNL) from July, 1991 through December, 2002. As part of this program, a 1:4 scale model of a prestressed concrete containment vessel (PCCV) was constructed and pressure tested to failure. The prototype for the model is the containment building of Unit 3 of the Ohi Nuclear Power Station in Japan. The design accident pressure, P_d , of both the prototype and the model is 0.39 MPa (57 psi). The objectives of the PCCV model test were to simulate some aspects of the severe accident loads on containment vessels, observe the model failure mechanisms, and obtain structural response data up to failure for comparison with analytical models.

The PCCV model was designed and constructed by NUPEC and its Japanese contractors, Mitsubishi Heavy Industries, Obayashi Corp., and Taisei Corp. SNL designed and installed the instrumentation and data acquisitions systems and conducted the overpressurization tests. ANATECH Consulting Engineers conducted the pre- and posttest analyses of the model under contract to SNL.

Nearly 1500 transducers were installed on the PCCV model to monitor displacements, liner, rebar, concrete and tendon strains and tendon anchor forces. This instrumentation suite was augmented by the Soundprint[®] acoustic monitoring system, video, and still photography.

Low pressure testing, including a Structural Integrity Test to $1.125 P_d$, and an Integrated Leak Rate Test at $0.9 P_d$, was conducted in September, 2000. The Limit State Test (LST) of the model was conducted on September 27-28, 2000 by slowly pressurizing the model using nitrogen gas. A leak, presumably through a tear in the liner, was first detected at a pressure of $2.5 P_d$ and a leak rate of 1.5% mass/day was estimated. The test was terminated when the model reached a pressure of $3.3 P_d$. At this pressure, the leak rate was nearly 1000% mass/day, exceeding the capacity of the pressurization system. Posttest inspections revealed 26 tears in the 1.6mm (1/16") steel liner as the source of the leaks.

Since only limited damage and inelastic response occurred during the LST, the interior was resealed with an elastomeric membrane. The PCCV was then filled nearly full with water and repressurized on November 14, 2001. This Structural Failure Mode Test reached a maximum pressure of $3.6 P_d$ when the model ruptured violently by failure of the prestressing tendons and then the reinforcing steel.

The resulting data from all the tests are provided for comparison with pretest and posttest analyses.

CONTENTS

ABSTRACT	iii
EXECUTIVE SUMMARY	xiii
ACKNOWLEDGMENTS	xvii
ABBREVIATIONS	xix
1. INTRODUCTION	1-1
1.1 Background	1-2
1.2 Scope	1-3
1.2.1 Model Features and Scale	1-3
1.2.2 Loading	1-4
1.2.3 Response	1-5
1.3 Project Organization	1-6
1.4 Project Schedule	1-7
2. DESIGN AND CONSTRUCTION OF THE PCCV MODEL	2-1
2.1 Design	2-1
2.1.1 Liner Design Considerations	2-3
2.1.2 Concrete Design Considerations	2-4
2.1.3 Prestressing Design Considerations	2-7
2.2 Construction	2-12
2.2.1 General Construction	2-12
2.2.2 Material Properties	2-17
2.2.3 Prestressing Operations	2-31
3. INSTRUMENTATION	3-1
3.1 Background	3-1
3.1.1 Design Considerations	3-1
3.2 Types of Measurements	3-4
3.2.1 Pressure	3-4
3.2.2 Temperature	3-5
3.2.3 Displacement	3-6
3.2.4 Concrete Cracking	3-9
3.2.5 Strain Measurements	3-10
3.2.6 Tendon Measurements	3-16
3.2.7 Visual Observations	3-20
3.2.8 Acoustic Monitoring	3-20
3.3 Instrument Installation	3-22
3.3.1 Instrument Locations	3-22
3.3.2 Quality Assurance and Control	3-24
4. DATA ACQUISITION	4-1
4.1 Objectives	4-1
4.2 Hardware Description	4-1
4.2.1 Hardware Specifications	4-3
4.2.2 Gage Wiring	4-4
4.3 Software Description	4-4
4.3.1 Software Structure	4-4
4.3.2 Software Module Specifics	4-5
4.3.3 Input/Output File Structure	4-5
4.4 Miscellaneous DAS Issues	4-6
4.4.1 Loss of Power	4-6

4.4.2	Integration of DAS with Other Systems	4-6
5.	TESTING	5-1
5.1	Test Planning	5-1
5.1.1	Pressurization System Design and Operation	5-2
5.2	Test Operations	5-3
5.2.1	System Functionality Test	5-4
5.2.2	Structural Integrity Test and Integrated Leak Rate Test	5-5
5.2.3	Limit State Test	5-13
5.2.4	Structural Failure Mode Test	5-18
5.3	Test Results	5-27
5.3.1	Data Files	5-27
5.3.2	Limit State Test Results	5-32
5.3.3	Structural Failure Mode Test Results	5-73
6.	SUMMARY AND CONCLUSION	6-1
6.1	Model Design	6-1
6.1.1	Scale Artifacts	6-1
6.1.2	Material Properties	6-2
6.1.3	Prestressing System	6-2
6.2	Instrumentation and Data Acquisition	6-3
6.2.1	Displacements	6-3
6.2.2	Liner Strains	6-4
6.2.3	Rebar/Concrete Strains	6-4
6.2.4	Tendon Strains/Forces	6-5
6.2.5	Acoustic	6-5
6.2.6	Video/Still Photography	6-6
6.2.7	Data Acquisition	6-6
6.3	Testing	6-7
6.3.1	Loading	6-7
6.3.2	Failure Criteria	6-7
6.3.3	Leak Rate Measurements	6-7
7.	REFERENCES	7-1
Appendix A:	PCCV Model Design Drawings	A-1
Appendix B:	PCCV Model Material Properties	B-1
Appendix C:	As-Built Model Survey Data	C-1
Appendix D:	Final PCCV Instrumentation List	D-1
Appendix E:	PCCV Instrumentation Layout Drawings	E-1
Appendix F:	Prestressed Concrete Containment Vessel Data Acquisition System/Instrumentation Schematic	F-1
Appendix G:	Posttest Data Correction	G-1
Appendix H:	SFMT Instrumentation List	H-1
Appendix I:	Data File Index	I-1
Appendix J:	Data Correction for Ambient Thermal Response	J-1
Appendix K:	LST Soundprint® Acoustic System Reports	K-1
Appendix L:	Metallurgical Analysis of PCCV Liner Tears	L-1

FIGURES

Figure 1.1	Ohi Nuclear Power Station, Ohi-cho, Fukui, Japan	1-2
Figure 1.2	PCCV Model Elevation and Cross-Section	1-4
Figure 1.3	Plan of Containment Technology Test Facility-West	1-8
Figure 2.1	Elevation of PCCV Prototype and Potential Failure Locations	2-2
Figure 2.2	Liner Anchor Layout	2-4
Figure 2.3	PCCV Prototype Equipment Hatch Arrangement	2-6
Figure 2.4	PCCV Prototype Personnel Airlock Arrangement	2-6
Figure 2.5	PCCV Prototype Main Steam Penetration Arrangement	2-6
Figure 2.6	PCCV Prototype Feed Water Penetration Arrangement	2-6
Figure 2.7	PCCV Concrete Lifts and Strengths	2-8
Figure 2.8	Arrangement of Reinforcing in the PCCV Prototype and Model at the Wall-Base Junction	2-9
Figure 2.9	PCCV Prototype and Model Tendon Design Stress Profiles	2-13
Figure 2.10	PCCV Model Layout	2-15
Figure 2.11	Aerial View of CTTF-West during PCCV Construction (March, 1999)	2-16
Figure 2.12	Placement of PCCV Mudmat	2-18
Figure 2.13	Basemat Rebar Support Frame	2-18
Figure 2.14	Basemat Bottom Bars and Vertical Ties	2-18
Figure 2.15	Measuring Rebar Location	2-18
Figure 2.16	F1 Formwork	2-19
Figure 2.17	Placing F1 Concrete	2-19
Figure 2.18	Measuring Concrete Slump	2-19
Figure 2.19	Concrete Test Cylinders and Beams	2-19
Figure 2.20	F2 Rebar Erection	2-20
Figure 2.21	F3 Rebar	2-20
Figure 2.22	F3 Rebar and Formwork	2-20
Figure 2.23	Basemat Top Rebar (F3) and Wall Dowels	2-20
Figure 2.24	F3 Concrete Placement	2-21
Figure 2.25	F4 Concrete	2-21
Figure 2.26	Wall Mock-Up Rebar	2-21
Figure 2.27	Wall Mock-up Form w/ Concrete 'Window'	2-21
Figure 2.28	Delivery of Liner Panels	2-22
Figure 2.29	Liner Panels after 'Uncrating'	2-22
Figure 2.30	Instrumentation Frame Column 'Trees'	2-22
Figure 2.31	Instrumentation Frame Erection	2-22
Figure 2.32	Instrument Frame Erection	2-23
Figure 2.33	Completed Instrument Frame	2-23
Figure 2.34	Liner Panel Erection	2-23
Figure 2.35	Dome Liner Erection	2-23
Figure 2.36	Liner Panels with Jigs	2-24
Figure 2.37	Liner Panel Instrumentation	2-24
Figure 2.38	Liner Strain Gages after Welding	2-24
Figure 2.39	Close-Up of Liner Strain Gages near Weld	2-24
Figure 2.40	Inner Rebar at M/S Penetrations	2-25
Figure 2.41	Installation of Inner Dome Rebar	2-25
Figure 2.42	Tendon Sheath Support Frame	2-25
Figure 2.43	Dome Tendon Sheaths and Support Frame	2-25
Figure 2.44	PCCV Model Tendon Sheaths	2-26
Figure 2.45	Outer Rebar for C1	2-27
Figure 2.46	C1 Formwork Installation	2-27
Figure 2.47	Placing C1 Concrete	2-27
Figure 2.48	Installation of Instrumented Hoop Tendon	2-27
Figure 2.49	C2 Formwork	2-28
Figure 2.50	C4 Concrete Placement	2-28
Figure 2.51	D1 Formwork Erection	2-28

Figure 2.52	D3 Concrete Placement	2-28
Figure 2.53	Final Basemat Concrete Lifts	2-29
Figure 2.54	Completed PCCV Model	2-30
Figure 2.55	Pulling Hoop Tendons	2-32
Figure 2.56	PCCV Model Tensioning Sequence	2-34
Figure 2.57	Tensioning Hoop Tendons	2-37
Figure 2.58	Tensioning Hardware Assembly and Load Cell	2-37
Figure 2.59	Tendon H11 Tensioning Force Time History	2-38
Figure 2.60	Tendon H35 Tensioning Force Time History	2-38
Figure 2.61	Tendon H53 Tensioning Force Time History	2-39
Figure 2.62	Tendon H67 Tensioning Force Time History	2-39
Figure 2.63	Tendon H68 Tensioning Force Time History	2-40
Figure 2.64	Tendon V37 Tensioning Force Time History	2-40
Figure 2.65	Tendon V46 Tensioning Force Time History	2-41
Figure 2.66	Tendon V85 Tensioning Force Time History	2-41
Figure 2.67	H11 Tendon Force Distribution, Elev. 1854	2-43
Figure 2.68	H35 Tendon Force Distribution, Elev. 4572	2-43
Figure 2.69	H53 Tendon Force Distribution, Elev. 6579	2-44
Figure 2.70	H67 Tendon Force Distribution, Elev. 8153	2-44
Figure 2.71	H68 Tendon Force Distribution, Elev. 8280	2-45
Figure 2.72	V37 Tendon Force Distribution, Azimuth 240 Degrees	2-45
Figure 2.73	V46 Tendon Force Distribution, Azimuth 135 Degrees	2-46
Figure 2.74	V85 Tendon Force Distribution, Azimuth 325 Degrees	2-46
Figure 3.1	Cardinal Instrumentation Layout Lines	3-3
Figure 3.2	CPOT Mounted on Instrumentation Frame and Attachment to PCCV Liner	3-7
Figure 3.3	LVDTs at Wall-Base Junction (Azimuth 324 degrees, Elev. 0.0 and 250.0)	3-8
Figure 3.4	TLDT Mounted on Instrumentation Frame and Attachment to PCCV Liner	3-9
Figure 3.5	External LVDT Measuring Displacement between Basemat and Mudmat	3-10
Figure 3.6	Rebar Strain Gage	3-12
Figure 3.7	Rebar Strain Gages Installed in PCCV Model	3-12
Figure 3.8	Concrete Strain Gage Bars	3-13
Figure 3.9	Sample Rebar and Gage Bar Strain Gages	3-13
Figure 3.10	SOFO Fiber Optic Strain Gage	3-15
Figure 3.11	Liner and Liner Anchor Strain Gages	3-16
Figure 3.12	Grid Layout around Inside of E/H	3-17
Figure 3.13	HBM Load Cell (a) Installation Jig, (b) In-Place	3-19
Figure 3.14	Geokon Load Cell (a) Installation Jig, (b) In-Place	3-19
Figure 3.15	Tendon Strain Instrumentation Arrangement	3-21
Figure 3.16	Video and Camera Layout	3-22
Figure 3.17	Interior and Exterior Acoustic Sensor (clamps during installation only)	3-22
Figure 3.18	Displacement Instrumentation Locations	3-25
Figure 3.19	Rebar Instrumentation Locations	3-26
Figure 3.20	Liner and Liner Anchor Instrumentation Locations	3-27
Figure 3.21	Tendon Instrumentation Locations	3-28
Figure 3.22	Concrete Instrumentation Locations	3-29
Figure 3.23	Temperature Instrumentation Locations	3-30
Figure 4.1	PCCV/DAS Hardware Configuration	4-2
Figure 4.2	DAS Software Tree	4-5
Figure 4.3	Top-Down Data File Folder Structure	4-7
Figure 4.4	Basic PCCV Data Flow Diagram	4-8
Figure 5.1	Original Pressurization and Depressurization Sequence	5-1
Figure 5.2	Final Pressurization Plan	5-2
Figure 5.3	Pressurization System Schematic	5-3
Figure 5.4	PCCV Test Organization	5-4
Figure 5.5	System Functionality Test Pressure Time History	5-5
Figure 5.6	System Functionality Test Leak Rates	5-6

Figure 5.7 Structural Integrity and ILRT Pressure and Temperature Time Histories	5-6
Figure 5.8 Concrete Crack Map Grid	5-8
Figure 5.9 Integrated Leak Rate Test Leak Rates	5-9
Figure 5.10 Pre-SIT Cracks at Azimuth. 350 degrees, Elev. 4680 to 6200 (Grid 45)	5-10
Figure 5.11 Post-SIT Cracks at Azimuth. 350 degrees, Elev. 4680 to 6200 (Grid 45)	5-11
Figure 5.12 SIT/ILRT Radial Displacement at Cylinder Midheight (Elev. 4680)	5-11
Figure 5.13 SIT/ILRT Vertical Displacement at Springline (Elev. 10750)	5-12
Figure 5.14 PCCV SIT/ILRT, LST, SFMT Exclusion Zone	5-12
Figure 5.15 Limit State Test Pressure and Average Temperature	5-13
Figure 5.16 LST Calculated Leak Rates at 1.5, 2.0 and 2.5 P_d	5-14
Figure 5.17 Internal Acoustic Sensor Signals at the E/H	5-15
Figure 5.18 LST Pressure Time History, 2.5 to 3.3 P_d	5-15
Figure 5.19 LST Pressure and Flow Rates at Maximum Pressure	5-16
Figure 5.20 LST - Estimated Leak Rates (2.5-3.1 P_d)	5-17
Figure 5.21 LST Estimated Terminal Leak Rates	5-17
Figure 5.22 Post-LST Cracks at Azimuth 350 degrees, Elev. 4680 to 6200 (grid 45)	5-18
Figure 5.23 LST Radial Displacement at Azimuth 135 degrees, Elev. 4680	5-19
Figure 5.24 PCCV Structural Failure Mode Test Concept	5-20
Figure 5.25 Test Specimen of Elastomeric Lining	5-21
Figure 5.26 SFMT Displacement Transducer Layout	5-22
Figure 5.27 Pre-SFMT Leak Test Pressure and Temperature	5-23
Figure 5.28 Pre-SFMT Leak Rate Test	5-24
Figure 5.29 Pre-SFMT Leak Test Acoustic Data	5-24
Figure 5.30 Pre-SFMT Hydrostatic Pressures	5-25
Figure 5.31 SFMT Pressure Time Histories	5-26
Figure 5.32 SFMT Wire Break Events vs. Pressure vs. Displacement	5-26
Figure 5.33 SFMT Pressurization System Data	5-27
Figure 5.34 SFMT: Rupture of the PCCV Model	5-28
Figure 5.35 PCCV Model after the SFMT	5-29
Figure 5.36 PCCV Test Data File Matrix	5-30
Figure 5.37 Radial Displacement at Azimuth 135 degrees, Elev. 6200	5-31
Figure 5.38 Radial Displacement History at Azimuth 135 degrees, Elev. 6200 (DT-R-Z6-01)	5-31
Figure 5.39 LST - Radial Displacement at Azimuth 135 degrees	5-34
Figure 5.40 LST - Radial Displacement at Azimuth 324 degrees	5-34
Figure 5.41 LST - Radial Displacement (DOR) at EL 4680	5-35
Figure 5.42 LST - Vertical Displacements (DOR) at Springline, El. 10750	5-35
Figure 5.43 LST - Deformation at Azimuth 90 degrees and 135 degrees (D and Z) $\times 100$	5-38
Figure 5.44 LST - Deformation at Azimuth 240 degrees and 324 degrees (I and L) $\times 100$	5-39
Figure 5.45 LST - Deformation at Elev. 4680 (5) $\times 100$	5-40
Figure 5.46 LST - Free-Field Liner Hoop Strains	5-42
Figure 5.47 Liner Tear (#15) at E/H	5-42
Figure 5.48 Equipment Hatch Liner Strain Gage Layout (Inside View)	5-43
Figure 5.49 E/H Liner Strains at 'Left' Edge of Embossment	5-43
Figure 5.50 E/H Liner Strains at 'Right' Edge of Embossment	5-44
Figure 5.51 E/H Liner Strains at 'Left' Corners of Embossment	5-44
Figure 5.52 Liner Strains (DOR) at M/S (Ref. D-SN-P-220)	5-45
Figure 5.53 Liner Strains (DOR) at F/W (Ref. D-SN-P-220)	5-46
Figure 5.54 Liner Tear (#3) and Strain Gages at F/W Penetration	5-46
Figure 5.55 Horizontal Stiffener Detail at Vertical Seam Weld ('Rathole') near D7	5-47
Figure 5.56 Liner Strains (DOR) at D7 Anchor Detail (Ref. R-SN-P-209, a.4)	5-48
Figure 5.57 Comparison of Strain at Z6 (Azimuth 135 degrees, Elev. 6280)	5-49
Figure 5.58 Arrangement of Gage Bar Strain Gages at Azimuth 135 degrees	5-50
Figure 5.59 LST Gage Bars Strain at Azimuth 135 degrees (due to pressure only)	5-51
Figure 5.60 LST - Vertical Load Cells	5-53
Figure 5.61 LST - Hoop Load Cells at 90 degrees	5-53
Figure 5.62 LST - Hoop Load Cells at 270 degrees	5-54

Figure 5.63	LST - H68 Tendon Strains	5-54
Figure 5.64	H11 Tendon Force Distribution, El. 1854	5-55
Figure 5.65	H35 Tendon Force Distribution, Elev. 4572	5-55
Figure 5.66	H53 Tendon Force Distribution, Elev. 6579	5-56
Figure 5.67	H67 Tendon Force Distribution, Elev. 8153	5-56
Figure 5.68	H68 Tendon Force Distribution, Elev. 8280	5-57
Figure 5.69	V37 Tendon Force Distribution, Azimuth 240 degrees	5-58
Figure 5.70	V46 Tendon Force Distribution, Azimuth 135 degrees	5-59
Figure 5.71	V85 Tendon Force Distribution, Azimuth 325 degrees	5-59
Figure 5.72	LST - Tendon Ping Acoustic Events	5-60
Figure 5.73	LST - Tendon Ping Event vs. Pressure Histogram	5-60
Figure 5.74	LST - Concrete Cracking Acoustic Events	5-61
Figure 5.75	LST - Concrete Cracking Events vs. Pressure Histogram	5-61
Figure 5.76	Post-LST Concrete Crack Map	5-62
Figure 5.77	Post-LST Liner Tears	5-64
Figure 5.78	Liner Tears and Acoustic Event Locations	5-65
Figure 5.79	Post-LST Liner Tear (#2) and Liner Buckling	5-66
Figure 5.80	Tear #7 at E/H	5-66
Figure 5.81	Tear #12 at E/H	5-67
Figure 5.82	Tear #13 at E/H	5-67
Figure 5.83	Tear #15 at E/H	5-68
Figure 5.84	Tear #2, Free-Field	5-68
Figure 5.85	Tear #16 at Rathole Detail	5-69
Figure 5.86	Close-Up of Tear #13 after Removal of Paint	5-70
Figure 5.87	Liner Specimen at Tear #2	5-70
Figure 5.88	Liner Specimen at Tear #15	5-71
Figure 5.89	E/H Displacement at Grid	5-72
Figure 5.90	E/H Post-LST Displacement	5-72
Figure 5.91	SFMT - Radial Displacement at Azimuth 135 degrees (Z)	5-73
Figure 5.92	SFMT - Radial Displacement at Azimuth 325 degrees (L)	5-74
Figure 5.93	SFMT - Radial Displacement at Elev. 4680 (5)	5-74
Figure 5.94	SFMT - Radial Displacement at Azimuth 135 degrees, Elev. 6200	5-75
Figure 5.95	SFMT - Vertical Displacement at Apex	5-76
Figure 5.96	SFMT Vertical Displacements at Springline (El. 10750) and Apex	5-77
Figure 5.97	SFMT - Deformation at Azimuth 135 Degrees (Z) $\times 100$	5-78
Figure 5.98	SFMT - Deformation at Azimuth 324 Degrees (L) $\times 100$	5-79
Figure 5.99	SFMT - Deformation at Elev. 4680 (5) $\times 100$ - $0P_d$ to $3.63 P_d$	5-80
Figure 5.100	SFMT - Deformation at Elev. 4680 (5) $\times 100$ - $3.0P_d$ to $3.63 P_d$	5-81
Figure 5.101	SFMT Exterior Liner Strains	5-82
Figure 5.102	SFMT - Free-Field Hoop Rebar Strains	5-82
Figure 5.103	SFMT - Free-Field Meridional Rebar Strains	5-83
Figure 5.104	SFMT - Meridional Rebar Strains at Wall-Base Junction	5-83
Figure 5.105	SFMT - Concrete (SOFO) Strains	5-84
Figure 5.106	SFMT - Instrumented Hoop Tendon Anchor Forces	5-85
Figure 5.107	SFMT - Instrumented Vertical Tendon Anchor Forces	5-85
Figure 5.108	SFMT - Tendon H53 Strains	5-86
Figure 5.109	SFMT - Tendon H68 Strain	5-87
Figure 5.110	SFMT - Tendon V46 Strains	5-87
Figure 5.111	SFMT - Tendon H11 Force Distribution (Elev. 1854)	5-88
Figure 5.112	SFMT - Tendon H35 Force Distribution (Elev. 4572)	5-88
Figure 5.113	SFMT - Tendon H53 Force Distribution (Elev. 6579)	5-89
Figure 5.114	SFMT - Tendon H67 Force Distribution (Elev. 8153)	5-89
Figure 5.115	SFMT - Tendon H68 Force Distribution (Elev. 8280)	5-90
Figure 5.116	SFMT - Tendon H35 Computed and Measured Force Distribution	5-91
Figure 5.117	SFMT - Tendon V37 Force Distribution at Azimuth 240 Degrees	5-91
Figure 5.118	SFMT - Tendon V46 Force Distribution at Azimuth 135 Degrees	5-92

Figure 5.119 SFMT - Tendon V85 Force Distribution at Azimuth 325 Degrees	5-92
Figure 5.120 SFMT - Wire Break Map	5-93
Figure 5.121 SFMT - Acoustic Event and Pressure Time History	5-94
Figure 5.122 SFMT - Rupture Map	5-95
Figure 5.123 SFMT - Rebar and Tendon Strands at the Rupture Line	5-96
Figure 5.124 SFMT - Model Displacements	5-97
Figure 5.125 SFMT - Debris Map	5-98

TABLES

Table 2.1 Properties of Liner Materials	2-3
Table 2.2 JIS G 3112 Reinforcing Steel Properties	2-8
Table 2.3 JIS G 3112 Bar Properties	2-8
Table 2.4 PCCV Model Tendon Strand Properties	2-10
Table 2.5 PCCV Model Design Prestressing Anchor Forces	2-11
Table 2.6 PCCV Model Average Concrete Properties	2-31
Table 2.7 Model Prestressing Schedule	2-35
Table 2.8 Instrumented Tendon Gage Performance during Prestressing	2-42
Table 2.9 Prestressing Data Summary	2-42
Table 3.1 Instrumentation Objectives	3-2
Table 3.2 Pressure Transducer Specifications	3-4
Table 3.3 Thermocouple Specifications	3-5
Table 3.4 RTD Specifications	3-6
Table 3.5 Displacement Transducer Specifications (CPOT)	3-7
Table 3.6 LVDT Specifications	3-8
Table 3.7 Temposonics Linear Displacement Transducer Specifications (TLDT)	3-9
Table 3.8 Strain Gage Specifications (Rebar & Tendon wire)	3-11
Table 3.9 Strain Gage Specifications (Concrete Gage Bars)	3-14
Table 3.10 Strain Gage Specifications (Fiber Optic Gages)	3-14
Table 3.11 Strain Gage Specifications (Liner & Liner Anchor)	3-15
Table 3.12 Load Cell Specifications	3-18
Table 3.13 Tensmeg Gage Specifications	3-19
Table 3.14 Instrumentation List Format	3-23
Table 3.15 Gage Type Nomenclature	3-23
Table 3.16 PCCV Instrument Summary	3-24
Table 3.17 PCCV Instrumentation Procedures Summary	3-24
Table 4.1 Description of Raw and Reduced Data for the PCCV Test	4-7
Table 5.1 PCCV Test Personnel Matrix	5-4
Table 5.2 Summary of ASME B&PV Code SIT Instrumentation Requirements	5-7
Table 5.3 Date File (Excel®) Format	5-33
Table 5.4 LST Liner Strain Summary	5-41
Table 5.5 Rebar Strain Summary	5-48
Table 5.6 SFMT Video Event Times	5-95

EXECUTIVE SUMMARY

Introduction

The Nuclear Power Engineering Corporation (NUPEC) of Japan and the U.S. Nuclear Regulatory Commission (NRC), Office of Nuclear Regulatory Research co-sponsored and jointly funded a cooperative containment research program at Sandia National Laboratories¹ (SNL). Tests of two containment models were authorized under this program. The first model, a mixed-scale model of an Improved Mark-II type steel containment vessel (SCV) for a Boiling Water Reactor (BWR), was tested in December 1996. The second model tested was a 1:4-scale model of the prestressed concrete containment vessel (PCCV) of an actual nuclear power plant in Japan, Ohi-3. Ohi-3 is an 1127 MWe Pressurized Water Reactor (PWR) unit, one of four units comprising the Ohi Nuclear Power station located in Fukui Prefecture, owned and operated by Kansai Electric Power Company. The scale of the PCCV model was a uniform 1:4, with minor exceptions to accommodate fabrication and construction concerns. This was judged to be the minimum scale that would allow the steel liner to be constructed from prototypical materials and fabricated with details and procedures that were representative of the prototype.

By definition, the scope of this program was limited to addressing the capacity of containment vessels to loads beyond the design basis, the so-called severe accident loads. Design accident loads for light water reactor containment vessels are typically based on the loss-of-coolant accident (LOCA) and are defined by bounding pressure and temperature transients. The design accident pressure, P_d , of both the prototype and the model is 0.39 MPa (57 psi). The term “severe accidents” is used to describe an array of conditions that could result in loads, in excess of the design basis loads, on the containment. The definition of severe accident loads, which is not as rigorous as the design basis loads definition, results from a consideration of various postulated failure scenarios of the primary nuclear system, up to and including a complete core meltdown and breach of the reactor pressure vessel. The resulting pressure and thermal loading characteristics depend on the unique features of the nuclear steam supply (NSS) system and the containment structure in addition to the postulated accident.

For this test program, it was necessary to decide whether both thermal and pressure loads would be applied to the model, either separately or simultaneously, what the pressurization medium should be, and whether the transient characteristics of these loads should be considered. Programmatically, the decision to perform a *static pneumatic* overpressurization test at *ambient temperature* was dictated by risk and cost considerations and previous experience.

Design and Construction

Within the cooperative framework agreed on by NUPEC and the NRC, NUPEC and its Japanese contractors designed and constructed the PCCV model at SNL’s Containment Technology Test Facility-West (CTTF-W). This test facility was specially constructed by SNL on land temporarily permitted for this purpose on Kirtland Air Force Base (KAFB), Albuquerque, New Mexico, USA. The prime contractor to NUPEC for the construction of the PCCV model was Mitsubishi Heavy Industries (MHI), who also designed and constructed the prototype plant, Ohi-3. In addition to overall design and construction, MHI designed, fabricated and erected the steel liner and all primary steel pressure-retaining components. Supporting MHI for the reinforced concrete portions of the model and ancillary structures were several subcontractors. Obayashi Corp., a large Japanese Architect/Engineer (A/E) and construction company, performed the detailed design of the PCCV model and Taisei Corp, another large A/E/Contractor, was the construction manager. Taisei retained the U.S. construction firm, Hensel Phelps Construction Co., Greeley, CO for general construction work and management of day-to-day construction operations. MHI pre-fabricated portions of the steel liner and the penetrations at their Kobe Shipyard and transported these components to the CTTF-W for final erection. The balance of the model was constructed on-site.

¹ This work is jointly sponsored by the Nuclear Power Engineering Corporation and the U.S. Nuclear Regulatory Commission. The work of the Nuclear Power Engineering Corporation is performed under the auspices of the Ministry of Economy, Trade and Industry, Japan. Sandia is a multiprogram laboratory operated by Sandia Corporation, a Lockheed Martin Company, for the U.S. Department of Energy under Contract Number DE-AC04-94AL85000

Instrumentation and Data Acquisition

NUPEC funded SNL to provide programmatic and model design support, instrument the model, and design and assemble the data acquisition system. The PCCV model instrumentation suite was designed to measure the global behavior in free-field locations of the model and the local structural response of the model near discontinuities. Global response measurements included both displacements referenced to a global or fixed reference and strain measurements at a regular pattern of azimuths and elevations to characterize the overall shape of the model. Local response measurements consisted of strain measurements of individual structural elements (i.e. liner, rebar, tendons, concrete) to characterize the force distribution near structural discontinuities. In areas absent of structural discontinuities or where membrane behavior was expected to dominate the response, relatively simple arrays of transducers were specified. Where structural discontinuities were judged to be significant more complex arrays of strain gages were utilized. Both hoop and meridional strains were measured.

Pressure measurement requirements included careful measurement of the PCCV interior pressure for purposes of leak detection, and to a lesser extent, leak rate measurement, characterization of the mechanical response as a function of pressure and to control the pressurization rate. It should be noted, that while measurement of leak rates was not a primary objective, detection of the onset of leakage requires the calculation of very small leak rates with relatively high accuracy.

As implied by the name, the unique feature of the PCCV model is the prestressing system, comprised of the vertical and hoop tendons and associated hardware. Special efforts were made to monitor the response of the prestressing system, both prior to and during pressure testing. An extensive effort was undertaken to develop and demonstrate the reliability of the tendon instrumentation. The resulting system was comprised of two types of strain gages to monitor the strain, and by calculation, the force distribution along the length of selected tendons along with load cells to measure the forces at the tendon anchors. Since the behavior of the tendons and the overall response of the model to the pressure load would be directly affected by the initial prestressing forces, the response of the PCCV model was monitored continuously from the start of prestressing through the subsequent pressure tests.

While these force, strain and displacement measurements provide accurate information on the response of the model at discrete locations, it was desirable to have some method to monitor the overall response of the model in the (likely) event that some significant response occurs at locations remote from any transducer. The displacement transducers reflect, to a greater extent than the strain or force transducers, the overall response of the model but might still miss other local response modes. This deficiency was addressed by including an extensive array of acoustic and, to a lesser degree, video/photographic monitoring of the PCCV model. While more qualitative in nature than the discrete response measurements, some quantitative information could be obtained from these monitoring systems. The acoustic system, in particular, was designed to detect the onset of liner tearing and leakage, along with concrete cracking and rupture of tendon wires or rebar. Similarly, video and still photography was used to document the development and distribution of concrete cracking, detect liner tearing at discrete locations during pressure testing and capture any unanticipated response modes.

Analysis

NRC funded SNL to perform preliminary, pre- and posttest analyses of the model. This analytical work was subcontracted by SNL to ANATECH Consulting Engineers, San Diego, CA. The preliminary analyses supported design studies, identified critical response modes and assisted in locating instrumentation. The pretest analysis consisted of the development and analysis of detailed numerical models in an attempt to predict the response of the PCCV to the test pressures and predict the capacity and most probable failure mode. The posttest analysis compared the test results to the pretest predictions, investigated and demonstrated changes in the modeling methods to improve the comparison with the test results and provided insights into the response observed during the pressure tests. The pre- and posttest analyses have been reported separately and are not included in this report.

NUPEC and NRC also jointly provided funding to share the costs associated with organizing and conducting a pretest Round Robin analysis. The Round Robin analysis euphemistically refers to an activity where a number of nuclear safety research organizations from government, industry and academia in the United States, Japan and other countries are provided with a common set of data on the model test (design drawings, material properties, test specifications, etc.) and then complete independent predictions of the model response, failure mode and pressure capacity. SNL was the focal

point for this effort in terms of disseminating and consolidating the work of the participating organizations. Seventeen independent organizations, including NUPEC and SNL, participated in this effort, performing pretest analyses and meeting before and after the PCCV model test to discuss and compare analysis results. The efforts of these Round Robin participants are documented in separate NUREG Contractor Reports. While a formal posttest Round Robin exercise was not conducted for the PCCV, most of the participants attended a posttest workshop and have reported the results of their posttest analyses independently.

Testing

NRC funded the planning and conduct of test operations. After extensive discussions between NUPEC, the NRC and SNL, a detailed Test Plan was developed by SNL to describe the conduct of the pressurization tests of the PCCV model. A final series of three tests were agreed upon:

- A leak check and System Functionality Test (SFT) @ $0.5 P_d$ (2.0 kgf/cm² or 28.4 psig)
- A Structural Integrity Test (SIT) @ $1.125 P_d$ followed by an Integrated Leak Rate Test (ILRT) @ $0.9 P_d$
- A Limit State Test (LST) to the static pressure capacity of the PCCV model (or the pressurization system, whichever comes first)

The *pneumatic* Limit State Test was the final test in the original program plan. This test was terminated following a functional failure, i.e. a leak, in the PCCV model, with only limited structural damage occurring. Subsequently, it was decided to re-pressurize the PCCV model, prior to demolition, in an attempt to observe larger inelastic response and, possibly, a global structural failure. This Structural Failure Mode Test (SFMT) was a combined *pneumatic-hydrostatic* test, where the PCCV model was filled nearly full with water, to reduce the volume of gas to be pressurized, and nitrogen gas was used to generate the overpressure.

The SFT was conducted beginning approximately 9:00 AM, July 18, 2000. The model was pressurized using nitrogen to $0.5 P_d$ (0.2 MPa or 28.4 psig) in three increments holding pressure for one hour or longer at each step, depending on the duration needed to perform all system functionality and leak checks. The model was then isolated and a leak rate check was performed by monitoring the model pressure and temperature for approximately 18 hours. After 18 hours, the calculated leak rate was 0.15% mass/day, which was interpreted as confirming that the model was leak-tight. After the model leak rate check, the model was allowed to depressurize through a pair of orifice plates calibrated to leak rates of 1% and 10% mass/day to perform a calibration test on the leak rate measurement instrumentation. The calculated leak rates for each test were 0.87% and 7.86%, respectively, indicating that the leak rate instrumentation was capable of accurately detecting a leak of 1% mass per day, which is the goal specified for the ILRT. The SFT was concluded on July 20 by opening the vent valve, allowing the model to depressurize.

The Structural Integrity Test and the Integrated Leak Rate Test were conducted on September 12-14, 2002 as a combined test, with the ILRT following immediately after the SIT. The SIT/ILRT reproduced the pre-operational tests conducted at the prototype plant and allows for a comparison of the model's elastic response characteristics and leak behavior with the prototype and pretest analyses. The SIT test pressure, P_{SIT} , was $1.125 P_d$. After the SIT pressure was maintained for one hour, the PCCV model was depressurized to the ILRT pressure, $0.9 P_d$. The calculated leakage rate at P_{ILRT} , L_{tm} , after 24 hours at $0.9 P_d$, was 0.06% mass/day.

The Limit State Test (LST) was designed to fulfill the primary objectives of the PCCV test program, i.e. to investigate the response of representative models of nuclear containment structures to pressure loading beyond the design basis accident and to compare analytical predictions to measured behavior. The LST was conducted after the SIT and ILRT were completed and the data from these tests evaluated. The PCCV model was depressurized between the SIT/ILRT and the LST. The LST began at 10:00 AM, Tuesday, September, 26, 2000 and continued, without depressurization, until the test was terminated just before 5:00 PM on Wednesday, September 27. The model was pressurized in increments of approximately $0.2 P_d$ to $1.5 P_d$ when a leak check was conducted yielding a leak rate of 0.48% mass/day. Pressurization of the model continued in increments of approximately $0.1 P_d$ to $2.0 P_d$ when a second leak check resulted in a calculated leak rate of 0.003%, i.e. essentially zero. Pressurization of the model resumed in increments of $0.1 P_d$ to $2.5 P_d$. At $2.4 P_d$, the acoustic system operator reported hearing a change in the acoustic output which might indicate that "something had happened". The model was isolated for a third leak check and after approximately 1-1/2 hours, a fairly stable leak rate

of 1.63% mass per day was calculated, indicating that the model was leaking, most likely from a tear in the liner in the vicinity of the E/H. The average hoop strain at $2.5P_d$, coinciding with the onset of liner tearing and leakage was 0.18%.

After concluding that the model had functionally failed between 2.4 and $2.5 P_d$, the next goal was to continue to pressurize the model as high as possible to collect data on the inelastic response of the structure and to observe, if possible, a structural failure mode. Pressurization continued in increments of $0.05 P_d$. The pressure was increased to slightly over $3.3 P_d$ before the leak rate exceeded the capacity of the pressurization system and the test was terminated. After the model had completely depressurized, it was purged with fresh air, the E/H was removed and a detailed inspection of the inside of the model revealed 26 discrete tears in the liner, all located at vertical field welds. Extensive examination and metallurgical analysis of the liner after the test revealed that fabrication defects contributed to nearly all of the liner tears.

Almost immediately after the completion of the LST, there was a recognition that while the PCCV model had demonstrated its capacity to resist pressures well above the design pressure and had exhibited liner tearing and leaking as the functional failure mode, the test objectives were not fully met with respect to observing large inelastic deformations, for comparison with analyses. NUPEC and NRC approved a concept proposed by SNL to seal the interior surface of the liner with an elastomeric membrane, fill the model with water to 1.5m (5') from the dome apex, approximately 97% of the interior, and repressurize the remaining gas pocket with nitrogen until the model failed or pressure could not be maintained.

The Structural Failure Mode Test (SFMT) began shortly after 10:00 AM on Wednesday, November 14, 2001. The model was continuously pressurized at a rate of approximately 0.035 MPa/min (5 psi/min). All active sensors were continuously scanned at intervals of approximately 30 seconds and the video cameras were continuously recording the response of the model. As the pressure was increased, evidence of leakage was visible by increasing wetting of the concrete surface. At 10:38 AM, the effective pressure in the model equaled the peak pressure achieved during the LST, $3.3 P_d$. At approximately 10:39 AM, the acoustic system recorded a very high noise level event which was interpreted as the breaking of a tendon wire. At this point in the test, events occurred very quickly. Shortly after detecting the wire break, a small spray of water was observed at approximately 0° azimuth and additional tendon wire breaks were detected by the acoustic system with increasing frequency. The rate of pressurization was decreasing and the nitrogen flow rate was increased to maintain the pressurization rate. Pressurization of the model continued until a second spray of water was observed and then, suddenly, at 10:46:12.3, at an effective pressure of $3.63 P_d$ (1.42 MPa or 206.4 psig) the PCCV model ruptured violently at $\sim 6^\circ$ azimuth near the mid-height of the cylinder. The maximum average hoop strain at the peak pressure of $3.63 P_d$ was 1.02%. The model continued to expand after reaching the peak pressure and the maximum hoop strain recorded just prior to rupture was 1.65%.

Conclusions

The over-pressurization tests of the 1:4-scale PCCV model represent a significant advance in understanding the capacity of nuclear power plant containments to loads associated with severe accidents. The data collected during the tests, as well as the response and failure modes exhibited, will be used for many years to come to benchmark numerical simulation methods used to predict the response of concrete containment structures. While lessons for actual plants can and should be drawn from this and previous large scale containment model tests, these insights are beyond the scope of this report and will be addressed in a future effort. The reader is cautioned *not* to draw direct conclusions regarding the pressure capacity of actual plants from these tests or interpret these results as a demonstration of the prototype capacity. The PCCV model tests have demonstrated the importance of the unique details and as-built characteristics of the model on the ultimate capacity. Any efforts to estimate the capacity of an actual containment must address the unique features of the plant under consideration.

With the completion of the PCCV tests, restoration of the test site and submittal of the test reports, the NUPEC/NRC Cooperative Containment Research Program was formally concluded on December 31, 2002.

ACKNOWLEDGMENTS

No one person was responsible for the success of the PCCV Test Project. Without the dedicated efforts of a team including the project sponsors, partners and contractors and supporting organizations, the outcome of this project would have been far less successful than it has proven to be. It is, however, difficult to acknowledge everyone who contributed to this project without unconsciously omitting some individuals. I would like to begin therefore by apologizing to those anonymous, but no less important contributors I may have overlooked.

But the contributions of some individuals are too significant to overlook. I would like to begin, therefore, by acknowledging the program managers of the sponsoring organizations, NUPEC and the U.S. NRC. Dr. James F. Costello, U.S. NRC, has been the guiding force behind the containment integrity research conducted at SNL for over 25 years, including this project. His perseverance, support, and guidance has been invaluable and it is no overstatement to say that this project may never have happened without his involvement. Similarly, the NUPEC project directors: Dr. Kenji Takumi, Dr. Hideo Ogasawara and Dr. Takshi Kiguchi; and the project managers: Mr. Akira Nonaka, Mr. Tomoyuki Matsumoto, Mr. Masaki Iriyama and Mr. Satoru Shibata ensured that this program had the financial and technical resources to meet the program objectives in order to make a significant contribution to the international nuclear power industry.

There were many Japanese colleagues who, as primary contractors or subcontractors to NUPEC, contributed to the planning, design, and construction of the PCCV model. These included, from Mitsubishi Heavy Industries: Toshisada Kato, Kaoru Nagata, Kazutoshi Hayashi, Nozumo Watanabe, Tomoyuki Kitani, Hiroshi Urakawa, Ryuichi Oshima, and Hiroshi Matsuoka; from Obayashi Corporation: Katsuhiko Umeki, Katsuyoshi Imoto, and Takako Kashiwase; and from Taisei Corporation: Yasuyuki Murazumi, Yutaka Kobayashi, and Shiro Mitsugi. General Construction of the model was managed by Hensel Phelps Construction Company whose on-site staff included: Guy Mills, Tina Connelly, Subba Padmendra and Norman 'Butch' Brackett.

SNL management support was provided by Walter von Riesemann and Dennis Berry. I am especially indebted to Brad Parks who was the initial program manager responsible for the planning and organization of an excellent project team. The dedication and professionalism exhibited by the SNL project team was unsurpassed in my experience and I am fortunate and proud to have had the opportunity to work with such an outstanding group of individuals. The primary project team included Dave Pace (PCCV Lead Engineer), L. Dwight Lambert (Site Manager and Instrumentation Leader), Eric Klamerus (Instrumentation and Pressurization System Engineer), Gina Rightley (DAS Lead Engineer), Mike Rightley (DAS and Instrumentation Design), Mike Luker (DAS and Instrumentation Engineer), Vincent Luk (Analysis and Round Robin Coordinator), Ken Eckelmeyer (Liner Inspection and Metallurgical Analysis) and a team of outstanding technicians consisting of Mike Ramirez, Bob Smyth, Ed Baynes, Bob Eyers, Raymond Davis, Roy Morgan, John Mulder, Richard Padilla, Jack Pantuso, Ed Vieth, Richard Klingler, and Larry Yellowhorse. Kimberly Brower assisted in the posttest data processing and analysis. Management and Administrative support was provided by Berlinda Gonzalez, Yolanda Aragon, Viola Madrid, Mary Campos, Rebecca Campbell, Linda Flores, Barbara Meloche and Barbara Hawkins. Site support was provided by SNL's Facilities Department members Walter Heimer, Paul Schlavin, George Greer, Ed Sanchez and Dave Hendrix. Nadine Williams was responsible for all permits and land-use issues. Dave Sparks and Russ Adams from SNL's Video Services Department taped the construction and testing of the model. Environmental, Safety and Health support was provided by Daniel 'Mac' MacLaughlin.

In addition to SNL's in-house staff, vital support was provided by several key sub-contractors, especially from ANATECH Consulting Engineers: Bob Dameron (Lead Analyst), Yusef Rashid, Jason Maxwell and Brian Hanson; from Pure Technologies, Ltd. Peter Paulson and Monroe Thomas; and from the University of New Mexico's ATR Institute, Lary Lenke. Faith Puffer (Tech Reps) was the technical editor responsible for producing this report.

The direction and planning of the project was greatly assisted by special advisors to the project. In Japan, NUPEC's Structural Advisory Committee included Prof. Hiroshi Akiyama, Prof. Katsuki Takiguchi and Prof. Noriyuki Miyazaki. The NRC's Peer Review Panel consisted of Tom Ahl, Bryan Erler, Ted Johnson, Richard Orr, Mete Sozen, John Stevenson, H.T. Tang, Walt von Riesemann, Richard White, Lyle Gerdes, Harold Townsend and Joseph Ucifferro.

It is very difficult to adequately describe the contribution of all these individuals in this short space, but to each of them, I would like to express my heartfelt thanks.

Thank you.

Michael F. Hessheimer, P.E.

Project Manager
NUPEC/NRC Cooperative Containment Program
Sandia National Laboratories

December 2002

ABBREVIATIONS

A/L	air lock
A/E	Architect/Engineer
AO	Acoustic System Operator
ASME	American Society of Mechanical Engineers
BWR	Boiling Water Reactor
CE	fiber optic gages
CONV	converted data
COR	corrected data
CPOT	Cable Potentiometer
CTTF	Containment Technology Test Facility
CVDT	converted
DA	data analyst
DAS	Data Acquisition System
DET	Division of Engineering Technology
DISP	displacement
DO	Data Acquisition System Operator
DOE	Department of Energy
DOR	data of record
DT	displacement
DYN	dynamic
E/H	equipment hatch
EPRI	Electric Power Research Institute
ES&H	Environmental Safety and Health
F/W	feedwater
GBST	gage bar strains
GFAC	gage-specific factors
ILRT	Integrated Leak Rate Test
KAFB	Kirtland Air Force Base
LI	liner strain gage
LINST	liner strains
LOCA	loss-of-coolant accident
LST	Limit State Test
LVDT	Linear Variable Differential Transformer
M/S	main steam
METI	Ministry of Economy, Trade and Industry
MHI	Mitsubishi Heavy Industries
NO	Nitrogen Supply Operator
NRC	U.S. Nuclear Regulatory Commission
NSS	nuclear steam supply
NUPEC	Nuclear Power Engineering Corporation
PCCV	prestressed concrete containment vessel
PLC	Programmable logic controller
PRES	pressure
PWR	Pressurized Water Reactor
REBST	rebar strain
RES	Office of Nuclear Regulatory Research
RS	rebar strain gages
RTD	Resistance Temperature Detectors
SCV	steel containment vessel
SFMT	Structural Failure Mode Test
SFT	System Functionality Test
SIT	Structural Integrity Test
SNL	Sandia National Laboratories
SOL	Standard Output Location

T/C	thermocouple
TC	test conductor
TEMP	temperature
UTS	ultimate strength
YS	yield strength

1. INTRODUCTION

The Nuclear Power Engineering Corporation (NUPEC) of Japan and the U.S. Nuclear Regulatory Commission (NRC), Office of Nuclear Regulatory Research have cosponsored and jointly funded a cooperative containment research program at Sandia National Laboratories (SNL). NUPEC was founded in 1976 as the Nuclear Power Engineering Center under the initiative of academia and private corporations. Supported by the Agency for Natural Resources and Environment of the Ministry of Economy, Trade and Industry (METI), NUPEC is mandated to advance the performance and public acceptance of commercial nuclear power plants through engineering tests, safety analyses, information acquisition and analyses, and public relations activities. Within NUPEC, the Systems Safety Department is conducting research on the integrity of reactor containment vessels during severe accidents. Containment integrity tests include experiments and analyses of debris cooling phenomena, hydrogen combustion behavior, fission products transport behavior, and containment structural behavior. In addition, the department coordinates the cooperative containment program with the NRC and manages program activities with SNL and other subcontractors.

The Office of Nuclear Regulatory Research (RES) at U.S. NRC plans, recommends, and implements programs of nuclear regulatory research, standards development, and resolution of safety issues for nuclear power plants and other facilities regulated by the NRC. Within RES, the Division of Engineering Technology (DET) plans, develops, and directs comprehensive research programs and standards development for nuclear and materials safety. In the nuclear safety area, there are programs for the design, qualification, construction, maintenance, inspection, and testing of current and advanced nuclear power plants. For materials safety, program activities include material characteristics, aging, and seismic and engineering aspects of these facilities and materials. Within DET, the Engineering Research Applications Branch has the lead for determining adequacy of structures and systems and for the coordinating and interfacing activities associated with the American Society of Mechanical Engineers (ASME) Code Section III. This branch coordinates the cooperative containment program with NUPEC and manages SNL activities.

SNL is a multi-program national security laboratory, operated by Sandia Corporation, a subsidiary of Lockheed Martin Company, for the National Nuclear Security Administration, U.S. Department of Energy (DOE). SNL's Nuclear Energy Technology Center has provided engineering and scientific support in the areas of reactor safety and safeguards to the NRC and the DOE for more than 20 years. A significant area of support has included analytical and experimental efforts to address issues related to severe accidents and containment integrity.

This cooperative containment program builds on the combined expertise of these organizations and continues to advance the understanding of nuclear containment structure's response to pressure loading beyond the design basis accident and the ability to predict, analytically, the structural behavior. This is accomplished by conducting static, pneumatic overpressurization tests at ambient temperature of scale models of actual containment vessels for nuclear power plants in Japan. NUPEC and the NRC formulated the overall scope of the program, and NUPEC, under contract with METI, is responsible for designing and constructing the models. SNL is funded by NUPEC to develop and operate a facility for conducting these tests, review the model designs and provide design support, instrument the models and collect data during the pressure tests, and report the results of the test. The NRC is funding SNL to perform pre- and posttest analyses of the models and to conduct the pressure tests. All funding is directed to SNL through agreements with the DOE's Work-for-Others Office in the Science and Technology Transfer Division.

Tests of two containment models were authorized under this program. The first model, a mixed-scale model of an Improved Mark-II type steel containment vessel (SCV) for a Boiling Water Reactor (BWR), was tested in December 1996. The results of the SCV tests and analyses have been published [1-5]. The second model tested was a 1:4-scale model of the prestressed concrete containment vessel (PCCV) of an actual nuclear power plant in Japan, Ohi-3 (Figure 1.1). Ohi-3 is an 1127 MWe Pressurized Water Reactor (PWR) unit, one of four units comprising the Ohi Nuclear Power station located in Fukui Prefecture and owned and operated by Kansai Electric Power Company.

This report describes the design, construction, and instrumentation of the PCCV model, the conduct of the pressure tests, and the results of those tests. The pre- and posttest analyses performed by ANATECH Corp (San Diego, CA) under contract to SNL are reported separately [6, 7]. Independent pretest analyses, conducted by a number of international organizations, were also conducted and presented in a summary report [8].



Figure 1.1. Ohi Nuclear Power Station, Ohi-cho, Fukui, Japan

1.1 Background

Containment vessels in nuclear power plants comprise, with the penetrations and other pressure boundary components, the final barrier between the environment and the nuclear steam supply system. The functions of the containment are to:

- contain any radioactive material that might be released from the primary system (reactor vessel, steam generators, piping) in the event of an accident;
- act as a supporting structure for operational equipment.

Containment buildings have been an integral part of commercial nuclear power plants in Japan and the United States since the first units were constructed in the 1960s. For U.S. containments, the design loads and their combinations, as well as the response limits, are specified in the ASME Boiler and Pressure Vessel Code [9]. Initially, severe accidents were not part of the design basis due to their perceived low probability of occurrence, and pressure relief valves were not required. In Japan, METI Directives control the design of nuclear power plants, and the design standards for containments are specified in the METI Notification No. 501 and in JEAG4601.

After the accident at Three Mile Island in the United States in 1979, attention turned to the capacity of containment systems beyond their design basis. SNL conducted a preliminary study [10], commissioned by the NRC, to identify experiments conducted to investigate this issue, but concluded that the scope of the tests and the data did not provide sufficient insight into the problem. As a result, a program, including scale model tests coupled with detailed structural analysis, was formulated by the NRC to investigate the integrity of containment systems beyond their design basis. The primary objective of the NRC program was, and continues to be, the validation of analytical methods used to predict the performance of light water reactor containment systems when subjected to loads beyond those specified in the design codes. While some insights could be gained into structural response and failure mechanisms of actual containments, it was also recognized that the capacity of actual containments could not be determined solely from tests of simplified scale models. The results of this program, as summarized by Parks [11], concluded that there was significant reserve capacity in the containment vessels to resist loads above the design basis and that although the analytical efforts were encouraging, uncertainties remained about structural response and failure mechanisms.

Remaining uncertainties regarding the response of containment structures led to discussions among NUPEC, the NRC, and SNL that culminated in a 1991 agreement to start the NUPEC/NRC Cooperative Containment Program. In parallel with this cooperative program, there are independent efforts sponsored and conducted by both NRC and NUPEC. These efforts include investigating the response of penetrations [12,13], the effects of aging on containment structure capacity [14], and the seismic capacity of containment structures [15, 16].

1.2 Scope

Nuclear power plants in Japan and the U.S. generally utilize one of two types of light water reactor systems; BWR and PWR. The containment vessels for the pressurized water reactors in Japan and the U.S. are typically free-standing reinforced concrete shells with an integral steel liner. A few have only regular steel reinforcing bars (rebar); however, the majority use both regular and posttensioned reinforcing. (For this report, the terms prestressed and posttensioned are used synonymously, even though the reinforcing is, technically, posttensioned; i.e. tensioning of the reinforcing is conducted after the concrete has been placed and cured to the specified minimum strength.) A variety of prestressed reinforcing or tendon configurations are represented in the fleet of PWR containments. However, the evolution of prestressed containment designs has been toward the use of longer, continuous tendons, culminating in the two-buttress containment with meridional 'hairpin' tendons and 360-degree hoop tendons, represented by the Ohi-3 design. No two-buttress prestressed concrete containments were constructed in the U.S. (although some were planned prior to the TMI-2 accident); however, many of the features of the Ohi-3 containment are similar to features in existing U.S. plants and the design philosophy is similar. As a result, NUPEC and the NRC agreed on a scale model of the Ohi-3 containment for the second test subject in the Cooperative Containment Program.

1.2.1 Model Features and Scale

The Ohi-3 containment is a thin prestressed concrete cylindrical shell with a hemispherical dome and a continuous steel liner anchored to a reinforced concrete basemat that extends beyond the containment to support other plant structures. Consistent with the objectives of the sponsoring organizations, the features and scale of the PCCV model were chosen so that the response of the model would mimic the global behavior of the prototype, and local details, particularly those around penetrations, would be represented. One of the primary considerations in determining the scale of the model was the desire to utilize nearly identical construction materials to the material used in the construction of the prototype. Preliminary design studies, conducted to determine the appropriate scale of the model, initially focused on a mixed scale model where the scale on the overall geometry would be 1:6, while the scale on the liner thickness would be 1:3. These preliminary studies indicated, however, that use of this mixed scale might upset the relationship between failure modes that might be expected in the prototype. In particular, the use of a steel liner, which was twice as thick, relative to the prestressed concrete shell, as the prototype, might retard the onset of liner tearing (leakage) failure modes and increase the likelihood of a structural failure mode occurring. As a result, it was decided that the scale of the model would be a uniform 1:4, with minor exceptions to accommodate fabrication and construction concerns. This was judged to be the minimum scale that would allow the steel liner to be constructed from prototypical materials and fabricated with details and procedures representative of the prototype. The overall geometry and dimensions of the PCCV model are shown in Figure 1.2.

Although both NUPEC and SNL (under NRC sponsorship) had conducted component tests of both full-size and scaled penetrations [12-13, 17], the PCCV model included both a functional representation of the major penetrations, namely the equipment hatch (E/H) and the personnel air lock (A/L), and nonfunctional representation of the main steam (M/S) and feedwater (F/W) penetrations. The E/H and A/L penetrations were fully-functional, one-fourth scale models of the penetrations in the prototype, while only the penetration sleeves of the M/S and F/W penetrations, terminated with pressure seating blind flanges, were included in the model. The liner and concrete reinforcing details around these penetrations were also retained in the model.

During construction and instrumentation of the model, primary access to the interior was through the E/H, while the A/L was used to provide heating, cooling, and ventilation for personnel working inside the model. The M/S and F/W penetrations provided portals for interior instrumentation cabling, power and, during testing, the pressurization medium. Prior to testing, after the E/H cover was installed and sealed, the A/L provided the means for final egress and sealing of the model with a specially-designed pressure seating cover that could be closed from the outside.

Details of the design and fabrication of the PCCV model are described in Chapters 2 and 3.

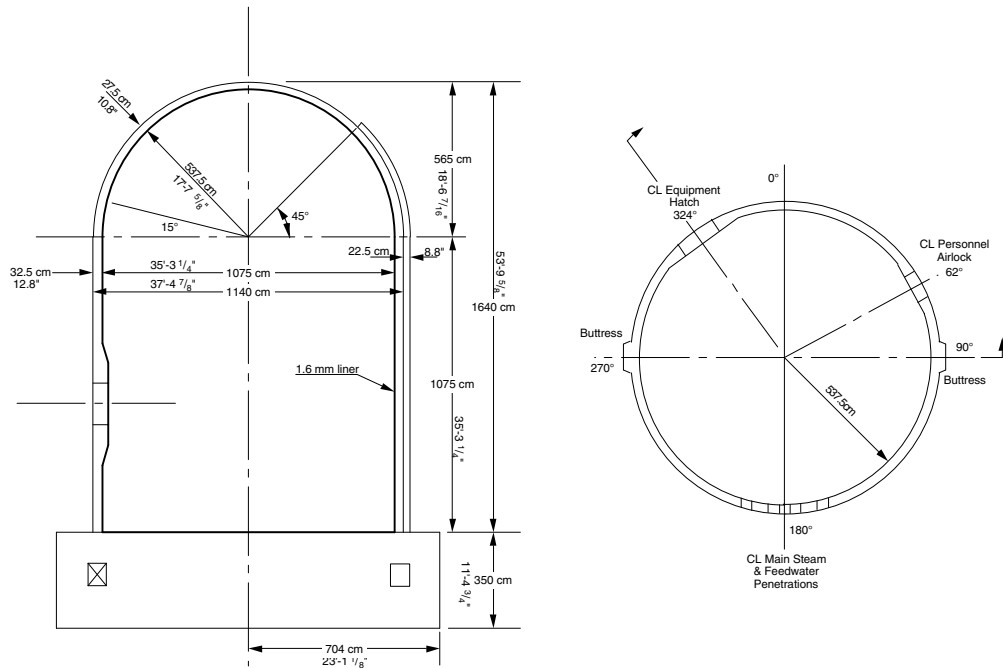


Figure 1.2 PCCV Model Elevation and Cross-Section

1.2.2 Loading

By definition, the scope of this program was limited to addressing the capacity of containment vessels to loads beyond the design basis, the so-called severe accident loads. Design accident loads for light water reactor containment vessels are typically based on the loss-of-coolant accident (LOCA) and are defined by a “bounding” pressure and temperature transients. The term “severe accidents” is used to describe an array of conditions that could result in loads exceeding the design basis on the containment. The definition of severe accident loads, which is not as rigorous as the design basis loads definition, results from considering of various postulated failure scenarios of the primary nuclear system, up to and including a complete core meltdown and breach of the reactor pressure vessel. The resulting pressure and thermal loading characteristics depend on the unique features of the nuclear steam supply (NSS) system and the containment structure, in addition to the postulated accident.

For this test program, it was necessary to decide whether both thermal and pressure loads would be applied to the model, either separately or simultaneously; what the pressurization medium should be; and whether the transient characteristics of these loads should be considered. Programmatically, the decision to perform a *static, pneumatic* overpressurization test at *ambient temperature* was dictated by risk and cost considerations and previous experience.

The effects of severe accident *temperature* loads on the structural response of the containment building are primarily limited to (1) the effects of elevated temperatures on the mechanical properties of the materials and (2) the mechanical loads resulting from differential or constrained thermal expansion. The effects of temperature on the material properties can be determined from standard material tests methods. These test results could be incorporated into the evaluation of the prototypical containment vessels without adding this complexity and cost (in terms of generating the thermal environment and protecting the instrumentation) to the PCCV model test. Regarding the stresses imposed by differential thermal expansion, there are only a few locations in a steel and/or concrete containment building where these effects are significant, notably at the junction of the containment wall and the basemat or, in the case of the PCCV model, the differential thermal expansion between the steel liner and the concrete shell under non-steady-state thermal conditions. Again, the added complexity and cost of simulating the thermal environments to reproduce these local effects was judged not justified for the PCCV model. It was further concluded that the effects of temperature could be addressed using

analytical methods that had been benchmarked against the pressure tests. Therefore, the decision was made to conduct the PCCV model test at *ambient temperature*.

The containment atmosphere during a severe accident consists of air, steam, and other by-products of the accident, including hydrogen and particulates (aerosols). The program's primary interest is in observing and measuring the structural response of the containment to pressure loads, and identifying failure modes. Containment failure (see Section 1.2.3) includes both functional failure, i.e. leakage, and structural failure, i.e., rupture of the pressure-resisting elements. There is not a rigorous distinction between functional and structural failure, and it is conceivable that they might occur simultaneously. Conventional wisdom holds, however, that local, limited structural failure (i.e. liner tearing) and leakage will occur prior to, and at pressures well below those required to cause extensive structural failure. As a result, *detection* of leakage, which indicates a tear in the steel liner or failure of a penetration seal, not *measurement* of actual leak rates for real containment atmospheres (see Section 1.2.3), is the objective of the test. Hence, there is no need to reproduce the containment atmosphere resulting from a severe accident. The choice of a pressurization medium, then, becomes somewhat arbitrary and is dictated by safety and operational considerations. Hydrostatic testing is preferable from a safety viewpoint; however, it raises operational problems and requires protection of sensitive electronics and wiring from the water under high pressure. *Pneumatic* testing, while more dangerous, does not present any risks that cannot be managed cost-effectively and does not require any unusual measures to protect the instrumentation. Nitrogen gas was chosen as the pressurization medium for the PCCV model tests primarily for operational considerations. Fairly large quantities could be delivered at the test site in liquid form with a limited amount of fixed equipment. Nitrogen gas also has the advantage of being dry for instrumentation considerations, and it allows simpler and more accurate calculations to detect a small leak.

The test plan and conduct of the pressure tests, along with the design and operation of the pressurization system, are described in Chapter 5.

It should be noted that the *pneumatic* Limit State Test (LST) was the final test in the original program plan. This test was terminated following a functional failure, i.e. a leak, in the PCCV model, with only limited structural damage occurring. Subsequently, it was decided to repressurize the PCCV model, prior to demolition, in an attempt to observe larger inelastic response and, possibly, a global structural failure. This test was a combined *pneumatic-hydrostatic* test, where the PCCV model was sealed inside with an elastomeric membrane and filled nearly full with water to reduce the volume of gas to be pressurized, and nitrogen gas was used to generate the overpressure. The rationale and design of this Structural Failure Mode Test (SFMT) are also described in Chapter 5.

1.2.3 Response

One important aspect of the PCCV model response in the high pressure tests is the concept of *failure*. In the U.S., the functional failure for the prototypical containment is defined in the regulations as containment leak rates exceeding 0.1 to 0.5% of the containment mass per day [18], considering maximum offsite dose rates due to fission product released to the environment. In Japan, the functional failure is defined in design specifications made by the utility company, not the regulations. (The specified leak rate for the PCCV prototype is 0.1% mass/day.) The functional failure criteria are not particularly useful to test the structural capacity of a containment vessel model, especially when one of the objectives is to generate large inelastic response modes for comparison with analytical predictions, which may be well beyond the levels required to cause functional failure; and secondly to gain some insight into design margins, i.e. the functional and structural capacity beyond the specified design load conditions. In the case of the PCCV model test, the pressurization system allows the model to be pressurized to levels significantly above those expected to cause local strains in the model to exceed the ultimate strain limits of the materials. The test(s) were terminated when the model and the pressurization system were incapable of maintaining or increasing the model pressure due to excessive leakage or gross rupture. In this report, the maximum pressure achieved prior to the termination of the tests will *not* be identified as the *failure pressure*, since failure is defined in terms of some acceptance criteria, not the operational inability to maintain pressure in the model.

The PCCV model instrumentation suite was designed to measure the global behavior in free-field locations of the model and the local structural response of the model near discontinuities. Global response measurements included both displacements referenced to a global or fixed reference, and strain measurements at a regular pattern of azimuths and elevations to characterize the overall shape of the model. Local response measurements consisted of individual structural element (i.e. liner, rebar, tendons, concrete) strain measurements to characterize the force distribution in the free field and near structural discontinuities. In areas without structural discontinuities or where membrane behavior was expected to dominate the response, relatively simple arrays of transducers were specified. Where structural discontinuities were

judged to be significant, more complex arrays of strain gages were utilized. Both hoop and meridional strains were measured.

Pressure measurement requirements included careful measurement of the PCCV interior pressure for leak detection (to a lesser extent); leak rate measurement; characterization of the mechanical response as a function of pressure; and controlling the pressurization rate. Note that while measurement of leak rates was not a primary objective, detecting the onset of leakage requires calculating very small leak rates with relatively high accuracy.

While there was no attempt to simulate severe accident temperature conditions, a fairly extensive set of thermal measurements were taken to measure both the interior and exterior atmospheric temperature for accurate leak rate calculation. Given the large volume of the PCCV model, gas temperatures inside the model could vary significantly and multiple measurements were required to limit errors resulting from nonuniform gas temperatures. During pressurization steps, large thermal gradients could occur as the gas inside the model was compressed. Furthermore, since the model was exposed to the environment, ambient thermal variations, both spatial and temporal, affected the interior gas temperature and could affect the accuracy of the leak rate calculations if not considered. Similarly, ambient thermal effects could affect the model response measurements. Multiple measurements of the model temperature using both embedded and surface mounted temperature transducers were employed to account for this effect.

As implied by the name, the unique feature of the PCCV model is the prestressing system, comprised of the vertical and hoop tendons and associated hardware. Special efforts were made to monitor the response of the prestressing system, both prior to and during pressure testing. An extensive effort was undertaken to develop and demonstrate the reliability of the tendon instrumentation. The resulting system was comprised of two types of gages to monitor the strain, and, by calculation, the force distribution along the length of selected tendons along with load cells to measure the forces at the tendon anchors. Since the behavior of the tendons and the overall response of the model to the pressure load would be directly affected by the initial prestressing forces, the response of the PCCV model was monitored continuously from the start of prestressing through the subsequent pressure tests.

While these force, strain, and displacement measurements provide accurate information on the response of the model at discrete locations, it is desirable to monitor the overall response of the model in the (likely) event that some significant response occurs at locations remote from any transducer. The displacement transducers reflect, to a greater extent than the strain or force transducers, the overall response of the model, but might still miss other local response modes. This deficiency was addressed by including an extensive array of acoustic and, to a lesser degree, video/photographic monitoring of the PCCV model. While more qualitative in nature than the discrete response measurements, some quantitative information could be obtained from these monitoring systems. The acoustic system, in particular, was designed to detect the onset of liner tearing and leakage, along with concrete cracking and rupture of tendon wires or rebar. Similarly, video and still photography were used to document the development and distribution of concrete cracking, detect liner tearing at discrete locations during pressure testing, and capture any unanticipated response modes.

The design and implementation of the model instrumentation suite are described in Chapter 3. Performance requirements and features of the data acquisition system and data management are summarized in Chapter 4. A summary and discussion of the high pressure tests and posttest inspections are provided in Chapter 5. The test results are also summarized in Chapter 5 and the corrected test data, including a description of the corrections applied to the raw data, are included in the appendices.

1.3 Project Organization

As noted above, NUPEC and the NRC are the sponsoring organizations for this cooperative containment research program. Programmatic authorization to pursue this area of research is provided to these organizations by the ministerial or executive offices of their respective national governments, as dictated by statute. Technical guidance was provided by panels of expert advisers from academia and industry in each country. In Japan, the Structural Advisory Committee met regularly with NUPEC personnel to review the program plans and status, while in the U.S., a special Peer Review Panel provided the same support to NRC and SNL personnel.

Within the cooperative framework agreed to by NUPEC and the NRC, NUPEC and its Japanese contractors designed and constructed the PCCV model at SNL's Containment Technology Test Facility-West (CTTF-W). This test facility was specially constructed by SNL on land temporarily permitted for this purpose by Kirtland Air Force Base (KAFB), Albuquerque, New Mexico, USA. This 'West' facility is distinct from the CTTF used for the previous large-scale model tests conducted for the U.S. NRC in the 1980s. The 'East' facility was not considered suitable for continued large-scale

model testing due to the identification of previous environmental contamination (not associated with the containment test operations) and subsequent clean-up operations that might interfere with the Cooperative program operations. The CTTF-West Land-Use Permit required NUPEC and the NRC, through their contracts with SNL, to remove all improvements within the permit boundaries and return the site to near its original condition at the conclusion of all test operations.

NUPEC and its Japanese contractors were authorized to construct the model at the CTTF-W under a specially negotiated Premise Access Agreement with SNL and the DOE. This agreement required NUPEC and its contractors to abide by all environmental health and safety regulations typically required for all capital construction activities managed by SNL, and authorized SNL to perform construction safety inspection to ensure that all requirements were being satisfied. The prime contractor to NUPEC for the construction of the PCCV model was Mitsubishi Heavy Industries (MHI), who also designed and constructed the prototype plant, Ohi-3. In addition to overall design and construction, MHI designed, fabricated, and erected the steel liner and all primary steel pressure-retaining components. Supporting MHI for the reinforced concrete portions of the model and ancillary structures were several subcontractors. Obayashi Corp., a large Japanese Architect/Engineer (A/E) and construction company, performed the detailed design of the PCCV model, and Taisei Corp, another large A/E/Contractor, was the construction manager. Taisei retained the U.S. construction firm, Hensel Phelps Construction Co., Greeley, CO for general construction work and management of day-to-day construction operations. MHI prefabricated portions of the steel liner and the penetrations at their Kobe Shipyard and transported these components to the CTTF-W for final erection. The balance of the model was constructed on-site.

NUPEC also funded SNL to provide programmatic and model design support, instrument the model, and design and assemble the data acquisition system.

NRC funded SNL to perform preliminary, pre- and posttest analyses of the model. This analytical work was subcontracted by SNL to ANATECH Consulting Engineers, San Diego, CA. The decision to subcontract this work to ANATECH was based, in part, on a successful history of collaboration on previous containment model tests [19, 20] and ANATECH's experience in developing sophisticated concrete models and related efforts for the Electric Power Research Institute (EPRI), Palo Alto, CA [21]. The preliminary analyses supported design studies, identified critical response modes, and assisted in the locating instrumentation. The pretest analysis consisted of developing and analyzing detailed numerical models in an attempt to predict the response of the PCCV to the test pressures and predict the capacity and most probable failure mode. The posttest analysis compared the test results to the pretest predictions, investigated and demonstrated changes in the modeling methods to improve comparison with the test results, and provided insights into the response observed during the pressure tests. The pre- and posttest analyses are reported separately [6,7] and are not included in this report.

NRC also funded the planning and conduct of test operations.

NUPEC and NRC also jointly provided funding to share the costs associated with organizing and conducting a pretest Round Robin analysis. The Round Robin analysis euphemistically refers to an activity where a number of nuclear safety research organizations from government, industry, and academia in the U.S., Japan, and other countries, are provided with a common set of data on the model test (design drawings, material properties, test specifications, etc.) and complete independent predictions of the model response, failure mode, and pressure capacity. SNL was the focal point for this effort in terms of disseminating and consolidating the work of the participating organizations. Seventeen independent organizations, including NUPEC and SNL, participated in this effort, performing pretest analyses and meeting before and after the PCCV model test to discuss and compare analysis results. The efforts of these Round Robin participants are documented in separate NUREG Contractor Reports [8]. While a formal posttest Round Robin exercise was not conducted for the PCCV, most of the participants attended a posttest workshop and have reported the results of their posttest analyses independently.

Regular Technical Working Group meetings were held in both Japan and the U.S., involving program personnel from NUPEC, (including its contractors), the NRC, and SNL. These meetings planned and coordinated program activities and resolve technical issues. Separate meetings were held to discuss administrative issues related to cost and schedule.

1.4 Project Schedule

The NUPEC/NRC Cooperative Containment Research Program commenced in June 1991. The tests were conducted at the CTTF-W at SNL. Figure 1.3 illustrates the layout of the test site. A safety zone consisting of a circular area with

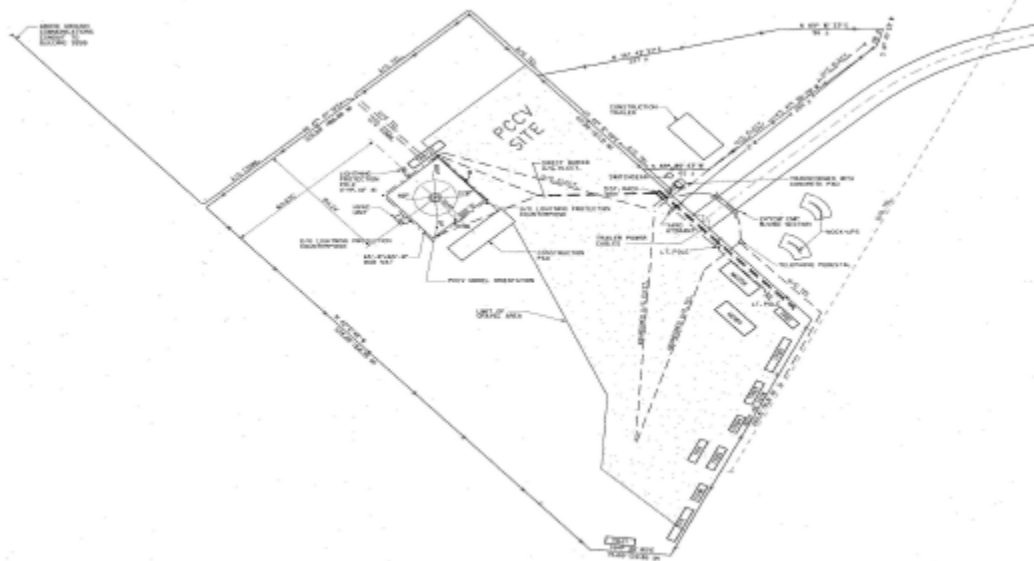


Figure 1.3 Plan of Containment Technology Test Facility-West

radius of 600 m (2000 ft) was maintained and monitored throughout the high-pressure test. The command center in Building 9950, located outside the exclusion zone, served as headquarters for conducting the high-pressure tests.

The high-pressure test of the SCV was completed on December 12, 1996. Construction of the PCCV model commenced January 3, 1997 with initial site preparation. Milestones in the construction and testing of the PCCV model included the following:

- 12 February 1997; First Basemat Pour (F1)
- 19 June 1997; First Liner Panel Installed
- 15 April 1999; Final Dome Pour (D3)
- 12-14 October 1999; Pretest Round Robin Meeting
- 8 March-3 May 2000; Prestressing
- 25 June 2000; PCCV Construction Completed
- 12-14 September 2000; Structural Integrity and Integrated Leak Rate Test
- 27-28 September 2000; Limit State Test
- 22 August 2001; Posttest Round Robin Meeting
- 14 November 2001; Structural Failure Mode Test
- 3 May 2002; PCCV Demolition and Site Restoration Completed

With the completion of the PCCV tests, restoration of the test site, and publication of the test reports, the NUPEC/NRC Cooperative Containment Research Program was formally concluded on December 31, 2002.

2. DESIGN AND CONSTRUCTION OF THE PCCV MODEL

2.1 Design

The PCCV model design was directed by NUPEC with overall responsibility for the design and construction contracted to MHI, Tokyo. Responsibility for the design of the liner and penetrations was assigned to MHI's Kobe Shipyard and Machinery Works while the concrete portions of the model were subcontracted to Obayashi Corp., Tokyo.

The basic philosophy guiding the design of the PCCV model was agreed upon very early in the program [22]. Key elements of this design philosophy included:

1. The PCCV model would be a uniform 1:4-scale model of the prototype or actual prestressed concrete containment vessel of Ohi Unit 3.
2. Elements of the model that would affect the ultimate strength would be equivalent to the prototype. The model liner would be one-fourth the thickness of the prototype liner. Reinforcing ratios would be maintained and the number and arrangement of the prestressing tendons would, to the extent possible, be identical to the prototype.
3. The model would be capable of reproducing the failure modes postulated for the prototype, including
 - a. Hoop tensile failure of the cylinder wall
 - b. Bending-shear failure at the junction of the cylinder wall with the basemat
 - c. Shear failure in the basemat above the tendon gallery
 - d. Bearing failure at the tendon anchors
 - e. Bending-shear failure at the large penetrations
 - f. Bending-shear at the small penetrations
 - g. Liner tearing due to strain concentrations at local discontinuities (stiffeners/anchors, thickened reinforcing plates at penetrations and embedments)
 - h. Leakage at penetration seals due to ovalization or distortion of the sealing surfaces.

Furthermore, to the extent possible, introduction of non-representative failure modes as a result of scaling or other modeling artifacts was to be avoided.

The general arrangement and representative failure mode locations are shown in Figure 2.1.

While the PCCV model was not 'designed' in the conventional sense, it's features were scaled directly from the Ohi-3 design with some simplifications to facilitate construction without compromising the objectives of the test. The prototype, Ohi-3, was designed in accordance with the "Draft Technical Code for Concrete Containment Vessels in Nuclear Power Plants" issued by Ministry of International Trade and Industry/Agency for Natural Resources and Energy (MITI/ANRE) in November, 1981 [23]. This draft code was formally adopted in 1993 as MITI Notification No. 452. The code is not identical to the American Society of Mechanical Engineers/American Concrete Institute (ASME/ACI) code [9], which governs the design of concrete containments in the U.S.; however, the basic design philosophies are similar, i.e., to ensure that all elements of the containment structure respond elastically (with some minor exceptions for secondary stresses) to the specified design loading conditions.

Construction of the prototype was also governed by Japanese Architectural Standard Specifications No. 5 and 5N for Reinforced Concrete Work at Nuclear Power Plants [24, 25]. Construction specifications for the PCCV model also followed these standards to the extent possible; however, modifications were made to adapt the specifications to U.S. construction practices.

The final design drawings for the PCCV model are provided in Appendix A. While it is beyond the scope of this report to include all the details of the design and construction specifications, a discussion of those features relevant to the model's response is appropriate and is included below.

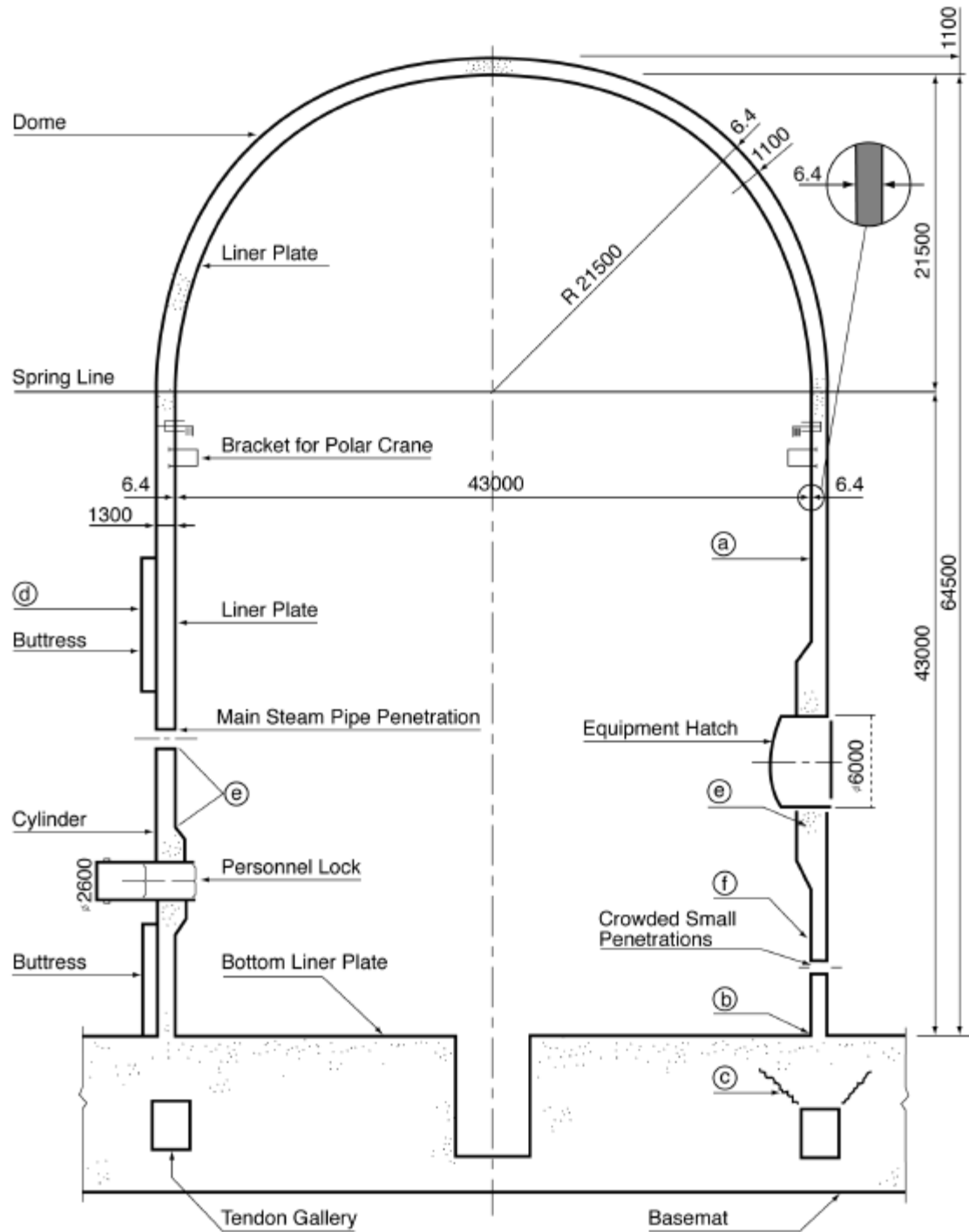


Figure 2.1. Elevation of PCCV Prototype and Potential Failure Locations

2.1.1 Liner Design Considerations

Design and fabrication/erection of the liner and penetrations was performed by MHI. The detailed specifications and practices are included in the project files. Essentially, the 1.6 mm (1/16") model liner was scaled from the 6.4 mm (~1/4") prototype liner. The as-built model liner thickness was 1.8 mm (0.070"), the extra 0.2 mm (0.008") providing a fabrication allowance. The model and prototype liner were both fabricated from SGV 410¹ carbon steel. JIS G3118 does not specify plate material under 6mm in thickness. The PCCV liner plate was fabricated to the same specifications as SGV410. Liner anchors and stiffeners were fabricated from SS 400². Penetration assemblies were fabricated from SGV 410. The nominal properties of SGV 410 and SS 400 are given in Table 2.1. Miscellaneous non-structural components, e.g. back-up bars, were fabricated from U.S. common bar stock, typically ASTM A36 carbon steel.

Table 2.1 Properties of Liner Materials

Nominal Properties	Liner Plate	Liner Anchors
	SGV 410	SS 400
Yield Strength	225 Mpa (33 ksi)	235 Mpa (34 ksi)
Tensile Strength	410 MPa (59 ksi)	392 Mpa (57 ksi)

The liner material was procured in Japan, and liner panels were prefabricated and welded at MHI's Kobe Shipyard. Jigs, to support the liner panels and facilitate field erection and assembly, were attached to the liner panels prior to shipping them to the test site in Albuquerque, NM. Note that these jigs are unique to the construction of the model. The prototype liner is thick enough to be self-supporting without the use of any jigs. All vertical and horizontal liner weld seams in the prototype were reproduced in the model. Typically, the panel assemblies for the cylinder wall fabricated in Kobe encompassed three vertical rings of individual plate segments, resulting in assemblies approximately 3 m². Dome segments and penetration assemblies were typically smaller, individual plate segments. All welding of the assemblies in Kobe, including attachment of the anchors and stiffeners, was done by computer-controlled automatic welders. All shop welding was done without the use of back-up bars.

Standard coupons were made from the liner and liner anchor materials, and these specimens were tested for quality control purposes and to determine the actual material properties. The results of these tests are summarized in Appendix B.

The general arrangement of the liner anchors on the PCCV model is shown in the design drawings and is illustrated in Figure 2.2. The vertical liner anchors in the prototype consisted of 'T-anchors' spaced 600 mm (24") on-center throughout the cylinder wall and dome. These anchors are built-up sections, continuously welded to the liner plate with double-sided fillet welds. Horizontal bar stiffeners are provided above and below each horizontal weld seam to stiffen the liner during construction. The model liner anchors and stiffeners are 1:4-scale of the prototype. At 1:4-scale, the vertical anchor spacing would be 150 mm (6"); however, because the liner anchors are, in general, ineffective at resisting pressure and facilitating fabrication, the vertical anchor spacing was increased to 450 mm (18") except near discontinuities in the liner, such as the wall-base junction, around the E/H, A/L, M/S, and F/W penetrations and around the crane rail bracket embedments, as shown in Figure 2.2. Furthermore, the vertical liner anchors were not extended into the dome. T-stiffeners were used at the perimeter of the dome liner segments, but interior T-anchors were replaced with small stud-type anchors, as shown on the drawings. Again, since the strains in the dome were expected to be well below those experienced by the cylinder wall, this modification was not judged to affect the pressure capacity of the model.

As noted previously, the majority of the liner anchors were shop-welded to the liner using welding machines. One additional deviation from the prototype was the use of intermittent, staggered fillet welds to attach the anchors and stiffeners to the liner plate. There was a concern that these 'stitch' welds might generate additional local strain concentrations from the weld geometry itself. Therefore, anchors and stiffeners adjacent to other local liner discontinuities were continuously welded to reduce the possibility of premature liner tearing.

¹ Japanese Industrial Standard (JIS) G 3118, "Carbon Steel Plates for Pressure Vessels for Intermediate and Moderate Temperature Service," Japanese Standards Association.

² JIS G 3101, "Rolled Steel for General Structure," Japanese Standards Association.

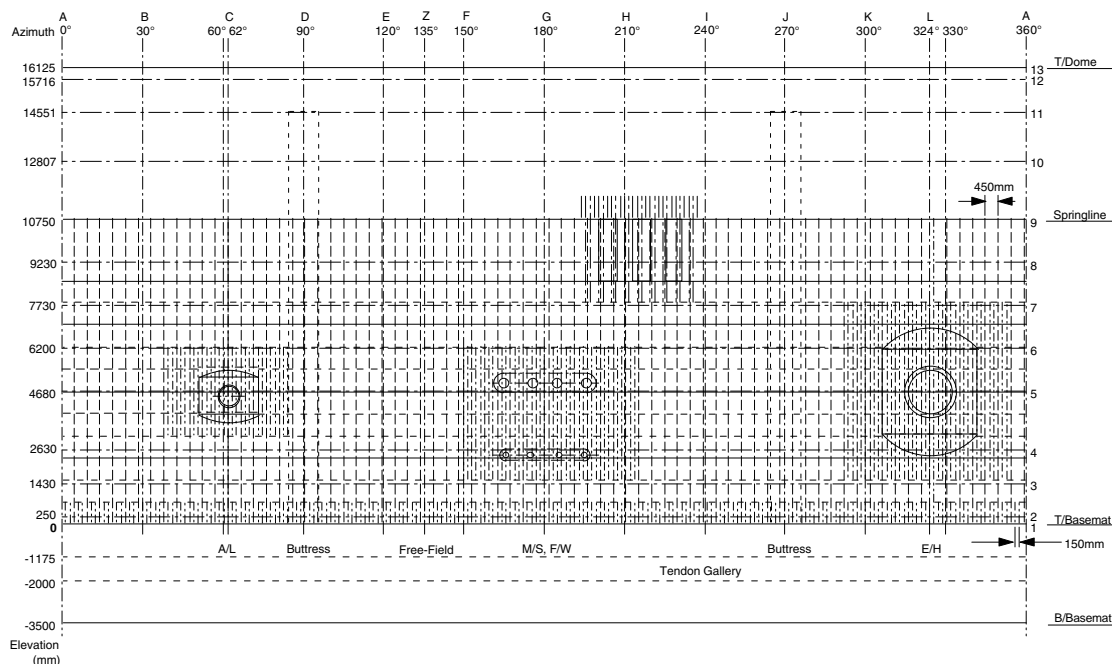


Figure 2.2 Liner Anchor Layout

While all the penetrations in the prototype were not included in the model, the major penetrations, consisting of the E/H, A/L, M/S, and F/W penetrations, were included in the model. These penetrations were representative of all the penetrations in the prototype and would be capable of reproducing the local strain concentrations in the structure and the liner. The E/H and A/L penetration assemblies in the model are 1:4-scale functional representations of the prototype assemblies, except that the A/L assembly includes only a single pressure seating cover and the interior doors are not reproduced. The model M/S and F/W penetration assemblies only included the penetration sleeve and reinforcing plates and were equipped with an interior flange and sealed with bolted pressure seating blind cover. No attempt was made to simulate the constraint conditions that might be imposed by the M/S or F/W piping. All the penetration sealing surfaces were milled and machined with grooves for double O-ring gaskets. The prototype penetration assemblies are shown in Figures 2.3 to 2.6 for comparison to the model penetration assemblies shown in the design drawings. The model did not include the polar crane rail or brackets; however, a set of three adjacent bracket embedments were included to reproduce the local discontinuities in the liner.

The erection, field welding, and quality control of the liner are described in Section 2.2.

2.1.2 Concrete Design Considerations

2.1.2.1 Geometry

While the basic geometric scale of 1:4 was maintained throughout the PCCV model, some exceptions and modifications were required. Most significantly, the configuration of the model basemat had to be determined. The thickness of the model basemat at 1:4 scale is 3.5 m (11' 5-3/4"). The primary design consideration of the model basemat is that the rotational stiffness at the wall-base junction is equivalent to the prototype, since this affects the bending-shear failure mode at this location. The prototype containment basemat is continuous with the mat for the surrounding structures and includes a large reactor cavity at the center of the containment. Simplified three-dimensional finite element analyses of both the prototype and model subjected to pressure loading were performed to select the dimensions and reinforcement for the model basemat that would yield the desired response characteristics. The scaled basemat thickness of 3.5 m was maintained and, with the reactor cavity eliminated from the model, the radius of 7.2 m (23' 7 1/2") and reinforcing were selected to match rotational stiffness of the prototype.

The location and size of the tendon gallery were scaled from the prototype. However, some modification of the construction sequence was required to accommodate this decision. Since the vertical prestressing tendons could not be inserted and tensioned inside a roughly 1-m² (2'-1" × 2'-8") tunnel, the portion of the basemat outside and below the tendon gallery was not constructed until after the tendons had been tensioned. This resulted in a somewhat different state of stress in the model basemat after prestressing; however, this difference was not significant and was unavoidable. Four access 'tunnels' to the tendon gallery were also included at 0 degrees, 90 degrees, 180 degrees, and 270 degrees to allow for visual inspection of the vertical tendon anchors and to ventilate the tendon gallery to minimize moisture that might affect the tendon anchors and the instrumentation.

Finally, some minor modifications in the geometry of the hoop tendon buttresses were required to accommodate the prestressing hardware. These were again judged to be insignificant with respect to the model's response to pressure.

2.1.2.2 Concrete Mix

The fundamental requirement of the PCCV model concrete was that it exhibit the same properties as the concrete used in the prototype. Based on prior experience with the construction and testing of a 1:6-scale reinforced concrete containment model at SNL, the approach to achieving this requirement was to specify a mix, using local (New Mexico) materials that would have the same 91-day³ compressive strength (f'_c) as the prototype concrete and then test the trial mix(es) to ensure they exhibited the same mechanical and chemical properties.

Two different concrete strengths were used in the prototype: 300 kg/cm² (4300 psi) for the majority of the basemat and 450 kg/cm² (6400 psi) for the cylinder wall, dome, and the portion of the basemat above the tendon gallery. The location of each mix, along with the lifts used in the construction of the model, are shown in Figure 2.7. Note that concrete lifts were not scaled from the prototype and are unique to the model.

The mix designs for the PCCV model consisted of Type I-II cement, air-entrained with 20% Class 2 Flyash and superplasticizer. Cement, aggregate, flyash, and water were all obtained locally and were batched by a supplier and mixed in transit. Maximum aggregate size was 10 mm (3/8"). Water/cement ratio for the 300 and 450 kg/cm² mixes were 0.43% and 0.34%, respectively.

Corrosion due to the presence of chlorides and alkalis in the mix was a concern for the prototype due to the close proximity of the plant to the ocean; however, this was not judged to be a major concern for the model, although the chemical composition of the mix would be tested. Flyash was specified for the trial mix, since the use of flyash is standard practice in the construction of Japanese nuclear power plants and minimizes possible reaction and expansion of the aggregate. (Use of flyash is not permitted in construction of U.S. nuclear power plants). Superplasticizers were specified to facilitate placement of the concrete by pumping in congested areas. A maximum slump of 10 cm (4") before and 20 cm (8") after adding superplasticizers at the site was specified.

The trial mixes were batched and tested by Construction Technologies Laboratories, Skokie, IL to determine if they met the project specifications. The properties determined from trial mix specimens are summarized in Appendix B. In lieu of actual material property data, the trial mix properties were used for the pretest analysis of the PCCV model.

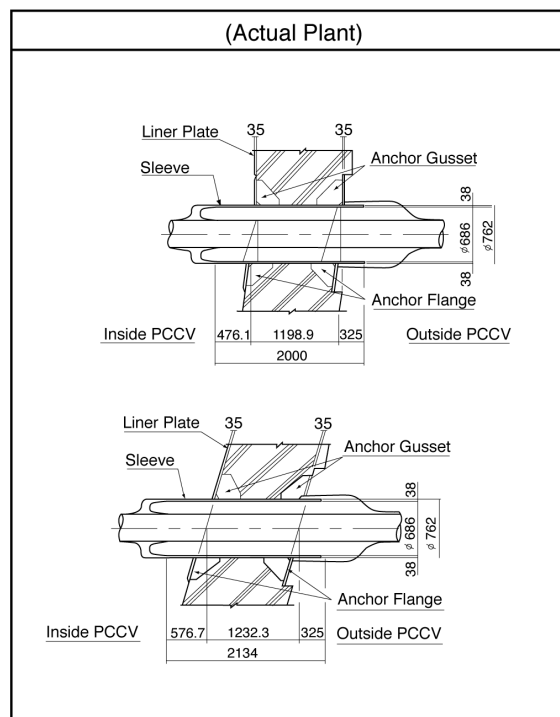
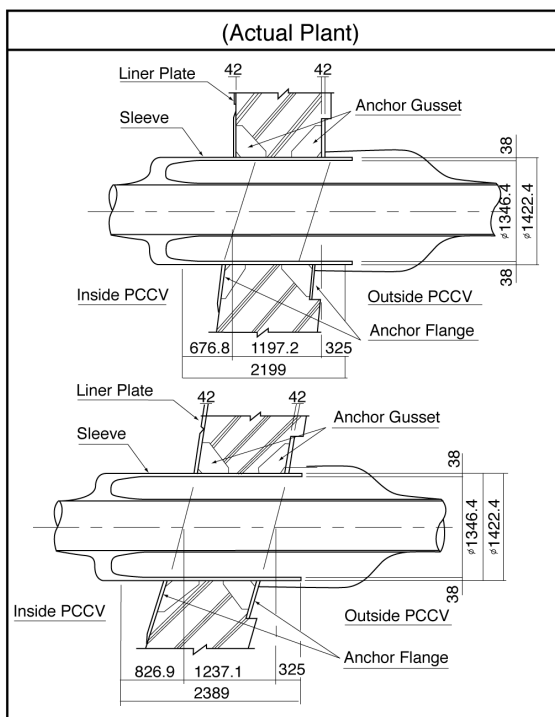
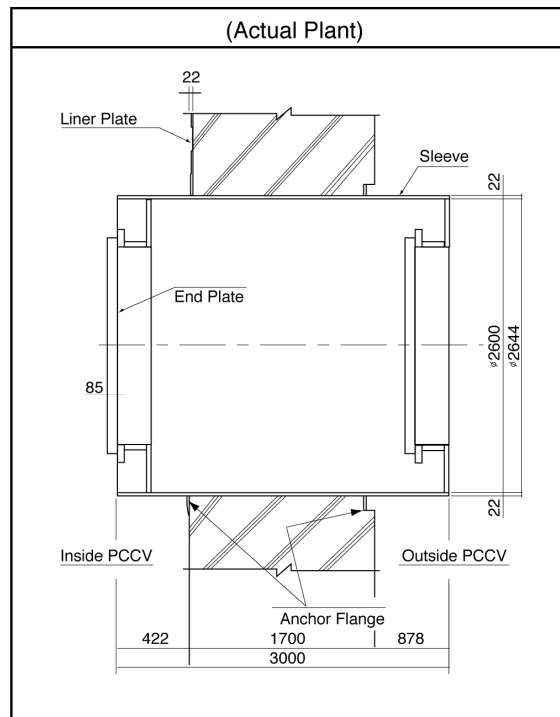
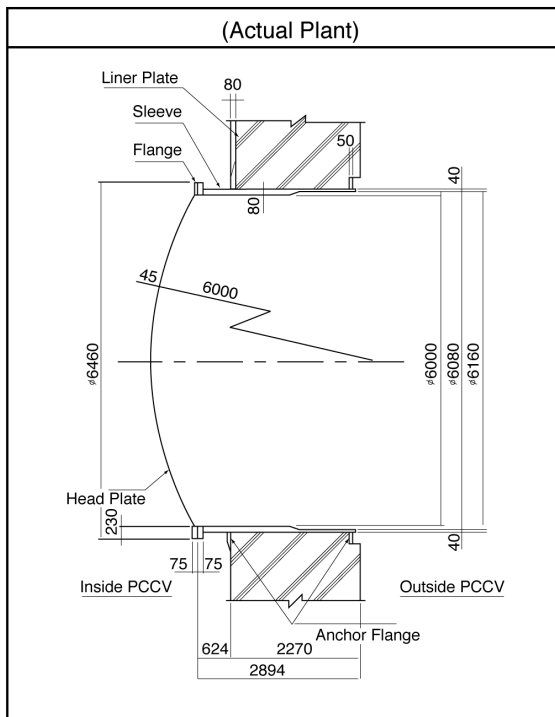
Quality control and material property test results for the concrete used to construct the model are described in Section 2.2 and summarized in Appendix B.

2.1.2.3 Reinforcing Steel (Rebar)

Normal, i.e. non-tensioned reinforcing steel for the prototype included grade SD490, SD390, and SD345 deformed bars⁴. The same grade steels were used to manufacture the rebar for the model in the U.S. (Cascade Steel, McMinnville, OR) in accordance with JIS Standards. The nominal properties for the rebar used in the model are summarized in Tables 2.2 and 2.3.

³ JIS A 1108, "Method of Test for Compressive Strength of Concrete," allows specification of design strength at four weeks (28 days) or 13 weeks (91 days). Project specifications for the PCCV prototype and model specified the design strength f'_c at 91 days.

⁴ JIS G 3112, "Steel Bars for Concrete Reinforcement."



In order to minimize rebar congestion in the model, all splices were originally intended to be made using swaged threaded couplers or position threaded couplers⁵. Swaged in-place couplers were not considered practical for the model due to limited clearance for the hand press. However, field considerations required some limited use of this type of coupler⁶.

Samples of all the rebar used in the model were tested for quality control and to determine mechanical properties for analysis according to JIS and ASTM methods. Tests were also conducted of both the threaded and position-threaded couplers used in the model construction. (No tests were conducted of the swaged in-place couplers.) ‘Dumbbell’ specimens were machined from SD390 D16, and D22 bars to measure the basic material properties. Finally, a series of bars were tested with strain gages installed in the same manner as the instrumented bars in the model to calibrate the strains with a standard extensometer. The results of all these tests are summarized in Appendix B.

While the basic reinforcing ratios in the model were nearly the same as the prototype, the reinforcing in the model differed from the prototype. Individual bars in the model were not scaled directly from the prototype. Generally, in the containment shell (i.e. the cylinder wall and dome), the rebar was placed in one layer in each direction on each face. Figure 2.8 compares the arrangement of the reinforcing at the base of the cylinder wall in the prototype with the model. In-plane spacing of the rebar in the model is based on the arrangement of the prestressing tendons (2 degrees on center circumferentially and 112.5 mm (4.4") on center vertically). Bar sizes were then selected to reproduce as closely as possible, within the limits of the standard bar sizes available, the reinforcing ratio of the prototype.

Tolerances on formed surfaces and placement of rebar were developed by considering the 1:4-scaled tolerances for the prototype and then adjusting these to accommodate practical construction limitations, such as congestion and clearance for concrete placement. These tolerances are specified in the model construction specifications along with the as-built records. The deviations from the nominal design dimensions were not judged significant enough to affect the response of the model and, accordingly, are not included in this report.

Additional reinforcing was also provided around the penetrations in the model. However, where prototype penetrations were eliminated, no additional reinforcing was included in the model.

2.1.3 Prestressing Design Considerations

Since the unique feature of the PCCV model, compared to previous large-scale containment model tests, was the prestressing system, particular attention was paid to the design, construction, and instrumentation of this component. An unbonded, seven-wire strand prestressing system⁷ was used in both the PCCV prototype and model. The tendons in the prototype consisted of 55, 12.7mm (½ in) diameter seven-wire strands⁸. The number and arrangement of the tendons in the model were kept the same as the prototype. The arrangement of the tendons is shown in Appendix A.

Both the prototype and model tendons were inserted in galvanized metal sheath or ducts after the concrete had been placed and allowed to cure, then tensioned. The model ducts were, generally, 35 mm (1-3/8") in diameter and were not ‘greased’ after tensioning. (The prototype tendon ducts were, as typical of most unbonded tendons, injected with a heavy grease after tensioning to protect the tendons from corrosion. Since the model tendons would only be in use for a relatively short time (< 2 years), they were not greased, although an anti-corrosion ‘shop-coat’ was brushed on prior to insertion in the ducts. Not greasing the tendons also facilitated the placement of instrumentation on selected tendons.)

In order to maintain the correct scaled cross-sectional area, the model tendons consisted of three, 13.7-mm (0.54") seven-wire strands. These model strands were custom-manufactured by the vendor for the model and nominal properties are not defined in the Japanese standard specifications, although the basic wire material was the same used for the prototype tendons⁹. The minimum properties of the model strands per the project specifications are given in Table 2.4. Extensive testing of individual strands as well as the tendon system were conducted for quality control and to determine the mechanical properties of the tendons. The results of these tests are summarized in Appendix B.

⁵ Grip-Twist® System, manufactured by BarSplice Products Co., Dayton OH.

⁶ Bar-Grip® System, *ibid*

⁷ VSL Multistrand Posttensioning System^a, VSL Corporation, Japan

⁸ JIS G 3536, “Uncoated Stress-Relieved Steel Wires and Strands for Prestressed Concrete.”

⁹ JIS G 3502, “Piano Wire Rod.”

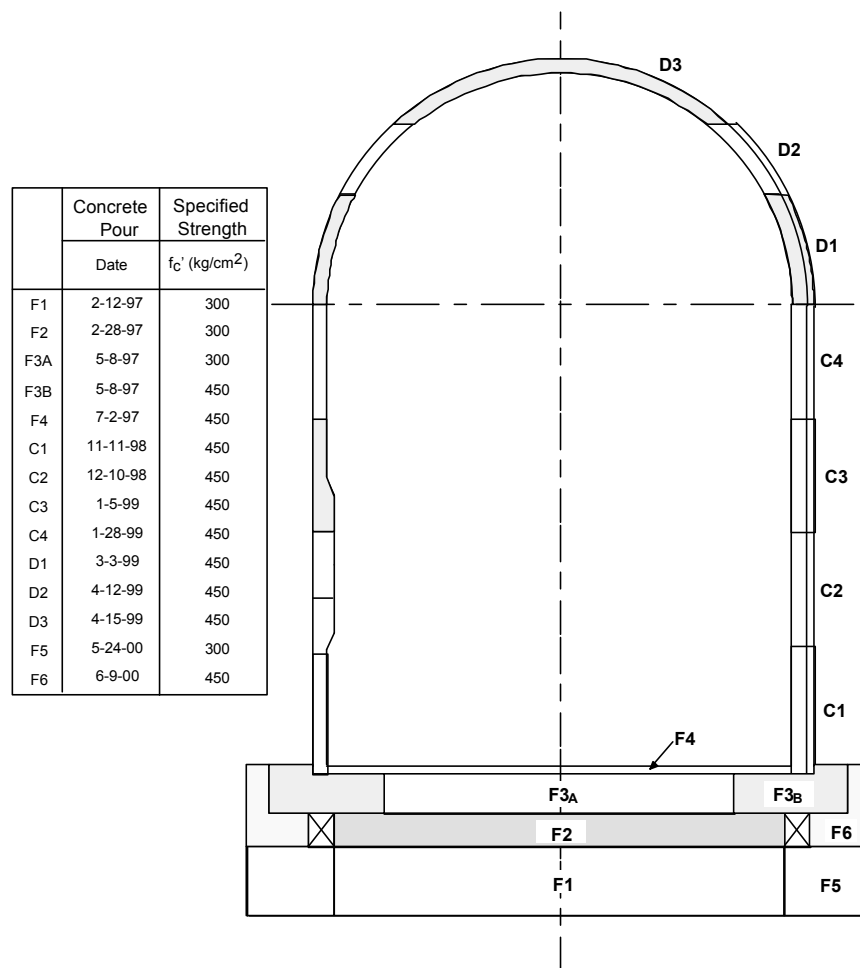


Figure 2.7 PCCV Concrete Lifts and Strengths

Table 2.2 JIS G 3112 Reinforcing Steel Properties

Grade	SD345	SD390	SD490
Model Location	Shell shear ties	Shell main bars, basemat shear bars	Basemat main bars
F_y min	343MPa ~50 ksi	392MPa ~57 ksi	490MPa ~71 ksi
F_t min	490MPa ~71 ksi	559MPa ~81 ksi	618MPa ~90 ksi
Elong.	18-20%	16-18%	12-14%

Table 2.3 JIS G 3112 Bar Properties
(Comparison with ASTM Standard Rebar)

	Nom. Diameter (d)		Nom. Area		Nom. Weight	
	millimeters	in	cm ²	in ²	kg/m	lb/ft
D6 (#2)	6.35	0.25	0.317	0.05	0.25	0.17
D10 (#3)	9.53	0.375	0.713	0.11	0.56	0.38
D13 (#4)	12.7	0.5	1.267	0.2	1	0.67
D16 (#5)	15.9	0.626	1.986	0.31	1.56	1.05
D19 (#6)	19.1	0.752	2.865	0.44	2.25	1.51
D22 (#7)	22.2	0.874	3.871	0.6	3.04	2.04

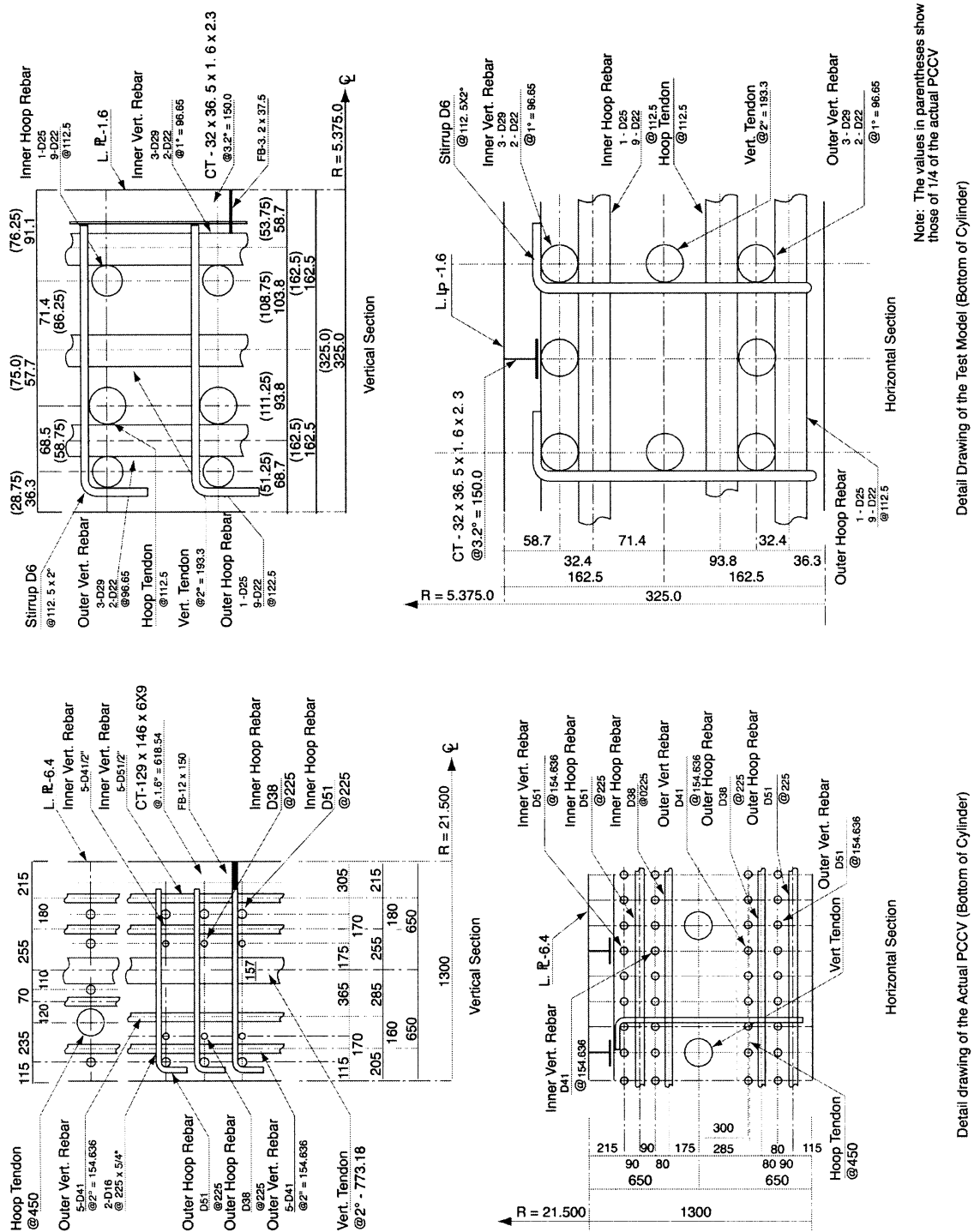


Figure 2.8 Arrangement of Reinforcing in the PCCV Prototype and Model at the Wall-Base Junction

Table 2.4 PCCV Model Tendon Strand Properties

Diameter:min	13.5 millimeters	0.531 in
nom	13.7 millimeters	0.539 in
max	14.1 millimeters	0.555 in
Area	1.131 cm ²	0.175 in ²
Yield Strength*	190 kN	42.7 kips
Tensile Strength	210 kN	47.2 kips
Min. Elongation	4.5%	4.5%

*Load at 0.2% elongation

Given the properties and arrangement of the tendons, the tensioning forces were specified to achieve the same effect in the model as the prototype, considering the unique features of the model prestressing system that do not scale. Three basic criteria were used to establish equivalence between the prototype and model prestressing.

1. First, the state of prestressing in the model should reflect the predicted state of stress in the prototype after reaching its 40-year design life. Since the model was tested approximately six months after tensioning the tendons, it was necessary to adjust the initial tensioning forces to account for the expected creep and relaxation losses in the prototype.
2. Second, the effective hoop compressive stress due to prestressing should be the same in the model as the prototype. This relates directly to the requirement that the hoop tensile response and failure mode in the cylinder wall be accurately modeled.
3. Third, the vertical compressive stress in the concrete at the base of the cylinder wall should be the same in the model and the prototype. This relates directly to the requirement that the bending/shear response and failure mode at the base of the cylinder wall be accurately modeled.

Given these criteria, the following factors were considered:

1. Tendon friction: Tendon stresses decrease from the point where the tension load is applied, i.e., the anchor, due to friction between the tendon and the sheath and between the strands themselves. Two components of friction are considered in the design; ‘wobble’ friction, λ , which results from the internal friction between the tendon strands and ducts, and angular friction, μ , which occurs as a result of sweeping the tendons around a curve. The tendon stress at any point, σ_x , along the length of the tendon is given by:

$$\sigma_x = \sigma_0 e^{-(\mu\alpha + \lambda l)}$$

where σ_0 is the applied tension, α is the arc length, and l is the distance from the anchor along the tendon.

The values of μ and λ used in the design of the prototype were 0.14 and 0.001, respectively. Since the model strands were actually larger in diameter than those used in the prototype (and therefore stiffer) and bent to a ‘4x’ tighter radius, tests of the model tendons resulted in values for angular and wobble friction coefficients of

$$\mu = 0.21, \lambda = 0.001$$

2. Setting Losses: After the tendons are tensioned, the tensioning forces are locked in by seating the strands in the anchor blocks using tapered wedges. During this process, there is some loss of anchor force due to slipping and settling of the anchor components. The tensioning hardware (anchors, wedges, jacks, etc.) cannot be scaled and as a result, the maximum setting loss specified for the model, 5 mm (0.2"), is larger than the scaled setting loss and nearly equal to the actual setting loss specified for the prototype. (The setting loss, specified in terms of length, is the measured change in length of the projecting tails of the tendons strands before and after anchoring.)

The larger setting loss, coupled with the higher friction coefficients for the model, result in stress profiles in the model tendons that are much less uniform than those in the prototype.

3. Gravity: For geometric scaling, mass densities are not scaled correctly if the same materials are used to construct the model and the prototype. For static tests, this only affects the dead load stresses, which, typically, are only a small percentage of the total stress. For the static overpressurization tests of the PCCV, this scaling artifact would not significantly affect on the model response, except, possibly, at the wall-base junction. Compressive stresses due to dead load are larger at the base of the cylinder wall than anywhere else in the model, and this stress may be an important response component for a bending/shear failure mode. Consequently, vertical tendon design loads were increased in the PCCV model to compensate for the reduced stress due to dead load at the wall-base junction.

The final tendon design stress profiles are shown in Figure 2.9. The profiles are given for a typical hoop tendon in the cylinder wall and for the longest and shortest vertical hairpin tendons. The stress distribution for the shorter hoop tendons in the dome and for both hoop and vertical tendons deflected around penetrations are not shown but can be calculated in a similar manner. (Note that the design tensioning and anchor forces for ‘deflected’ tendons are not adjusted in either the prototype or the model, to account for additional friction losses due to ‘in-plane’ curvature.) The corresponding design anchor forces are given in Table 2.5. These values were included in the model prestressing specifications. The as-built prestressing results are summarized in Section 2.2.3.

Table 2.5 PCCV Model Design Prestressing Anchor Forces

Tendons	Tensioning Force	Lift-Off Force	Losses (Creep and Relaxation)*	At Test
Vertical Tendons	49.6 tonnes (109.3 kips)	46.3 (102.1)	3.1 (6.8)	43.2 (95.3)
Hoop Tendons	44.4 tonnes (97.9 kips)	34.1 (75.2)	3.1 (6.8)	31 -68.4

*Losses evaluated at six months.

Considering the design tendon stress profiles, the prestressing design criteria can be satisfied. For the prototype, the average hoop tendon stress after 40 years is 85.3 kg_f/mm² (121.3 ksi). Calculating the equivalent pressure, p_{eqv} :

$$p_{eqv} = \frac{\sigma a}{R s} = \frac{(85.3 \text{ kg}_f/\text{mm}^2)(5429 \text{ mm}^2)}{(2150 \text{ cm})(45 \text{ cm})} = 4.8 \text{ kg}_f/\text{cm}^2 (68 \text{ psi})$$

where

a = the area of the tendon,

R = the inside radius of the containment, and

s = the hoop tendon spacing.

For the model, the average hoop stress after six months is 85.7 kg_f/mm² (121.8 ksi) and the equivalent pressure is:

$$p_{eqv} = \frac{\sigma a}{R s} = \frac{(85.7 \text{ kg}_f/\text{mm}^2)(339.3 \text{ mm}^2)}{(537.5 \text{ cm})(11.25 \text{ cm})} = 4.8 \text{ kg}_f/\text{cm}^2 (68 \text{ psi})$$

which is essentially identical to the prototype. Comparing the design pressure, P_d , the hoop prestressing is equivalent to applying a counterbalancing pressure of 120% of the design pressure.

$$\frac{P_{eqv}}{P_d} = \frac{4.8 \text{ kg}_f/\text{cm}^2}{4.0 \text{ kg}_f/\text{cm}^2} = 1.20$$

Comparing the concrete compressive stress at the base of the wall:

For the prototype after 40 years:

$$\sigma_c = \frac{\sigma_a}{t s} = \frac{(106.3 \text{ kg/mm}^2)(5429 \text{ mm}^2)}{(130 \text{ cm})(77.32 \text{ cm})} = 57.4 \text{ kg/cm}^2 (817 \text{ psi})$$

Concrete compressive stress due to Dead Load 15.2 kg/cm² (216 psi)

Total compressive stress in Concrete 72.6 kg/cm² (1,033 psi)

where t is the thickness of the containment wall and s is the vertical tendon spacing.

For the model after 6 months:

$$\sigma_c = \frac{\sigma_a}{t s} = \frac{(127.5 \text{ kg/mm}^2)(339.3 \text{ mm}^2)}{(32.5 \text{ cm})(19.33 \text{ cm})} = 68.9 \text{ kg/cm}^2 (980 \text{ psi})$$

Concrete compressive stress due to dead load 3.2 kg/cm² (46 psi)

Total compressive stress in concrete 72.1 kg/cm² (1025 psi)

Therefore, the higher vertical tendon stress in the model, when combined with the dead load stress, yields nearly the same compressive stress in the concrete as the prototype.

2.2 Construction

2.2.1 General Construction

Prior to construction of the PCCV model, during the initial development of the containment test site in 1993, the location of the PCCV model was selected, the surface soil was removed, and the existing subgrade was excavated to a depth of over 8 m (25') and replaced with a compacted engineered backfill. The allowable bearing capacity, based on limiting soil settlement to 25 mm (1") or less, is 3.11 kN/m² (6.5 ksf) [26].

The overall site plan was shown in Figure 1.3. A detail of the areas surrounding the PCCV model is shown in Figure 2.10. The model was oriented so the E/H opening was facing due south. (This was primarily for operational considerations rather than any test requirement.) An aerial view of the test site during construction is shown in Figure 2.11.

On-site construction of the model by Hensel Phelps Construction Co. commenced on January 3, 1997 with construction of a 19.8 m × 19.8 m × 30 centimeters thick (65' × 65' × 1') mudmat placed on the engineered back-fill (Figure 2.12). This mudmat was constructed of 'lean' concrete and reinforced with welded wire fabric to provide a level working surface on which to construct the model. Benchmark monuments were constructed of small concrete pads at each of the four cardinal azimuths (0 degrees, 90 degrees, 180 degrees, and 270 degrees) outside the perimeter of the construction zone. These control points were subsequently used for the model's layout.

After the mudmat concrete had cured, a steel frame to support the basemat rebar was erected (Figure 2.13) and the rebar for the first basemat lift (F1) was erected (Figure 2.14). After verifying the position of the rebar (Figure 2.15), the formwork was set (Figure 2.16) and the F1 concrete placed (Figure 2.17). While F1 concrete was placed directly on the mudmat, there was no positive connection between the two.

Most of the model reinforcing was prefabricated by Border Steel Co., El Paso, TX, although some field fabrication was required as the construction progressed. All concrete was batched by Lafarge Construction Materials (formerly doing business as Western Mobile NM), Albuquerque, NM, mixed in transit and placed by pumping. All sampling and quality control tests were conducted by AGRA Earth and Environmental, Inc., Albuquerque, NM. Slump (Figure 2.18) and air entrainment tests were conducted on each batch/truck of concrete delivered to the site and standard cylinders and beams

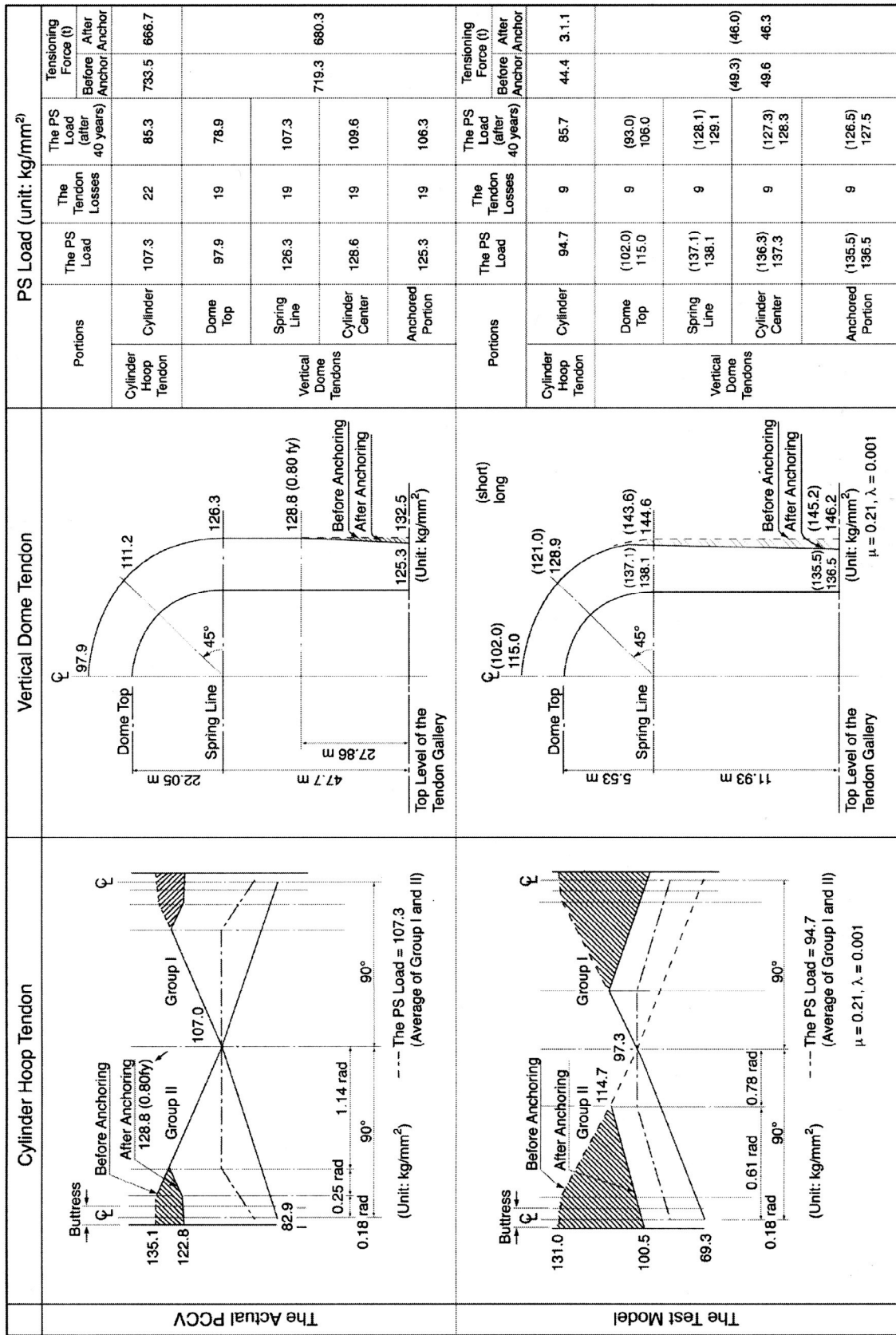


Figure 2.9 PCCV Prototype and Model Tendon Design Stress Profiles

were cast (Figure 2.19) for testing at seven, 28, and 91 days and at the time of tensioning and pressure testing. Both standard-cure, SC, (two to four days in a water bath, then stored in a humidity controlled chamber until testing), and field-cured (FC) specimens (two to seven days in a water bath, then stored on-site until testing) were produced and tested.

Installation of rebar and concrete placement for F2, F3, and F4 followed a similar sequence (Figures 2.20-2.25). Strain gages and thermocouples (T/Cs) were mounted on some of the rebar prior to installation and the lead wires were routed through the forms prior to concrete placement. As noted previously, the concrete outside the tendon gallery was not placed, thus allowing access for insertion and tensioning of the vertical tendons. The bottom basemat rebar that extended beyond the initial basemat lifts was covered with a temporary plywood deck to protect it from damage during construction until the final basemat pours (F5 and F6) were made. Other rebar that extended beyond lifts F1 to F4 were terminated and equipped with mechanical splices.

Prior to construction of the cylinder wall, a mock-up of the wall, incorporating the E/H embossment, vertical buttress, tendon sheaths, and the liner, was constructed to develop and demonstrate the erection sequence and method for placing the cylinder wall concrete (Figure 2.26). Since the wall lifts were approximately 3 m (10') in height, form 'windows' were located at mid-height (Figure 2.27) to limit the drop height of the wet concrete. Due to the dense rebar pattern, the trunk of the concrete pump could not be inserted into the forms. After placing the concrete through the form window and using spud-type vibrators to consolidate the concrete and prevent voids, the windows were blocked and placement of concrete continued at the top of the mock-up. After the concrete had cured and the exterior form was removed, the mock-up was cored to inspect for voids in the concrete. None were discovered. While this sequence of construction was not completely identical to the sequence for the model wall (e.g. continuing vertical wall reinforcing would limit placement at the top of each lift), the mock-up demonstrated that the planned construction sequence would be successful.

Since New Mexico is subject to severe summer lightning storms and the PCCV model is in an exposed desert terrain, a lightning protection system, consisting of four 30 m (100') poles connected to a buried copper cable counterpoise, was installed around the model. The lightning protection system provides an alternate path to ground around the model, thereby preventing direct lightning strikes that might damage the instruments, wires, and data acquisition components. Until the dome was completed, only two of the poles at 0 degrees and 180 degrees could be installed to accommodate crane operations, thereby providing only partial protection. Nevertheless, the protection system appears to have functioned successfully, since no direct lightning strikes were ever recorded on the model, even though there was a strike on the chain-link fence surrounding the site that damaged unprotected telephone lines strung along the fence.

While the basemat and wall mock-up construction was being completed, the liner panels, which had been fabricated by MHI in Kobe, Japan, were shipped to the test site. The liner panels arrived at the site in June, 1997 (Figure 2.28). Prior to shipping the panels to the U.S., all the cylinder wall panels were temporarily erected in Kobe to ensure that they would fit. Typical liner panels with support jigs are shown in Figure 2.29.

At the same time the liner panels were being shipped, an internal structural steel frame was fabricated (in the U.S.) and also delivered to the test site. This structure, known as the instrumentation frame, provided the support structure from which to hang the liner panels, with jigs, prior to welding; provided internal support during concrete placement; and provided a work platform during liner welding and installation of the internal instrumentation. During testing, this internal frame also acted as the reference structure for measuring model displacements. Components and erection of the instrumentation frame are shown in Figures 2.30-2.33.

Beginning in September, 1997, the liner panels were erected and bolted to the frame (Figures 2.34-2.36). After all the panels were assembled, a crew of welders from MHI began welding the liner seams. First, the basemat liner plates were welded to the embedded anchors. The liner erection plan then called for the seam between the first liner ring and the basemat to be welded, followed by the horizontal seam between the first and second liner rings. After this, the vertical seams for the first ring were completed. The liner erection and welding specifications defined overall and local dimensional tolerances and nondestructive inspection criteria. All liner welds were radiographed and inspected for flaws (undercutting, inclusions, and porosity). Initial difficulties welding the 1.6 mm liner in the field resulted in most of first ring's liner welds is being rejected. These welds were then ground out and repair welds were made. While there was some improvement, some of the repair welds contained flaws that exceeded the welding specifications. After additional repairs, inspection, and laboratory tests of welded liner specimens, it was decided that the original welding specifications were overly conservative and the criteria on flaws were relaxed. (The original weld flaw acceptance criteria had been scaled from the prototype welding specifications.)

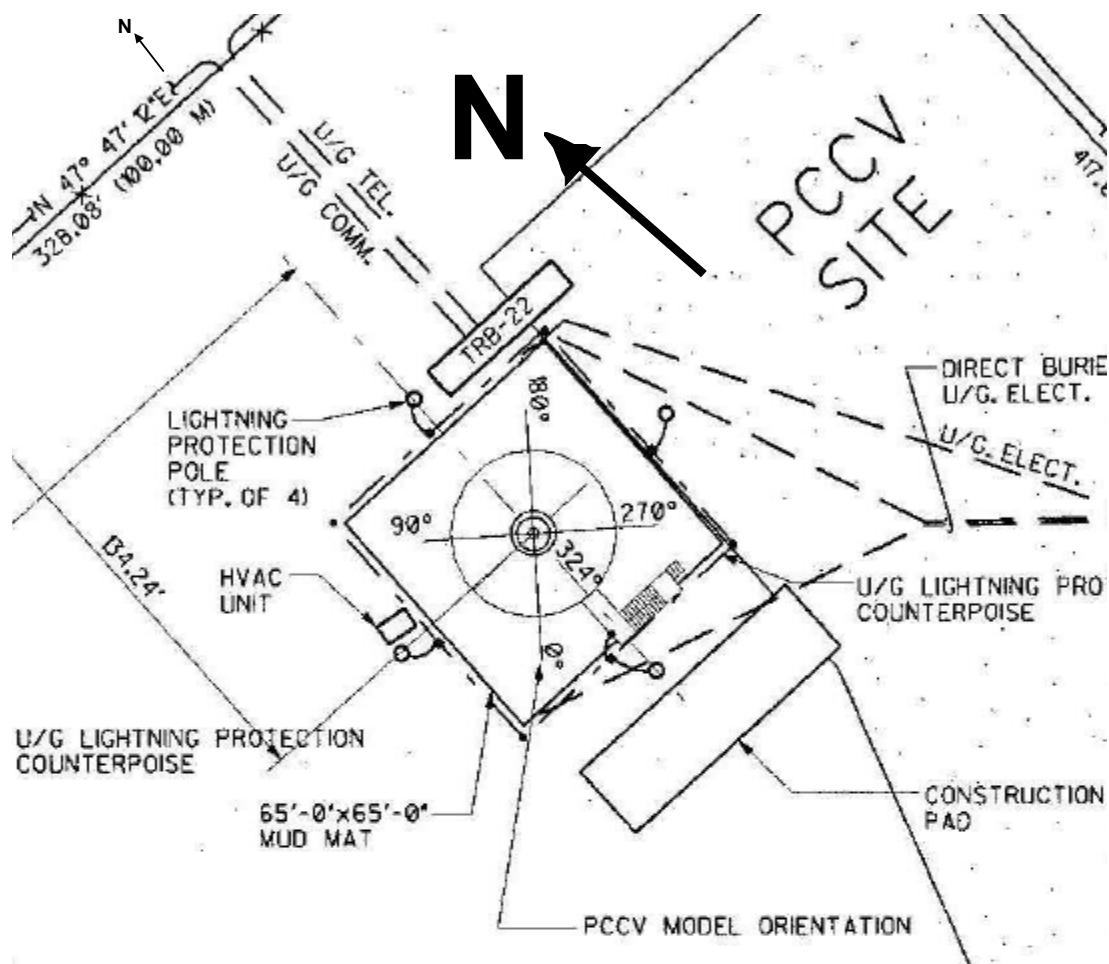


Figure 2.10 PCCV Model Layout

For the 6.4 mm (1/4") thick liner in the prototype, the liner seam welds could be made using double-sided full penetration welds. However, this method of welding could not be used for the 1.6 mm (1/16") thick model liner welds. The field welds in the model liner required back-up bars or, in some locations, back-up tape, and the full penetration welds were made from one side. Where welds were ground out and repaired, it was sometimes necessary to remove a section of the back-up bar and replace it with another segment. (Note that this created some local discontinuities in the model liner that became important during the pressure tests, but which were not representative of details in the prototype.) In areas where liner strains were expected to be high due to geometric discontinuities, the back-up bars were removed after the liner welds were completed to maintain the similarity with the prototype. In some locations, the weld bead was ground to reduce its profile, as well.

Both of these cosmetic post-weld treatments may have caused local thinning of the liner. Unfortunately, no measurements of the post-weld liner thickness were made. After the liner seam welds were completed, the penetration insert assemblies were welded to the liner and the stiffener, and liner anchor welds were completed.

To expedite the liner strain gage installation and the model's erection, a number of strain gages on the exterior surface of the liner, i.e. the concrete side of the liner, were installed prior to erection and welding of the liner panels. Since heat input from the welding operations could damage strain gages near the weld seams, only those gages over 10 cm (4") from the weld seams were installed prior to erection. This included gages on the liner anchors and stiffeners. Figure 2.36 shows two liner panels during installation of the strain gages. After the liner panels were erected and welded, the exterior



Figure 2.11 Aerial View of CTTF-West during PCCV Construction (March, 1999)

strain gages near the liner weld seams were installed. Figures 2.38 and 2.39 show typical strain gage installations near weld seams.

After all weld inspection criteria had been satisfied, construction of the model proceeded with the installation of inner horizontal and vertical rebar layers in the cylinder and dome (Figures 2.40-2.41). All instrumented rebar for these two layers was installed concurrently with the remainder of the reinforcing steel.

Next, the tendon sheath support frame, consisting of steel angles with support pins to correctly position the tendon sheaths, was installed (Figure 2.42). Except for the instrumented hoop tendons, which were preassembled with the sheath, all the tendon sheaths were all installed prior to outer reinforcing and shear reinforcing (Figures 2.43 and 2.44). The model construction then proceeded by lifts; C1 through C4 in the cylinder, and D1 to D3 in the dome. For each lift, the outer and radial rebar, including instrumented rebar and any instrumented hoop tendons, were installed first. Lead wires for the liner, rebar and tendon strain gages, embedded T/Cs, and fiber optic strain gages, were then routed through PVC ducts that had been placed in the previous lift. After checking that the gages and lead wires had not been damaged and were still functioning, the outer concrete forms were installed and concrete for each lift was placed. After the concrete had cured sufficiently, the outer forms were stripped and the cycle was repeated until the final dome pour was completed. The final dome pour, D3, was completed without the use of external forms. The plasticizer was not added for this lift, so a low slump was maintained and the final surface was hand finished, aided by a wooden template that defined the outer surface. This sequence of construction is illustrated in Figures 2.45 through 2.52.

After the D3 concrete achieved its specified strength, the liner jigs were cut loose from the liner, detached from the interior frame, and removed. This freed the containment wall from the interior frame, making both structures independent of each other. The instrumentation frame then functioned as a work platform and as the reference frame for measuring shell displacements.

After the liner jigs were removed, model construction was temporarily suspended while SNL assumed control of the model for installing of the interior instrumentation. Details of the instrumentation installation are provided in Chapter 3. Prior to installing the interior instrumentation, the interior of the liner surface was cleaned and painted white. Cardinal lines were surveyed and marked on the liner as reference for the installation of the interior instrumentation. The as-built radii at the intersections of the cardinal lines were also determined, and the results are tabulated in Appendix C.

Prior to beginning the interior instrumentation, interior lighting, power, and ventilation were installed. Structural steel stairs to the top of the basemat and E/H were erected, and a vestibule with locking doors for access control was installed over the E/H opening. Machined flange covers were installed over the M/S and F/W penetration sleeves. Six of these covers were drilled for the sealed instrumentation feedthroughs and the remaining two were equipped for the power feedthrough and the pressurization line.

While the interior instrumentation was completed, construction activities resumed after an approximately six-month hiatus with the insertion of prestressing tendons into the sheaths. After the interior instrumentation was completed and verified ready for operation, the DAS was started prior to tensioning the tendons. Details of the prestressing operations and results are described in Section 2.2.3. After prestressing was completed, model construction concluded with the placement of the final basemat concrete lifts, F5 and F6 (Figure 2.53). After the forms were stripped, Mitsubishi and Hensel Phelps demobilized and turned the model over to SNL on July 28, 2000. The completed PCCV model is shown in Figure 2.54.

2.2.2 Material Properties

Properties of all the PCCV model construction materials, except for the model concrete, were determined from tests prior to construction and summarized in Section 2.1. Model concrete properties were determined by testing standard specimens (cylinders and beams) cast during placement of each concrete lift.

All concrete testing was conducted according to ASTM standards¹⁰ and the results are summarized in Appendix B. Quality control tests, consisting of standard 6-inch cylinder, unconfined compressive strength tests, were performed by AGRA Earth and Environmental, Inc. Specimens were cast from nearly every truck of concrete placed in the model. (Each truck contained approximately 7.6 m³ (10 cubic yards.)) Standard Cured (SC) specimens were cured in a water bath for two to four days (depending on weekends) and stored in a humidity-controlled chamber until tested. FC specimens were also cured in a water bath for two to four days, then stored at the site, under blankets, until tested. Compression tests¹¹ of both SC and FC cylinders were conducted at seven, 28, and 91 days. 91-day strengths were compared to the specified design strengths.

The average 91-day FC strength results for the first two cylinder wall lifts, C1 = 389kg_f/cm² (5527 psi) and C2 = 436kg_f/cm² (6200 psi), failed to meet the minimum specified design strength of 450 kg_f/cm² (6400 psi). This may have resulted from cold weather conditions, which might have retarded the curing rate. Analysis of the test data suggested that the concrete would reach the specified minimum design strength by the time prestressing was scheduled to occur, so no action was deemed necessary. Nevertheless, the curing method of FC specimens for lifts C4 through D3 and F5 and F6 was modified to keep the cylinders in the water bath for seven days. This modified field curing method is designated FC' in the material data summary.

While the strength of the concrete in C1 and C2 was deemed adequate, there was a concern that the low strength might cause higher creep losses than anticipated in the prestressing design calculations. Creep tests¹² of two specimens each from C1 and C2 were conducted at the University of New Mexico and compared to the results of the trial mix creep tests

¹⁰ *Annual Book of ASTM Standards*, American Society for Testing and Materials (ASTM), Philadelphia, PA.

¹¹ ASTM C39-94, "Standard Test Method for Compressive Strength of Cylindrical Concrete Specimens."

¹² ASTM C512-87, "Standard Test Method for Creep of Concrete in Compression" (modified).



Figure 2.12 Placement of PCCV Mudmat



Figure 2.13 Basemat Rebar Support Frame



Figure 2.14 Basemat Bottom Bars and Vertical Ties

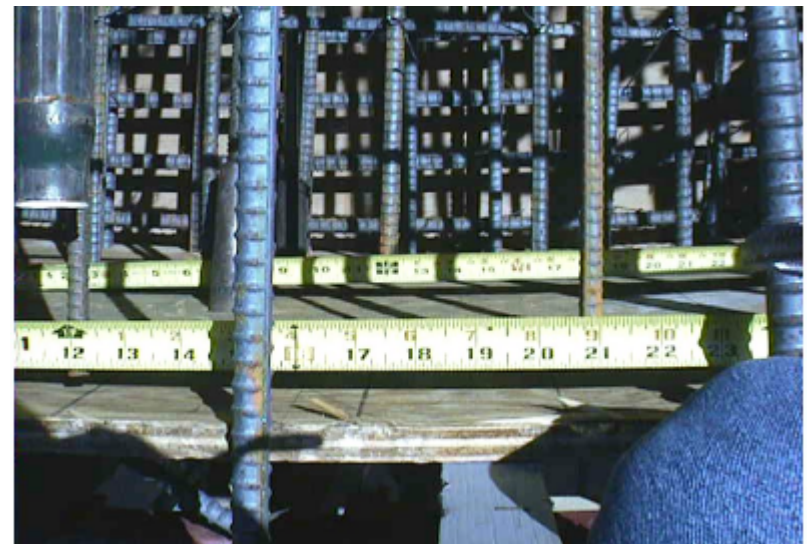


Figure 2.15 Measuring Rebar Location



Figure 2.16 F1 Formwork



Figure 2.17 Placing F1 Concrete



Figure 2.18 Measuring Concrete Slump



Figure 2.19 Concrete Test Cylinders and Beams



Figure 2.20 F2 Rebar Erection

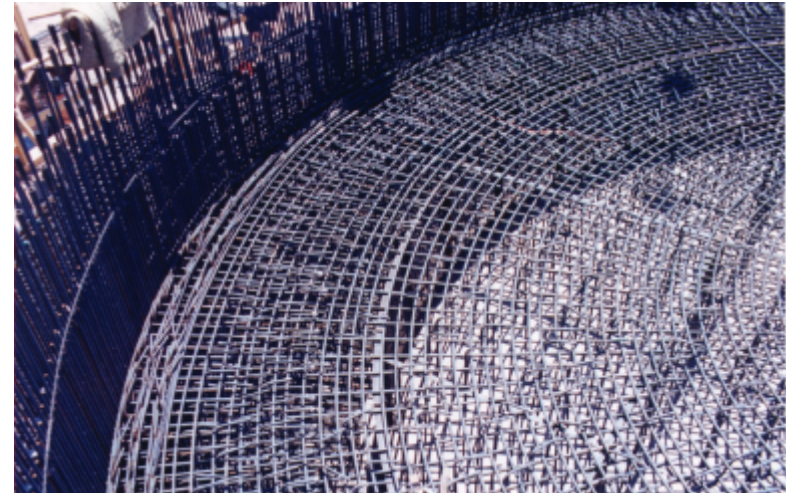


Figure 2.21 F3 Rebar



Figure 2.22 F3 Rebar and Formwork



Figure 2.23 Basemat Top Rebar (F3) and Wall Dowels



Figure 2.24 F3 Concrete Placement



Figure 2.25 F4 Concrete



Figure 2.26 Wall Mock-Up Rebar



Figure 2.27 Wall Mock-up Form w/ Concrete 'Window'



Figure 2.28 Delivery of Liner Panels



Figure 2.29 Liner Panels after 'Uncrating'



Figure 2.30 Instrumentation Frame Column 'Trees'



Figure 2.31 Instrumentation Frame Erection



Figure 2.32 Instrument Frame Erection



Figure 2.33 Completed Instrument Frame



Figure 2.34 Liner Panel Erection



Figure 2.35 Dome Liner Erection



Figure 2.36 Liner Panels with Jigs



Figure 2.37 Liner Panel Instrumentation

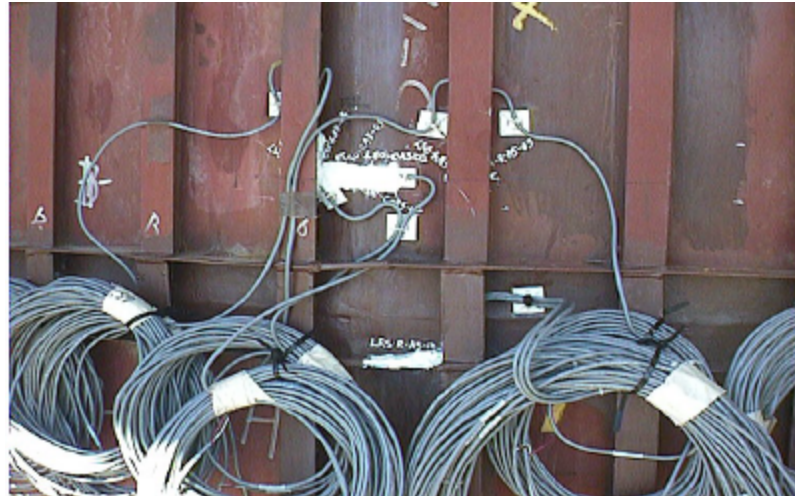


Figure 2.38 Liner Strain Gages after Welding



Figure 2.39 Close-Up of Liner Strain Gages near Weld



Figure 2.40 Inner Rebar at M/S Penetrations



Figure 2.41 Installation of Inner Dome Rebar

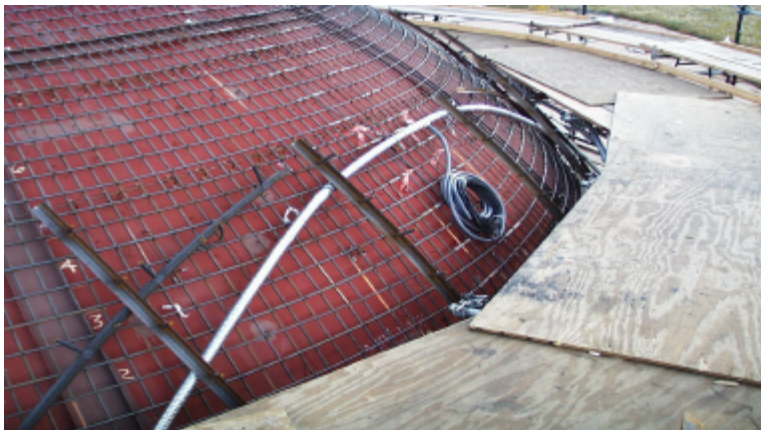


Figure 2.42 Tendon Sheath Support Frame



Figure 2.43 Dome Tendon Sheaths and Support Frame



Figure 2.44 PCCV Model Tendon Sheaths



Figure 2.45 Outer Rebar for C1



Figure 2.46 C1 Formwork Installation



Figure 2.47 Placing C1 Concrete



Figure 2.48 Installation of Instrumented Hoop Tendon.



Figure 2.49 C2 Formwork



Figure 2.50 C4 Concrete Placement



Figure 2.51 D1 Formwork Erection



Figure 2.52 D3 Concrete Placement



Figure 2.53 Final Basemat Concrete Lifts

[27]. These results, presented in Appendix B, showed higher amounts of creep and shrinkage than the trial mix data and indicated that creep losses in the prestressing might be higher than expected. This data was considered in specifying the tensioning forces for the tendons in Table 2.5.

More extensive material property tests for FC specimens were conducted around the time the model was being tensioned and just prior to the Limit State Test (LST). These tests provided more accurate material property data for concrete constitutive models used in the pre- and posttest analyses to predict and simulate the model response to pressure. These tests were also conducted at the University of New Mexico and included unconfined compression tests, compression tests to determine modulus of elasticity and Poisson's ratio¹³, split cylinder tensile strength¹⁴, and modulus of rupture¹⁵. The unit weight of the specimens was also determined and, since prediction of concrete cracking was one of the pretest analysis milestone objectives, a limited number of direct tension tests were conducted on specimens from the cylinder wall. The results of these tests and the direct tension test procedure are detailed in Reference [28] and summarized in Appendix B. A summary is also provided in Table 2.6.

A few other observations on the model concrete are worth noting:

1. The Coefficient of Variation (COV) in the compressive strength of the FC model concrete was 15.9% at 91-days and 13% at the time of prestressing. This COV is larger than typically observed for concrete from a central batch plant and indicates a significant degree of variation in the model concrete properties.
2. Compressive failure strains in the concrete specimens were typically in the range of 0.25 to 0.30%. While the tensile failure strain was not determined, the direct tension tests performed by the University yielded critical crack opening displacement data, which could be utilized in a fracture mechanics approach.
3. The modulus of elasticity in compression, determined from test data, is significantly lower than values usually computed from 'rules-of-thumb.' For example, ACI 318¹⁶ recommends that $E_c = 57,000 \sqrt{f'_c}$ in psi. Using 9300 psi as the average strength of the field cured cylinder/dome specimens yields an elastic modulus of 5.51×10^6 psi, compared to the measured value of 3.90×10^6 psi, a reduction of nearly 30%. If the modulus were based on the specified minimum strength of 6400 psi, the resulting value would be 4.56×10^6 psi, still higher than the measured value by 15%.

¹³ ASTM C469-94, "Standard Test Method for Static Modulus of Elasticity and Poisson's Ratio of Concrete in Compression."

¹⁴ ASTM 496-96, "Standard Test Method for Splitting Tensile Strength of Cylindrical Concrete Specimens."

¹⁵ ASTM C78-94, "Standard Test Method for Flexural Strength of Concrete (Using Simple Beam with Third-Point Loading)."

¹⁶ *Building Code Requirements for Structural Concrete*, ACI 318-02, American Concrete Institute, Farmington Hills, MI.



Figure 2.54 Completed PCCV Model

2.2.3 Prestressing Operations

With the majority of the model instrumentation suite installed, model construction resumed in February, 2000 with the insertion of noninstrumented tendon strands into the sheaths embedded in the model. Prior to insertion, the strands were coated with an anti-corrosive agent, but there was no other treatment. Insertion was achieved by feeding a ‘puller cable’ through the sheath equipped with a wire gripping sleeve that tightened on the strands as it was tensioned to pull them through the sheath (Figure 2.55). Except for a few minor obstacles, e.g. grout which had penetrated the sheath splices and had to be cleared, the sheaths were clear and insertion was accomplished without any difficulty.

Table 2.6 PCCV Model Average Concrete Properties

Design Compressive Strength		300kg _f /cm ²	(4300 psi)	450kg _f /cm ²	(6400 psi)
<u>@ Prestressing</u>					
Compressive Strength,	FC	570	(8102)	559	(7956)
	FC'	NA	NA	680	(9665)
Young's Modulus		25.7 GPa	(3.7 × 10 ⁶ psi)	27.2 GPa	(4.0 × 10 ⁶ psi)
<u>@ Limit State Test</u>					
Compressive Strength,	FC	562	(7998)	615	(8750)
	FC'	NA	NA	700	(9953)
Young's Modulus		27.2 GPa	(3.9 × 10 ⁶ psi)	26.9 GPa	(3.9 × 10 ⁶ psi)
Poisson's Ratio		0.21		0.22	
Split Tensile Strength		35	(497)	36	(519)
Direct Tensile Strength		NA	NA	23	(320)
Modulus of Rupture		NA	NA	42	(594)
Density		2186kg _f /m ³	(136.4 pcf)	2176kg _f /m ³	(135.8 pcf)

The suite of gages installed on the model prior to prestressing and installing the DAS cleared the final system checks, and the DAS was put into operation at 11:48 AM, March, 3, 2000. The initial data scan represented the initial or ‘zero’ reading for all the model transducers. All subsequent readings, through the LST until the DAS was shut down in October, are referenced to this initial scan. The model was scanned hourly for seven days to provide baseline information on the response to ambient temperature variations prior to tensioning the model and to verify the operational readiness of the DAS in attended and unattended modes.

Model prestressing began on March 10, 2000. The arrangement of the model tendons is shown in Appendix A. The nomenclature for identifying individual tendons consisted of an alpha designator ‘H’ for hoop tendons and ‘V’ for vertical tendons, followed by a numerical designator (1 through 98 for the hoop tendons and 1 through 90 for the vertical tendons). The hoop tendons were numbered consecutively from 1, the lowest tendon in the cylinder wall, to 98, at the midpoint of the dome. Even-numbered hoop tendons (H2, H4, H6,..., H98) were anchored at the 90 degree buttress and odd-numbered hoop tendons (H1, H3,..., H97) were anchored at the 270 degree buttress. Vertical tendons were numbered consecutively from V1 at 45 degrees, clockwise to V90 at 223 degrees. The vertical tendons were arranged in two orthogonal groups, with V1 through V45 spanning the dome in a plane (nearly) parallel to the 90 to 270 degree axis and V46 through V90 in an orthogonal plane approximately 0 to 180 degrees. This arrangement is illustrated more clearly in the design drawings and shown in Figure 2.44.



Figure 2.55 Pulling Hoop Tendons

Prestressing operations were defined by MHI in the project construction specifications¹⁷. The overall sequence of tensioning is illustrated in Figure 2.56. This sequence is identical to that used for the prototype and is intended to apply balanced prestressing forces to the model to prevent excessive local deformation or damage. The actual tensioning schedule is shown in Table 2.7. Prestressing operations were completed on May 3, 2000.

Thirty-four of the 188 tendons were instrumented with load cells at the anchors, and eight of these tendons, five hoop and three vertical, were also instrumented with strain gages at discrete locations along their length in an attempt to monitor and record the force distribution for comparison with the design calculations. The instrumented tendons are identified in Table 2.7 and their locations are illustrated in Figure 3.21. Details of the tendon instrumentation are given in Chapter 3.

Only one tendon was tensioned at a time (Figure 2.56). The procedure was to assemble the tensioning hardware at each end of the tendon. The tensioning hardware consisted of the tendon anchor and wedges, tensioning chair, hydraulic jack, and tensioning anchor. For the instrumented tendons, a pair of bearing plates, spherical washers, and the load cell was inserted between the tendon anchor and the bearing plate embedded in the model. This arrangement is shown in Figure 2.58. After the tensioning hardware was assembled, one end of the tendon, designated the 'B' end, was tensioned to 10% of the design load while the jack on the 'A' end was locked off. Then the B-end jack was locked off and the tensioning force was applied continuously by the jack at the A end until the jack pressure gage indicated that the force specified in Table 2.5 had been reached. (The jacks were calibrated prior to the start of prestressing and the conversion between hydraulic pressure and force was established for each jack.) In most cases, the tendon 'stretch' exceeded the maximum stroke of the jack and the strands had to be regripped to complete tensioning. When the A end was at the maximum load, the force at the B end was recorded and the friction coefficients for the tendon were computed and compared to the design values. (If the friction deviated from the design values by more than a specified range, the tendon was retensioned or, in some instances, the tendon was removed and new strands were inserted.) The B end was then tensioned to the specified force. When both ends were at the specified force, the anchors were seated.

¹⁷ MH-K10-29, "Prestressing Work Procedure," Rev. 1, Mitsubishi Heavy Industries, May, 1999.

The seating loss, defined in terms of length, was measured as the difference between the length of the tendon extending beyond the anchor, before and after seating. This indicates the loss of elongation (and hence tension) in the tendon as the load is transferred from the jack grips to the tendon anchors. The measured seating loss was compared to the maximum design seating loss of 5 mm (0.2"), and, if it was excessive, the tendon was retensioned. After seating the tendon, each end was subjected to a 'lift-off' test in which the tendons were regripped and pulled until the tendon anchor lifted off the bearing plate enough to insert a feeler gage between them. The measured lift-off force was also compared to the value specified in Table 2.5.

The instrumented tendons, those with load cells only and those with strain gages, were closely monitored during tensioning but the load cell data was not reported to the tensioning contractor, VStructural, LLC., during prestressing. The tensioning procedure was modified for the eight instrumented tendons with strain gages. Since the lead wires for these gages would be damaged if the tendon was pulled in one direction first and then the other, causing the gages and the lead wires to travel back and forth in the sheath, these tendon were tensioned simultaneously at both the A and B ends. The tensioning forces were applied in small load increments and the tendon gages were monitored continuously during tensioning. The responses of the instrumented tendons are shown as force time histories in Figures 2.59 through 2.66.

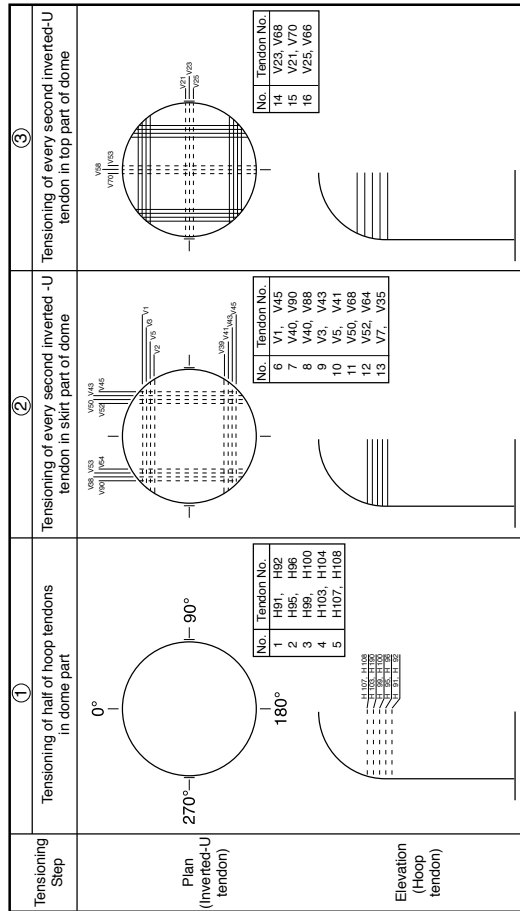
These figures show the response of the load cells at each end of the tendons and the response of the surviving strain gages (converted to force by multiplying the strain by the nominal tendon area and elastic modulus of the strand). The strain gages on these tendons suffered a high mortality rate during prestressing, as shown in Table 2.8. Nevertheless, a high mortality rate was expected, and in most cases the surviving strain gages provided insight into the behavior of the tendons during prestressing and subsequent pressure testing.

The figures illustrate the range of strain in individual strand wires at a given measurement position, and also show when some of the strain gages failed. The data was not plotted after a gage had failed. It is interesting to note that the Tensmeg gages (TT) typically gave lower strain readings than the bonded foil gages (TF) mounted on individual wire strands. This is likely due to the Tensmeg end blocks slipping relative to the strand, resulting in an inaccurate measure of the strand strain. For most future discussions of the tendon response, only the data from the TF gages is considered as a reliable measure of the tendon strain and the TT data is ignored.

Figure 2.62 illustrates how the stages of the prestressing procedure are reflected in the test data. In the figure for H67, the surviving strain gages at each measurement position along the length of the tendon were averaged before converting them to a tendon force. This was done to simplify the plot, but this also recognizes that the force in individual wires in the tendon strands vary and the load cells (TL) forces and average forces from the strain gages (TF or TT) are plotted as a function of time. The force time history shows the load being applied incrementally at both ends of the tendon until the specified tensioning force was achieved and load was stable. Note that at a force of approximately 30T, the tendon was anchored and regripped when the stroke of the jacks was exceeded. After stabilizing at the maximum force, the tendons were seated, with the corresponding drop in load at and near the anchors. The slight increase in force at the anchors after seating reflects the lift-off test. (This shows that the force required to lift-off the anchor is slightly higher than the seated anchor force.)

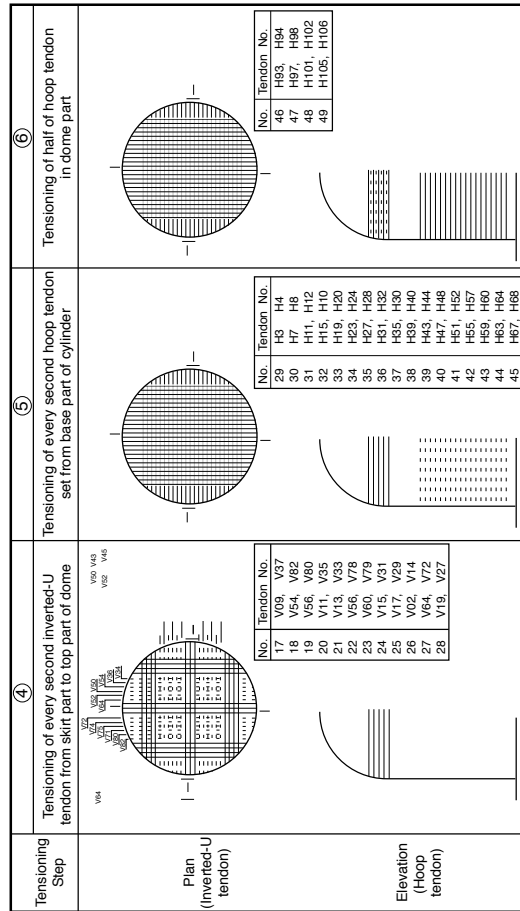
Note also that the strain gages were most likely to fail near the tendon anchors and less likely to fail at the tendon mid-point. This occurs because the strands near the anchors travel the furthest during tensioning, increasing the likelihood that the gages or their lead wires were crushed against the sheath wall or another strand.

Considering Figure 2.62, it can be seen that the general force distribution along the length of the tendons is consistent with the design assumption, i.e., the highest tendon force is near the anchor and the lowest force is at the mid-point of the tendon. Figures 2.67 through 2.74 compare the measured force distribution in the tendons during and after tensioning with the design assumptions shown in Figure 2.9. The data for the horizontal tendons generally confirms the assumed design force distribution. The surviving gages do not provide enough data points to fully define the shape of the force distribution curve, notably where the effect of the anchor set loss disappears. Due to the discontinuities in the hoop tendon force distribution, only the data points are shown and no attempt was made to interpolate the hoop tendon force between measurement locations. In general, the data is consistent with the design assumptions and does not appear to contradict the predicted response.



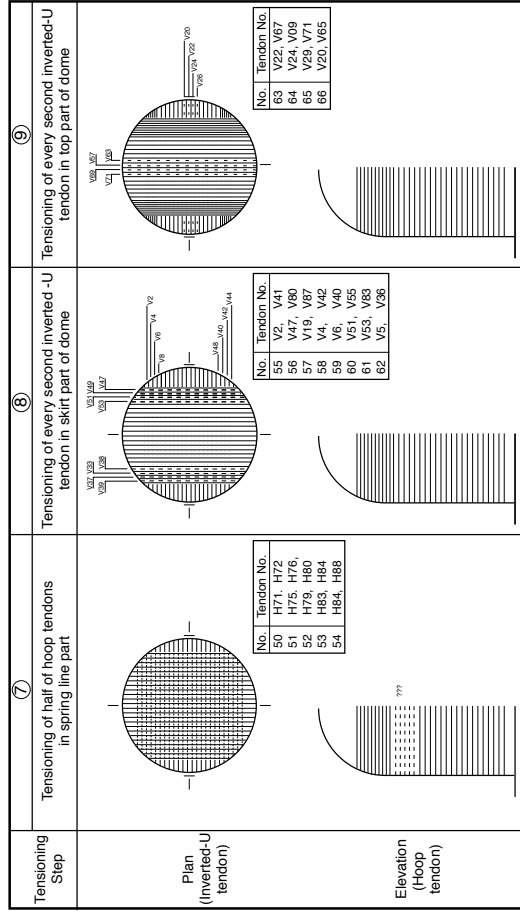
Tensioning Sequence (1/4)

Note: 1. Solid line shows tendon tensioned fully in the previous step.
2. Broken line shows tendon to be tensioned in this step.



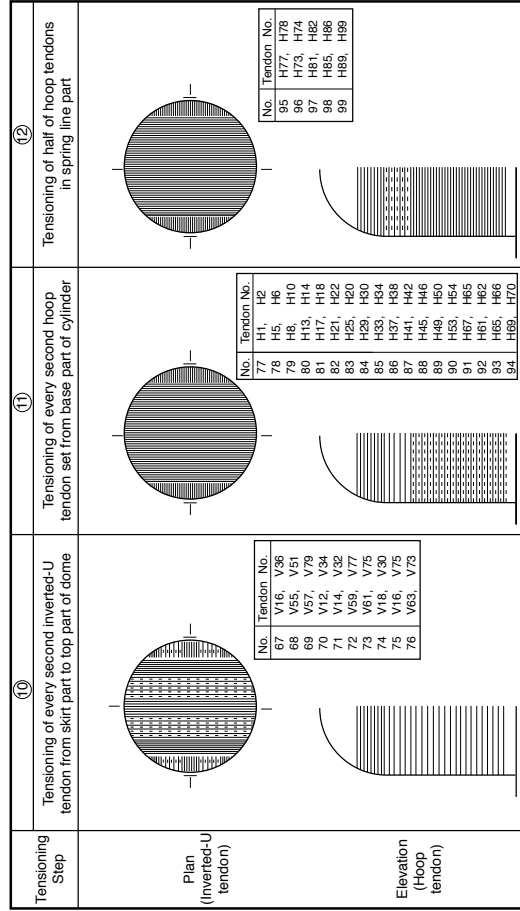
Tensioning Sequence (2/4)

Note: 1. Solid line shows tendon tensioned fully in the previous step.
2. Broken lines show tendon to be tensioned in this step.



Tensioning Sequence (3/4)

Note: 1. Solid line shows tendon tensioned fully in the previous step.
2. Broken lines show tendon to be tensioned in this step.



Tensioning Sequence (4/4)

Note: 1. Solid line shows tendon tensioned fully in the previous step.
2. Broken lines show tendon to be tensioned in this step.

Figure 2.56 PCCV Model Tensioning Sequence

Table 2.7 Model Prestressing Schedule

Sun	Mon	Tue	Wed	Thr	Fri	Sat
5-Mar	6-Mar	7-Mar	8-Mar	9-Mar	10-Mar	11-Mar
					H91 H92	
						V45
Sun	Mon	Tue	Wed	Thr	Fri	Sat
12-Mar	13-Mar	14-Mar	15-Mar	16-Mar	17-Mar	18-Mar
	H95 H96 H99 H100 H103	H103* H104 H107* H108* V1	V1* V45* V90	V46 V48 V88 V3 V43	V5 V41(1) V50	V86(2) V52 V84 V7
		*retensioning required				V54
Sun	Mon	Tue	Wed	Thr	Fri	Sat
19-Mar	20-Mar	21-Mar	22-Mar	23-Mar	24-Mar	25-Mar
	V39 V23 V68 V21 V70 V25(3) V66	V66* V25 (3) V9	V37 NUPEC AUDIT INSP. V54 V82 V56* V80	V11 PRP SITE VISIT V35* V13 V33 V58 V78 V60	V76* V15 V31 V17 V29	V62 V74 V64 V72 V19 V27
						H11
Sun	Mon	Tue	Wed	Thr	Fri	Sat
26-Mar	27-Mar	28-Mar	29-Mar	30-Mar	31-Mar	1-Apr
	H3 H4 H7* H8 H12	H11 H16 (4) H15	H16 H19 H20 H23 H24 H27 H28 H31	H32 H36 H35(5) H40	PS Op's suspended due to high winds.	H63
Sun	Mon	Tue	Wed	Thr	Fri	Sat
2-Apr	3-Apr	4-Apr	5-Apr	6-Apr	7-Apr	8-Apr
	H39* H44 H43 H48 H47 H52 H51	H56 H55 H60 H59 H64 H63*	H63 H67 H68	H93 H94 H97 H98 H102 H101	H105 H106	V49

Load Cell

Schedule Impact

Instrumented

**Tendon to be replaced

Completed

Weekend Milestone

Sequence			
1	H91	58	H4
2	H92	59	H7**
3	H95	60	H8**
4	H96	61	H11
5	H99	62	H12
6	H100	63	H15
7	H103	64	H16
8	H104	65	H19
9	H107	66	H20
10	H108	67	H23
11	V1	68	H24
12	V45	69	H27
13	V46	70	H28
14	V90	71	H31
15	V48	72	H32
16	V88	73	H35
17	V3	74	H36
18	V43	75	H39
19	V5	76	H40
20	V41	77	H43
21	V50	78	H44
22	V86**	79	H47
23	V52	80	H48
24	V84	81	H51
25	V7	82	H52
26	V39	83	H55
27	V23	84	H56
28	V68	85	H59
29	V21	86	H60
30	V70	87	H63
31	V25	88	H64
32	V66	89	H67
33	V9	90	H68
34	V37	91	H93
35	V54	92	H94
36	V82	93	H97
37	V56	94	H98
38	V80	95	H101
39	V11	96	H102
40	V35	97	H105
41	V13	98	H106
42	V33	99	H71
43	V58	100	H72
44	V78	101	H75
45	V60	102	H76
46	V76	103	H79
47	V15	104	H80
48	V31	105	H83
49	V17	106	H84
50	V29	107	H87
51	V62	108	H88
52	V74	109	V2
53	V64	110	V44
54	V72	111	V47
55	V19	112	V89
56	V27	113	V49
57	H3		

Table 2.7 Model Prestressing Schedule (continued)

							Sequence								
Sun	Mon	Tue	Wed	Thr	Fri	Sat	114	V87	157	H9**					
9-Apr	10-Apr	11-Apr	12-Apr	13-Apr	14-Apr	15-Apr	115	V4	158	H10					
	Jack Re- calibration	PS Op's suspended due to high winds.	H71	H87	V87		116	V42	159	H13					
			H72	H88	V4		117	V6(1)	160	H14					
			H75	V2	V42		118	V40(2)	161	H17					
			H76	V44	V6(1)		119	V51	162	H18					
			H79	V47*	V40(2)		120	V85	163	H21					
			H80	V89	V51		121	V53	164	H22					
			H83	V49			122	V83	165	H25					
			H84		V12		123	V8	166	H26					
Sun	Mon	Tue	Wed	Thr	Fri	Sat	124	V38	167	H29					
16-Apr	17-Apr	18-Apr	19-Apr	20-Apr	21-Apr	22-Apr	125	V22	168	H30					
	V85 Op Error damaged 19/31 gages. Op's suspended	Op's suspended	V85	V8*	V26*	V36(6)	126	V67	169	H33					
			V53	V38	V71	V55	127	V24	170	H34					
			V83	V22	V20	V81	128	V69	171	H37					
				V67*	V65	V57	129	V26	172	H38					
				V24	V10		130	V71	173	H41					
				V69	V36		131	V20	174	H42					
							132	V65	175	H45					
					H22	133	V10	176	H46						
Sun	Mon	Tue	Wed	Thr	Fri	Sat	134	V36	177	H49					
23-Apr	24-Apr	25-Apr	26-Apr	27-Apr	28-Apr	29-Apr	135	V55	178	H50					
	V79* V12 V34 V14 V32(6) V59	V77	H1	H17	H41		136	V81	179	H53					
		V61*	H2	H18	H42		137	V57	180	H54					
		V75	H5	H21	H45		138	V79	181	H57					
		V16	H6	H22	H46		139	V12	182	H58					
		V30	H9	H25	H49		140	V34	183	H61					
		V18	H10	H26	H50		141	V14	184	H62					
		V28	H13	H29			142	V32	185	H65					
		V63	H14	H30			143	V59	186	H66					
		V73		H33			144	V77	187	H69					
				H34			145	V61	188	H70					
				H37			146	V75	189	H73					
				H38			147	V16	190	H74					
									148	V30	191	H77			
Sun	Mon	Tue	Wed	Thr	Fri	Sat	149	V18	192	H78					
30-Apr	1-May	2-May	3-May	4-May	5-May	6-May	150	V28	193	H81					
	H54 H53 H57	H58	H85				151	V63	194	H82					
		H61	H86				152	V73	195	H85					
		H62	H89				153	H1	196	H86					
		H65	H90				154	H2	197	H89					
		H66					155	H5	198	H90					
		H69													
		H70													
		H73													
		H74													
		H77													
		H78													
		H81													
		H82													
								H90							

Notes:

- (1) V41 removed and replaced with V6. V41 set-loss, friction and loft-off were high.
- (2) V86 (mock-up tendon) removed and replaced with V40 tendon.
- (3) Remove V25, friction loss too high (>0.25), detension, remove LC's, remove and replace strand, reinstall LC's tomorrow (3/21) AM.
- (4) Remove and replace tendon due to lift-off force too high.
- (5) Tensioning of H35 delayed due to water in LC connectors, connectors removed and hardwired
- (6) V36 removed and replaced, friction not within specifications.



Figure 2.57 Tensioning Hoop Tendons



Figure 2.58 Tensioning Hardware Assembly and Load Cell

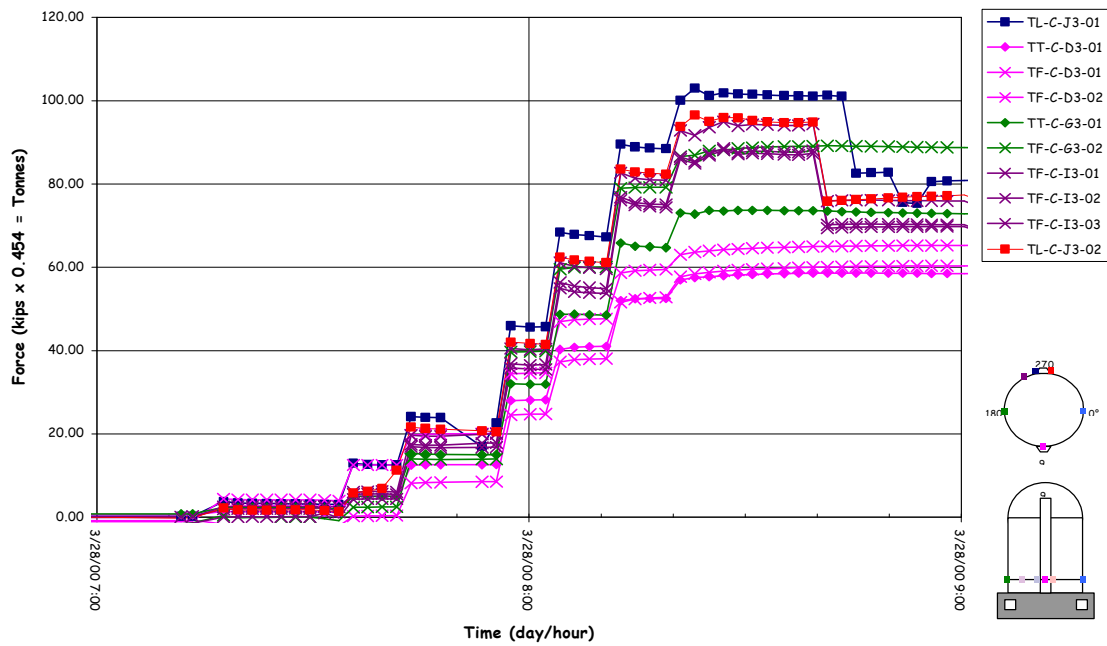


Figure 2.59 Tendon H11 Tensioning Force Time History

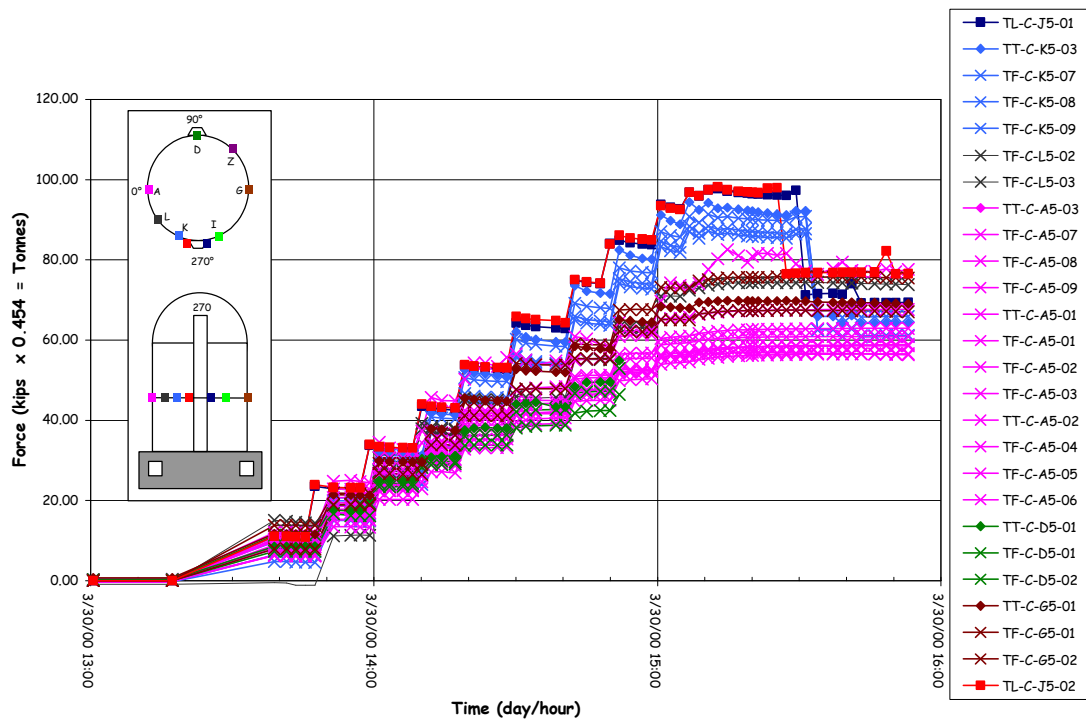


Figure 2.60 Tendon H35 Tensioning Force Time History

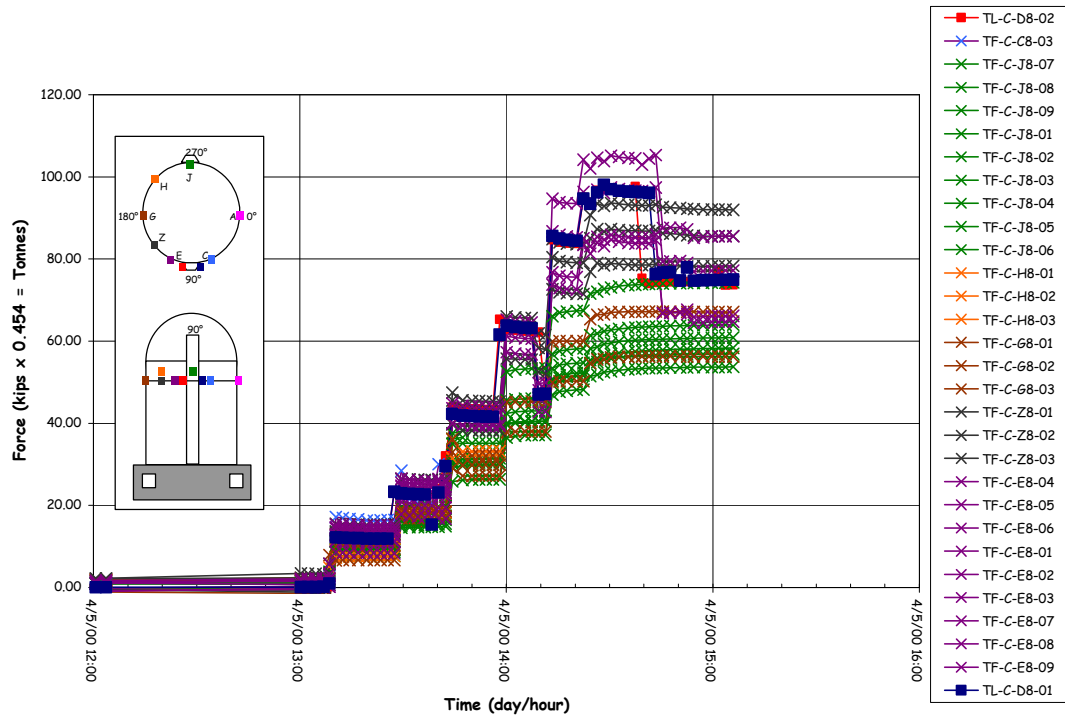


Figure 2.61 Tendon H53 Tensioning Force Time History

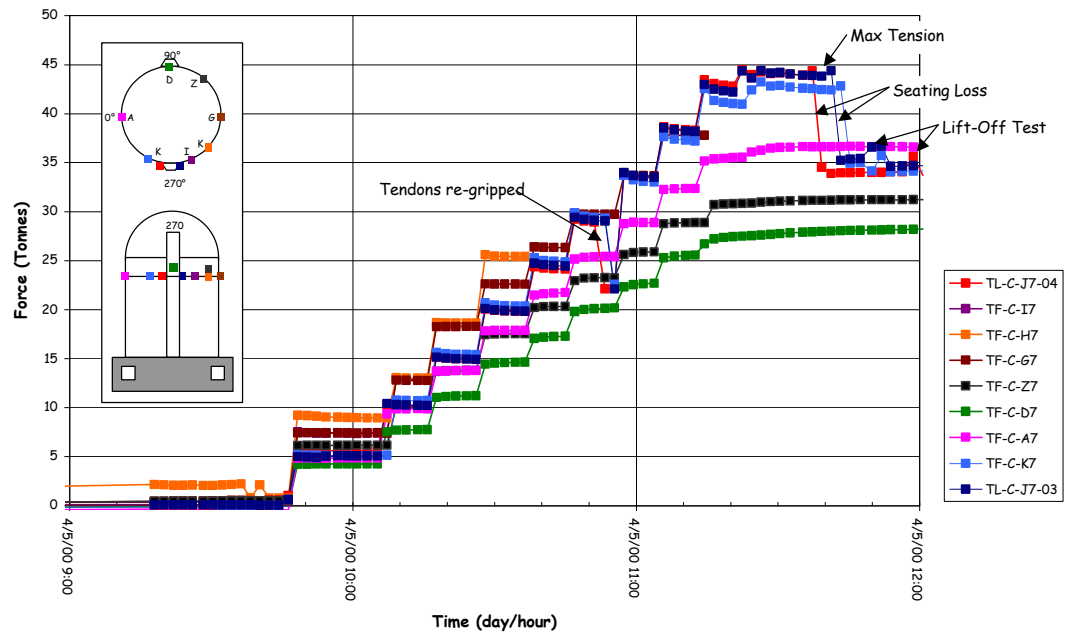


Figure 2.62 Tendon H67 Tensioning Force Time History

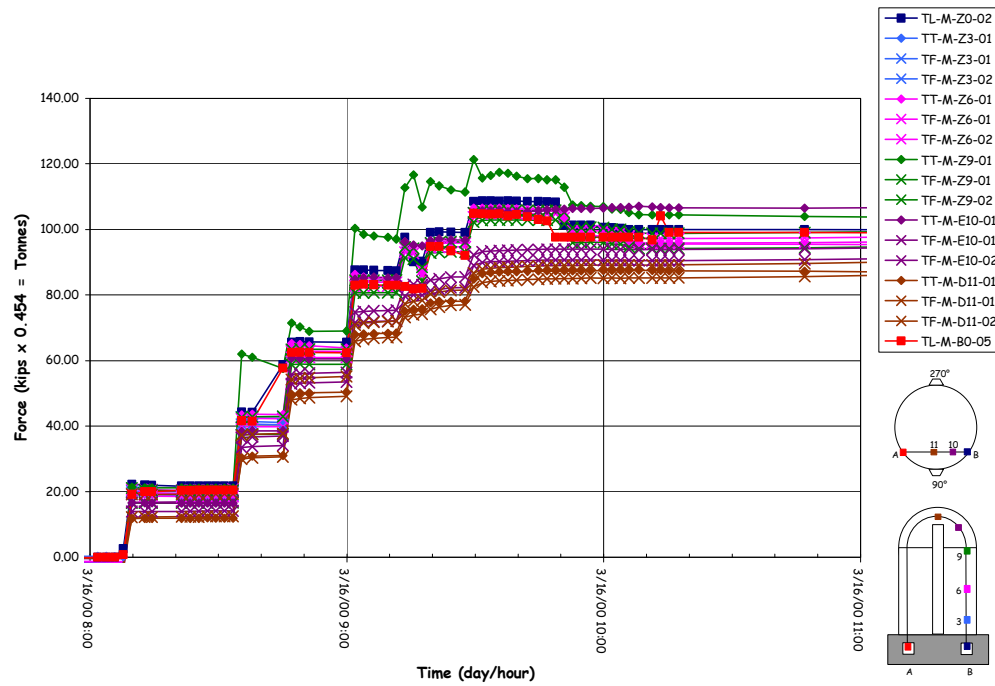


Figure 2.63 Tendon H68 Tensioning Force Time History

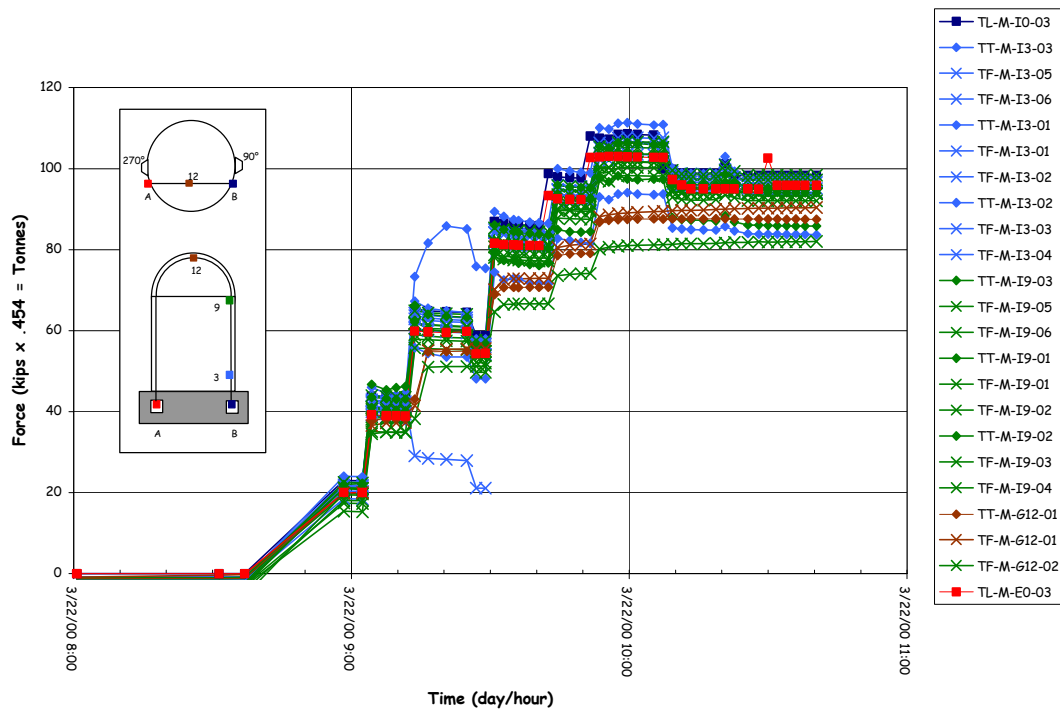


Figure 2.64 Tendon V37 Tensioning Force Time History

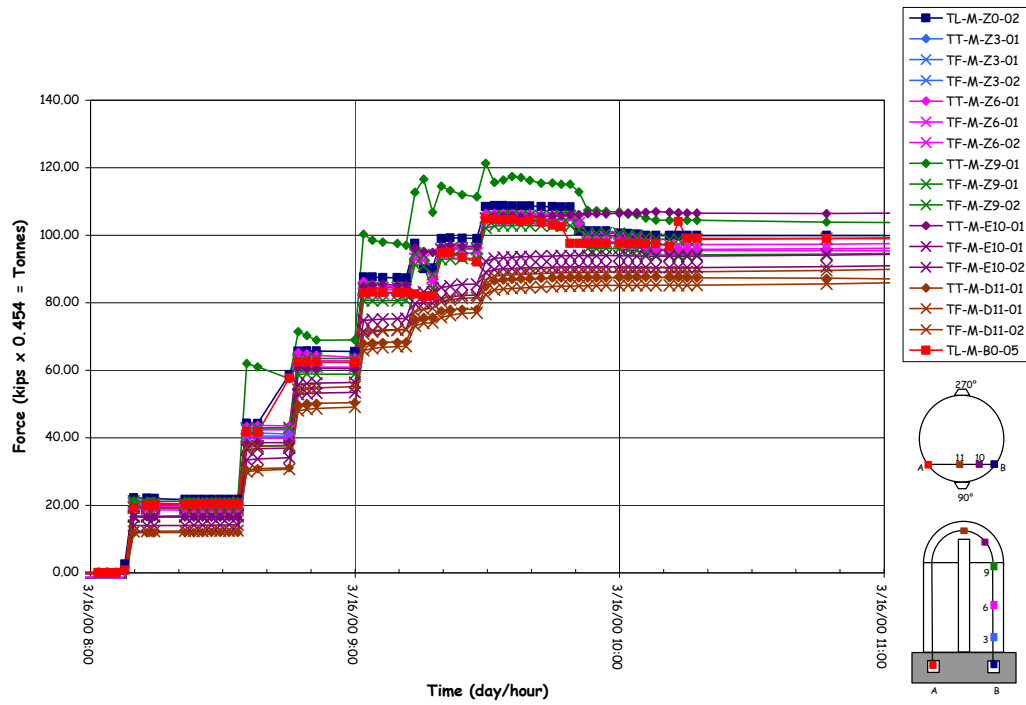


Figure 2.65 Tendon V46 Tensioning Force Time History

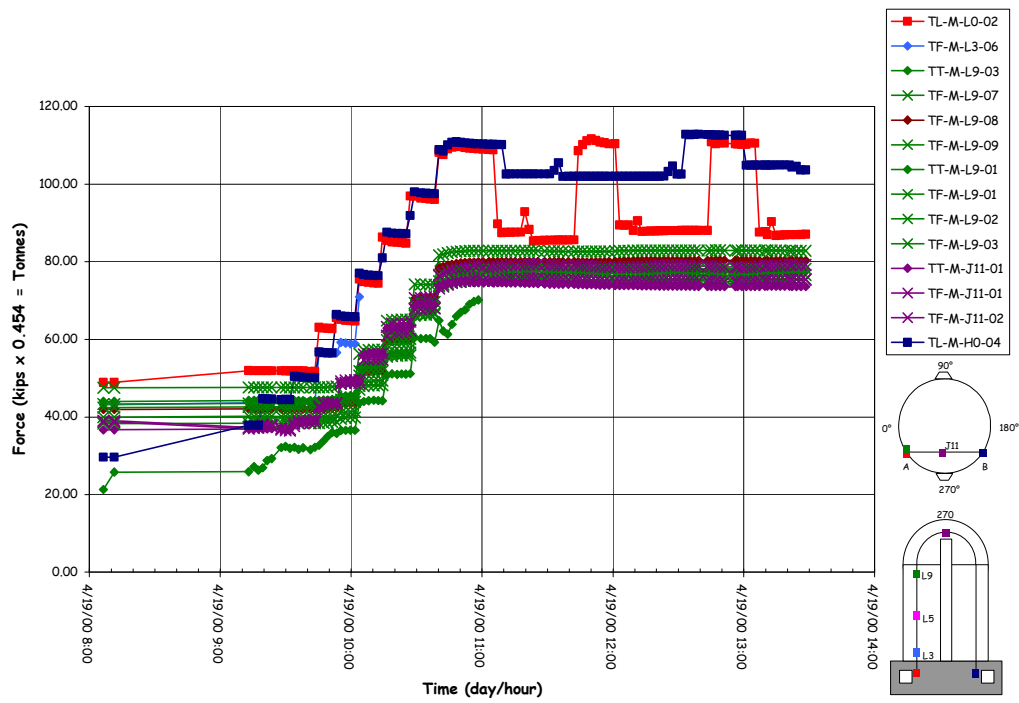


Figure 2.66 Tendon V85 Tensioning Force Time History

Table 2.8 Instrumented Tendon Gage Performance during Prestressing

H11:	4/12 strain gages failed	33% mortality
H35:	23/39 strain gages failed	59% mortality
H53:	14/22 strain gages failed	59% mortality
H67:	11/21 strain gages failed	52% mortality
H68:	18/33 strain gages failed	54% mortality
V46:	3/15 strain gages failed	20 % mortality
V85:	20/30 strain gages failed	67% mortality (operator error)
Overall*:	96/193 strain gages failed	50% mortality
*Six additional gages failed prior to pressure testing: (102/193, 53%)		

The vertical tendon data, however, appears to suggest that the wobble friction in the straight portion of the cylinder wall may be underestimated, while the angular friction in the dome may be overestimated. Since the majority of the strain gages on V37 and V46 survived and the force distribution is more nearly a continuous function, a curve was fitted through the test data to facilitate interpreting and comparing the design assumptions. Unfortunately, due to operator error prior to the start of prestressing operations, most of the gages on V85 (which is deflected around the E/H), were damaged. While the force distribution around the penetration was not obtained, it is apparent that deflecting the tendon around the penetration results in additional losses, as expected.

Finally, the prestressing contractor's data and the load cell data was summarized for comparison with the design specification in Table 2.9.

Table 2.9 Prestressing Data Summary

	<u>Hoop Tendons</u>		<u>Vertical Tendons</u>	
Average Tension Force:				
Design:	44.41 T	97.9 kips	49.57 T	109.3 kips
Jack:	43.53 T	95.97 kips	49.02 T	108.07 kips
Jack (w/ Load Cells only):	43.61 T	96.14 kips	49.09 T	108.23 kips
Load Cells:	43.21 T	95.27 kips	48.20 T	106.27 kips
Average Lift-off Force:				
Design:	34.11 T	75.2 kips	46.31 T	102.1 kips
Jacks:	34.02 T	75.01 kips	44.22 T	97.49 kips
Average Friction Coefficient:	0.18		0.22	
Average Seating Loss:	3.95 mm	0.16"	4.9 mm	0.19"
Jack:	9.51 T	20.96 kips	4.80 T	10.58 kips
Load Cell:	9.86 T	21.75 kips	4.64 T	10.23 kips
Average Final Load Cell Force:	33.34 T	73.52 kips	43.56 T	96.04 kips
Average Elastic Loss:	0.27 T	0.59 kips	0.58 T	1.29 kips

One Tonne = 1000 kg_r = 9.807 kN = 2.205 kips

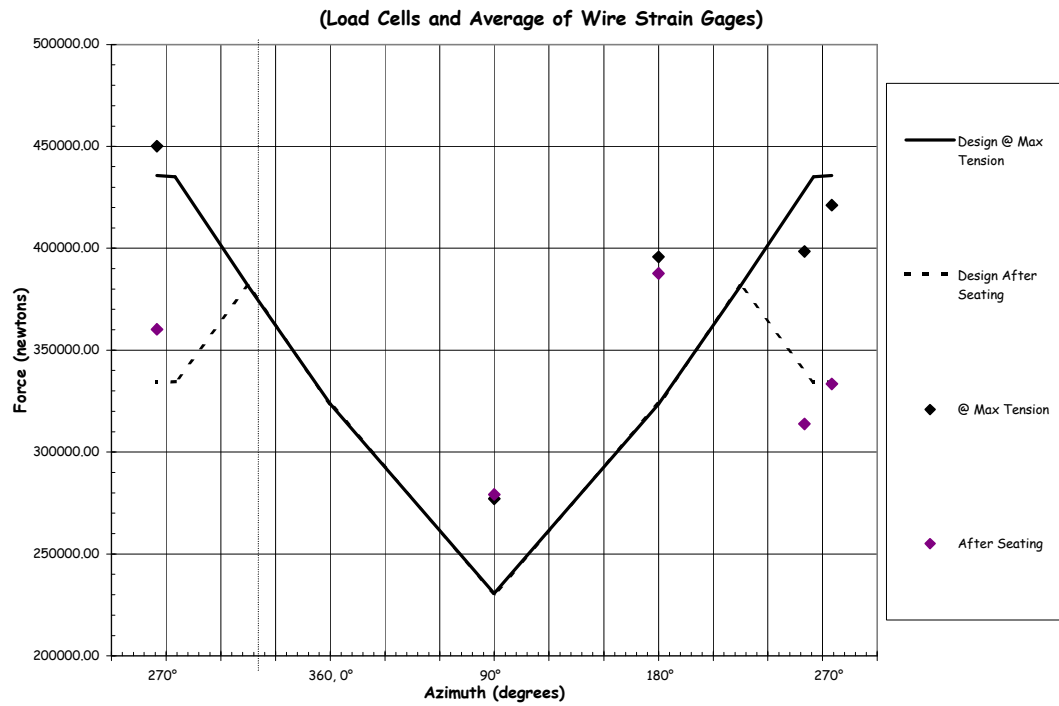


Figure 2.67 H11 Tendon Force Distribution, Elev. 1854

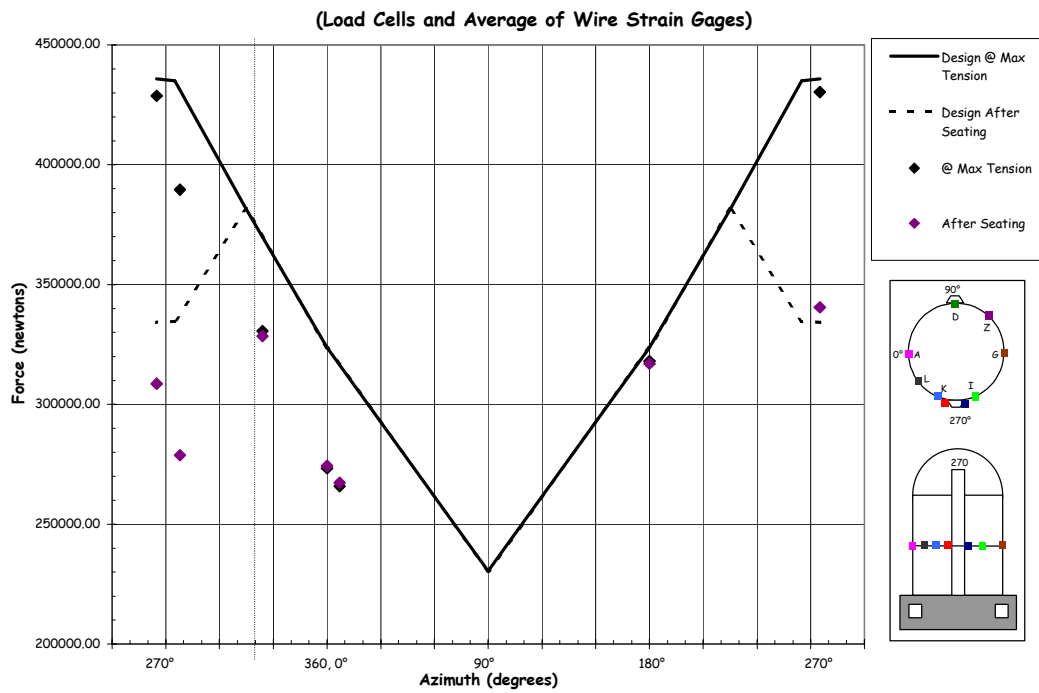


Figure 2.68 H35 Tendon Force Distribution, Elev. 4572

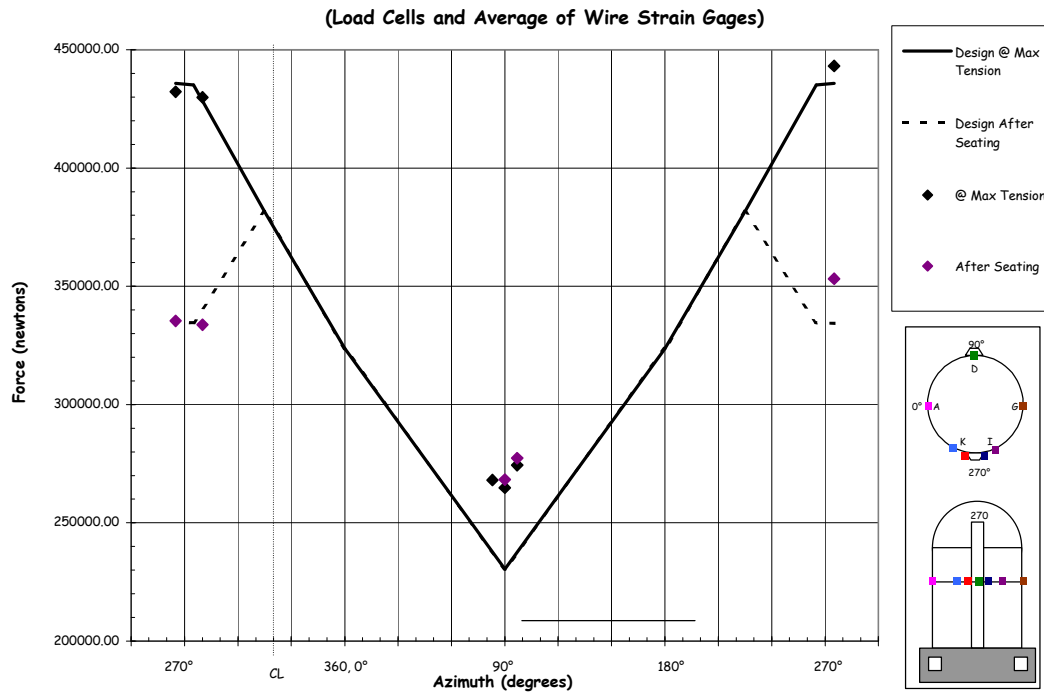


Figure 2.69 H53 Tendon Force Distribution, Elev. 6579

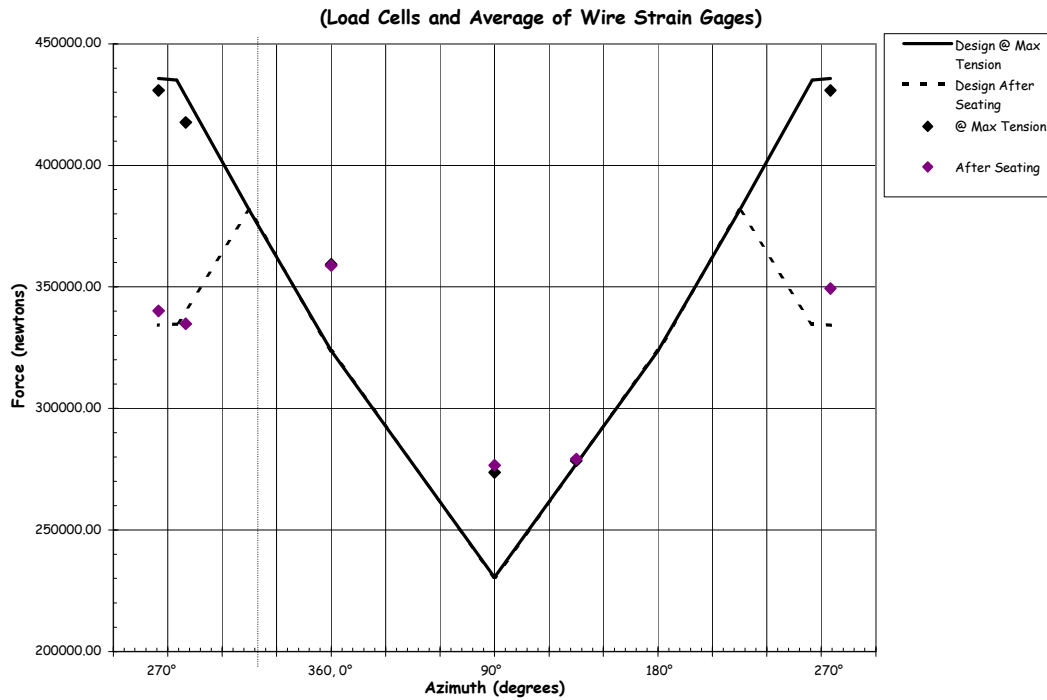


Figure 2.70 H67 Tendon Force Distribution, Elev. 8153

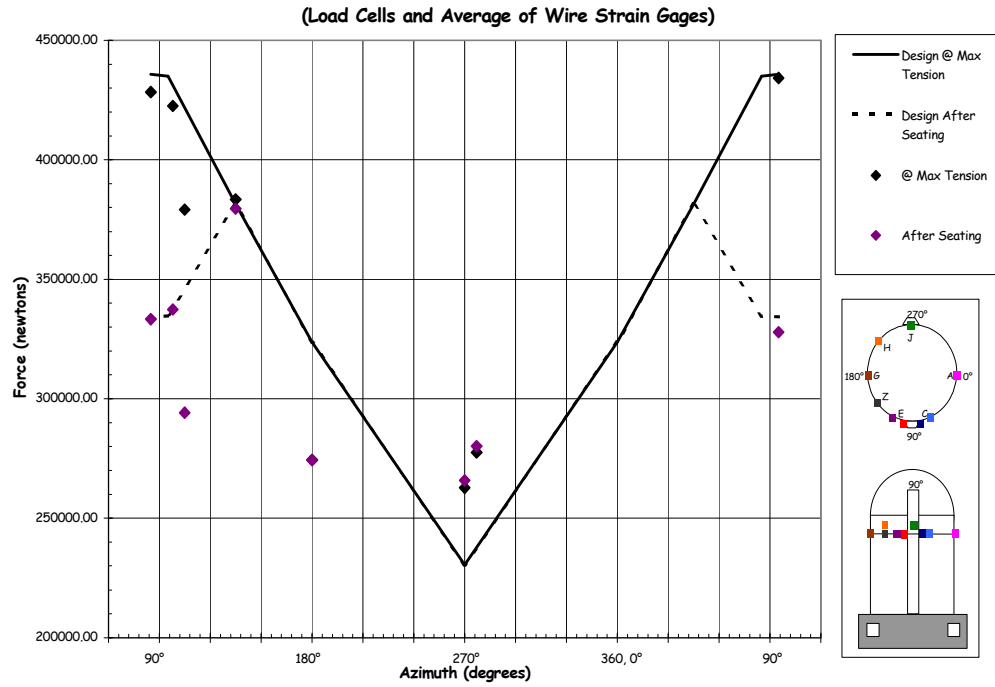


Figure 2.71 H68 Tendon Force Distribution, Elev. 8280

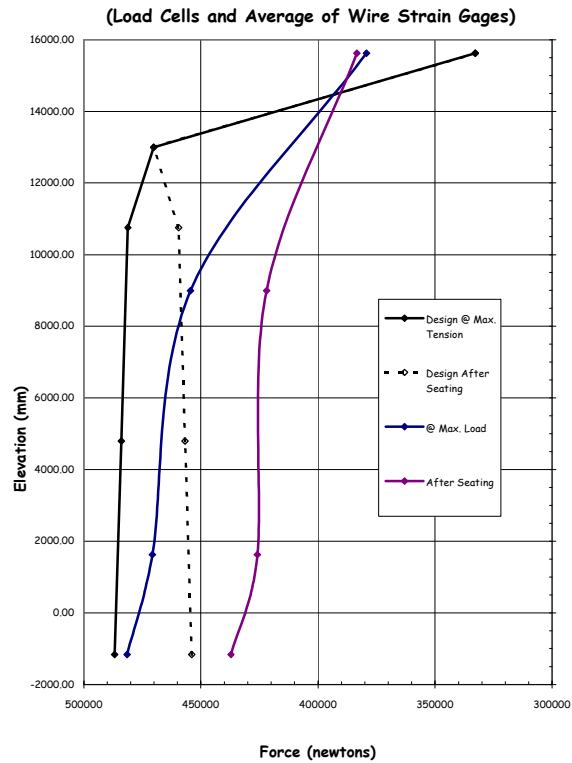


Figure 2.72 V37 Tendon Force Distribution, Azimuth 240 Degrees

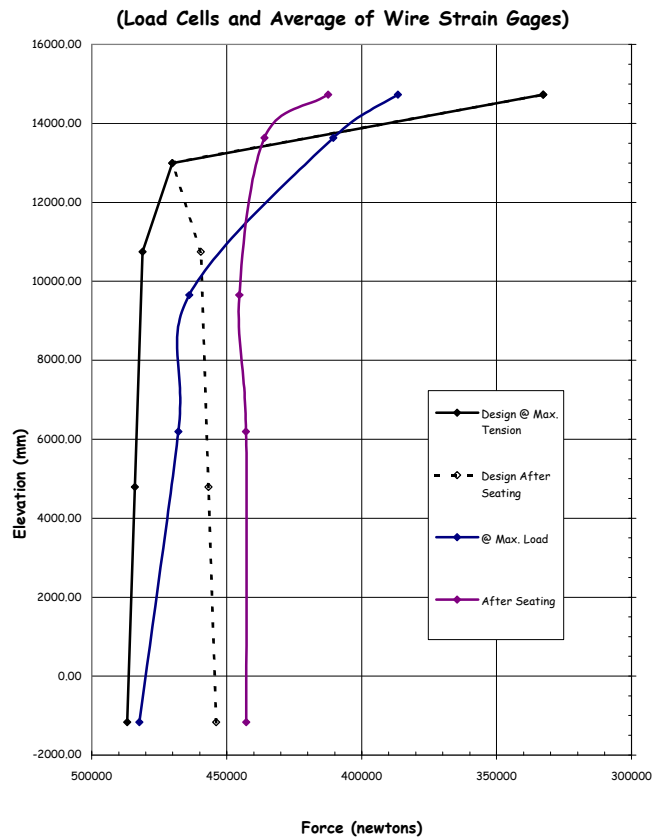


Figure 2.73 V46 Tendon Force Distribution, Azimuth 135 Degrees

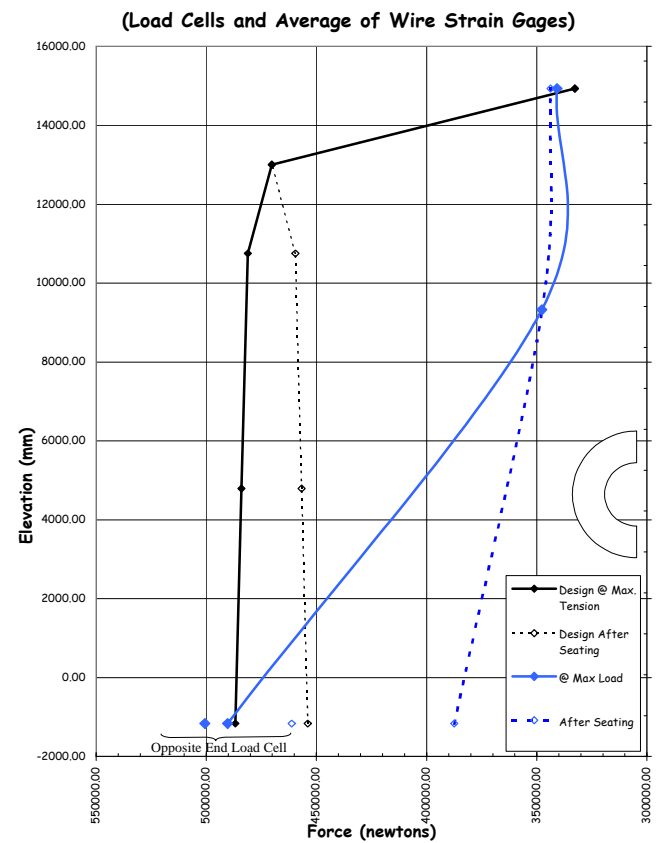


Figure 2.74 V85 Tendon Force Distribution, Azimuth 325 Degrees

3. INSTRUMENTATION

3.1 Background

The instrumentation suite installed on the PCCV model was designed to support the test program objectives, i.e., to provide data on the response of model to internal pressure loading well into the inelastic regime, for comparison with analytical models; and to provide insight and information into response and failure mechanisms that may be representative of actual nuclear power plant containment structures.

Since most types of instrumentation are only capable of measuring a single response parameter at a discrete location, the task of designing the instrumentation suite consisted of identifying critical response parameters and locations from which the overall and local response of the model could be inferred, selecting transducers with the requisite accuracy and range, meeting other operating constraints (pressure, temperature, size, etc.) and integrating them with the other transducers and the data acquisition system. The design of the instrumentation suite also required the specification of quality control procedures to ensure the transducers would perform as designed and that the output could be reliably interpreted in terms of the response parameters of interest.

This chapter describes the considerations given in the design of the instrumentation, gives specifications for the transducers selected, and provides a list of all the transducers installed on the model, along with details of the location, installation, and quality control procedures.

3.1.1 Design Considerations

The basic instrumentation plan was outlined by NUPEC in early 1992 during the initial planning for the PCCV model test [29]. After extensive discussions between NUPEC, its subcontractors, the NRC, and SNL, the details of the instrumentation were agreed upon and documented [30, 31]. Preliminary analyses of the PCCV model guided the selection and location of the final suite of measurements [32]. The detailed PCCV Instrumentation Plan provides a complete description of the instrumentation system and was updated throughout the model design and construction, finally reflecting the ‘as-built’ configuration employed during the pressure tests.

Considering the basic design philosophy, described in Section 2.1, the basic instrumentation plan identified the following measurements to be taken during the PCCV pressure tests:

1. load (internal pressure),
2. displacement,
3. rebar strain,
4. concrete strain,
5. concrete crack width,
6. liner and liner anchor strain,
7. tendon force, and
8. temperature.

These parameters would be measured at a number of locations to characterize both the global and local response of the model. The basic plan also called for the instrumentation to provide information regarding the potential failure modes identified in Section 2.1. Table 3.1 shows the relationship between instrument location, instrument type, measurement type, and measurement objective. The measurement objectives are either to capture global or local response at specified locations in the PCCV or to measure the behavior of potential failure modes, as shown above. The measurement types and the various instrument types to be specified are discussed in Section 3.2. Installation and locations of the instruments are discussed in Section 3.3.

The basic instrumentation plan also specified a grid of azimuths and elevations which would form the basis for the instrumentation layout and provide a scheme for incorporating the nominal gage locations in the individual gage IDs. This basic grid of cardinal lines is shown in Figure 3.1.

Thirteen cardinal elevations were established, from 1 at the top of the basemat (elev. 0.00) to 13 at the dome apex. Twelve cardinal azimuths, spaced roughly 30 degrees apart, were established with A at 0 degrees (or 360 degrees) to L at 324 degrees. A thirteenth cardinal azimuth was established at 135 degrees and designated Z. This azimuth was selected to represent the global axisymmetric response of the containment based on preliminary analysis results. While the PCCV model is not axisymmetric in terms of geometry and stiffness, Azimuth Z is reasonably distant from any major structural discontinuities and the net hoop prestressing force is close to the average.

The cardinal lines of the model were selected because they correspond to the measurement locations for the prototype Structural Integrity Test (SIT). The SITs were carried out on the containments of the Ohi Nuclear Power Station (Units 3 and 4) in 1991 and 1992. Comparison of the SIT results from the prototype with the model SIT results might be useful for investigating the similarity between the structures. The SIT for both the Ohi containment and the model were performed at 1.125 times design pressure.

Table 3.1 Instrumentation Objectives

Location	Material	Measurement Type	Instrument Type	Measurement Objective
Free-Field Cylinder and	Liner	Strain	Strain gage	Response and Liner failure
Dome	Liner anchor	Strain	Strain gage	Response
	Rebar	Strain	Strain gage	Response
	Tendon	Strain	Tensmeg & Strain gage	Response and Tendon failure
		Force	Load cells	Response
	Concrete	Strain	Strain gage	Response
		Cracking	Video	Response
	All	Displacement	CPOT and TLDT	Response
Wall-Basemat	Liner	Strain	Strain gage	Liner failure
Juncture	Liner anchor	Strain	Strain gage	Liner failure
	Rebar	Strain	Strain gage	Shear failure
	Concrete	Strain	Gage bars	Shear failure
		Cracking	Video	Shear failure
On E/H or A/L	Steel hatch	Strain	Strain Gage	E/H or A/L failure
		Displacement	LVDT	Response
Around E/H or	Plate and Liner	Strain	Strain gage	Liner failure
A/L	Liner anchor	Strain	Strain gage	Liner failure
	Concrete	Cracking	Video	Response
Other	Steel Plate	Strain	Strain gage	Penetration failure
Penetrations	Liner	Strain	Strain gage	Liner failure
	Liner anchor	Strain	Strain gage	Liner failure
Basemat/ Tendon	Tendons	Force	Load cell	Response and Tendon failure
Gallery	Rebar	Strain	Strain gage	Shear failure
	Concrete	Uplift Displacement	LVDT	Response
Buttress	Liner	Strain	Strain gage	Response and Liner failure
	Rebar	Strain	Strain gage	Response
	Tendon	Force	Load cell	Response and Tendon failure

CPOT - Cable Potentiometer

LVDT - Linear Variable Differential Transformer

TLDT – Temposonics Linear Displacement Transducer

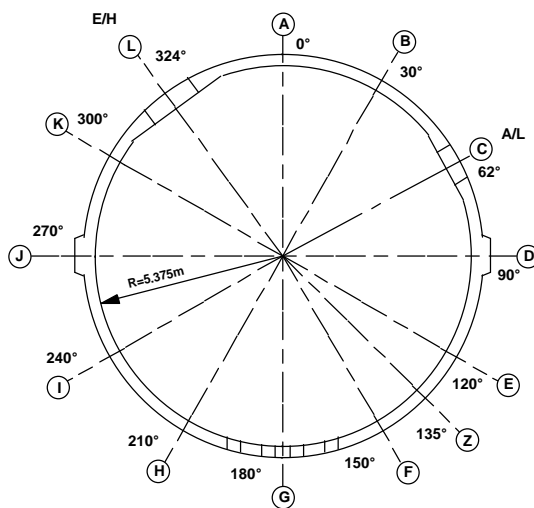
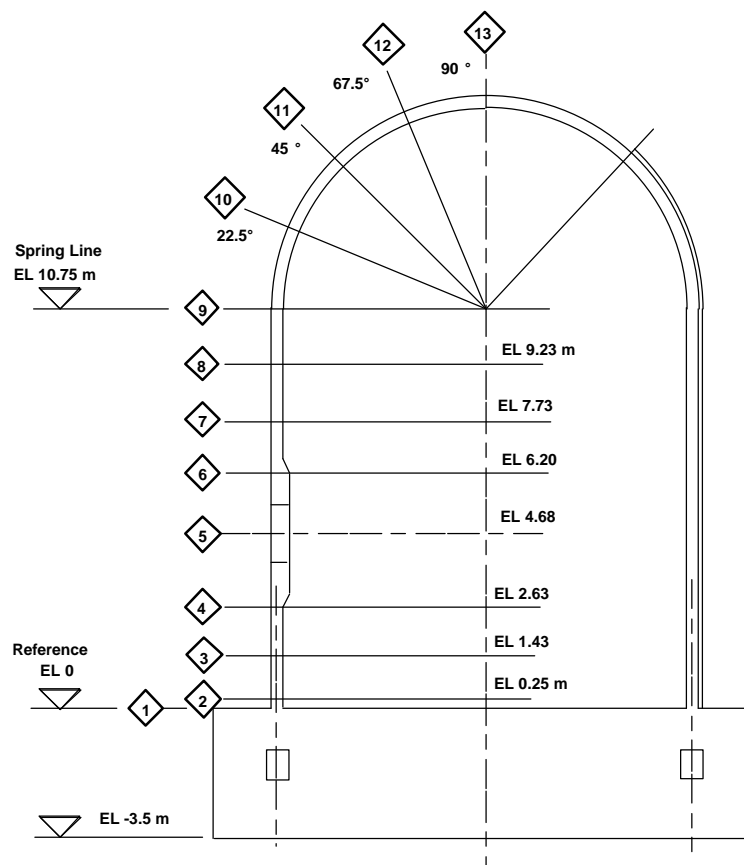


Figure 3.1 Cardinal Instrumentation Layout Lines

3.2 Types of Measurements

This section summarizes the types of measurements required to meet the PCCV test objectives. Details of what and why measurements were taken are included. These measurement types correspond to those shown previously in Table 3.1.

3.2.1 Pressure

Accurate measurement of the internal gas pressure in the PCCV during pressure tests was necessary for several reasons. First, the pressurization of the vessel for the test needed to be carefully controlled and accurately recorded to allow comparison of model response with pre- and posttest analytical results as a function of pressure. Next, accurate calculation of the integrated gross leak rate of the vessel during low pressure testing and detection of leaks and leak rate estimation during high pressure testing dictated the need for accurate pressure and temperature data. These data, along with knowledge of the gas properties in the vessel, allow calculation of leak rates during the tests.

The specifications for the pressure sensors are presented in Table 3.2. The accuracy requirements dictate voltage output devices (rather than millivolt output) with integrated signal conditioning electronics included.

Table 3.2 Pressure Transducer Specifications

Specification Item	Data
Type of measurement required	Gage pressure inside PCCV model
Anticipated exposure conditions	Non-purified nitrogen gas at pressures from ambient to approx. 2.1 Mpa-g (300 psig) for durations no more than 20 days (500 hours)
Operational range	1% of full scale < P_{op} < 2.4 Mpa-g (350 psig) (125% of anticipated rupture pressure)
Desired output	Amplified voltage
Total desired accuracy (i.e., linearity, repeatability, hysteresis, sensitivity)	Less than or equal to 0.1% of span
Temperature effect	< 0.05% full scale per /F over temperature compensated range
Logistics (electrical connection, cabling requirements, etc.)	Pressure taps from vessel will be installed so the transducer housing will represent part of the pressure boundary, typical four wire connection with independent power supply required (i.e., not provided by VXI mainframes), specifications for power supply dependent on type of pressure transducer (i.e., input voltage needs)

Two high-accuracy pressure transducers, Mensor Model 4040 high-accuracy digital units¹⁸, were installed in the vessel to provide redundancy in the measurements. Although the predicted failure pressure of the model was not known with certainty, preliminary calculations indicated it would be in the range of 1.6MPa-g (230 psig). The pressurization system and all equipment was designed for an upper-bound capacity estimate of 2.1Mpa-g (300 psig). Applying an overpressure margin of 15%, the specified range for the pressure transducers was 2.4 MPa-g (350 psig).

¹⁸ Mensor Corporation, 201 Barnes Drive, San Marcos, Texas, 78666.
(http://www.mensor.com/Digital_Pressure_Transducer_4000.htm)

(An independent pressure transducer was supplied with the pressurization system to control test operations. This transducer was independently calibrated; however, all test results are reported against the ‘official’ pressure transducers.)

3.2.2 Temperature

Both model material and internal gas temperatures were measured. Material temperature measurements were made to provide data for thermal compensation of all strain gages within the PCCV model and to provide data to correlate the response of the model to changes in ambient thermal conditions and the effects of direct radiant heating. Two types of T/Cs were used: Omega Model SA1-T T/Cs were placed on the inside surface of the PCCV liner, while Omega Model TQSS-116 were embedded within the concrete¹⁹. Due to the low sensitivity of the strain gages to temperatures around 23/C and the anticipated low temperature gradients along the inside surface of the model, low cost thermocouples were installed so that one T/C compensated several gages. Therefore, only a relatively small number of T/Cs were required to fulfill the temperature compensation requirements for the entire suite of strain gages. These were uniformly distributed, along with additional liner T/Cs near the E/H and A/L.

Internal gas temperature measurements were required to evaluate the integrated leak rate from the vessel prior to and during the pressure tests. High accuracy transducers were required for this purpose due to the small magnitude of the overall leak rate compared to the large volume of the vessel. Resistance temperature detectors (RTDs), Omega Model RD 805 precision gas temperature monitoring units¹⁹, were used for this purpose. The RTDs were distributed fairly uniformly throughout the model so that the tributary volumes associated with each sensor were approximately equal. These temperature measurements, in conjunction with the pressure measurements, provided data to detect leaks and estimate leak rates. Fans were available to circulate the gas inside the model in order to minimize thermal stratification during testing. A single RTD was also located outside the model (on the north side, i.e., in the shade) to provide ambient air temperature data.

The requirements for each of the two temperature monitoring instruments are provided in Tables 3.3 and 3.4. For the PCCV tests, three wire, lead-resistance-compensation-type sensors with low self-heating errors were used.

Table 3.3 Thermocouple Specifications

Specification Item	Data
Type of measurement required	Temperature measurements of inside surface of PCCV model
Anticipated exposure conditions	Nitrogen, from ambient to 2.1 MPa-g (300 psig), expected maximum temp. range from -5 to 50/C
Operational range	-10 to 100 /C
Desired accuracy	< 2% of total input range
Temporal response times	Unspecified, not critical
Junction characteristics	Ungrounded, sheathed
Logistics (electrical connection, cabling requirements, etc.)	Two-wire twisted, insulated leads of same material as thermoelement junction pair, junctions at pin-type pressure feedthroughs (requires pins of same materials as conductors)

¹⁹Omega Engineering, Inc., One Omega Drive, Stamford, Conn. 06907-0047. (<http://www.omega.com/temperature/tsc.html>)

Table 3.4 RTD Specifications

Specification Item	Data
Type of measurement required	PCCV internal gas temperature measurements
Anticipated exposure conditions	Nitrogen, ambient to 2.1 MPa-g (300 psig)
Operational range	-10 to 100/C
Desired accuracy	< 2% of total input range
Desired sensitivity	N/A
Logistics (electrical connection, cabling requirements, etc.)	Four-wire twisted, insulated leads. Requires constant current source (typically 1ma).

3.2.3 Displacement

Displacements were measured at discrete locations to compare with analysis and allow construction of the global response of the model. The types of displacement measured included:

1. radial displacements of the cylinder wall at regular azimuths and elevations relative to a reference point on the instrumentation frame,
2. vertical displacements at the springline at regular azimuths relative to the top of the basemat liner,
3. horizontal and vertical displacements in the dome at regular azimuths and elevations relative to the instrumentation frame,
4. vertical displacements at the apex of the dome relative to the instrumentation frame,
5. changes in internal diameter (i.e. ovalization) of the E/H and A/L barrels,
6. vertical displacement or uplift of the basemat relative to the mudmat.

The range of displacements to be measured included small, elastic deformations during prestressing and subsequent changes due to ambient temperature variation, creep, etc., through large inelastic deformations during pressure testing.

For the PCCV model test, three types of displacement transducers allowed a wide range of expected displacement to be measured. Overall global deformations at the cardinal points were typically measured using CPOT Celesco Model PT 101²⁰ (Figure 3.2). Where deformations were expected to be small, such as at the wall-junction or where higher precision was desirable, such as measuring local deformations at penetrations, Schaevitz HCD series²¹ LVDTs with ranges on the order of 4" or less were used (Figure 3.3). In some locations where both high accuracy and long range were required, Temposonics® magnetostrictive high-accuracy TLDTs²² were used (Figure 3.4). The specifications for each of these displacement transducers are provided in Tables 3.5, 3.6, and 3.7.

Note that all displacement data represents the relative motion between the point of interest and a reference point. Ideally, the reference point is fixed and not influenced by the loads applied to the test structure; however, in most cases, this is impractical. For the case of the PCCV model, most displacements were measured internally and referenced to the instrumentation frame or the top of the basemat. Since the basemat was judged to be, essentially, a rigid mass, the only consideration required for the instrumentation frame was its response to variations in internal temperature. A set of transducers were mounted on the instrumentation frame to measure changes in height and plan dimensions and determine if there was any effect on the cylinder or dome displacements. These frame displacement transducers consisted of

²⁰ Celesco Transducer Products, Inc., 20630 Plummer St., Chatsworth, CA, 91311. (<http://www.celesco.com/cet/index.html>)

²¹ Measurement Specialties, Inc., Sensor Products Division, 950 Forge Ave. Bldg B, Norristown, PA 19403. (<http://www.msusa.com/schaevitz/products/LVDT/index.html>)

²² MTS Systems Corp., Sensors Group, 3001 Sheldon Drive, Cary, NC 27513. (<http://www.mtssensors.com/>)

CPOTs and two Spectron Model SSY0140 dual-axis inclinometers²³ to monitor tilt of the frame due to possible basemat curvature.

In addition, the internal displacement transducers were attached to the liner surface, assuming that the liner was ‘perfectly’ bonded to the concrete. This assumption, while valid in most cases, was incorrect in a number of cases (which will be discussed in Chapter 5) and it is worth remembering that all internal displacement data represents the position or motion of the liner, not necessarily the concrete wall.

Similarly, uplift of the basemat was measured relative to the mudmat (Figure 3.5) and, as was previously identified, any motion of the mudmat would affect the uplift data.

Table 3.5 Displacement Transducer Specifications (CPOT)

Specification Item	Data
Type of measurement required	Radial or vertical displacement of internal surface of the PCCV model
Anticipated exposure conditions	Nitrogen, from ambient to 2.1 MPa-g (300 psig)
Operational range	5 cm, 12.5 cm, 25 cm, and 38 cm (2", 5", 10" and 15")
Desired accuracy (linearity and repeatability)	0.15 to 0.25% full scale
Logistics (electrical connection, cabling requirements, etc.)	Power supply required (not included on VXI card), multi-pin cable connector needed



Figure 3.2 CPOT Mounted on Instrumentation Frame and Attachment to PCCV Liner

²³ Spectron Systems Technology, Inc., 595 Old Willets Path, Hauppauge, NY 11788.
(<http://www.spectronsensors.com/inclinomter.htm>)

Table 3.6 LVDT Specifications

Specification Item	Data
Type of measurement required	Radial or vertical displacement of internal surface of the PCCV model Ovalization of equipment hatch and personnel airlock, basemat uplift
Anticipated exposure conditions	Nitrogen, from ambient to approx. 2.1 MPa-g (300 psig)
Operational range	2.5 and 10 cm (1" and 4")
Desired sensitivity	< 1% total input range
Deviation from linearity	0.25% full scale
Logistics (electrical connection, cabling requirements, etc.)	Same as CPOT requirements

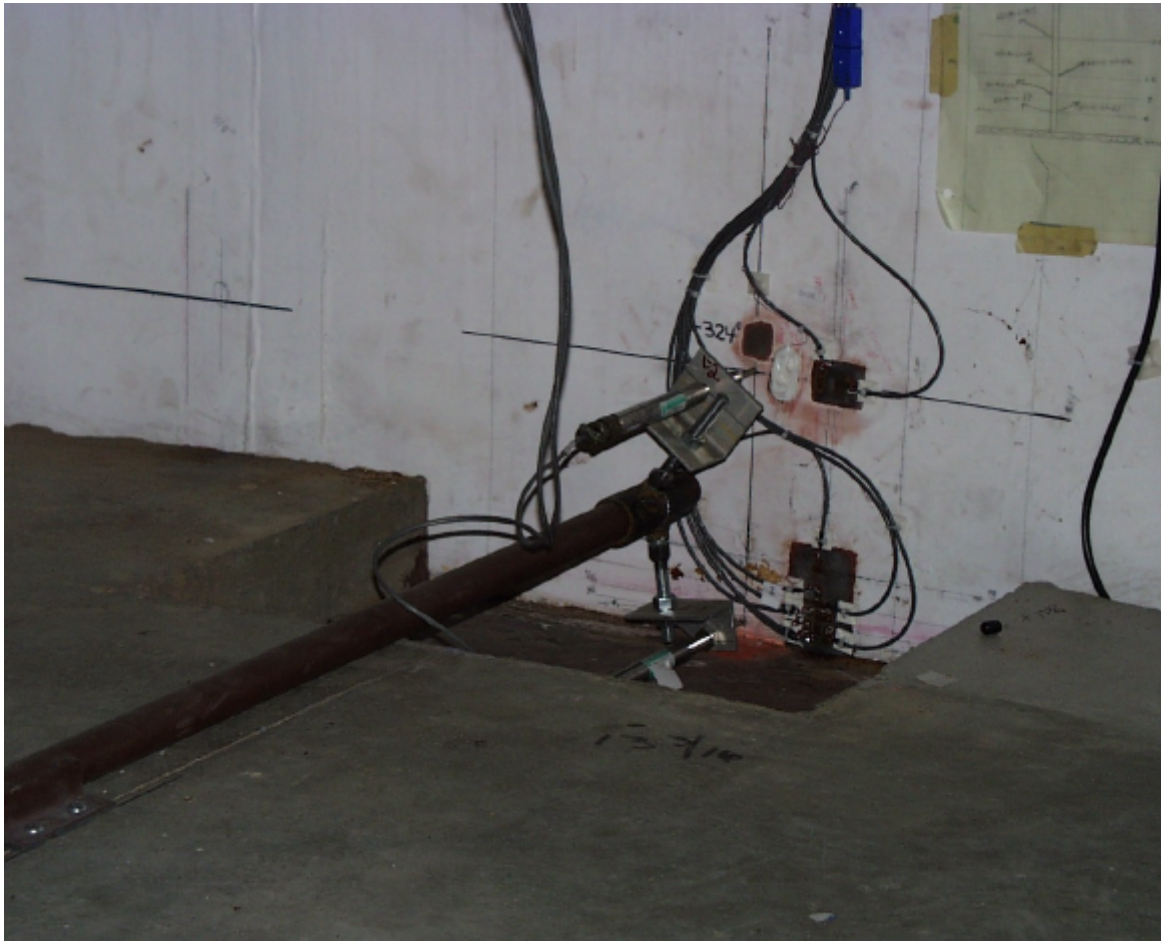


Figure 3.3 LVDTs at Wall-Base Junction (Azimuth 324 degrees, Elev. 0.0 and 250.0)

Table 3.7 Temposonics Linear Displacement Transducer Specifications (TLDT)

Specification Item	Data
Type of measurement required	Accurate and high range measurements of linear displacement of internal surface of PCCV model
Anticipated exposure conditions	Nitrogen, from ambient to approx. 2.1 MPa-g (300 psig)
Operational range	38 cm (15")
Desired sensitivity	< 1% total input range
Deviation from linearity	0.02% full scale (min 13 mm)
Logistics (electrical connection, cabling requirements, etc.)	Same as CPOT requirements



Figure 3.4 TLDT Mounted on Instrumentation Frame and Attachment to PCCV Liner

3.2.4 Concrete Cracking

The basic instrumentation plan identified the relationship between concrete cracking and load or pressure as one of the response mechanisms to observe during the PCCV test. In order to thoroughly model and understand concrete cracking mechanisms, several parameters to measure were identified:

1. the strain in the concrete,
2. when and where a crack first occurs,
3. crack propagation, and
4. crack width.

Measurement of discrete concrete crack width is, however, difficult to perform in practice. A discrete crack must be identified prior to placing a gage at the crack location. However, since most cracks of interest will not form until the test pressure exceeds the design pressure (and the prestressing load), safety constraints prohibit the installation of gages during testing. Several schemes for measuring concrete crack width were considered, including pre-cracking the model, placing crack width gages at a number of shrinkage cracks, or using high resolution video monitoring. However, none of these schemes was considered to be practical or cost-effective. The decision was made to abandon requirements to measure concrete crack width and focus on crack detection and crack propagation.



Figure 3.5 External LVDT Measuring Displacement between Basemat and Mudmat

Crack initiation and propagation were monitored by performing detailed visual inspection to construct crack maps in areas of interest following critical load steps. These crack maps are supported by photographic records of all the areas inspected. Detection of crack initiation during pressure testing was also attempted via acoustic monitoring, described in Section 3.2.8.

Concrete strain measurements are discussed in Section 3.2.5.2.

3.2.5 Strain Measurements

Strain gages applied to individual structural elements provide information on the discrete strain in the element being interrogated and are also capable, when used in groups, of providing insight into local and global strain fields in the structure. Extensive experience through the previous history of containment testing at SNL and elsewhere formed the basis for the specification of strain gage requirements for the PCCV experiment. Standard electrical-resistance type, bonded strain gages were chosen for their simplicity and accuracy, as well as low relative cost. All foil-type strain gages used on the PCCV model were high-elongation-type EP Micro-Measurements gages constructed of annealed constantan on a polyimide backing.²⁴ These gages were used to measure strains in the rebar, concrete, liner, liner anchor, hatches and penetrations, and tendons. In some cases, noted below, special types of strain gages were used in addition to the bonded foil gages to provide additional response information.

Care must be exercised, however, when interpreting strain gage output, since very small gage length strain gages are highly susceptible to the influence of local structural discontinuities or as-built conditions and positioning of the gage in areas with high strain gradients can significantly affect the results. These factors should be considered when comparing strain data with analysis results at discrete points in a structure. Furthermore, the application of the strain gage to the structural element may perturb the strain fields in the vicinity of the gage and these effects should, if present, also be considered.

²⁴ Micro-Measurements Division, Vishay Measurements Group, Inc., Raleigh, NC 27611.
(http://www.vishay.com/brands/measurements_group/strain_gages/mm.htm)

3.2.5.1 Reinforcing Bar Strain

Strain gages, mounted to meridional, hoop, and transverse reinforcing steel, were used to measure the global ‘free-field’ or local membrane, bending and shearing strains in the model as a function of pressure. Reinforcing strain measurements were generally not made in areas where the reinforcing was highly congested, such as around penetrations, or to determine local strain concentrations. Exceptions to the latter case included the wall-basemat intersection and around the tendon gallery. In areas of highly congested reinforcing, rebar strains were measured at the perimeter of the reinforcing grid to confirm boundary conditions for comparison with pretest analyses. Typical reinforcing strain measurements included:

1. Free-field strain measurements of meridional and hoop reinforcing steel at regular azimuths and elevations in the cylinder wall and dome for comparison with pretest axisymmetric and global 3D analyses and to determine the global strains at which local failures were expected to occur. Typically, both inner and outer reinforcing strains were measured to resolve membrane and bending behavior.
2. Near-field strain measurements of meridional and hoop reinforcing steel at the boundaries of local reinforcing areas, e.g. E/H, A/L, etc., were acquired for confirm boundary conditions for local submodels in pretest and posttest analyses.
3. Near-field strain measurements of radial ties in the vicinity of structural discontinuities where large shears or large bending moments were predicted to occur, and to measure triaxial state of strain (stress) for evaluating failure models. In addition, inclined gage bars were used, based on the predicted orientation of principal tensile stresses.

The specifications for the rebar (and tendon wire) strain gages are summarized in Table 3.8. Figures 3.6 and 3.7 show a typical rebar strain gage after mounting on the bar and in place in the model, with protective epoxy cover.

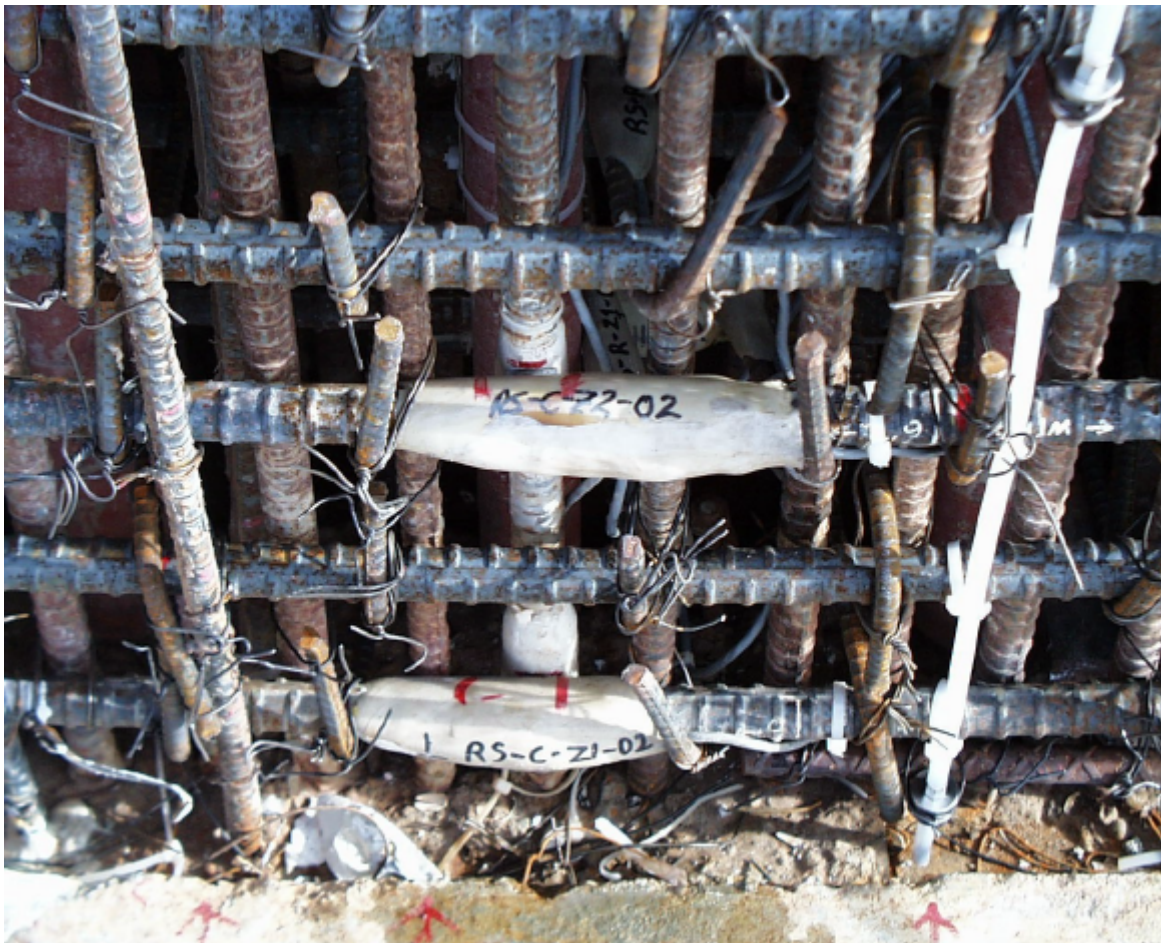
Understanding the method of mounting the strain gages on the rebar is important to interpreting the rebar strain data. One of the first considerations is that the surface of the rebar to which the gage is to be bonded must be ground smooth. This typically removes a portion of the bar’s cross-section, which can result in a local strain concentration in the bar. This phenomenon is described in more detail in Section 5.3.2.1.5. Second, requirements to protect the strain gages during erection and concrete placement locally debond the rebar from the concrete, so that local strains between the rebar and concrete may not be compatible. Finally, strain gages on rebar are located away from the ends of bars or mechanical splices to ensure the bars are fully developed and to avoid end effects. However, in some cases, end effects may be a factor and the location of the gage relative to the bar end should be known.

Table 3.8 Strain Gage Specifications (Rebar & Tendon wire)

Specification Item	Data
Type of measurement required	Point strain (approx.) in the “hoop,” “meridional,” and “radial” directions attached to the reinforcing steel and the prestressing tendon strand wires.
Anticipated exposure conditions	Concrete placement, curing, long term exposure, temperatures from -5 to 50/C
Operational range	Wire gages: 4 - 6% Rebar gages: 5 - 10%
Desired strain sensitivity (gage factor, k)	$1 < k < 2$ (all gages)
Transverse sensitivity, k_t	$k_t < 2\%$ (all gages)
Mounting configuration	Strain gages will be adhesively bonded to the reinforcing steel and tendon wire strands
Logistics (installation, electrical connection, cabling requirements, etc.)	Three wire twisted, insulated cables



Figure 3.6 Rebar Strain Gage



**Figure 3.7 Rebar Strain Gages Installed in PCCV Model
(Note SOFO Fiber Optic Concrete Strain Gage at right)**

3.2.5.2 Concrete Strain

As noted above, since rebar gages are susceptible to local strain concentration and may be debonded from the concrete, rebar strains may not provide an accurate indication of the concrete strain. Measurement of concrete strains, therefore, may require the use of independent gages designed specifically for this purpose. Based on experience during previous model tests, commercially-available concrete strain gages were not judged reliable or cost-effective. Measurement of global concrete strain can be most accurately and reliably be determined from displacement data using the kinematic relationship $\epsilon = \Delta r/R$. Specially fabricated bars, or gage bars, which are not part of the normal reinforcing, along with long-gage length fiber-optic gages, were installed to help measure local concrete strains, such as where significant bending occurs (e.g. at the wall base junction, adjacent to the buttresses and near penetrations) and for comparison with rebar strain measurements.

Specifications for the gage bar strain gages are summarized in Tables 3.9. The configuration of the gage bars is illustrated in Figure 3.8. Sample rebar and gage bar strain gages are compared in Figure 3.9.

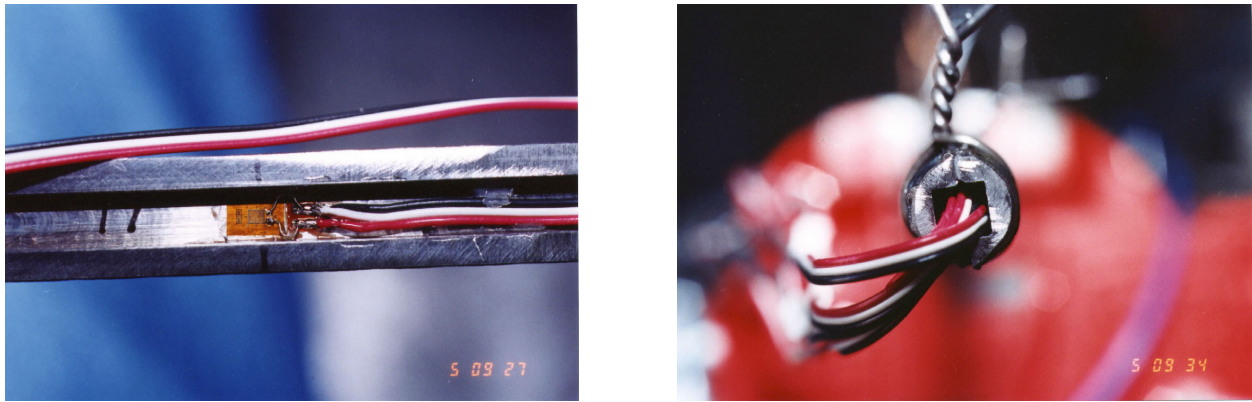


Figure 3.8 Concrete Strain Gage Bars



Figure 3.9 Sample Rebar and Gage Bar Strain Gages

Table 3.9 Strain Gage Specifications (Concrete Gage Bars)

Specification Item	Data
Type of measurement required	Point strain (approx.) in the “hoop” and “meridional” directions, embedded in the concrete.
Anticipated exposure conditions	Concrete placement, curing, long term exposure, temperatures from -5 to 50/C
Operational range	5 – 10%
Desired strain sensitivity (gage factor, k)	$1 < k < 2$ (all gages)
Transverse sensitivity, k_t	$k_t < 2\%$ (all gages)
Mounting configuration	Attached to the reinforcing steel prior to concrete placement
Logistics (installation, electrical connection, cabling requirements, etc.)	Three wire twisted, insulated cables

Specifications for the fiber optic gages SOFO Model 500²⁵ are summarized in Table 3.10. The SOFO gage, prior to installation, is shown in Figure 3.10. The active gage length is between the two ‘anchors,’ shown at the bottom, and the remainder is the fiber optic transmission cable. The installed SOFO gage was shown in Figure 3.7.

Table 3.10 Strain Gage Specifications (Fiber Optic Gages)

Specification Item	Data
Type of measurement required	Global or ‘near-field’ strain in the “hoop” and “meridional” directions in the concrete
Anticipated exposure conditions	Concrete placement, curing, long term exposure, temperatures from -5 to 50/C
Operational range	50 cm (20") gage length, 1 – 2%
Desired strain sensitivity (gage factor, k)	NA
Transverse sensitivity, k_t	NA
Mounting configuration	Place between reinforcing steel prior to concrete placement
Logistics (installation, electrical connection, cabling requirements, etc.)	Fiber optic leads running to 10 channel SOFO DAS reader

3.2.5.3 Liner and Liner Anchor Strain

Both the membrane and bending strains in the liner, as well as strains in the liner anchors, were measured. Strain gages were used to measure both free-field and local strains near liner discontinuities where strain concentrations might occur. Liner anchor strain measurements were included to investigate shear transfer across anchor, pullout force on anchor, and reinforcement contribution in the axial direction of the liner anchor. The specifications for the liner and liner anchor strain gages are summarized in Table 3.11.

At particular details and locations, arrays of gages were applied to allow characterization of the local strain fields and provide insight into the mechanism that tears the liner. Note that gages located adjacent to tears often exhibit much lower strains than expected since the tear acts as a strain relief mechanism on the surrounding structure. In areas where bending strains were likely to occur, strain gages were applied to both sides of the liner to allow them to be resolved into bending and membrane components. In areas where bending was unlikely, strain gages were only applied to the inside surface of the liner. Typical interior and exterior liner and liner anchor gages are shown in Figure 3.11.

²⁵SMARTTEC SA, Via Pobbiette 11, 6928 Manno, Switzerland. (<http://www.smartec.ch/Home.htm>)

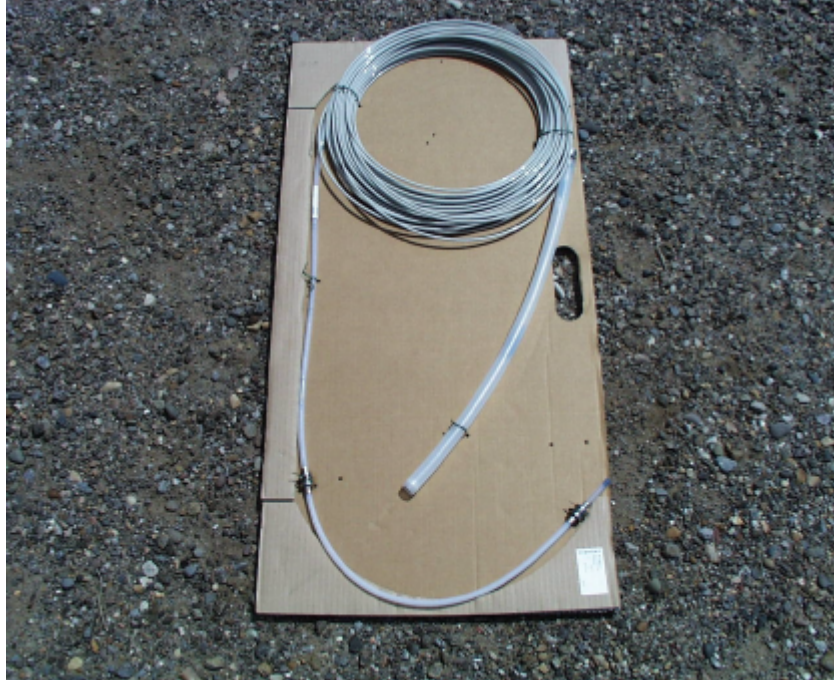


Figure 3.10 SOFO Fiber Optic Strain Gage

Table 3.11 Strain Gage Specifications (Liner & Liner Anchor)

Specification Item	Data
Type of measurement required	Point strain (approx.) in the “hoop,” “meridional,” and “radial” directions, both internal and external on the liner, liner anchors, and stiffeners embedded in the concrete.
Anticipated exposure conditions	Internal: non-purified nitrogen gas at pressures from ambient to approx. 2.1 MPa-g (300 psig), duration of elevated pressures not more than 20 days (500 hours), temperatures from -5 to 50/C. External: concrete placement, curing, and long term exposure
Operational range	Strip gages (2-10 elements): 20% 0-45-90 rosettes (3 elements): 20% single gages: 10 - 20%
Desired strain sensitivity (gage factor, k)	$1 < k < 2$ (all gages)
Transverse sensitivity, k_t	$k_t < 2\%$ (all gages)
Mounting configuration	Carrier matrix material bonded to surface of liner (both internal and external), model liner material is carbon steel, painted internally
Logistics (installation, electrical connection, cabling requirements, etc.)	Three wire twisted, insulated cable, junctions to pin-type pressure feedthroughs



Figure 3.11 Liner and Liner Anchor Strain Gages

3.2.5.4 Residual Liner Strain

Considering pretest analysis results that predicted high liner strain concentrations around the E/H insert plate and ranked them most likely to tear the liner, an attempt was made to measure the residual strain fields in the liner at this location after high pressure testing. This was performed by placing a grid on the interior liner surface and, using a digital position mapping tool, recording the position of the grid points before and after testing. Based on the change in position, coupled with strain data from liner strain gages located within the grid, it was hoped that a more accurate map of the strain field could be obtained. The grid placed around the E/H is shown in Figure 3.12

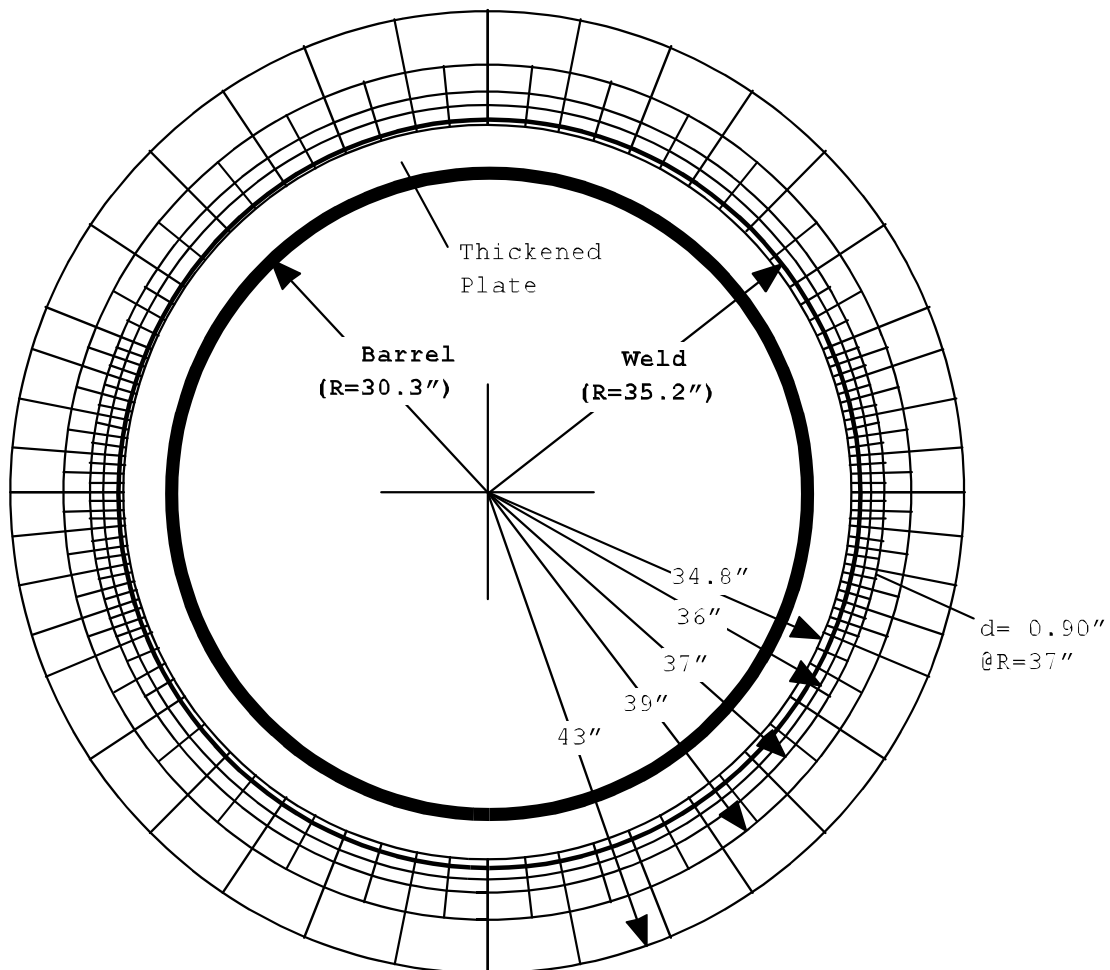
3.2.6 Tendon Measurements

Tendon strain and force measurements were discussed Section 2.2.3 in the context of prestressing operations. The basic instrumentation plan called only for tendon anchor forces to be measured during the tests. It was, however, desirable to measure the force at points along the tendon length to confirm the design force distribution described in Section 2.1.3, both initially, after prestressing, and during pressure testing as the PCCV model deformed.

3.2.6.1 Tendon Anchor Force (At Ends)

Load cells were installed at both ends of selected hoop tendons and meridional hairpin tendons to measure the anchor forces during and after prestressing and during pressure testing. Due to the relatively high cost of the load cells, only approximately one-sixth of the model tendons were monitored with load cells. The load cells were inserted between the tendon anchor and the bearing plate embedded in the concrete to measure the compressive force.

GRID LAYOUT



E/H Inside View

5 radial Circles
120 radial Lines
480 points
Smallest grid ~ 1" x 1"

Figure 3.12 Grid Layout around Inside of E/H

From this data, tensile stresses at each end of the tendons were computed. All loads cells were installed just prior to the prestressing operations and measurements were taken throughout the prestressing operations. The requirements for the load cells are provided in Table 3.12.

Table 3.12 Load Cell Specifications

Specification Item	Data
Type of measurement required	Tendon load at both ends
Anticipated exposure conditions	Ambient outdoor temperatures and humidity
Operational range	0 to 890 kN (200 kips)
Desired accuracy	1% of total input range
Temporal response times	Unspecified, not critical
Logistics (electrical connection, cabling requirements, etc.)	Six wire, twisted insulated pairs

Due to limited availability and to reduce cost, two different load cells were used in the model. Higher accuracy (and higher cost) HBM Model C6-100t load cells²⁶ were used for the instrumented tendons, while somewhat lower accuracy (and less expensive) Geokon Model GK-3000-200-2.0²⁷ load cells were used for the remaining tendons. The HBM load cell with spherical washers (provided to balance the force applied to the load cell) and bearing plates are shown in Figure 3.13. Both the installation jig used for positioning the load cells for the hoop tendons and the arrangement for the vertical tendons is shown. The Geokon load cell with the bearing plates is shown in Figure 3.14. Although the Geokon load cells came equipped with spherical washers provided by the manufacturer, laboratory calibration tests showed the output was more accurate if very thick bearing plates were used in place of the spherical washers. (Also, the spherical washers exhibited an unfortunate tendency to shatter at loads below the load cell capacity, ejecting fragments in a highly energetic manner.) Both the installation jig used for positioning the load cells for the hoop tendons and the arrangement for the vertical tendons is shown.

3.2.6.2 Tendon Force Distribution (Along Length)

The tendon force distribution was determined by measuring the strain at discrete points of individual wires and strands comprising the tendon. Extensive research was conducted to investigate the efficacy of commercially-available transducers to provide the desired data. Laboratory and mock-up testing of tendon strands were conducted to investigate the performance of the gages and led to a scheme utilizing two types of gages. These tests were also used to develop calibration relationships between wire or strand strain and tendon force, and demonstrate methods to protect the gages from damage during construction and tensioning.

In addition to standard strain gages placed directly on the wires (specified in Table 3.8), strain gages specially designed to measure the axial strain in seven-wire strands, Tensmeg®²⁸ gages, were used. Tensmeg gages are a single wire gage attached with rubber end-blocks around a tendon strand to measure uniaxial strain in the tendon. The specifications for the Tensmeg gages are summarized in Table 3.13.

Based on the laboratory and mock-up tests that demonstrated the variability of strain from wire to wire within a given strand and from strand to strand, along with the likelihood of a high mortality rate for the strain gages, each measurement location used combinations of wire and strand strain gages, along with special hardware, to protect the gages and lead wires. Special handling and tensioning procedures were also employed to minimize damage to the tendon strain gages.

²⁶ HBM, Inc., 19 Bartlett Street, Marlborough, MA 01752. (<http://www.hbm.com>)

²⁷ Geokon, Inc., 48 Spencer Street, Lebanon, NH 03766. (<http://www.geokon.com/>)

²⁸ Roctest Ltd., 665 Pine Avenue, Saint-Lambert, Quebec, Canada J4P 2P4. (<http://www.roctest.com/roctelemac/product/product/tensmeg.htm>)

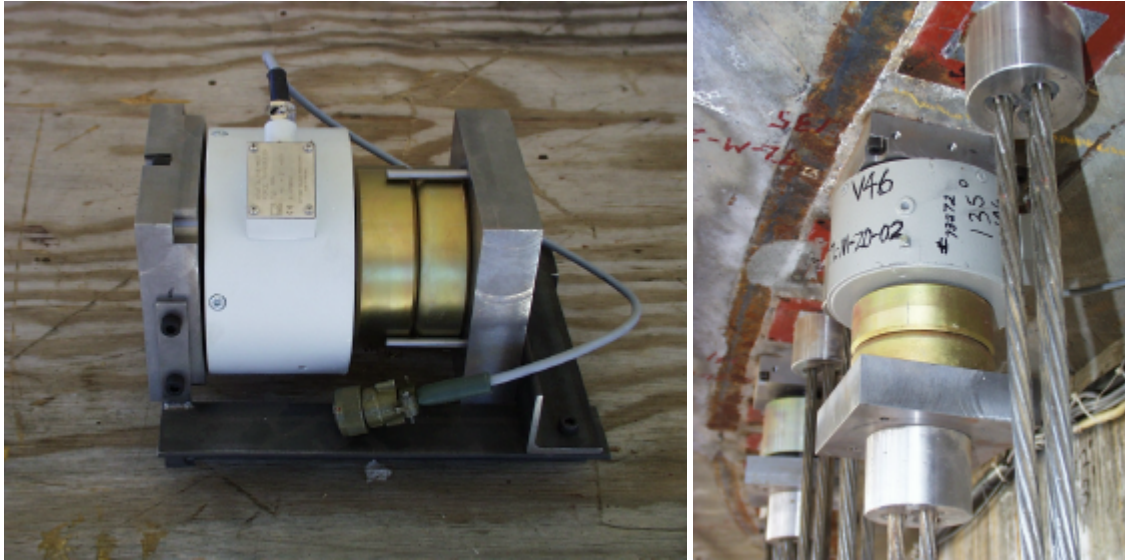


Figure 3.13 HBM Load Cell (a) Installation Jig, (b) In-Place



Figure 3.14 Geokon Load Cell (a) Installation Jig, (b) In-Place

Table 3.13 Tensmeg Gage Specifications

Specification Item	Data
Type of measurement required	Point strain (approx.) in the “hoop” and “meridional” directions, inside the tendon ducts, embedded in the concrete
Anticipated exposure conditions	Concrete placement, curing, and long term exposure
Operational range	4 – 6%
Desired strain sensitivity (gage factor, k)	$1 < k < 2$ (all gages)
Transverse sensitivity, k_t	$k_t < 2\%$ (all gages)
Mounting configuration	Gages will be adhesively bonded directly on each strand
Logistics (installation, electrical connection, cabling requirements, etc.)	Three wire twisted, insulated cable

A set of representative hoop and vertical hairpin tendons were instrumented with gages along the length of the tendon. Five hoop tendons were instrumented: H11 near the base of the cylinder wall, H53 near the mid-height, H35 (which is deflected around the E/H and A/L penetrations), and a pair of tendons H67 and H68 halfway between the cylinder mid-height and springline, which were not equipped with the protective hardware. Three vertical tendons were also instrumented: V46, which had the shortest radius in the dome, V37, which had the largest radius in the dome, and V85, which was also deflected around the E/H penetration.

The typical arrangement of the strain gages at a measurement location is shown in Figure 3.15. This figure also illustrates the positioning of the load blocks on the tendons to protect the gages from damage. The specific arrangement of gages at a given measurement location is described in Section 3.3.

3.2.7 Visual Observations

Both video and still photography was employed inside and outside of the PCCV model at locations where large deformation or other signs of damage, such as liner tearing, concrete cracking, or crushing might be expected to occur. These observations were intended to supplement the discrete measurements obtained by the other transducers. Visually monitoring the model with live video during the test was also a safety requirement. It was important to observe various sections of the model visually to properly conduct the high-pressure test.

The video cameras were placed outside the model to monitor the overall behavior, while some were placed close to the model to monitor specific areas, such as the E/H, A/L, and wall-basemat junction. Interior video cameras monitored the liner behavior. A sketch of the video and camera layout is shown in Figure 3.16. In addition, several still cameras were placed near the outside of the model to record snap-shots at each pressure step during the test. Based on the pseudostatic nature of the pressure tests and the unlikelihood of a catastrophic rupture, the video cameras were of normal speed (30 frames/sec) and there were no requirements to use high-speed video cameras during testing.

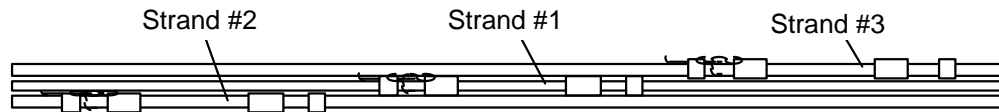
3.2.8 Acoustic Monitoring

Acoustic monitoring was not specified in the basic instrumentation plan, but incorporated into the final instrumentation plan to allow monitoring of the entire structure and identify damage that could occur at locations not monitored via other methods. The specific goals of the acoustic monitoring system were to:

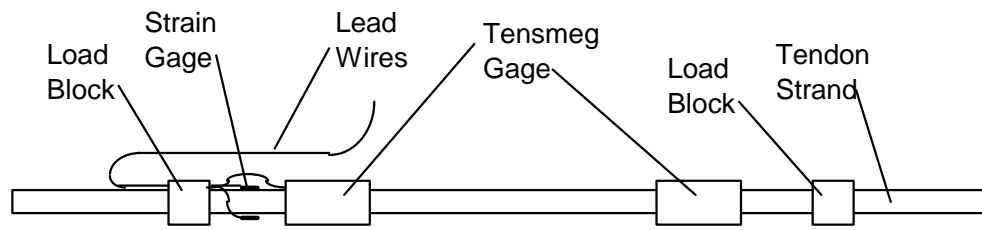
1. detect tendon wire breaks,
2. detect rebar breaks,
3. detect concrete cracking and crushing, and
4. detect liner tearing and leakage.

Acoustic monitoring of the PCCV model during both the prestressing and low and high pressure tests was performed by Pure Technologies Inc. of Calgary, Canada under a turn-key contract. Pure Technologies developed the SoundPrint® acoustic monitoring system²⁹ and has extensive experience in acoustically monitoring structures, especially prestressed concrete structures, such as parking garages and bridges. This system was run independently of the main data acquisition system (DAS). The system consisted of acoustic sensors, essentially piezo-electric accelerometers, bonded to the structure and connected to a separate DAS. One unique feature of this system is the capability to perform real-time data processing and analysis to identify event types and locations. Thirty-two sensors were glued to the external surface of the model and 16 sensors were placed inside the model. The sensors are shown in Figure 3.17.

²⁹Pure Technologies Ltd., 705 11th Avenue SW, Calgary, AB, Canada T2R 0E3 (<http://www.soundprint.com/>)



(a) Tendon Instrumentation Layout (Typical)



(b) Strand Instrumentation Layout (Typical)



(c) Tensmeg End Block and Wire Strain Gage

Figure 3.15 Tendon Strain Instrumentation Arrangement

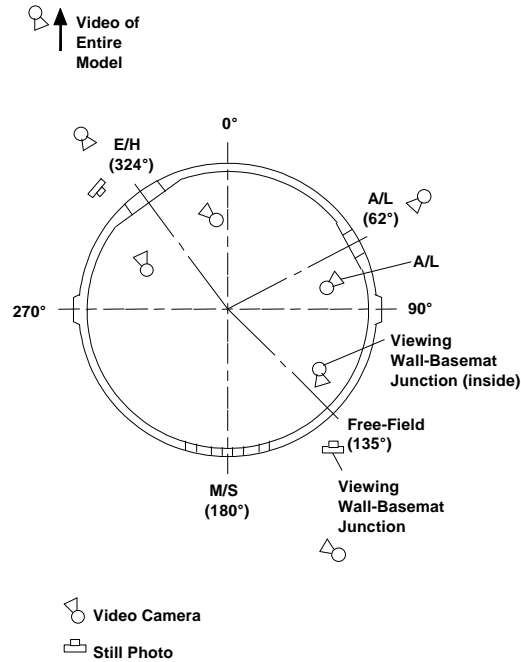


Figure 3.16 Video and Camera Layout

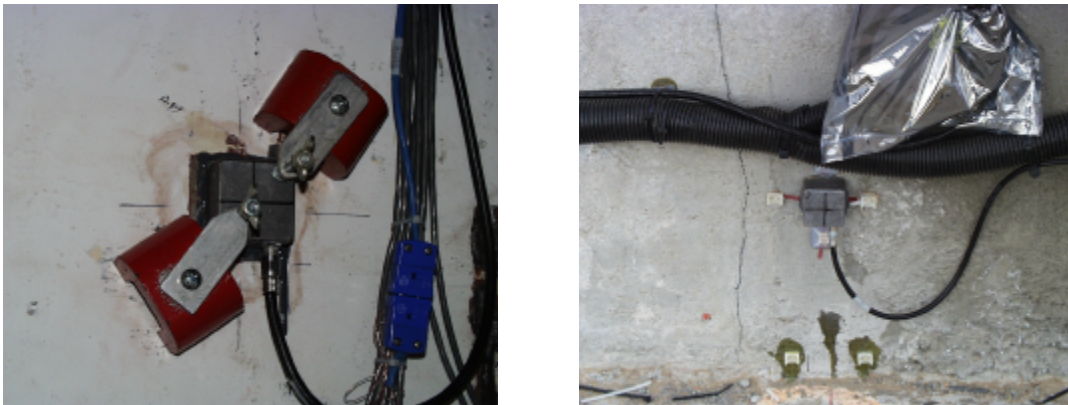


Figure 3.17 Interior and Exterior Acoustic Sensor (clamps during installation only)

3.3 Instrument Installation

3.3.1 Instrument Locations

The final list of gages installed on the PCCV model is provided in Appendix D. This list identifies every gage installed on the model and any gages that were damaged during construction or testing. The format of the tables in Appendix D is given in Table 3.14.

Because of the large number of transducers and the DAS requirement to have a unique address or label, a Gage ID scheme was developed to provide basic information about the type of gage and its orientation and location while providing each gage with a unique identity for subsequent reference and data management. A set of gage type abbreviations were developed to form the first part of the name. These abbreviations are listed in Table 3.15.

Table 3.14 Instrumentation List Format

Column	Description
1	Gage ID (name) AAA-B-CC-DD AAA Type abbreviation (Table 3.15) B Orientation (R-radial, M-meridional, C-circumferential) CC General location designator (azimuth <i>letter</i> / elevation <i>number</i> from Figure 3.1) DD Sequential numbering (for each similar type and location)
2	Azimuth
3	Vertical Elevation
4	Radial Distance (from centerline of containment)
5	Transducer Designation (for procurement)
6	Location Drawing No. (Appendix E)
7	Details Drawing No.
8	Basic Mark Number (construction designation)
9	Modified Mark Number (instrumented designation)
10	Comments
11	Calibration (pre- and post-calibration status)

Table 3.15 Gage Type Nomenclature

Type Abbreviation	Description
RS	rebar strain, single element gage
GB	gage bar, multiple elements
CE	concrete strain, embedded fiber optic gage
LSI	liner strain, single element gage, inside surface
LRI	liner strain, rosette gage, inside surface
LSO	liner strain, single element gage, outside surface
LRO	liner strain, rosette gage, outside surface
LSA	liner strain, single gage, on anchor
LRA	liner strain, rosette gage, on anchor
LSS	liner strain, single gage, on stiffener
LRS	liner strain, rosette gage, on stiffener
DL	linear variable differential transformer displacement transducer
DT	Temposonics linear displacement transducer
CP	cable potentiometer displacement transducer
IT	inclinometer displacement transducer
TC	thermocouple, embedded in concrete basemat, type K
TW	thermocouple, embedded in cylinder wall, type T
TI	thermocouple, inside liner surface, type T
RT	resistance temperature detector
PG	pressure gauge
TL	tendon load cells
TT	tendon strain, Tensmeg
TF	tendon strain, foil

The location designation is based on the cardinal azimuth and elevation lines shown in Figure 3.1. For example, gage DT-R-Z6-01 is easily recognized as a Temposonics displacement transducer (DT) measuring the radial displacement ® at Azimuth 135 degrees (Z), Elevation 6200 (6). Since there is only one transducer at this location, it is by default number one (01). These gage IDs are used in reporting and discussing the test data in Chapter 5.

The nominal location of the gages are shown in Figures 3.18 to 3.23. A set of detailed instrumentation drawings is provided in Appendix E. The total number of each type of instrument installed on the PCCV Model is shown in Table 3.16.

Table 3.16 PCCV Instrument Summary

Instrument Type		Number of Gages
Strain	Liner	559
	Rebar	391
	Tendons (Tensmeg)	37
	Tendons (wire)	156
	Concrete	94
Displacements		101
Load Cells (1/3 of Tendons)		68
Temperature and Pressure		100
Acoustic		54
Total		1560

3.3.2 Quality Assurance and Control

The PCCV Instrumentation QA Task Plan [33] describes and documents the SNL process for installing instrumentation on the PCCV model. The Task Plan addresses transducer calibration, installation, and wiring to the terminal boards, instrument check-out procedures, and compliance records. In addition, personnel roles, responsibilities, and training appropriate to accomplish the PCCV instrumentation installation task are described. As-installed measurements were made and the exact location of each instrument was recorded as a permanent quality record for the experiment. The tasks, objectives, and responsible project team member described in the Task Plan are summarized in Table 3.17.

Table 3.17 PCCV Instrumentation Procedures Summary

Tasks	Objectives	Responsible Member
1. Provide Instrumentation Drawings for: Transducer Location Deliver As-Built Drawings	Assure proper sensor location to match predicted deformation analysis Assure correct channel assignment to terminal board Assure integrity of instrumentation installation	Instrumentation Engineer
2. Instrument the PCCV Model	Monitor PCCV deformation behavior	Instrumentation Leader
3. Develop/Issue Environmental Safety and Health (ES&H) Operating Procedure	Control hazardous material/processes	Test Leader
4. Install Terminal Boards/Sensor Wiring	Maintain channel assignments	Instrumentation Leader
5. Check Instrument Functionality	Assure sensor integrity	Instrumentation Leader
6. Obtain Required Transducer Calibrations	Assure data accuracy/acceptance	Instrumentation Engineer
7. Complete All Documentation	Assure integrity/traceability of acquired data	Instrumentation Engineer

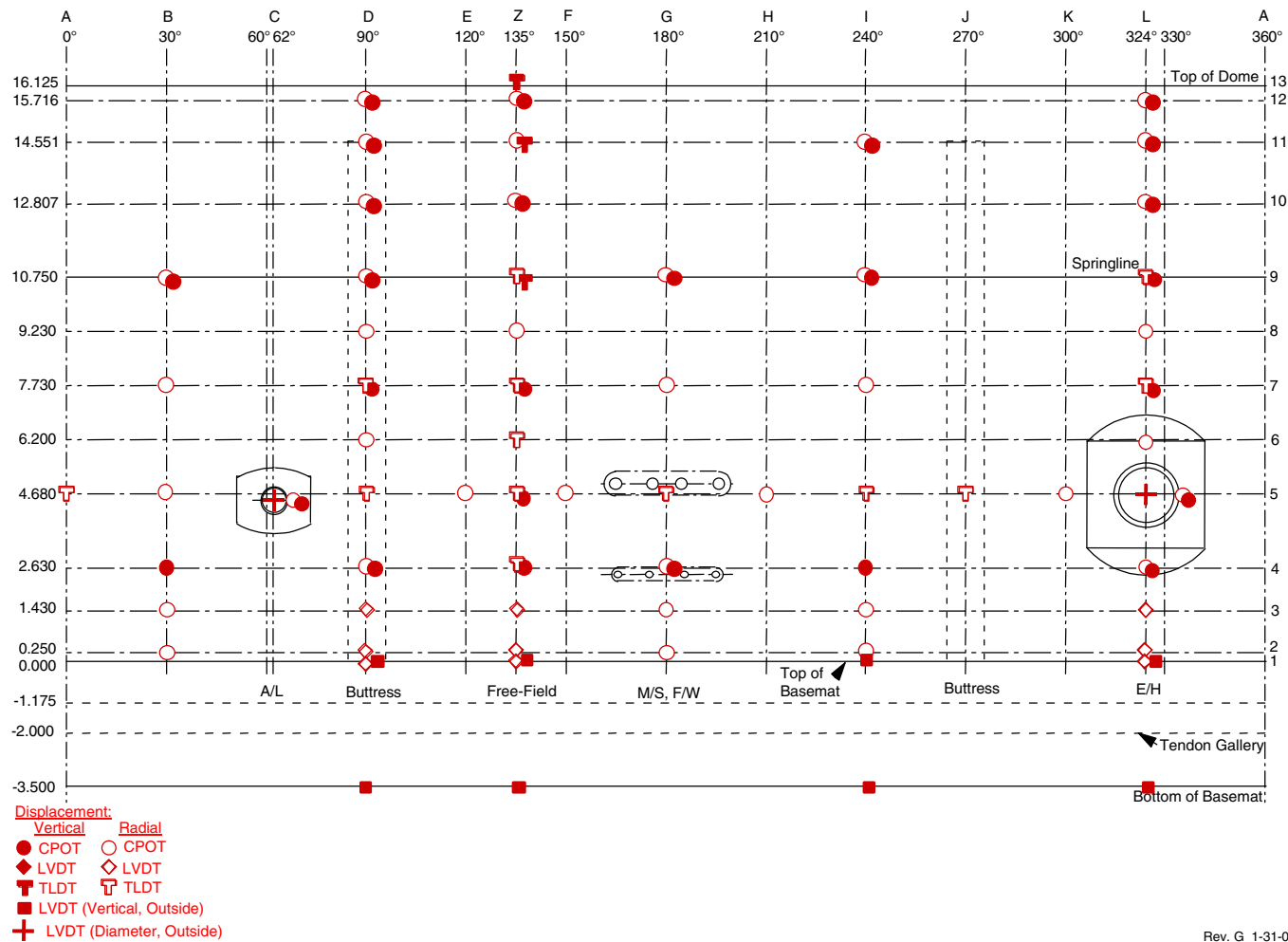


Figure 3.18. Displacement Instrumentation Locations

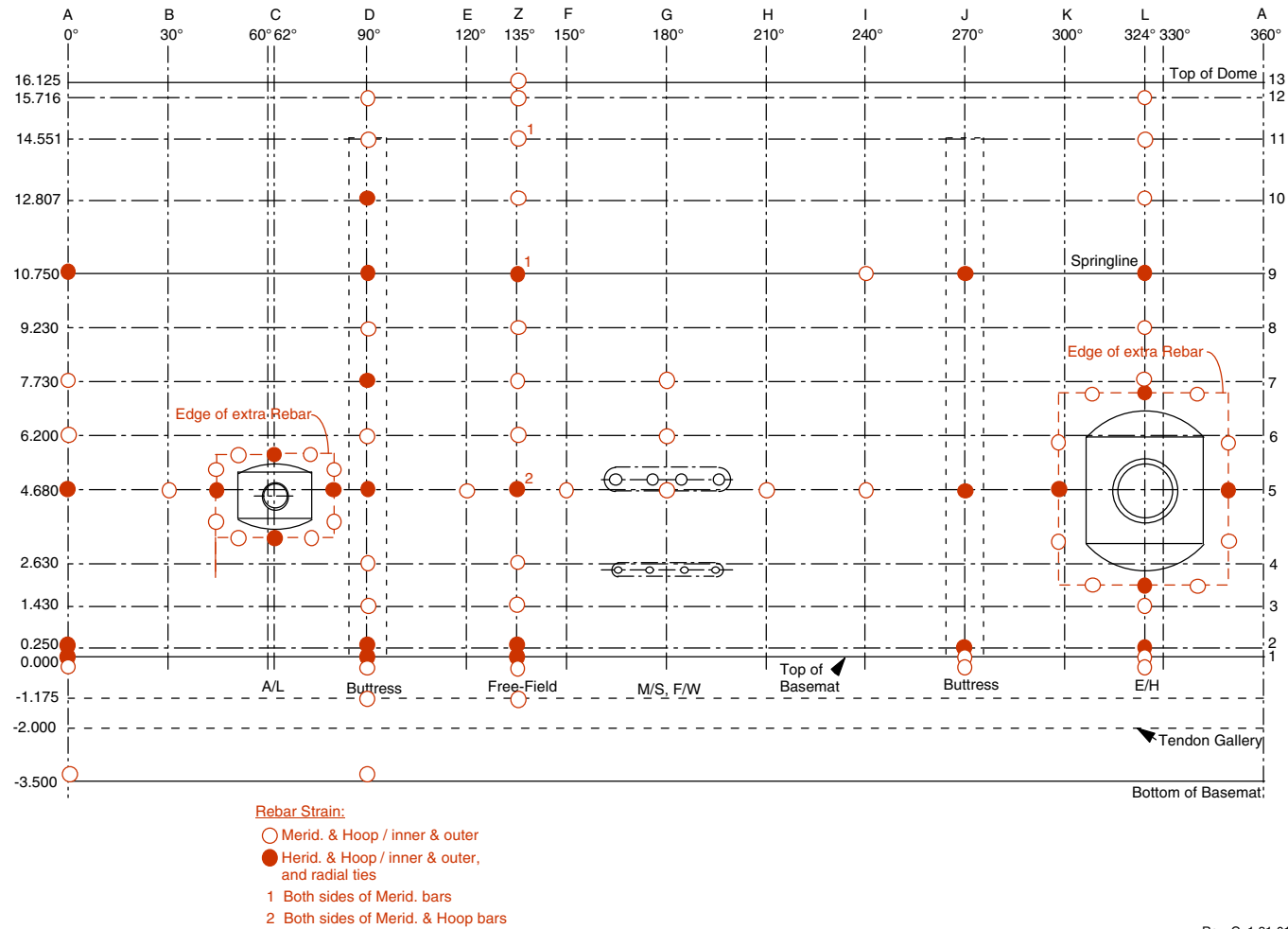


Figure 3.19. Rebar Instrumentation Locations

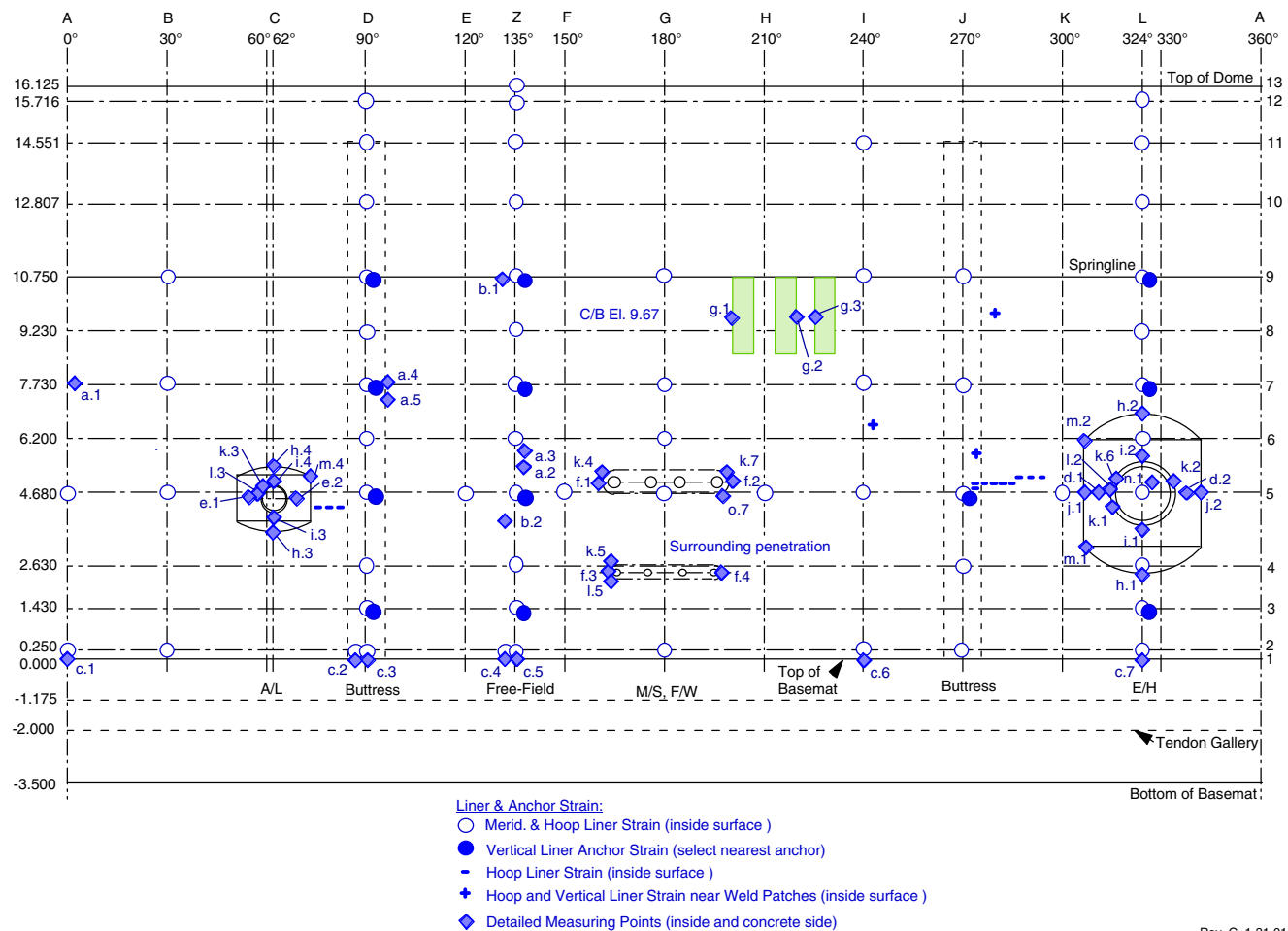


Figure 3.20. Liner and Liner Anchor Instrumentation Locations

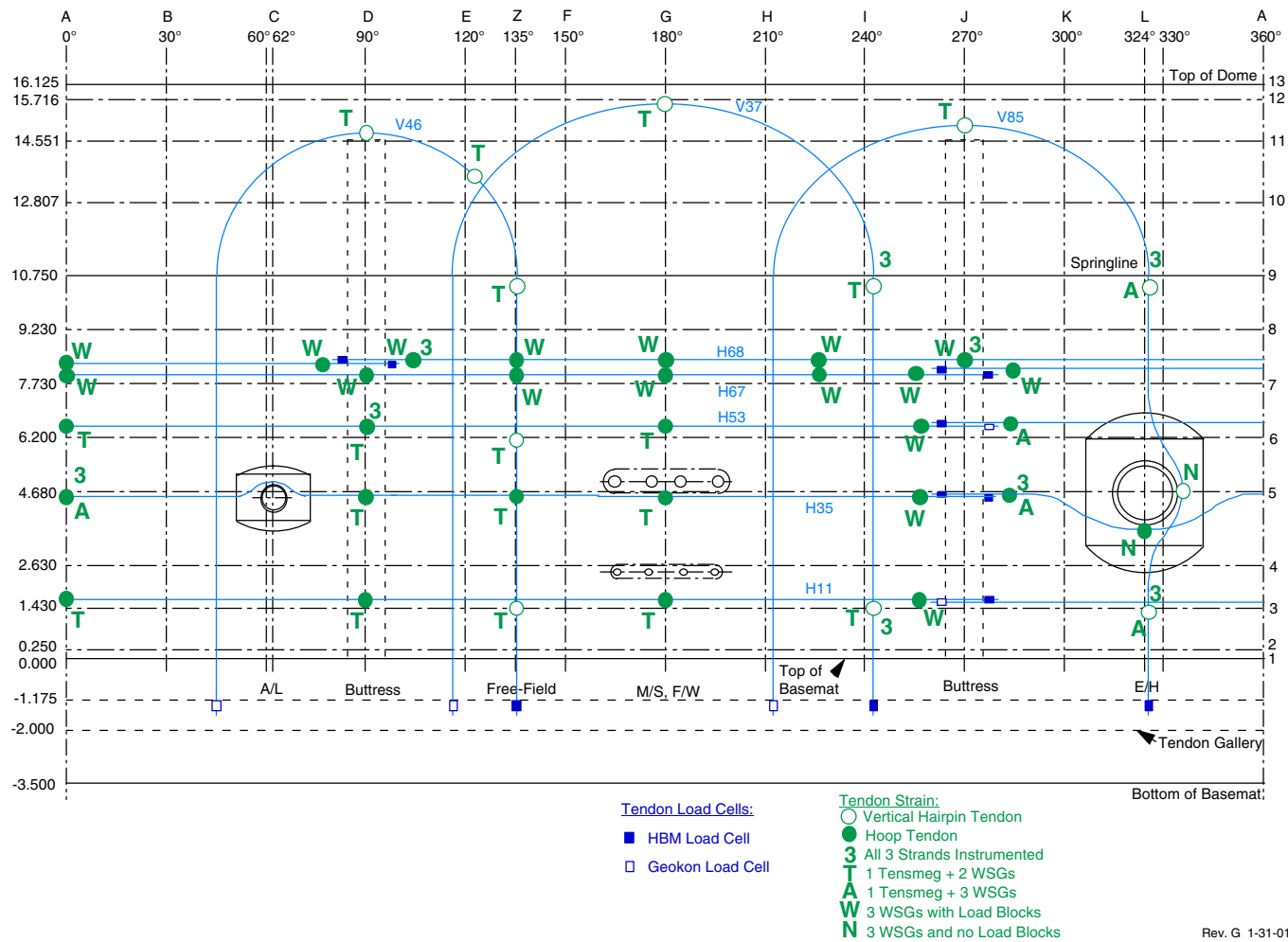


Figure 3.21. Tendon Instrumentation Locations

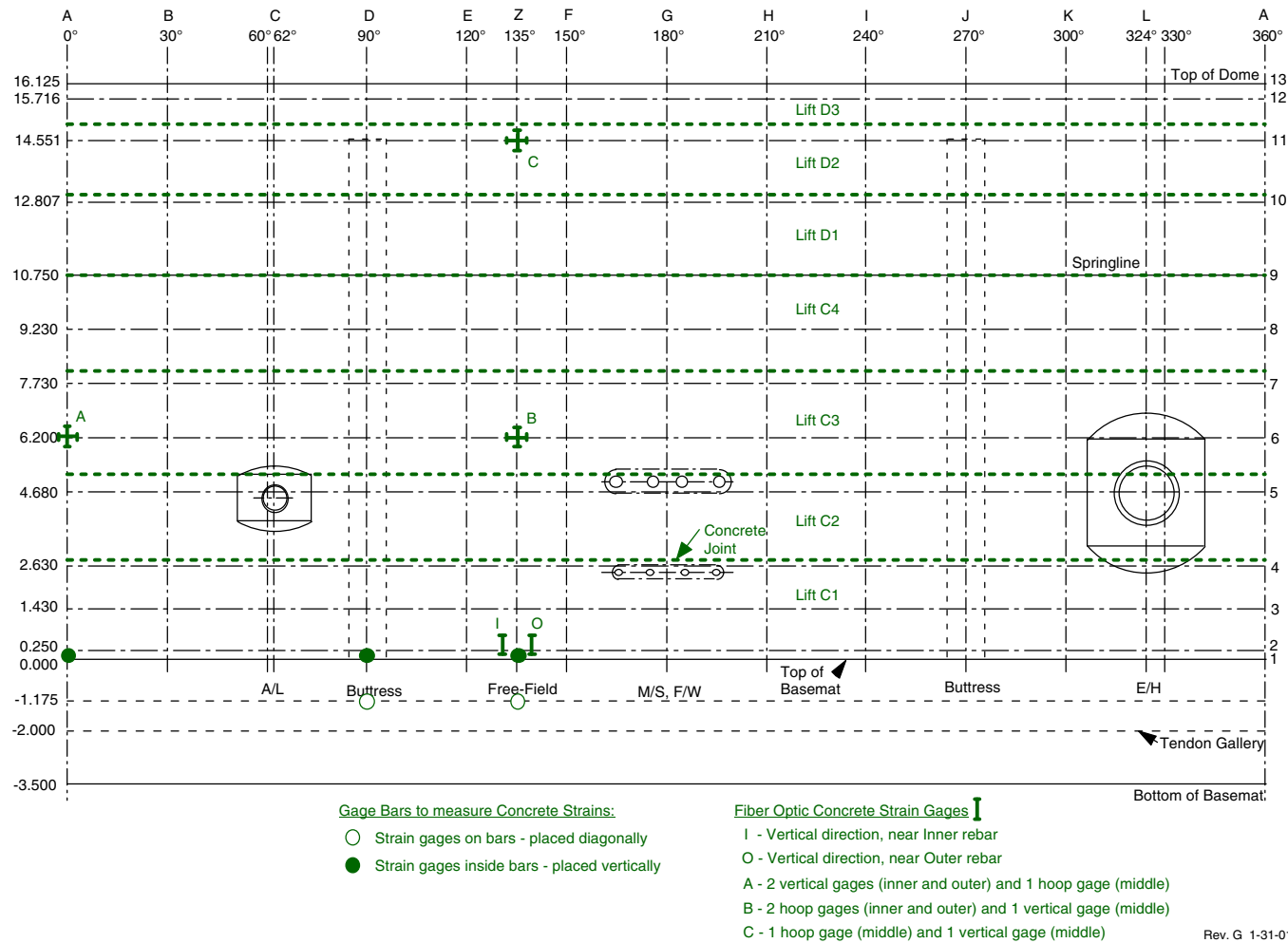
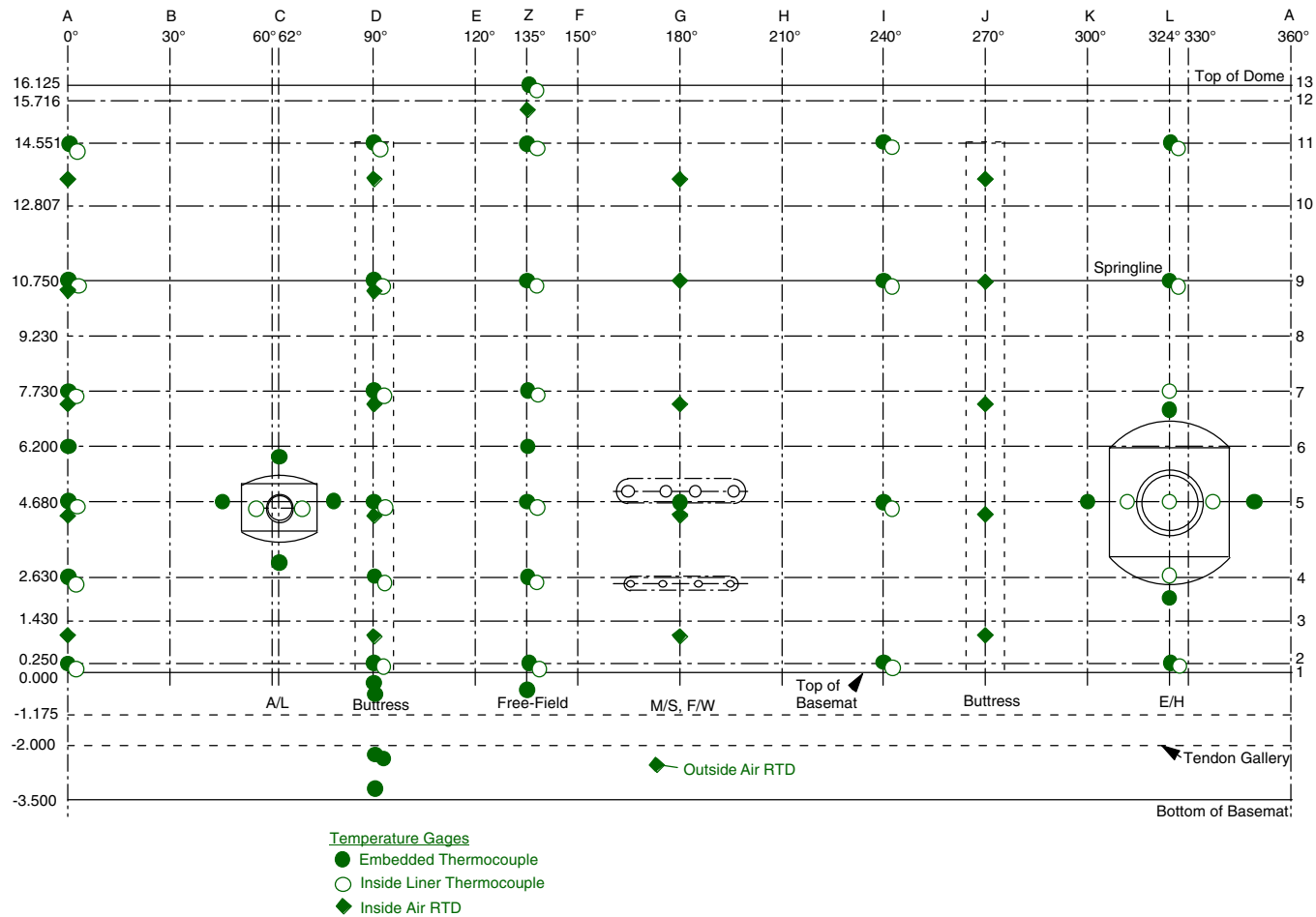


Figure 3.22. Concrete Instrumentation Locations



Rev. G 1-31-01

Figure 3.23. Temperature Instrumentation Locations

4. DATA ACQUISITION

The DAS comprises integrated hardware and software components to acquire, interpret, record, display, correct, and archive data from the suite of transducers installed on the PCCV model. The basic data acquisition requirements were specified by NUPEC and, after discussions with the NRC and SNL, a detailed DAS Plan [29] was developed and approved. The DAS Plan specified the objectives, performance requirements, and basic architecture of the DAS. A DAS QA Task Plan [30] specified and documented the detailed procedures that guaranteed the DAS satisfied the operational specifications. The key elements of the DAS Plan and QA Task Plan are summarized in this chapter.

4.1 Objectives

The primary program objectives the DAS must satisfy included the following.

1. The DAS must be fully functional, verified, and approved at the time of model prestressing. This means that the output signal from all operational sensors can be read, that the source and location of all output signals was known with certainty, and that the output signal can be converted to accurate engineering measurement units within the tolerances specified in the Instrumentation Plan.
2. During prestressing operation, the DAS must:
 - a. be capable of monitoring all instruments, including all strain gages, displacement transducers, and T/Cs, except those gages in the uncompleted portion of the basemat,
 - b. provide a real-time display of selected sensor output (especially load cells and tendon gages) in engineering units to monitor prestressing operations, and
 - c. retain a record of final data after prestressing as initial conditions for subsequent readings.
3. The DAS must be capable of periodic data acquisition between prestressing and testing phases.
4. During low and high pressure testing, the DAS must be capable of scanning all active sensor data and storing dynamic data and data of record (DoR) data. The DAS must be capable of providing real-time displays of any sensor output (uncorrected) in engineering units and facilitating comparison with pretest predictions to guide the conduct of the test. The DAS may also be integrated with other systems controlling and monitoring the test, such as the pressurization system, acoustic monitoring system, visual monitoring system (video and still photography), lighting systems, and audio systems.
5. The DAS must record the data in a manner that facilitates timely and accurate correction of the raw data after the test is complete.

4.2 Hardware Description

The PCCV hardware configuration for both the instrumentation system and the DAS is shown in Figure 4.1. A more detailed schematic is provided in Appendix F. This schematic not only graphically “maps” all component classifications important to the data acquisition effort, but also provides details on where documentation pertaining to each component of the system may be found. This documentation includes installation, wiring, and quality control information. For the PCCV tests, there were approximately 1500 instruments mounted on the model. Each of these gages had lead wires extending from the gage itself to a terminal board. From the terminal board, the gage’s signal was carried to a specific channel on a card located in a mainframe. The channel location defined the General Purpose Interface Bus (GPIB) address for that gage. This address was used for acquisition, tracking, and recording of the gage’s data. There were 13 mainframes located in a DAS trailer. From the mainframes, a fiber optic cable carried the signals from all of the gages to the data acquisition computer located in the control room (9950). The hardware from the gages to the front side of the terminal boards made up the instrumentation system. The remaining hardware (shown on the right of Figure 4.1) made up the DAS. The data acquisition computers stored the data on redundant media and also made the data available to the display computer. The display computer allowed test personnel to track the behavior of the gages in real time. The stored data were protected and used for posttest data analysis.

The primary hardware component involved in the data gathering was the Hewlett Packard 75000 Series B system, which included the HP1302A VXI Mainframe and its associated 5 ½ digit multimeter (HP1326B). Analog signals from the instruments were sent to plug-in cards installed into the mainframe housing. An analog bus jumper connected the signals to the digital multimeter where the analog-to-digital (A-D) conversion occurred.

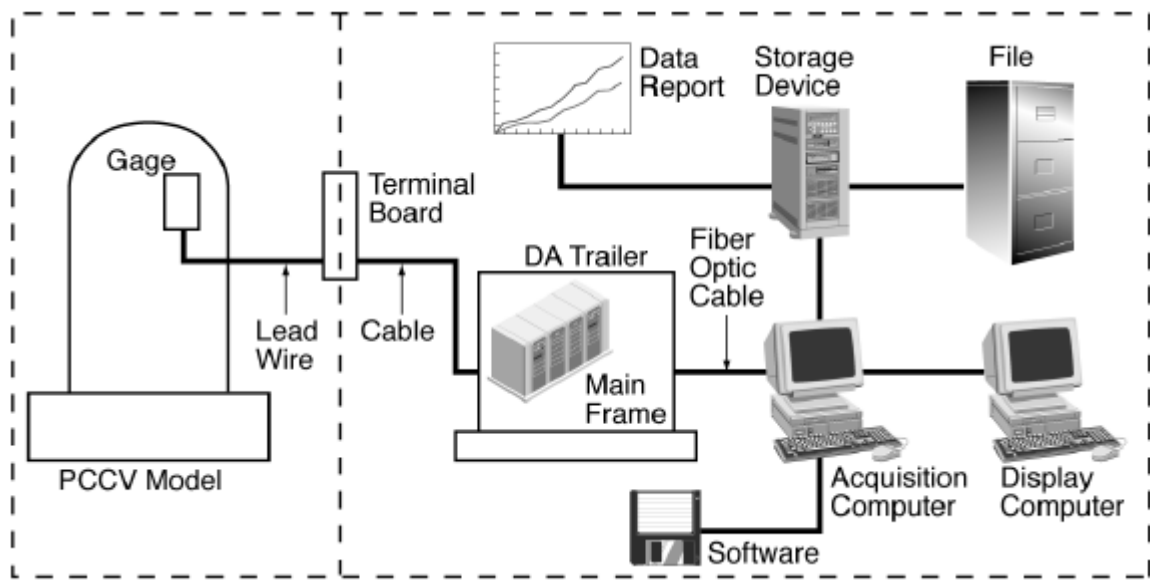


Figure 4.1 PCCV/DAS Hardware Configuration

Data were then stored in input/output (I/O) buffers dedicated to the multimeter, or in the RAM of the mainframe, for eventual transfer over a standard GPIB cable to the data acquisition computer. The mainframe was able to manage the channel switching and data transfer operations as well as respond to controller commands over the GPIB. In addition, the status of the data transfer operations was monitored.

The digital multimeter can be used as a stand-alone device through the VXI bus. However, for this test, it was connected through the analog bus jumper to a series of relay multiplexers. It measured and converted five types of input signals: DC voltage, RMS AC voltage, 2-wire resistance, 4-wire resistance, and electrically-based temperature sensing devices (T/Cs and RTDs).

The characteristics of the multiplexer cards varied based on the type of signal they carried. This experiment used three types of cards: 350 Ω and 120 Ω strain gage cards (Wheatstone quarter-bridge circuits, 8-channel capacity) and a 16-channel voltage card (i.e., non-bridged voltage producing device). To service the different types of instruments installed on the PCCV model, 137 350 Ω cards, 26 120 Ω cards, and 23 voltage cards were used. Two types of VXI mainframes were used. One accepted seven multiplexer cards, and the other type accepted 16 cards. There were no basic differences between these mainframes other than their card capacities. In order to accommodate the cards needed, 13 mainframes were utilized.

Strain gage multiplexer cards are designed to measure the voltage produced in a bridge circuit due to resistance changes in a strain gage. Consequently, these circuits require excitation voltage, which is provided by external power supplies. The strain gage multiplexer cards provide excitation and scale the output of the strain gages. The 1326B digital multimeter measures the voltage and converts the reading to strain units. Thus, the raw data received by the data acquisition computer is in strain units.

The data are held in the VXI bus buffer until the GPIB controller-in-charge (the data acquisition computers) commands a transfer. The mainframes were located in a data analysis trailer situated near the mudmat of the PCCV model and an opening to the Tendon Gallery tunnel, as well as the small penetrations that would feed all internal instrumentation cables (180 degrees). The location, near 180 degrees, was chosen as it allowed cable lengths to be as short as reasonable, thus preserving signal integrity. The data acquisition computers were located remotely at the 9950 site. Adapting the standard GPIB cable to a fiber-optic bundle minimized digital signal loss and degradation. This cable could be extended over long distances and eventually readapted to standard GPIB format for installation into GPIB cards on the DAS computer chassis.

From the perspective of the data acquisition computers, each mainframe/multimeter pair represents a single GPIB instrument. One GPIB card is capable of controlling seven GPIB instruments. For the PCCV experiment, two GPIB interface cards and two data acquisition computers were used, as more than eight GPIB instruments were needed.

The data acquisition software used for the PCCV test was designed as a general instrumentation monitoring system, with a single GPIB card and controlled by a single data acquisition computer. This implies that any computer running the acquisition software can scan any instrumentation suite with an accurate configuration file. Thus, each data acquisition computer scanned approximately half of the instruments on the model. Each data acquisition computer operated independently of the other. The display computer read data from both computers, one at a time.

The final major piece of hardware involved in the DAS was a display computer. This computer read the experimental data from the data acquisition computers upon demand and presented it in optional formats (plot form, array form, comparison form). The display computer provided the test conductor information to help make real-time decisions during the test.

The display computer had additional monitors allowing observers (located outside the test control room) to view the display.

Additionally, the DAS included two separate data storage devices (one connected to each data acquisition computer). These stored redundant copies of the data files to ensure data protection.

4.2.1 Hardware Specifications

Manuals and hardware specifications for each DAS component were included in the DAS Plan. All of the hardware chosen for the PCCV data acquisition effort was expected to meet requirements for the overall system operation.

The total time required for the actual acquisition of data from the VXI mainframes was governed by two primary factors: the switching and settling time of the on-board multiplexer and the aperture setting for each sampled channel. This statement assumes very short times for I/O from the controller to the multimeters. By far, the largest of these components is the aperture setting for a static DAS with unfiltered data signals. (The settling time for the mechanical relays in the PCCV's VXI mainframes is on the order of μ seconds.) For the PCCV tests, the aperture time was set to 16.5 ms, which ensures electrical filtering of common 60 Hz noise sources. Decreasing the aperture time allows for more rapid data acquisition, but significantly increases signal noise, particularly for unfiltered data. Signal degradation is further complicated by the moderate to long cable lengths, which are necessary in a test of this sort. Therefore, the default 16.5 ms aperture for each channel was used. This setting results in a maximum possible sampling frequency of 60 Hz. This value is decreased incrementally by the relay operation and I/O to the controller.

Scan time is defined as including: 1) the time required for the GPIB-based READ command to reach the mainframe from the control computer; 2) the time for the command module in the appropriate mainframes to receive the request for data and set the multiplexer for operation; 3) the time for multiplexer switching and the multimeter aperture delay for each configured channel; and 4) the time required to transfer all the data from the controller buffer back to the DAS computers. Thus, the scan time was larger than the product of the sampling frequency multiplied by the number of gages scanned, because of the time required to transfer the large controller buffer contents via the GPIB. Scan times were slightly different for the two DAS computers, with PCCV1 requiring approximately 50 seconds and PCCV2 requiring approximately 70 seconds.

Cycle time includes the scan time plus the time to store the data on the requested storage devices. The plan was to immediately generate two copies of the data, one on an internal hard disk and one on a removable disk. The storage required the largest amount of time by far. To shorten this as much as possible, the DAS software was written to facilitate this operation (i.e., separation of data display and data acquisition computers, up-front creation and preparation of data files, use of binary high-speed I/O data file formats rather than ASCII, termination of all unnecessary processing during data storage, etc.) and the data storage hardware was chosen to minimize disk seek time, transfer rate, and access time. Cycle time was approximately 120 seconds during system checkout, a setting that was used for the remainder of the testing.

4.2.2 Gage Wiring

The criteria to determine from which opening each gage's wires left the model was based solely on the route requiring the shortest length of wire. Thus, in the majority of cases, each gage's wires exited the model from the opening closest to the gage itself. Once the wires exited the model, they went to one of several terminal boards. The wires leaving the terminal boards entered the DAS trailer and connected to the data acquisition mainframe cards.

As stated, lead wires were as short as reasonable while still enabling the needed connections. All gage/wire combinations were reviewed, and corrections to gage factors were made posttest, as per Appendix G.

4.3 Software Description

The software used to control the DAS and display the acquired data during the experiment was developed using National Instrument's Labview™ software package.³⁰ The basic building block of Labview™ is called the virtual instrument (VI). A VI is similar to a subprogram or a module of code.

The data acquisition program is made up of VI trees, each representing a code module with a specific purpose. Graphics objects (such as knobs, dials, switches, etc.) visible on the screen during the data acquisition process can adjust instrument and data acquisition control parameters. Users may manipulate these objects with mouse commands.

The PCCV/DAS software is separated into three major groups: the primary program group used to gather and store the data during the experiment, a secondary program group to display the data during the experiment, and a utility group of programs used either before or after the test. These utility routines were designed to accomplish several tasks:

1. Form the configuration file and channel set-up,
2. Run DAS diagnostics and self-testing,
3. Perform channel and instrument integrity evaluations,
4. Evaluate noise, and
5. Present posttest data and storage to customer-defined formats.

4.3.1 Software Structure

The software was separated into two main groups of programs and a group of utility routines. (The term "group" refers to a series of linked subprograms existing as separate files.)

The data acquisition software (the primary group) was used to both gather and store the data during each of the tests (e.g., pre-stressing, SIT, final). This program group required input in the form of configuration files and was primarily responsible for data scanning, immediate redundant data storage, and fault limit detection and announcement.

The data display software (the secondary group) used the data gathered by the primary group. The display software did not access the stored data files on the acquisition computer, but rather global variables that were shared by the acquisition and display computers. In Labview™, global variables are used to easily access a set of values from any active VI. This allows values to be shared between Labview™ programs without requiring any other connections between the programs. This software group was responsible for displaying the experimental data on demand in the form requested by the user. Several different display modes were developed to meet the need of the PCCV experiments. These included a stability review, strain and displacement distributions, and a primary graphical user interface.

The utility group provided the necessary input channel configuration information to the main group software. There were many other secondary tasks the utility group performed as needs arose.

³⁰ National Instruments Corporation, Austin, TX (<http://amp.ni.com/niwc/labview/what.jsp?node=1381>)

4.3.2 Software Module Specifics

The three PCCV DAS software groups were divided into seven main modules. Modules 1, 2, and 4a composed the main acquisition group. Module 4b was the main display software group. Modules 3, 5, 6, and 7 composed the Utility Group. Figure 4.2 shows a schematic of the modules and how they were grouped.

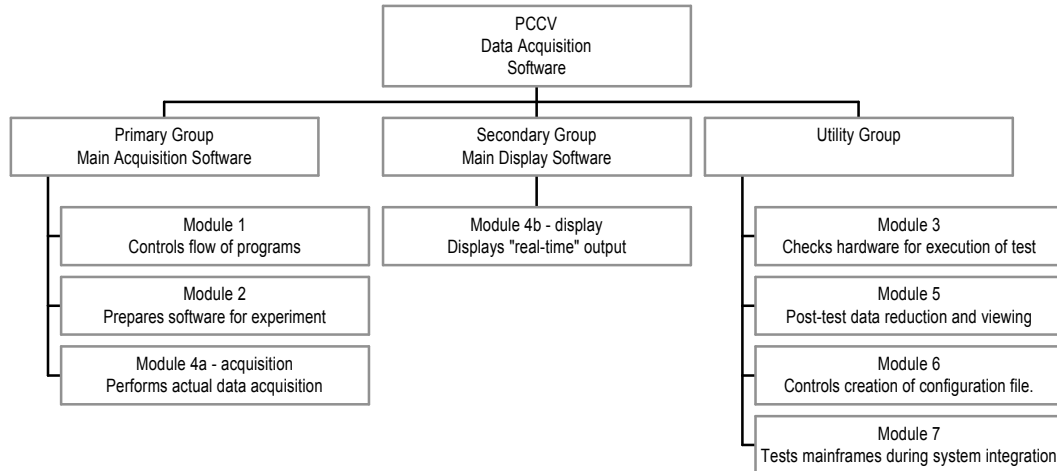


Figure 4.2. DAS Software Tree

The modules are listed below with a brief description of each.

- Module 1: Controls flow of program through Modules 2, 3, and 4a.
- Module 2: Prepares the software package to conduct a test including configuration information input to the acquisition software.
- Module 3: Prepares the hardware for executing the test. Includes checking the GPIB bus for the configured listeners and card layouts, and diagnosing the status (electronically) of the mainframes, digital multimeters (DMMs), and any other hardware.
- Module 4a: Performs the actual data acquisition, including readings during non-steady-state operation as well as the steady-state (DOR) scans. Includes writing raw data to disk as soon as possible. Provides continuous pressure information as well.
- Module 4b: Allows the user to select and display the desired real-time output.
- Module 5: Provides posttest data reduction and viewing.
- Module 6: Simplifies creating the configuration file and putting configuration information into the configuration file to minimize errors.
- Module 7: Facilitates mainframe testing during system integration. Easily configurable to rapidly indicate status of connected instruments.

4.3.3 Input/Output File Structure

4.3.3.1 File Structure Description

The two basic sets of I/O files necessary in the DAS software package were:

1. A configuration that file that provided the necessary input data to the DAS software, and
2. Data files into which the recorded data were placed.

Data File Structure

The design of the output data file structure allowed standard plotting software to select segments of data for plotting.

The output data file structure:

- Provided users with a clear map between the columns of numbers in a data file and the location and type of instrument originating the data,
- Used nomenclature for naming the files that provided the nature of the data contained and the types of instruments represented in the files,
- Generated an easily accessible set of files for archival purposes, anticipating future inquiries for analysis and presentation, and
- Facilitated rapid data correction and post-processing.

Two levels of folders below a “main” data folder were required to properly organize the data files. These levels are shown in Figure 4.3.

All data from this experiment was stored as *raw* data signals (i.e., the output of the A-D conversion step in the DAS process). Posttest data reduction converted the raw data into standard engineering units.

Table 4-1 lists the raw and reduced data units for the instruments in the PCCV experiment.

Note that the term “raw” in this table indicates the nature of the data signal after hardwired, “firmware” processing, which occurred automatically within the digital multimeter of the HP VXI Mainframe.

The data from some instruments was used to compensate or correct the raw data from other instruments. Details on this practice are found in Appendix G. Figure 4-4 illustrates the basic data flow diagram for the PCCV project.

4.4 Miscellaneous DAS Issues

4.4.1 Loss of Power

During the verification and validation testing, the results of losing electrical power to the DAS computers were determined. This determination involved actually shutting down electrical power to the computers while the DAS software was running. Several iterations of this were done, each at a different point in the acquisition process. It was necessary that data be maintained in the event of a power outage.

4.4.2 Integration of DAS with Other Systems

In general, the DAS was independent of all other systems involved in the PCCV experiments. There were two exceptions: still camera operation and the activation of redundant interior model lights. It was possible from the main data acquisition screen to operate the still cameras positioned throughout the PCCV model. Similarly, the interior model lighting was controlled from the main data acquisition screen. It was possible to turn the redundant lights on or off from the DAS computer.

The Soundprint acoustic monitoring system and the SOFO fiber-optic gages were equipped with their own independent DASs, also located in the data acquisition trailer. The only interface between these systems and the main DAS was manual synchronization of clock time. This provided the correlation between gage output and pressure subsequently used to analyze the test data.

Table 4.1. Description of Raw and Reduced Data for the PCCV Test

Instrument Type	Raw Data Units	Reduced Data Units
Strain gage (includes Tensmegs gages)	strain or microstrain (depending on gage factor format)	Strain
Cable-type displacement transducer	DC volts	Displacement (mm)
LVDT	DC volts	Displacement (mm)
Temposonic	DC volts	Displacement (mm)
Inclinometer-type displacement transducer	DC volts	Tilt angle (degrees)
Thermocouple	temperature (°C)	Same as raw
RTD	temperature (°C)	Same as raw
Pressure gage	DC volts	Pressure (MPa)
Load cells	DC volts	Load (Newtons)
Power supplies	DC volts	Same as raw (data used to reduce instrument voltages to CPOT distances)

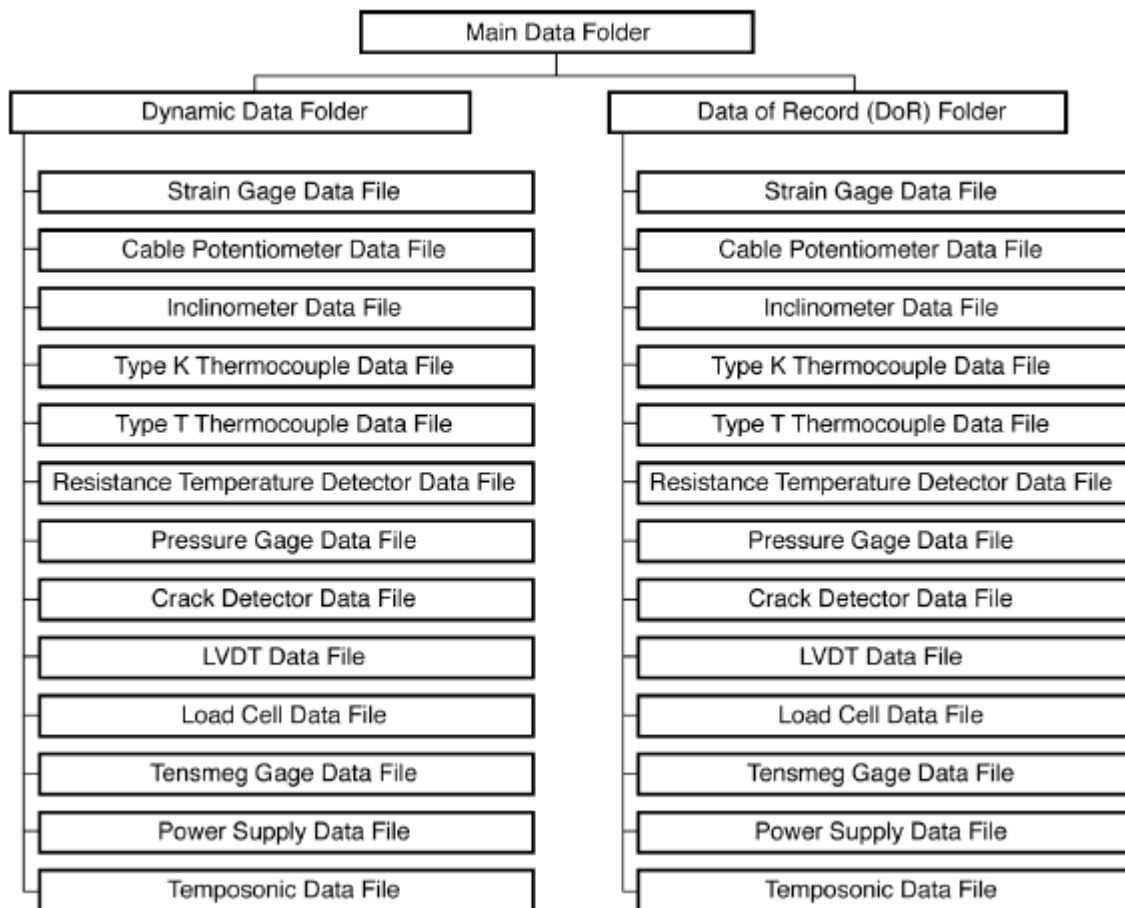


Figure 4.3 Top-Down Data File Folder Structure

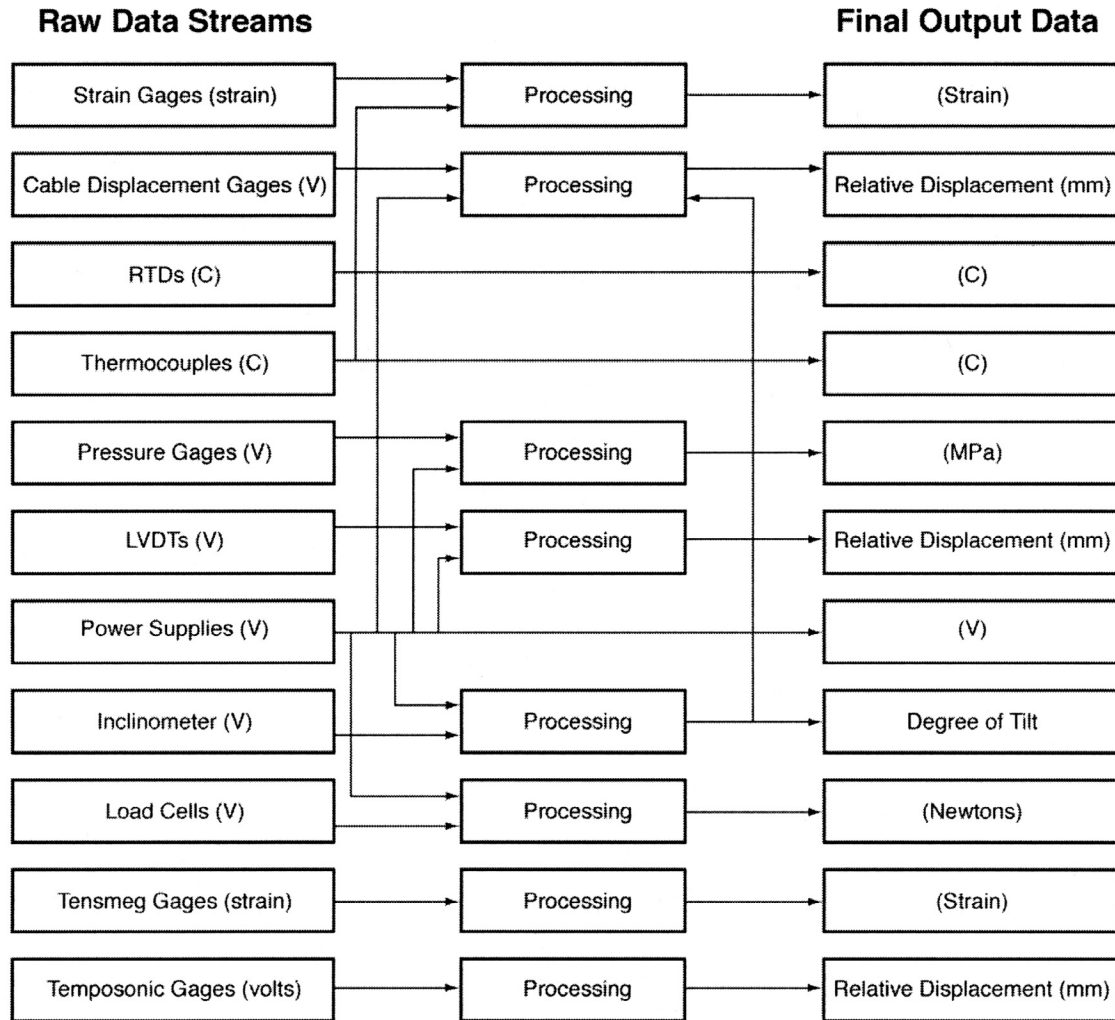


Figure 4.4 Basic PCCV Data Flow Diagram

5. TESTING

5.1 Test Planning

The basic objectives of the PCCV test were specified by NUPEC in the Master Project Plan [34]. The stated objective of this plan was to... “investigate the ultimate behavior of PCCV under pressure beyond the design basis accident and to prove the pressure retaining capacity of PCCV.” NUPEC originally specified a series of five tests, illustrated in Figure 5.1: 1) trial pressurization to 0.4 kg_f/cm² (5.7 psig or 0.1 P_d), 2) structural integrity and integrated leak rate tests to 4.5 and 3.6 kg_f/cm² (64.1 and 51.2 psig or 1.125 and 0.9 P_d), respectively, 3) two design pressure tests to 4.0 kg_f/cm² (57 psig or 1.0 P_d), and 4) a Limit State Test (LST) terminating with excessive leakage or structural failure.

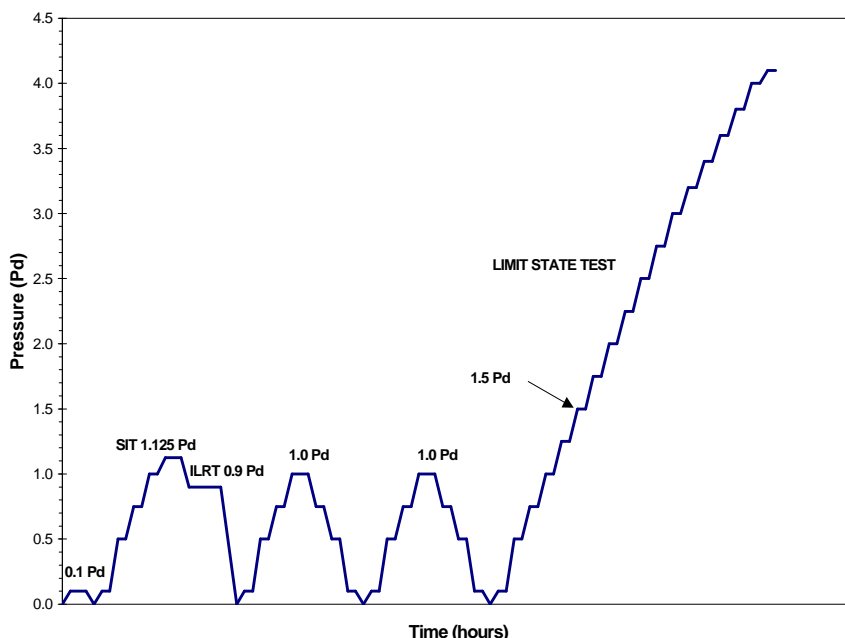


Figure 5.1 Original Pressurization and Depressurization Sequence [34]

After extensive discussions between NUPEC, the NRC and SNL, a detailed Test Plan [35] was developed by SNL to describe the conduct of the PCCV model’s pressurization tests. Additional procedures that addressed the safe conduct of the tests were defined in the Operating Procedure [36]. The Test Plan includes:

- procedures to be conducted prior to tests to assure that all systems are ready;
- a list of test personnel required to conduct the tests and an outline of functions and checklists assigned to each person;
- procedures to be followed during the tests, including the general test philosophy;
- procedures to be conducted after pressure tests are completed.

Detailed checklists were prepared to ensure that all test operations were conducted as planned and completed in the appropriate sequence. Detailed procedural logs, stored in the project files, were generated to document the conduct of each test. A summary of the test plan is included in this chapter.

A final series of three tests were agreed upon. These tests are defined as follows and are illustrated in Figure 5.2.

1. A leak check and System Functionality Test (SFT) at 0.5 P_d (2.0 kg_f/cm² or 28.4 psig)

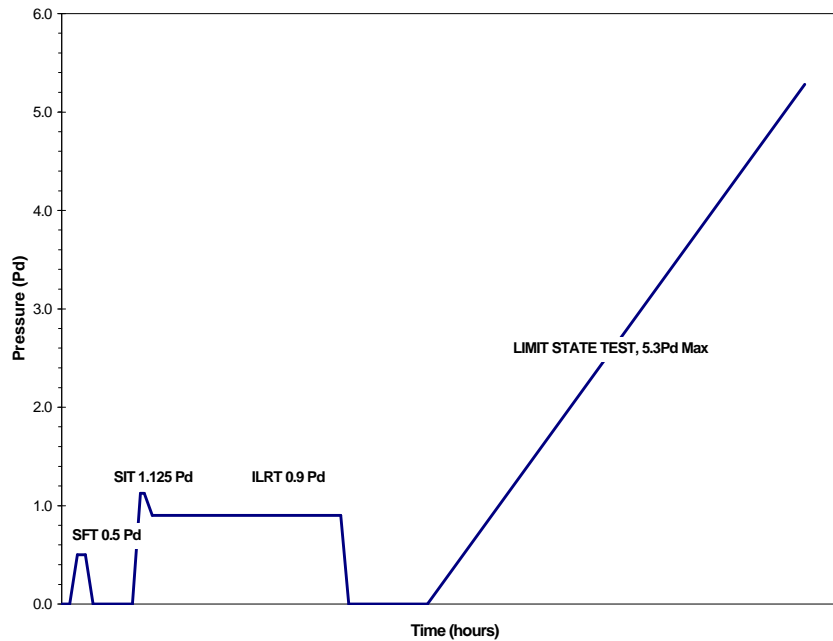


Figure 5.2 Final Pressurization Plan

2. A Structural Integrity Test (SIT) at 1.125 P_d followed by an Integrated Leak Rate Test (ILRT) at 0.9 P_d
3. An Limit State Test (LST) to the static pressure capacity of the PCCV model (or the pressurization system, whichever comes first)

A fourth test was added to the test program after the conclusion of the LST. After careful evaluation of the LST results, NUPEC, the NRC, SNL, and their technical advisors concluded that not all of the program's objectives were met after the LST. SNL was tasked with designing and conducting a test that would allow the PCCV model to be pressurized beyond the level reached during the LST in an attempt to observe greater inelastic response of the model and, hopefully, generate a structural failure mode. This Structural Failure Mode Test (SFMT) is described in Section 5.2.4.

5.1.1 Pressurization System Design and Operation

The pressurization system for the PCCV model test consisted of a pressure source, a valve gallery (consisting of several valves, a flow meter, and several sensors) used to control the flow of nitrogen, a programmable logic controller (PLC), control computer, and high pressure piping which interconnects all the components. A schematic of the pressurization system is shown in Figure 5.3

For the SFT, SIT/ILRT, and SFMT, the pressure source consisted of a pressurized nitrogen tube trailer. The trailer was located adjacent to the PCCV model, next to the valve gallery with a short flexible hose connecting them. For the LST, the pressure source consisted of a truck with liquid nitrogen that was gasified and regulated to a constant pressure and temperature. This source was located more than 600 m (2000') away from the PCCV model for safety reasons, near Building 9950. The pressurized nitrogen gas was piped aboveground onto the CTTF site and into the valve gallery.

In addition to the temperature being controlled at the source location during the pressure testing, the gas was heated in the piping prior to entering the PCCV model. These heaters helped increase the temperature of the gas prior to entering the PCCV model. Several additional heaters were located inside the model to help maintain temperatures to within ± 5 degree C of the average ambient temperature ($\sim 15^\circ \text{C}$) outside the PCCV model.

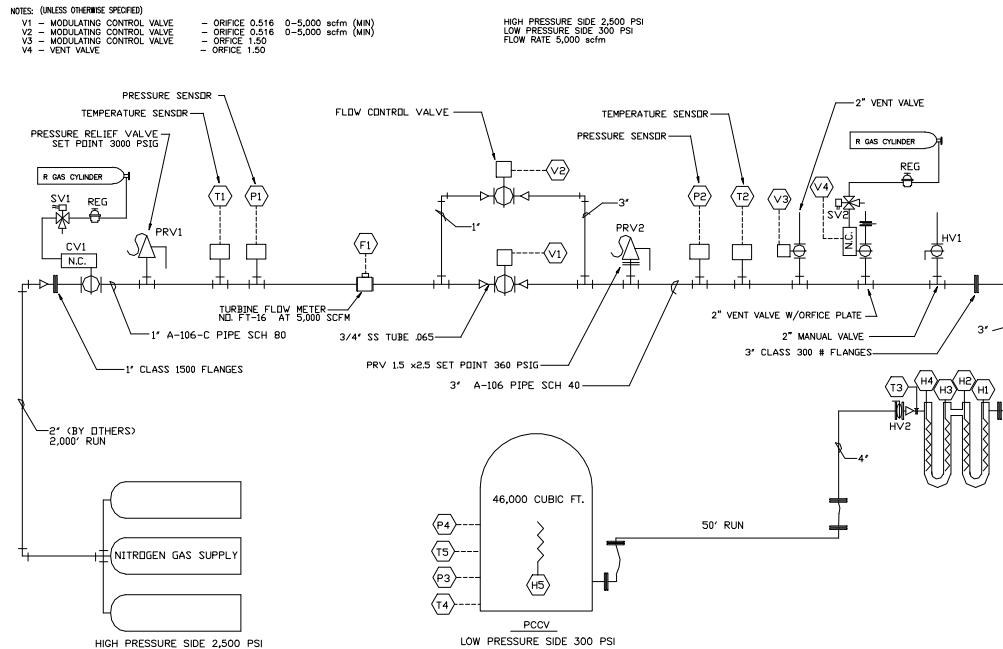


Figure 5.3 Pressurization System Schematic

The pressurization system was controlled by the PLC, which was located on the valve gallery skid next to the PCCV model. Communication with the PLC was performed by the control computer located in Building 9950. A more detailed description of the entire pressurization system is provided in the PCCV Pressurization System Data Package [37].

The entire pressurization system was designed and fabricated by an outside contractor (Rupert Plumbing and Heating Company, Inc., Albuquerque, NM). Initial testing of the system (primarily the valve gallery and heaters) was performed by the contractor prior to delivery to the CTTF site. After the system was installed at the site, the system was tested again before connecting to the PCCV model and conducting the pressure tests of the model.

The system tests performed by the contractor were approved by SNL personnel and encompassed all possible conditions the system might have to deal with during both the low- and high-pressure testing. These system tests checked all wiring, valve functionality, instrument functionality, and the control hardware and software.

After the system was installed and tested, the piping into the PCCV model was hooked up. All pressure lines connected to the valve gallery and the PCCV model were clean and dry before they were connected. Before the flex hose and flange were connected to the PCCV model, the line was “blown out” to clean it. The pressure source line up to the valve gallery was also blown out prior to the final hook-up.

5.2 Test Operations

The over-pressurization tests of the PCCV model were conducted at the CTTF-W, shown in Figure 1.3.

Building 9950, an ancillary facility for the test site (shown in the background in Figure 2.11), was the headquarters for conducting the pressure tests. It housed the control room and the observation room. During the test, key project members were inside the control room to execute the test plan and monitor the response of the model. Visitors observed the test progress and received periodic information on test status in the observation room.

The basic test team for each test is shown in Figure 5.4. The test team was only fully staffed for the LST and the SFMT. Test staffing for prestressing and the low-pressure tests is shown in Table 5.1.

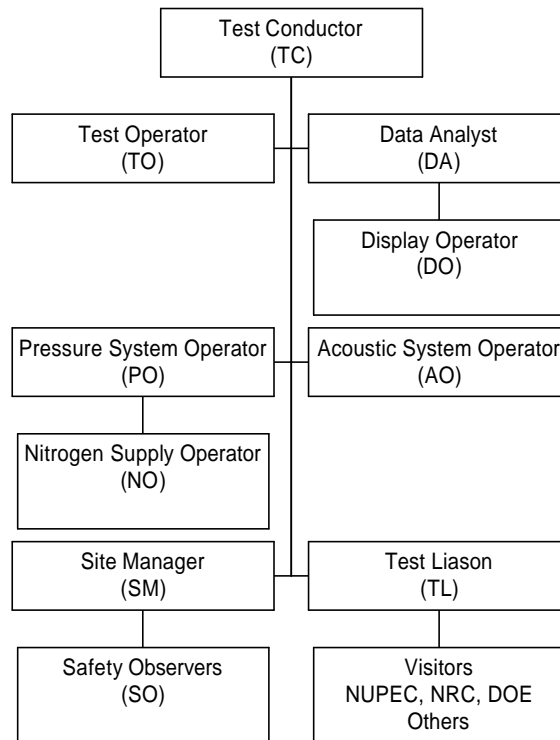


Figure 5.4 PCCV Test Organization

Table 5.1 PCCV Test Personnel Matrix

Position	Prestressing	SFT	SIT/ILRT	LST	SFMT
Test Conductor	X*	X	X	X	X
Test Operator	X	X	X	X	X
Data Analyst				X	X
Display Operator			X	X	X
Pressure System Operator		X	X	X	X
Acoustic System Operator	X	X	X	X	X
Site Manager	X	X	X	X	X
Safety Observers			X	X	X
Nitrogen Supply Operators		X	X	X	X
Test Liaison			X	X	
Visitors			X	X	X

*Part-time

5.2.1 System Functionality Test

The system functionality test and leak check was designed to verify the functionality of all the systems (instrumentation, data acquisition, pressurization, etc.) and the initial leak-tightness of the PCCV model (especially the sealing of the penetrations) prior to the performance of the pressure tests. Controlled leak tests were included to determine the accuracy of the leak detection instrumentation during the ILRT and LST.

The SFT was conducted beginning approximately 9:00 AM, July 18, 2000. The model was pressurized using nitrogen to 0.5 P_d (0.2 MPa or 28.4 psig) in three increments holding pressure for one hour or longer at each step, depending on the duration needed to perform all system functionality and leak checks. The model was then isolated and a leak rate check was performed by monitoring the model pressure and temperature for approximately 18 hours. After 18 hours, the calculated leak rate was 0.15% mass/day, which confirmed that the model was leak-tight. After the model leak rate check, the model was allowed to depressurize through a pair of orifice plates calibrated to leak rates of 1% and 10% mass/day to perform a calibration test on the leak rate measurement instrumentation. The calculated leak rates for each test were 0.87% and 7.86%, respectively, indicating that the leak rate instrumentation accurately detected a leak of 1% mass per day, which is the goal specified for the ILRT. The SFT was concluded on July 20 by opening the vent valve, allowing the model to depressurize. The SFT pressure time history and leak rates are shown in Figures 5.5 and 5.6.

5.2.2 Structural Integrity Test and Integrated Leak Rate Test

The SIT and the ILRT were conducted on September 12-14, 2000 as a combined test, with the ILRT following immediately after the SIT. The SIT/ILRT reproduced the preoperational tests conducted at the prototype plant and allows for a comparison of the model's elastic response characteristics and leak behavior with the prototype and pretest analyses. The pressure and average temperature time histories measured during the test are shown in Figure 5.7.

5.2.2.1 Structural Integrity Test

The SIT followed the procedures specified by Japanese Standard JEAC 4203-1994 [38] and the ASME Boiler and Pressure Vessel Code, Section III, Division 2, Article CC-6000, "Structural Integrity Test of Concrete Containments." [9]

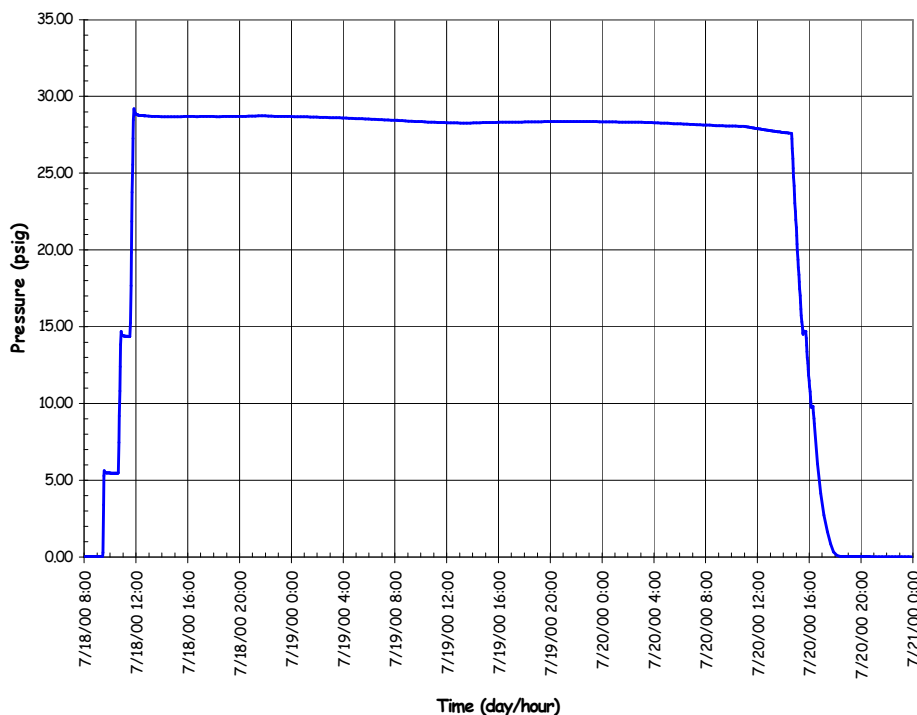


Figure 5.5 System Functionality Test Pressure Time History

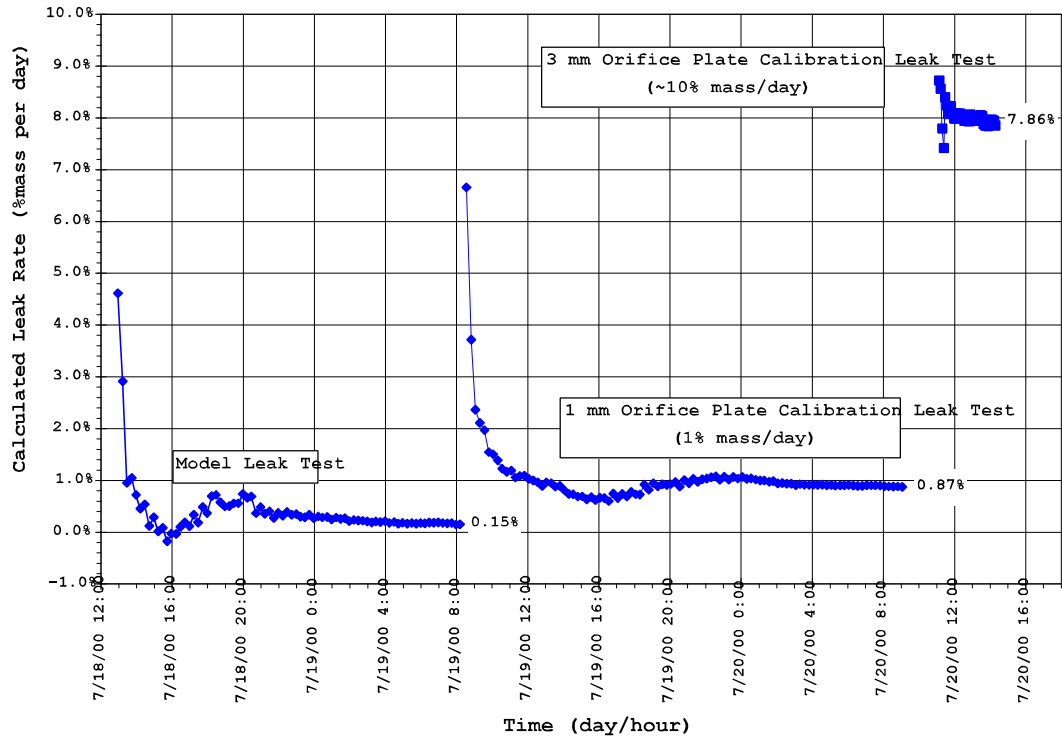


Figure 5.6 System Functionality Test Leak Rates

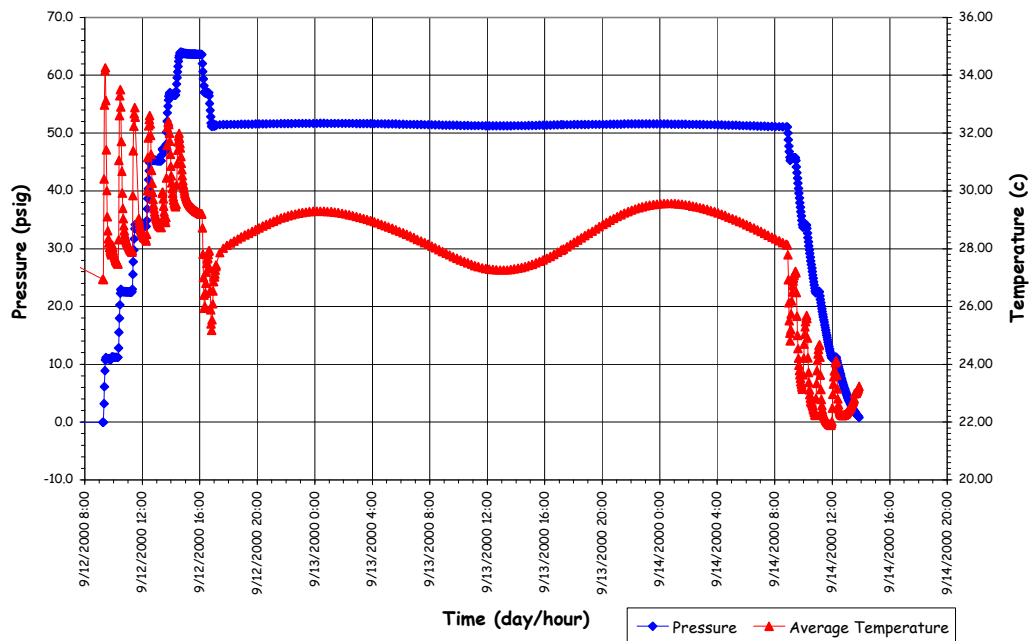


Figure 5.7 Structural Integrity and ILRT Pressure and Temperature Time Histories

Per MITI Code 501, Article 104 [39], the SIT test pressure, P_{SIT} , was $1.125 P_d$ (0.44 MPa or 64 psig). The PCCV model was pressurized in five equal increments at a rate of 20% of the test pressure per hour. (CC-6110 requires pressurization to $1.5 P_d$.) Per CC-6340, the response of the model was recorded at each pressure step (including $0 P_d$). Data of Record (DOR) was recorded when the following stability criterion was achieved:

$$\frac{Q_t - Q_{t-\Delta t}}{Q_{t-\Delta t}} \leq 0.02 \quad (5.1)$$

where Q_t and $Q_{t-\Delta t}$ are the data at the current and the previous time interval, respectively. The next pressure increment followed only after this criterion was satisfied or the total step duration reached one hour.

All active gages in or on the model were recorded at each step. The locations of the gages were selected to allow for direct comparison of the PCCV model response to the prototype at the SIT pressure in addition to the primary objective of monitoring the response of the model to ultimate pressure. Table 5.2 summarizes the ASME code requirements for SIT measurements.

Table 5.2 Summary of ASME B&PV Code SIT Instrumentation Requirements

	Measurements	Accuracy/Range	Pressure	Acceptance Criteria
Cracking	CC-6350 Cracks > 0.01"x 6" @ specified locations	CC-6225 >0.005" @ 0.003"	CC-6350 Before test @ P_{SIT} After test	CC-6420 Review by Designer
Strains	CC-6370: (Concrete Strains) @ Wall/Slab @ E/H @ Shell Discontinuities @ Restraints @ Steel/Concrete Trans.	CC-6224 $\pm 5\% \epsilon_{max}$ or $10 \mu\epsilon$ Gage Length > 4"	CC-6371 1. Baseline-Continuously for 24 hrs prior to test CC-6340 2. @ P_0 (Atmospheric press.) 3. During pressurization @ 20% P_{SIT} 40% P_{SIT} 60% P_{SIT} 80% P_{SIT} 100% P_{SIT} 4. @ PSIT + 1 hour 5. During depressurization @ 80% P_{SIT} 60% P_{SIT} 40% P_{SIT} 20% P_{SIT} @ P_0	CC-6410 (a) No rebar yielding (b) No visible liner or concrete damage (c-2) Residual displacements: @ Pts of Max. δ_R & δ_V : $\delta_{res} < 20\% \delta_{max} * @ P_{SIT} + 0.01"$ (*measured or predicted) Avg. δ_R @ each elevation: $\delta_{res} < 20\% \delta_{max} * @ P_{SIT} + 0.01"$
Displacements	CC-6361: δ_R @ 20% H & 0°, 90°, 180°, 270° δ_R @ 40% H & 0°, 90°, 180°, 270° δ_R @ 60% H & 0°, 90°, 180°, 270° δ_R @ 80% H & 0°, 90°, 180°, 270° δ_R @ 100% H & 0°, 90°, 180°, 270° δ_R @ E/H (12 points) δ_V @ Springline & 0°, 90°, 180°, 270° δ_V @ Apex δ_V @ two pts. Bet. Apex & Springline	CC-6223 $\pm 5\% \delta_{max}$ or 0.01"		
Temperature	CC-6380 Concrete @ Specified locations for Strain Correction Gas @ Interior & Exterior	CC-6226 $\pm 2^\circ F$ Range: Expected temp.		
Pressure		CC-6222: $\pm 2\% P_{SIT}$ Range < 4 P_{SIT}		

In general, the model instrumentation satisfied all of the requirements summarized in Table 5.2 with the following exceptions or modifications.

- The entire surface of the cylinder was mapped for cracks prior to the test; however, crack widths were not measured. No crack mapping was performed during the SIT. After the SIT, additional cracks within selected areas of the cylinder wall were identified but the widths were not measured. The crack map grid is shown in Figure 5.8
- Model strains were measured primarily using the gages mounted directly to the rebar and liner. Only a limited number of concrete strains were measured directly.
- Displacements were measured at all specified locations with the exception of the points around the largest penetration (i.e. the E/H)

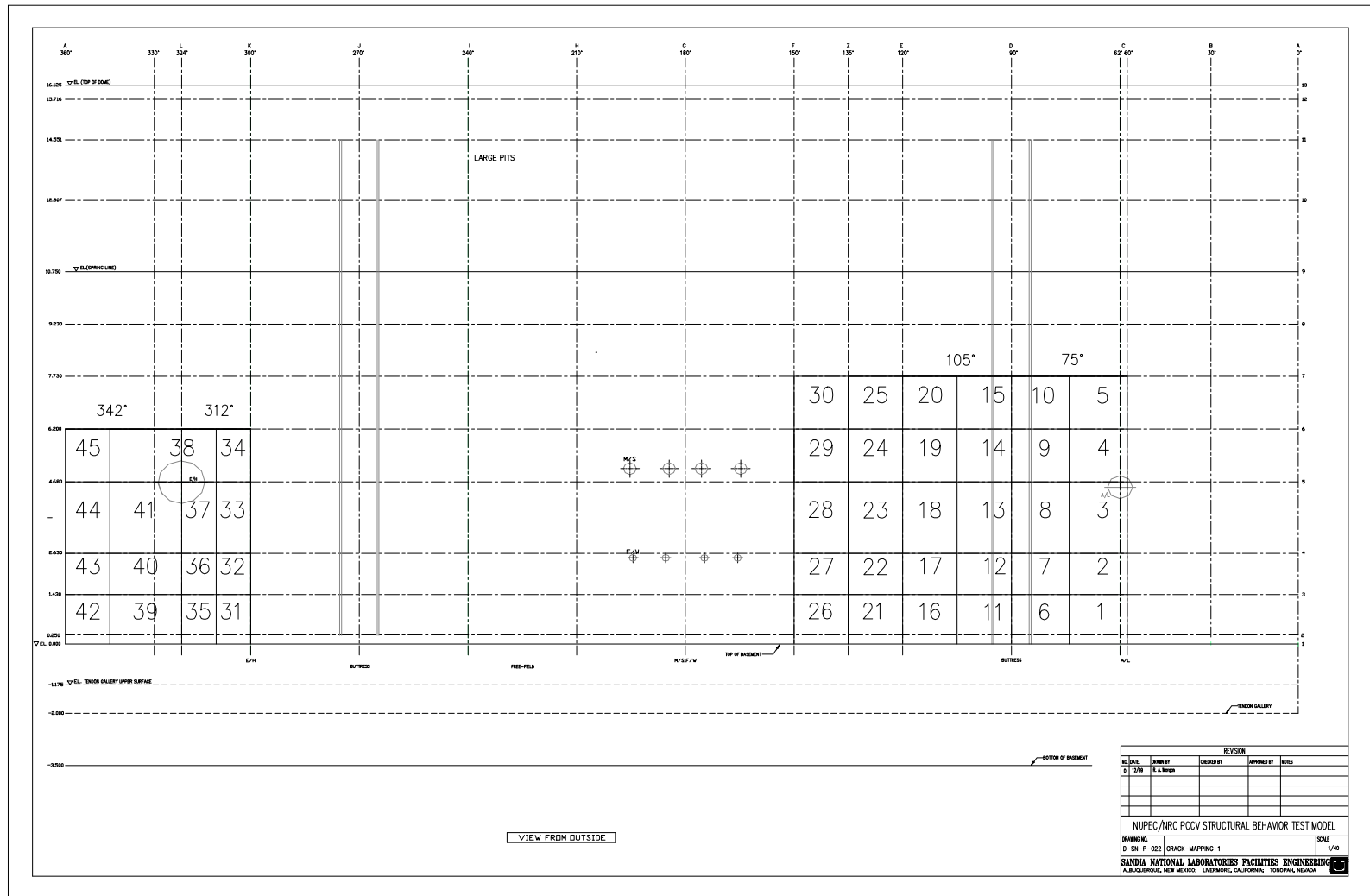


Figure 5.8 Concrete Crack Map Grid

After the SIT pressure was maintained for the required minimum of one hour per CC-6320, the PCCV model was depressurized to the ILRT pressure. First, the model was depressurized to Pd, for comparison with the pressurization phase, before depressurizing to the ILRT pressure (0.9Pd).

The temperature inside the model was specified to be maintained at approximately 25 °C (77 °F) during the test with a maximum range of 10 °C to 38 °C (50 °F to 100 °F). The average temperature during the SIT, recorded by the RTDs, was closer to 30 °C (86 °F). The ambient air temperature outside the model was measured near the base of the model.

5.2.2.2 Integrated Leak Rate Test

The ILRT requirements for Japanese containments are specified in JEAC 4203-1994 [38]. The ILRT requirements for U.S. containment vessels are specified in 10CFR50, Appendix J “Primary Reactor Containment Leakage Testing for Water-Cooled Power Reactors,” [40] which references the tests procedures in American National Standards ANSI/ANS N45.2-1974 “Leakage Rate Testing of Containment Structures for Nuclear Reactors [41] and ANSI/ANS N56.9-1987 “Containment System Leakage Testing Requirements.” [42]

The ILRT for the PCCV model was a hybrid of these procedures. The ILRT pressure, P_{ILRT} , was 0.9 Pd (0.35 MPa or 51.2 psig) based on JEAC 4203 and the Absolute Method for a Type A Test per ANSI/ANS N56.9 (Section 5.0) was followed. After depressurizing from the P_{SIT} to P_{ILRT} , the model was held at P_{ILRT} for approximately one hour to allow the model atmosphere to stabilize before the start of the leakage rate test. The ILRT commenced after all stabilization criteria were achieved and the duration of the test was “sufficient to enable adequate data to be accumulated and statistically analyzed so that a leakage rate ... can be accurately determined” but no less than 24 hours. Data was collected at least once every hour. The measured leakage rate at P_{ILRT} , L_{tm} , was determined using both the (a) total time analysis and (b) point-to-point analysis techniques. The nominal atmospheric pressure at the elevation of the test site (verified by checking the Sandia Photovoltaics Weather Station reading) was used for leak rate calculations. The calculated leak rate after 24 hours at 0.9 P_d , was 0.059% mass/day.

After the ILRT was completed, the model was initially depressurized by venting through the 1mm orifice plate, calibrated for a leak rate of 1% mass/day. After approximately 16 hours, a stable leak rate of 0.996% mass per day was calculated, again confirming the accuracy of the leak rate instrumentation.

The calculated leak rates during and after the ILRT are shown in Figure 5.9.

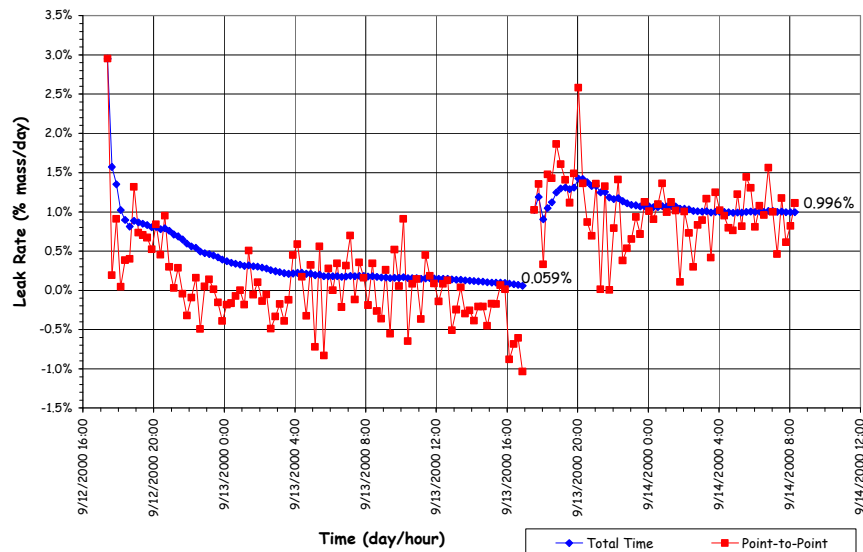


Figure 5.9 Integrated Leak Rate Test Leak Rates

Per JEAC 4203, the maximum leak rate at the ILRT pressure should be less than 0.1% mass/day. Similarly, per 10 CFR 50, the specified maximum allowable leak rate, L_a , at the design accident pressure, P_d , for the prototype containment is 0.1% mass/day. The maximum leak rate at the ILRT pressure level, L_t , is

$$L_t = L_a (P_{ILRT}/P_d) = 0.09\% \text{ mass/day}$$

Normally, the measured leak rate, L_{tm} , should be less than $0.75L_t$ (0.07% mass/day). For the PCCV model, this translates into measuring a change in pressure of approximately $0.001 \text{ kg}_f/\text{cm}^2$ (0.02 psi), which is beyond the capability of the instrumentation to resolve. While the calculated leak rates are within the limits specified in the standards, the accuracy of these leak rate estimates is questionable. Using the instruments selected for the high pressure test, however, the PCCV model exhibited a leak rate which was less than 1% mass/day, which corresponds to a pressure drop of 0.004 MPa (0.6 psi) over 24 hours.

While holding at the ILRT pressure, a limited amount of crack mapping was performed. This was accomplished by tracing all new cracks in predetermined areas and taking still photos of these areas. Cracks in the area to the left of the E/H prior to the SIT were traced in black and are shown in Figure 5.10. New cracks, traced in blue during the ILRT, are shown in Figure 5.11. Cracks widths were not measured.



Figure 5.10 Pre-SIT Cracks at Azimuth. 350 degrees, Elev. 4680 to 6200 (Grid 45)

Model response data was also recorded during and after the SIT/ILRT. Figures 5.12 and 5.13 show the radial and vertical displacement of the model as a function of time.

The initial displacements represent the net effect of prestressing, creep, shrinkage, etc. from the 'zero' reading in March to the start of the SIT in September. The cyclic response during the ILRT is an indication of the model's response to variation in ambient temperature and direct heating.

After the leak rate calibration, the PCCV model was depressurized at approximately the same rate and increments as the initial pressurization phase to compare the responses at the same pressure levels.

An exclusion zone was established for the SIT, consisting of a circular area with radius of 600 m (2,000'), centered at the PCCV model. The exclusion zone, as shown in Figure 5.14, was marked, and signs were posted to identify this area. The safety observers monitored the exclusion zone at all times during the test to make sure that no intruder entered this area. No exclusion zone was required for the ILRT because the model pressure was below the design pressure ($0.9P_d$).

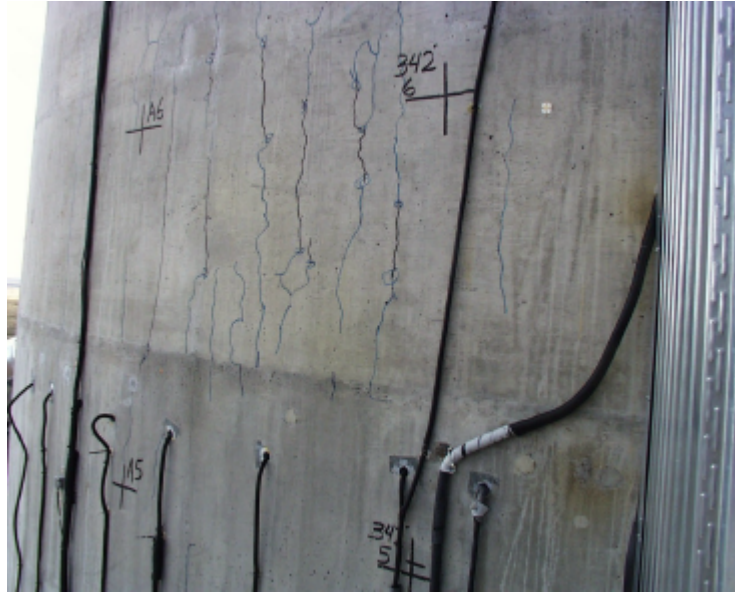


Figure 5.11 Post-SIT Cracks at Azimuth. 350 degrees, Elev. 4680 to 6200 (Grid 45)

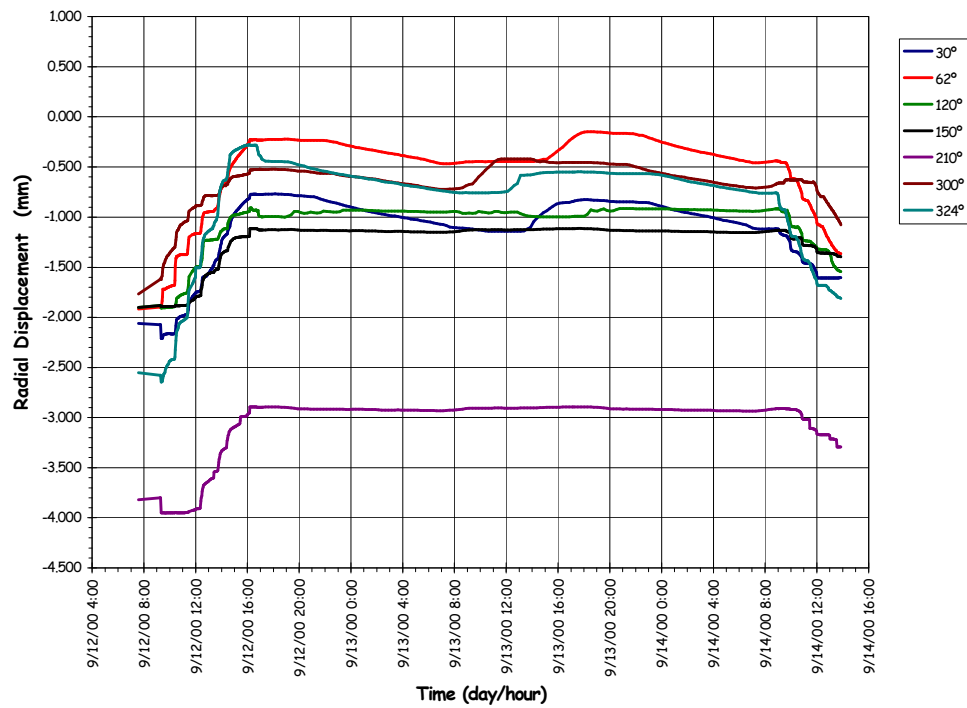


Figure 5.12 SIT/ILRT Radial Displacements at Cylinder Midheight (Elev. 4680)

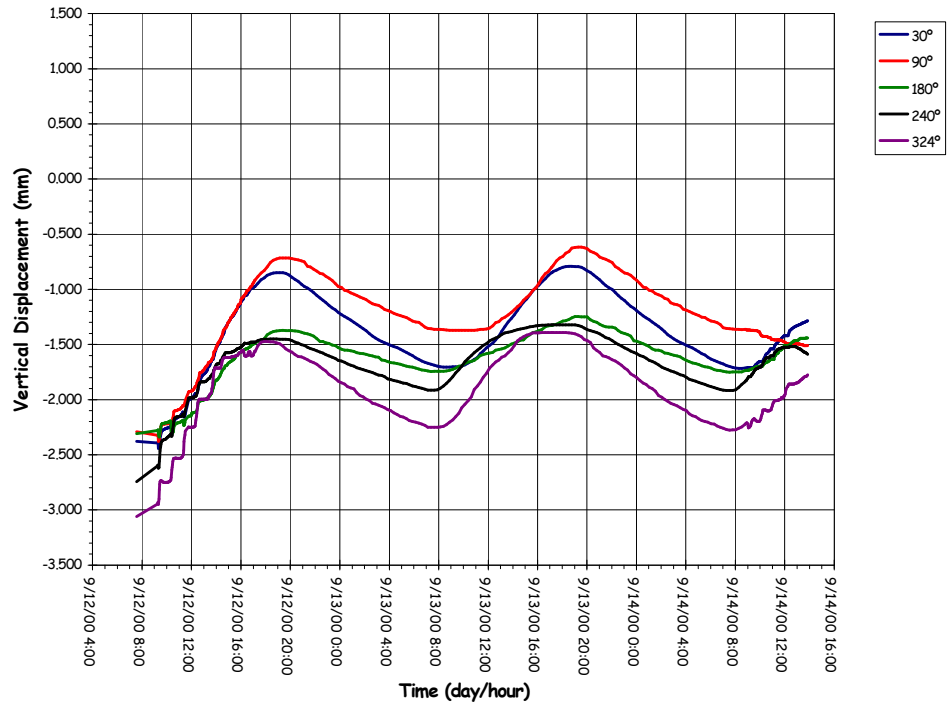


Figure 5.13 SIT/ILRT Vertical Displacements at Springline (Elev. 10750)

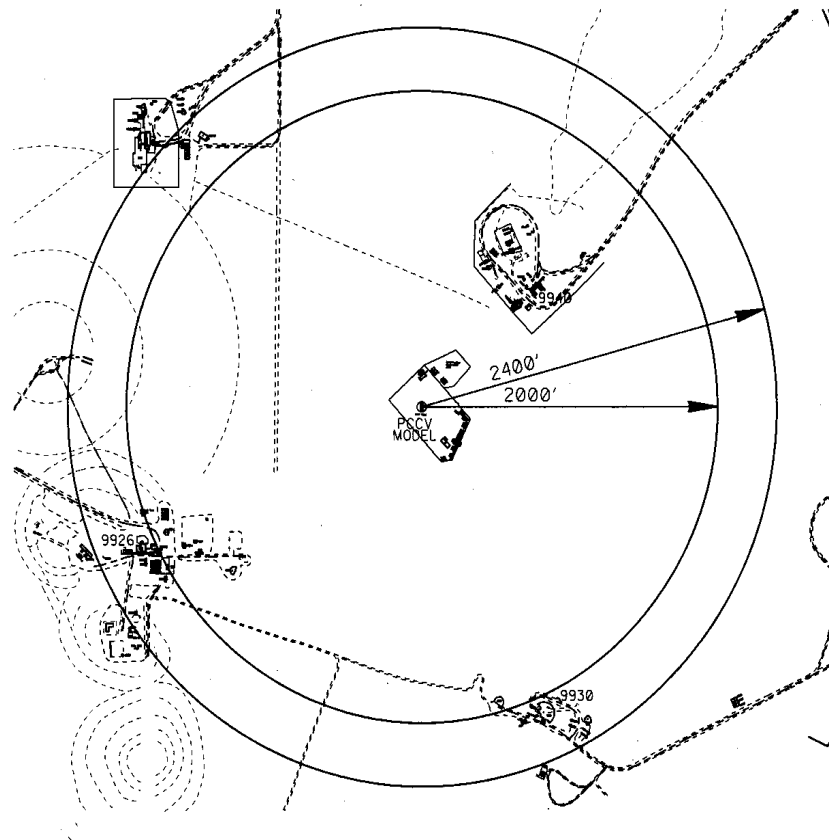


Figure 5.14 PCCV SIT/ILRT, LST, SFMT Exclusion Zone

Personnel were permitted to approach the model after the pressure has stabilized and the test conductor (TC) determined that it was safe to approach the model.

5.2.3 Limit State Test

The LST was designed to fulfill the primary objectives of the PCCV test program, i.e. to investigate the response of representative models of nuclear containment structures to pressure loading beyond the design basis accident and to compare analytical predictions to measured behavior. The LST was conducted after the SIT and ILRT were completed and the data from these tests evaluated. The PCCV model was depressurized between the SIT/ILRT and the LST. The LST began at 10:00 AM, Tuesday, September, 26, 2000, and continued, without depressurization, until the test was terminated just before 5:00 PM on Wednesday, September 27.

The exclusion zone for the LST covered the same circular area of radius 600 m (2,000'), centered at the PCCV model, as shown in Figure 5.14. At this radius, the estimated peak free-field overpressure due to a sudden burst at an internal pressure 2.1 MPa or 300 psig [34] is 1.66 kPa (0.24 psi). This is below the free-field allowable whole body exposure of 3.4 kPa (0.5psi) specified by SNL Environmental Safety and Health (ES&H) regulations. The safety observers monitored the exclusion zone at all times during the LST to make sure no intruder entered this area. In addition, the safety observers monitored the area above the model for aircraft. If an aircraft had approached the exclusion zone, pressurization of the model would have been suspended or held until the aircraft cleared the exclusion zone.

The pressure and average temperature time histories during the LST, including depressurization, are plotted in Figure 5.15. The LST followed the planned pressurization sequence up to the point where the model began leaking.

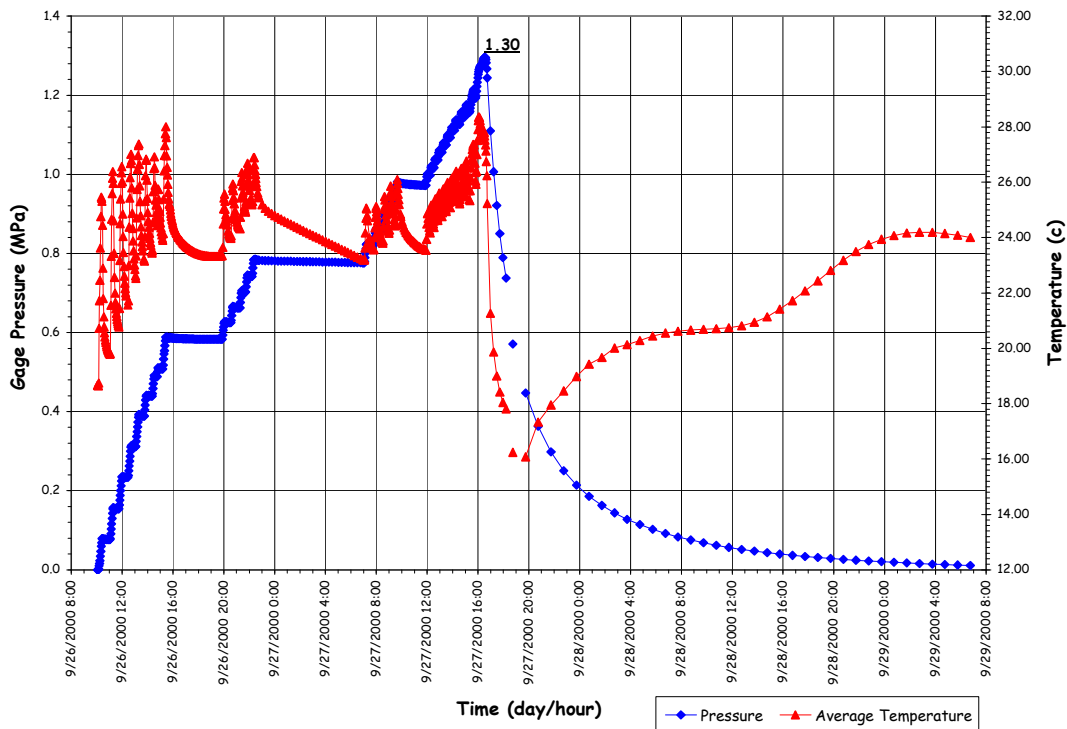


Figure 5.15 Limit State Test Pressure and Average Temperature

Initially, the model pressurization sequence matched the pressurization steps followed for the SIT to allow for comparison of the model response to two identical cycles of loading. The gage stability criteria used during the SIT (i.e. Equation 5.1) was also applied during the LST. Pressurization continued in increments of approximately $0.2P_d$ until a pressure of $1.5 P_d$ ($6.0 \text{ kg}_f/\text{cm}^2$ or 85.3 psig) was reached at approximately 4:30 PM. At this pressure, the first planned leak check was conducted by isolating the model and monitoring the temperature and pressure. After approximately three hours, a leak rate of 0.48% mass/day was calculated. Considering previous experience from the ILRT, which

demonstrated that thermal expansion of the model during the day yielded apparent leak rates in this range, the results were interpreted to indicate that the PCCV model was leak-tight.

Pressurization of the model continued in increments of approximately $0.1P_d$ until a pressure of $2.0P_d$ ($8.0 \text{ kg}_f/\text{cm}^2$ or 113.8 psig) was reached at approximately 11:00 PM. At this pressure the model was again isolated to perform a planned leak check. This leak check was also planned to be held for 8 hours to allow the test team to partially stand down for a rest period. A ‘skeleton crew’ consisting of the TC, Data Acquisition System Operator (DO), and Nitrogen Supply Operator (NO) continued to monitor the response of the model and all other systems until approximately 7:00 AM on September 27. This pressure hold and leak check was also selected below the lower bound prediction for the onset of structural yielding (i.e. yielding of the rebar or tendons) to ensure the model would remain relatively stable during this period. After approximately eight hours, the calculated leak rate was 0.003%, i.e., essentially zero. This confirmed the interpretation of the leak check results at $1.5 P_d$ and also demonstrated the greater accuracy of the leak rate results when the model is thermally stable.

Pressurization of the model resumed at 7:00 AM in increments of $0.1P_d$, with increasing dwell time between pressure steps (~30 minutes) required to meet the gage stability criteria. As the pressure was increased to the next planned leak check at $2.5P_d$, liner strain gages in the vicinity of the E/H (LSI-C-K5-12) began registering rapidly increasing strains in excess of 1%. At $2.4P_d$, the acoustic system operator (AO) reported hearing a change in the acoustic output which might indicate that “something had happened.” At approximately 10:00 AM at a pressure of $2.5P_d$ ($10.0 \text{ kg}_f/\text{cm}^2$ or 142.2 psig), the model was isolated for the third planned leak check. After approximately 1-1/2 hours, a fairly stable leak rate of 1.628% mass per day was calculated. The leak rate calculations at 1.5, 2.0, and $2.5P_d$ are plotted in Figure 5.16. Coupled with the acoustic data that continued to confirm some new event had occurred, it became clear that the model was leaking, most likely from a tear in the liner in the vicinity of the E/H. Plots of the output of the four internal acoustic sensors surrounding the E/H at 2.3, 2.4, and $2.5 P_d$ are shown in Figure 5.17.

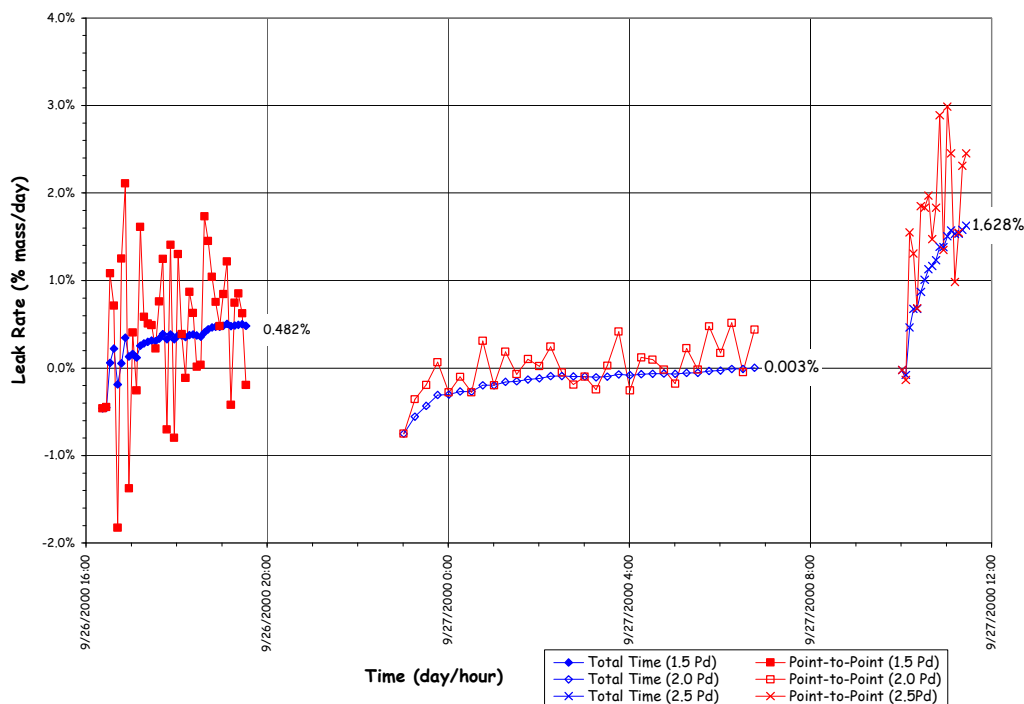


Figure 5.16 LST Calculated Leak Rates at 1.5, 2.0 and $2.5 P_d$

After consulting with NUPEC and the NRC, the TC concluded that the model had functionally failed between 2.4 and $2.5 P_d$ and directed a change in the pressurization plan. Since the model was leaking, the next goal was to pressurize the model as highly as possible to collect data on the inelastic response of the structure and to observe, if possible, a structural failure mode. Pressurization continued in increments of $0.05 P_d$, as planned. However, the gage stability criteria was abandoned and the hold time at each pressure step was reduced to less than 10 minutes.

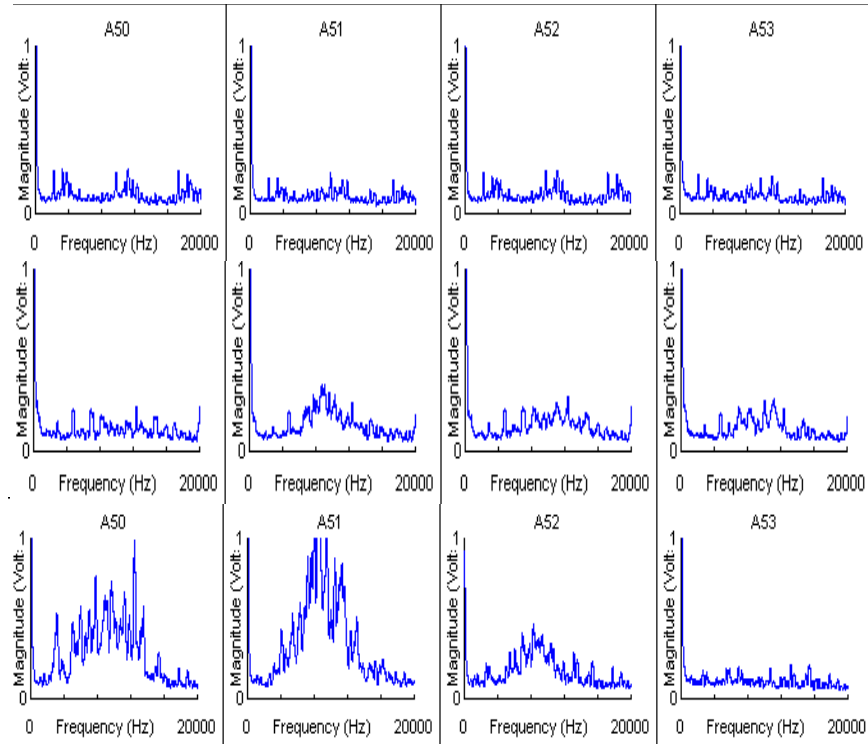


Figure 5.17 Internal Acoustic Sensor Signals at the E/H

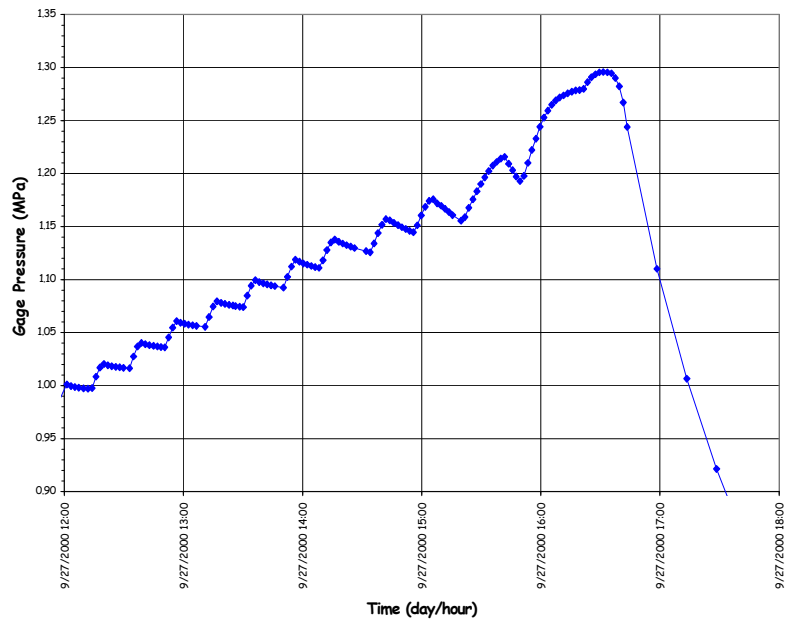


Figure 5.18 LST Pressure Time History, 2.5 to 3.3 P_d

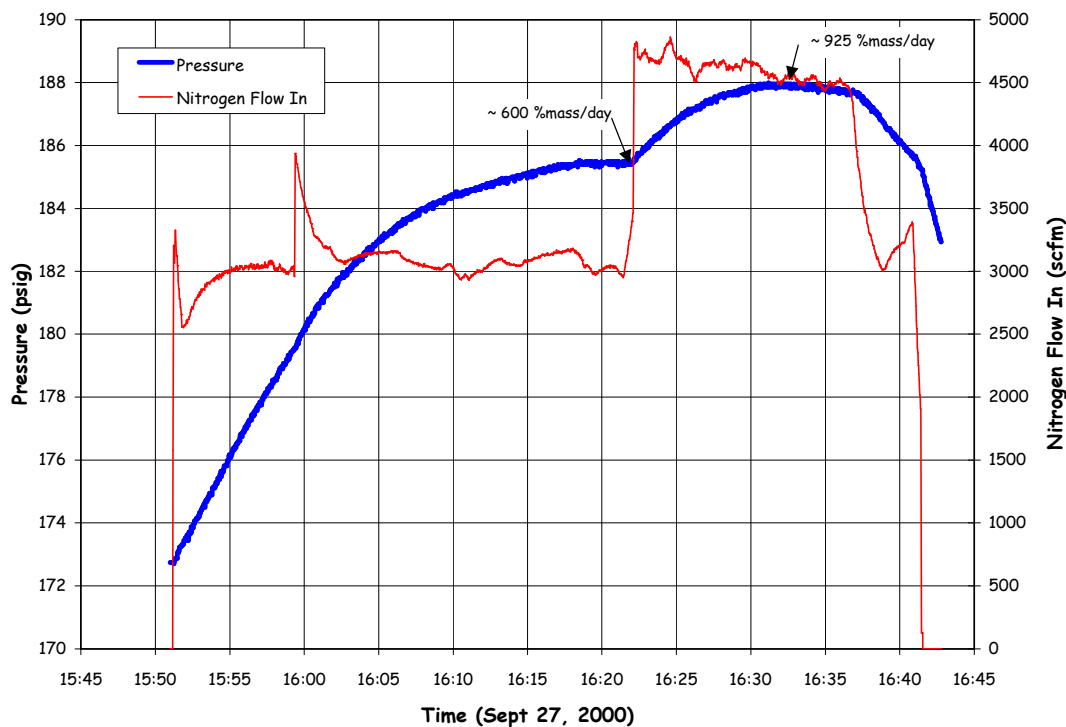


Figure 5.19 LST Pressure and Flow Rates at Maximum Pressure

The PCCV model was pressurized to approximately $3.0P_d$, with increasing evidence of leakage and increasing liner strains. At $3.0P_d$, it became increasingly difficult to pressurize the model, and the nitrogen flow rate was increased to 99 std.m³/min (3500 scfm). At this flow rate, the pressure in the model was increased to $3.1P_d$. However, the pressure dropped steadily after reaching this pressure. The leak rate at this point was estimated to be 100%.

The nitrogen flow rate was increased to the maximum capacity of the pressurization system, 142 std.m³/min (5000 scfm), and the pressure was increased to slightly over $3.3P_d$ before the leak rate exceeded the capacity of the pressurization system. The pressure time history and flow rates during the final phase of the test are shown in Figures 5.18 and 5.19. Since it was no longer possible to increase the pressure in the model and the supply of nitrogen was nearly exhausted, the TC decided to begin terminating the test.

The isolation valve was closed and the model was allowed to depressurize on its own. The terminal leak rate was estimated to be on the order of 900% mass/day. (The maximum flow rate of nitrogen, 5000 scfm, is equivalent to a leak rate of 1000% mass/day.) Estimated leak rates during the final pressurization and depressurization phases are shown in Figures 5.20 and 5.21.

After the model pressure was reduced to $1.0P_d$, test personnel were able to inspect the model close-up. Nitrogen gas was observed (heard and felt) escaping through many small cracks in the concrete around the penetration sleeves and at the tendon anchors. It was speculated that the liner acted as a leak chase, allowing nitrogen gas escaping through a tear or tears in the liner to travel between the liner and the concrete until it found an exit path through a crack in the concrete or a conduit in the tendon duct.

At maximum pressure, local liner strains of up to 6.5% were recorded and global hoop strains (computed from the radial displacement) at the mid-height of the cylinder averaged 0.4%. While large liner strains were observed, causing suspicion that the liner might have torn in several locations, the remainder of the structure appeared to suffer very little damage with the exception of more extensive concrete cracking at some locations. The largest crack was observed to the left of the E/H, shown in Figure 5.22. This is the same location as the crack photos shown in Figures 5.10 and 5.11. There was no indication of tendon or rebar failure. The detailed results of the LST are discussed in Section 5.3.2.1.

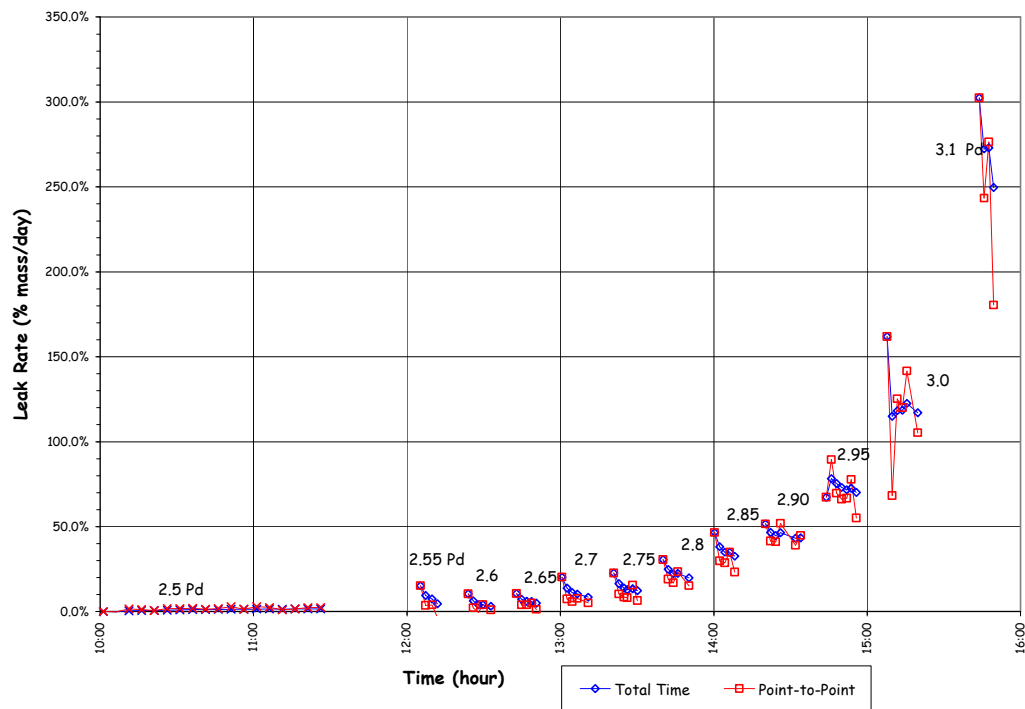


Figure 5-20. LST - Estimated Leak Rates (2.5-3.1 P_d)

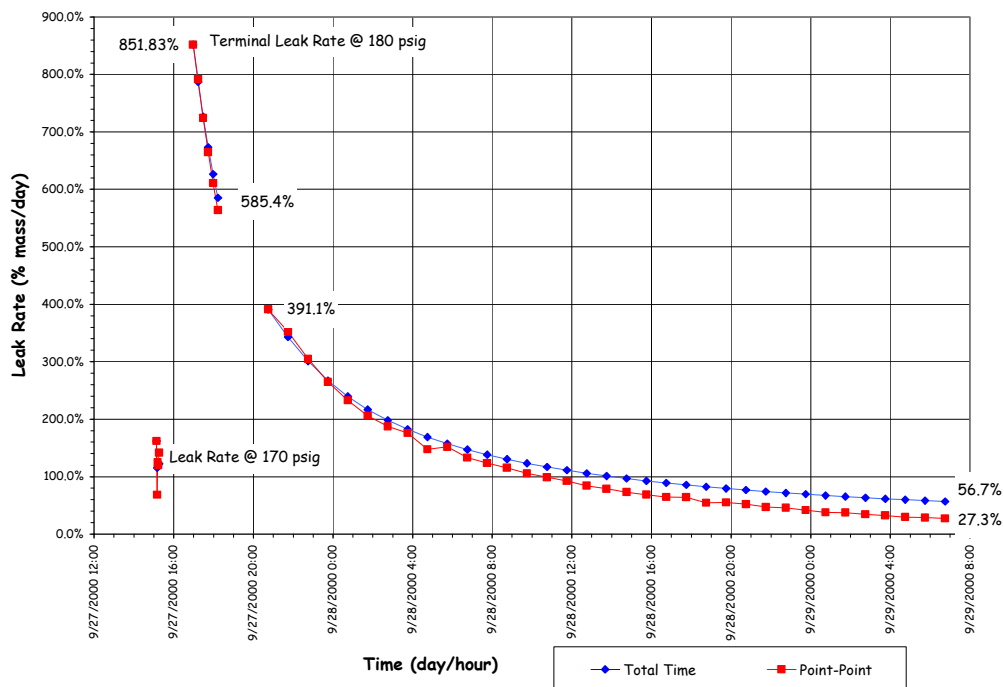


Figure 5.21 LST Estimated Terminal Leak Rates

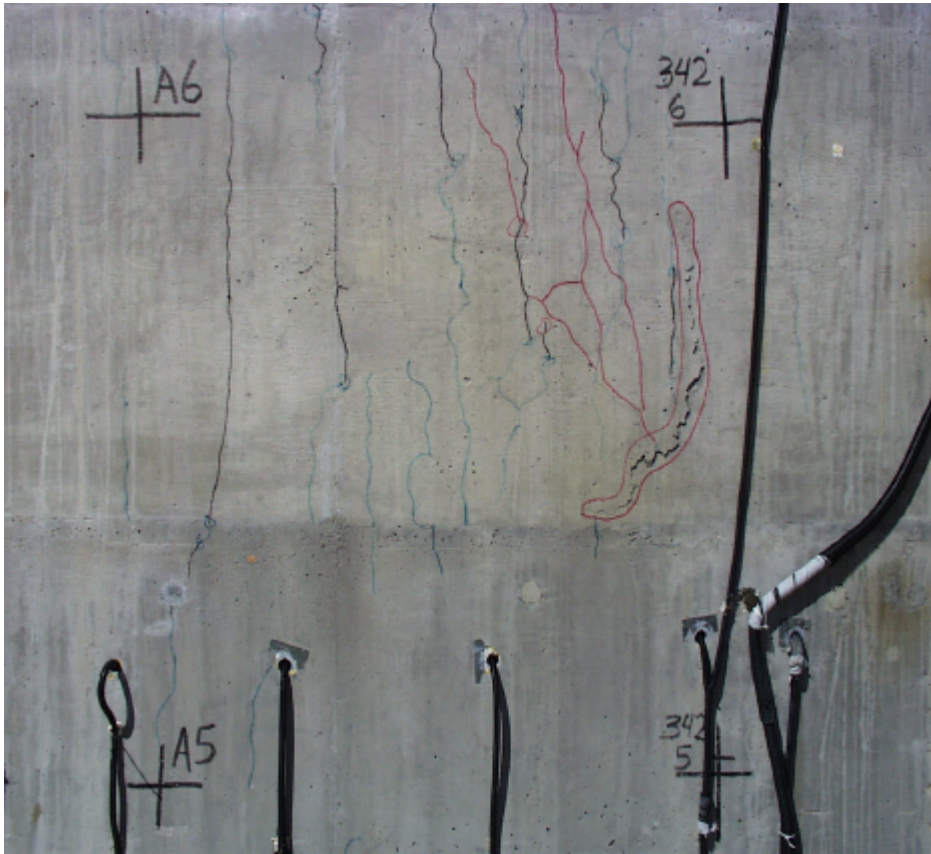


Figure 5.22 Post-LST Cracks at Azimuth 350 degrees, Elev. 4680 to 6200 (Grid 45)

After the model had completely depressurized, it was purged with fresh air, the E/H was removed, and detailed posttest inspection of the inside of the model began. A cursory inspection of the model identified 26 discrete tears at 18 separate locations. A detailed posttest inspection plan was developed, and the results of this inspection are described in Section 5.3.2.1

5.2.4 Structural Failure Mode Test

Almost immediately after the completion of the LST, it was recognized that while the PCCV model had demonstrated its capacity to resist pressures well above the design pressure and confirmed, arguably, liner tearing and leaking as the functional failure mode, the test objectives were not fully met with respect to observing large inelastic deformations for comparison with analyses, and witnessing the structural failure mode of the PCCV model. SNL was tasked by NUPEC and the NRC with investigating the possibility of conducting a second LST.

Two issues needed to be addressed to determine the technical feasibility of reloading the PCCV model. First was the question of whether the LST had caused damage to the structure such that any data obtained by reloading the structure would be compromised and of limited value for comparison with analytical results. The LST data was thoroughly reviewed and, with the exception of the liner and cracking of the concrete, there was no evidence of excessive structural damage. There was also no indication that the tendons had been strained beyond their yield limit and, except for a few isolated measurements, the same was true for the rebar. (Only 27 of the rebar gages registered strains in excess of 0.4% with a maximum of 1.7%—which likely reflects the local perturbation caused by the presence of the gage.) Comparing the radial displacement at the mid-height of the cylinder to the pretest Round Robin predictions in Figure 5.23 clearly illustrates that the structure was on the verge of global yielding but had not undergone a significant amount of inelastic

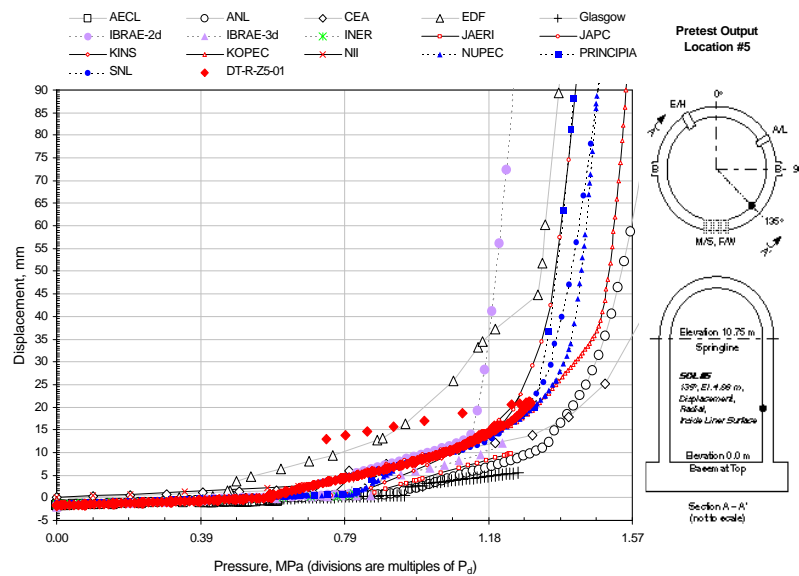


Figure 5.23 LST Radial Displacement at Azimuth 135 degrees, Elev. 4680

deformation. (In this context, only the yielding of the steel and rebar is addressed. Obviously, the loss in stiffness that occurs with global concrete cracking at approximately $1.5P_d$ cannot be recovered.) This was a positive finding for the prospect of reloading the model since most, if not all, of the capacity of the rebar and tendons was still available. Another important conclusion from the consideration of the LST data was that if, in fact, the model was on the verge of global structural yielding, the additional pressure required to cause larger; inelastic deformations was not very large; perhaps only on the order of a few tenths to half the design pressure, i.e. an additional 1.0 to $2.0 \text{ kg}_f/\text{cm}^2$ (14 to 30 psig).

The second issue was the requirement to reseal the model in order to repressurize it. Since large sections of the liner were removed as part of the post-LST inspection, the liner was no longer capable of providing an effective membrane to prevent premature leakage. Furthermore, even if the liner tears and cutouts were locally repaired or sealed, it was clear that other areas of the liner were susceptible to tearing at the same pressures (or perhaps even at lower pressures) that caused the liner to tear during the LST. It was necessary, therefore, to devise a cost-effective method of completely replacing the liner function in order to proceed with plans to repressurize the PCCV. The replacement 'liner' was also required to ensure that the model could be repressurized to a level beyond the maximum pressure achieved during the LST. (A corollary of this conclusion was that there was no further need to investigate the response of the liner, and the instrumentation applied to the liner could be abandoned.)

Furthermore, the SFMT had to be completed within the current program budget and schedule. The concept developed to repressurize the PCCV model is illustrated in Figure 5.24.

The concept consists of sealing the interior surface of the liner with an elastomeric membrane after removing all interior transducers on the liner. After closing the E/H and A/L, the model would be filled with water to 1.5 m (5') from the dome apex, approximately 97% of the interior volume $1,591,000 \text{ ltr}$ (350,000 gal). Filling the model with water would provide several advantages:

1. The leak rate of water through any tears in the liner is much less than the corresponding leak rate of gas. Therefore, even if a leak path developed, the flow rate capacity of the pressurization system should be adequate to compensate for the leak.
2. By maintaining a gas pocket in the model, the pressurization system used for the LST, with nitrogen gas as the pressurization medium, could be used for the SFMT without any major modifications. The only modification required would be installing additional piping inside the model to allow the gas to be introduced at the dome apex and to fill (and drain, if necessary) the model. Reducing the volume of gas to be pressurized lowered the demand on the pressurization system in the event of a leak, as well as the volume of gas required to conduct the test. In the

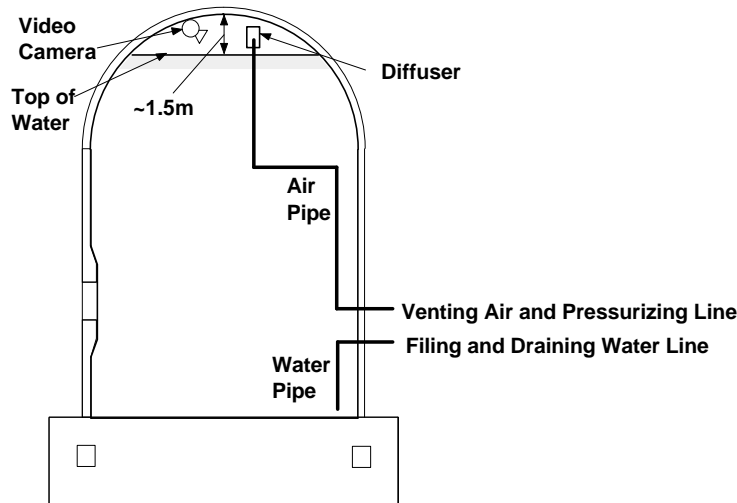


Figure 5.24 PCCV Structural Failure Mode Test Concept

case of the SFMT, a pressurized tube trailer could be used instead of the more expensive liquid nitrogen source required for the LST.

3. Since the pressurization system could compensate for small leaks, it is not essential that the elastomeric liner be completely leak-tight, only that the leaks would be small enough to allow the model to be pressurized to the desired level.
4. Water leaks would be readily visible, compared to gas leaks.
5. In the event of a catastrophic PCCV model rupture, the energy stored in the model nearly filled with water is much less than the stored energy if pressurized to the same level with gas. As a result, the safety exclusion zone around the model could be reduced, if necessary.

At the same time, filling the model with water would have some disadvantages:

1. Any instruments or other electrically-powered components (lights, cameras, etc.) inside the model would have to be removed or completely sealed.
2. The internal pressure would not be uniform due to the hydrostatic head, approximately 1.4 kg/cm^2 (20 psig).

These disadvantages, however, were not deemed significant, and efforts focused on selection of a suitable liner. A number of vendors were contacted, and two proposals for sealing the liner were considered. One proposal was to prefabricate a 5 mm (200 mil) PVC sheet liner, which would be installed inside the model by heat welding the seams and sealing around the penetrations using ring clamps. The second proposal was to spray on a two-part polyurea coating, also a minimum of 5 mm (200 mil) thick. After considering both proposals, the sprayed-on lining was selected since it could be more readily adapted to the irregular liner surface and had significant cost and schedule advantages. The elastomeric liner was installed by Ershigs Corporation³¹ in August, 2001 after the interior model inspection was completed and all the surface instrumentation was removed. The application of a test sprayed-on liner is shown in Figure 5.25.

After the elastomeric liner was installed, the interior instrumentation for the SFMT was installed. A reduced set of instruments was selected, allowing one data acquisition computer to scan all the gages in less than 60 seconds to support 'rapid' pressurization of the model. The instrumentation suite for the SFMT consisted of the following (A complete list of all the SFMT gages is provided in Appendix H):

³¹ Ershigs, 742 Marine Drive, PO Box 1707, Bellingham, WA 98277, (<http://www.ershigs.com/>)

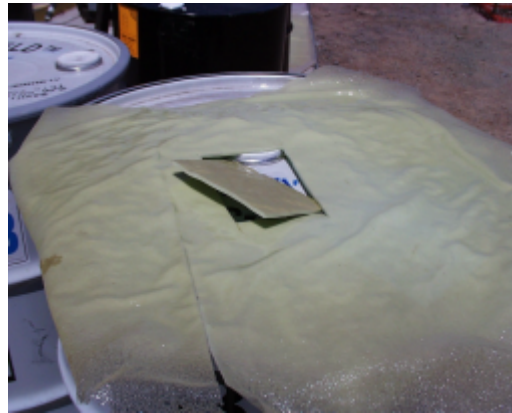


Figure 5-25. Test Specimen of Elastomeric Lining

1. All interior gages used for the LST were removed or abandoned. These were replaced by 20 waterproof LVDTs, 17 radial and three vertical, located as shown in Figure 5.26.
2. Five interior pressure transducers, three below water at the base, cylinder mid-height, and springline, and two to measure the gas pressure.
3. Two interior video cameras and lights to monitor the E/H and the water surface.
4. 18 exterior liner strain gages
 - a. 14 at meridional at wall-base junction
 - b. Four at hoop stiffener details
5. 82 rebar strain gages (Standard Output Locations (SOLs)).
 - a. 35 rebar gages (all 22 SOL plus 13 meridional at wall-base junction)
 - b. 47 gage bars (all surviving)
6. All surviving tendon strain gages and all load cells.
7. Soundprint® acoustic monitoring (external sensors only).
8. Concrete strain (six SOFO gages).
9. Four external digital video cameras at 0 degrees, 90 degrees, 270 degrees, and 360 degrees, completely covering the PCCV cylinder wall.

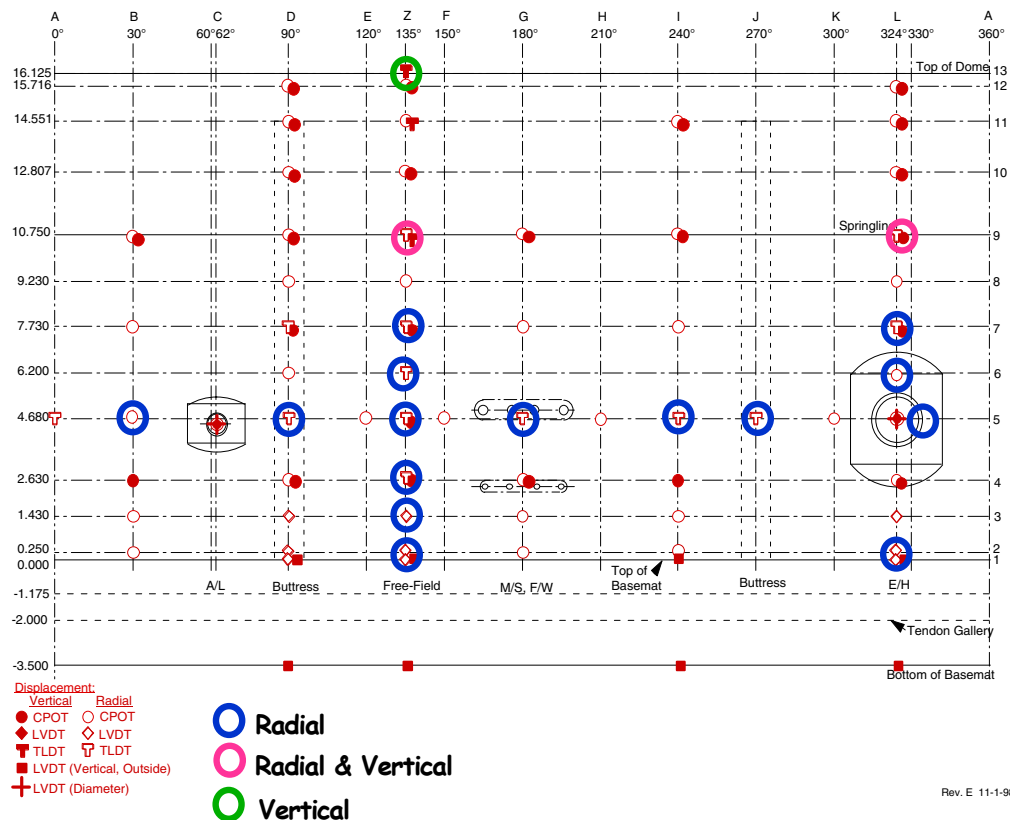


Figure 5.26 SFMT Displacement Transducer Layout

After completing the installation and all test-readiness checks, the E/H cover was installed and sealed. A low pressure pneumatic test was conducted to check for leaks on October 3, 2001. The pressure and temperature time histories for the leak test are shown in Figure 5.27. The leak test began at approximately 09:30 and a leak was detected (via the acoustic system) at approximately 0.2 Pd (~12 psig). Pressure was increased to the target pressure of 0.5Pd (30 psig), at which time the vessel was isolated and monitored for a 24-hour leak test. The acoustic system (multiple sensors) continued to output signals consistent with a leak in the model and several potential leak locations were identified.

Once the model was deemed stable, the nitrogen supply was isolated and a close inspection of the model was conducted. Through a combination of visual/auditory inspection, hand-held acoustic monitoring, and the application of soap-water solution, a number of locations were discovered where nitrogen gas was leaking from the model.

- The largest apparent leak was from a crack on the left-hand side of the 90-degree buttress at an elevation of approximately 6 m (20') above the top of the basemat (Level 6 in the cardinal coordinate system). This leak was the first detected by the acoustic system and was immediately confirmed during the close-up inspection.
- Secondary leaks, identified by the acoustic system, were confirmed at 150 degrees/3 and 6 m (10 and 20') and 210 degrees/4.5 m (15'). These leaks appeared to be through previously existing cracks in the concrete. The leak at 150 degrees was along the horizontal construction joints between C1, C2, and C3 as well as along a vertical crack extending between C2 and C3. The leak at 210 degrees also appeared to be through a previous crack.
- The acoustic system also suggested leaks at 300 degrees/1 to 2 m (3 to 6-1/2') and 360 degrees/0 m, but close-up examination could not confirm leakage at either location.
- During the close-up inspection, a leak was also detected at 30 degrees/5 m (16') which was not initially identified by the acoustic system.
- Close-up inspection of the penetrations also revealed leakage at the F/W penetrations. There was no evidence of leakage at the E/H, A/L, or M/S penetrations.

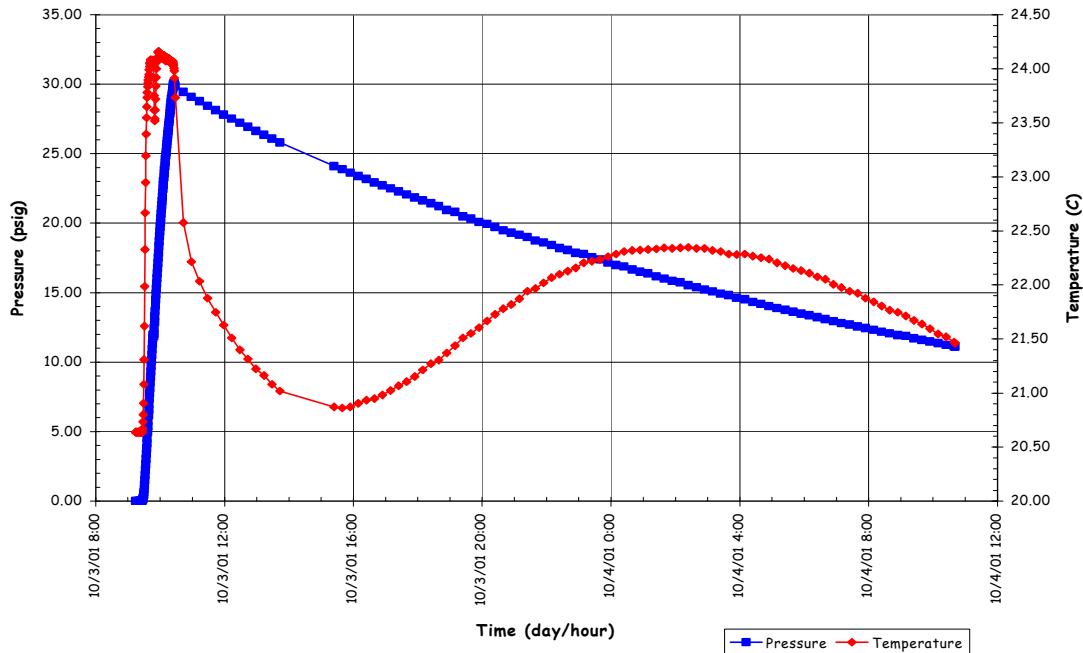


Figure 5.27 Pre-SFMT Leak Test Pressure and Temperature

These results indicated that, in spite of the manufacturer's quality control procedures coupled with detailed visual inspection (individual locations that appeared suspect were also sealed with silicone sealant prior to closing the model), the sprayed-on liner was not impermeable. Once the gas escaped through the sprayed-on and steel liners, it migrated between the steel and concrete until it found an exit path. The pressure did not appear high enough to tear the sprayed-on liner when a leak was first detected.

The calculated leak rate, shown in Figure 5.28, was initially 70% mass/day at the maximum pressure of 2.1 kg/cm² (psi) decaying to 45% at 0.77 kg/cm² (11 psi) over 24 hours. The sound levels as detected by the SoundPrint system (shown in Figure 5.29), which are roughly proportional to the rate of gas escaping, indicated a stable leak rate that was, to a large extent, independent of the pressure.

Based on these results, it was concluded that the leak was most likely due to a pre-existing hole(s) in the sprayed on liner which did not increase (or decrease) significantly during pressurization or during the leak test. (The equivalent orifice size reduced from about 6 mm (0.25") at 2.1 kg/cm² (30 psi) to 5 mm (0.20") at 0.8 kg/cm² (12 psi), based on the calculated leak rates.) As a result, the SFMT could be conducted without repairing the sprayed-on liner while maintaining a reasonable chance that the leak would not grow significantly and overwhelm the capacity of the pressurization system. (Nevertheless, during an unscheduled one-month postponement of the SFMT, the surface was retested with a 'spark-tester,' and a few small holes were discovered and sealed. The model was then resealed and readied for filling with water.)

Filling the PCCV with water and the SFMT began at approximately 09:00 November 6, after the initial data scan was taken, and continued until November 8, 2001. Slow water leaks were initially observed late November 6, after the model was about one-quarter full, however, the amount of water leaking was insignificant. The pressure time histories at various elevations in the model from the start of filling to the SFMT are shown in Figure 5.30. This figure illustrates the hydrostatic head and also reflects the slight loss of water due to leaks. The water level was 'topped off' on November 12, prior to the start of the SFMT.

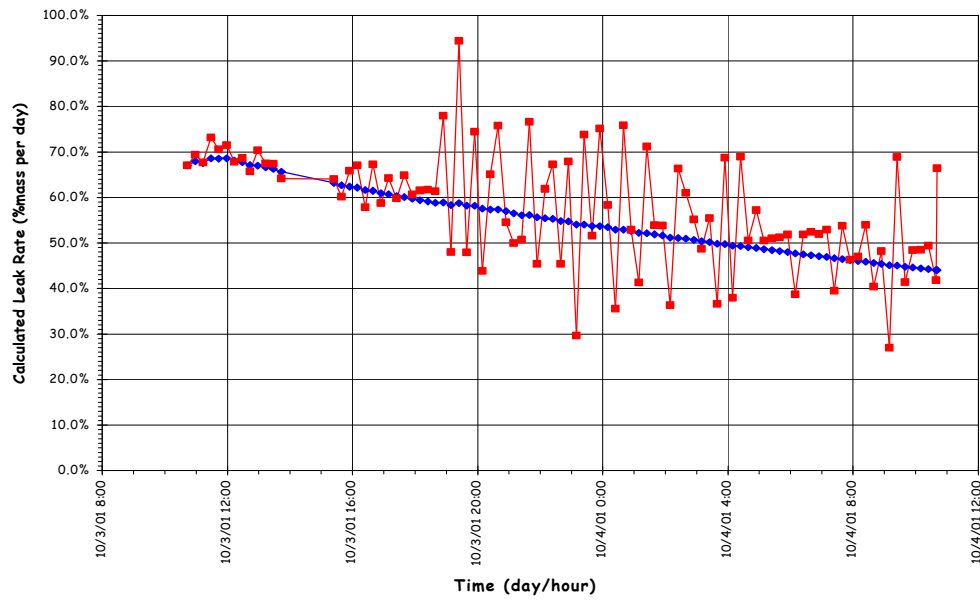


Figure 5.28 Pre-SFMT Leak Rate Test

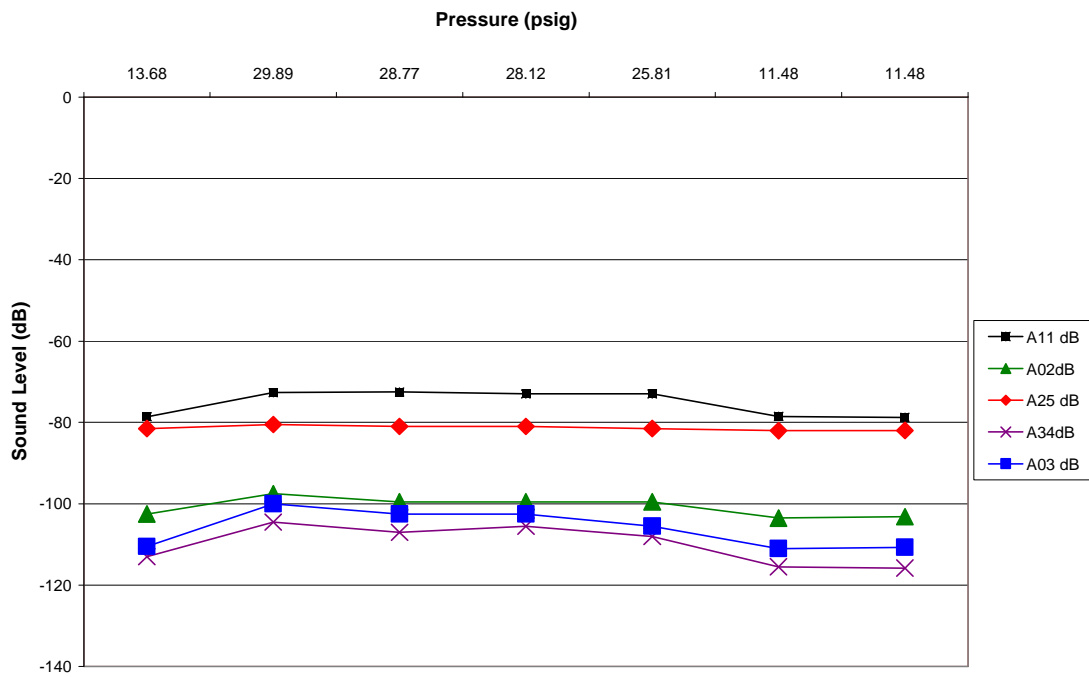


Figure 5.29 Pre-SFMT Leak Test Acoustic Data

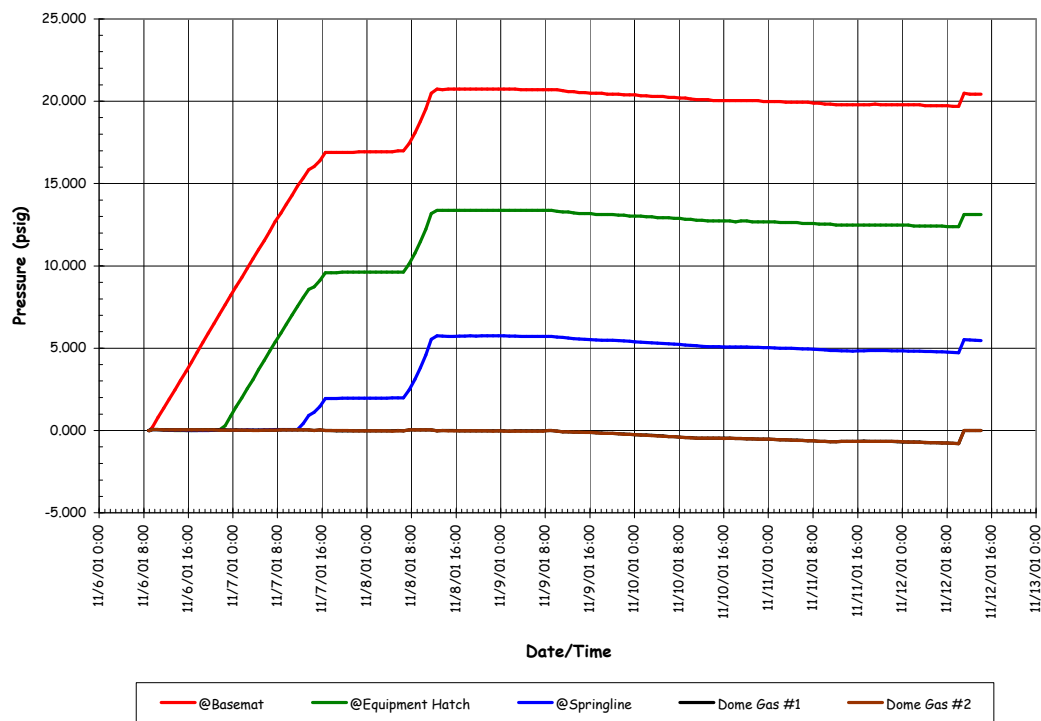


Figure 5.30 Pre-SFMT Hydrostatic Pressures

The test sequence planned for the SFMT was to rapidly pressurize the model using nitrogen gas to compensate for the known leaks in the model. The minimum flow rate capacity of pressurization system, 14 std.m³/min (500 scfm), would increase pressure in the reduced void space at a rate of about 0.35 kg_f/cm² (5 psi) every minute. At this rate, the model could be pressurized to failure in less than an hour.

The SFMT began shortly after 10:00 AM on Wednesday, November 14, 2001. The pressure time histories are shown in Figure 5.31. The pressure time history of all five gages are shown along with the effective model pressure, which is calculated as a volume-weighted average. Any references to the SFMT pressures are to the effective pressure, unless noted otherwise.

The model was continuously pressurized at a rate of approximately 0.35 kg_f/cm² (5psi)/min. All active sensors were continuously scanned at intervals of approximately 30 seconds and the video cameras continuously recorded the response of the model. As the pressure increased, evidence of leakage was visible as increasing wetting of the concrete surface. At 10:38 AM, the effective pressure in the model equaled the peak pressure achieved during the LST, 3.3 Pd (1.29 MPa or 188 psig). At approximately 10:39 AM, the acoustic system recorded a very high noise level event, which was interpreted as the breaking of a tendon wire. At this point in the test, events occurred very quickly. Shortly after detecting the wire break, a small spray of water was observed at approximately 0 degrees Azimuth and additional tendon wire breaks were detected by the acoustic system with increasing frequency. The wire break events are plotted in Figure 5.32, along with the effective pressure and the radial displacement at Azimuth L (324 degrees), elev. 6 (6280), as a function of time.

The rate of pressurization decreased and the nitrogen flow rate was increased to maintain the pressurization rate. The gas pressure and flow rates are shown in Figure 5.33. The water surface inside the model, viewed through the internal video camera, was dropping slowly, but it was unclear if this was due to leakage or radial expansion of the vessel.

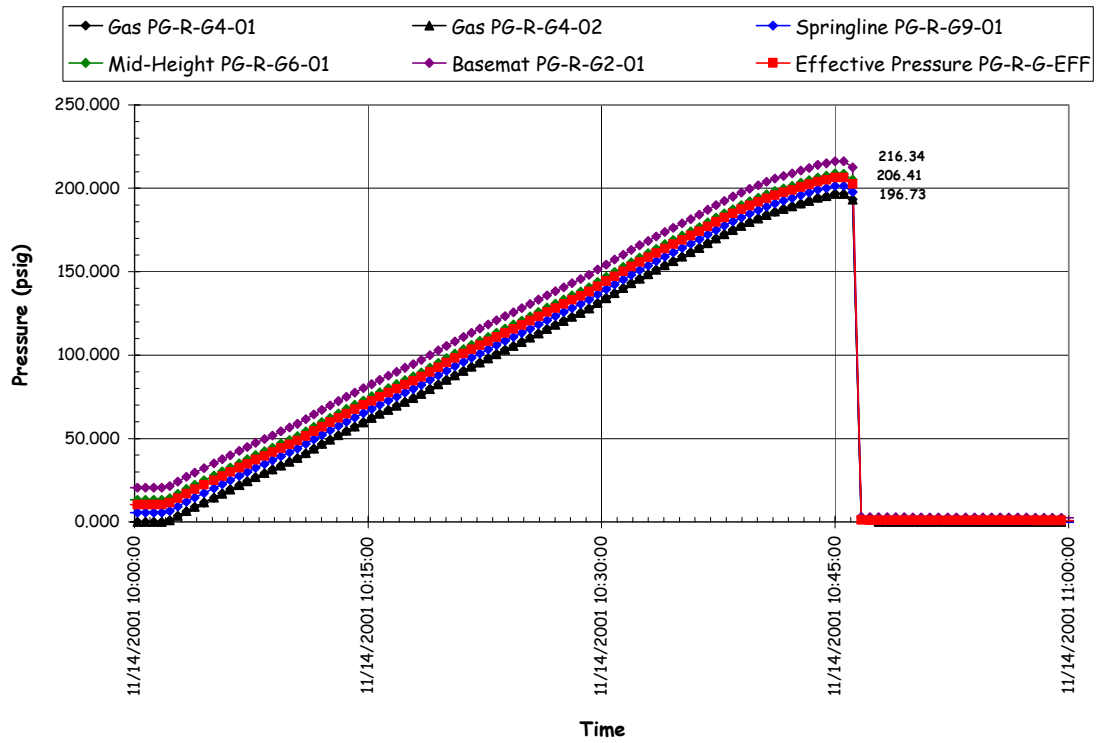


Figure 5.31 SFMT Pressure Time Histories

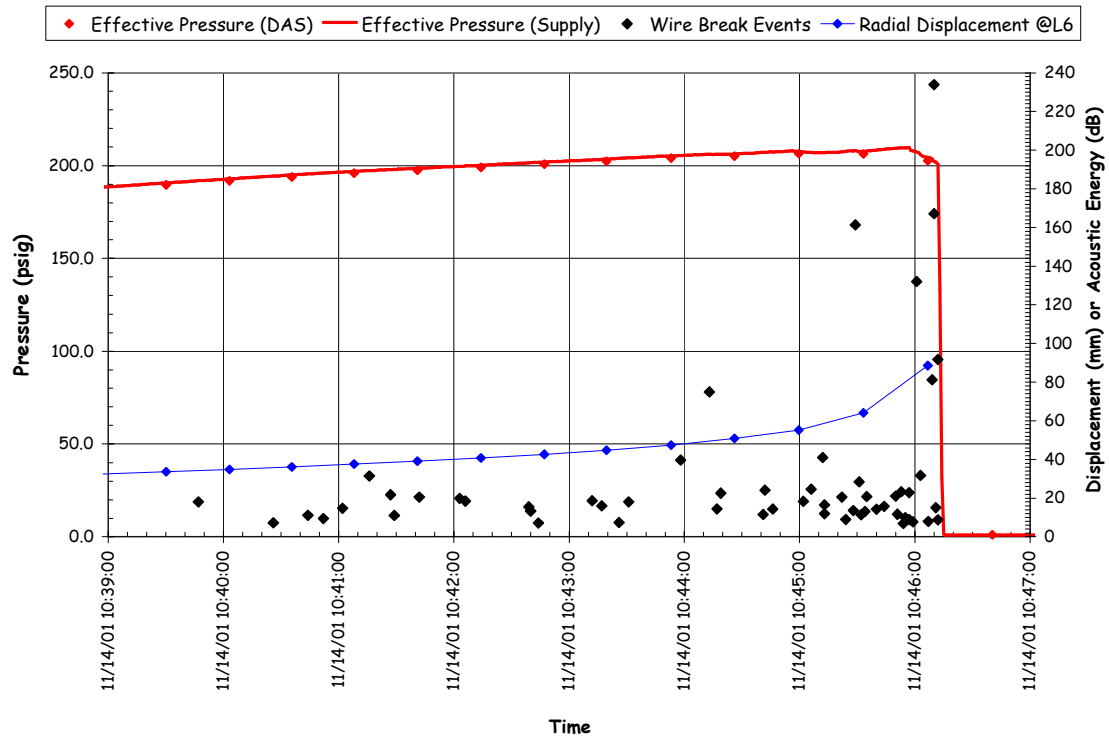


Figure 5.32 SFMT Wire Break Events vs. Pressure vs. Displacement

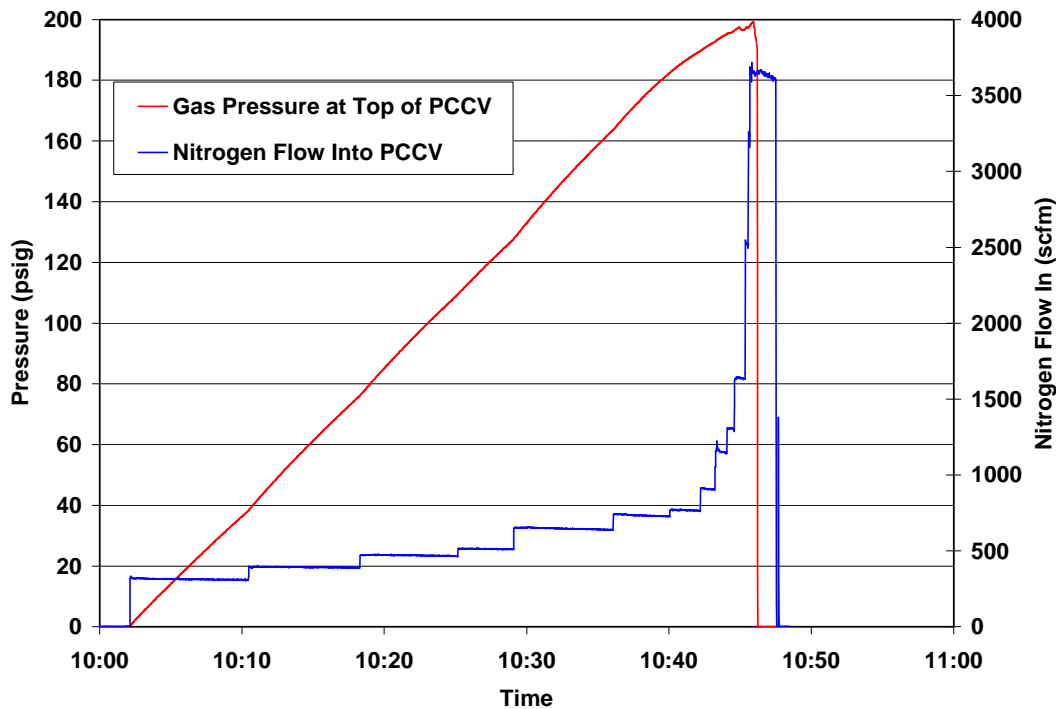


Figure 5.33 SFMT Pressurization System Data

Pressurization of the model continued until a second spray of water was observed and suddenly, at 10:46:12.3, at an effective pressure of $3.63 P_d$ (1.42 MPa or 206.4 psig), the PCCV model ruptured violently at ~6 degrees azimuth near the mid-height of the cylinder. The rupture propagated vertically in both directions and then radiated circumferentially about 2 m above the top of the basemat, shearing off the cylinder wall. The dome and cylinder wall then came to rest on the instrumentation frame, which apparently prevented the model from toppling over. The entire collapse was over in slightly more than one second. The entire SFMT, including the sequence of rupture and collapse, was recorded by the digital video cameras. A short movie (.mpg) file showing the rupture of the model is included on the enclosed data CD. The moment of rupture is shown from all four angles in Figure 5.34. The video recorded failure of the tendons, including ejection of tendon anchors. The condition of the model after the SFMT is shown in Figure 5.35.

The detailed results of the SFMT are discussed in Section 5.3.3, along with observations from the posttest inspection of the model. In the case of the SFMT, posttest inspection was limited to visual inspection due to the obvious damage and restricted access for safety.

Because of program schedule constraints, demolition of the PCCV model commenced in December, 2001 and was completed in April, 2002. During this period, attempts were made to further inspect the model and characterize the damage caused by the SFMT. However, these efforts were of limited value due to the difficulty of discriminating the damage caused during the SFMT from the demolition process. A few specimens from the model were retrieved, however, more for sentimental value than for providing any further technical insight into the behavior of the model.

5.3 Test Results

5.3.1 Data Files

The response of the model was continuously recorded beginning March 3, 2000, prior to prestressing, through October 11, 2000, following the LST. Additional data was recorded using a modified instrumentation suite from November 6 to 14, 2001 for the SFMT. Data for each set of transducers was saved in individual files and a data management and file



(a) 0 degrees Azimuth



(b) 90 degrees Azimuth



(a) 180 degrees Azimuth



(b) 270 degrees Azimuth

Figure 5.34 SFMT: Rupture of the PCCV Model



Figure 5.35 PCCV Model after the SFMT

naming scheme was developed to facilitate access and utilization of the data. A summary of the data file structure is shown in Figure 5.36.

The basic data was recorded as the output voltage (strain for strain gages, °C for temperature sensors) for each instrument at discrete time steps. This basic data is referred to as the raw, dynamic data. Note that the time reported in the data files is the DAS clock time at the start of a data scan. Since it took up to two minutes to complete a data scan (one minute for the SFMT), the actual time the data was recorded may be up to two minutes later than the recorded time. For pseudo-static loading, this is not a significant issue, but it may have some effect on the response recorded near the end of the LST and SFMT. The raw data is stored as ASCII, tab-delimited text files (.dat)

The raw, DOR is a subset of the raw, dynamic data. The concept of the DOR was defined to facilitate comparison of the data with analysis results. Typically, the analysis results are described as a function of pressure. The DOR is intended to provide a single, stable response value at each pressure step. The DOR were recorded separately from the dynamic data when the gage stability criteria (Eq. 5.1) was met, or at the direction of the test conductor.

The concept of dynamic and DOR data is illustrated in Figure 5.37. In this figure, the dynamic data during and after the LST is plotted along with the DOR for the radial displacement at the cylinder mid-height at 135 degrees. At lower pressures, the data are essentially identical; however, at higher pressures, the drift due to model creep and/or leakage is apparent. Furthermore, the DOR set does not capture the maximum pressure. In subsequent discussions of the DOR, the response at the maximum pressure from the dynamic data has been appended to the DOR for completeness.

Due to the extended length of time over which the data was recorded, the raw data files were separated into individual files by time periods. These periods were chosen to correspond with distinct loading periods, as shown in Figure 5.36. The acronyms for each period were used in the file naming scheme. The full response time history (from March 3 to October 11) for any transducer can be reconstructed by combining the data from the individual files, as illustrated in Figure 5.38 for the radial displacement at the cylinder mid-height at 135 degrees. Gaps in the data represent times when the DAS was shut down for maintenance or when temporary malfunctions (e.g. loss of power, etc.) corrupted the data. Times when the corrupted data was removed from the files are duly noted in the Excel® spreadsheets.

	Before Prestressing	Prestressing	Post Prestressing	System Functionality Test		Post SFT	SIT/ILRT	Post SIT/ILRT	Limit State Test	Post LST	Structural Failure Mode Test
Start	3/3/00	3/10/00	5/5/00	7/18/00		8/7/00	9/12/00	9/14/00	9/26/00	9/27/00	11/6/01
End	3/9/00	5/5/00	7/18/00	7/21/00		9/11/00	9/14/00	9/26/00	9/27/00	10/11/00	11/14/01
	BPS	PS	PPS	SFT		PSFT	SITILRT	PSITILRT	LST	PLST	SFMT
RAW	DYNAMIC	DYNAMIC	DYNAMIC	DYNAMIC	DAS SHUTDOWN FOR MAINTENANCE	DYNAMIC	DYNAMIC	DYNAMIC	DYNAMIC	DYNAMIC	DYNAMIC
	*.dat	*.dat	*.dat	*.dat		*.dat	*.dat	*.dat	*.dat	*.dat	*.dat
	DOR	DOR		DOR			DOR		DOR		
	*.dat	*.dat		*.dat			*.dat		*.dat		
CONVERTED	DYNAMIC	DYNAMIC	DYNAMIC	DYNAMIC		DYNAMIC	DYNAMIC	DYNAMIC	DYNAMIC	DYNAMIC	DYNAMIC
	*.dat	*.dat	*.dat	*.dat		*.dat	*.dat	*.dat	*.dat	*.dat	*.dat
	*.xls	*.xls	*.xls	*.xls		*.xls	*.xls	*.xls	*.xls	*.xls	*.xls
	DOR	DOR		DOR			DOR		DOR		
	*.dat	*.dat		*.dat			*.dat		*.dat		
	*.xls	*.xls		*.xls			*.xls		*.xls		
CORRECTED									DYNAMIC		
									*.xls		
									DOR		

Figure 5.36 PCCV Test Data File Matrix

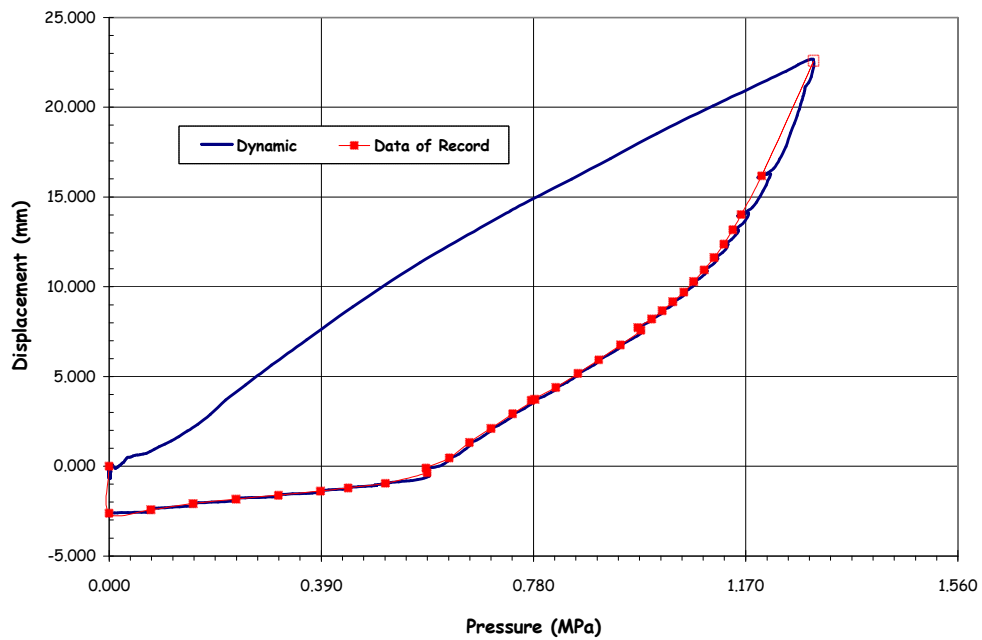


Figure 5.37 Radial Displacement at Azimuth 135 degrees, Elev. 6200

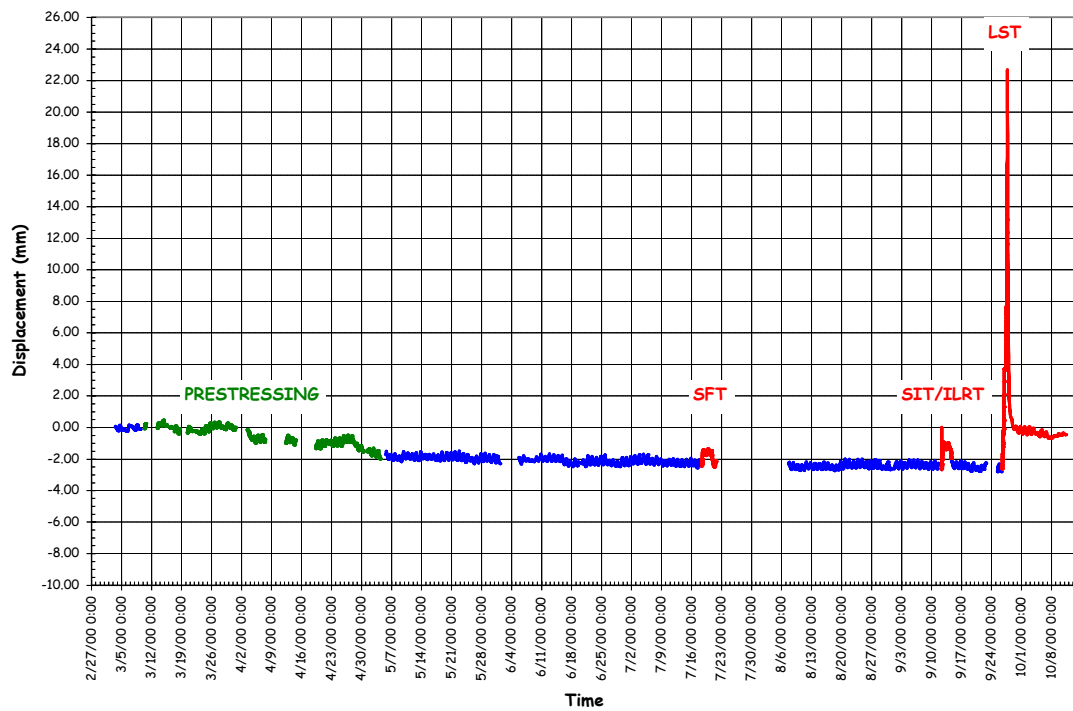


Figure 5.38 Radial Displacement History at Azimuth 135 degrees, Elev. 6200 (DT-R-Z6-01)

After the raw data was stored, it was converted using utility programs constructed as part of the DAS software. The conversion process was described in Chapter 4 and consisted of applying gage specific-gage factors (GFAC) obtained from the manufacturer or from gage calibration test data, correcting for actual gage power supply voltages. This converted data (CONV) was also stored as ASCII, tab-delimited text files (.dat) for each type of gage and loading period.

To simplify access to the data, the converted data files were further reorganized and stored in Microsoft Excel® spreadsheet format (.xls). The data files were grouped by response variable type according to the scheme shown in Table 5.3. Each data file was further subdivided by grouping similar gages on separate worksheets, as shown. Units for each response variable/gage are also shown. The converted data files in Excel® format are provided with this report on a CD. Appendix I provides a complete list of the data files on the disk. The format of each data file consists of the time (at the start of the data scan) in the first column followed by the response for each of the gages, identified by gage name in the following columns. The Excel® data files were also modified to add the average pressure at each time step where appropriate, (i.e., for the pressure tests), the nominal azimuth, elevation, and, in some cases, radius of the gage, and additional information (such as references to an instrumentation drawing detail or tendon number), where applicable.

The data file naming scheme consists of

- the gage type acronym,
- the data type acronym,
- a designation for dynamic (DYN) or DOR, and
- the loading period acronym.

For example, the file:

DISP_CVTD_DYN_LST.xls

contains the converted (CVTD) DYN displacement (DISP) during the LST in Excel® format (.xls).

One final set of data files, corrected data (COR), is also provided. The model was exposed to variations in ambient temperature, both temporal (day/night, seasonal) and spatial (due to direct solar heating), and responded accordingly. Since the converted test data includes the response to ambient thermal conditions, as well as prestressing and pressure loads, and the analyses, typically, do not, an attempt was made to correct the test data and 'remove' the effect of the temperature transient. This correction is described in Appendix J and was only applied to the LST data files.

In addition to the basic data files described above, additional data was collected by the pressurization system, acoustic system, and from visual observation and photographic (still and video records). This data is described in the following sections.

5.3.2 Limit State Test Results

5.3.2.1 Test Data

The LST data (DYN and DOR) is provided on the enclosed data CD in Excel® spreadsheets, as noted in Section 5.3.1. The response of every functioning transducer is provided. The following sections present a synthesis of the data focusing on the critical response measurements.

5.2.3.1.1 Displacements

The displacement data provides the most comprehensive view of the overall or global response of the model. Figures 5.39 through 5.42 show the displacement response as a function of pressure at various azimuths and elevations.

Table 5.3 Data File (Excel®) Format

Gage Type	Gage Type Acronym	Worksheet Label
Displacements	DISP	Unit: millimeters
		Radial
		Meridional
		Hatches
		Instrumentation Frame
Gage Bar Strains	GBST	Unit: strain
		Wall-Base 90 deg
		Wall-Base 135 deg
		Wall-Base 350 deg
		Above Tendon Gallery
Liner Strains	LINST	Unit: strain
		Free-Field Hoop
		Free-Field Merid
		Free-Field Merid Anchors
		E-H Details
		A-L Details
		M-S Details
		F-W Details
		Wall-Base
		Misc Details
Pressure	PRES	Unit: MegaPascal
Rebar Strain	REBST	Unit: strain
		Free-Field Hoop
		Free-Field Merid
		Free-Field Radial Bar
		Basemat
		E-H Bars
		A-L Bars
Temperature	TEMP	Unit: °Celsius
		Inside Air (includes outside air temperature)
		Inside Liner
		Embedded Concrete
Tendons	TENDON	Unit: Newtons/strain
		Load Cells (grouped by tendon)
		Tensmegs (grouped by tendon)
		Strain Gages (grouped by tendon)
Concrete Strain*	SOFO*	Unit: strain

*Concrete strains by SOFO gages were only measured during prestressing and pressure tests.

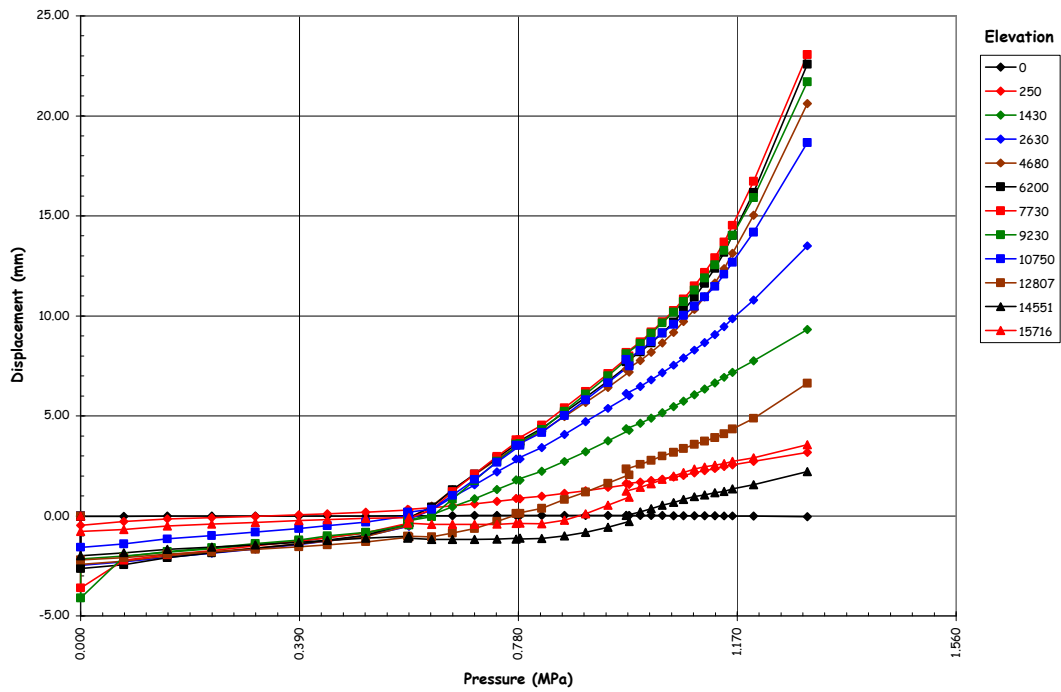


Figure 5.39 LST - Radial Displacement at Azimuth 135 degrees

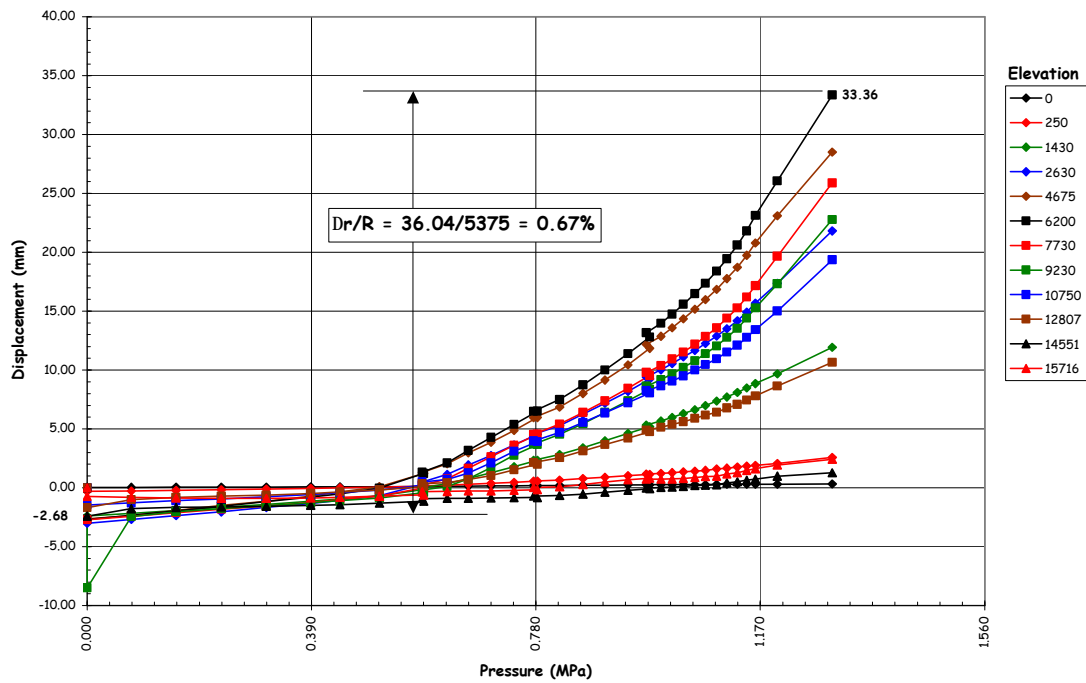


Figure 5.40 LST - Radial Displacement at Azimuth 324 degrees

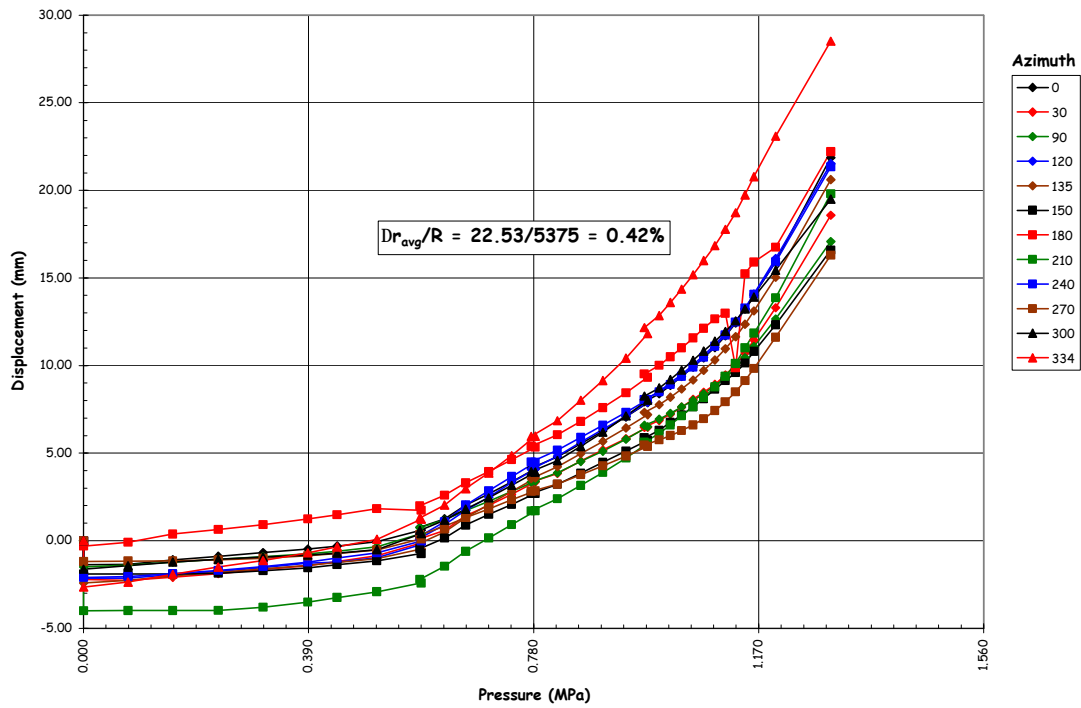


Figure 5.41 LST-Radial Displacement (DOR) at EL 4680

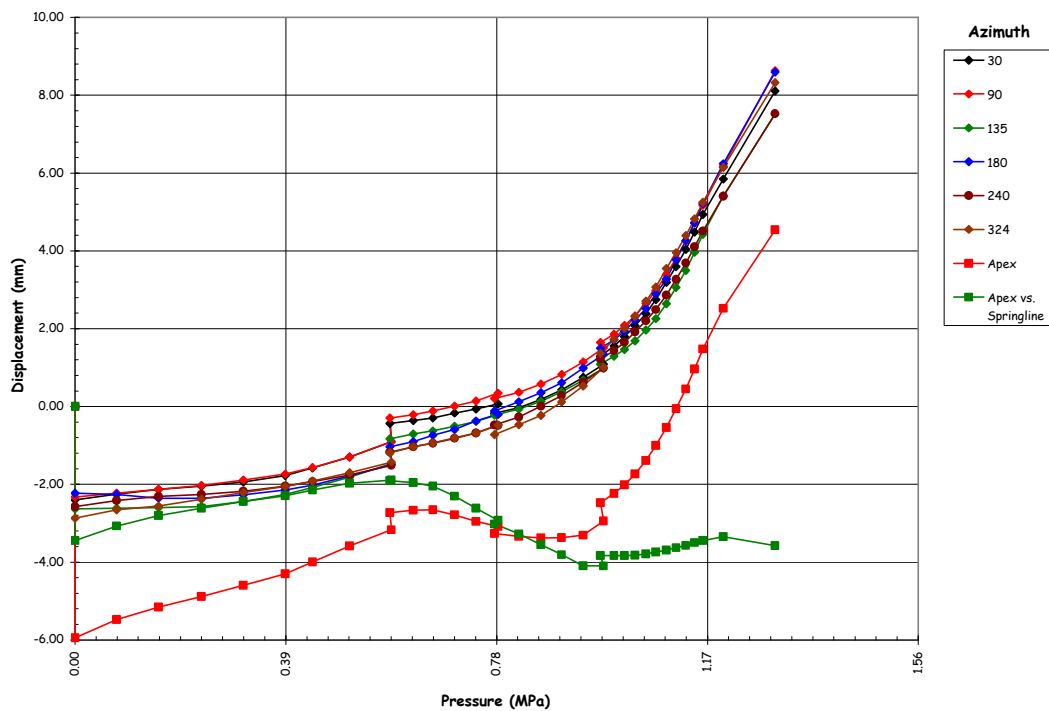


Figure 5.42 LST-Vertical Displacements (DOR) at Springline, EL. 10750

The radial displacement of the model at the cardinal elevations along Azimuth 135 degrees, selected to represent the ‘free-field’ or axisymmetric response of the model, is shown in Figure 5.39. This plot illustrates several features of the response data that should be noted. The initial values (i.e. at P=0) reflect the inside surface motion of the liner between March 3rd and the start of the LST, thereby reflecting the influence of prestressing, changes in ambient temperature, creep, etc. The response due to pressure alone is the reported displacement minus the displacement at the start of the LST (i.e., at P=0 on 10:03 a.m., 26 September, 2000).

The initial data also suggests that the liner most likely separated from the concrete wall at some locations, as evidenced by the relatively large displacements that occurred during the first pressure step. At these locations, the first increment of pressure ‘pushed’ the liner back into contact with the concrete surface. This behavior can also be observed in the SFT and SIT/ILRT data, including a restoration of the gap after depressurization. The liner separation is most likely a result of differential thermal expansion and prestressing, resulting in compressive stresses that may have bowed or slightly buckled the liner.

The response remains essentially elastic up to 1.3 to 1.5 P_d , after overcoming the prestress ($\sim 1.2 P_d$) and tensile cracking of the concrete. It is interesting to note that even though drying and shrinkage cracks were present prior to pressure testing, the onset of generalized concrete tensile cracking is quite distinct. Beyond 1.5 P_d to approximately 2 to 2.5 P_d , the response is still linear, although the loss of concrete tensile stiffness is quite distinct. Beyond 2.5 P_d , the response becomes increasingly nonlinear, particularly in the mid-section of the cylinder, as the model exhibits generalized yielding in the hoop direction.

The data also exhibits some apparent discontinuities at 1.5, 2.0, and 2.5 P_d . These apparent discontinuities coincide with the leak checks of the model and reflect, primarily, the response to changes in ambient thermal conditions over the time the model was isolated. The jump in displacement at 2.5 P_d , however, most likely includes creep effects, since the temperature was stable over the relatively short (1-1/2 hour) hold at this pressure.

Figure 5.40 displays the displacements at Azimuth 324 degrees, which coincides with the centerline of the E/H. The largest radial displacement recorded during the LST, 33.36 mm, occurred at this Azimuth at El. 6200, above the E/H. Computing the equivalent hoop strain due to pressure at this location from kinematics,

$$@P_{\max} = \frac{\Delta r}{R} = \frac{(33.36 + 2.68)}{5375} = 0.67\%$$

Similarly, calculating the local hoop strain in the vicinity of the equipment hatch at 2.5 P_d , corresponding with the onset of liner tearing and leakage, yields a value of approximately 0.28%.

Figure 5.40 again illustrates the liner separation phenomena, previously described, at elev. 9230. In this case the large magnitude of the displacement clearly indicates that the liner buckled. (A review of the post-prestressing data indicates that this occurred shortly after the completion of prestressing, most likely in conjunction with thermally-induced compressive strains.) This behavior did not, however, compromise the integrity of the liner and no tears were discovered at this location.

Figure 5.41 compares the displacement response as a function of Azimuth at elev. 4680, nominally the mid-height of the cylinder and the centerline of the E/H, A/L, and M/S penetrations. Ignoring some variation in initial conditions, reflecting some ‘out-of-roundness’ following prestressing, the response is fairly uniform, i.e. axisymmetric, except at 324 degrees, where largest deflections were already noted to occur. Averaging the radial deformation due to pressure yields a nominal average hoop strain of 0.42% at the peak pressure 3.3 P_d . Similarly, the average hoop strain at 2.5 P_d , coinciding with the onset of liner tearing and leakage, was 0.18%.

Figure 5.42 shows the vertical displacement of the springline at various azimuths. The vertical displacement at the apex and the differential displacement between the average springline displacement and the apex are also plotted. The vertical displacement exhibits similar behavior to the hoop displacements. In the vertical direction, however, the loss of stiffness due to concrete cracking occurs around 2.5 P_d . Yielding in the vertical direction does not appear to occur. This is due to the higher level of vertical prestress in the cylinder wall and the lower tensile forces induced by the pressure. The

vertical displacement is nearly uniform at the springline and the average meridional strain in the cylinder wall is less than 0.1%.

$$@P_{\max} = 3.3P_d: \quad \frac{\Delta l}{L} = \frac{(8.00 + 2.50)}{10750} = 0.10\%$$

The vertical displacements illustrate, much more dramatically, the effect of ambient temperature and creep during the leak checks.

Figure 5.42 also shows that beginning around $1.5P_d$, the dome apex deflects downward relative to the springline, most likely due to increasing force in the vertical tendons once the initial prestressing force is overcome by the pressure. (The vertical prestressing applies a compressive force on the cylinder wall approximately equal to the tensile force exerted by a pressure of $1.88P_d$.)

Deformed profiles of the PCCV model, constructed from the displacement data, are shown in Figures 5.43 through 5.45. These figures provide a more illuminating view of the model behavior than the pressure histories. The figures were constructed by applying the displacement data (exaggerated by a factor of 100) to the initial configuration of the model. The initial conditions were defined by the as-built model survey data (Appendix C). While these measurements were made in July, 1999, it was assumed that any changes in the position of the cardinal points by March, 2000 could be neglected without significant error. The motion of the cardinal points without displacement transducers were computed by linear interpolation. Both radial and vertical displacements were applied to the cardinal points and out-of-plane (i.e. circumferential) motion of the was not measured or considered.

The as-built position of the PCCV model is plotted along with the deformed shapes at the start of the LST ($P = 0$), at approximately $1.0P_d$ (0.398 MPa/57 psi), $2.0 P_d$ (0.776 MPa/113 psi), $2.5 P_d$ (0.978 MPa/142 psi), $3.0 P_d$ (1.162 MPa/169 psi), and $3.3 P_d$ (1.295 MPa/188 psi).

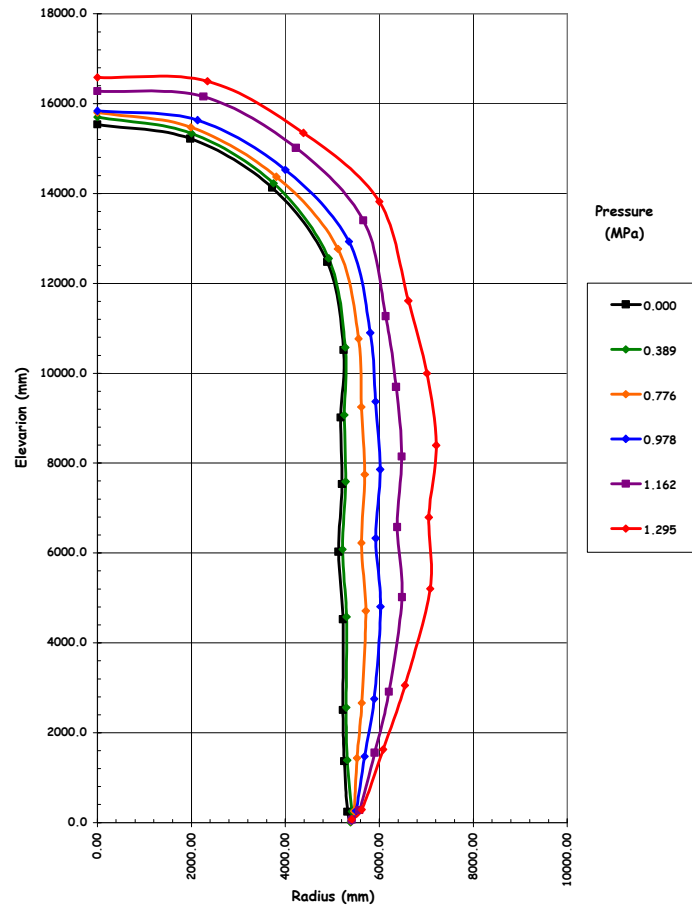
The figures illustrate a few interesting points about the behavior of the PCCV model.

First, and most importantly, the radial deformations are smallest at the buttresses (90 degrees and 270 degrees) and larger between the buttresses (0 degrees and 180 degrees), illustrating the stiffening effect of the buttresses even though the net hoop prestressing force is smallest at the buttress. The largest radial deformations are at the E/H and A/L penetrations, showing the reduced stiffness of these regions in spite of thickening and added conventional reinforcing. This reduction in stiffness is due to the lower prestressing forces as the tendons are deflected around the penetrations in addition to the opening itself.

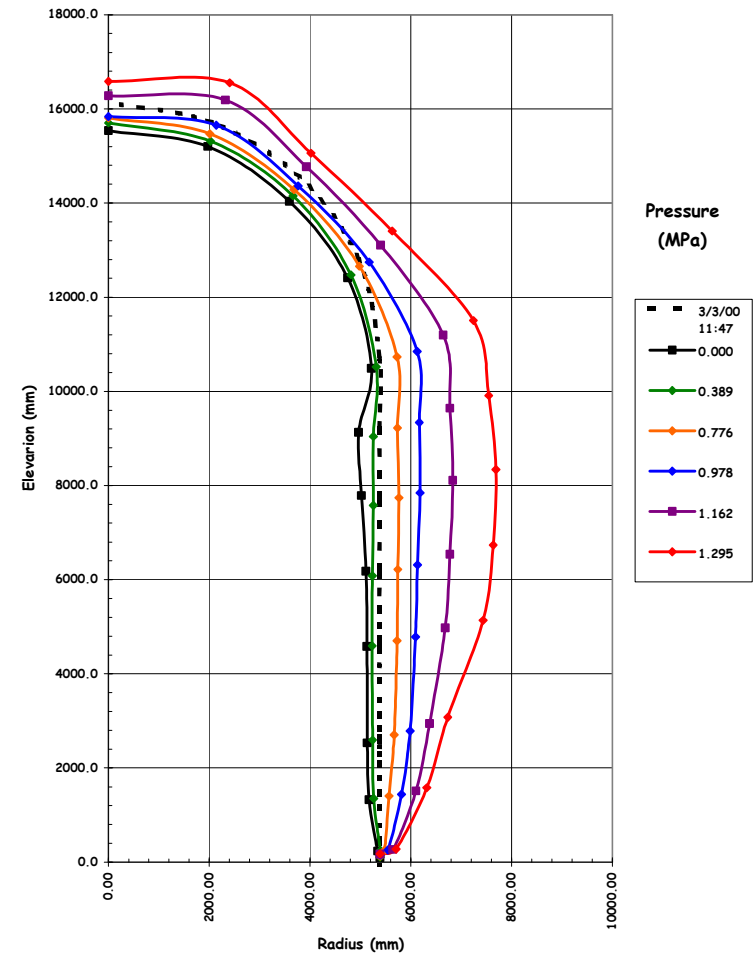
Secondly, the vertical profiles do not show any reverse curvature at the wall-base junction and seem to imply the presence of a hinge forming at this location. While a hinge may have occurred, this deformation pattern may be more reflective of an instrumentation artifact than the model's behavior in this region. The displacement transducers at the wall-base junction were anchored to the base liner immediately adjacent to the wall, while the displacements above this point were measure relative to the instrumentation frame. It is likely that the differential displacement measured at the wall-base junction does not accurately reflect the total displacement in this region, and the data should be viewed with this limitation in mind.

Finally, a few other minor observations:

- The unusual deformation patten in the dome at 135 degrees and 324 degrees coincides with the regions where the East-West and North-South sets of vertical tendons overlap with the hoop tendons in the dome, where higher prestressing forces are present than in other regions of the dome.
- The initial buckling of the liner at Azimuth 324 degrees, elev. 9230 is clearly shown in Figure 5.44.

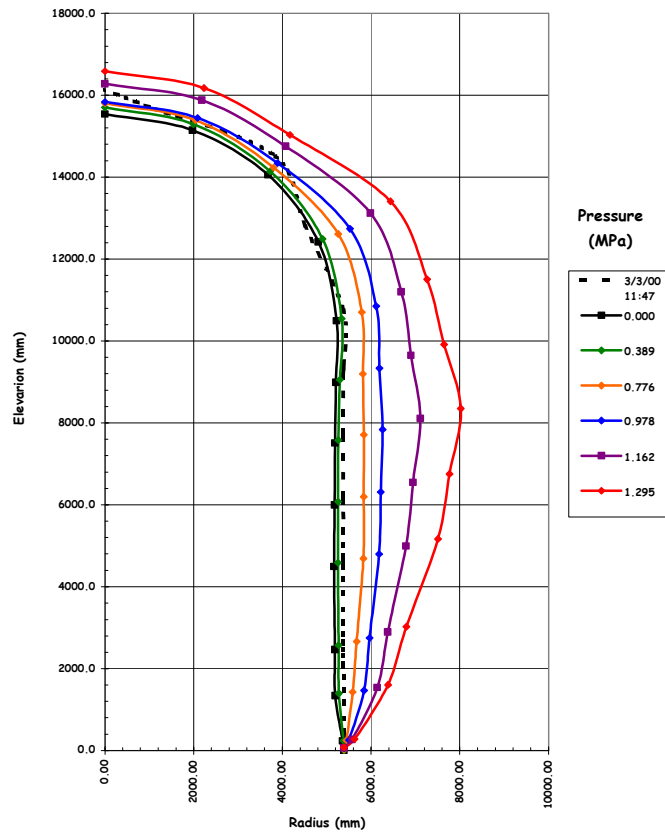


(90°)

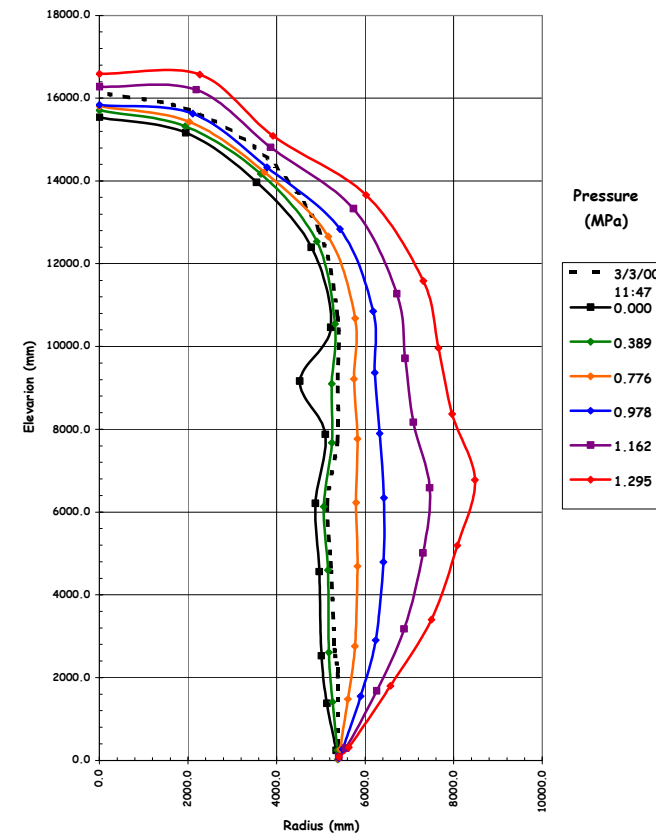


(135°)

Figure 5.43 LST - Deformation at Azimuth 90 degrees and 135 degrees (D and Z) $\times 100$



(240°)



(324°)

Figure 5.44 LST - Deformation at Azimuth 240 degrees and 324 degrees (I and L) $\times 100$

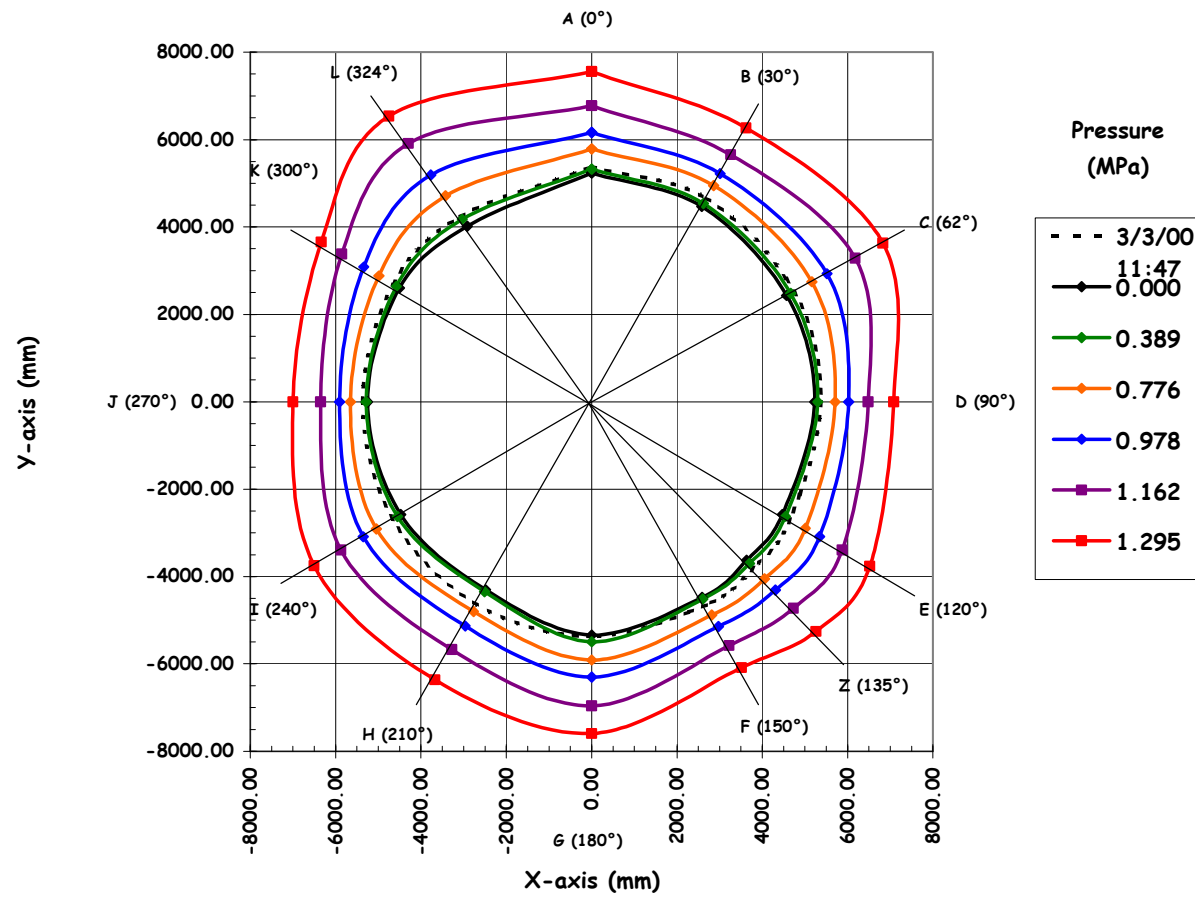


Figure 5.45 LST - Deformation at Elev. 4680 (5) \times 100

5.3.2.1.2 Liner Strains

Five hundred and fifty-nine strain gages were placed on both surfaces of the liner to measure both the meridional and hoop free-field liner strains, as well as local strains at the penetrations, the wall-base junction, liner anchor, and stiffeners where discontinuities might result in high local strains prior to the liner tearing. The data for each of these gages is provided on the enclosed CD. The majority of these gages did not record significant strains, however, gages at a number of locations deserve closer inspection. Table 5.4 summarizes the maximum strains recorded during the LST at locations of interest.

Before considering several of these locations in detail, it is worth noting that individual strain gages can provide misleading information due to their sensitivity to local as-built conditions, particularly in areas of sharp discontinuities and high strain gradients. As a result, it is more meaningful to consider sets of gages in these locations, thus providing a more realistic view of the strain field in a particular area.

Figure 5.46 shows all the free-field liner hoop strain gages that exceeded 0.5% at the end of the test. It is interesting to note that up to 2.5 Pd, the free-field liner strain hoop strains were almost all below 0.2%, which compares favorably with the average hoop strain computed from the displacements, 0.18%.

Nearly all the free-field liner and liner anchor meridional strain gages were below 0.1%, which is also consistent with the displacement data.

Considering the liner strains near penetrations and other discontinuities, the strains in the vicinity of the E/H are of primary interest since there were indications during the LST that the liner initially tore in this region. Posttest inspection of the liner, described in Section 5.3.2.2, revealed several tears at the edges of the embossment (Figure 5.47), but no apparent damage near the insert plate. The layout of the liner strain gages is shown on Drawing D-SN-P-218 (Appendix E), and reproduced in Figure 5.48 for reference. The highest strains in this region were at the left and right edges of the embossment. The strains adjacent to the insert plate (#19 to #67) were small, nearly all less than 0.2% at maximum pressure, with only a few near the ends of anchors or stiffeners reaching 0.5%.

Table 5.4 LST Liner Strain Summary

Maximum Free-Field Hoop Strain	0.90%
Maximum Free-Field Meridional Strain	0.14%
Maximum Meridional Anchor Strain	0.10%
Maximum Equipment Hatch Strain	3.88%
Maximum Personnel Airlock Strain	0.75%
Maximum Main Steam Penetration Strain	4.54%
Maximum Feedwater Penetration Strain	6.39%
Maximum Wall-Base Junction Strain	1.97%
Maximum Miscellaneous Liner Details Strain	5.75%

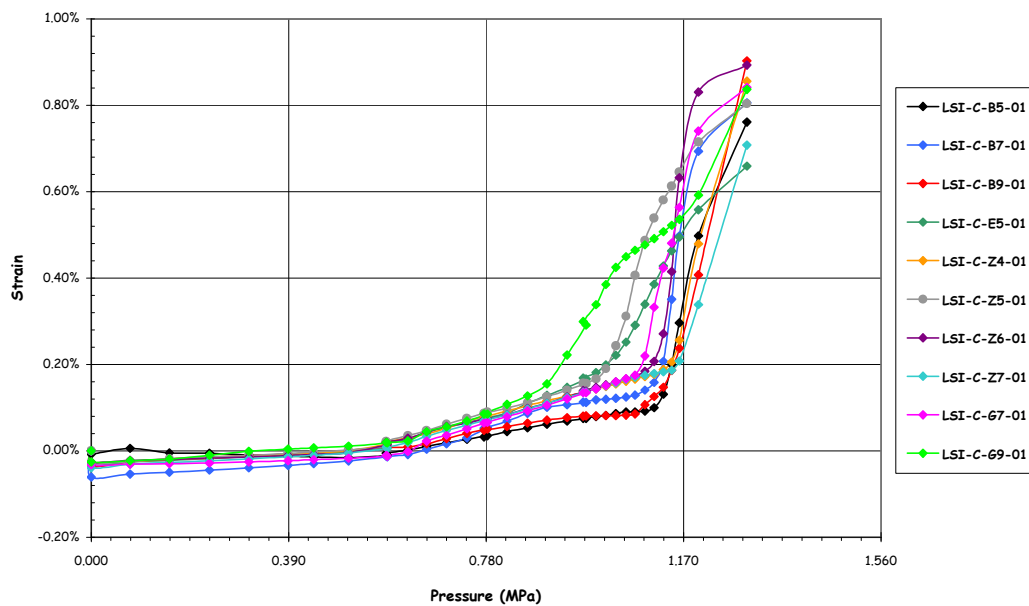


Figure 5.46 LST – Free-Field Liner Hoop Strains



Figure 5.47 Liner Tear (#15) at E/H

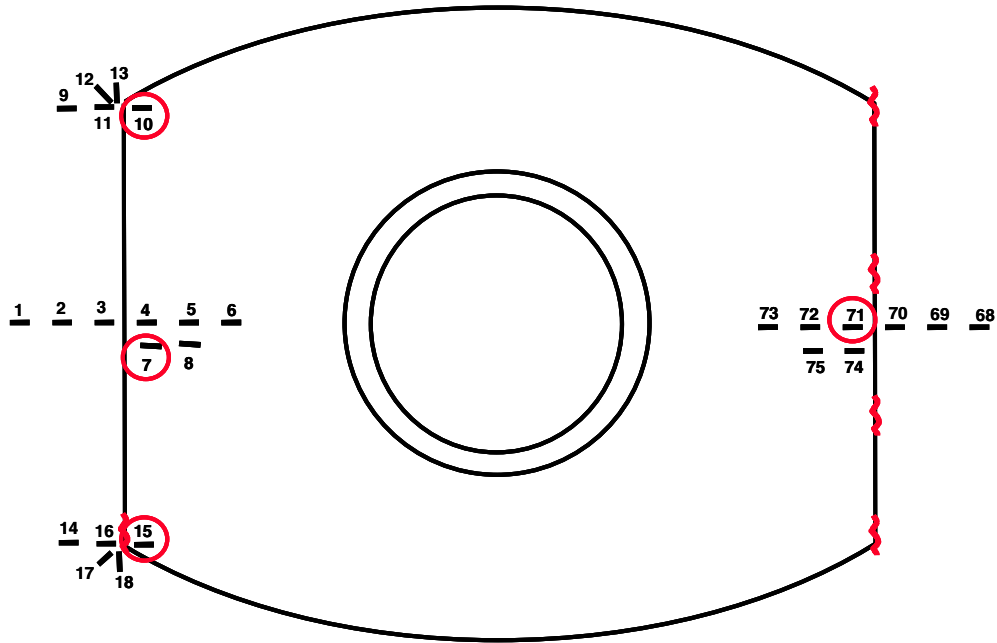


Figure 5.48 Equipment Hatch Liner Strain Gage Layout (Inside View)

The strains at the middle of the ‘left’ (#1-8) and right (#68-75) edges of the embossment are shown in Figures 5.49 and 5.50. The strains at the upper and lower ‘left’ corners are shown in Figure 5.51. With the exception of gage #7, the strains at the mid-sides of the embossment are all very small until global yielding of the model occurs just below $3P_d$. At the corners, however, liner strains begin increasing earlier, with gage #10 showing increasing strains beginning at $1.5P_d$, while most of the other gages show significant increases beginning at $2.5P_d$, when liner tearing was believed to

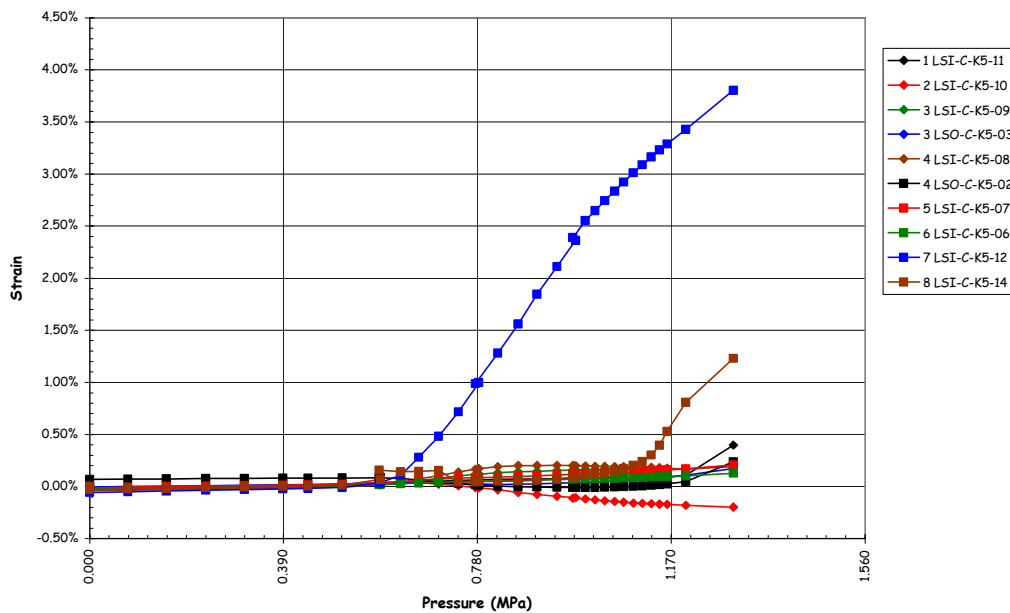


Figure 5.49 E/H Liner Strains at ‘Left’ Edge of Embossment

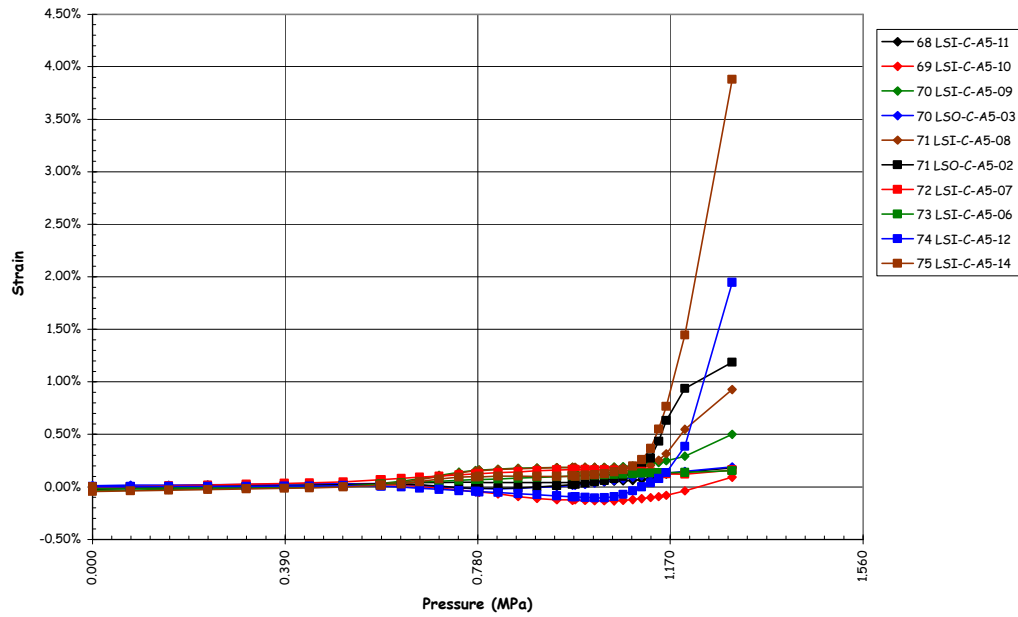


Figure 5.50 E/H Liner Strains at 'Right' Edge of Embossment

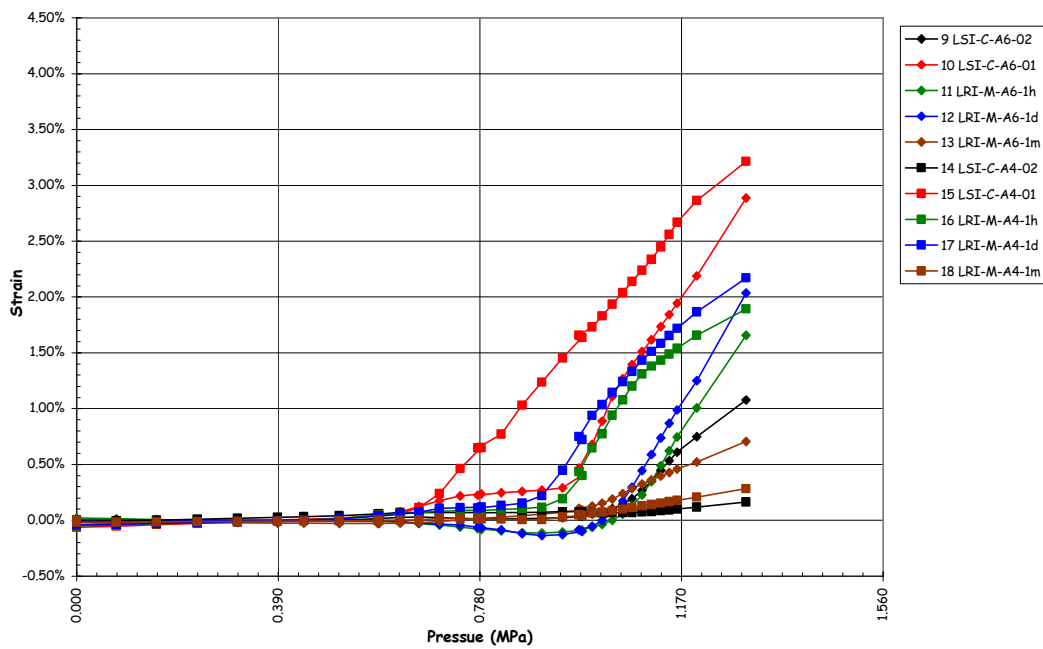


Figure 5.51 E/H Liner Strains at 'Left' Corners of Embossment

have occurred. At first glance, it appears unfortunate that the liner tore on the opposite side from the strain gages (pretest analyses suggested the highest strains would occur on the 'left' side). However, it has been found that strain gages near tears often see lower strains than would be expected, since the tear acts as a strain relief mechanism. While it is apparent that the strains on the 'right' side were higher, it is unlikely that gages at those locations would have recorded higher strains than those on the left side. This is demonstrated by comparing gages #7 on the left and its mirror image, #74, on the right.

Note that at the pressure $2.5 P_d$, when the liner tearing is believed to have begun, the measured strains were only on the order of 0.75% to 1.50%.

The liner strain at the A/L shows a similar pattern to those at the E/H, with a peak tensile strain at the corner of the embossment of 0.75%. However, no tears occurred at this penetration.

Liner strains at the M/S and F/W penetrations are shown in Figures 5.52 and 5.53. The layout of the liner strain gages is shown on Drawing D-SN-P-220 (Appendix E).

Several large tears occurred at each end of the F/W penetration, beginning at the weld between the thickened insert plate and the liner; however, no tears occurred at the M/S penetration event, though the free-field hoop strains at the M/S are higher since it is closer to the mid-height of the cylinder. There are a number of reasons why this occurred, primarily liner fabrication issues discussed in Section 5.3.2.2. It is interesting to note that even though the strain gages at the F/W penetration were located near the tear (see Figure 5.54), measured strains were relatively low until the very end of the LST, when some strains increased very rapidly. This might indicate that a tear in the vicinity of a strain gage can act as a strain relief mechanism on the surrounding material. The 'jump' in the strain near the end of the test may also be due to material distortion in the vicinity of the tear as the tear propagated. On the other hand, the strains recorded at the M/S penetration begin to climb rapidly at 2.0 to $2.5 P_d$, reaching values as high as 4.5% without resulting in any liner tearing. Detailed inspections of this location did not reveal any evidence of the fabrication problems that were present at the F/W penetration.

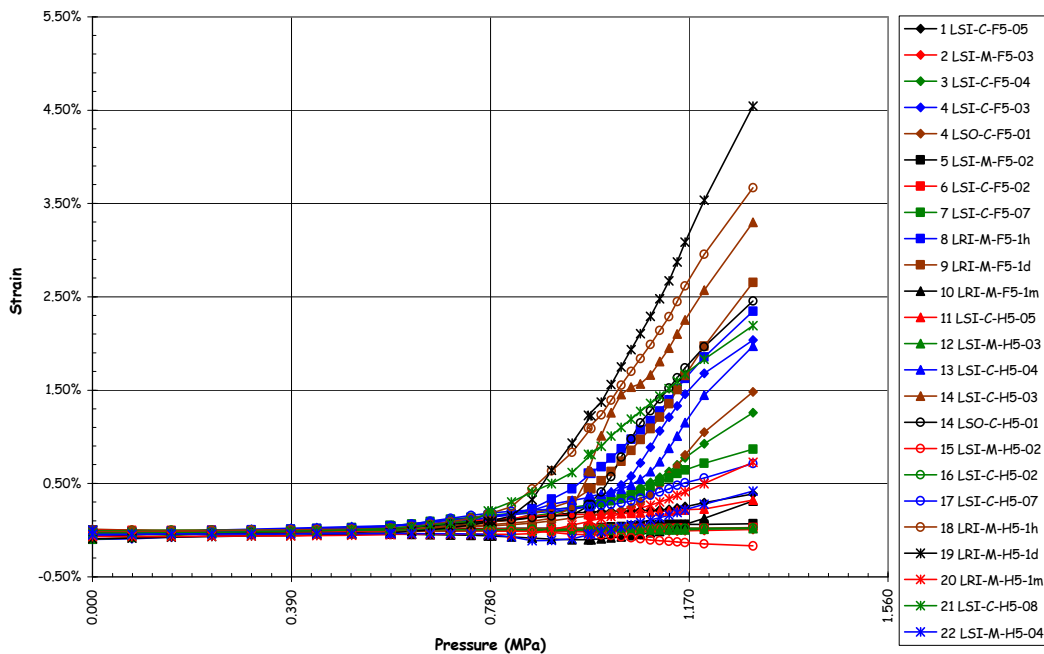


Figure 5.52 Liner Strains (DOR) at M/S (Ref. D-SN-P-220)

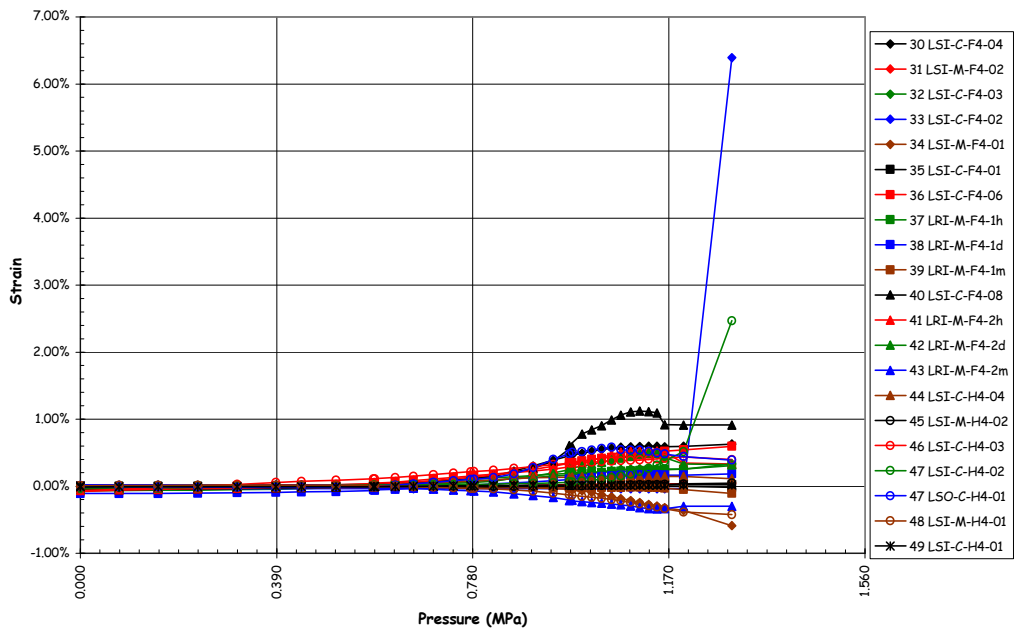


Figure 5.53 Liner Strains (DOR) at F/W (F=Ref. D-SN-P-220)

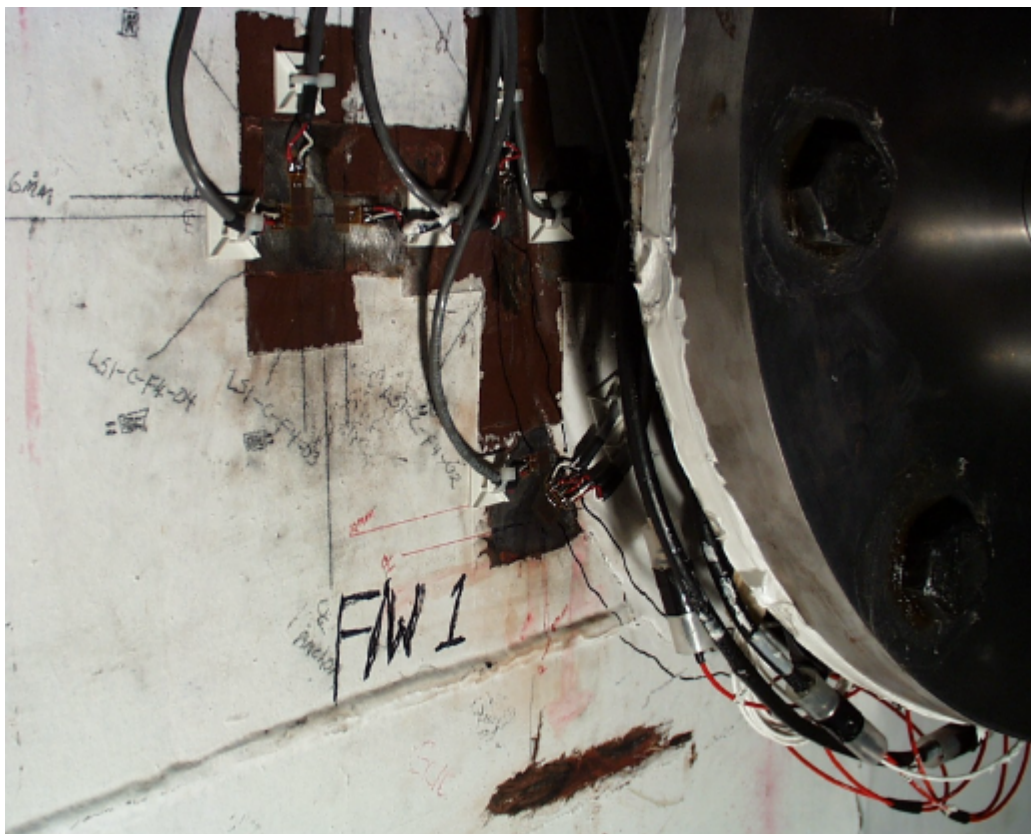


Figure 5.54 Liner Tear (#3) and Strain Gages at F/W Penetration

A number of other details believed to create potential strain concentrations in the liner were also instrumented and monitored during the test. One of these details occurs throughout the model: a gap is left in a horizontal stiffener or vertical anchor where it crosses a liner seam welds (Figure 5.55), euphemistically called a ‘rathole.’ In previous containment model tests, this detail caused significant strain concentrations when the surrounding liner began to yield. In fact, a number of the liner tears found after the test occurred at these details. One such detail that was instrumented was located near the intersection of cardinal lines D7 (Azimuth 90 degrees, elev. 7730). Although a tear occurred in a similar detail above this location, the liner did not tear at this rathole and the strains recorded at this location provided valuable information regarding the behavior of this detail for comparison with analyses.

The interior strain gages at D7 are also shown after the LST in Figure 5.56. The arrangement of these gages is shown on Drawing D-SN-P-209, Detail a.4 (Appendix E). Strains begin increasing between 2.0 and 2.5Pd, reaching a maximum of 5.7% at the maximum pressure. Nevertheless, the liner did not tear. A subsequent comparison of this detail to similar rathole details that did tear, but were not instrumented, revealed a lack of any weld repairs, which was not true of the other locations. This detail appears to demonstrate that the liner is capable of undergoing significant local strain without tearing in the absence of any other factors that might degrade the liner.

5.3.2.1.3 Rebar and Concrete Strains

The reinforcing steel strains are summarized in Table 5.5. Typically, after the onset of global yielding, the rebar strains were higher than the corresponding strains computed from displacements and the free-field liner strains. This phenomena was recognized during gage calibration and occurs due to a local reduction in cross-section from grinding away a portion of the bar to mount the strain gage. The effect of this local cross-section reduction causes the bar to yield at the gage location slightly before the rest of the bar yields. The effect on the rebar strain readings is to introduce an artificial strain increment, on the order of 0.5% strain, after the bar has yielded, compared to the strain that would occur if the gage were not present. This artifact can be illustrated by considering the hoop strain measurements at Z6 shown in Figure 5.57. Attempts were made to develop an algorithm to correct for this gage artifact; however, the results were not particularly useful. The rebar strain data included on the data CD were not corrected for this artifact, which any interpretation of this data should consider.

Figure 5.57 compares the hoop strains recorded at the mid-height of the cylinder wall (Z6: Azimuth 135 degrees, elev. 6280) by the fiber optic gages (CE), rebar strain gages (RS), liner strain gage (LI) and computed from the displacement (DT). The strains track each other very well until local yielding occurs in the liner and, shortly after, in the rebar. The fiber optic gage continues to track the displacement and provides a much more accurate measure of the hoop strain in the wall than the LI or RS gages.



Figure 5.55 Horizontal Stiffener Detail at Vertical Seam Weld (‘Rathole’) near D7

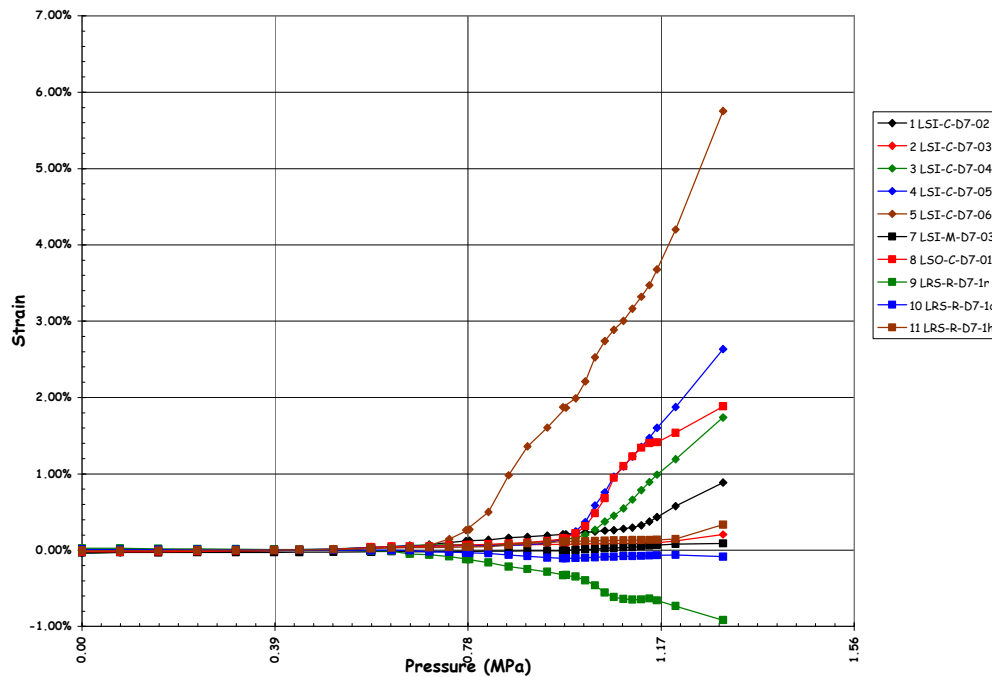


Figure 5.56 Liner Strains (DOR) at D7 Anchor Detail (Ref. R-SN-P-209, a.4)

Table 5.5 Rebar Strain Summary

Maximum Free Field Hoop Rebar Strain	1.68%
Maximum Free Field Meridional Rebar Strain*	0.47%
Maximum Free Field Radial Rebar Strain	0.88%
Maximum Basemat Rebar Strain	0.84%
Maximum Rebar Strain at E/H	1.62%
Maximum Rebar Strain at A/L	1.50%

* One gage (RS-M-A0-07) recorded a maximum strain of 6.11%. However, the initial strain of the start of the LST was 5.85%, yielding a change in strain of 0.27%. The initial high strain reading was due to an increase in resistance not associated with strain of the bar.

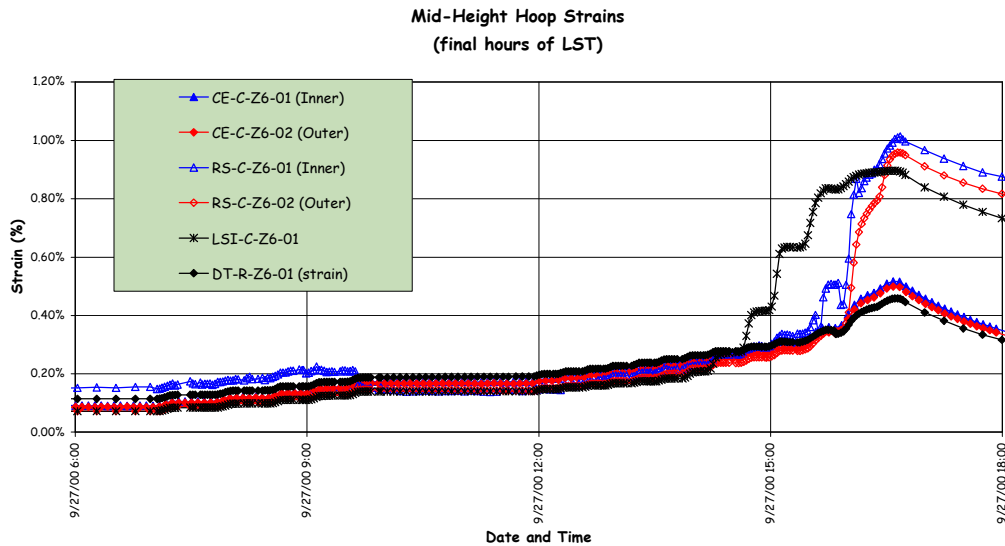


Figure 5.57 Comparison of Strain at Z6 (Azimuth 135 degrees, Elev. 6280)

Strain gages were also installed on specially fabricated ‘gage bars,’ which were located at several azimuths (90 degrees, 135 degrees and 350 degrees) at the wall-base junction in an attempt to get a more accurate picture of the strain fields at this location due to the presence of large bending forces under pressure (Figure 5.58). Unfortunately, a large number of these gages were damaged during construction and only very limited data was obtained. (Since the gage bars were embedded in the basemat, they were placed at the time of the final basemat lift and left exposed for almost two years until the first cylinder wall lift was placed. During this time, they were exposed to the weather and some rough handling by the construction workers.) However, enough gages survived at 135 degrees that it is possible to construct a picture of the strain history at this location. Figure 5.59 shows the distribution of strain *due to pressure only* at four elevations (86, 201, 312, and 427) above the top of the basemat. Only the strain due to pressure is plotted, since the initial strains due to dead load and prestressing are somewhat ambiguous and mask the pressure response. The strains recorded by the surviving gages at each elevation are plotted at pressure levels corresponding to $1P_d$, $2P_d$, $2.5P_d$, $3P_d$, and $3.3P_d$. While these results are incomplete, they do show the increasing curvature of the cross-section as a function of pressure, especially at elev. 427.

Some gage bars were also located in the basemat, above the tendon gallery, in an attempt to measure tensile strains that might develop at this location. However, there was no indication of any damage in this region and, with a few ambiguous exceptions, the gages did not record any response to the pressure loads.

Overall, in spite of the significant effort (and expense) involved in the application and installation of the rebar strain gages, the resulting data is only marginally useful and any future tests of a similar nature would be advised to consider the method of installing strain gages on rebar and to limit the number of gages to a few, critical locations.

5.3.2.1.4 Tendon Forces and Strains

Since the unique feature of this model, compared to previous large-scale containment models tested at SNL, is the prestressing system, and the behavior of this system to pressure loads beyond design levels is of particular interest, a significant effort was made to measure the response of the tendons. Both tendon anchor forces, as well as strains along the length of the tendons, were measured. Unfortunately, as noted in Chapter 2, approximately 50% of the strain gages installed on the tendons strands were damaged during construction and/or prestressing. Furthermore, data from the Tensmeg gages indicates the likelihood that these gages de-bonded or slipped relative to the tendon strands, casting some doubt on the accuracy of the data.

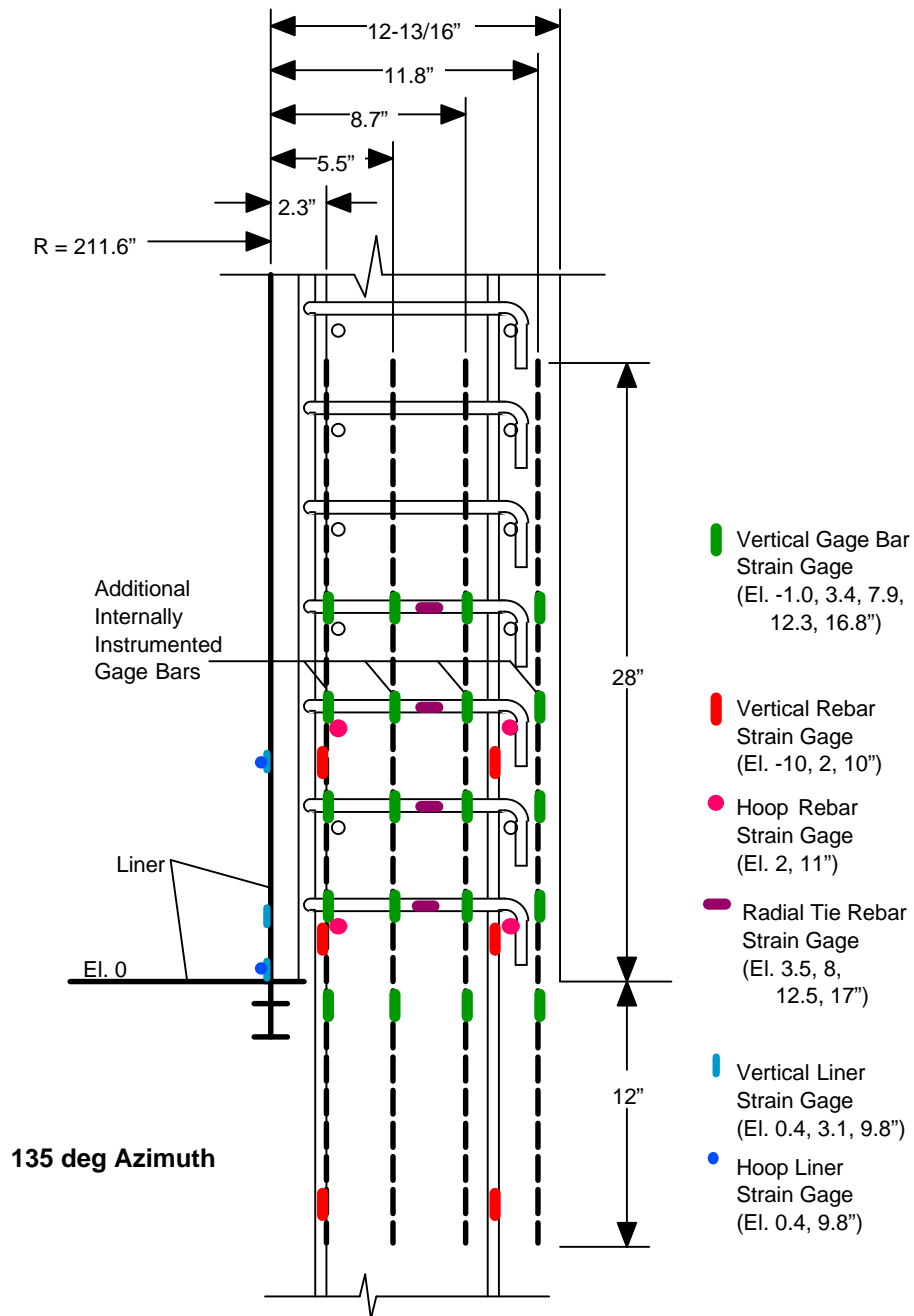


Figure 5.58 Arrangement of Gage Bar Strain Gages at Azimuth 135 degrees

Nevertheless, the surviving gages provide some significant insight into the response of the tendons to the pressure loading. All of the tendon data (load cells and strain gages) is provided on the enclosed CD, as described in Section 5.3.1. A summary of the data and a discussion of the LST results follows.

One-sixth of the tendons in the model were equipped with load cells at each anchor prior to prestressing. Figures 5.60 through 5.62 illustrate the tendon anchor forces during the LST. The anchor forces for the vertical tendons with load cells are shown in Figure 5.60. The anchor forces are shown for the maximum tensioning force during prestressing, after the completion of prestressing (on 5/4/00) and during the LST at $0.0P_d$, $1.0P_d$, $2.0P_d$, $2.5P_d$, $3.0P_d$ and at maximum pressure, $3.3P_d$. Similarly, Figures 5.61 and 5.62 show the anchor forces for the hoop tendons anchored at the 90 degree

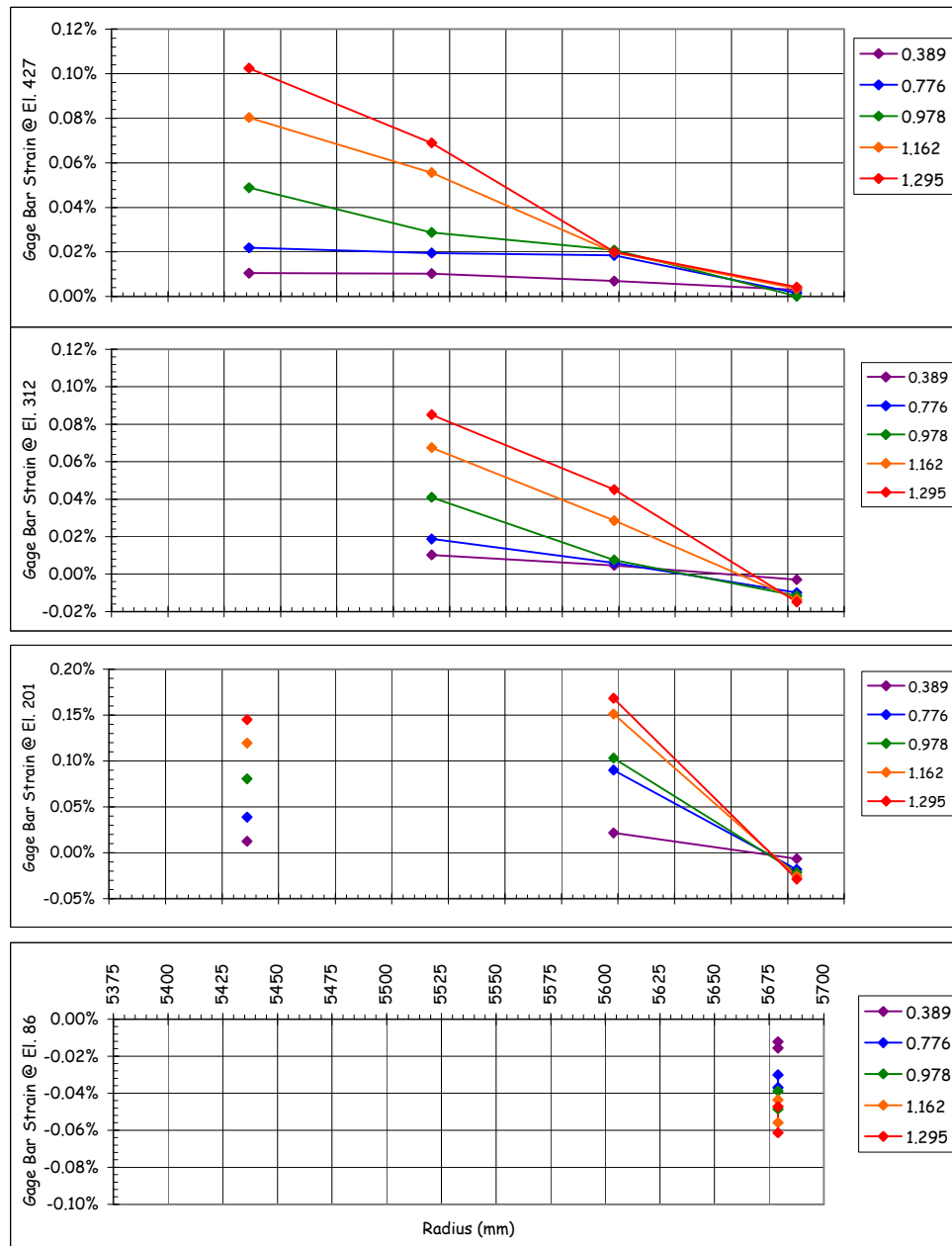


Figure 5.59 LST Gage Bars Strains at Azimuth 135 degrees (due to pressure only)

and 270 degree buttresses. In general, the vertical tendon anchor forces did not exceed the initial tensioning force. The average vertical tendon force at the peak pressure of $3.3P_d$ was 466 kN (104.7 kips) compared to the average tensioning force of 472 kN (106.3 kips). The hoop tendon anchor forces, however, did exceed the initial tensioning force of 424 kN (95.3 kips). The maximum anchor force recorded at the peak pressure of $3.3P_d$ was 550 kN (123.64 kips) for tendon H53. The average anchor force for all the hoop tendons at the peak pressure was 496 kN (111.6 kips). The tendon yield strength (0.2% offset) is approximately 590 kN (132.6 kips), so hoop tendon forces at the anchors were approaching, but had not exceeded their yield strength.

Eight tendons, five hoop tendons (H11, H35, H53, H67, and H68) and three vertical tendons (V37, V46, and V85), were instrumented along their length by placing strain gages on individual strand wires at specified locations. The surviving bonded foil gages are believed to have provided the most reliable data on the strain in the tendons. Figure 5.63 plots the strain history during the LST of the surviving gages on tendon H68. This plot illustrates the variability between strains in different strand wires at roughly the same position along the tendon. Nevertheless, considering an average strain of approximately 0.40% at the start of the LST, the increase in the average strain to 0.80% is nearly identical to the average hoop strain computed from the displacements, at 0.42%.

A more useful way of analyzing the tendon response data is by constructing the tendon force profiles at pressures during the LST, similar to the force profiles constructed for the prestressing loads (see Figures 2.66-2.73). The tendon force profiles for the five instrumented hoop tendons are shown in Figures 5.64 to 5.68. The force profiles include the design and measured values at maximum tension and after seating, and the recorded response during the LST at $0.0P_d$, $1.0P_d$ (0.389 MPa/56.4 psi), $2.0P_d$ (0.776 MPa/112.5 psi), $2.5P_d$ (0.978 MPa/141.8 psi), $3.0P_d$ (1.162 MPa/168.5 psi), and at the maximum pressure, $3.3P_d$ (1.295 MPa/187.8 psi). The profiles are also shown during depressurization at approximately $2.5P_d$, $2.0P_d$, $1.0P_d$, and $0.0P_d$. These force profiles were constructed by converting the average strain from all the foil strain gages at a given position to a force using the actual tendon force-strain test data and combining the computed forces with load cell data. When only a single strain gage survived at a given position, it is noted on the profile.

There is not adequate data to assume the shape of the hoop tendon force profile between the surviving measurement positions, so only the force at the measurement locations are shown. There is enough data to suggest, however, that the tendon force distribution tends to become more uniform, with the largest increase in strain occurring near the mid-point of the tendon, where the initial prestressing force was the smallest. This may be due to a combination of local yielding and/or slipping as the tendons try to maintain equilibrium and local deformation of the cylinder wall. Comparing the differential strain at the midpoint of the tendons to the hoop strain calculated from the wall displacement at that location (see Figures 5.66 and 5.67) indicates that the tendon strain is greater than what would be expected if the tendon did not slip relative to the wall. After unloading, however, the initial tendon force profile (at the start of the LST) is almost completely recovered, which implies that any redistribution occurring during the LST is entirely elastic. This is not a completely satisfying observation, since it would seem likely that any redistribution of tendon forces due to slipping would remain after depressurizing. This reinforces the observation that the change in tendon forces is also due to the local elastic deformation of the wall.

The force profiles for the vertical tendons, constructed in the same manner as the hoop tendon profiles, are shown in Figures 5.69 to 5.71. Again, since the gage mortality was lower for the vertical tendons than the hoop tendons and the force profile is more nearly a continuous function, curves were fit through the data to facilitate interpretation and comparison of the data with the design assumptions. The data again shows that the vertical tendon force distribution becomes more uniform as the pressure increases, and the largest relative increase occurs at the mid-point of the tendon, i.e. the apex, for the vertical tendons. This suggests that the tendons must slip relative to the concrete wall to allow the forces to redistribute; however, as with the hoop tendons, recovery of the initial tendon force distribution is nearly complete after depressurization. In this case, however, it is difficult to argue that the tendon force distribution is dominated by the local radial deformation of the concrete wall/dome, since those in the dome are much smaller than those in the cylinder wall, which is inconsistent with the observed change in the force distribution.

While the tendon response measurements provided new insight into the behavior of unbonded tendons under limit load conditions, some apparent paradoxes were identified that might be answered by further testing and analysis. One conclusion is apparent and undeniable, however. The change in tendon anchor forces is not a reliable indicator, by itself, of the change in force along the length of the tendons, and any attempts to preclude tendon rupture by measuring only the anchor force will not be adequate.

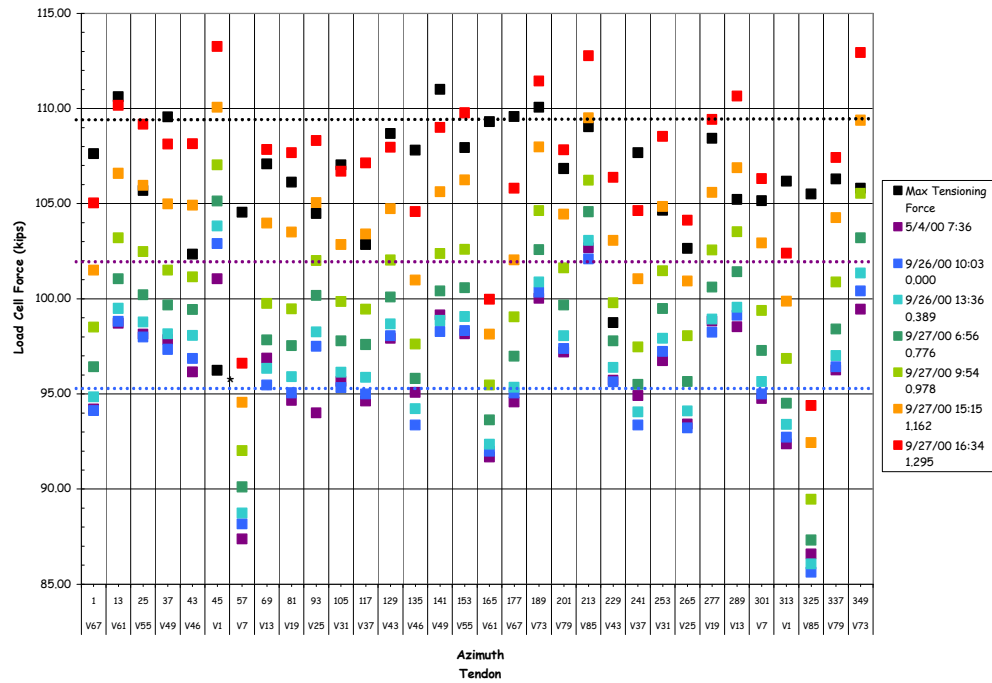


Figure 5.60 LST - Vertical Load Cells

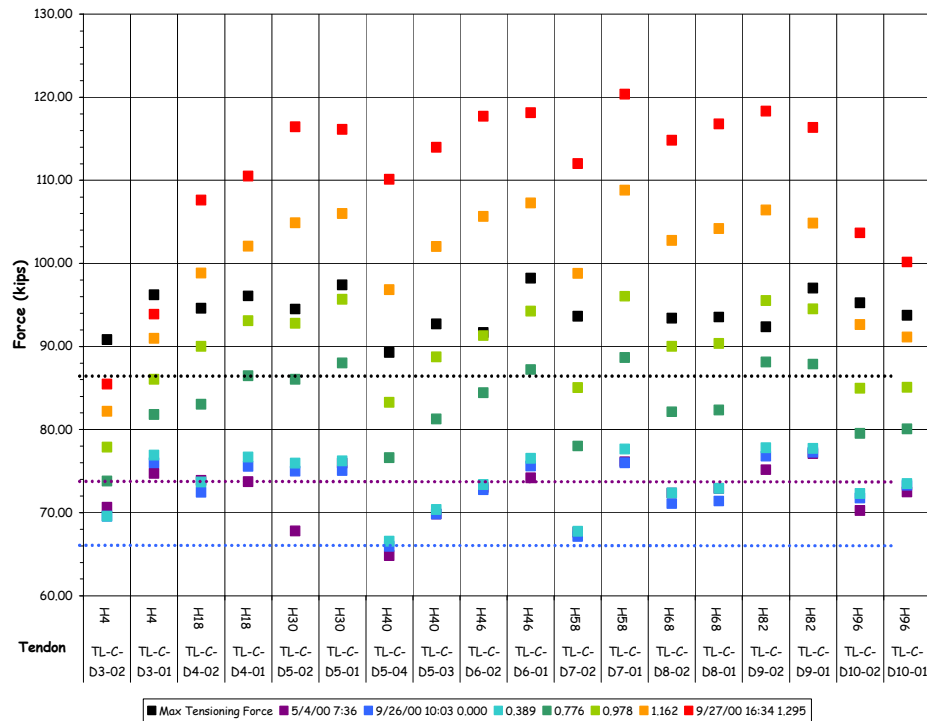


Figure 5.61 LST - Hoop Load Cells at 90 degrees

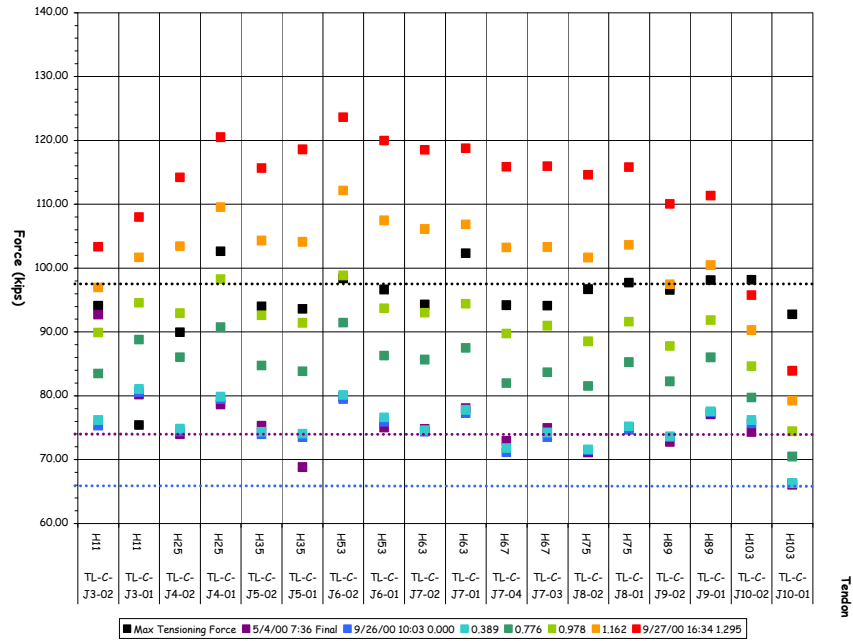


Figure 5.62 LST - Hoop Load Cells at 270 degrees

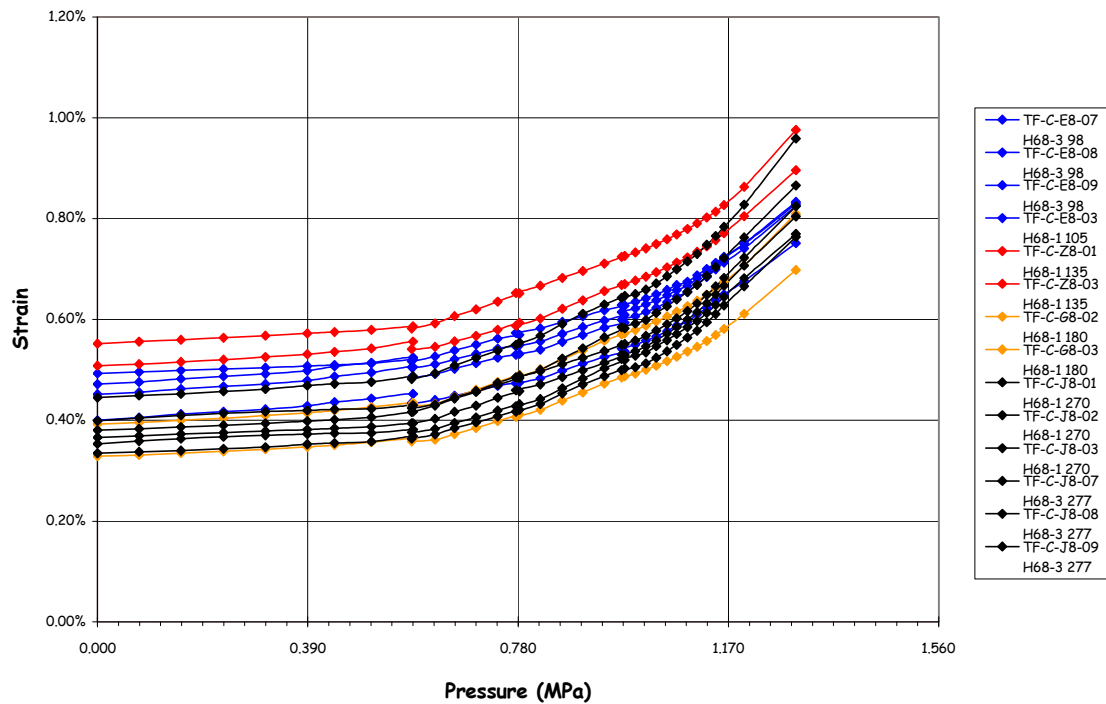


Figure 5.63 LST - H68 Tendon Strains

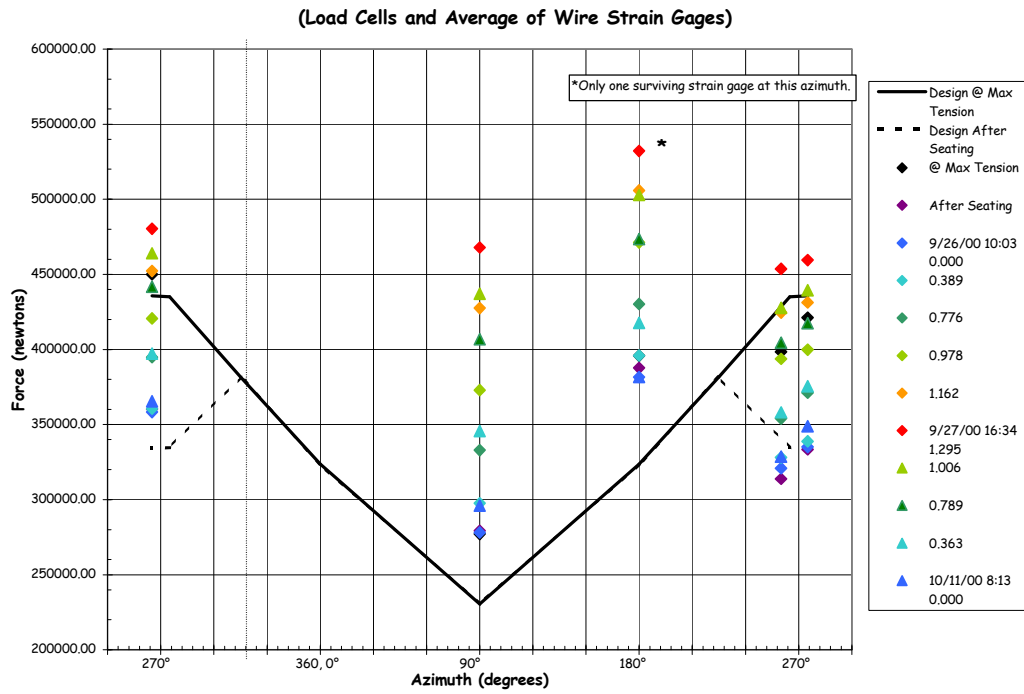


Figure 5.64 H11 Tendon Force Distribution, El. 1854

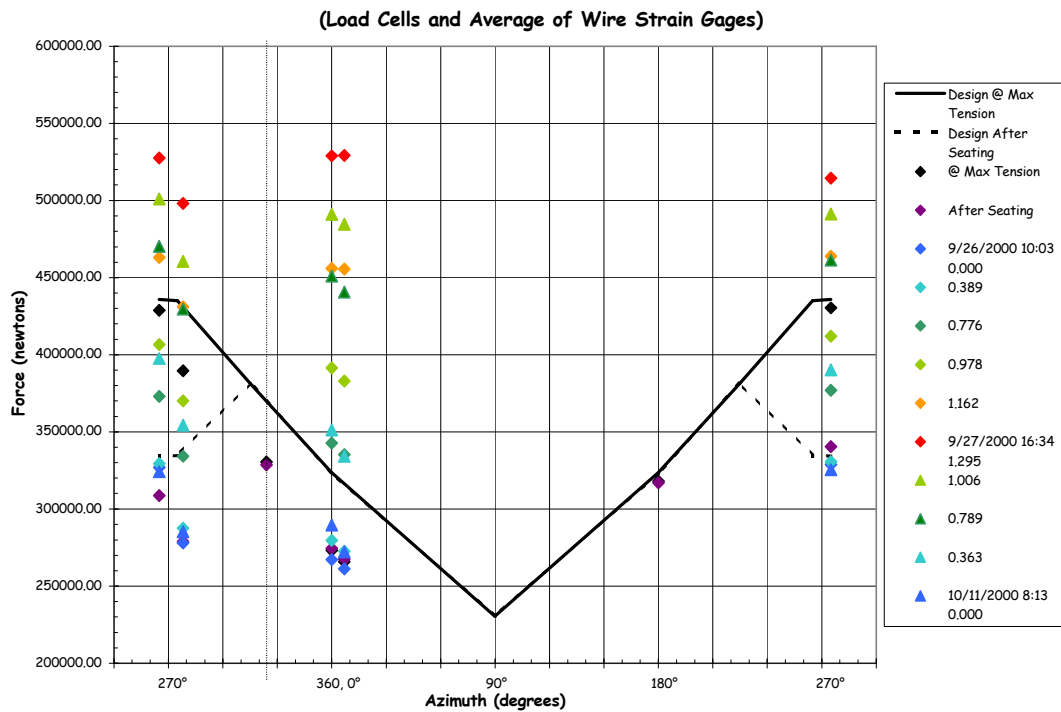


Figure 5.65 H35 Tendon Force Distribution, Elev. 4572

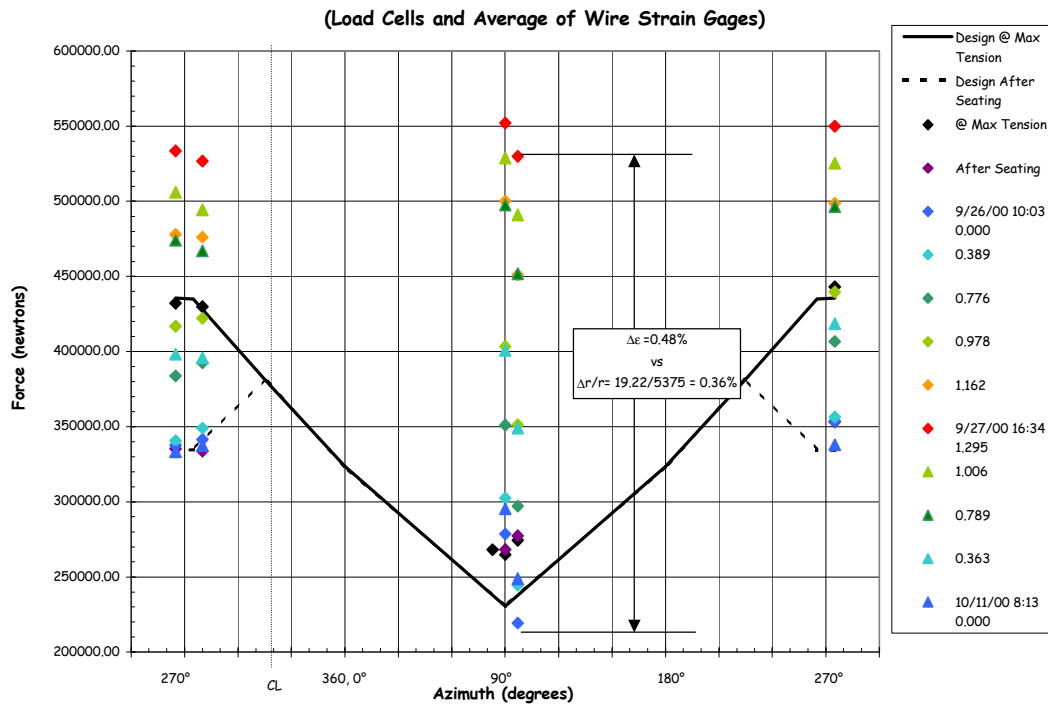


Figure 5.66 H53 Tendon Force Distribution, Elev. 6579

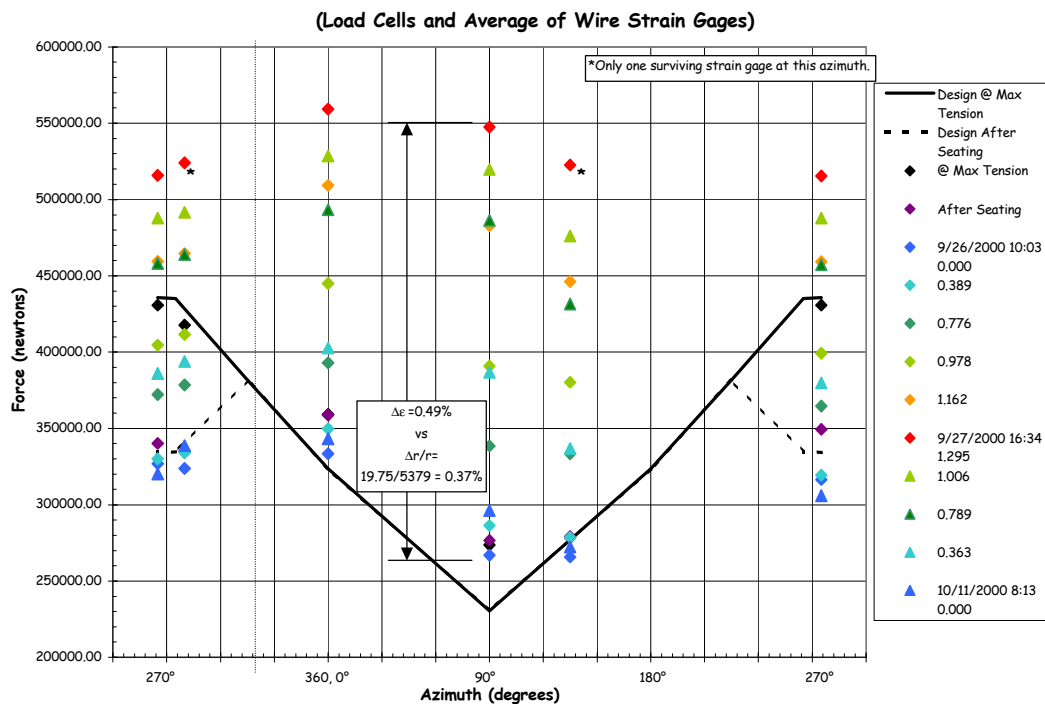


Figure 5.67 H67 Tendon Force Distribution, Elev. 8153

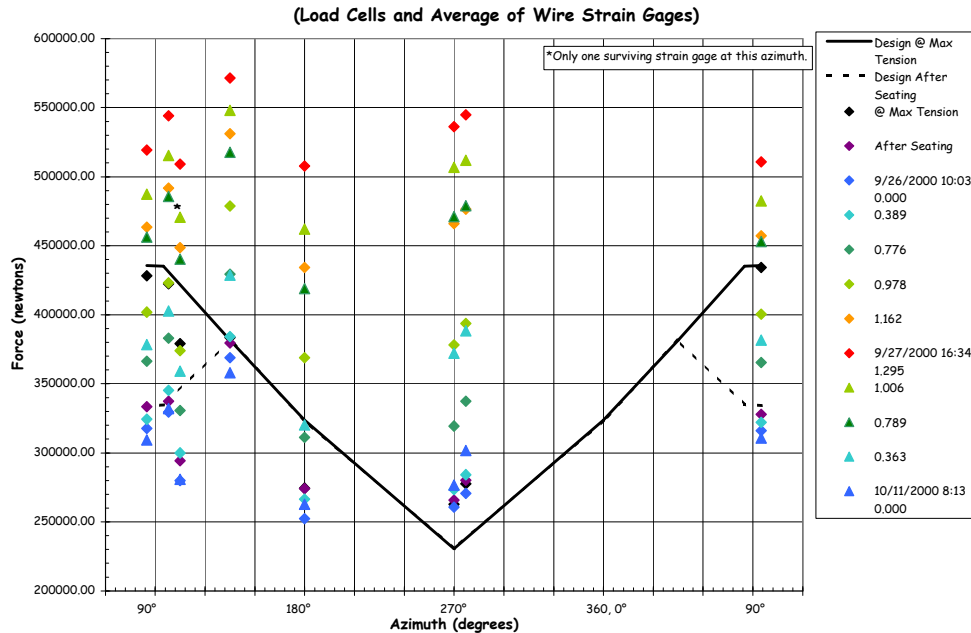


Figure 5.68 H68 Tendon Force Distribution, Elev. 8280

5.3.2.1.5 Acoustic Response

The complete reports from the Acoustic System Operator, Pure Technologies, are provided in Appendix K. As stated in Section 3.2.8, the objectives for the acoustic system were to detect tendon or rebar breaks, concrete cracking or crushing, and liner tearing/leakage. The acoustic system response data, which helped to identify when the PCCV model began leaking, was described in Section 5.2.2 (see Figure 5.17).

There were no tendon wire or rebar breaks during the LST; however, events defined as tendon ‘pings’ were reported. These tendon pings were interpreted as a readjustment or reseating of the tendon wires/strands as they were tensioned, but the magnitude of these acoustic events are much lower than those associated with a wire break. Figure 5.72 shows the location of the tendon pings are concentrated at the buttresses. Whether this is indicative of source of these events or merely reflects that any tendon events will be transmitted more rapidly along the tendon strands to the acoustic sensors on the buttresses is speculative, but reasonable. A histogram of the tendon ping events as a function of pressure is shown in Figure 5.73. The fact that the majority of tendon pings occurred around $2.0P_d$ is noteworthy, but the reason for physical significance of this is not obvious. It may be that a certain level of tension must be applied to reseat the strands, or it may simply be that this pressure was held for almost eight hours and the number of events that accumulated at this time appears to be significant.

A total of 489 cracking events were detected from March 3 to September 27, 2000. Two-hundred twenty nine of these events were recorded during the LST. These cracking events represent distinct acoustic events, as distinguished from the ubiquitous ‘crackling’ which occurred nearly continuously during the period the PCCV was monitored by the acoustic system. This crackling is believed to be the acoustic manifestation of microcracking and shearing in response to environmental and pressure loading. The acoustic events identified as cracking represent the formation or extension of discrete macrocracks in response to the applied pressure or other loads. Figure 5.74 maps the location of the cracking events during the LST, grouped by pressure bands. No obvious pattern emerges from this map except that the majority of cracks occurred in the middle section of the cylinder wall, where the strains and displacements were greatest. A histogram of the cracking events as a function of pressure, shown in Figure 5.75, however, reveals the majority of cracking events occurring in the range of 1.5 to $2.0P_d$ where the initial loss of stiffness, presumed to be due to concrete cracking, was already noted.

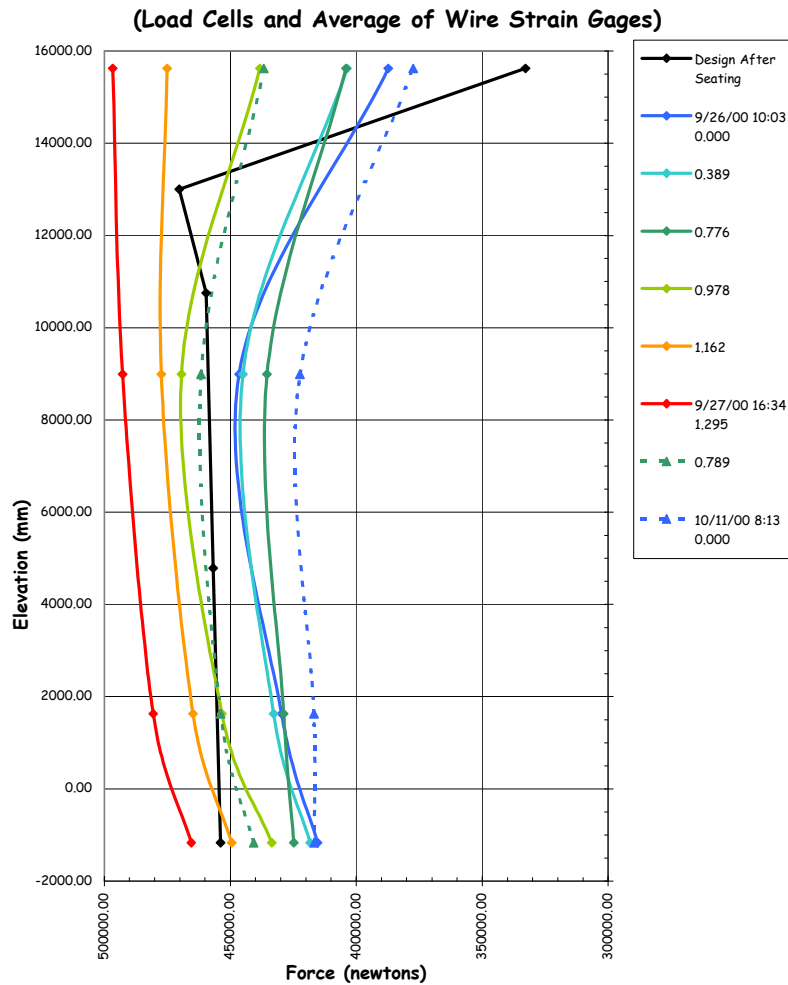


Figure 5.69 V37 Tendon Force Distribution, Azimuth 240 degrees

5.3.2.2 Posttest Inspection

Post-LST inspection of the PCCV model consisted of external crack mapping, visual inspection of the liner and metallurgical examination of the liner tears, and posttest measurements around the E/H.

5.3.2.2.1 Crack Mapping

New cracks and extensions of existing cracks within the crack mapping zones resulting from the LST (see Fig. 5.8) were traced in red and the surface was photographed to document the crack locations (e.g. Fig 5.22). The cracks were then transferred to the crack map drawing, shown in Figure 5.76, which shows all the major cracks identified after various loading stages. In general, concrete cracking was not extensive or very severe, with the exception of some areas around the E/H and some of the smaller penetrations. As noted in Chapter 3, there was no effort to measure crack widths. While it can be observed that some of the larger cracks around the E/H are near the liner tear locations, there was no further effort to correlate the crack locations with other events or data.

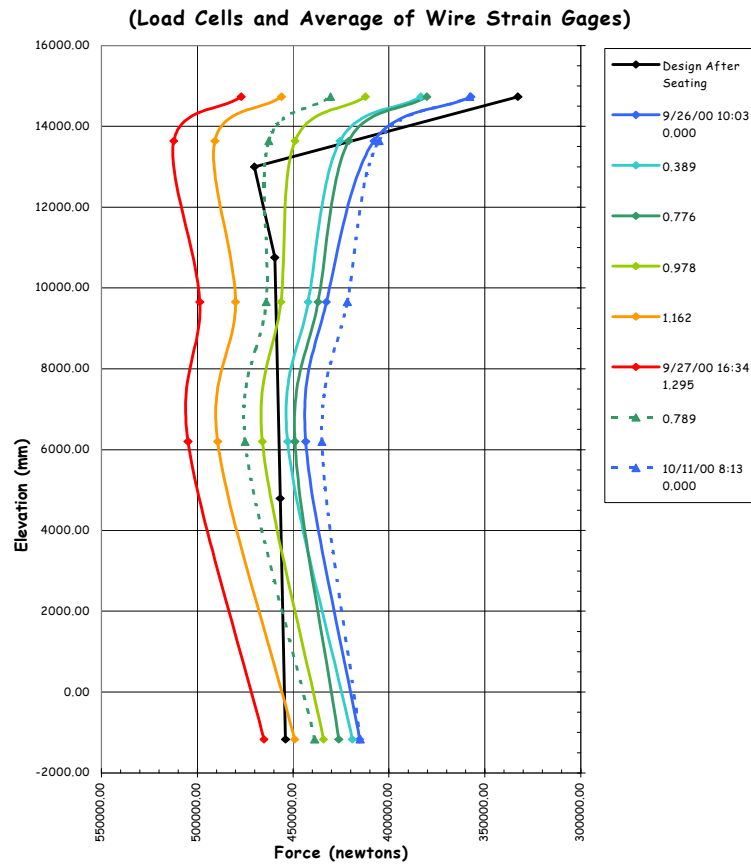


Figure 5.70 V46 Tendon Force Distribution, Azimuth 135 degrees

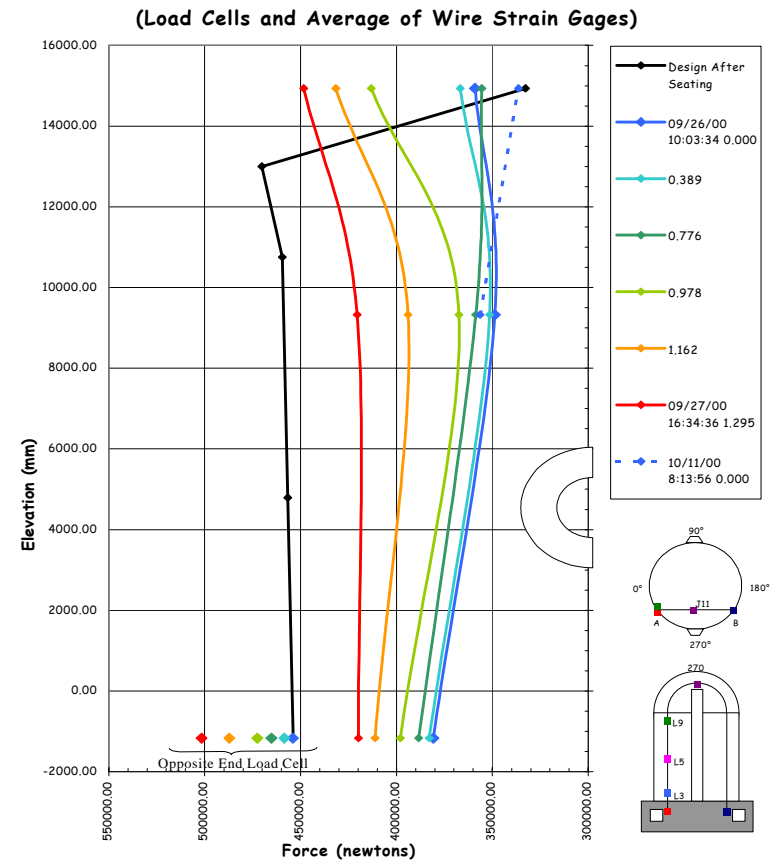


Figure 5.71 V85 Tendon Force Distribution, Azimuth 325 degrees

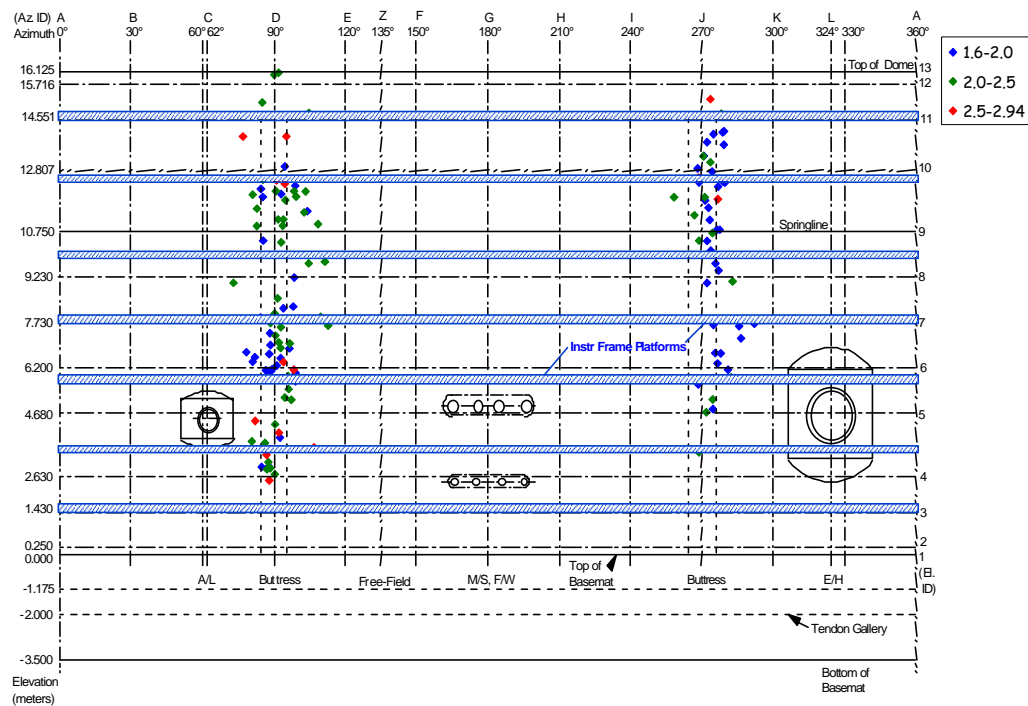


Figure 5.72 LST – Tendon Ping Acoustic Events

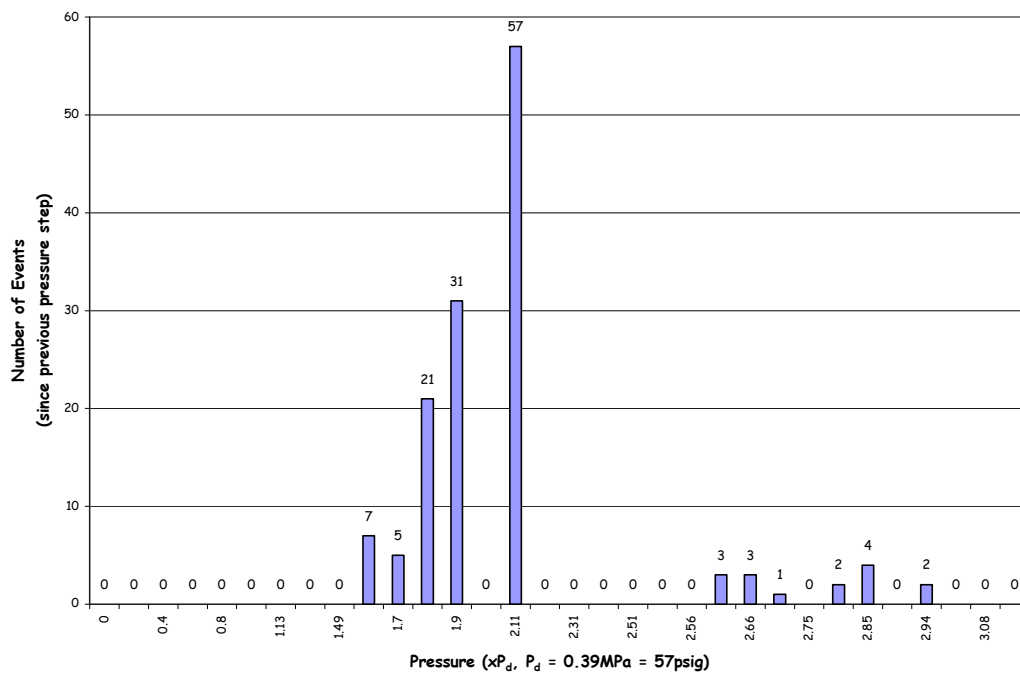


Figure 5.73 LST – Tendon Ping Event vs. Pressure Histogram

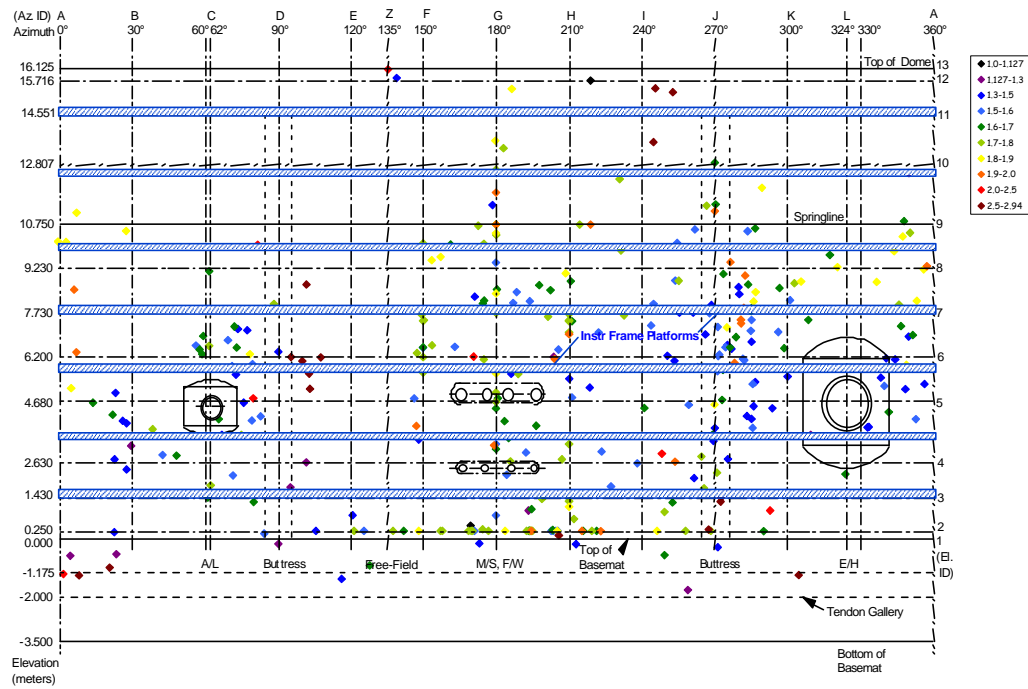


Figure 5.74 LST – Concrete Cracking Acoustic Events

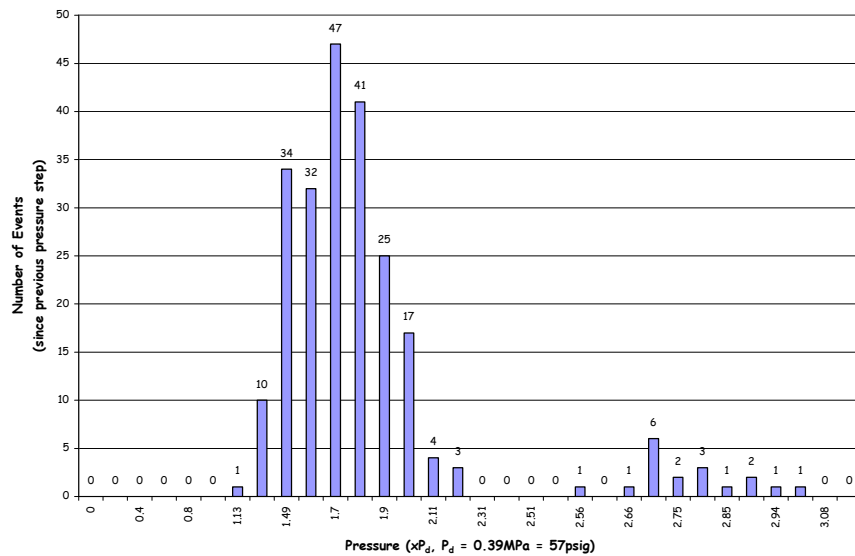


Figure 5.75 LST – Concrete Cracking Events vs. Pressure Histogram

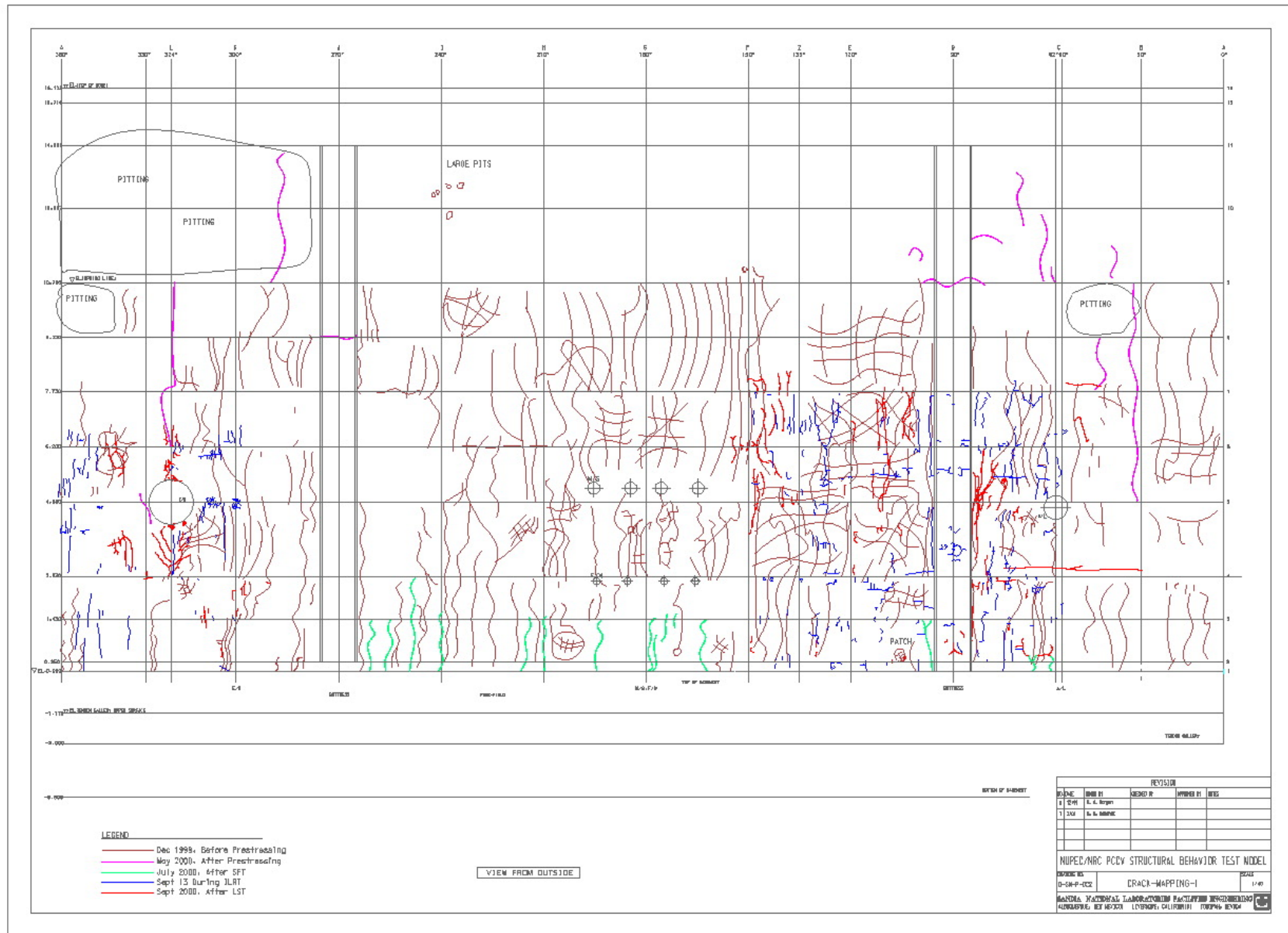


Figure 5.76 Post-LST Concrete Crack Map

5.3.2.2.2 Liner Inspection

As noted in Section 5.2.3, after entering the model following the LST, the liner surface was examined carefully and 26 discrete tears were found at 18 different locations, the grouping by location being somewhat arbitrary. The location of the tears are mapped in Figure 5.77. The location numbers are subsequently used to identify the tears.

One immediate observation was that each liner tear was at or very near a field weld seam in the liner. No tears were found in the undisturbed parent material or at a shop weld.

The acoustic events, later associated with the sound of the nitrogen gas escaping through the liner tears, are superimposed on the tear map in Figure 5.78, along with the approximate pressure levels when these events were first detected. The first tearing event appears to be clearly associated with the tears along the edge of the E/H embossment (#7, #12, #13, and #15), although it is arguable which of these occurred first. The other acoustic tearing events cannot be as clearly identified with any specific tear or tears, and, near the end of the test, it may have been difficult to distinguish the separate 'tearing' events from each other since gas continued to escape through each tear after it occurred.

A typical liner tear (#2) as it appeared during the initial inspection is shown in Figure 5.79. In addition to the liner tears, a pattern of buckling appeared throughout the middle section of the cylinder wall. The buckling pattern, also illustrated in Figure 5.79, is believed to have occurred during depressurization, when the permanently stretched liner could not accommodate the elastic recovery of the cylinder wall.

After the initial inspection of the liner, a more methodical inspection was undertaken. Each tear was photographed and matched with photographs of the 'backside' of the liner before the concrete was placed. (One early program decision was to photograph the entire length of every field weld made during the fabrication of the liner. While this was a very time-consuming and painstaking task, the benefit obtained in understanding the causes of the liner tearing was worth the effort.) A sample of the pre-LST exterior condition compared to the post-LST interior condition for Tears #7, #12, #13 and #15 at the E/H, #2 at a free-field weld seam, and #16 at a 'rathole' detail are shown in Figures 5.80 to 5.85.

The paint was then removed from each tear, allowing the liner tear to be seen without being obscured by the paint. Each tear was then photographed again for documentation. Figure 5.86 shows an close-up of Tear #13 after removing the paint. With the paint removed, it was clear that the weld was repaired or had been reworked by grinding at nearly every tear. Note the grind marks in Figure 5.86, which occurred during erection and welding of the liner. (The paint was removed by using chemical strippers; no paint was removed by mechanical methods.)

While this initial inspection was being completed, a detailed posttest liner inspection plan was being developed. After reviewing the plan with NUPEC and the NRC, the plan, consisting of the following elements, was implemented.

1. In-situ examination:
 - a. In addition to the visual/photographic records, ultrasonic thickness measurements were made at each tear location and at several baseline locations where tears did not occur.
2. Destructive examination:
 - a. Twenty-five liner specimens were removed from the model (see Figures 5.87 and 5.88).
 - b. Eighteen of the liner specimens were subjected to metallographic analysis.
 - c. Sample weld specimens were subjected to metallographic analysis.
 - d. After the liner specimens were examined by SNL, the unused portions were sent to NUPEC for further examination. The results of NUPEC's examination have been reported separately.

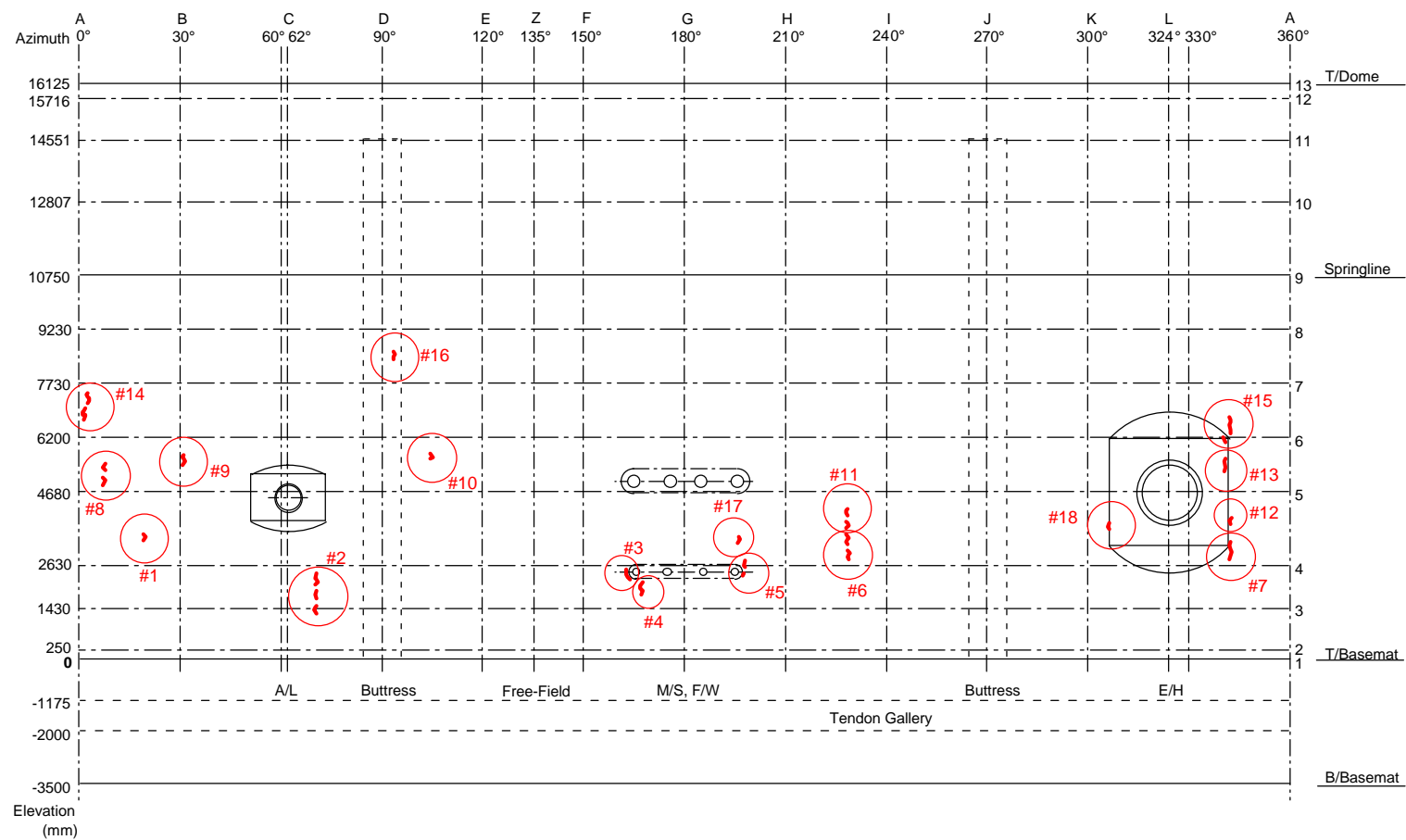
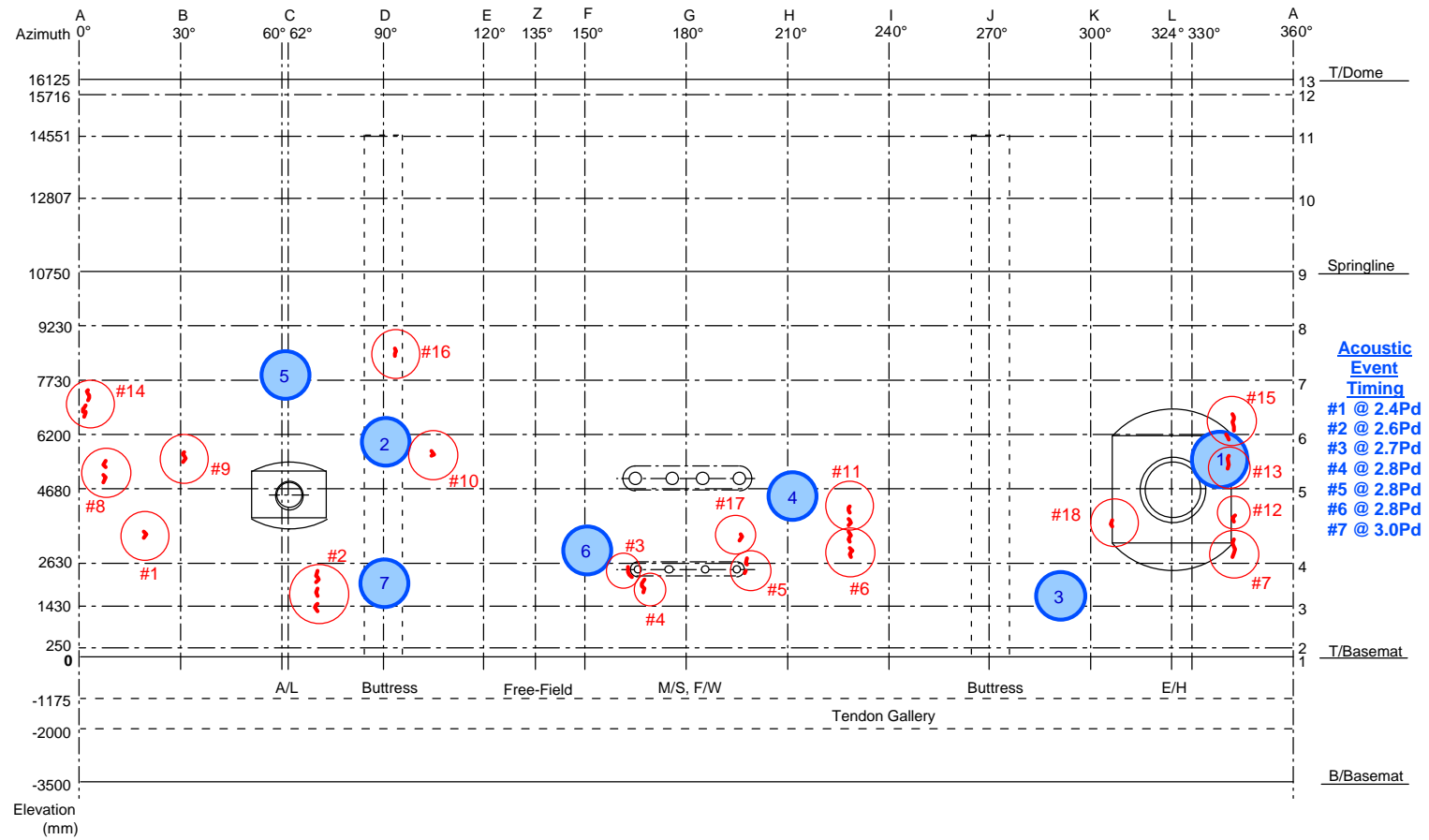


Figure 5.77 Post-LST Liner Tears



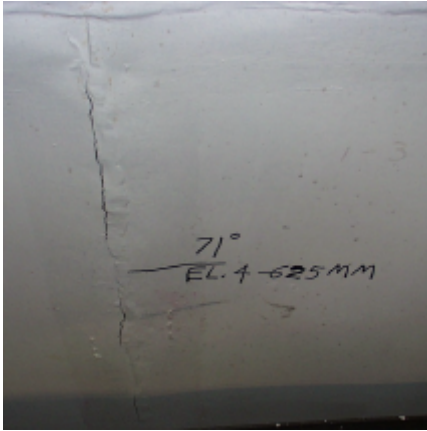


Figure 5.79 Post-LST Liner Tear (#2) and Liner Buckling

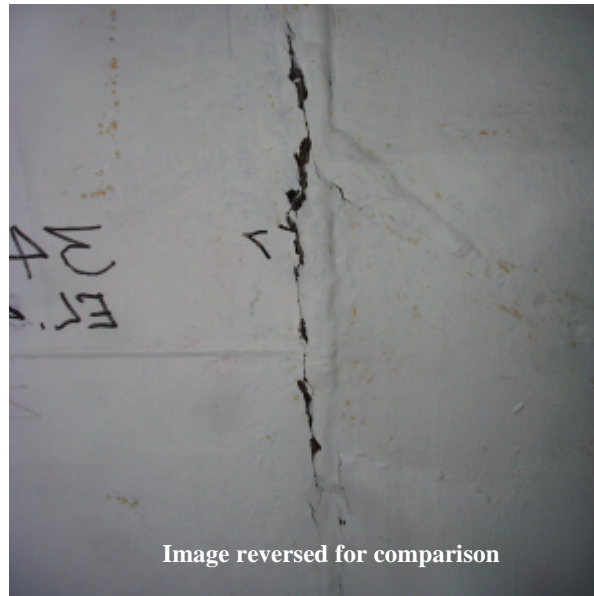


Image reversed for comparison

Figure 5.80 Tear #7 at E/H



Figure 5.81 Tear #12 at E/H



Figure 5.82 Tear #13 at E/H

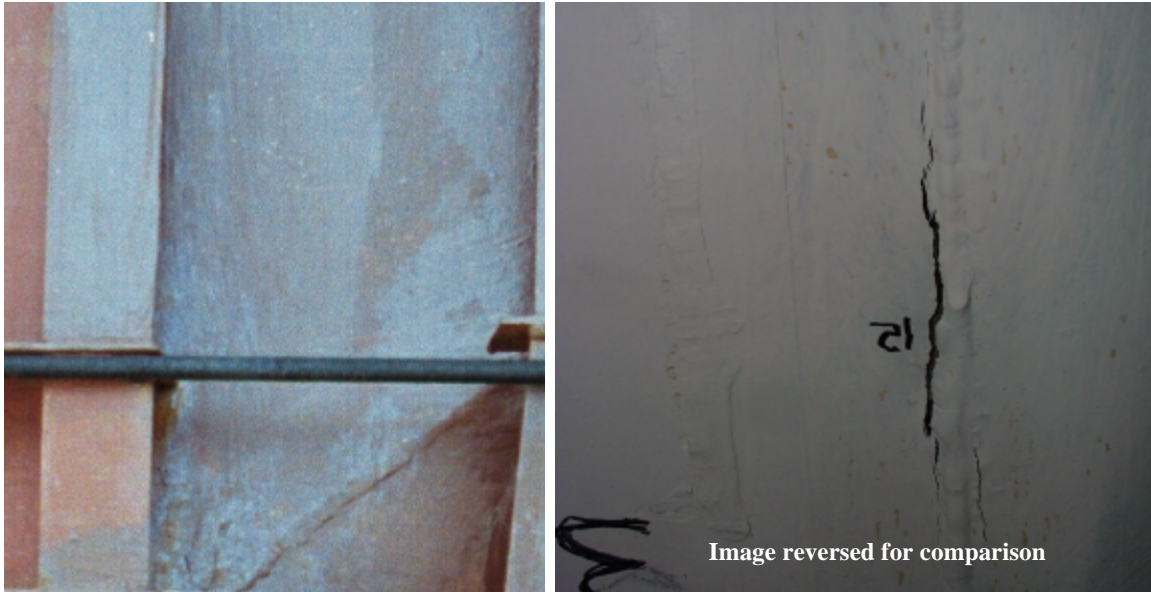


Figure 5.83 Tear #15 at E/H



Figure 5.84 Tear #2, Free-Field



Figure 5.85 Tear #16 at Rathole Detail

The results of the liner inspection are detailed in Appendix L. The conclusions of the inspection and metallographic analysis are repeated below.

1. Nearly all of the tears occurred in areas where the liner thickness was reduced ~25% or more by grinding done in association with repair welding. Extensive localized plastic deformation culminating in ductile tearing occurred in these thinned areas as the structure was being tested. This appears to have been the most prevalent cause of liner failure.
2. In samples where quantification was possible, it appears that the reduced thickness at the point of failure was up to 50% of the local material thickness.
3. At the E/H
 - a. #15: 50%-60% reduction by grinding
 - b. #13: 25% reduction by grinding
 - c. #12: >10% reduction by grinding
 - d. #7: 25% reduction by grinding
4. @ the Free-Field
 - a. #16-1 (D7): no tear, no repair ~10% reduction in thickness (post-LST)
 - b. #16-2: tear, single weld repair, thickness reduction on both sides of weld
5. Geometric features may also have contributed to the formation of some tears. These include structural transitions, such as those at the feedwater penetration and the equipment hatch transition boundaries, discontinuities in horizontal stiffeners, and discontinuities in weld back-up bars. A missing segment in a horizontal back-up bar appears to have been primarily responsible for one tear (#16).
6. Only one tear occurred in association with a material or weld defect. A lack-of fusion weld defect was found at the initiation site of tear #1.
7. The specially produced quarter-scale liner material exhibited mechanical properties that may have made it particularly prone to plastic strain localization and tearing. While nearly conforming to the specifications for full-thickness material, the quarter-thickness plate exhibited a yield strength much higher than the specified minimum (383 MPa compared with 225 MPa) and an unusually high yield-to-ultimate-strength (YS/UTS) ratio (0.77). This high YS/UTS ratio is qualitatively consistent with extensive localized plastic strain culminating in ductile tearing in regions where more than ~25% of the liner thickness had been ground off, as was observed near most of the tears.

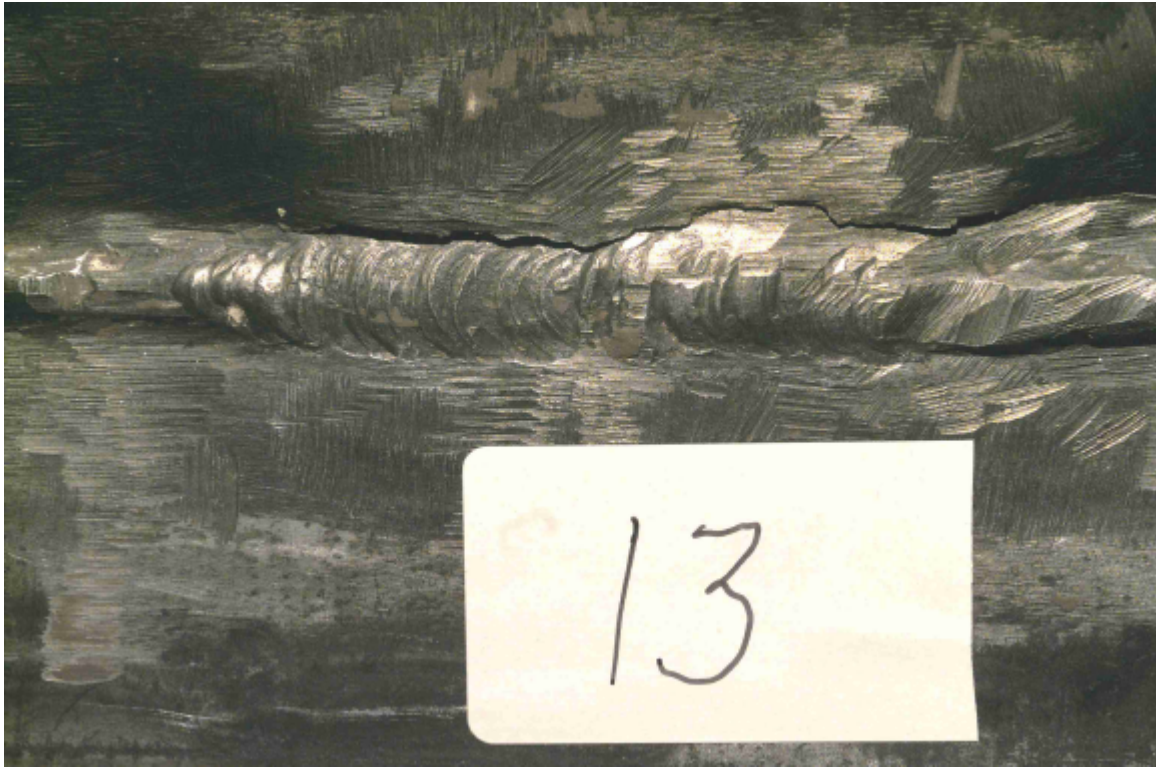


Figure 5.86 Close-Up of Tear #13 after Removal of Paint



Figure 5.87 Liner Specimen at Tear #2



Figure 5.88 Liner Specimen at Tear #15

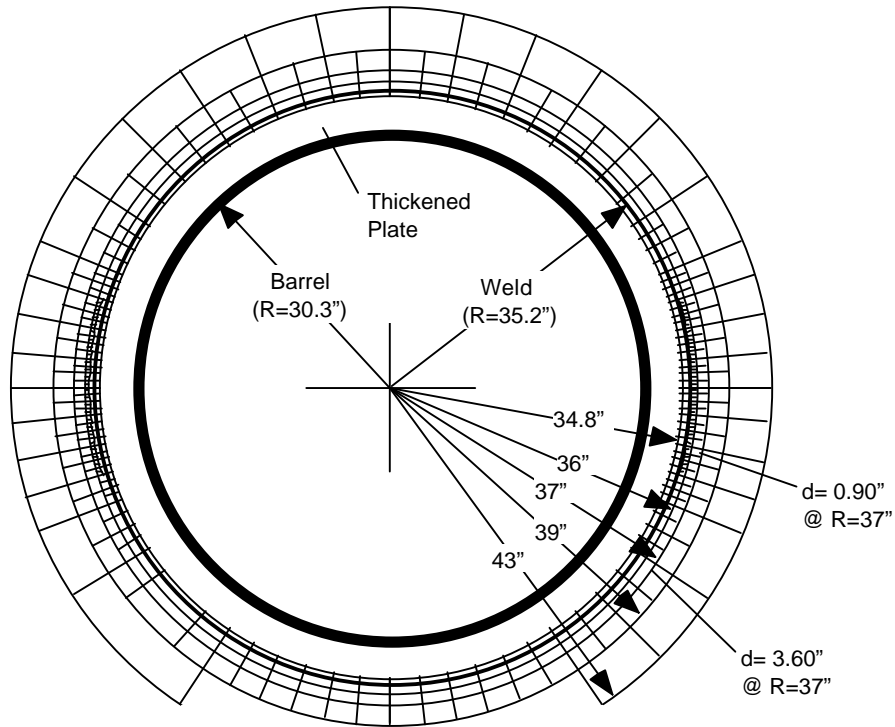
8. Tensile and hardness tests on welded test samples indicated that modest amounts of plastic strain localization should be expected in the weld-heat-affected zones, but to a much lesser extent than observed in association with the liner tears. Consistent with this, smaller (but significant) amounts of localized plastic strain were observed adjacent to some welds that had not been repaired or ground. These strains were sufficient to initiate necking in the most severely strained regions. However, with the possible exception of tear #12, there was no indication that tearing was imminent in regions other than those where repair welding and substantial grinding had been done.
9. The mechanical testing results did not suggest that deficiencies in the properties of either the base metal or weld metal, nor excessive softening in the weld-heat-affected zones, could account for the extensive localized plastic deformation culminating in tearing that appeared to occur in the liner.

In summary, it is apparent that the onset of liner tearing at $2.5P_d$ resulted, to a significant degree, from the difficulty of field welding the very thin liner. The conditions that led to the liner tearing would not be present to the same degree in the prototype, and the initiation of tearing might be delayed until a higher pressure was achieved. Nevertheless, in spite of the liner welding difficulties, it is also apparent that the near field strains in the vicinity of a liner discontinuity must be large enough to initiate a tear because all the tears were initiated at vertical weld seams within the middle portion of the cylinder wall.

5.3.2.2.3 Posttest Measurements

As described in Section 3.2.5.4, a grid was constructed around the E/H to measure the residual strain field after the test. The pretest analysis predicted large strains near the perimeter of the thickened insert plate surrounding the E/H barrel and near the anchors and stiffeners that terminated near the insert. The grid, shown in Figure 5.89, was drawn, and the position of the grid points was obtained using a 3D digital position mapping tool. After the LST, the grid points were mapped again and the pre- and posttest positions were plotted in Figure 5.90.

Unfortunately, as noted previously, the strains in this region were very small and the resulting residual displacements are barely distinguishable from the pretest positions, given the precision of the digital probe. As a result, no useful information was obtained by this effort.



E/H Inside View

Figure 5.89 E/H Displacement Grid

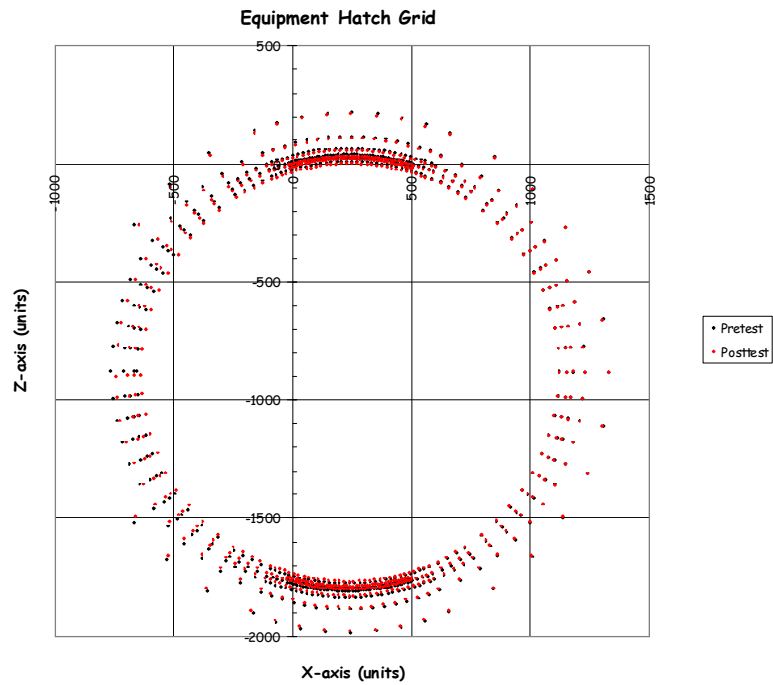


Figure 5.90 E/H Post-LST Displacement

5.3.3 Structural Failure Mode Test Results

5.3.3.1 Test Data

The Structural Failure Mode Test data (DYN only) is provided on the enclosed data CD in Excel® spreadsheets, as noted in Section 5.3.1. The response of every functioning transducer in the revised instrumentation suite is provided. The following sections present a synthesis of the data focusing on the critical response measurements.

5.3.3.1.1 Displacements

As for the LST, the displacement data provides the most comprehensive view of the overall or global response of the model. Since the displacement transducers had to be waterproof, a reduced suite of gages was used during the SFMT. Based on the results of the LST, two vertical arrays at Azimuth 135 degrees and 324 degrees, and one horizontal array at Elev. 4680, were employed for the SFMT, as shown in Figure 5.26. Figures 5.91 through 5.93 show the radial displacement response as a function of pressure along these cardinal lines. Since the displacement transducers had to be removed after the LST to install the elastomeric liner and new transducers were installed for the SFMT, the displacements were ‘zeroed’ prior to the start of the SFMT on November 6, before filling the vessel with water. The displacements therefore reflect only the response to pressure (including the hydrostatic pressure) and not the effects of prestressing, nor any other previous loading. Note that the pressures shown are the effective pressure, i.e. the volume weighted average pressure in the model.

During the SFMT, the displacement response of the model is essentially linear to just beyond 3.0 Pd, when global yielding begins to occur prior to rupture. The initial stiffness of the model, however, is less than the initial stiffness during the LST. Figure 5.94 compares the response at the mid-height of the cylinder (Z6) during the LST and the SFMT. (The SFMT response was offset in this figure by adding the residual displacement at the end of the LST to facilitate comparison.) This figure shows that the hoop stiffness during the SFMT is essentially identical to the post-cracking stiffness during and after the LST. It also shows that the SFMT displacement is nearly identical to the LST displacement at the maximum LST pressure, suggesting that, if the LST had continued, the response would have been virtually

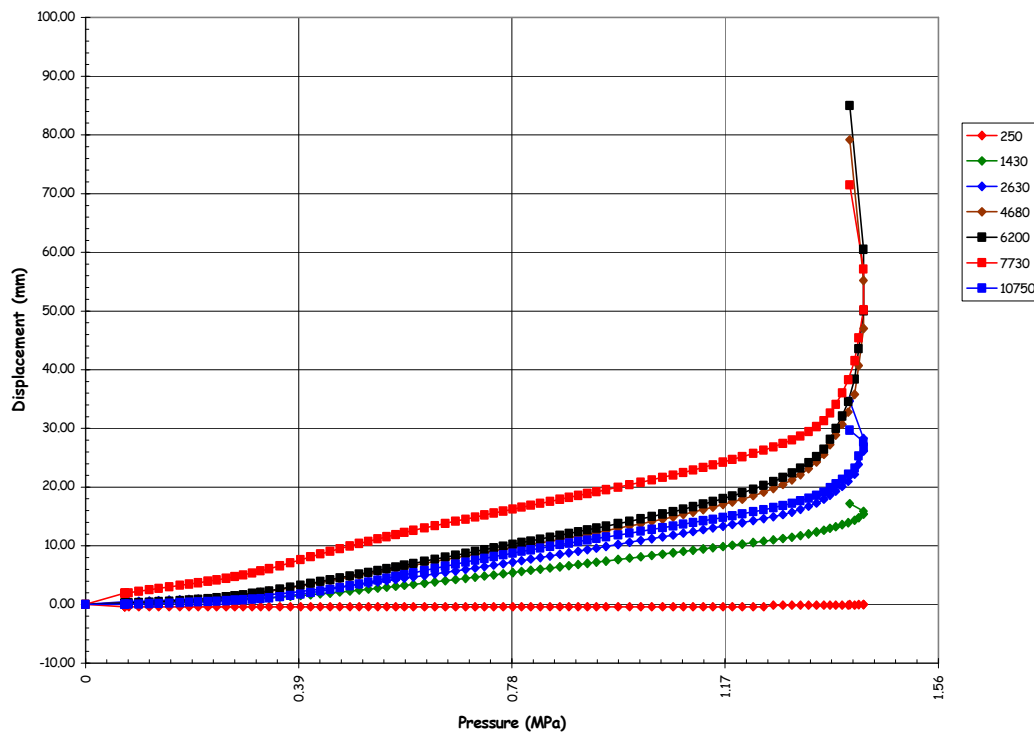


Figure 5.91 SFMT – Radial Displacement at Azimuth 135 degrees (Z)

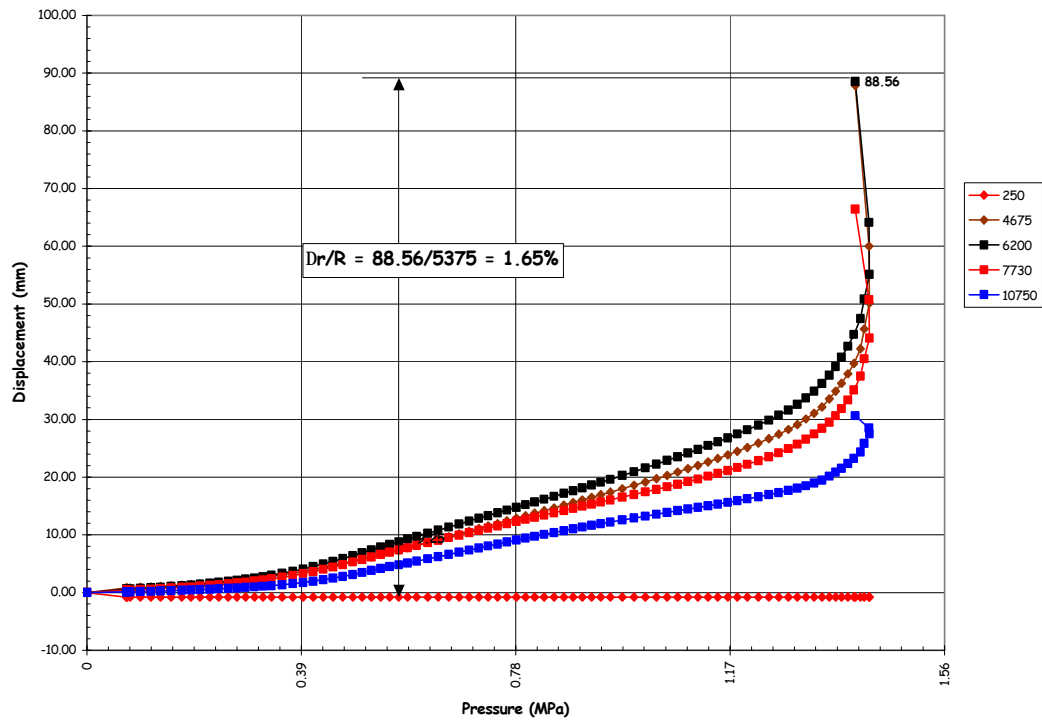


Figure 5.92 SFMT – Radial Displacement at Azimuth 324 degrees (L)

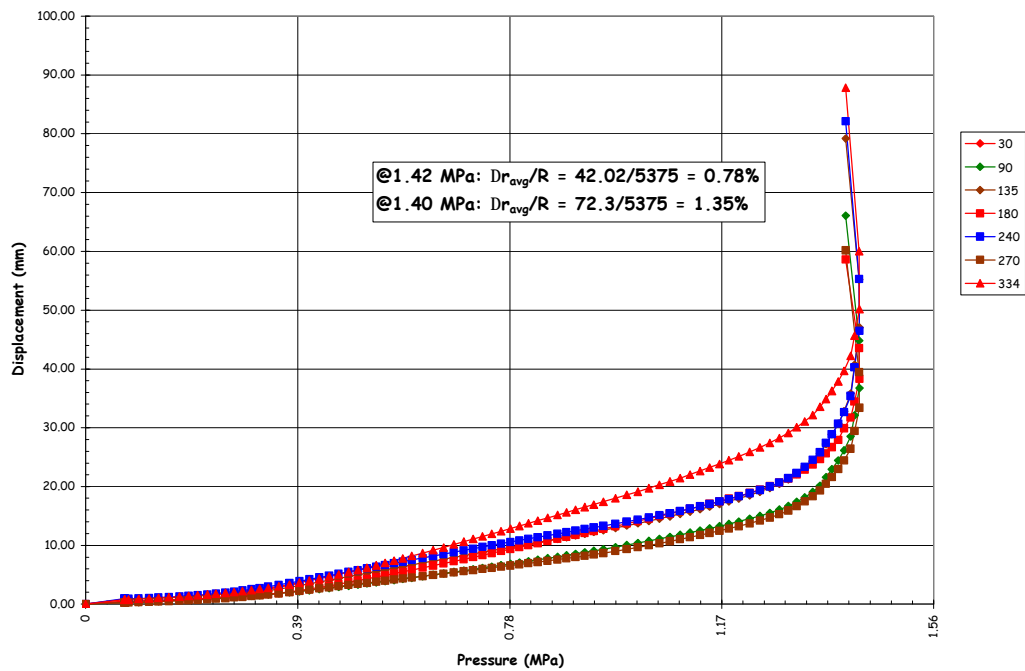


Figure 5.93 SFMT – Radial Displacement at Elev. 4680 (5)

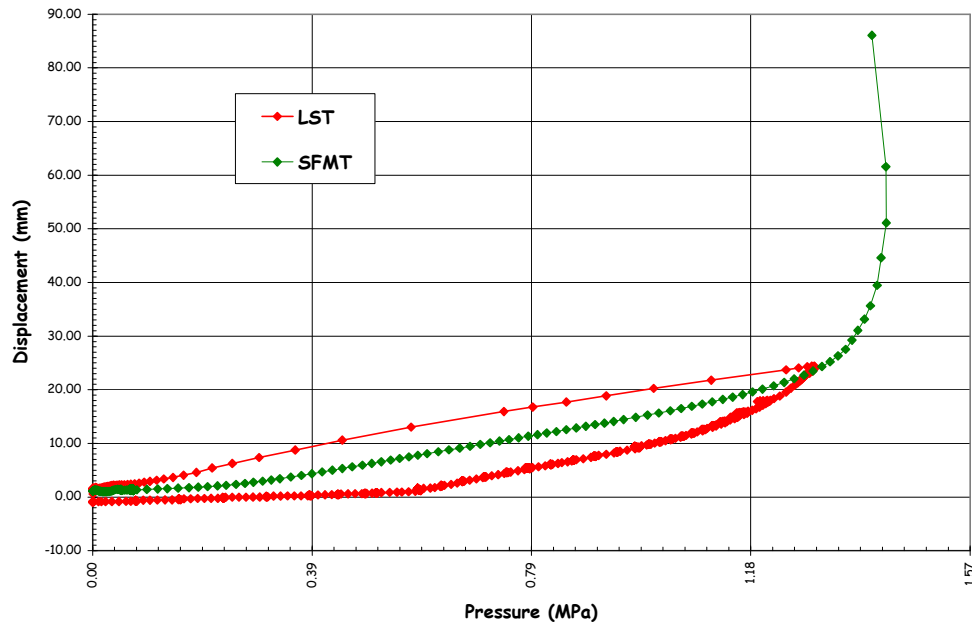


Figure 5.94 SFMT – Radial Displacement at Azimuth 135 degrees, Elev. 6200

identical to that measured during the SFMT. Similarly, the vertical displacements at the apex (offset again) are compared in Figure 5.95.

Since the SFMT was conducted as a continuous pressure test with no holds for gage stability of leak checks, there were no discontinuities in the response histories.

The peak displacements shown in the plots were the final readings obtained before the model ruptured and the gages were destroyed. The pressure values at and beyond the peak were recorded at the beginning of the data scan. Since each scan took approximately 30 seconds, the pressure may have increased (or decreased) during the scan. Note that a few data scans were completed after the peak pressure was reached. The post-peak values may indicate some ‘softening’ of the model. However, it is more likely that the plots reflect the drop in pressure due to the rapid expansion and increasing leakage just prior to rupture.

Figure 5.92 displays the displacements at Azimuth 324 degrees, which coincides with the centerline of the E/H. The largest radial displacement recorded during the SFMT, 88.56 mm, again occurred at this azimuth at elev. 6200, above the E/H. Computing the equivalent hoop strain due to pressure at this location from kinematics,

$$@P_{\text{final}} = 3.58P_d: \quad \frac{\Delta r}{R} = \frac{88.56}{5376} = 1.65\% .$$

At the peak pressure, $3.65P_d$, the displacement was 55.12 mm, yielding an equivalent hoop strain of 1.02%

Figure 5.93 compares the displacement response as a function of azimuth at elev. 4680, nominally the mid-height of the cylinder and the centerline of the E/H, A/L, and M/S penetrations. The response is not as uniform as was observed during the LST. Nonetheless, averaging the radial deformation due to pressure yields a nominal average hoop strain of 0.78% at the peak pressure $3.65P_d$. Similarly, the average hoop strain at $3.58P_d$, just prior to rupture, was 1.35%.

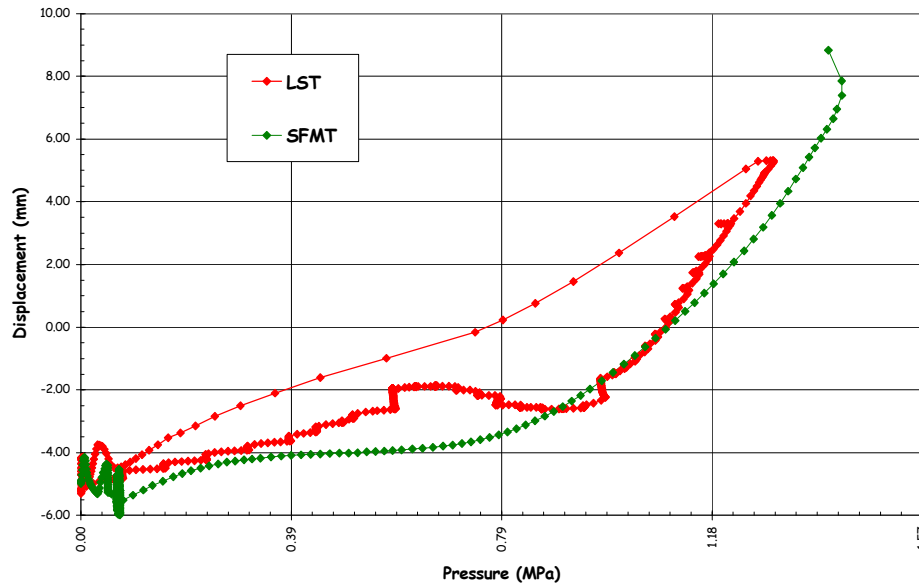


Figure 5.95 SFMT – Vertical Displacement at Apex

The vertical displacements are shown in Figure 5.96. The maximum vertical displacement at the springline was 10.84 mm at Azimuth 135 degrees, essentially the same as during the LST, and 5.94 mm at Azimuth 324 degrees, less than during the LST. The reason for the small displacement at 324 degrees is not immediately obvious; however, it might be the stiffening effect of the E/H embossment, although this was not observed during the LST. Nevertheless, it is clear that the vessel did not yield in the vertical direction and the vertical strains were still on the order of 0.1%.

Deformed profiles of the PCCV model, constructed from the displacement data in a similar manner as those constructed for the LST, are shown in Figures 5.97 through 5.100. For the SFMT, the initial position was again assumed to be defined by the as-built model survey data (Appendix C). However, since the gages were zeroed prior to the start of the SFMT, any deformations of the liner surface or the wall are not reflected in the data.

The as-built position of the PCCV model is plotted in the first portion of the figures, along with the deformed shapes due to the hydrostatic pressure (H_2O) and at approximately $1.0P_d$, $2.0P_d$, $2.5P_d$, $3.0P_d$, $3.5P_d$, and $P_{max} = 3.63P_d$. The second portion of each figure provides a more refined breakdown between $3.0P_d$ and $3.63P_d$ and the profile at $P_{final} = 3.57P_d$, immediately prior to rupture of the vessel. These figures dramatically illustrate the large deformations that occur as the vessel yields, even though the pressure is dropping. The displacement nearly doubles as the pressure drops from $3.63P_d$ to $3.57P_d$.

A most provocative observation after considering the displacement data and the global response of the model is that the relatively small pressure increase between the LST and the SFMT, from $3.3P_d$ to $3.6P_d$ (approximately 10%), made the vessel go from a relatively benign and only slightly damaged step to total collapse. It is reasonable to speculate what the response of the model might have been if the liner had not torn and leaked at $2.5P_d$, arguably prematurely, and it had been possible to pressurize it to $3.6P_d$ pneumatically.

5.3.3.1.2 Liner Strains

Since the liner was damaged during the LST and large portions were removed for metallographic analysis, the response of the liner was not a critical objective during the SFMT. Nevertheless, 18 exterior gages (the interior ones were

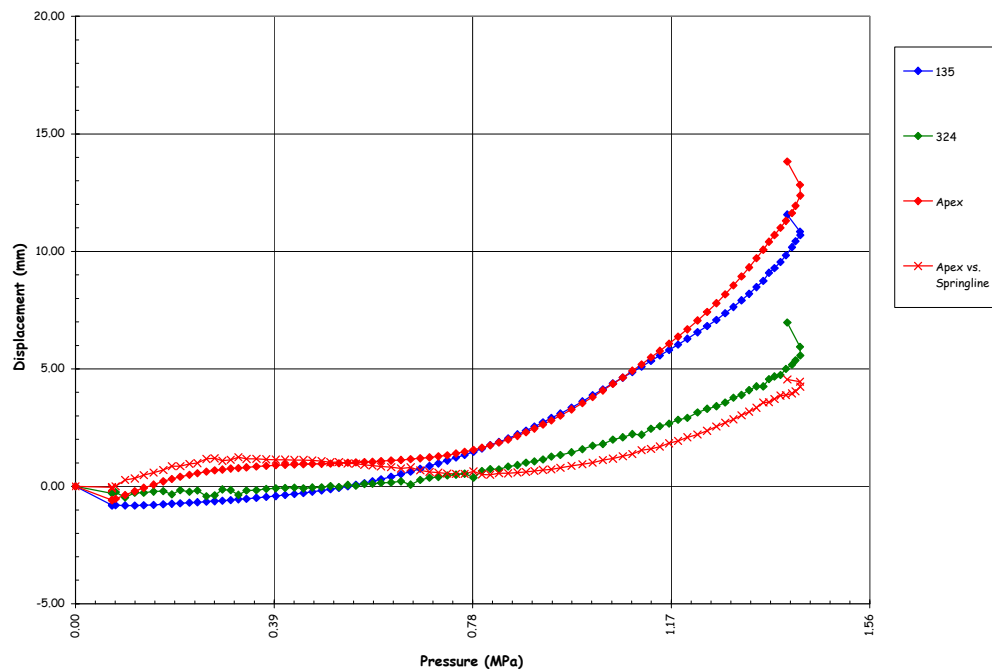


Figure 5.96 SFMT Vertical Displacements at Springline (El. 10750) and Apex

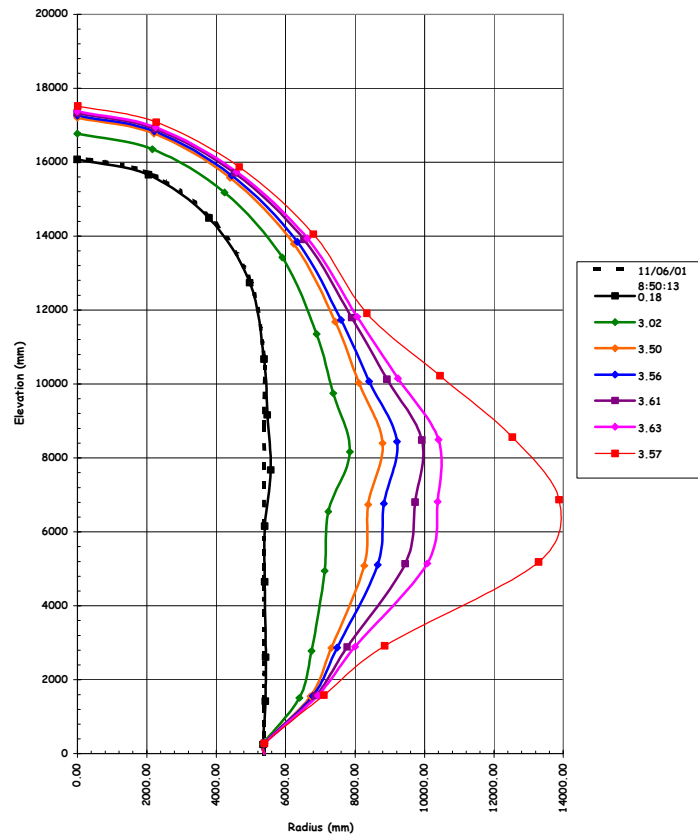
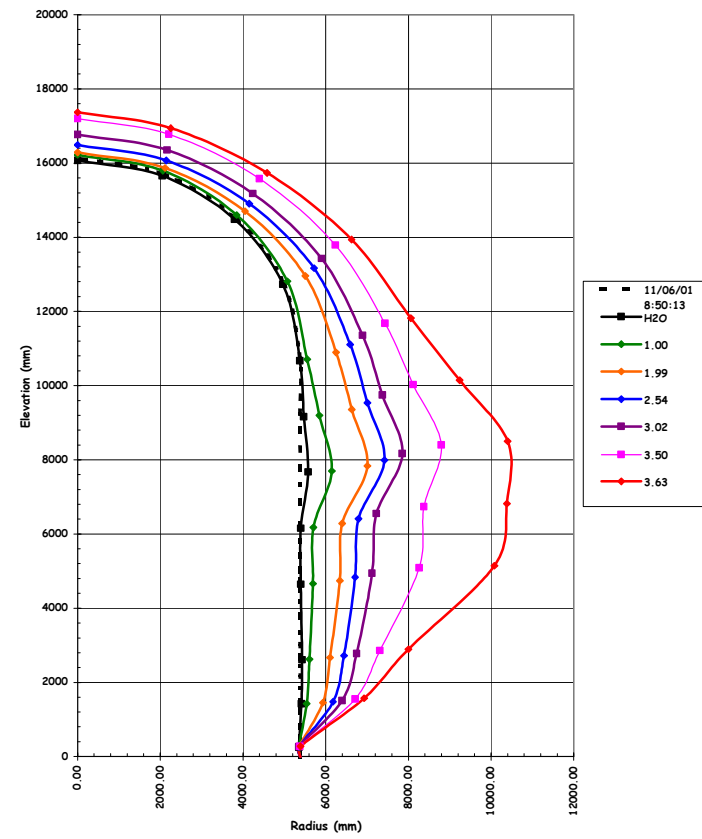
removed prior to installing the elastomeric liner) were monitored during the SFMT to provide some information on the liner response at higher pressures and for comparison with other instruments. Of the 18 strain gages selected, three failed

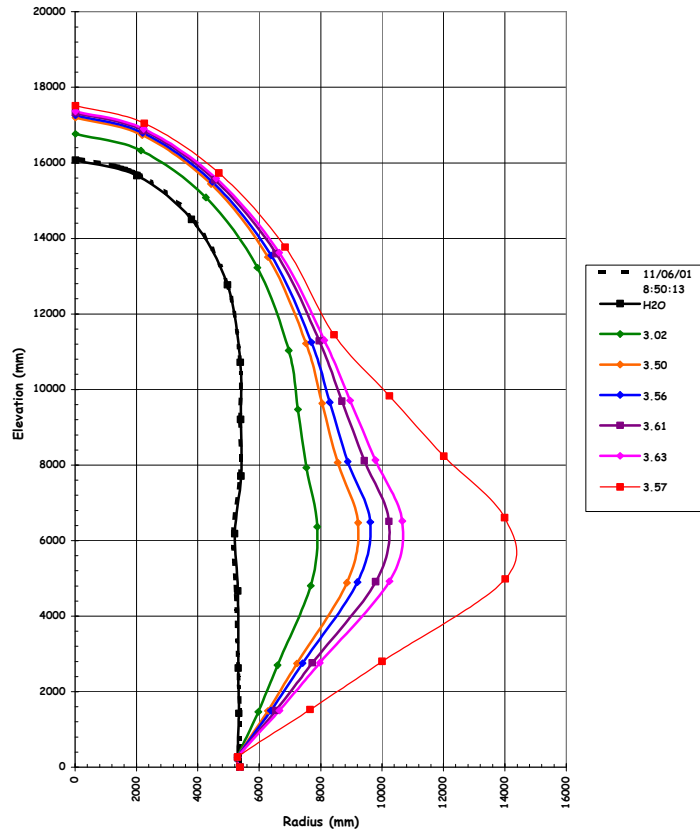
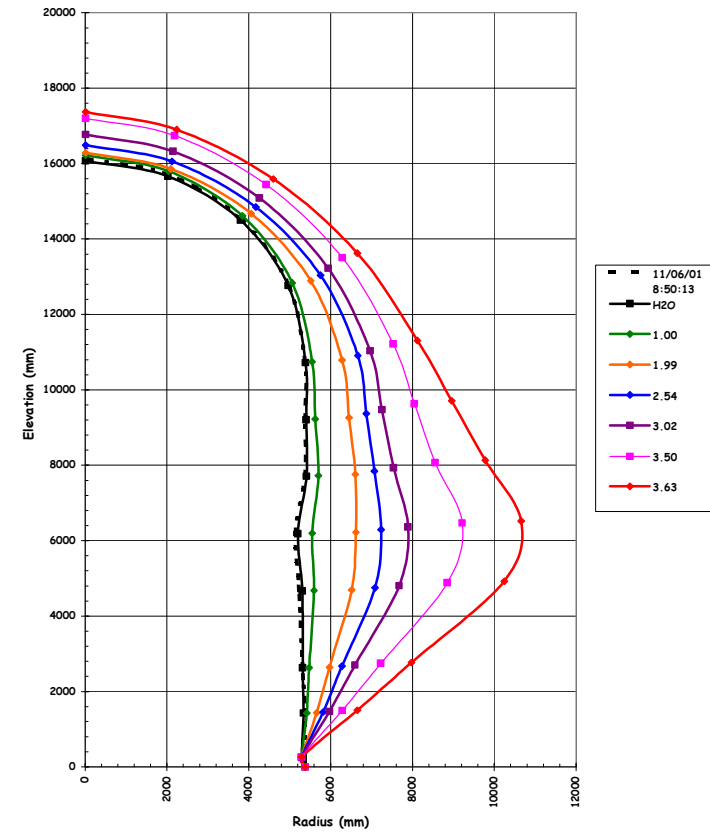
before filling the model with water. The remaining gages at the wall-base junction and the two external gages at D7 also appeared to have been damaged prior to the test, possibly by water leaking from the model. As a result, meaningful data was only obtained for three liner strain gages.

The strain histories for the surviving gages are plotted in Figure 5.101. These gages measured the hoop liner strain inside a rathole (see drawing D-SN-P-209, Appendix E) at Azimuth 0 degrees, elev. 7730 (A7) and Azimuth 135 degrees, elev. 4680 and 6200 (Z5 and Z6) at the mid-height of the cylinder. The maximum liner strains at Z5 (1.9%) and Z6 (1.5%) are consistent with the strains calculated from the displacements. At A7, nearest the location where the model ruptured, the hoop strains were consistently lower than those at Z5 and Z6, even going into compression, until the peak pressure was reached, when the strain increased rapidly to a maximum of 1.5% tension. While these were not free-field gages, they nevertheless gave some indication of the hoop strains in the liner.

5.3.3.1.3 Rebar and Concrete Strains

Eighty-two rebar and gage bar gages were selected for monitoring during the SFMT. Of these, four of the main rebar strain gages and all the gage bar strain gages appear to have failed before $0.5P_d$. The strain histories for all 31 surviving rebar gages are shown in Figures 5.102 to 5.104. The maximum free-field hoop rebar strain was 1.4% (RS-C-Z6-02). The maximum free-field meridional rebar strain was 0.3% (RS-M-D6-02). These values are consistent with the global strains based on displacement data. The rebar strains at the wall-base junction show the effect of bending but combined with the other meridional strains, confirm that the model was still essentially elastic in the vertical direction.

(a) $0P_d$ to $3.63P_d$ (b) $3.0P_d$ to $3.63P_d$ Figure 5.97 SFMT - Deformation at Azimuth 135 Degrees (Z) $\times 100$

(a) $0P_d$ to $3.63P_d$ (b) $3.0P_d$ to $3.63P_d$ Figure 5.98 SFMT - Deformation at Azimuth 324 Degrees (L) $\times 100$

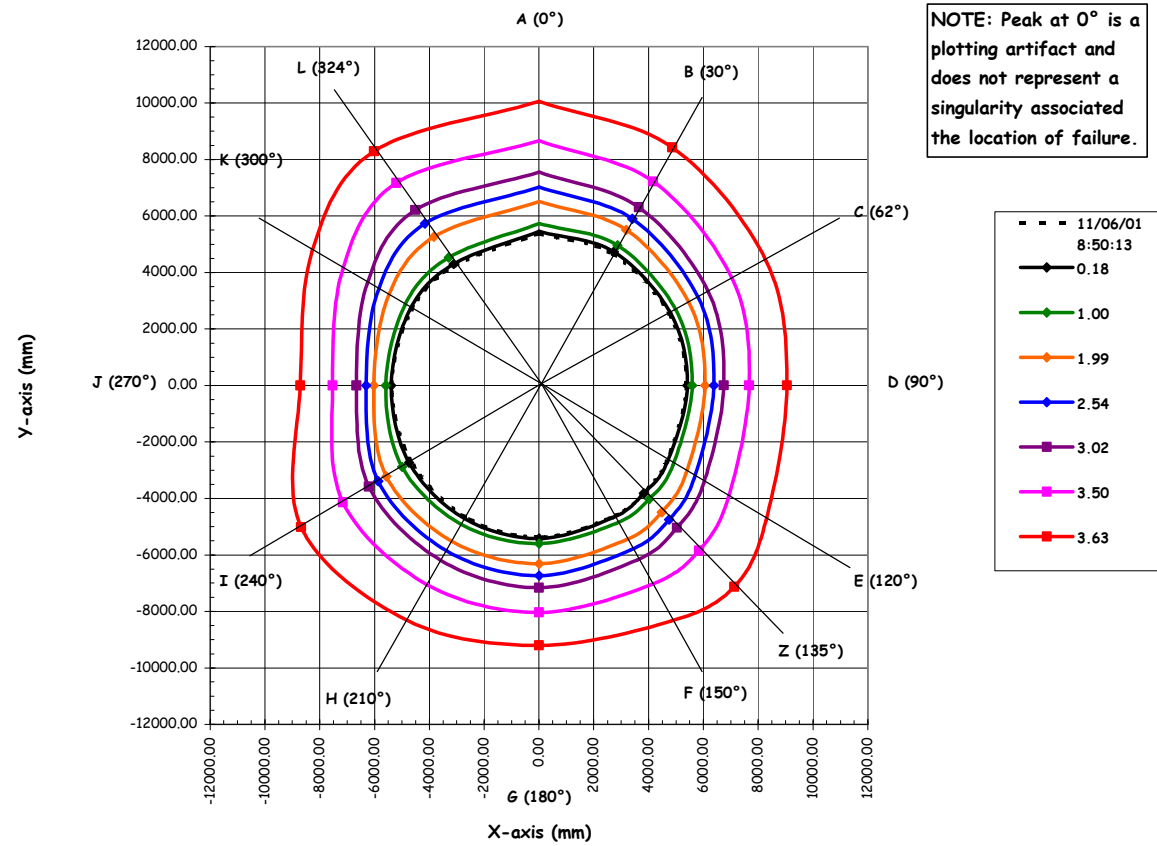


Figure 5.99 SFMT - Deformation at Elev. 4680 (5) \times 100 - 0P_d to 3.63P_d

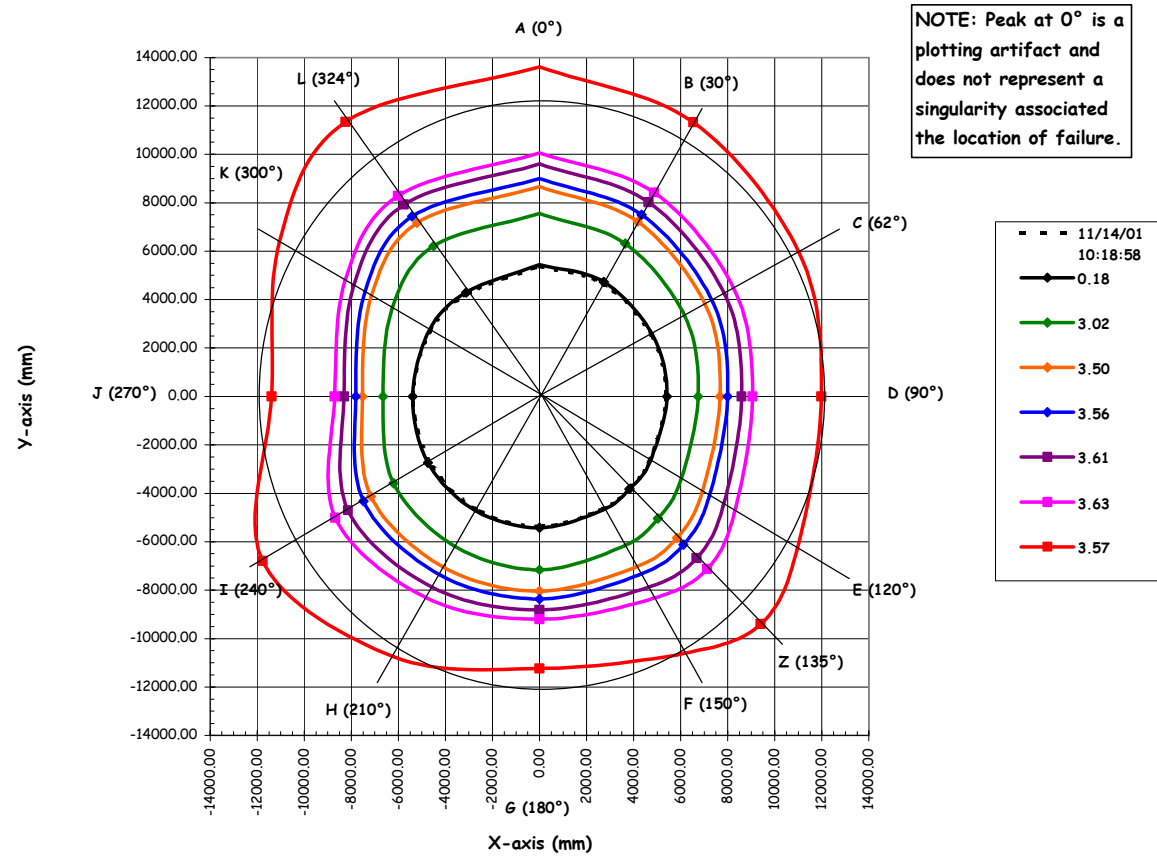


Figure 5.100 SFMT - Deformation at Elev. 4680 (5) \times 100 – 3.0 P_d to 3.63 P_d

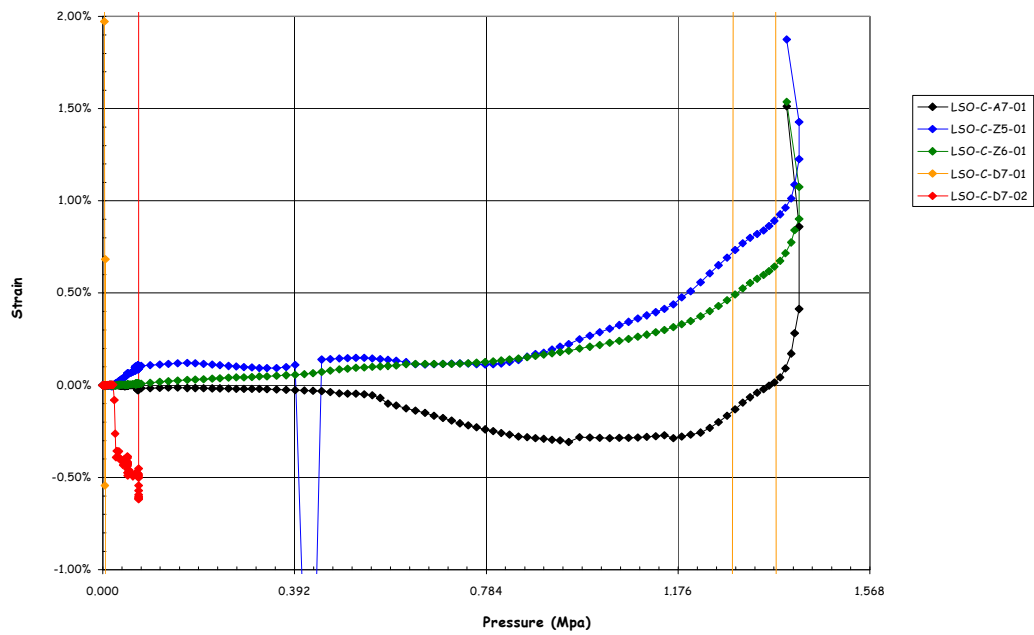


Figure 5.101 SFMT Exterior Liner Strains

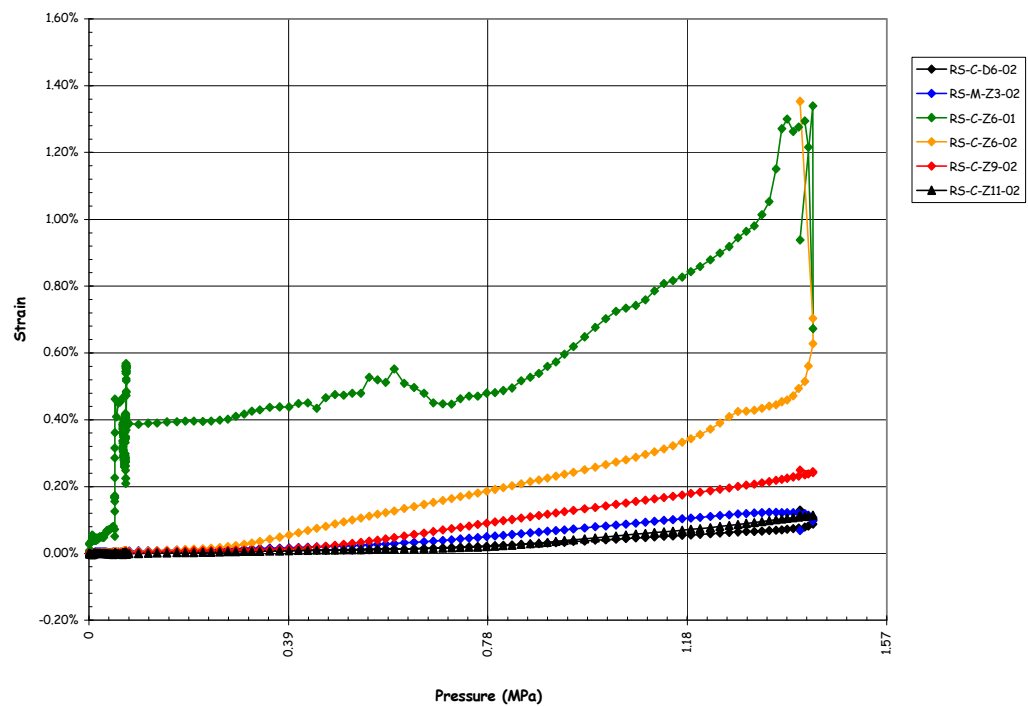


Figure 5.102 SFMT – Free-Field Hoop Rebar Strains

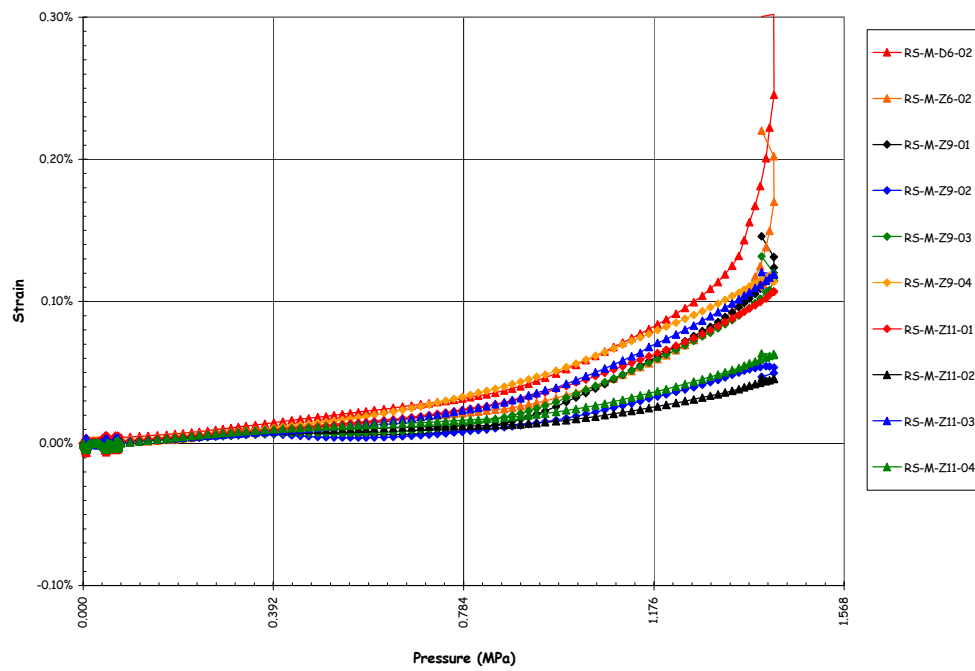


Figure 5.103 SFMT – Free-Field Meridional Rebar Strains

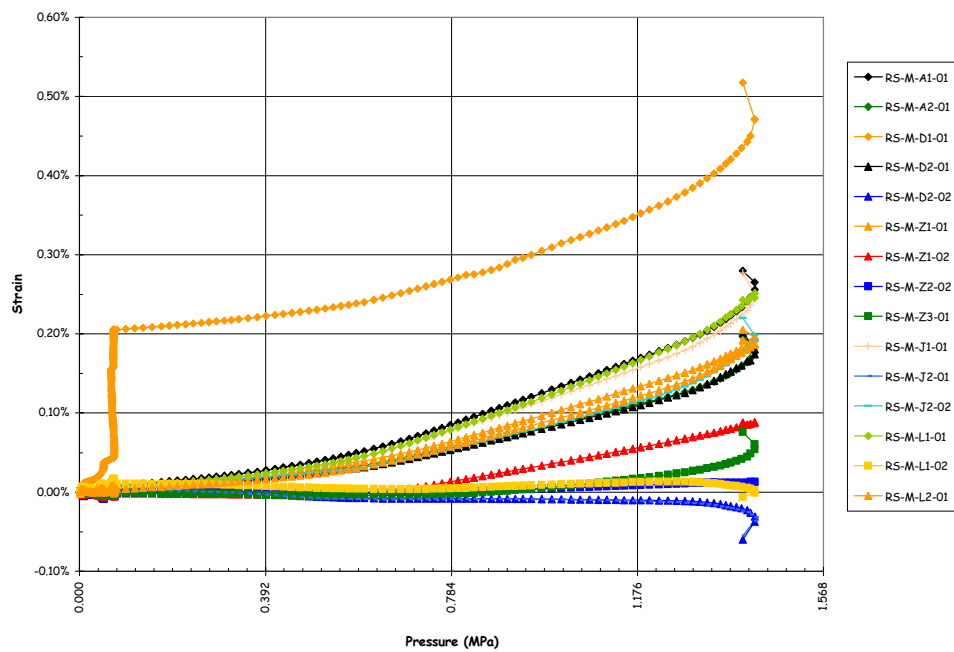


Figure 5.104 SFMT – Meridional Rebar Strains at Wall-Base Junction

Concrete strains, measured by the surviving SOFO fiber-optic gages, are plotted in Figure 5.105. The maximum hoop strain in the concrete, 1.1% (CE-C-Z6-01) at the mid-height of the cylinder, is a little lower than the displacement-based or rebar strains, but overall the concrete strains are consistent with the other measurements.

5.3.3.1.4 Tendon Forces and Strains

All the tendon load cells and strain gages that survived the LST were still functioning at the start of the SFMT and all were monitored during the test. Several load cells and tendon strain gages failed after filling the PCCV with water or early during the SFMT, presumably due to water leaks from the model damaging the gage or shorting out the wiring. The data for all the gages that were functioning at the start of the test are provided, however.

Figures 5.106 and 5.107 show the anchor forces for the instrumented tendons during the SFMT. These anchor forces are representative examples of all the tendon anchors. With the exception of one anchor on H53, the hoop tendon anchor forces increase to nearly 600 kN, which is close to the breaking strength of straight tendons in laboratory tests. It is reasonable to expect that the breaking strength of the curved tendons under field conditions would be lower than the laboratory breaking strength. Load cell TL-C-J6-01 on H53 exhibits an artificially high force near the beginning of the SFMT, most likely from moisture affecting the gage. However, the increased force due to pressure tracks very closely with the other load cells. The vertical tendon anchor forces do not show as large an increase, and the average maximum force only approaches 500 kN, well below the breaking strength. This is consistent with response during the LST and the observation that the vertical tendons did not fail prior to the rupture of the model.

Near the end of the test, sudden decreases in load were observed for several hoop tendon load cells and interpreted as individual strand wires breaking. After reaching the peak pressure, all the load cell readings dropped sharply as the tendons and the model ruptured.

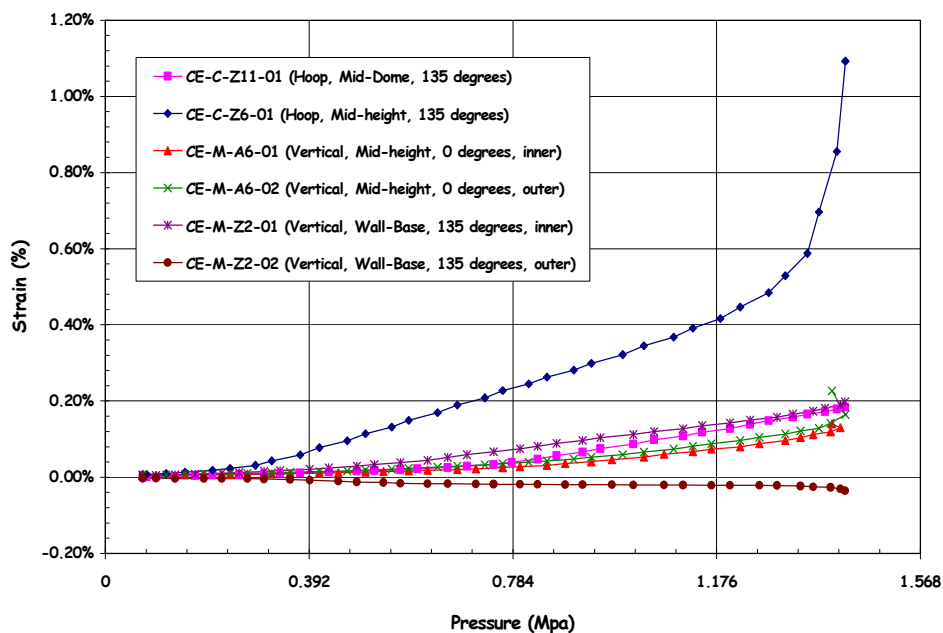


Figure 5.105 SFMT – Concrete (SOFO) Strains

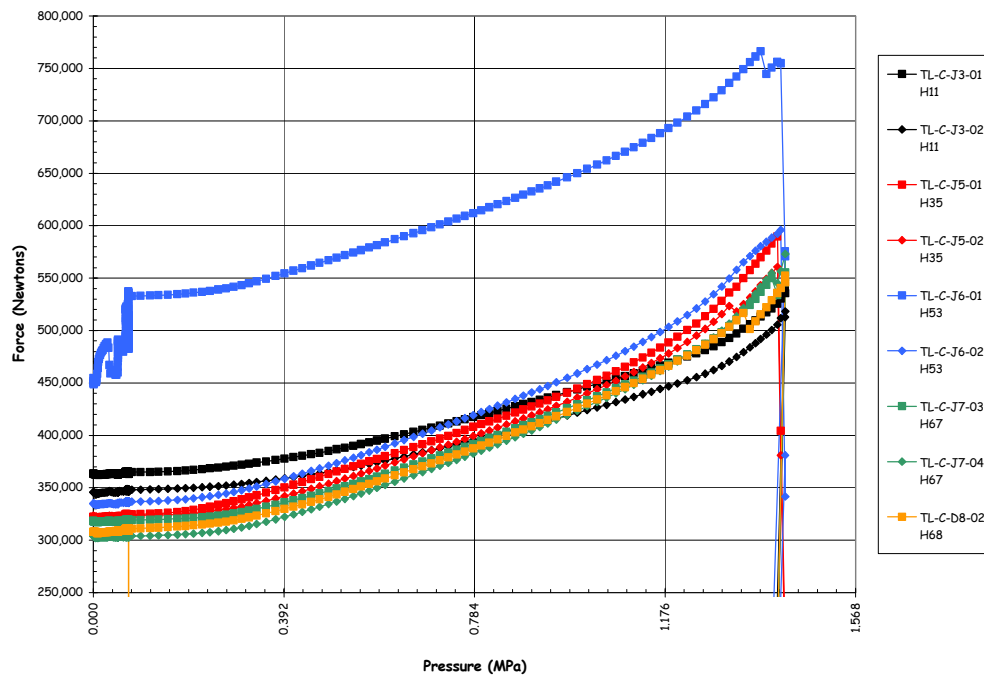


Figure 5.106 SFMT – Instrumented Hoop Tendon Anchor Forces

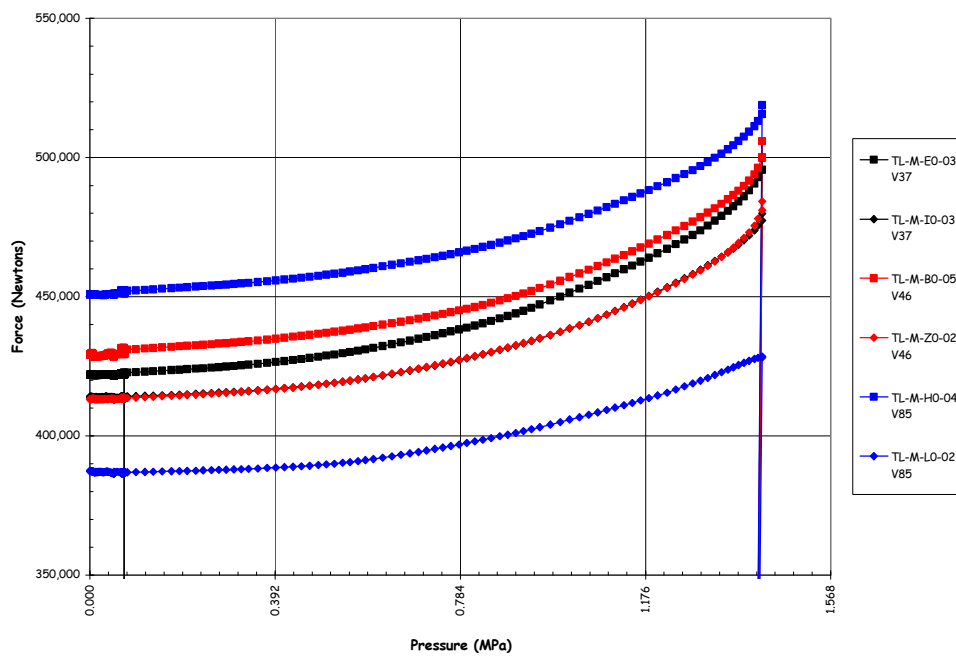


Figure 5.107 SFMT – Instrumented Vertical Tendon Anchor Forces

Tendon strains were also recorded using the surviving foil gages mounted on individual strand wires. Figures 5.108 and 5.109 show the strains for hoop tendons H53 and H68, and Figure 5.110 shows the strains for vertical tendon V46. These results are typical of the other instrumented tendons, although the magnitude of the strains vary. Since the strain gages were 're-zeroed' before the SFMT, only the strain due to pressure is plotted. The total tendon strain is the measured strain plus the residual prestressing strain, typically on the order of 0.4% for the hoop tendons and 0.6% for the vertical tendons. The hoop tendon strains at maximum pressure were therefore on the order of 1.0%, 0.4% due to prestressing plus 0.6% due to the maximum pressure of $3.65P_d$. Similarly, the maximum hoop tendon strain measure prior to rupture is on the order of 1.4% to 1.5%. There may be some local strain concentrations that were not captured by the strain gages, but this limiting tendon strain is significantly less than the ultimate strain obtained from laboratory tests of a straight tendon sample, typically on the order of 4% for the tendon and 7% for individual strands. Furthermore, none of the model tendons ruptured at the anchors where strain concentrations might be expected, but all ruptured where the deformation of the model was greatest, approximately azimuth 6 degrees.

Similarly, the strain in the vertical tendons at the maximum pressure are on the order of 0.1 to 0.2%, and the total strain is on the order of 0.7% to 0.8%. Both are well below the strain at which the hoop tendons were believed to have ruptured, reinforcing the belief that the vertical tendons did not fail prior to the rupture of the vessel.

The tendon force profiles, previously constructed for prestressing and the LST, were also constructed for the SFMT. Since the tendon strains were re-zeroed for the SFMT, it was assumed that the residual strain for each gage after the LST was the initial strain at the start of the SFMT. These residual strain values were added to the SFMT strain data and the force distribution profiles were constructed in the same manner as before. Figures 5.111 to 5.115 show the force profiles for the five instrumented hoop tendons.

One point deserves mentioning. The tendon anchor forces appear to drop off at or just beyond the peak pressure. This is an artifact of rupture occurring during a data scan. The pressure and strain values were recorded near the beginning of the scan, while the load cells were among the last instruments scanned. If rupture, which occurred in a few seconds, took place during the 30 second data scan, the DAS would associate the pressure before rupture with the load cell reading after rupture, giving the appearance that the tendon anchor forces dropped before the model ruptured.

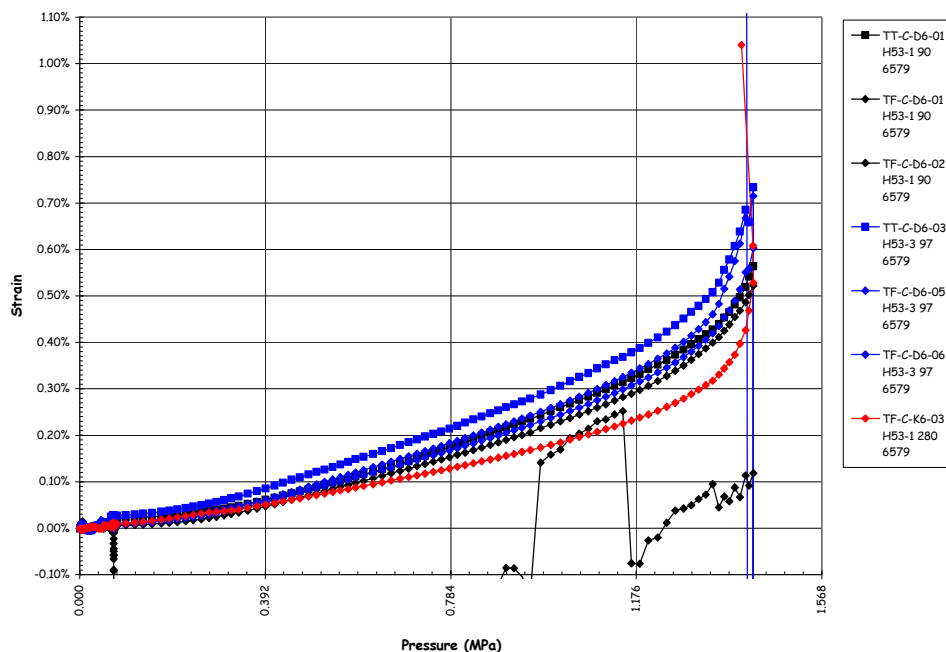


Figure 5.108 SFMT – Tendon H53 Strains

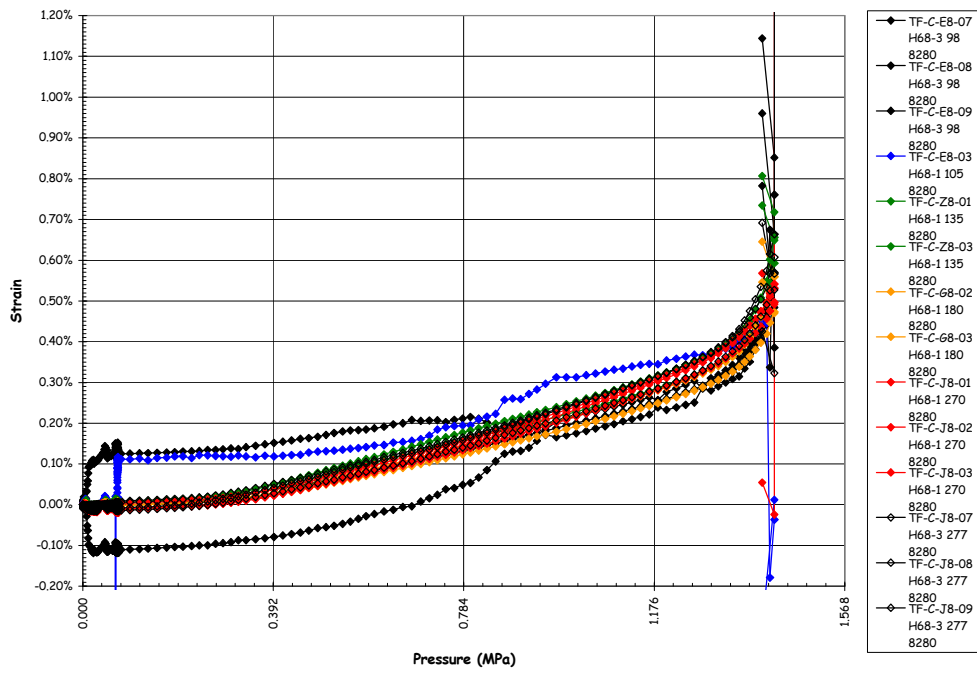


Figure 5.109 SFMT – Tendon H68 Strain

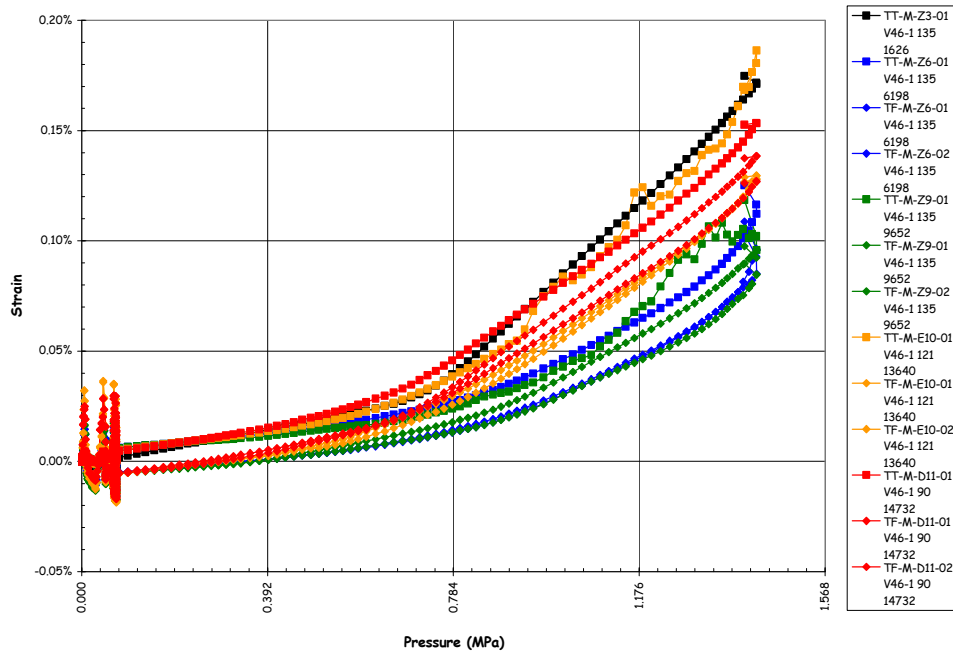


Figure 5.110 SFMT – Tendon V46 Strains

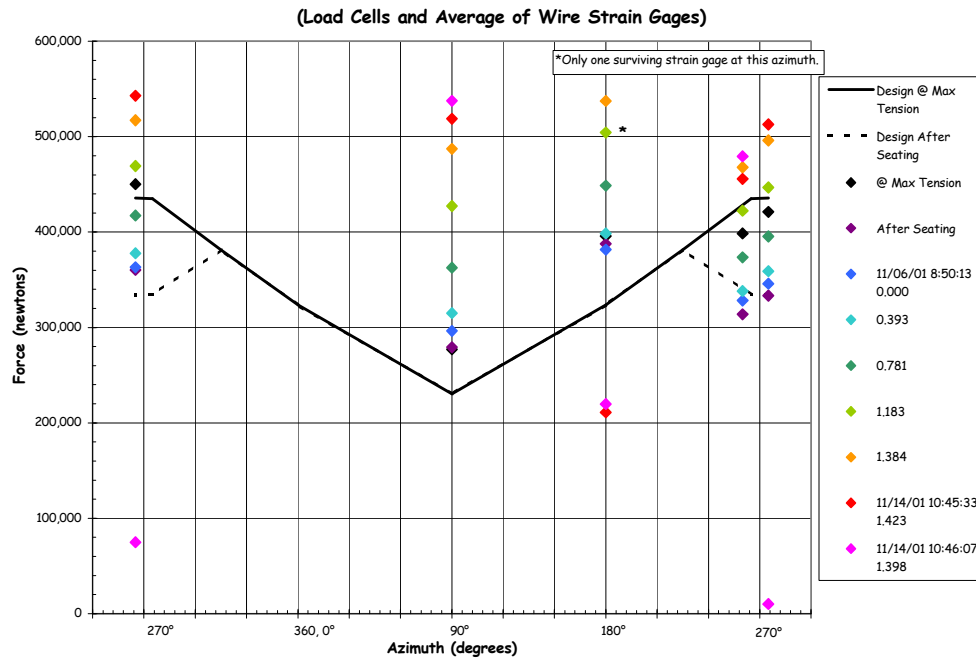


Figure 5.111 SFMT – Tendon H11 Force Distribution (Elev. 1854)

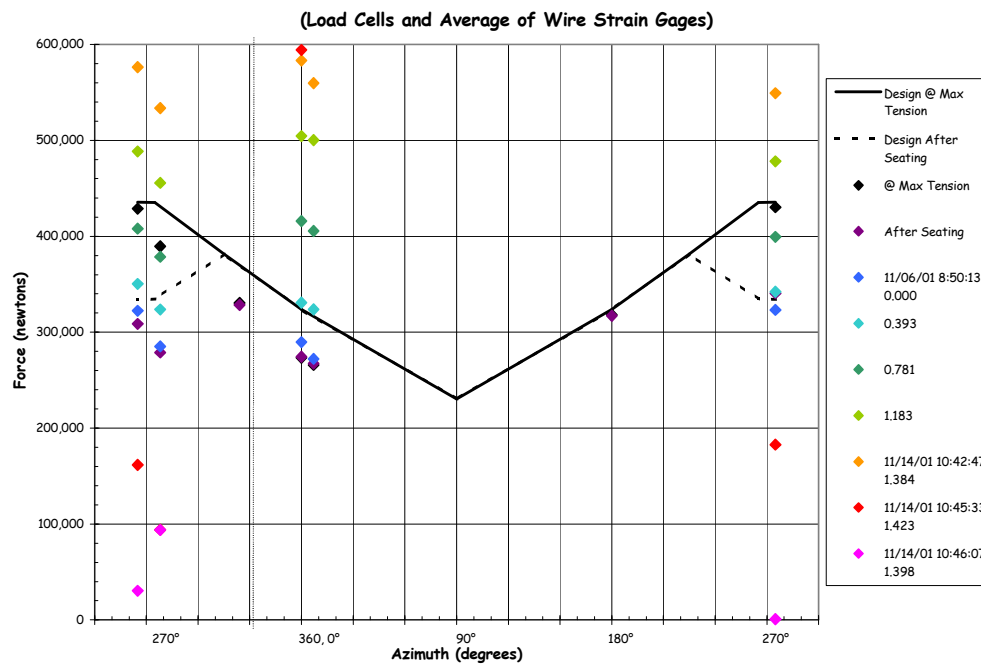


Figure 5.112 SFMT - Tendon H35 Force Distribution (Elev. 4572)

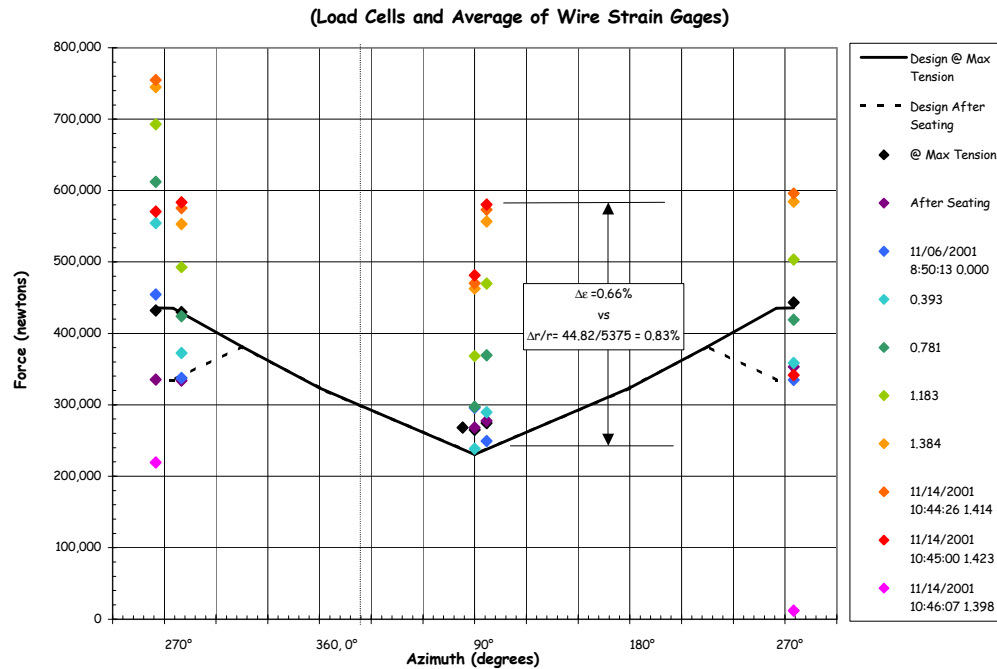


Figure 5.113 SFMT - Tendon H53 Force Distribution (Elev. 6579)

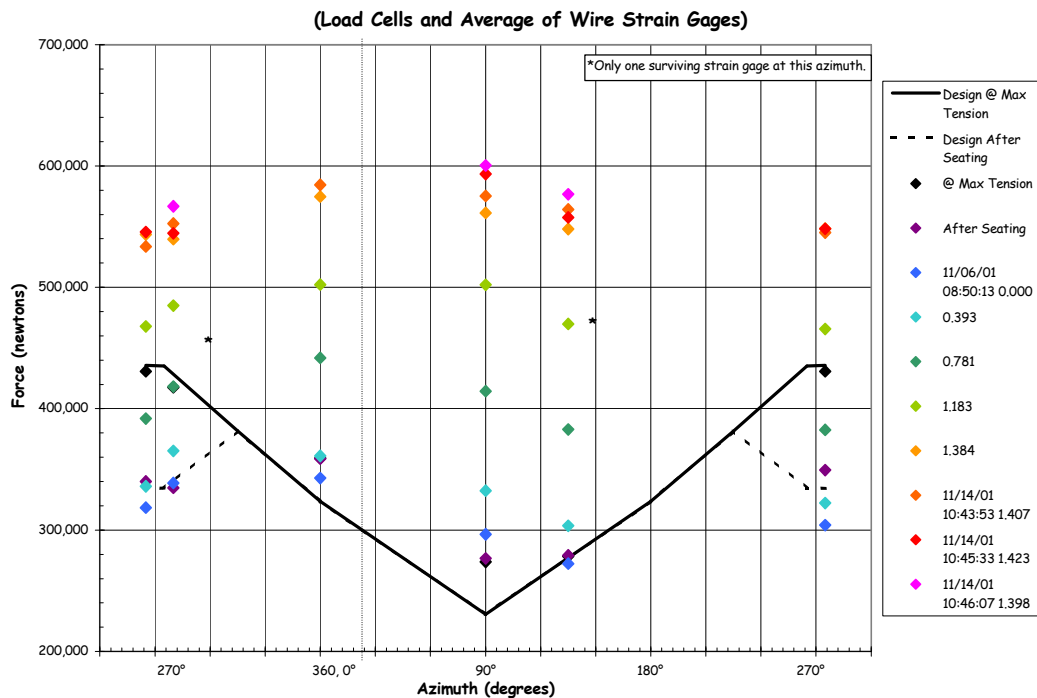


Figure 5.114 SFMT - Tendon H67 Force Distribution (Elev. 8153)

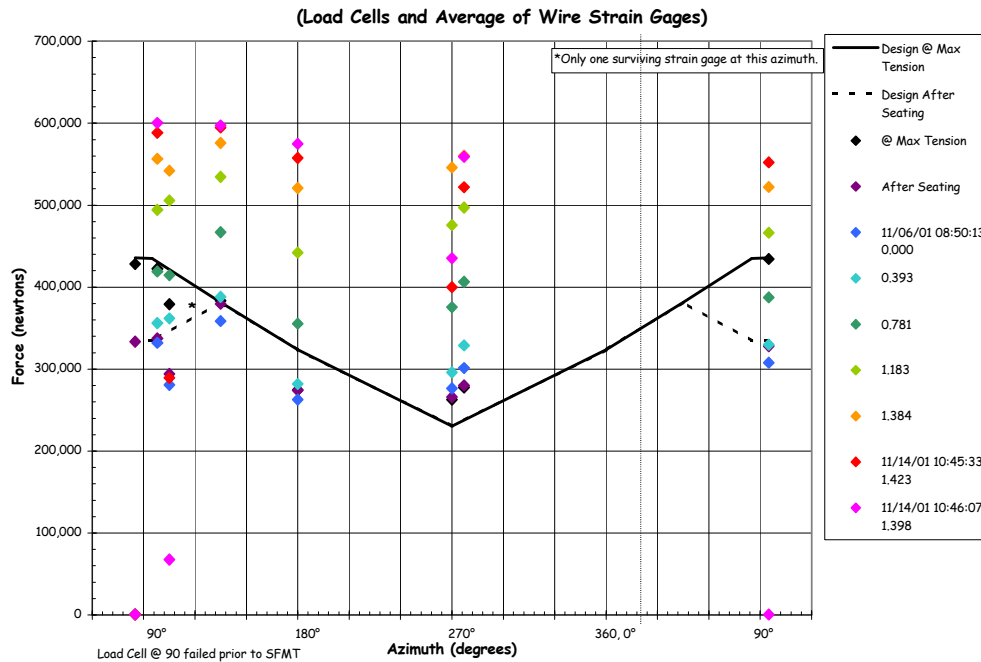


Figure 5.115 SFMT - Tendon H68 Force Distribution (Elev. 8280)

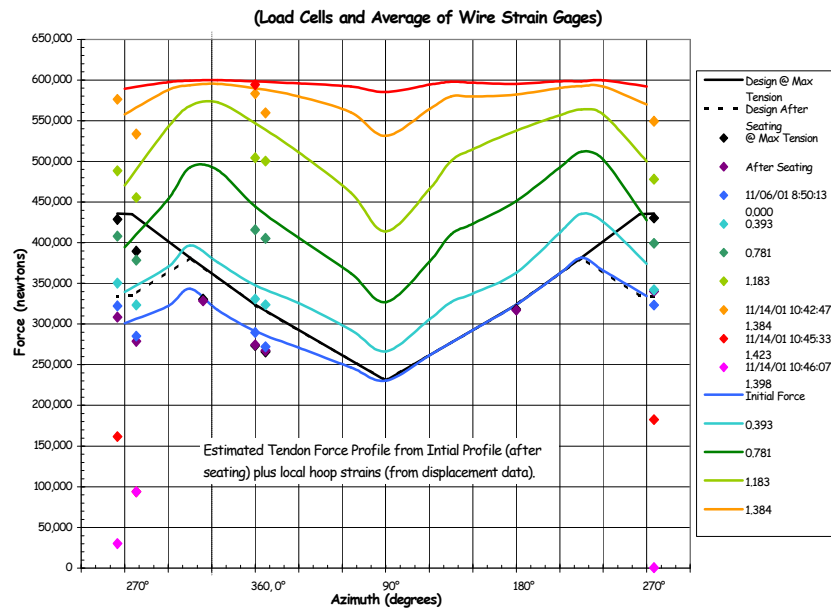
Again, the data is not adequate to assume the shape of the hoop tendon force profile between the surviving measurement positions, and only the force at the measurement locations are plotted, with no attempt to interpolate the strain between the measurement locations. As the pressure is increased, however, and generalized yielding of the model and the tendons occurs, all the plots indicate that the tendon force becomes more uniform along the length, approaching a limiting value of approximately 600 kN (135 kips). One unresolved issue is whether the tendon force equilibrates by slipping relative to the sheath or if the friction is high enough to effectively bond the tendon to the concrete.

An attempt was made to determine this by calculating the local, displacement-based strain in the wall and, assuming the tendon behaved as if bonded, adding it to the initial prestressing strains and computing the force profile from these strains. Figure 5.116 compares the force distribution obtained in this manner with the forces based on the tendon strain measurements for tendon H35 near elev. 4680 where the displacements were measured. The results compare favorably and seem to reinforce the idea that the tendons behave as if they were bonded after prestressing. While this is a compelling argument, it must also be admitted that these results are not entirely conclusive and further tests may be required to resolve this issue.

Figures 5.117 to 5.119 show the force profiles for the instrumented vertical tendons. Again, as was observed with the response during the LST, the force profile appears to become more uniform with pressure. Since the vertical tendons do not yield, tendons must slip relative to the sheath or concrete wall, even in the dome where the tendons are curved. This counters the observation made for the hoop tendons that the tendons behave as if they were bonded to the concrete. No explanation for this apparent inconsistency has been proposed, reiterating the need for further investigation of this behavior, including additional testing.

5.3.3.1.5 Acoustic Response

The acoustic monitoring system used during the LST was also employed for the SFMT, minus the interior sensors, which were removed to install elastomeric liner. Since the SFMT was not focused on detecting liner tearing/leaks, this was not a significant compromise. The focus of the acoustic system during the SFMT was to detect tendon wire breaks and any other events that might indicate structural damage. The acoustic monitoring system was put into operation at the same time the main DAS was started, prior to filling the vessel with water. (As noted in Section 5.2, it was also employed during the pneumatic leak check of the elastomeric liner.)



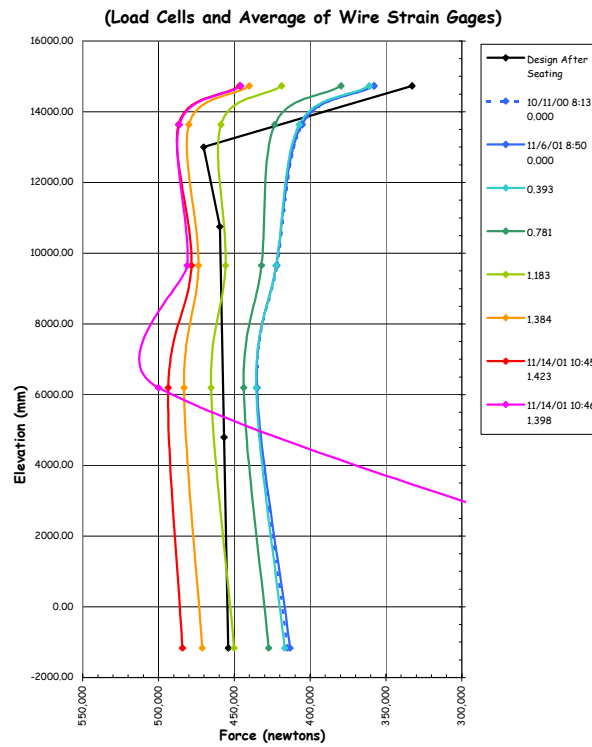


Figure 5.118 SFMT - Tendon V46 Force Distribution at Azimuth 135 Degrees

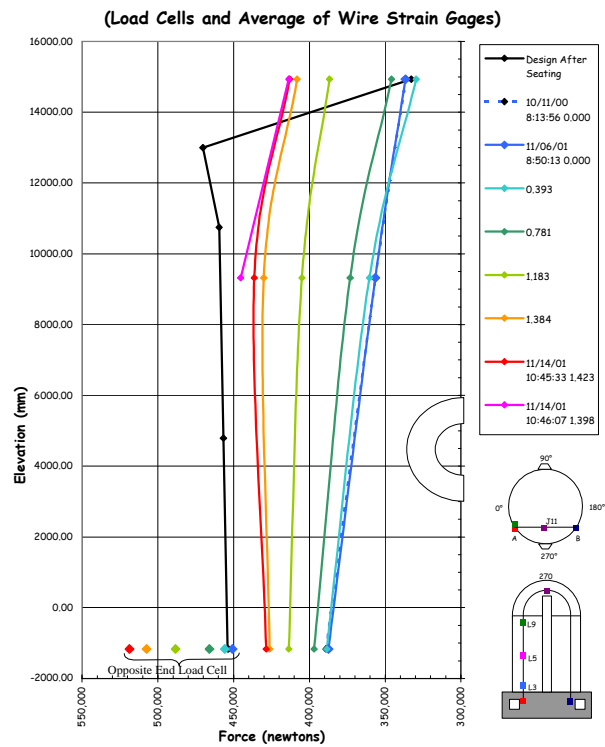


Figure 5.119 SFMT - Tendon V85 Force Distribution at Azimuth 325 Degrees

The post-SFMT reports from Pure Technologies are included in Appendix K. The acoustic event data is also included with the SFMT response data files in Appendix I (data CD). Along with a .wav file of the combined acoustic output during the final minute leading up to, and including, the rupture of the PCCV model. In addition to background noise associated with leaking, deformation, and microcracking of the model, the system identified distinct acoustic events which were categorized as concrete cracking, tendon gallery events, tendon pings, and tendon wire breaks.

Only 27 distinct concrete cracking events were recorded during the SFMT prior to rupture, continuing the trend observed during the LST, i.e., the bulk of the concrete cracking events occurred between 1.0 and 2.3P_d. The tendon pings were confined to the vertical buttresses and the tendon gallery, as during the LST, suggesting the tendons and anchors continued to readjust or reseal themselves. Since all the tendon pings occurred during the final minutes of the SFMT (10:39:30 to 10:45:26), it may also suggest some slipping at the anchors.

The tendon gallery events were all limited to the tendon gallery between 10:43:37 and 10:46:03, implying something occurred with the vertical tendons. The acoustic characteristic of these events is different from the tendon pings and suggested a different mechanism. However, no physical explanation for these events was offered or identified during posttest inspection or demolition of the model.

Fifty-seven actual or probable wire break events were identified between 10:39:47 and rupture of the model at 10:46:12. The wire-break event locations are mapped in Figure 5.120.

Other than observing the discontinuities in the tendon load cell and strain time histories that might indicate a wire break, there were no other efforts to correlate the probable wire breaks identified by the acoustic system with the other test data. While it is arguable that the probable wire break events were actual wire breaks, at least a dozen or so were confirmed by the visual records. Figure 5.121 plots the time history of all the acoustic events along with the effective pressure time history. It is readily apparent that the frequency and magnitude of the wire break events increases just prior to rupture.

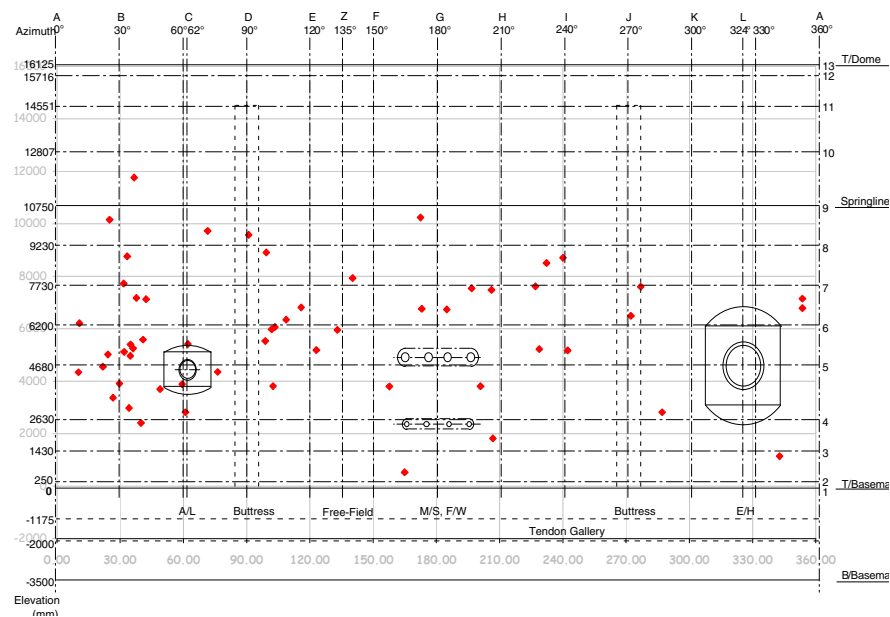


Figure 5.120 SFMT – Wire Break Map

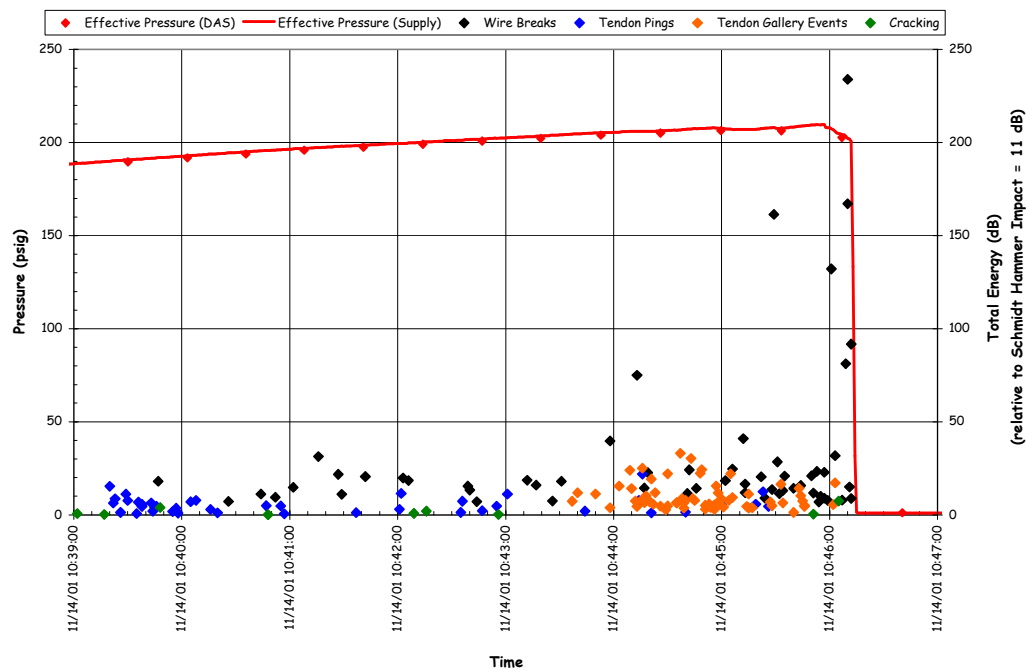


Figure 5.121 SFMT – Acoustic Event and Pressure Time History

5.3.3.1.6 Video

Due to the dynamic nature of the PCCV model rupture at the end of the SFMT, the video images were a valuable diagnostic resource for understanding the failure sequence. Four exterior digital video cameras at 0 degrees, 90 degrees, 180 degrees, and 270 degrees and two interior video cameras at the E/H and at the top of the dome monitored the model throughout the SFMT. Viewing the images in slow motion revealed that the model rupture began at the mid-height of the cylinder at approximately 6 degrees azimuth. The rupture propagated vertically in both directions until it reached a point approximately 2 m above the top of the basemat. The cylinder wall then began to open up, shearing itself from the basemat circumferentially in both directions, and meeting on the back side at 180 degrees. The vessel then ‘telescoped’ over the stem of the cylinder wall before coming to rest on the instrumentation frame.

The interior view of the E/H was distorted by the water and the resulting images were not useful. However, the camera in the dome showed the water surface dropping just prior to the rupture of the vessel, which was captured by all four external video cameras. A video file (.mpg) showing the PCCV model during the final minute of the SFMT and posttest images is included on the data CD in Appendix I. This video includes the acoustic system recording synchronized with the visual images. From close inspection of the video file, visible event times were documented in Table 5.6. The same event may have been observed at slightly different times depending on the camera viewing the event.

5.3.3.2 Posttest Inspection

Since the model was severely damaged and unstable, inspection after the SFMT was limited to an exterior survey. The exterior surface was photographed and the debris field was roughly mapped to document the model fragment locations.

The rupture lines are roughly mapped in Figure 5.122. This figure shows the approximate location of major vertical and horizontal rupture lines along with secondary tears at the E/H and adjacent to the main vertical rupture. These secondary tears are most likely associated with previous liner tears and/or cutouts.

The hoop rebar and tendons along the main rupture line were also inspected for evidence of any discontinuity or other defects that may have accounted for the location of rupture. The close-up photographs of the rebar and tendon strands in Figure 5.123 clearly show ‘necking’ of the bars and wires, indicating that they failed in a ductile manner with large local strains occurring before failure. These photographs are typical of all the tendons and bars at the rupture. The hoop

Table 5.6 SFMT Video Event Times

Time	0° Camera	90° Camera	180° Camera	270° Camera
hour:min:sec:1/30th sec (Video camera speed: 30 frames/second)				
10:45:55:28		H40 wedge ejected, strand broken		
10:45:56:01			H40 wedge ejected, strand broken(?)	
10:45:56:15		Something begins falling @ 100°, El. 5000 toward 5 o'clock		
10:45:56:26	Concrete spall above E/H			
10:45:57:00				Concrete spall (?) @ E/H
10:46:01:24		H42 wedges ejected, strand broken	H42 wedge ejected, strand broken	
10:46:03:10	Water stream starts @ 30°			
10:46:09:09		H64 strand broken/ejected		
10:46:09:12			H64 strand ejected	
10:46:11:21		Spurt of water(?) from H48 anchor		
10:46:11:26	H37 strand ejected			H37 strand ejected
10:46:12:00	Rupture initiated @ 6° (Collapse over in less than 2 seconds)			
10:46:12:01			H40 second strand ejected H37 strand ejected	Rupture
10:46:12:06			Rupture, multiple strands ejected	

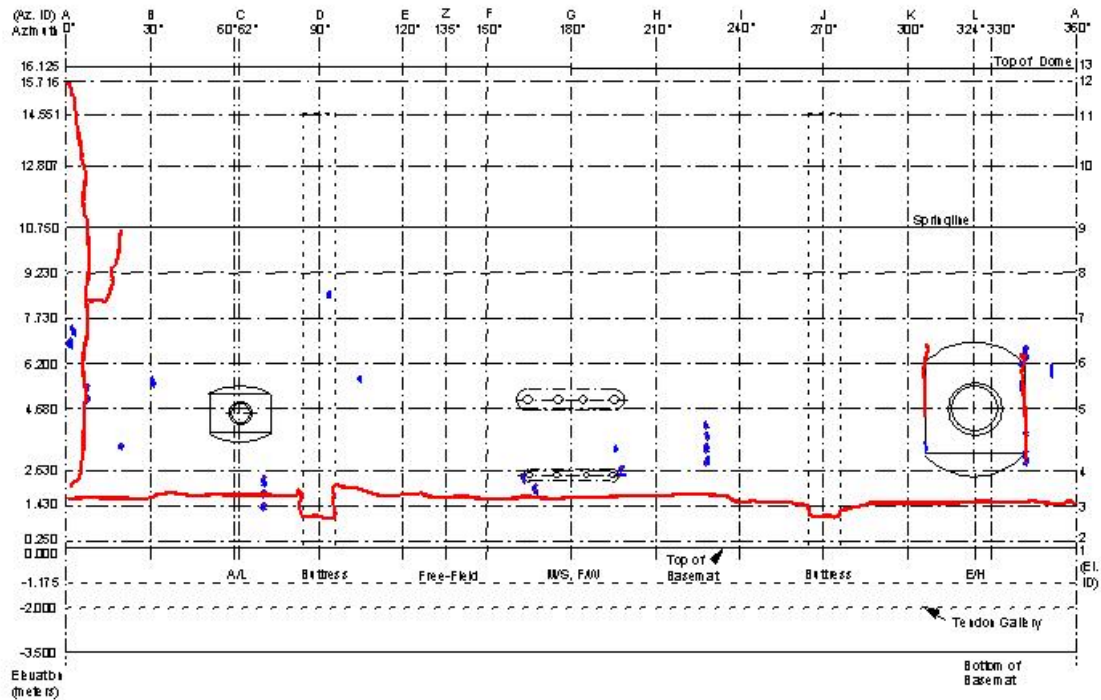


Figure 5.122 SFMT – Rupture Map

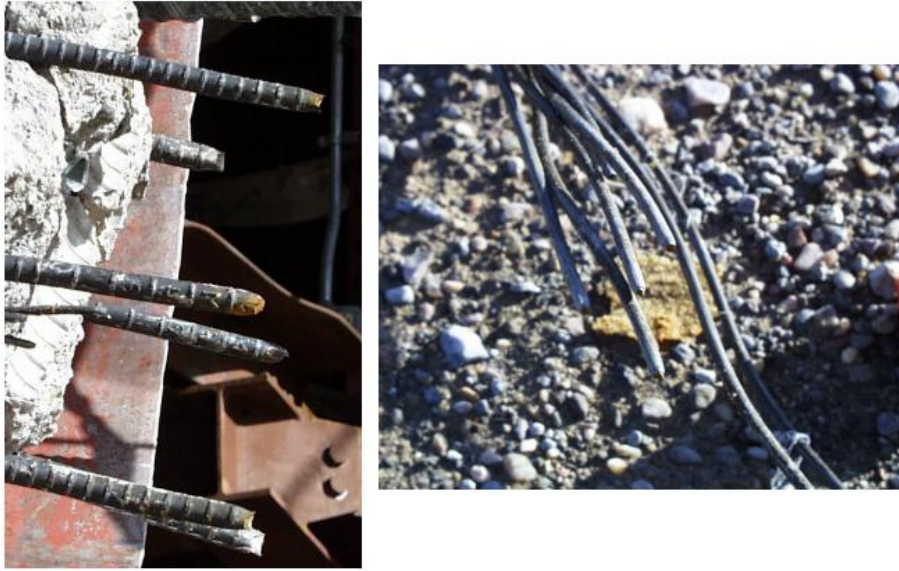


Figure 5.123 SFMT – Rebar and Tendon Strands at the Rupture Line

bars were spliced mechanically very near the rupture, but there was no evidence that any of the mechanical splices failed or that these in any way biased the location where failure began.

The position of the model after the SFMT was also noted. Figure 5.124 shows that the model displaced approximately 3" horizontally and tipped in the opposite direction of the rupture. Six tendons were completely ejected from the model and the final location of major pieces of debris were mapped on the site plan, as shown in Figure 5.125. The location of the debris was not only due to the initial rupture, but also by the flow of 350,000 gallons of water escaping from the model.

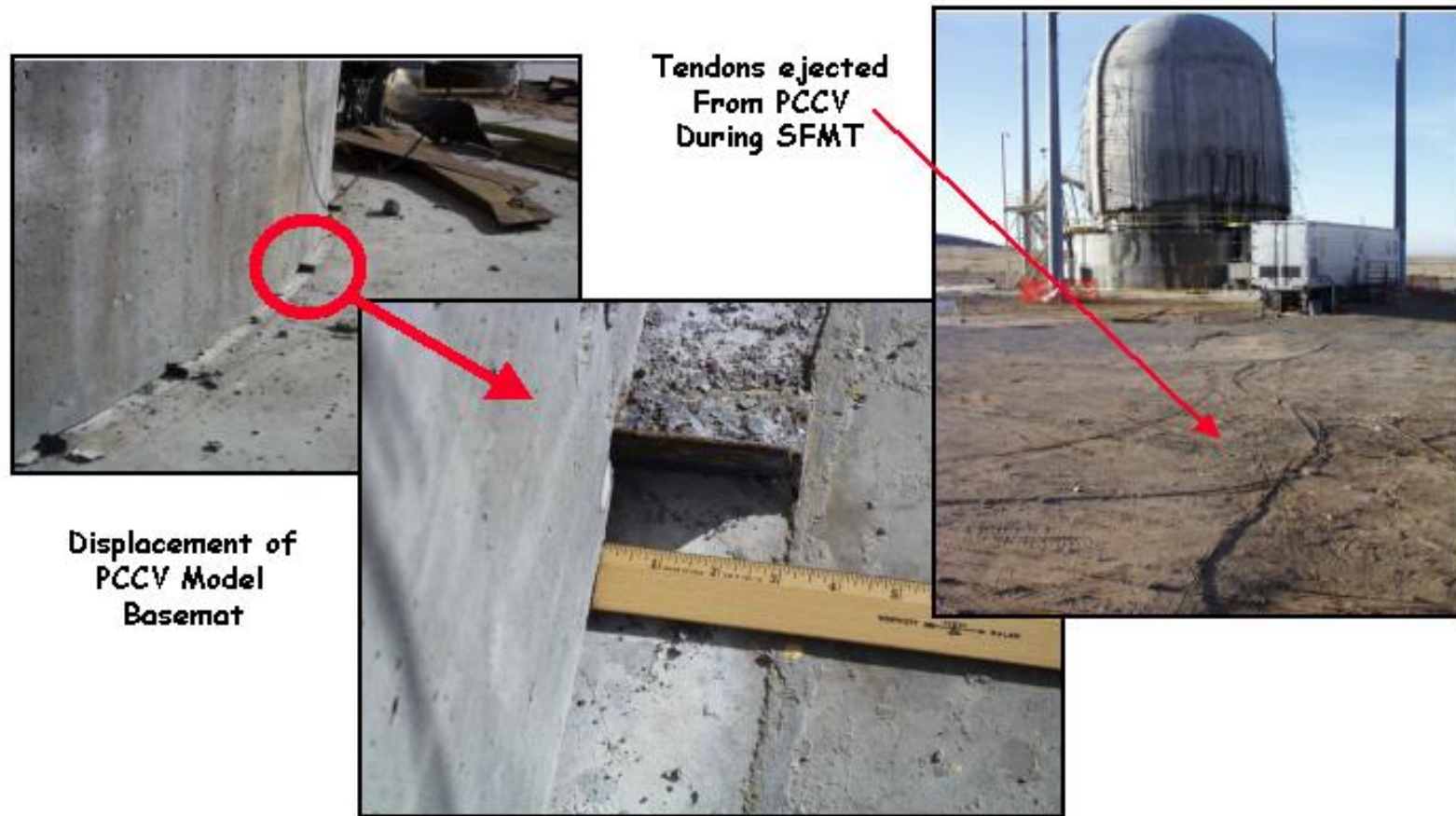


Figure 5.124 SFMT – Model Displacements

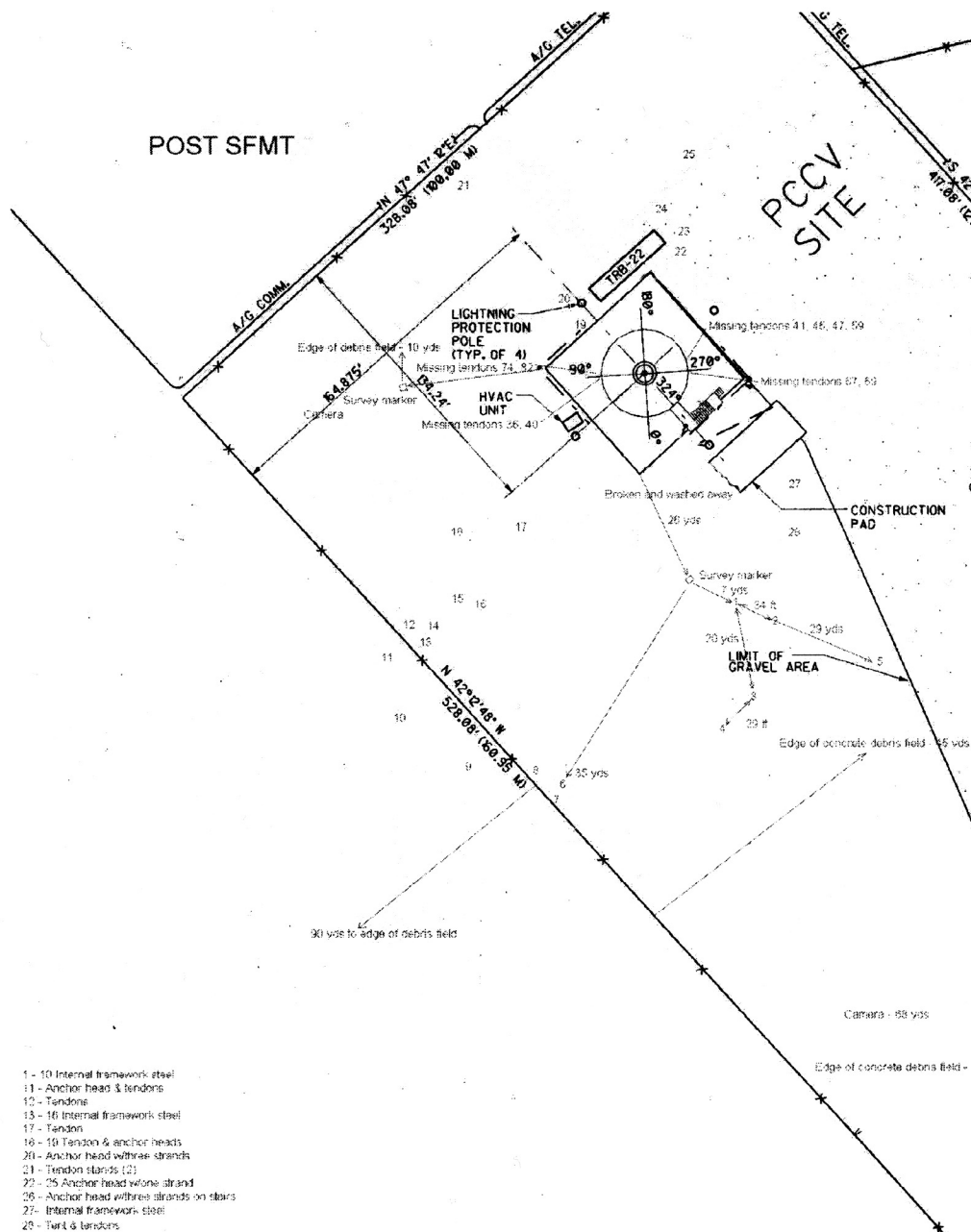


Figure 5.125 SFMT - Debris Map

6. SUMMARY AND CONCLUSION

The overpressurization tests of the 1:4-scale PCCV model represent a significant advance in understanding the capacity of nuclear power plant containments to withstand loads associated with severe accidents. The data collected during the tests, as well as the response and failure modes exhibited, will be useful to benchmark numerical simulation methods used to predict the response of concrete containment structures. One important observation, which should not be overlooked by focusing on the technical results, is that this program not only demonstrated that international collaboration on large-scale experiments is technically and programmatically feasible, but also desirable. The experience and expertise of the Japanese and U.S. partners, along with those of the Round Robin participants and other international support, contributed to the success of the project and resulted in a much more meaningful and productive effort.

While lessons for actual plants can and should be drawn from this and previous large-scale containment model tests, such insights are beyond the scope of this report and will be addressed in a future effort. (A program has been initiated by the NRC at SNL to apply the results of the test programs to the design and operation of actual plants.) The reader is cautioned *not* to draw direct conclusions regarding the pressure capacity of actual plants from these tests or interpret these results as a demonstration of the prototype capacity. The PCCV model tests demonstrated the importance of the unique details and as-built characteristics of the model on the ultimate capacity. Any efforts to estimate the capacity of an actual containment must address the unique features of the plant under consideration.

Furthermore, no conclusions were drawn in this report regarding the analytical methods used to predict or simulate the response of the model or actual containments. These are addressed separately in the pre- and posttest analysis reports [6, 7, and 8].

The conclusions drawn from the PCCV tests in this report will be limited to a discussion of the model, instrumentation, and test design, and their adequacy in meeting the objectives of the program. Where appropriate, recommendations for further investigation are made.

6.1 Model Design

6.1.1 Scale Artifacts

The results of the test clearly demonstrate the necessity of conducting model tests at a scale large enough to:

- utilize materials that exhibit the characteristics of those in the prototype,
- represent the design details and construction methods used in the prototype, and
- avoid the presence of non-representative details and as-built conditions.

At 1:4-scale, the PCCV model achieved most of these criteria. However, even at this scale, the results of the test were subject to scale-related artifacts, most notably in the response of the liner. A variety of compromises were made in the selection of the liner material (which was similar, but not identical, to the prototype), fabrication methods, and details. The decision to scale the weld acceptance criteria (porosity, inclusion, flaw size) might have, in hindsight, contributed to possible premature liner tearing. Since it was nearly impossible to meet the weld acceptance criteria for the field welds, most were rejected and repaired, resulting in local thinning and strain localization in the vicinity of the welds. When the acceptance criteria were later relaxed, the resulting welds appeared to perform much better than those that were repaired (in that no tears were discovered at unrepaired welds). Other factors, such as using intermittent back-up bars and modified liner anchor and stiffener details, may have further contributed to the localized tearing of the liner.

This observation could lead one to conclude that the initial plan of a mixed-scale model, with a thicker liner, might have been preferable. However, that option is also fraught with difficulties. A thicker liner, which might have delayed liner tearing and leakage, could have resulted in a catastrophic failure (as witnessed during the SFMT), when it is more than likely that an actual liner would have torn before reaching the structural limit of $3.6 P_d$.

Suffice it to say that the selection of the model scale is a critical decision which should be guided by a thorough understanding of the prototype design. One must exercise care when introducing any model artifacts that could affect the results of the test.

6.1.2 Material Properties

As a corollary to the previous point, it is worth making a few observations regarding the data from tests used to define the properties of construction materials. Typically, the properties are obtained from standardized tests of small or representative samples of the construction materials. These test methods assure that the construction materials meet a minimum quality standard. Experience has shown that if these minimum standards are met, the structure will meet the design requirements. This is subtly, but significantly, different from characterizing the *in-situ* properties of a structure's constitutive elements.

Nevertheless, these standardized test results are usually all that is available, and most engineers would be happy to have actual material data rather than minimum specified properties. The difficulty arises when the properties of these sample tests are used to develop mathematical material models to predict the response of structures well beyond their design limits, especially when they include inelastic behavior and failure conditions.

The SFMT clearly demonstrated that the tendons failed shortly after the cylinder wall and measured tendon strains were approximately 1%, much less than the 4 to 7% strain obtained from laboratory tests of tendon specimens. Similarly, the measured (and calculated) liner strains at the pressure level where the liner tore were well below the ultimate strain of the liner coupons, even considering local strain concentrations.

This raises the question, then, of whether current standard material test methods are being used to perform a function for which they were not originally intended and if they are adequate for the task. If not, can alternate test methods be devised to provide a better basis for constitutive models? There have been significant advances in the computational methods used to simulate structural response, but no comparable advances in the measurement and characterization of material models on which these computational methods depend.

A second question related to the material properties is the type and amount of data considered adequate to calculate the response of actual containments. A fairly extensive suite of material tests were conducted for the PCCV model, and actual properties were used in all cases. It is not clear if this level of information would be available for all containments. If not, the quality of the capacity predictions may be reduced, with a corresponding increase in uncertainty. One way to address this question might be to use the specified properties of the PCCV model and compare the resulting capacity prediction with those based on the measured properties.

These questions pertain to the use of all structural model test data, and it is not possible to answer these questions on the basis of the PCCV test results alone. However, they are worthy of considering when the results of the PCCV model tests are utilized.

6.1.3 Prestressing System

As the critical feature of the PCCV model, the prestressing tendons deserve special attention. Again, because of the scale limitations, several compromises were made in the design of the model prestressing. Although each tendon in the prototype was represented in the model, the individual strands were larger than the prototype tendons. In addition, the tensioning and anchoring hardware could not be scaled, resulting in higher friction losses and a force profile that deviated significantly from the prototype.

It is not obvious from the test results whether the deviations from the prototype had any significant effect on the capacity of the PCCV. However, the test results, while somewhat inconclusive, did indicate that the assumptions used to predict the tendon force distribution and losses might require further investigation. This appears to be particularly true for the vertical tendons, where the losses due to wobble friction appeared to be underestimated and the losses due to angular friction appeared to be overestimated.

The test also indicated that the tendon force distribution becomes more uniform as the pressure is increased, especially beyond the elastic limits of the model. However, the mechanism by which this adjustment occurs was not clearly demonstrated. The question of whether the tendons behaved as if they were unbonded (and achieved the ‘load leveling’ by slipping relative to the concrete wall) or bonded (resulting in local yielding and increased local deformation) may be an important modeling consideration and should be investigated in more detail, especially if opportunities exist for additional large-scale testing.

It was also noted that, although the vertical tendons were initially tensioned to a higher level than the hoop tendons (nearly 25% higher after anchoring), the challenge to the vertical tendons was minor compared to the hoop tendons. (The level of the vertical prestressing is typically governed by the stress at the apex, where the effective prestressing is calculated to be significantly less than at the base.) This apparent discrepancy between the expected and observed behavior suggests that a review of the design method for the vertical tendons may be in order.

6.2 Instrumentation and Data Acquisition

In spite of a higher-than-expected gage mortality, in most cases from damage during construction, the instrumentation and data acquisition systems performed up to specifications and provided most of the data necessary to understand the response of the model and to compare with analyses. Some observations and lessons learned are warranted.

6.2.1 Displacements

The displacement data provided the most reliable source of information and insight into the model’s overall response to the pressure loads. Nevertheless, the tests demonstrated some factors that should have been considered in the design of the instrumentation and might have improved the quality of the data.

Displacement transducers are relatively inexpensive to procure and install. In hindsight, it might have been useful to install more displacement transducers, even at the cost of eliminating some other gages.

The primary difficulty in measuring displacements is finding a stable global reference point. For small structures, this may be relatively simple; but for large, exposed structures, this can be a significant challenge. In the case of the PCCV, most of the model displacements were measured relative to the stiff instrumentation frame, which was mounted on the fairly rigid basemat. This proved to be a good choice and internal measurements of the frame motion confirm that it did not move significantly as a result of basemat uplift or thermal expansion. (One minor problem discovered after prestressing was that the displacement transducers were attached to the liner, assuming it was ‘bonded’ to the concrete wall, which turned out not to be the case. This was recognized fairly quickly, but could have been avoided if the locations of the displacement measurements corresponded with liner anchor locations, or if small anchors had been attached to the liner at the displacement measurement locations before placing concrete.)

Some transducers were not or could not be mounted on the reference frame, and an incomplete understanding of the interaction between the reference and measurement locations resulted in misleading data. The most notable example of this was the measurement of uplift at the edge of the basemat. In this case, the vertical motion of the basemat’s outside bottom edge was measured relative to the top of the mudmat. This arrangement failed to recognize that the mudmat’s stiffness was insignificant compared to the basemat and that any deformation of the basemat was reflected by the mudmat. As a result, no differential displacement was measured and the initial conclusion was that no basemat uplift had occurred. While comparing this response with the analyses, which did predict some uplift would occur, the flaw in the transducers’ placement was recognized. Unfortunately, no data was obtained to confirm the analytical results. If this phenomenon had been recognized in advance, a more stable reference location could have been identified or constructed.

Other examples of such difficulty include the measurement of the radial and vertical displacement at the wall-base junction, where again some minor modifications could have eliminated all or most of the problem and ensured the desired data was obtained. The point of this discussion is not to fault the design of the instrumentation system, but to point out the importance of carefully considering the stability of the physical reference frame and interpreting the data with a thorough understanding of its practical limitations.

In designing the instrumentation for the PCCV model, efforts were made to obtain independent displacement measurements with a stable fixed reference frame. A number of optical and laser tracking systems were considered, but none of them provided a cost-effective solution with the required accuracy in harsh environmental conditions. Advances in these or other systems may, however, yield viable options for future large scale tests.

6.2.2 Liner Strains

With 559 installed on the PCCV model, the liner strain gages accounted for over one-third the total number of transducers on the model. While strain gages are relatively inexpensive to purchase, the installation, monitoring, and processing of the data represented a significant portion of the project's cost. This naturally leads to the question of whether the data obtained justified the expense.

The liner strain gages were intended to measure:

- the global or free-field hoop and meridional strains,
- the local strains near liner discontinuities, and
- the local strains in the liner anchors and stiffeners.

The free-field strain gages yielded larger maximum strains than those derived from the displacement data. For example, at the maximum LST pressure ($3.3P_d$), the liner hoop strain at Z6 was 0.90%, compared to approximately 0.5% computed from the displacement data. The difficulty of measuring global or even near-field strains from liner strain data is in the sensitivity of small gage length strain gages to local discontinuities or variations in the liner, even when these discontinuities are not readily apparent. It does not appear that these free-field liner strains reliably indicate the free-field strains in the wall. This problem might have been reduced by installing larger gage-length strain gages for the free-field measurements, thus minimizing the effect of local variations, but these are more difficult to install and even at larger gage lengths (e.g. 50 mm or 2 in) the problem is not completely eliminated.

The strain gages located near the liner discontinuities (e.g. near anchors and stiffeners, fold lines, and inserts) registered higher strains than the surrounding material and provided some valuable information for comparison with local liner analysis. Direct comparison was difficult, however, since the problem of local variations and discontinuities was exacerbated by the high local strain gradients and as-built conditions which may not be modeled. In this case, the gage length of the strain gages may have been too large to measure the peak liner strains. Individual strain gage data can be misleading, and multiple gages are required to construct a map of the strain fields in the vicinity of the discontinuity.

One other problem with local liner strain measurements is well known, but difficult to avoid. Strain gages placed near a tear typically measure smaller strains than strain gages placed in a similar location without a tear, because the tear acts as a strain relief mechanism. This phenomenon was demonstrated by the strain gages located near the E/H and M/S penetrations.

The liner anchor strain gages were generally consistent with the free-field meridional gages and the average vertical strain in the cylinder wall calculated from the displacements. In fact, the peak liner anchor strain of 0.1% is identical to the average strain derived from the displacements. This makes sense when considering that the anchors are bonded better to the concrete than the liner, suggesting that the free-field strains can be measured more accurately by mounting strain gages on the anchors and hoop stiffeners if they can be isolated from other discontinuities.

6.2.3 Rebar/Concrete Strains

The strain gages were mounted on the main reinforcing steel and on specially fabricated gage bars, expecting that these rebar strains would be an accurate measure of the local strains in the wall due to membrane and bending forces. A few fiber-optic strain gages were installed to independently measure the concrete wall strains at a few selected locations to corroborate this assumption. The test data indicates that the rebar strains are a reliable measure of the wall strains up to the onset of local yielding. At this point, the method to mount the strain gages on the rebar, which removes a small portion of the bar to provide a smooth surface on which the gage is bonded, forms a 'structural fuse.' This structural fuse

yields before the rest of the bar yields and experiences artificially higher strains, up to 0.5%, beyond yield. For the PCCV test, the post-yield behavior was of primary interest and this artifact corrupted the rebar strain data beyond roughly $1.5P_d$. Improved methods of measuring rebar strains that avoid the structural fuse problem would make rebar strain measurements more reliable indicators of the wall strain.

Overall, the displacement data provided a much more accurate and reliable measure of the local membrane wall strains than the rebar gages. The displacement data could not, however, provide any insight into the local bending strains in the wall at locations such as the wall-base junction, the springline, and the buttresses.

The fiber-optic gages yielded much better results; however, these gages are relatively expensive and experienced a fairly high mortality rate. Improvements in the installation technique and reduction in hardware costs would make these gages a much more attractive option for future tests.

Most of the gage bars were damaged during construction or after prolonged exposure to the elements. The surviving gage bars did provide some useful data and demonstrated that the concept was sound. The expense of fabrication and difficulty of installation, however, do not make this an attractive option, compared to the fiber-optic gages, for future tests.

6.2.4 Tendon Strains/Forces

The major instrumentation challenge posed to SNL for the PCCV model test was to measure the force distribution in the tendons during prestressing and pressure testing. Efforts in previous testing programs to collect force distribution data on unbonded tendons had been generally unsuccessful. A significant effort was made to investigate, develop, and demonstrate the feasibility of measuring the tendon strains within the program schedule and budget constraints. Since this was not an instrumentation development program, the effort focused on adapting or modifying ‘off-the-shelf’ components for this task. SNL was also limited to using transducers that would not require any modification in the basic structural components or their arrangement. (Some minor modifications, such as increasing the instrumented tendon duct diameter from 35 to 40 mm, were accepted to accommodate the instrumentation.) While the results were not completely satisfactory due to the high mortality rate (>50%) of the strain gages, a significant amount of data unique for prestressed concrete structures was collected, and the feasibility of measuring the variation in tendon strain, and indirectly force, along the length was demonstrated.

As noted above, the data obtained during the test did not conclusively provide an understanding of the tendon response mechanism beyond yield to ultimate load. Future tests, if conducted, might resolve this issue using improved tendon instrumentation. The biggest challenge for the instrumentation was surviving the harsh mechanical environment imposed on the sensors and lead wires during the prestressing operations. A number of promising non-contact sensors were investigated for the PCCV test to avoid this problem, but they were ultimately abandoned due to cost, reliability problems, or difficulty integrating them into the model. If future tests are planned, improvements in these sensors or new types of sensors might make them an attractive alternative to the methods employed in the PCCV test, and should be considered seriously. The lessons learned and the techniques developed for the PCCV test provide a solid basis for the next step in understanding unbonded tendon behavior.

6.2.5 Acoustic

The Soundprint® acoustic monitoring system provided the only quantitative monitoring of the entire model as opposed to the individual transducers that monitored discrete model elements. The acoustic monitoring system detected concrete cracking, liner tearing and leakage, and tendon wire or rebar breaks. The system successfully met all of these objectives at a relatively low cost, and almost immediately detected a liner leak at the leak rate threshold established for the test, 1% mass/day. To a lesser extent, it was also able to identify the general location of the first liner tear/leak, although detection and location of the subsequent tears/leaks was less conclusive.

Posttest analysis of the acoustic data also suggested that it might be a viable means of detecting the onset of global tensile cracking (and associated loss of stiffness). Although the acoustic capabilities to locate events were degraded during the SFMT due to the existing concrete damage and the elimination of interior sensors, the Soundprint® system was still able to detect tendon wire breaks. Because of the extensive damage caused when the model ruptured, posttest inspection was

unable to confirm the number or location of the reported wire break events. However, the wire break events that did occur were detected.

Further analysis of the extensive acoustic data obtained from prestressing through all of the pressure tests might provide further insights into the capabilities of acoustic monitoring systems to monitor containments and similar structures.

6.2.6 Video/Still Photography

Each phase of the model construction, instrumentation, and testing was photographed in detail to provide a record that could subsequently aid in the interpretation of the model response to applied loads. Thousands of still photographs and hours of video were recorded and archived for future use. In spite of this effort, there were still some features of the model or procedures that could have been documented in more detail. Nevertheless, these records, which were obtained at a relatively low cost, proved invaluable.

The best example of the records' value was in providing a partial explanation of the liner tearing mechanisms. While it was a particularly painstaking effort, the decision to photograph the exterior surface of all the liner field welds in the cylinder wall and dome before placing the rebar and concrete provided graphic evidence of the local discontinuities influence on the response and tearing of the liner. After the tears were located on the inside of the model, the photographic database provided detailed information on the condition of the backside. This information was subsequently used in the posttest examination and analysis of the liner.

In a similar, although less dramatic, manner, photographs of the transducer installations also assisted the interpretation of some test data, especially with regard to the effect of placement and mounting details. Crack mapping of the concrete wall after prestressing and pressure testing was also greatly facilitated by tracing and photographing the surface.

Since the tests were essentially static in nature (except for the SFMT), no high-speed film or video photography was used. Use of standard video cameras during the LST was limited to providing visual input of the model response for test operations. Observing a few critical locations inside the model with close-up video in an attempt to observe local damage, e.g. liner tearing, was not successful, since the locations observed did not exhibit any visible damage.

The external digital cameras used during the SFMT, however, were invaluable in capturing the sequence of rupture and damage progression of the model. Even with normal speed video, the failure of several tendons and the location where the rupture started were recorded. It is unlikely that without this visual record the sequence of the model failure would have been as clearly understood. The interior video camera that observed the water surface also gave an early indication of the model rupture, as the water surface was observed to drop rapidly just prior to rupture, although this was not immediately recognized.

6.2.7 Data Acquisition

The DAS was specifically *not* designed as a high-speed DAS, but was designed to provide accurate, real-time information on the model's response during the application of relatively slow loading over an extended period of time, to operate unattended, and to efficiently manage the large volumes of data obtained. It performed this function admirably, and the robustness of the system was demonstrated several times during power outages and other challenges such as lightning strikes. The few minor system 'failures' that occurred did not take place during critical test periods, and recovery and restart of the system was always accomplished quickly and with a minimal loss of data.

The DAS was adapted to the challenge of the rapid loading during the SFMT with only some minor difficulties noted near the end of the test, when correlation of the pressure with a specific response value introduced some error due to the relatively slow scan rate (30 sec) compared to the time over which the model rupture occurred (<1 sec). This error is insignificant as long as the time lag is recognized. However, it does point out the need to ask if rapid data acquisition capabilities are required, should future tests be conducted.

6.3 Testing

The successful completion of the tests within the programmatic constraints, i.e. cost and schedule, attest to the adequacy of the test plans and procedures. However, a few points may require further consideration and discussion.

6.3.1 Loading

The reasons for conducting static, pneumatic overpressurization tests at ambient temperature were discussed in Section 1.2.2. While the tests successfully obtained data on the response to pressurization and, secondarily, to prestressing, the application and interpretation of these results should recall that the test load does not faithfully represent the complex loading environment that will exist during a severe accident. The effects of temperature, the temporal relationship between pressure and temperature, the composition of the internal atmosphere, and the rate of loading may all affect the response and failure modes and the sequence of these events and should be considered in any evaluation of containment capacity.

Other containment model tests [45] have attempted to consider some or all of these aspects of severe accident loads. Future efforts should consider evaluating the effects of these other loads on the response of the PCCV model and possibly the prototype, and the results of these efforts may indicate a need for additional testing that includes these loads.

6.3.2 Failure Criteria

As noted in Section 1.2.3, it was not the goal of these tests to establish failure criteria, either functional or structural, for prototypical containments. Nevertheless, the test did provide some insight into issues that should be considered when establishing failure criteria for actual containments.

First, the primary functional failure criteria defined in terms of a maximum leak rate cannot be applied directly to conventional mechanistic models of containment structures that output response in terms of displacement, strain, force, stress, etc. As a result, design philosophies have focused on limiting these response variables to ensure that no leakage occurs. Further study of the relationship between leakage and structural response may provide some insights that could be applied to regulations and design requirements based on functional criteria.

Secondly, predictions of containment capacity have often been based on the structural capacity of the components used in the construction; for example, using the ultimate strength or elongation of samples of prestressing tendons, liner, rebar, etc., as the limit criteria. The PCCV model test demonstrated, as noted in the discussion on material properties, that the strain levels measured at failure can be much lower than the limiting values obtained from standard tests of sample specimens. The test results should provide some guidance on the development of appropriate failure criteria for use in future capacity calculations.

6.3.3 Leak Rate Measurements

The SIT/ILRT data, conducted in accordance with the specified procedures currently used in both Japan and the U.S., demonstrated the difficulty of accurately measuring leak rates to guarantee that they do not exceed the specified limits. Even with the relatively simple, controlled structure represented by the PCCV model and the extensive suite of instruments available during testing, it was not possible to accurately measure leak rates on the order of 0.1% mass/day. An apparent leak rate of 0.5% mass/day at 1.5P_d during the LST was due to thermal expansion of the model in response to ambient temperature changes and the model's direct heating. In light of these results, a review of leak rate measurement methods and the leak rate test criteria should be considered.

One area to explore might be the use of acoustic monitoring to detect, locate, and, possibly, measure leak rates. The acoustic monitoring system was able to readily detect a leak rate of 1% mass/day. Further evaluation of the data and refinement of the monitoring system might determine the feasibility of detecting even smaller leaks and possibly correlating the acoustic signal levels with leak rate.

7. REFERENCES

1. Luk, V. K., M. F. Hessheimer, G. S. Rightley, L. D. Lambert and E. W. Klammerus, *Design, Instrumentation, and Testing of a Steel Containment Vessel Model*, NUREG/CR-5679, SAND98-2701, Sandia National Laboratories, Albuquerque, NM, January 1999.
2. Porter, V. L., P. A. Carter and S. W. Key, *Pretest Analysis of the Steel Containment Vessel Model*, NUREG/CR-6516, SAND96-2877, Sandia National Laboratories, Albuquerque, NM, January, 1999.
3. Luk, V. K., and E. W. Klammerus, *Round Robin Pretest Analysis of a Steel Containment Vessel Model and Contact Structure Assembly Subject to Static Internal Pressurization*, NUREG/CR-6517, SAND96-2899, Sandia National Laboratories, Albuquerque, NM, August, 1998.
4. Ludwigsen, J. S., V. K. Luk, M. F. Hessheimer, and J. F. Costello, *Posttest Analyses of the Steel Containment Vessel Model*, NUREG/CR-6649, SAND99-2954, Sandia National Laboratories, Albuquerque, NM, February 2000.
5. Luk, V. K., and E. W. Klammerus, *Round Robin Posttest Analysis of a Steel Containment Vessel Model*, NUREG/CR-5678, SAND98-700, Sandia National Laboratories, Albuquerque, NM, January, 2000.
6. Dameron, R. A., L. Zhang, Y. R. Rashid, and M. S. Vargas, *Pretest Analysis of a 1:4-Scale Prestressed Concrete Containment Vessel Model*, NUREG/CR-6685, SAND2000-2093, ANATECH Corporation, San Diego, CA and Sandia National Laboratories, Albuquerque, NM, October, 2000.
7. Dameron, R. A., Hanson, B. E., Parker, D. R., and Rashid, Y. R. 2003. *Posttest Analysis of a 1:4 Scale Prestressed Concrete Containment Vessel Model*, NUREG/CR-6809, SAND2003-0839P, ANA-01-0330, ANATECH Corporation, San Diego, CA and Sandia National Laboratories, Albuquerque, NM, February, 2003.
8. Luk, V. K., *Pretest Round Robin Analysis of a Prestressed Concrete Containment Vessel Model*, NUREG/CR-6678, SAND00-1535, Sandia National Laboratories, Albuquerque, NM, August, 2000.
9. American Society of Mechanical Engineers, Boiler and Pressure Vessel Code, Section III, Division 2, Code for Concrete Reactor Vessels and Containments.
10. Blejwas, T. E., et. al., *Background Study and Preliminary Plans for a Program on the Safety Margins of Containments*, NUREG/CR-2549, SAND82-0324, Sandia National Laboratories, Albuquerque, NM, May 1982.
11. Parks, M. B., Horschel, D. S., and von Riesemann, W. A., "Summary of NRC-Sponsored Research on Containment Integrity," *Proceedings of the 11th International Conference on Structural Mechanics in Reactor Technology*, August 18-23, 1991, Tokyo, Japan.
12. Parks, M.B., H.P. Walther, and L.D. Lambert. "Experiments to Determine the Leakage Behavior of Pressure-Unseating Equipment Hatches," *Proceedings of the 11th International Conference on Structural Mechanics in Reactor Technology*, Tokyo, Japan, August 1991.
13. Lambert, L.D. and M.B. Parks. *Experimental Results from Containment Piping Bellows Subjected to Severe Accident Conditions*. NUREG/CR-6154, SAND94-1711, Vol. 1. Sandia National Laboratories, Albuquerque, NM. September 1994.
14. Cherry, J. "Analysis of Containment Structures with Corrosion Damage," *Proceedings of the 24th Water Reactor Safety Information Meeting*, Vol. 1, pp. 333-352, Bethesda, Maryland, October 21-23, 1996.
15. Nakamura, S., Y. Sasaki, K. Horibe, M. Nakajima, K. Hoshino, T. Takahashi, T. Hagesawa, T. Kei, T. Meida, K. Takigushi, and H. Akiyama. "Plan of the Seismic Proving Test for Reinforced Concrete Containment Vessel: Test Plan and Test Model Design," *Proceedings of the 14th International Conference in Structural Mechanics on Reactor Technology*, Vol. 11, pp. 83-90, Lyon, France, August 17-22, 1997.
16. James, R.J., Y.R. Rashid, J. Cherry, N.C. Chokshi, S. Nakamura. "Analytical Prediction of the Seismic Response of a Prestressed Concrete Containment Vessel," *Proceedings of the 14th International Conference in Structural Mechanics in Reactor Technology*, Vol. 7, pp. 151-160, Lyon, France, August 17-22, 1997.
17. Arai, S., T. Matsumoto, M. Goto, Y. Naruse, T. Mieda, and H. Yamanaka. "Pressurization Test on the Equipment Hatch Model," *Proceedings of the 14th International Conference on Structural Mechanics in Reactor Technology*, Lyon, France, August, 1997.
18. Lobner, P., C. Donahoe, and C. Vavallin, *Overview and Comparison of U.S. Commercial Nuclear Power Plants*. NUREG/CR-5640, SAIC-89/1541. San Diego, CA: Science Application International Corporation, September 1990.
19. R. A. Dameron, R. S. Dunham, Y. R. Rashid, M. F. Sullaway, H. T. Tang, "Analytical Correlation and Post-Test Analysis of the Sandia 1:6 Scale Reinforced Concrete Containment Test," *Proceedings of the Fourth Workshop on Containment Integrity*, NUREG/CP-0095, SAND88-1836, June 1988, pp. 441-458.

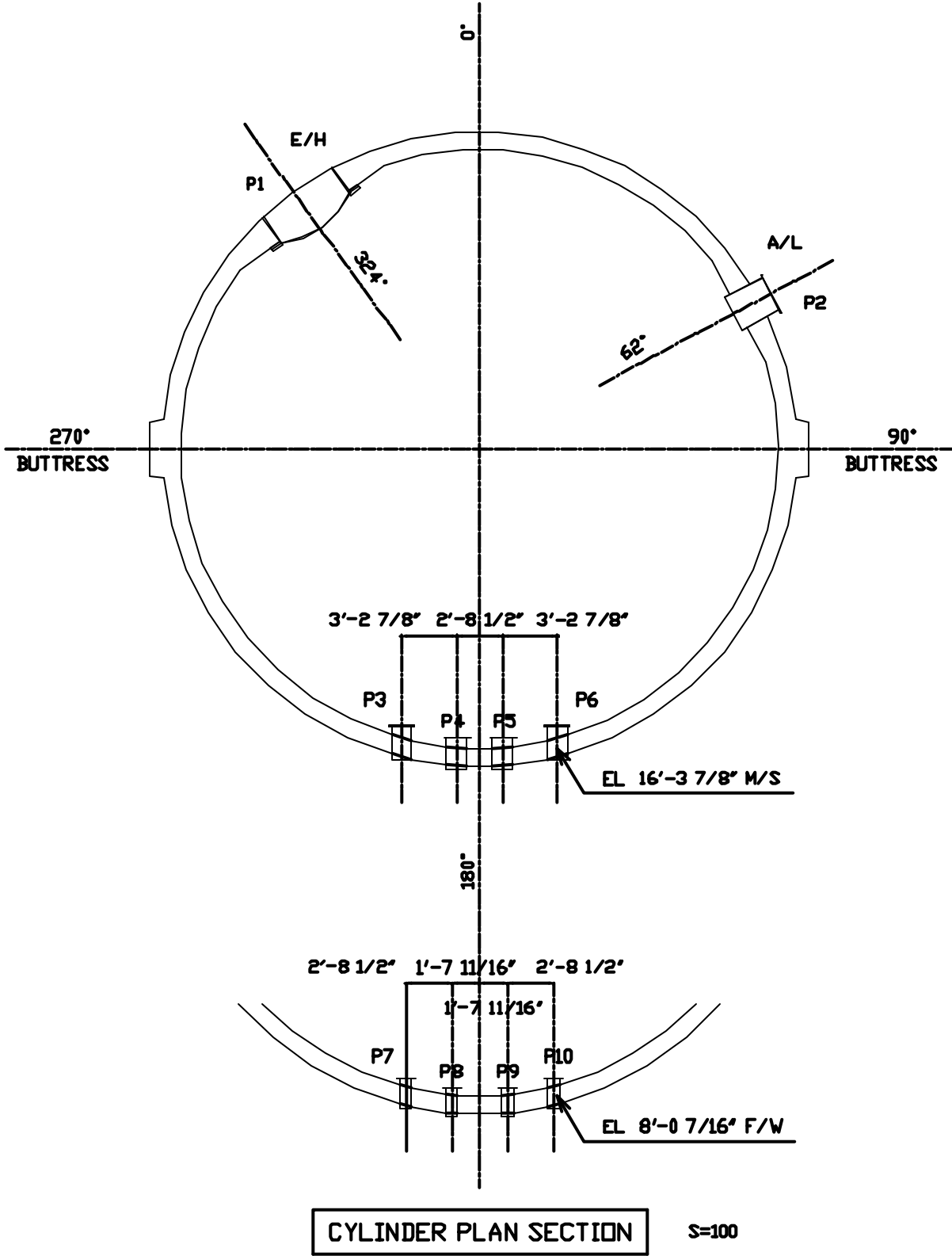
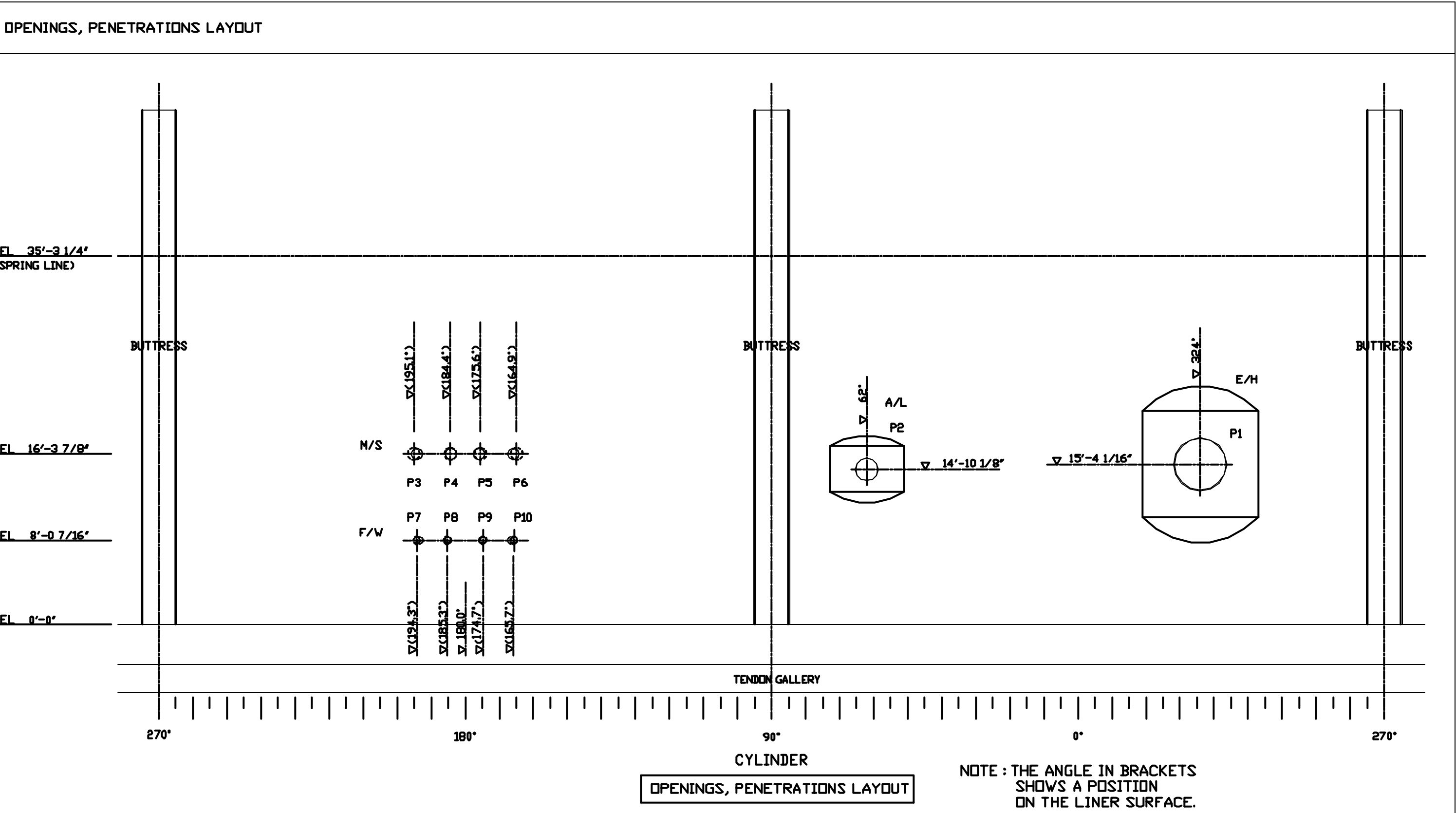
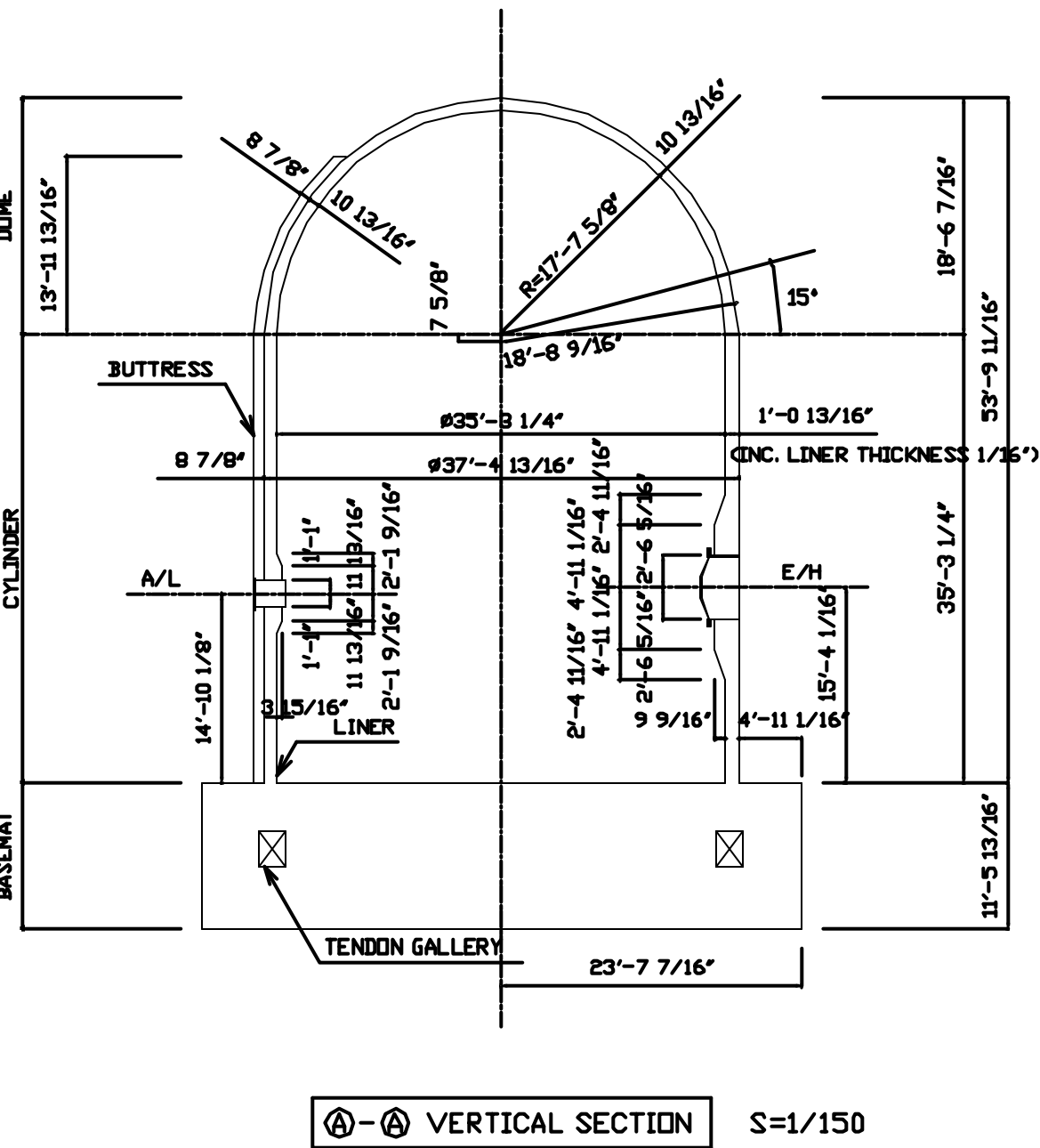
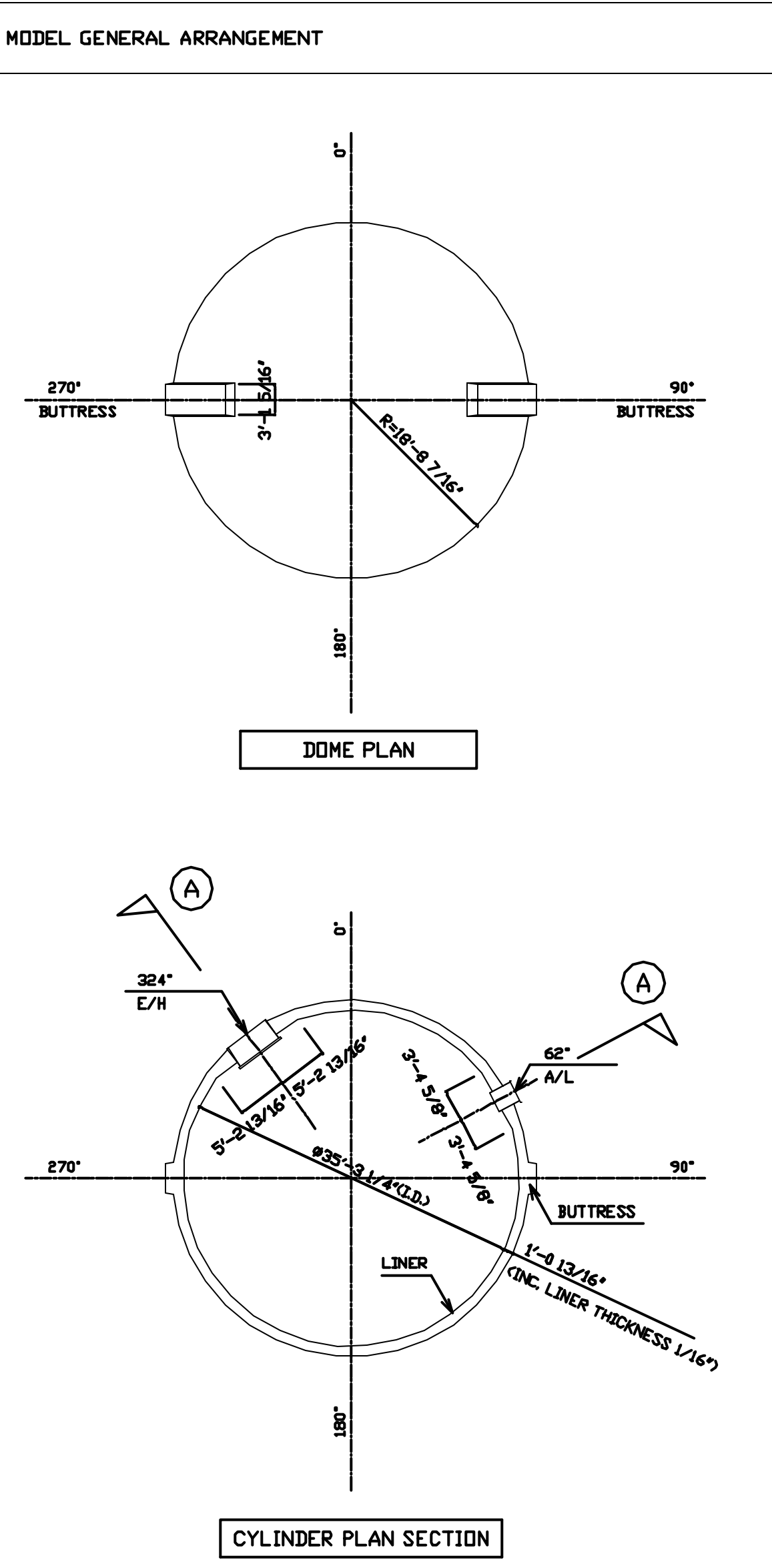
20. R. A. Dameron, Y. R. Rashid, M. F. Sullaway, "Pretest Predictions of 1:10 Scale Model Test of the Sizewell-B Containment Building," *ANATECH Report to Sandia National Labs*, June 1989.
21. R. A. Dameron, R. S. Dunham, Y. R. Rashid, H. T. Tang, "Conclusions of the EPRI Concrete Containment Research Program," *Proceedings of the 3rd International Seminar on Containment of Nuclear Reactors*, August 1989, pp. 189-218.
22. Design Policy of the Test Model (Concrete Body), CTG-09-06, NUPEC, June 1993.
23. Draft Technical Code for Concrete Containment Vessels in Nuclear Power Plants, Ministry of International Trade and Industry, Agency for Natural Resources and Energy, Tokyo, Japan, 1981.
24. Reinforced Concrete Work, Japanese Architectural Standard Specification 5, Architectural Institute of Japan, Tokyo.
25. Reinforced Concrete Work at Nuclear Power Plants, Japanese Architectural Standard Specification 5N, Architectural Institute of Japan, Tokyo.
26. Miller, C. M., "Geotechnical Investigation for the Containment Technology Test Facility-West," Job No. 1-20904, Geo-Test, Inc., Albuquerque, NM, October, 1992.
27. Grush, M., Lenke, L. R. and Escobedo, T., "Strength and Creep Testing of Concrete Used in the Cylindrical Portion of the NUPEC/NRC Prestressed Concrete Containment Vessel," ATR Institute, University of New Mexico, Albuquerque, NM, January, 2000.
28. Lenke, L. R. and Gerstle, W., "Mechanical Property Evaluation of Concrete Used in the NUPEC/NRC Prestressed Concrete Containment Vessel: Prestress and Limit State Test Results," ATR Institute, University of New Mexico, Albuquerque, NM, June, 2001.
29. "PCCV Structural Behavior Test, Basic Plan of Instrumentation for the Test," Nuclear Power Engineering Center, Tokyo, Japan, March, 1992.
30. "Revised Basic Instrumentation Plan for the 1/4 PCCV Model (CTG-12-16)," Nuclear Power Engineering Corporation, Tokyo, Japan, March 16, 1994.
31. R-SN-P-001, "PCCV Instrumentation Plan," Rev. G, Sandia National Laboratories, Albuquerque, NM, February 28, 2001.
32. Dameron, R. A., Zhang, L., Rashid, Y. R., Maxwell, J. S., Vargas, M. S., "Preliminary Analytical Studies of A 1:4-Scale Model of a Prestressed Concrete Containment Vessel Model," R-SI-P-018, ANATECH Corp., San Diego, CA, November, 1997.
33. R-SI-P-002, "PCCV Instrumentation Task Plan," Rev. 2, Sandia National Laboratories, Albuquerque, NM, June, 1999.
34. JPN-12-A-1, "PCCV Structural Behavior Proving Test, Master Plan of the Project," Revision 1, Nuclear Power Engineering Corporation, Tokyo, Japan, June 22, 1994.
35. R-SN-P-007, "Prestressed Concrete Containment Vessel Model Test Plan," Revision B, Sandia National Laboratories, Albuquerque, NM, September, 2000.
36. R-SI-P-005, "ES&H Operating Procedure - Testing of the Prestressed Concrete Containment Vessel (PCCV) Model," Revision B, Sandia National Laboratories, Albuquerque, NM, October 2000.
37. R-SI-P-006, "PCCV Pressurization System Data Package," Revision B, Sandia National Laboratories, Albuquerque, NM, October 2001.
38. Japanese Standard JEAC 4203-1994.
39. MITI Code 501, Article 104.
40. 10CFR50, Appendix J "Primary Reactor Containment Leakage Testing for Water-Cooled Power Reactors."
41. American National Standards. "Leakage Rate Testing of Containment Structures for Nuclear Reactors." ANSI/ANS N45.2-1974.
42. American National Standards "Containment System Leakage Testing Requirements." ANSI/ANS N56.9-1987.
43. NUPEC Liner Examination Report (in Japanese)
44. Procedure of Equipment Hatch Cover Installation, Mitsubishi Heavy Industries, LTD, MH-K12-15, May 26, 2000.
45. Hessheimer, M. F., R. A. Dameron and W. A. von Riesenmann, "A Summary of Containment Integrity Research," Presented at the *Seminar on Containment of Nuclear Reactors* held in conjunction with the 14th International Conference on Structural Mechanics in Reactor Technology (SMiRT 14), Saclay, France, August 15-26, 1997.

Appendix A: PCCV Model Design Drawings

List of PCCV Design Drawings

Number	Date	Rev	Description
PCCV-QCON-01	12/20/96	2	Model-General Arrangement Basemat Rebar Arrangement
PCCV-QCON-02	12/20/96	1	Basemat Tendon Gallery Access Tunnel Rebar Arrangement
PCCV-QCON-03	12/20/96	1	Prestressing Tendon General Arrangement
PCCV-QCON-04	12/20/96	1	Cylinder Prestressing Tendon Arrangement
PCCV-QCON-05	12/20/96	1	Cylinder Prestressing Tendon Arrangement
PCCV-QCON-06	12/20/96	1	Cylinder Prestressing Tendon Arrangement
PCCV-QCON-07	12/20/96	1	Prestressing Tendon Details (Equipment Hatch [E/H]) (Vertical Dome)
PCCV-QCON-08	12/20/96	1	Prestressing Tendon Details (E/H) (HOOP)
PCCV-QCON-09	12/20/96	1	Prestressing Tendon Details (Airlock [A/L])
PCCV-QCON-10	12/20/96	1	Prestressing Tendon Details (Main Steam [M/S] Feedwater [F/W])
PCCV-QCON-11	12/20/96	1	Dome Prestressing Tendon Arrangement-Prestressing System Hardware
PCCV-QCON-12	12/20/96	1	Cylinder & Dome Rebar General Arrangement (1)
PCCV-QCON-13	12/20/96	1	Cylinder & Dome Rebar General Arrangement (2)
PCCV-QCON-14	12/20/96	1	Cylinder & Dome Rebar Details
PCCV-QCON-15	12/20/96	2	Buttress Rebar Details
PCCV-QCON-16	12/20/96	1	Opening Rebar Details (E/H)
PCCV-QCON-17	12/20/96	2	Opening Rebar Details (A/L)
PCCV-QCON-18	12/20/96	3	Penetration Rebar Details (M/S F/W)
PCCV-QCON-19	12/20/96	2	Crane Bracket Rebar Details Rebar Arrangement Standards
M1-ZCD1001A		3	Liner General Arrangement
M1-ZCD1002A		0	Cylinder Liner Anchor Details
M1-ZCD1006A		0	Liner Plate Block Layout of Cylinder Portion
M1-ZCD1007A		2	Cylinder Liner Anchor Details #2-5 Blocks (0-90 Degrees)
M1-ZCD1008A		2	Cylinder Liner Anchor Details #2-5 Blocks (90-270 Degrees)
M1-ZCD1009A		2	Cylinder Liner Anchor Details #2-5 Blocks (270-360 Degrees)
M1-ZCD1010A		0	Cylinder Liner Anchor Details #2-5 Blocks (E/H)
M1-ZCD1011A		0	Cylinder Liner Anchor Details #2-5 Blocks (A/L)
M1-ZCD1012A		0	Cylinder Liner Anchor Details #2-5 Blocks (M/S)
M1-ZCD1013A		0	Cylinder Liner Anchor Details #2-5 Blocks (F/W)
M1-ZCD1014A		0	Cylinder Liner Anchor Details Polar Crane Bracket Details
M1-ZCD1015A		0	Liner Plate Block Layout of Dome
M1-ZCD1016A		0	Stud Layout of Dome
M1-ZCD1018A		0	Liner Plate Block and Stud Details of Dome Portion #6 Tiers
M1-ZCD1019A		0	Liner Plate Block and Stud Details of Dome Portion #7-8 Tiers
M1-ZCD1020A		0	Liner Plate Block and Stud Details of Dome Portion #9-10 Tiers
M1-ZCD1025A	03/26/97	1	Base Liner Plate Detail

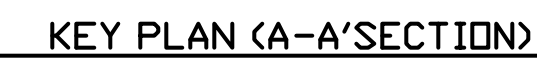
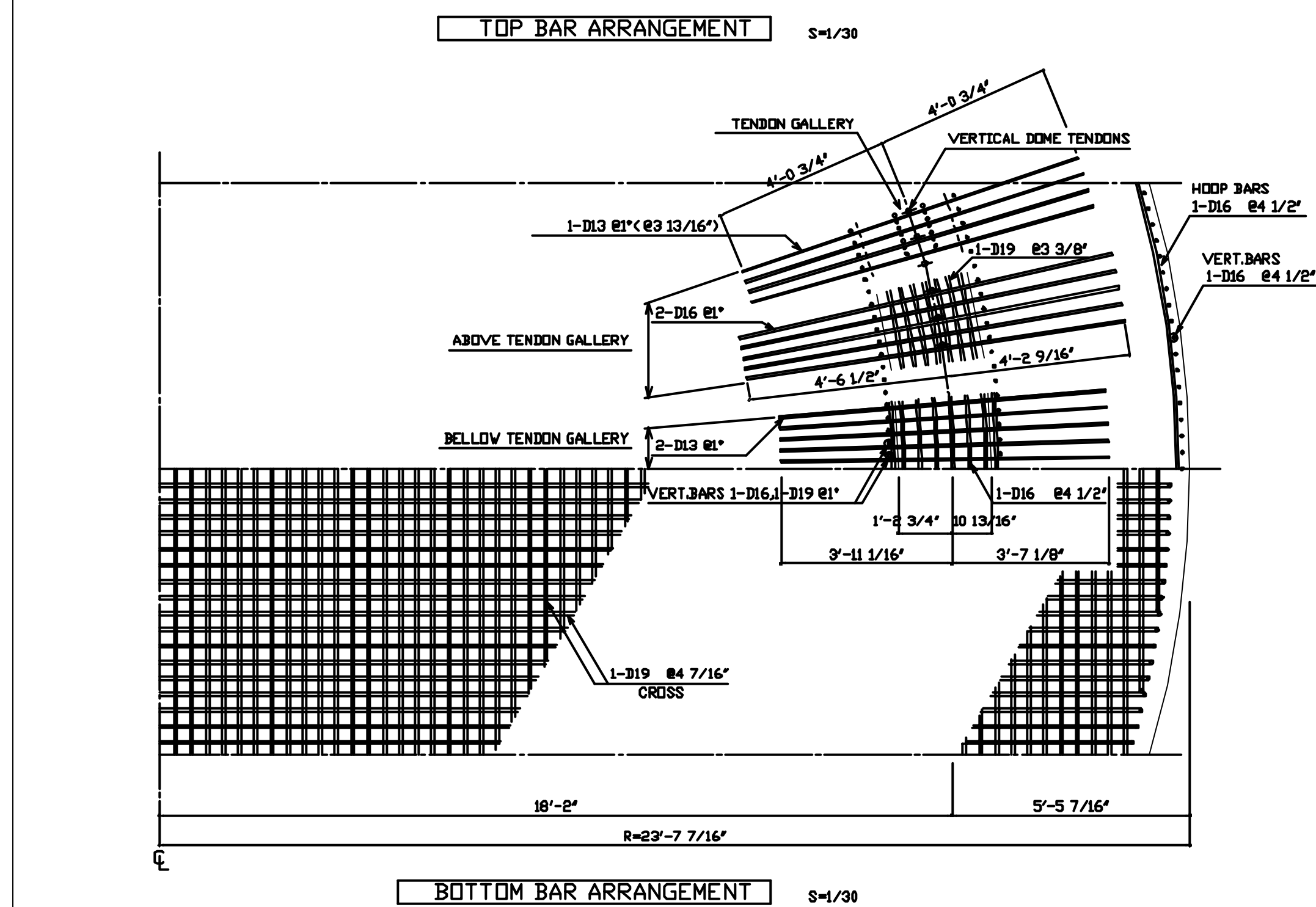
DESIGN SPECIFICATIONS						
STRUCTURE TYPE			REINFORCED CONCRETE PRESTRESSED CONCRETE			
TOP HEIGHT			EL. 53'-9 11/16'			
FOUNDATION SPEC.	TYPE		BASEMAT			
	BOTTOM LEVEL		EL. -11'-5 13/16'			
	BEARING CAPACITY		LONG TERM 0.34MPa (SHORT TERM 0.34MPa)			
	GROUND LINE PREPERATION		CONCRETE WITHOUT REINFORCING			
CONCRETE SPEC.						
PORTION			TYPE		Fc	
BASEMAT	GENERAL PORTION		NORMAL CONCRETE		Fc= 29.42MPa	
	AROUND TENDON GALLERY		NORMAL CONCRETE HIGH STRENGTH		Fc= 44.13MPa	
P C C V			NORMAL CONCRETE HIGH STRENGTH		Fc= 44.13MPa	
REBAR SPEC.						
PORTION			GRADE		JOINT TYPE	
			S#490	S#390	S#345	SPLICE
BASEMAT	MAIN BAR		○		○	
	SHEAR BAR			○	○	○
	BAR AROUND OPENING		○		○	
P C C V	MAIN BAR			○	○	
	BAR AROUND OPENING					
	RADIAL TIE			○		
TENDON SPEC.						
PORTION				SPEC.		
P C C V	VERTICAL DOME TENDONS		45×2=90 (Ø2")		•POST TENSIONING SYSTEM(VSL) •13.7mm Ø×3 (ORDERED STRAND)	
	HOOP CYLINDER TENDONS		45×2=90 (Ø4 7/16')			
	HOOP DOME TENDONS		9×2=18 (Ø2.5")			
PS LOAD (KIPS)						
P C C V	TYPE		BEFORE ANCHORING		AFTER ANCHORING	
	VERT. DOME TENDON		113.1		105.8	
	HOOP TENDON		101.9		78.7	



OPENINGS, PENETRATIONS SCHEDULE			
No.	SLEEVE O.D.		REMARKS
	NOMINAL DIAMETER	SIZE Ø	
P1	4'-11 1/16"	3'-0 5/8"	E/H
P2	2'-1 9/16"	2'-2"	A/L
P3	-	1'-1"	M/S
P4	-	1'-1"	M/S
P5	-	1'-1"	M/S
P6	-	1'-1"	M/S
P7	-	7 1/2"	F/V
P8	-	7 1/2"	F/V
P9	-	7 1/2"	F/V
P10	-	7 1/2"	F/V

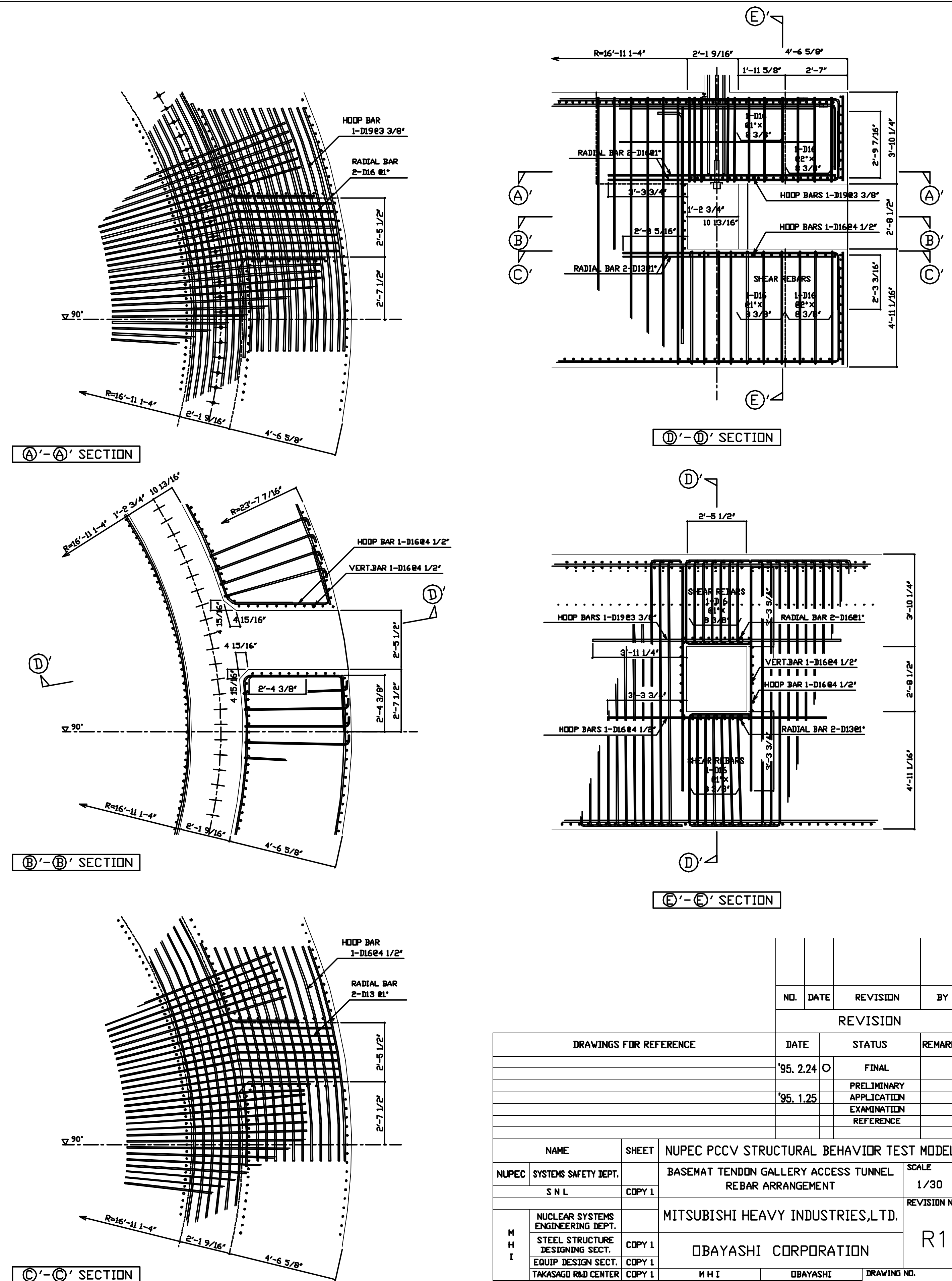
NUMBER OF OPENINGS, PENETRATIONS	
OPENINGS, PENETRATIONS	NUMBER
E/H	1
A/L	1
M/S , F/V	8

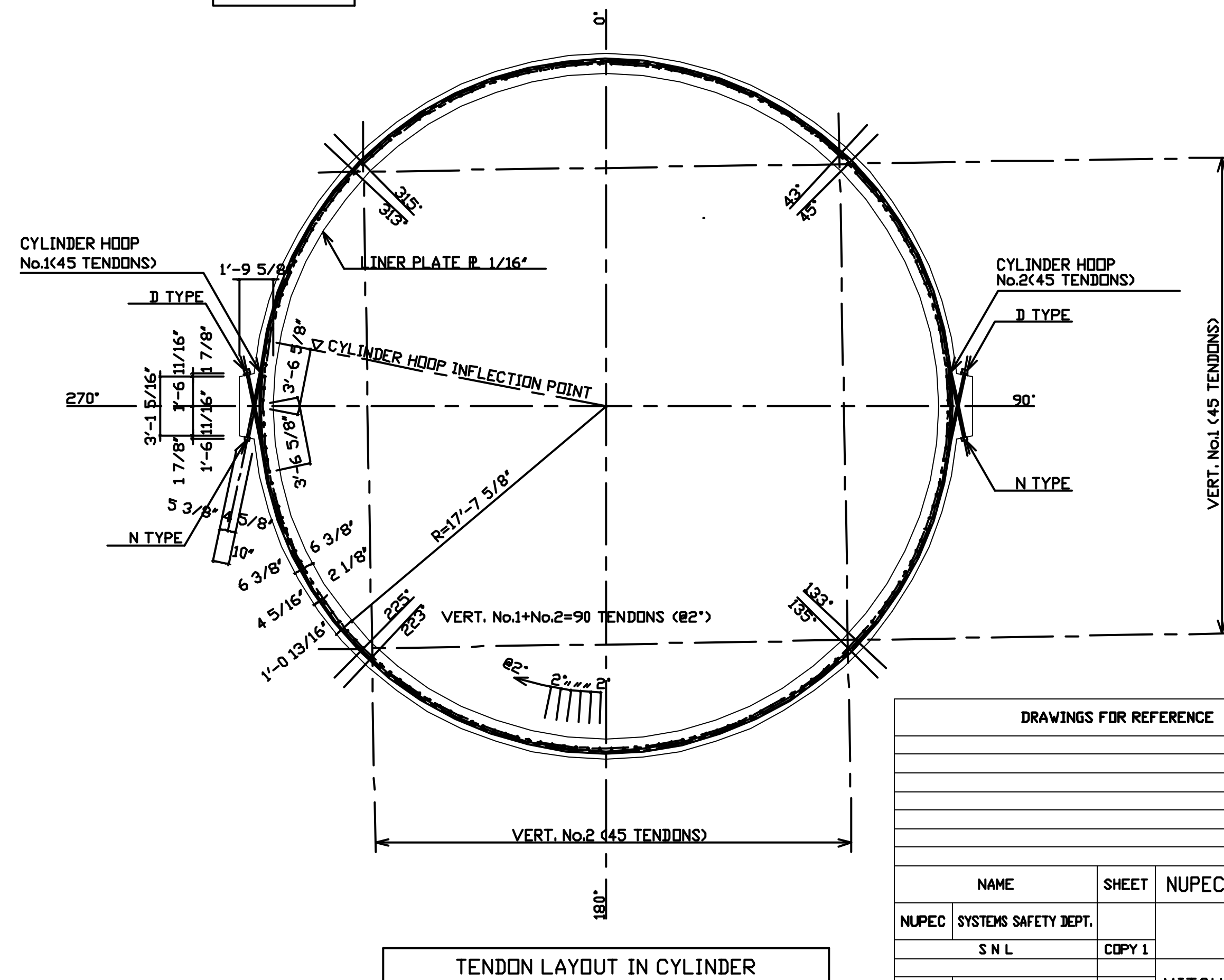
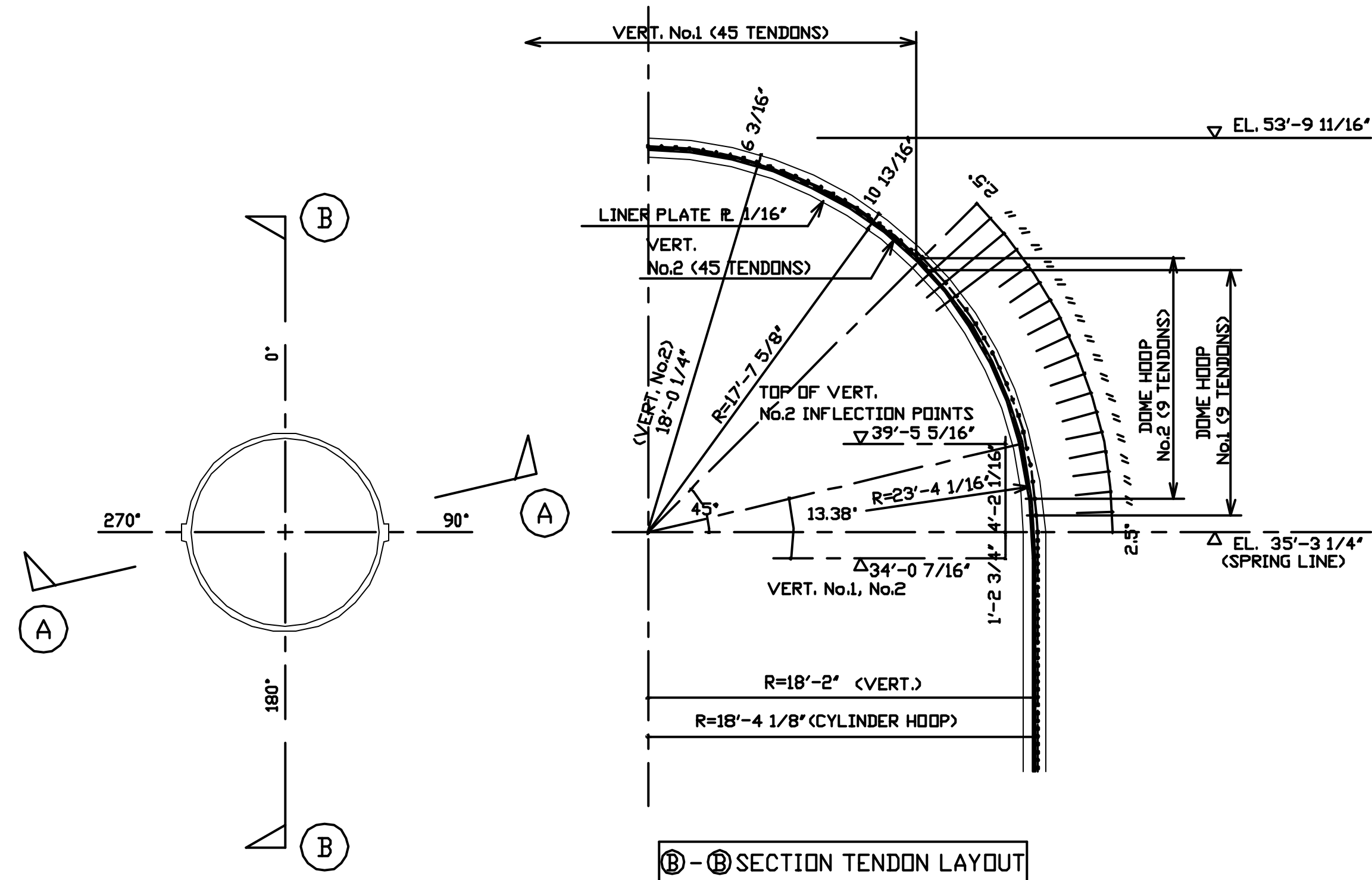
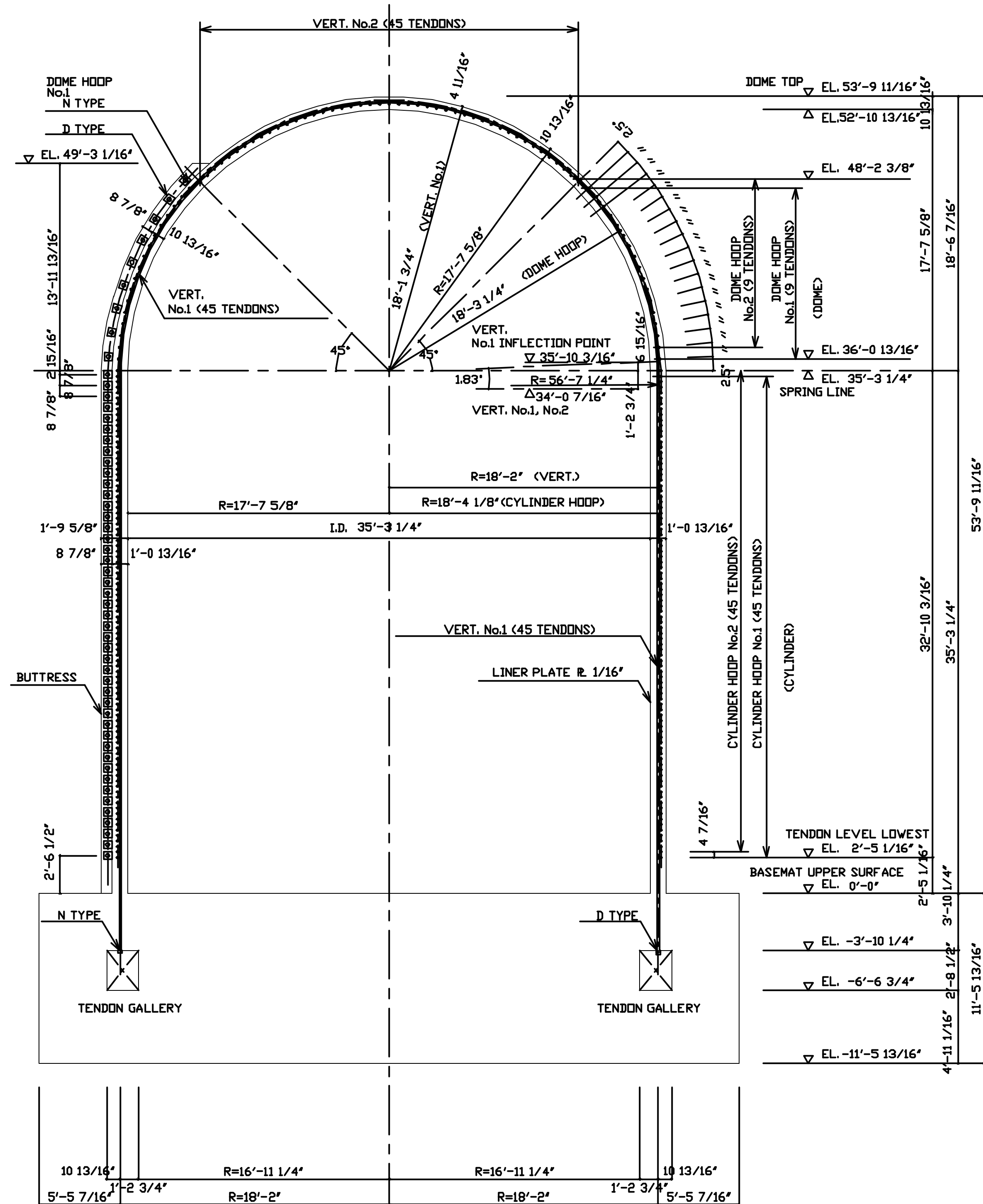
R2		'95 8.1	PS LOAD UPDATED M/S/F/V O.D. UPDATED	
NO.		DATE	REVISION	BY
REVISION				
DRAWINGS FOR REFERENCE		DATE	STATUS	REMARKS
		'95. 2.24	○	FINAL
		'95. 1.25		PRELIMINARY
		'94.11.17		APPLICATION
				EXAMINATION
				REFERENCE
NAME		SHEET	NUPEC PCCV STRUCTURAL BEHAVIOR TEST MODEL	
NUPEC	SYSTEMS SAFETY DEPT.		MODEL-GENERAL ARRANGEMENT	
S N L		COPY 1	MITSUBISHI HEAVY INDUSTRIES,LTD.	
M H I	NUCLEAR SYSTEMS ENGINEERING DEPT.		OBAYASHI CORPORATION	
	STEEL STRUCTURE DESIGNING SECT.	COPY 1		
	EQUIP DESIGN SECT.	COPY 1		
	TAKASAGO R&D CENTER	COPY 1		
T A I S E I		COPY 1	DRAWING NO. PCCV-QCON-01	
OBAYASHI		ORIG.		
			M H I	OBAYASHI T. Arai K. Umada H. Murano



		NO.	DATE	REVISION		BY	
		REVISION					
DRAWINGS FOR REFERENCE				DATE		STATUS	
				'95. 2.24		O FINAL	
						PRELIMINARY	
				'95. 1.25		APPLICATION	
				'94.11.17		EXAMINATION	
						REFERENCE	
NAME		SHEET		NUPEC PCCV STRUCTURAL BEHAVIOR TEST MODEL			
NUPEC	SYSTEMS SAFETY DEPT.			BASEMAT REBAR ARRANGEMENT			SCALE 1/10 1/30
S N L		COPY 1					REVISION NO.
M H I	NUCLEAR SYSTEMS ENGINEERING DEPT.			MITSUBISHI HEAVY INDUSTRIES,LTD.			R1
	STEEL STRUCTURE DESIGNING SECT.	COPY 1		Oabayashi CORPORATION			
	EQUIP DESIGN SECT.	COPY 1					
	TAKASAGO R&D CENTER	COPY 1					
	T A I S E I	COPY 1					
Oabayashi		ORIG.		M H I		Oabayashi T. Ito K. Umehashi H. Munaga	DRAWING NO. PCCV-QCON-02

90°, 270° TENDON GALLERY ACCESS TUNNEL REBAR ARRANGEMENT

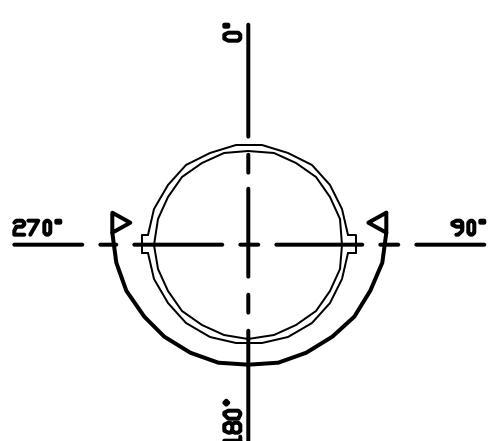




NO.	DATE	REVISION	BY

DRAWINGS FOR REFERENCE	DATE	STATUS	REMARKS
	'95. 2.24	O FINAL	
	'95. 1.25	PRELIMINARY	
	'94.11.17	APPLICATION	
		EXAMINATION	
		REFERENCE	

NAME		SHEET	NUPEC PCVY STRUCTURAL BEHAVIOR TEST MODEL		
NUPEC	SYSTEMS SAFETY DEPT.		PRESTRESSING TENDON GENERAL ARRANGEMENT		SCALE 1/60
S N L		COPY 1			
M H I	NUCLEAR SYSTEMS ENGINEERING DEPT.		MITSUBISHI HEAVY INDUSTRIES, LTD.		
	STEEL STRUCTURE DESIGNING SECT.	COPY 1	OBAYASHI CORPORATION		
	EQUIP DESIGN SECT.	COPY 1			
	TAKASAGO R&D CENTER	COPY 1	M H I	OBAYASHI	DRAWING NO.
T A I S E I		COPY 1	<i>T. Jima K. Umehashi H. Murawano</i>		PCCV-QCON-04
OBAYASHI		ORIG.			

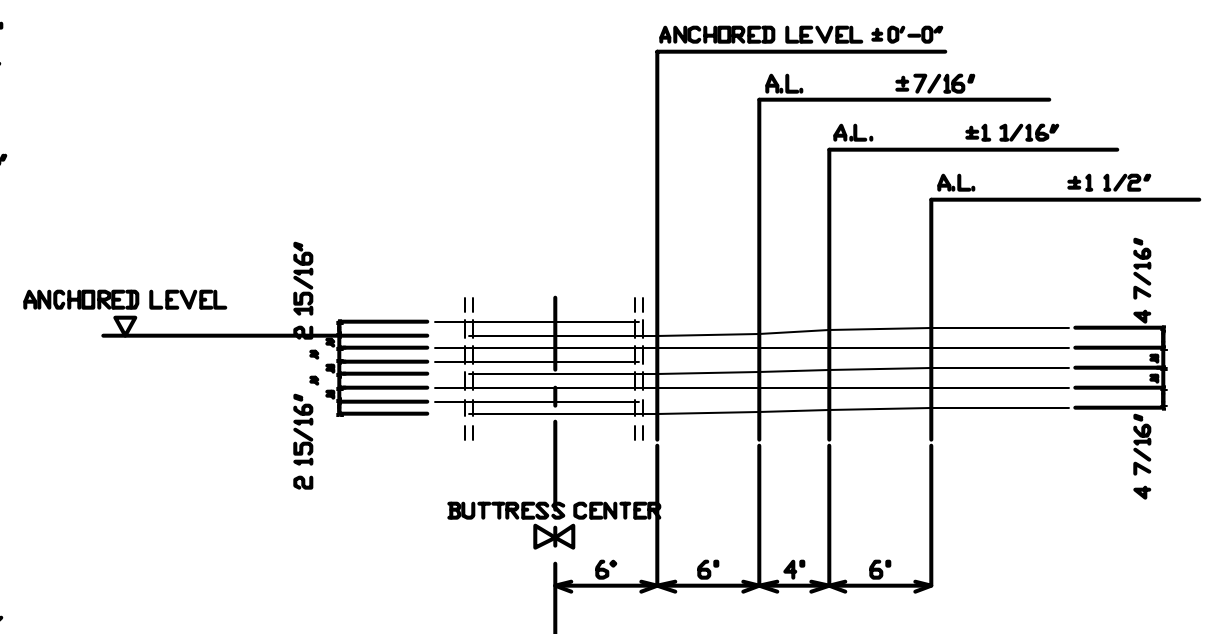


1. PARALLEL SHEATH PITCH IS NOT LESS THAN 2 15/16".
2. THE DISTANCE BETWEEN SHEATH CENTER AND PENETRATION SLEEVE OUTER PORTION IS NOT LESS THAN
 - ① E/H : 5 7/8"
 - ② A/L : 4 15/16"
 - ③ N/SF/W : 2 7/16"
3. THE CLEARANCE BETWEEN SHEATH OUTER PORTION AND SLEEVE STIFFENER IS NOT LESS THAN 9/16".
4. THE CLEARANCE BETWEEN SHEATH OUTER PORTION AND CRANE BRACKET IS NOT LESS THAN 1".
5. THE CLEARANCE BETWEEN BEARING PLATES IS NOT LESS THAN 3/16".

V81 V87 V43	V80 V86 V44		
$\langle +1.0^\circ \rangle$	$\langle -1.0^\circ \rangle$	EL.	$34^\circ - 0.7/16''$
$\langle +1.2^\circ \rangle$	$\langle -1.2^\circ \rangle$	EL.	$33^\circ - 0.3/16''$
$\langle +1.4^\circ \rangle$	$\langle -1.4^\circ \rangle$	EL.	$31^\circ - 11.7/8''$
$\langle +1.4^\circ \rangle$	$\langle -1.4^\circ \rangle$	EL.	$30^\circ - 10.1/16''$
$\langle +1.2^\circ \rangle$	$\langle -1.2^\circ \rangle$	EL.	$29^\circ - 9.3/4''$
$\langle +1.0^\circ \rangle$	$\langle -1.0^\circ \rangle$	EL.	$28^\circ - 9.1/2''$

(+1.2") : SHOWS A DEVIATION FROM \mathbb{C}

VERTICAL DOME TENDON LAYOUT NEAR CRANE BRACKET
(COMMON IN 3 BRACKETS)

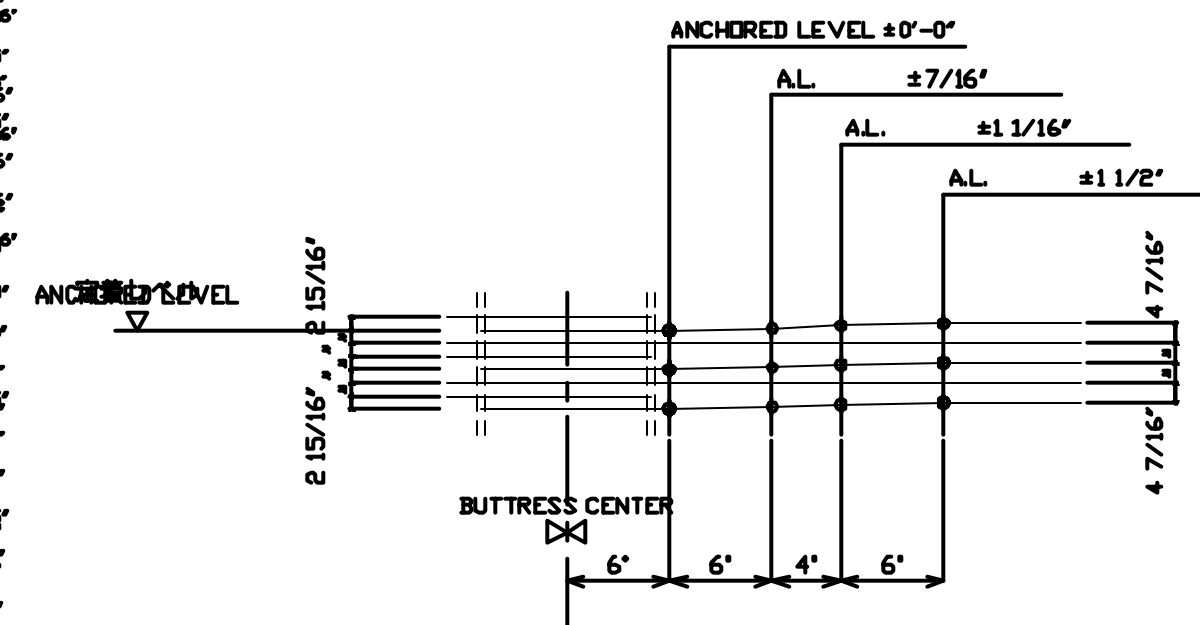
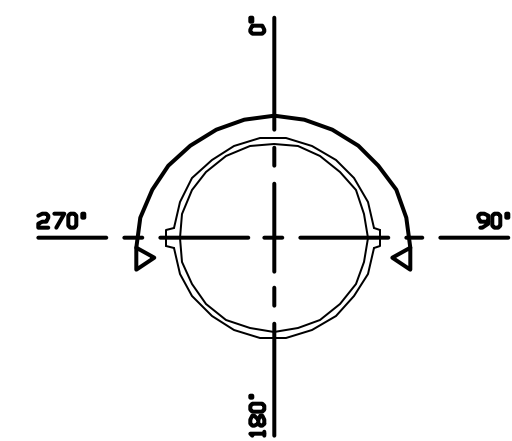
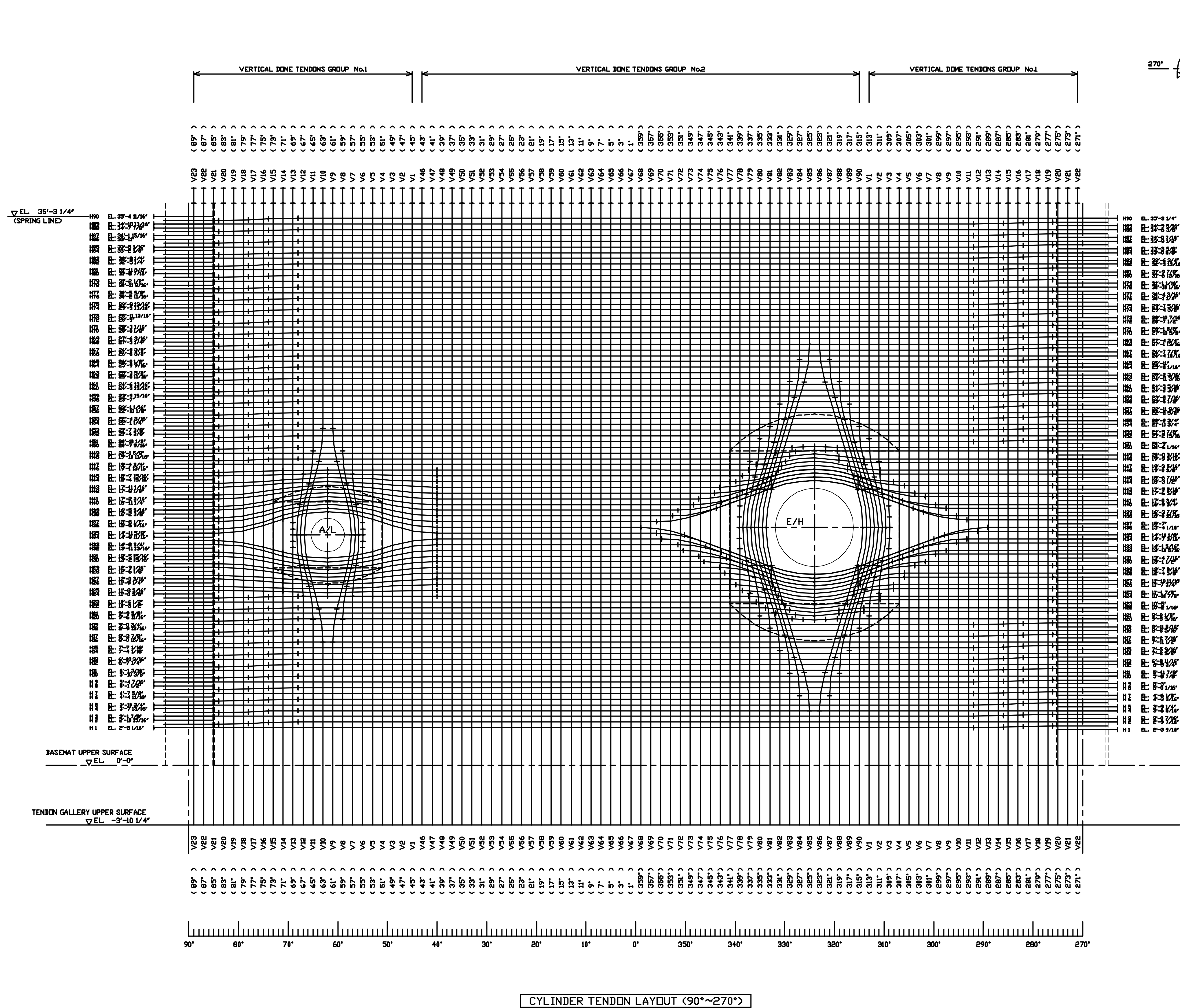


CYLINDER HOOP TENDON LAYOUT NEAR BUTTRESS

NO.	DATE	REVISION	BY

DRAWINGS FOR REFERENCE				DATE		STATUS		REMARKS	
				'95. 2.24		O FINAL			
				'95. 1.25		PRELIMINARY APPLICATION			
				'94.11.17		EXAMINATION			
						REFERENCE			
NAME			SHEET	NUPEC PCCV STRUCTURAL BEHAVIOR TEST MODEL					
NUPEC		SYSTEMS SAFETY DEPT.		CYLINDER PRESTRESSING TENDON ARRANGEMENT (270°~90°)					SCALE 1/40
		S N L	COPY 1						REVISION NO.
M H I	NUCLEAR SYSTEMS ENGINEERING DEPT.			MITSUBISHI HEAVY INDUSTRIES, LTD.					R1
	STEEL STRUCTURE DESIGNING SECT.		COPY 1						
	EQUIP DESIGN SECT.		COPY 1	OBAYASHI CORPORATION					
	TAKASAGO R&D CENTER		COPY 1	M H I		OBAYASHI		DRAWING NO.	
	T A I S E I		COPY 1			T. Iba, K. Umeki, H. Murano		PCCV-QCON-05	
		OBAYASHI	ORIG.						

CYLINDER TENDON LAYOUT (270°~90°)

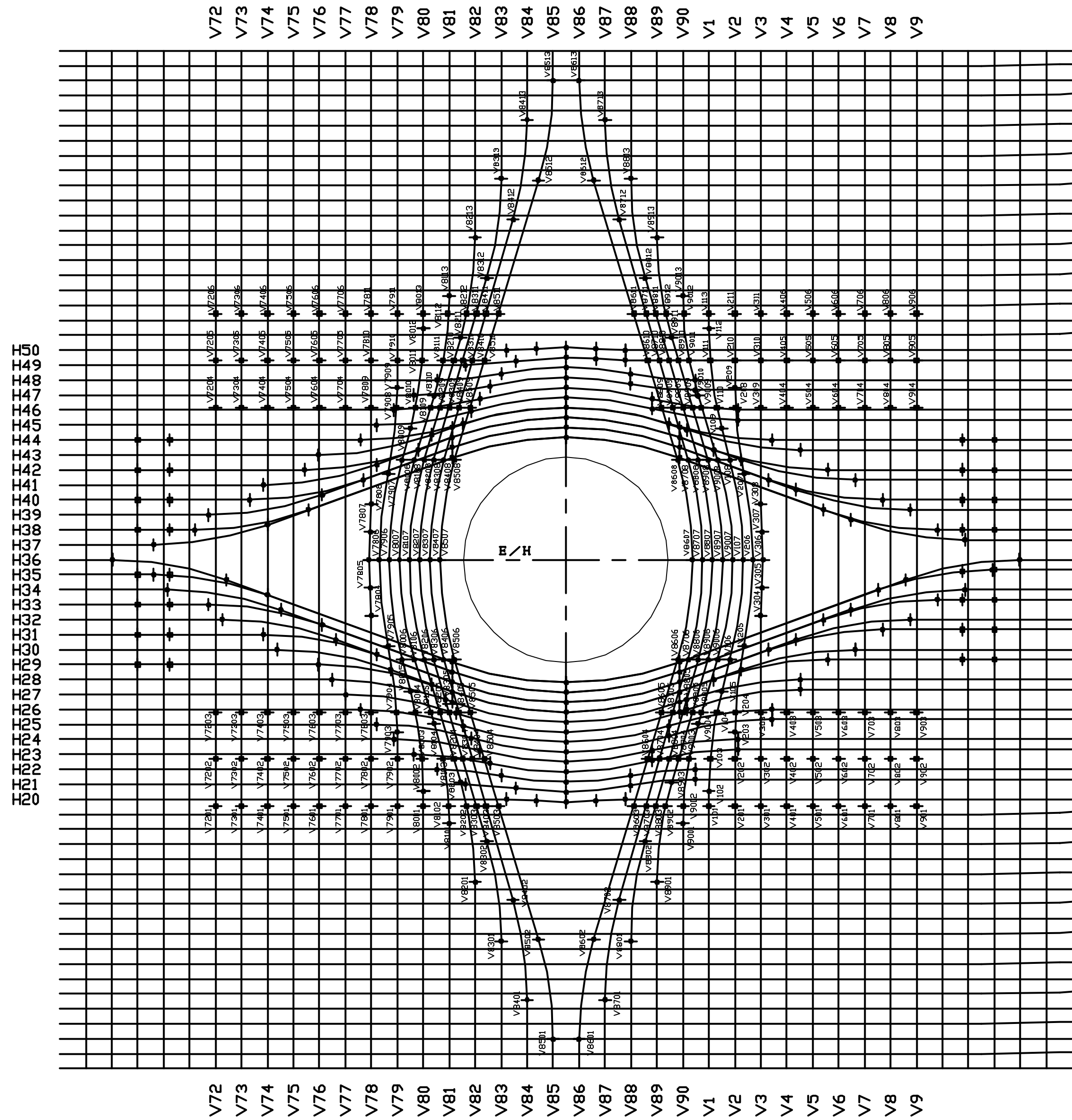


CYLINDER HOOP TENDON LAYOUT NEAR BUTTRESS




				NO.	DATE	REVISION	BY
				REVISION			
DRAWINGS FOR REFERENCE				DATE	STATUS		REMARKS
				'95.2.24	○	FINAL	
						PRELIMINARY	
				'95.1.25		APPLICATION	
				'94.11.17		EXAMINATION	
						REFERENCE	
NAME		SHEET	NUPEC PCCV STRUCTURAL BEHAVIOR TEST MODEL				
NUPEC	SYSTEMS SAFETY DEPT.		CYLINDER PRESTRESSING TENDON ARRANGEMENT(90°~270°)				SCALE 1/40
S N L		COPY 1					REVISION NO.
			MITSUBISHI HEAVY INDUSTRIES,LTD.				R1
M H I	NUCLEAR SYSTEMS ENGINEERING DEPT.						
	STEEL STRUCTURE DESIGNING SECT.	COPY 1	OBAYASHI CORPORATION				
	EQUIP DESIGN SECT.	COPY 1					
	TAKASAGO R&D CENTER	COPY 1					
T A I S E I		COPY 1	M H I	OBAYASHI		DRAWING NO.	
OBAYASHI		ORIG.			T. Obayashi, K. Umada H. Murano		PCCV-QCON-06

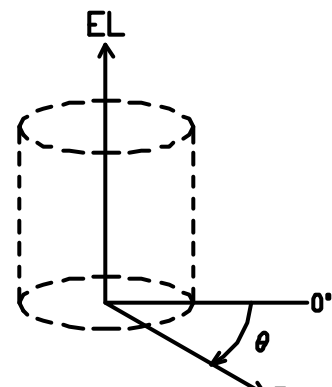
TENNION NO	FORM NO	01			02			03			04			05			06			07			08			09			10			11			12			13		
		EL	θ	R	EL	θ	R	EL	θ	R	EL	θ	R	EL	θ	R	EL	θ	R	EL	θ	R	EL	θ	R	EL	θ	R	EL	θ	R	EL	θ	R	EL	θ	R			
V9		9'-3 1/4"	297'		10'-5 1/8"	297'	18'-1 7/8"	11'-7"	297'	18'-1 11/16"	19'-1 1/8"	297'	18'-1 11/16"	20'-3"	297'	18'-1 7/8"	21'-4 7/8"	297'																						
V8		9'-3 1/4"	299'		10'-5 1/8"	299'	18'-1 5/16"	11'-7"	299'	18'-1 5/16"	19'-1 1/8"	299'	18'-1 5/16"	20'-3"	299'	18'-1 11/16"	21'-4 7/8"	299'																						
V7		9'-3 1/4"	301'		10'-5 1/8"	301'	18'-1 1/2"	11'-7"	301'	18'-1"	19'-1 1/8"	301'	18'-1"	20'-3"	301'	18'-1 1/2"	21'-4 7/8"	301'																						
V6		9'-3 1/4"	303'		10'-5 1/8"	303'	18'-1 3/8"	11'-7"	303'	18'-0 11/16"	19'-1 1/8"	303'	18'-0 11/16"	20'-3"	303'	18'-1 3/8"	21'-4 7/8"	303'																						
V5		9'-3 1/4"	305'		10'-5 1/8"	305'	18'-0 7/16"	11'-7"	305'	18'-0 7/16"	19'-1 1/8"	305'	18'-1 1/4"	20'-3"	305'	18'-1 1/4"	21'-4 7/8"	305'																						
V4		9'-3 1/4"	307'		10'-5 1/8"	307'	18'-1 1/8"	11'-7"	307'	18'-0 3/16"	19'-1 1/8"	307'	18'-0 3/16"	20'-3"	307'	18'-1 1/8"	21'-4 7/8"	307'																						
V3		9'-3 1/4"	309'		10'-5 1/8"	309'	18'-1"	11'-7"	309'	17'-11 15/16"	13'-11 9/16"	309'	17'-11 15/16"	14'-7 13/16"	308.91'	18'	15'-4 1 1/8"	308.92'	18'	16'-0 5/16"	308.91'	18'	16'-0 9/16"	309'	17'-11 15/16"	19'-1 1/8"	309'	17'-11 15/16"	20'-3"	309'	18'-1"	21'-4 7/8"	309'							
V2		9'-3 1/4"	311'		10'-5 1/8"	311'	18'-0 7/8"	11'-1 1/8"	311'	17'-11 13/16"	11'-7"	310.96'	17'-11 3/4"	13'-2 9/16"	310.30'	17'-11 13/16"	15'-4 1/16"	309.60'	17'-11 7/8"	17'-5 1/2"	310.30'	17'-11 13/16"	19'-1 1/8"	310.96'	17'-11 3/4"	19'-7"	311'	17'-11 13/16"	20'-3"	311'	18'-0 7/8"	21'-4 7/8"	311'							
V1		9'-3 1/4"	313'		9'-7 5/8"	313'	18'-1 15/16"	10'-5 1/8"	312.96'	17'-11 13/16"	11'-7"	312.98'	17'-11 3/4"	13'-3 1/16"	312.01'	17'-11 13/16"	15'-0 1/16"	311.37'	17'-11 3/4"	15'-3 1/2"	310.38'	17'-11 13/16"	17'-9 9/16"	311.37'	17'-11 3/4"	18'-6 15/16"	312.06'	17'-11 11/16"	19'-1 1/8"	312.98'	17'-11 5/8"	20'-3"	312.90'	18'-0 13/16"	21'-0 1/2"	313'	18'-1 15/16"	21'-4 7/8"	313'	
V90		6'-10"	315'		9'-3 1/4"	314.97'			314.98'	18'-0 3/4"	11'-3 9/16"	313.84'	17'-11 5/8"	11'-7"	313.57'	17'-11 9/16"	18'-10 1/2"	312.32'	17'-11 5/8"	15'-4 1/16"	311.16'	17'-11 3/4"	17'-9 9/16"	312.32'	17'-11 11/16"	19'-1 1/8"	313.57'	17'-11 9/16"	19'-4 9/16"	313.84'	17'-11 5/8"	20'-3"	314.52'	18'-0 3/4"	21'-4 7/8"	314.97'				
V89		7'-4 11/16"	317'		9'-3 1/4"	316.35'			315.02'	18'-0 3/4"	11'-3 9/16"	315.25'	18'-0 3/4"	11'-7"	314.27'	17'-11 1/2"	17'-11 5/8"	313.06'	17'-11 5/8"	15'-4 1/16"	311.94'	17'-11 3/4"	17'-9 9/16"	313.06'	17'-11 5/8"	19'-1 1/8"	314.27'	17'-11 1/2"	17'-11 5/8"	315.25'	18'-0 3/4"	20'-9 7/8"	315.02'	18'-1 1/16"	21'-4 7/8"	316.35'				
V88		8'-11 1/																																						

CYLINDER HOOP TENDON POSITION, IN CASE OF BLANK)



S=1/25

- 1)  : INFLECTION POINT (IN-PLANE)
- 2)  : INFLECTION POINT (OUT OF PLANE)
- 3)  POINT NO.
TENDON NO.
- 4) CYLINDRICAL COORDINATES

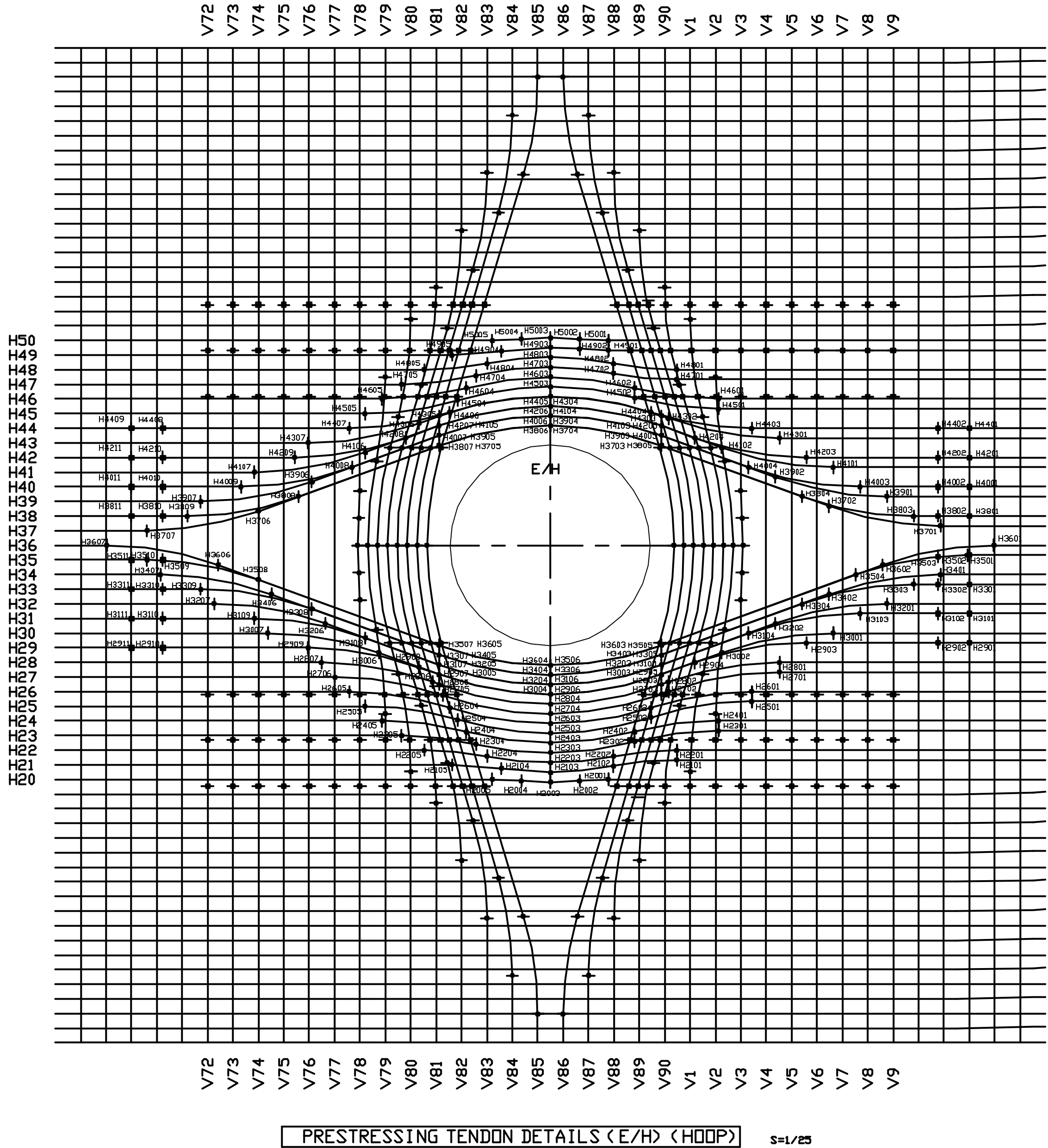


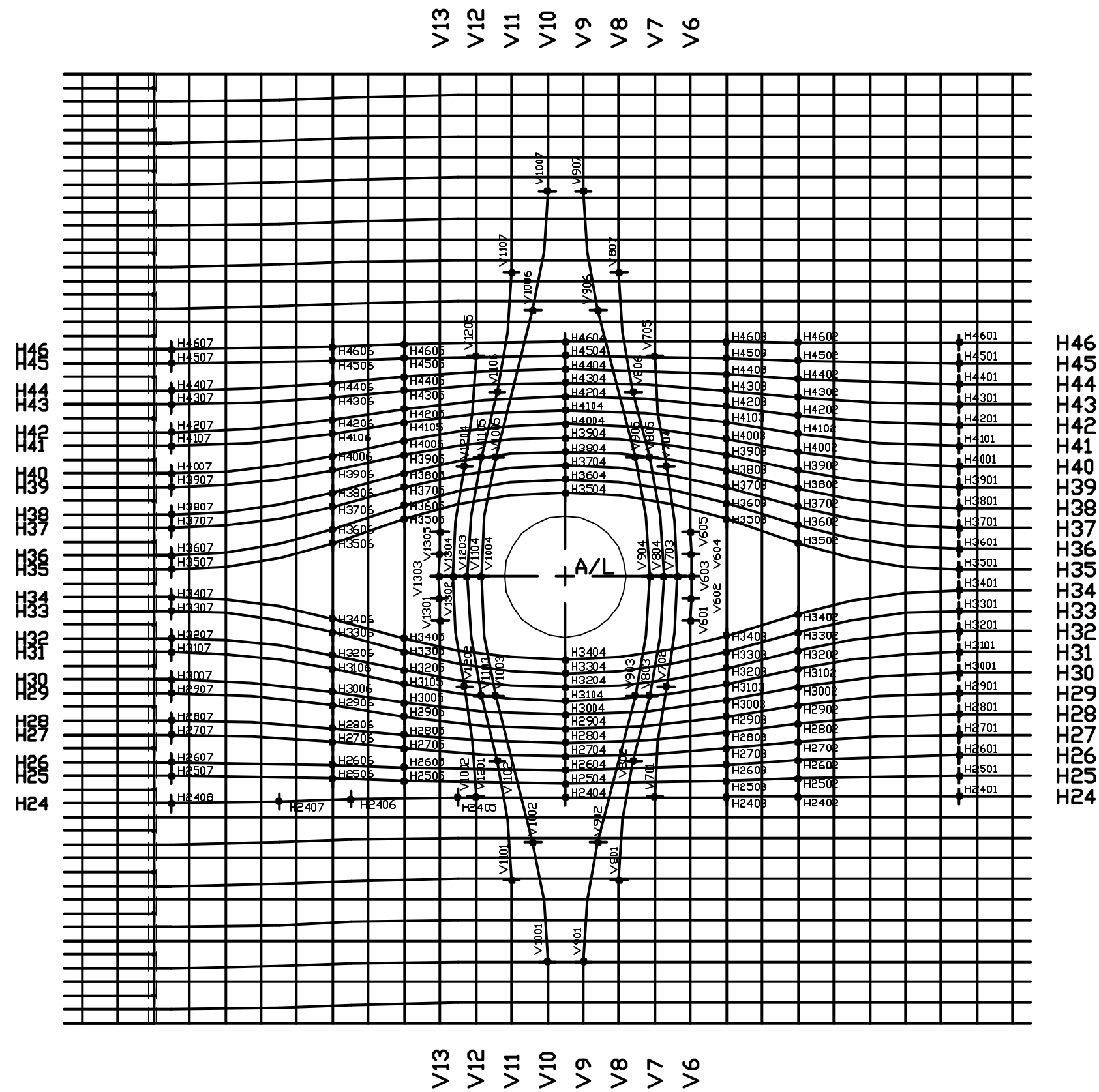
		NO.		DATE		REVISION	
						BY	
				REVISION			
DRAWINGS FOR REFERENCE				DATE		STATUS	
				'95.2.24		O FINAL	
						PRELIMINARY	
				'95.1.25		APPLICATION	
				'94.11.17		EXAMINATION	
						REFERENCE	
NAME		SHEET		NUPEC PCCV STRUCTURAL BEHAVIOR TEST MODEL			
NUPEC	SYSTEMS SAFETY DEPT.				PRESTRESSING TENDON DETAILS (E/H) (VERTICAL DOME)		SCALE 1/25
S N L		COPY 1				REVISION NO.	
				MITSUBISHI HEAVY INDUSTRIES,LTD.			
M H I	NUCLEAR SYSTEMS ENGINEERING DEPT.				O B A Y A S H I C O R P O R A T I O N		R 1
	STEEL STRUCTURE DESIGNING SECT.		COPY 1				
	EQUIP DESIGN SECT.		COPY 1				
	TAKASAGO R&D CENTER		COPY 1				
	T A I S E I		COPY 1				
O B A Y A S H I		ORIG.		M H I	O B A Y A S H I	DRAWING NO.	
				T. Ito K. Umeha H. Murano		PCCV-QCON-07	

THE INFLECTION POINTS IN CYLINDRICAL COORDINATES (HOOP)

POINT NO. TENDON NO.	01				02				03				04				05				06				07				08				09				10				11																																																																																																																																																																																																																																																																																																																																																																																																
	EL	θ		R	EL	θ		R	EL	θ		R	EL	θ		R	EL	θ		R	EL	θ		R	EL	θ		R	EL	θ		R	EL	θ		R	EL	θ		R																																																																																																																																																																																																																																																																																																																																																																																																	
H20	9'-5 3/16"	319.42°			9'-4 13/16"	321.71°			9'-4 3/8"	324°			9'-4 13/16"	326.29°			9'-5 3/16"	328.58°																																																																																																																																																																																																																																																																																																																																																																																																																							
H21	9'-11 1/8"	314.06°			9'-9 3/16"	319.03°			9'-7 3/8"	324°			9'-8 1/2"	327.87°			9'-9 5/8"	331.75°																																																																																																																																																																																																																																																																																																																																																																																																																							
H22	10'-2 1/16"	314.06°			10'-0 3/16"	319.03°			9'-10 5/16"	324°			10'-0 3/16"	328.97°			10'-2 1/16"	333.94°																																																																																																																																																																																																																																																																																																																																																																																																																							
H23	10'-7 15/16"	310.75°			10'-4 5/8"	317.38°			10'-1 1/4"	324°			10'-3 7/8"	329.86°			10'-6 1/2"	335.72°																																																																																																																																																																																																																																																																																																																																																																																																																							
H24	10'-10 7/8"	310.75°			10'-7 9/16"	317.38°			10'-4 3/16"	324°			10'-7 9/16"	330.62°			10'-10 7/8"	337.25°																																																																																																																																																																																																																																																																																																																																																																																																																							
H25	11'-4 13/16"	308.16°			10'-11 15/16"	316.08°			10'-7 3/16"	324°			10'-11 1/4"	331.30°			11'-3 5/16"	336.61°																																																																																																																																																																																																																																																																																																																																																																																																																							
H26	11'-7 3/4"	308.16°			11'-2 15/16"	316.08°			10'-10 1/8"	324°			11'-2 15/16"	331.92°			11'-7 3/4"	339.84°																																																																																																																																																																																																																																																																																																																																																																																																																							
H27	12'-1 11/16"	305.96°			11'-7 3/4"	314.72°			11'-7"	315.24°			11'-1 1/16"	324°			11'-6 5/8"	332.49°			12'-0 3/16"	340.98°																																																																																																																																																																																																																																																																																																																																																																																																																			
H28	12'-4 5/8"	305.96°			11'-10 11/16"	314.72°			11'-9 15/16"	315.24°			11'-4"	324°			11'-9 15/16"	332.76°			12'-0 11/16"	333.28°			12'-4 5/8"	348.04°																																																																																																																																																																																																																																																																																																																																																																																																															
H29	12'-10 1/2"	291°			12'-10 1/2"	293.48°	18'-3 7/8"		12'-10 1/2"	303.84°	18'-2 1/16"		12'-4 9/16"	312.61°	18'-1"		12'-0 15/16"	315.24°	18'-0 15/16"		11'-7"	324°	18'-0 11/16"	12'-0 15/16"	332.76°	18'-0 15/16"	12'-3 1/8"	334.34°	18'-1 1/16"	12'-9 1/16"	343.10°	18'-1 15/16"	12'-9 1/16"	354.52°	18'-3 7/8"	12'-9 1/16"	357°																																																																																																																																																																																																																																																																																																																																																																																																				
H30	13'-1 1/2"	301.73°			12'-7 9/16"	310.50°			12'-0 15/16"	315.24°			11'-7"	324°			12'-7 9/16"	337.51°			12'-7 9/16"	337.51°	13'-1 1/2"	346.27°	13'-3 1/8"	346.27°	13'-3 1/8"	346.27°	13'-3 1/8"	346.27°	13'-3 1/8"	346.27°	13'-3 1/8"	346.27°	13'-3 1/8"	346.27°	13'-3 1/8"	346.27°	13'-3 1/8"	346.27°	13'-3 1/8"	346.27°	13'-3 1/8"	346.27°	13'-3 1/8"	346.27°	13'-3 1/8"	346.27°	13'-3 1/8"	346.27°	13'-3 1/8"	346.27°	13'-3 1/8"	346.27°	13'-3 1/8"	346.27°	13'-3 1/8"	346.27°	13'-3 1/8"	346.27°	13'-3 1/8"	346.27°	13'-3 1/8"	346.27°	13'-3 1/8"	346.27°	13'-3 1/8"	346.27°	13'-3 1/8"	346.27°	13'-3 1/8"	346.27°	13'-3 1/8"	346.27°	13'-3 1/8"	346.27°	13'-3 1/8"	346.27°	13'-3 1/8"	346.27°	13'-3 1/8"	346.27°	13'-3 1/8"	346.27°	13'-3 1/8"	346.27°	13'-3 1/8"	346.27°	13'-3 1/8"	346.27°	13'-3 1/8"	346.27°	13'-3 1/8"	346.27°	13'-3 1/8"	346.27°	13'-3 1/8"	346.27°	13'-3 1/8"	346.27°	13'-3 1/8"	346.27°	13'-3 1/8"	346.27°	13'-3 1/8"	346.27°	13'-3 1/8"	346.27°	13'-3 1/8"	346.27°	13'-3 1/8"	346.27°	13'-3 1/8"	346.27°	13'-3 1/8"	346.27°	13'-3 1/8"	346.27°	13'-3 1/8"	346.27°	13'-3 1/8"	346.27°	13'-3 1/8"	346.27°	13'-3 1/8"	346.27°	13'-3 1/8"	346.27°	13'-3 1/8"	346.27°	13'-3 1/8"	346.27°	13'-3 1/8"	346.27°	13'-3 1/8"	346.27°	13'-3 1/8"	346.27°	13'-3 1/8"	346.27°	13'-3 1/8"	346.27°	13'-3 1/8"	346.27°	13'-3 1/8"	346.27°	13'-3 1/8"	346.27°	13'-3 1/8"	346.27°	13'-3 1/8"	346.27°	13'-3 1/8"	346.27°	13'-3 1/8"	346.27°	13'-3 1/8"	346.27°	13'-3 1/8"	346.27°	13'-3 1/8"	346.27°	13'-3 1/8"	346.27°	13'-3 1/8"	346.27°	13'-3 1/8"	346.27°	13'-3 1/8"	346.27°	13'-3 1/8"	346.27°	13'-3 1/8"	346.27°	13'-3 1/8"	346.27°	13'-3 1/8"	346.27°	13'-3 1/8"	346.27°	13'-3 1/8"	346.27°	13'-3 1/8"	346.27°	13'-3 1/8"	346.27°	13'-3 1/8"	346.27°	13'-3 1/8"	346.27°	13'-3 1/8"	346.27°	13'-3 1/8"	346.27°	13'-3 1/8"	346.27°	13'-3 1/8"	346.27°	13'-3 1/8"	346.27°	13'-3 1/8"	346.27°	13'-3 1/8"	346.27°	13'-3 1/8"	346.27°	13'-3 1/8"	346.27°	13'-3 1/8"	346.27°	13'-3 1/8"	346.27°	13'-3 1/8"	346.27°	13'-3 1/8"	346.27°	13'-3 1/8"	346.27°	13'-3 1/8"	346.27°	13'-3 1/8"	346.27°	13'-3 1/8"	346.27°	13'-3 1/8"	346.27°	13'-3 1/8"	346.27°	13'-3 1/8"	346.27°	13'-3 1/8"	346.27°	13'-3 1/8"	346.27°	13'-3 1/8"	346.27°	13'-3 1/8"	346.27°	13'-3 1/8"	346.27°	13'-3 1/8"	346.27°	13'-3 1/8"	346.27°	13'-3 1/8"	346.27°	13'-3 1/8"	346.27°	13'-3 1/8"	346.27°	13'-3 1/8"	346.27°	13'-3 1/8"	346.27°	13'-3 1/8"	346.27°	13'-3 1/8"	346.27°	13'-3 1/8"	346.27°	13'-3 1/8"	346.27°	13'-3 1/8"	346.27°	13'-3 1/8"	346.27°	13'-3 1/8"	346.27°	13'-3 1/8"	346.27°	13'-3 1/8"	346.27°	13'-3 1/8"	346.27°	13'-3 1/8"	346.27°	13'-3 1/8"	346.27°	13'-3 1/8"	346.27°	13'-3 1/8"	346.27°	13'-3 1/8"	346.27°	13'-3 1/8"	346.27°	13'-3 1/8"	346.27°	13'-3 1/8"	346.27°	13'-3 1/8"	346.27°	13'-3 1/8"	346.27°	13'-3 1/8"	346.27°	13'-3 1/8"	346.27°	13'-3 1/8"	346.27°	13'-3 1/8"	346.27°	13'-3 1/8"	346.27°	13'-3 1/8"	346.27°	13'-3 1/8"	346.27°	13'-3 1/8"	346.27°	13'-3 1/8"	346.27°	13'-3 1/8"	346.27°	13'-3 1/8"	346.27°	13'-3 1/8"	346.27°	13'-3 1/8"	346.27°	13'-3 1/8"	346.27°	13'-3 1/8"	346.27°	13'-3 1/8"	346.27°	13'-3 1/8"	346.27°	13'-3 1/8"	346.27°	13'-3 1/8"	346.27°	13'-3 1/8"	346.27°	13'-3 1/8"	346.27°	13'-3 1/8"	346.27°	13'-3 1/8"	346.27°	13'-3 1/8"	346.27°	13'-3 1/8"	346.27°	13'-3 1/8"	346.27°	13'-3 1/8"	346.27°	13'-3 1/8"	346.27°	13'-3 1/8"	346.27°	13'-3 1/8"	346.27°	13'-3 1/8"	346.27°	13'-3 1/8"	346.27°	13'-3 1/8"	346.27°	13'-3 1/8"	346.27°	13'-3 1/8"	346.27°	13'-3 1/8"	346.27°	13'-3 1/8"	346.27°	13'-3 1/8"	346.27°	13'-3 1/8"	346.27°	13'-3 1/8"	346.27°	13'-3 1/8"	346.27°	13'-3 1/8"	346.27°	13'-3 1/8"	346.27°	13'-3 1/8"	346.27°	13'-3 1/8"	346.27°	13'-3 1/8"	346.27°	13'-3 1/8"	346.27°	13'-3 1/8"	346.27°	13'-3 1/8"	346.27°	13'-3 1/8"	346.27°	13'-3 1/8"	346.27°	13'-3 1/8"	346.27°	13'-3 1/8"	346.27°	13'-3 1/8"	346.27°	13'-3 1/8"	346.27°	13'-3 1/8"	346.27°	13'-3 1/8"	346.27°	13'-3 1/8"	346.27°	13'-3 1/8"	346.27°	13'-3 1/8"	346.27°	13'-3 1/8"	346.27°	13'-3 1/8"	346.27°	13'-3 1/8"	346.27°	13'-3 1/8"	346.27°	13'-3 1/8"	346.27°	13'-3 1/8"</

EL: LEVEL
 θ : AZIMUTH ANGLE
R: RADIUS < R SHOULD BE 18'-4 1/8", NORMAL
CYLINDER HOOP TENDON POSITION, IN CASE OF BLANK >





PRESTRESSING TENDON DETAILS (A/L) S=1/25

THE INFLECTION POINTS IN CYLINDRICAL COORDINATES (VERTICAL DOME TENDONS)

POINT NO.	01		02		03		04		05		06		07	
TENDON NO.	EL	θ	EL	θ	EL	θ	EL	θ	EL	θ	EL	θ	EL	θ
V6	14'-0 5/8"	55°	14'-3 3/8"	54.97°	14'-10 1/8"	54.94°	15'-2 15/16"	54.97°	15'-7 11/16"	55°				
V7	10'-10 7/8"	57°	12'-10 1/2"	56.36°	14'-10 1/8"	55.72°	16'-9 3/4"	56.36°	18'-9 7/16"	57°				
V8	9'-4 15/16"	59°	11'-6 1/2"	58.20°	12'-8 9/16"	57.30°	14'-10 1/8"	56.50°	16'-11 3/4"	57.30°	18'-1 13/16"	58.20°	20'-3 3/8"	59°
V9	7'-11 1/2"	61°	10'-1 1/16"	60.17°	12'-8 9/16"	58.11°	14'-10 1/8"	57.28°	16'-11 3/4"	58.11°	19'-7 1/4"	60.17°	21'-8 13/16"	61°
V10	7'-11 1/2"	63°	10'-1 1/16"	63.83°	12'-8 9/16"	65.89°	14'-10 1/8"	66.72°	16'-11 3/4"	65.89°	19'-7 1/4"	63.83°	21'-8 13/16"	63°
V11	9'-4 15/16"	65°	11'-6 1/2"	65.80°	12'-8 9/16"	66.70°	14'-10 1/8"	67.50°	16'-11 3/4"	66.70°	18'-1 13/16"	65.80°	20'-3 3/8"	65°
V12	10'-10 7/8"	67°	12'-10 1/2"	67.64°	14'-10 1/8"	68.28°	16'-9 3/4"	67.64°	18'-9 7/16"	67°				
V13	14'-0 5/8"	69°	14'-3 3/8"	69.03°	14'-10 1/8"	69.06°	15'-2 15/16"	69.03°	15'-7 11/16"	69°				

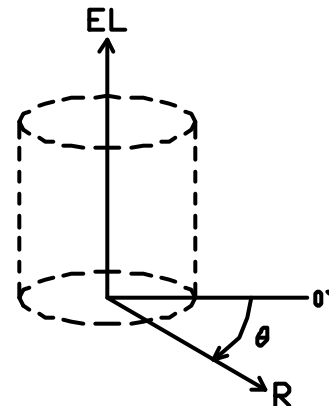
EL : LEVEL
θ : AZIMUTH ANGLE
R : 18'-2"

THE INFLECTION POINTS IN CYLINDRICAL COORDINATES (HOOP TENDONS)

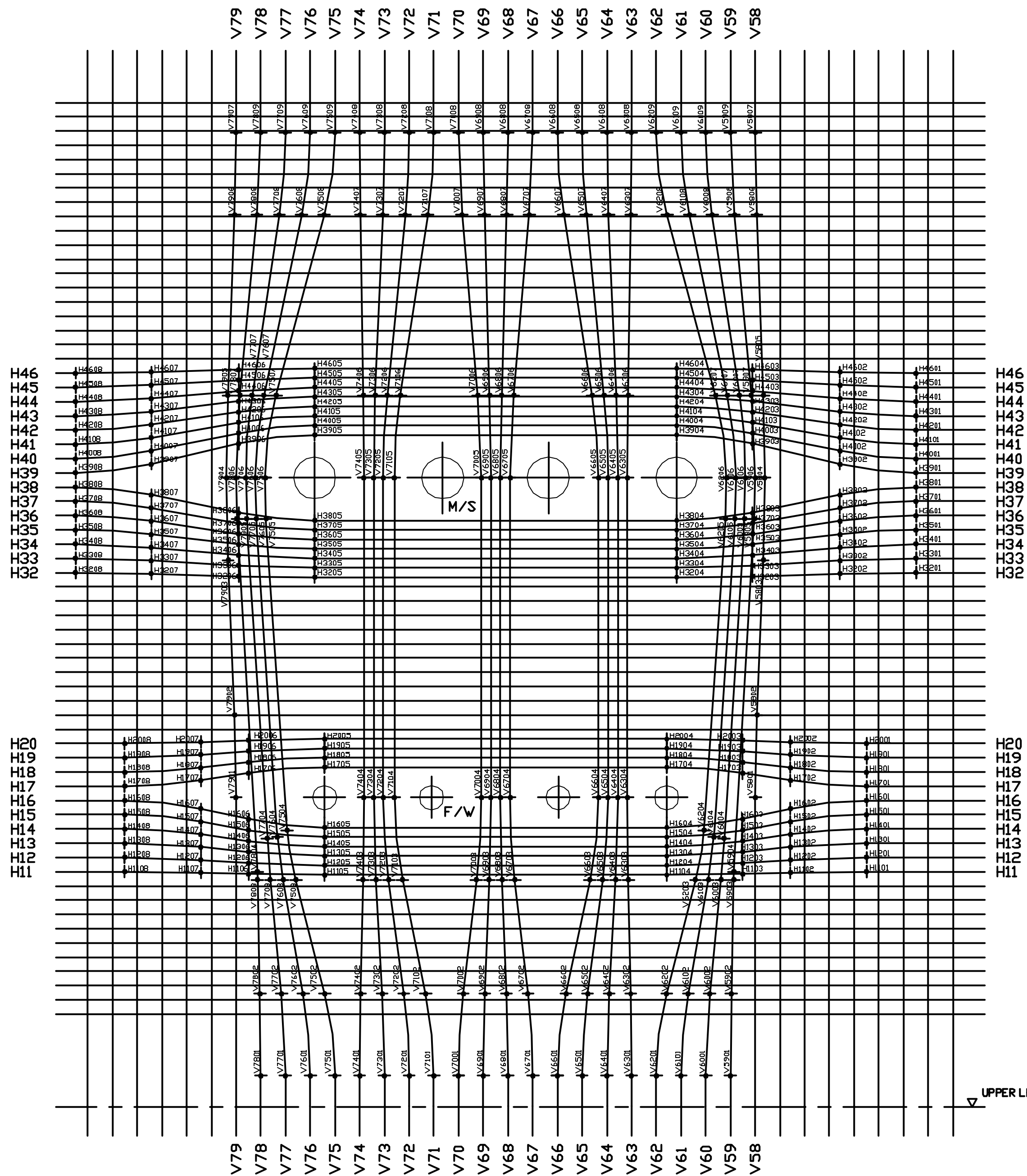
POINT NO.	01		02		03		04		05		06		07		08	
TENDON NO.	EL	θ	EL	θ	EL	θ	EL	θ	EL	θ	EL	θ	EL	θ	EL	θ
H24	10'-10 7/8"	40°	10'-10 13/16"	49°	10'-10 3/4"	53°	10'-10 11/16"	62°	10'-10 11/16"	68°	10'-10 5/16"	74°	10'-9 13/16"	78°	10'-9 7/16"	84°
H25	11'-3 5/16"	40°	11'-2 3/4"	49°	11'-2 3/16"	53°	11'-1 5/8"	62°	11'-2 3/16"	71°	11'-2 3/4"	75°	11'-3 5/16"	84°		
H26	11'-7 3/4"	40°	11'-6 11/16"	49°	11'-5 11/16"	53°	11'-4 5/8"	62°	11'-5 3/16"	71°	11'-5 11/16"	75°	11'-6 5/16"	84°		
H27	12'-0 3/16"	40°	11'-10 5/8"	49°	11'-9 1/8"	53°	11'-7 9/16"	62°	11'-9 1/8"	71°	11'-10 5/8"	75°	12'-0 3/16"	84°		
H28	12'-4 5/8"	40°	12'-2 1/2"	49°	12'-0 5/8"	53°	11'-10 1/2"	62°	12'-0 1/8"	71°	12'-1 9/16"	75°	12'-3 1/8"	84°		
H29	12'-9 1/16"	40°	12'-6 7/16"	49°	12'-4 1/16"	53°	12'-1 7/16"	62°	12'-4 1/16"	71°	12'-6 7/16"	75°	12'-9 1/16"	84°		
H30	13'-1 1/2"	40°	12'-10 5/16"	49°	12'-7 9/16"	53°	12'-4 3/8"	62°	12'-7"	71°	12'-9 3/8"	75°	13'	84°		
H31	13'-5 15/16"	40°	13'-2 1/4"	49°	12'-11"	53°	12'-7 3/8"	62°	12'-11"	71°	13'-2 1/4"	75°	13'-5 15/16"	84°		
H32	13'-10 5/16"	40°	13'-6 3/16"	49°	13'-2 7/16"	53°	12'-10 5/16"	62°	13'-1 15/16"	71°	13'-5 1/4"	75°	13'-8 7/8"	84°		
H33	14'-2 3/4"	40°	13'-10 1/8"	49°	13'-5 15/16"	53°	13'-1 1/4"	62°	13'-5 15/16"	71°	13'-10 1/8"	75°	14'-2 3/4"	84°		
H34	14'-7 3/16"	40°	14'-2 1/16"	49°	13'-9 3/8"	53°	13'-4 3/16"	62°	13'-8 7/8"	71°	14'-1 1/16"	75°	14'-5 3/4"	84°		
H35	14'-11 5/8"	40°	15'-3 1/4"	49°	15'-10 7/16"	53°	16'-4 1/16"	62°	15'-10 7/16"	71°	15'-5 1/4"	75°	14'-11 5/8"	84°		
H36	15'-4 1/16"	40°	15'-9 3/16"	49°	16'-1 7/8"	53°	16'-7 1/16"	62°	16'-1 3/8"	71°	15'-8 1/4"	75°	15'-2 9/16"	84°		
H37	15'-8 1/2"	40°	16'-1 1/8"	49°	16'-5 5/16"	53°	16'-10"	62°	16'-5 5/16"	71°	16'-1 1/8"	75°	15'-8 1/2"	84°		
H38	16'-0 15/16"	40°	16'-5 1/16"	49°	16'-8 13/16"	53°	17'-0 15/16"	62°	16'-8 1/4"	71°	16'-4 1/8"	75°	15'-11 7/16"	84°		
H39	16'-5 5/16"	40°	16'-9"	49°	17'-0 1/4"	53°	17'-3 7/8"	62°	17'-0 3/4"	71°	16'-9"	75°	16'-5 5/16"	84°		
H40	16'-9 3/4"	40°	17'-0 15/16"	49°	17'-3 11/16"	53°	17'-6 7/8"	62°	17'-3 3/16"	71°	16'-11 15/16"	75°	16'-8 5/16"	84°		
H41	17'-2 3/16"	40°	17'-4 13/16"	49°	17'-7 3/16"	53°	17'-9 13/16"	62°	17'-7 3/16"	71°	17'-4 13/16"	75°	17'-2 3/16"	84°		
H42	17'-6 5/8"	40°	17'-8 3/4"	49°	17'-10 5/8"	53°	18'-0 3/4"	62°	17'-10 1/8"	71°	17'-7 3/4"	75°	17'-5 1/8"	84°		
H43	17'-11 1/16"	40°	18'-0 5/8"	49°	18'-2 1/8"	53°	18'-3 11/16"	62°	18'-2 1/8"	71°	18'-0 5/8"	75°	17'-11 1/16"	84°		
H44	18'-3 1/2"	40°	18'-4 9/16"	49°	18'-5 9/16"	53°	18'-6 11/16"	62°	18'-5 1/16"	71°	18'-3 5/8"	75°	18'-2"	84°		
H45	18'-7 15/16"	40°	18'-8 1/2"	49°	18'-9 1/16"	53°	18'-9 5/8"	62°	18'-9 1/16"	71°	18'-8 1/2"	75°	18'-7 15/16"	84°		
H46	19'-0 3/8"	40°	19'-0 7/16"	49°	19'-0 1/2"	53°	19'-0 9/16"	62°	19'	71°	18'-11 7/16"	75°	18'-10 7/8"	84°		

EL : LEVEL
θ : AZIMUTH ANGLE
R : 18'-4 1/8"

- NOTE :
- 1) Φ : INFLECTION POINT (IN-PLANE)
 - 2) $\begin{matrix} \text{H00 00} \\ \text{POINT NO.} \\ \text{TENDON NO.} \end{matrix}$
 - 3) $\begin{matrix} \text{V00 00} \\ \text{POINT NO.} \\ \text{TENDON NO.} \end{matrix}$
 - 4) CYLINDRICAL COORDINATES



REVISION			
NO.	DATE	REVISION	BY
DRAWINGS FOR REFERENCE			
		DATE	STATUS
		'95.2.24	FINAL
		'95.1.25	PRELIMINARY
		'94.11.17	EXAMINATION
			REFERENCE
REMARKS			
NUPEC PCCV STRUCTURAL BEHAVIOR TEST MODEL			
NAME		SHEET	SCALE
NUPEC SYSTEMS SAFETY DEPT.			1/25
S N L		COPY 1	REVISION NO.
NUCLEAR SYSTEMS ENGINEERING DEPT.			R1
STEEL STRUCTURE DESIGNING SECT.		COPY 1	
EQUIP DESIGN SECT.		COPY 1	
TAKASAGO R&D CENTER		COPY 1	
T A I S E I		COPY 1	
OBAYASHI		DRIG.	
M H I		OBAYASHI	DRAWING NO.
		T. Ito, K. Umehashi, H. Murano	PCCV-QCON-09



THE INFLECTION POINTS IN CYLINDRICAL COORDINATES (VERTICAL DOME TENDONS)

POINT NO.	01		02		03		04		05		06		07		08		09	
TENDON NO.	EL	θ	EL	θ	EL	θ	EL	θ	EL	θ	EL	θ	EL	θ	EL	θ	EL	θ
V58	8'-0 7/16"	159°	10'-2 1/16"	158.87°	14'-2 1/4"	158.36°	16'-3 7/8"	158.22°	18'-5 7/16"	158.08°	23'-1 9/16"	158.08°	25'-3 1/8"	159°	23'-1 9/16"	160.69°	25'-3 1/8"	161°
V59	9 13/16"	161°	2'-11 7/16"	160.93°	5'-10 7/8"	160.73°	6'-11 5/8"	160.72°	15'-3 1/16"	159.07°	16'-3 7/8"	159.00°	18'-5 7/16"	159.31°	23'-1 9/16"	162.50°	25'-3 1/8"	163°
V60	9 13/16"	163°	2'-11 7/16"	162.67°	5'-10 7/8"	161.77°	6'-11 5/8"	161.52°	15'-3 1/16"	159.85°	16'-3 7/8"	159.78°	18'-5 7/16"	160.28°	23'-1 9/16"	164.31°	25'-3 1/8"	165°
V61	9 13/16"	165°	2'-11 7/16"	164.42°	5'-10 7/8"	162.80°	7'-0 3/16"	162.35°	15'-3 1/16"	160.63°	16'-3 7/8"	160.56°	18'-5 7/16"	161.25°	23'-1 9/16"	164.31°	25'-3 1/8"	166°
V62	9 13/16"	167°	2'-11 7/16"	166.17°	5'-10 7/8"	163.83°	7'-2 1/8"	163.13°	15'-3 1/16"	161.41°	16'-3 7/8"	161.34°	18'-5 7/16"	162.22°	23'-1 9/16"	166.12°	25'-3 1/8"	167°
V63	9 13/16"	169°	2'-11 7/16"	165.07°	5'-10 7/8"	162.87°	8'-0 7/16"	163.34°	16'-3 7/8"	163.94°	18'-5 7/16"	163.29°	23'-1 9/16"	165.05°	25'-3 1/8"	169°		
V64	9 13/16"	171°	2'-11 7/16"	170.82°	5'-10 7/8"	170.30°	8'-0 7/16"	170.12°	16'-3 7/8"	170.12°	18'-5 7/16"	170.26°	23'-1 9/16"	170.86°	25'-3 1/8"	171°		
V65	9 13/16"	173°	2'-11 7/16"	172.56°	5'-10 7/8"	171.94°	8'-0 7/16"	170.90°	16'-3 7/8"	170.90°	18'-5 7/16"	171.23°	23'-1 9/16"	172.67°	25'-3 1/8"	173°		
V66	9 13/16"	175°	2'-11 7/16"	174.31°	5'-10 7/8"	172.37°	8'-0 7/16"	171.68°	16'-3 7/8"	171.68°	18'-5 7/16"	172.20°	23'-1 9/16"	174.48°	25'-3 1/8"	175°		
V67	9 13/16"	177°	2'-11 7/16"	173.38°	5'-10 7/8"	178.45°	8'-0 7/16"	178.83°	16'-3 7/8"	178.83°	18'-5 7/16"	178.54°	23'-1 9/16"	177.29°	25'-3 1/8"	177°		
V68	9 13/16"	179°	2'-11 7/16"	179.13°	5'-10 7/8"	179.48°	8'-0 7/16"	179.61°	16'-3 7/8"	179.61°	18'-5 7/16"	179.31°	23'-1 9/16"	179.10°	25'-3 1/8"	179°		
V69	9 13/16"	181°	2'-11 7/16"	180.87°	5'-10 7/8"	180.52°	8'-0 7/16"	180.39°	16'-3 7/8"	180.39°	18'-5 7/16"	180.49°	23'-1 9/16"	180.90°	25'-3 1/8"	181°		
V70	9 13/16"	183°	2'-11 7/16"	182.62°	5'-10 7/8"	181.55°	8'-0 7/16"	181.17°	16'-3 7/8"	181.17°	18'-5 7/16"	181.46°	23'-1 9/16"	182.71°	25'-3 1/8"	183°		
V71	9 13/16"	185°	2'-11 7/16"	185.69°	5'-10 7/8"	187.63°	8'-0 7/16"	188.32°	16'-3 7/8"	188.32°	18'-5 7/16"	188.80°	23'-1 9/16"	185.52°	25'-3 1/8"	185°		
V72	9 13/16"	187°	2'-11 7/16"	187.44°	5'-10 7/8"	188.66°	8'-0 7/16"	189.10°	16'-3 7/8"	189.10°	18'-5 7/16"	188.77°	23'-1 9/16"	187.33°	25'-3 1/8"	187°		
V73	9 13/16"	189°	2'-11 7/16"	189.18°	5'-10 7/8"	189.70°	8'-0 7/16"	189.88°	16'-3 7/8"	189.88°	18'-5 7/16"	189.74°	23'-1 9/16"	189.14°	25'-3 1/8"	189°		
V74	9 13/16"	191°	2'-11 7/16"	190.93°	5'-10 7/8"	190.73°	8'-0 7/16"	190.66°	16'-3 7/8"	190.66°	18'-5 7/16"	190.71°	23'-1 9/16"	190.95°	25'-3 1/8"	191°		
V75	9 13/16"	193°	2'-11 7/16"	193.83°	5'-10 7/8"	196.17°	7'-2 1/8"	196.87°	15'-3 1/16"	196.59°	16'-3 7/8"	196.66°	18'-5 7/16"	197.78°	23'-1 9/16"	193.88°	25'-3 1/8"	193°
V76	9 13/16"	195°	2'-11 7/16"	195.58°	5'-10 7/8"	197.20°	7'-0 3/16"	197.65°	15'-3 1/16"	197.31°	16'-3 7/8"	199.44°	18'-5 7/16"	196.75°	23'-1 9/16"	195.69°	25'-3 1/8"	195°
V77	9 13/16"	197°	2'-11 7/16"	197.33°	5'-10 7/8"	198.23°	6'-11 5/8"	198.48°	15'-3 1/16"	200.17°	16'-3 7/8"	200.22°	18'-5 7/16"	199.72°	23'-1 9/16"	197.50°	25'-3 1/8"	197°
V78	9 13/16"	199°	2'-11 7/16"	199.07°	5'-10 7/8"	199.27°	6'-11 5/16"	199.28°	15'-3 1/16"	200.93°	16'-3 7/8"	201.00°	18'-5 7/16"	200.69°	23'-1 9/16"	199.31°	25'-3 1/8"	199°
V79	8'-0 7/16"	201°	10'-2 1/16"	201.13°	14'-2 1/4"	201.64°	16'-3 7/8"	201.78°	18'-5 7/16"	201.66°	23'-1 9/16"	201.12°	25'-3 1/8"	201°				

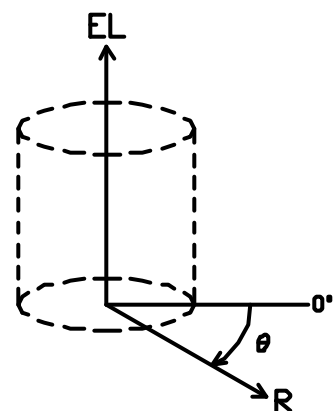
EL : LEVEL
 θ : AZIMUTH ANGLE
R : 18'-2"

THE INFLECTION POINTS IN CYLINDRICAL COORDINATES (HOOP TENDONS)

POINT NO.	01	02	03	04	05	06	07	08
TENDON NO.	EL	θ	EL	θ	EL	θ	EL	θ
H11	6'-1 3/16"	150°	6'-1 1/16"	156.15°	6'-0 5/8"	160.01°	6'-0 5/16"	166.16°
H12	6'-3 3/4"	150°	6'-3"	156.15°	6'-4 1/16"	160.01°	6'-3 5/16"	166.16°
H13	6'-10 3/16"	150°	6'-9"	156.15°	6'-7 7/16"	160.01°	6'-6 1/4"	166.16°
H14	7'-2 5/8"	150°	7'-0 15/16"	156.15°	6'-10 7/8"	160.01°	6'-9 3/16"	166.16°
H15	7'-7 1/16"	150°	7'-4 15/16"	156.15°	7'-2 1/4"	160.01°	7'-0 1/8"	166.16°
H16	7'-11 1/2"	150°	7'-8 15/16"	156.15°	7'-5 5/8"	160.01°	7'-3 1/8"	166.16°
H17	8'-3 7/8"	150°	8'-5 11/16"	156.15°	8'-8"	160.01°	8'-9 13/16"	166.16°
H18	8'-8 5/16"	150°	8'-9 11/16"	156.15°	8'-11 3/8"	160.01°	9'-0 3/4"	166.16°
H19	9'-0 3/4"	150°	9'-1 11/16"	156.15°	9'-2 13/16"	160.01°	9'-3 11/16"	166.16°
H20	9'-5 3/16"	150°	9'-5 11/16"	156.15°	9'-6 3/16"	160.01°	9'-6 11/16"	166.16°
H32	13'-10 5/16"	146°	13'-10"	152.15°	13'-9 3/16"	159.21°	13'-8 7/8"	165.36°
H33	14'-2 3/4"	146°	14'-2 1/16"	152.15°	14'-0 1/2"	159.21°	13'-11 13/16"	165.36°
H34	14'-7 3/16"	146°	14'-6 3/16"	152.15°	14'-3 13/16"	159.21°	14'-2 3/4"	165.36°
H35	14'-11 5/8"	146°	14'-10 1/4"	152.15°	14'-7 1/16"	159.21°	14'-5 3/4"	165.36°
H36	15'-4 1/16"	146°	15'-2 5/16"	152.15°	14'-10 3/8"	159.21°	14'-8 11/16"	165.36°
H37	15'-8 1/2"	146°	15'-6 7/16"	152.15°	15'-1 11/16"	159.21°	14'-11 5/8"	165.36°
H38	16'-0 15/16"	146°	15'-10 1/2"	152.15°	15'-4 15/16"	159.21°	15'-2 9/16"	165.36°
H39	16'-5 5/16"	146°	16'-8 1/16"	152.15°	17'-2 7/16"	159.21°	17'-5 1/8"	165.36°
H40	16'-9 3/4"	146°	17'-0 3/16"	152.15°	17'-3 3/4"	159.21°	17'-8 1/8"	165.36°
H41	17'-2 3/16"	146°	17'-4 1/4"	152.15°	17'-9"	159.21°	17'-11 1/16"	165.36°
H42	17'-6 5/8"	146°	17'-8 3/8"	152.15°	18'-0 5/16"	159.21°	18'-2"	165.36°
H43	17'-11 1/16"	146°	18'-0 7/16"	152.15°	18'-3 5/8"	159.21°	18'-4 15/16"	165.36°
H44	18'-3 1/2"	146°	18'-4 1/2"	152.15°	18'-6 7/8"	159.21°	18'-7 15/16"	165.36°
H45	18'-7 15/16"	146°	18'-8 5/8"	152.15°	18'-10 3/16"	159.21°	18'-10 7/8"	165.36°
H46	19'-0 3/8"	146°	19'-0 11/16"	152.15°	19'-1 1/2"	159.21°	19'-1 13/16"	165.36°

EL : LEVEL
 θ : AZIMUTH ANGLE
R : 18'-4 1/8"

- NOTE :
- 1) Φ : INFLECTION POINT (IN-PLANE)
 - 2) H00 00 : POINT NO. TENDON NO.
 - 3) V00 00 : POINT NO. TENDON NO.
 - 4) CYLINDRICAL COORDINATES

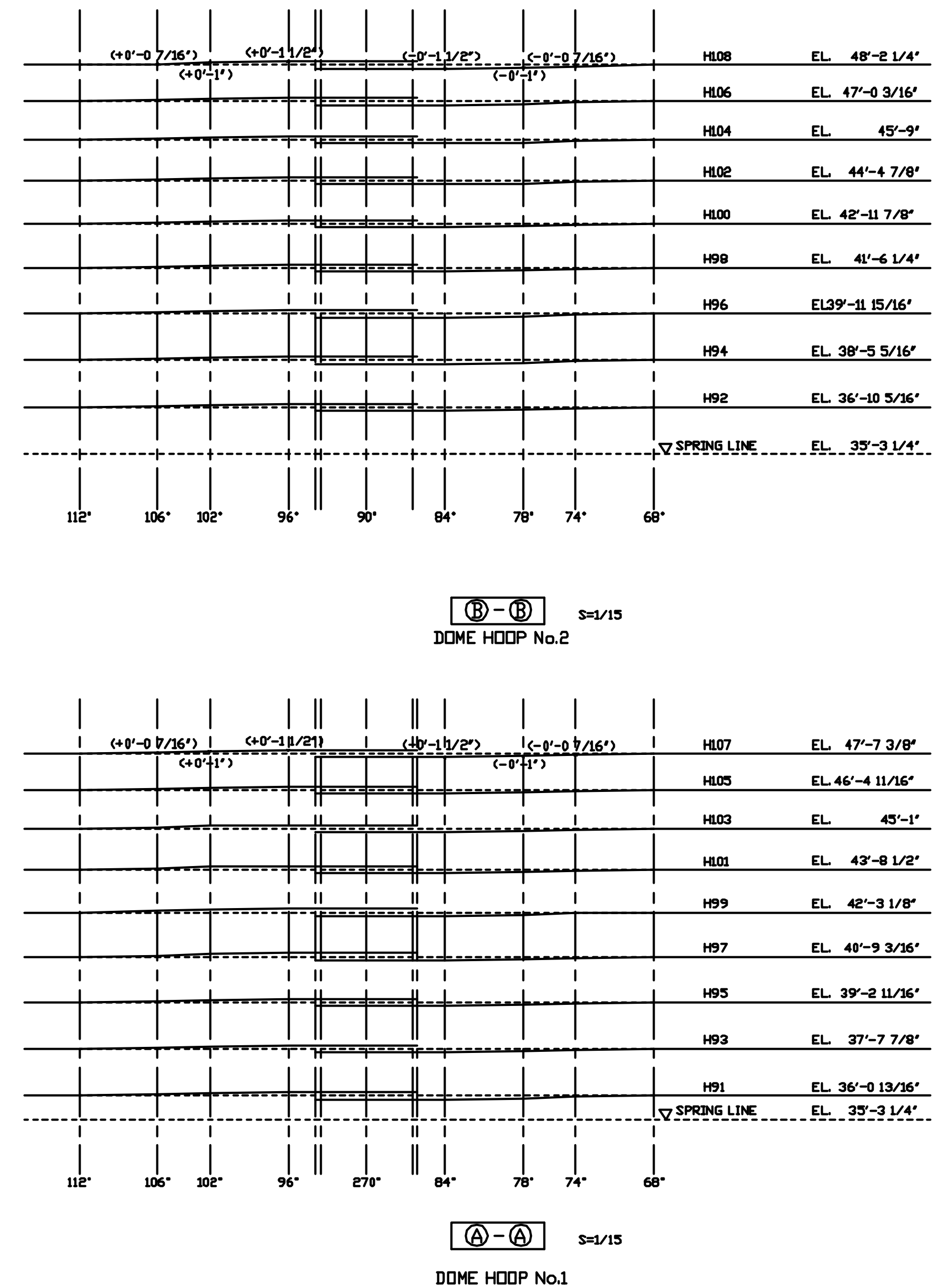


NO.	DATE	REVISION	BY

REVISION

DRAWINGS FOR REFERENCE	DATE	STATUS	REMARKS
	'95.2.24	O	FINAL
	'95.1.25		PRELIMINARY
	'94.11.17		APPLICATION
			EXAMINATION
			REFERENCE

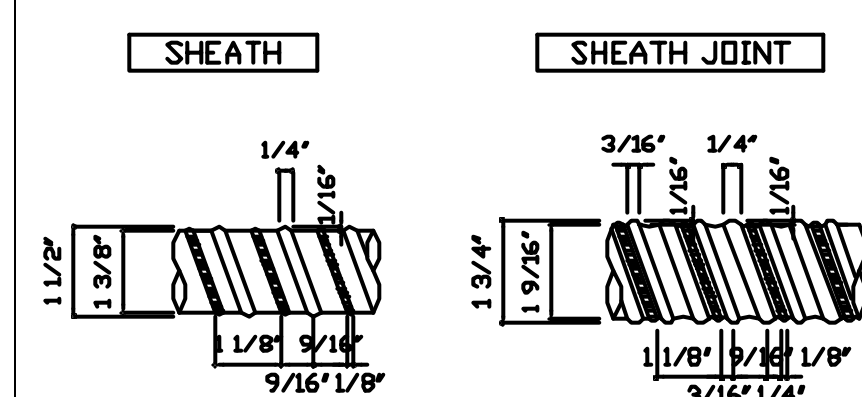
NAME	SHEET	NUPEC PCCV STRUCTURAL BEHAVIOR TEST MODEL	SCALE
NUPEC SYSTEMS SAFETY DEPT.		PRESTRESSING TENDON DETAILS (M/S • F/W)	1/25
S N L	COPY 1		REVISION NO.
M H I		MITSUBISHI HEAVY INDUSTRIES, L.T.D.	
NUCLEAR SYSTEMS ENGINEERING DEPT.			
STEEL STRUCTURE DESIGNING SECT.	COPY 1	OBAYASHI CORPORATION	R1
EQUIP DESIGN SECT.	COPY 1		
TAKASAGO R&D CENTER	COPY 1		
T A S E I	COPY 1		
OBAYASHI	ORIG.		
		M H I	OBAYASHI
			T. Oba, K. Umada, H. Murano
		DRAWING NO.	PCCV-QCON-10



NOTE :

- 1) SHEATH CENTERS ARE SHOWN
- 2) () , OFFSET VALUE FROM NOMAL POSITION AT HOOP TENDON ANCHORED PORTIONS

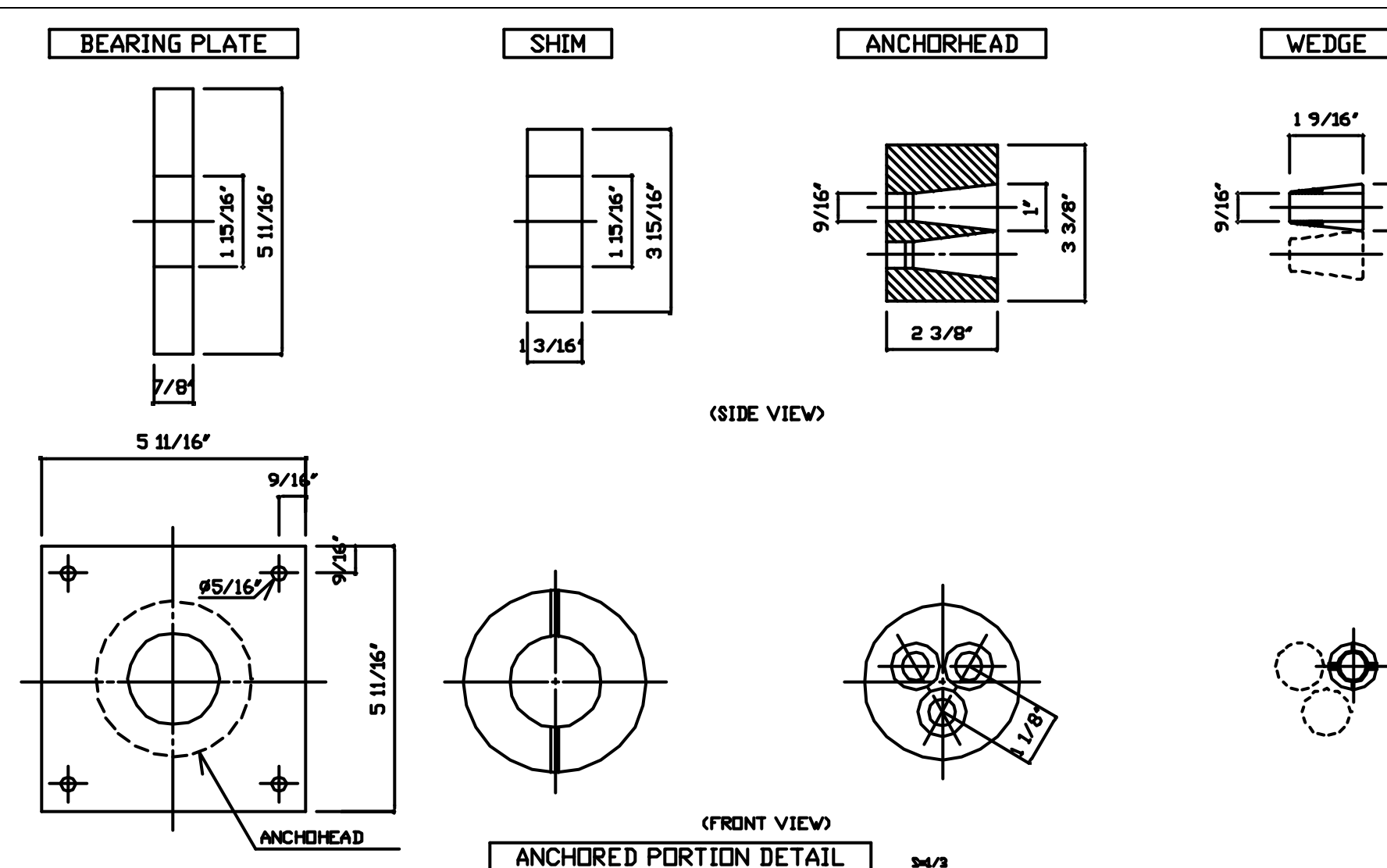
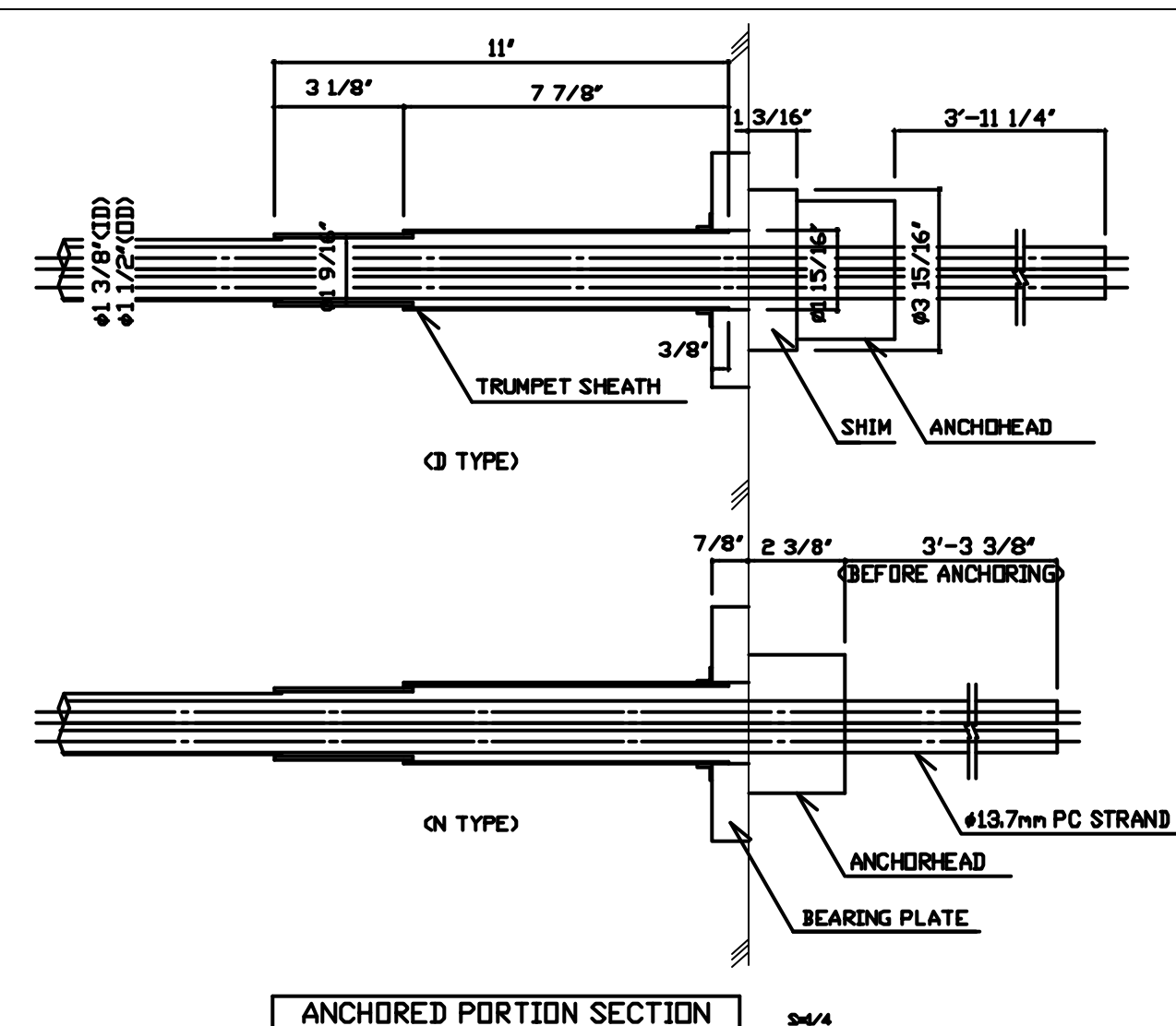
PS SYSTEM HARDWARE



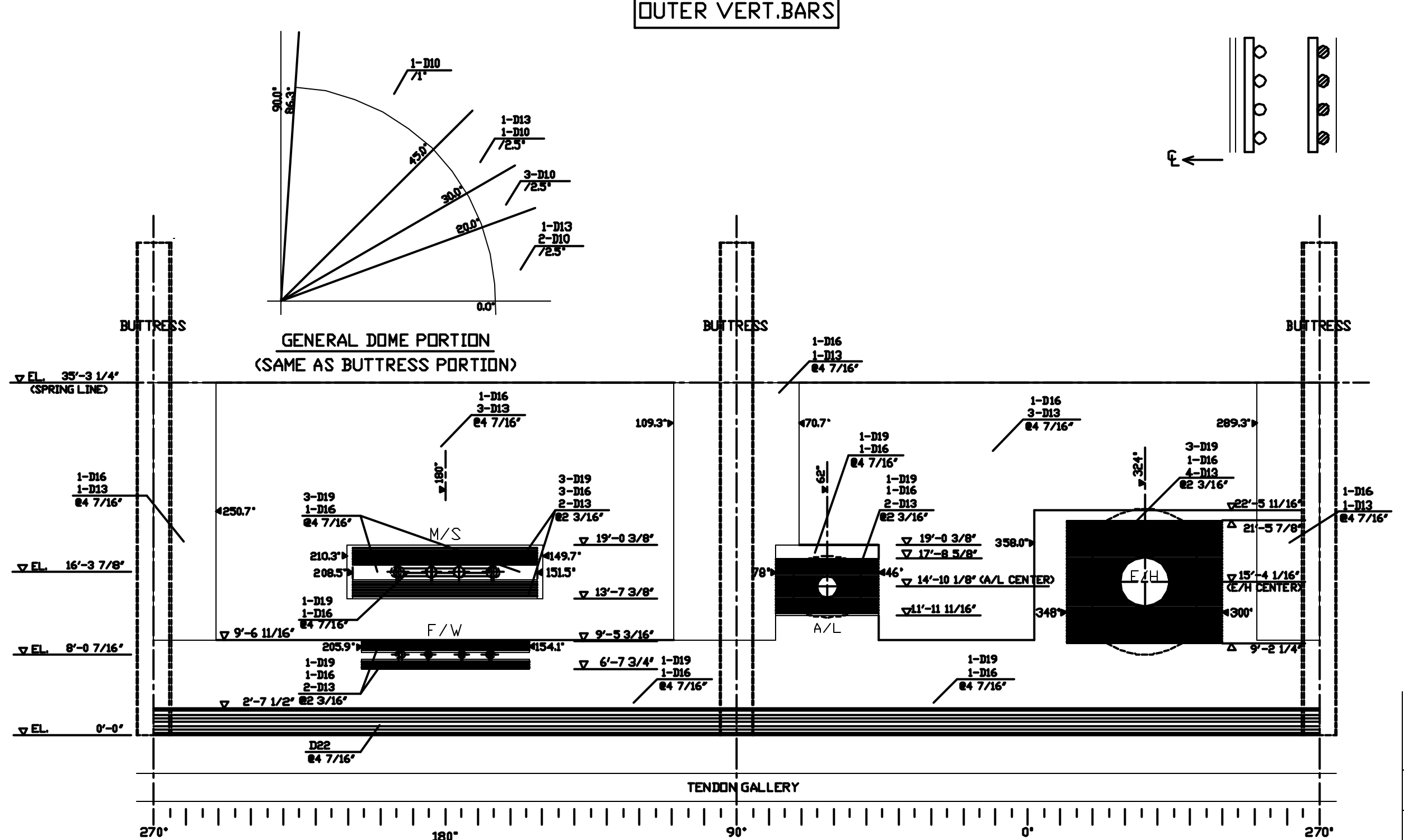
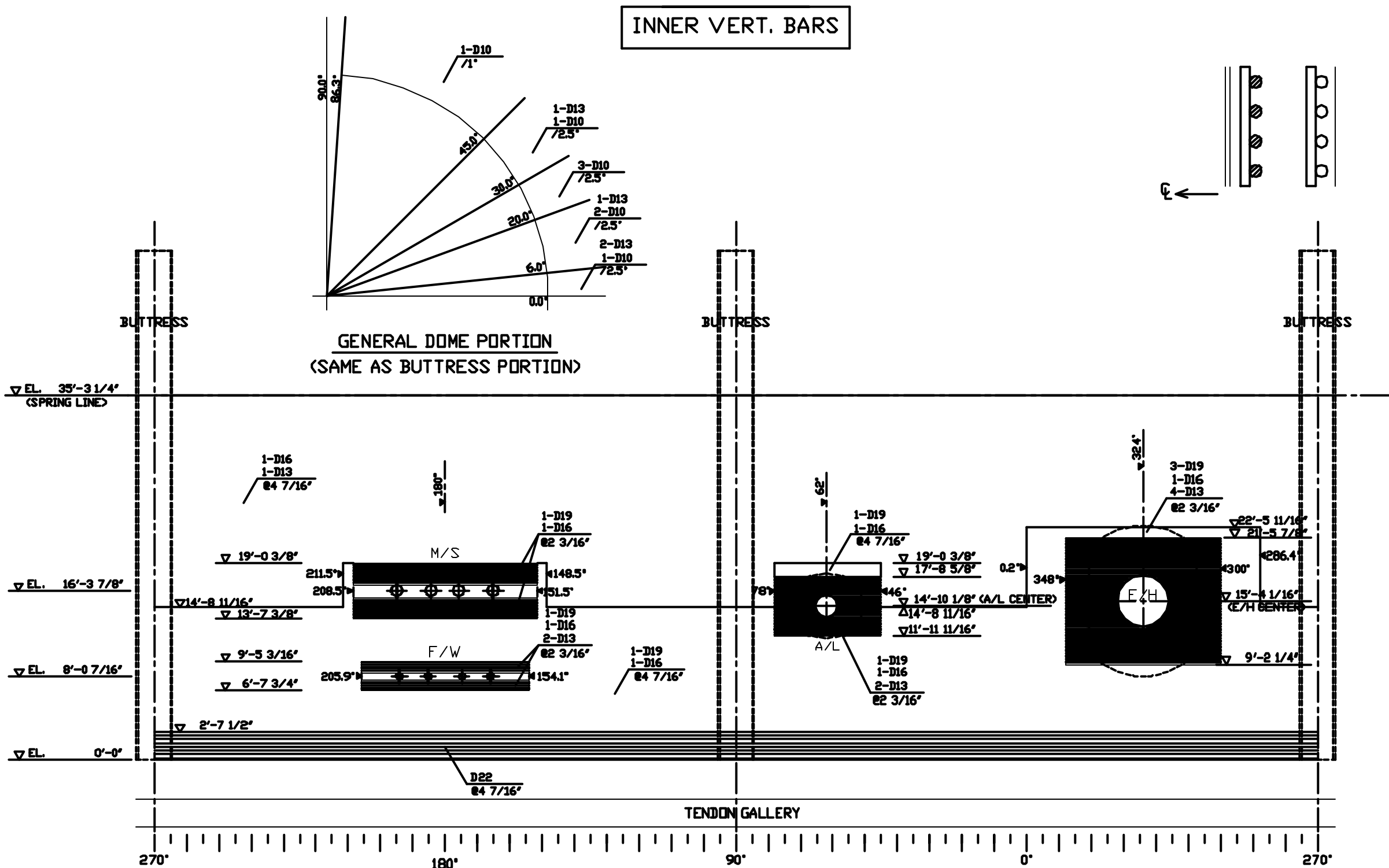
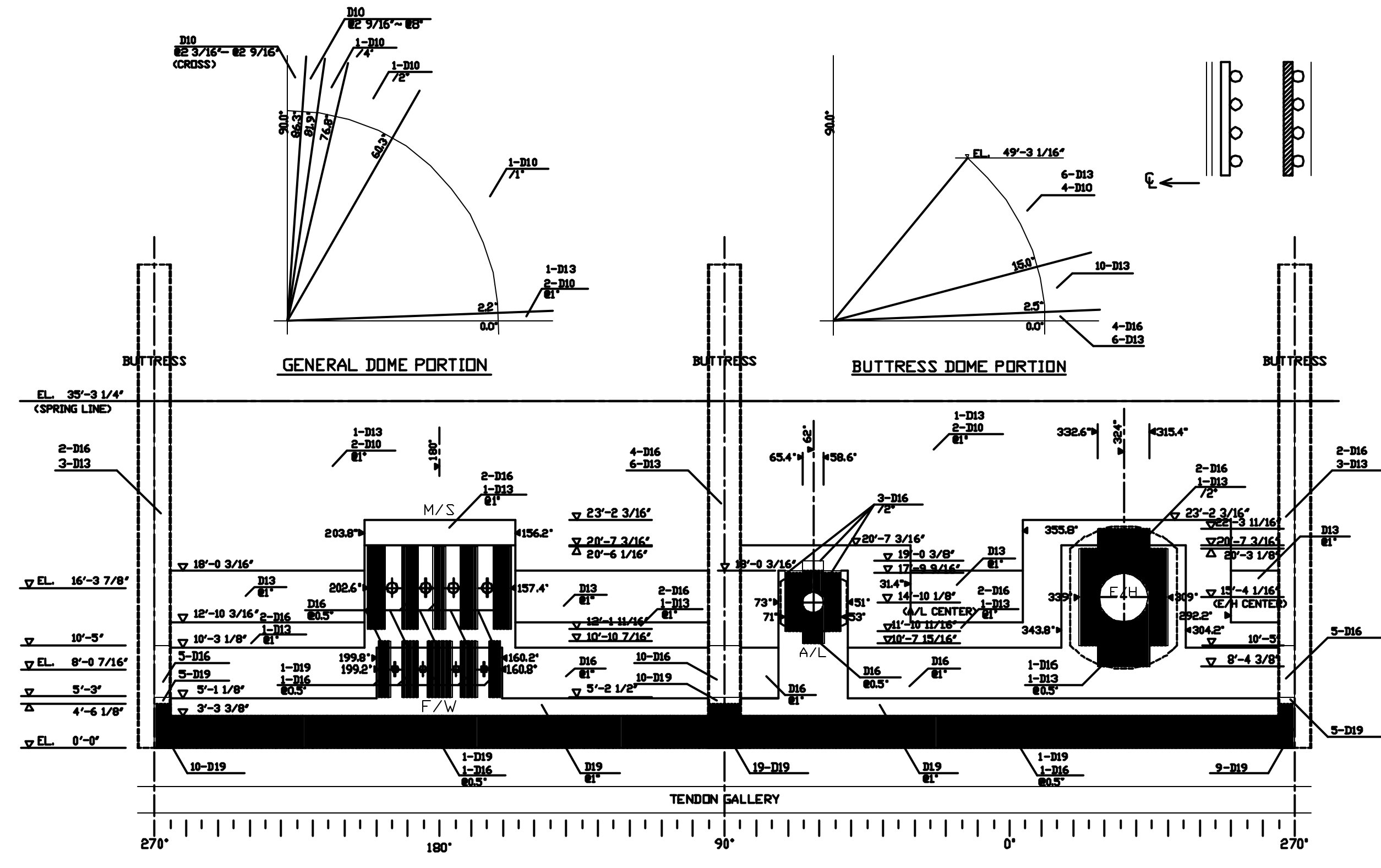
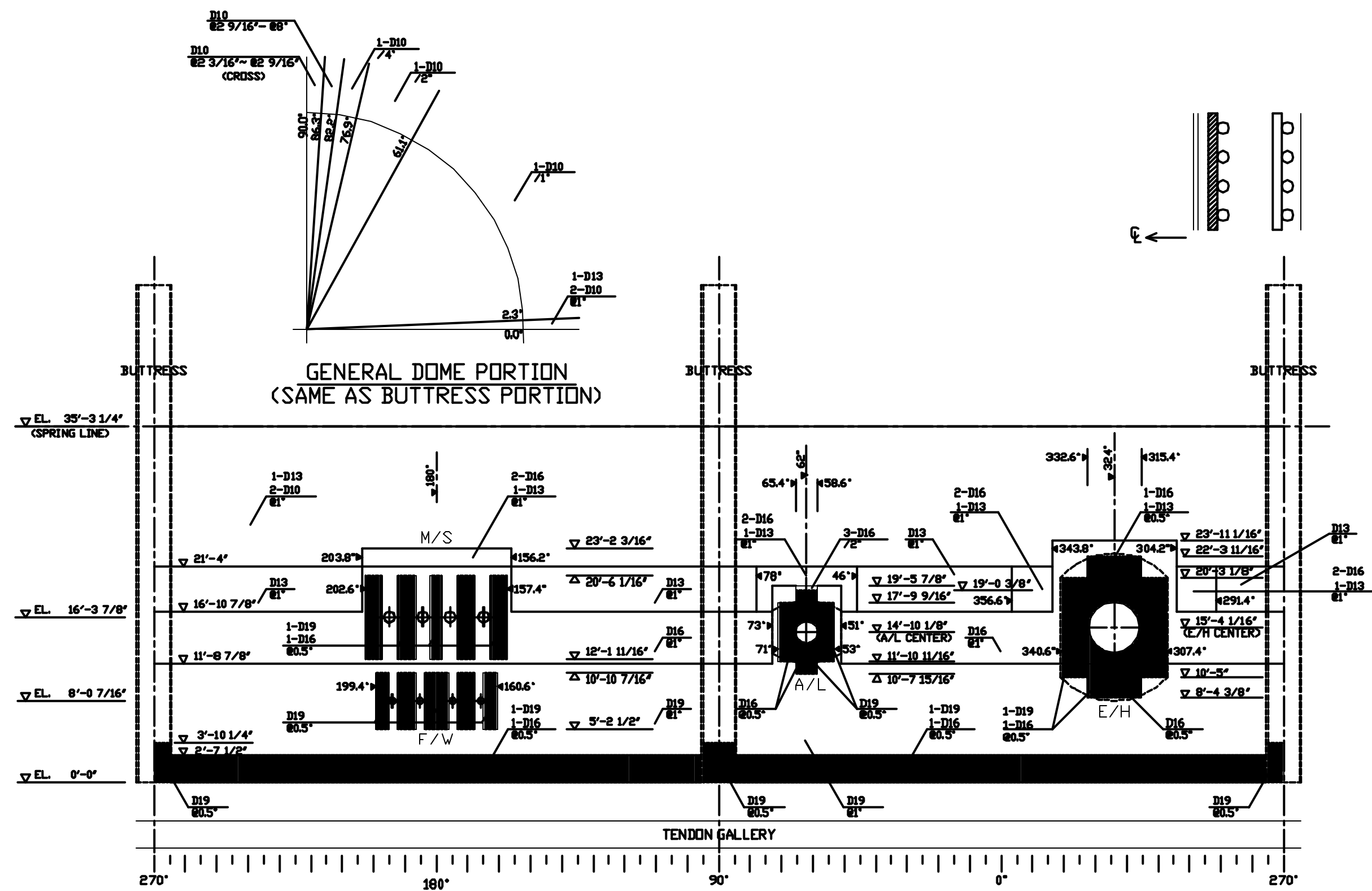
SHEATH DETAIL

• MATERIAL SPECIFICATIONS

ANCHORHEAD	:SS5C	JIS G 405
BEARING PLATE	:SS400	JIS G 3103
WEDGE	:SCM415	JIS G 4105
SHEATH	:SGCC	JIS G 3301
TRUMPET SHEATH	:SGCV	JIS G 3441
SHIM	:SS400	JIS G 3103



				NO.		DATE		REVISION		BY	
				REVISION							
DRAWINGS FOR REFERENCE				DATE		STATUS		REMARKS			
				'95. 2.24		○		FINAL			
								PRELIMINARY			
				'95. 1.25				APPLICATION			
				'94.11.17				EXAMINATION			
								REFERENCE			
NAME			SHEET	NUPEC PCCV STRUCTURAL BEHAVIOR TEST MODEL							
NUPEC	SYSTEMS SAFETY DEPT.			DOME PRESTRESSING TENDON ARRANGEMENT • PRESTRESSING SYSTEM HARDWARE				SCALE 1/40, 1/3 1/4			
S N L			COPY 1					REVISION NO.			
M H I	NUCLEAR SYSTEMS ENGINEERING DEPT.			MITSUBISHI HEAVY INDUSTRIES, LTD.				R1			
	STEEL STRUCTURE DESIGNING SECT.		COPY 1	OBAYASHI CORPORATION							
	EQUIP. DESIGN SECT.		COPY 1								
	TAKASAGO R&D CENTER		COPY 1								
		T A I S E I		COPY 1	M H I		OBAYASHI		DRAWING NO.		
		PRAYASHI		PTG.			T. Iba K. Umeki H. Munaga		PCCV-QCON-11		

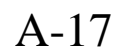


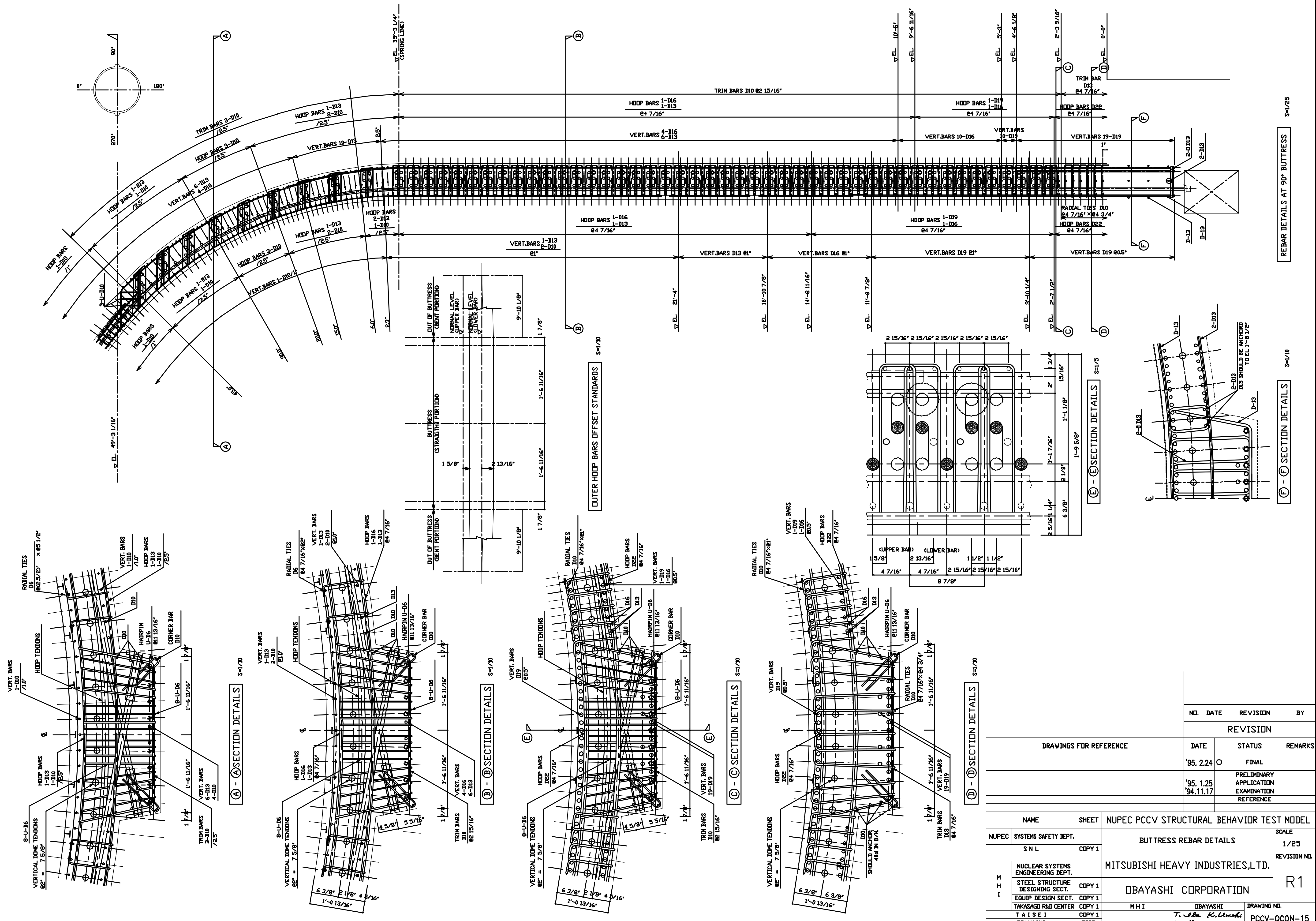
REBAR ARRANGEMENT GENERAL DESCRIPTION

(TYPICALS)

- 1-D13
2-D10
E1 EACH D13, D10, D10 PITCH 1" EACH
- 1-D13
2-D10
7/25 EACH D13, D10, D10 PER 2.5"
- 1-D19
1-D16
2-D19
E2 3/16 EACH D19, D16, D13, D13 PITCH 56.25 EACH
- 1-D10
7/4 EACH D10, D10 PER 2.5"

DRAWINGS FOR REFERENCE			DATE	STATUS	REMARKS
			'95.2.24	O	FINAL
			'95.1.25		PRELIMINARY
			'94.11.17		APPLICATION
					EXAMINATION
					REFERENCE
NAME		SHEET	NUPEC PCCV STRUCTURAL BEHAVIOR TEST MODEL		
NUPEC	SYSTEMS SAFETY DEPT.		CYLINDER & DOME REBAR GENERAL ARRANGEMENT (C)		SCALE 1/120
S N L		COPY 1			REVISION NO.
M H I	NUCLEAR SYSTEMS ENGINEERING DEPT.		MITSUBISHI HEAVY INDUSTRIES,LTD.		R1
	STEEL STRUCTURE DESIGNING SECT.	COPY 1	OBAYASHI CORPORATION		
	EQUIP DESIGN SECT.	COPY 1			
	TAKASAGO R&D CENTER	COPY 1			
	T A I S E I	COPY 1			
OBAYASHI		DRIG.	M H I	OBAYASHI <i>T. Iba K. Umehara H. Murano</i>	DRAWING NO. PCCV-QCON-12





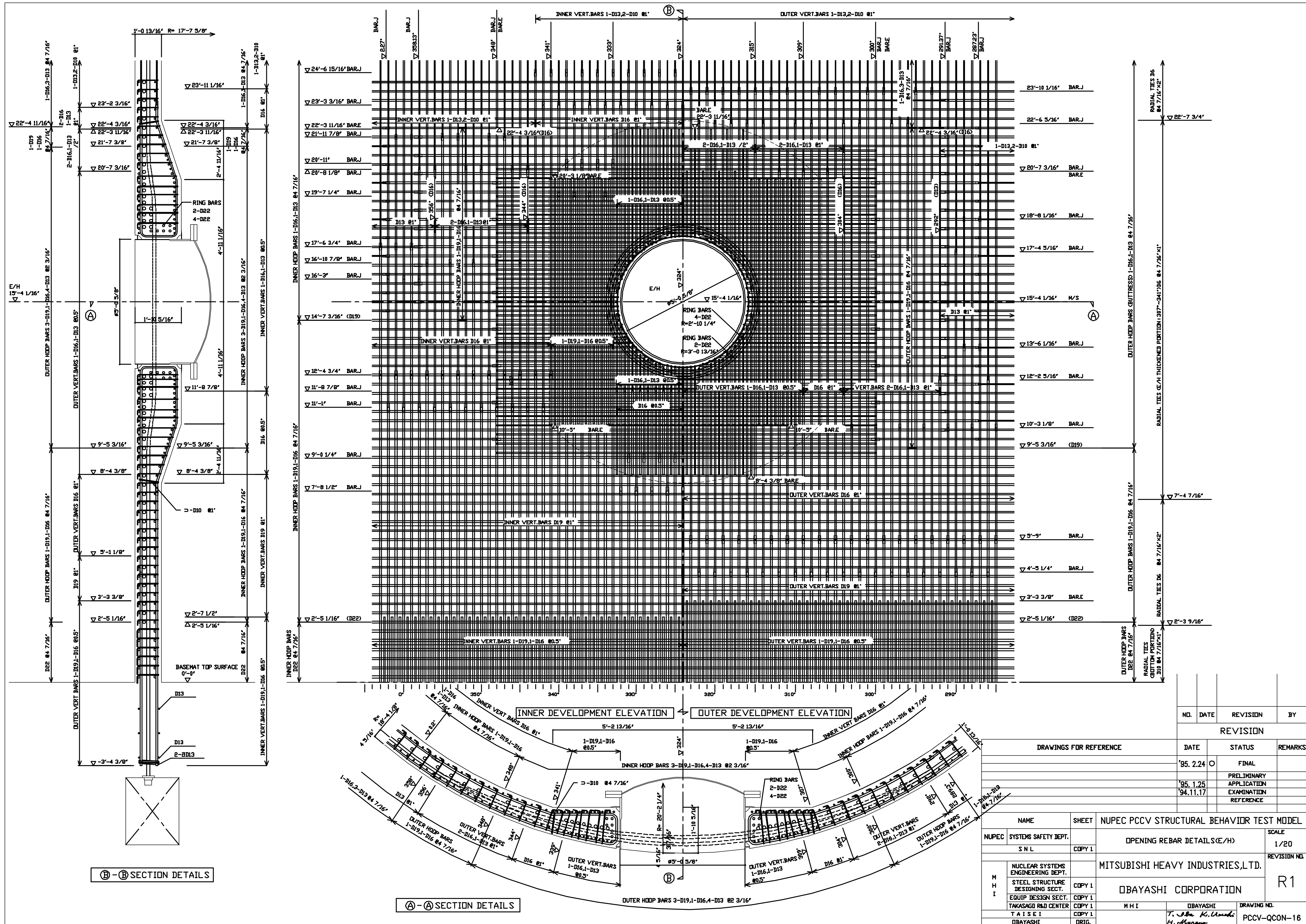
S-4/25

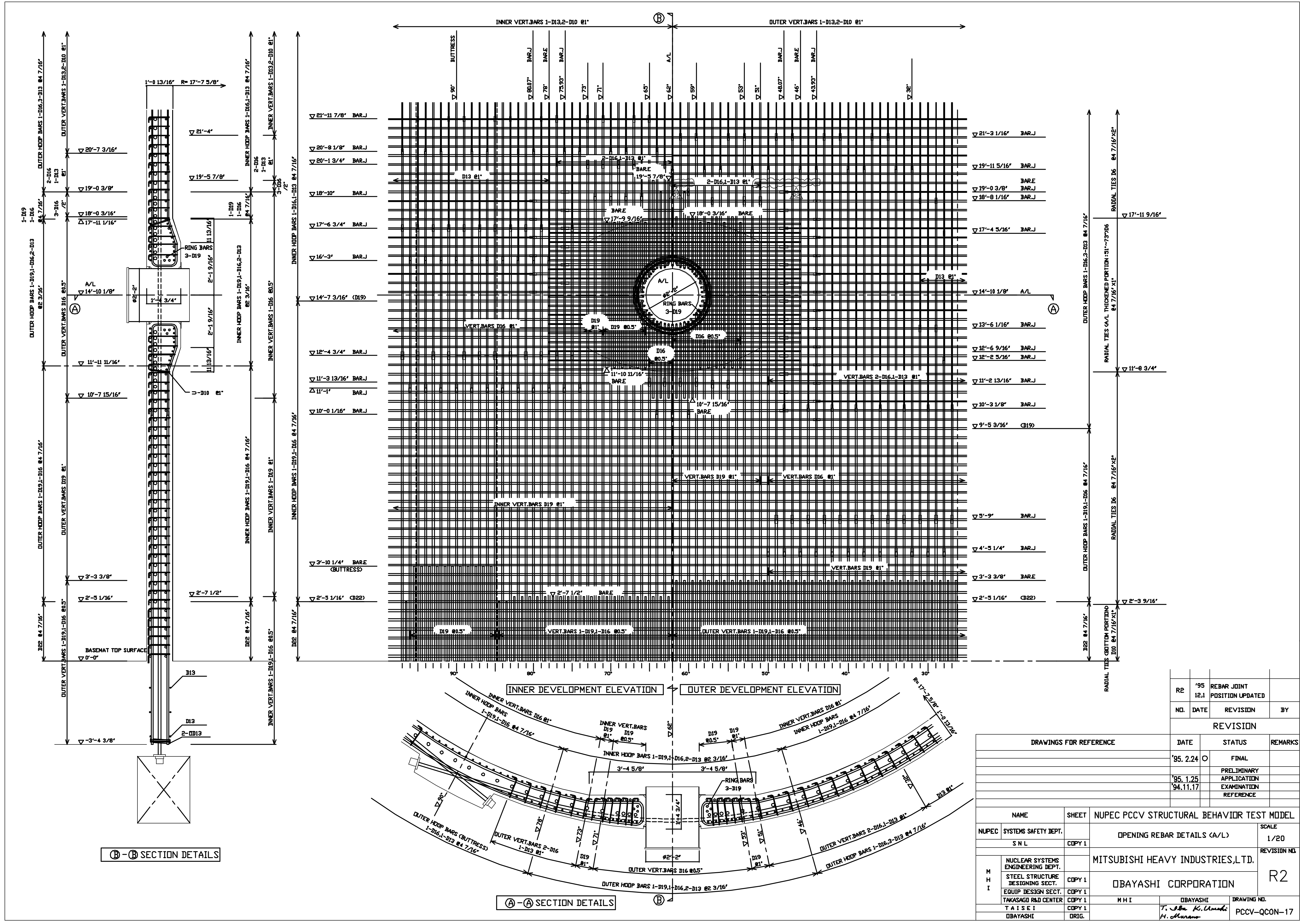
S-4/10

REBAR DETAILS AT 90° BUTTRESS

REVISION			
NO.	DATE	REVISION	BY
DRAWINGS FOR REFERENCE			
	DATE	STATUS	REMARKS
	'95.2.24	FINAL	
	'95.1.25	PRELIMINARY	
	'94.11.17	APPLICATION	
		EXAMINATION	
		REFERENCE	

NAME		SHEET		NUPEC PCCV STRUCTURAL BEHAVIOR TEST MODEL	
NUPEC SYSTEMS SAFETY DEPT.		COPY 1		BUTTRESS REBAR DETAILS	
S.N.L.		COPY 1		MITSUBISHI HEAVY INDUSTRIES, L.T.D.	
NUCLEAR SYSTEMS ENGINEERING DEPT.		COPY 1		OBAYASHI CORPORATION	
STEEL STRUCTURE DESIGNING SECT.		COPY 1		M.H.I.	
EQUIP DESIGN SECT.		COPY 1		OBAYASHI	
TAKASAGO R&D CENTER		COPY 1		T. Obayashi, K. Umehara	
T.A.I.S.E.I.		COPY 1		H. Muramatsu	
OBAYASHI		ORIG.		DRAWING NO. PCCV-QCON-15	



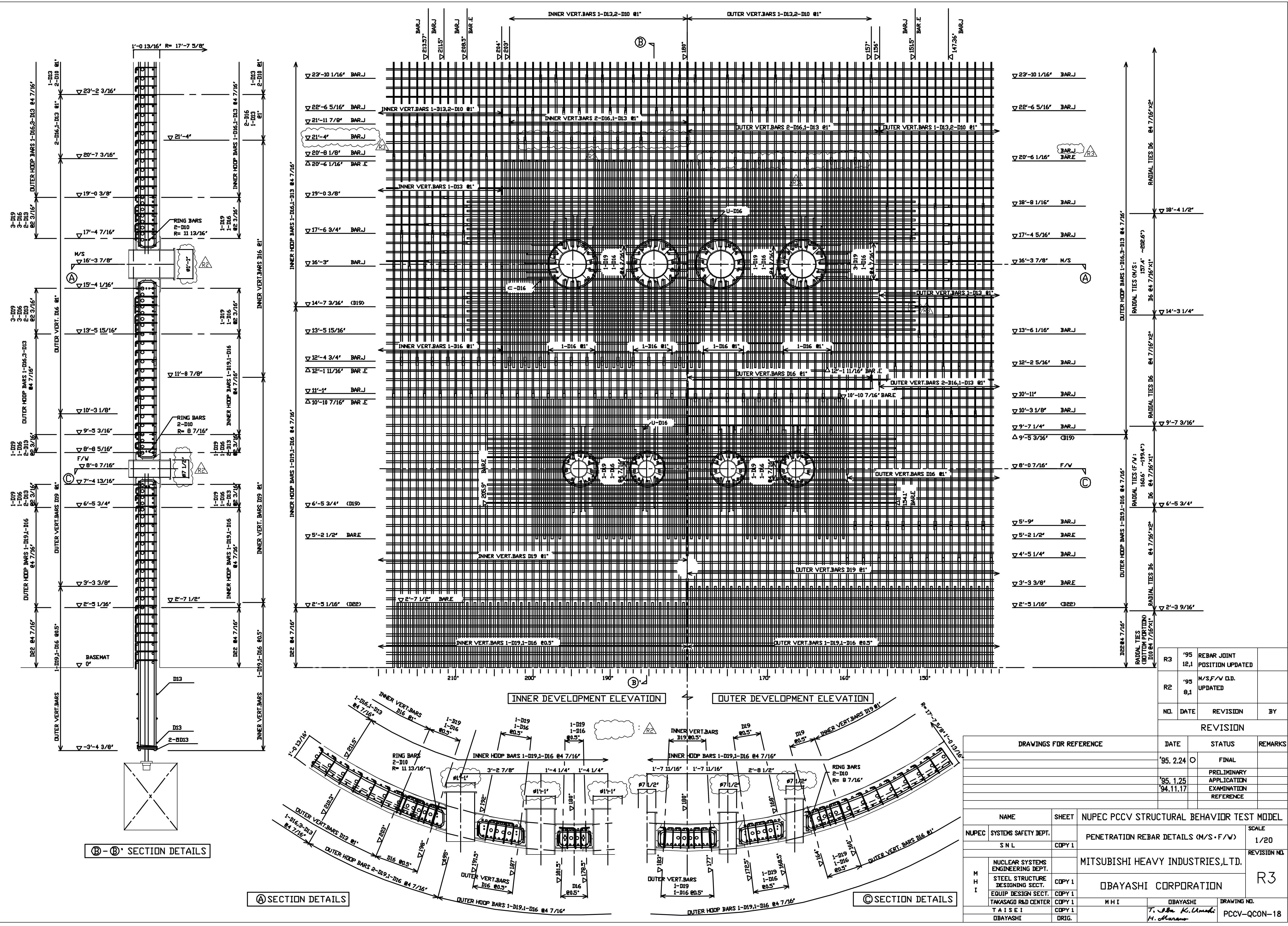


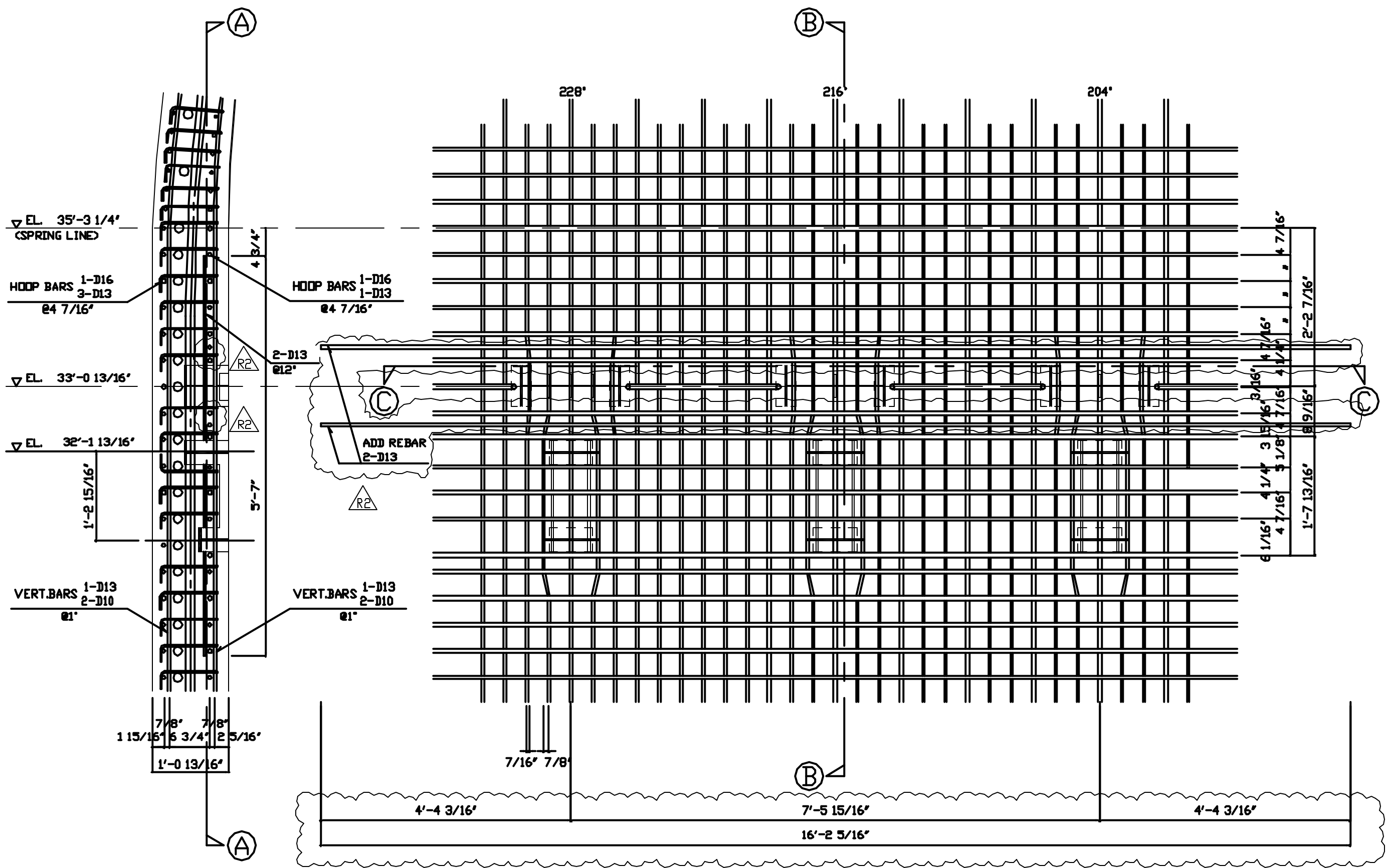
R2	'95 12.1	REBAR JOINT POSITION UPDATED	
NO.	DATE	REVISION	BY

REVISION

DRAWINGS FOR REFERENCE	DATE	STATUS	REMARKS
	'95. 2.24	O	FINAL
	'95. 1.25		PRELIMINARY
	'94. 11.17		APPLICATION
			EXAMINATION
			REFERENCE

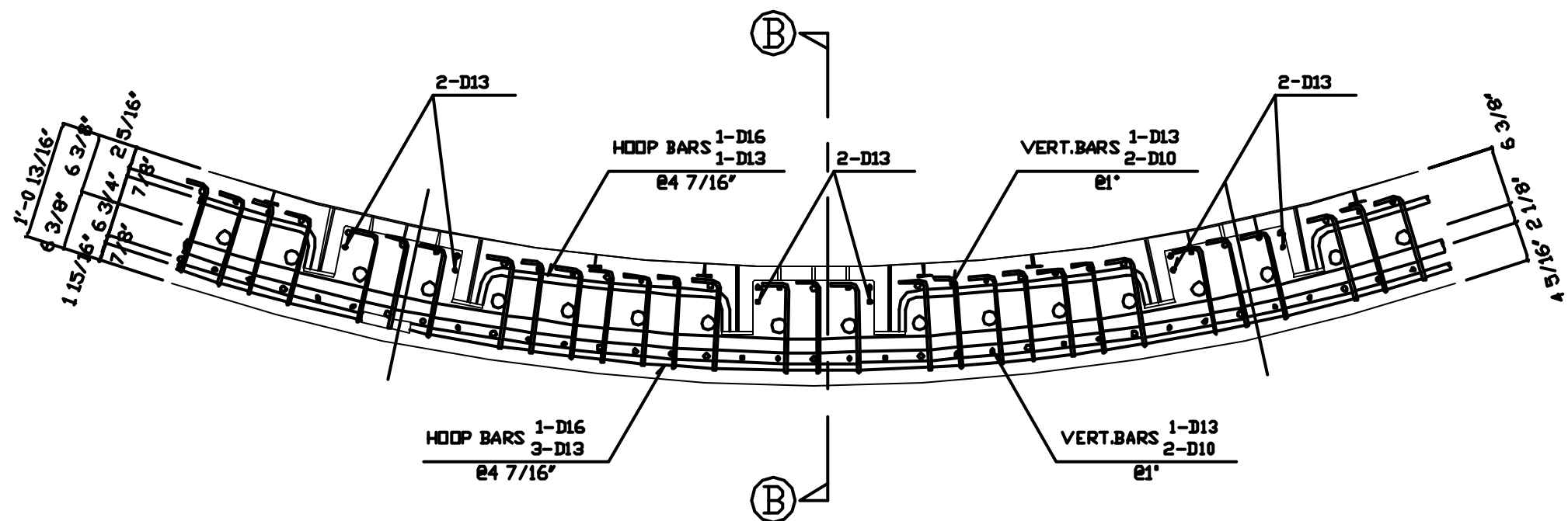
NAME		SHEET	NUPEC PCCV STRUCTURAL BEHAVIOR TEST MODEL		
NUPEC	SYSTEMS SAFETY DEPT.		OPENING REBAR DETAILS (A/L)		SCALE
S N L		COPY 1			1/20
M H I	NUCLEAR SYSTEMS ENGINEERING DEPT.		MITSUBISHI HEAVY INDUSTRIES,LTD.		REVISION NO.
	STEEL STRUCTURE DESIGNING SECT.	COPY 1	OBAYASHI CORPORATION		R2
	EQUIP DESIGN SECT.	COPY 1			
	TAKASAGO R&D CENTER	COPY 1			
	T A I S E I	COPY 1	M H I	OBAYASHI	DRAWING NO.
OBAYASHI	ORIG.		T. Obayashi H. Murano	PCCV-QCON-17	





Ⓑ-Ⓑ SECTION DETAILS

Ⓐ-Ⓐ SECTION DETAILS



Ⓒ-Ⓒ SECTION DETAILS

1. GENERAL DESCRIPTION

1.1 MATERIALS

- REBARS: SD345, SD390, SD490, DEFORMED BARS (JIS G3112)
- CONCRETE: $F_c = 29.4\text{MPa}$, $F_c = 44.13\text{MPa}$
- PORTIONS: REFER TO DESIGN SPEC. AT "PCCV-QCON-01 MODEL-GENERAL ARRANGEMENT"

2. REBAR PREPARATIONS

2.1 BENDING STANDARDS & EXTRA LENGTH

- BENDING SHAPES & DIMENSIONS AT END PORTIONS
 - RADIAL TIE END PORTION: L.E. D10
 - BASEMAT SHEAR BAR END PORTION: L.E. D16

TABLE 2-1 HOOK BENDING SHAPES & DIMENSIONS

ANGLES	SHAPE	GRADE	PIN DIAMETER (D)	EXTRA LENGTH	PORTIONS
180°		SD345	4d	G.E. 4d	
		SD390	5d	G.E. 4d	
135°		SD345	4d	G.E. 6d	
		SD390	5d	G.E. 6d	
90°		SD345	4d	G.E. 8d	RADIAL TIES
		SD390	5d	G.E. 8d	

NOTE: d=NOMINAL DIAMETER

2.2 BENDING SHAPES & DIMENSIONS AT INTERMEDIATE PORTION

TABLE 2-2 BENDING SHAPES & DIMENSIONS AT INTERMEDIATE PORTION

ANGLES	SHAPE	PORTION	REBAR DIAMETER	GRADE	PIN DIAMETER (D)
L.E. 90°		U BAR	D6~D16	SD390	G.E. 4d
		TRIM BAR			
		REBAR (AT CORNERS)	D19~D22	SD490	G.E. 6d
		WALL REBAR			
		BASEMAT RADIAL BAR			
		REBAR ANCHORED PORTION AT THE UPPER PART OF TENDON GALLERY			

3. REBAR ANCHORING & JOINT

3.1 REBAR ANCHORING

IN CASE OF BENT ANCHORING, REBAR SHOULD BE BENT BEYOND THE MEMBER CENTER LINE.

TABLE 3-1 MINIMUM ANCHORED LENGTH

PORTION	GRADE	CONCRETE STRENGTH $F_c(\text{MPa})$	REBAR DIAMETER	ANCHORED LENGTH
BASEMAT	SD390	29.4MPa	D16	58d
		44.13MPa		45d
	SD490	29.4MPa	D10~D19	63d
		44.13MPa		52d

NOTE: REBAR ANCHORED LENGTH SHOULD REFER TO DETAIL DRAWINGS

3.2 REBAR JOINT

- EXTRA PROBLEMS SHOULD BE SOLVED WITH NUPEC.
- TABLE 3-2; JOINT PROPER USE
- TABLE 3-3; LAP LENGTH
- REBAR SPLICE SPACING DISTANCES

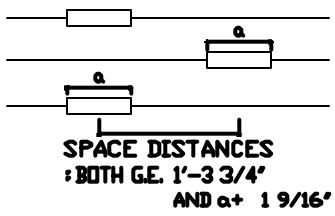


TABLE 3-2 PORTIONS

PORTIONS	REBAR DIA.	L.E. D22
PCCV		SPLICE
BASEMAT		BASICALLY SPLICE BUT LAP ACCEPTABLE

TABLE 3-3 MINIMUM LAP LENGTH

PORTION	GRADE	CONCRETE STRENGTH $F_c(\text{MPa})$	REBAR DIAMETER	LAP LENGTH
BASEMAT	SD390	29.4MPa	D10~D19	45d
		44.13MPa		

4. REBAR COVER DEPTH

4.1 MINIMUM COVER DEPTH

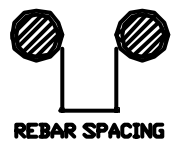
MINIMUM COVER DEPTH SHOULD BE THE MAXIMUM VALUE AMONG THOSE VALUES DESCRIBED BELOW.
1) REQUIRED DEPTH DEPENDS ON REBAR DIAMETER

TABLE 4-1 MINIMUM REBAR COVER DEPTH (UNIT: INCH)

REBAR DIAMETER	D6	D10	D13	D16	D19	D22
COVER DEPTH	3/8"	9/16"	13/16"	1"	1 3/16"	1 3/8"

2) REQUIRED DEPTH DEPENDS ON THE MAXIMUM AGGREGATE DIAMETER
3/8"

5. REBAR SPACING



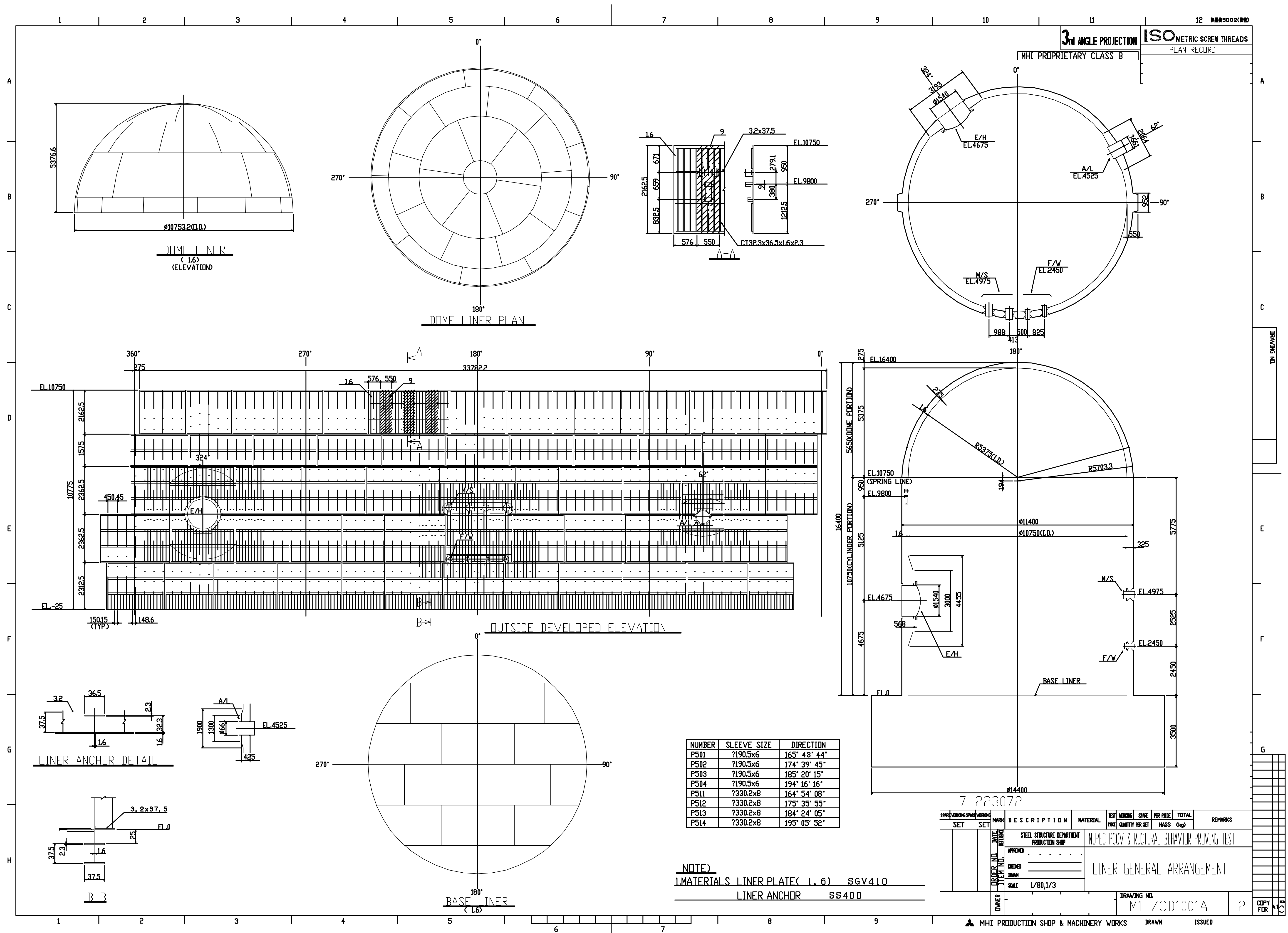
REBAR SPACING: GE. 1.5 TIMES THE MAX COARSE AGGREGATE DIAMETER
GE. 9/16"
GE. 1.5 TIMES THE NOMINAL REBAR DIAMETER

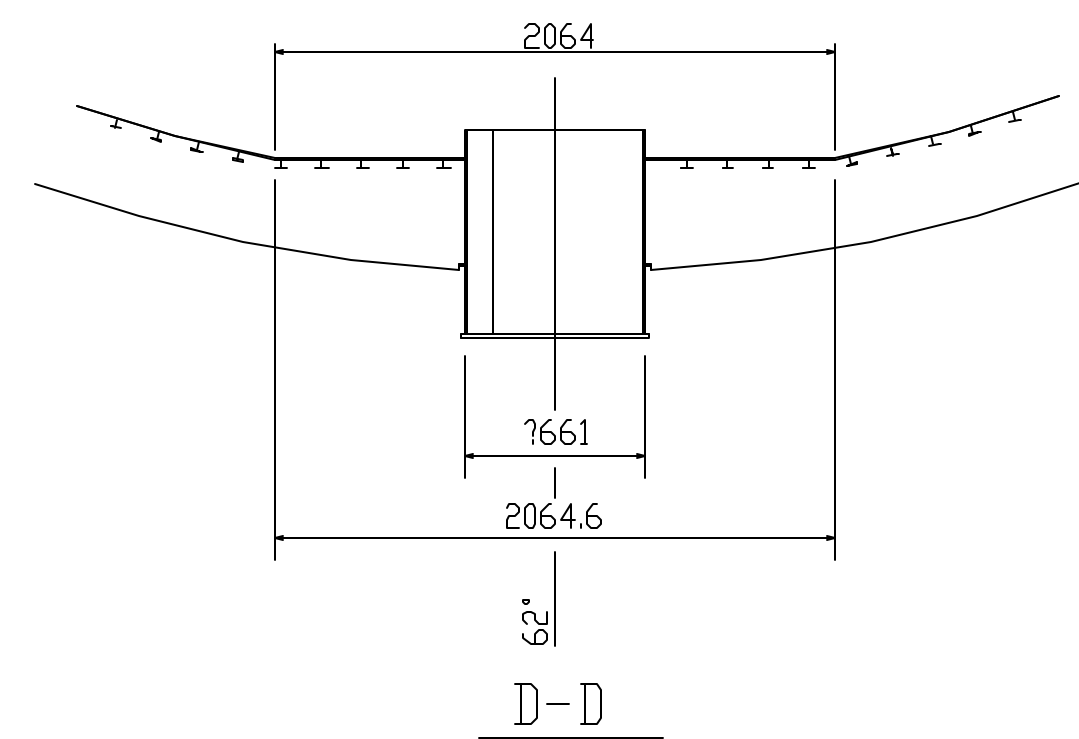
R2	'95.8.1	CRANE BRACKET ANCHOR - HOOP REBAR WELDING TERMINATED 2-REBARS ADDED 2-REBARS DIA. CHANGED	
NO.	DATE	REVISION	BY

REVISION

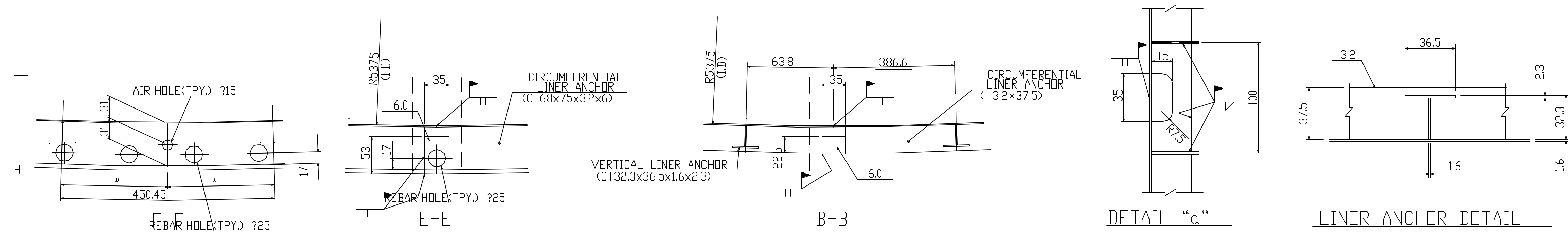
DRAWINGS FOR REFERENCE	DATE	STATUS	REMARKS
	'95.2.24	O	FINAL
			PRELIMINARY
	'95.1.25		APPLICATION
	'94.11.17		EXAMINATION
			REFERENCE


NAME	SHEET	NUPEC PCCV STRUCTURAL BEHAVIOR TEST MODEL	
NUPEC SYSTEMS SAFETY DEPT.		CRANE BRACKET REBAR DETAILS	
S.N.L.	COPY 1	REBAR ARRANGEMENT STANDARDS	
		SCALE 1/15	
		REVISION NO.	
MHI	NUCLEAR SYSTEMS ENGINEERING DEPT.	MITSUBISHI HEAVY INDUSTRIES, L.T.D.	
	STEEL STRUCTURE DESIGNING SECT.	OBAYASHI CORPORATION	
	EQUIP DESIGN SECT.	R2	
	TAKASAGO R&D CENTER		
T.A.S.E.I.	COPY 1		
OBAYASHI	ORIG.		
		MHI	OBAYASHI
		T. Obayashi	H. Murano
		DRAWING NO. PCCV-QCON-19	

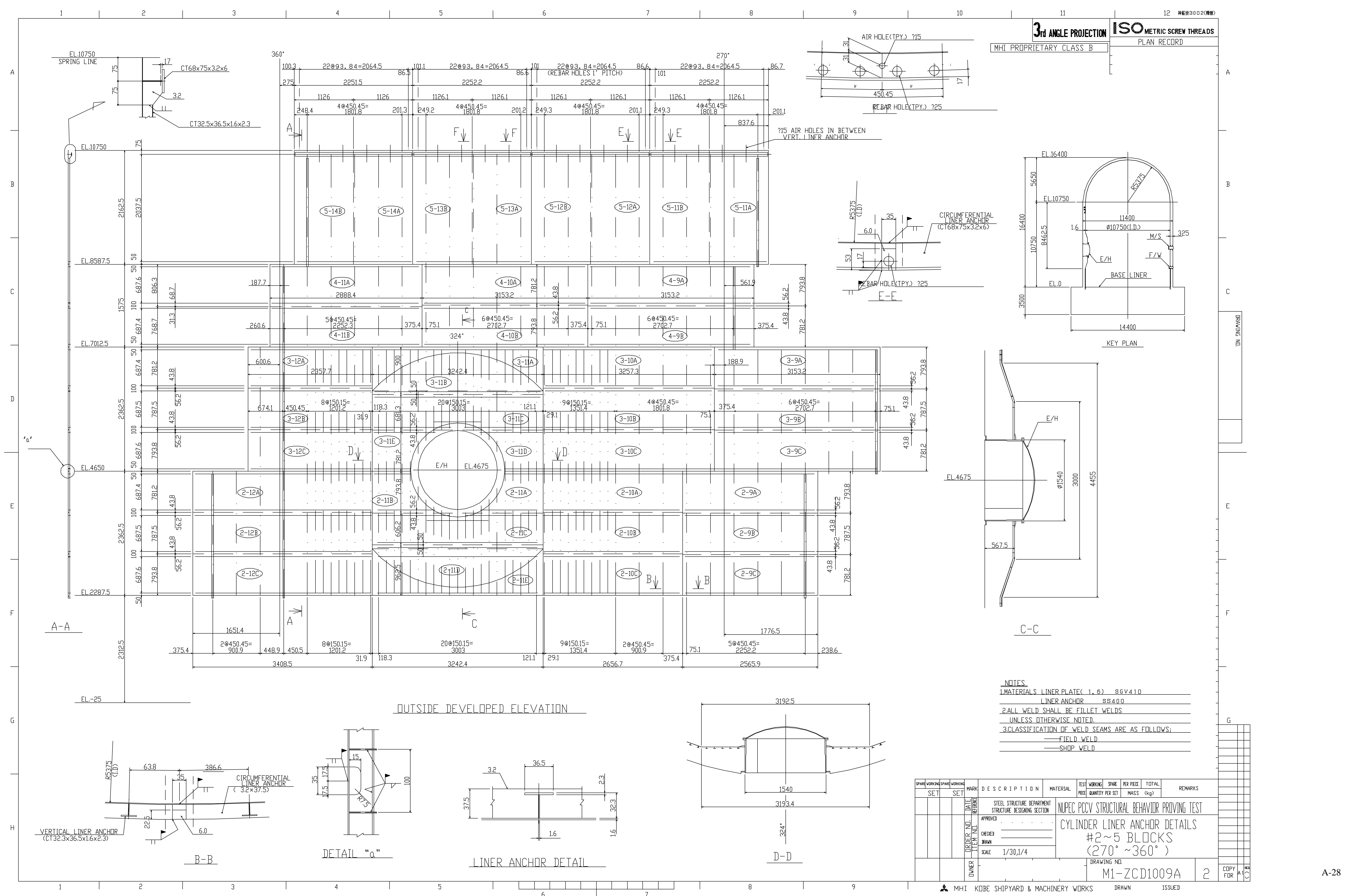


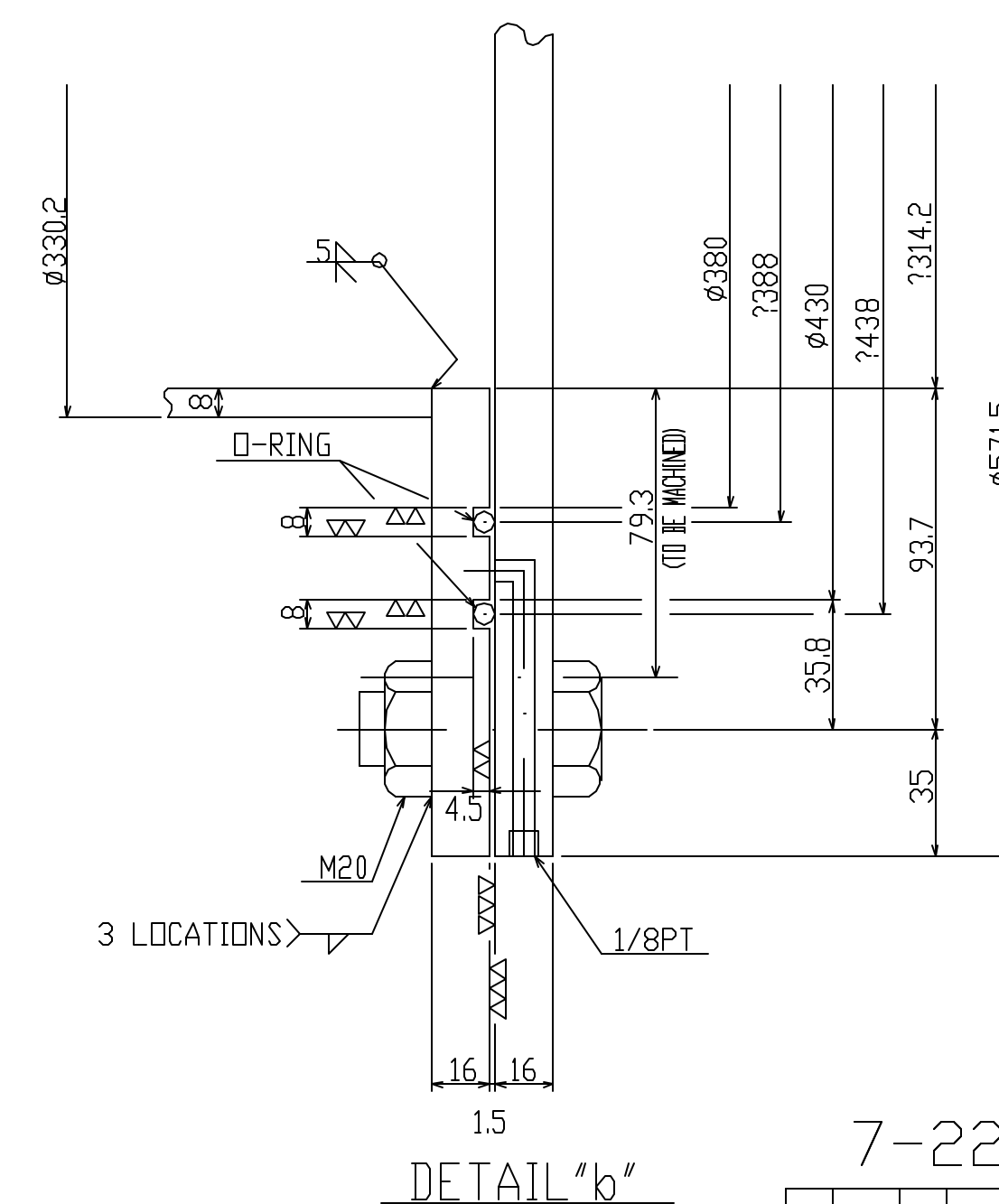
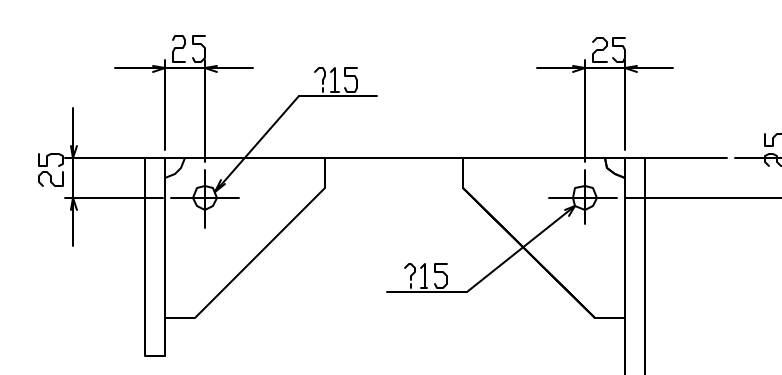
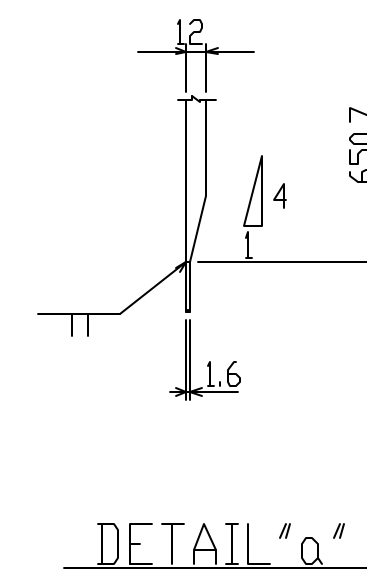
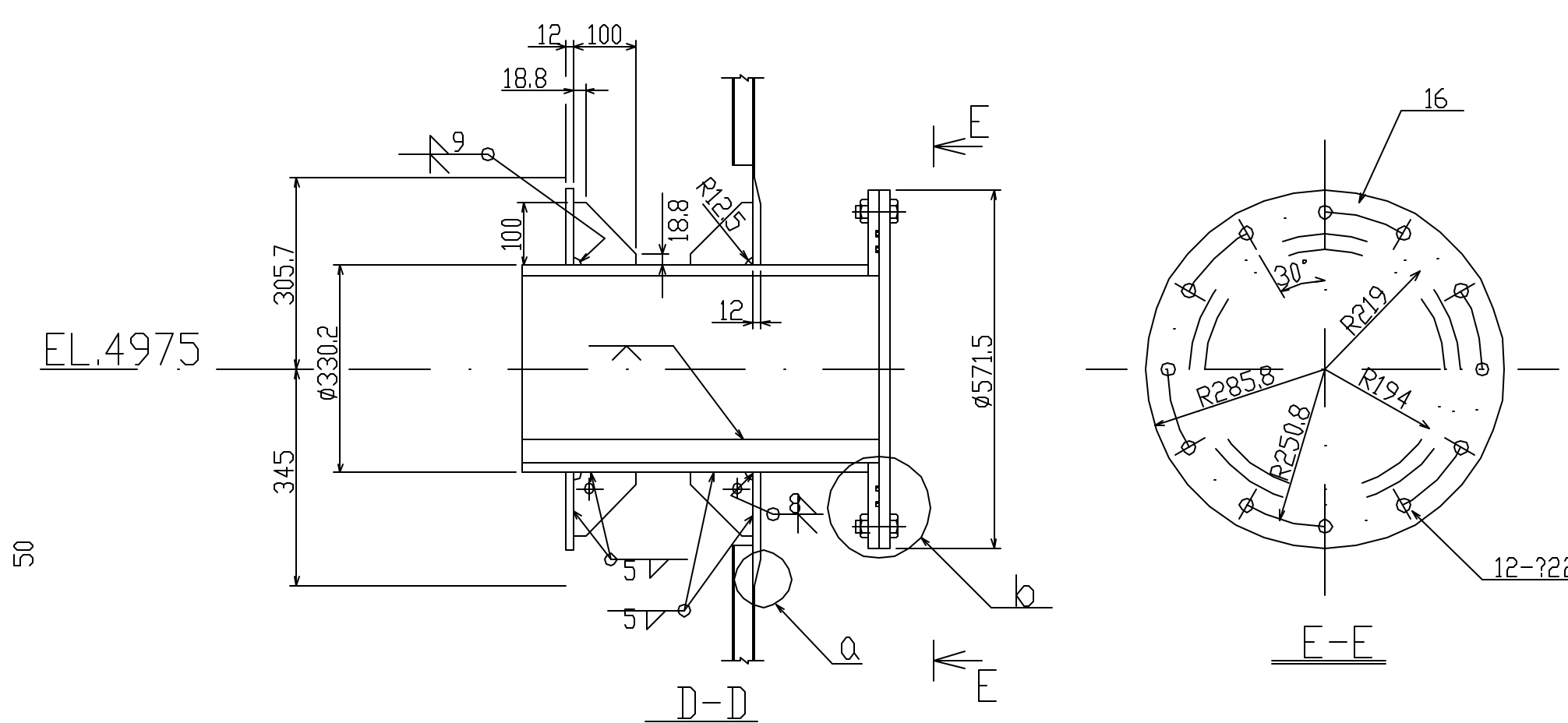
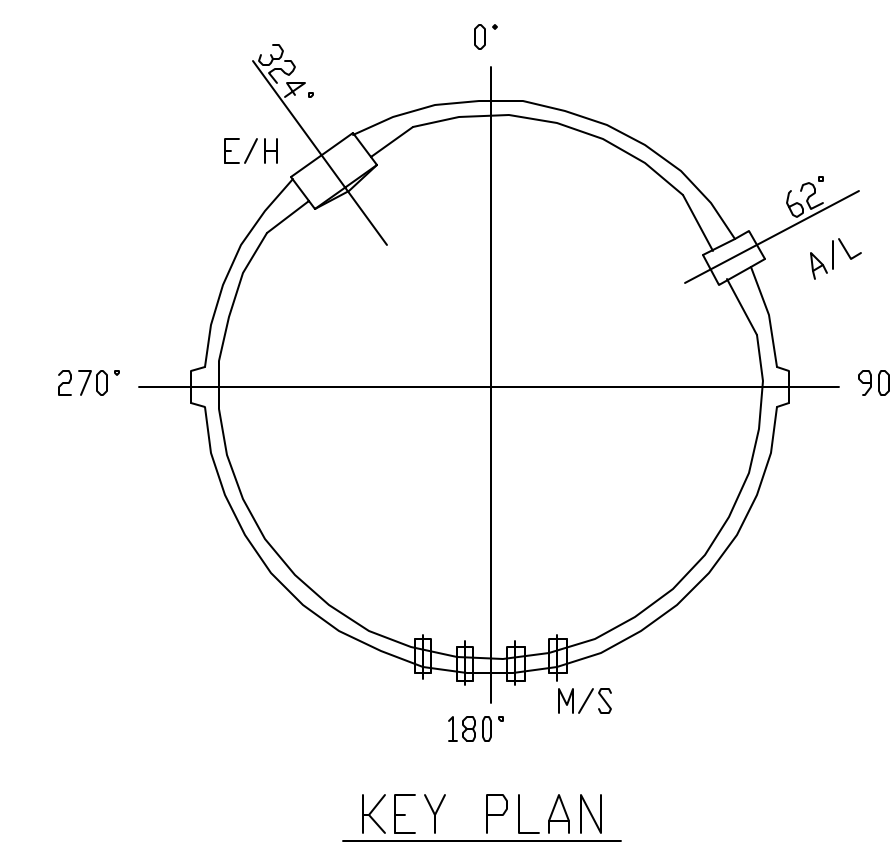


- NOTES:
- | | |
|---|---------|
| 1. MATERIALS LINER PLATE (1.6) | SGV 410 |
| LINER ANCHOR | SS 400 |
| 2. ALL WELD SHALL BE FILLET WELDS | |
| UNLESS OTHERWISE NOTED. | |
| 3. CLASSIFICATION OF WELD SEAMS ARE AS FOLLOWS; | |
| — FIELD WELD | |
| — SHOP WELD | |



7-223072																										
SPARE WORKING		SPARE WORKING		MARK		DESCRIPTION			MATERIAL		TEST WORKING		SPARE		PER PIECE		TOTAL		REMARKS							
SET		SET									PIECE		QUANTITY PER SET		MASS		(kg)									
				DATE		STEEL STRUCTURE DEPARTMENT STRUCTURE DESIGNING SECTION			NUPEC PCCV STRUCTURAL BEHAVIOR PROVING TEST																	
				ORDER NO.		APPROVED			CYLINDER LINER ANCHOR DETAILS																	
				ITEM NO.		CHECKED			#2~5 BLOCKS																	
						DRAWN			(0° ~ 90°)																	
						SCALE 1/30,1/4																				
				OWNER					DRAWING NO.																	
									M1-ZCD1007A								2		COPY FOR							
 MHI KOBE SHIPYARD & MACHINERY WORKS															DRAWN					ISSUED						



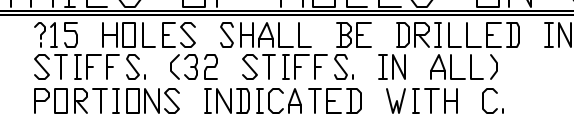
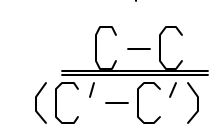
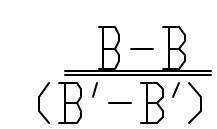
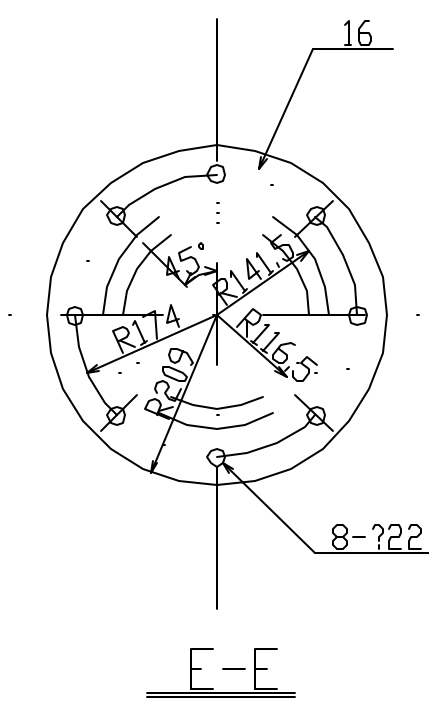
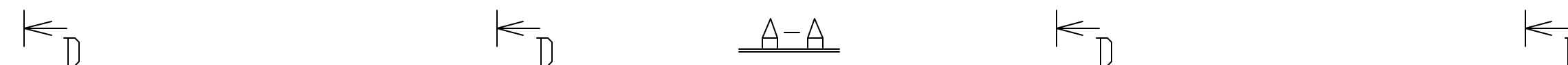
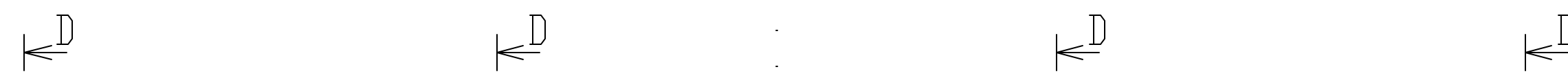


NOTES

1. MATERIALS LINER PLATE(1, 6) SGV410
LINER ANCHOR SS400

2. ALL WELD SHALL BE FILLET WELDS UNLESS
OTHERWISE NOTED.

7-222072																																																																																																																																																																																																																																																																																																																																																																																																																																																																																																																																																																																																																																																																																																																																																																																																																																																																																																																																																																																																																																																																																																																																																																																																																																																																																																																																																																																																																																																																																																																																																																																					</
----------	--	--	--	--	--	--	--	--	--	--	--	--	--	--	--	--	--	--	--	--	--	--	--	--	--	--	--	--	--	--	--	--	--	--	--	--	--	--	--	--	--	--	--	--	--	--	--	--	--	--	--	--	--	--	--	--	--	--	--	--	--	--	--	--	--	--	--	--	--	--	--	--	--	--	--	--	--	--	--	--	--	--	--	--	--	--	--	--	--	--	--	--	--	--	--	--	--	--	--	--	--	--	--	--	--	--	--	--	--	--	--	--	--	--	--	--	--	--	--	--	--	--	--	--	--	--	--	--	--	--	--	--	--	--	--	--	--	--	--	--	--	--	--	--	--	--	--	--	--	--	--	--	--	--	--	--	--	--	--	--	--	--	--	--	--	--	--	--	--	--	--	--	--	--	--	--	--	--	--	--	--	--	--	--	--	--	--	--	--	--	--	--	--	--	--	--	--	--	--	--	--	--	--	--	--	--	--	--	--	--	--	--	--	--	--	--	--	--	--	--	--	--	--	--	--	--	--	--	--	--	--	--	--	--	--	--	--	--	--	--	--	--	--	--	--	--	--	--	--	--	--	--	--	--	--	--	--	--	--	--	--	--	--	--	--	--	--	--	--	--	--	--	--	--	--	--	--	--	--	--	--	--	--	--	--	--	--	--	--	--	--	--	--	--	--	--	--	--	--	--	--	--	--	--	--	--	--	--	--	--	--	--	--	--	--	--	--	--	--	--	--	--	--	--	--	--	--	--	--	--	--	--	--	--	--	--	--	--	--	--	--	--	--	--	--	--	--	--	--	--	--	--	--	--	--	--	--	--	--	--	--	--	--	--	--	--	--	--	--	--	--	--	--	--	--	--	--	--	--	--	--	--	--	--	--	--	--	--	--	--	--	--	--	--	--	--	--	--	--	--	--	--	--	--	--	--	--	--	--	--	--	--	--	--	--	--	--	--	--	--	--	--	--	--	--	--	--	--	--	--	--	--	--	--	--	--	--	--	--	--	--	--	--	--	--	--	--	--	--	--	--	--	--	--	--	--	--	--	--	--	--	--	--	--	--	--	--	--	--	--	--	--	--	--	--	--	--	--	--	--	--	--	--	--	--	--	--	--	--	--	--	--	--	--	--	--	--	--	--	--	--	--	--	--	--	--	--	--	--	--	--	--	--	--	--	--	--	--	--	--	--	--	--	--	--	--	--	--	--	--	--	--	--	--	--	--	--	--	--	--	--	--	--	--	--	--	--	--	--	--	--	--	--	--	--	--	--	--	--	--	--	--	--	--	--	--	--	--	--	--	--	--	--	--	--	--	--	--	--	--	--	--	--	--	--	--	--	--	--	--	--	--	--	--	--	--	--	--	--	--	--	--	--	--	--	--	--	--	--	--	--	--	--	--	--	--	--	--	--	--	--	--	--	--	--	--	--	--	--	--	--	--	--	--	--	--	--	--	--	--	--	--	--	--	--	--	--	--	--	--	--	--	--	--	--	--	--	--	--	--	--	--	--	--	--	--	--	--	--	--	--	--	--	--	--	--	--	--	--	--	--	--	--	--	--	--	--	--	--	--	--	--	--	--	--	--	--	--	--	--	--	--	--	--	--	--	--	--	--	--	--	--	--	--	--	--	--	--	--	--	--	--	--	--	--	--	--	--	--	--	--	--	--	--	--	--	--	--	--	--	--	--	--	--	--	--	--	--	--	--	--	--	--	--	--	--	--	--	--	--	--	--	--	--	--	--	--	--	--	--	--	--	--	--	--	--	--	--	--	--	--	--	--	--	--	--	--	--	--	--	--	--	--	--	--	--	--	--	--	--	--	--	--	--	--	--	--	--	--	--	--	--	--	--	--	--	--	--	--	--	--	--	--	--	--	--	--	--	--	--	--	--	--	--	--	--	--	--	--	--	--	--	--	--	--	--	--	--	--	--	--	--	--	--	--	--	--	--	--	--	--	--	--	--	--	--	--	--	--	--	--	--	--	--	--	--	--	--	--	--	--	--	--	--	--	--	--	--	--	--	--	--	--	--	--	--	--	--	--	--	--	--	--	--	--	--	--	--	--	--	--	--	--	--	--	--	--	--	--	--	--	--	--	--	--	--	--	--	--	--	--	--	--	--	--	--	--	--	--	--	--	--	--	--	--	--	--	--	--	--	--	--	--	--	--	--	--	--	--	--	--	--	--	--	--	--	--	--	--	--	--	--	--	--	--	--	--	--	--	--	--	--	--	--	--	--	--	--	--	--	--	--	--	--	--	--	--	--	--	--	--	--	--	--	--	--	--	--	--	--	--	--	--	--	--	--	--	--	--	--	--	--	--	--	--	--	--	--	--	--	--	--	--	--	--	--	--	--	--	--	--	--	--	--	--	--	--	--	--	--	--	--	--	--	--	--	--	--	--	--	--	--	--	--	--	--	--	--	--	--	--	--	--	--	--	--	--	--	--	--	--	--	--	--	--	--	--	--	--	--	--	--	--	--	--	--	--	--	--	--	--	--	--	--	--	--	--	--	--	--	--	--	--	--	--	--	--	--	--	--	--	--	--	--	--	--	--	--	--	--	--	--	--	--	--	--	--	--	--	--	--	--	--	--	--	--	--	--	--	--	--	--	--	--	--	--	--	--	--	--	--	--	--	--	--	--	--	--	--	--	--	--	--	--	--	--	--	--	--	--	--	--	--	--	--	--	--	--	--	--	--	--	--	--	--	--	--	--	--	--	--	--	--	--	--	--	--	--	--	--	--	--	--	--	--	--	--	--	--	--	--	--	--	--	--	--	--	--	--	--	--	--	--	--	--	--	--	--	--	--	--	--	--	--	--	--	--	--	--	--	--	--	--	--	--	--	--	--	--	--	--	--	--	--	--	--	--	--	--	--	--	--	--	--	--	--	--	--	--	--	--	--	--	--	--	--	--	--	--	--	--	--	--	--	--	--	--	--	--	--	--	--	--	--	--	--	--	--	--	--	--	--	--	--	--	--	--	--	--	--	--	--	--	--	--	--	--	--	--	--	--	--	--	--	--	--	--	--	--	--	--	--	--	--	--	--	--	--	--	--	--	--	--	--	--	--	--	--	--	--	--	--	--	--	--	--	--	--	--	--	--	--	--	--	--	--	--	--	--	--	--	--	--	--	--	--	--	--	--	--	--	--	--	--	--	--	--	--	--	--	--	--	--	--	--	--	--	--	--	--	--	--	--	--	--	--	--	--	--	--	--	--	--	--	--	--	--	--	--	--	--	--	--	--	--	--	--	--	--	--	--	--	--	--	--	--	--	--	--	--	--	--	--	--	--	--	--	--	--	--	--	--	--	--	--	--	--	--	--	--	--	--	--	--	--	--	--	--	--	--	--	--	--	--	--	--	--	--	--	--	--	--	--	--	--	--	--	--	--	--	--	--	--	--	--	--	--	--	--	--	--	--	--	--	--	--	--	--	--	--	--	--	--	--	----



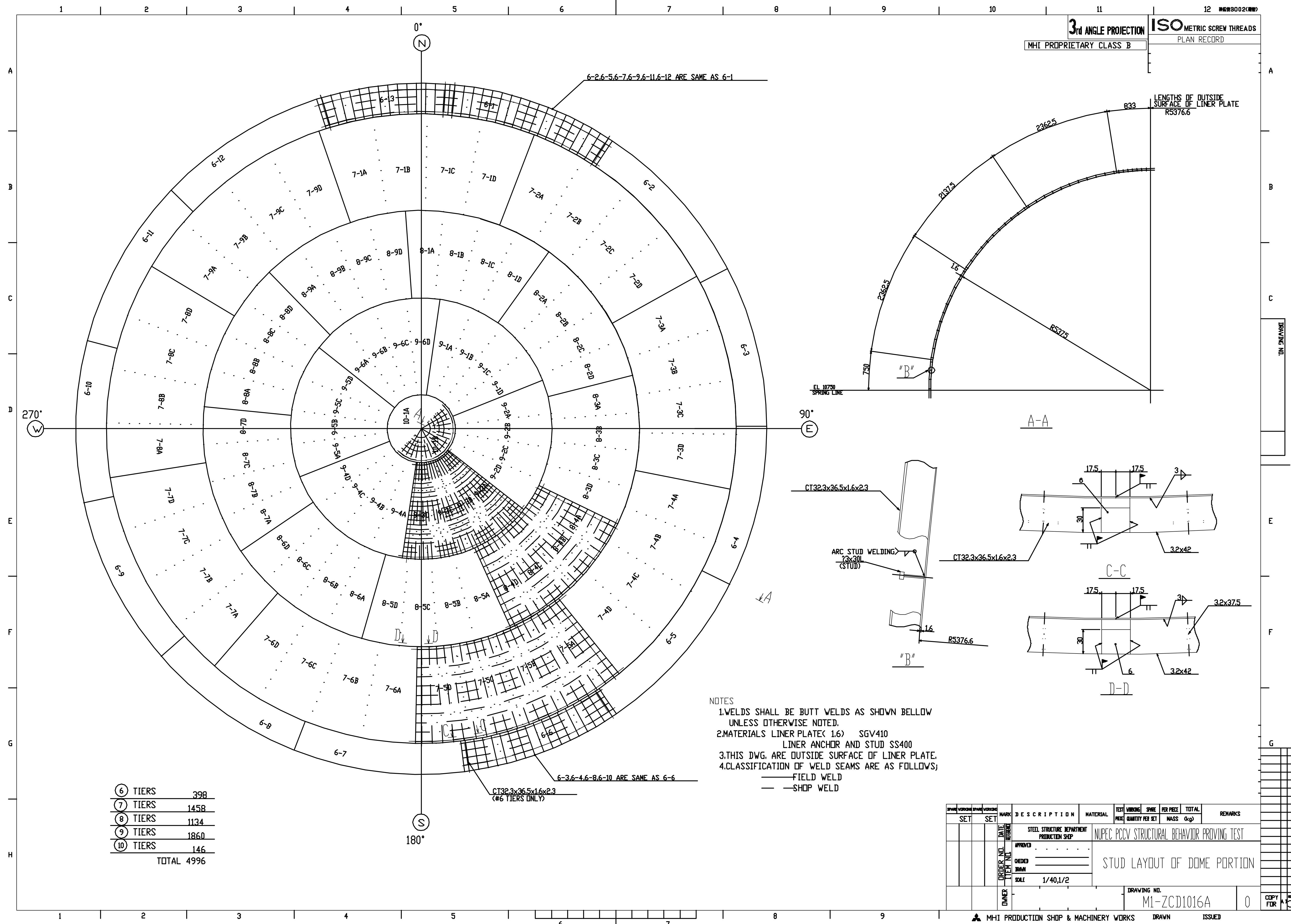
1. MATERIALS LINER PLATE(1, 6) SGV410
LINER ANCHOR SS400
2. ALL WELD SHALL BE FILLET WELDS UNLESS
OTHERWISE NOTED.

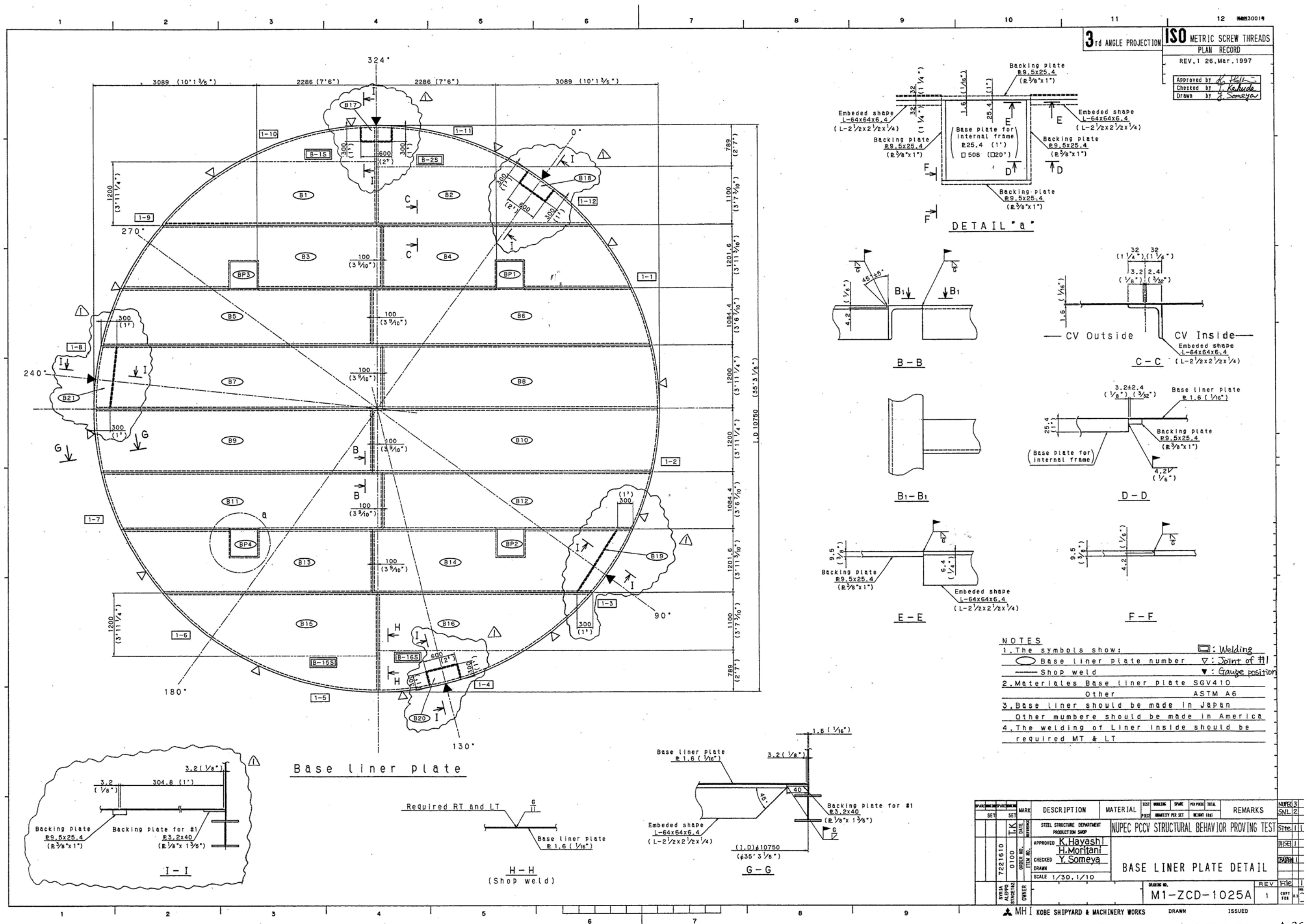
[illegible]



1. THIS DWG. INDICATES LINER PLATE BLOCK LAYOUT OF DOME PORTION.
2. CIRCUMFERENTIAL DIMENSIONS SHOWN ON THIS DWG. ARE ARC LENGTHS OF OUTSIDE SURFACE OF LINER PLATE.
3. MARKS' IN () AND () INDICATE TIER NUMBERS AND LINER PLATE BLOCK MARKS.
4. WELDS SHALL BE BUTT WELDS AS SHOWN BELLOW UNLESS OTHERWISE NOTED.
5. MATERIALS LINER PLATE (16) SGV410
6. CLASSIFICATION OF WELD SEAMS ARE AS FOLLOWS;
——— FIELD WELD
——— SHOP WELD

SPARE WORKING		SPARE WORKING		MARK SET	DESCRIPTION	MATERIAL	TEST	WORKING	SPARE	PER PIECE	TOTAL	REMARKS			
SET		SET					PRICE	QUANTITY PER SET	MASS	(kg)					
				DATE	STEEL STRUCTURE DEPARTMENT PRODUCTION SHOP		NUPEC PCCV STRUCTURAL BEHAVIOR PROVING TEST								
				REFERENCE			APPROVED		LINER PLATE BLOCK LAYOUT OF DOME PORTION						
				ORDER NO.	CHECKED										
				ITEM NO.	DRAWN										
					SCALE	1/40									
				OWNER			DRAWING NO.								
							M1-ZCD1015A					0		COPY FOR	REC'D





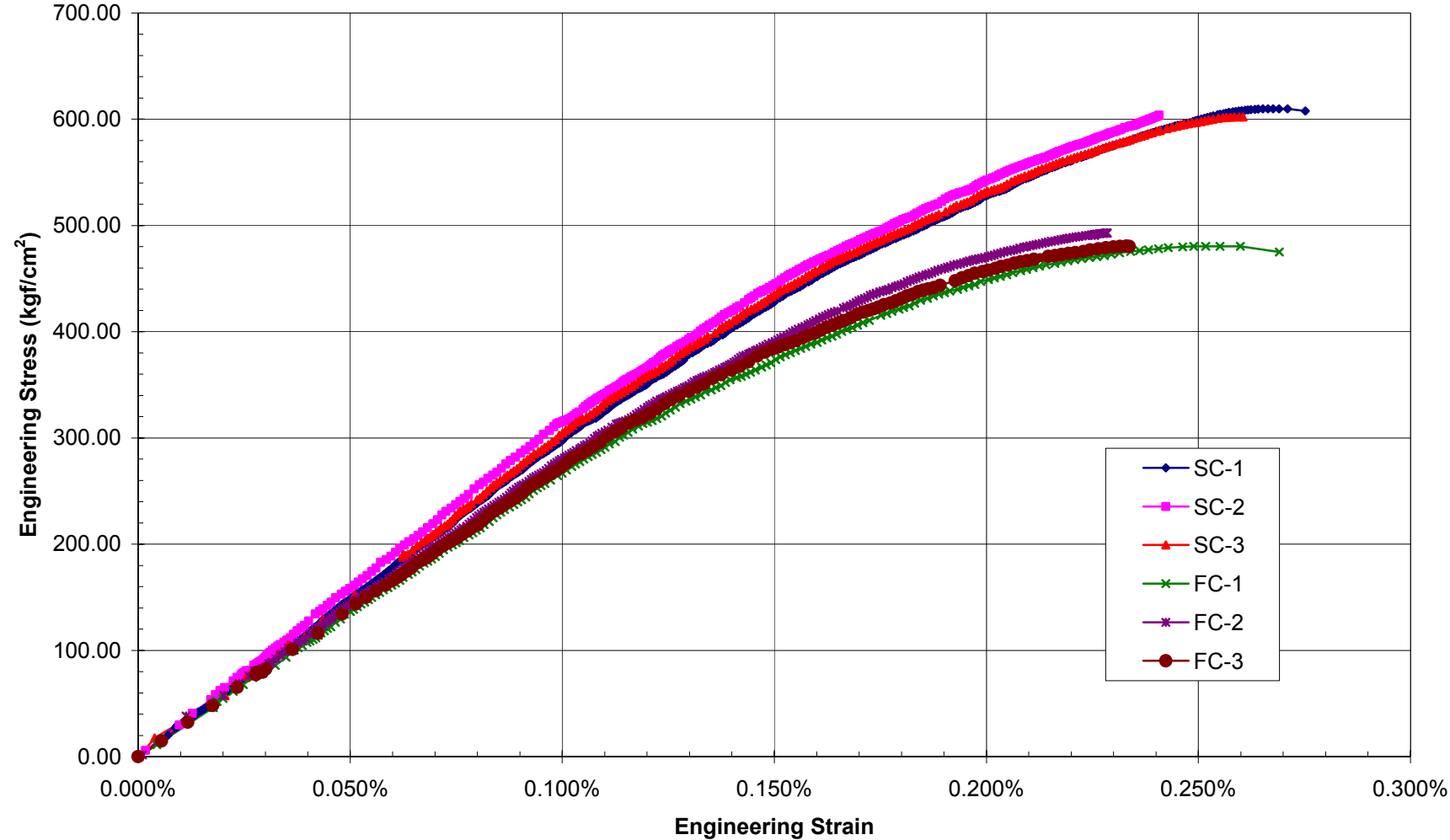
Appendix B: PCCV Model Material Properties

Section i. Trial Mix Concrete

Trial Concrete Mixture Test (METRIC)														
Procedures & Specifications														
JPN-14-T-1-6, Trial Concrete Mixture, Procedure, Rev. 1; 5/14/96														
Data & Test Reports														
(A) JPN-22-T-1, Ancillary Test Report, October 3, 1997														
(B) JPN-22-T-1(Rev.1), Ancillary Test Report, March 9, 1998														
(C) MH-K10-39, Concrete Creep Coeff. & Drying Shrinkage Test Report														
Test Items														
Fresh Concrete														
			300 kgf/cm ²		450 kgf/cm ²									
Slump w/o superplasticizers (cm)	ASTM C143-90a	(A)	16.8		10.8									
		(B)	9.2		8.9									
Slump w/ superplasticizers (cm)		(A)	19.4		20.7									
		(B)	16.2		18.7									
Air Content (%)	ASTM C231-91b	(A)	4.50		4.85									
		(B)	5.50		5.00									
Quantity of Chloride (%)	ASTM C1152-90	(A)	0.001		0.002									
		(B)	0.003		0.002									
Hardened Concrete														
			300 kgf/cm ²		450 kgf/cm ²		300 kgf/cm ²		450 kgf/cm ²		300 kgf/cm ²		450 kgf/cm ²	
Specimens	ASTM C31-91		SC	FC	SC	FC	SC	FC	SC	FC	SC	FC	SC	FC
			1 week				4 weeks				13 weeks			
Compressive Strength (kgf/cm ²)	ASTM C39-86 or -94(?)	(A)	343	300	399	418	411	341	507	492	524.00	425.00	614.00	498.00
		(B)	-	-	-	-	484	426	545	544	601.00	480.00	657.00	630.00
Split Tensile Strength (kgf/cm ²)	ASTM C496-90	(A)									40.10	34.40	42.90	35.20
		(B)									40.60	40.60	45.50	39.20
Flexural Strength (kgf/cm ²)	ASTM C-78-84	(A)									54.80	40.80	56.90	56.20
		(B)									57.40	60.20	58.80	44.80
Young's Modulus (kgf/cm ² x 10 ⁵)	ASTM C469-87	(A)									2.96	2.85	3.26	2.75
		(B)									3.04	2.73	3.02	2.97
Poisson's Ratio	ASTM C469-87	(A)									0.20	0.18	0.20	0.18
		(B)									0.22	0.23	0.23	0.23
Unit Weight (ton/m ³)	<u>weight of cylinders</u>	(A)									2.25	2.21	2.26	2.19
	<u>nominal volume</u>	(B)									2.25	2.23	2.24	2.23
Stress-Strain Relation	TTP-08, Rev. 1, 9/19/97	(A)*												
	using strain gages	(B)									X(B)	X(B)	X(B)	X(B)
Creep Coefficient	ASTM C512-87	(loaded at 175.8 kgf/cm ²)											X(C)	
Drying Shrinkage	ASTM C512-87	(w/o loading)											X(C)	
*For test A, stress-strain results were obtained up to about 40% of the maximum stress														

Trial Concrete Mixture Test (ENGLISH)														
Procedures & Specifications														
JPN-14-T-1-6, Trial Concrete Mixture, Procedure, Rev. 1; 5/14/96														
Data & Test Reports														
(A) JPN-22-T-1, Ancillary Test Report, October 3, 1997														
(B) JPN-22-T-1(Rev.1), Ancillary Test Report, March 9, 1998														
(C) MH-K10-39, Concrete Creep Coeff. & Drying Shrinkage Test Report														
Test Items														
Fresh Concrete														
			4300 psi		6400 psi									
Slump w/o superplasticizers (in)	ASTM C143-90a	(A)	6.6		4.3									
		(B)	3.6		3.5									
Slump w/ superplasticizers (cm)		(A)	7.6		8.1									
		(B)	6.4		7.4									
Air Content (%)	ASTM C231-91b	(A)	4.50		4.85									
		(B)	5.50		5.00									
Quantity of Chloride (%)	ASTM C1152-90	(A)	0.001		0.002									
		(B)	0.003		0.002									
Hardened Concrete														
			4300 psi		6400 psi		4300 psi		6400 psi		4300 psi		6400 psi	
Specimens	ASTM C31-91		SC	FC	SC	FC	SC	FC	SC	FC	SC	FC	SC	FC
			1 week				4 weeks				13 weeks			
Compressive Strength (psi)	ASTM C39-86 or -94(?)	(A)	4877	4266	5674	5944	5844	4849	7210	6996	7451	6044	8731	7082
		(B)	-	-	-	-	6882	6058	7750	7736	8546	6826	9343	8959
Split Tensile Strength (psi)	ASTM C496-90	(A)									570	489	610	501
		(B)									577	577	647	557
Flexural Strength (psi)	ASTM C-78-84	(A)									779	580	809	799
		(B)									816	856	836	637
Young's Modulus (psi x 10 ⁶)	ASTM C469-87	(A)									4.2	4.1	4.6	3.9
		(B)									4.3	3.9	4.3	4.2
Poisson's Ratio	ASTM C469-87	(A)									0.20	0.18	0.20	0.18
		(B)									0.22	0.23	0.23	0.23
Unit Weight (pcf)	weight of cylinders	(A)									140	138	141	137
	nominal volume	(B)									140	139	140	139
Stress-Strain Relation	TTP-08, Rev. 1, 9/19/97	(A)*												
	using strain gages	(B)									X(B)	X(B)	X(B)	X(B)
Creep Coefficient	ASTM C512-87	(loaded at 2500 psi)											X(C)	
Drying Shrinkage	ASTM C512-87	(w/o loading)											X(C)	
*For test A, stress-strain results were obtained up to about 40% of the maximum stress														

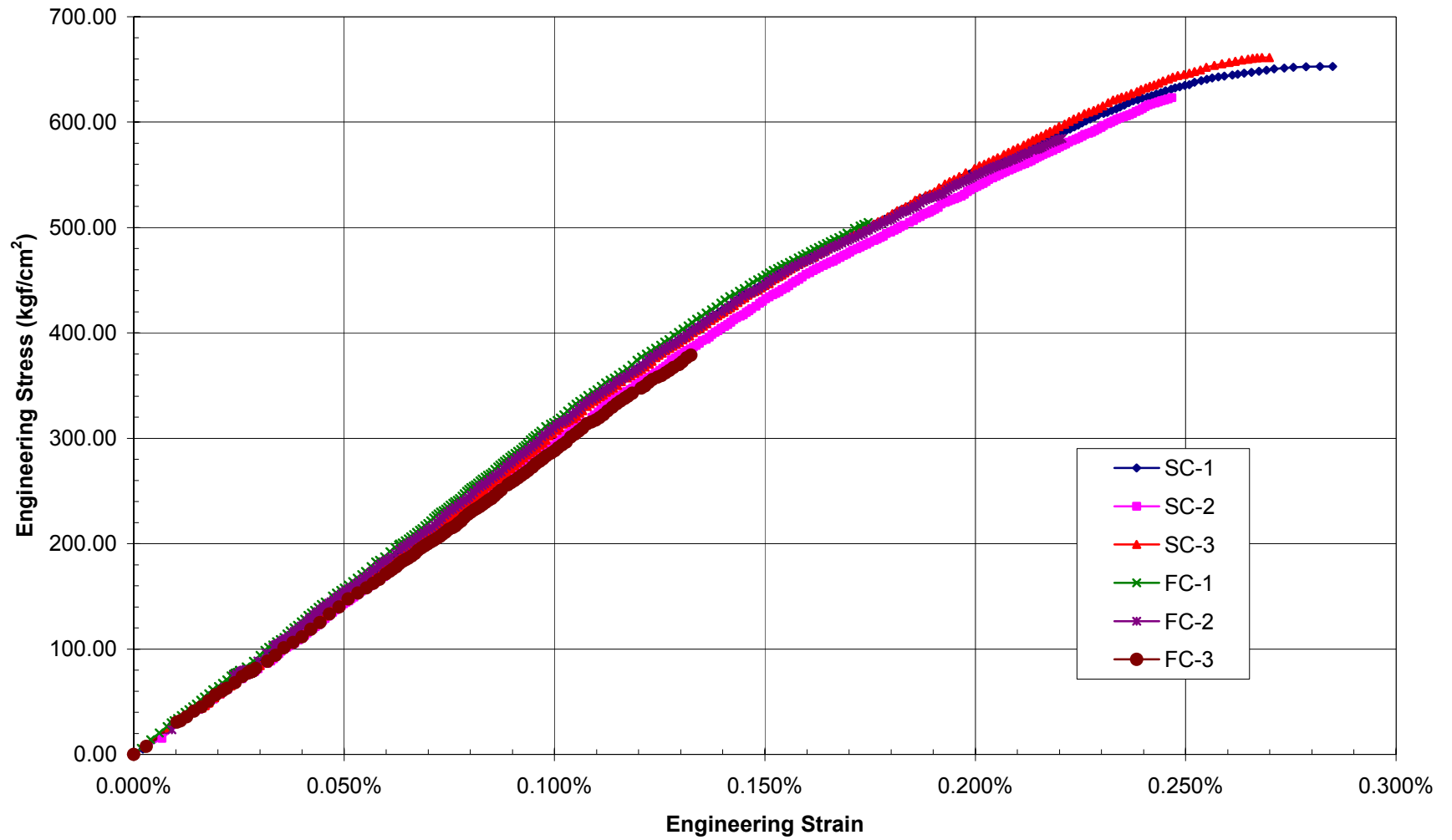
Trial Concrete Mix Stress-Strain @ 13 weeks (300 kg_f/cm²) - Series B



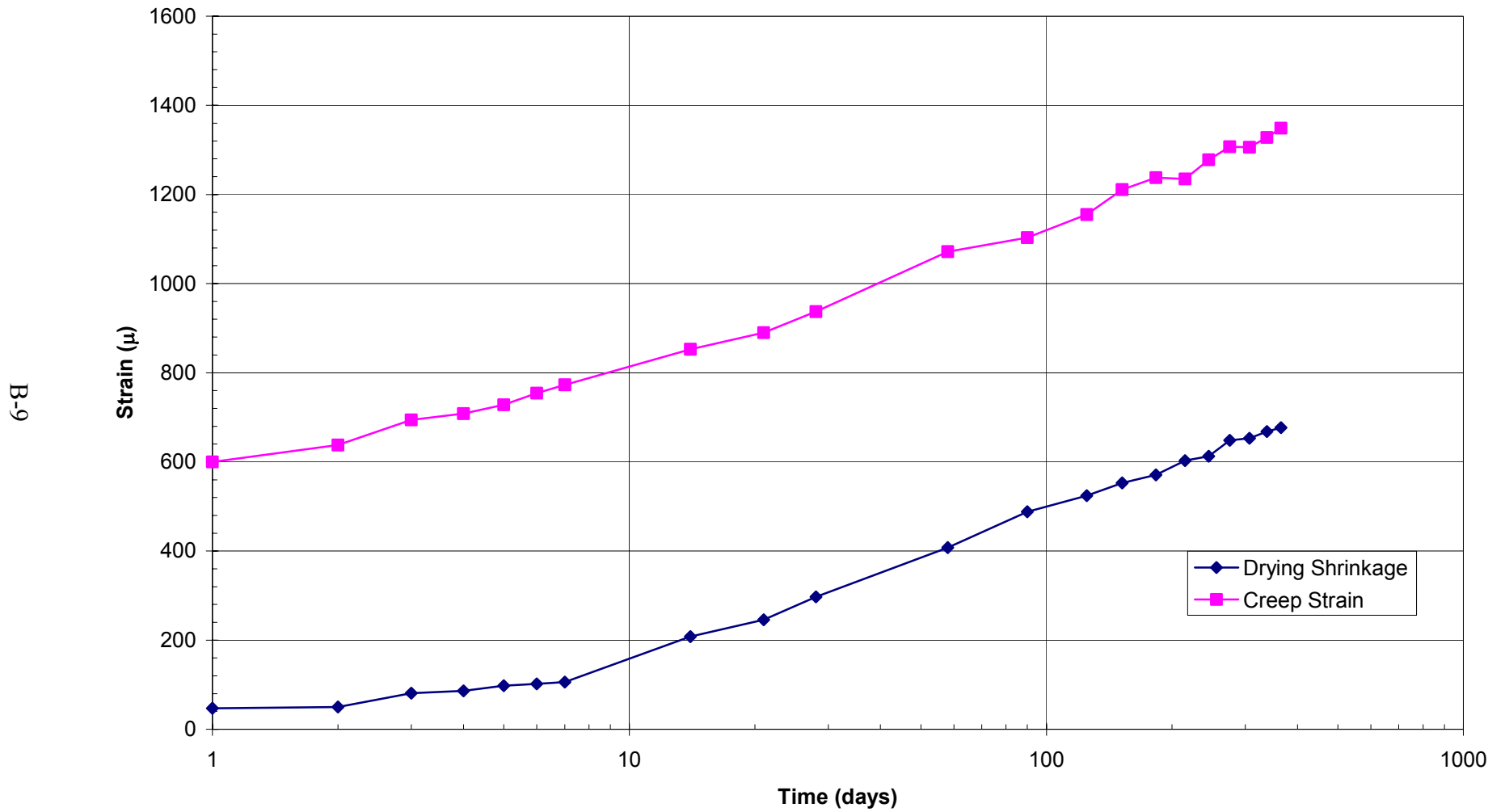
B-7

Trial Concrete Mix Stress-Strain @ 13 weeks (450 kgf/cm²) - Series B

B-8



Concrete Creep and Shrinkage Strain



Section ii. Model Concrete

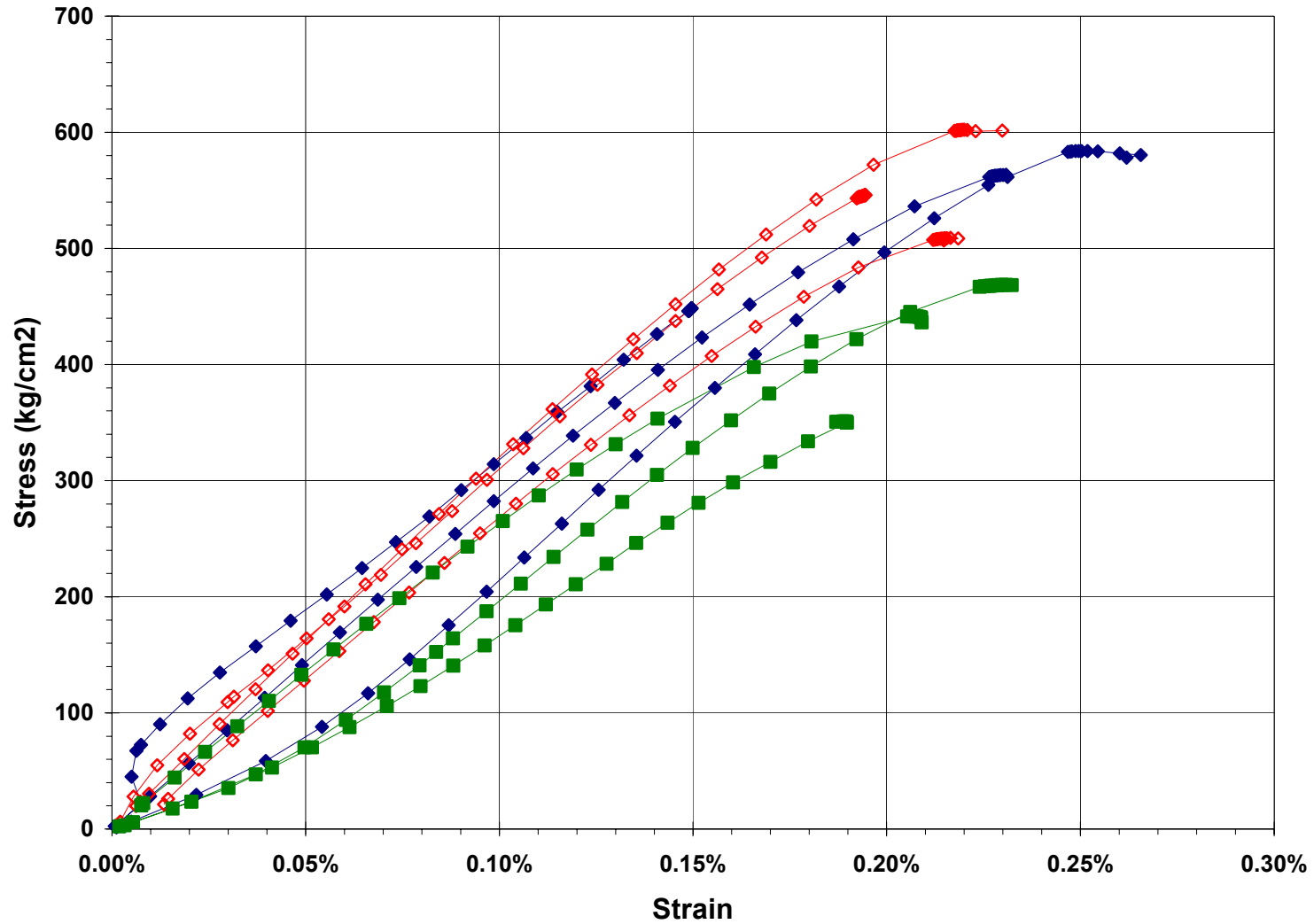
PCCV Model Concrete Tests (METRIC)																
Procedures & Specifications																
Spec.-T-03-1(E) Specification for Concrete Work; Rev.2																
JPN-14-T-1-8; Concrete Material Test Procedure; Rev. 1; 6/14/96																
Submittal : T-03-1 (E) 2.17.0; Revised 10/30/97																
Data & Test Reports																
(A)* AGRA Reports of Compression Test Results, *NUPEC to issue Test Report																
(B) JPN-22-T-1 (Rev.1), Ancillary Test Report, 9 March 1998																
(C) "Strength and Creep Testing of Concrete in PCCV", ATR/UNM, 31 Jan. 2000																
(D) MH-K11-37: PCCV Stress-Strain Tests, CTL, 15 Feb 2000																
(E) "Mechanical Property Evaluation of Concrete Used in the NUPEC/NRC PCCV: Prestress and Limit State Test Results", Lenke & Gerstle, ATR Institute/UNM, 30 June 2001.																
(F)Draft "Standard Test Method for Determination of Direct Tension Properties of Hardened Concrete using the Stiff Tensile Test (STT) Apparatus", Feb. 2000																
	Specification	Lift:	F1	F2	F3a	F3b	F4	C1	C2	C3	C4	D1	D2	D3	F5	F6
			300	300	300	450	450	450	450	450	450	450	450	450	300	450
Quality Control Tests																
Specimens	ASTM C31-91															
At Placement			X(A)	X(A)	X(A)	X(A)	X(A)	X(A)	X(A)	X(A)	X(A)	X(A)	X(A)	X(A)	X(A)	X(A)
Date (M/D/Y)			02/12/97	02/28/97	05/08/97	05/08/97	07/02/97	11/11/98	12/10/98	01/05/99	01/28/99	03/03/99	04/12/99	04/15/99	05/24/00	06/09/00
Slump (cm)	ASTM C143-90a		14.5	16.8	18.3	14.2	16.5	18.3	23.5	21.4	21.9	21.7	24.6	10.8	9.7	9.7
Air Content (%)	ASTM C231-91b		6.5	7.2	6.0	5.7	6.4	4.6	4.6	4.6	4.6	4.6	4.6	4.6	4.0	3.6
Unit Weight (kgf/m ³)			2159.5	2206.0	2196.3	2178.7	2159.5	2212.4	2216.2	2235.3	2244.9	2232.7	2215.6	2214.8		
Temperature (C)			22.2	21.1	27.2	28.3	28.9	22.2	20.4	22.3	17.4	23.6	23.9	21.4	27.7	27.8
1 Week			X(B)	X(B)	X(B)	X(B)	X(B)				X(A)	X(A)	X(A)	X(A)	X(A)	X(A)
Date (M/D/Y)			02/19/97	03/07/97		05/15/97					02/03/99	03/10/99	04/19/99	04/22/99	05/31/00	06/16/00
Compressive Strength (kgf/cm ²)	ASTM C39-86	SC	347	320	-	404	-					370	363	400	334	365
		FC	-	-	-	-	-				378					
		FC*									430	353	360	386		
4 Weeks			X(B)	X(B)	X(B)	X(B)	X(B)	X(A)	X(A)	X(A)	X(A)	X(A)	X(A)	X(A)	X(A)	X(A)
Date (M/D/Y)			03/05/97	03/28/97	06/05/97	06/05/97	07/30/97	12/09/98	01/07/99	02/02/99	02/24/99	03/31/99	05/10/99	05/13/99	06/21/00	07/07/00
Compressive Strength (kgf/cm ²)	ASTM C39-86	SC	392	404	401	490	370	372	386	419	488	474	451	483	407	460
		FC	389	461	342	438	496	339	336	395	423					
		FC*									460	459	435	499	422	459
13 Weeks			X(B)	X(B)	X(B)	X(B)	X(B)	X(A)	X(A)	X(A)	X(A)	X(A)	X(A)	X(A)		
Date (M/D/Y)				05/30/97	08/07/97	08/07/97	10/01/97	02/10/99	03/11/99	04/06/99	04/28/99	06/02/99	07/12/99	07/15/99		
Compressive Strength (kgf/cm ²)	ASTM C39-86	SC	479	480	488	560	449	480	498	496	545	553	489	629		
		FC	395	438	391	483	516	389	436	450	484					
		FC*									516	577	529	629		
Mean Comp. Strength (kgf/cm ²)	ASTM C469-87	FC						X(C)	X(C)							
Young's Modulus (kgf/cm ² x 10 ⁶)	ASTM C469-87	FC						2.05	2.30							
Stress-Strain	ASTM C469-87	FC						X(C)	X(C)							
Poisson's Ratio	ASTM C469-87	FC						0.19	0.22							
Creep Test Data																
Creep Coefficient	ASTM C512-87			FC					X(C)							
Specific Creep (in/in/psi)	(loaded to 61.5 kgf/cm ² @ 28 days)			FC					X(C)							
Drying Shrinkage strain (in/in)	(relative to 28 days)			FC					X(C)							

PCCV Model Concrete Tests (METRIC)																
Procedures & Specifications																
Spec.-T-03-1(E) Specification for Concrete Work; Rev.2																
JPN-14-T-1-8; Concrete Material Test Procedure; Rev. 1; 6/14/96																
Submittal : T-03-1 (E) 2.17.0; Revised 10/30/97																
Data & Test Reports																
(A)* AGRA Reports of Compression Test Results, *NUPEC to issue Test Report																
(B) JPN-22-T-1 (Rev.1), Ancillary Test Report, 9 March 1998																
(C) "Strength and Creep Testing of Concrete in PCCV", ATR/UNM, 31 Jan. 2000																
(D) MH-K11-37: PCCV Stress-Strain Tests, CTL, 15 Feb 2000																
(E) "Mechanical Property Evaluation of Concrete Used in the NUPEC/NRC PCCV: Prestress and Limit State Test Results", Lenke & Gerstle, ATR Institute/UNM, 30 June 2001.																
(F)Draft "Standard Test Method for Determination of Direct Tension Properties of Hardened Concrete using the Stiff Tensile Test (STT) Apparatus", Feb. 2000																
	Specification	Lift:	F1	F2	F3a	F3b	F4	C1	C2	C3	C4	D1	D2	D3	F5	F6
			300	300	300	450	450	450	450	450	450	450	450	450	300	450
Design Data Tests																
@ Prestressing																
Date (M/D/Y)			01/31/00	01/31/00	01/31/00	01/31/00	01/31/00	01/31/00	01/31/00	01/31/00	01/31/00	01/31/00	01/31/00	01/31/00		
Compressive Strength (kgf/cm ²)	ASTM C39-96	FC	532	553	421	606	672	621	581	516						
		FC*									630	727	517	581		
			X(E)	X(E)	X(E)	X(E)	X(E)	X(E)	X(E)	X(E)	X(E)	X(E)	X(E)	X(E)		
Date (M/D/Y)			03/08/00	03/08/00	03/08/00	03/08/00	03/08/00	03/08/00	03/08/00	03/08/00	03/08/00	03/08/00	03/08/00	03/08/00		
Compressive Strength (kgf/cm ²)	ASTM C39-86	FC	600	558	551	553	629	553	534	528						
		FC*									730	665	624	700		
			X(D)	X(D)	X(D)	X(D)	X(D)	X(D)	X(D)	X(D)	X(D)	X(D)	X(D)	X(D)		
Young's Modulus (kgf/cm ² x 10 ⁵)	ASTM C39-96		2.66	2.92	2.27	2.87	3.03	2.77	2.86	2.53	2.98	3.12	2.43	2.41		
Young's Modulus (GPa)			26.1	28.6	22.3	28.1	29.7	27.2	28.0	24.8	29.2	30.6	23.8	23.6		
Poisson's Ratio			NA	NA	NA	NA	NA	NA	NA	NA	NA	NA	NA	NA		
Unit Weight			NA	NA	NA	NA	NA	NA	NA	NA	NA	NA	NA	NA		
@ Limit State Test			X(E)	X(E)	X(E)	X(E)	X(E)	X(E)	X(E)	X(E)	X(E)	X(E)	X(E)	X(E)	X(E)	X(E)
Unit Weight (kgf/m ³)			2167.5	2194.7	2170.7	2185.1	2181.9	2111.4	2095.4	2175.5	2186.7	2214.0	2181.9	2231.6	2210.8	2199.5
Date (M/D/Y)								08/24/00	08/24/00	08/24/00		08/24/00	08/24/00	08/24/00		09/28/00
Mean Comp. Strength (kgf/cm ²)	ASTM C39-86	FC						499	481	598						
		FC*										626	578	649		581
Date (M/D/Y)			10/05/00	10/07/00	10/09/00	10/12/00	10/12/00	10/09/00	10/09/00	10/10/00	10/10/00	10/11/00	10/11/00	10/11/00	10/11/00	10/11/00
Mean Comp. Strength (kgf/cm ²)	ASTM C469-87	FC	574	575	538	659	662	573	572	610						
		FC*									665	734	676	760	592	665
Young's Modulus (kgf/cm ² x 10 ⁵)	ASTM C469-87		2.86	2.97	2.62	2.89	2.78	2.51	2.55	2.60	2.83	2.94	2.78	2.96	2.64	2.59
Young's Modulus (GPa)			28.0	29.2	25.7	28.3	27.2	24.6	25.0	25.5	27.8	28.8	27.2	29.0	25.9	25.4
Poisson's Ratio	ASTM C469-87		0.22	0.22	0.20	0.22	0.22	0.21	0.22	0.22	0.22	0.22	0.21	0.22	0.21	0.22
Stress-Strain																
Date (M/D/Y)			08/23/00	08/23/00	08/23/00	08/23/00	08/23/00	08/23/00	08/23/00	08/23/00	09/27/00	08/23/00	08/24/00	08/24/00	09/28/00	09/27/00
Split Tensile Strength (kgf/cm2)	ASTM C496-90		35	34	35	33	41	34	31	37	40	38	35	37	35	40
Date (M/D/Y)						10/12/00		10/18/00	10/20/00	10/23/00	10/23/00	10/25/00				
Direct Tension (kgf/cm2)	Draft ASTM Standard (F)					29		21	17	22	24	22				
Date (M/D/Y)						08/22/00		08/21/00	08/21/00	08/21/00	08/21/00	08/22/00	08/22/00	08/22/00		09/28/00
Modulus of Rupture (kgf/cm2)	ASTM C-78-84					41		37	41	38	43	44	44	45		41

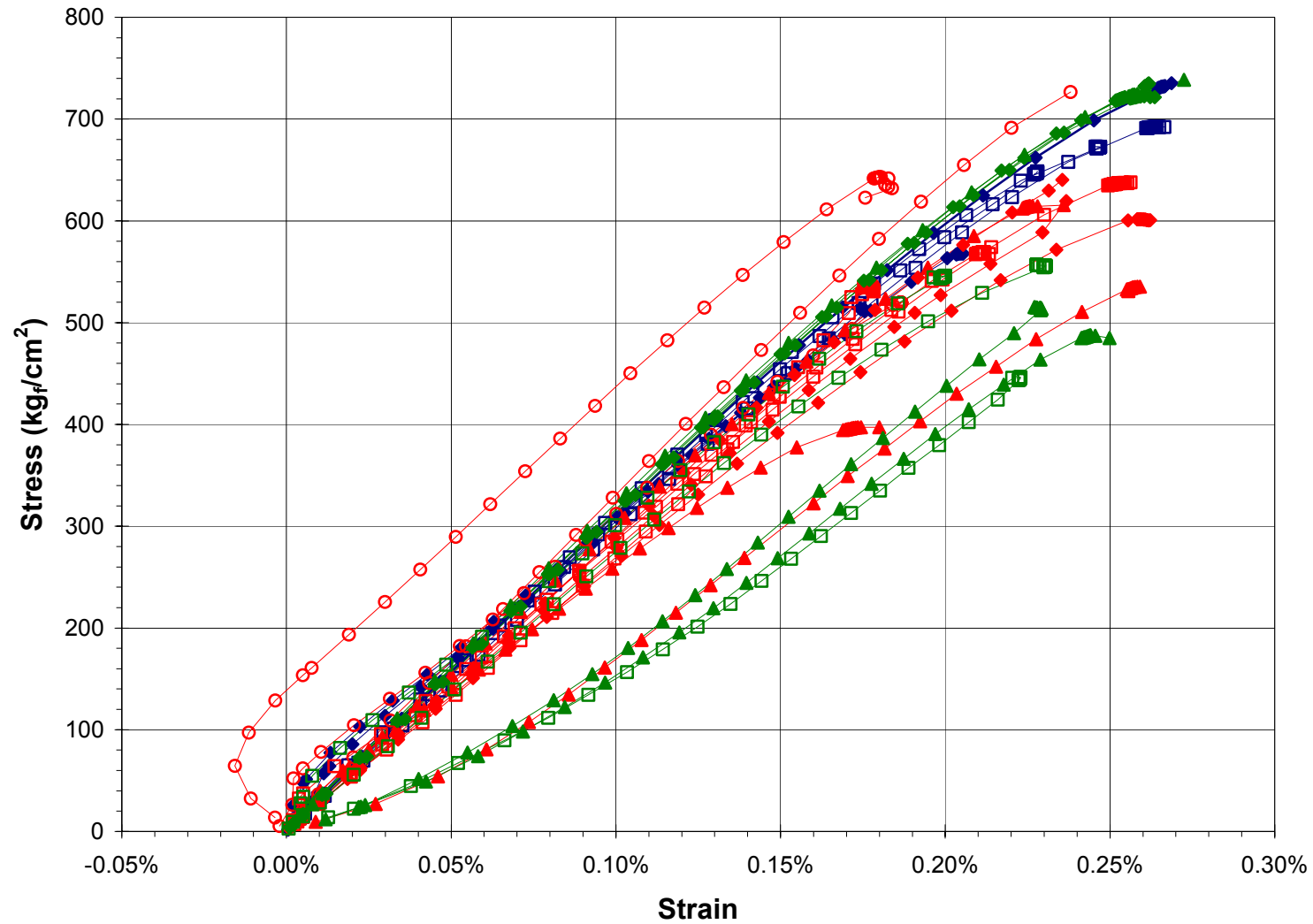
PCCV Model Concrete Tests (ENGLISH)																
Procedures & Specifications																
Spec.-T-03-1(E) Specification for Concrete Work; Rev.2																
JPN-14-T-1-8; Concrete Material Test Procedure; Rev. 1; 6/14/96																
Submittal : T-03-1 (E) 2.17.0; Revised 10/30/97																
Data & Test Reports																
(A)* AGRA Reports of Compression Test Results, *NUPEC to issue Test Report																
(B) JPN-22-T-1 (Rev.1), Ancillary Test Report, 9 March 1998																
(C) "Strength and Creep Testing of Concrete in PCCV", ATR/UNM, 31 Jan. 2000																
(D) MH-K11-37: PCCV Stress-Strain Tests, CTL, 15 Feb 2000																
(E) "Mechanical Property Evaluation of Concrete Used in the NUPEC/NRC PCCV: Prestress and Limit State Test Results", Lenke & Gerstle, ATR Institute/UNM, 30 June 2001.																
(F)Draft "Standard Test Method for Determination of Direct Tension Properties of Hardened Concrete using the Stiff Tensile Test (STT) Apparatus", Feb. 2000																
	Specification	Lift:	F1	F2	F3a	F3b	F4	C1	C2	C3	C4	D1	D2	D3	F5	F6
			4300	4300	4300	6400	6400	6400	6400	6400	6400	6400	6400	6400	4300	6400
Quality Control Tests																
Specimens	ASTM C31-91															
At Placement			X(A)	X(A)	X(A)	X(A)	X(A)	X(A)	X(A)	X(A)	X(A)	X(A)	X(A)	X(A)	X(A)	X(A)
Date (M/D/Y)			02/12/97	02/28/97	05/08/97	05/08/97	07/02/97	11/11/98	12/10/98	01/05/99	01/28/99	03/03/99	04/12/99	04/15/99	05/24/00	06/09/00
Slump (cm)	ASTM C143-90a		14.5	16.8	18.3	14.2	16.5	18.3	23.5	21.4	21.9	21.7	24.6	10.8	9.7	9.7
Air Content (%)	ASTM C231-91b		6.5	7.2	6.0	5.7	6.4	4.6	4.6	4.6	4.6	4.6	4.6	4.6	4.0	3.6
Unit Weight (pcf)			134.8	137.7	137.1	136.0	134.8	138.1	138.3	139.5	140.1	139.4	138.3	138.3		
Temperature (°F)			72.0	70.0	81.0	83.0	84.0	72.0	68.8	72.2	63.3	74.4	75.0	70.5	81.9	82.0
1 Week			X(B)	X(B)	X(B)	X(B)	X(B)				X(A)	X(A)	X(A)	X(A)	X(A)	X(A)
Date (M/D/Y)			02/19/97	03/07/97		05/15/97					02/03/99	03/10/99	04/19/99	04/22/99	05/31/00	06/16/00
Compressive Strength (psi)	ASTM C39-86	SC	4934	4550	-	5745	-					5266	5166	5688	4746	5184
		FC	-	-	-	-	-				5377					
		FC*									6111	5022	5121	5485		
4 Weeks			X(B)	X(B)	X(B)	X(B)	X(B)	X(A)	X(A)	X(A)	X(A)	X(A)	X(A)	X(A)	X(A)	X(A)
Date (M/D/Y)			03/05/97	03/28/97	06/05/97	06/05/97	07/30/97	12/09/98	01/07/99	02/02/99	02/24/99	03/31/99	05/10/99	05/13/99	06/21/00	07/07/00
Compressive Strength (psi)	ASTM C39-86	SC	5568	5739	5702	6963	5259	5296	5491	5965	6941	6746	6419	6868	5785	6536
		FC	5537	6562	4861	6234	7058	4820	4776	5621	6009					
		FC*									6547	6530	6181	7090	6001	6524
13 Weeks			X(B)	X(B)	X(B)	X(B)	X(B)	X(A)	X(A)	X(A)	X(A)	X(A)	X(A)	X(A)		
Date (M/D/Y)				05/30/97	08/07/97	08/07/97	10/01/97	02/10/99	03/11/99	04/06/99	04/28/99	06/02/99	07/12/99	07/15/99		
Compressive Strength (psi)	ASTM C39-86	SC	6815	6822	6940	7957	6386	6823	7076	7053	7750	7865	6949	8942		
		FC	5613	6234	5560	6865	7342	5527	6200	6403	6887					
		FC*									7335	8210	7519	8944		
								X(C)	X(C)							
Mean Comp. Strength (psi)	ASTM C469-87	FC						5628	6390							
Young's Modulus (psi * 10 ⁶)	ASTM C469-87	FC						2.91	3.28							
Stress-Strain	ASTM C469-87	FC						X(C)	X(C)							
Poisson's Ratio	ASTM C469-87	FC						0.19	0.22							
Creep Test Data																
Creep Coefficient	ASTM C512-87			FC					X(C)							
Specific Creep (in/in/psi)	(loaded to 875 psi @ 28 days)			FC					X(C)							
Drying Shrinkage strain (in/in)	(relative to 28 days)			FC					X(C)							

PCCV Model Concrete Tests (ENGLISH)																
Procedures & Specifications																
Spec.-T-03-1(E) Specification for Concrete Work; Rev.2																
JPN-14-T-1-8; Concrete Material Test Procedure; Rev. 1; 6/14/96																
Submittal : T-03-1 (E) 2.17.0; Revised 10/30/97																
Data & Test Reports																
(A)* AGRA Reports of Compression Test Results, *NUPEC to issue Test Report																
(B) JPN-22-T-1 (Rev.1), Ancillary Test Report, 9 March 1998																
(C) "Strength and Creep Testing of Concrete in PCCV", ATR/UNM, 31 Jan. 2000																
(D) MH-K11-37: PCCV Stress-Strain Tests, CTL, 15 Feb 2000																
(E) "Mechanical Property Evaluation of Concrete Used in the NUPEC/NRC PCCV: Prestress and Limit State Test Results", Lenke & Gerstle, ATR Institute/UNM, 30 June 2001.																
(F)Draft "Standard Test Method for Determination of Direct Tension Properties of Hardened Concrete using the Stiff Tensile Test (STT) Apparatus", Feb. 2000																
	Specification	Lift:	F1	F2	F3a	F3b	F4	C1	C2	C3	C4	D1	D2	D3	F5	F6
			4300	4300	4300	6400	6400	6400	6400	6400	6400	6400	6400	6400	4300	6400
Design Data Tests																
@ Prestressing																
Date (M/D/Y)			01/31/00	01/31/00	01/31/00	01/31/00	01/31/00	01/31/00	01/31/00	01/31/00	01/31/00	01/31/00	01/31/00	01/31/00		
Compressive Strength (psi)	ASTM C39-96	FC	7566	7857	5980	8617	9549	8825	8263	7339						
		FC*									630	727	517	581		
			X(E)	X(E)	X(E)	X(E)	X(E)	X(E)	X(E)	X(E)	X(E)	X(E)	X(E)	X(E)		
Date (M/D/Y)			03/08/00	03/08/00	03/08/00	03/08/00	03/08/00	03/08/00	03/08/00	03/08/00	03/08/00	03/08/00	03/08/00	03/08/00		
Compressive Strength (psi)	ASTM C39-86	FC	8525	7940	7840	7870	8950	7860	7590	7510						
		FC*									10380	9455	8875	9950		
			X(D)	X(D)	X(D)	X(D)	X(D)	X(D)	X(D)	X(D)	X(D)	X(D)	X(D)	X(D)		
Young's Modulus (psi x 10 ⁵)	ASTM C39-96		3.78	4.15	3.23	4.08	4.31	3.94	4.06	3.60	4.24	4.43	3.45	3.42		
Poisson's Ratio			NA	NA	NA	NA	NA	NA	NA	NA	NA	NA	NA	NA		
Unit Weight			NA	NA	NA	NA	NA	NA	NA	NA	NA	NA	NA	NA		
@ Limit State Test																
			X(E)	X(E)	X(E)	X(E)	X(E)	X(E)	X(E)	X(E)	X(E)	X(E)	X(E)	X(E)	X(E)	X(E)
Unit Weight (pcf)			135.3	137.0	135.5	136.4	136.2	131.8	130.8	135.8	136.5	138.2	136.2	139.3	138.0	137.3
Date (M/D/Y)								08/24/00	08/24/00	08/24/00		08/24/00	08/24/00	08/24/00		09/28/00
Mean Comp. Strength (psi)	ASTM C39-86	FC						7097	6840	8507						
		FC*										8895	8217	9230		8260
Date (M/D/Y)			10/05/00	10/07/00	10/09/00	10/12/00	10/12/00	10/09/00	10/09/00	10/10/00	10/10/00	10/11/00	10/11/00	10/11/00	10/11/00	10/11/00
Mean Comp. Strength (psi)	ASTM C469-87	FC	8160	8183	7650	9367	9420	8148	8137	8680						
		FC*									9461	10433	9613	10805	8420	9453
Young's Modulus (psi x 10 ⁵)	ASTM C469-87		4.06	4.23	3.72	4.11	3.95	3.57	3.63	3.70	4.03	4.18	3.95	4.21	3.76	3.68
Poisson's Ratio	ASTM C469-87		0.22	0.22	0.20	0.22	0.22	0.21	0.22	0.22	0.22	0.22	0.21	0.22	0.21	0.22
Stress-Strain																
Date (M/D/Y)			08/23/00	08/23/00	08/23/00	08/23/00	08/23/00	08/23/00	08/23/00	08/23/00	09/27/00	08/23/00	08/24/00	08/24/00	09/28/00	09/27/00
Split Tensile Strength (psi)	ASTM C496-90		498	485	500	468	585	483	435	527	568	537	492	525	503	565
Date (M/D/Y)						10/12/00		10/18/00	10/20/00	10/23/00	10/23/00	10/25/00				
Direct Tension (kgf/cm2)	Draft ASTM Standard (F)					409		303	235	318	337	316				
Date (M/D/Y)						08/22/00		08/21/00	08/21/00	08/21/00	08/21/00	08/22/00	08/22/00	08/22/00		09/28/00
Modulus of Rupture (kgf/cm2)	ASTM C-78-84					590		532	587	543	613	628	628	638		590

PCCV Model Concrete Stress-Strain @ Prestressing

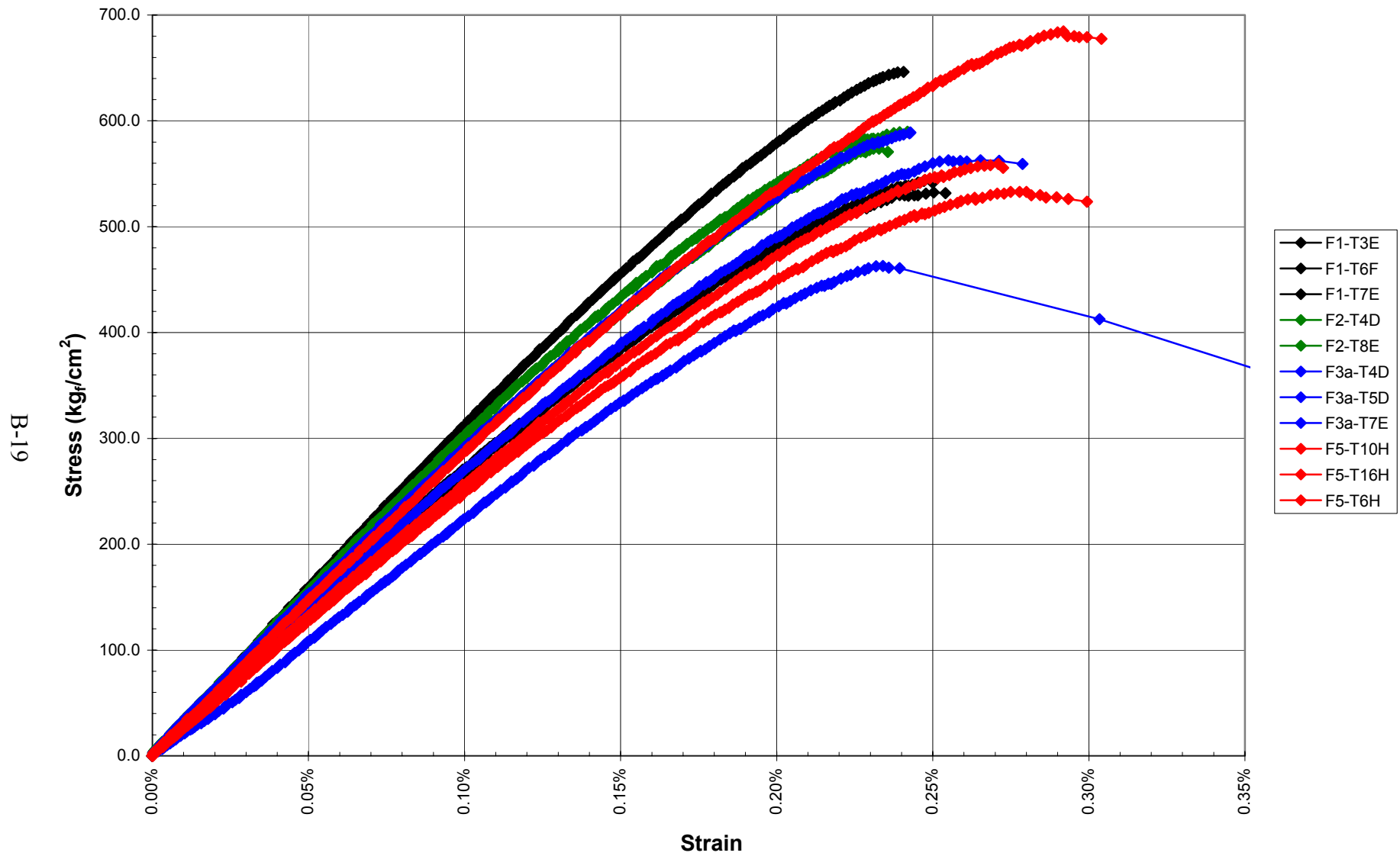


PCCV Model Concrete Stress-Strain @ Prestressing

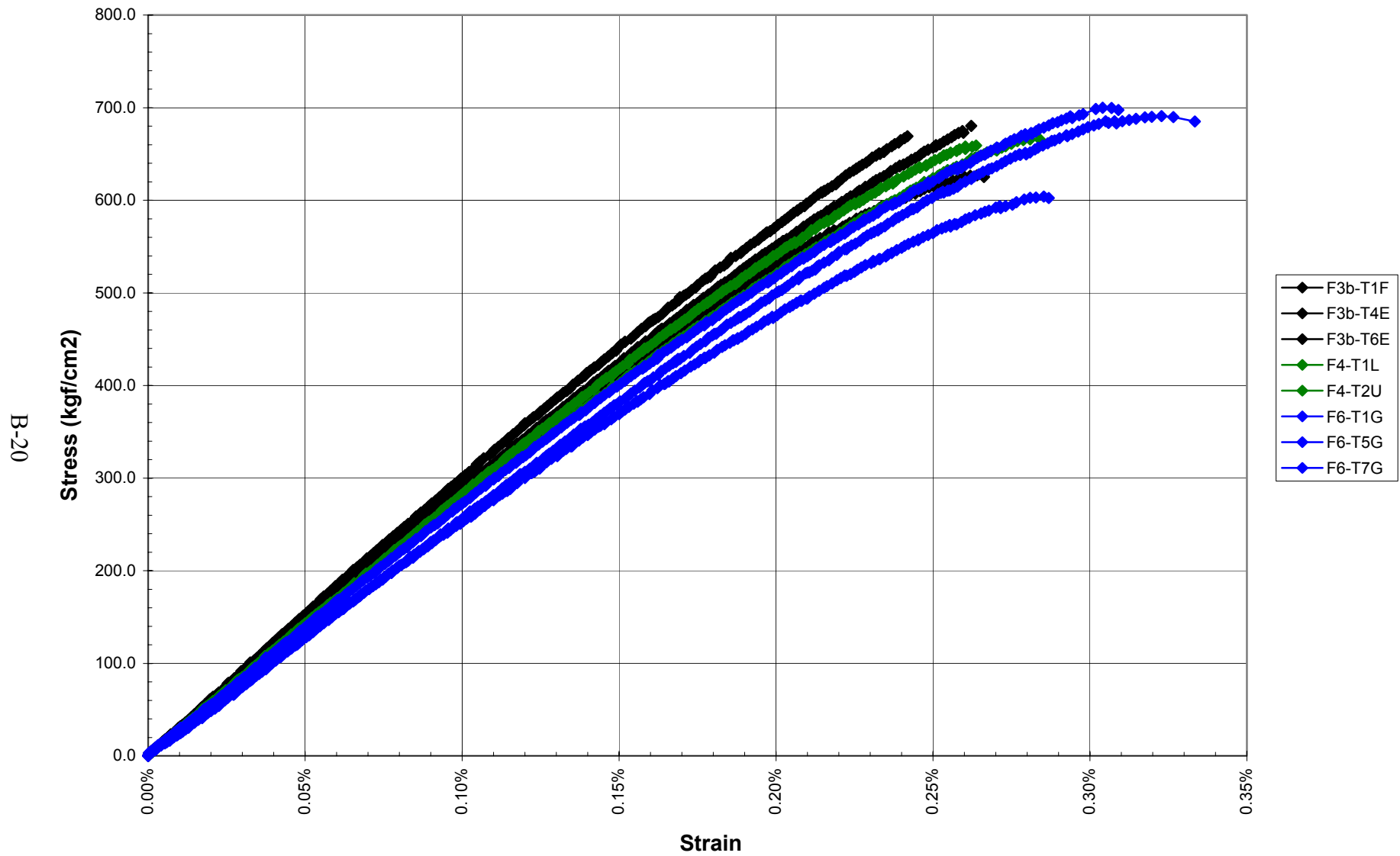


- F3BT2
- F3BT3
- F3BT7
- F4T1
- F4T2
- F4T2B
- C1T2
- C1T5
- C1T6
- C2T1
- C2T3
- C2T4
- C3T1
- C3T3
- C3T5
- C4T1
- C4T2
- C4T3
- D1T2
- D1T3
- D1T4
- D2T2
- D2T3
- D2T4
- D3T1
- D3T2
- D3T2B

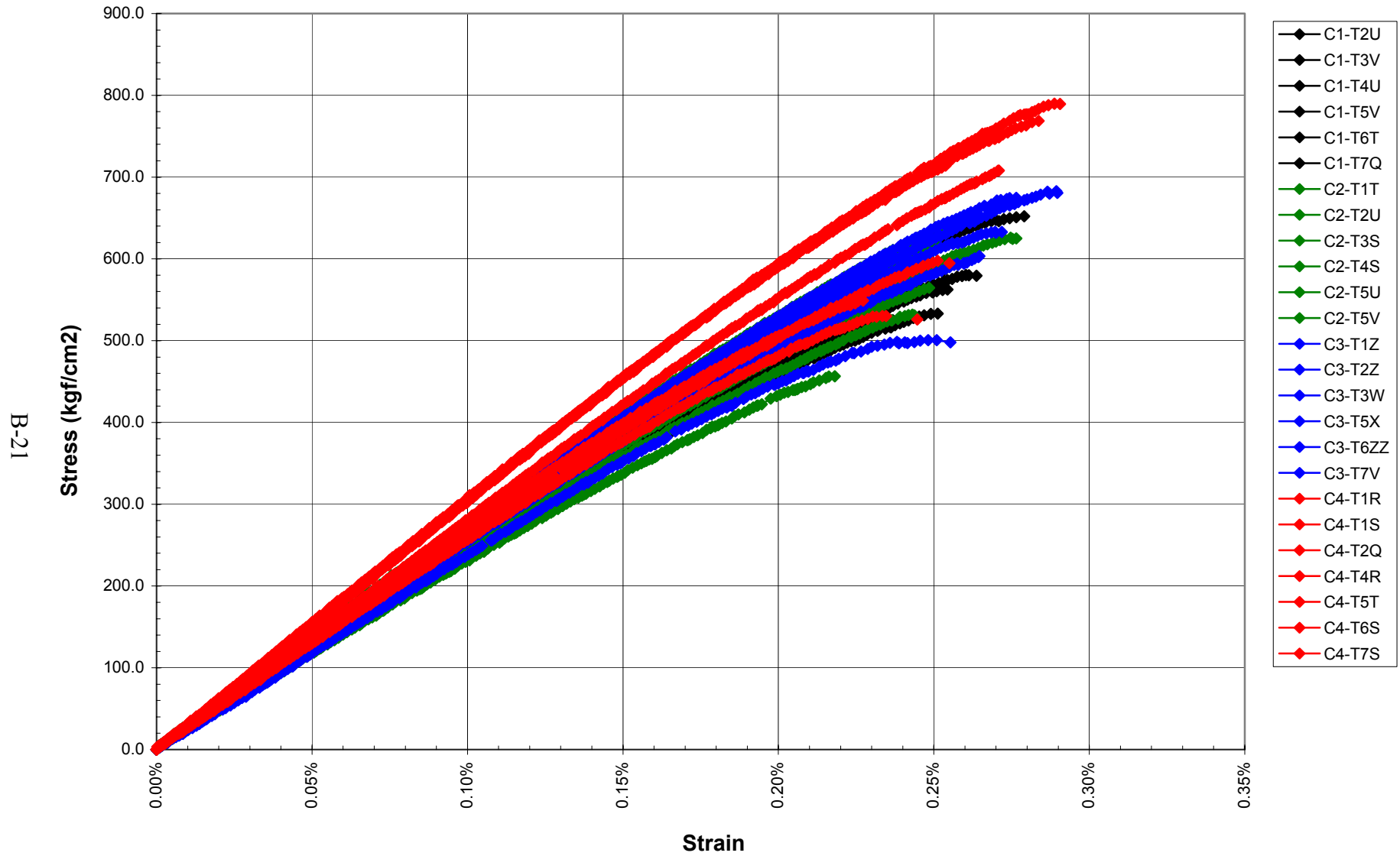
PCCV Concrete Properties @ Limit State Test



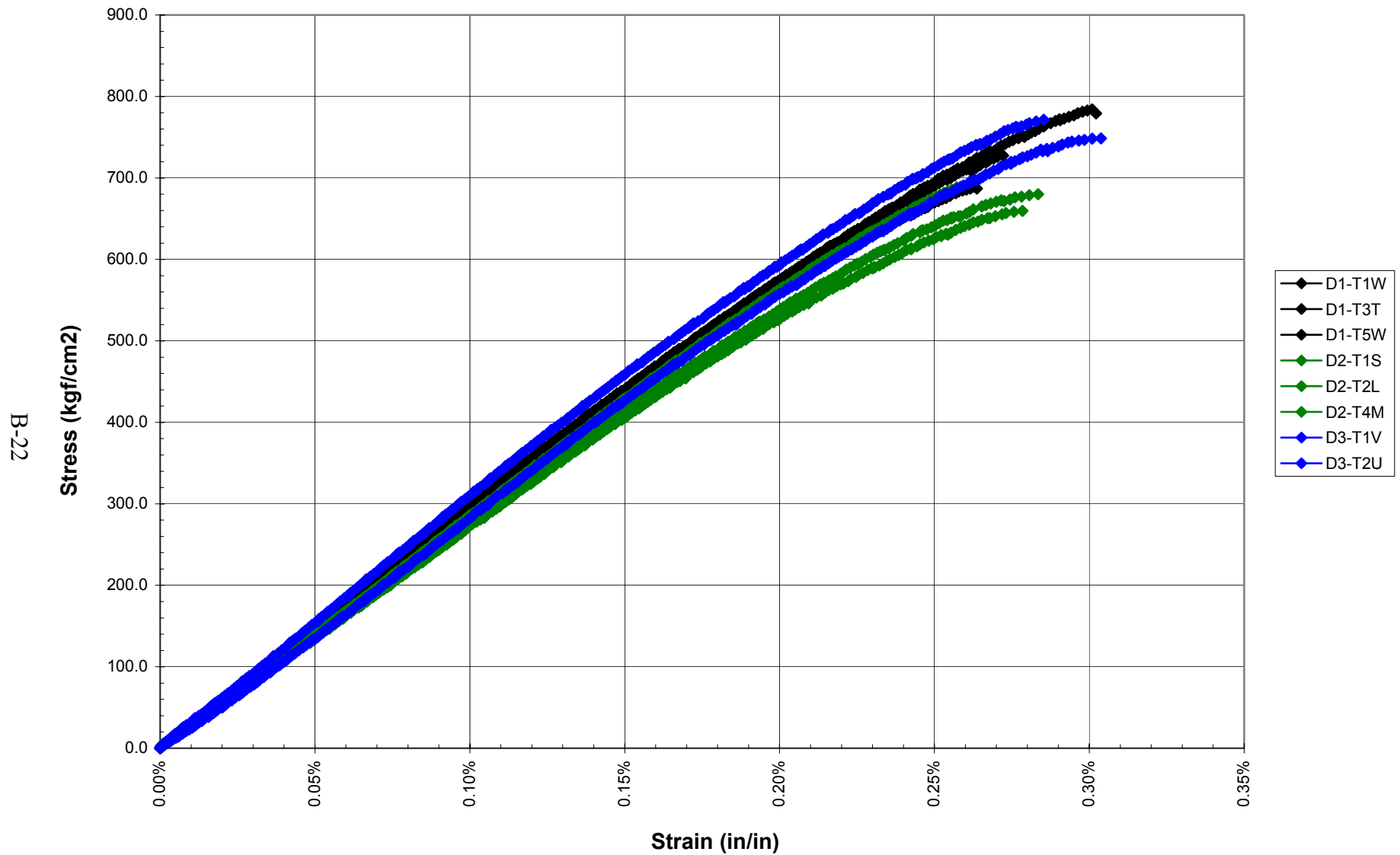
PCCV Concrete Properties @ Limit State Test



PCCV Concrete Properties @ Limit State Test

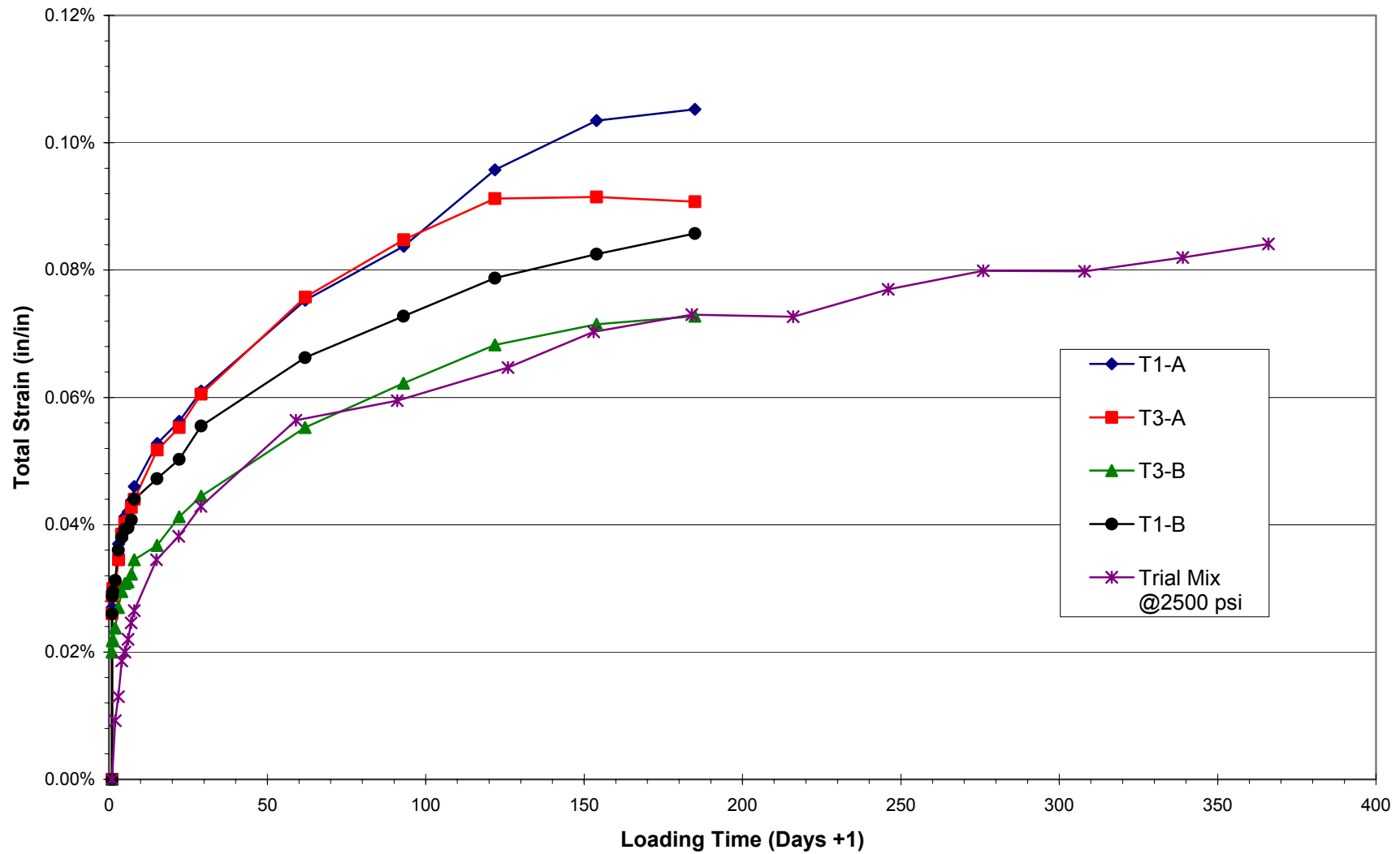


PCCV Concrete Properties @ Limit State Test



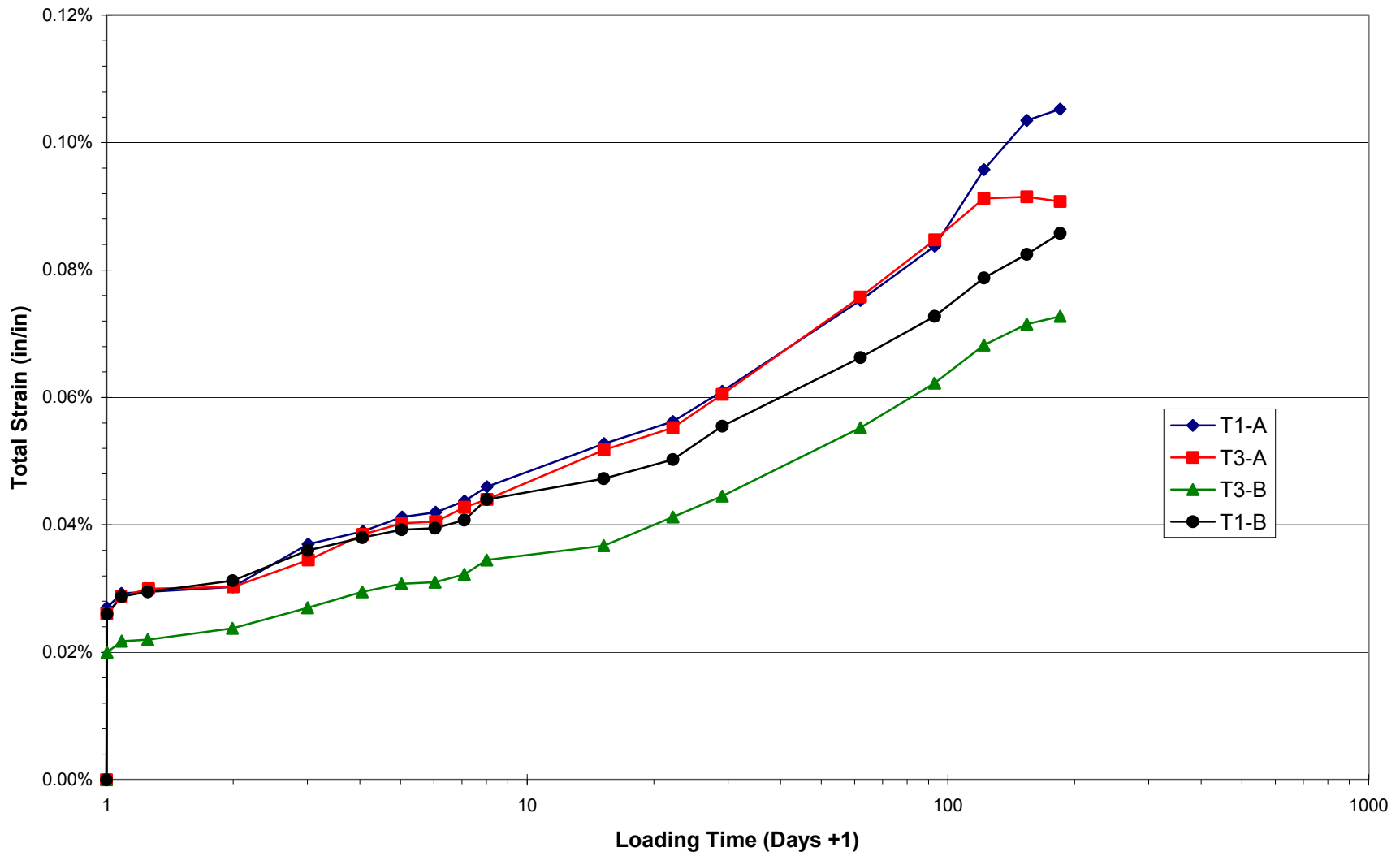
PCCV Model Concrete Creep
Lift C2 (loaded to ~850 psi @ 104 days)

B-23



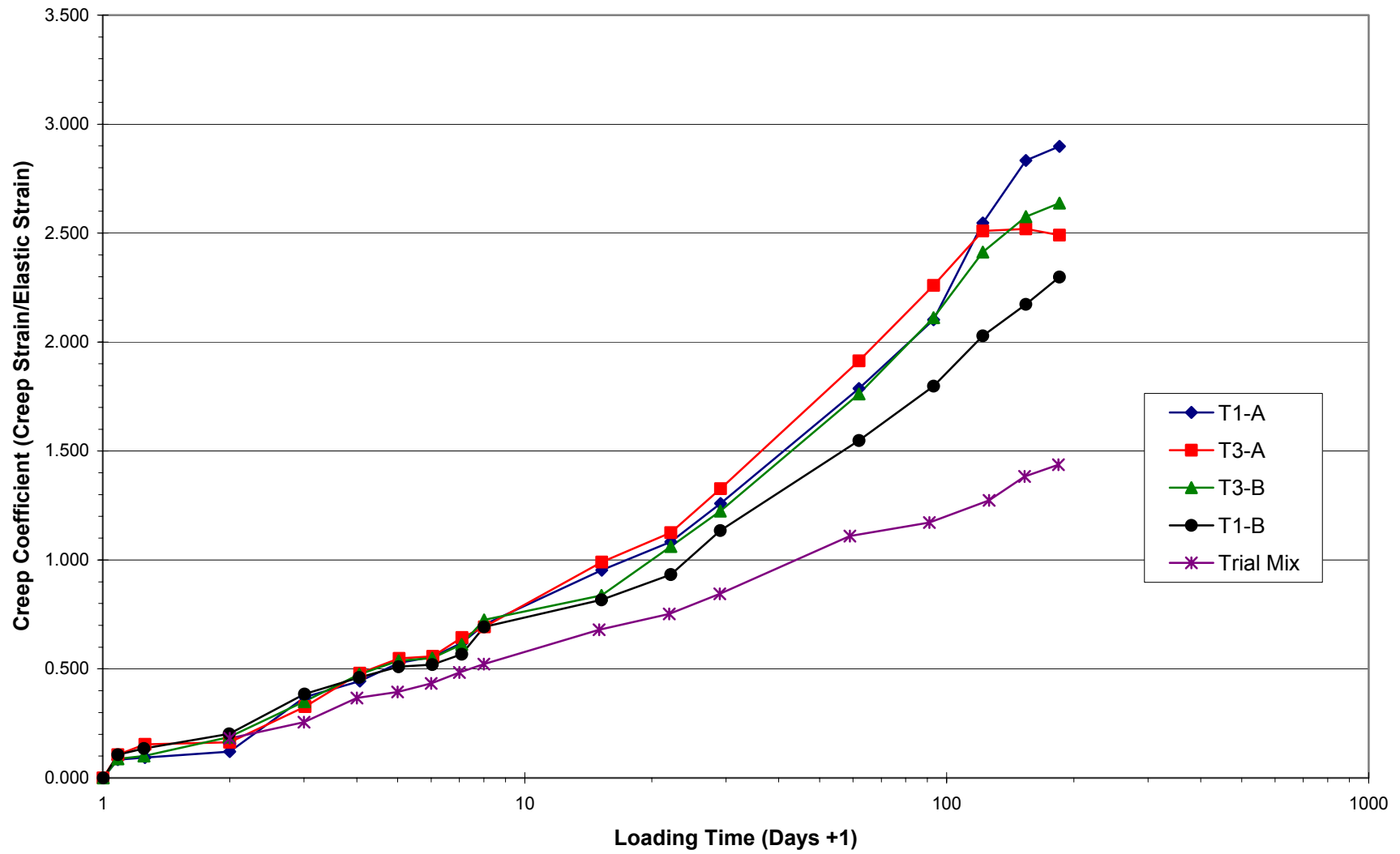
PCCV Model Concrete Creep
Lift C2 (loaded to ~850 psi @ 104 days)

B-24

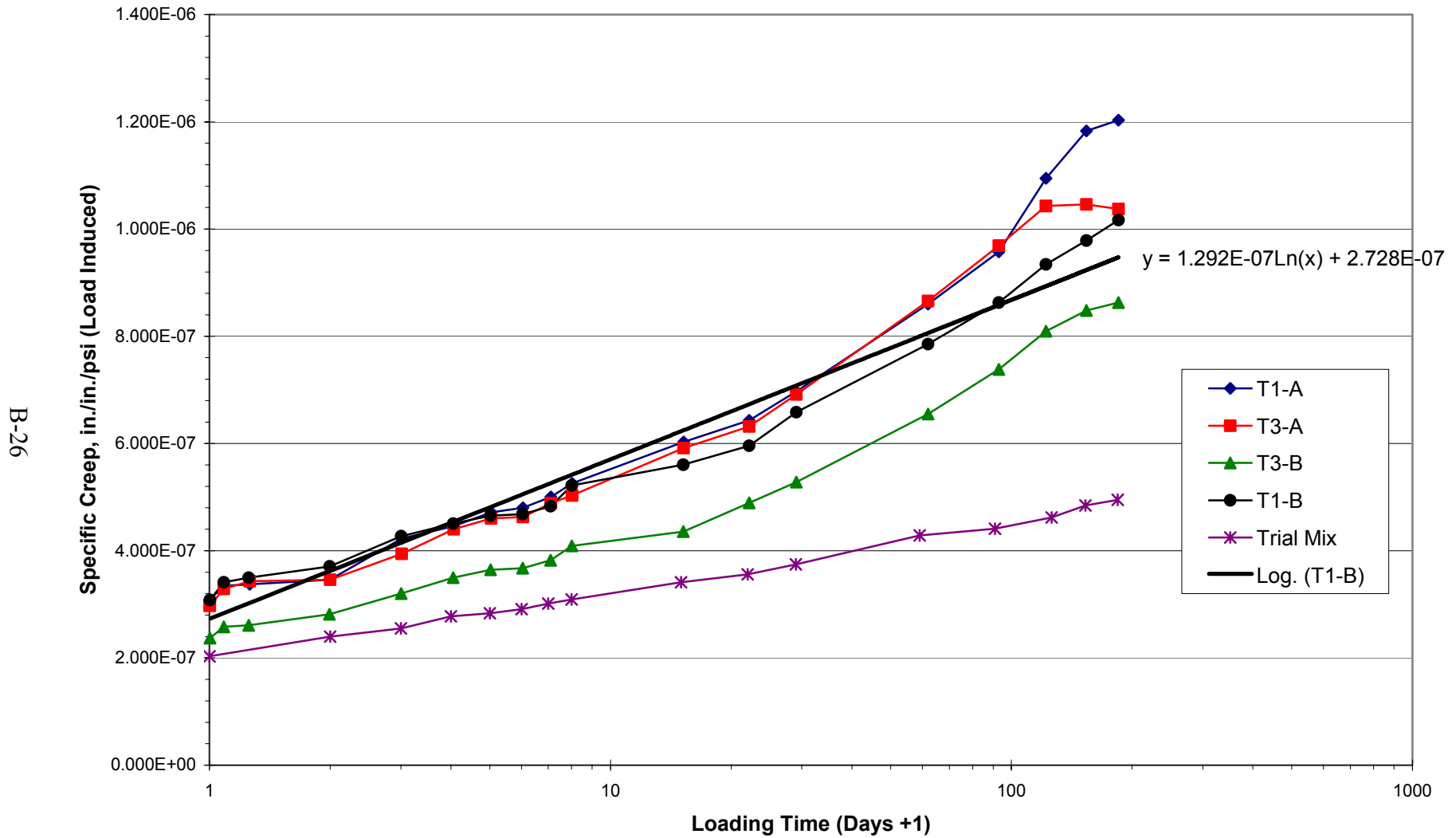


PCCV Model Concrete Creep
Lift C2 (loaded to ~850 psi @ 104 days)

B-25



PCCV Model Concrete Creep
Lift C2 (loaded to ~850 psi @ 104 days)



Section iii. Liner

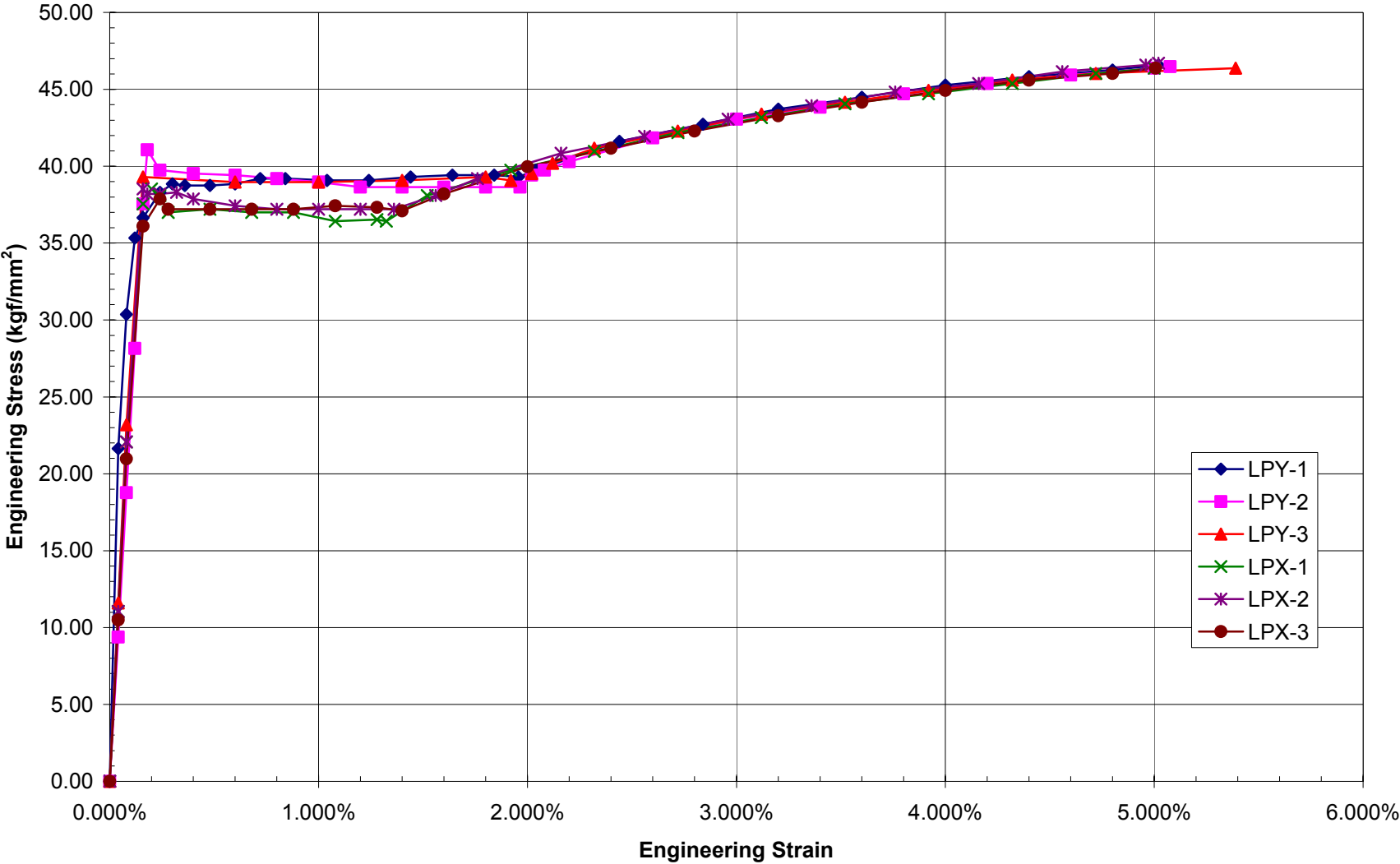
PCCV Liner Material Tests (METRIC)						
Procedures & Specifications						
PCCV Liner Construction Procedure, MH-K9-25A, Rev. 1, Apr. 25, 1997						
Dimension Tolerance for PCCV Liner Installation, MH-K9-26A, Rev. 2, 5/29/97						
Liner Dimension Measurement Procedure, MH-K9-31, Rev. 1						
Procedure for Nondestructive Examinations (RT and PT) and Leak Testing, UGS-L9-970200A, Rev. 2, Apr. 16, 1997						
Repairing Procedure for 5-9 Liner Panel, MH-K9-36, Rev. 0						
Liner Welding Re-Confirmation Test, MH-K9-37, Rev. 1						
Alteration of RT Acceptance Criteria; MH-K9-39						
JIS-Carbon Steel Plates for Pressure Vessels for Intermediate and Moderate Temperature Service, JIS G 3118, 1987						
JIS-Rolled Steels for General Structure, JIS G 3101, 1995						
Data & Test Reports						
(A)Results of Liner Material (SGV410) Test; MH-K9-45, February 1998						
(B)Welded Joint Tensile Test Results; MH-K9-43;9/12						
(C)JPN-16-M-1; Ancillary Test/Liner Material Test, September 1995						
(D)Liner Anchor Test Report; JPN-15-M-2, March 1995						
(E)Results of Liner Welding Re-Confirmation Test, MH-K9-38						
(F)The Repair of 5-9 Liner Panel, MH-K9-41						
(G)Liner Dimensional Inspection Record, MH-K9-46						
	Mat'l Spec.	Yield Stress	Ultimate Stress	Elongation	Elastic Modulus	Stress-Strain
Liner Plate	SGV410	kgf/mm ²	kgf/mm ²		kgf/mm ²	
Nominal (JIS G 3118-1987)	min.	22.9	41.8	21.0%		
	max.		50.0			
Test (JIS Z 2241)		X(A)	X(A)	X(A)	X(A)	X(A)
(T*W*G=25.1*1.84*50mm)						
Meridional	LPY-1	38.9	50.5	33.8%	2.21E+04	
	LPY-2	41.1	50.8	33.0%	2.23E+04	
	LPY-3	39.3	50.7	33.6%	2.29E+04	
	Average	39.8	50.7	33.5%	2.24E+04	
Hoop	LPX-1	38.5	50.9	33.0%	2.17E+04	
	LPX-2	38.5	51.0	33.0%	2.32E+04	
	LPX-3	37.8	50.7	33.0%	2.19E+04	
	Average	38.3	50.9	33.0%	2.23E+04	

PCCV Liner Material Tests (METRIC)						
Procedures & Specifications						
PCCV Liner Construction Procedure, MH-K9-25A, Rev. 1, Apr. 25, 1997						
Dimension Tolerance for PCCV Liner Installation, MH-K9-26A, Rev. 2, 5/29/97						
Liner Dimension Measurement Procedure, MH-K9-31, Rev. 1						
Procedure for Nondestructive Examinations (RT and PT) and Leak Testing, UGS-L9-970200A, Rev. 2, Apr. 16, 1997						
Repairing Procedure for 5-9 Liner Panel, MH-K9-36, Rev. 0						
Liner Welding Re-Confirmation Test, MH-K9-37, Rev. 1						
Alteration of RT Acceptance Criteria; MH-K9-39						
JIS-Carbon Steel Plates for Pressure Vessels for Intermediate and Moderate Temperature Service, JIS G 3118, 1987						
JIS-Rolled Steels for General Structure, JIS G 3101, 1995						
Data & Test Reports						
(A)Results of Liner Material (SGV410) Test; MH-K9-45, February 1998						
(B)Welded Joint Tensile Test Results; MH-K9-43;9/12						
(C)JPN-16-M-1; Ancillary Test/Liner Material Test, September 1995						
(D)Liner Anchor Test Report; JPN-15-M-2, March 1995						
(E)Results of Liner Welding Re-Confirmation Test, MH-K9-38						
(F)The Repair of 5-9 Liner Panel, MH-K9-41						
(G)Liner Dimensional Inspection Record, MH-K9-46						
		Yield Stress	Ultimate Stress	Elongation	Elastic Modulus	Stress-Strain
		kgf/mm ²	kgf/mm ²		kgf/mm ²	
Welded (SMAW) Liner Plate						
(JIS Z 3121, Test Piece 1A)		X(B)	X(B)	X(B)		X(B)
	As-welded (avg.)	39.4	51.7	19.1%		
	Repaired (avg.)	37.9	51.4	18.4%		
	w/o Back-up bar (avg.)	39.2	51.7	17.9%		
	w/ Back-up bar (avg.)	38.1	51.4	19.7%		
	Mat'l Spec.	Yield Stress	Ultimate Stress	Elongation	Elastic Modulus	Stress-Strain
Liner Anchor	SS400	kgf/mm ²	kgf/mm ²		kgf/mm ²	
Nominal						
	JIS G 3101-1995	min.	25.0	40.8	21.0%	
		max.		52.0		
Test		X(C)	X(C)	X(C)	X(C)	
	vertical	29.5	46.5	33.0%	2.12E+04	
	horizontal	31.5	45.3	38.0%	2.20E+04	
		fc'	Max. Load	Max. Disp.	Initial Stiffness	Force-Deflection
		kgf/cm ²	kgf	mm	kgf/mm	
Liner Anchor Force-Deflection		X(D)	X(D)	X(D)	X(D)	X(D)
	Tension, prestressed	410	4,433	0.100	127,333	
	Tension, non-prestressed	410	3,20	0.129	52,667	
	Shear, prestressed	410	14,700	2.865	59,267	
	Shear, non-prestressed	410	11,100	1.155	39,667	

PCCV Liner Material Tests (ENGLISH)						
Procedures & Specifications						
PCCV Liner Construction Procedure, MH-K9-25A, Rev. 1, Apr. 25, 1997						
Dimension Tolerance for PCCV Liner Installation, MH-K9-26A, Rev. 2, 5/29/97						
Liner Dimension Measurement Procedure, MH-K9-31, Rev. 1						
Procedure for Nondestructive Examinations (RT and PT) and Leak Testing, UGS-L9-970200A, Rev. 2, Apr. 16, 1997						
Repairing Procedure for 5-9 Liner Panel, MH-K9-36, Rev. 0						
Liner Welding Re-Confirmation Test, MH-K9-37, Rev. 1						
Alteration of RT Acceptance Criteria; MH-K9-39						
JIS-Carbon Steel Plates for Pressure Vessels for Intermediate and Moderate Temperature Service, JIS G 3118, 1987						
JIS-Rolled Steels for General Structure, JIS G 3101, 1995						
Data & Test Reports						
(A)Results of Liner Material (SGV410) Test; MH-K9-45, February 1998						
(B)Welded Joint Tensile Test Results; MH-K9-43;9/12						
(C)JPN-16-M-1; Ancillary Test/Liner Material Test, September 1995						
(D)Liner Anchor Test Report; JPN-15-M-2, March 1995						
(E)Results of Liner Welding Re-Confirmation Test, MH-K9-38						
(F)The Repair of 5-9 Liner Panel, MH-K9-41						
(G)Liner Dimensional Inspection Record, MH-K9-46						
	Mat'l Spec.	Yield Stress	Ultimate Stress	Elongation	Elastic Modulus	Stress-Strain
Liner Plate	SGV410	psi	psi		psi	
Nominal (JIS G 3118-1987)	min.	32,626	59,451	21.0%		
	max.		71,052			
Test (JIS Z 2241)		X(A)	X(A)	X(A)	X(A)	X(A)
(T*W*G=25.1*1.84*50mm)						
Meridonal	LPY-1	55,316	71,811	33.8%	3.143E+07	
	LPY-2	58,444	72,238	33.0%	3.171E+07	
	LPY-3	55,885	72,095	33.6%	3.256E+07	
	Average	56,548	72,048	33.5%	3.190E+07	
Hoop	LPX-1	54,747	72,380	33.0%	3.086E+07	
	LPX-2	54,747	72,522	33.0%	3.299E+07	
	LPX-3	53,752	72,095	33.0%	3.114E+07	
	Average	54,415	72,332	33.0%	3.166E+07	

PCCV Liner Material Tests (ENGLISH)						
Procedures & Specifications						
PCCV Liner Construction Procedure, MH-K9-25A, Rev. 1, Apr. 25, 1997						
Dimension Tolerance for PCCV Liner Installation, MH-K9-26A, Rev. 2, 5/29/97						
Liner Dimension Measurement Procedure, MH-K9-31, Rev. 1						
Procedure for Nondestructive Examinations (RT and PT) and Leak Testing, UGS-L9-970200A, Rev. 2, Apr. 16, 1997						
Repairing Procedure for 5-9 Liner Panel, MH-K9-36, Rev. 0						
Liner Welding Re-Confirmation Test, MH-K9-37, Rev. 1						
Alteration of RT Acceptance Criteria; MH-K9-39						
JIS-Carbon Steel Plates for Pressure Vessels for Intermediate and Moderate Temperature Service, JIS G 3118, 1987						
JIS-Rolled Steels for General Structure, JIS G 3101, 1995						
Data & Test Reports						
(A)Results of Liner Material (SGV410) Test; MH-K9-45, February 1998						
(B)Welded Joint Tensile Test Results; MH-K9-43;9/12						
(C)JPN-16-M-1; Ancillary Test/Liner Material Test, September 1995						
(D)Liner Anchor Test Report; JPN-15-M-2, March 1995						
(E)Results of Liner Welding Re-Confirmation Test, MH-K9-38						
(F)The Repair of 5-9 Liner Panel, MH-K9-41						
(G)Liner Dimensional Inspection Record, MH-K9-46						
		Yield Stress	Ultimate Stress	Elongation	Elastic Modulus	Stress-Strain
		psi	psi		psi	
Welded (SMAW) Liner Plate						
(JIS Z 3121, Test Piece 1A)		X(B)	X(B)	X(B)		X(B)
	As-welded (avg.)	55,971	73,517	19.1%		
	Repaired (avg.)	53,941	73,082	18.4%		
	w/o Back-up bar (avg.)	55,681	73,517	17.9%		
	w/ Back-up bar (avg.)	54,231	73,082	19.7%		
	Mat'l Spec.	Yield Stress	Ultimate Stress	Elongation	Elastic Modulus	Stress-Strain
Liner Anchor	SS400	psi	psi		psi	
Nominal						
	JIS G 3101-1995	min.	35,526	58,001	21.0%	
		max.	-	73,952		
Test		X(C)	X(C)	X(C)	X(C)	
	vertical	41,906	66,122	33.0%	3.016E+07	
	horizontal	44,806	64,382	38.0%	3.132E+07	
		fc'	Max. Load	Max. Disp.	Initial Stiffness	Force-Deflection
		psi	lbs	in.	lb/in.	
Liner Anchor Force-Deflection		X(D)	X(D)	X(D)	X(D)	X(D)
	Tension, prestressed	5835	9,774	0.004	7,130,375	
	Tension, non-prestressed	5835	7,070	0.005	2,949,213	
	Shear, prestressed	5835	32,408	0.113	3,318,797	
	Shear, non-prestressed	5835	24,471	0.045	2,221,242	

Liner Stress-Strain



B-33

Section iv. Rebar and Couplers

PCCV Rebar/Coupler Material Tests (METRIC)												
Procedures & Specifications												
JPN-14-T-1-3; Rebar Material Test Procedure; 6/14/96												
JPN-14-T-1-4; Rebar Connection Test Procedure; 6/14/96												
Spec.-T-04-2(E) Rev. 2; Specification for Reinforcement Material												
Spec.-T-04-3(E) Rev. 2; Specification for Mechanical Joint												
Data & Test Reports												
(A)JPN-21-T-5, Ancillary Test Report, Rebar Joint Test, May 20, 1997												
(B) TAP 9702; Material Property data for a mechanical model used in pre/post analyses, 4/21/97												
(C) JPN-21-T-4, Ancillary Test Report, Rebar Material Test, May 20, 1997												
(D) MH-K10-37, Tensile Test Result for #3 Position Threaded Coupler												
(E) MH-K10-38, Tensile Test Result for #6 Position Threaded Coupler												
(F) SNL Rebar Calibration Tests, February, 1999												
Component		Design Data Tests										
Mat'l Spec.												
Reinforcing Steel			Diameter	Area	Yield Stress	Ultimate Stress	Gage Length	Elongation ¹	Elastic Modulus	Stress-Strain ²		
			(mm)	(mm ²)	(kN)	(MPa)	(kN)	(MPa)	Initial	Final	(%)	(N/mm ²)
Nominal (JIS G 3112)	SD345											
min.					345.0		490.0			18.0%		
max.					390.0							
Test (JIS Z 2241)			X(B)	X(B)	X(B)	X(B)	X(B)	X(B)	X(B)	X(B)	X(B)	X(B)
(ASTM E8M-93)	D6	1	6.35	31.67	12.1	382.1	15.5	489.4	47.7	62.5	31.0%	1.68E+05
(G=8D, Grip=10D)		2	6.35	31.67	11.5	363.1	15.5	489.4	47.7	62.0	30.0%	1.71E+05
		3	6.35	31.67	11.5	363.1	15.5	489.4	47.8	62.2	30.1%	1.67E+05
		mean	6.35	31.67	11.7	369.4	15.5	489.4	47.7	62.2	30.4%	1.69E+05
D10		1	9.53	71.33	26.3	368.7	39.2	549.6	79.7	97.5	22.3%	1.82E+05
(G=8D, Grip=10D)		2	9.53	71.33	26.6	372.9	39.9	559.4	80.0	98.6	23.3%	1.85E+05
		3	9.53	71.33	26.5	371.5	39.2	549.6	80.0	100.7	25.9%	1.80E+05
		mean	9.53	71.33	26.5	371.0	39.4	552.8	79.9	98.9	23.8%	1.82E+05
		¹ Elongation @ ultimate load based on gage length of broken bars.										
		² Stress-Strain relationship measured by 2 dia. opposed strain gages located @ center of gage length.										
		JIS Z 2441 references use of extensometer for strain measurement.										

Reinforcing Steel			Diameter	Area	Yield Stress		Ultimate Stress		Gage Length		Elongation ¹	Elastic Modulus	Stress-Strain ²
			(mm)	(mm2)	(kN)	(MPa)	(kN)	(MPa)	Initial	Final	(%)	(N/mm2)	
Nominal (JIS G 3112)	SD390												
min.					390.0		539.0				16.0%		
	max.				490.0								
Test (JIS Z 2241)			X(B)	X(B)	X(B)	X(B)	X(B)	X(B)	X(B)	X(B)	X(B)	X(B)	X(B)
(ASTM E8M-93)	D10	1	9.53	71.33	33.2	465.4	46.7	654.7	80.2	94.1	17.3%	1.83E+05	
(G=8D, Grip=10D)		2	9.53	71.33	34.4	482.3	47.0	658.9	79.5	97.7	22.9%	1.85E+05	
		3	9.53	71.33	33.6	471.1	46.0	644.9	79.7	96.6	21.2%	1.82E+05	
		mean	9.53	71.33	33.7	472.9	46.6	652.8	79.8	96.1	20.5%	1.83E+05	
D13		1	12.7	126.7	53.4	421.5	77.2	609.3	104.0	129.4	24.4%	1.83E+05	
(G=8D, Grip=10D)		2	12.7	126.7	55.8	440.4	77.5	611.7	103.9	128.4	23.6%	1.83E+05	
		3	12.7	126.7	55.1	434.9	77.4	610.9	104.0	129.6	24.6%	1.84E+05	
		mean	12.7	126.7	54.8	432.3	77.4	610.6	104.0	129.1	24.2%	1.83E+05	
D16		1	15.9	198.6	90.9	457.7	122.5	616.8	128.0	146.6	19.4%	1.82E+05	
(G=8D, Grip=10D)		2	15.9	198.6	91.3	459.7	123.0	619.3	128.2	147.4	24.1%	1.84E+05	
		3	15.9	198.6	90.4	455.2	121.8	613.3	127.9	146.5	22.7%	1.84E+05	
		mean	15.9	198.6	90.9	457.5	122.4	616.5	128.0	146.8	22.1%	1.83E+05	
D16		1	12.5	122.7	66.0	537.9	87.8	715.6	49.7	63.5	27.8%	2.09E+05	
(dumbbell)		2	12.5	122.7	63.8	520.0	88.2	718.8	50.0	63.0	26.0%	2.09E+05	
(D x G = 12.5 x 50)		3	12.5	122.7	63.4	516.7	87.8	715.6	50.0	63.7	27.4%	2.09E+05	
		mean	12.5	122.7	64.4	524.9	87.9	716.7	49.9	63.4	27.1%	2.09E+05	
D19		1	19.1	286.5	135.2	471.9	188.2	656.9	152.2	181.5	19.3%	1.83E+05	
(G=8D, Grip=10D)		2	19.1	286.5	135.6	473.3	188.8	659.0	152.2	183.9	20.8%	1.83E+05	
		3	19.1	286.5	135.8	474.0	188.8	659.0	151.9	187.2	23.2%	1.86E+05	
		mean	19.1	286.5	135.5	473.1	188.6	658.3	152.1	184.2	21.1%	1.84E+05	
D22		1	22.2	387.1	176.6	456.2	263.7	681.2	176.0	200.3	16.8%	1.90E+05	
(G=8D, Grip=10D)		2	22.2	387.1	177.9	459.6	263.9	681.7	176.0	202.3	20.0%	1.91E+05	
		3	22.2	387.1	178.5	461.1	263.0	679.4	176.1	202.1	19.1%	1.92E+05	
		mean	22.2	387.1	177.7	459.0	263.5	680.8	176.0	201.6	18.7%	1.91E+05	
D22		1	14	153.9	73.0	474.5	113.7	739.0	50.8	63.7	25.4%	2.10E+05	
(dumbbell)		2	14	153.9	73.4	476.8	112.0	728.0	50.6	63.8	26.1%	2.08E+05	
(D x G = 14 x 50)		3	14	153.9	70.8	460.2	115.0	747.0	51.3	64.8	26.3%	2.08E+05	
		mean	14	153.9	72.4	470.5	113.6	738.0	50.9	64.1	25.9%	2.09E+05	
			¹ Elongation @ ultimate load based on gage length of broken bars.										
			² Stress-Strain relationship measured by 2 dia.opossed strain gages located @ center of gage length.										
			JIS Z 2441 references use of extensometer for strain measurement.										

Reinforcing Steel		Diameter	Area	Yield Stress		Ultimate Stress		Gage Length		Elongation ¹	Elastic Modulus	Stress-Strain ²
		(mm)	(mm ²)	(kN)	(MPa)	(kN)	(MPa)	Initial	Final	(%)	(N/mm ²)	
Nominal (JIS G 3112)	SD490											
	min.				490.0		618.0			12.0%		
	max.				620.0							
Test (JIS Z 2241)			X(B)	X(B)	X(B)	X(B)	X(B)	X(B)	X(B)	X(B)	X(B)	X(B)
(ASTM E8M-93)	D10	1	9.53	71.33	35.1	492.1	47.6	667.3	79.7	97.9	22.8%	1.86E+05
(G=8D, Grip=10D)		2	9.53	71.33	35.0	490.7	47.2	661.7	79.8	95.5	19.7%	1.87E+05
		3	9.53	71.33	35.0	490.7	47.7	668.7	80.0	97.4	21.8%	1.87E+05
	mean		9.53	71.33	35.0	491.1	47.5	665.9	79.8	96.9	21.4%	1.87E+05
	D13	1	12.7	126.7	69.2	546.2	94.8	748.2	104.0	122.7	18.0%	1.83E+05
(G=8D, Grip=10D)		2	12.7	126.7	69.2	546.2	95.1	750.6	103.9	121.5	16.9%	1.85E+05
		3	12.7	126.7	70.0	552.5	95.7	755.3	104.0	119.0	14.4%	1.85E+05
	mean		12.7	126.7	69.5	548.3	95.2	751.4	104.0	121.1	16.4%	1.84E+05
	D16	1	15.9	198.6	96.2	544.9	134.3	676.2	128.2	143.3	17.0%	1.84E+05
(G=8D, Grip=10D)		2	15.9	198.6	102.3	544.9	138.9	699.4	128.0	143.1	15.2%	1.86E+05
		3	15.9	198.6	99.3	551.2	136.9	689.3	128.0	144.6	19.0%	1.84E+05
	mean		15.9	198.6	99.3	547.0	136.7	688.3	128.1	143.7	17.1%	1.85E+05
	D16	1	12.5	122.7	69.2	544.9	97.3	793.0	49.6	62.1	25.2%	2.12E+05
(dumbbell)		2	12.5	122.7	67.4	544.9	96.8	788.9	50.2	62.1	23.7%	2.10E+05
(D x G = 12.5 x 50)		3	12.5	122.7	68.3	551.2	95.7	780.0	49.9	62.2	24.6%	2.09E+05
	mean		12.5	122.7	68.3	547.0	96.6	787.3	49.9	62.1	24.5%	2.10E+05
	D19	1	19.1	286.5	146.4	511.0	203.4	709.9	151.7	178.6	17.7%	1.85E+05
(G=8D, Grip=10D)		2	19.1	286.5	147.2	513.8	202.8	707.9	151.9	177.5	16.9%	1.87E+05
		3	19.1	286.5	146.6	511.7	203.8	711.3	151.8	180.2	18.7%	1.86E+05
	mean		19.1	286.5	146.7	512.2	203.3	709.7	151.8	178.8	17.8%	1.86E+05
		¹ Elongation @ ultimate load based on gage length of broken bars.										
		² Stress-Strain relationship measured by 2 dia.opossed strain gages located @ center of gage length.										
		JIS Z 2441 references use of extensometer for strain measurement.										

[illegible]

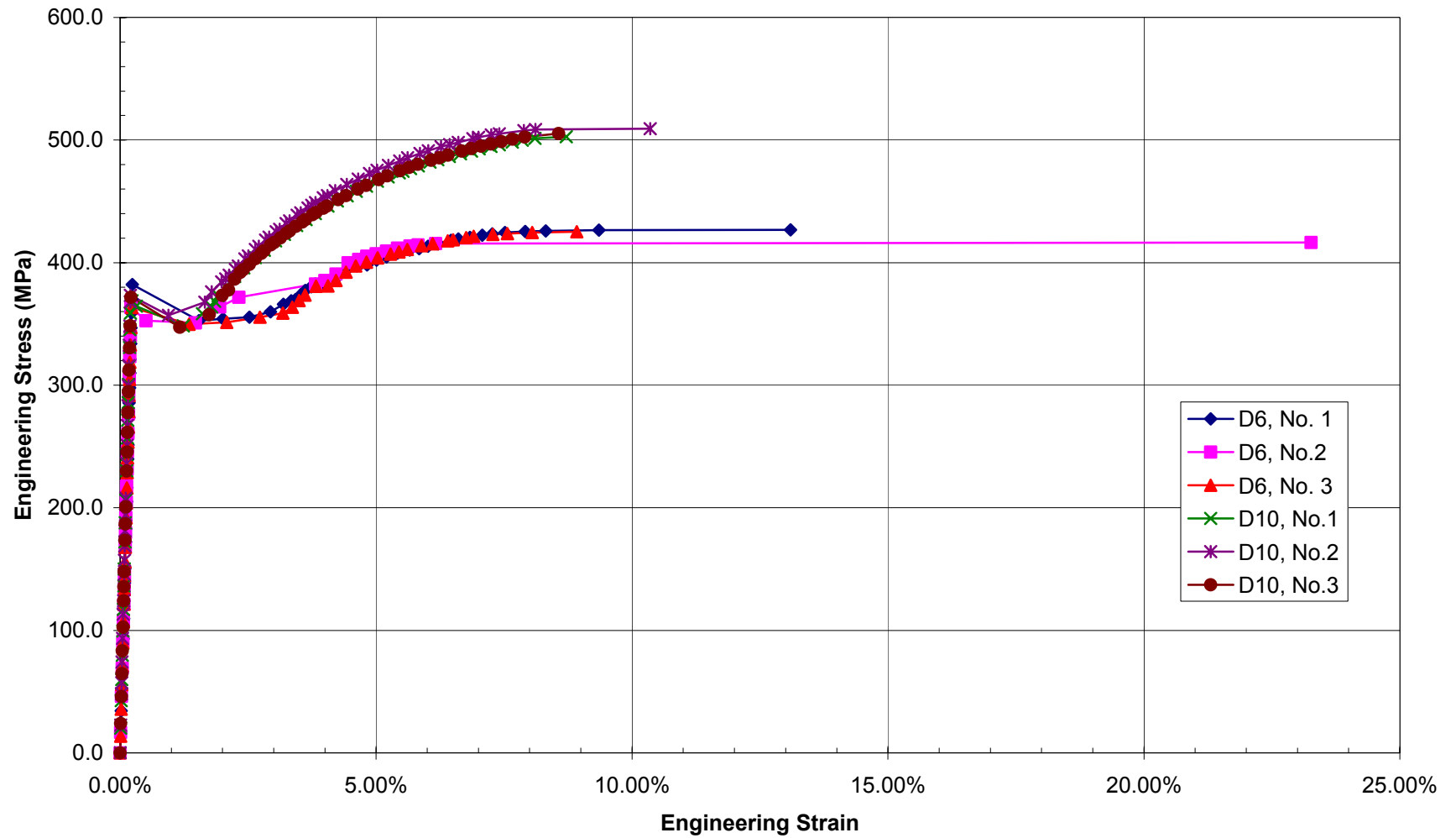
PCCV Rebar/Coupler Material Tests (ENGLISH)													
Procedures & Specifications													
JPN-14-T-1-3; Rebar Material Test Procedure; 6/14/96													
JPN-14-T-1-4; Rebar Connection Test Procedure; 6/14/96													
Spec.-T-04-2(E) Rev. 2; Specification for Reinforcement Material													
Spec.-T-04-3(E) Rev. 2; Specification for Mechanical Joint													
Data & Test Reports													
(A)JPN-21-T-5, Ancillary Test Report, Rebar Joint Test, May 20, 1997													
(B) TAP 9702; Material Property data for a mechanical model used in pre/post analyses, 4/21/97													
(C) JPN-21-T-4, Ancillary Test Report, Rebar Material Test, May 20, 1997													
(D) MH-K10-37, Tensile Test Result for #3 Position Threaded Coupler													
(E) MH-K10-38, Tensile Test Result for #6 Position Threaded Coupler													
(F) SNL Rebar Calibration Tests, February, 1999													
Component		Design Data Tests											
Mat'l Spec.													
Reinforcing Steel			Diameter	Area	Yield Stress		Ultimate Stress		Gage Length		Elongation ¹	Elastic Modulus	Stress-Strain ²
			(in.)	(in ²)	(kips)	(ksi)	(kips)	(ksi)	Initial	Final	(%)	(psi)	
Nominal (JIS G 3112)	SD345												
min.					50.03		71.05				18.0%		
max.					56.55								
Test (JIS Z 2241)			X(B)	X(B)	X(B)	X(B)	X(B)	X(B)	X(B)	X(B)	X(B)	X(B)	X(B)
(ASTM E8M-93)	D6	0.250	0.049	2.72	55.40	3.48	70.96	1.878	2.461	31.0%	2.44E+07	1.68E+05	
(G=8D, Grip=10D)		2	0.250	0.049	2.59	52.65	3.48	70.96	1.878	2.441	30.0%	2.48E+07	
		3	0.250	0.049	2.59	52.65	3.48	70.96	1.882	2.449	30.1%	2.42E+07	
		mean	0.250	0.049	2.63	53.56	3.48	70.96	1.878	2.449	30.4%	2.45E+07	
D10		1	0.375	0.111	5.91	53.46	8.81	79.69	3.138	3.839	22.3%	2.64E+07	
(G=8D, Grip=10D)		2	0.375	0.111	5.98	54.07	8.97	81.11	3.150	3.882	23.3%	2.68E+07	
		3	0.375	0.111	5.96	53.87	8.81	79.69	3.150	3.965	25.9%	2.61E+07	
		mean	0.375	0.111	5.95	53.80	8.86	80.16	3.146	3.894	23.8%	2.64E+07	
		¹ Elongation @ ultimate load based on gage length of broken bars.											
		² Stress-Strain relationship measured by 2 dia. opposed strain gages located @ center of gage length.											
		JIS Z 2441 references use of extensometer for strain measurement.											

Reinforcing Steel			Diameter	Area	Yield Stress		Ultimate Stress		Gage Length		Elongation ¹	Elastic Modulus	Stress-Strain ²
			(in.)	(in ²)	(kips)	(ksi)	(kips)	(ksi)	Initial	Final	(%)	(psi)	
Nominal (JIS G 3112)	SD390												
	min.				56.55		78.16				16.0%		
	max.			71.05									
Test (JIS Z 2241)			X(B)	X(B)	X(B)	X(B)	X(B)	X(B)	X(B)	X(B)	X(B)	X(B)	X(B)
(ASTM E8M-93)	D10	0.375	0.111	7.46	67.48	10.50	94.93	3.157	3.705	17.3%	2.65E+07	1.83E+05	
(G=8D, Grip=10D)	2	0.375	0.111	7.73	69.93	10.57	95.54	3.130	3.846	22.9%	2.68E+07		
	3	0.375	0.111	7.55	68.31	10.34	93.51	3.138	3.803	21.2%	2.64E+07		
	mean	0.375	0.111	7.58	68.57	10.47	94.66	3.142	3.783	20.5%	2.65E+07		
D13 (#4)	1	0.500	0.196	12.00	61.12	17.35	88.35	4.094	5.094	24.4%	2.65E+07		
(G=8D, Grip=10D)	2	0.500	0.196	12.54	63.86	17.42	88.70	4.091	5.055	23.6%	2.65E+07		
	3	0.500	0.196	12.39	63.06	17.40	88.58	4.094	5.102	24.6%	2.67E+07		
	mean	0.500	0.196	12.31	62.68	17.39	88.54	4.094	5.083	24.2%	2.65E+07		
D16 (#5)	1	0.626	0.308	20.43	66.37	27.54	89.44	5.039	5.772	19.4%	2.64E+07		
(G=8D, Grip=10D)	2	0.626	0.308	20.52	66.66	27.65	89.80	5.047	5.803	24.1%	2.67E+07		
	3	0.626	0.308	20.32	66.00	27.38	88.93	5.035	5.768	22.7%	2.67E+07		
	mean	0.626	0.308	20.43	66.34	27.52	89.39	5.039	5.780	22.1%	2.65E+07		
D16 (#5)	1	0.492	0.190	14.84	78.00	19.74	103.76	1.957	2.500	27.8%	3.03E+07		
(dumbbell)	2	0.492	0.190	14.34	75.40	19.83	104.23	1.969	2.480	26.0%	3.03E+07		
(D x G = 0.5 x 2.0)	3	0.492	0.190	14.25	74.92	19.74	103.76	1.969	2.508	27.4%	3.03E+07		
	mean	0.492	0.190	14.48	76.11	19.77	103.92	1.965	2.496	27.1%	3.03E+07		
D19 (#6)	1	0.752	0.444	30.39	68.43	42.31	95.25	5.992	7.146	19.3%	2.65E+07		
(G=8D, Grip=10D)	2	0.752	0.444	30.48	68.63	42.44	95.56	5.992	7.240	20.8%	2.65E+07		
	3	0.752	0.444	30.53	68.73	42.44	95.56	5.980	7.370	23.2%	2.70E+07		
	mean	0.752	0.444	30.46	68.60	42.40	95.45	5.988	7.252	21.1%	2.67E+07		
D22 (#7)	1	0.874	0.600	39.70	66.15	59.28	98.77	6.929	7.886	16.8%	2.76E+07		
(G=8D, Grip=10D)	2	0.874	0.600	39.99	66.64	59.32	98.85	6.929	7.965	20.0%	2.77E+07		
	3	0.874	0.600	40.13	66.86	59.12	98.51	6.933	7.957	19.1%	2.78E+07		
	mean	0.874	0.600	39.95	66.56	59.23	98.72	6.929	7.937	18.7%	2.77E+07		
D22 (#7)	1	0.551	0.239	16.41	68.80	25.56	107.16	2.000	2.508	25.4%	3.05E+07		
(dumbbell)	2	0.551	0.239	16.50	69.14	25.18	105.56	1.992	2.512	26.1%	3.02E+07		
(D x G = 0.5 x 2.0)	3	0.551	0.239	15.92	66.73	25.85	108.32	2.020	2.551	26.3%	3.02E+07		
	mean	0.551	0.239	16.28	68.22	25.54	107.01	2.004	2.524	25.9%	3.03E+07		
		¹ Elongation @ ultimate load based on gage length of broken bars.											
		² Stress-Strain relationship measured by 2 dia.opossed strain gages located @ center of gage length.											
		JIS Z 2441 references use of extensometer for strain measurement.											

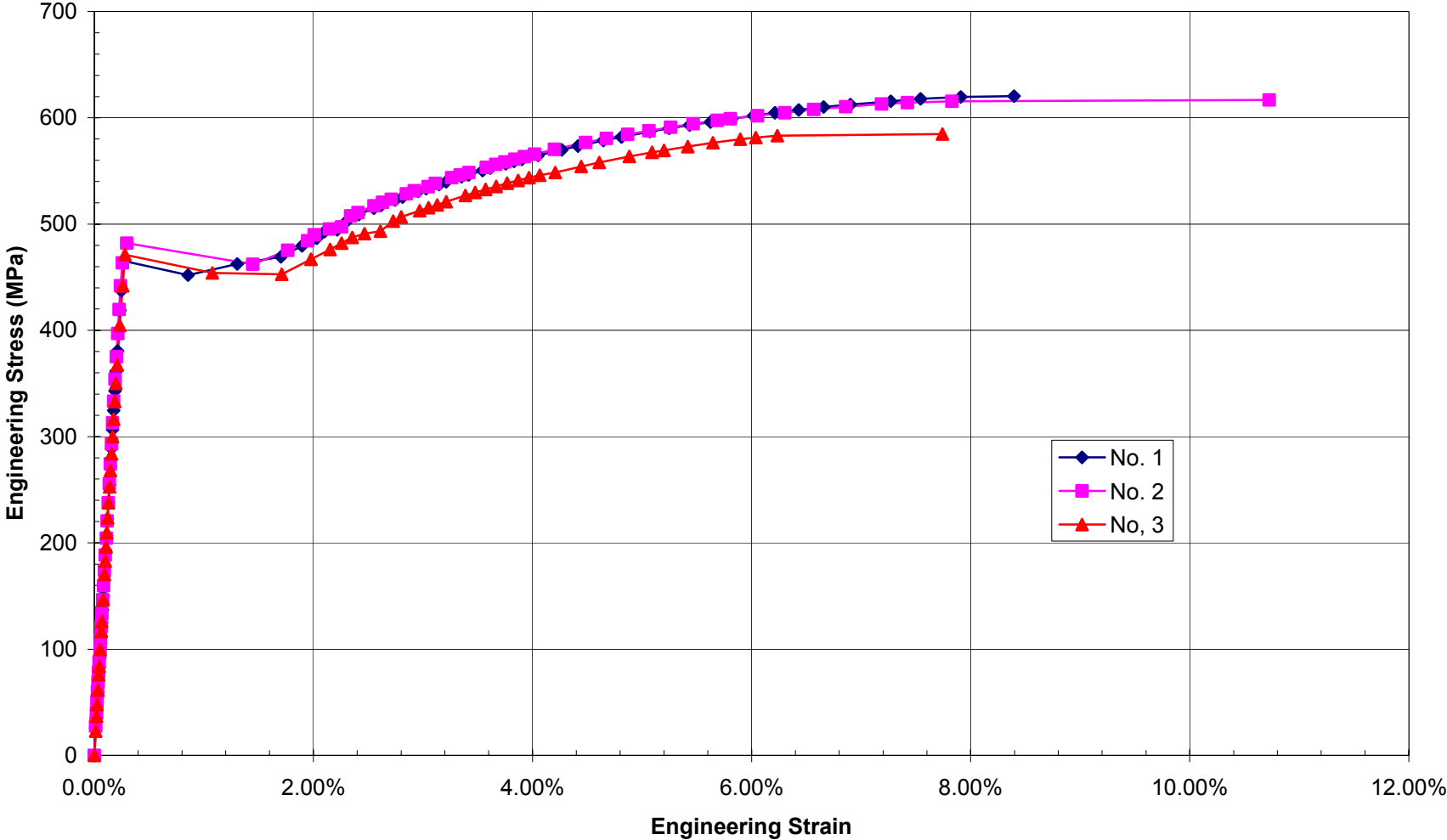
Reinforcing Steel			Diameter	Area	Yield Stress		Ultimate Stress		Gage Length		Elongation ¹	Elastic Modulus	Stress-Strain ²
			(in.)	(in ²)	(kips)	(ksi)	(kips)	(ksi)	Initial	Final	(%)	(psi)	
Nominal (JIS G 3112)	SD490												
min.					71.05		89.61				12.0%		
max.					89.90								
Test (JIS Z 2241)			X(B)	X(B)	X(B)	X(B)	X(B)	X(B)	X(B)	X(B)	X(B)	X(B)	X(B)
(ASTM E8M-93)	D10	0.375	0.111	7.89	71.35	10.70	96.76	3.138	3.854	22.8%	2.70E+07	1.86E+05	
(G=8D, Grip=10D)		2	0.375	0.111	7.87	71.15	10.61	95.95	3.142	3.760	19.7%	2.71E+07	
		3	0.375	0.111	7.87	71.15	10.72	96.96	3.150	3.835	21.8%	2.71E+07	
		mean	0.375	0.111	7.87	71.21	10.68	96.56	3.142	3.815	21.4%	2.71E+07	
D13		1	0.500	0.196	15.56	79.20	21.31	108.49	4.094	4.831	18.0%	2.65E+07	
(G=8D, Grip=10D)		2	0.500	0.196	15.56	79.20	21.38	108.84	4.091	4.783	16.9%	2.68E+07	
		3	0.500	0.196	15.74	80.11	21.51	109.52	4.094	4.685	14.4%	2.68E+07	
		mean	0.500	0.196	15.62	79.50	21.40	108.95	4.094	4.768	16.4%	2.67E+07	
D16		1	0.626	0.308	21.63	79.01	30.19	98.05	5.047	5.642	17.0%	2.67E+07	
(G=8D, Grip=10D)		2	0.626	0.308	23.00	79.01	31.22	101.41	5.039	5.634	15.2%	2.70E+07	
		3	0.626	0.308	22.32	79.92	30.78	99.95	5.039	5.693	19.0%	2.67E+07	
		mean	0.626	0.308	22.32	79.32	30.73	99.80	5.043	5.657	17.1%	2.68E+07	
D16		1	0.492	0.190	15.56	79.01	21.87	114.99	1.953	2.445	25.2%	3.07E+07	
(dumbbell)		2	0.492	0.190	15.15	79.01	21.76	114.39	1.976	2.445	23.7%	3.05E+07	
(D x G = 12.5 x 50)		3	0.492	0.190	15.35	79.92	21.51	113.10	1.965	2.449	24.6%	3.03E+07	
		mean	0.492	0.190	15.35	79.32	21.72	114.16	1.965	2.445	24.5%	3.05E+07	
D19		1	0.752	0.444	32.91	74.10	45.72	102.94	5.972	7.031	17.7%	2.68E+07	
(G=8D, Grip=10D)		2	0.752	0.444	33.09	74.50	45.59	102.65	5.980	6.988	16.9%	2.71E+07	
		3	0.752	0.444	32.96	74.20	45.81	103.14	5.976	7.094	18.7%	2.70E+07	
		mean	0.752	0.444	32.98	74.27	45.70	102.91	5.976	7.039	17.8%	2.70E+07	
			¹ Elongation @ ultimate load based on gage length of broken bars.										
			² Stress-Strain relationship measured by 2 dia.opposed strain gages located @ center of gage length.										
			JIS Z 2441 references use of extensometer for strain measurement.										

[illegible]

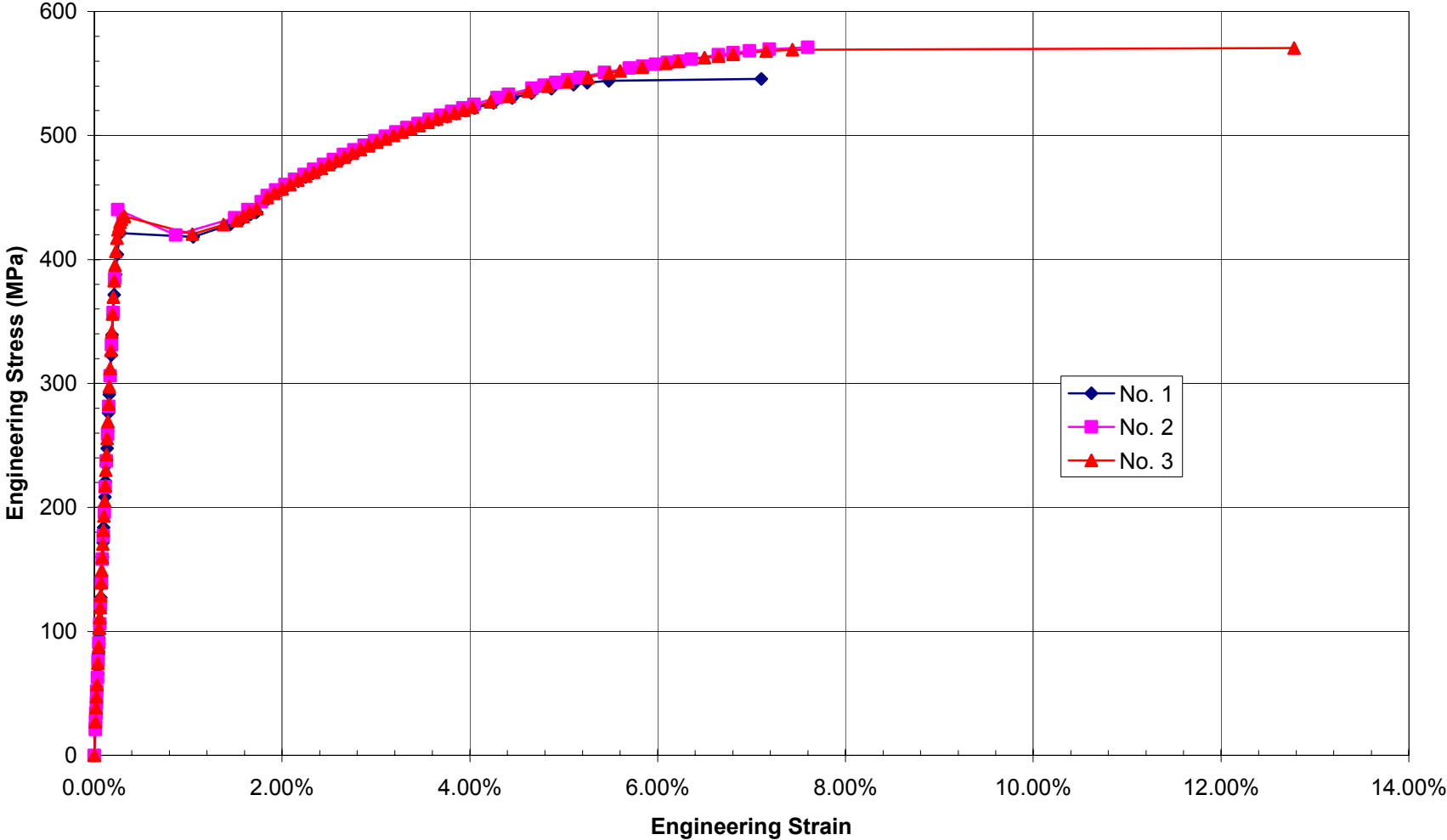
SD345, D6 (#2) & D10 (#3) Stress-Strain



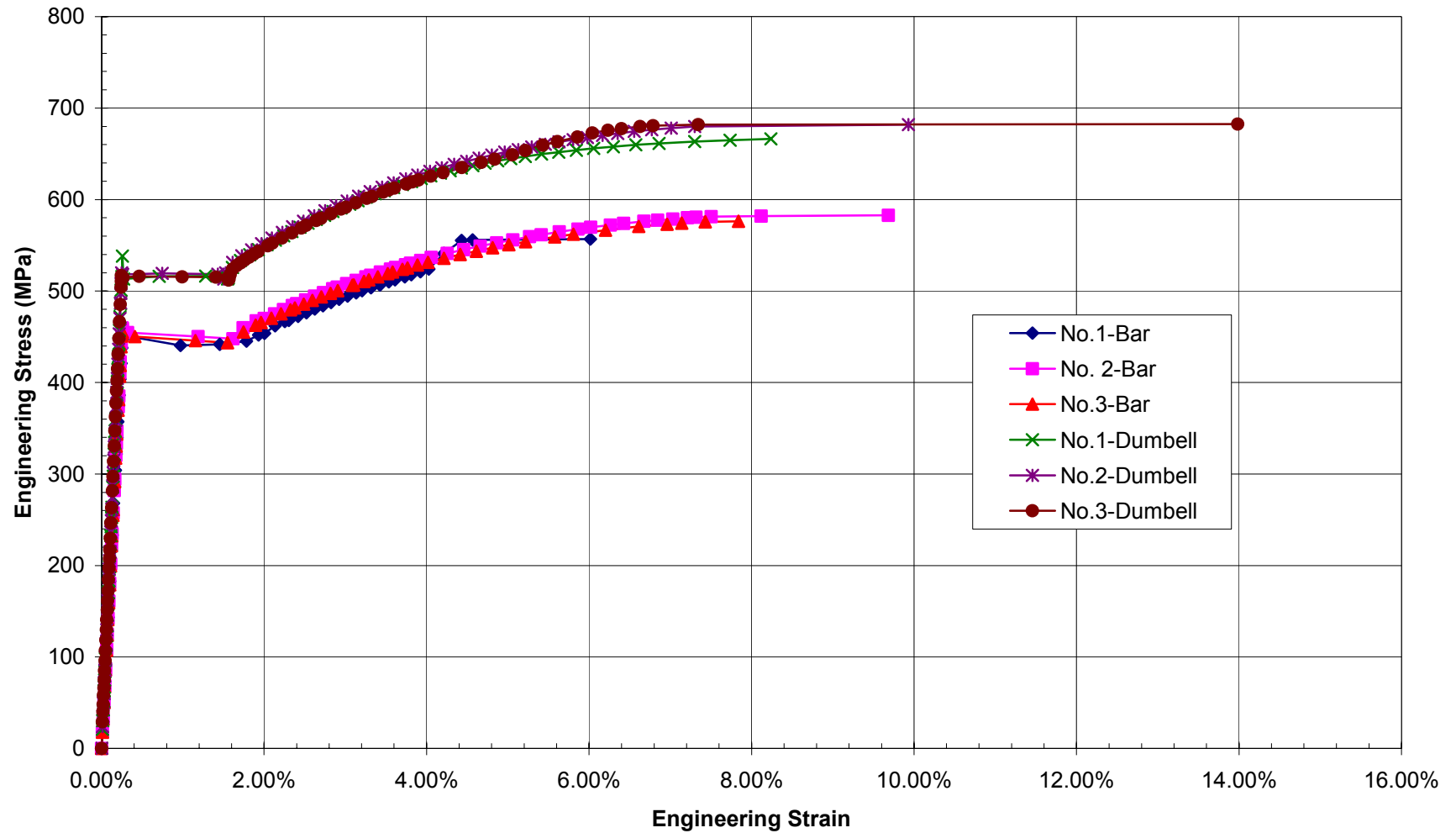
SD390, D10 (#3) Stress-Strain



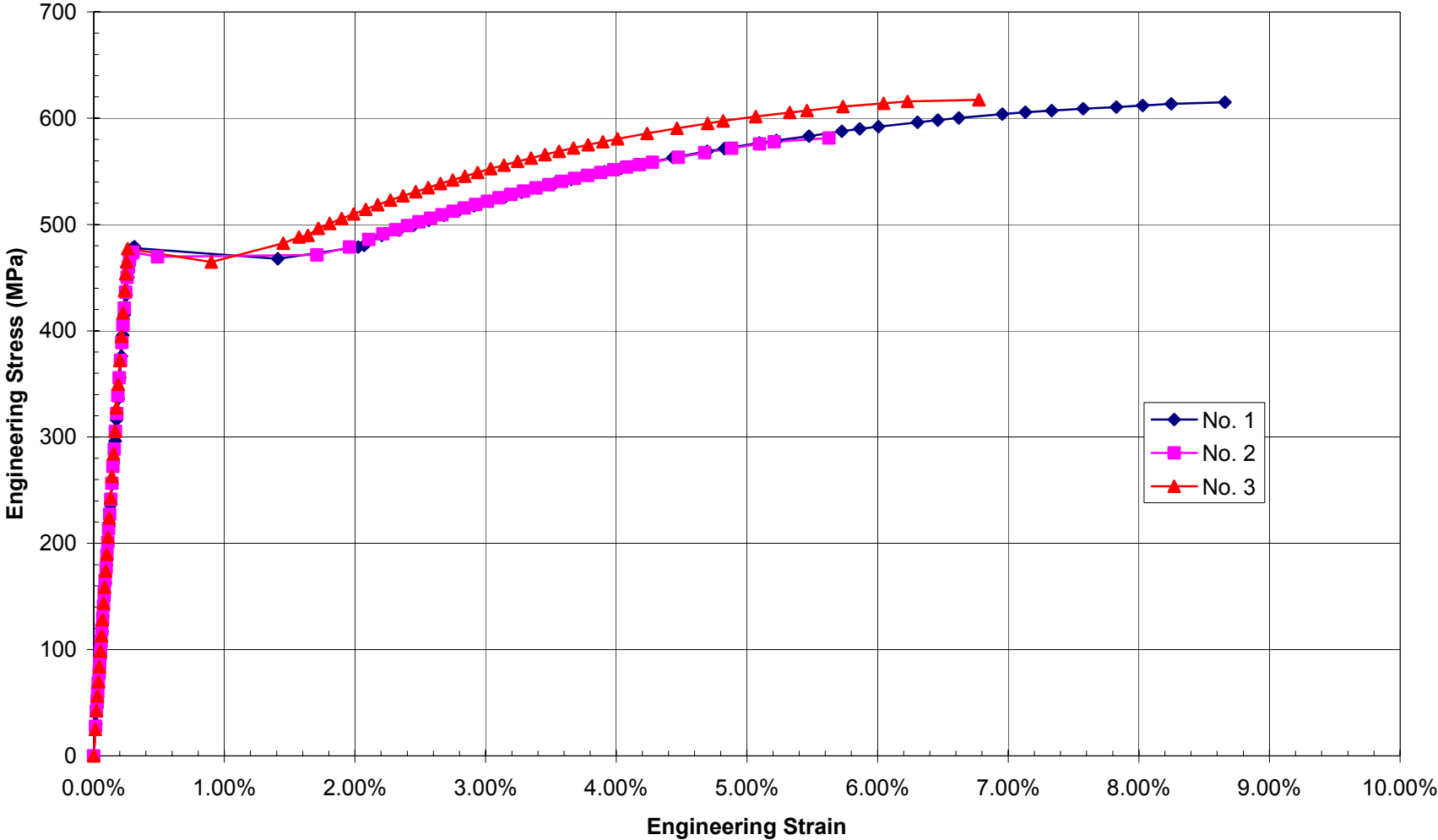
SD390, D13 (#4) Stress-Strain



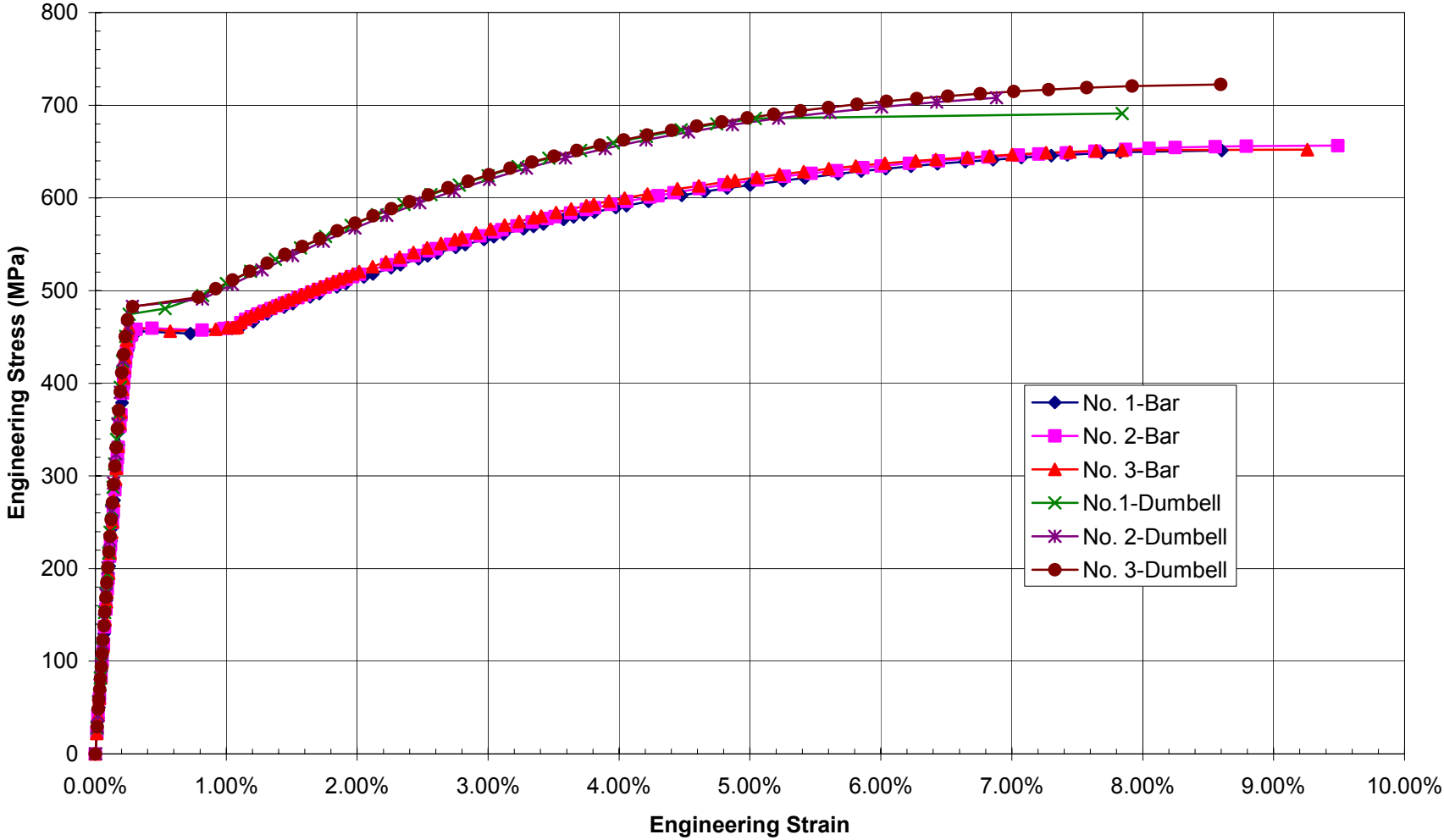
SD390, D16 (#5) Stress-Strain



SD390, D19 (#6) Stress-Strain

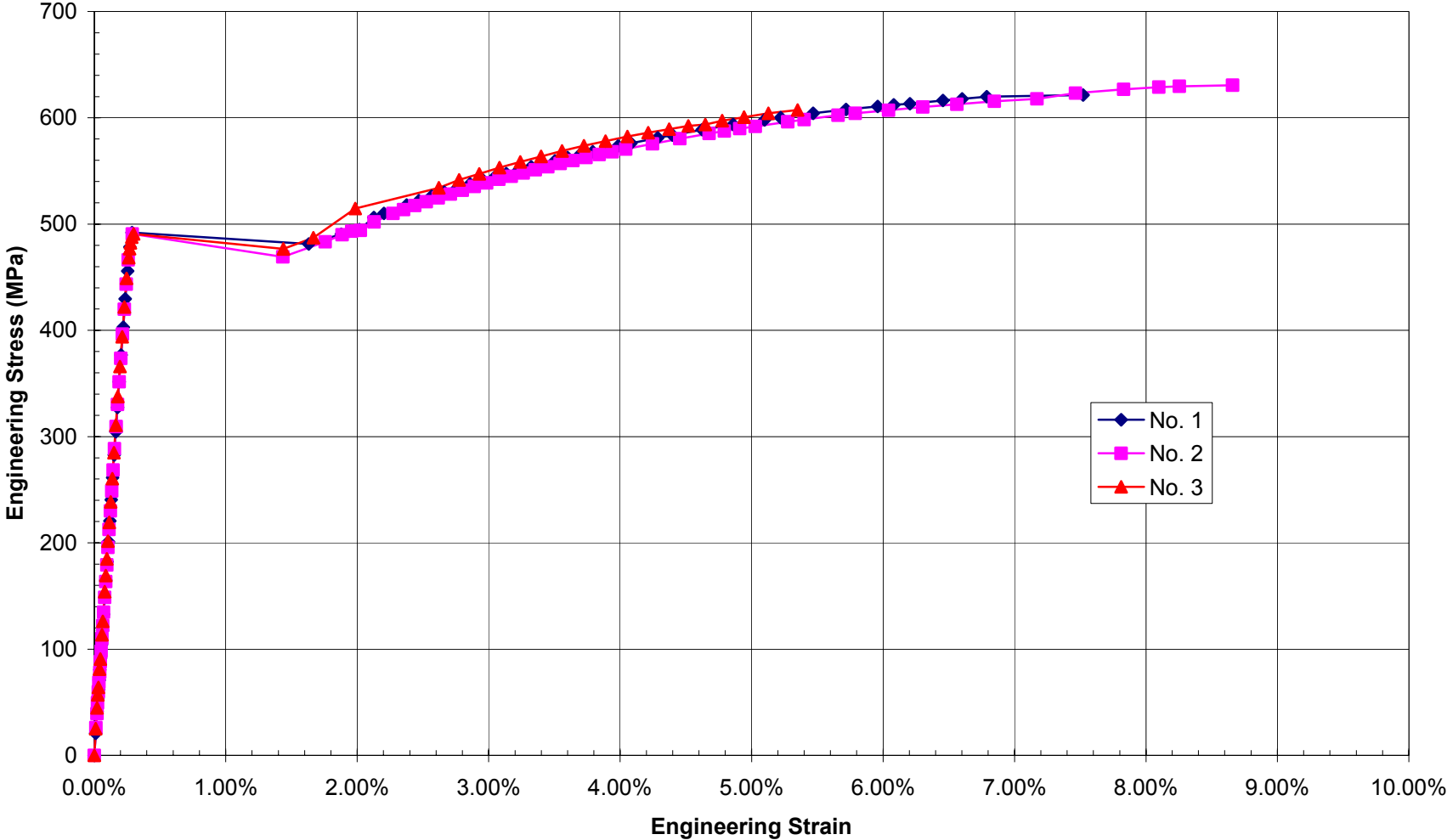


SD390, D22 (#7) Stress-Strain



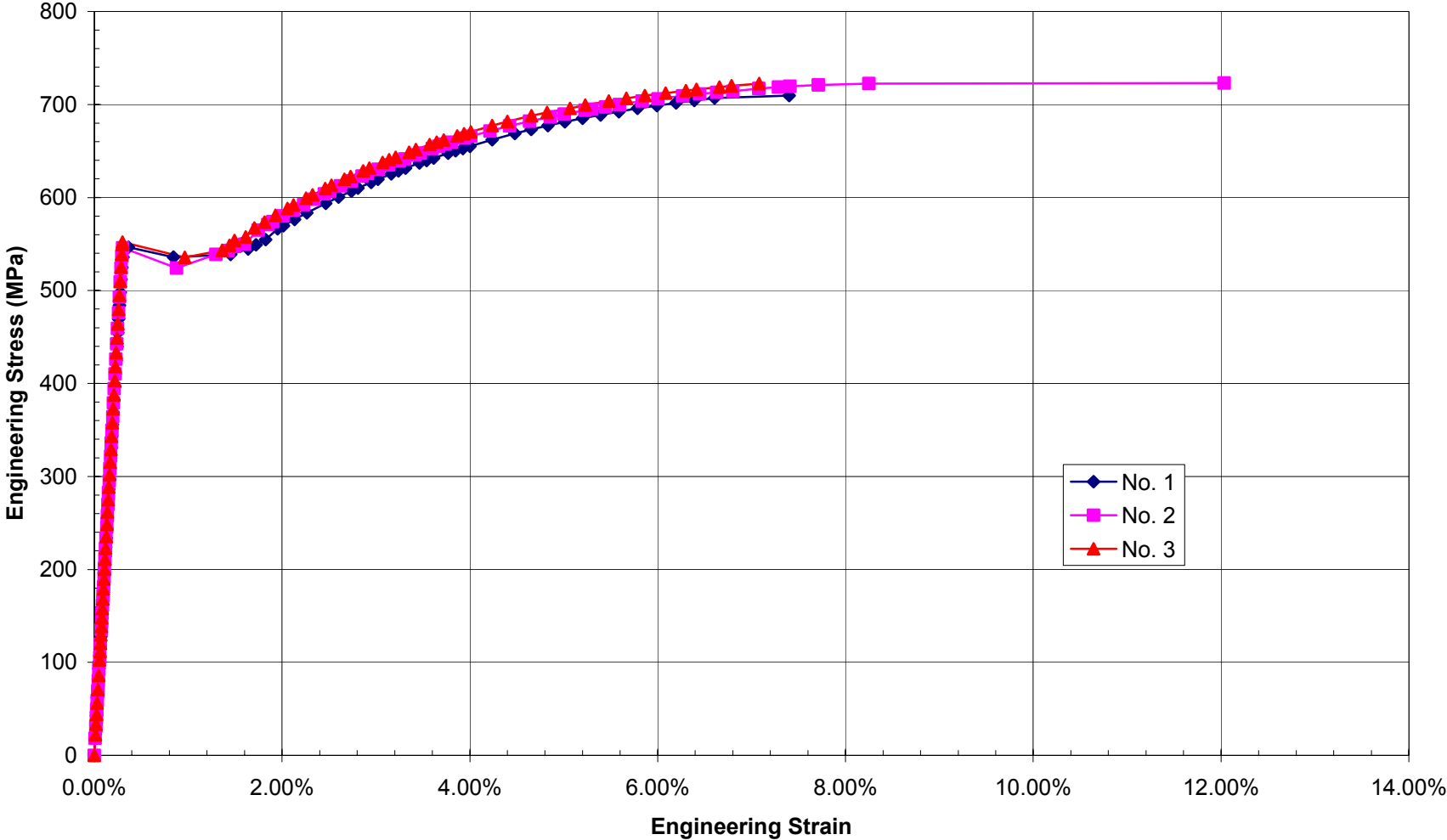
B-50

SD490, D10 (#3) Stress-Strain



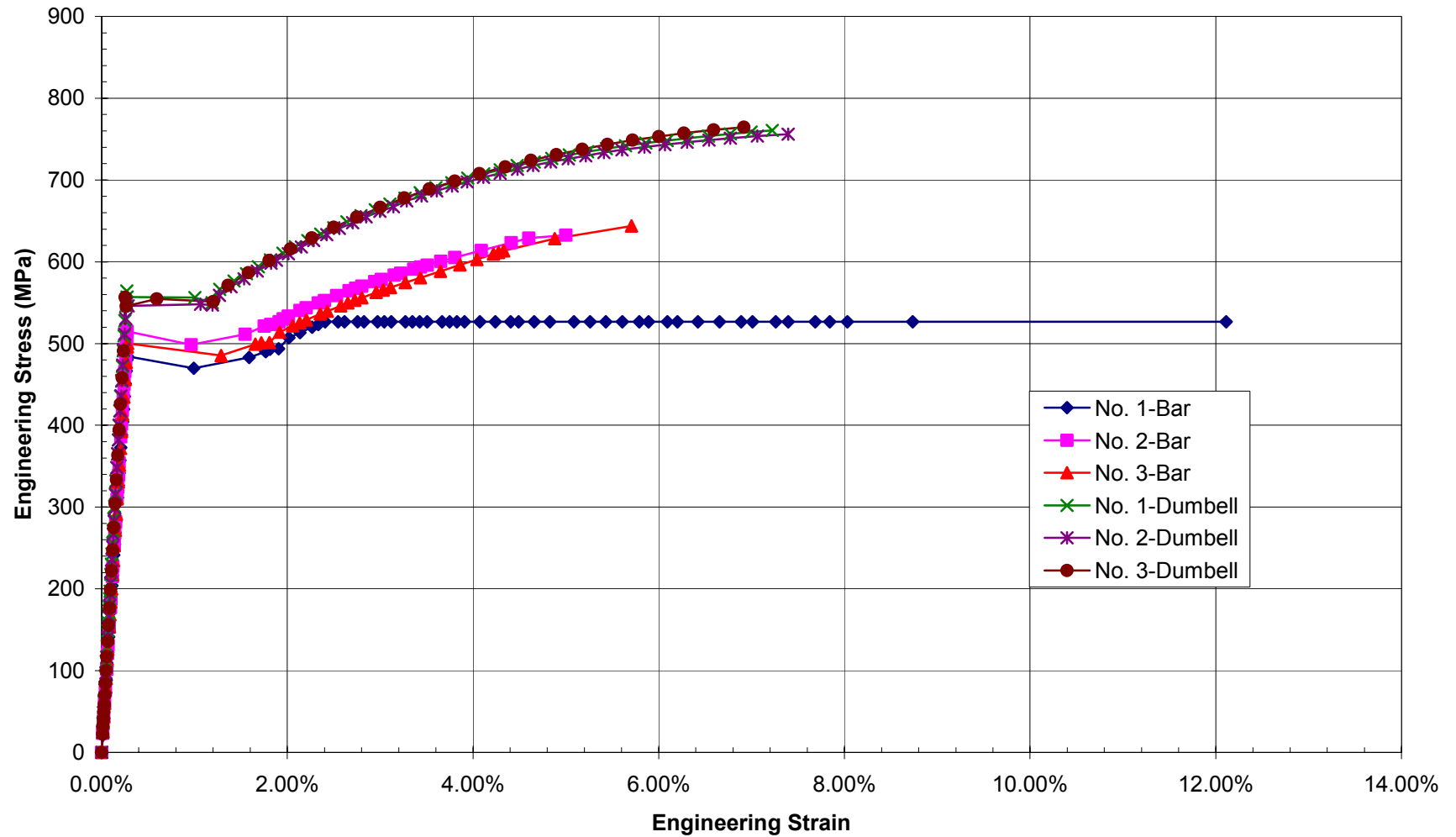
B-51

SD490, D13 (#4) Stress-Strain

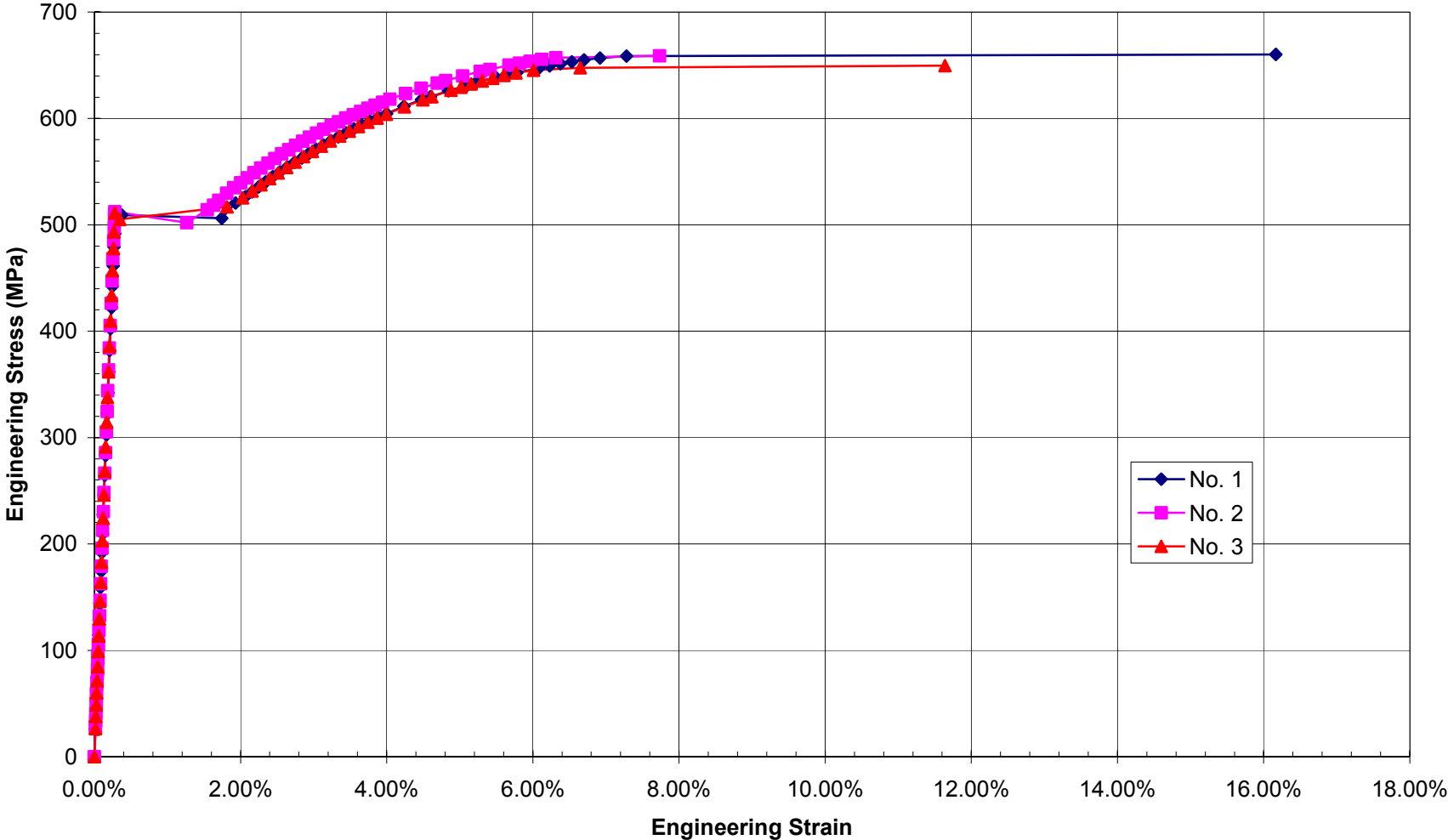


B-52

SD490, D16 (#5) Stress-Strain



SD490, D19 (#6) Stress-Strain



Section v. Tendons

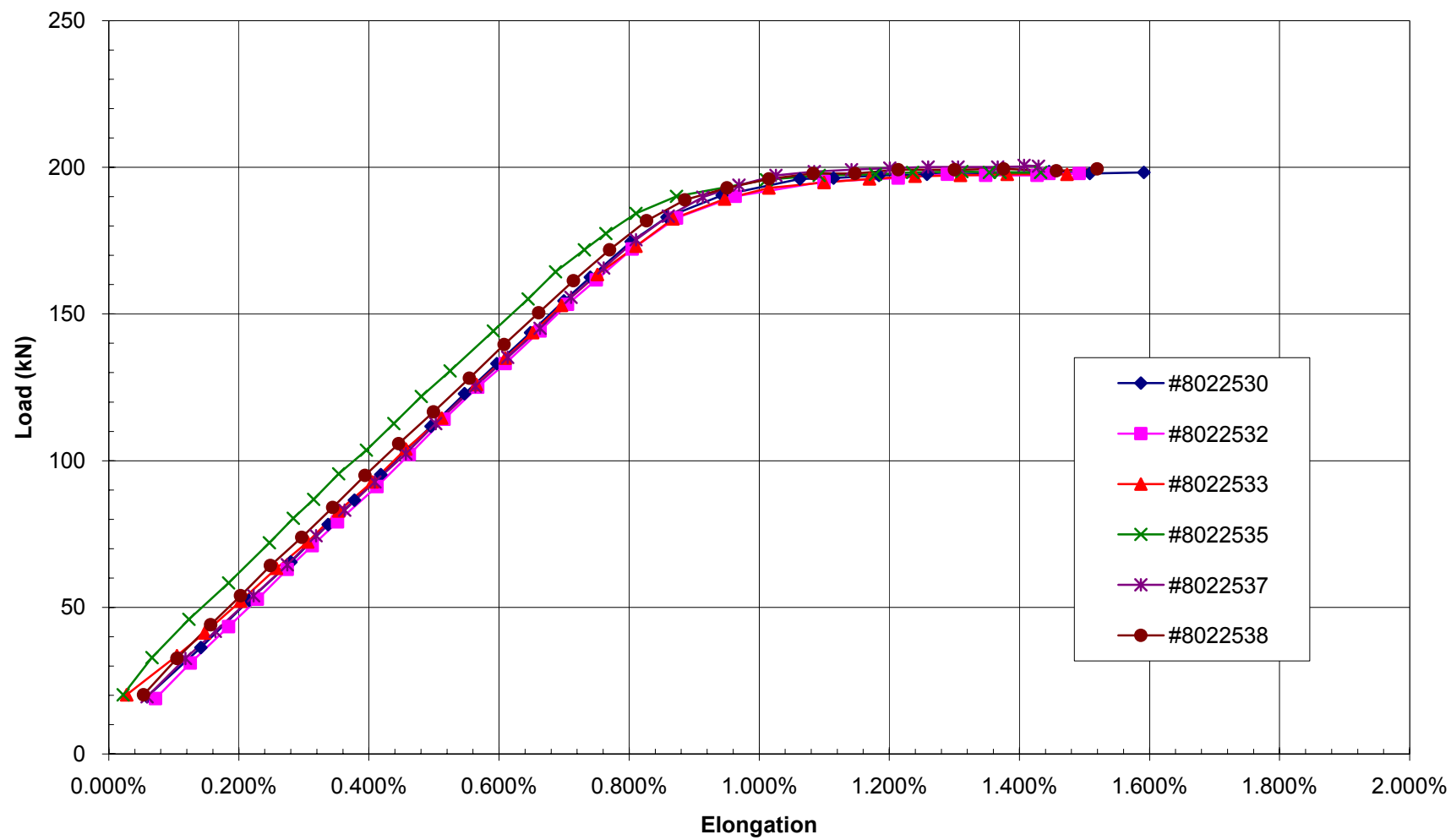
PCCV Tendon Material Tests (METRIC)												
Procedures & Specifications						Data & Test Reports						
1. JPN-12-T-2: Outline of Ancillary Tests						(A) JPN-12-T-3: "The Result of Trial Manufacturing of Tendon System" Electronic Data on the Server						
2. JPN-14-T-1-5; Tendon Material Test Procedure;Rev.1;9/30/96						(B) JPN-18-T-4; Tendon Friction Coefficient and Set Loss Verification Test; 5/14/96						
3. JPN-14-T-1-7; Prestressing Tendon Tensile Test Procedure;Rev.1; 9/30/96						(C)MH-K10-26 Tendon Material Test Report; June 1998						
4. Spec.-T-05-2(E), Rev.1; Specification for PC Materials						(D) MH-K10-40, Tendon System Test Report						
Component	Material Specifications											
			Diameter (mm)	Pitch	Dia. Diff. (mm)	Weight (kg)	Yield ¹ (kN)	Ultimate (kN)	Elongation ² (%)	Relaxation (% per 1000 hr)		
Raw Material:	SWRS82B per JIS G3502	min.	13.5	12	0.08		190	210	4.50%			
Strand:	SWPR7BL per JIS G3536	nom.	13.7									
		max.	14.1	18						1.50%		
Sample Tendon System Test (1, A)										Load-Elong. ³		
										Stress-Strain		
Tendon Strand Material Test (2, C)												
JIS G 3536 (G=600mm)		8022530	13.62	14.1	0.10	2565	197	213	8.4%	Elong. Only		
		8022531	13.60	14.1	0.10	2561						
		8022532	13.60	14.1	0.09	2561	196	214	8.0%	Elong. Only		
		8022533	13.61	14.0	0.11	2563	195	214	8.3%	Elong. & Strain		
		8022534	13.60	14.1	0.10	2553						
		8022535	13.61	14.2	0.10	2565	197	214	8.3%	Elong. Only		
		8022536	13.60	14.2	0.11	2561						
		8022537	13.60	14.0	0.10	2564	199	214	8.3%	Elong. & Strain		
		8022538	13.60	14.1	0.10	2559	198	214	8.3%	Elong. Only		
		¹ Load at 0.2% permanent Elongation										
		² [(Stroke @ breakage - Stroke @10%Min. Strength)/Initial Distance bet. Grips]+0.1%										
		³ Elongation determined from stroke of testing machine(?); Strain from strain gages mounted on individual wires.										
Tendon Sytem Test (3, D)						Ultimate		Displacement		Elongation ¹		
Anchorhead:	S55CN per JIS G4051		Diameter	Pitch	Dia. Diff.	Jack	Load Cell	Load End	Fixed End		Elastic Modulus	
Bearing Plate	SS400 per JIS G3101		(mm)		(mm)	(kN)	(kN)	(mm)	(mm)	(%)	(kN/mm2)	
Sheath:	SGCC per JIS G3302	min.	13.5	12	0.08		210			4.50%		
Wedge:	SCM415 per JIS G4105	nom.	13.7									
Strand:	SWPR7BL per JIS G3536	max.	14.1	18								
Strand:	JIS G 3536 (G=600mm)		13.6	14.2	0.11		215			7.7%	191	
Tendon:		min.				630	630			2.0%		
												Load-Elong. ²
												Stress-Strain
		1				653	641	286.49	5.02	3.94%	Elong. & Strain	
		2				647	637	281.27	4.92	3.87%	Elong. & Strain	
		3				647	637	267.25	4.98	3.67%	Elong. & Strain	
		Avg.				649	638	278.34	4.97	3.83%		
		¹ Elongation = (Load End Displacement - Fixed End Displacement)/(7150mm)										
² Strain measured using three strain gages each on wires of three strands, not corrected for pitch of wire.												

Tendon Friction and Set Loss Test (B)											
Average Friction Coefficient:		0.21									
Setting Loss			Anchor Force			Set					
		Tendon	Before	After	Loss	Strand 1	Strand 2	Strand 3	Avg.		
			(kN)	(kN)	(kN)	(mm)	(mm)	(mm)	(mm)		
		#1	481.4	383.2	98.2	4.7	5.1	4.1	4.6		
		#2	464.5	374.2	90.3	4.7	4.9	4.7	4.8		
		#3	473.8	385.9	87.9	4.8	4.4	4.9	4.7		
		Average:			92.1				4.7		
Tendon Strand Calibration Tests											
JIS G 3536 (G=600mm)			Diameter	Yield ¹	Ultimate	Elongation			Elastic Modulus ⁵		
			(mm)	(kN)	(kN)	Stroke ²	Tensmeg ³	WSG ⁴	(N/mm2)		
					(%)	(%)	(%)				
Strand:	SWPR7BL per JIS G3536	min.	13.5	190	210	4.50%					
		nom.	13.7								
		max.	14.1								
		1		191.3	208.4	5.6%	4.2%	4.2%	203448		
		2 ⁷		189.9	192.5	3.6%	1.5%	1.6%	193103		
		3		191.7	209.7	6.1%	4.4%	4.5%	200000		
		4		191.3	210.8	6.6%	4.5%	4.9%	197931		
		5 ⁸	13.6								
		6 ⁸	13.6								
		7		191.3	210.7	6.5%	4.9%	5.0%	200000		
		8		190.8	210.0	5.8%	4.5%	4.5%	195172		
		9		191.3	210.5	6.4%	na	4.9%	195862		
		10		191.3	209.1	5.7%	na	4.3%	201379		
		Average	13.6	191.3	209.9	6.1%	4.5%	4.6%	199113		
		¹ Load at 0.2% permanent Elongation using Offset Method									
		² [(Stroke @ breakage - Stroke @10%Min. Strength)/Initial Distance bet. Grips]+0.1%									
		³ Final Tensmeg reading									
		⁴ Final average wire strain gage (WSG) reading									
		⁵ Slope of Stress versus Extensometer Strain between 140 MPa and 1400 MPa									
⁶ Elongation & Strain determined from calibrated extensometer											
⁷ Strand #2 experienced some grip slippage causing premature failure (data not included in averages)											
⁸ Strands #5 and #6 will be tested just prior to PCCV pressure testing											

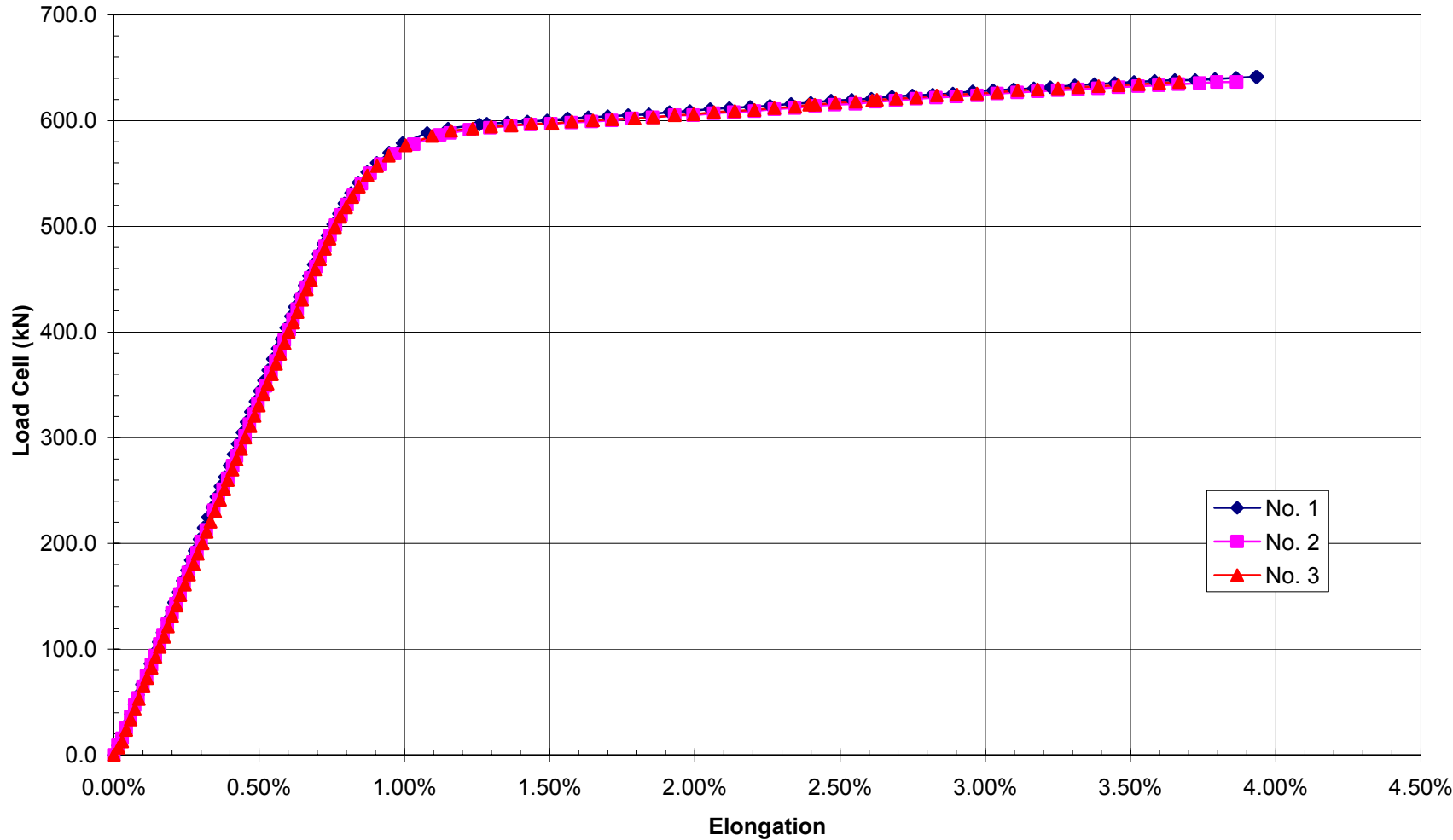
PCCV Tendon Material Tests (ENGLISH)												
Procedures & Specifications						Data & Test Reports						
1. JPN-12-T-2: Outline of Ancillary Tests						(A) JPN-12-T-3: "The Result of Trial Manufacturing of Tendon System" Electronic Data on the Server						
2. JPN-14-T-1-5; Tendon Material Test Procedure;Rev.1;9/30/96						(B) JPN-18-T-4; Tendon Friction Coefficient and Set Loss Verification Test; 5/14/96						
3. JPN-14-T-1-7; Prestressing Tendon Tensile Test Procedure;Rev.1; 9/30/96						(C)MH-K10-26 Tendon Material Test Report; June 1998						
4. Spec.-T-05-2(E), Rev.1; Specification for PC Materials						(D) MH-K10-40, Tendon System Test Report						
Component	Material Specifications		Diameter (in)	Pitch	Dia. Diff. (in)	Weight (lbs)	Yield ¹ (kips)	Ultimate (kips)	Elongation ² (%)	Relaxation (% per 1000 hr)		
Raw Material:	SWRS82B per JIS G3502	min.	0.531	12	0.003		42.7	47.2	4.50%			
Strand:	SWPR7BL per JIS G3536	nom.	0.539									
		max.	14.1	0.555	18					1.50%		
Sample Tendon System Test (1, A)										Load-Elong. ³		
										Stress-Strain		
Tendon Strand Material Test (2, C)												
JIS G 3536 (G=600mm)		8022530	0.536	14.1	0.004	5655	44.3	47.9	8.4%	Elong. Only		
		8022531	0.535	14.1	0.004	5646						
		8022532	0.535	14.1	0.004	5646	44.1	48.1	8.0%	Elong. Only		
		8022533	0.536	14.0	0.004	5650	43.8	48.1	8.3%	Elong. & Strain		
		8022534	0.535	14.1	0.004	5628						
		8022535	0.536	14.2	0.004	5655	44.3	48.1	8.3%	Elong. Only		
		8022536	0.535	14.2	0.004	5646						
		8022537	0.535	14.0	0.004	5653	44.7	48.1	8.3%	Elong. & Strain		
	8022538	0.535	14.1	0.004	5642	44.5	48.1	8.3%	Elong. Only			
¹ Load at 0.2% permanent Elongation												
² [(Stroke @ breakage - Stroke @10%Min. Strength)/Initial Distance bet. Grips]+0.1%												
³ Elongation determined from stroke of testing machine(?); Strain from strain gages mounted on individual wires.												
Tendon Sytem Test (3, D)						Ultimate		Displacement		Elongation ¹		
Anchorhead:	S55CN per JIS G4051		Diameter (in)	Pitch	Dia. Diff. (in)	Jack (kips)	Load Cell (kips)	Load End (in)	Fixed End (in)	(%)	Elastic Modulus (kN/mm2)	
Bearing Plate	SS400 per JIS G3101											
Sheath:	SGCC per JIS G3302	min.	0.531	12	0.003		47.2			4.50%		
Wedge:	SCM415 per JIS G4105	nom.	0.539									
Strand:	SWPR7BL per JIS G3536	max.	0.555	18								
Strand:	JIS G 3536 (G=600mm)		0.535	14.2	0.004		48.3			7.7%	27695	
Tendon:		min.				141.6	141.6			2.0%		
											Load-Elong. ²	
											Stress-Strain	
		1					146.8	144.1	11.279	0.198	3.94%	Elong. & Strain
		2					145.4	143.2	11.074	0.194	3.87%	Elong. & Strain
		3					145.4	143.2	10.522	0.196	3.67%	Elong. & Strain
		Avg.					145.9	143.5	10.958	0.196	3.83%	
¹ Elongation = (Load End Displacement - Fixed End Displacement)/(7150mm)												
² Strain measured using three strain gages each on wires of three strands. not corrected for pitch of wire.												

Tendon Friction and Set Loss Test (B)											
Average Friction Coefficient:		0.21									
Setting Loss			Anchor Force			Set					
		Tendon	Before	After	Loss	Strand 1	Strand 2	Strand 3	Avg.		
			(kips)	(kips)	(kips)	(in)	(in)	(in)	(in)		
		#1	108.2	86.1	22.1	0.184	0.200	0.162	0.182		
		#2	104.4	84.1	20.3	0.186	0.193	0.187	0.189		
		#3	106.5	86.8	19.8	0.187	0.174	0.191	0.184		
		Average:			20.7				0.185		
Tendon Strand Calibration Tests											
JIS G 3536 (G=600mm)			Diameter	Yield ¹	Ultimate	Elongation		Elastic Modulus ⁵			
			(in)	(kips)	(kips)	Stroke ²	Tensmeg ³	WSG ⁴	(ksi)		
						(%)	(%)	(%)			
Strand:	SWPR7BL per JIS G3536	min.	0.531	42.7	47.2	4.50%					
		nom.	0.539								
		max.	0.555								
		1		43.0	46.85	5.6%	4.2%	4.2%	29500		
		2 ⁷		42.7	43.27	3.6%	1.5%	1.6%	28000		
		3		43.1	47.14	6.1%	4.4%	4.5%	29000		
		4		43.0	47.38	6.6%	4.5%	4.9%	28700		
		5 ⁸	0.535								
		6 ⁸	0.535								
		7		43.0	47.36	6.5%	4.9%	5.0%	29000		
		8		42.9	47.21	5.8%	4.5%	4.5%	28300		
		9		43.0	47.31	6.4%	na	4.9%	28400		
		10		43.0	47.00	5.7%	na	4.3%	29200		
		Average	0.535	43.0	47.18	6.1%	4.5%	4.6%	28871		
		¹ Load at 0.2% permanent Elongation using Offset Method									
		² [(Stroke @ breakage - Stroke @10%Min. Strength)/Initial Distance bet. Grips]+0.1%									
		³ Final Tensmeg reading									
		⁴ Final average wire strain gage (WSG) reading									
⁵ Slope of Stress versus Extensometer Strain between 140 MPa and 1400 MPa											
⁶ Elongation & Strain determined from calibrated extensometer											
⁷ Strand #2 experienced some grip slippage causing premature failure (data not included in averages)											
⁸ Strands #5 and #6 will be tested just prior to PCCV pressure testing											

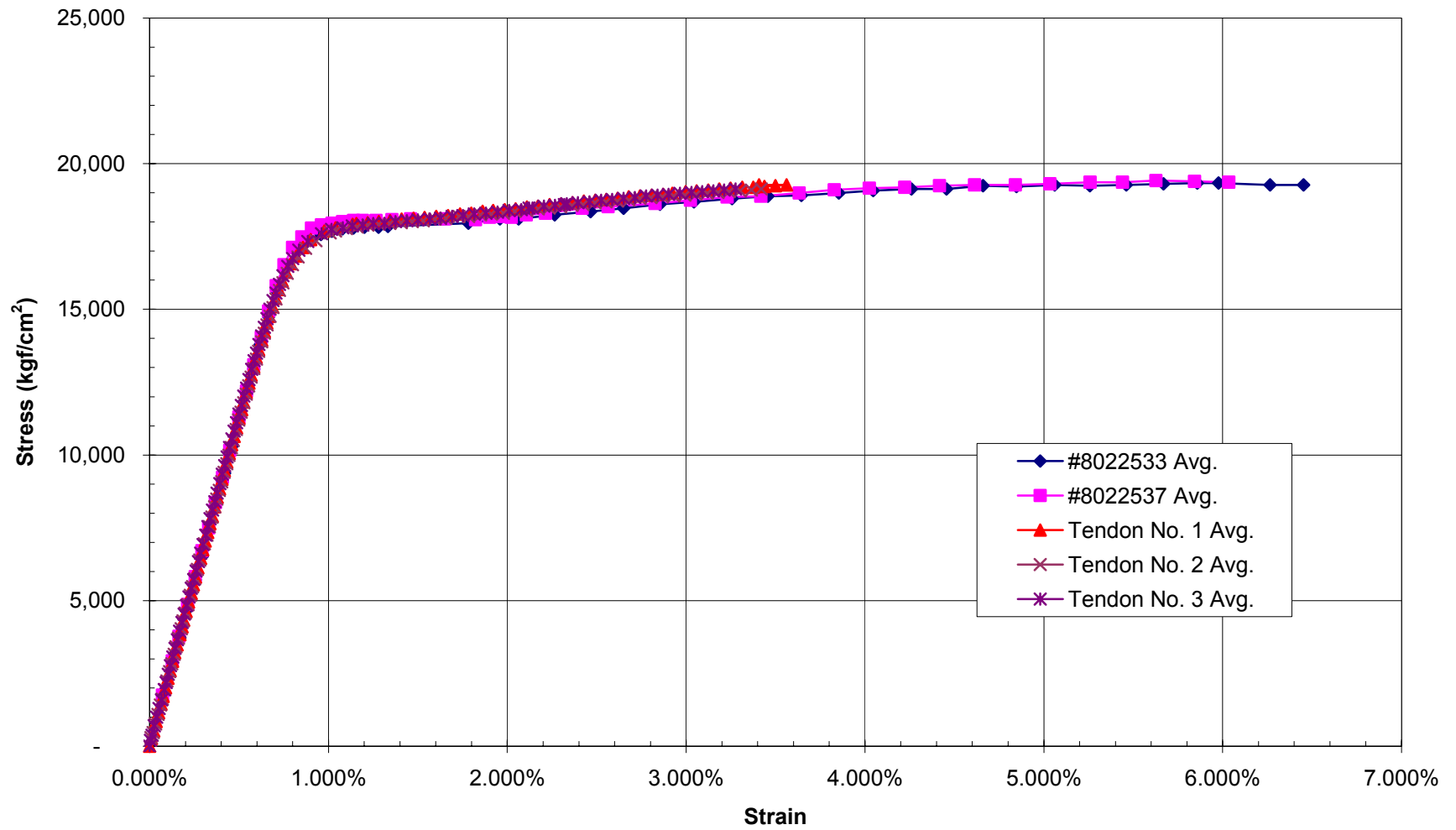
Tendon Strand (SWPR7BL), Load-Elongation



Tendon System Load-Elongation



Strand & Tendon Stress-Strain



Appendix C: As-Built Model Survey Data

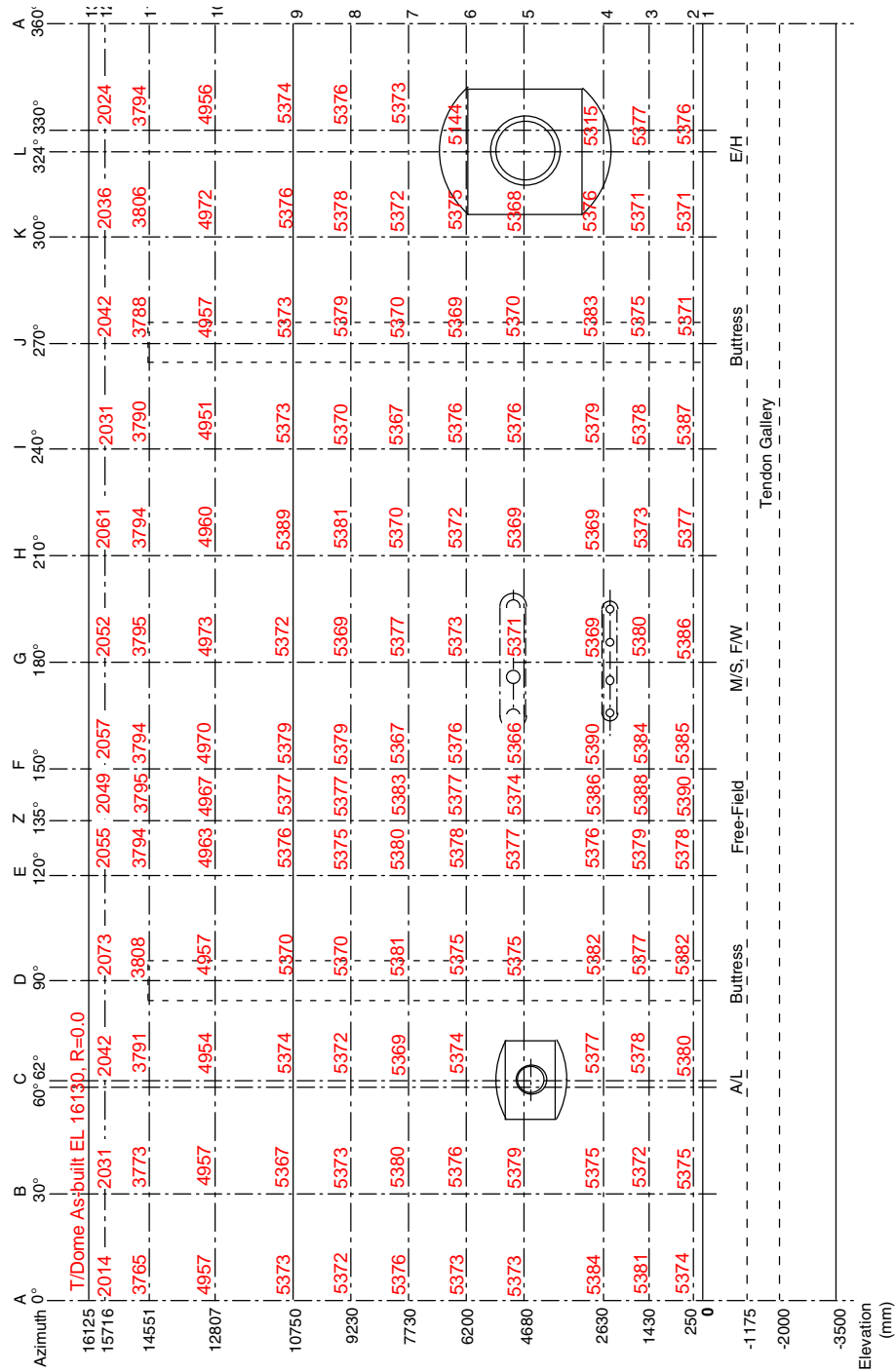


Figure C.1. As-Built Inside Radius of Cardinal Points, July 1999.

PNO	NORTHING	EASTING	STATION ELEV.	RAD. DIST FROM C/L	DESCRIPTION	NAME / LOCATION
1	838.102	299.999	-4.506		CONCRETE CONTROL TRIANGLES	CP-1
2	804.615	296.647	5.421	5.705	EQUIP. HATCH, TOP OUTSIDE	E-2
3	804.617	296.646	3.904	5.707	EQUIP. HATCH, BOTTOM OUTSIDE	E-3
4	799.993	261.886	-3.337		CONCRETE CONTROL TRIANGLES	CP-4
5	804.031	297.071	5.410	4.983	EQUIP. HATCH, TOP INSIDE	E-5
6	804.032	297.070	3.912	4.984	EQUIP. HATCH, BOTTOM INSIDE	E-6
7			-3.414		CONC. BASE 324 LIGHTNING POLE	BM-1
8			3.642		"SQUARE" PEN MARK ON STEEL	TBM @ LEVEL "C"
9			-0.003		OUTSIDE COLLAR	0-00
10			0.001		OUTSIDE COLLAR	0-90
11			-0.003		OUTSIDE COLLAR	0-180
12			0.005		OUTSIDE COLLAR	0-270
13			0.001		OUTSIDE COLLAR	0-324
14	887.561	236.383	-3.059		#5 REBAR W/ALUM. CAP	HATCHLINE SOUTH
15	829.197	278.787	-3.995		#5 REBAR W/ALUM. CAP	HATCHLINE NORTH
16	800.000	300.000	0.131	0.000	CONCRETE BASE MARK	RADIUS PT. CENTERLINE MODEL
17	*****					
18	*****					
19	*****					
20	*****					
21			-0.005		STEEL PLATE, 0.6m x 0.6m	1 -- 130
22			-0.004		STEEL PLATE, 0.6m x 0.6m	1 -- 0
23			-0.003		STEEL RIM	1 -- 30
24			0.002		STEEL RIM	1 -- 62
25			-0.004		STEEL PLATE, 0.6m x 0.6m	1 -- 90
26			-0.004		STEEL RIM	1 -- 120
27			-0.005		STEEL RIM	1 -- 135
28			-0.005		STEEL RIM	1 -- 150
29			0.001		STEEL RIM	1 -- 180
30			-0.002		STEEL RIM	1 -- 210
31			0.001		STEEL PLATE, 0.6m x 0.6m	1 -- 240
32			-0.003		STEEL RIM	1 -- 270
33			0.004		STEEL RIM	1 -- 300
34			0.000		STEEL PLATE, 0.6m x 0.6m	1 -- 324
35	805.374	300.000	0.250	5.374	2'x2' "+" ON INSIDE STEEL WALL	2 -- 0
36	804.655	302.688	0.250	5.375	2'x2' "+" ON INSIDE STEEL WALL	2 -- 30
37	802.526	304.750	0.250	5.380	2'x2' "+" ON INSIDE STEEL WALL	2 -- 62
38	800.000	305.382	0.250	5.382	2'x2' "+" ON INSIDE STEEL WALL	2 -- 90
39	797.311	304.657	0.250	5.378	2'x2' "+" ON INSIDE STEEL WALL	2 -- 120
40	796.188	303.811	0.250	5.390	2'x2' "+" ON INSIDE STEEL WALL	2 -- 135
41	795.336	302.693	0.250	5.385	2'x2' "+" ON INSIDE STEEL WALL	2 -- 150
42	794.614	300.000	0.250	5.386	2'x2' "+" ON INSIDE STEEL WALL	2 -- 180
43	795.343	297.312	0.250	5.377	2'x2' "+" ON INSIDE STEEL WALL	2 -- 210
44	797.307	295.335	0.250	5.387	2'x2' "+" ON INSIDE STEEL WALL	2 -- 240
45	800.000	294.629	0.250	5.371	2'x2' "+" ON INSIDE STEEL WALL	2 -- 270
46	802.686	295.349	0.250	5.371	2'x2' "+" ON INSIDE STEEL WALL	2 -- 300
47	804.349	296.840	0.250	5.376	2'x2' "+" ON INSIDE STEEL WALL	2 -- 324
48	805.381	300.000	1.430	5.381	2'x2' "+" ON INSIDE STEEL WALL	3 -- 0
49	804.652	302.686	1.430	5.372	2'x2' "+" ON INSIDE STEEL WALL	3 -- 30
50	802.525	304.748	1.430	5.378	2'x2' "+" ON INSIDE STEEL WALL	3 -- 62
51	800.000	305.377	1.430	5.377	2'x2' "+" ON INSIDE STEEL WALL	3 -- 90
52	797.311	304.658	1.430	5.379	2'x2' "+" ON INSIDE STEEL WALL	3 -- 120
53	796.190	303.810	1.430	5.388	2'x2' "+" ON INSIDE STEEL WALL	3 -- 135
54	795.337	302.691	1.430	5.384	2'x2' "+" ON INSIDE STEEL WALL	3 -- 150
55	794.620	300.000	1.430	5.380	2'x2' "+" ON INSIDE STEEL WALL	3 -- 180
56	795.347	297.314	1.430	5.373	2'x2' "+" ON INSIDE STEEL WALL	3 -- 210
57	797.311	295.343	1.430	5.378	2'x2' "+" ON INSIDE STEEL WALL	3 -- 240
58	800.000	294.625	1.430	5.375	2'x2' "+" ON INSIDE STEEL WALL	3 -- 270
59	802.686	295.349	1.430	5.371	2'x2' "+" ON INSIDE STEEL WALL	3 -- 300
60	804.350	296.839	1.430	5.377	2'x2' "+" ON INSIDE STEEL WALL	3 -- 324
61	805.384	300.000	2.630	5.384	2'x2' "+" ON INSIDE STEEL WALL	4 -- 0
62	804.655	302.688	2.630	5.375	2'x2' "+" ON INSIDE STEEL WALL	4 -- 30
63	802.524	304.748	2.630	5.377	2'x2' "+" ON INSIDE STEEL WALL	4 -- 62
64	800.000	305.382	2.630	5.382	2'x2' "+" ON INSIDE STEEL WALL	4 -- 90
65	797.311	304.656	2.630	5.376	2'x2' "+" ON INSIDE STEEL WALL	4 -- 120
66	796.192	303.808	2.630	5.386	2'x2' "+" ON INSIDE STEEL WALL	4 -- 135
67	795.332	302.695	2.630	5.390	2'x2' "+" ON INSIDE STEEL WALL	4 -- 150
68	794.631	300.000	2.630	5.369	2'x2' "+" ON INSIDE STEEL WALL	4 -- 180
69	795.350	297.316	2.630	5.369	2'x2' "+" ON INSIDE STEEL WALL	4 -- 210
70	797.311	295.342	2.630	5.379	2'x2' "+" ON INSIDE STEEL WALL	4 -- 240
71	800.000	294.617	2.630	5.383	2'x2' "+" ON INSIDE STEEL WALL	4 -- 270
72	802.688	295.344	2.630	5.376	2'x2' "+" ON INSIDE STEEL WALL	4 -- 300
73	804.300	296.876	2.630	5.315	2'x2' "+" ON INSIDE STEEL WALL	4 -- 324
74	805.373	300.000	4.680	5.373	2'x2' "+" ON INSIDE STEEL WALL	5 -- 0
75	804.658	302.690	4.680	5.379	2'x2' "+" ON INSIDE STEEL WALL	5 -- 30
76					"+" FALLS IN HATCH OPENING	5 -- 62 @ PERSONEL HATCH
77	800.000	305.375	4.680	5.375	2'x2' "+" ON INSIDE STEEL WALL	5 -- 90

PNO	NORTHING	EASTING	STATION ELEV.	RAD. DIST FROM C/L	DESCRIPTION	NAME / LOCATION
78	797.312	304.657	4.680	5.377	2'x2' "+" ON INSIDE STEEL WALL	5 -- 120
79	796.200	303.800	4.680	5.374	2'x2' "+" ON INSIDE STEEL WALL	5 -- 135
80	795.352	302.681	4.680	5.366	2'x2' "+" ON INSIDE STEEL WALL	5 -- 150
81	794.629	300.000	4.680	5.371	2'x2' "+" ON INSIDE STEEL WALL	5 -- 180
82	795.350	297.316	4.680	5.369	2'x2' "+" ON INSIDE STEEL WALL	5 -- 210
83	797.312	295.344	4.680	5.376	2'x2' "+" ON INSIDE STEEL WALL	5 -- 240
84	800.000	294.630	4.680	5.370	2'x2' "+" ON INSIDE STEEL WALL	5 -- 270
85	802.684	295.351	4.680	5.368	2'x2' "+" ON INSIDE STEEL WALL	5 -- 300
86					"+" FALLS IN HATCH OPENING	5 -- 324 @ EQUIPMENT HATCH
87	805.373	300.000	6.200	5.373	2'x2' "+" ON INSIDE STEEL WALL	6 -- 0
88	804.656	302.688	6.200	5.376	2'x2' "+" ON INSIDE STEEL WALL	6 -- 30
89	802.523	304.745	6.200	5.374	2'x2' "+" ON INSIDE STEEL WALL	6 -- 62
90	800.000	305.375	6.200	5.375	2'x2' "+" ON INSIDE STEEL WALL	6 -- 90
91	797.311	304.657	6.200	5.378	2'x2' "+" ON INSIDE STEEL WALL	6 -- 120
92	796.198	303.802	6.200	5.377	2'x2' "+" ON INSIDE STEEL WALL	6 -- 135
93	795.344	302.688	6.200	5.376	2'x2' "+" ON INSIDE STEEL WALL	6 -- 150
94	794.627	300.000	6.200	5.373	2'x2' "+" ON INSIDE STEEL WALL	6 -- 180
95	795.348	297.314	6.200	5.372	2'x2' "+" ON INSIDE STEEL WALL	6 -- 210
96	797.312	295.344	6.200	5.376	2'x2' "+" ON INSIDE STEEL WALL	6 -- 240
97	800.000	294.631	6.200	5.369	2'x2' "+" ON INSIDE STEEL WALL	6 -- 270
98	802.688	295.345	6.200	5.375	2'x2' "+" ON INSIDE STEEL WALL	6 -- 300
99	804.162	296.976	6.200	5.144	2'x2' "+" ON INSIDE STEEL WALL	6 -- 324
100	805.376	300.000	7.730	5.376	2'x2' "+" ON INSIDE STEEL WALL	7 -- 0
101	804.659	302.690	7.730	5.380	2'x2' "+" ON INSIDE STEEL WALL	7 -- 30
102	802.521	304.740	7.730	5.369	2'x2' "+" ON INSIDE STEEL WALL	7 -- 62
103	800.000	305.381	7.730	5.381	2'x2' "+" ON INSIDE STEEL WALL	7 -- 90
104	797.310	304.659	7.730	5.380	2'x2' "+" ON INSIDE STEEL WALL	7 -- 120
105	796.194	303.806	7.730	5.383	2'x2' "+" ON INSIDE STEEL WALL	7 -- 135
106	795.352	302.684	7.730	5.367	2'x2' "+" ON INSIDE STEEL WALL	7 -- 150
107	794.623	300.000	7.730	5.377	2'x2' "+" ON INSIDE STEEL WALL	7 -- 180
108	795.350	297.315	7.730	5.370	2'x2' "+" ON INSIDE STEEL WALL	7 -- 210
109	797.317	295.352	7.730	5.367	2'x2' "+" ON INSIDE STEEL WALL	7 -- 240
110	800.000	294.630	7.730	5.370	2'x2' "+" ON INSIDE STEEL WALL	7 -- 270
111	802.686	295.348	7.730	5.372	2'x2' "+" ON INSIDE STEEL WALL	7 -- 300
112	804.347	296.842	7.730	5.373	2'x2' "+" ON INSIDE STEEL WALL	7 -- 324
113	805.372	300.000	9.230	5.372	2'x2' "+" ON INSIDE STEEL WALL	8 -- 0
114	804.654	302.687	9.230	5.374	2'x2' "+" ON INSIDE STEEL WALL	8 -- 30
115	802.522	304.743	9.230	5.372	2'x2' "+" ON INSIDE STEEL WALL	8 -- 62
116	800.000	305.370	9.230	5.370	2'x2' "+" ON INSIDE STEEL WALL	8 -- 90
117	797.313	304.655	9.230	5.375	2'x2' "+" ON INSIDE STEEL WALL	8 -- 120
118	796.198	303.802	9.230	5.377	2'x2' "+" ON INSIDE STEEL WALL	8 -- 135
119	795.342	302.689	9.230	5.379	2'x2' "+" ON INSIDE STEEL WALL	8 -- 150
120	794.631	300.001	9.230	5.369	2'x2' "+" ON INSIDE STEEL WALL	8 -- 180
121	795.340	297.310	9.230	5.381	2'x2' "+" ON INSIDE STEEL WALL	8 -- 210
122	797.315	295.349	9.230	5.370	2'x2' "+" ON INSIDE STEEL WALL	8 -- 240
123	800.000	294.621	9.230	5.379	2'x2' "+" ON INSIDE STEEL WALL	8 -- 270
124	802.689	295.343	9.230	5.378	2'x2' "+" ON INSIDE STEEL WALL	8 -- 300
125	804.349	296.840	9.230	5.376	2'x2' "+" ON INSIDE STEEL WALL	8 -- 324
126	805.373	300.000	10.750	5.373	2'x2' "+" ON INSIDE STEEL WALL	9 -- 0
127	804.648	302.684	10.750	5.367	2'x2' "+" ON INSIDE STEEL WALL	9 -- 30
128	802.523	304.745	10.750	5.374	2'x2' "+" ON INSIDE STEEL WALL	9 -- 62
129	800.000	305.370	10.750	5.370	2'x2' "+" ON INSIDE STEEL WALL	9 -- 90
130	797.312	304.656	10.750	5.376	2'x2' "+" ON INSIDE STEEL WALL	9 -- 120
131	796.198	303.802	10.750	5.377	2'x2' "+" ON INSIDE STEEL WALL	9 -- 135
132	795.342	302.689	10.750	5.379	2'x2' "+" ON INSIDE STEEL WALL	9 -- 150
133	794.628	300.000	10.750	5.372	2'x2' "+" ON INSIDE STEEL WALL	9 -- 180
134	795.333	297.306	10.750	5.389	2'x2' "+" ON INSIDE STEEL WALL	9 -- 210
135	797.314	295.347	10.750	5.373	2'x2' "+" ON INSIDE STEEL WALL	9 -- 240
136	800.000	294.627	10.750	5.373	2'x2' "+" ON INSIDE STEEL WALL	9 -- 270
137	802.688	295.344	10.750	5.376	2'x2' "+" ON INSIDE STEEL WALL	9 -- 300
138	804.348	296.841	10.750	5.374	2'x2' "+" ON INSIDE STEEL WALL	9 -- 324
139	804.957	300.000	12.807	4.957	2'x2' "+" ON INSIDE STEEL WALL	10 -- 0
140	804.294	302.478	12.807	4.957	2'x2' "+" ON INSIDE STEEL WALL	10 -- 30
141	802.326	304.374	12.807	4.954	2'x2' "+" ON INSIDE STEEL WALL	10 -- 62
142	800.002	304.957	12.807	4.957	2'x2' "+" ON INSIDE STEEL WALL	10 -- 90
143	797.518	304.298	12.807	4.963	2'x2' "+" ON INSIDE STEEL WALL	10 -- 120
144	796.488	303.512	12.807	4.967	2'x2' "+" ON INSIDE STEEL WALL	10 -- 135
145	795.696	302.485	12.807	4.970	2'x2' "+" ON INSIDE STEEL WALL	10 -- 150
146	795.027	300.000	12.807	4.973	2'x2' "+" ON INSIDE STEEL WALL	10 -- 180
147	795.705	297.519	12.807	4.960	2'x2' "+" ON INSIDE STEEL WALL	10 -- 210
148	797.525	295.712	12.807	4.951	2'x2' "+" ON INSIDE STEEL WALL	10 -- 240
149	800.004	295.043	12.807	4.957	2'x2' "+" ON INSIDE STEEL WALL	10 -- 270
150	802.486	295.694	12.807	4.972	2'x2' "+" ON INSIDE STEEL WALL	10 -- 300
151	804.009	297.087	12.807	4.956	2'x2' "+" ON INSIDE STEEL WALL	10 -- 324
152	803.765	300.000	14.511	3.765	2'x2' "+" ON INSIDE STEEL WALL	11 -- 0
153	803.266	301.888	14.511	3.773	2'x2' "+" ON INSIDE STEEL WALL	11 -- 30
154	801.777	303.349	14.511	3.791	2'x2' "+" ON INSIDE STEEL WALL	11 -- 62

PNO	NORTHING	EASTING	STATION ELEV.	RAD. DIST FROM C/L	DESCRIPTION	NAME / LOCATION
155	799.997	303.808	14.511	3.808	2'x2' "+" ON INSIDE STEEL WALL	11 -- 90
156	798.103	303.286	14.511	3.794	2'x2' "+" ON INSIDE STEEL WALL	11 -- 120
157	797.316	302.682	14.511	3.795	2'x2' "+" ON INSIDE STEEL WALL	11 -- 135
158	796.714	301.896	14.511	3.794	2'x2' "+" ON INSIDE STEEL WALL	11 -- 150
159	796.205	300.000	14.511	3.795	2'x2' "+" ON INSIDE STEEL WALL	11 -- 180
160	796.713	298.106	14.511	3.794	2'x2' "+" ON INSIDE STEEL WALL	11 -- 210
161	798.102	296.720	14.511	3.790	2'x2' "+" ON INSIDE STEEL WALL	11 -- 240
162	799.997	296.212	14.511	3.788	2'x2' "+" ON INSIDE STEEL WALL	11 -- 270
163	801.903	296.704	14.511	3.806	2'x2' "+" ON INSIDE STEEL WALL	11 -- 300
164	803.069	297.770	14.511	3.794	2'x2' "+" ON INSIDE STEEL WALL	11 -- 324
165	802.014	300.000	15.716	2.014	2'x2' "+" ON INSIDE STEEL WALL	12 -- 0
166	801.759	301.016	15.716	2.031	2'x2' "+" ON INSIDE STEEL WALL	12 -- 30
167	800.959	301.803	15.716	2.042	2'x2' "+" ON INSIDE STEEL WALL	12 -- 62
168	800.000	302.073	15.716	2.073	2'x2' "+" ON INSIDE STEEL WALL	12 -- 90
169	798.973	301.780	15.716	2.055	2'x2' "+" ON INSIDE STEEL WALL	12 -- 120
170	798.551	301.449	15.716	2.049	2'x2' "+" ON INSIDE STEEL WALL	12 -- 135
171	798.219	301.029	15.716	2.057	2'x2' "+" ON INSIDE STEEL WALL	12 -- 150
172	797.948	300.000	15.716	2.052	2'x2' "+" ON INSIDE STEEL WALL	12 -- 180
173	798.215	298.970	15.716	2.061	2'x2' "+" ON INSIDE STEEL WALL	12 -- 210
174	798.985	298.241	15.716	2.031	2'x2' "+" ON INSIDE STEEL WALL	12 -- 240
175	800.000	297.958	15.716	2.042	2'x2' "+" ON INSIDE STEEL WALL	12 -- 270
176	801.018	298.237	15.716	2.036	2'x2' "+" ON INSIDE STEEL WALL	12 -- 300
177	801.637	298.810	15.716	2.024	2'x2' "+" ON INSIDE STEEL WALL	12 -- 324
178	800.000	300.000	16.130	0.000	DOME TOP CENTERLINE MARK	RADIUS PT.- CENTERLINE MODE
179	794.813	301.330	2.545	5.355	TOP OF PIPE @ WALL- LEVEL"B"	ACCESS PIPE
180	794.671	300.507	2.544	5.353	TOP OF PIPE @ WALL- LEVEL"B"	ACCESS PIPE
181	794.671	299.507	2.544	5.352	TOP OF PIPE @ WALL- LEVEL"B"	ACCESS PIPE
182	794.821	298.682	2.544	5.344	TOP OF PIPE @ WALL- LEVEL"B"	ACCESS PIPE
183	794.852	301.396	5.134	5.334	TOP OF PIPE @ WALL- LEVEL"C"	ACCESS PIPE
184	794.682	300.407	5.131	5.333	TOP OF PIPE @ WALL- LEVEL"C"	ACCESS PIPE
185	794.677	299.580	5.131	5.340	TOP OF PIPE @ WALL- LEVEL"C"	ACCESS PIPE
186	794.851	298.599	5.130	5.336	TOP OF PIPE @ WALL- LEVEL"C"	ACCESS PIPE
187	802.432	304.590	4.193	5.195	INSIDE INVERT OF PIPE	CL. PERSONEL HATCH

Appendix D: Final PCCV Instrumentation List

Rebar Strain Instrumentation List

Labeling	Azimuthal	Vertical	Radial	Transducer	Location	Details	Basic	Modified	Comnts	Calibration
I D	Angle	Elevation	Distance	Designation	Drawing #	Drawing #	Mark #	Mark #		
(name)	(deg)	(in)	(in)							
RS-R-A0-01	0	-135.0	48.0	EP-08-250BF-350	D-SN-P-127		F1XY063	F1XY063A	(basemat	NoCal
RS-R-A0-02	0	-135.0	168.0	EP-08-250BF-350	D-SN-P-127		F1XY063	F1XY063A	bottom)	NoCal
RS-R-D0-01	90	-135.0	48.0	EP-08-250BF-350	D-SN-P-127		F1XYA63	F1XYA63A		NoCal
RS-R-D0-02	90	-135.0	168.0	EP-08-250BF-350	D-SN-P-127		F1XYA63	F1XYA63A		NoCal
RS-R-A0-03	0	-4.0	48.0	EP-08-250BF-350	D-SN-P-127		F8R012	F8R012A	(basemat	NoCal
RS-R-A0-04	0	-4.0	168.0	EP-08-250BF-350	D-SN-P-127		F8R016	F8R016A	top)	NoCal
RS-R-A0-05	0	-4.0	206.0	EP-08-250BF-350	D-SN-P-127		F8R016	F8R016A		NoCal
RS-R-A0-06	0	-4.0	218.0	EP-08-250BF-350	D-SN-P-127		F8R016	F8R016A		NoCal
RS-R-D0-03	90	-4.0	48.0	EP-08-250BF-350	D-SN-P-127		F8R001	F8R001A		NoCal
RS-R-D0-04	90	-4.0	168.0	EP-08-250BF-350	D-SN-P-127		F8R015	F8R015A		NoCal
RS-R-D0-05	90	-4.0	206.0	EP-08-250BF-350	D-SN-P-127		F8R015	F8R015A		NoCal
RS-R-D0-06	90	-4.0	218.0	EP-08-250BF-350	D-SN-P-127		F8R015	F8R015A		NoCal
RS-R-Z0-01	135	-4.0	48.0	EP-08-250BF-350	D-SN-P-127		F8R006	F8R006A		NoCal
RS-R-Z0-02	135	-4.0	168.0	EP-08-250BF-350	D-SN-P-127		F8R016	F8R016B		NoCal
RS-R-Z0-03	135	-4.0	206.0	EP-08-250BF-350	D-SN-P-127		F8R016	F8R016B		NoCal
RS-R-Z0-04	135	-4.0	218.0	EP-08-250BF-350	D-SN-P-127		F8R016	F8R016B		NoCal
RS-C-D0-07	90	-47.0	202.0	EP-08-250BF-350	D-SN-P-127		F3C001	F3C001A	(tendon	NoCal
RS-C-D0-08	90	-47.0	231.0	EP-08-250BF-350	D-SN-P-127		F3C003	F3C003A	gallery)	NoCal
RS-R-D0-09	90	-44.0	197.0	EP-08-250BF-350	D-SN-P-127		F4R001	F4R001A		NoCal
RS-R-D0-10	90	-44.0	235.0	EP-08-250BF-350	D-SN-P-127		F4R001	F4R001A		NoCal
RS-R-D0-11	90	-28.0	205.0	EP-08-250BF-350	D-SN-P-127		F5R002	F5R002A		NoCal
RS-M-D0-12	90	-40.0	201.0	EP-08-250BF-350	D-SN-P-127		F3Z002	F3Z002A		NoCal
RS-M-D0-13	90	-23.0	201.0	EP-08-250BF-350	D-SN-P-127		F3Z002	F3Z002A		NoCal
RS-M-D0-14	90	-40.0	232.0	EP-08-250BF-350	D-SN-P-127		F3Z004	F3Z004A		NoCal
RS-C-Z0-05	135	-47.0	202.0	EP-08-250BF-350	D-SN-P-127		F3C001	F3C001A		NoCal
RS-C-Z0-06	135	-47.0	231.0	EP-08-250BF-350	D-SN-P-127		F3C003	F3C003A		NoCal
RS-R-Z0-07	135	-44.0	197.0	EP-08-250BF-350	D-SN-P-127		F4R001	F4R001B		NoCal
RS-R-Z0-08	135	-44.0	235.0	EP-08-250BF-350	D-SN-P-127		F4R001	F4R001B		NoCal
RS-R-Z0-09	135	-28.0	205.0	EP-08-250BF-350	D-SN-P-127		F5R002	F5R002B		NoCal
RS-M-Z0-10	135	-40.0	201.0	EP-08-250BF-350	D-SN-P-127		F3Z002	F3Z002B		NoCal
RS-M-Z0-11	135	-23.0	201.0	EP-08-250BF-350	D-SN-P-127		F3Z002	F3Z002B		NoCal
RS-M-Z0-12	135	-40.0	232.0	EP-08-250BF-350	D-SN-P-127		F3Z004	F3Z004B		NoCal
GB-D-D0-01	90	-40.0	198.0	EP-08-250BF-350	D-SN-P-127		-	G13D0A	(Inclined	NoCal
GB-D-D0-02	90	-31.5	206.5	EP-08-250BF-350	D-SN-P-127		-	G13D0A	gage bars	NoCal
GB-D-D0-03	90	-23.0	215.0	EP-08-250BF-350	D-SN-P-127		-	G13D0A	above	NoCal
GB-D-D0-04	90	-40.0	238.0	EP-08-250BF-350	D-SN-P-127		-	G13D0B	gallery)	NoCal
GB-D-D0-05	90	-31.5	229.5	EP-08-250BF-350	D-SN-P-127		-	G13D0B		NoCal
GB-D-D0-06	90	-23.0	221.0	EP-08-250BF-350	D-SN-P-127		-	G13D0B		NoCal
GB-D-D0-07	90	-39.0	189.0	EP-08-250BF-350	D-SN-P-127		-	G14D0A		NoCal
GB-D-D0-08	90	-30.5	197.5	EP-08-250BF-350	D-SN-P-127		-	G14D0A		NoCal
GB-D-D0-09	90	-22.0	206.0	EP-08-250BF-350	D-SN-P-127		-	G14D0A		NoCal
GB-D-D0-10	90	-13.5	214.5	EP-08-250BF-350	D-SN-P-127		-	G14D0A		NoCal
GB-D-Z0-01	135	-40.0	198.0	EP-08-250BF-350	D-SN-P-127		-	G13Z0A		NoCal
GB-D-Z0-02	135	-31.5	206.5	EP-08-250BF-350	D-SN-P-127		-	G13Z0A		NoCal
GB-D-Z0-03	135	-23.0	215.0	EP-08-250BF-350	D-SN-P-127		-	G13Z0A		NoCal
GB-D-Z0-04	135	-40.0	238.0	EP-08-250BF-350	D-SN-P-127		-	G13Z0B		NoCal
GB-D-Z0-05	135	-31.5	229.5	EP-08-250BF-350	D-SN-P-127		-	G13Z0B		NoCal
GB-D-Z0-06	135	-23.0	221.0	EP-08-250BF-350	D-SN-P-127		-	G13Z0B		NoCal
GB-D-Z0-07	135	-39.0	189.0	EP-08-250BF-350	D-SN-P-127		-	G14Z0A		NoCal
GB-D-Z0-08	135	-30.5	197.5	EP-08-250BF-350	D-SN-P-127		-	G14Z0A		NoCal
GB-D-Z0-09	135	-22.0	206.0	EP-08-250BF-350	D-SN-P-127		-	G14Z0A		NoCal
GB-D-Z0-10	135	-13.5	214.5	EP-08-250BF-350	D-SN-P-127		-	G14Z0A		NoCal

Rebar Strain Instrumentation List

Labeling	Azimuthal	Vertical	Radial	Transducer	Location	Details	Basic	Modified	Comnts	Calibration
I D	Angle	Elevation	Distance	Designation	Drawing #	Drawing #	Mark #	Mark #		
(name)	(deg)	(in)	(in)							
GB-M-A1-01	350	-1.0	214.0	EP-08-062AQ-350	D-SN-P-125		-	G15A1A	(vertical	NoCal
GB-M-A1-02	350	3.4	214.0	EP-08-062AQ-350	D-SN-P-125		-	G15A1A	gage bars	NoCal
GB-M-A1-03	350	7.9	214.0	EP-08-062AQ-350	D-SN-P-125		-	G15A1A	at wall	NoCal
GB-M-A1-04	350	12.3	214.0	EP-08-062AQ-350	D-SN-P-125		-	G15A1A	basemat	NoCal
GB-M-A1-05	350	16.8	214.0	EP-08-062AQ-350	D-SN-P-125		-	G15A1A	junction)	NoCal
GB-M-A1-06	350	-1.0	217.2	EP-08-062AQ-350	D-SN-P-125		-	G15A1B		NoCal
GB-M-A1-07	350	3.4	217.2	EP-08-062AQ-350	D-SN-P-125		-	G15A1B		NoCal
GB-M-A1-08	350	7.9	217.2	EP-08-062AQ-350	D-SN-P-125		-	G15A1B		NoCal
GB-M-A1-09	350	12.3	217.2	EP-08-062AQ-350	D-SN-P-125		-	G15A1B		NoCal
GB-M-A1-10	350	16.8	217.2	EP-08-062AQ-350	D-SN-P-125		-	G15A1B		NoCal
GB-M-A1-11	350	-1.0	220.4	EP-08-062AQ-350	D-SN-P-126		-	G15A1C		NoCal
GB-M-A1-12	350	3.4	220.4	EP-08-062AQ-350	D-SN-P-126		-	G15A1C		NoCal
GB-M-A1-13	350	7.9	220.4	EP-08-062AQ-350	D-SN-P-126		-	G15A1C		NoCal
GB-M-A1-14	350	12.3	220.4	EP-08-062AQ-350	D-SN-P-126		-	G15A1C		NoCal
GB-M-A1-15	350	16.8	220.4	EP-08-062AQ-350	D-SN-P-126		-	G15A1C		NoCal
GB-M-A1-16	350	-1.0	223.6	EP-08-062AQ-350	D-SN-P-126		-	G15A1D		NoCal
GB-M-A1-17	350	3.4	223.6	EP-08-062AQ-350	D-SN-P-126		-	G15A1D		NoCal
GB-M-A1-18	350	7.9	223.6	EP-08-062AQ-350	D-SN-P-126		-	G15A1D		NoCal
GB-M-A1-19	350	12.3	223.6	EP-08-062AQ-350	D-SN-P-126		-	G15A1D		NoCal
GB-M-A1-20	350	16.8	223.6	EP-08-062AQ-350	D-SN-P-126		-	G15A1D		NoCal
GB-M-A1-21	351	-1.0	223.6	EP-08-062AQ-350	D-SN-P-126		-	G15A1E	Added	NoCal
GB-M-A1-22	351	3.4	223.6	EP-08-062AQ-350	D-SN-P-126		-	G15A1E	Added	NoCal
GB-M-D1-01	90	-1.0	214.0	EP-08-062AQ-350	D-SN-P-125		-	G15D1A		NoCal
GB-M-D1-02	90	3.4	214.0	EP-08-062AQ-350	D-SN-P-125		-	G15D1A		NoCal
GB-M-D1-03	90	7.9	214.0	EP-08-062AQ-350	D-SN-P-125		-	G15D1A		NoCal
GB-M-D1-04	90	12.3	214.0	EP-08-062AQ-350	D-SN-P-125		-	G15D1A		NoCal
GB-M-D1-05	90	16.8	214.0	EP-08-062AQ-350	D-SN-P-125		-	G15D1A		NoCal
GB-M-D1-06	90	-1.0	220.0	EP-08-062AQ-350	D-SN-P-125		-	G15D1B		NoCal
GB-M-D1-07	90	3.4	220.0	EP-08-062AQ-350	D-SN-P-125		-	G15D1B		NoCal
GB-M-D1-08	90	7.9	220.0	EP-08-062AQ-350	D-SN-P-125		-	G15D1B		NoCal
GB-M-D1-09	90	12.3	220.0	EP-08-062AQ-350	D-SN-P-125		-	G15D1B		NoCal
GB-M-D1-10	90	16.8	220.0	EP-08-062AQ-350	D-SN-P-125		-	G15D1B		NoCal
GB-M-D1-11	90	-1.0	226.0	EP-08-062AQ-350	D-SN-P-126		-	G15D1C		NoCal
GB-M-D1-12	90	3.4	226.0	EP-08-062AQ-350	D-SN-P-126		-	G15D1C		NoCal
GB-M-D1-13	90	7.9	226.0	EP-08-062AQ-350	D-SN-P-126		-	G15D1C		NoCal
GB-M-D1-14	90	12.3	226.0	EP-08-062AQ-350	D-SN-P-126		-	G15D1C		NoCal
GB-M-D1-15	90	16.8	226.0	EP-08-062AQ-350	D-SN-P-126		-	G15D1C		NoCal
GB-M-D1-16	90	-1.0	232.0	EP-08-062AQ-350	D-SN-P-126		-	G15D1D		NoCal
GB-M-D1-17	90	3.4	232.0	EP-08-062AQ-350	D-SN-P-126		-	G15D1D		NoCal
GB-M-D1-18	90	7.9	232.0	EP-08-062AQ-350	D-SN-P-126		-	G15D1D		NoCal
GB-M-D1-19	90	12.3	232.0	EP-08-062AQ-350	D-SN-P-126		-	G15D1D		NoCal
GB-M-D1-20	90	16.8	232.0	EP-08-062AQ-350	D-SN-P-126		-	G15D1D		NoCal
GB-M-Z1-01	135	-1.0	214.0	EP-08-062AQ-350	D-SN-P-125		-	G15Z1A		NoCal
GB-M-Z1-02	135	3.4	214.0	EP-08-062AQ-350	D-SN-P-125		-	G15Z1A		NoCal
GB-M-Z1-03	135	7.9	214.0	EP-08-062AQ-350	D-SN-P-125		-	G15Z1A		NoCal
GB-M-Z1-04	135	12.3	214.0	EP-08-062AQ-350	D-SN-P-125		-	G15Z1A		NoCal
GB-M-Z1-05	135	16.8	214.0	EP-08-062AQ-350	D-SN-P-125		-	G15Z1A		NoCal
GB-M-Z1-06	135	-1.0	217.2	EP-08-062AQ-350	D-SN-P-125		-	G15Z1B		NoCal
GB-M-Z1-07	135	3.4	217.2	EP-08-062AQ-350	D-SN-P-125		-	G15Z1B		NoCal
GB-M-Z1-08	135	7.9	217.2	EP-08-062AQ-350	D-SN-P-125		-	G15Z1B		NoCal
GB-M-Z1-09	135	12.3	217.2	EP-08-062AQ-350	D-SN-P-125		-	G15Z1B		NoCal
GB-M-Z1-10	135	16.8	217.2	EP-08-062AQ-350	D-SN-P-125		-	G15Z1B		NoCal
GB-M-Z1-11	135	-1.0	220.4	EP-08-062AQ-350	D-SN-P-126		-	G15Z1C		NoCal
GB-M-Z1-12	135	3.4	220.4	EP-08-062AQ-350	D-SN-P-126		-	G15Z1C		NoCal
GB-M-Z1-13	135	7.9	220.4	EP-08-062AQ-350	D-SN-P-126		-	G15Z1C		NoCal

Rebar Strain Instrumentation List

Labeling I D (name)	Azimuthal Angle (deg)	Vertical Elevation (in)	Radial Distance (in)	Transducer Designation	Location Drawing #	Details Drawing #	Basic Mark #	Modified Mark #	Comnts	Calibration
GB-M-Z1-14	135	12.3	220.4	EP-08-062AQ-350	D-SN-P-126		-	G15Z1C		NoCal
GB-M-Z1-15	135	16.8	220.4	EP-08-062AQ-350	D-SN-P-126		-	G15Z1C		NoCal
GB-M-Z1-16	135	-1.0	223.6	EP-08-062AQ-350	D-SN-P-126		-	G15Z1D		NoCal
GB-M-Z1-17	135	3.4	223.6	EP-08-062AQ-350	D-SN-P-126		-	G15Z1D		NoCal
GB-M-Z1-18	135	7.9	223.6	EP-08-062AQ-350	D-SN-P-126		-	G15Z1D		NoCal
GB-M-Z1-19	135	12.3	223.6	EP-08-062AQ-350	D-SN-P-126		-	G15Z1D		NoCal
GB-M-Z1-20	135	16.8	223.6	EP-08-062AQ-350	D-SN-P-126		-	G15Z1D		NoCal
GB-M-Z1-21	136	-1.0	223.6	EP-08-062AQ-350	D-SN-P-126		-	G15Z1E	Added	NoCal
GB-M-Z1-22	136	3.4	223.6	EP-08-062AQ-350	D-SN-P-126		-	G15Z1E	Added	NoCal
RS-M-A0-07	0	-10.0	214.0	EP-08-250BF-350	D-SN-P-125		S2V002	S2V002A	(free-	NoCal
RS-M-A0-08	0	-10.0	221.5	EP-08-250BF-350	D-SN-P-126		S6V002	S6V002A	field	NoCal
RS-M-A1-01	0	2.0	214.0	EP-08-250BF-350	D-SN-P-125		S2V002	S2V002A	vertical	NoCal
RS-M-A1-02	0	2.0	221.5	EP-08-250BF-350	D-SN-P-126		S6V002	S6V002A	bars)	NoCal
RS-M-A2-01	0	10.0	214.0	EP-08-250BF-350	D-SN-P-125		S2V002	S2V002A		NoCal
RS-M-A2-02	0	10.0	221.5	EP-08-250BF-350	D-SN-P-126		S6V002	S6V002A		NoCal
RS-M-A5-01	1	184.0	214.0	EP-08-250BF-350	D-SN-P-125		S2V006	S2V006A		NoCal
RS-M-A5-02	0	184.0	221.5	EP-08-250BF-350	D-SN-P-126		S6VC13	S6VC13A		NoCal
RS-M-A6-01	1	244.0	214.0	EP-08-250BF-350	D-SN-P-125		S2V011	S2V011C		NoCal
RS-M-A6-02	1	244.0	221.5	EP-08-250BF-350	D-SN-P-126		S6VA15	S6VA15A		NoCal
RS-M-A7-01	1	304.0	214.0	EP-08-250BF-350	D-SN-P-125		S2V013	S2V013A		NoCal
RS-M-A7-02	1	304.0	221.5	EP-08-250BF-350	D-SN-P-126		S6VA15	S6VA15A		NoCal
RS-M-A9-01	1	423.0	214.0	EP-08-250BF-350	D-SN-P-125		S2V013	S2V013A		NoCal
RS-M-A9-02	1	423.0	221.5	EP-08-250BF-350	D-SN-P-126		S6V015	S6V015A		NoCal
RS-M-B5-01	29	184.0	214.0	EP-08-250BF-350	D-SN-P-125		S2V006	S2V006B		NoCal
RS-M-B5-02	30	184.0	221.5	EP-08-250BF-350	D-SN-P-126		S6VC13	S6VC13B		NoCal
RS-M-D0-15	90	-10.0	214.0	EP-08-250BF-350	D-SN-P-125		S1VA02	S1VA02A		NoCal
RS-M-D0-16	89	-10.0	230.0	EP-08-250BF-350	D-SN-P-126		SB1VA04	SB1VA04A		NoCal
RS-M-D1-01	90	2.0	214.0	EP-08-250BF-350	D-SN-P-125		S1VA02	S1VA02A		NoCal
RS-M-D1-02	89	2.0	230.0	EP-08-250BF-350	D-SN-P-126		SB1VA04	SB1VA04A		NoCal
RS-M-D2-01	90	10.0	214.0	EP-08-250BF-350	D-SN-P-125		S1VA02	S1VA02A		NoCal
RS-M-D2-02	89	10.0	230.0	EP-08-250BF-350	D-SN-P-126		SB1VA04	SB1VA04A		NoCal
RS-M-D3-01	90	56.0	214.0	EP-08-250BF-350	D-SN-P-125		S1VB02	S1VB02A		NoCal
RS-M-D3-02	89	56.0	230.0	EP-08-250BF-350	D-SN-P-126		SB1VB04	SB1VB04A		NoCal
RS-M-D4-01	90	104.0	214.0	EP-08-250BF-350	D-SN-P-125		S1VB02	S1VB02A		NoCal
RS-M-D4-02	89	104.0	230.0	EP-08-250BF-350	D-SN-P-126		SB1V006	SB1V006A		NoCal
RS-M-D5-01	91	184.0	214.0	EP-08-250BF-350	D-SN-P-125		S1V004	S1V004A		NoCal
RS-M-D5-02	89.5	184.0	230.0	EP-08-250BF-350	D-SN-P-126		SB1V008	SB1V008A		NoCal
RS-M-D6-01	90	244.0	214.0	EP-08-250BF-350	D-SN-P-125		S1V005	S1V005A		NoCal
RS-M-D6-02	89.5	244.0	230.0	EP-08-250BF-350	D-SN-P-126		SB2V002	SB2V002A		NoCal
RS-M-D7-01	90	304.0	214.0	EP-08-250BF-350	D-SN-P-125		S1V005	S1V005A		NoCal
RS-M-D7-02	89.5	304.0	230.0	EP-08-250BF-350	D-SN-P-126		SB2V002	SB2V002A		NoCal
RS-M-D8-01	90	363.0	214.0	EP-08-250BF-350	D-SN-P-125		S1V005	S1V005A		NoCal
RS-M-D8-02	89	363.0	230.0	EP-08-250BF-350	D-SN-P-126		SB2V006	SB2V006A		NoCal
RS-M-D9-01	91	423.0	214.0	EP-08-250BF-350	D-SN-P-125		S1V007	S1V007A		NoCal
RS-M-D9-02	89	423.0	230.0	EP-08-250BF-350	D-SN-P-126		SB2V006	SB2V006A		NoCal
RS-M-D10-01	90	504.0	198.0	EP-08-250BF-350	D-SN-P-125		D2V001	D2V001A		NoCal
RS-M-D10-02	89.5	504.0	214.0	EP-08-250BF-350	D-SN-P-126		DB1V002	DB1V002A		NoCal
RS-M-D11-01	90	573.0	152.0	EP-08-250BF-350	D-SN-P-125		D2V001	D2V001A		NoCal
RS-M-D11-02	89.5	573.0	170.0	EP-08-250BF-350	D-SN-P-126		DB1V008	DB1V008A		NoCal
RS-M-D12-01	91	619.0	83.0	EP-08-250BF-350	D-SN-P-125		D2V011	D2V011A		NoCal
RS-M-D12-02	91	619.0	101.0	EP-08-250BF-350	D-SN-P-126		D5V011	D5V011A		NoCal
RS-M-E5-01	119	184.0	214.0	EP-08-250BF-350	D-SN-P-125		S1V004	S1V004B		NoCal
RS-M-E5-02	119	184.0	221.5	EP-08-250BF-350	D-SN-P-126		S5V008	S5V008A		NoCal

Rebar Strain Instrumentation List

Labeling I D (name)	Azimuthal Angle (deg)	Vertical Elevation (in)	Radial Distance (in)	Transducer Designation	Location Drawing #	Details Drawing #	Basic Mark #	Modified Mark #	Comnts	Calibration
RS-M-Z0-13	135	-10.0	214.0	EP-08-250BF-350	D-SN-P-125		S1VA02	S1VA02B		NoCal
RS-M-Z0-14	135	-10.0	221.5	EP-08-250BF-350	D-SN-P-126		S5VA03	S5VA03A		NoCal
RS-M-Z1-01	135	2.0	214.0	EP-08-250BF-350	D-SN-P-125		S1VA02	S1VA02B		NoCal
RS-M-Z1-02	135	2.0	221.5	EP-08-250BF-350	D-SN-P-126		S5VA03	S5VA03A		NoCal
RS-M-Z2-01	135	10.0	214.0	EP-08-250BF-350	D-SN-P-125		S1VA02	S1VA02B		NoCal
RS-M-Z2-02	135	10.0	221.5	EP-08-250BF-350	D-SN-P-126		S5VA03	S5VA03A		NoCal
RS-M-Z3-01	135	56.0	214.0	EP-08-250BF-350	D-SN-P-125		S1VA03	S1VA03A		NoCal
RS-M-Z3-02	135	56.0	221.5	EP-08-250BF-350	D-SN-P-126		S5VB03	S5VB03A		NoCal
RS-M-Z4-01	135	104.0	214.0	EP-08-250BF-350	D-SN-P-125		S1VA03	S1VA03A		NoCal
RS-M-Z4-02	135	104.0	221.5	EP-08-250BF-350	D-SN-P-126		S5V005	S5V005A		NoCal
RS-M-Z5-01	135	184.0	214.0	EP-08-250BF-350	D-SN-P-125		S1V004	S1V004C		NoCal
RS-M-Z5-02	135	184.0	221.5	EP-08-250BF-350	D-SN-P-126		S5VB07	S5VB07A		NoCal
RS-M-Z5-03	135	184.0	214.0	EP-08-250BF-350	D-SN-P-125		S1V004	S1V004C		NoCal
RS-M-Z5-04	135	184.0	221.5	EP-08-250BF-350	D-SN-P-126		S5VB07	S5VB07A		NoCal
RS-M-Z6-01	135	244.0	214.0	EP-08-250BF-350	D-SN-P-125		S1V005	S1V005B		NoCal
RS-M-Z6-02	135	244.0	221.5	EP-08-250BF-350	D-SN-P-126		S5VA07	S5VA07A		NoCal
RS-M-Z7-01	135	304.0	214.0	EP-08-250BF-350	D-SN-P-125		S1V005	S1V005B		NoCal
RS-M-Z7-02	135	304.0	221.5	EP-08-250BF-350	D-SN-P-126		S5VA07	S5VA07A		NoCal
RS-M-Z8-01	135	363.0	214.0	EP-08-250BF-350	D-SN-P-125		S1V005	S1V005B		NoCal
RS-M-Z8-02	135	363.0	221.5	EP-08-250BF-350	D-SN-P-126		S5V007	S5V007A		NoCal
RS-M-Z9-01	135	423.0	214.0	EP-08-250BF-350	D-SN-P-125		S1V005	S1V005B		NoCal
RS-M-Z9-02	135	423.0	221.5	EP-08-250BF-350	D-SN-P-126		S5V007	S5V007A		NoCal
RS-M-Z9-03	135	423.0	214.0	EP-08-250BF-350	D-SN-P-125		S1V005	S1V005B		NoCal
RS-M-Z9-04	135	423.0	221.5	EP-08-250BF-350	D-SN-P-126		S5V007	S5V007A		NoCal
RS-M-Z10-01	135	504.0	198.0	EP-08-250BF-350	D-SN-P-125		D1V003	D1V003A		NoCal
RS-M-Z10-02	135	504.0	206.0	EP-08-250BF-350	D-SN-P-126		D4V003	D4V003A		NoCal
RS-M-Z11-01	135	573.0	152.0	EP-08-250BF-350	D-SN-P-125		D1V003	D1V003A		NoCal
RS-M-Z11-02	135	573.0	162.0	EP-08-250BF-350	D-SN-P-126		D4VA03	D4VA03A		NoCal
RS-M-Z11-03	135	573.0	152.0	EP-08-250BF-350	D-SN-P-125		D1V003	D1V003A		NoCal
RS-M-Z11-04	135	573.0	162.0	EP-08-250BF-350	D-SN-P-126		D4VA03	D4VA03A		NoCal
RS-M-Z12-01	135	619.0	83.0	EP-08-250BF-350	D-SN-P-125		D1V003	D1V003A		NoCal
RS-M-Z12-02	135	619.0	90.0	EP-08-250BF-350	D-SN-P-126		D4VA03	D4VA03A		NoCal
RS-M-Z13-01	-	637.0	0.0	EP-08-250BF-350	D-SN-P-125		D1V004	D1V004A		NoCal
RS-M-Z13-02	-	644.0	0.0	EP-08-250BF-350	D-SN-P-126		D4V004	D4V004A		NoCal
RS-M-Z13-03	-	637.0	0.0	EP-08-250BF-350	D-SN-P-125		D2V004	D2V004A		NoCal
RS-M-Z13-04	-	644.0	0.0	EP-08-250BF-350	D-SN-P-126		D5V004	D5V004A		NoCal
RS-M-F5-01	149	184.0	214.0	EP-08-250BF-350	D-SN-P-125		S1V004	S1V004D		NoCal
RS-M-F5-02	149	184.0	221.5	EP-08-250BF-350	D-SN-P-126		S5V008	S5V008B		NoCal
RS-M-G5-01	180	184.0	214.0	EP-08-250BF-350	D-SN-P-125		S1PV016	S1PV016A		NoCal
RS-M-G5-02	180	184.0	221.5	EP-08-250BF-350	D-SN-P-126		S5PV022	S5PV022A		NoCal
RS-M-G6-01	180	244.0	214.0	EP-08-250BF-350	D-SN-P-125		S1PV016	S1PV016A		NoCal
RS-M-G6-02	181	244.0	221.5	EP-08-250BF-350	D-SN-P-126		S5PV021	S5PV021A		NoCal
RS-M-G7-01	180	304.0	214.0	EP-08-250BF-350	D-SN-P-125		S1PVA38	S1PVA38A		NoCal
RS-M-G7-02	180	304.0	221.5	EP-08-250BF-350	D-SN-P-126		S5PVA47	S5PVA47A		NoCal
RS-M-H5-01	209	184.0	214.0	EP-08-250BF-350	D-SN-P-125		S1V004	S1V004E		NoCal
RS-M-H5-02	209	184.0	221.5	EP-08-250BF-350	D-SN-P-126		S5V008	S5V008C		NoCal
RS-M-I5-01	239	184.0	214.0	EP-08-250BF-350	D-SN-P-125		S1V004	S1V004F		NoCal
RS-M-I5-02	239	184.0	221.5	EP-08-250BF-350	D-SN-P-126		S5V008	S5V008D		NoCal
RS-M-I9-01	239	423.0	214.0	EP-08-250BF-350	D-SN-P-125		S1V007	S1V007B		NoCal
RS-M-I9-02	239	423.0	221.5	EP-08-250BF-350	D-SN-P-126		S5V009	S5V009A		NoCal
RS-M-J0-01	270	-10.0	214.0	EP-08-250BF-350	D-SN-P-125		S2V002	S2V002B		NoCal
RS-M-J0-02	269	-10.0	230.0	EP-08-250BF-350	D-SN-P-126		SB1V004	SB1V004B		NoCal
RS-M-J1-01	270	2.0	214.0	EP-08-250BF-350	D-SN-P-125		S2V002	S2V002B		NoCal

Rebar Strain Instrumentation List

Labeling I D (name)	Azimuthal Angle (deg)	Vertical Elevation (in)	Radial Distance (in)	Transducer Designation	Location Drawing #	Details Drawing #	Basic Mark #	Modified Mark #	Comnts	Calibration
RS-M-J1-02	269	2.0	230.0	EP-08-250BF-350	D-SN-P-126		SB1V004	SB1V004B		NoCal
RS-M-J2-01	270	10.0	214.0	EP-08-250BF-350	D-SN-P-125		S2V002	S2V002B		NoCal
RS-M-J2-02	269	10.0	230.0	EP-08-250BF-350	D-SN-P-126		SB1V004	SB1V004B		NoCal
RS-M-J5-01	270	184.0	214.0	EP-08-250BF-350	D-SN-P-125		S2V006	S2V006C		NoCal
RS-M-J5-02	269.5	184.0	230.0	EP-08-250BF-350	D-SN-P-126		SB1V008	SB1V008B		NoCal
RS-M-J9-01	271	423.0	214.0	EP-08-250BF-350	D-SN-P-125		S2V013	S2V013B		NoCal
RS-M-J9-02	269	423.0	230.0	EP-08-250BF-350	D-SN-P-126		SB2V006	SB2V006B		NoCal
RS-M-L0-01	324	-10.0	214.0	EP-08-250BF-350	D-SN-P-125		S2VA02	S2VA02A		NoCal
RS-M-L0-02	324	-10.0	221.5	EP-08-250BF-350	D-SN-P-126		S6V002	S6V002B		NoCal
RS-M-L1-01	324	2.0	214.0	EP-08-250BF-350	D-SN-P-125		S2VA02	S2VA02A		NoCal
RS-M-L1-02	324	2.0	221.5	EP-08-250BF-350	D-SN-P-126		S6V002	S6V002B		NoCal
RS-M-L2-01	324	10.0	214.0	EP-08-250BF-350	D-SN-P-125		S2VA02	S2VA02A		NoCal
RS-M-L2-02	324	10.0	221.5	EP-08-250BF-350	D-SN-P-126		S6V002	S6V002B		NoCal
RS-M-L3-01	324	56.0	214.0	EP-08-250BF-350	D-SN-P-125		S2PVA10	S2PVA10A		NoCal
RS-M-L3-02	324	60.0	221.5	EP-08-250BF-350	D-SN-P-126		P2V007	P2V007A		NoCal
RS-M-L7-01	324	304.0	214.0	EP-08-250BF-350	D-SN-P-125		S2PV034	S2PV034A		NoCal
RS-M-L7-02	324	304.0	221.5	EP-08-250BF-350	D-SN-P-126		S6PVA15	S6PVA15A		NoCal
RS-M-L8-01	324	363.0	214.0	EP-08-250BF-350	D-SN-P-125		S2PV034	S2PV034A		NoCal
RS-M-L8-02	324	363.0	221.5	EP-08-250BF-350	D-SN-P-126		S6V020	S6V020A		NoCal
RS-M-L9-01	323	423.0	214.0	EP-08-250BF-350	D-SN-P-125		S2PV033	S2PV033A		NoCal
RS-M-L9-02	323	423.0	221.5	EP-08-250BF-350	D-SN-P-126		S6V015	S6V015B		NoCal
RS-M-L10-01	324	504.0	198.0	EP-08-250BF-350	D-SN-P-125		D1V001	D1V001A		NoCal
RS-M-L10-02	323	504.0	206.0	EP-08-250BF-350	D-SN-P-126		D4V003	D4V003B		NoCal
RS-M-L11-01	324	573.0	152.0	EP-08-250BF-350	D-SN-P-125		D1V001	D1V001A		NoCal
RS-M-L11-02	324	573.0	162.0	EP-08-250BF-350	D-SN-P-126		D4VA01	D4VA01A		NoCal
RS-M-L12-01	323	619.0	83.0	EP-08-250BF-350	D-SN-P-125		D1V003	D1V003B		NoCal
RS-M-L12-02	323	619.0	90.0	EP-08-250BF-350	D-SN-P-126		D4VA03	D4VA03B		NoCal
RS-M-C5-01	44	147.0	214.0	EP-08-250BF-350	D-SN-P-125		S2V006	S2V006D	(A/L	NoCal
RS-M-C5-02	45	147.0	221.5	EP-08-250BF-350	D-SN-P-126		S6VC13	S6VC13C	vertical	NoCal
RS-M-C5-03	44	184.0	214.0	EP-08-250BF-350	D-SN-P-125		S2V006	S2V006D	bars)	NoCal
RS-M-C5-04	44	184.0	221.5	EP-08-250BF-350	D-SN-P-126		S6V010	S6V010A		NoCal
RS-M-C5-05	44	209.0	214.0	EP-08-250BF-350	D-SN-P-125		S2V011	S2V011A		NoCal
RS-M-C5-06	44	209.0	221.5	EP-08-250BF-350	D-SN-P-126		S6V010	S6V010A		NoCal
RS-M-C5-07	51	125.0	214.0	EP-08-250BF-350	D-SN-P-125		S2V021	S2V021A		NoCal
RS-M-C5-08	52	125.0	221.5	EP-08-250BF-350	D-SN-P-126		S6PVA05	S6PVA05A		NoCal
RS-M-C5-09	61	125.0	214.0	EP-08-250BF-350	D-SN-P-125		S2PV021	S2PV021A		NoCal
RS-M-C5-10	61	125.0	221.5	EP-08-250BF-350	D-SN-P-126		S6PVA06	S6PVA06A		NoCal
RS-M-C5-11	73	125.0	214.0	EP-08-250BF-350	D-SN-P-125		S2V021	S2V021B		NoCal
RS-M-C5-12	72	125.0	221.5	EP-08-250BF-350	D-SN-P-126		S6PVA05	S6PVA05B		NoCal
RS-M-C5-13	51	230.0	214.0	EP-08-250BF-350	D-SN-P-125		S2V004	S2V004A		NoCal
RS-M-C5-14	52	230.0	221.5	EP-08-250BF-350	D-SN-P-126		S6V018	S6V018A		NoCal
RS-M-C5-15	62	230.0	214.0	EP-08-250BF-350	D-SN-P-125		P3VA06	P3VA06A		NoCal
RS-M-C5-16	62	230.0	221.5	EP-08-250BF-350	D-SN-P-126		P3VA06	P3VA06A		NoCal
RS-M-C5-17	73	230.0	214.0	EP-08-250BF-350	D-SN-P-125		S2V004	S2V004B		NoCal
RS-M-C5-18	72	230.0	221.5	EP-08-250BF-350	D-SN-P-126		S6V018	S6V018B		NoCal
RS-M-C5-19	80	147.0	214.0	EP-08-250BF-350	D-SN-P-125		S2V006	S2V006E		NoCal
RS-M-C5-20	80	147.0	221.5	EP-08-250BF-350	D-SN-P-126		S6VC10	S6VC10A		NoCal
RS-M-C5-21	80	184.0	214.0	EP-08-250BF-350	D-SN-P-125		S2V006	S2V006E		NoCal
RS-M-C5-22	80	184.0	221.5	EP-08-250BF-350	D-SN-P-126		S6VA10	S6VA10A		NoCal
RS-M-C5-23	80	209.0	214.0	EP-08-250BF-350	D-SN-P-125		S2V011	S2V011B		NoCal
RS-M-C5-24	80	209.0	221.5	EP-08-250BF-350	D-SN-P-126		S6VA10	S6VA10A		NoCal
RS-M-K5-01	299	131.0	214.0	EP-08-250BF-350	D-SN-P-125		S2V021	S2V021C	(E/H	NoCal
RS-M-K5-02	299	131.0	221.5	EP-08-250BF-350	D-SN-P-126		S6V007	S6V007A	vertical	NoCal
RS-M-K5-03	299	184.0	214.0	EP-08-250BF-350	D-SN-P-125		S2V018	S2V018A	bars)	NoCal
RS-M-K5-04	299	184.0	221.5	EP-08-250BF-350	D-SN-P-126		S6VB09	S6VB09A		NoCal

Rebar Strain Instrumentation List

Labeling I D (name)	Azimuthal Angle (deg)	Vertical Elevation (in)	Radial Distance (in)	Transducer Designation	Location Drawing #	Details Drawing #	Basic Mark #	Modified Mark #	Comnts	Calibration
RS-M-K5-05	299	237.0	214.0	EP-08-250BF-350	D-SN-P-125		S2V018	S2V018A		NoCal
RS-M-K5-06	299	237.0	221.5	EP-08-250BF-350	D-SN-P-126		S6V009	S6V009A		NoCal
RS-M-L4-01	308	79.0	214.0	EP-08-250BF-350	D-SN-P-125		S2PV002	S2PV002A		NoCal
RS-M-L4-02	308	79.0	221.5	EP-08-250BF-350	D-SN-P-126		S6VA12	S6VA12A		NoCal
RS-M-L4-03	324	79.0	214.0	EP-08-250BF-350	D-SN-P-125		S2PVA10	S2PVA10A		NoCal
RS-M-L4-04	324	79.0	221.5	EP-08-250BF-350	D-SN-P-126		P2V007	P2V007A		NoCal
RS-M-L4-05	340	79.0	214.0	EP-08-250BF-350	D-SN-P-125		S2PV002	S2PV002B		NoCal
RS-M-L4-06	340	79.0	221.5	EP-08-250BF-350	D-SN-P-126		S6VA12	S6VA12B		NoCal
RS-M-L6-01	308	289.0	214.0	EP-08-250BF-350	D-SN-P-125		S2PV033	S2PV033B		NoCal
RS-M-L6-02	308	289.0	221.5	EP-08-250BF-350	D-SN-P-126		S6V024	S6V024A		NoCal
RS-M-L6-03	324	289.0	214.0	EP-08-250BF-350	D-SN-P-125		S2PV034	S2PV034A		NoCal
RS-M-L6-04	324	289.0	221.5	EP-08-250BF-350	D-SN-P-126		S6PVA15	S6PVA15A		NoCal
RS-M-L6-05	340	289.0	214.0	EP-08-250BF-350	D-SN-P-125		S2PV033	S2PV033C		NoCal
RS-M-L6-06	340	289.0	221.5	EP-08-250BF-350	D-SN-P-126		S6V024	S6V024B		NoCal
RS-M-A5-03	349	131.0	214.0	EP-08-250BF-350	D-SN-P-125		S2V021	S2V021D		NoCal
RS-M-A5-04	349	131.0	221.5	EP-08-250BF-350	D-SN-P-126		S6V007	S6V007B		NoCal
RS-M-A5-05	349	184.0	214.0	EP-08-250BF-350	D-SN-P-125		S2V018	S2V018B		NoCal
RS-M-A5-06	349	184.0	221.5	EP-08-250BF-350	D-SN-P-126		S6VB09	S6VB09B		NoCal
RS-M-A5-07	349	237.0	214.0	EP-08-250BF-350	D-SN-P-125		S2V018	S2V018B		NoCal
RS-M-A5-08	349	237.0	221.5	EP-08-250BF-350	D-SN-P-126		S6V009	S6V009B		NoCal
RS-C-A1-01	0	2.0	215.0	EP-08-250BF-350	D-SN-P-125		S4HA01	S4HA01A	(free-	NoCal
RS-C-A1-02	0	2.0	223.0	EP-08-250BF-350	D-SN-P-126		S8H001	S8H001A	field	NoCal
RS-C-A2-01	0	11.0	215.0	EP-08-250BF-350	D-SN-P-125		S4HA01	S4HA01B	Hoop	NoCal
RS-C-A2-02	0	11.0	223.0	EP-08-250BF-350	D-SN-P-126		S8H001	S8H001B	bars)	NoCal
RS-C-A5-01	2	184.0	215.0	EP-08-250BF-350	D-SN-P-125		S4H013	S4H013A		NoCal
RS-C-A5-02	0	184.0	223.0	EP-08-250BF-350	D-SN-P-126		S8HB16	S8HB16A		NoCal
RS-C-A6-01	2	246.0	215.0	EP-08-250BF-350	D-SN-P-125		S4H022	S4H022A		NoCal
RS-C-A6-02	0	246.0	223.0	EP-08-250BF-350	D-SN-P-126		S8HA21	S8HA21A		NoCal
RS-C-A7-01	0	308.0	215.0	EP-08-250BF-350	D-SN-P-125		S4H028	S4H028A		NoCal
RS-C-A7-02	0	308.0	223.0	EP-08-250BF-350	D-SN-P-126		S8H029	S8H029B		NoCal
RS-C-A9-01	0	423.0	215.0	EP-08-250BF-350	D-SN-P-125		S4H028	S4H028C		NoCal
RS-C-A9-02	0	423.0	223.0	EP-08-250BF-350	D-SN-P-126		S8H028	S8H028A		NoCal
RS-C-B5-01	30	184.0	215.0	EP-08-250BF-350	D-SN-P-125		S4H013	S4H013A		NoCal
RS-C-B5-02	30	184.0	223.0	EP-08-250BF-350	D-SN-P-126		S8HA16	S8HA16A		NoCal
RS-C-D1-01	90	2.0	215.0	EP-08-250BF-350	D-SN-P-125		S4H001	S4H001C		NoCal
RS-C-D1-02	90	2.0	223.0	EP-08-250BF-350	D-SN-P-126		S8H002	S8H002A		NoCal
RS-C-D2-01	90	11.0	215.0	EP-08-250BF-350	D-SN-P-125		S4H001	S4H001D		NoCal
RS-C-D2-02	90	11.0	223.0	EP-08-250BF-350	D-SN-P-126		S8H002	S8H002B		NoCal
RS-C-D3-01	90	56.0	215.0	EP-08-250BF-350	D-SN-P-125		S4H003	S4H003A		NoCal
RS-C-D3-02	90	56.0	223.0	EP-08-250BF-350	D-SN-P-126		S8H006	S8H006A		NoCal
RS-C-D4-01	90	104.0	215.0	EP-08-250BF-350	D-SN-P-125		S4H002	S4H002A		NoCal
RS-C-D4-02	90	104.0	223.0	EP-08-250BF-350	D-SN-P-126		S8H008	S8H008A		NoCal
RS-C-D5-01	90	184.0	215.0	EP-08-250BF-350	D-SN-P-125		S4H015	S4H015A		NoCal
RS-C-D5-02	90	184.0	223.0	EP-08-250BF-350	D-SN-P-126		S8H019	S8H019B		NoCal
RS-C-D6-01	90	246.0	215.0	EP-08-250BF-350	D-SN-P-125		S4HA24	S4HA24A		NoCal
RS-C-D6-02	90	246.0	223.0	EP-08-250BF-350	D-SN-P-126		S8H033	S8H033A		NoCal
RS-C-D7-01	90	304.0	215.0	EP-08-250BF-350	D-SN-P-125		S4H023	S4H023A		NoCal
RS-C-D7-02	90	304.0	223.0	EP-08-250BF-350	D-SN-P-126		S8H031	S8H031A		NoCal
RS-C-D8-01	90	361.0	215.0	EP-08-250BF-350	D-SN-P-125		S4H024	S4H024D		NoCal
RS-C-D8-02	90	361.0	223.0	EP-08-250BF-350	D-SN-P-126		S8H032	S8H032A		NoCal
RS-C-D9-01	90	423.0	215.0	EP-08-250BF-350	D-SN-P-125		S4H024	S4H024E		NoCal
RS-C-D9-02	90	423.0	223.0	EP-08-250BF-350	D-SN-P-126		S8H033	S8H033B		NoCal
RS-C-D10-01	91	504.0	199.0	EP-08-250BF-350	D-SN-P-125		D3H027	D3H027A		NoCal
RS-C-D10-02	91	504.0	207.0	EP-08-250BF-350	D-SN-P-126		D6H027	D6H027A		NoCal
RS-C-D11-01	89	573.0	153.0	EP-08-250BF-350	D-SN-P-125		D3H048	D3H048A		NoCal

Rebar Strain Instrumentation List

Labeling	Azimuthal	Vertical	Radial	Transducer	Location	Details	Basic	Modified	Comnts	Calibration
I D	Angle	Elevation	Distance	Designation	Drawing #	Drawing #	Mark #	Mark #		
(name)	(deg)	(in)	(in)							
RS-C-D11-02	89	573.0	163.0	EP-08-250BF-350	D-SN-P-126		D6H048	D6H048A		NoCal
RS-C-D12-01	90	619.0	85.0	EP-08-250BF-350	D-SN-P-125		D3H070	D3H070A		NoCal
RS-C-D12-02	90	619.0	92.0	EP-08-250BF-350	D-SN-P-126		D6H070	D6H070A		NoCal
RS-C-E5-01	120	184.0	215.0	EP-08-250BF-350	D-SN-P-125		S3H014	S3H014A		NoCal
RS-C-E5-02	120	184.0	223.0	EP-08-250BF-350	D-SN-P-126		S7HA20	S7HA20A		NoCal
RS-C-Z1-01	135	2.0	215.0	EP-08-250BF-350	D-SN-P-125		S3H001	S3H001A		NoCal
RS-C-Z1-02	135	2.0	223.0	EP-08-250BF-350	D-SN-P-126		S7H001	S7H001A		NoCal
RS-C-Z2-01	135	11.0	215.0	EP-08-250BF-350	D-SN-P-125		S3H001	S3H001B		NoCal
RS-C-Z2-02	135	11.0	223.0	EP-08-250BF-350	D-SN-P-126		S7H001	S7H001B		NoCal
RS-C-Z3-01	135	56.0	215.0	EP-08-250BF-350	D-SN-P-125		S3H003	S3H003A		NoCal
RS-C-Z3-02	135	56.0	223.0	EP-08-250BF-350	D-SN-P-126		S7H003	S7H003A		NoCal
RS-C-Z4-01	135	104.0	215.0	EP-08-250BF-350	D-SN-P-125		S3H004	S3H004A		NoCal
RS-C-Z4-02	135	104.0	223.0	EP-08-250BF-350	D-SN-P-126		S7H005	S7H005A		NoCal
RS-C-Z5-01	135	184.0	215.0	EP-08-250BF-350	D-SN-P-125		S3H014	S3H014A		NoCal
RS-C-Z5-02	135	184.0	223.0	EP-08-250BF-350	D-SN-P-126		S7HA20	S7HA20A		NoCal
RS-C-Z5-03	135	184.0	215.0	EP-08-250BF-350	D-SN-P-125		S3H014	S3H014A		NoCal
RS-C-Z5-04	135	184.0	223.0	EP-08-250BF-350	D-SN-P-126		S7HA20	S7HA20A		NoCal
RS-C-Z6-01	135	246.0	215.0	EP-08-250BF-350	D-SN-P-125		S3H026	S3H026A		NoCal
RS-C-Z6-02	135	246.0	223.0	EP-08-250BF-350	D-SN-P-126		S7H031	S7H031A		NoCal
RS-C-Z7-01	135	304.0	215.0	EP-08-250BF-350	D-SN-P-125		S3H018	S3H018A		NoCal
RS-C-Z7-02	135	304.0	223.0	EP-08-250BF-350	D-SN-P-126		S7H036	S7H036A		NoCal
RS-C-Z8-01	135	361.0	215.0	EP-08-250BF-350	D-SN-P-125		S3H016	S3H016A		NoCal
RS-C-Z8-02	135	361.0	223.0	EP-08-250BF-350	D-SN-P-126		S7H038	S7H038A		NoCal
RS-C-Z9-01	135	423.0	215.0	EP-08-250BF-350	D-SN-P-125		S3H016	S3H016B		NoCal
RS-C-Z9-02	135	423.0	223.0	EP-08-250BF-350	D-SN-P-126		S7H036	S7H036B		NoCal
RS-C-Z10-01	135	504.0	199.0	EP-08-250BF-350	D-SN-P-125		D3H027	D3H027A		NoCal
RS-C-Z10-02	135	504.0	207.0	EP-08-250BF-350	D-SN-P-126		D6H027	D6H027A		NoCal
RS-C-Z11-01	135	573.0	153.0	EP-08-250BF-350	D-SN-P-125		D3H048	D3H048B		NoCal
RS-C-Z11-02	135	573.0	163.0	EP-08-250BF-350	D-SN-P-126		D6H048	D6H048B		NoCal
RS-C-Z12-01	135	619.0	85.0	EP-08-250BF-350	D-SN-P-125		D3H070	D3H070A		NoCal
RS-C-Z12-02	135	619.0	92.0	EP-08-250BF-350	D-SN-P-126		D6H070	D6H070A		NoCal
RS-C-F5-01	152	184.0	215.0	EP-08-250BF-350	D-SN-P-125		S3PH007	S3PH007A		NoCal
RS-C-F5-02	150	184.0	223.0	EP-08-250BF-350	D-SN-P-126		S7HA20	S7HA20A		NoCal
RS-C-G5-01	180	184.0	215.0	EP-08-250BF-350	D-SN-P-125		S3PH007	S3PH007A		NoCal
RS-C-G5-02	180	184.0	223.0	EP-08-250BF-350	D-SN-P-126		S7HA20	S7HA20A		NoCal
RS-C-G6-01	180	246.0	215.0	EP-08-250BF-350	D-SN-P-125		S3H026	S3H026A		NoCal
RS-C-G6-02	180	246.0	223.0	EP-08-250BF-350	D-SN-P-126		S7H031	S7H031A		NoCal
RS-C-G7-01	180	304.0	215.0	EP-08-250BF-350	D-SN-P-125		S3H018	S3H018A		NoCal
RS-C-G7-02	180	304.0	223.0	EP-08-250BF-350	D-SN-P-126		S7H036	S7H036A		NoCal
RS-C-H5-01	208	184.0	215.0	EP-08-250BF-350	D-SN-P-125		S3PH007	S3PH007A		NoCal
RS-C-H5-02	210	184.0	223.0	EP-08-250BF-350	D-SN-P-126		S7H028	S7H028A		NoCal
RS-C-I5-01	240	184.0	215.0	EP-08-250BF-350	D-SN-P-125		S3H019	S3H019A		NoCal
RS-C-I5-02	240	184.0	223.0	EP-08-250BF-350	D-SN-P-126		S7H028	S7H028A		NoCal
RS-C-I9-01	240	423.0	215.0	EP-08-250BF-350	D-SN-P-125		S3H020	S3H020A		NoCal
RS-C-I9-02	240	423.0	223.0	EP-08-250BF-350	D-SN-P-126		S7H040	S7H040A		NoCal
RS-C-J1-01	270	2.0	215.0	EP-08-250BF-350	D-SN-P-125		S3H002	S3H002A		NoCal
RS-C-J1-02	270	2.0	223.0	EP-08-250BF-350	D-SN-P-126		S7H006	S7H006A		NoCal
RS-C-J2-01	270	11.0	215.0	EP-08-250BF-350	D-SN-P-125		S3H002	S3H002B		NoCal
RS-C-J2-02	270	11.0	223.0	EP-08-250BF-350	D-SN-P-126		S7H006	S7H006B		NoCal
RS-C-J5-01	270	184.0	215.0	EP-08-250BF-350	D-SN-P-125		S3H019	S3H019A		NoCal
RS-C-J5-02	270	184.0	223.0	EP-08-250BF-350	D-SN-P-126		S7H028	S7H028A		NoCal

Rebar Strain Instrumentation List

Labeling I D (name)	Azimuthal Angle (deg)	Vertical Elevation (in)	Radial Distance (in)	Transducer Designation	Location Drawing #	Details Drawing #	Basic Mark #	Modified Mark #	Comnts	Calibration
RS-C-J9-01	270	423.0	215.0	EP-08-250BF-350	D-SN-P-125		S3H020	S3H020A		NoCal
RS-C-J9-02	270	423.0	223.0	EP-08-250BF-350	D-SN-P-126		S7HB41	S7HB41A		NoCal
RS-C-L1-01	324	2.0	215.0	EP-08-250BF-350	D-SN-P-125		S4HA01	S4HA01A		NoCal
RS-C-L1-02	324	2.0	223.0	EP-08-250BF-350	D-SN-P-126		S8H001	S8H001A		NoCal
RS-C-L2-01	324	11.0	215.0	EP-08-250BF-350	D-SN-P-125		S4HA01	S4HA01B		NoCal
RS-C-L2-02	324	11.0	223.0	EP-08-250BF-350	D-SN-P-126		S8H001	S8H001B		NoCal
RS-C-L3-01	324	56.0	215.0	EP-08-250BF-350	D-SN-P-125		S4HA03	S4HA03A		NoCal
RS-C-L3-02	324	56.0	223.0	EP-08-250BF-350	D-SN-P-126		S8H005	S8H005A		NoCal
RS-C-L7-01	324	308.0	215.0	EP-08-250BF-350	D-SN-P-125		S4H028	S4H028A		NoCal
RS-C-L7-02	324	308.0	223.0	EP-08-250BF-350	D-SN-P-126		S8H029	S8H029B		NoCal
RS-C-L8-01	324	361.0	215.0	EP-08-250BF-350	D-SN-P-125		S4H028	S4H028B		NoCal
RS-C-L8-02	324	361.0	223.0	EP-08-250BF-350	D-SN-P-126		S8H029	S8H029C		NoCal
RS-C-L9-01	324	423.0	215.0	EP-08-250BF-350	D-SN-P-125		S4H028	S4H028C		NoCal
RS-C-L9-02	324	423.0	223.0	EP-08-250BF-350	D-SN-P-126		S8H028	S8H028A		NoCal
RS-C-L10-01	324	504.0	199.0	EP-08-250BF-350	D-SN-P-125		D3H027	D3H027B		NoCal
RS-C-L10-02	324	504.0	207.0	EP-08-250BF-350	D-SN-P-126		D6H027	D6H027B		NoCal
RS-C-L11-01	324	573.0	153.0	EP-08-250BF-350	D-SN-P-125		D3H048	D3H048C		NoCal
RS-C-L11-02	324	573.0	163.0	EP-08-250BF-350	D-SN-P-126		D6H048	D6H048C		NoCal
RS-C-L12-01	324	619.0	85.0	EP-08-250BF-350	D-SN-P-125		D3H070	D3H070B		NoCal
RS-C-L12-02	324	619.0	92.0	EP-08-250BF-350	D-SN-P-126		D6H070	D6H070B		NoCal
RS-C-C5-01	44	149.0	215.0	EP-08-250BF-350	D-SN-P-125		S4PH018	S4PH018A	(A/L	NoCal
RS-C-C5-02	44	149.0	223.0	EP-08-250BF-350	D-SN-P-126		S8H016	S8H016B	hoop	NoCal
RS-C-C5-03	44	184.0	215.0	EP-08-250BF-350	D-SN-P-125		S4H013	S4H013A	bars)	NoCal
RS-C-C5-04	44	184.0	223.0	EP-08-250BF-350	D-SN-P-126		S8HA16	S8HA16A		NoCal
RS-C-C5-05	44	211.0	215.0	EP-08-250BF-350	D-SN-P-125		S4H013	S4H013B		NoCal
RS-C-C5-06	44	211.0	223.0	EP-08-250BF-350	D-SN-P-126		S8HA15	S8HA15A		NoCal
RS-C-C5-07	52	126.0	215.0	EP-08-250BF-350	D-SN-P-125		S4H003	S4H003C		NoCal
RS-C-C5-08	52	126.0	223.0	EP-08-250BF-350	D-SN-P-126		S8H017	S8H017A		NoCal
RS-C-C5-09	62	126.0	215.0	EP-08-250BF-350	D-SN-P-125		S4H003	S4H003C		NoCal
RS-C-C5-10	62	126.0	223.0	EP-08-250BF-350	D-SN-P-126		S8H017	S8H017A		NoCal
RS-C-C5-11	72	126.0	215.0	EP-08-250BF-350	D-SN-P-125		S4H003	S4H003C		NoCal
RS-C-C5-12	72	126.0	223.0	EP-08-250BF-350	D-SN-P-126		S8H017	S8H017A		NoCal
RS-C-C5-13	52	232.0	215.0	EP-08-250BF-350	D-SN-P-125		S4H025	S4H025A		NoCal
RS-C-C5-14	52	232.0	223.0	EP-08-250BF-350	D-SN-P-126		S8H013	S8H013A		NoCal
RS-C-C5-15	62	232.0	215.0	EP-08-250BF-350	D-SN-P-125		S4H025	S4H025A		NoCal
RS-C-C5-16	62	232.0	223.0	EP-08-250BF-350	D-SN-P-126		S8H013	S8H013A		NoCal
RS-C-C5-17	72	232.0	215.0	EP-08-250BF-350	D-SN-P-125		S4H025	S4H025A		NoCal
RS-C-C5-18	72	232.0	223.0	EP-08-250BF-350	D-SN-P-126		S8H013	S8H013A		NoCal
RS-C-C5-19	80	149.0	215.0	EP-08-250BF-350	D-SN-P-125		S4PH018	S4PH018A		NoCal
RS-C-C5-20	80	149.0	223.0	EP-08-250BF-350	D-SN-P-126		S8H019	S8H019A		NoCal
RS-C-C5-21	80	184.0	215.0	EP-08-250BF-350	D-SN-P-125		S4H015	S4H015A		NoCal
RS-C-C5-22	80	184.0	223.0	EP-08-250BF-350	D-SN-P-126		S8H019	S8H019B		NoCal
RS-C-C5-23	80	211.0	215.0	EP-08-250BF-350	D-SN-P-125		S4H015	S4H015B		NoCal
RS-C-C5-24	80	211.0	223.0	EP-08-250BF-350	D-SN-P-126		S8H019	S8H019C		NoCal
RS-C-K5-01	299	131.0	215.0	EP-08-250BF-350	D-SN-P-125		S4PH006	S4PH006A	(E/H	NoCal
RS-C-K5-02	299	131.0	223.0	EP-08-250BF-350	D-SN-P-126		S8PH002	S8PH002A	hoop	NoCal
RS-C-K5-03	299	184.0	215.0	EP-08-250BF-350	D-SN-P-125		P5H016	P5H016A	bars)	NoCal
RS-C-K5-04	299	184.0	223.0	EP-08-250BF-350	D-SN-P-126		P5H016	P5H016A		NoCal
RS-C-K5-05	299	237.0	215.0	EP-08-250BF-350	D-SN-P-125		S4PH008	S4PH008A		NoCal
RS-C-K5-06	299	237.0	223.0	EP-08-250BF-350	D-SN-P-126		S8PH005	S8PH005A		NoCal
RS-C-L4-01	308	79.0	215.0	EP-08-250BF-350	D-SN-P-125		S4HA02	S4HA02A		NoCal
RS-C-L4-02	308	79.0	223.0	EP-08-250BF-350	D-SN-P-126		S8H007	S8H007A		NoCal
RS-C-L4-03	324	79.0	215.0	EP-08-250BF-350	D-SN-P-125		S4HA02	S4HA02A		NoCal
RS-C-L4-04	324	79.0	223.0	EP-08-250BF-350	D-SN-P-126		S8H007	S8H007A		NoCal
RS-C-L4-05	340	79.0	215.0	EP-08-250BF-350	D-SN-P-125		S4HA02	S4HA02A		NoCal

Rebar Strain Instrumentation List

Labeling	Azimuthal	Vertical	Radial	Transducer	Location	Details	Basic	Modified	Comnts	Calibration
I D	Angle	Elevation	Distance	Designation	Drawing #	Drawing #	Mark #	Mark #		
(name)	(deg)	(in)	(in)							
RS-C-L4-06	340	79.0	223.0	EP-08-250BF-350	D-SN-P-126		S8H007	S8H007A		NoCal
RS-C-L6-01	308	289.0	215.0	EP-08-250BF-350	D-SN-P-125		S4H030	S4H030A		NoCal
RS-C-L6-02	308	289.0	223.0	EP-08-250BF-350	D-SN-P-126		S8H029	S8H029A		NoCal
RS-C-L6-03	324	289.0	215.0	EP-08-250BF-350	D-SN-P-125		S4H030	S4H030A		NoCal
RS-C-L6-04	324	289.0	223.0	EP-08-250BF-350	D-SN-P-126		S8H029	S8H029A		NoCal
RS-C-L6-05	340	289.0	215.0	EP-08-250BF-350	D-SN-P-125		S4H030	S4H030A		NoCal
RS-C-L6-06	340	289.0	223.0	EP-08-250BF-350	D-SN-P-126		S8H029	S8H029A		NoCal
RS-C-A5-03	349	131.0	215.0	EP-08-250BF-350	D-SN-P-125		S4PH006	S4PH006A		NoCal
RS-C-A5-04	349	131.0	223.0	EP-08-250BF-350	D-SN-P-126		S8PH002	S8PH002A		NoCal
RS-C-A5-05	349	184.0	215.0	EP-08-250BF-350	D-SN-P-125		P5HA16	P5HA16A		NoCal
RS-C-A5-06	349	184.0	223.0	EP-08-250BF-350	D-SN-P-126		P5HA16	P5HA16A		NoCal
RS-C-A5-07	349	237.0	215.0	EP-08-250BF-350	D-SN-P-125		S4PH008	S4PH008A		NoCal
RS-C-A5-08	349	237.0	223.0	EP-08-250BF-350	D-SN-P-126		S8PH005	S8PH005A		NoCal
RS-R-A1-01	0	3.5	218.0	EP-08-250BF-350	D-SN-P-126		S10R002	S10R002A	(radial	NoCal
RS-R-A1-02	0	8.0	218.0	EP-08-250BF-350	D-SN-P-126		S10R002	S10R002B	shear	NoCal
RS-R-A2-01	0	12.5	218.0	EP-08-250BF-350	D-SN-P-126		S10R002	S10R002C	ties)	NoCal
RS-R-A2-02	0	17.0	218.0	EP-08-250BF-350	D-SN-P-126		S10R002	S10R002D		NoCal
RS-R-A5-01	0	184.0	218.0	EP-08-062AQ-350	D-SN-P-126		S10R001	S10R001A		NoCal
RS-R-A9-01	0	423.0	218.0	EP-08-062AQ-350	D-SN-P-126		S10R001	S10R001B		NoCal
RS-R-D1-01	90	3.5	222.0	EP-08-250BF-350	D-SN-P-126		SB5R001	SB5R001A		NoCal
RS-R-D1-02	90	8.0	222.0	EP-08-250BF-350	D-SN-P-126		SB5R001	SB5R001B		NoCal
RS-R-D2-01	90	12.5	222.0	EP-08-250BF-350	D-SN-P-126		SB5R001	SB5R001C		NoCal
RS-R-D2-02	90	17.0	222.0	EP-08-250BF-350	D-SN-P-126		SB5R001	SB5R001D		NoCal
RS-R-D5-01	90	184.0	222.0	EP-08-062AQ-350	D-SN-P-126		SB5U01A	SB5U01AA		NoCal
RS-R-D7-01	90	304.0	222.0	EP-08-062AQ-350	D-SN-P-126		SB5U01A	SB5U01AB		NoCal
RS-R-D9-01	90	423.0	222.0	EP-08-062AQ-350	D-SN-P-126		SB5U01A	SB5U01AC		NoCal
RS-R-D10-01	90	504.0	206.0	EP-08-062AQ-350	D-SN-P-126		DB1U05A	DB1U05AA		NoCal
RS-R-Z1-01	135	3.5	218.0	EP-08-250BF-350	D-SN-P-126		S9R002	S9R002A		NoCal
RS-R-Z1-02	135	8.0	218.0	EP-08-250BF-350	D-SN-P-126		S9R002	S9R002B		NoCal
RS-R-Z2-01	135	12.5	218.0	EP-08-250BF-350	D-SN-P-126		S9R002	S9R002C		NoCal
RS-R-Z2-02	135	17.0	218.0	EP-08-250BF-350	D-SN-P-126		S9R002	S9R002D		NoCal
RS-R-Z5-01	135	184.0	218.0	EP-08-062AQ-350	D-SN-P-126		S9R001	S9R001A		NoCal
RS-R-Z9-01	135	423.0	218.0	EP-08-062AQ-350	D-SN-P-126		S9R001	S9R001B		NoCal
RS-R-J2-01	270	12.5	222.0	EP-08-250BF-350	D-SN-P-126		SB5R001	SB5R001E		NoCal
RS-R-J5-01	270	184.0	222.0	EP-08-062AQ-350	D-SN-P-126		SB5U02A	SB5U02AA		NoCal
RS-R-J9-01	270	423.0	222.0	EP-08-062AQ-350	D-SN-P-126		SB5U02A	SB5U02AB		NoCal
RS-R-L2-01	324	12.5	218.0	EP-08-250BF-350	D-SN-P-126		S10R002	S10R002E		NoCal
RS-R-L9-01	324	423.0	218.0	EP-08-062AQ-350	D-SN-P-126		S10R001	S10R001C		NoCal
RS-R-C5-01	44	184.0	218.0	EP-08-062AQ-350	D-SN-P-126		S10R001	S10R001D		NoCal
RS-R-C5-02	62	125.0	218.0	EP-08-062AQ-350	D-SN-P-126		S10R001	S10R001E		NoCal
RS-R-C5-03	62	230.0	218.0	EP-08-062AQ-350	D-SN-P-126		S10R001	S10R001F		NoCal
RS-R-C5-04	80	184.0	218.0	EP-08-062AQ-350	D-SN-P-126		S10R001	S10R001G		NoCal
RS-R-K5-01	299	184.0	218.0	EP-08-062AQ-350	D-SN-P-126		S10R001	S10R001H		NoCal
RS-R-L4-01	324	79.0	218.0	EP-08-062AQ-350	D-SN-P-126		S10R001	S10R001I		NoCal
RS-R-L6-01	324	289.0	218.0	EP-08-062AQ-350	D-SN-P-126		S10R001	S10R001J		NoCal
RS-R-A5-02	349	184.0	218.0	EP-08-062AQ-350	D-SN-P-126		S10R001	S10R001K		NoCal

NoCal - No calibration was performed on this instrument before or after model testing

Liner Strain Instrumentation List

Labeling	Azimuthal	Vertical	Radial	Transducer	Location	Details	Basic	Modified	Comnts	Calibration
I D	Angle	Elevation	Distance	Designation	Drawing #	Drawing #	Mark #	Mark #		
(name)	(deg)	(in)	(in)			D-SN-P-				
LSI-C-A2-01	0	9.8	211.6	EP-08-250BF-350	D-SN-P-130	206/(2)	1-12C	1-12C	(Free	NoCal
LSI-M-A2-01	0	9.8	211.6	EP-08-250BF-350	D-SN-P-130	206/(2)	1-12C	1-12C	Field	NoCal
LSI-C-A5-01	0	187.0	211.6	EP-08-250BF-350	D-SN-P-130	206/(2)	3-12C	3-12C	Inside	NoCal
LSI-M-A5-01	0	187.0	211.6	EP-08-250BF-350	D-SN-P-130	206/(2)	3-12C	3-12C	Gages)	NoCal
LSI-C-B2-01	30	9.8	211.6	EP-08-250BF-350	D-SN-P-130	206/(2)	1-12C	1-12C		NoCal
LSI-M-B2-01	30	9.8	211.6	EP-08-250BF-350	D-SN-P-130	206/(2)	1-12C	1-12C		NoCal
LSI-C-B5-01	30	187.0	211.6	EP-08-250BF-350	D-SN-P-130	206/(2)	3-12C	3-12C		NoCal
LSI-M-B5-01	30	187.0	211.6	EP-08-250BF-350	D-SN-P-130	206/(2)	3-12C	3-12C		NoCal
LSI-C-B7-01	30	303.1	211.6	EP-08-250BF-350	D-SN-P-130	206/(2)	4-11B	4-11B		NoCal
LSI-M-B7-01	30	303.1	211.6	EP-08-250BF-350	D-SN-P-130	206/(2)	4-11B	4-11B		NoCal
LSI-C-B9-01	30	422.2	211.6	EP-08-250BF-350	D-SN-P-130	206/(2)	5-1A	5-1A		NoCal
LSI-M-B9-01	30	422.2	211.6	EP-08-250BF-350	D-SN-P-130	206/(2)	5-1A	5-1A		NoCal
LSI-C-D2-01	88.9	9.8	211.6	EP-08-250BF-350	D-SN-P-130	206/(2)	1-3C	1-3C		NoCal
LSI-M-D2-01	88.9	9.8	211.6	EP-08-250BF-350	D-SN-P-130	206/(2)	1-3C	1-3C		NoCal
LSI-C-D2-02	89.6	9.8	211.6	EP-08-250BF-350	D-SN-P-130	206/(2)	1-3C	1-3C		NoCal
LSI-M-D2-02	89.6	9.8	211.6	EP-08-250BF-350	D-SN-P-130	206/(2)	1-3C	1-3C		NoCal
LSI-C-D3-01	90	55.1	211.6	EP-08-250BF-350	D-SN-P-130	206/(2)	1-3B	1-3B		NoCal
LSI-M-D3-01	90	55.1	211.6	EP-08-250BF-350	D-SN-P-130	206/(2)	1-3B	1-3B		NoCal
LSI-C-D4-01	90	103.5	211.6	EP-08-250BF-350	D-SN-P-130	206/(2)	2-3C	2-3C		NoCal
LSI-M-D4-01	90	103.5	211.6	EP-08-250BF-350	D-SN-P-130	206/(2)	2-3C	2-3C		NoCal
LSI-C-D5-01	90	187.0	211.6	EP-08-250BF-350	D-SN-P-130	206/(2)	3-4C	3-4C		NoCal
LSI-M-D5-01	90	187.0	211.6	EP-08-250BF-350	D-SN-P-130	206/(2)	3-4C	3-4C		NoCal
LSI-C-D6-01	90	241.1	211.6	EP-08-250BF-350	D-SN-P-130	206/(2)	3-4B	3-4B		NoCal
LSI-M-D6-01	90	241.1	211.6	EP-08-250BF-350	D-SN-P-130	206/(2)	3-4B	3-4B		NoCal
LSI-C-D7-01	90	303.1	211.6	EP-08-250BF-350	D-SN-P-130	206/(2)	4-3B	4-3B		NoCal
LSI-M-D7-01	90	303.1	211.6	EP-08-250BF-350	D-SN-P-130	206/(2)	4-3B	4-3B		NoCal
LSI-C-D8-01	90	363.4	211.6	EP-08-250BF-350	D-SN-P-130	206/(2)	5-4B	5-4B		NoCal
LSI-M-D8-01	90	363.4	211.6	EP-08-250BF-350	D-SN-P-130	206/(2)	5-4B	5-4B		NoCal
LSI-C-D9-01	90	422.2	211.6	EP-08-250BF-350	D-SN-P-130	206/(2)	5-4B	5-4B		NoCal
LSI-M-D9-01	90	422.2	211.6	EP-08-250BF-350	D-SN-P-130	206/(2)	5-4B	5-4B		NoCal
LSI-C-D10-01	90	504.2	195.5	EP-08-250BF-350	D-SN-P-130	206/(2)	7-3C	7-3C		NoCal
LSI-M-D10-01	90	504.2	195.5	EP-08-250BF-350	D-SN-P-130	206/(2)	7-3C	7-3C		NoCal
LSI-C-D11-01	90	572.9	149.6	EP-08-250BF-350	D-SN-P-130	206/(2)	8-3C	8-3C		NoCal
LSI-M-D11-01	90	572.9	149.6	EP-08-250BF-350	D-SN-P-130	206/(2)	8-3C	8-3C		NoCal
LSI-C-D12-01	90	618.7	81.0	EP-08-250BF-350	D-SN-P-130	206/(2)	9-2B	9-2B		NoCal
LSI-M-D12-01	90	618.7	81.0	EP-08-250BF-350	D-SN-P-130	206/(2)	9-2B	9-2B		NoCal
LSI-C-E5-01	120	187.0	211.6	EP-08-250BF-350	D-SN-P-130	206/(2)	3-5C	3-5C		NoCal
LSI-M-E5-01	120	187.0	211.6	EP-08-250BF-350	D-SN-P-130	206/(2)	3-5C	3-5C		NoCal
LSI-C-Z2-01	129.5	9.8	211.6	EP-08-250BF-350	D-SN-P-130	206/(2)	1-4C	1-4C		NoCal
LSI-M-Z2-01	129.5	9.8	211.6	EP-08-250BF-350	D-SN-P-130	206/(2)	1-4C	1-4C		NoCal
LSI-C-Z2-02	130.4	9.8	211.6	EP-08-250BF-350	D-SN-P-130	206/(2)	1-4C	1-4C		NoCal
LSI-M-Z2-02	130.4	9.8	211.6	EP-08-250BF-350	D-SN-P-130	206/(2)	1-4C	1-4C		NoCal
LSI-C-Z3-01	135	55.1	211.6	EP-08-250BF-350	D-SN-P-130	206/(2)	1-4B	1-4B		NoCal
LSI-M-Z3-01	135	55.1	211.6	EP-08-250BF-350	D-SN-P-130	206/(2)	1-4B	1-4B		NoCal
LSI-C-Z4-01	135	103.5	211.6	EP-08-250BF-350	D-SN-P-130	206/(2)	2-5C	2-5C		NoCal
LSI-M-Z4-01	135	103.5	211.6	EP-08-250BF-350	D-SN-P-130	206/(2)	2-5C	2-5C		NoCal
LSI-C-Z5-01	135	187.0	211.6	EP-08-250BF-350	D-SN-P-130	206/(2)	3-5C	3-5C		NoCal
LSI-M-Z5-01	135	187.0	211.6	EP-08-250BF-350	D-SN-P-130	206/(2)	3-5C	3-5C		NoCal
LSI-C-Z6-01	135	241.1	211.6	EP-08-250BF-350	D-SN-P-130	206/(2)	3-5B	3-5B		NoCal
LSI-M-Z6-01	135	241.1	211.6	EP-08-250BF-350	D-SN-P-130	206/(2)	3-5B	3-5B		NoCal
LSI-C-Z7-01	135	303.1	211.6	EP-08-250BF-350	D-SN-P-130	206/(2)	4-5B	4-5B		NoCal
LSI-M-Z7-01	135	303.1	211.6	EP-08-250BF-350	D-SN-P-130	206/(2)	4-5B	4-5B		NoCal
LSI-C-Z8-01	135	363.4	211.6	EP-08-250BF-350	D-SN-P-130	206/(2)	5-6B	5-6B		NoCal
LSI-M-Z8-01	135	363.4	211.6	EP-08-250BF-350	D-SN-P-130	206/(2)	5-6B	5-6B		NoCal
LSI-C-Z9-01	135	422.2	211.6	EP-08-250BF-350	D-SN-P-130	206/(2)	5-6B	5-6B		NoCal
LSI-M-Z9-01	135	422.2	211.6	EP-08-250BF-350	D-SN-P-130	206/(2)	5-6B	5-6B		NoCal
LSI-C-Z10-01	135	504.2	195.5	EP-08-250BF-350	D-SN-P-130	206/(2)	7-4C	7-4C		NoCal

Liner Strain Instrumentation List

Labeling	Azimuthal	Vertical	Radial	Transducer	Location	Details	Basic	Modified	Comnts	Calibration
I D	Angle	Elevation	Distance	Designation	Drawing #	Drawing #	Mark #	Mark #		
(name)	(deg)	(in)	(in)			D-SN-P-				
LSI-M-Z10-01	135	504.2	195.5	EP-08-250BF-350	D-SN-P-130	206/(2)	7-4C	7-4C		NoCal
LSI-C-Z11-01	135	572.9	149.6	EP-08-250BF-350	D-SN-P-130	206/(2)	8-4B	8-4B		NoCal
LSI-M-Z11-01	135	572.9	149.6	EP-08-250BF-350	D-SN-P-130	206/(2)	8-4B	8-4B		NoCal
LSI-C-Z12-01	135	618.7	81.0	EP-08-250BF-350	D-SN-P-130	206/(2)	9-3A	9-3A		NoCal
LSI-M-Z12-01	135	618.7	81.0	EP-08-250BF-350	D-SN-P-130	206/(2)	9-3A	9-3A		NoCal
LSI-C-Z13-01	135	634.8	0.0	EP-08-250BF-350	D-SN-P-130	206/(2)	10-1B	10-1B		NoCal
LSI-M-Z13-01	135	634.8	0.0	EP-08-250BF-350	D-SN-P-130	206/(2)	10-1B	10-1B		NoCal
LSI-C-F5-01	150	187.0	211.6	EP-08-250BF-350	D-SN-P-130	206/(2)	3-6C	3-6C		NoCal
LSI-M-F5-01	150	187.0	211.6	EP-08-250BF-350	D-SN-P-130	206/(2)	3-6C	3-6C		NoCal
LSI-C-G2-01	180	9.8	211.6	EP-08-250BF-350	D-SN-P-130	206/(2)	1-6C	1-6C		NoCal
LSI-M-G2-01	180	9.8	211.6	EP-08-250BF-350	D-SN-P-130	206/(2)	1-6C	1-6C		NoCal
LSI-C-G5-01	180	187.0	211.6	EP-08-250BF-350	D-SN-P-130	206/(2)	3-7C	3-7C		NoCal
LSI-M-G5-01	180	187.0	211.6	EP-08-250BF-350	D-SN-P-130	206/(2)	3-7C	3-7C		NoCal
LSI-C-G6-01	180	241.1	211.6	EP-08-250BF-350	D-SN-P-130	206/(2)	3-7C	3-7C		NoCal
LSI-M-G6-01	180	241.1	211.6	EP-08-250BF-350	D-SN-P-130	206/(2)	3-7C	3-7C		NoCal
LSI-C-G7-01	180	303.1	211.6	EP-08-250BF-350	D-SN-P-130	206/(2)	4-6B	4-6B		NoCal
LSI-M-G7-01	180	303.1	211.6	EP-08-250BF-350	D-SN-P-130	206/(2)	4-6B	4-6B		NoCal
LSI-C-G9-01	180	422.2	211.6	EP-08-250BF-350	D-SN-P-130	206/(2)	5-8B	5-8B		NoCal
LSI-M-G9-01	180	422.2	211.6	EP-08-250BF-350	D-SN-P-130	206/(2)	5-8B	5-8B		NoCal
LSI-C-H5-01	210	187.0	211.6	EP-08-250BF-350	D-SN-P-130	206/(2)	3-8C	3-8C		NoCal
LSI-M-H5-01	210	187.0	211.6	EP-08-250BF-350	D-SN-P-130	206/(2)	3-8C	3-8C		NoCal
LSI-C-I2-01	239.4	9.8	211.6	EP-08-250BF-350	D-SN-P-130	206/(2)	1-8C	1-8C		NoCal
LSI-M-I2-01	239.4	9.8	211.6	EP-08-250BF-350	D-SN-P-130	206/(2)	1-8C	1-8C		NoCal
LSI-C-I5-01	240	187.0	211.6	EP-08-250BF-350	D-SN-P-130	206/(2)	3-9C	3-9C		NoCal
LSI-M-I5-01	240	187.0	211.6	EP-08-250BF-350	D-SN-P-130	206/(2)	3-9C	3-9C		NoCal
LSI-C-I7-01	240	303.1	211.6	EP-08-250BF-350	D-SN-P-130	206/(2)	4-8B	4-8B		NoCal
LSI-M-I7-01	240	303.1	211.6	EP-08-250BF-350	D-SN-P-130	206/(2)	4-8B	4-8B		NoCal
LSI-C-I9-01	240	422.2	211.6	EP-08-250BF-350	D-SN-P-130	206/(2)	5-10B	5-10B		NoCal
LSI-M-I9-01	240	422.2	211.6	EP-08-250BF-350	D-SN-P-130	206/(2)	5-10B	5-10B		NoCal
LSI-C-I11-01	240	572.9	149.6	EP-08-250BF-350	D-SN-P-130	206/(2)	8-4D	8-4D		NoCal
LSI-M-I11-01	240	572.9	149.6	EP-08-250BF-350	D-SN-P-130	206/(2)	8-4D	8-4D		NoCal
LSI-C-J2-01	270	9.8	211.6	EP-08-250BF-350	D-SN-P-130	206/(2)	1-9C	1-9C		NoCal
LSI-M-J2-01	270	9.8	211.6	EP-08-250BF-350	D-SN-P-130	206/(2)	1-9C	1-9C		NoCal
LSI-C-J4-01	270	103.5	211.6	EP-08-250BF-350	D-SN-P-130	206/(2)	2-9C	2-9C		NoCal
LSI-M-J4-01	270	103.5	211.6	EP-08-250BF-350	D-SN-P-130	206/(2)	2-9C	2-9C		NoCal
LSI-C-J5-01	270	187.0	211.6	EP-08-250BF-350	D-SN-P-130	206/(2)	3-9C	3-9C		NoCal
LSI-M-J5-01	270	187.0	211.6	EP-08-250BF-350	D-SN-P-130	206/(2)	3-9C	3-9C		NoCal
LSI-C-J7-01	270	303.1	211.6	EP-08-250BF-350	D-SN-P-130	206/(2)	4-9B	4-9B		NoCal
LSI-M-J7-01	270	303.1	211.6	EP-08-250BF-350	D-SN-P-130	206/(2)	4-9B	4-9B		NoCal
LSI-C-J9-01	270	422.2	211.6	EP-08-250BF-350	D-SN-P-130	206/(2)	5-11A	5-11A		NoCal
LSI-M-J9-01	270	422.2	211.6	EP-08-250BF-350	D-SN-P-130	206/(2)	5-11A	5-11A		NoCal
LSI-C-K5-01	300	187.0	211.6	EP-08-250BF-350	D-SN-P-130	206/(2)	3-10C	3-10C		NoCal
LSI-M-K5-01	300	187.0	211.6	EP-08-250BF-350	D-SN-P-130	206/(2)	3-10C	3-10C		NoCal
LSI-C-L2-01	324.6	9.8	211.6	EP-08-250BF-350	D-SN-P-130	206/(2)	1-11C	1-11C		NoCal
LSI-M-L2-01	324.6	9.8	211.6	EP-08-250BF-350	D-SN-P-130	206/(2)	1-11C	1-11C		NoCal
LSI-C-L3-01	324	55.1	211.6	EP-08-250BF-350	D-SN-P-130	206/(2)	1-11B	1-11B		NoCal
LSI-M-L3-01	324	55.1	211.6	EP-08-250BF-350	D-SN-P-130	206/(2)	1-11B	1-11B		NoCal
LSI-C-L4-01	324	103.5	211.6	EP-08-250BF-350	D-SN-P-130	206/(2)	2-11D	2-11D		NoCal
LSI-M-L4-01	324	103.5	211.6	EP-08-250BF-350	D-SN-P-130	206/(2)	2-11D	2-11D		NoCal
LSI-C-L6-01	324	241.1	211.6	EP-08-250BF-350	D-SN-P-130	206/(2)	3-11B	3-11B		NoCal
LSI-M-L6-01	324	241.1	211.6	EP-08-250BF-350	D-SN-P-130	206/(2)	3-11B	3-11B		NoCal
LSI-C-L7-01	324	303.1	211.6	EP-08-250BF-350	D-SN-P-130	206/(2)	4-10B	4-10B		NoCal
LSI-M-L7-01	324	303.1	211.6	EP-08-250BF-350	D-SN-P-130	206/(2)	4-10B	4-10B		NoCal
LSI-C-L8-01	324	363.4	211.6	EP-08-250BF-350	D-SN-P-130	206/(2)	5-13B	5-13B		NoCal
LSI-M-L8-01	324	363.4	211.6	EP-08-250BF-350	D-SN-P-130	206/(2)	5-13B	5-13B		NoCal
LSI-C-L9-01	324	422.2	211.6	EP-08-250BF-350	D-SN-P-130	206/(2)	5-13B	5-13B		NoCal
LSI-M-L9-01	324	422.2	211.6	EP-08-250BF-350	D-SN-P-130	206/(2)	5-13B	5-13B		NoCal
LSI-C-L10-01	324	504.2	195.5	EP-08-250BF-350	D-SN-P-130	206/(2)	7-9B	7-9B		NoCal

Liner Strain Instrumentation List

Labeling	Azimuthal	Vertical	Radial	Transducer	Location	Details	Basic	Modified	Comnts	Calibration
I D	Angle	Elevation	Distance	Designation	Drawing #	Drawing #	Mark #	Mark #		
(name)	(deg)	(in)	(in)			D-SN-P-				
LSI-M-L10-01	324	504.2	195.5	EP-08-250BF-350	D-SN-P-130	206/(2)	7-9B	7-9B		NoCal
LSI-C-L11-01	324	572.9	149.6	EP-08-250BF-350	D-SN-P-130	206/(2)	8-9A	8-9A		NoCal
LSI-M-L11-01	324	572.9	149.6	EP-08-250BF-350	D-SN-P-130	206/(2)	8-9A	8-9A		NoCal
LSI-C-L12-01	324	618.7	81.0	EP-08-250BF-350	D-SN-P-130	206/(2)	9-6B	9-6B		NoCal
LSI-M-L12-01	324	618.7	81.0	EP-08-250BF-350	D-SN-P-130	206/(2)	9-6B	9-6B		NoCal
LSI-C-D5-02	76.8	168.0	211.6	EP-08-250BF-350	D-SN-P-130	206/(2)	2-3A	2-3A	(Extra	NoCal
LSI-C-D5-03	78.4	168.0	211.6	EP-08-250BF-350	D-SN-P-130	206/(2)	2-3A	2-3A	Hoop	NoCal
LSI-C-D5-04	80	168.0	211.6	EP-08-250BF-350	D-SN-P-130	206/(2)	2-3A	2-3A	gages)	NoCal
LSI-C-J5-02	286	200.0	211.6	EP-08-250BF-350	D-SN-P-130	206/(2)	3-10B	3-10B		NoCal
LSI-C-J5-03	288.5	200.0	211.6	EP-08-250BF-350	D-SN-P-130	206/(2)	3-10B	3-10B		NoCal
LSI-C-J5-04	291	200.0	211.6	EP-08-250BF-350	D-SN-P-130	206/(2)	3-10B	3-10B		NoCal
LSA-M-D3-01	90	53.1	212.0	EP-08-250BF-350	D-SN-P-129	206/(1)	1-3B	1-3B	(Free	NoCal
LSA-M-D5-01	90	194.9	212.0	EP-08-250BF-350	D-SN-P-129	206/(1)	3-4C	3-4C	Field	NoCal
LSA-M-D7-01	90	301.2	212.0	EP-08-250BF-350	D-SN-P-129	206/(1)	4-3B	4-3B	Anchor	NoCal
LSA-M-D9-01	90	411.4	212.0	EP-08-250BF-350	D-SN-P-129	206/(1)	5-4B	5-4B	Gages)	NoCal
LSA-M-Z3-01	129	53.1	212.0	EP-08-250BF-350	D-SN-P-129	206/(1)	1-4B	1-4B		NoCal
LSA-M-Z5-01	128	194.9	212.0	EP-08-250BF-350	D-SN-P-129	206/(1)	3-5C	3-5C		NoCal
LSA-M-Z7-01	138	301.2	212.0	EP-08-250BF-350	D-SN-P-129	206/(1)	4-5B	4-5B		NoCal
LSA-M-Z9-01	129	411.4	212.0	EP-08-250BF-350	D-SN-P-129	206/(1)	5-6B	5-6B		NoCal
LSA-M-J5-01	268	194.9	212.0	EP-08-250BF-350	D-SN-P-129	206/(1)	3-9C	3-9C		NoCal
LSA-M-L3-01	325	53.1	212.0	EP-08-250BF-350	D-SN-P-129	206/(1)	1-11B	1-11B		NoCal
LSA-M-L7-01	325	301.2	212.0	EP-08-250BF-350	D-SN-P-129	206/(1)	4-10B	4-10B		NoCal
LSA-M-L9-01	325	411.4	212.0	EP-08-250BF-350	D-SN-P-129	206/(1)	5-13B	5-13B		NoCal
LSO-C-A7-01	1.8	305.3	211.7	EP-08-125AC-350	D-SN-P-129	209/(a.1)	4-1B	4-1B	(Vert.	NoCal
LRS-R-A7-1r	1.7	305.1	212.0	EP-08-125RA-120	D-SN-P-129	209/(a.1)	4-1B	4-1B	Weld)	NoCal
LRS-R-A7-1d	1.7	305.1	212.0	EP-08-125RA-120	D-SN-P-129	209/(a.1)	4-1B	4-1B		NoCal
LRS-R-A7-1h	1.7	305.1	212.0	EP-08-125RA-120	D-SN-P-129	209/(a.1)	4-1B	4-1B		NoCal
LSI-C-Z5-02	137.3	216.2	211.6	EP-08-125AC-350	D-SN-P-130	209/(a.2)	3-6B	3-6B		NoCal
LSI-C-Z5-03	137.4	216.2	211.6	EP-08-125AC-350	D-SN-P-130	209/(a.2)	3-6B	3-6B		NoCal
LSI-C-Z5-04	137.5	216.2	211.6	EP-08-125MW-120	D-SN-P-130	209/(a.2)	3-6B	3-6B		NoCal
LSI-C-Z5-05	137.6	216.2	211.6	EP-08-125MW-120	D-SN-P-130	209/(a.2)	3-6B	3-6B		NoCal
LSI-C-Z5-06	137.8	216.2	211.6	EP-08-125AC-350	D-SN-P-130	209/(a.2)	3-6B	3-6B		NoCal
LSI-M-Z5-03	137.6	216.4	211.6	EP-08-125AC-350	D-SN-P-130	209/(a.2)	3-6B	3-6B		NoCal
LSO-C-Z5-01	137.5	216.2	211.7	EP-08-125AC-350	D-SN-P-129	209/(a.2)	3-6B	3-6B		NoCal
LRS-R-Z5-1r	137.4	216.0	212.0	EP-08-125RA-120	D-SN-P-129	209/(a.2)	3-6B	3-6B		NoCal
LRS-R-Z5-1d	137.4	216.0	212.0	EP-08-125RA-120	D-SN-P-129	209/(a.2)	3-6B	3-6B		NoCal
LRS-R-Z5-1h	137.4	216.0	212.0	EP-08-125RA-120	D-SN-P-129	209/(a.2)	3-6B	3-6B		NoCal
LSI-C-Z6-02	137.3	229.7	211.6	EP-08-125AC-350	D-SN-P-130	209/(a.3)	3-6B	3-6B		NoCal
LSI-C-Z6-03	137.4	229.7	211.6	EP-08-125AC-350	D-SN-P-130	209/(a.3)	3-6B	3-6B		NoCal
LSI-C-Z6-04	137.5	229.7	211.6	EP-08-125MW-120	D-SN-P-130	209/(a.3)	3-6B	3-6B		NoCal
LSI-C-Z6-05	137.6	229.7	211.6	EP-08-125MW-120	D-SN-P-130	209/(a.3)	3-6B	3-6B		NoCal
LSI-C-Z6-06	137.8	229.7	211.6	EP-08-125AC-350	D-SN-P-130	209/(a.3)	3-6B	3-6B		NoCal
LSI-M-Z6-03	137.6	229.9	211.6	EP-08-125AC-350	D-SN-P-130	209/(a.3)	3-6B	3-6B		NoCal
LSO-C-Z6-01	137.5	229.7	211.7	EP-08-125AC-350	D-SN-P-129	209/(a.3)	3-6B	3-6B		NoCal
LSI-C-D7-02	95.6	305.3	211.6	EP-08-125AC-350	D-SN-P-130	209/(a.4)	4-3B	4-3B		NoCal
LSI-C-D7-03	95.7	305.3	211.6	EP-08-125AC-350	D-SN-P-130	209/(a.4)	4-3B	4-3B		NoCal
LSI-C-D7-04	95.8	305.3	211.6	EP-08-125MW-120	D-SN-P-130	209/(a.4)	4-3B	4-3B		NoCal
LSI-C-D7-05	95.9	305.3	211.6	EP-08-125MW-120	D-SN-P-130	209/(a.4)	4-3B	4-3B		NoCal
LSI-C-D7-06	96.1	305.3	211.6	EP-08-125AC-350	D-SN-P-130	209/(a.4)	4-3B	4-3B		NoCal
LSI-M-D7-03	95.9	305.5	211.6	EP-08-125AC-350	D-SN-P-130	209/(a.4)	4-3B	4-3B		NoCal
LSO-C-D7-01	95.8	305.3	211.7	EP-08-125AC-350	D-SN-P-129	209/(a.4)	4-3B	4-3B		NoCal
LRS-R-D7-1r	95.7	305.1	212.0	EP-08-125RA-120	D-SN-P-129	209/(a.4)	4-3B	4-3B		NoCal

Liner Strain Instrumentation List

Labeling	Azimuthal	Vertical	Radial	Transducer	Location	Details	Basic	Modified	Comnts	Calibration
I D	Angle	Elevation	Distance	Designation	Drawing #	Drawing #	Mark #	Mark #		
(name)	(deg)	(in)	(in)			D-SN-P-				
LRS-R-D7-1d	95.7	305.1	212.0	EP-08-125RA-120	D-SN-P-129	209/(a.4)	4-3B	4-3B		NoCal
LRS-R-D7-1h	95.7	305.1	212.0	EP-08-125RA-120	D-SN-P-129	209/(a.4)	4-3B	4-3B		NoCal
LSI-C-D7-07	95.6	291.5	211.6	EP-08-125AC-350	D-SN-P-130	209/(a.5)	4-3B	4-3B		NoCal
LSI-C-D7-08	95.7	291.5	211.6	EP-08-125AC-350	D-SN-P-130	209/(a.5)	4-3B	4-3B		NoCal
LSI-C-D7-09	95.8	291.5	211.6	EP-08-125MW-120	D-SN-P-130	209/(a.5)	4-3B	4-3B		NoCal
LSI-C-D7-10	95.9	291.5	211.6	EP-08-125MW-120	D-SN-P-130	209/(a.5)	4-3B	4-3B		NoCal
LSI-C-D7-11	96.1	291.5	211.6	EP-08-125AC-350	D-SN-P-130	209/(a.5)	4-3B	4-3B		NoCal
LSI-M-D7-05	95.9	291.7	211.6	EP-08-125AC-350	D-SN-P-130	209/(a.5)	4-3B	4-3B		NoCal
LSO-C-D7-02	95.8	291.5	211.7	EP-08-125AC-350	D-SN-P-129	209/(a.5)	4-3B	4-3B		NoCal
LSI-C-Z9-02	128.7	422.8	211.6	EP-08-125AC-350	D-SN-P-130	209/(b.1)	5-6B	5-6B	(Horiz.	NoCal
LSI-C-Z9-03	128.7	422.3	211.6	EP-08-125AC-350	D-SN-P-130	209/(b.1)	5-6B	5-6B	Weld)	NoCal
LSI-M-Z9-02	128.8	422.8	211.6	EP-08-125AC-350	D-SN-P-130	209/(b.1)	5-6B	5-6B		NoCal
LSI-M-Z9-04	128.8	422.3	211.6	EP-08-125AC-350	D-SN-P-130	209/(b.1)	5-6B	5-6B		NoCal
LSI-C-Z5-07	128.7	151.9	211.6	EP-08-125AC-350	D-SN-P-130	209/(b.2)	2-4B	2-4B		NoCal
LSI-C-Z5-08	128.7	151.4	211.6	EP-08-125AC-350	D-SN-P-130	209/(b.2)	2-4B	2-4B		NoCal
LSI-M-Z5-04	128.8	151.9	211.6	EP-08-125AC-350	D-SN-P-130	209/(b.2)	2-4B	2-4B		NoCal
LSI-M-Z5-06	128.8	151.4	211.6	EP-08-125AC-350	D-SN-P-130	209/(b.2)	2-4B	2-4B		NoCal
LSI-C-A1-01	0.1	0.4	211.6	EP-08-125AC-350	D-SN-P-130	208/(c.1)	1-12C	1-12C	(Basemat	NoCal
LSI-C-A1-02	0.1	1.2	211.6	EP-08-125AC-350	D-SN-P-130	208/(c.1)	1-12C	1-12C	Liner	NoCal
LSI-M-A1-01	0	0.4	211.6	EP-08-125MW-120	D-SN-P-130	208/(c.1)	1-12C	1-12C	Conn.)	NoCal
LSI-M-A1-02	0	0.5	211.6	EP-08-125MW-120	D-SN-P-130	208/(c.1)	1-12C	1-12C		NoCal
LSI-M-A1-03	0	0.8	211.6	EP-08-125AC-350	D-SN-P-130	208/(c.1)	1-12C	1-12C		NoCal
LSI-M-A1-04	0	1.2	211.6	EP-08-125AC-350	D-SN-P-130	208/(c.1)	1-12C	1-12C		NoCal
LSI-M-A1-05	0	2.0	211.6	EP-08-125AC-350	D-SN-P-130	208/(c.1)	1-12C	1-12C		NoCal
LSI-M-A1-06	0	3.1	211.6	EP-08-125AC-350	D-SN-P-130	208/(c.1)	1-12C	1-12C		NoCal
LSO-M-A1-01	0	-0.7	211.7	EP-08-125MW-120	D-SN-P-129	208/(c.1)	1-12C	1-12C		NoCal
LSO-M-A1-02	0	-0.2	211.7	EP-08-125MW-120	D-SN-P-129	208/(c.1)	1-12C	1-12C		NoCal
LSO-M-A1-03	0	0.4	211.7	EP-08-125MW-120	D-SN-P-129	208/(c.1)	1-12C	1-12C		NoCal
LSO-M-A1-04	0	0.5	211.7	EP-08-125MW-120	D-SN-P-129	208/(c.1)	1-12C	1-12C		NoCal
LSI-C-A1-03	0.1	0.0	210.0	EP-08-125AC-350	D-SN-P-130	208/(c.1)	1-12C	1-12C		NoCal
LSI-C-A1-04	0.1	0.0	207.7	EP-08-125AC-350	D-SN-P-130	208/(c.1)	1-12C	1-12C		NoCal
LSI-R-A1-01	0	0.0	211.2	EP-08-125AC-350	D-SN-P-130	208/(c.1)	1-12C	1-12C		NoCal
LSI-R-A1-02	0	0.0	210.0	EP-08-125AC-350	D-SN-P-130	208/(c.1)	1-12C	1-12C		NoCal
LSI-R-A1-03	0	0.0	209.6	EP-08-125AC-350	D-SN-P-130	208/(c.1)	1-12C	1-12C		NoCal
LSI-R-A1-04	0	0.0	207.7	EP-08-125AC-350	D-SN-P-130	208/(c.1)	1-12C	1-12C		NoCal
LSI-C-D1-01	89.7	0.4	211.6	EP-08-125AC-350	D-SN-P-130	208/(c.2)	1-3C	1-3C		NoCal
LSI-C-D1-02	89.7	1.2	211.6	EP-08-125AC-350	D-SN-P-130	208/(c.2)	1-3C	1-3C		NoCal
LSI-M-D1-01	89.6	0.4	211.6	EP-08-125MW-120	D-SN-P-130	208/(c.2)	1-3C	1-3C		NoCal
LSI-M-D1-02	89.6	0.5	211.6	EP-08-125MW-120	D-SN-P-130	208/(c.2)	1-3C	1-3C		NoCal
LSI-M-D1-03	89.6	0.8	211.6	EP-08-125AC-350	D-SN-P-130	208/(c.2)	1-3C	1-3C		NoCal
LSI-M-D1-04	89.6	1.2	211.6	EP-08-125AC-350	D-SN-P-130	208/(c.2)	1-3C	1-3C		NoCal
LSI-M-D1-05	89.6	2.0	211.6	EP-08-125AC-350	D-SN-P-130	208/(c.2)	1-3C	1-3C		NoCal
LSI-M-D1-06	89.6	3.1	211.6	EP-08-125AC-350	D-SN-P-130	208/(c.2)	1-3C	1-3C		NoCal
LSO-M-D1-01	89.6	-0.7	211.7	EP-08-125MW-120	D-SN-P-129	208/(c.2)	1-3C	1-3C		NoCal
LSO-M-D1-02	89.6	-0.2	211.7	EP-08-125MW-120	D-SN-P-129	208/(c.2)	1-3C	1-3C		NoCal
LSO-M-D1-03	89.6	0.4	211.7	EP-08-125MW-120	D-SN-P-129	208/(c.2)	1-3C	1-3C		NoCal
LSO-M-D1-04	89.6	0.5	211.7	EP-08-125MW-120	D-SN-P-129	208/(c.2)	1-3C	1-3C		NoCal
LSI-C-D1-03	89	0.4	211.6	EP-08-125AC-350	D-SN-P-130	207/(c.3)	1-3C	1-3C		NoCal
LSI-C-D1-04	89	1.2	211.6	EP-08-125AC-350	D-SN-P-130	207/(c.3)	1-3C	1-3C		NoCal
LSI-M-D1-07	88.9	0.4	211.6	EP-08-125MW-120	D-SN-P-130	207/(c.3)	1-3C	1-3C		NoCal
LSI-M-D1-08	88.9	0.5	211.6	EP-08-125MW-120	D-SN-P-130	207/(c.3)	1-3C	1-3C		NoCal
LSI-M-D1-09	88.9	0.8	211.6	EP-08-125AC-350	D-SN-P-130	207/(c.3)	1-3C	1-3C		NoCal

Liner Strain Instrumentation List

Labeling	Azimuthal	Vertical	Radial	Transducer	Location	Details	Basic	Modified	Comnts	Calibration
I D	Angle	Elevation	Distance	Designation	Drawing #	Drawing #	Mark #	Mark #		
(name)	(deg)	(in)	(in)			D-SN-P-				
LSI-M-D1-10	88.9	1.2	211.6	EP-08-125AC-350	D-SN-P-130	207/(c.3)	1-3C	1-3C		NoCal
LSI-M-D1-11	88.9	2.0	211.6	EP-08-125AC-350	D-SN-P-130	207/(c.3)	1-3C	1-3C		NoCal
LSI-M-D1-12	88.9	3.1	211.6	EP-08-125AC-350	D-SN-P-130	207/(c.3)	1-3C	1-3C		NoCal
LSO-M-D1-05	88.9	-0.7	211.7	EP-08-125MW-120	D-SN-P-129	207/(c.3)	1-3C	1-3C		NoCal
LSO-M-D1-06	88.9	-0.2	211.7	EP-08-125MW-120	D-SN-P-129	207/(c.3)	1-3C	1-3C		NoCal
LSO-M-D1-07	88.9	0.4	211.7	EP-08-125MW-120	D-SN-P-129	207/(c.3)	1-3C	1-3C		NoCal
LSO-M-D1-08	88.9	0.5	211.7	EP-08-125MW-120	D-SN-P-129	207/(c.3)	1-3C	1-3C		NoCal
LRA-R-D1-1r	88.8	0.5	212.0	EP-08-125RA-120	D-SN-P-129	207/(c.3)	1-3C	1-3C		NoCal
LRA-R-D1-1d	88.8	0.5	212.0	EP-08-125RA-120	D-SN-P-129	207/(c.3)	1-3C	1-3C		NoCal
LRA-R-D1-1m	88.8	0.5	212.0	EP-08-125RA-120	D-SN-P-129	207/(c.3)	1-3C	1-3C		NoCal
LRA-R-D1-2r	88.8	2.1	212.0	EP-08-125RA-120	D-SN-P-129	207/(c.3)	1-3C	1-3C		NoCal
LRA-R-D1-2d	88.8	2.1	212.0	EP-08-125RA-120	D-SN-P-129	207/(c.3)	1-3C	1-3C		NoCal
LRA-R-D1-2m	88.8	2.1	212.0	EP-08-125RA-120	D-SN-P-129	207/(c.3)	1-3C	1-3C		NoCal
LSI-C-Z1-01	129.6	0.4	211.6	EP-08-125AC-350	D-SN-P-130	208/(c.4)	1-4C	1-4C		NoCal
LSI-C-Z1-02	129.6	1.2	211.6	EP-08-125AC-350	D-SN-P-130	208/(c.4)	1-4C	1-4C		NoCal
LSI-M-Z1-01	129.5	0.4	211.6	EP-08-125MW-120	D-SN-P-130	208/(c.4)	1-4C	1-4C		NoCal
LSI-M-Z1-02	129.5	0.5	211.6	EP-08-125MW-120	D-SN-P-130	208/(c.4)	1-4C	1-4C		NoCal
LSI-M-Z1-03	129.5	0.8	211.6	EP-08-125AC-350	D-SN-P-130	208/(c.4)	1-4C	1-4C		NoCal
LSI-M-Z1-04	129.5	1.2	211.6	EP-08-125AC-350	D-SN-P-130	208/(c.4)	1-4C	1-4C		NoCal
LSI-M-Z1-05	129.5	2.0	211.6	EP-08-125AC-350	D-SN-P-130	208/(c.4)	1-4C	1-4C		NoCal
LSI-M-Z1-06	129.5	3.1	211.6	EP-08-125AC-350	D-SN-P-130	208/(c.4)	1-4C	1-4C		NoCal
LSO-M-Z1-01	129.5	-0.7	211.7	EP-08-125MW-120	D-SN-P-129	208/(c.4)	1-4C	1-4C		NoCal
LSO-M-Z1-02	129.5	-0.2	211.7	EP-08-125MW-120	D-SN-P-129	208/(c.4)	1-4C	1-4C		NoCal
LSO-M-Z1-03	129.5	0.4	211.7	EP-08-125MW-120	D-SN-P-129	208/(c.4)	1-4C	1-4C		NoCal
LSO-M-Z1-04	129.5	0.5	211.7	EP-08-125MW-120	D-SN-P-129	208/(c.4)	1-4C	1-4C		NoCal
LSI-C-Z1-03	130.5	0.4	211.6	EP-08-125AC-350	D-SN-P-130	207/(c.5)	1-4C	1-4C		NoCal
LSI-C-Z1-04	130.5	1.2	211.6	EP-08-125AC-350	D-SN-P-130	207/(c.5)	1-4C	1-4C		NoCal
LSI-M-Z1-07	130.4	0.4	211.6	EP-08-125MW-120	D-SN-P-130	207/(c.5)	1-4C	1-4C		NoCal
LSI-M-Z1-08	130.4	0.5	211.6	EP-08-125MW-120	D-SN-P-130	207/(c.5)	1-4C	1-4C		NoCal
LSI-M-Z1-09	130.4	0.8	211.6	EP-08-125AC-350	D-SN-P-130	207/(c.5)	1-4C	1-4C		NoCal
LSI-M-Z1-10	130.4	1.2	211.6	EP-08-125AC-350	D-SN-P-130	207/(c.5)	1-4C	1-4C		NoCal
LSI-M-Z1-11	130.4	2.0	211.6	EP-08-125AC-350	D-SN-P-130	207/(c.5)	1-4C	1-4C		NoCal
LSI-M-Z1-12	130.4	3.1	211.6	EP-08-125AC-350	D-SN-P-130	207/(c.5)	1-4C	1-4C		NoCal
LSO-M-Z1-05	130.4	-0.7	211.7	EP-08-125MW-120	D-SN-P-129	207/(c.5)	1-4C	1-4C		NoCal
LSO-M-Z1-06	130.4	-0.2	211.7	EP-08-125MW-120	D-SN-P-129	207/(c.5)	1-4C	1-4C		NoCal
LSO-M-Z1-07	130.4	0.4	211.7	EP-08-125MW-120	D-SN-P-129	207/(c.5)	1-4C	1-4C		NoCal
LSO-M-Z1-08	130.4	0.5	211.7	EP-08-125MW-120	D-SN-P-129	207/(c.5)	1-4C	1-4C		NoCal
LRA-R-Z1-1r	130.3	0.5	212.0	EP-08-125RA-120	D-SN-P-129	207/(c.5)	1-4C	1-4C		NoCal
LRA-R-Z1-1d	130.3	0.5	212.0	EP-08-125RA-120	D-SN-P-129	207/(c.5)	1-4C	1-4C		NoCal
LRA-R-Z1-1m	130.3	0.5	212.0	EP-08-125RA-120	D-SN-P-129	207/(c.5)	1-4C	1-4C		NoCal
LRA-R-Z1-2r	130.3	2.1	212.0	EP-08-125RA-120	D-SN-P-129	207/(c.5)	1-4C	1-4C		NoCal
LRA-R-Z1-2d	130.3	2.1	212.0	EP-08-125RA-120	D-SN-P-129	207/(c.5)	1-4C	1-4C		NoCal
LRA-R-Z1-2m	130.3	2.1	212.0	EP-08-125RA-120	D-SN-P-129	207/(c.5)	1-4C	1-4C		NoCal
LSI-C-Z1-05	130.5	0.0	210.0	EP-08-125AC-350	D-SN-P-130	207/(c.5)	1-4C	1-4C		NoCal
LSI-C-Z1-06	130.5	0.0	207.7	EP-08-125AC-350	D-SN-P-130	207/(c.5)	1-4C	1-4C		NoCal
LSI-R-Z1-05	130.4	0.0	211.2	EP-08-125AC-350	D-SN-P-130	207/(c.5)	1-4C	1-4C		NoCal
LSI-R-Z1-06	130.4	0.0	210.0	EP-08-125AC-350	D-SN-P-130	207/(c.5)	1-4C	1-4C		NoCal
LSI-R-Z1-07	130.4	0.0	209.6	EP-08-125AC-350	D-SN-P-130	207/(c.5)	1-4C	1-4C		NoCal
LSI-R-Z1-08	130.4	0.0	207.7	EP-08-125AC-350	D-SN-P-130	207/(c.5)	1-4C	1-4C		NoCal
LSI-C-I1-01	239.5	0.4	211.6	EP-08-125AC-350	D-SN-P-130	207/(c.6)	1-8C	1-8C		NoCal
LSI-C-I1-02	239.5	1.2	211.6	EP-08-125AC-350	D-SN-P-130	207/(c.6)	1-8C	1-8C		NoCal
LSI-M-I1-01	239.4	0.4	211.6	EP-08-125MW-120	D-SN-P-130	207/(c.6)	1-8C	1-8C		NoCal
LSI-M-I1-02	239.4	0.5	211.6	EP-08-125MW-120	D-SN-P-130	207/(c.6)	1-8C	1-8C		NoCal
LSI-M-I1-03	239.4	0.8	211.6	EP-08-125AC-350	D-SN-P-130	207/(c.6)	1-8C	1-8C		NoCal
LSI-M-I1-04	239.4	1.2	211.6	EP-08-125AC-350	D-SN-P-130	207/(c.6)	1-8C	1-8C		NoCal

Liner Strain Instrumentation List

Labeling	Azimuthal	Vertical	Radial	Transducer	Location	Details	Basic	Modified	Comnts	Calibration
I D	Angle	Elevation	Distance	Designation	Drawing #	Drawing #	Mark #	Mark #		
(name)	(deg)	(in)	(in)			D-SN-P-				
LSI-M-I1-05	239.4	2.0	211.6	EP-08-125AC-350	D-SN-P-130	207/(c.6)	1-8C	1-8C		NoCal
LSI-M-I1-06	239.4	3.1	211.6	EP-08-125AC-350	D-SN-P-130	207/(c.6)	1-8C	1-8C		NoCal
LSO-M-I1-01	239.4	-0.7	211.7	EP-08-125MW-120	D-SN-P-129	207/(c.6)	1-8C	1-8C		NoCal
LSO-M-I1-02	239.4	-0.2	211.7	EP-08-125MW-120	D-SN-P-129	207/(c.6)	1-8C	1-8C		NoCal
LSO-M-I1-03	239.4	0.4	211.7	EP-08-125MW-120	D-SN-P-129	207/(c.6)	1-8C	1-8C		NoCal
LSO-M-I1-04	239.4	0.5	211.7	EP-08-125MW-120	D-SN-P-129	207/(c.6)	1-8C	1-8C		NoCal
LRA-R-I1-1r	239.3	0.5	212.0	EP-08-125RA-120	D-SN-P-129	207/(c.6)	1-8C	1-8C		NoCal
LRA-R-I1-1d	239.3	0.5	212.0	EP-08-125RA-120	D-SN-P-129	207/(c.6)	1-8C	1-8C		NoCal
LRA-R-I1-1m	239.3	0.5	212.0	EP-08-125RA-120	D-SN-P-129	207/(c.6)	1-8C	1-8C		NoCal
LRA-R-I1-2r	239.3	2.1	212.0	EP-08-125RA-120	D-SN-P-129	207/(c.6)	1-8C	1-8C		NoCal
LRA-R-I1-2d	239.3	2.1	212.0	EP-08-125RA-120	D-SN-P-129	207/(c.6)	1-8C	1-8C		NoCal
LRA-R-I1-2m	239.3	2.1	212.0	EP-08-125RA-120	D-SN-P-129	207/(c.6)	1-8C	1-8C		NoCal
LSI-C-L1-01	324.7	0.4	211.6	EP-08-125AC-350	D-SN-P-130	208/(c.7)	1-11C	1-11C		NoCal
LSI-C-L1-02	324.7	1.2	211.6	EP-08-125AC-350	D-SN-P-130	208/(c.7)	1-11C	1-11C		NoCal
LSI-M-L1-01	324.6	0.4	211.6	EP-08-125MW-120	D-SN-P-130	208/(c.7)	1-11C	1-11C		NoCal
LSI-M-L1-02	324.6	0.5	211.6	EP-08-125MW-120	D-SN-P-130	208/(c.7)	1-11C	1-11C		NoCal
LSI-M-L1-03	324.6	0.8	211.6	EP-08-125AC-350	D-SN-P-130	208/(c.7)	1-11C	1-11C		NoCal
LSI-M-L1-04	324.6	1.2	211.6	EP-08-125AC-350	D-SN-P-130	208/(c.7)	1-11C	1-11C		NoCal
LSI-M-L1-05	324.6	2.0	211.6	EP-08-125AC-350	D-SN-P-130	208/(c.7)	1-11C	1-11C		NoCal
LSI-M-L1-06	324.6	3.1	211.6	EP-08-125AC-350	D-SN-P-130	208/(c.7)	1-11C	1-11C		NoCal
LSO-M-L1-01	324.6	-0.7	211.7	EP-08-125MW-120	D-SN-P-129	208/(c.7)	1-11C	1-11C		NoCal
LSO-M-L1-02	324.6	-0.2	211.7	EP-08-125MW-120	D-SN-P-129	208/(c.7)	1-11C	1-11C		NoCal
LSO-M-L1-03	324.6	0.4	211.7	EP-08-125MW-120	D-SN-P-129	208/(c.7)	1-11C	1-11C		NoCal
LSO-M-L1-04	324.6	0.5	211.7	EP-08-125MW-120	D-SN-P-129	208/(c.7)	1-11C	1-11C		NoCal
LSI-C-K5-02	315.2	184.0	211.6	EP-08-125AC-350	D-SN-P-218	210/(d.1)	3-11D	3-11D	(E/H	NoCal
LSI-C-K5-03	314.2	184.0	211.6	EP-08-125AC-350	D-SN-P-218	210/(d.1)	3-11D	3-11D	Liner	NoCal
LSI-C-K5-04	312.8	189.0	211.6	EP-08-125AC-350	D-SN-P-218	210/(d.1)	3-11D	3-11D	Horiz.)	NoCal
LSI-C-K5-05	312.6	189.0	211.6	EP-08-125AC-350	D-SN-P-218	210/(d.1)	3-11D	3-11D		NoCal
LSO-C-K5-01	314.2	184.0	211.7	EP-08-125AC-350	D-SN-P-129	210/(d.1)	3-11D	3-11D		NoCal
LSA-R-K5-01	312.7	189.0	212.0	EP-08-125AC-350	D-SN-P-129	210/(d.1)	3-11D	3-11D		NoCal
LSA-R-K5-02	312.7	189.0	212.0	EP-08-125AC-350	D-SN-P-129	210/(d.1)	3-11D	3-11D		NoCal
LSI-C-K5-06	308.1	189.0	211.6	EP-08-125AC-350	D-SN-P-218	210/(d.1)	3-11D	3-11D		NoCal
LSI-C-K5-07	307.9	189.0	211.6	EP-08-125AC-350	D-SN-P-218	210/(d.1)	3-11D	3-11D		NoCal
LSI-C-K5-08	306.8	189.0	211.6	EP-08-125AC-350	D-SN-P-218	210/(d.1)	3-11D	3-11D		NoCal
LSI-C-K5-09	306.6	189.0	211.6	EP-08-125AC-350	D-SN-P-218	210/(d.1)	3-11D	3-11D		NoCal
LSI-C-K5-10	306.4	189.0	211.6	EP-08-125AC-350	D-SN-P-218	210/(d.1)	3-11D	3-11D		NoCal
LSI-C-K5-11	306.2	189.0	211.6	EP-08-125AC-350	D-SN-P-218	210/(d.1)	3-11D	3-11D		NoCal
LSO-C-K5-02	306.8	189.0	211.6	EP-08-125AC-350	D-SN-P-129	210/(d.1)	3-11D	3-11D		NoCal
LSO-C-K5-03	306.6	189.0	211.6	EP-08-125AC-350	D-SN-P-129	210/(d.1)	3-11D	3-11D		NoCal
LSA-R-K5-03	308	189.0	212.0	EP-08-125AC-350	D-SN-P-129	210/(d.1)	3-11D	3-11D		NoCal
LSA-R-K5-04	308	189.0	212.0	EP-08-125AC-350	D-SN-P-129	210/(d.1)	3-11D	3-11D		NoCal
LSA-R-K5-05	306.3	189.0	212.0	EP-08-125AC-350	D-SN-P-129	210/(d.1)	3-11D	3-11D		NoCal
LSA-R-K5-06	306.3	189.0	212.0	EP-08-125AC-350	D-SN-P-129	210/(d.1)	3-11D	3-11D		NoCal
LSI-C-K5-15	314.2	187.0	211.6	EP-08-125AC-350	D-SN-P-218	210/(d.1)	3-11D	3-11D		NoCal
LSI-C-A5-02	332.8	184.0	211.6	EP-08-125AC-350	D-SN-P-218	210/(d.2)	3-11E	3-11E		NoCal
LSI-C-A5-03	333.8	184.0	211.6	EP-08-125AC-350	D-SN-P-218	210/(d.2)	3-11E	3-11E		NoCal
LSI-C-A5-04	335.2	189.0	211.6	EP-08-125AC-350	D-SN-P-218	210/(d.2)	3-11E	3-11E		NoCal
LSI-C-A5-05	335.4	189.0	211.6	EP-08-125AC-350	D-SN-P-218	210/(d.2)	3-11E	3-11E		NoCal
LSO-C-A5-01	333.8	184.0	211.7	EP-08-125AC-350	D-SN-P-129	210/(d.2)	3-11E	3-11E		NoCal
LSA-R-A5-01	335.3	189.0	212.0	EP-08-125AC-350	D-SN-P-129	210/(d.2)	3-11E	3-11E		NoCal
LSA-R-A5-02	335.3	189.0	212.0	EP-08-125AC-350	D-SN-P-129	210/(d.2)	3-11E	3-11E		NoCal
LSI-C-A5-06	339.9	189.0	211.6	EP-08-125AC-350	D-SN-P-218	210/(d.2)	3-11E	3-11E		NoCal
LSI-C-A5-07	340.1	189.0	211.6	EP-08-125AC-350	D-SN-P-218	210/(d.2)	3-11E	3-11E		NoCal
LSI-C-A5-08	341.2	189.0	211.6	EP-08-125AC-350	D-SN-P-218	210/(d.2)	3-11E	3-11E		NoCal
LSI-C-A5-09	341.4	189.0	211.6	EP-08-125AC-350	D-SN-P-218	210/(d.2)	3-11E	3-11E		NoCal

Liner Strain Instrumentation List

Labeling	Azimuthal	Vertical	Radial	Transducer	Location	Details	Basic	Modified	Comnts	Calibration
I D	Angle	Elevation	Distance	Designation	Drawing #	Drawing #	Mark #	Mark #		
(name)	(deg)	(in)	(in)			D-SN-P-				
LSI-C-A5-10	341.6	189.0	211.6	EP-08-125AC-350	D-SN-P-218	210/(d.2)	3-11E	3-11E		NoCal
LSI-C-A5-11	341.8	189.0	211.6	EP-08-125AC-350	D-SN-P-218	210/(d.2)	3-11E	3-11E		NoCal
LSO-C-A5-02	341.2	189.0	211.6	EP-08-125AC-350	D-SN-P-129	210/(d.2)	3-11E	3-11E		NoCal
LSO-C-A5-03	341.4	189.0	211.6	EP-08-125AC-350	D-SN-P-129	210/(d.2)	3-11E	3-11E		NoCal
LSA-R-A5-03	340	189.0	212.0	EP-08-125AC-350	D-SN-P-129	210/(d.2)	3-11E	3-11E		NoCal
LSA-R-A5-04	340	189.0	212.0	EP-08-125AC-350	D-SN-P-129	210/(d.2)	3-11E	3-11E		NoCal
LSA-R-A5-05	341.7	189.0	212.0	EP-08-125AC-350	D-SN-P-129	210/(d.2)	3-11E	3-11E		NoCal
LSA-R-A5-06	341.7	189.0	212.0	EP-08-125AC-350	D-SN-P-129	210/(d.2)	3-11E	3-11E		NoCal
LSI-C-A5-15	333.8	187.0	211.6	EP-08-125AC-350	D-SN-P-218	210/(d.2)	3-11E	3-11E		NoCal
LSI-C-C5-02	58.3	178.1	211.6	EP-08-125AC-350	D-SN-P-219	211/(e.1)	2-2A	2-2A	(A/L	NoCal
LSI-C-C5-03	57.9	178.1	211.6	EP-08-125AC-350	D-SN-P-219	211/(e.1)	2-2A	2-2A	Liner	NoCal
LSI-C-C5-04	56.9	178.1	211.6	EP-08-125AC-350	D-SN-P-219	211/(e.1)	2-2A	2-2A	Horiz.)	NoCal
LSI-C-C5-05	56.7	178.1	211.6	EP-08-125AC-350	D-SN-P-219	211/(e.1)	2-2A	2-2A		NoCal
LSO-C-C5-01	57.9	178.1	211.7	EP-08-125AC-350	D-SN-P-129	211/(e.1)	2-2A	2-2A		NoCal
LSA-R-C5-01	56.8	178.1	212.0	EP-08-125AC-350	D-SN-P-129	211/(e.1)	2-2A	2-2A		NoCal
LSA-R-C5-02	56.8	178.1	212.0	EP-08-125AC-350	D-SN-P-129	211/(e.1)	2-2A	2-2A		NoCal
LSI-C-C5-12	65.7	178.1	211.6	EP-08-125AC-350	D-SN-P-219	211/(e.2)	2-2A	2-2A		NoCal
LSI-C-C5-13	66.1	178.1	211.6	EP-08-125AC-350	D-SN-P-219	211/(e.2)	2-2A	2-2A		NoCal
LSI-C-C5-14	66.4	178.1	211.6	EP-08-125AC-350	D-SN-P-219	211/(e.2)	2-2A	2-2A		NoCal
LSI-C-C5-15	66.6	178.1	211.6	EP-08-125AC-350	D-SN-P-219	211/(e.2)	2-2A	2-2A		NoCal
LSO-C-C5-02	66.1	178.1	211.7	EP-08-125AC-350	D-SN-P-129	211/(e.2)	2-2A	2-2A		NoCal
LSA-R-C5-04	66.5	178.1	212.0	EP-08-125AC-350	D-SN-P-129	211/(e.2)	2-2A	2-2A		NoCal
LSI-C-C5-16	72.6	178.1	211.6	EP-08-125AC-350	D-SN-P-219	211/(e.2)	2-2A	2-2A		NoCal
LSI-C-C5-17	GAGE	REMOVED								
LSI-C-C5-18	72.9	178.1	211.6	EP-08-125AC-350	D-SN-P-219	211/(e.2)	2-2A	2-2A		NoCal
LSI-C-C5-19	73.1	178.1	211.6	EP-08-125AC-350	D-SN-P-219	211/(e.2)	2-2A	2-2A		NoCal
LSI-C-C5-20	74.3	178.1	211.6	EP-08-125AC-350	D-SN-P-219	211/(e.2)	2-2A	2-2A		NoCal
LSI-C-C5-21	74.5	178.1	211.6	EP-08-125AC-350	D-SN-P-219	211/(e.2)	2-2A	2-2A		NoCal
LSI-C-F5-02	162.1	195.9	211.6	EP-08-125AC-350	D-SN-P-220	212/(f.1)	3-7C	3-7C	(M/S &	NoCal
LSI-C-F5-03	161.4	195.9	211.6	EP-08-125AC-350	D-SN-P-220	212/(f.1)	3-7C	3-7C	F/W	NoCal
LSI-C-F5-04	160.9	195.9	211.6	EP-08-125AC-350	D-SN-P-220	212/(f.1)	3-7C	3-7C	Liner	NoCal
LSI-C-F5-05	160.7	195.9	211.6	EP-08-125AC-350	D-SN-P-220	212/(f.1)	3-7C	3-7C	Horiz.)	NoCal
LSI-M-F5-02	161.4	196.0	211.6	EP-08-125AC-350	D-SN-P-220	212/(f.1)	3-7C	3-7C		NoCal
LSI-M-F5-03	160.7	196.0	211.6	EP-08-125AC-350	D-SN-P-220	212/(f.1)	3-7C	3-7C		NoCal
LSO-C-F5-01	161.4	195.9	211.7	EP-08-125AC-350	D-SN-P-129	212/(f.1)	3-7C	3-7C		NoCal
LSI-C-H5-02	197.5	195.9	211.6	EP-08-125AC-350	D-SN-P-220	212/(f.2)	3-7C	3-7C		NoCal
LSI-C-H5-03	198.6	195.9	211.6	EP-08-125AC-350	D-SN-P-220	212/(f.2)	3-7C	3-7C		NoCal
LSI-C-H5-04	199.1	195.9	211.6	EP-08-125AC-350	D-SN-P-220	212/(f.2)	3-7C	3-7C		NoCal
LSI-C-H5-05	199.3	195.9	211.6	EP-08-125AC-350	D-SN-P-220	212/(f.2)	3-7C	3-7C		NoCal
LSI-M-H5-02	198.6	196.0	211.6	EP-08-125AC-350	D-SN-P-220	212/(f.2)	3-7C	3-7C		NoCal
LSI-M-H5-03	199.3	196.0	211.6	EP-08-125AC-350	D-SN-P-220	212/(f.2)	3-7C	3-7C		NoCal
LSO-C-H5-01	198.6	195.9	211.7	EP-08-125AC-350	D-SN-P-129	212/(f.2)	3-7C	3-7C		NoCal
LSI-C-F4-01	163.8	96.5	211.6	EP-08-125AC-350	D-SN-P-220	212/(f.3)	2-6C	2-6C		NoCal
LSI-C-F4-02	163.3	96.5	211.6	EP-08-125AC-350	D-SN-P-220	212/(f.3)	2-6C	2-6C		NoCal
LSI-C-F4-03	162.3	96.5	211.6	EP-08-125AC-350	D-SN-P-220	212/(f.3)	2-6C	2-6C		NoCal
LSI-C-F4-04	162.1	96.5	211.6	EP-08-125AC-350	D-SN-P-220	212/(f.3)	2-6C	2-6C		NoCal
LSI-M-F4-01	163.3	96.6	211.6	EP-08-125AC-350	D-SN-P-220	212/(f.3)	2-6C	2-6C		NoCal
LSI-M-F4-02	162.1	96.6	211.6	EP-08-125AC-350	D-SN-P-220	212/(f.3)	2-6C	2-6C		NoCal
LSO-C-F4-01	163.3	96.5	211.7	EP-08-125AC-350	D-SN-P-129	212/(f.3)	2-6C	2-6C		NoCal
LSI-C-H4-01	196.2	96.5	211.6	EP-08-125AC-350	D-SN-P-220	212/(f.4)	2-6C	2-6C		NoCal
LSI-C-H4-02	196.7	96.5	211.6	EP-08-125AC-350	D-SN-P-220	212/(f.4)	2-6C	2-6C		NoCal
LSI-C-H4-03	197.7	96.5	211.6	EP-08-125AC-350	D-SN-P-220	212/(f.4)	2-6C	2-6C		NoCal

Liner Strain Instrumentation List

Labeling	Azimuthal	Vertical	Radial	Transducer	Location	Details	Basic	Modified	Comnts	Calibration
I D	Angle	Elevation	Distance	Designation	Drawing #	Drawing #	Mark #	Mark #		
(name)	(deg)	(in)	(in)			D-SN-P-				
LSI-C-H4-04	197.9	96.5	211.6	EP-08-125AC-350	D-SN-P-220	212/(f.4)	2-6C	2-6C		NoCal
LSI-M-H4-01	196.7	96.6	211.6	EP-08-125AC-350	D-SN-P-220	212/(f.4)	2-6C	2-6C		NoCal
LSI-M-H4-02	197.9	96.6	211.6	EP-08-125AC-350	D-SN-P-220	212/(f.4)	2-6C	2-6C		NoCal
LSO-C-H4-01	196.7	96.5	211.7	EP-08-125AC-350	D-SN-P-129	212/(f.4)	2-6C	2-6C		NoCal
LSI-C-G8-01	201.4	378.0	211.6	EP-08-125AC-350	D-SN-P-130	213/(g.1)	5-9A	5-9A	(Crane	NoCal
LSI-C-G8-02	200.9	378.0	211.6	EP-08-125AC-350	D-SN-P-130	213/(g.1)	5-9A	5-9A	Bracket	NoCal
LSI-C-G8-03	200.7	378.0	211.6	EP-08-125AC-350	D-SN-P-130	213/(g.1)	5-9A	5-9A	Liner)	NoCal
LSI-C-G8-04	200.5	378.0	211.6	EP-08-125AC-350	D-SN-P-130	213/(g.1)	5-9A	5-9A		NoCal
LSO-C-G8-01	200.9	378.0	211.7	EP-08-125AC-350	D-SN-P-129	213/(g.1)	5-9A	5-9A		NoCal
LSI-C-H8-01	218.5	378.0	211.6	EP-08-125AC-350	D-SN-P-130	213/(g.2)	5-9E	5-9E		NoCal
LSI-C-H8-02	219	378.0	211.6	EP-08-125AC-350	D-SN-P-130	213/(g.2)	5-9E	5-9E		NoCal
LSI-C-H8-03	219.9	378.0	211.6	EP-08-125AC-350	D-SN-P-130	213/(g.2)	5-9E	5-9E		NoCal
LSI-C-H8-04	220.1	378.0	211.6	EP-08-125AC-350	D-SN-P-130	213/(g.2)	5-9E	5-9E		NoCal
LSO-C-H8-01	219	378.0	211.7	EP-08-125AC-350	D-SN-P-129	213/(g.2)	5-9E	5-9E		NoCal
LSI-C-H8-05	225.3	378.0	211.6	EP-08-125AC-350	D-SN-P-130	213/(g.3)	5-9E	5-9E		NoCal
LSI-C-H8-06	224.8	378.0	211.6	EP-08-125AC-350	D-SN-P-130	213/(g.3)	5-9E	5-9E		NoCal
LSI-C-H8-07	224.6	378.0	211.6	EP-08-125AC-350	D-SN-P-130	213/(g.3)	5-9E	5-9E		NoCal
LSI-C-H8-08	224.4	378.0	211.6	EP-08-125AC-350	D-SN-P-130	213/(g.3)	5-9E	5-9E		NoCal
LSO-C-H8-02	224.8	378.0	211.7	EP-08-125AC-350	D-SN-P-129	213/(g.3)	5-9E	5-9E		NoCal
LSI-C-L4-02	324.1	95.1	211.6	EP-08-125AC-350	D-SN-P-218	213/(h.1)	2-11D	2-11D	(E/H &	NoCal
LSI-C-L4-04	324.1	96.0	211.6	EP-08-125AC-350	D-SN-P-218	213/(h.1)	2-11D	2-11D	A/L	NoCal
LSI-M-L4-02	324	95.1	211.6	EP-08-125AC-350	D-SN-P-218	213/(h.1)	2-11D	2-11D	Liner	NoCal
LSI-M-L4-03	324	95.6	211.6	EP-08-125AC-350	D-SN-P-218	213/(h.1)	2-11D	2-11D	Vert.)	NoCal
LSI-M-L4-05	324	96.0	211.6	EP-08-125AC-350	D-SN-P-218	213/(h.1)	2-11D	2-11D		NoCal
LSI-M-L4-06	324	96.6	211.6	EP-08-125AC-350	D-SN-P-218	213/(h.1)	2-11E	2-11E		NoCal
LSI-M-L4-07	324	96.9	211.6	EP-08-125AC-350	D-SN-P-218	213/(h.1)	2-11E	2-11E		NoCal
LRA-R-L4-1r	324	95.1	212.0	EP-08-125RA-120	D-SN-P-129	213/(h.1)	2-11D	2-11D		NoCal
LRA-R-L4-1d	324	95.1	212.0	EP-08-125RA-120	D-SN-P-129	213/(h.1)	2-11D	2-11D		NoCal
LRA-R-L4-1m	324	95.1	212.0	EP-08-125RA-120	D-SN-P-129	213/(h.1)	2-11D	2-11D		NoCal
LSI-C-L6-04	324.1	272.1	211.6	EP-08-125AC-350	D-SN-P-218	213/(h.2)	3-11B	3-11B		NoCal
LSI-M-L6-05	324	272.1	211.6	EP-08-125AC-350	D-SN-P-218	213/(h.2)	3-11B	3-11B		NoCal
LSI-M-L6-06	324	271.5	211.6	EP-08-125AC-350	D-SN-P-218	213/(h.2)	3-11A	3-11A		NoCal
LRA-R-L6-1r	324	273.0	212.0	EP-08-125RA-120	D-SN-P-129	213/(h.2)	3-11B	3-11B		NoCal
LRA-R-L6-1d	324	273.0	212.0	EP-08-125RA-120	D-SN-P-129	213/(h.2)	3-11B	3-11B		NoCal
LRA-R-L6-1m	324	273.0	212.0	EP-08-125RA-120	D-SN-P-129	213/(h.2)	3-11B	3-11B		NoCal
LSI-C-C4-03	61.7	140.4	211.6	EP-08-125AC-350	D-SN-P-219	213/(h.3)	2-2B	2-2B		NoCal
LSI-M-C4-04	61.6	140.4	211.6	EP-08-125AC-350	D-SN-P-219	213/(h.3)	2-2B	2-2B		NoCal
LSI-M-C4-05	61.6	141.0	211.6	EP-08-125AC-350	D-SN-P-219	213/(h.3)	2-2C	2-2C		NoCal
LRA-R-C4-1r	61.6	139.5	212.0	EP-08-125RA-120	D-SN-P-129	213/(h.3)	2-2B	2-2B		NoCal
LRA-R-C4-1d	61.6	139.5	212.0	EP-08-125RA-120	D-SN-P-129	213/(h.3)	2-2B	2-2B		NoCal
LRA-R-C4-1m	61.6	139.5	212.0	EP-08-125RA-120	D-SN-P-129	213/(h.3)	2-2B	2-2B		NoCal
LSI-C-C6-03	61.7	215.9	211.6	EP-08-125AC-350	D-SN-P-219	213/(h.4)	3-3D	3-3D		NoCal
LSI-M-C6-04	61.6	215.9	211.6	EP-08-125AC-350	D-SN-P-219	213/(h.4)	3-3D	3-3D		NoCal
LSI-M-C6-05	61.6	215.3	211.6	EP-08-125AC-350	D-SN-P-219	213/(h.4)	3-3C	3-3C		NoCal
LRA-R-C6-1r	61.6	216.8	212.0	EP-08-125RA-120	D-SN-P-129	213/(h.4)	3-3D	3-3D		NoCal
LRA-R-C6-1d	61.6	216.8	212.0	EP-08-125RA-120	D-SN-P-129	213/(h.4)	3-3D	3-3D		NoCal
LRA-R-C6-1m	61.6	216.8	212.0	EP-08-125RA-120	D-SN-P-129	213/(h.4)	3-3D	3-3D		NoCal
LSI-C-L5-03	324.1	147.3	211.6	EP-08-125AC-350	D-SN-P-218	214/(i.1)	2-11C	2-11C	(E/H &	NoCal
LSI-M-L5-02	324	148.7	211.6	EP-08-125AC-350	D-SN-P-218	214/(i.1)	2-11C	2-11C	A/L	NoCal
LSI-M-L5-03	324	147.3	211.6	EP-08-125AC-350	D-SN-P-218	214/(i.1)	2-11C	2-11C	Liner	NoCal

Liner Strain Instrumentation List

Labeling	Azimuthal	Vertical	Radial	Transducer	Location	Details	Basic	Modified	Comnts	Calibration
I D	Angle	Elevation	Distance	Designation	Drawing #	Drawing #	Mark #	Mark #		
(name)	(deg)	(in)	(in)			D-SN-P-				
LSI-M-L5-04	324	146.9	211.6	EP-08-125AC-350	D-SN-P-218	214/(i.1)	2-11C	2-11C	Vert.)	NoCal
LSO-M-L5-01	324	149.1	211.7	EP-08-125AC-350	D-SN-P-129	214/(i.1)	2-11C	2-11C		NoCal
LSO-M-L5-02	324	148.7	211.7	EP-08-125AC-350	D-SN-P-129	214/(i.1)	2-11C	2-11C		NoCal
LRA-R-L5-1r	324	149.9	212.0	EP-08-125RA-120	D-SN-P-129	214/(i.1)	2-11C	2-11C		NoCal
LRA-R-L5-1d	324	149.9	212.0	EP-08-125RA-120	D-SN-P-129	214/(i.1)	2-11C	2-11C		NoCal
LRA-R-L5-1m	324	149.9	212.0	EP-08-125RA-120	D-SN-P-129	214/(i.1)	2-11C	2-11C		NoCal
LSI-C-L5-06	324.1	219.9	211.6	EP-08-125AC-350	D-SN-P-218	214/(i.2)	3-11C	3-11C		NoCal
LSI-M-L5-05	324	219.4	211.6	EP-08-125AC-350	D-SN-P-218	214/(i.2)	3-11C	3-11C		NoCal
LSI-M-L5-06	324	219.9	211.6	EP-08-125AC-350	D-SN-P-218	214/(i.2)	3-11C	3-11C		NoCal
LSI-M-L5-07	324	220.3	211.6	EP-08-125AC-350	D-SN-P-218	214/(i.2)	3-11C	3-11C		NoCal
LSO-M-L5-03	324	219.0	211.7	EP-08-125AC-350	D-SN-P-129	214/(i.2)	3-11C	3-11C		NoCal
LSO-M-L5-04	324	219.4	211.7	EP-08-125AC-350	D-SN-P-129	214/(i.2)	3-11C	3-11C		NoCal
LRA-R-L5-2r	324	218.2	212.0	EP-08-125RA-120	D-SN-P-129	214/(i.2)	3-11C	3-11C		NoCal
LRA-R-L5-2d	324	218.2	212.0	EP-08-125RA-120	D-SN-P-129	214/(i.2)	3-11C	3-11C		NoCal
LRA-R-L5-2m	324	218.2	212.0	EP-08-125RA-120	D-SN-P-129	214/(i.2)	3-11C	3-11C		NoCal
LSI-C-C5-23	61.7	162.9	211.6	EP-08-125AC-350	D-SN-P-219	214/(i.3)	2-2A	2-2A		NoCal
LSI-M-C5-02	62	163.3	211.6	EP-08-125AC-350	D-SN-P-219	214/(i.3)	2-2A	2-2A		NoCal
LSI-M-C5-03	61.6	162.9	211.6	EP-08-125AC-350	D-SN-P-219	214/(i.3)	2-2A	2-2A		NoCal
LSI-M-C5-04	61.6	162.5	211.6	EP-08-125AC-350	D-SN-P-219	214/(i.3)	2-2A	2-2A		NoCal
LSO-M-C5-01	62	163.7	211.7	EP-08-125AC-350	D-SN-P-129	214/(i.3)	2-2A	2-2A		NoCal
LSO-M-C5-02	62	163.3	211.7	EP-08-125AC-350	D-SN-P-129	214/(i.3)	2-2A	2-2A		NoCal
LSI-C-C5-26	61.7	193.4	211.6	EP-08-125AC-350	D-SN-P-219	214/(i.4)	3-3D	3-3D		NoCal
LSI-M-C5-05	62	193.0	211.6	EP-08-125AC-350	D-SN-P-219	214/(i.4)	3-3D	3-3D		NoCal
LSI-M-C5-06	61.6	193.4	211.6	EP-08-125AC-350	D-SN-P-219	214/(i.4)	3-3D	3-3D		NoCal
LSI-M-C5-07	61.6	193.8	211.6	EP-08-125AC-350	D-SN-P-219	214/(i.4)	3-3D	3-3D		NoCal
LSO-M-C5-03	62	192.6	211.7	EP-08-125AC-350	D-SN-P-129	214/(i.4)	3-3D	3-3D		NoCal
LSO-M-C5-04	62	193.0	211.7	EP-08-125AC-350	D-SN-P-129	214/(i.4)	3-3D	3-3D		NoCal
LSI-C-K5-12	306.8	185.2	211.6	EP-08-125AC-350	D-SN-P-218	214/(j.1)	2-10A	2-10A	(E/H	NoCal
LSI-C-K5-14	306.9	185.2	211.6	EP-08-125AC-350	D-SN-P-218	214/(j.1)	2-10A	2-10A	Liner	NoCal
LRS-R-K5-1r	307	185.0	212.0	EP-08-125RA-120	D-SN-P-129	214/(j.1)	2-10A	2-10A	Bend	NoCal
LRS-R-K5-1d	307	185.0	212.0	EP-08-125RA-120	D-SN-P-129	214/(j.1)	2-10A	2-10A	Horiz.)	NoCal
LRS-R-K5-1h	307	185.0	212.0	EP-08-125RA-120	D-SN-P-129	214/(j.1)	2-10A	2-10A		NoCal
LSI-C-A5-12	341.2	185.2	211.6	EP-08-125AC-350	D-SN-P-218	214/(j.2)	2-12A	2-12A		NoCal
LSI-C-A5-14	341.1	185.2	211.6	EP-08-125AC-350	D-SN-P-218	214/(j.2)	2-12A	2-12A		NoCal
LRS-R-A5-1r	341	185.0	212.0	EP-08-125RA-120	D-SN-P-129	214/(j.2)	2-12A	2-12A		NoCal
LRS-R-A5-1d	341	185.0	212.0	EP-08-125RA-120	D-SN-P-129	214/(j.2)	2-12A	2-12A		NoCal
LRS-R-A5-1h	341	185.0	212.0	EP-08-125RA-120	D-SN-P-129	214/(j.2)	2-12A	2-12A		NoCal
LSI-C-L5-09	314.2	178.6	211.6	EP-08-125AC-350	D-SN-P-218	215/(k.1)	2-11B	2-11B	(Anchor	NoCal
LRI-M-L5-1h	314.3	178.6	211.6	EP-08-125RA-120	D-SN-P-218	215/(k.1)	2-11B	2-11B	Ends	NoCal
LRI-M-L5-1d	314.3	178.6	211.6	EP-08-125RA-120	D-SN-P-218	215/(k.1)	2-11B	2-11B	near	NoCal
LRI-M-L5-1m	314.3	178.6	211.6	EP-08-125RA-120	D-SN-P-218	215/(k.1)	2-11B	2-11B	Plate)	NoCal
LSI-C-L5-11	333.8	189.4	211.6	EP-08-125AC-350	D-SN-P-218	215/(k.2)	3-11E	3-11E		NoCal
LRI-M-L5-2h	333.7	189.4	211.6	EP-08-125RA-120	D-SN-P-218	215/(k.2)	3-11E	3-11E		NoCal
LRI-M-L5-2d	333.7	189.4	211.6	EP-08-125RA-120	D-SN-P-218	215/(k.2)	3-11E	3-11E		NoCal
LRI-M-L5-2m	333.7	189.4	211.6	EP-08-125RA-120	D-SN-P-218	215/(k.2)	3-11E	3-11E		NoCal
LSI-C-C5-29	58.3	185.8	211.6	EP-08-125AC-350	D-SN-P-219	215/(k.3)	2-2A	2-2A		NoCal
LRI-M-C5-1h	58.4	185.8	211.6	EP-08-125RA-120	D-SN-P-219	215/(k.3)	2-2A	2-2A		NoCal
LRI-M-C5-1d	58.4	185.8	211.6	EP-08-125RA-120	D-SN-P-219	215/(k.3)	2-2A	2-2A		NoCal
LRI-M-C5-1m	58.4	185.8	211.6	EP-08-125RA-120	D-SN-P-219	215/(k.3)	2-2A	2-2A		NoCal

Liner Strain Instrumentation List

Labeling	Azimuthal	Vertical	Radial	Transducer	Location	Details	Basic	Modified	Comnts	Calibration
I D	Angle	Elevation	Distance	Designation	Drawing #	Drawing #	Mark #	Mark #		
(name)	(deg)	(in)	(in)			D-SN-P-				
LSI-C-F5-07	162.4	205.4	211.6	EP-08-125AC-350	D-SN-P-220	215/(k.4)	3-7C	3-7C		NoCal
LRI-M-F5-1h	162.5	205.4	211.6	EP-08-125RA-120	D-SN-P-220	215/(k.4)	3-7C	3-7C		NoCal
LRI-M-F5-1d	162.5	205.4	211.6	EP-08-125RA-120	D-SN-P-220	215/(k.4)	3-7C	3-7C		NoCal
LRI-M-F5-1m	162.5	205.4	211.6	EP-08-125RA-120	D-SN-P-220	215/(k.4)	3-7C	3-7C		NoCal
LSI-C-F4-06	163.7	102.3	211.6	EP-08-125AC-350	D-SN-P-220	215/(k.5)	2-6C	2-6C		NoCal
LRI-M-F4-1h	163.8	102.3	211.6	EP-08-125RA-120	D-SN-P-220	215/(k.5)	2-6C	2-6C		NoCal
LRI-M-F4-1d	163.8	102.3	211.6	EP-08-125RA-120	D-SN-P-220	215/(k.5)	2-6C	2-6C		NoCal
LRI-M-F4-1m	163.8	102.3	211.6	EP-08-125RA-120	D-SN-P-220	215/(k.5)	2-6C	2-6C		NoCal
LSI-C-L5-23	314.2	189.4	211.6	EP-08-125AC-350	D-SN-P-218	215/(k.6)	3-11D	3-11D		NoCal
LRI-M-L5-5h	314.3	189.4	211.6	EP-08-125RA-120	D-SN-P-218	215/(k.6)	3-11D	3-11D		NoCal
LRI-M-L5-5d	314.3	189.4	211.6	EP-08-125RA-120	D-SN-P-218	215/(k.6)	3-11D	3-11D		NoCal
LRI-M-L5-5m	314.3	189.4	211.6	EP-08-125RA-120	D-SN-P-218	215/(k.6)	3-11D	3-11D		NoCal
LSI-C-H5-07	197.6	205.4	211.6	EP-08-125AC-350	D-SN-P-220	215/(k.7)	3-7C	3-7C		NoCal
LRI-M-H5-1h	197.5	205.4	211.6	EP-08-125RA-120	D-SN-P-220	215/(k.7)	3-7C	3-7C		NoCal
LRI-M-H5-1d	197.5	205.4	211.6	EP-08-125RA-120	D-SN-P-220	215/(k.7)	3-7C	3-7C		NoCal
LRI-M-H5-1m	197.5	205.4	211.6	EP-08-125RA-120	D-SN-P-220	215/(k.7)	3-7C	3-7C		NoCal
LSI-C-L5-13	333.8	184.5	211.6	EP-08-125AC-350	D-SN-P-218	215/(l.1)	3-11D	3-11D	(Stiff.	NoCal
LRI-M-L5-3h	333.9	185.0	211.6	EP-08-125RA-120	D-SN-P-218	215/(l.1)	3-11D	3-11D	Ends	NoCal
LRI-M-L5-3d	333.9	185.0	211.6	EP-08-125RA-120	D-SN-P-218	215/(l.1)	3-11D	3-11D	near	NoCal
LRI-M-L5-3m	333.9	185.0	211.6	EP-08-125RA-120	D-SN-P-218	215/(l.1)	3-11D	3-11D	Plate)	NoCal
LSI-C-L5-15	314.2	184.5	211.6	EP-08-125AC-350	D-SN-P-218	215/(l.2)	3-11E	3-11E		NoCal
LRI-M-L5-4h	314.1	185.0	211.6	EP-08-125RA-120	D-SN-P-218	215/(l.2)	3-11E	3-11E		NoCal
LRI-M-L5-4d	314.1	185.0	211.6	EP-08-125RA-120	D-SN-P-218	215/(l.2)	3-11E	3-11E		NoCal
LRI-M-L5-4m	314.1	185.0	211.6	EP-08-125RA-120	D-SN-P-218	215/(l.2)	3-11E	3-11E		NoCal
LSI-C-C5-31	57.9	180.6	211.6	EP-08-125AC-350	D-SN-P-219	215/(l.3)	2-2A	2-2A		NoCal
LRI-M-C5-2h	57.8	181.1	211.6	EP-08-125RA-120	D-SN-P-219	215/(l.3)	2-2A	2-2A		NoCal
LRI-M-C5-2d	57.8	181.1	211.6	EP-08-125RA-120	D-SN-P-219	215/(l.3)	2-2A	2-2A		NoCal
LRI-M-C5-2m	57.8	181.1	211.6	EP-08-125RA-120	D-SN-P-219	215/(l.3)	2-2A	2-2A		NoCal
LSI-C-C5-33	66.1	180.6	211.6	EP-08-125AC-350	D-SN-P-219	215/(l.4)	2-2A	2-2A		NoCal
LRI-M-C5-3h	66.2	181.1	211.6	EP-08-125RA-120	D-SN-P-219	215/(l.4)	2-2A	2-2A		NoCal
LRI-M-C5-3d	66.2	181.1	211.6	EP-08-125RA-120	D-SN-P-219	215/(l.4)	2-2A	2-2A		NoCal
LRI-M-C5-3m	66.2	181.1	211.6	EP-08-125RA-120	D-SN-P-219	215/(l.4)	2-2A	2-2A		NoCal
LSI-C-F4-08	163.6	92.7	211.6	EP-08-125AC-350	D-SN-P-220	215/(l.5)	2-6C	2-6C		NoCal
LRI-M-F4-2h	163.5	92.2	211.6	EP-08-125RA-120	D-SN-P-220	215/(l.5)	2-6C	2-6C		NoCal
LRI-M-F4-2d	163.5	92.2	211.6	EP-08-125RA-120	D-SN-P-220	215/(l.5)	2-6C	2-6C		NoCal
LRI-M-F4-2m	163.5	92.2	211.6	EP-08-125RA-120	D-SN-P-220	215/(l.5)	2-6C	2-6C		NoCal
LSI-C-A4-01	306.8	125.2	211.6	EP-08-125AC-350	D-SN-P-218	216/(m.1)	2-11D	2-11D	(Re-	NoCal
LSI-C-A4-02	306.5	125.0	211.6	EP-08-125AC-350	D-SN-P-218	216/(m.1)	2-12B	2-12B	Entrant	NoCal
LRI-M-A4-1h	306.7	125.0	211.6	EP-08-125RA-120	D-SN-P-218	216/(m.1)	2-12B	2-12B	Corners)	NoCal
LRI-M-A4-1d	306.7	125.0	211.6	EP-08-125RA-120	D-SN-P-218	216/(m.1)	2-12B	2-12B		NoCal
LRI-M-A4-1m	306.7	125.0	211.6	EP-08-125RA-120	D-SN-P-218	216/(m.1)	2-12B	2-12B		NoCal
LSI-C-A6-01	306.8	242.9	211.6	EP-08-125AC-350	D-SN-P-218	216/(m.2)	3-11B	3-11B		NoCal
LSI-C-A6-02	306.5	243.1	211.6	EP-08-125AC-350	D-SN-P-218	216/(m.2)	3-12B	3-12B		NoCal
LRI-M-A6-1h	306.7	243.1	211.6	EP-08-125RA-120	D-SN-P-218	216/(m.2)	3-12B	3-12B		NoCal
LRI-M-A6-1d	306.7	243.1	211.6	EP-08-125RA-120	D-SN-P-218	216/(m.2)	3-12B	3-12B		NoCal
LRI-M-A6-1m	306.7	243.1	211.6	EP-08-125RA-120	D-SN-P-218	216/(m.2)	3-12B	3-12B		NoCal
LSI-C-C5-36	72.9	203.5	211.6	EP-08-125AC-350	D-SN-P-219	216/(m.4)	3-3D	3-3D		NoCal

Liner Strain Instrumentation List

Labeling	Azimuthal	Vertical	Radial	Transducer	Location	Details	Basic	Modified	Comnts	Calibration
I D	Angle	Elevation	Distance	Designation	Drawing #	Drawing #	Mark #	Mark #		
(name)	(deg)	(in)	(in)			D-SN-P-				
LSI-C-C5-37	73.2	203.7	211.6	EP-08-125AC-350	D-SN-P-219	216/(m.4)	3-2C	3-2C		NoCal
LRI-M-C5-5h	73	203.7	211.6	EP-08-125RA-120	D-SN-P-219	216/(m.4)	3-2C	3-2C		NoCal
LRI-M-C5-5d	73	203.7	211.6	EP-08-125RA-120	D-SN-P-219	216/(m.4)	3-2C	3-2C		NoCal
LRI-M-C5-5m	73	203.7	211.6	EP-08-125RA-120	D-SN-P-219	216/(m.4)	3-2C	3-2C		NoCal
LSI-C-L5-16	324.1	184.0	191.0	EP-08-125AC-350	D-SN-P-218	217/(n.1)	E/H	E/H	(Equip-	NoCal
LSI-C-L5-17	324.1	213.2	194.0	EP-08-125AC-350	D-SN-P-218	217/(n.1)	E/H	E/H	ment	NoCal
LSI-C-L5-18	331.9	184.0	194.0	EP-08-125AC-350	D-SN-P-218	217/(n.1)	E/H	E/H	Hatch)	NoCal
LSI-M-L5-08	324	184.0	191.0	EP-08-125AC-350	D-SN-P-218	217/(n.1)	E/H	E/H		NoCal
LSI-M-L5-09	324	213.2	194.0	EP-08-125AC-350	D-SN-P-218	217/(n.1)	E/H	E/H		NoCal
LSI-M-L5-10	331.9	184.4	194.0	EP-08-125AC-350	D-SN-P-218	217/(n.1)	E/H	E/H		NoCal
LSI-M-L5-11	324	214.4	196.0	EP-08-125AC-350	D-SN-P-218	217/(n.1)	E/H	E/H		NoCal
LSI-M-L5-12	324	214.4	198.0	EP-08-125AC-350	D-SN-P-218	217/(n.1)	E/H	E/H		NoCal
LSI-M-L5-13	332.2	184.0	196.0	EP-08-125AC-350	D-SN-P-218	217/(n.1)	E/H	E/H		NoCal
LSI-M-L5-14	332.2	184.0	198.0	EP-08-125AC-350	D-SN-P-218	217/(n.1)	E/H	E/H		NoCal
LSI-C-L5-19	323.9	214.4	196.0	EP-08-125AC-350	D-SN-P-218	217/(n.1)	E/H	E/H		NoCal
LSI-C-L5-20	323.9	214.4	198.0	EP-08-125AC-350	D-SN-P-218	217/(n.1)	E/H	E/H		NoCal
LSI-C-L5-21	332.2	184.4	196.0	EP-08-125AC-350	D-SN-P-218	217/(n.1)	E/H	E/H		NoCal
LSI-C-L5-22	332.2	184.4	198.0	EP-08-125AC-350	D-SN-P-218	217/(n.1)	E/H	E/H		NoCal
LSI-M-H5-04	197	183.5	211.6	EP-08-125AC-350	D-SN-P-220	217/(o.1)	M/S	M/S	Weld	NoCal
LSI-C-H5-08	196.9	183.3	211.6	EP-08-125AC-350	D-SN-P-220	217/(o.1)	M/S	M/S	Detail	NoCal
LSI-C-J5-05	271.9	187.0	211.6	EP-08-125AC-350	D-SN-P-130	130	3-9C	3-9C	Buttress	NoCal
LSI-C-J5-06	271.9	185.0	211.6	EP-08-125AC-350	D-SN-P-130	130	3-9C	3-9C	Strains	NoCal
LSI-C-J5-07	274.0	187.0	211.6	EP-08-250BF-350	D-SN-P-130	130	3-10C	3-10C		NoCal
LSI-C-J5-08	276.0	187.0	211.6	EP-08-250BF-350	D-SN-P-130	130	3-10C	3-10C		NoCal
LSI-C-J5-09	278.0	187.0	211.6	EP-08-250BF-350	D-SN-P-130	130	3-10C	3-10C		NoCal
LSI-C-J5-10	280.0	187.0	211.6	EP-08-250BF-350	D-SN-P-130	130	3-10C	3-10C		NoCal
LRI-C-J6-1h	273.8	229.0	211.6	EP-08-125RA-120	D-SN-P-130	130			Near	NoCal
LRI-M-J6-1m	273.8	229.0	211.6	EP-08-125RA-120	D-SN-P-130	130			Liner	NoCal
LRI-C-I6-1h	241.0	259.5	211.6	EP-08-125RA-120	D-SN-P-130	130			Repairs	NoCal
LRI-M-I6-1m	241.0	259.5	211.6	EP-08-125RA-120	D-SN-P-130	130				NoCal
LRI-C-J8-1h	278.3	381.4	211.6	EP-08-125RA-120	D-SN-P-130	130				NoCal
LRI-M-J8-1m	278.3	381.4	211.6	EP-08-125RA-120	D-SN-P-130	130				NoCal

NoCal - No calibration was performed on this instrument before or after model testing

Tendon Instrumentation List

Labeling	Azimuthal	Vertical	Radial	Transducer	Location	Details	Basic	Modified	Comnts	Calibration
I D	Angle	Elevation	Distance	Designation	Drawing #	Drawing #	Mark #	Mark #		
(name)	(deg)	(in)	(in)							
TT-M-Z3-01	135	64.0	218.0	TENSMEG-120	D-SN-P-128		V46	V46-1	Vert.	NoCal
TT-M-Z6-01	135	244.0	218.0	TENSMEG-120	D-SN-P-128		V46	V46-1	Tensmeg	NoCal
TT-M-Z9-01	135	380.0	218.0	TENSMEG-120	D-SN-P-128		V46	V46-1		NoCal
TT-M-E10-01	121	537.0	178.0	TENSMEG-120	D-SN-P-128		V46	V46-1		NoCal
TT-M-D11-01	90	580.0	141.0	TENSMEG-120	D-SN-P-128		V46	V46-1		NoCal
TT-M-I3-01	241	64.0	218.0	TENSMEG-120	D-SN-P-128		V37	V37-1		NoCal
TT-M-I3-02	241	90.0	218.0	TENSMEG-120	D-SN-P-128		V37	V37-2		NoCal
TT-M-I3-03	241	38.0	218.0	TENSMEG-120	D-SN-P-128		V37	V37-3		NoCal
TT-M-I9-01	241	380.0	218.0	TENSMEG-120	D-SN-P-128		V37	V37-1		NoCal
TT-M-I9-02	241	406.0	218.0	TENSMEG-120	D-SN-P-128		V37	V37-2		NoCal
TT-M-I9-03	241	354.0	218.0	TENSMEG-120	D-SN-P-128		V37	V37-3		NoCal
TT-M-G12-01	180	615.0	87.0	TENSMEG-120	D-SN-P-128		V37	V37-1		NoCal
TT-M-L3-01	325	64.0	218.0	TENSMEG-120	D-SN-P-128		V85	V85-1		NoCal
TT-M-L3-02	325	90.0	218.0	TENSMEG-120	D-SN-P-128		V85	V85-2		NoCal
TT-M-L3-03	325	38.0	218.0	TENSMEG-120	D-SN-P-128		V85	V85-3		NoCal
TT-M-L9-01	325	380.0	218.0	TENSMEG-120	D-SN-P-128		V85	V85-1		NoCal
TT-M-L9-02	325	406.0	218.0	TENSMEG-120	D-SN-P-128		V85	V85-2		NoCal
TT-M-L9-03	325	354.0	218.0	TENSMEG-120	D-SN-P-128		V85	V85-3		NoCal
TT-M-J11-01	270	588.0	132.0	TENSMEG-120	D-SN-P-128		V85	V85-1		NoCal
TT-C-A3-01	0	73.0	220.0	TENSMEG-120	D-SN-P-128		H11	H11-1	Hoop	NoCal
TT-C-D3-01	90	73.0	220.0	TENSMEG-120	D-SN-P-128		H11	H11-1	Tensmeg	NoCal
TT-C-G3-01	180	73.0	220.0	TENSMEG-120	D-SN-P-128		H11	H11-1		NoCal
TT-C-A5-01	0	180.0	220.0	TENSMEG-120	D-SN-P-128		H35	H35-1		NoCal
TT-C-A5-02	7	180.0	220.0	TENSMEG-120	D-SN-P-128		H35	H35-2		NoCal
TT-C-A5-03	353	180.0	220.0	TENSMEG-120	D-SN-P-128		H35	H35-3		NoCal
TT-C-D5-01	90	180.0	220.0	TENSMEG-120	D-SN-P-128		H35	H35-1		NoCal
TT-C-Z5-01	135	180.0	220.0	TENSMEG-120	D-SN-P-128		H35	H35-1		NoCal
TT-C-G5-01	180	174.0	220.0	TENSMEG-120	D-SN-P-128		H35	H35-1		NoCal
TT-C-K5-01	285	180.0	220.0	TENSMEG-120	D-SN-P-128		H35	H35-1		NoCal
TT-C-K5-02	292	180.0	220.0	TENSMEG-120	D-SN-P-128		H35	H35-2		NoCal
TT-C-K5-03	278	180.0	220.0	TENSMEG-120	D-SN-P-128		H35	H35-3		NoCal
TT-C-A6-01	0	259.0	220.0	TENSMEG-120	D-SN-P-128		H53	H53-1		NoCal
TT-C-D6-01	90	259.0	220.0	TENSMEG-120	D-SN-P-128		H53	H53-1		NoCal
TT-C-D6-02	83	259.0	220.0	TENSMEG-120	D-SN-P-128		H53	H53-2		NoCal
TT-C-D6-03	97	259.0	220.0	TENSMEG-120	D-SN-P-128		H53	H53-3		NoCal
TT-C-G6-01	180	259.0	220.0	TENSMEG-120	D-SN-P-128		H53	H53-1		NoCal
TT-C-K6-01	280	259.0	220.0	TENSMEG-120	D-SN-P-128		H53	H53-1		NoCal
TF-M-Z3-01	135	64.0	218.0	EP-08-062AQ-350	D-SN-P-128		V46	V46-1	Vert.	NoCal
TF-M-Z3-02	135	64.0	218.0	EP-08-062AQ-350	D-SN-P-128		V46	V46-1	Foil	NoCal
TF-M-Z6-01	135	244.0	218.0	EP-08-062AQ-350	D-SN-P-128		V46	V46-1	Gages	NoCal
TF-M-Z6-02	135	244.0	218.0	EP-08-062AQ-350	D-SN-P-128		V46	V46-1		NoCal
TF-M-Z9-01	135	380.0	218.0	EP-08-062AQ-350	D-SN-P-128		V46	V46-1		NoCal
TF-M-Z9-02	135	380.0	218.0	EP-08-062AQ-350	D-SN-P-128		V46	V46-1		NoCal
TF-M-E10-01	121	537.0	178.0	EP-08-062AQ-350	D-SN-P-128		V46	V46-1		NoCal
TF-M-E10-02	121	537.0	178.0	EP-08-062AQ-350	D-SN-P-128		V46	V46-1		NoCal
TF-M-D11-01	90	580.0	141.0	EP-08-062AQ-350	D-SN-P-128		V46	V46-1		NoCal
TF-M-D11-02	90	580.0	141.0	EP-08-062AQ-350	D-SN-P-128		V46	V46-1		NoCal
TF-M-I3-01	241	64.0	218.0	EP-08-062AQ-350	D-SN-P-128		V37	V37-1		NoCal
TF-M-I3-02	241	64.0	218.0	EP-08-062AQ-350	D-SN-P-128		V37	V37-1		NoCal
TF-M-I3-03	241	90.0	218.0	EP-08-062AQ-350	D-SN-P-128		V37	V37-2		NoCal
TF-M-I3-04	241	90.0	218.0	EP-08-062AQ-350	D-SN-P-128		V37	V37-2		NoCal
TF-M-I3-05	241	38.0	218.0	EP-08-062AQ-350	D-SN-P-128		V37	V37-3		NoCal

Tendon Instrumentation List

Labeling	Azimuthal	Vertical	Radial	Transducer	Location	Details	Basic	Modified	Comnts	Calibration
I D	Angle	Elevation	Distance	Designation	Drawing #	Drawing #	Mark #	Mark #		
(name)	(deg)	(in)	(in)							
TF-M-I3-06	241	38.0	218.0	EP-08-062AQ-350	D-SN-P-128		V37	V37-3		NoCal
TF-M-I9-01	241	380.0	218.0	EP-08-062AQ-350	D-SN-P-128		V37	V37-1		NoCal
TF-M-I9-02	241	380.0	218.0	EP-08-062AQ-350	D-SN-P-128		V37	V37-1		NoCal
TF-M-I9-03	241	406.0	218.0	EP-08-062AQ-350	D-SN-P-128		V37	V37-2		NoCal
TF-M-I9-04	241	406.0	218.0	EP-08-062AQ-350	D-SN-P-128		V37	V37-2		NoCal
TF-M-I9-05	241	354.0	218.0	EP-08-062AQ-350	D-SN-P-128		V37	V37-3		NoCal
TF-M-I9-06	241	354.0	218.0	EP-08-062AQ-350	D-SN-P-128		V37	V37-3		NoCal
TF-M-G12-01	180	615.0	87.0	EP-08-062AQ-350	D-SN-P-128		V37	V37-1		NoCal
TF-M-G12-02	180	615.0	87.0	EP-08-062AQ-350	D-SN-P-128		V37	V37-1		NoCal
TF-M-L3-01	325	64.0	218.0	EP-08-062AQ-350	D-SN-P-128		V85	V85-1		NoCal
TF-M-L3-02	325	64.0	218.0	EP-08-062AQ-350	D-SN-P-128		V85	V85-1		NoCal
TF-M-L3-03	325	64.0	218.0	EP-08-062AQ-350	D-SN-P-128		V85	V85-1		NoCal
TF-M-L3-04	325	90.0	218.0	EP-08-062AQ-350	D-SN-P-128		V85	V85-2		NoCal
TF-M-L3-05	325	90.0	218.0	EP-08-062AQ-350	D-SN-P-128		V85	V85-2		NoCal
TF-M-L3-06	325	90.0	218.0	EP-08-062AQ-350	D-SN-P-128		V85	V85-2		NoCal
TF-M-L3-07	325	38.0	218.0	EP-08-062AQ-350	D-SN-P-128		V85	V85-3		NoCal
TF-M-L3-08	325	38.0	218.0	EP-08-062AQ-350	D-SN-P-128		V85	V85-3		NoCal
TF-M-L3-09	325	38.0	218.0	EP-08-062AQ-350	D-SN-P-128		V85	V85-3		NoCal
TF-M-L5-01	334	184.0	218.0	EP-08-062AQ-350	D-SN-P-128		V85	V85-1		NoCal
TF-M-L5-02	334	184.0	218.0	EP-08-062AQ-350	D-SN-P-128		V85	V85-1		NoCal
TF-M-L5-03	334	184.0	218.0	EP-08-062AQ-350	D-SN-P-128		V85	V85-1		NoCal
TF-M-L9-01	325	380.0	218.0	EP-08-062AQ-350	D-SN-P-128		V85	V85-1		NoCal
TF-M-L9-02	325	380.0	218.0	EP-08-062AQ-350	D-SN-P-128		V85	V85-1		NoCal
TF-M-L9-03	325	380.0	218.0	EP-08-062AQ-350	D-SN-P-128		V85	V85-1		NoCal
TF-M-L9-04	325	406.0	218.0	EP-08-062AQ-350	D-SN-P-128		V85	V85-2		NoCal
TF-M-L9-05	325	406.0	218.0	EP-08-062AQ-350	D-SN-P-128		V85	V85-2		NoCal
TF-M-L9-06	325	406.0	218.0	EP-08-062AQ-350	D-SN-P-128		V85	V85-2		NoCal
TF-M-L9-07	325	354.0	218.0	EP-08-062AQ-350	D-SN-P-128		V85	V85-3		NoCal
TF-M-L9-08	325	354.0	218.0	EP-08-062AQ-350	D-SN-P-128		V85	V85-3		NoCal
TF-M-L9-09	325	354.0	218.0	EP-08-062AQ-350	D-SN-P-128		V85	V85-3		NoCal
TF-M-J11-01	270	588.0	132.0	EP-08-062AQ-350	D-SN-P-128		V85	V85-1		NoCal
TF-M-J11-02	270	588.0	132.0	EP-08-062AQ-350	D-SN-P-128		V85	V85-1		NoCal
TF-C-A3-01	0	73.0	220.0	EP-08-062AQ-350	D-SN-P-128		H11	H11-1	Hoop	NoCal
TF-C-A3-02	0	73.0	220.0	EP-08-062AQ-350	D-SN-P-128		H11	H11-1	Foil	NoCal
TF-C-D3-01	90	73.0	220.0	EP-08-062AQ-350	D-SN-P-128		H11	H11-1	Gages	NoCal
TF-C-D3-02	90	73.0	220.0	EP-08-062AQ-350	D-SN-P-128		H11	H11-1		NoCal
TF-C-G3-01	180	73.0	220.0	EP-08-062AQ-350	D-SN-P-128		H11	H11-1		NoCal
TF-C-G3-02	180	73.0	220.0	EP-08-062AQ-350	D-SN-P-128		H11	H11-1		NoCal
TF-C-I3-01	260	73.0	220.0	EP-08-062AQ-350	D-SN-P-128		H11	H11-1		NoCal
TF-C-I3-02	260	73.0	220.0	EP-08-062AQ-350	D-SN-P-128		H11	H11-1		NoCal
TF-C-I3-03	260	73.0	220.0	EP-08-062AQ-350	D-SN-P-128		H11	H11-1		NoCal
TF-C-A5-01	0	180.0	220.0	EP-08-062AQ-350	D-SN-P-128		H35	H35-1		NoCal
TF-C-A5-02	0	180.0	220.0	EP-08-062AQ-350	D-SN-P-128		H35	H35-1		NoCal
TF-C-A5-03	0	180.0	220.0	EP-08-062AQ-350	D-SN-P-128		H35	H35-1		NoCal
TF-C-A5-04	7	180.0	220.0	EP-08-062AQ-350	D-SN-P-128		H35	H35-2		NoCal
TF-C-A5-05	7	180.0	220.0	EP-08-062AQ-350	D-SN-P-128		H35	H35-2		NoCal
TF-C-A5-06	7	180.0	220.0	EP-08-062AQ-350	D-SN-P-128		H35	H35-2		NoCal
TF-C-A5-07	353	180.0	220.0	EP-08-062AQ-350	D-SN-P-128		H35	H35-3		NoCal
TF-C-A5-08	353	180.0	220.0	EP-08-062AQ-350	D-SN-P-128		H35	H35-3		NoCal
TF-C-A5-09	353	180.0	220.0	EP-08-062AQ-350	D-SN-P-128		H35	H35-3		NoCal
TF-C-D5-01	90	180.0	220.0	EP-08-062AQ-350	D-SN-P-128		H35	H35-1		NoCal
TF-C-D5-02	90	180.0	220.0	EP-08-062AQ-350	D-SN-P-128		H35	H35-1		NoCal
TF-C-Z5-01	135	180.0	220.0	EP-08-062AQ-350	D-SN-P-128		H35	H35-1		NoCal
TF-C-Z5-02	135	180.0	220.0	EP-08-062AQ-350	D-SN-P-128		H35	H35-1		NoCal

Tendon Instrumentation List

Labeling	Azimuthal	Vertical	Radial	Transducer	Location	Details	Basic	Modified	Comnts	Calibration
I D	Angle	Elevation	Distance	Designation	Drawing #	Drawing #	Mark #	Mark #		
(name)	(deg)	(in)	(in)							
TF-C-G5-01	180	174.0	220.0	EP-08-062AQ-350	D-SN-P-128		H35	H35-1		NoCal
TF-C-G5-02	180	174.0	220.0	EP-08-062AQ-350	D-SN-P-128		H35	H35-1		NoCal
TF-C-I5-01	260	180.0	220.0	EP-08-062AQ-350	D-SN-P-128		H35	H35-1		NoCal
TF-C-I5-02	260	180.0	220.0	EP-08-062AQ-350	D-SN-P-128		H35	H35-1		NoCal
TF-C-I5-03	260	180.0	220.0	EP-08-062AQ-350	D-SN-P-128		H35	H35-1		NoCal
TF-C-K5-01	285	180.0	220.0	EP-08-062AQ-350	D-SN-P-128		H35	H35-1		NoCal
TF-C-K5-02	285	180.0	220.0	EP-08-062AQ-350	D-SN-P-128		H35	H35-1		NoCal
TF-C-K5-03	285	180.0	220.0	EP-08-062AQ-350	D-SN-P-128		H35	H35-1		NoCal
TF-C-K5-04	292	180.0	220.0	EP-08-062AQ-350	D-SN-P-128		H35	H35-2		NoCal
TF-C-K5-05	292	180.0	220.0	EP-08-062AQ-350	D-SN-P-128		H35	H35-2		NoCal
TF-C-K5-06	292	180.0	220.0	EP-08-062AQ-350	D-SN-P-128		H35	H35-2		NoCal
TF-C-K5-07	278	180.0	220.0	EP-08-062AQ-350	D-SN-P-128		H35	H35-3		NoCal
TF-C-K5-08	278	180.0	220.0	EP-08-062AQ-350	D-SN-P-128		H35	H35-3		NoCal
TF-C-K5-09	278	180.0	220.0	EP-08-062AQ-350	D-SN-P-128		H35	H35-3		NoCal
TF-C-L5-01	324	148.0	220.0	EP-08-062AQ-350	D-SN-P-128		H35	H35-1		NoCal
TF-C-L5-02	324	148.0	220.0	EP-08-062AQ-350	D-SN-P-128		H35	H35-1		NoCal
TF-C-L5-03	324	148.0	220.0	EP-08-062AQ-350	D-SN-P-128		H35	H35-1		NoCal
TF-C-A6-01	0	259.0	220.0	EP-08-062AQ-350	D-SN-P-128		H53	H53-1		NoCal
TF-C-A6-02	0	259.0	220.0	EP-08-062AQ-350	D-SN-P-128		H53	H53-1		NoCal
TF-C-D6-01	90	259.0	220.0	EP-08-062AQ-350	D-SN-P-128		H53	H53-1		NoCal
TF-C-D6-02	90	259.0	220.0	EP-08-062AQ-350	D-SN-P-128		H53	H53-1		NoCal
TF-C-D6-03	83	259.0	220.0	EP-08-062AQ-350	D-SN-P-128		H53	H53-2		NoCal
TF-C-D6-04	83	259.0	220.0	EP-08-062AQ-350	D-SN-P-128		H53	H53-2		NoCal
TF-C-D6-05	97	259.0	220.0	EP-08-062AQ-350	D-SN-P-128		H53	H53-3		NoCal
TF-C-D6-06	97	259.0	220.0	EP-08-062AQ-350	D-SN-P-128		H53	H53-3		NoCal
TF-C-G6-01	180	259.0	220.0	EP-08-062AQ-350	D-SN-P-128		H53	H53-1		NoCal
TF-C-G6-02	180	259.0	220.0	EP-08-062AQ-350	D-SN-P-128		H53	H53-1		NoCal
TF-C-I6-01	260	259.0	220.0	EP-08-062AQ-350	D-SN-P-128		H53	H53-1		NoCal
TF-C-I6-02	260	259.0	220.0	EP-08-062AQ-350	D-SN-P-128		H53	H53-1		NoCal
TF-C-I6-03	260	259.0	220.0	EP-08-062AQ-350	D-SN-P-128		H53	H53-1		NoCal
TF-C-K6-01	280	259.0	220.0	EP-08-062AQ-350	D-SN-P-128		H53	H53-1		NoCal
TF-C-K6-02	280	259.0	220.0	EP-08-062AQ-350	D-SN-P-128		H53	H53-1		NoCal
TF-C-K6-03	280	259.0	220.0	EP-08-062AQ-350	D-SN-P-128		H53	H53-1		NoCal
TF-C-A7-01	0	321.0	220.0	EP-08-062AQ-350	D-SN-P-128		H67	H67-1		NoCal
TF-C-A7-02	0	321.0	220.0	EP-08-062AQ-350	D-SN-P-128		H67	H67-1		NoCal
TF-C-A7-03	0	321.0	220.0	EP-08-062AQ-350	D-SN-P-128		H67	H67-1		NoCal
TF-C-D7-01	90	321.0	220.0	EP-08-062AQ-350	D-SN-P-128		H67	H67-1		NoCal
TF-C-D7-02	90	321.0	220.0	EP-08-062AQ-350	D-SN-P-128		H67	H67-1		NoCal
TF-C-D7-03	90	321.0	220.0	EP-08-062AQ-350	D-SN-P-128		H67	H67-1		NoCal
TF-C-Z7-01	135	321.0	220.0	EP-08-062AQ-350	D-SN-P-128		H67	H67-1		NoCal
TF-C-Z7-02	135	321.0	220.0	EP-08-062AQ-350	D-SN-P-128		H67	H67-1		NoCal
TF-C-Z7-03	135	321.0	220.0	EP-08-062AQ-350	D-SN-P-128		H67	H67-1		NoCal
TF-C-G7-01	180	321.0	220.0	EP-08-062AQ-350	D-SN-P-128		H67	H67-1		NoCal
TF-C-G7-02	180	321.0	220.0	EP-08-062AQ-350	D-SN-P-128		H67	H67-1		NoCal
TF-C-G7-03	180	321.0	220.0	EP-08-062AQ-350	D-SN-P-128		H67	H67-1		NoCal
TF-C-H7-01	225	321.0	220.0	EP-08-062AQ-350	D-SN-P-128		H67	H67-1		NoCal
TF-C-H7-02	225	321.0	220.0	EP-08-062AQ-350	D-SN-P-128		H67	H67-1		NoCal
TF-C-H7-03	225	321.0	220.0	EP-08-062AQ-350	D-SN-P-128		H67	H67-1		NoCal
TF-C-I7-01	260	321.0	220.0	EP-08-062AQ-350	D-SN-P-128		H67	H67-1		NoCal
TF-C-I7-02	260	321.0	220.0	EP-08-062AQ-350	D-SN-P-128		H67	H67-1		NoCal
TF-C-I7-03	260	321.0	220.0	EP-08-062AQ-350	D-SN-P-128		H67	H67-1		NoCal
TF-C-K7-01	280	321.0	220.0	EP-08-062AQ-350	D-SN-P-128		H67	H67-1		NoCal
TF-C-K7-02	280	321.0	220.0	EP-08-062AQ-350	D-SN-P-128		H67	H67-1		NoCal
TF-C-K7-03	280	321.0	220.0	EP-08-062AQ-350	D-SN-P-128		H67	H67-1		NoCal
TF-C-A8-01	0	326.0	220.0	EP-08-062AQ-350	D-SN-P-128		H68	H68-1		NoCal

Tendon Instrumentation List

Labeling	Azimuthal	Vertical	Radial	Transducer	Location	Details	Basic	Modified	Comnts	Calibration
I D	Angle	Elevation	Distance	Designation	Drawing #	Drawing #	Mark #	Mark #		
(name)	(deg)	(in)	(in)							
TF-C-A8-02	0	326.0	220.0	EP-08-062AQ-350	D-SN-P-128		H68	H68-1		NoCal
TF-C-A8-03	0	326.0	220.0	EP-08-062AQ-350	D-SN-P-128		H68	H68-1		NoCal
TF-C-C8-01	80	326.0	220.0	EP-08-062AQ-350	D-SN-P-128		H68	H68-1		NoCal
TF-C-C8-02	80	326.0	220.0	EP-08-062AQ-350	D-SN-P-128		H68	H68-1		NoCal
TF-C-C8-03	80	326.0	220.0	EP-08-062AQ-350	D-SN-P-128		H68	H68-1		NoCal
TF-C-E8-01	105	326.0	220.0	EP-08-062AQ-350	D-SN-P-128		H68	H68-1		NoCal
TF-C-E8-02	105	326.0	220.0	EP-08-062AQ-350	D-SN-P-128		H68	H68-1		NoCal
TF-C-E8-03	105	326.0	220.0	EP-08-062AQ-350	D-SN-P-128		H68	H68-1		NoCal
TF-C-E8-04	112	326.0	220.0	EP-08-062AQ-350	D-SN-P-128		H68	H68-2		NoCal
TF-C-E8-05	112	326.0	220.0	EP-08-062AQ-350	D-SN-P-128		H68	H68-2		NoCal
TF-C-E8-06	112	326.0	220.0	EP-08-062AQ-350	D-SN-P-128		H68	H68-2		NoCal
TF-C-E8-07	98	326.0	220.0	EP-08-062AQ-350	D-SN-P-128		H68	H68-3		NoCal
TF-C-E8-08	98	326.0	220.0	EP-08-062AQ-350	D-SN-P-128		H68	H68-3		NoCal
TF-C-E8-09	98	326.0	220.0	EP-08-062AQ-350	D-SN-P-128		H68	H68-3		NoCal
TF-C-Z8-01	135	326.0	220.0	EP-08-062AQ-350	D-SN-P-128		H68	H68-1		NoCal
TF-C-Z8-02	135	326.0	220.0	EP-08-062AQ-350	D-SN-P-128		H68	H68-1		NoCal
TF-C-Z8-03	135	326.0	220.0	EP-08-062AQ-350	D-SN-P-128		H68	H68-1		NoCal
TF-C-G8-01	180	326.0	220.0	EP-08-062AQ-350	D-SN-P-128		H68	H68-1		NoCal
TF-C-G8-02	180	326.0	220.0	EP-08-062AQ-350	D-SN-P-128		H68	H68-1		NoCal
TF-C-G8-03	180	326.0	220.0	EP-08-062AQ-350	D-SN-P-128		H68	H68-1		NoCal
TF-C-H8-01	225	326.0	220.0	EP-08-062AQ-350	D-SN-P-128		H68	H68-1		NoCal
TF-C-H8-02	225	326.0	220.0	EP-08-062AQ-350	D-SN-P-128		H68	H68-1		NoCal
TF-C-H8-03	225	326.0	220.0	EP-08-062AQ-350	D-SN-P-128		H68	H68-1		NoCal
TF-C-J8-01	270	326.0	220.0	EP-08-062AQ-350	D-SN-P-128		H68	H68-1		NoCal
TF-C-J8-02	270	326.0	220.0	EP-08-062AQ-350	D-SN-P-128		H68	H68-1		NoCal
TF-C-J8-03	270	326.0	220.0	EP-08-062AQ-350	D-SN-P-128		H68	H68-1		NoCal
TF-C-J8-04	263	326.0	220.0	EP-08-062AQ-350	D-SN-P-128		H68	H68-2		NoCal
TF-C-J8-05	263	326.0	220.0	EP-08-062AQ-350	D-SN-P-128		H68	H68-2		NoCal
TF-C-J8-06	263	326.0	220.0	EP-08-062AQ-350	D-SN-P-128		H68	H68-2		NoCal
TF-C-J8-07	277	326.0	220.0	EP-08-062AQ-350	D-SN-P-128		H68	H68-3		NoCal
TF-C-J8-08	277	326.0	220.0	EP-08-062AQ-350	D-SN-P-128		H68	H68-3		NoCal
TF-C-J8-09	277	326.0	220.0	EP-08-062AQ-350	D-SN-P-128		H68	H68-3		NoCal
TL-M-A0-03	1	-46.0	218.0	GK-3000-200-2.0	D-SN-P-128		V67	V67	Vert.	PreCal
TL-M-A0-05	13	-46.0	218.0	GK-3000-200-2.0	D-SN-P-128		V61	V61	Load	PreCal
TL-M-B0-02	25	-46.0	218.0	GK-3000-200-2.0	D-SN-P-128		V55	V55	Cells	PreCal
TL-M-B0-04	37	-46.0	218.0	GK-3000-200-2.0	D-SN-P-128		V49	V49		PreCal
TL-M-B0-05	43	-46.0	218.0	GK-3000-200-2.0	D-SN-P-128		V46	V46		PreCal
TL-M-C0-01	45	-46.0	218.0	GK-3000-200-2.0	D-SN-P-128		V1	V1		PreCal
TL-M-C0-03	57	-46.0	218.0	GK-3000-200-2.0	D-SN-P-128		V7	V7		PreCal
TL-M-C0-05	69	-46.0	218.0	GK-3000-200-2.0	D-SN-P-128		V13	V13		PreCal
TL-M-D0-02	81	-46.0	218.0	GK-3000-200-2.0	D-SN-P-128		V19	V19		PreCal
TL-M-D0-04	93	-46.0	218.0	GK-3000-200-2.0	D-SN-P-128		V25	V25		PreCal
TL-M-E0-01	105	-46.0	218.0	GK-3000-200-2.0	D-SN-P-128		V31	V31		PreCal
TL-M-E0-03	117	-46.0	218.0	GK-3000-200-2.0	D-SN-P-128		V37	V37		PreCal
TL-M-Z0-01	129	-46.0	218.0	GK-3000-200-2.0	D-SN-P-128		V43	V43		PreCal
TL-M-Z0-02	135	-46.0	218.0	HBM-C6-100t	D-SN-P-128		V46	V46		PreCal
TL-M-Z0-03	141	-46.0	218.0	GK-3000-200-2.0	D-SN-P-128		V49	V49		PreCal
TL-M-F0-02	153	-46.0	218.0	GK-3000-200-2.0	D-SN-P-128		V55	V55		PreCal
TL-M-G0-01	165	-46.0	218.0	GK-3000-200-2.0	D-SN-P-128		V61	V61		PreCal
TL-M-G0-03	177	-46.0	218.0	GK-3000-200-2.0	D-SN-P-128		V67	V67		PreCal
TL-M-G0-05	189	-46.0	218.0	GK-3000-200-2.0	D-SN-P-128		V73	V73		PreCal
TL-M-H0-02	201	-46.0	218.0	GK-3000-200-2.0	D-SN-P-128		V79	V79		PreCal
TL-M-H0-04	213	-46.0	218.0	GK-3000-200-2.0	D-SN-P-128		V85	V85		PreCal
TL-M-I0-01	229	-46.0	218.0	GK-3000-200-2.0	D-SN-P-128		V43	V43		PreCal

Tendon Instrumentation List

Labeling	Azimuthal	Vertical	Radial	Transducer	Location	Details	Basic	Modified	Comnts	Calibration
I D	Angle	Elevation	Distance	Designation	Drawing #	Drawing #	Mark #	Mark #		
(name)	(deg)	(in)	(in)							
TL-M-I0-03	241	-46.0	218.0	HBM-C6-100t	D-SN-P-128		V37	V37		PreCal
TL-M-I0-05	253	-46.0	218.0	GK-3000-200-2.0	D-SN-P-128		V31	V31		PreCal
TL-M-J0-02	265	-46.0	218.0	GK-3000-200-2.0	D-SN-P-128		V25	V25		PreCal
TL-M-J0-04	277	-46.0	218.0	GK-3000-200-2.0	D-SN-P-128		V19	V19		PreCal
TL-M-K0-01	289	-46.0	218.0	GK-3000-200-2.0	D-SN-P-128		V13	V13		PreCal
TL-M-K0-03	301	-46.0	218.0	GK-3000-200-2.0	D-SN-P-128		V7	V7		PreCal
TL-M-K0-05	313	-46.0	218.0	GK-3000-200-2.0	D-SN-P-128		V1	V1		PreCal
TL-M-L0-02	325	-46.0	218.0	HBM-C6-100t	D-SN-P-128		V85	V85		PreCal
TL-M-L0-04	337	-46.0	218.0	GK-3000-200-2.0	D-SN-P-128		V79	V79		PreCal
TL-M-A0-01	349	-46.0	218.0	GK-3000-200-2.0	D-SN-P-128		V73	V73		PreCal
TL-C-D3-01	85	44.0	230.0	GK-3000-200-2.0	D-SN-P-128		H4	H4	Hoop	PreCal
TL-C-D3-02	95	41.0	230.0	GK-3000-200-2.0	D-SN-P-128		H4	H4	Load	PreCal
TL-C-D4-01	85	106.0	230.0	GK-3000-200-2.0	D-SN-P-128		H18	H18	Cells	PreCal
TL-C-D4-02	95	103.0	230.0	GK-3000-200-2.0	D-SN-P-128		H18	H18	90 Deg.	PreCal
TL-C-D5-01	85	159.0	230.0	GK-3000-200-2.0	D-SN-P-128		H30	H30		PreCal
TL-C-D5-02	95	156.0	230.0	GK-3000-200-2.0	D-SN-P-128		H30	H30		PreCal
TL-C-D5-03	85	203.0	230.0	GK-3000-200-2.0	D-SN-P-128		H40	H40		PreCal
TL-C-D5-04	95	200.0	230.0	GK-3000-200-2.0	D-SN-P-128		H40	H40		PreCal
TL-C-D6-01	85	230.0	230.0	GK-3000-200-2.0	D-SN-P-128		H46	H46		PreCal
TL-C-D6-02	95	227.0	230.0	GK-3000-200-2.0	D-SN-P-128		H46	H46		PreCal
TL-C-D7-01	85	283.0	230.0	GK-3000-200-2.0	D-SN-P-128		H58	H58		PreCal
TL-C-D7-02	95	280.0	230.0	GK-3000-200-2.0	D-SN-P-128		H58	H58		PreCal
TL-C-D8-01	85	327.0	230.0	HBM-C6-100t	D-SN-P-128		H68	H68		PreCal
TL-C-D8-02	95	324.0	230.0	HBM-C6-100t	D-SN-P-128		H68	H68		PreCal
TL-C-D9-01	85	389.0	230.0	GK-3000-200-2.0	D-SN-P-128		H82	H82		PreCal
TL-C-D9-02	95	386.0	230.0	GK-3000-200-2.0	D-SN-P-128		H82	H82		PreCal
TL-C-D10-01	85	481.0	230.0	GK-3000-200-2.0	D-SN-P-128		H96	H96		PreCal
TL-C-D10-02	95	478.0	230.0	GK-3000-200-2.0	D-SN-P-128		H96	H96		PreCal
TL-C-J3-01	265	75.0	230.0	GK-3000-200-2.0	D-SN-P-128		H11	H11	Hoop	PreCal
TL-C-J3-02	275	72.0	230.0	HBM-C6-100t	D-SN-P-128		H11	H11	Load	PreCal
TL-C-J4-01	265	137.0	230.0	GK-3000-200-2.0	D-SN-P-128		H25	H25	Cells	PreCal
TL-C-J4-02	275	134.0	230.0	GK-3000-200-2.0	D-SN-P-128		H25	H25	270 Deg	PreCal
TL-C-J5-01	265	181.0	230.0	HBM-C6-100t	D-SN-P-128		H35	H35		PreCal
TL-C-J5-02	275	178.0	230.0	HBM-C6-100t	D-SN-P-128		H35	H35		PreCal
TL-C-J6-01	265	261.0	230.0	HBM-C6-100t	D-SN-P-128		H53	H53		PreCal
TL-C-J6-02	275	258.0	230.0	GK-3000-200-2.0	D-SN-P-128		H53	H53		PreCal
TL-C-J7-01	265	305.0	230.0	GK-3000-200-2.0	D-SN-P-128		H63	H63		PreCal
TL-C-J7-02	275	302.0	230.0	GK-3000-200-2.0	D-SN-P-128		H63	H63		PreCal
TL-C-J7-03	265	323.0	230.0	HBM-C6-100t	D-SN-P-128		H67	H67		PreCal
TL-C-J7-04	275	320.0	230.0	HBM-C6-100t	D-SN-P-128		H67	H67		PreCal
TL-C-J8-01	265	358.0	230.0	GK-3000-200-2.0	D-SN-P-128		H75	H75		PreCal
TL-C-J8-02	275	355.0	230.0	GK-3000-200-2.0	D-SN-P-128		H75	H75		PreCal
TL-C-J9-01	265	420.0	230.0	GK-3000-200-2.0	D-SN-P-128		H89	H89		PreCal
TL-C-J9-02	275	417.0	230.0	GK-3000-200-2.0	D-SN-P-128		H89	H89		PreCal
TL-C-J10-01	265	543.0	230.0	GK-3000-200-2.0	D-SN-P-128		H103	H103		PreCal
TL-C-J10-02	275	540.0	230.0	GK-3000-200-2.0	D-SN-P-128		H103	H103		PreCal

NoCal - No calibration was performed on this instrument before or after model testing

PreCal - Calibration was performed on this instrument prior to model testing only

Displacement Instrumentation List

Labeling	Azimuthal	Vertical	Radial	Transducer	Location	Details	Initial	Modified	Comnts	Calibration
I D	Angle	Elevation	Distance	Designation	Drawing #	Drawing #	Offset	Mark #		
(name)	(deg)	(in)	(in)							
CP-M-B4-01	30	104.0	211.0	PT101-0002-111-1110	D-SN-P-131		+0.25	CPOT-2	CPOT	PostOK
CP-M-B9-01	30	423.0	211.0	PT101-0005-111-1110	D-SN-P-131		+0.5	CPOT-5	Vertical	PostOUT
CP-M-C5-01	66	178.0	200.0	PT101-0002-111-1110	D-SN-P-131		+0.25	CPOT-2	Disp.	PostOK
CP-M-D4-01	90	104.0	211.0	PT101-0002-111-1110	D-SN-P-131		+0.25	CPOT-2		PostOK
CP-M-D7-01	90	304.0	211.0	PT101-0002-111-1110	D-SN-P-131		+0.25	CPOT-2		PostOK
CP-M-D9-01	90	423.0	211.0	PT101-0002-111-1110	D-SN-P-131		+0.5	CPOT-2		PostOK
CP-M-D10-01	90	504.0	196.0	PT101-0002-111-1110	D-SN-P-131		+0.5	CPOT-2		PostOK
CP-M-D11-01	90	573.0	150.0	PT101-0005-111-1110	D-SN-P-131		+0.5	CPOT-5		PostOK
CP-M-D12-01	90	619.0	81.0	PT101-0015-111-1110	D-SN-P-131		+1	CPOT-15		PostOK
CP-M-Z4-01	135	104.0	211.0	PT101-0002-111-1110	D-SN-P-131		+0.25	CPOT-2		PostOK
CP-M-Z5-01	135	184.0	211.0	PT101-0002-111-1110	D-SN-P-131		+0.25	CPOT-2		PostOK
CP-M-Z7-01	135	304.0	211.0	PT101-0002-111-1110	D-SN-P-131		+0.25	CPOT-2		PostOK
CP-M-Z10-01	135	504.0	196.0	PT101-0002-111-1110	D-SN-P-131		+0.5	CPOT-2		PostOK
CP-M-Z12-01	135	619.0	81.0	PT101-0015-111-1110	D-SN-P-131		+1	CPOT-15		PostOK
CP-M-G4-01	180	104.0	211.0	PT101-0002-111-1110	D-SN-P-131		+0.25	CPOT-2		PostOK
CP-M-G9-01	180	423.0	211.0	PT101-0005-111-1110	D-SN-P-131		+0.5	CPOT-5		PostOUT
CP-M-I4-01	240	104.0	211.0	PT101-0002-111-1110	D-SN-P-131		+0.25	CPOT-2		PostOK
CP-M-I9-01	240	423.0	211.0	PT101-0002-111-1110	D-SN-P-131		+0.5	CPOT-2		PostOK
CP-M-I11-01	240	573.0	150.0	PT101-0005-111-1110	D-SN-P-131		+0.5	CPOT-5		PostOK
CP-M-L4-01	324	104.0	211.0	PT101-0002-111-1110	D-SN-P-131		+0.25	CPOT-2		PostOK
CP-M-L5-01	334	184.0	200.0	PT101-0002-111-1110	D-SN-P-131		+0.25	CPOT-2		PostOK
CP-M-L7-01	324	304.0	211.0	PT101-0002-111-1110	D-SN-P-131		+1.75	CPOT-2		PostOK
CP-M-L9-01	324	423.0	211.0	PT101-0005-111-1110	D-SN-P-131		+0.5	CPOT-5		PostOK
CP-M-L10-01	324	504.0	196.0	PT101-0002-111-1110	D-SN-P-131		+0.5	CPOT-2		PostOK
CP-M-L11-01	324	573.0	150.0	PT101-0005-111-1110	D-SN-P-131		+0.5	CPOT-5		PostOK
CP-M-L12-01	324	619.0	81.0	PT101-0015-111-1110	D-SN-P-131		+1	CPOT-15		PostOK
CP-R-B2-01	30	10.0	211.0	PT101-0002-111-1110	D-SN-P-131		+0.25	CPOT-2	CPOT	PostOK
CP-R-B3-01	30	56.0	211.0	PT101-0002-111-1110	D-SN-P-131		+0.25	CPOT-2	Radial	PostOK
CP-R-B5-01	30	184.0	211.0	PT101-0010-111-1110	D-SN-P-131		+0.5	CPOT-10	Disp.	PostOK
CP-R-B7-01	30	304.0	211.0	PT101-0010-111-1110	D-SN-P-131		+0.5	CPOT-10		PostOK
CP-R-B9-01	30	423.0	211.0	PT101-0005-111-1110	D-SN-P-131		+0.5	CPOT-5		PostOK
CP-R-C5-01	66	178.0	200.0	PT101-0010-111-1110	D-SN-P-131		+0.5	CPOT-10		PostOK
CP-R-D4-01	90	104.0	211.0	PT101-0002-111-1110	D-SN-P-131		+0.25	CPOT-2		PostOK
CP-R-D6-01	90	244.0	211.0	PT101-0010-111-1110	D-SN-P-131		+0.5	CPOT-10		PostOUT
CP-R-D8-01	90	363.0	211.0	PT101-0005-111-1110	D-SN-P-131		+0.5	CPOT-5		PostOK
CP-R-D9-01	90	423.0	211.0	PT101-0002-111-1110	D-SN-P-131		+0.25	CPOT-2		PostOK
CP-R-D10-01	90	504.0	196.0	PT101-0002-111-1110	D-SN-P-131		+0.25	CPOT-2		PostOK
CP-R-D11-01	90	573.0	150.0	PT101-0002-111-1110	D-SN-P-131		+0.25	CPOT-2		PostOK
CP-R-D12-01	90	619.0	81.0	PT101-0002-111-1110	D-SN-P-131		+0.25	CPOT-2		PostOK
CP-R-E5-01	120	184.0	211.0	PT101-0010-111-1110	D-SN-P-131		+0.5	CPOT-10		PostOK
CP-R-Z8-01	135	363.0	211.0	PT101-0005-111-1110	D-SN-P-131		+0.5	CPOT-5		PostOK
CP-R-Z10-01	135	504.0	196.0	PT101-0002-111-1110	D-SN-P-131		+0.25	CPOT-2		PostOK
CP-R-Z11-01	135	573.0	150.0	PT101-0002-111-1110	D-SN-P-131		+0.25	CPOT-2		PostOK
CP-R-Z12-01	135	619.0	81.0	PT101-0002-111-1110	D-SN-P-131		+0.25	CPOT-2		PostOK
CP-R-F5-01	150	184.0	211.0	PT101-0010-111-1110	D-SN-P-131		+0.5	CPOT-10		PostOK
CP-R-G2-01	180	10.0	211.0	PT101-0002-111-1110	D-SN-P-131		+0.25	CPOT-2		PostOK
CP-R-G3-01	180	56.0	211.0	PT101-0002-111-1110	D-SN-P-131		+0.25	CPOT-2		PostOK
CP-R-G4-01	180	104.0	211.0	PT101-0005-111-1110	D-SN-P-131		+0.5	CPOT-5		PostOK
CP-R-G7-01	180	304.0	211.0	PT101-0010-111-1110	D-SN-P-131		+0.5	CPOT-10		PostOK
CP-R-G9-01	180	423.0	211.0	PT101-0005-111-1110	D-SN-P-131		+0.5	CPOT-5		PostOUT
CP-R-H5-01	210	184.0	211.0	PT101-0010-111-1110	D-SN-P-131		+0.5	CPOT-10		PostOK
CP-R-I2-01	240	10.0	211.0	PT101-0002-111-1110	D-SN-P-131		+0.25	CPOT-2		PostOK
CP-R-I3-01	240	56.0	211.0	PT101-0002-111-1110	D-SN-P-131		+0.25	CPOT-2		PostOK
CP-R-I7-01	240	304.0	211.0	PT101-0010-111-1110	D-SN-P-131		+0.5	CPOT-10		PreCal
CP-R-I9-01	240	423.0	211.0	PT101-0005-111-1110	D-SN-P-131		+0.5	CPOT-5		PostOK
CP-R-I11-01	240	573.0	150.0	PT101-0002-111-1110	D-SN-P-131		+0.25	CPOT-2		PostOK

Displacement Instrumentation List

Labeling I D (name)	Azimuthal Angle (deg)	Vertical Elevation (in)	Radial Distance (in)	Transducer Designation	Location Drawing #	Details Drawing #	Initial Offset	Modified Mark #	Comnts	Calibration
CP-R-K5-01	300	184.0	211.0	PT101-0010-111-1110	D-SN-P-131		+0.5	CPOT-10		PostOK
CP-R-L4-01	324	104.0	211.0	PT101-0005-111-1110	D-SN-P-131		+0.5	CPOT-5		PostOK
CP-R-L5-01	334	184.0	200.0	PT101-0010-111-1110	D-SN-P-131		+0.5	CPOT-10		PostOK
CP-R-L6-01	324	244.0	211.0	PT101-0010-111-1110	D-SN-P-131		+0.5	CPOT-10		PostOK
CP-R-L8-01	324	363.0	211.0	PT101-0005-111-1110	D-SN-P-131		+0.5	CPOT-5		PostOK
CP-R-L10-01	324	504.0	196.0	PT101-0002-111-1110	D-SN-P-131		+0.25	CPOT-2		PostOK
CP-R-L11-01	324	573.0	150.0	PT101-0002-111-1110	D-SN-P-131		+0.25	CPOT-2		PostOK
CP-R-L12-01	324	619.0	81.0	PT101-0002-111-1110	D-SN-P-131		+0.25	CPOT-2		PostOK
DL-M-D0-01	90	-138.0	283.0	GCD-121-500	D-SN-P-131		-0.3	LVDT-1	LVDT	PostOK
DL-M-D1-01	90	0.0	283.0	GCD-121-2000-1283	D-SN-P-131		-1.5	LVDT-4	Outside	PostOK
DL-M-Z0-01	135	-138.0	283.0	GCD-121-500	D-SN-P-131		-0.3	LVDT-1	Vertical	PostOK
DL-M-Z1-01	135	0.0	283.0	GCD-121-2000-1283	D-SN-P-131		-1.5	LVDT-4	Disp.	PostOUT
DL-M-I0-01	240	-138.0	283.0	GCD-121-500	D-SN-P-131		-0.3	LVDT-1		PostOUT
DL-M-I1-01	240	0.0	283.0	GCD-121-2000-1283	D-SN-P-131		-1.5	LVDT-4		PreCal
DL-M-L0-01	324	-138.0	283.0	GCD-121-500	D-SN-P-131		-0.3	LVDT-1		PostOUT
DL-M-L1-01	324	0.0	283.0	GCD-121-2000-1283	D-SN-P-131		-1.5	LVDT-4		PostOUT
DL-R-D1-01	90	0.0	211.0	GCD-121-500	D-SN-P-131		-0.3	LVDT-1	LVDT	PostOUT
DL-R-D2-01	90	10.0	211.0	GCD-121-500	D-SN-P-131		-0.3	LVDT-1	Radial	PostOK
DL-R-D3-01	90	56.0	211.0	GCD-121-2000-1283	D-SN-P-131		-1.5	LVDT-4	Disp.	PostOUT
DL-R-Z1-01	135	0.0	211.0	GCD-121-500	D-SN-P-131		-0.3	LVDT-1		PostOUT
DL-R-Z2-01	135	10.0	211.0	GCD-121-500	D-SN-P-131		-0.3	LVDT-1		PostOK
DL-R-Z3-01	135	56.0	211.0	GCD-121-2000-1283	D-SN-P-131		-1.5	LVDT-4		PostOUT
DL-R-L1-01	324	0.0	211.0	GCD-121-500	D-SN-P-131		-0.3	LVDT-1		PostOK
DL-R-L2-01	324	10.0	211.0	GCD-121-500	D-SN-P-131		-0.3	LVDT-1		PostOK
DL-R-L3-01	324	56.0	211.0	GCD-121-2000-1283	D-SN-P-131		-1.5	LVDT-4		PostOUT
DL-M-C5-01	62	178.0	218.0	GCD-121-500	D-SN-P-131		-0.3	LVDT-1	LVDT	PostOUT
DL-C-C5-01	62	178.0	218.0	GCD-121-500	D-SN-P-131		-0.3	LVDT-1	Hatch	PostOK
DL-M-L5-01	324	184.0	218.0	GCD-121-2000-1283	D-SN-P-131		-1.5	LVDT-4	Diagonal	PostOK
DL-C-L5-01	324	184.0	218.0	GCD-121-2000-1283	D-SN-P-131		-1.5	LVDT-4	Disp.	PostOUT
DT-M-Z9-01	135	423.0	211.0	LSVD600U01001A0	D-SN-P-131		+1	TEMPO-10	Tempos.	PostOUT
DT-M-Z11-01	135	573.0	150.0	LSVD600U01001A0	D-SN-P-131		+1	TEMPO-10	Vertical	PostOUT
DT-M-Z13-01	-	635.0	0.0	LSVD600U01001A0	D-SN-P-131		+1	TEMPO-10	Disp.	PostOUT
DT-R-A5-01	0	184.0	211.0	LSVD600U01001A0	D-SN-P-131		+1	TEMPO-10	Tempos.	PostOK
DT-R-D5-01	90	184.0	211.0	LSVD600U01001A0	D-SN-P-131		+1	TEMPO-10	Radial	PostOUT
DT-R-D7-01	90	304.0	211.0	LSVD600U01001A0	D-SN-P-131		+1	TEMPO-10	Disp.	PostOUT
DT-R-Z4-01	135	104.0	211.0	LSVD600U01001A0	D-SN-P-131		+1	TEMPO-10		PostOUT
DT-R-Z5-01	135	184.0	211.0	LSVD600U01001A0	D-SN-P-131		+1	TEMPO-10		PostOK
DT-R-Z6-01	135	244.0	211.0	LSVD600U01001A0	D-SN-P-131		+1	TEMPO-10		PostOUT
DT-R-Z7-01	135	304.0	211.0	LSVD600U01001A0	D-SN-P-131		+1	TEMPO-10		PostOK
DT-R-Z9-01	135	423.0	211.0	LSVD600U01001A0	D-SN-P-131		+1	TEMPO-10		PostOK
DT-R-G5-01	180	184.0	211.0	LSVD600U01001A0	D-SN-P-131		+1	TEMPO-10		PostOK
DT-R-I5-01	240	184.0	211.0	LSVD600U01001A0	D-SN-P-131		+1	TEMPO-10		PostOK
DT-R-J5-01	270	184.0	211.0	LSVD600U01001A0	D-SN-P-131		+1	TEMPO-10		PostOK
DT-R-L7-01	324	304.0	211.0	LSVD600U01001A0	D-SN-P-131		+1	TEMPO-10		PostOUT
DT-R-L9-01	324	423.0	211.0	LSVD600U01001A0	D-SN-P-131		+1	TEMPO-10		PostOUT
CP-V-B3-01	30	50.0	200.0	PT101-0002-111-1110	N/A		+1	CPOT-2	Instr.	PostOK
CP-V-G3-01	180	50.0	200.0	PT101-0002-111-1110	N/A		+1	CPOT-2	Frame	PostOK
CP-V-Z11-01	-	570.0	0.0	PT101-0002-111-1110	N/A		+1	CPOT-2	Sens.	PostOK
CP-V-A9-01	9	390.0	130.0	PT101-0002-111-1110	N/A		+1	CPOT-2		PostOK
CP-V-D9-01	99	390.0	130.0	PT101-0002-111-1110	N/A		+1	CPOT-2		PostOK
CP-V-G9-01	189	390.0	130.0	PT101-0002-111-1110	N/A		+1	CPOT-2		PostOK
CP-V-J9-01	279	390.0	130.0	PT101-0002-111-1110	N/A		+1	CPOT-2		PostOK

Displacement Instrumentation List

Labeling	Azimuthal	Vertical	Radial	Transducer	Location	Details	Initial	Modified	Comnts	Calibration
I D	Angle	Elevation	Distance	Designation	Drawing #	Drawing #	Offset	Mark #		
(name)	(deg)	(in)	(in)							
CP-H-G5-01	189	218.0	130.0	PT101-0002-111-1110	N/A		+1	CPOT-2		PostOUT
CP-H-J5-01	279	218.0	130.0	PT101-0002-111-1110	N/A		+1	CPOT-2		PostOK
CP-H-G9-01	189	380.0	130.0	PT101-0002-111-1110	N/A		+1	CPOT-2		PostOK
CP-H-J9-01	279	380.0	130.0	PT101-0002-111-1110	N/A		+1	CPOT-2		PostOK
IT-H-A11-01	0	580.0	10.0	SSY0140	N/A		+0	TILT		PostOUT
IT-H-D11-01	90	580.0	10.0	SSY0140	N/A		+0	TILT		PostOUT

PreCal - Calibration was preformed on this instrument prior to model testing only

PostOK - Calibration was performed on this instrument Before and After model testing and remained within tolerance

PostOUT - Calibration was performed on this instrument Before and After model testing and difference was Out-of Tolerance

Other Instrumentation List

Labeling I D (name)	Azimuthal Angle (deg)	Vertical Elevation (in)	Radial Distance (in)	Transducer Designation	Location Drawing #	Details Drawing #	Basic Mark #	Modified Mark #	Comnts	Calibration
TC-R-D0-01	90	-134.0	48.0	K-24-2-505	D-SN-P-132	N/A	N/A	N/A	(Thermoc.	NoCal
TC-R-D0-02	90	-104.0	48.0	K-24-2-505	D-SN-P-132	N/A	N/A	N/A	embedded	NoCal
TC-R-D0-03	90	-104.0	200.0	K-24-2-505	D-SN-P-132	N/A	N/A	N/A	basemat)	NoCal
TC-R-D0-04	90	-6.0	48.0	CASS-116U-240	D-SN-P-132	N/A	N/A	N/A		NoCal
TC-R-D0-05	90	-36.0	214.0	CASS-116U-240	D-SN-P-132	N/A	N/A	N/A		NoCal
TC-R-Z0-01	135	-36.0	214.0	CASS-116U-240	D-SN-P-132	N/A	N/A	N/A		NoCal
TW-R-A2-01	0	10.0	218.0	TQSS-116U-180	D-SN-P-132	N/A	N/A	N/A	(Thermoc.	NoCal
TW-R-A4-01	0	104.0	218.0	TQSS-116U-72	D-SN-P-132	N/A	N/A	N/A	embedded	NoCal
TW-R-A5-01	0	184.0	218.0	TQSS-116U-72	D-SN-P-132	N/A	N/A	N/A	cylinder	NoCal
TW-R-A5-02	349	184.0	218.0	TQSS-116U-72	D-SN-P-132	N/A	N/A	N/A	& dome)	NoCal
TW-R-A6-01	0	244.0	218.0	TQSS-116U-72	D-SN-P-132	N/A	N/A	N/A		NoCal
TW-R-A7-01	0	304.0	218.0	TQSS-116U-72	D-SN-P-132	N/A	N/A	N/A		NoCal
TW-R-A9-01	0	423.0	218.0	TQSS-116U-72	D-SN-P-132	N/A	N/A	N/A		NoCal
TW-R-A11-01	0	573.0	158.0	TQSS-116U-240	D-SN-P-132	N/A	N/A	N/A		NoCal
TW-R-C5-01	44	184.0	218.0	TQSS-116U-96	D-SN-P-132	N/A	N/A	N/A		NoCal
TW-R-C5-02	62	125.0	218.0	TQSS-116U-96	D-SN-P-132	N/A	N/A	N/A		NoCal
TW-R-C5-03	62	230.0	218.0	TQSS-116U-96	D-SN-P-132	N/A	N/A	N/A		NoCal
TW-R-C5-04	80	184.0	218.0	TQSS-116U-96	D-SN-P-132	N/A	N/A	N/A		NoCal
TW-R-D2-01	90	10.0	222.0	TQSS-116U-180	D-SN-P-132	N/A	N/A	N/A		NoCal
TW-R-D4-01	90	104.0	222.0	TQSS-116U-96	D-SN-P-132	N/A	N/A	N/A		NoCal
TW-R-D5-01	90	184.0	222.0	TQSS-116U-96	D-SN-P-132	N/A	N/A	N/A		NoCal
TW-R-D7-01	90	304.0	222.0	TQSS-116U-96	D-SN-P-132	N/A	N/A	N/A		NoCal
TW-R-D9-01	90	423.0	222.0	TQSS-116U-72	D-SN-P-132	N/A	N/A	N/A		NoCal
TW-R-D11-01	62	180.0	220.0	TQSS-116U-240	D-SN-P-132	N/A	N/A	N/A	A/L	NoCal
TW-R-Z2-01	135	10.0	218.0	TQSS-116U-180	D-SN-P-132	N/A	N/A	N/A		NoCal
TW-R-Z4-01	135	104.0	218.0	TQSS-116U-72	D-SN-P-132	N/A	N/A	N/A		NoCal
TW-R-Z5-01	135	184.0	218.0	TQSS-116U-96	D-SN-P-132	N/A	N/A	N/A		NoCal
TW-R-Z6-01	135	244.0	218.0	TQSS-116U-96	D-SN-P-132	N/A	N/A	N/A		NoCal
TW-R-Z7-01	135	304.0	218.0	TQSS-116U-96	D-SN-P-132	N/A	N/A	N/A		NoCal
TW-R-Z9-01	135	423.0	218.0	TQSS-116U-72	D-SN-P-132	N/A	N/A	N/A		NoCal
TW-R-Z11-01	135	573.0	158.0	TQSS-116U-240	D-SN-P-132	N/A	N/A	N/A		NoCal
TW-R-Z13-01	-	640.0	0.0	TQSS-116U-480	D-SN-P-132	N/A	N/A	N/A		NoCal
TW-R-G5-01	180	184.0	218.0	TQSS-116U-96	D-SN-P-132	N/A	N/A	N/A		NoCal
TW-R-I2-01	240	10.0	218.0	TQSS-116U-180	D-SN-P-132	N/A	N/A	N/A		NoCal
TW-R-I5-01	240	184.0	218.0	TQSS-116U-96	D-SN-P-132	N/A	N/A	N/A		NoCal
TW-R-I9-01	240	423.0	218.0	TQSS-116U-72	D-SN-P-132	N/A	N/A	N/A		NoCal
TW-R-I11-01	324	184.0	220.0	TQSS-116U-240	D-SN-P-132	N/A	N/A	N/A	E/H	NoCal
TW-R-K5-01	299	184.0	218.0	TQSS-116U-96	D-SN-P-132	N/A	N/A	N/A		NoCal
TW-R-L2-01	324	10.0	218.0	TQSS-116U-180	D-SN-P-132	N/A	N/A	N/A		NoCal
TW-R-L4-01	324	79.0	218.0	TQSS-116U-96	D-SN-P-132	N/A	N/A	N/A		NoCal
TW-R-L7-01	324	289.0	218.0	TQSS-116U-96	D-SN-P-132	N/A	N/A	N/A		NoCal
TW-R-L9-01	324	423.0	218.0	TQSS-116U-72	D-SN-P-132	N/A	N/A	N/A		NoCal
TW-R-L11-01	324	573.0	158.0	TQSS-116U-240	D-SN-P-132	N/A	N/A	N/A		NoCal
TI-C-A2-01	0	10.0	211.0	SA1-T	D-SN-P-132	N/A	N/A	N/A	(Thermoc.	NoCal
TI-C-A4-01	0	104.0	211.0	SA1-T	D-SN-P-132	N/A	N/A	N/A	attached	NoCal
TI-C-A5-01	0	184.0	211.0	SA1-T	D-SN-P-132	N/A	N/A	N/A	to inside	NoCal
TI-C-A7-01	0	304.0	211.0	SA1-T	D-SN-P-132	N/A	N/A	N/A	liner)	NoCal
TI-C-A9-01	0	423.0	211.0	SA1-T	D-SN-P-132	N/A	N/A	N/A		NoCal

Other Instrumentation List

Labeling I D (name)	Azimuthal Angle (deg)	Vertical Elevation (in)	Radial Distance (in)	Transducer Designation	Location Drawing #	Details Drawing #	Basic Mark #	Modified Mark #	Comnts	Calibration
TI-C-A11-01	0	573.0	151.0	SA1-T	D-SN-P-132	N/A	N/A	N/A		NoCal
TI-C-C5-01	57	178.0	211.0	SA1-T	D-SN-P-132	N/A	N/A	N/A		NoCal
TI-C-C5-02	67	178.0	211.0	SA1-T	D-SN-P-132	N/A	N/A	N/A		NoCal
TI-C-D2-01	90	10.0	211.0	SA1-T	D-SN-P-132	N/A	N/A	N/A		NoCal
TI-C-D4-01	90	104.0	211.0	SA1-T	D-SN-P-132	N/A	N/A	N/A		NoCal
TI-C-D5-01	90	184.0	211.0	SA1-T	D-SN-P-132	N/A	N/A	N/A		NoCal
TI-C-D7-01	90	304.0	211.0	SA1-T	D-SN-P-132	N/A	N/A	N/A		NoCal
TI-C-D9-01	90	423.0	211.0	SA1-T	D-SN-P-132	N/A	N/A	N/A		NoCal
TI-C-D11-01	90	573.0	151.0	SA1-T	D-SN-P-132	N/A	N/A	N/A		NoCal
TI-C-Z2-01	135	10.0	211.0	SA1-T	D-SN-P-132	N/A	N/A	N/A		NoCal
TI-C-Z4-01	135	104.0	211.0	SA1-T	D-SN-P-132	N/A	N/A	N/A		NoCal
TI-C-Z5-01	135	184.0	211.0	SA1-T	D-SN-P-132	N/A	N/A	N/A		NoCal
TI-C-Z7-01	135	304.0	211.0	SA1-T	D-SN-P-132	N/A	N/A	N/A		NoCal
TI-C-Z9-01	135	423.0	211.0	SA1-T	D-SN-P-132	N/A	N/A	N/A		NoCal
TI-C-Z11-01	135	573.0	151.0	SA1-T	D-SN-P-132	N/A	N/A	N/A		NoCal
TI-C-Z13-01	-	634.0	0.0	SA1-T	D-SN-P-132	N/A	N/A	N/A		NoCal
TI-C-I2-01	240	10.0	211.0	SA1-T	D-SN-P-132	N/A	N/A	N/A		NoCal
TI-C-I5-01	240	184.0	211.0	SA1-T	D-SN-P-132	N/A	N/A	N/A		NoCal
TI-C-I9-01	240	423.0	211.0	SA1-T	D-SN-P-132	N/A	N/A	N/A		NoCal
TI-C-I11-01	240	573.0	151.0	SA1-T	D-SN-P-132	N/A	N/A	N/A		NoCal
TI-C-L2-01	324	10.0	211.0	SA1-T	D-SN-P-132	N/A	N/A	N/A		NoCal
TI-C-L4-01	324	104.0	211.0	SA1-T	D-SN-P-132	N/A	N/A	N/A		NoCal
TI-C-L5-01	324	184.0	211.0	SA1-T	D-SN-P-132	N/A	N/A	N/A		NoCal
TI-C-L5-02	314	184.0	211.0	SA1-T	D-SN-P-132	N/A	N/A	N/A		NoCal
TI-C-L5-03	334	184.0	211.0	SA1-T	D-SN-P-132	N/A	N/A	N/A		NoCal
TI-C-L7-01	324	304.0	211.0	SA1-T	D-SN-P-132	N/A	N/A	N/A		NoCal
TI-C-L9-01	324	423.0	211.0	SA1-T	D-SN-P-132	N/A	N/A	N/A		NoCal
TI-C-L11-01	324	573.0	151.0	SA1-T	D-SN-P-132	N/A	N/A	N/A		NoCal
RT-M-A3-01	0	40.0	150.0	RTD-805	D-SN-P-132	N/A	N/A	N/A	(RTD	NoCal
RT-M-A5-01	0	170.0	150.0	RTD-805	D-SN-P-132	N/A	N/A	N/A	inside	NoCal
RT-M-A7-01	0	290.0	150.0	RTD-805	D-SN-P-132	N/A	N/A	N/A	air	NoCal
RT-M-A9-01	0	423.0	150.0	RTD-805	D-SN-P-132	N/A	N/A	N/A	Temp.)	NoCal
RT-M-A10-01	0	533.0	120.0	RTD-805	D-SN-P-132	N/A	N/A	N/A		NoCal
RT-M-D3-01	90	40.0	150.0	RTD-805	D-SN-P-132	N/A	N/A	N/A		NoCal
RT-M-D5-01	90	170.0	150.0	RTD-805	D-SN-P-132	N/A	N/A	N/A		NoCal
RT-M-D7-01	90	290.0	150.0	RTD-805	D-SN-P-132	N/A	N/A	N/A		NoCal
RT-M-D9-01	90	423.0	150.0	RTD-805	D-SN-P-132	N/A	N/A	N/A		NoCal
RT-M-D10-01	90	533.0	120.0	RTD-805	D-SN-P-132	N/A	N/A	N/A		NoCal
RT-M-Z12-01	-	608.0	0.0	RTD-805	D-SN-P-132	N/A	N/A	N/A		NoCal
RT-M-G3-01	180	40.0	150.0	RTD-805	D-SN-P-132	N/A	N/A	N/A		NoCal
RT-M-G5-01	180	170.0	150.0	RTD-805	D-SN-P-132	N/A	N/A	N/A		NoCal
RT-M-G7-01	180	290.0	150.0	RTD-805	D-SN-P-132	N/A	N/A	N/A		NoCal
RT-M-G9-01	180	423.0	150.0	RTD-805	D-SN-P-132	N/A	N/A	N/A		NoCal
RT-M-G10-01	180	533.0	120.0	RTD-805	D-SN-P-132	N/A	N/A	N/A		NoCal
RT-M-J3-01	270	40.0	150.0	RTD-805	D-SN-P-132	N/A	N/A	N/A		NoCal
RT-M-J5-01	270	170.0	150.0	RTD-805	D-SN-P-132	N/A	N/A	N/A		NoCal
RT-M-J7-01	270	290.0	150.0	RTD-805	D-SN-P-132	N/A	N/A	N/A		NoCal
RT-M-J9-01	270	423.0	150.0	RTD-805	D-SN-P-132	N/A	N/A	N/A		NoCal

Other Instrumentation List

Labeling I D (name)	Azimuthal Angle (deg)	Vertical Elevation (in)	Radial Distance (in)	Transducer Designation	Location Drawing #	Details Drawing #	Basic Mark #	Modified Mark #	Comnts	Calibration
RT-M-J10-01	270	533.0	120.0	RTD-805	D-SN-P-132	N/A	N/A	N/A		NoCal
RT-R-G0-01	180	-60.0	400.0	RTD-805	D-SN-P-132	N/A	N/A	N/A	Outside	NoCal
PG-R-G4-01	180	96.5	230.0	4040	N/A	N/A	N/A	N/A	(pressure	PostOK
PG-R-G4-02	180	96.5	230.0	4040	N/A	N/A	N/A	N/A	gages)	PostOK
CE-M-Z2-01	135	10.0	214.0	SOFO-500	D-SN-P-125	N/A	684	684	(fiber	NoCal
CE-M-Z2-02	135	10.0	221.0	SOFO-500	D-SN-P-126	N/A	683	683	optic	NoCal
CE-M-A6-01	0	244.0	214.0	SOFO-500	D-SN-P-125	N/A	682	682	concrete	NoCal
CE-C-A6-01	0	244.0	218.0	SOFO-500	D-SN-P-125	N/A	737	737	strain	NoCal
CE-M-A6-02	0	244.0	221.0	SOFO-500	D-SN-P-126	N/A	738	738	gages)	NoCal
CE-C-Z6-01	135	244.0	214.0	SOFO-500	D-SN-P-125	N/A	685	685		NoCal
CE-M-Z6-01	135	244.0	218.0	SOFO-500	D-SN-P-125	N/A	686	686		NoCal
CE-C-Z6-02	135	244.0	221.0	SOFO-500	D-SN-P-126	N/A	687	687		NoCal
CE-M-Z11-01	135	573.0	157.0	SOFO-500	D-SN-P-125	N/A	775	775		NoCal
CE-C-Z11-01	135	573.0	157.0	SOFO-500	D-SN-P-125	N/A	776	776		NoCal
A00	0	423.0	224.0						Acoustic	PreCal
A01	0	304.0	224.0						Sensors	PreCal
A02	0	184.0	224.0						(Ext)	PreCal
A03	0	10.0	224.0							PreCal
A04	0	-79.0	206.0							PreCal
A05	62	423.0	224.0							PreCal
A06	62	304.0	224.0							PreCal
A07	60	10.0	224.0							PreCal
A08	60	-79.0	206.0							PreCal
A09	90	580.0	170.0							PreCal
A10	90	423.0	230.0							PreCal
A11	90	244.0	230.0							PreCal
A12	90	127.0	230.0							PreCal
A13	90	10.0	230.0							PreCal
A14	120	-79.0	206.0							PreCal
A15	150	423.0	224.0							PreCal
A16	150	304.0	224.0							PreCal
A17	150	184.0	224.0							PreCal
A18	150	10.0	224.0							PreCal
A19	180	644.0	0.0							PreCal
A20	180	184.0	224.0							PreCal
A21	180	10.0	224.0							PreCal
A22	180	-79.0	206.0							PreCal
A23	210	423.0	224.0							PreCal
A24	210	304.0	224.0							PreCal
A25	210	184.0	224.0							PreCal
A26	210	10.0	224.0							PreCal
A27	240	-79.0	206.0							PreCal
A28	270	580.0	170.0							PreCal
A29	270	423.0	230.0							PreCal
A30	270	244.0	230.0							PreCal
A31	270	127.0	230.0							PreCal
A32	270	10.0	230.0							PreCal
A33	285	304.0	224.0							PreCal
A34	285	56.0	224.0							PreCal
A35	300	-79.0	206.0							PreCal
A36	318	423.0	224.0							PreCal
A37	324	10.0	224.0							PreCal
A38	15	10.0	211.0						Acoustic	PreCal

Other Instrumentation List

Labeling	Azimuthal	Vertical	Radial	Transducer	Location	Details	Basic	Modified	Comnts	Calibration
I D	Angle	Elevation	Distance	Designation	Drawing #	Drawing #	Mark #	Mark #		
(name)	(deg)	(in)	(in)							
A39	57.1	196.0	205.0						Sensors	PreCal
A40	62	10.0	211.0						(Int)	PreCal
A41	66.9	196.0	205.0							PreCal
A42	105	10.0	211.0							PreCal
A43	150	244.0	211.0							PreCal
A44	150	10.0	211.0							PreCal
A45	210	244.0	211.0							PreCal
A46	210	10.0	211.0							PreCal
A47	240	10.0	211.0							PreCal
A48	295	10.0	211.0							PreCal
A49	313.7	222.0	200.0							PreCal
A50	313.7	146.0	200.0							PreCal
A51	334.3	222.0	200.0							PreCal
A52	334.3	146.0	200.0							PreCal
A53	330	10.0	211.0							PreCal

NoCal - No calibration was performed on this instrument before or after model testing

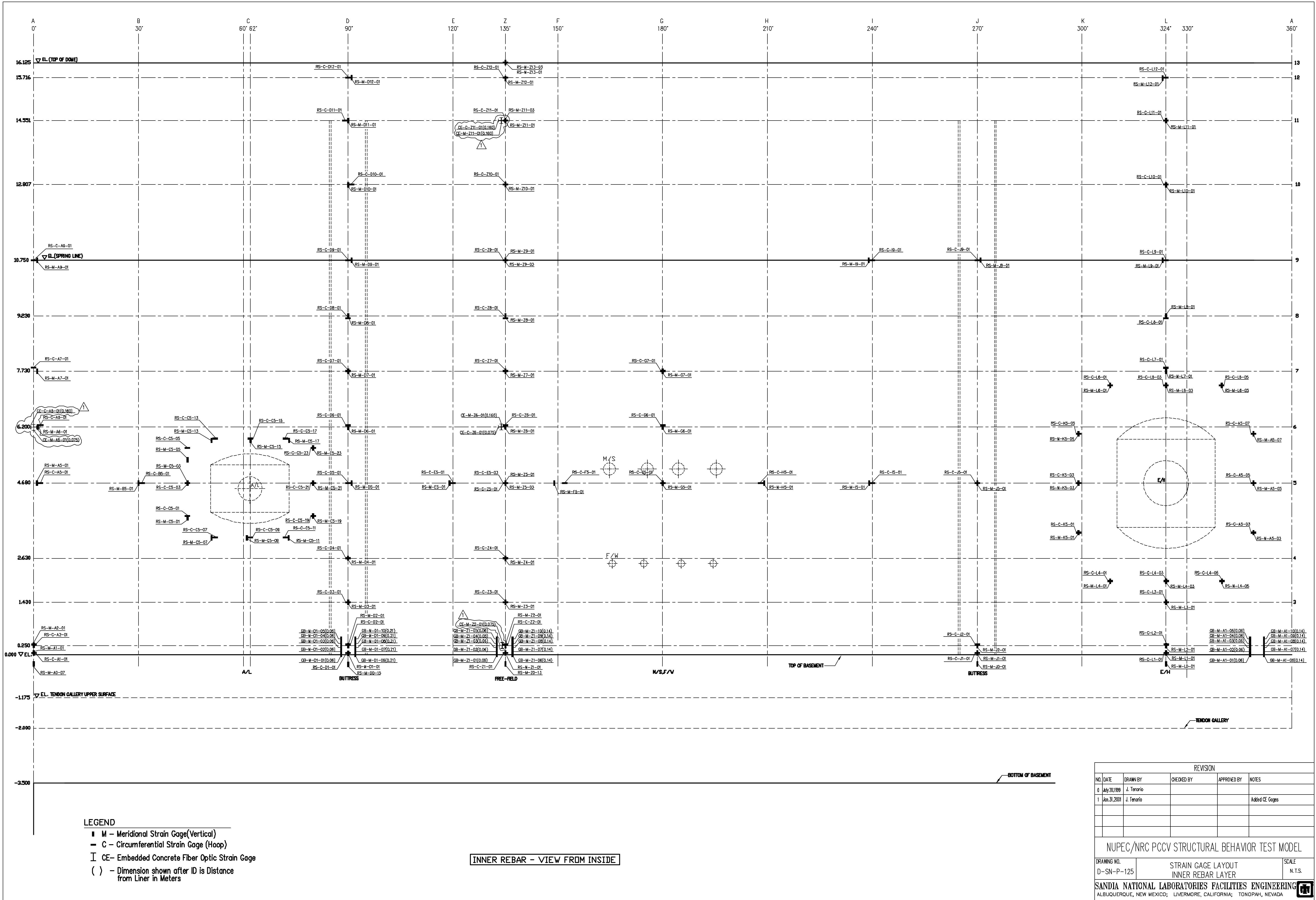
PreCal - Calibration was performed on this instrument prior to model testing only

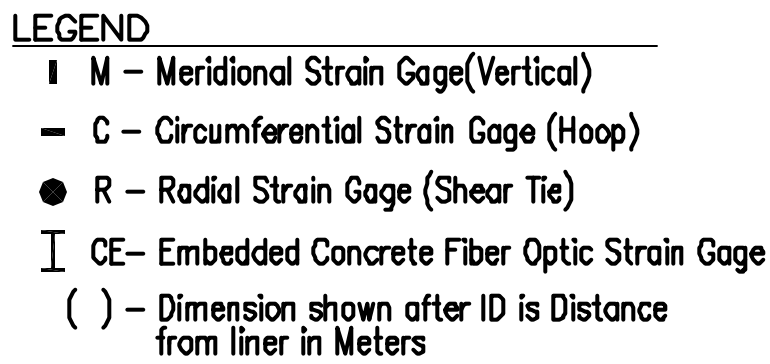
PostOK - Calibration was performed on this instrument Before and After model testing and remained within tolerance

Appendix E: PCCV Instrumentation Layout Drawings

List of PCCV Instrumentation Layout Drawings

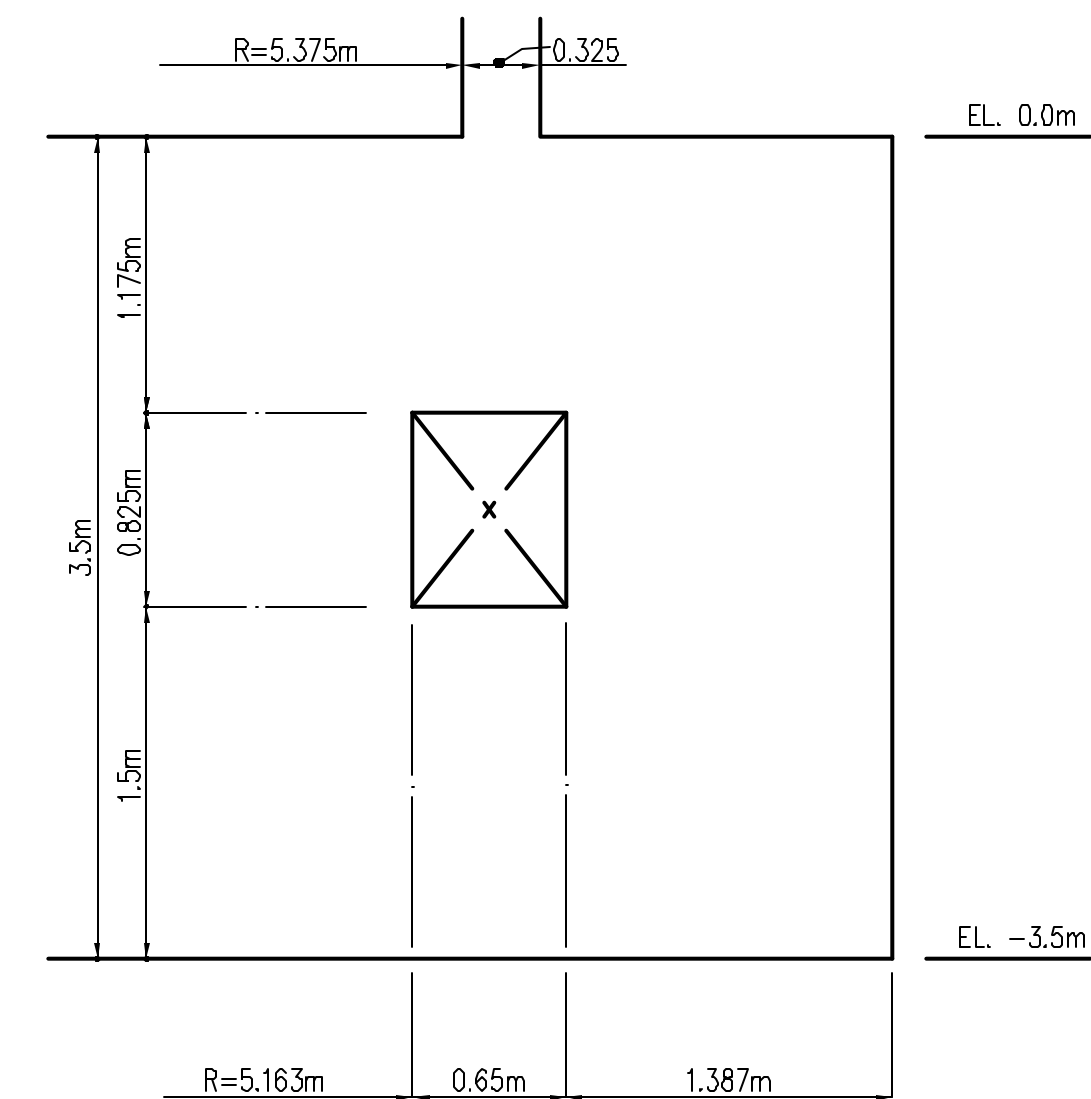
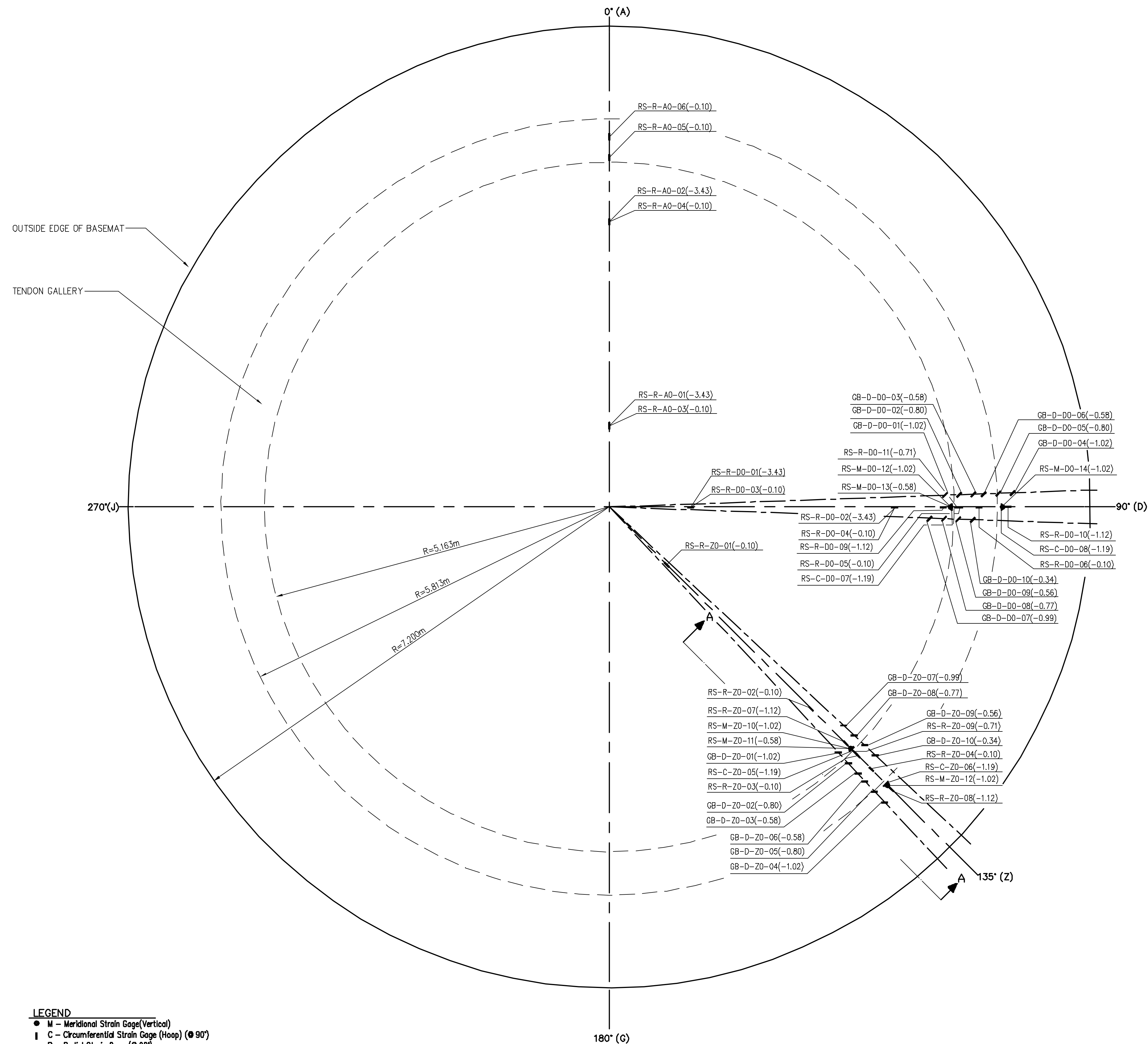
Number	Date	Rev	Description
D-SN-P-125	1/31/2001	1	Strain Gage Layout – Inner Rebar Layer
D-SN-P-126	1/31/2001	1	Strain Gage Layout – Outer Rebar Layers
D-SN-P-127	7/20/1999	0	Strain Gage Layout – Basemat Rebar
D-SN-P-128	1/31/2001	1	Strain Gage Layout – Tendons
D-SN-P-129	1/31/2002	1	Strain Gage Layout – Exterior Liner
D-SN-P-130	1/31/2002	1	Strain Gage Layout – Interior Liner
D-SN-P-131	1/31/2002	1	Displacement Transducer Layout
D-SN-P-132	1/31/2002	0	Temperature Sensor Layout
D-SN-P-133	1/31/2002	0	Displacement Transducer Fixtures
D-SN-P-206	7/20/1999	1	Instrumentation Liner Details – Gauges Installation Details
D-SN-P-207	7/20/1999	1	Instrumentation Liner Details – Basemat Liner Connection
D-SN-P-208	7/20/1999	1	Instrumentation Liner Details – Basemat Liner Connection
D-SN-P-209	7/20/1999	1	Instrumentation Liner Details – Detail a & b
D-SN-P-210	7/20/1999	1	Instrumentation Liner Details – Detail d
D-SN-P-211	7/20/1999	1	Instrumentation Liner Details – Detail e
D-SN-P-212	7/20/1999	1	Instrumentation Liner Details – Detail f
D-SN-P-213	7/20/1999	1	Instrumentation Liner Details – Detail g & h
D-SN-P-214	7/20/1999	1	Instrumentation Liner Details – Detail i & j
D-SN-P-215	7/20/1999	1	Instrumentation Liner Details – Detail k & l
D-SN-P-216	7/20/1999	1	Instrumentation Liner Details – Detail m
D-SN-P-217	7/20/1999	1	Instrumentation Liner Details – Detail n
D-SN-P-218	7/20/1999	0	Interior Liner Gage Layout – Equipment Hatch
D-SN-P-219	1/31/2001	1	Interior Liner Gage Layout – Airlock
D-SN-P-220	36360	0	Interior Liner Gage Layout – Main Steam and Feedwater





REVISION					
NO.	DATE	DRAWN BY	CHECKED BY	APPROVED BY	NOTES
0	July 20, 1999	J. Tamarlo			
1	Jan 31, 2001	J. Tamarlo			Added CE Gages

E-5



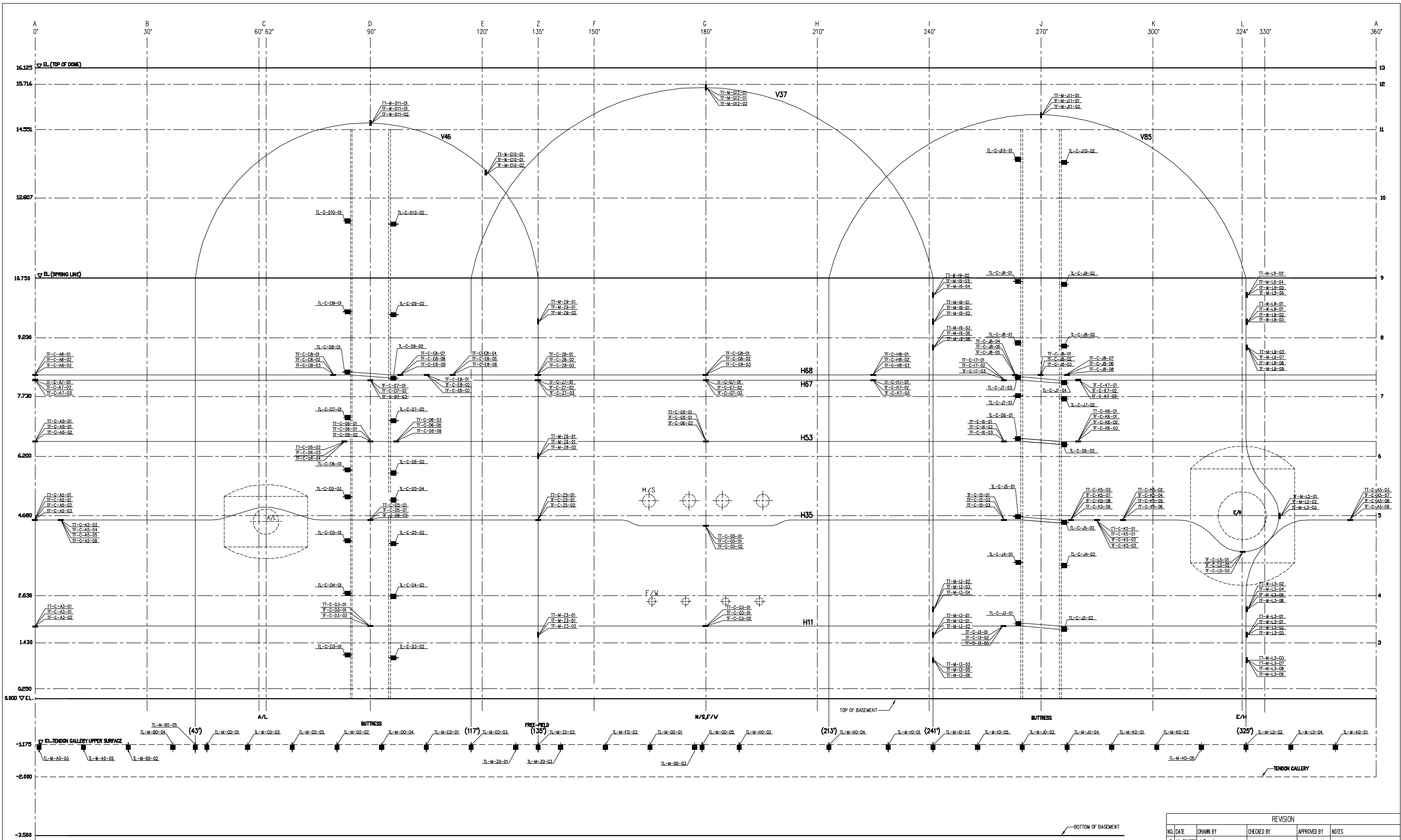
A-A SECTION
SCALE - 1/24

NOTE
VERTICAL ELEVATION SHOWN IN PARENTHESES (m).
0.0 ELEVATION IS TOP OF BASEMAT

- LEGEND**
- M - Meridional Strain Gage (Vertical)
 - ⊥ C - Circumferential Strain Gage (Hoop) (⊙ 90°)
 - R - Radial Strain Gage (⊙ 90°)
 - ⌵ D - Diagonal Gage Bar Strain Gage (⊙ 90°)

BASEMENT REBAR - VIEW FROM ABOVE

REVISION					
NO.	DATE	DRAWN BY	CHECKED BY	APPROVED BY	NOTES
0	July 20, 1999	J. Tenorio			
NUPEC/NRC PCCV STRUCTURAL BEHAVIOR TEST MODEL					
DRAWING NO. D-SN-P-127		STRAIN GAGE LAYOUT BASEMENT REBAR			SCALE 1/24
SANDIA NATIONAL LABORATORIES FACILITIES ENGINEERING					
ALBUQUERQUE, NEW MEXICO; LIVERMORE, CALIFORNIA; TONOPAH, NEVADA					



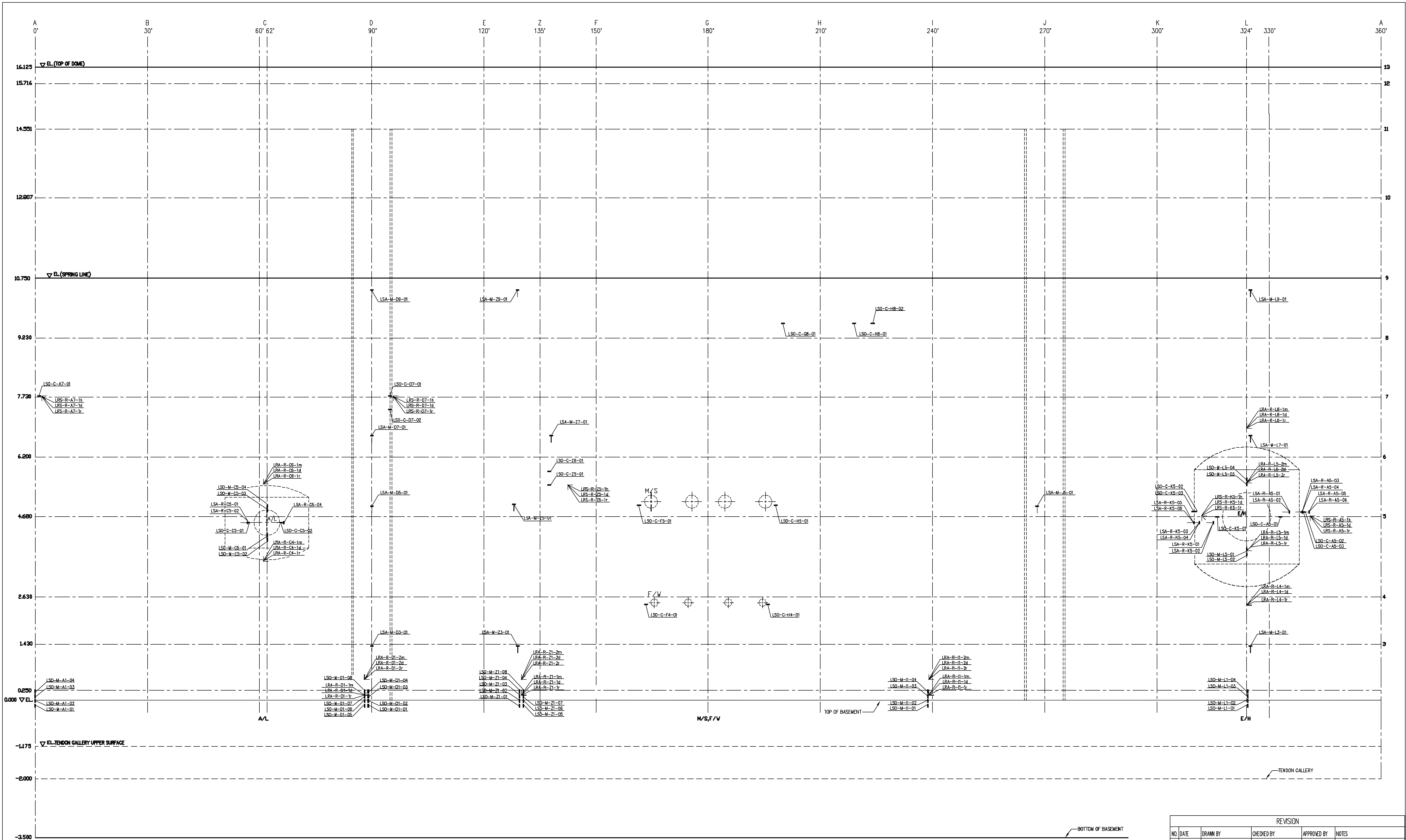
LEGEND

- M – Meridional (Hairpin) Tendon Strain Gage Location
- C – Circumferential (Hoop) Tendon Strain Gage Location
- M – Meridional (Hairpin) Load Cell
- C – Circumferential (Hoop) Load Cell

NOTE: If 3 Locations are close on same tendon: All 3 Tendon Strands are Instrumented. Otherwise, only the #1 strand is Instrumented.

STRAIN GAGES AND LOAD CELLS ON TENDONS – VIEW FROM INSIDE

REVISION				
NO.	DATE	DRAWN BY	CHECKED BY	APPROVED BY
0	July 20, 1999	J. Tenorio		
1	Jan. 31, 2001	J. Tenorio		
				Corrected Azimuth Lines
NUPEC/NRC PCCV STRUCTURAL BEHAVIOR TEST MODEL DRAWING NO. D-SN-P-128 STRAIN GAGE LAYOUT TENDONS SCALE N.T.S. SANDIA NATIONAL LABORATORIES ENGINEERING ALBUQUERQUE, NEW MEXICO; LIVERMORE, CALIFORNIA; TONOPAH, NEVADA				

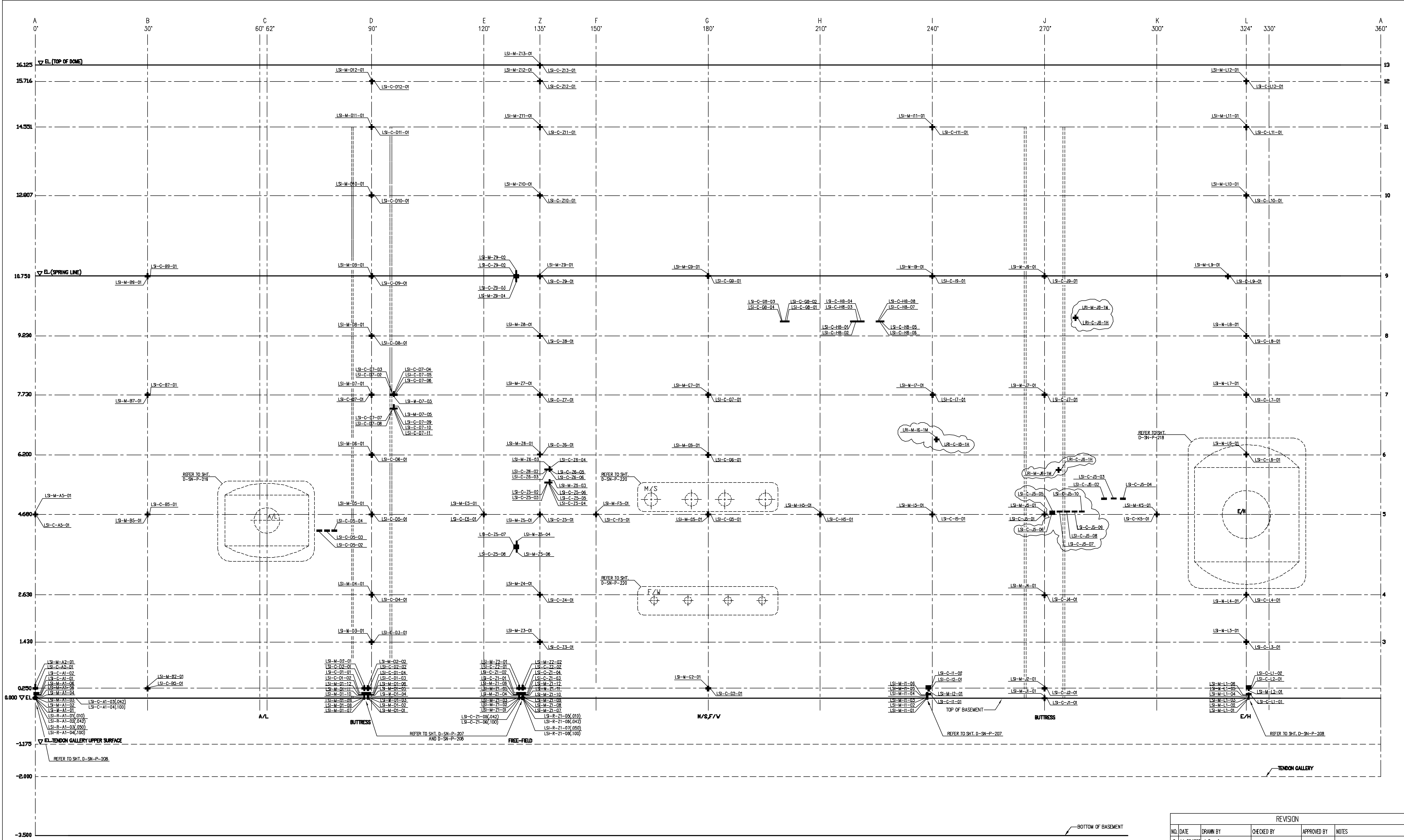


- LEGEND**
- LSO-M Meridional (Vertical) Liner Strain Gage
 - LSO-C Circumferential (Hoop) Liner Strain Gage
 - LSA-M Meridional (Vertical) Gage on Anchor Web.
 - LSA-R Radial Gage on Anchor Web
 - LRA - Rosette on Vertical Liner Anchor Web
 - LRS - Rosette on Horizontal Liner Stiffener

NOTE: For Rosette Gage ID's ending in:
m - meridional direction
h - hoop direction
r - radial direction
d - diagonal direction

STRAIN GAGES ON LINER EXTERIOR - VIEW FROM INSIDE

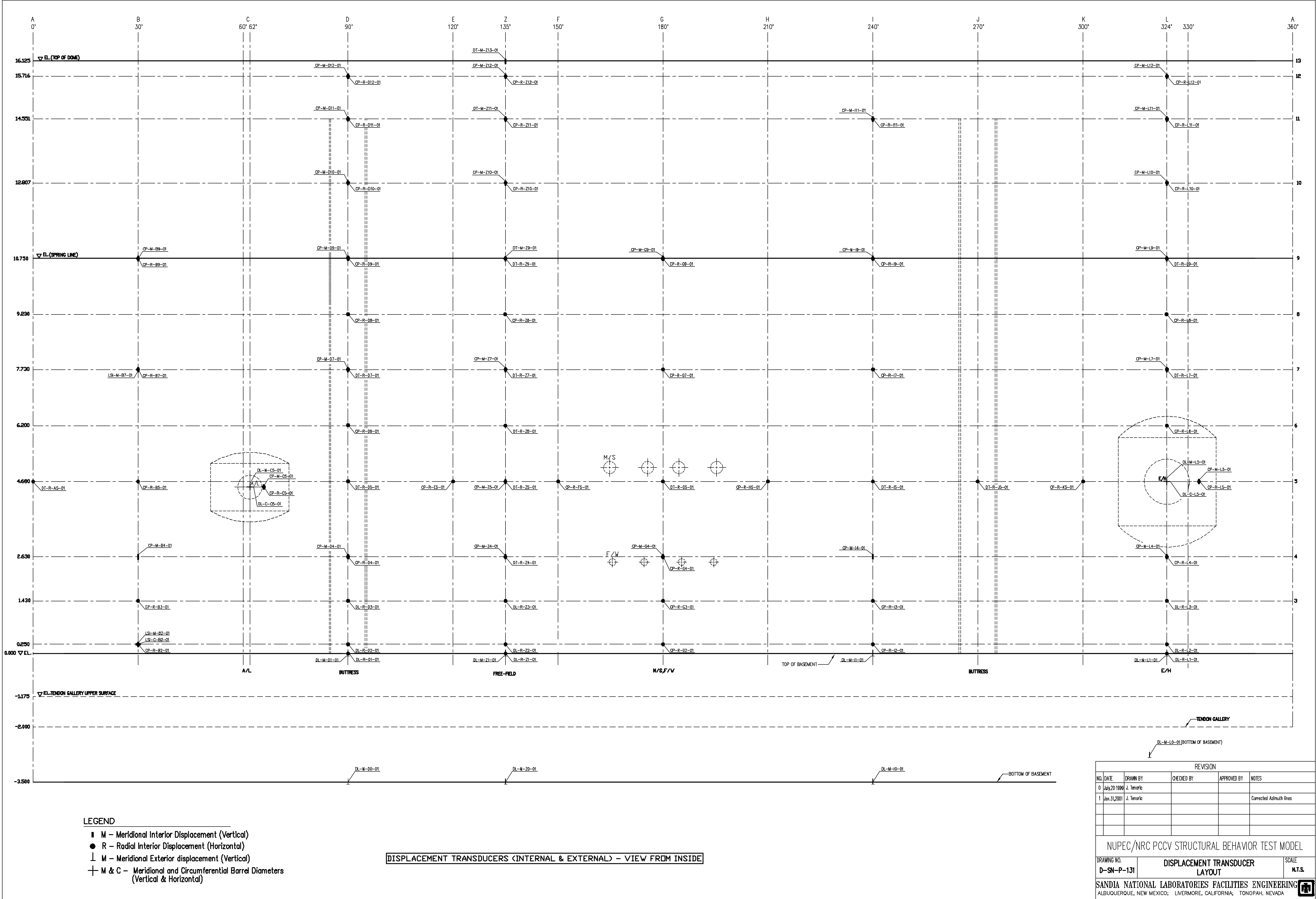
REVISION					
NO.	DATE	DRAWN BY	CHECKED BY	APPROVED BY	NOTES
0	July 20, 1996	J. Tenorio			
1	Jan. 31, 2001	J. Tenorio			Corrected Azimuth Lines
NUPEC/NRC PCCV STRUCTURAL BEHAVIOR TEST MODEL					
DRAWING NO. D-SN-P-129		STRAIN GAGE LAYOUT EXTERIOR LINER			SCALE N.T.S.
SANDIA NATIONAL LABORATORIES FACILITIES ENGINEERING ALBUQUERQUE, NEW MEXICO; LIVERMORE, CALIFORNIA; TONOPAH, NEVADA					



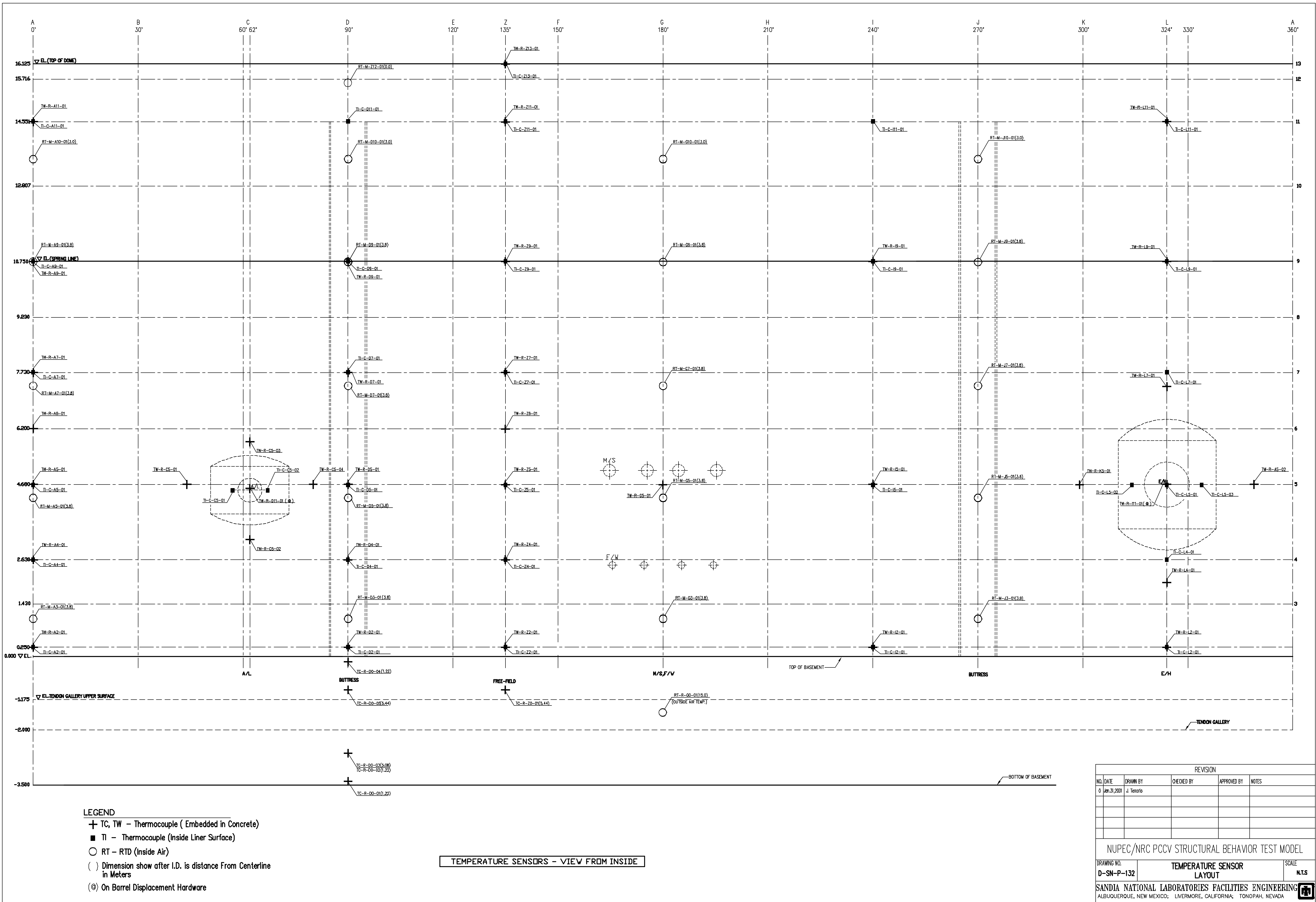
- LEGEND**
- M – Meridional Strain Gage (Vertical)
 - C – Circumferential Strain Gage (Hoop)
 - R – Radial Strain Gage (on Basement Liner Only)
 - () – Dimension shown after ID is Distance from Cylinder liner in Meters

STRAIN GAGES ON LINER INTERIOR – VIEW FROM INSIDE

REVISION					
NO.	DATE	DRAWN BY	CHECKED BY	APPROVED BY	NOTES
0	July 20, 1998	J. Tenorio			
1	Jan. 31, 2009	J. Tenorio			Added Gages
NUPEC/NRC PCCV STRUCTURAL BEHAVIOR TEST MODEL					
DRAWING NO. D-SN-P-130		STRAIN GAGE LAYOUT INTERIOR LINER			SCALE N.T.S.
SANDIA NATIONAL LABORATORIES FACILITIES ENGINEERING					
ALBUQUERQUE, NEW MEXICO; LIVERMORE, CALIFORNIA; TONOPAH, NEVADA					



REVISION					
NO.	DATE	DRAWN BY	CHECKED BY	APPROVED BY	NOTES
0	July 20, 1998	J. Tenorio			
1	Jan. 31, 2001	J. Tenorio			Corrected Asimuth lines
NUPEC/NRC PCCV STRUCTURAL BEHAVIOR TEST MODEL					
DRAWING NO. D-SN-P-131		DISPLACEMENT TRANSDUCER LAYOUT			SCALE N.T.S.
SANDIA NATIONAL LABORATORIES FACILITIES ENGINEERING					
ALBUQUERQUE, NEW MEXICO; LIVERMORE, CALIFORNIA; TONOPAH, NEVADA					



LEGEND

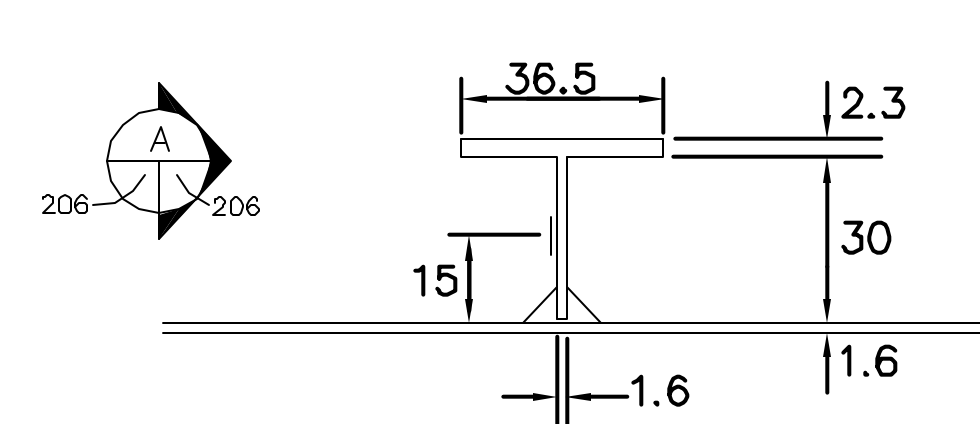
- + TC, TW - Thermocouple (Embedded in Concrete)
- TI - Thermocouple (Inside Liner Surface)
- RT - RTD (Inside Air)
- () Dimension show after I.D. is distance From Centerline in Meters
- (@) On Barrel Displacement Hardware

TEMPERATURE SENSORS - VIEW FROM INSIDE

REVISION					
NO.	DATE	DRAWN BY	CHECKED BY	APPROVED BY	NOTES
0	Jan. 31, 2009	J. Tenorio			
NUPEC/NRC PCCV STRUCTURAL BEHAVIOR TEST MODEL					
DRAWING NO. D-SN-P-132		TEMPERATURE SENSOR LAYOUT			SCALE N.T.S.
SANDIA NATIONAL LABORATORIES FACILITIES ENGINEERING					
ALBUQUERQUE, NEW MEXICO:		LIVERMORE, CALIFORNIA:		TONOPAH, NEVADA	

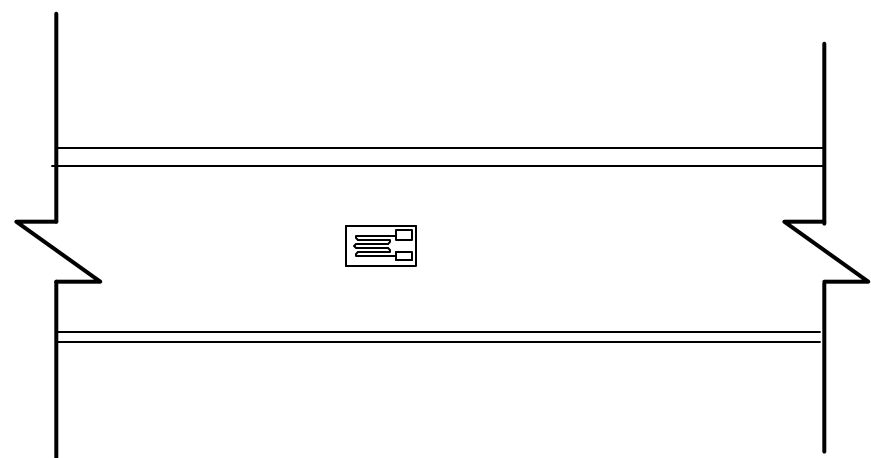


REVISION					
NO.	DATE	DRAWN BY	CHECKED BY	APPROVED BY	NOTES
0	Jan.31,2001	J. Tenorio			
NUPEC/NRC PCCV STRUCTURAL BEHAVIOR TEST MODEL					
DRAWING NO. D-SN-P-133		DISPLACEMENT TRANSDUCER FIXTURES			SCALE 1/1
SANDIA NATIONAL LABORATORIES FACILITIES ENGINEERING ALBUQUERQUE, NEW MEXICO; LIVERMORE, CALIFORNIA; TONOPAH, NEVADA					



1 TYPICAL ANCHOR WEB GAUGE

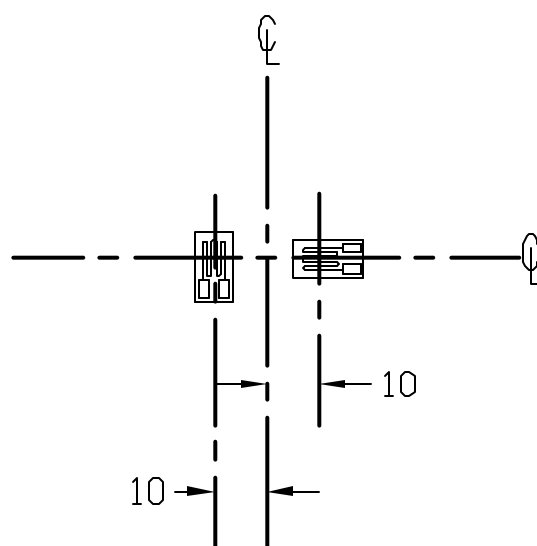
ZCD1002Ai
ZCD1007Ai
ZCD1008Ai
ZCD1009Ai
200
201
202
203
204



A SIDE VIEW

206

ANCHOR GAGE LOCATIONS			
LABELING ID	AZIMUTHAL ANGLE	VERTICAL ELEVATION	LINER MARK #
(name)	(deg)	(in)	
LSA-M-D3-01	90	53.1	1-3B
LSA-M-D5-01	90	194.9	3-4C
LSA-M-D7-01	90	301.2	4-3B
LSA-M-D9-01	90	411.4	5-4B
LSA-M-Z3-01	129	53.1	1-4B
LSA-M-Z5-01	128	194.9	3-5C
LSA-M-Z7-01	138	301.2	4-5B
LSA-M-Z9-01	129	411.4	5-6B
LSA-M-J5-01	268	194.9	3-9C
LSA-M-L3-01	325	53.1	1-11B
LSA-M-L7-01	325	301.2	4-10B
LSA-M-L9-01	325	411.4	5-13B



2 TYPICAL VERTICAL AND HOOP GAUGE

ZCD1002Ai
ZCD1007Ai
ZCD1008Ai
ZCD1009Ai
200
201
202
203
204

FREE FIELD LINER GAGE LOCATIONS								
LABELING ID	AZIMUTHAL ANGLE	VERTICAL ELEVATION	LABELING ID	AZIMUTHAL ANGLE	VERTICAL ELEVATION	LABELING ID	AZIMUTHAL ANGLE	VERTICAL ELEVATION
(name)	(deg)	(in)	(name)	(deg)	(in)	(name)	(deg)	(in)
LSI-C-A2-01	0	9.8	LSI-C-D11-01	90	572.9	LSI-C-G2-01	180	9.8
LSI-M-A2-01	0	9.8	LSI-M-D11-01	90	572.9	LSI-M-G2-01	180	9.8
LSI-C-A5-01	0	184.3	LSI-C-D12-01	90	618.7	LSI-C-G5-01	180	184.3
LSI-M-A5-01	0	184.3	LSI-M-D12-01	90	618.7	LSI-M-G5-01	180	184.3
LSI-C-B2-01	30	9.8	LSI-C-E5-01	120	184.3	LSI-C-G6-01	180	244.1
LSI-M-B2-01	30	9.8	LSI-M-E5-01	120	184.3	LSI-M-G6-01	180	244.1
LSI-C-B5-01	30	184.3	LSI-C-Z2-01	129.5	9.8	LSI-C-G7-01	180	304.3
LSI-M-B5-01	30	184.3	LSI-M-Z2-01	129.5	9.8	LSI-M-G7-01	180	304.3
LSI-C-B7-01	30	304.3	LSI-C-Z2-02	130.4	9.8	LSI-C-G9-01	180	423.2
LSI-M-B7-01	30	304.3	LSI-M-Z2-02	130.4	9.8	LSI-M-G9-01	180	423.2
LSI-C-B9-01	30	423.2	LSI-C-Z3-01	135	56.3	LSI-C-H5-01	210	184.3
LSI-M-B9-01	30	423.2	LSI-M-Z3-01	135	56.3	LSI-M-H5-01	210	184.3
LSI-C-C6-01	62	184.3	LSI-C-Z4-01	135	103.5	LSI-C-I2-01	239.4	9.8
LSI-M-C6-01	62	184.3	LSI-M-Z4-01	135	103.5	LSI-M-I2-01	239.4	9.8
LSI-C-D2-01	88.9	9.8	LSI-C-Z5-01	135	184.3	LSI-C-I5-01	240	184.3
LSI-M-D2-01	88.9	9.8	LSI-M-Z5-01	135	184.3	LSI-M-I5-01	240	184.3
LSI-C-D2-02	89.6	9.8	LSI-C-Z6-01	135	244.1	LSI-C-I7-01	240	304.3
LSI-M-D2-02	89.6	9.8	LSI-M-Z6-01	135	244.1	LSI-M-I7-01	240	304.3
LSI-C-D3-01	90	56.3	LSI-C-Z7-01	135	304.3	LSI-C-I9-01	240	423.2
LSI-M-D3-01	90	56.3	LSI-M-Z7-01	135	304.3	LSI-M-I9-01	240	423.2
LSI-C-D4-01	90	103.5	LSI-C-Z8-01	135	363.4	LSI-C-I11-01	240	572.9
LSI-M-D4-01	90	103.5	LSI-M-Z8-01	135	363.4	LSI-M-I11-01	240	572.9
LSI-C-D5-01	90	184.3	LSI-C-Z9-01	135	423.2	LSI-C-J1-01	270	0.0
LSI-M-D5-01	90	184.3	LSI-M-Z9-01	135	423.2	LSI-M-J1-01	270	0.0
LSI-C-D6-01	90	244.1	LSI-C-Z10-01	135	504.2	LSI-C-J2-01	270	9.8
LSI-M-D6-01	90	244.1	LSI-M-Z10-01	135	504.2	LSI-M-J2-01	270	9.8
LSI-C-D7-01	90	304.3	LSI-C-Z11-01	135	572.9	LSI-C-J4-01	270	103.5
LSI-M-D7-01	90	304.3	LSI-M-Z11-01	135	572.9	LSI-M-J4-01	270	103.5
LSI-C-D8-01	90	363.4	LSI-C-Z12-01	135	618.7	LSI-C-J5-01	270	184.3
LSI-M-D8-01	90	363.4	LSI-M-Z12-01	135	618.7	LSI-M-J5-01	270	184.3
LSI-C-D9-01	90	423.2	LSI-C-Z13-01	135	634.8	LSI-C-J7-01	270	304.3
LSI-M-D9-01	90	423.2	LSI-M-Z13-01	135	634.8	LSI-M-J7-01	270	304.3
LSI-C-D10-01	90	504.2	LSI-C-F5-01	150	184.3	LSI-C-J9-01	270	423.2
LSI-M-D10-01	90	504.2	LSI-M-F5-01	150	184.3	LSI-M-J9-01	270	423.2


HOOP ONLY GAGES		
LSI-C-D5-02	76.8	168
LSI-C-D5-03	78.4	168
LSI-C-D5-04	80	168
LSI-C-J5-02	286	200
LSI-C-J5-03	288.5	200
LSI-C-J5-04	291	200

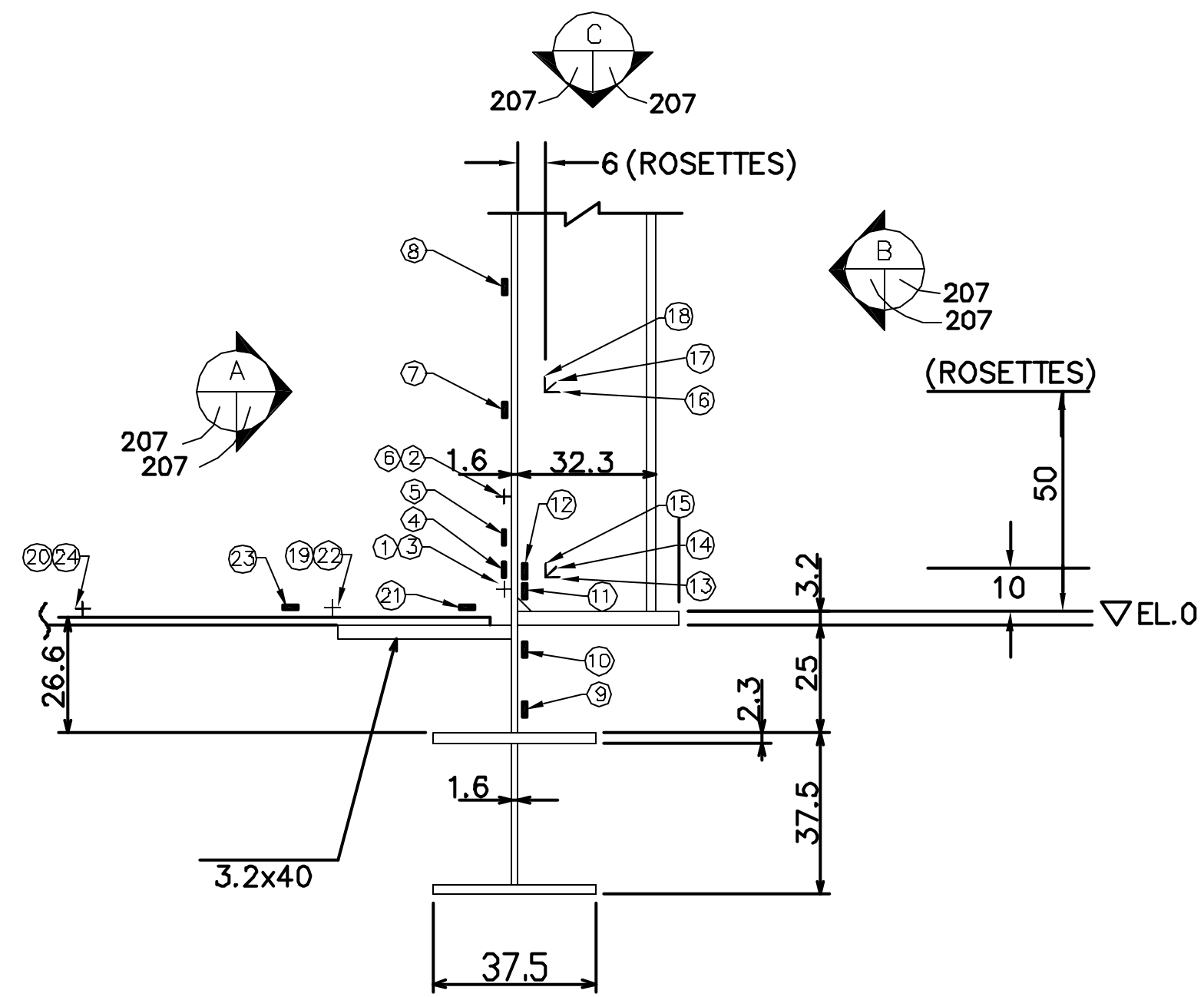
NOTE:

AHCHOR WEB GAUGE LOCATIONS SHOWN ON DRAWINGS ZCD1002Ai, ZCD1007Ai, ZCD1008Ai, AND ZCD1009Ai

ALL DIMENSIONS SHOWN IN MM

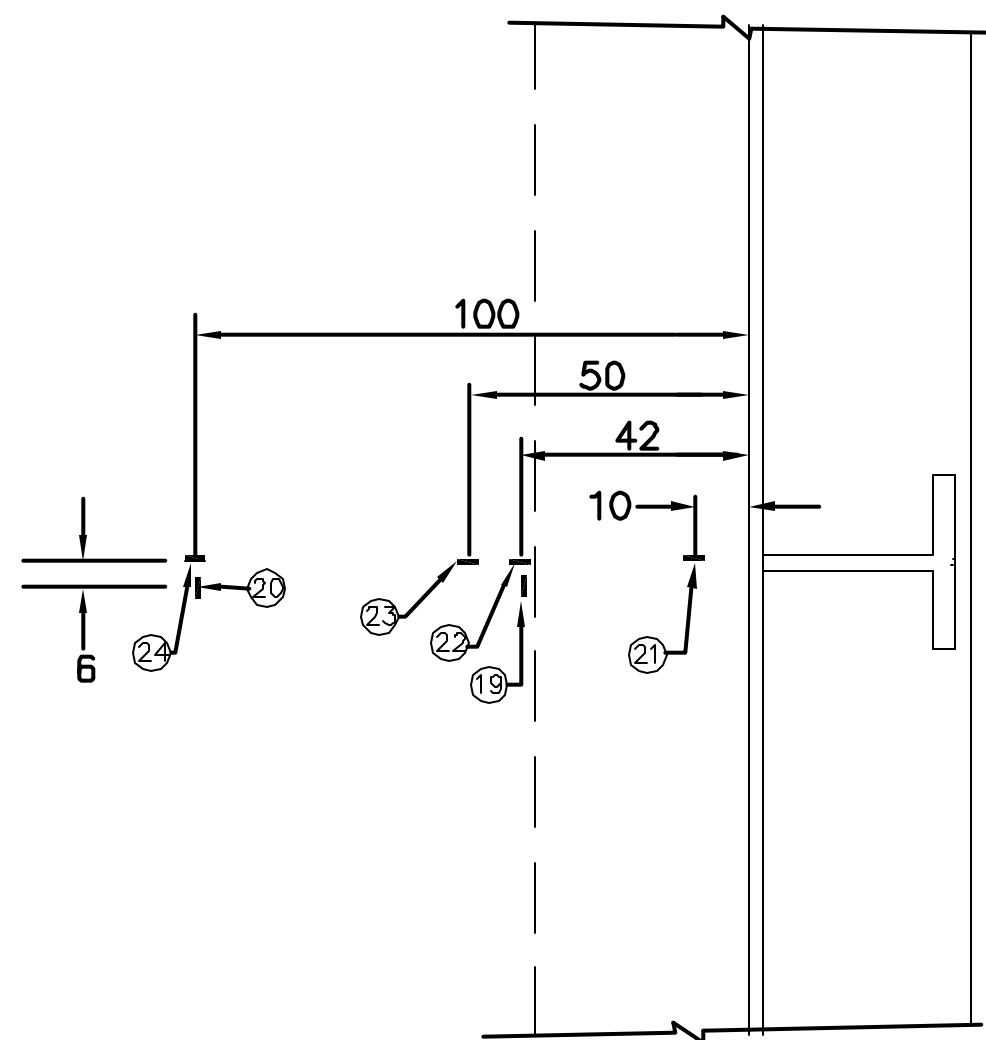
ASSURE GAUGES PLACED 300MM FROM EDGE OR ANY FUTURE WELDING LOCATIONS. AND 100MM AWAY FROM DISCONTINUITYS.

REVISION					
NO.	DATE	DRAWN BY	CHECKED BY	APPROVED BY	NOTES
0	May 15, 1997	T. Martinez			
1	July 20, 1999	J. Tenorio			Removed Gages
NUPEC/NRC PCCV STRUCTURAL BEHAVIOR TEST MODEL					
DRAWING NO.		INSTRUMENTATION LINER DETAILS			SCALE
D-SN-P-206		GAUGES INSTALLATION DETAILS			1/1
SANDIA NATIONAL LABORATORIES FACILITIES ENGINEERING					
ALBUQUERQUE, NEW MEXICO; LIVERMORE, CALIFORNIA; TONOPAH, NEVADA					



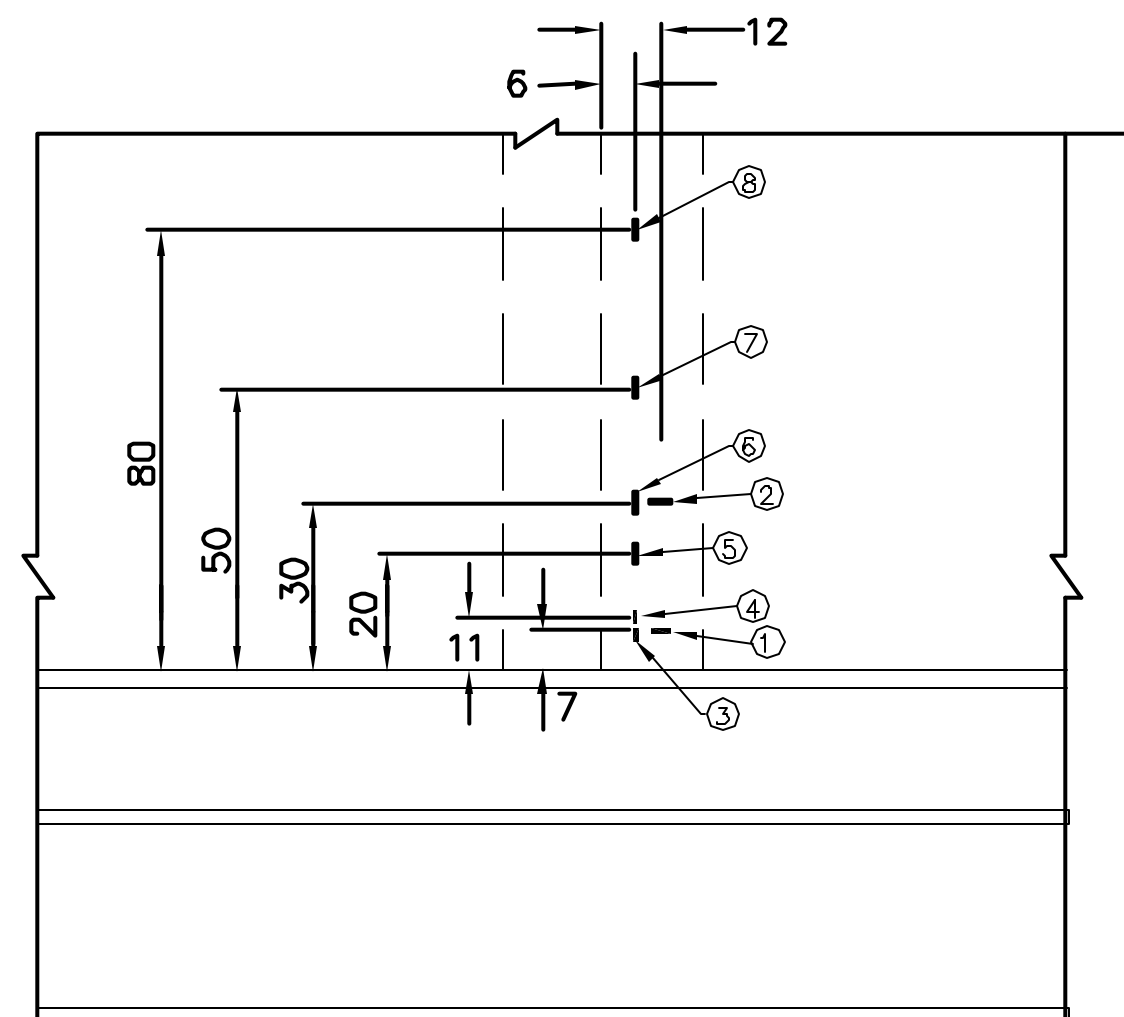
BASEMAT LINER CONNECTION DETAIL

ZCD1002Ai 200
207
ZCD1002Ai 201
c.3
c.5
c.6
207
ZCD1002Ai 202



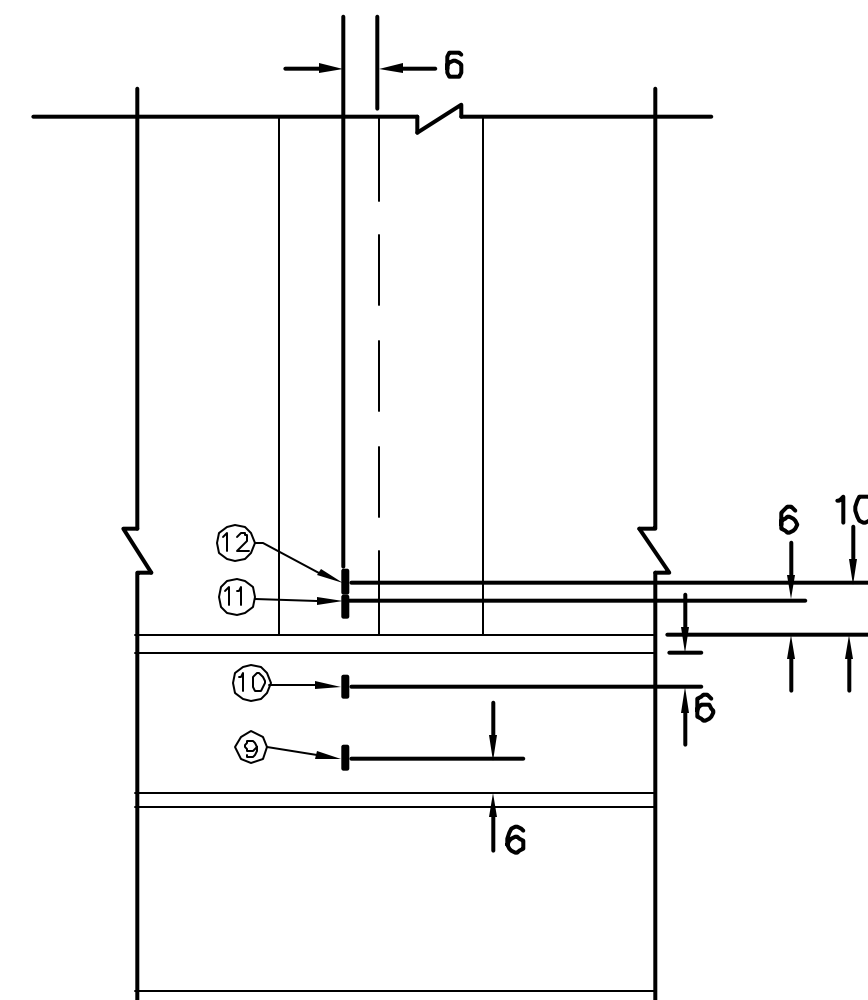
TOP VIEW (c.5 only)

207
C
207



INSIDE VIEW

207
A
207



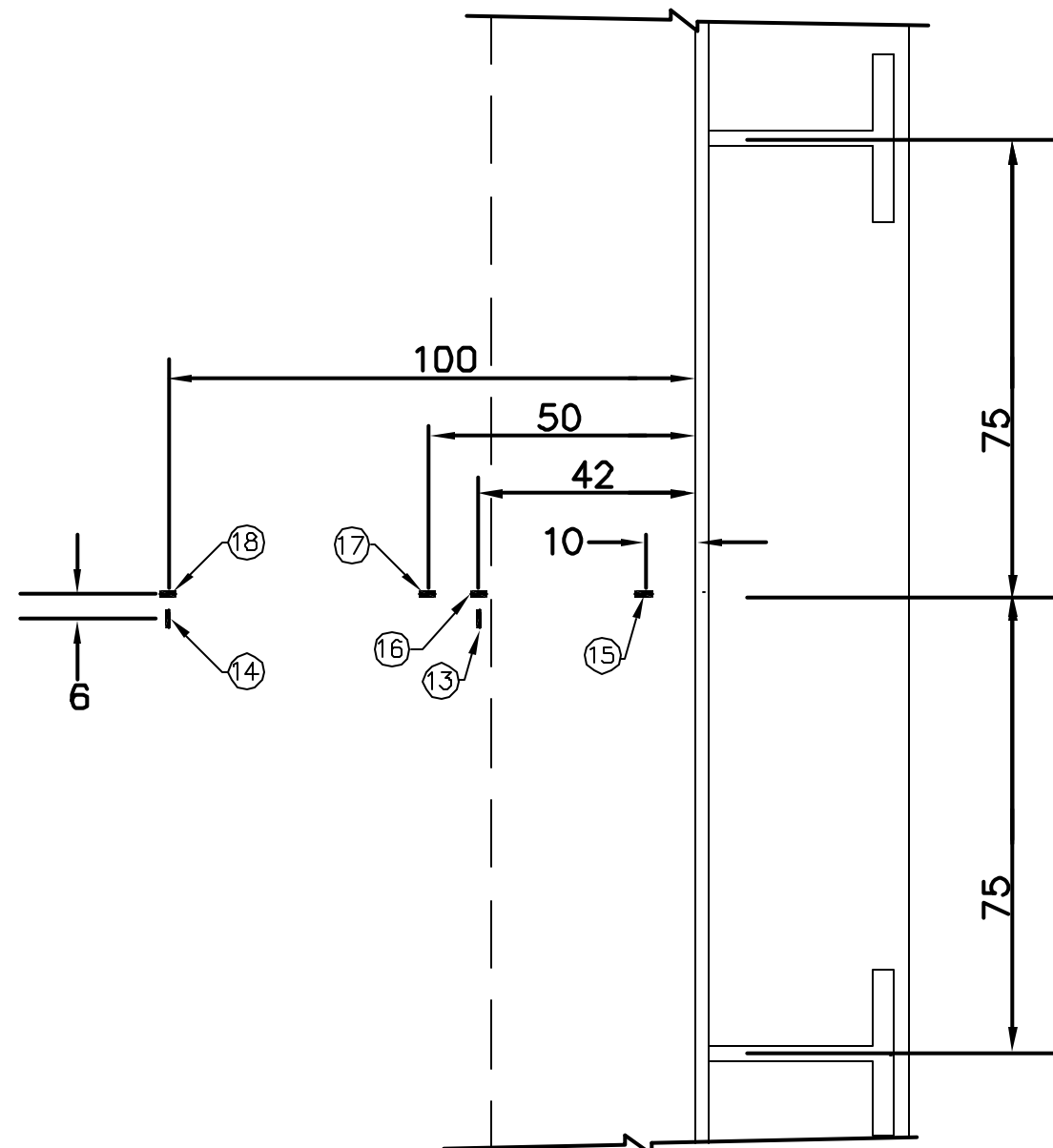
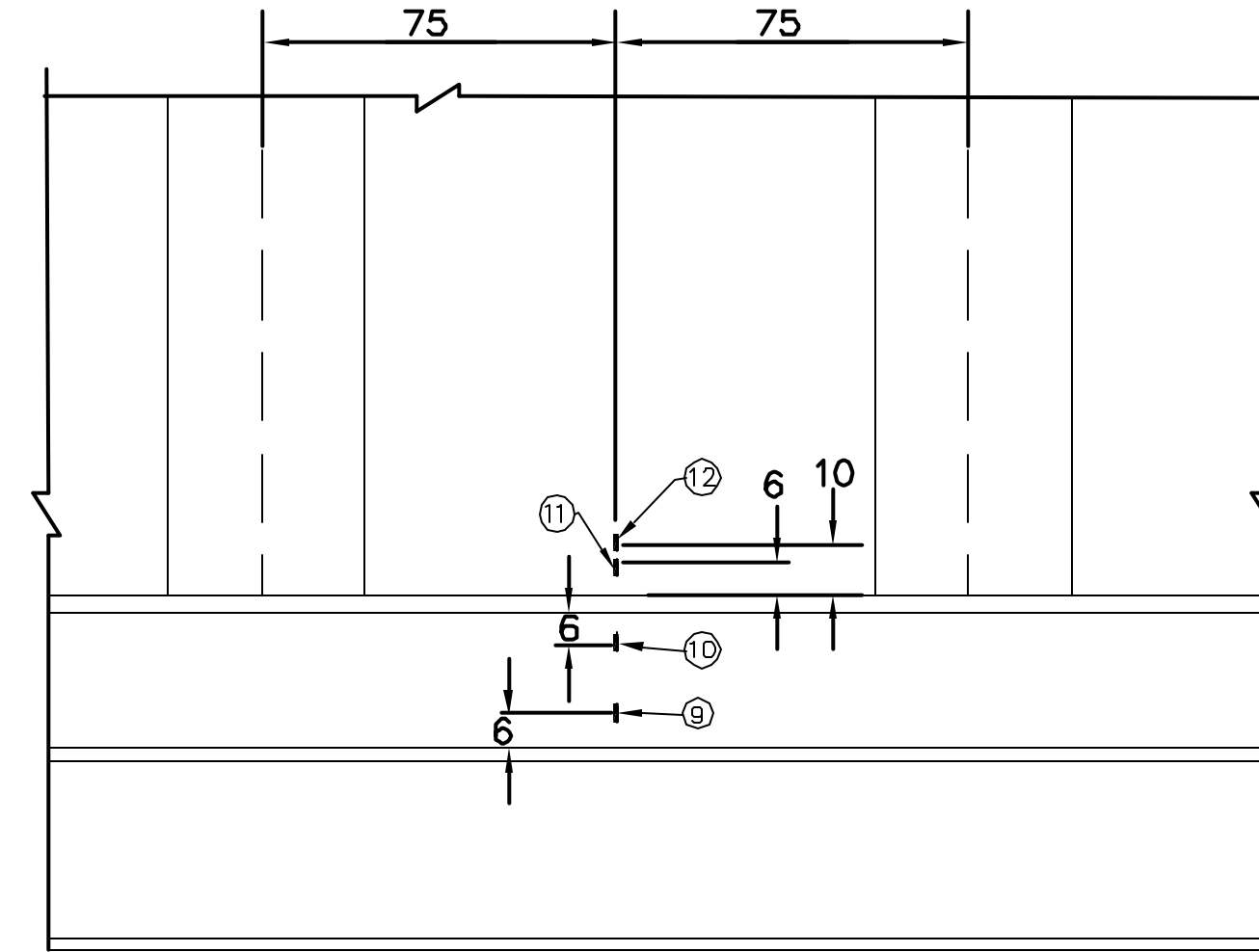
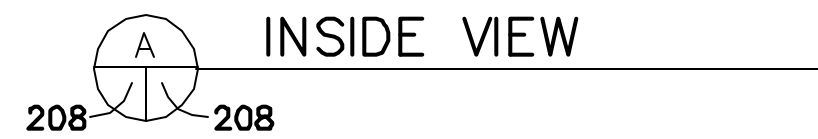
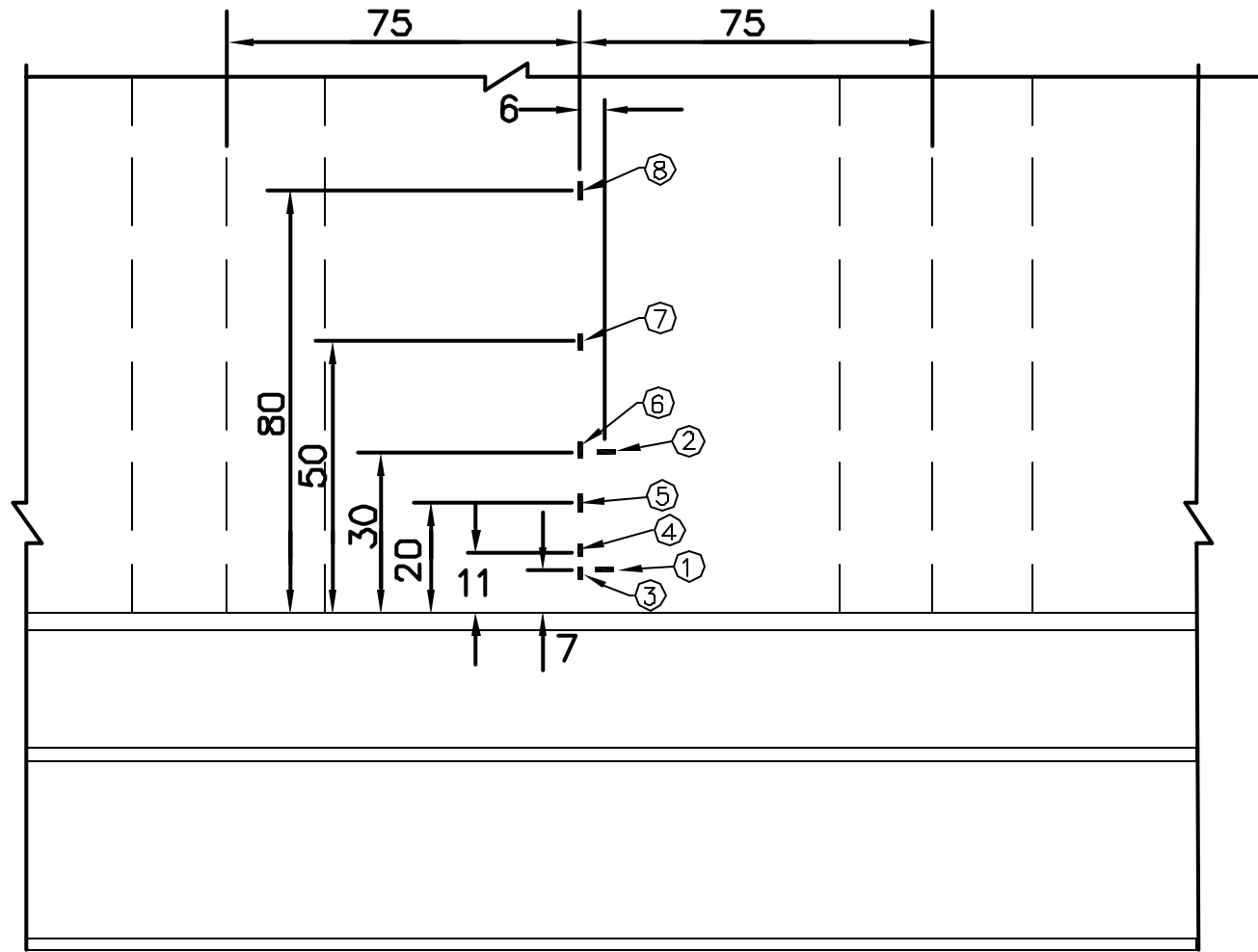
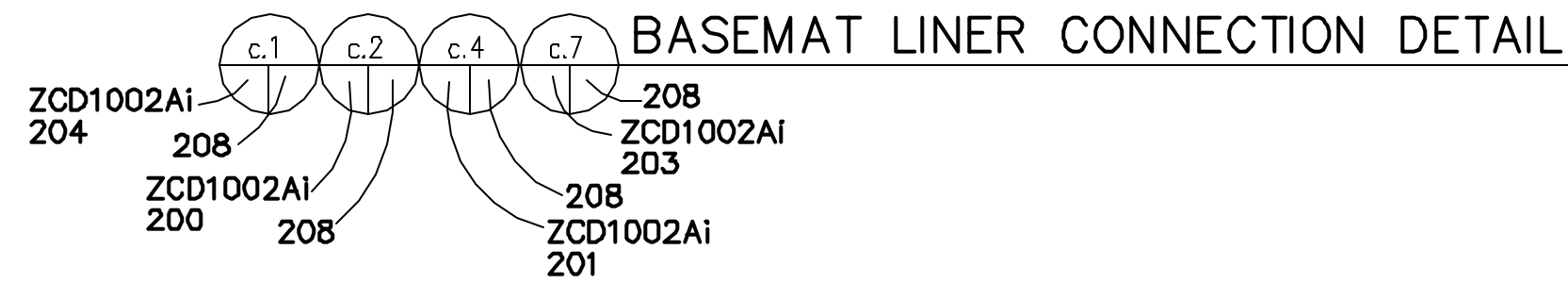
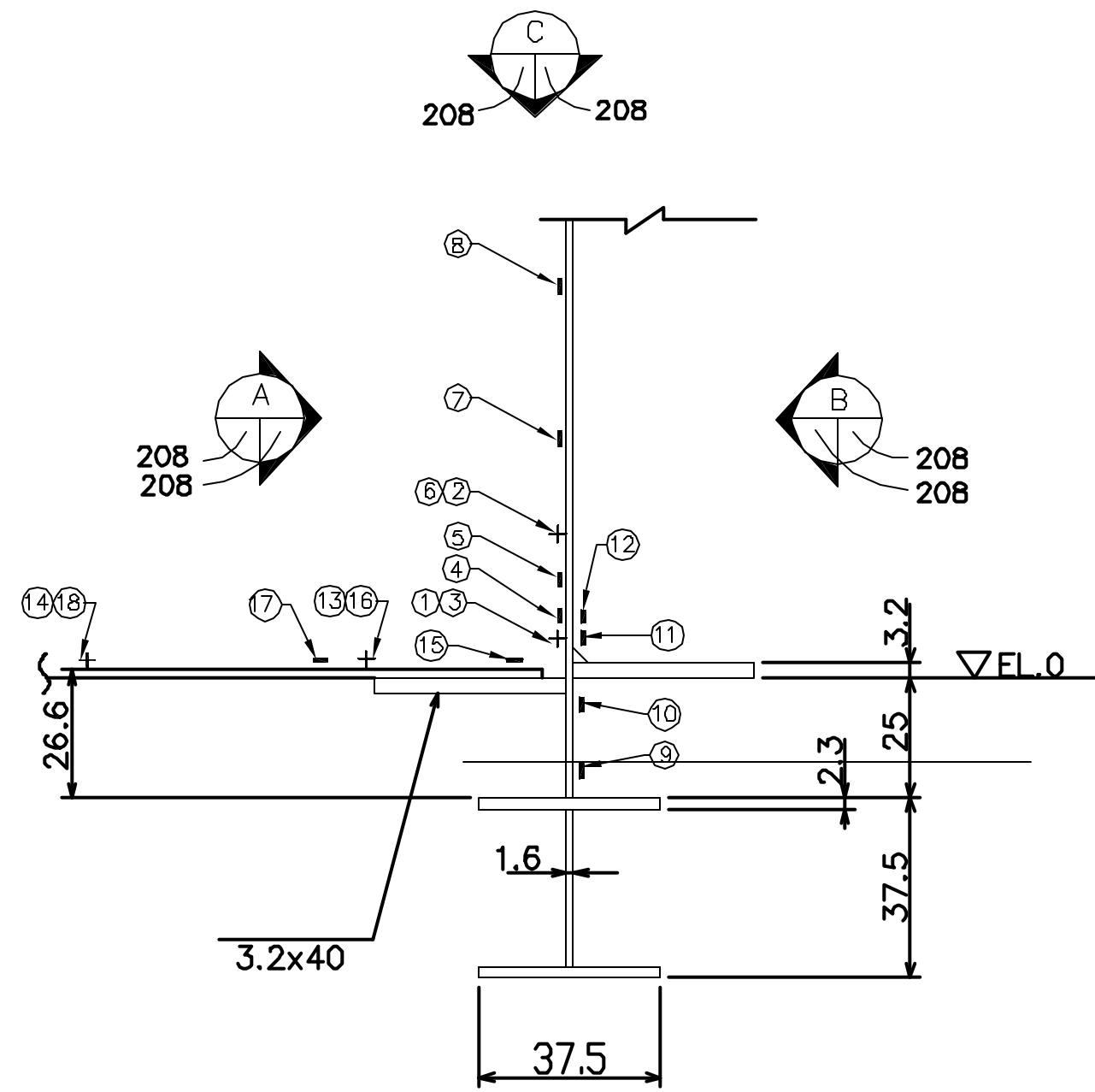
OUTSIDE VIEW

207
B
207

INSTRUMENTATION ID #			
Detail #	c.5	c.3	c.6
Azimuth	131	90	240
Elevation	0	0	0
Liner #	1-4C	1-3C	1-8C
Instr. #			
①	LSI-C-Z1-03	LSI-C-D1-03	LSI-C-I1-01
②	LSI-C-Z1-04	LSI-C-D1-04	LSI-C-I1-02
③	LSI-M-Z1-07	LSI-M-D1-07	LSI-M-I1-01
④	LSI-M-Z1-08	LSI-M-D1-08	LSI-M-I1-02
⑤	LSI-M-Z1-09	LSI-M-D1-09	LSI-M-I1-03
⑥	LSI-M-Z1-10	LSI-M-D1-10	LSI-M-I1-04
⑦	LSI-M-Z1-11	LSI-M-D1-11	LSI-M-I1-05
⑧	LSI-M-Z1-12	LSI-M-D1-12	LSI-M-I1-06
⑨	LSO-M-Z1-05	LSO-M-D1-05	LSO-M-I1-01
⑩	LSO-M-Z1-06	LSO-M-D1-06	LSO-M-I1-02
⑪	LSO-M-Z1-07	LSO-M-D1-07	LSO-M-I1-03
⑫	LSO-M-Z1-08	LSO-M-D1-08	LSO-M-I1-04
⑬	LRA-R-Z1-1r	LRA-R-D1-1r	LRA-R-I1-1r
⑭	LRA-R-Z1-1d	LRA-R-D1-1d	LRA-R-I1-1d
⑮	LRA-R-Z1-1m	LRA-R-D1-1m	LRA-R-I1-1m
⑯	LRA-R-Z1-2r	LRA-R-D1-2r	LRA-R-I1-2r
⑰	LRA-R-Z1-2d	LRA-R-D1-2d	LRA-R-I1-2d
⑱	LRA-R-Z1-2m	LRA-R-D1-2m	LRA-R-I1-2m
⑲	LSI-C-Z1-05	n/a	n/a
⑳	LSI-C-Z1-06	n/a	n/a
㉑	LSI-R-Z1-05	n/a	n/a
㉒	LSI-R-Z1-06	n/a	n/a
㉓	LSI-R-Z1-07	n/a	n/a
㉔	LSI-R-Z1-08	n/a	n/a

NOTE:
ALL DIMENSIONS SHOWN IN MM

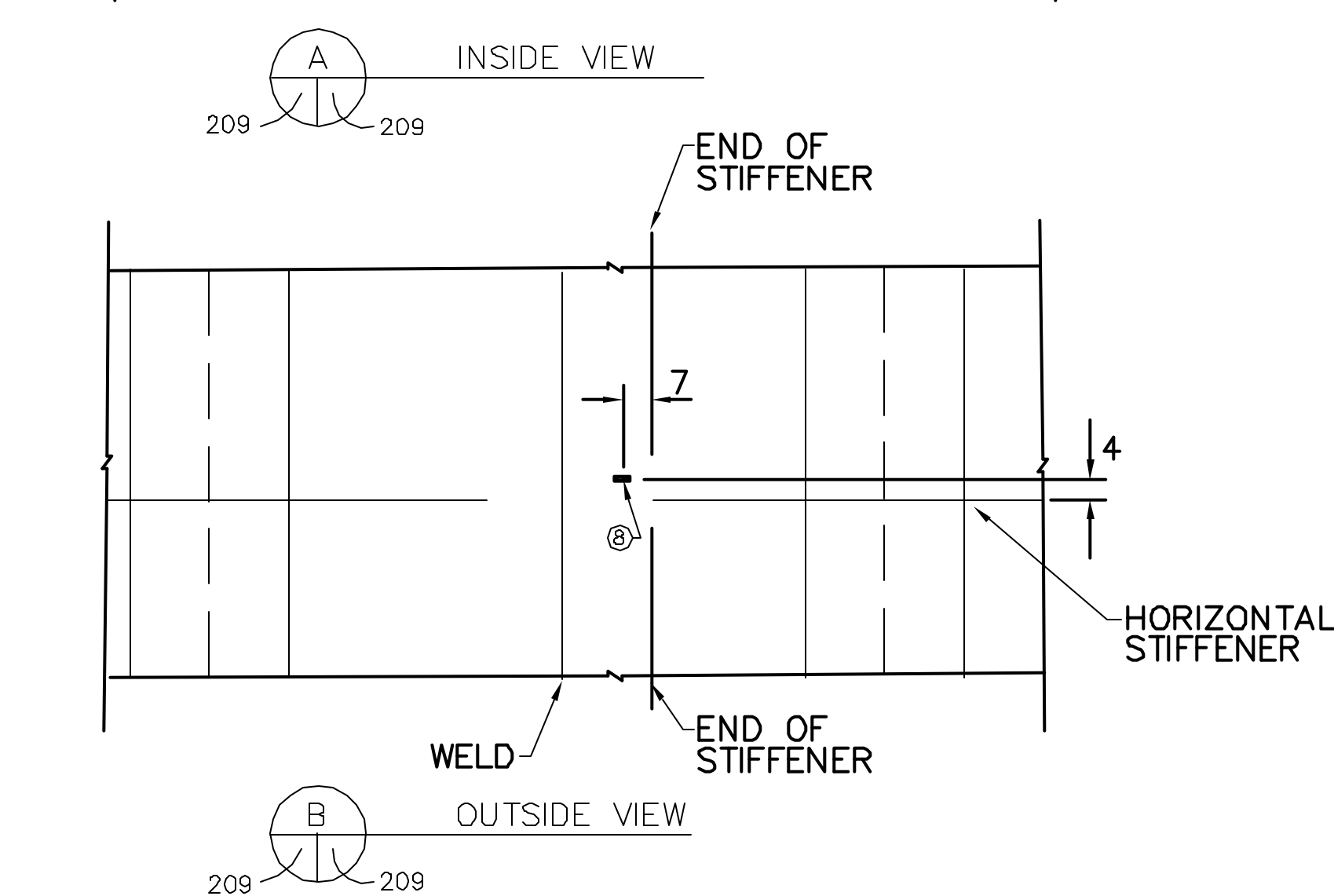
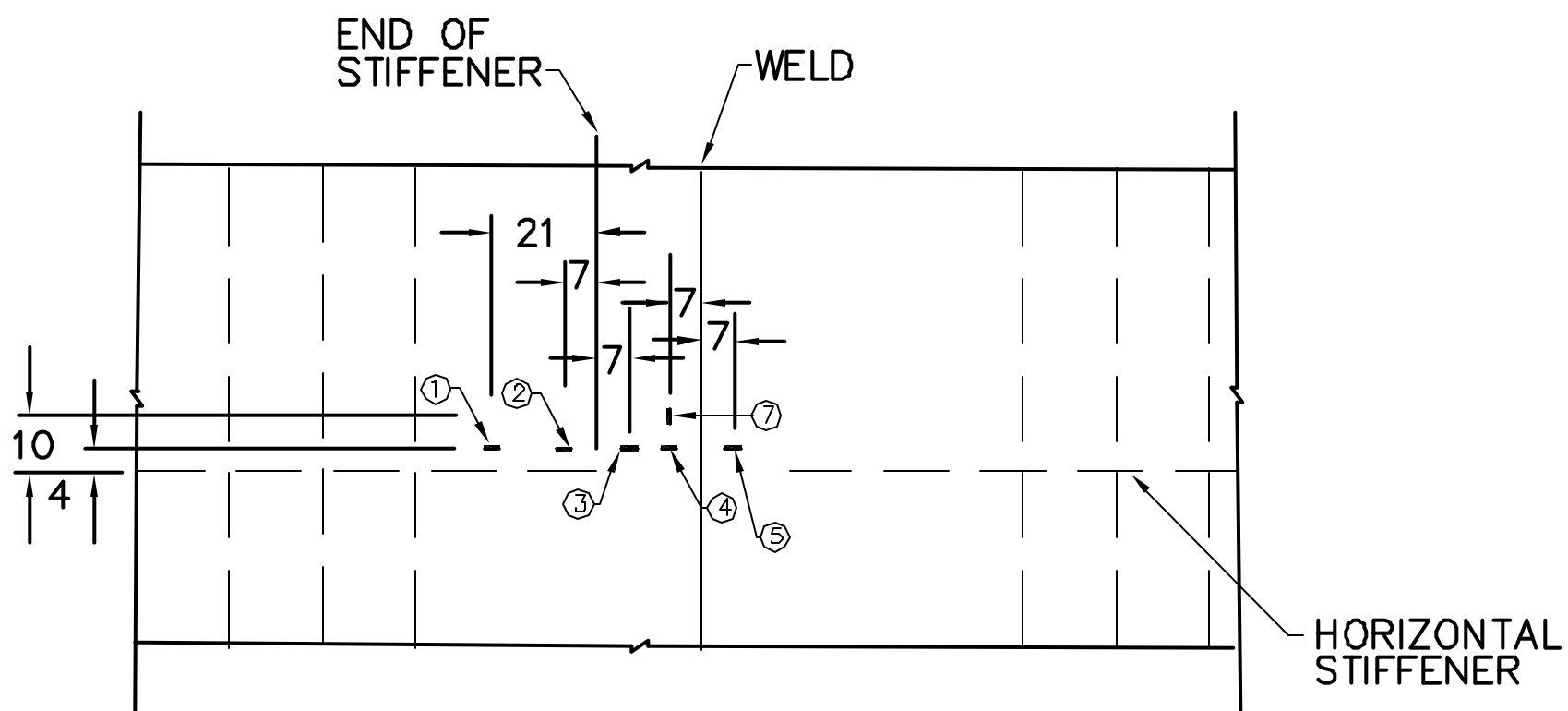
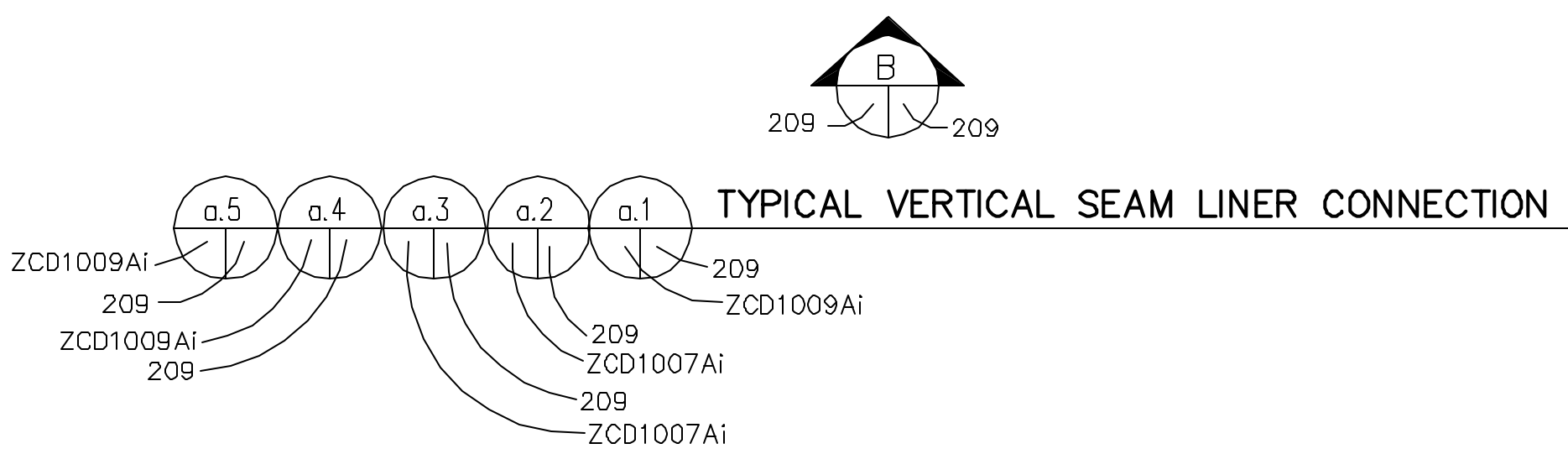
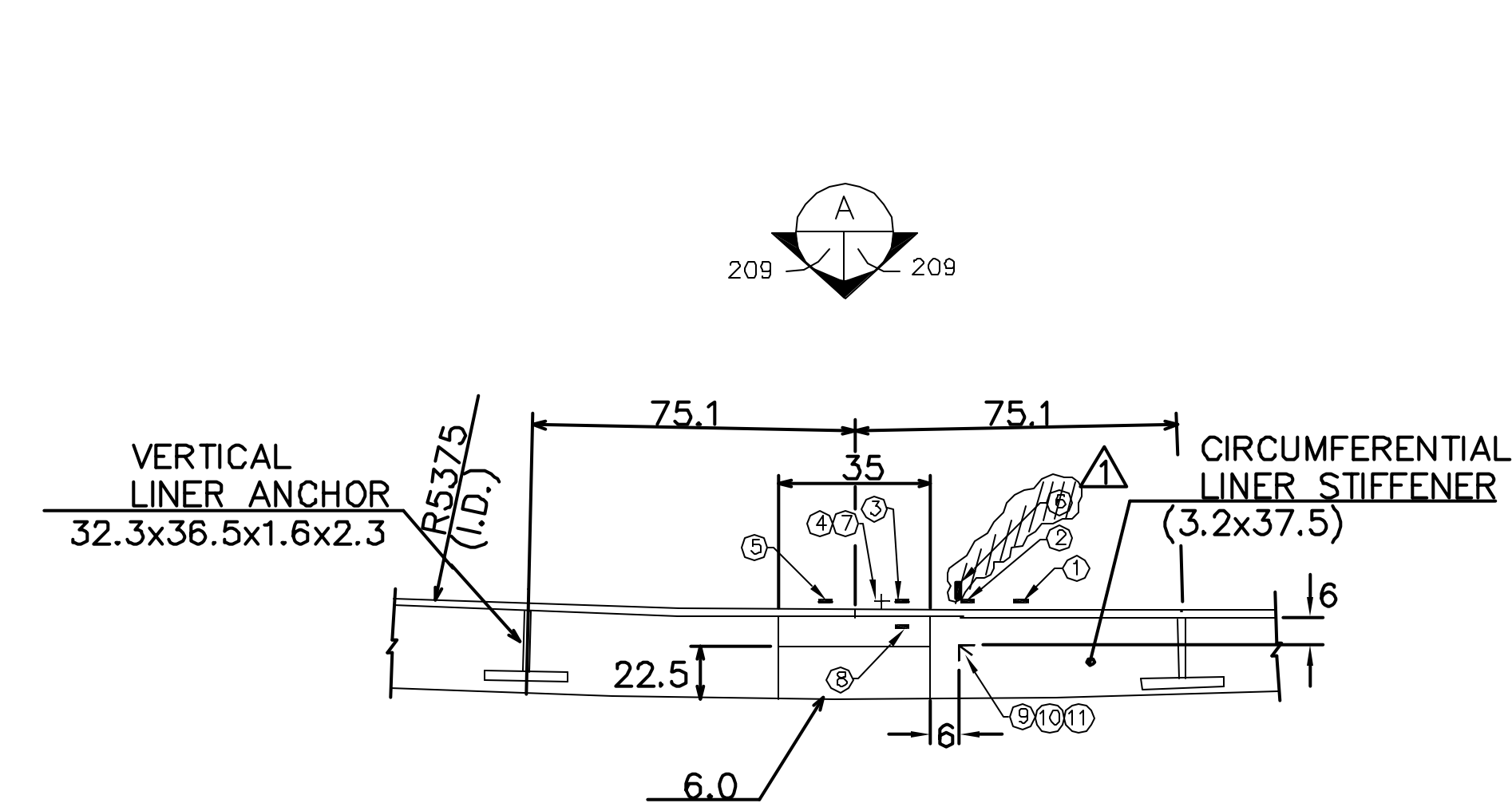
REVISION				
NO.	DATE	DRAWN BY	CHECKED BY	APPROVED BY
0	May 15, 1997	T. Martinez		
1	July 20, 1999	J. Tenorio		
NUPEC/NRC PCCV STRUCTURAL BEHAVIOR TEST MODEL DRAWING NO. D-SN-P-207 INSTRUMENTATION LINER DETAILS SCALE 1/1 BASEMAT LINER CONNECTION @ ANCHOR SANDIA NATIONAL LABORATORIES FACILITIES ENGINEERING ALBUQUERQUE, NEW MEXICO; LIVERMORE, CALIFORNIA; TONOPAH, NEVADA				



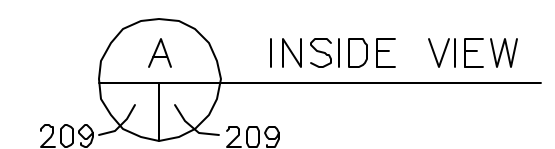
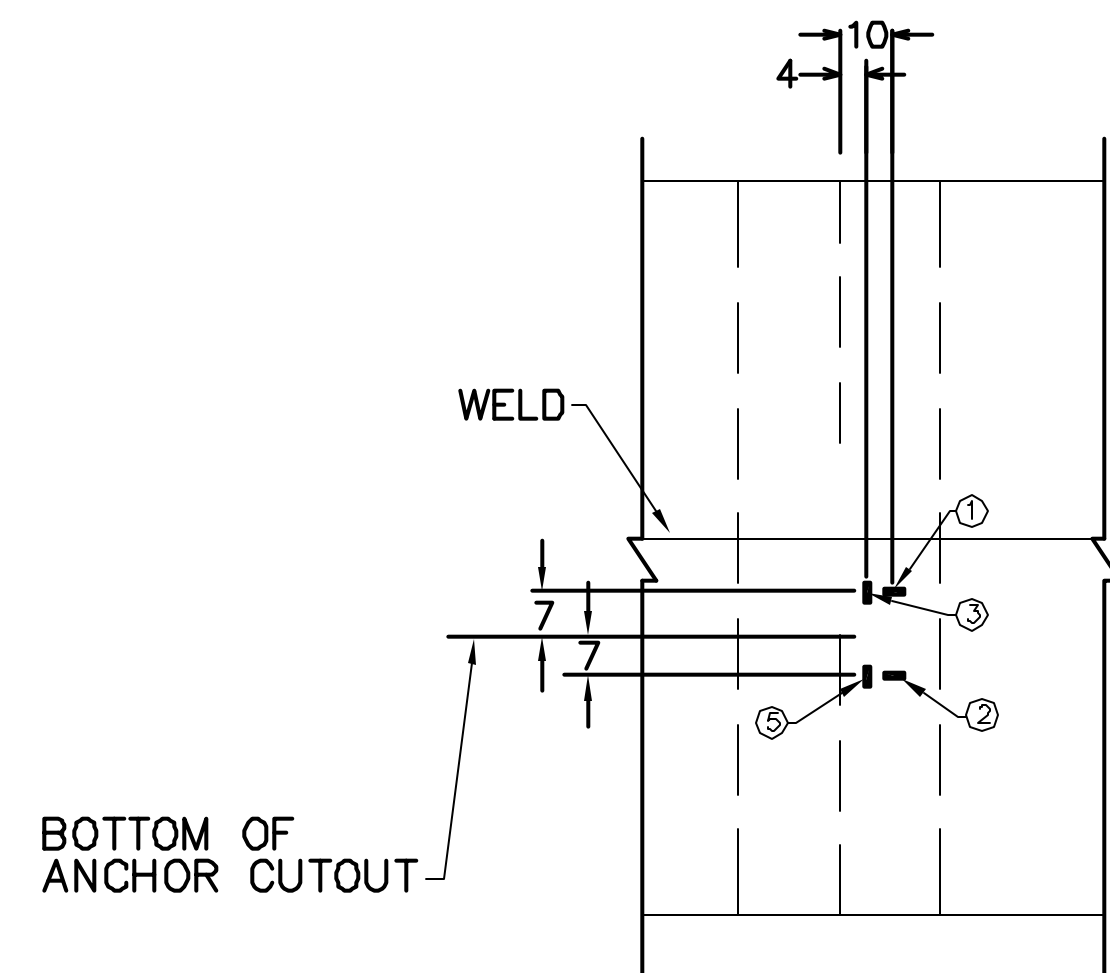
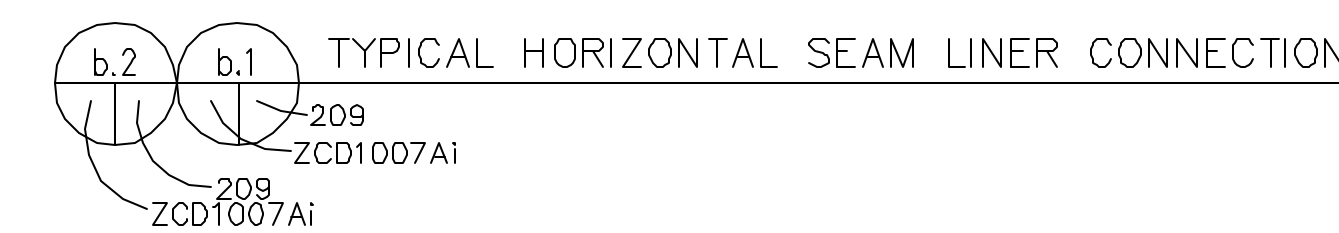
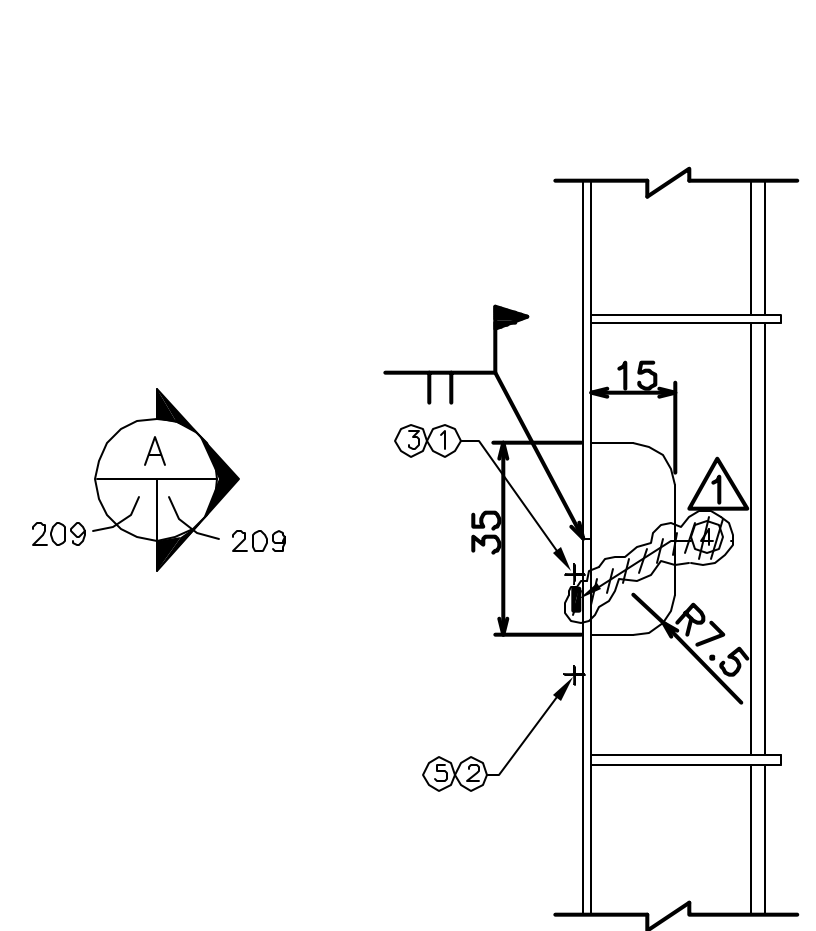
	INSTRUMENTATION ID #			
Detail #	c.1	c.2	c.4	c.7
Azimuth	0	89	130	324
Elevation	0	0	0	0
Liner #	1-12C	1-3C	1-4C	1-11C
Instr. #				
①	LSI-C-A1-01	LSI-C-D1-01	LSI-C-Z1-01	LSI-C-L1-01
②	LSI-C-A1-02	LSI-C-D1-02	LSI-C-Z1-02	LSI-C-L1-02
③	LSI-M-A1-01	LSI-M-D1-01	LSI-M-Z1-01	LSI-M-L1-01
④	LSI-M-A1-02	LSI-M-D1-02	LSI-M-Z1-02	LSI-M-L1-02
⑤	LSI-M-A1-03	LSI-M-D1-03	LSI-M-Z1-03	LSI-M-L1-03
⑥	LSI-M-A1-04	LSI-M-D1-04	LSI-M-Z1-04	LSI-M-L1-04
⑦	LSI-M-A1-05	LSI-M-D1-05	LSI-M-Z1-05	LSI-M-L1-05
⑧	LSI-M-A1-06	LSI-M-D1-06	LSI-M-Z1-06	LSI-M-L1-06
⑨	LSO-M-A1-01	LSO-M-D1-01	LSO-M-Z1-01	LSO-M-L1-01
⑩	LSO-M-A1-02	LSO-M-D1-02	LSO-M-Z1-02	LSO-M-L1-02
⑪	LSO-M-A1-03	LSO-M-D1-03	LSO-M-Z1-03	LSO-M-L1-03
⑫	LSO-M-A1-04	LSO-M-D1-04	LSO-M-Z1-04	LSO-M-L1-04
⑬	LSI-C-A1-03	n/a	n/a	n/a
⑭	LSI-C-A1-04	n/a	n/a	n/a
⑮	LSI-R-A1-01	n/a	n/a	n/a
⑯	LSI-R-A1-02	n/a	n/a	n/a
⑰	LSI-R-A1-03	n/a	n/a	n/a
⑱	LSI-R-A1-04	n/a	n/a	n/a

NOTE:
ALL DIMENSIONS SHOWN IN MM

REVISION					
NO.	DATE	DRAWN BY	CHECKED BY	APPROVED BY	NOTES
0	May 15, 1997	T. Martinez			
1	July 20, 1999	J. Tenorio			Drawing No.'s
NUPEC/NRC PCCV STRUCTURAL BEHAVIOR TEST MODEL					
DRAWING NO.		INSTRUMENTATION LINER DETAILS			SCALE
D-SN-P-208		BASEMAT LINER CONNECTION			1/1
SANDIA NATIONAL LABORATORIES FACILITIES ENGINEERING					
ALBUQUERQUE, NEW MEXICO;		LIVERMORE, CALIFORNIA;		TONOPAH, NEVADA	

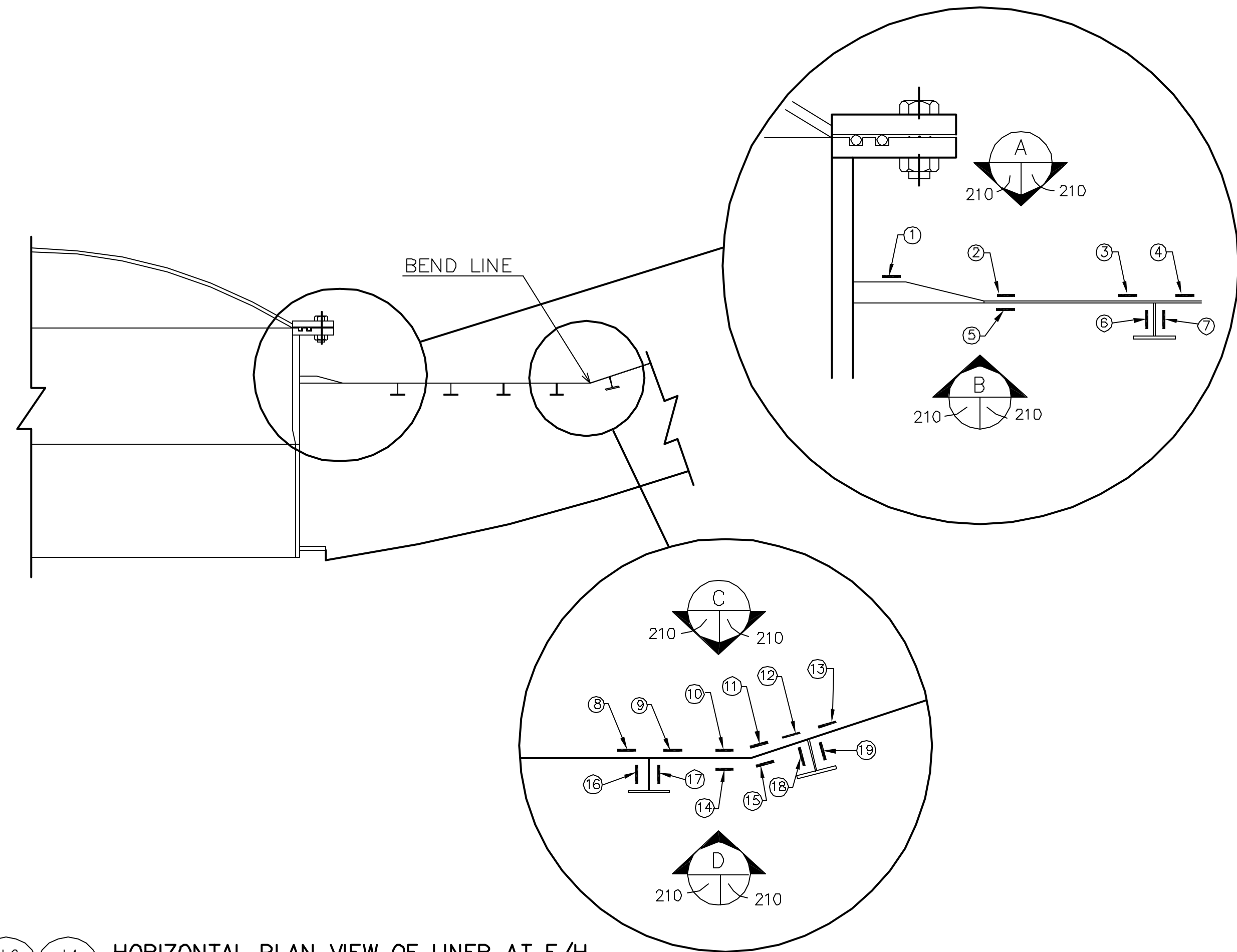


INSTRUMENTATION ID #					
Detail #	a.1	a.2	a.3	a.4	a.5
Azimuth	2	137	137	95	95
Elevation	7750	5487	5831	7750	7400
Liner #	4-1B	3-6B	3-6B	4-3B	4-3B
Instr. #					
①	LSI-C-A7-01	LSI-C-Z5-02	LSI-C-Z6-02	LSI-C-D7-02	LSI-C-D7-07
②	LSI-C-A7-02	LSI-C-Z5-03	LSI-C-Z6-03	LSI-C-D7-03	LSI-C-D7-08
③	LSI-C-A7-03	LSI-C-Z5-04	LSI-C-Z6-04	LSI-C-D7-04	LSI-C-D7-09
④	LSI-C-A7-04	LSI-C-Z5-05	LSI-C-Z6-05	LSI-C-D7-05	LSI-C-D7-10
⑤	LSI-C-A7-05	LSI-C-Z5-06	LSI-C-Z6-06	LSI-C-D7-06	LSI-C-D7-11
⑥	LSI-M-A7-01	LSI-M-Z5-02	LSI-M-Z6-02	LSI-M-D7-02	LSI-M-D7-04
⑦	LSI-M-A7-02	LSI-M-Z5-03	LSI-M-Z6-03	LSI-M-D7-03	LSI-M-D7-05
⑧	LSO-C-A7-01	LSO-C-Z5-01	LSO-C-Z6-01	LSO-C-D7-01	LSO-C-D7-02
⑨	LRS-R-A7-1r	LRS-R-Z5-1r	n/a	LRS-R-D7-1r	n/a
⑩	LRS-R-A7-1d	LRS-R-Z5-1d	n/a	LRS-R-D7-1d	n/a
⑪	LRS-R-A7-1h	LRS-R-Z5-1h	n/a	LRS-R-D7-1h	n/a



INSTRUMENTATION ID #					
Detail #	b.1	b.2	b.3	b.4	b.5
Azimuth	130	130	278	278	278
Elevation	10750	3869	7612	7612	7612
Liner #	5-6B	2-4B	3-5A	3-5A	3-5A
Instr. #					
①	LSI-C-Z9-02	LSI-C-Z5-07	LSI-C-D7-02	LSI-C-D7-03	LSI-C-D7-04
②	LSI-C-Z9-03	LSI-C-Z5-08	LSI-C-D7-05	LSI-C-D7-06	LSI-C-D7-07
③	LSI-M-Z9-02	LSI-M-Z5-04	LSI-M-D7-02	LSI-M-D7-03	LSI-M-D7-04
④	LSI-M-Z9-03	LSI-M-Z5-05	LSI-M-D7-05	LSI-M-D7-06	LSI-M-D7-07
⑤	LSI-M-Z9-04	LSI-M-Z5-06	LSI-M-D7-08	LSI-M-D7-09	LSI-M-D7-10

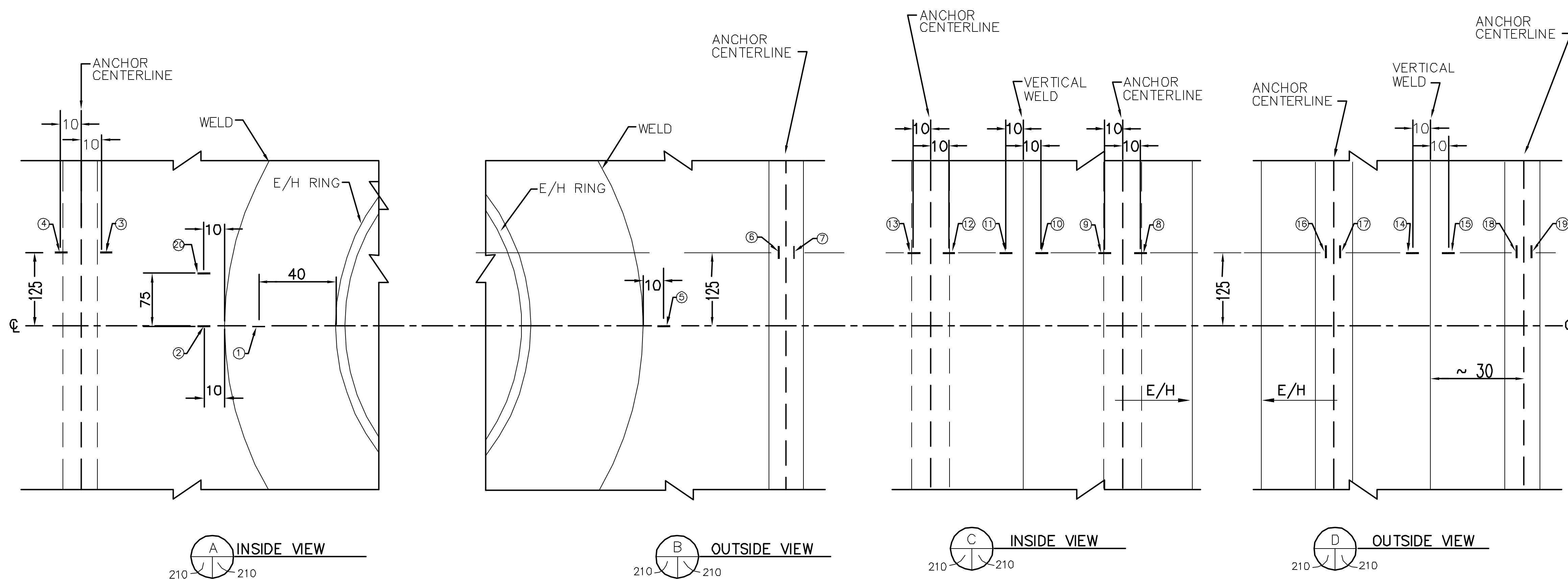
REVISION					
NO.	DATE	DRAWN BY	CHECKED BY	APPROVED BY	NOTES
0	Feb.4/1998	T. Martinez			
1	July 20/1999	J.Tenorio			Removed Gages
NUPEC/NRC PCCV STRUCTURAL BEHAVIOR TEST MODEL					
DRAWING NO.		INSTRUMENTATION LINER DETAILS			SCALE
D-SN-P-209		DETAIL a & b			1/1
SANDIA NATIONAL LABORATORIES FACILITIES ENGINEERING					
ALBUQUERQUE, NEW MEXICO; LIVERMORE, CALIFORNIA; TONOPAH, NEVADA					



HORIZONTAL PLAN VIEW OF LINER AT E/H

d.2
ZCD1010Ai
210

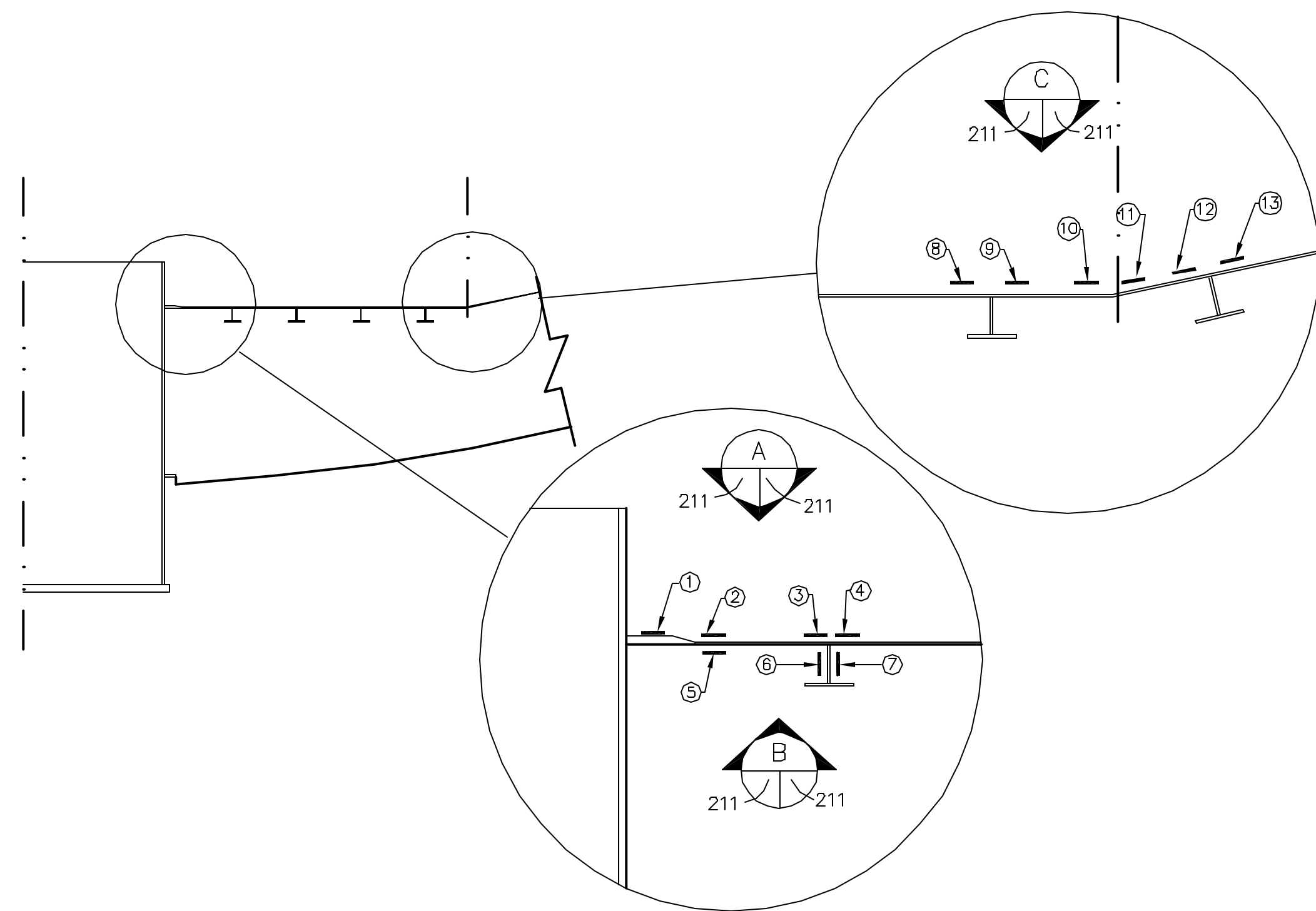
d.1
210
ZCD1010Ai



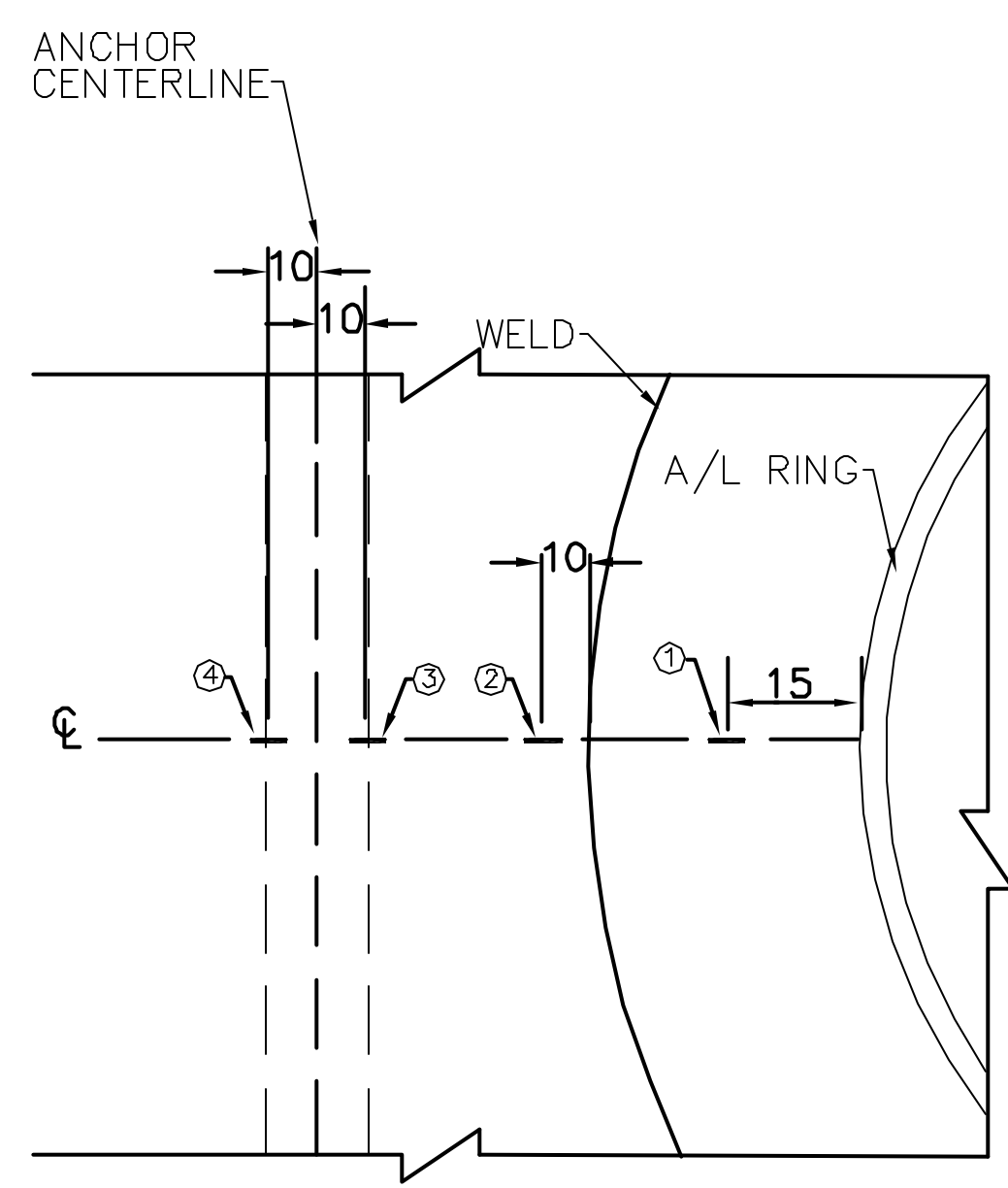
NOTE: CENTER LSA GAUGES ON ANCHOR WEB ORIENTED IN RADIAL DIRECTION (HORIZONTAL)

INSTRUMENTATION ID #		
Detail #	d.1	d.2
Azimuth	310	340
Elevation	4800	4800
Liner #	3-11D	3-11E
Instr. #		
①	LSI-C-K5-02	LSI-C-A5-02
②	LSI-C-K5-03	LSI-C-A5-03
③	LSI-C-K5-04	LSI-C-A5-04
④	LSI-C-K5-05	LSI-C-A5-05
⑤	LSO-C-K5-01	LSO-C-A5-01
⑥	LSA-R-K5-01	LSA-R-A5-01
⑦	LSA-R-K5-02	LSA-R-A5-02
⑧	LSI-C-K5-06	LSI-C-A5-06
⑨	LSI-C-K5-07	LSI-C-A5-07
⑩	LSI-C-K5-08	LSI-C-A5-08
⑪	LSI-C-K5-09	LSI-C-A5-09
⑫	LSI-C-K5-10	LSI-C-A5-10
⑬	LSI-C-K5-11	LSI-C-A5-11
⑭	LSO-C-K5-02	LSO-C-A5-02
⑮	LSO-C-K5-03	LSO-C-A5-03
⑯	LSA-R-K5-03	LSA-R-A5-03
⑰	LSA-R-K5-04	LSA-R-A5-04
⑱	LSA-R-K5-05	LSA-R-A5-05
⑲	LSA-R-K5-06	LSA-R-A5-06
⑳	LSI-C-K5-15	LSI-C-A5-15

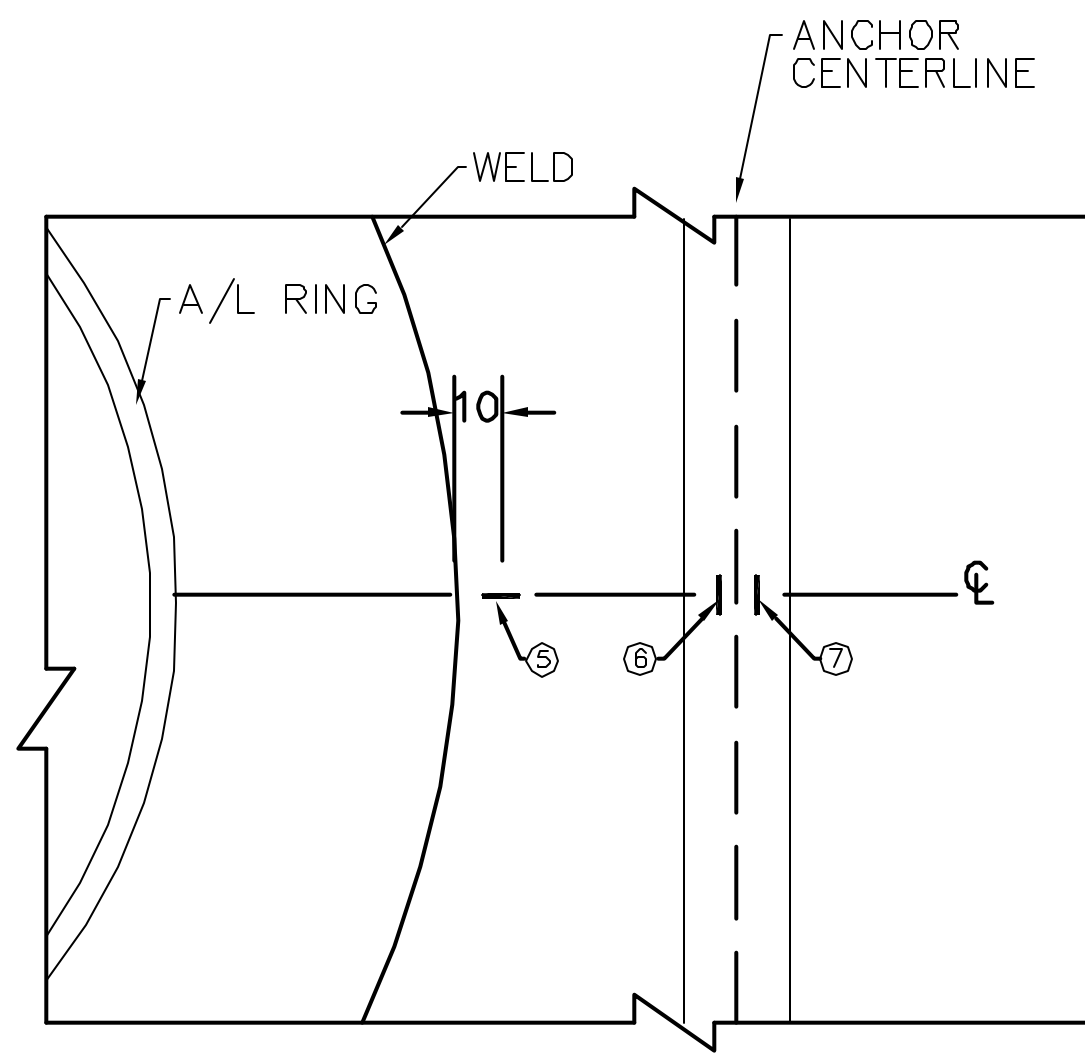
REVISION					
NO.	DATE	DRAWN BY	CHECKED BY	APPROVED BY	NOTES
0	Feb. 4, 1998	T. Martinez			
1	July 20, 1999	J. Tenorio			Moved Gages
NUPEC/NRC PCCV STRUCTURAL BEHAVIOR TEST MODEL					
DRAWING NO.		INSTRUMENTED LINER DETAILS			SCALE
D-SN-P-210		DETAIL d			1/1
SANDIA NATIONAL LABORATORIES FACILITIES ENGINEERING					
ALBUQUERQUE, NEW MEXICO;		LIVERMORE, CALIFORNIA;		TONOPAH, NEVADA	



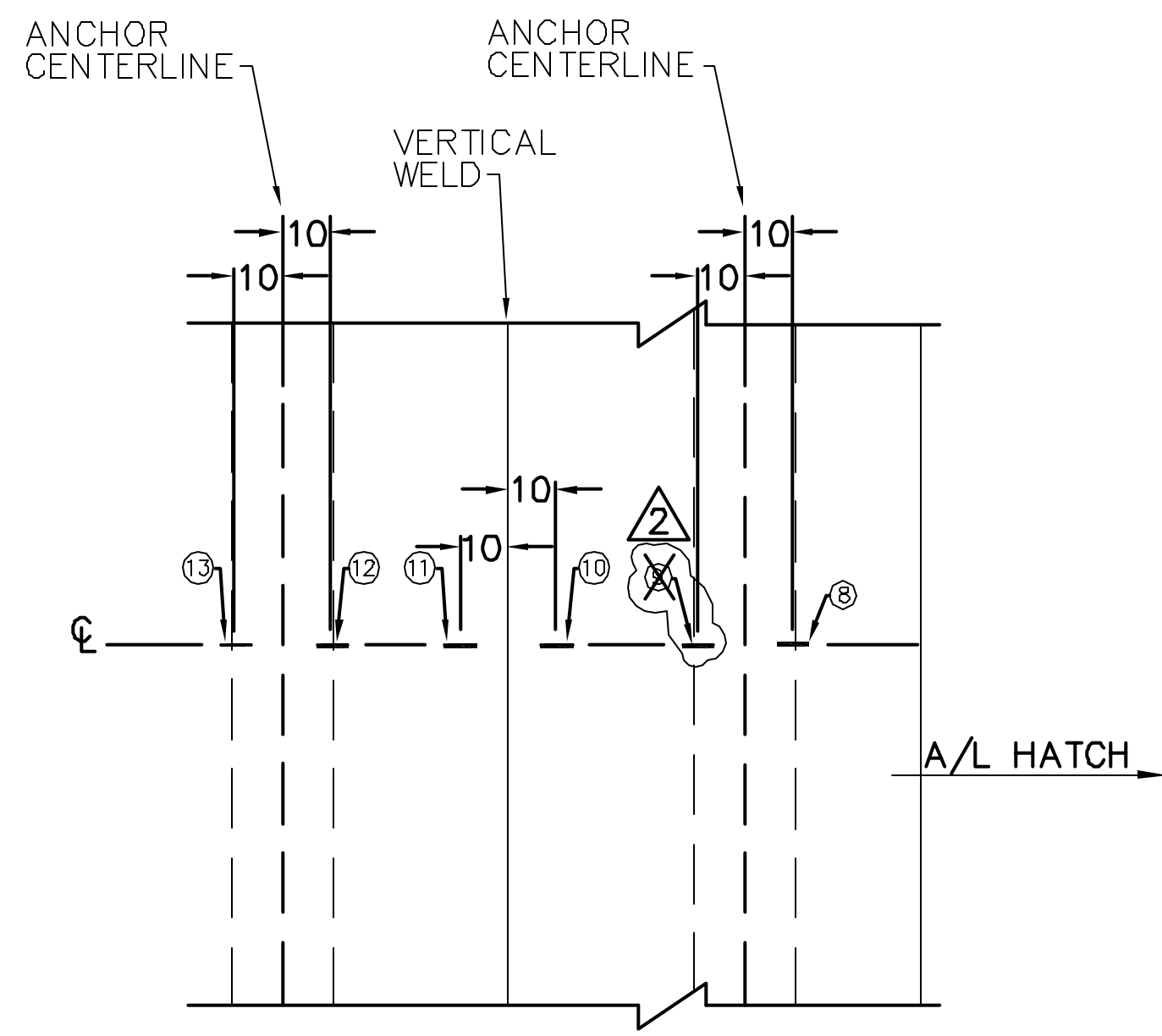
HORIZONTAL PLAN VIEW OF LINER AT A/L



INSIDE VIEW



OUTSIDE VIEW

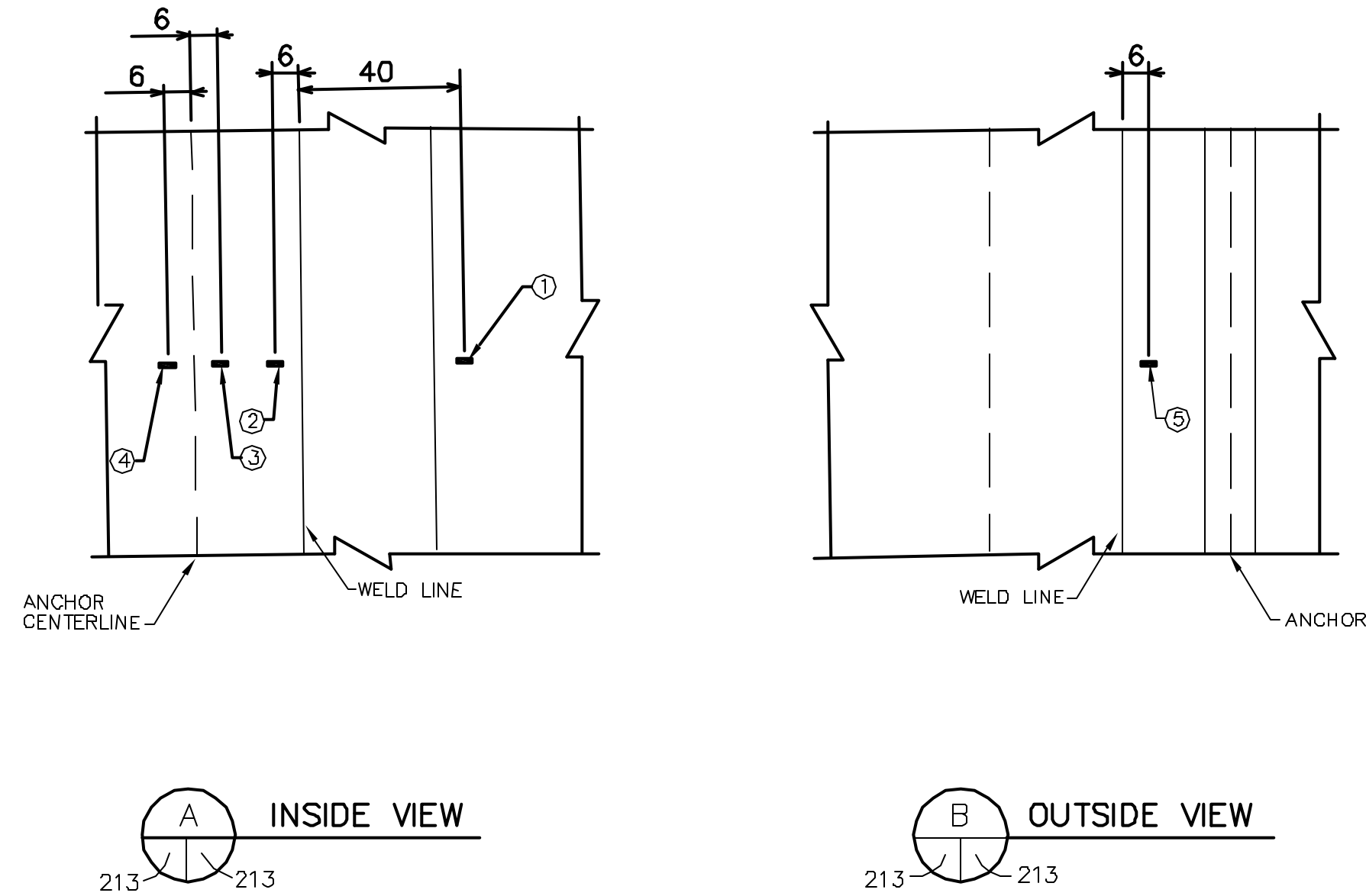
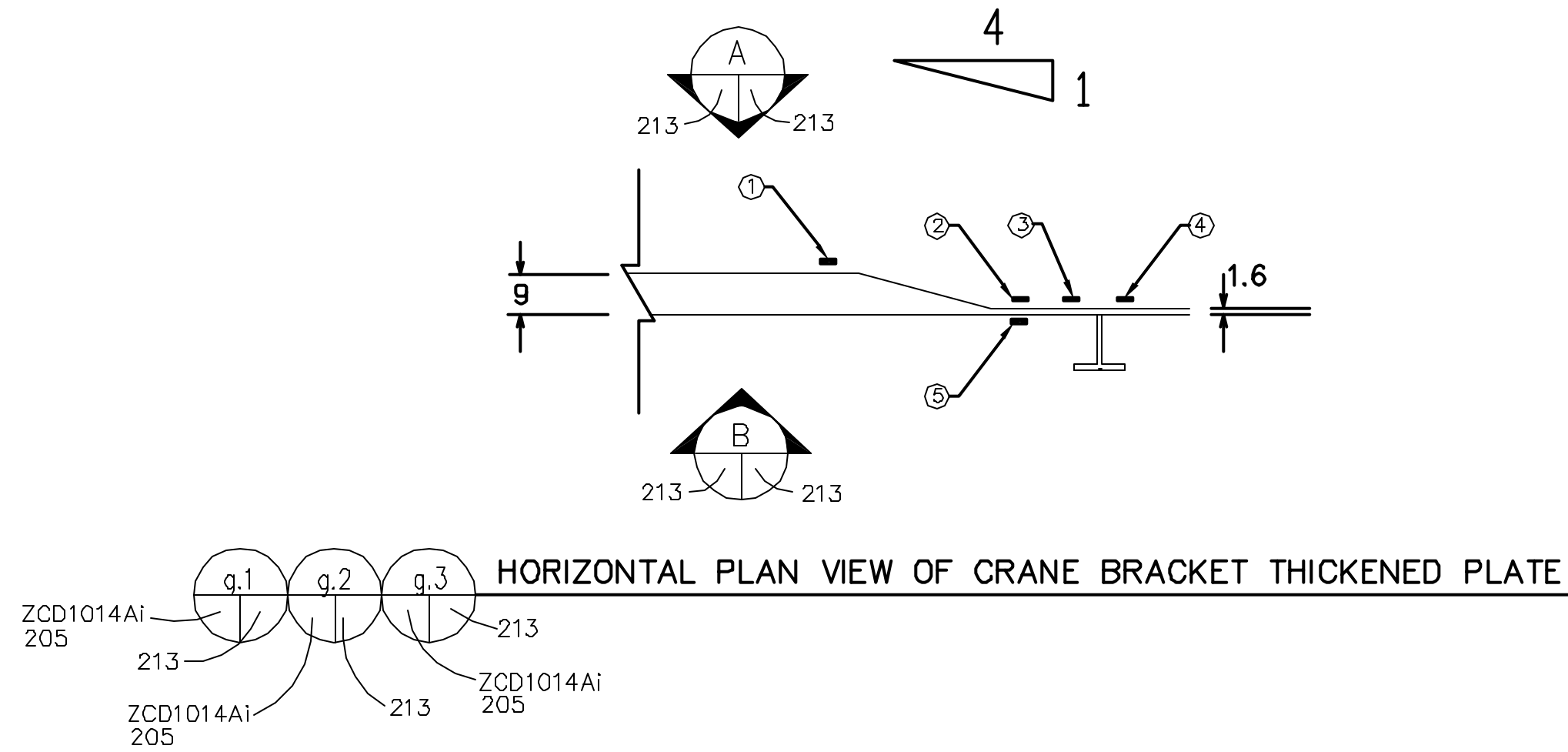


INSIDE VIEW

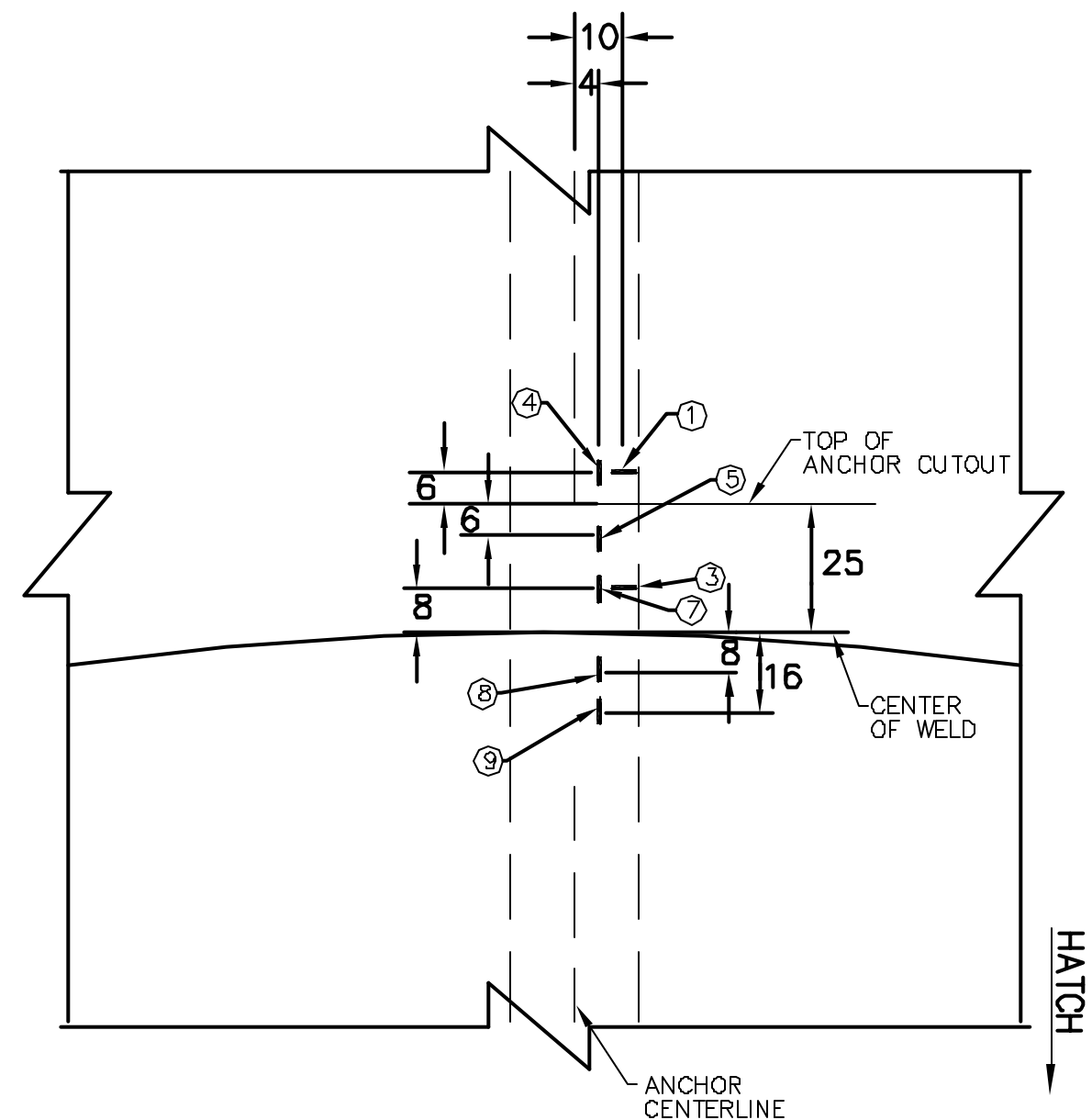
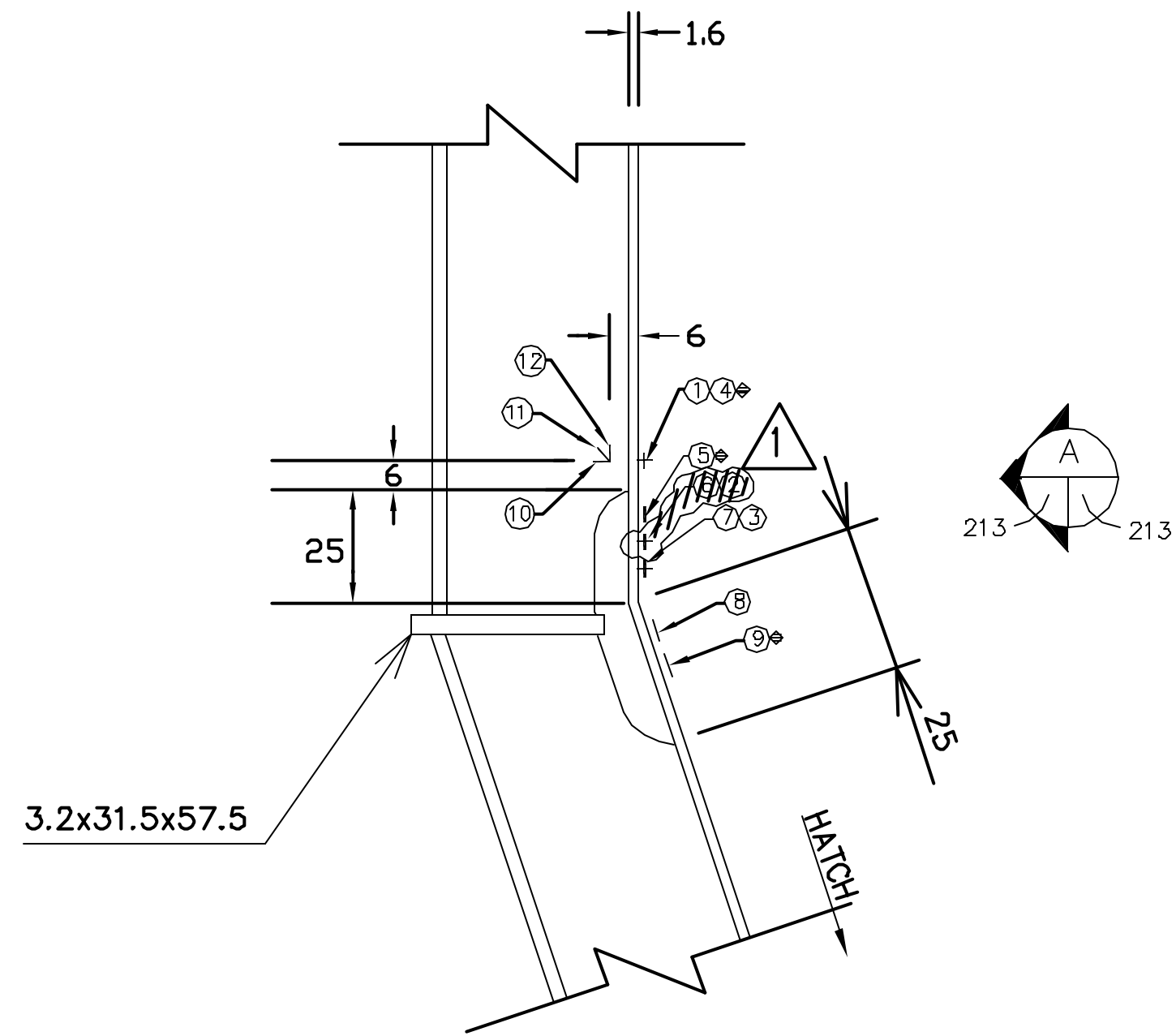
INSTRUMENTATION ID #		
Detail #	e.1	e.2
Azimuth	58	70
Elevation	4525	4525
Liner #	2-2A	2-2A
Instr. #		
①	LSI-C-C5-02	LSI-C-C5-12
②	LSI-C-C5-03	LSI-C-C5-13
③	LSI-C-C5-04	LSI-C-C5-14
④	LSI-C-C5-05	LSI-C-C5-15
⑤	LSO-C-C5-01	LSO-C-C5-02
⑥	LSA-R-C5-01	LSA-R-C5-03
⑦	LSA-R-C5-02	LSA-R-C5-04
⑧	LSI-C-C5-06	LSI-C-C5-16
⑨	LSI-C-C5-07	LSI-C-C5-17
⑩	LSI-C-C5-08	LSI-C-C5-18
⑪	LSI-C-C5-09	LSI-C-C5-19
⑫	LSI-C-C5-10	LSI-C-C5-20
⑬	LSI-C-C5-11	LSI-C-C5-21

NOTE: CENTER LSA GAUGES ON ANCHOR WEB ORIENTED IN RADIAL DIRECTION. (HORIZONTAL)

REVISION					
NO.	DATE	DRAWN BY	CHECKED BY	APPROVED BY	NOTES
0	Feb. 4, 1988	T. Martinez			
1	July 20, 1999	J. Tenorio			Removed Gages
2	Jan. 31, 2001	J. Tenorio			Addtl Gages Removed
NUPEC/NRC PCCV STRUCTURAL BEHAVIOR TEST MODEL					
DRAWING NO.		INSTRUMENTED LINER DETAILS			SCALE
D-SN-P-211		DETAIL e			1/1
SANDIA NATIONAL LABORATORIES FACILITIES ENGINEERING					
ALBUQUERQUE, NEW MEXICO:		LIVERMORE, CALIFORNIA:		TONOPAH, NEVADA	

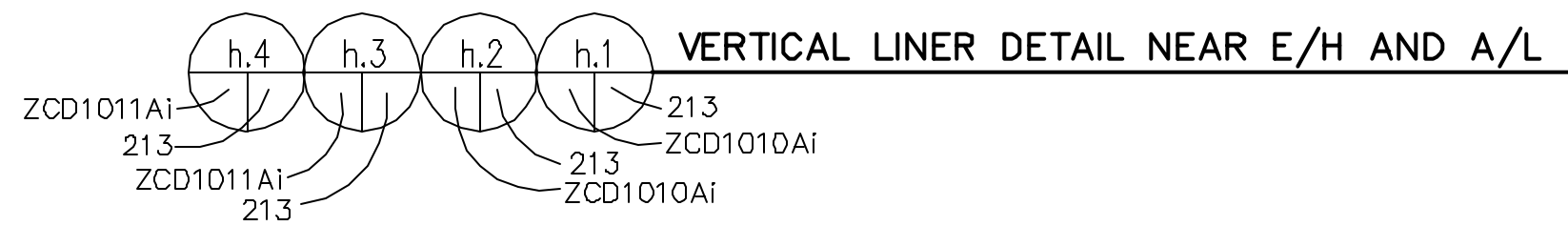


INSTRUMENTATION ID #			
Detail #	g.1	g.2	g.3
Azimuth	200	220	225
Elevation	9600	9600	9600
Liner #	5-9A	5-9E	5-9E
Instr. #			
①	LSI-C-G8-01	LSI-C-H8-01	LSI-C-H8-05
②	LSI-C-G8-02	LSI-C-H8-02	LSI-C-H8-06
③	LSI-C-G8-03	LSI-C-H8-03	LSI-C-H8-07
④	LSI-C-G8-04	LSI-C-H8-04	LSI-C-H8-08
⑤	LSO-C-G8-01	LSO-C-H8-01	LSO-C-H8-02

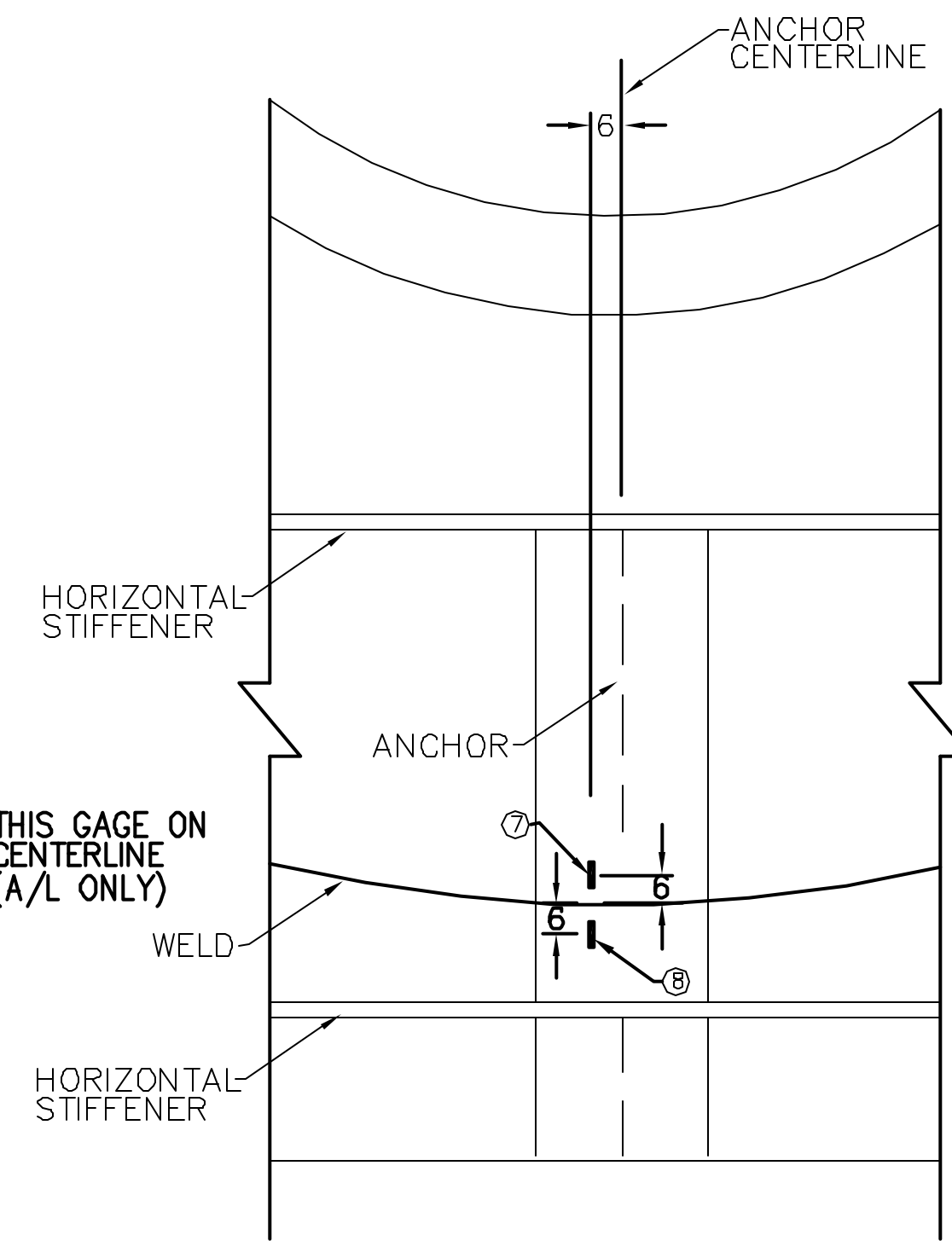
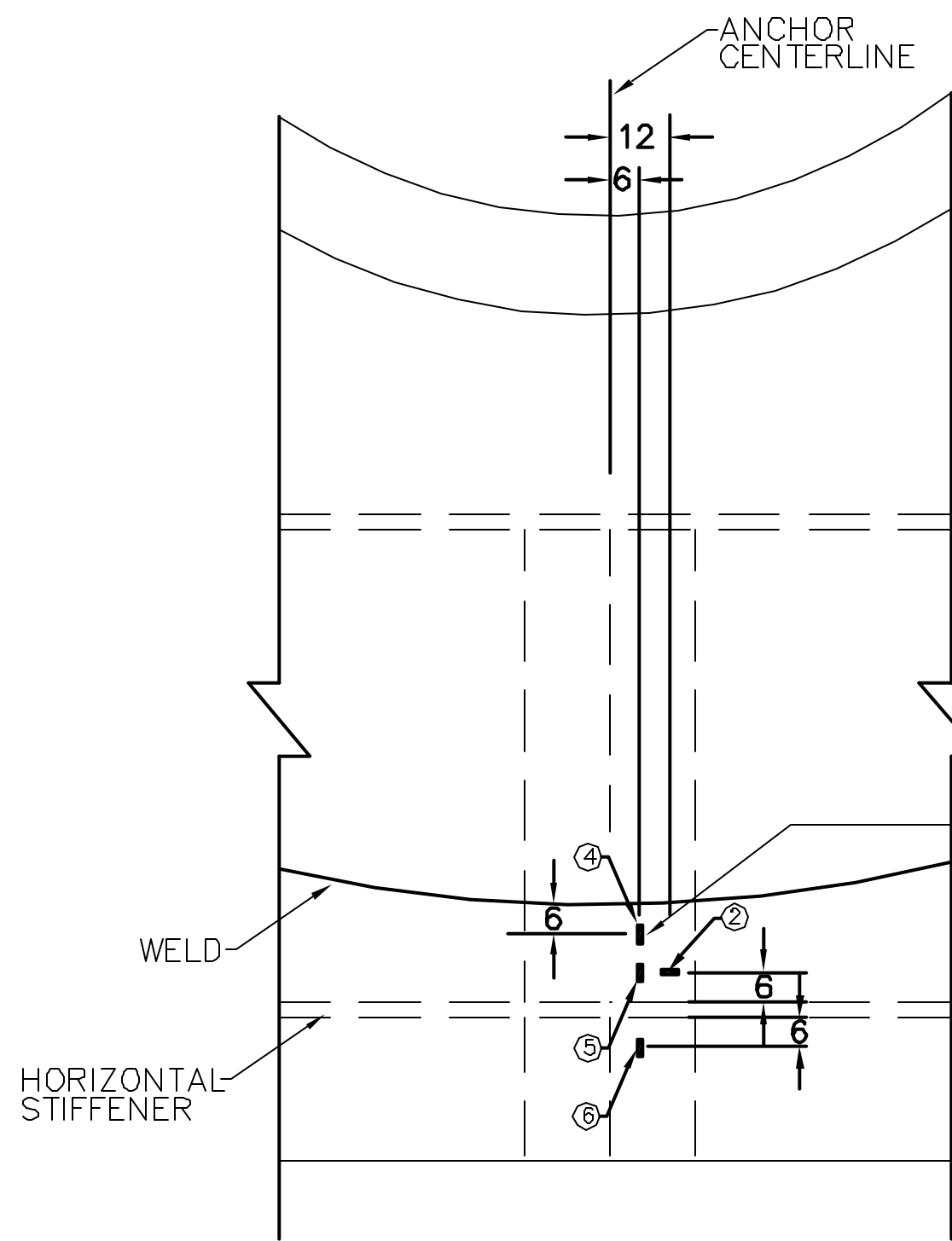
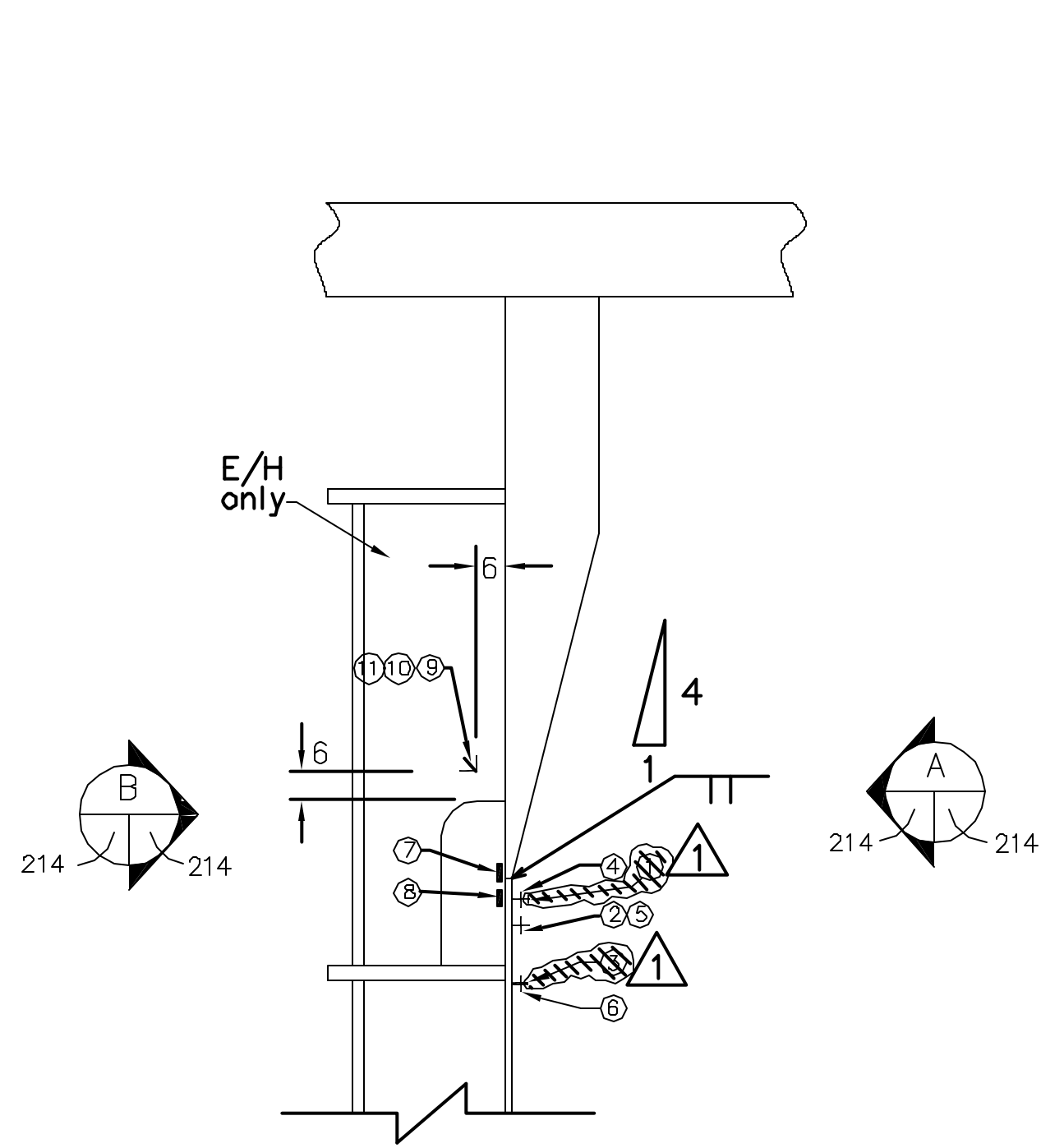


INSTRUMENTATION ID #				
Detail #	h.1	h.2	h.3	h.4
Azimuth	324	324	62	62
Elevation	2446	6904	3575	5475
Liner #	2-11D/2-11E	3-11B/3-11A	2-2B/2-2C	3-3D/3-3C
Instr. #				
①	LSI-C-L4-02	LSI-C-L6-02	LSI-C-C4-01	LSI-C-C6-01
②	LSI-C-L4-03	LSI-C-L6-03	LSI-C-C4-02	LSI-C-C6-02
③	LSI-C-L4-04	LSI-C-L6-04	LSI-C-C4-03	LSI-C-C6-03
④	LSI-M-L4-02	LSI-M-L6-02	LSI-M-C4-01	LSI-M-C6-01
⑤	LSI-M-L4-03	LSI-M-L6-03	LSI-M-C4-02	LSI-M-C6-02
⑥	LSI-M-L4-04	LSI-M-L6-04	LSI-M-C4-03	LSI-M-C6-03
⑦	LSI-M-L4-05	LSI-M-L6-05	LSI-M-C4-04	LSI-M-C6-04
⑧	LSI-M-L4-06	LSI-M-L6-06	LSI-M-C4-05	LSI-M-C6-05
⑨	LSI-M-L4-07	LSI-M-L6-07	LSI-M-C4-06	LSI-M-C6-06
⑩	LRA-R-L4-1r	LRA-R-L6-1r	LRA-R-C4-1r	LRA-R-C6-1r
⑪	LRA-R-L4-1d	LRA-R-L6-1d	LRA-R-C4-1d	LRA-R-C6-1d
⑫	LRA-R-L4-1m	LRA-R-L6-1m	LRA-R-C4-1m	LRA-R-C6-1m

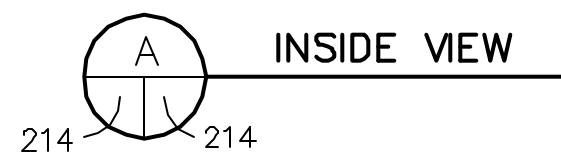
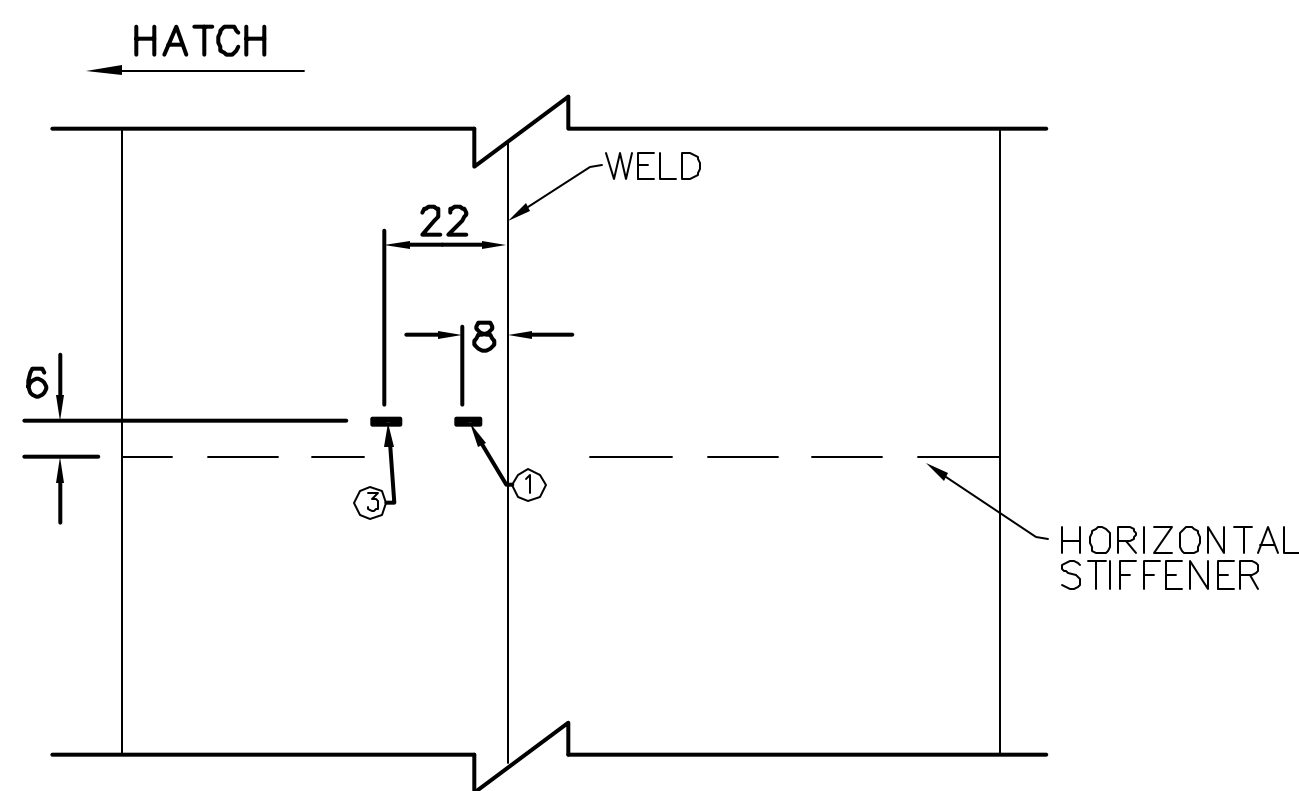
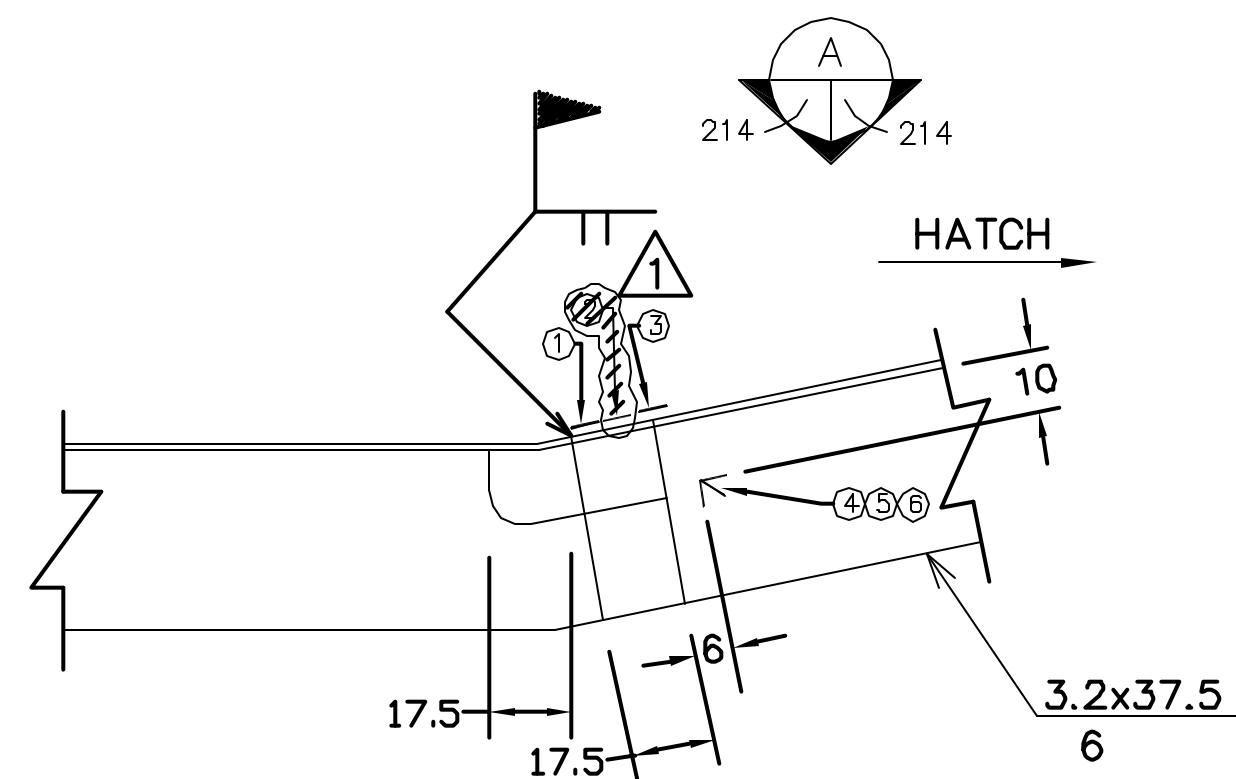
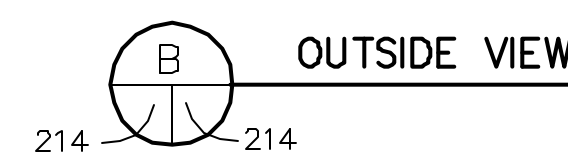
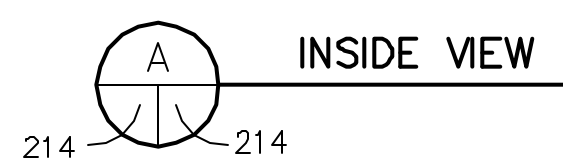
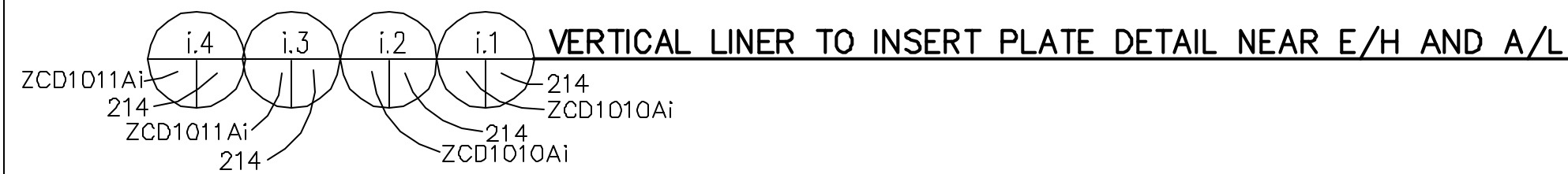
① = BELOW E/H ONLY



REVISION					
NO.	DATE	DRAWN BY	CHECKED BY	APPROVED BY	NOTES
0	Feb. 4, 1998	T. Martinez			
1	July 20, 1999	J. Tenorio			Gages Removed
NUPEC/NRC PCCV STRUCTURAL BEHAVIOR TEST MODEL					
DRAWING NO.		INSTRUMENTED LINER DETAILS			SCALE
D-SN-P-213		DETAIL g & h			1/1
SANDIA NATIONAL LABORATORIES FACILITIES ENGINEERING					
ALBUQUERQUE, NEW MEXICO; LIVERMORE, CALIFORNIA; TONOPAH, NEVADA					

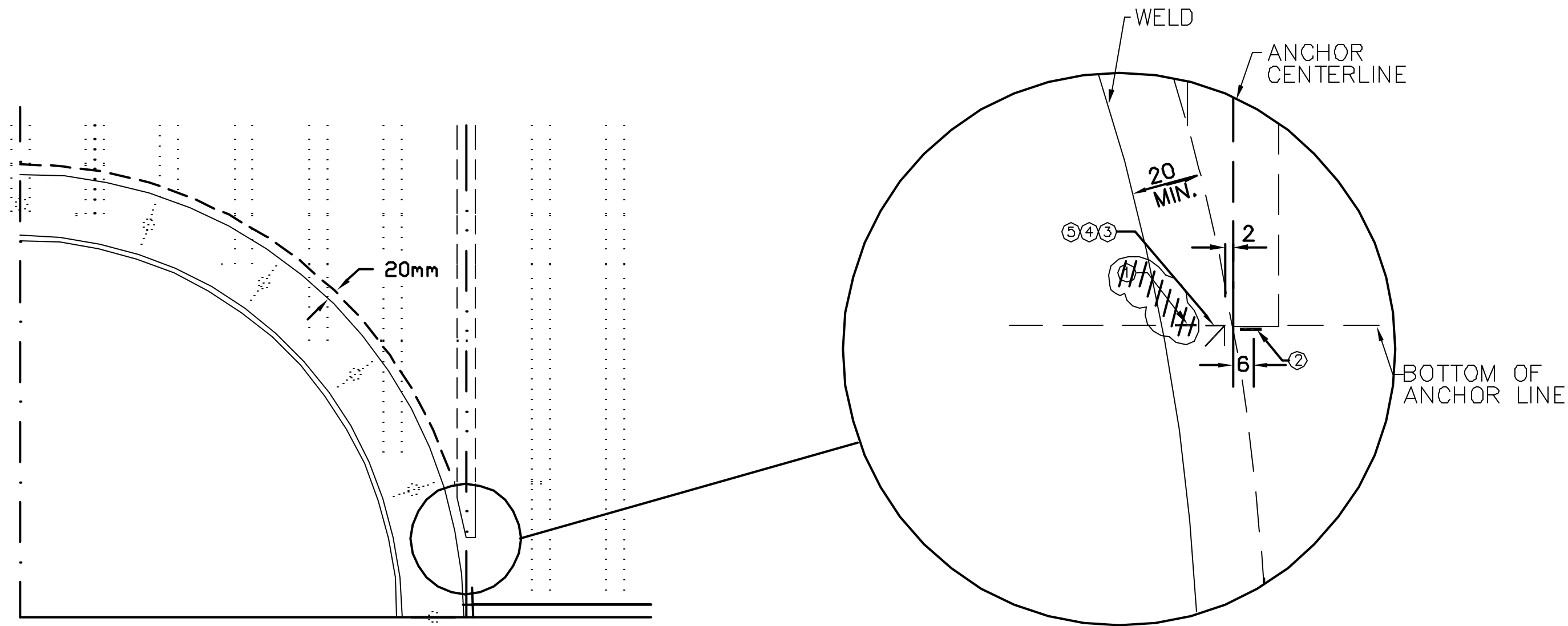


INSTRUMENTATION ID #				
Detail #	i.1	i.2	i.3	i.4
Azimuth	324	324	62	62
Elevation	3782	5568	4153	4897
Liner #	2-11C	3-11C	2-2A	3-3D
Instr. #				
①	LSI-C-L5-02	LSI-C-L5-05	LSI-C-C5-22	LSI-C-C5-25
②	LSI-C-L5-03	LSI-C-L5-06	LSI-C-C5-23	LSI-C-C5-26
③	LSI-C-L5-04	LSI-C-L5-07	LSI-C-C5-24	LSI-C-C5-27
④	LSI-M-L5-02	LSI-M-L5-05	LSI-M-C5-02	LSI-M-C5-05
⑤	LSI-M-L5-03	LSI-M-L5-06	LSI-M-C5-03	LSI-M-C5-06
⑥	LSI-M-L5-04	LSI-M-L5-07	LSI-M-C5-04	LSI-M-C5-07
⑦	LSO-M-L5-01	LSO-M-L5-03	LSO-M-C5-01	LSO-M-C5-03
⑧	LSO-M-L5-02	LSO-M-L5-04	LSO-M-C5-02	LSO-M-C5-04
⑨	LRA-R-L5-1r	LRA-R-L5-2r	N/A	N/A
⑩	LRA-R-L5-1d	LRA-R-L5-2d	N/A	N/A
⑪	LRA-R-L5-1m	LRA-R-L5-2m	N/A	N/A

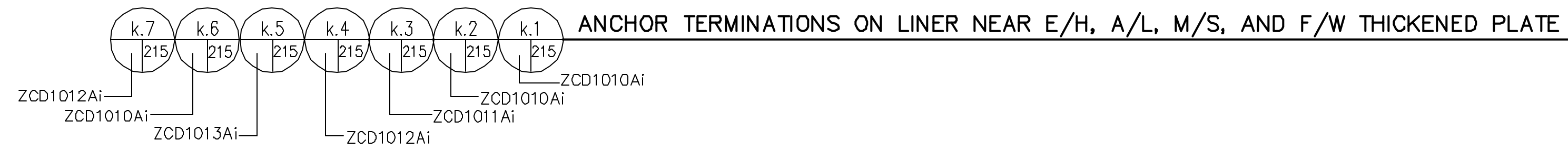


INSTRUMENTATION ID #		
Detail #	j.1	j.2
Azimuth	305	340
Elevation	4700	4700
Liner #	2-10A	2-12A
Instr. #		
①	LSI-C-K5-12	LSI-C-A5-12
②	LSI-C-K5-13	LSI-C-A5-13
③	LSI-C-K5-14	LSI-C-A5-14
④	LRS-R-K5-1r	LRS-R-A5-1r
⑤	LRS-R-K5-1d	LRS-R-A5-1d
⑥	LRS-R-K5-1h	LRS-R-A5-1h

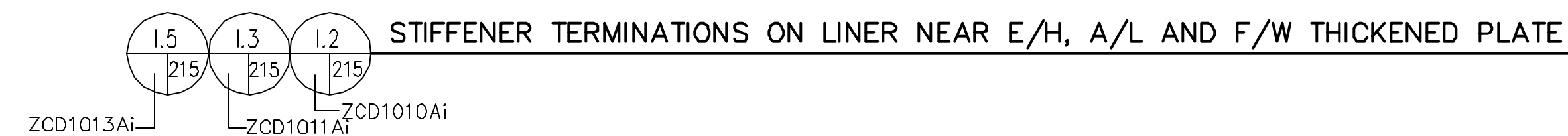
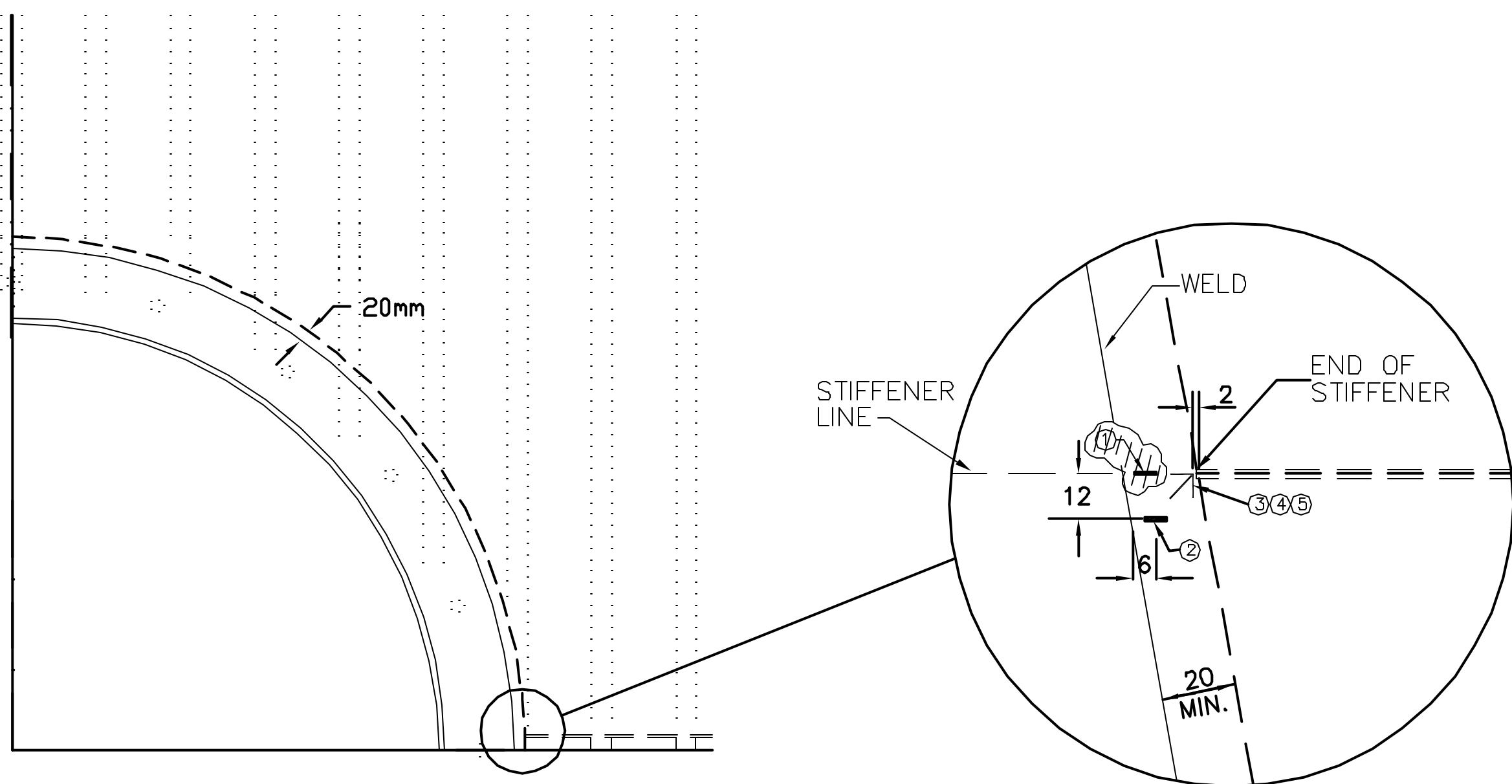
REVISION					
NO.	DATE	DRAWN BY	CHECKED BY	APPROVED BY	NOTES
0	Feb. 4, 1998	T. Martinez			
1	July 20, 1999	J. Tenorio			Removed Gages
NUPEC/NRC PCCV STRUCTURAL BEHAVIOR TEST MODEL					
DRAWING NO.		INSTRUMENTED LINER DETAILS			SCALE
D-SN-P-214		DETAIL i & j			1/1
SANDIA NATIONAL LABORATORIES FACILITIES ENGINEERING					
ALBUQUERQUE, NEW MEXICO;		LIVERMORE, CALIFORNIA;		TONOPAH, NEVADA	



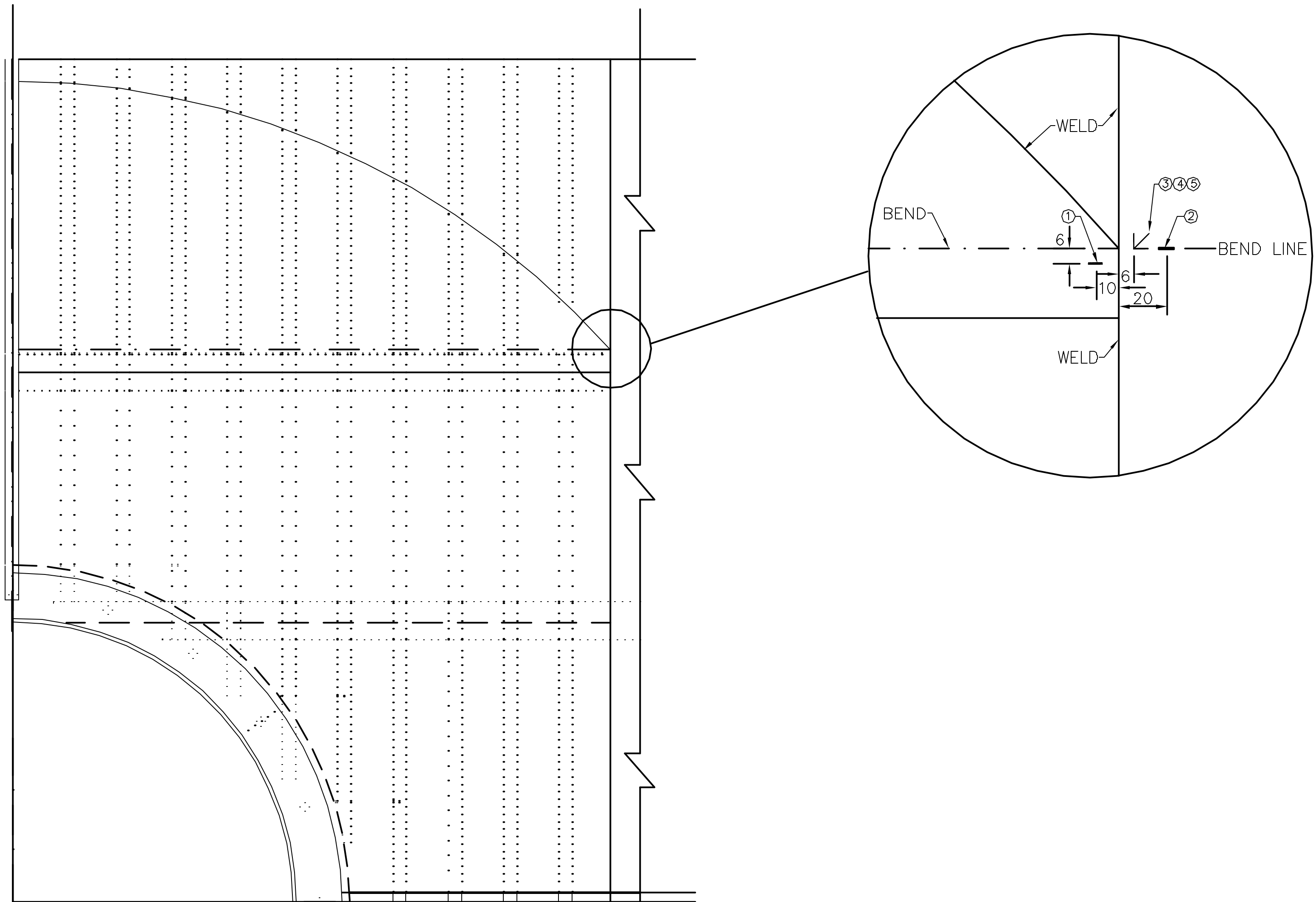
INSTRUMENTATION ID #						
Detail #	k.1	k.2	k.3	k.4	k.5	k.6
Azimuth	314	334	58	162	164	314
Elevation	4550	4800	4700	5200	2600	4800
Liner #	2-11A	3-11E	2-2A	3-7C	2-6C	3-11D
Instr. #	1	2	3	4	5	6
①	LSI-C-L5-08	LSI-C-L5-10	LSI-C-C5-28	LSI-C-F5-06	LSI-C-F4-06	LSI-C-L5-16
②	LSI-C-L5-09	LSI-C-L5-11	LSI-C-C5-29	LSI-C-F5-07	LSI-C-F4-06	LSI-C-L5-23
③	LRI-M-L5-1h	LRI-M-L5-2h	LRI-M-C5-1h	LRI-M-F5-1h	LRI-M-F4-1h	LRI-M-L5-5h
④	LRI-M-L5-1d	LRI-M-L5-2d	LRI-M-C5-1d	LRI-M-F5-1d	LRI-M-F4-1d	LRI-M-L5-5d
⑤	LRI-M-L5-1m	LRI-M-L5-2m	LRI-M-C5-1m	LRI-M-F5-1m	LRI-M-F4-1m	LRI-M-L5-5m



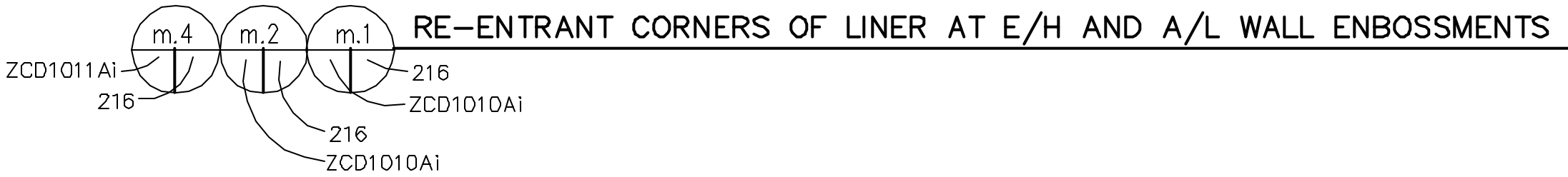
INSTRUMENTATION ID #				
Detail #	I.1	I.2	I.3	I.4
Azimuth	334	314	68	66
Elevation	4700	4700	4600	4600
Liner #	3-11D	3-11E	2-2A	2-2A
Instr. #	1	2	3	4
①	LSI-C-L5-12	LSI-C-L5-14	LSI-C-C5-30	LSI-C-C5-32
②	LSI-C-L5-13	LSI-C-L5-15	LSI-C-C5-31	LSI-C-C5-33
③	LRI-M-L5-3h	LRI-M-L5-4h	LRI-M-C5-2h	LRI-M-C5-3h
④	LRI-M-L5-3d	LRI-M-L5-4d	LRI-M-C5-2d	LRI-M-C5-3d
⑤	LRI-M-L5-3m	LRI-M-L5-4m	LRI-M-C5-2m	LRI-M-C5-3m



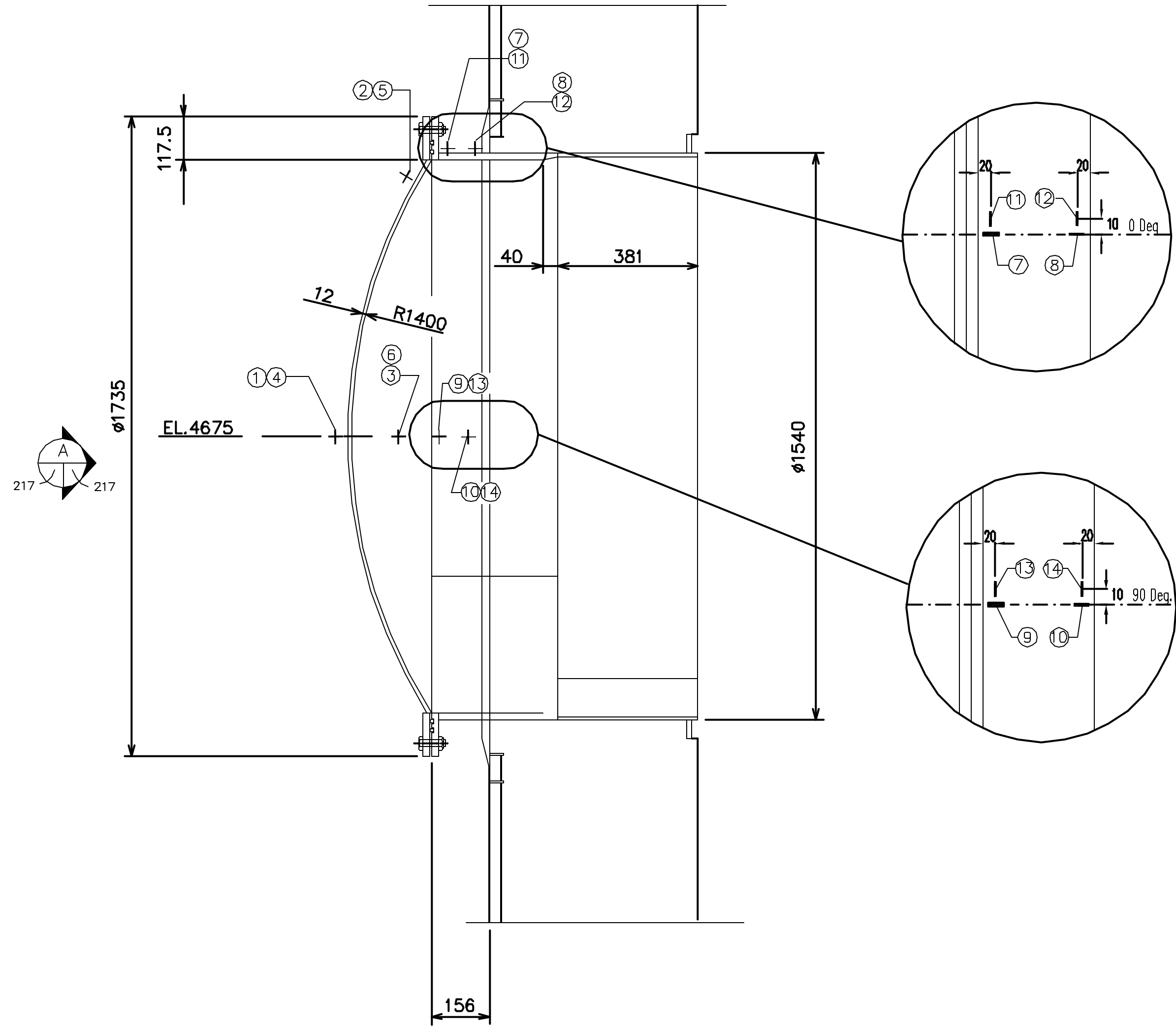
REVISION					
NO.	DATE	DRAWN BY	CHECKED BY	APPROVED BY	NOTES
0	Feb. 4, 1988	T. Martinez			
1	July 20, 1988	J. Tenorio			Modified Gages
NUPEC/NRC PCCV STRUCTURAL BEHAVIOR TEST MODEL					
DRAWING NO.		INSTRUMENTED LINER DETAILS			SCALE
D-SN-P-215		DETAIL k & l			1/1
SANDIA NATIONAL LABORATORIES FACILITIES ENGINEERING					
ALBUQUERQUE, NEW MEXICO;		LIVERMORE, CALIFORNIA;		TONOPAH, NEVADA	



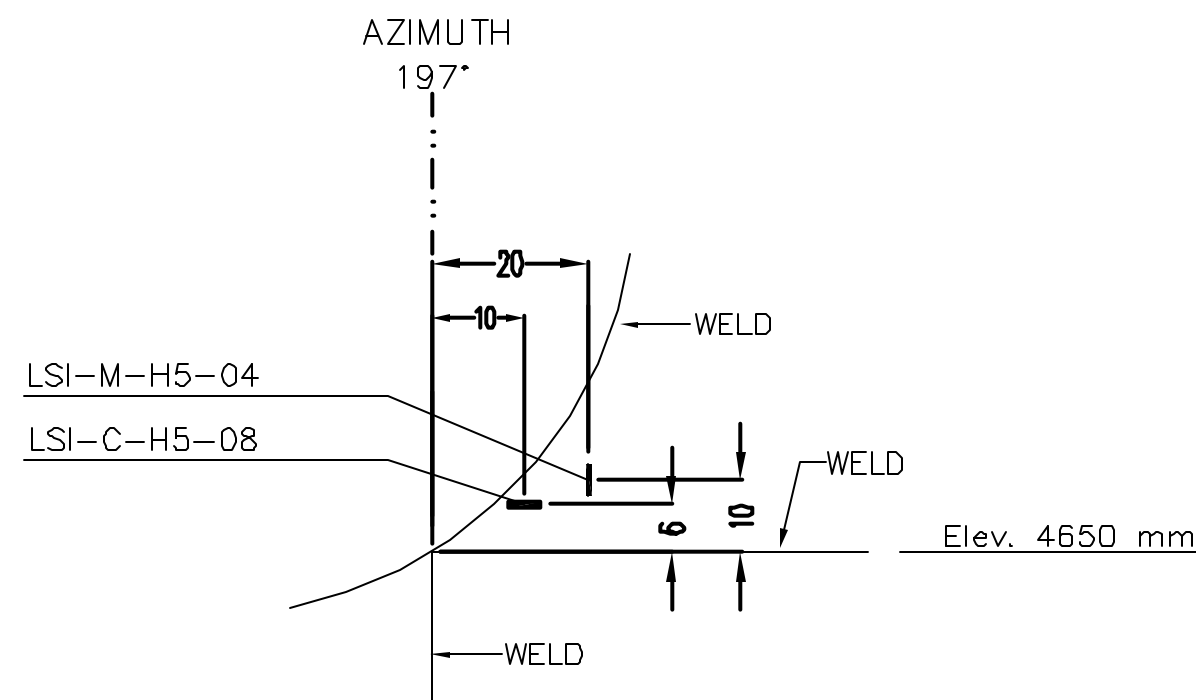
INSTRUMENTATION ID #				
Detail #	m.1	m.2	m.3	m.4
Azimuth	310	310	310	310
Elevation	3200	3150	3175	3175
Liner #	2-11D/2-12B	3-11B/3-12B	2-2B/2-1A	3-3D/3-2C
Instr. #				
①	LSI-C-A4-D1	LSI-C-A6-D1	LSI-C-C5-34	LSI-C-C5-36
②	LSI-C-A4-D2	LSI-C-A6-D2	LSI-C-C5-35	LSI-C-C5-37
③	LRI-M-A4-1h	LRI-M-A6-1h	LRI-M-C5-4h	LRI-M-C5-5h
④	LRI-M-A4-1d	LRI-M-A6-1d	LRI-M-C5-4d	LRI-M-C5-5d
⑤	LRI-M-A4-1m	LRI-M-A6-1m	LRI-M-C5-4m	LRI-M-C5-5m



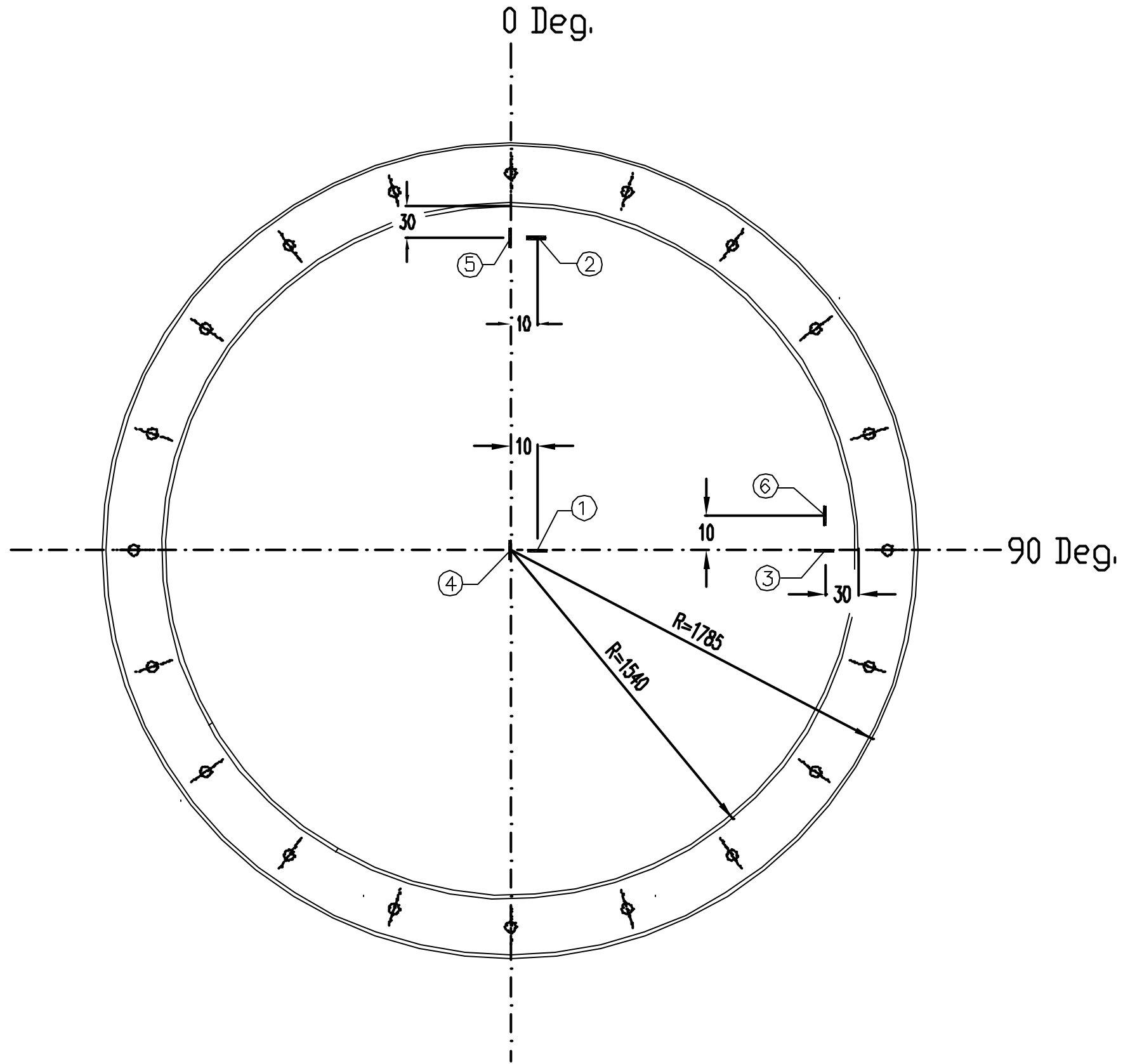
REVISION					
NO.	DATE	DRAWN BY	CHECKED BY	APPROVED BY	NOTES
0	Feb. 4, 1998	T. Martinez			
1	July 20, 1999	J. Tenorio			Removed Gages
NUPEC/NRC PCCV STRUCTURAL BEHAVIOR TEST MODEL					
DRAWING NO.		INSTRUMENTED LINER DETAILS			SCALE
D-SN-P-216		DETAIL m			1/1
SANDIA NATIONAL LABORATORIES FACILITIES ENGINEERING					
ALBUQUERQUE, NEW MEXICO;		LIVERMORE, CALIFORNIA;		TONOPAH, NEVADA	



E/H DETAIL
ZCD1010Ai-217




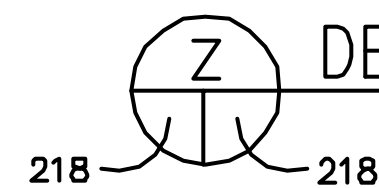
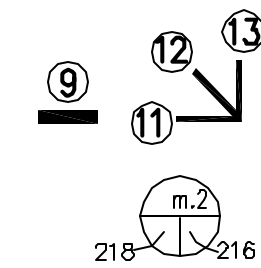
M/S CORNER WELD DETAIL (INSIDE VIEW)
217-217



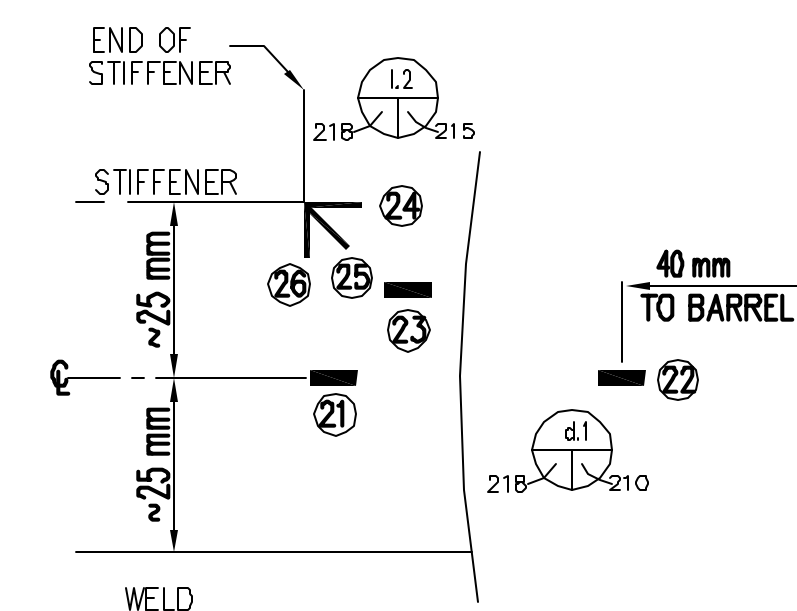
INSIDE VIEW
217-217

INSTRUMENTATION ID #				
Instr. #	Detail #	Azimuth	Elevation (mm)	Radial Dist.(mm)
①	LSI-C-L5-16	324	4675	4850
②	LSI-C-L5-17	324	5460	4930
③	LSI-C-L5-18	333	4675	4930
④	LSI-M-L5-08	324	4675	4850
⑤	LSI-M-L5-09	324	5460	4930
⑥	LSI-M-L5-10	333	4675	4930
⑦	LSI-M-L5-11	324	5460	4980
⑧	LSI-M-L5-12	324	5460	5030
⑨	LSI-M-L5-13	333	4675	4980
⑩	LSI-M-L5-14	333	4675	5030
⑪	LSI-C-L5-19	324	5460	4980
⑫	LSI-C-L5-20	324	5460	5030
⑬	LSI-C-L5-21	333	4675	4980
⑭	LSI-C-L5-22	333	4675	5030

REVISION					
NO.	DATE	DRAWN BY	CHECKED BY	APPROVED BY	NOTES
0	Feb 4, 1998	J. Tenorio			
1	July 20, 1998	J. Tenorio			Add Detail 0.1
NUPEC/NRC PCCV STRUCTURAL BEHAVIOR TEST MODEL					
DRAWING NO.		INSTRUMENTATION LINER DETAILS			SCALE
D-SN-P-217		DETAIL - n			1/6
SANDIA NATIONAL LABORATORIES FACILITIES ENGINEERING					
ALBUQUERQUE, NEW MEXICO; LIVERMORE, CALIFORNIA; TONOPAH, NEVADA					
					




INSTRUMENTATION GAGES									
Instr.	Labeling		Details		Instr.	Labeling		Details	
#	I.D.		Drawing #		#	I.D.		Drawing #	
	(Name)		D-SN-P-			(Name)		D-SN-P-	
(1)	LSI-C-K5-11	210/(d.1)	(46)	LSI-M-L5-12	217/(n.1)				
(2)	LSI-C-K5-10	210/(d.1)	(47)	LSI-C-L5-19	217/(n.1)				
(3)	LSI-C-K5-09	210/(d.1)	(48)	LSI-C-L5-20	217/(n.1)				
(4)	LSI-C-K5-08	210/(d.1)	(49)	LSI-M-L5-08	217/(n.1)				
(5)	LSI-C-K5-07	210/(d.1)	(50)	LSI-C-L5-16	217/(n.1)				
(6)	LSI-C-K5-06	210/(d.1)	(51)	LSI-C-L5-18	217/(n.1)				
(7)	LSI-C-K5-12	214/(j.1)	(52)	LSI-M-L5-10	217/(n.1)				
(8)	LSI-C-K5-14	214/(j.1)	(53)	LSI-M-L5-13	217/(n.1)				
(9)	LSI-C-A6-02	216/(m.2)	(54)	LSI-M-L5-14	217/(n.1)				
(10)	LSI-C-A6-01	216/(m.2)	(55)	LSI-C-L5-21	217/(n.1)				
(11)	LRI-M-A6-1h	216/(m.2)	(56)	LSI-C-L5-22	217/(n.1)				
(12)	LRI-M-A6-1d	216/(m.2)	(57)	LSI-M-L5-02	214/(i.1)				
(13)	LRI-M-A6-1m	216/(m.2)	(58)	LSI-M-L5-03	214/(i.1)				
(14)	LSI-C-A4-02	216/(m.1)	(59)	LSI-C-L5-03	214/(i.1)				
(15)	LSI-C-A4-01	216/(m.1)	(60)	LSI-M-L5-04	214/(i.1)				
(16)	LRI-M-A4-1h	216/(m.1)	(61)	LSI-M-L4-07	213/(h.1)				
(17)	LRI-M-A4-1d	216/(m.1)	(62)	LSI-M-L4-06	213/(h.1)				
(18)	LRI-M-A4-1m	216/(m.1)	(63)	LSI-M-L4-05	213/(h.1)				
(19)	LSI-C-K5-05	210/(d.1)	(64)	LSI-C-L4-04	213/(h.1)				
(20)	LSI-C-K5-04	210/(d.1)	(65)	LSI-M-L4-03	213/(h.1)				
(21)	LSI-C-K5-03	210/(d.1)	(66)	LSI-M-L4-02	213/(h.1)				
(22)	LSI-C-K5-02	210/(d.1)	(67)	LSI-C-L4-02	213/(h.1)				
(23)	LSI-C-L5-15	215/(l.2)	(68)	LSI-C-A5-11	210/(d.2)				
(24)	LRI-M-L5-4h	215/(l.2)	(69)	LSI-C-A5-10	210/(d.2)				
(25)	LRI-M-L5-4d	215/(l.2)	(70)	LSI-C-A5-09	210/(d.2)				
(26)	LRI-M-L5-4m	215/(l.2)	(71)	LSI-C-A5-08	210/(d.2)				
(27)	LSI-C-L5-23	215/(k.6)	(72)	LSI-C-A5-07	210/(d.2)				
(28)	LRI-M-L5-5h	215/(k.6)	(73)	LSI-C-A5-06	210/(d.2)				
(29)	LRI-M-L5-5d	215/(k.6)	(74)	LSI-C-A5-12	214/(j.2)				
(30)	LRI-M-L5-5m	215/(k.6)	(75)	LSI-C-A5-14	214/(j.2)				
(31)	LSI-C-L5-09	215/(k.1)	(76)	LSI-C-A5-05	210/(d.2)				
(32)	LRI-M-L5-1h	215/(k.1)	(77)	LSI-C-A5-04	210/(d.2)				
(33)	LRI-M-L5-1d	215/(k.1)	(78)	LSI-C-A5-03	210/(d.2)				
(34)	LRI-M-L5-1m	215/(k.1)	(79)	LSI-C-A5-02	210/(d.2)				
(35)	LSI-C-K5-15	210/(d.1)	(80)	LSI-C-L5-13	215/(l.1)				
(36)	LSI-M-L6-05	213/(h.2)	(81)	LRI-M-L5-3h	215/(l.1)				
(37)	LSI-C-L6-04	213/(h.2)	(82)	LRI-M-L5-3d	215/(l.1)				
(38)	LSI-M-L6-06	213/(h.2)	(83)	LRI-M-L5-3m	215/(l.1)				
(39)	LSI-M-L5-07	214/(i.2)	(84)	LSI-C-A5-15	210/(d.2)				
(40)	LSI-M-L5-06	214/(i.2)	(85)	LSI-C-L5-11	215/(k.2)				
(41)	LSI-C-L5-06	214/(i.2)	(86)	LRI-M-L5-2h	215/(k.2)				
(42)	LSI-M-L5-05	214/(i.2)	(87)	LRI-M-L5-2d	215/(k.2)				
(43)	LSI-M-L5-09	217/(n.1)	(88)	LRI-M-L5-2m	215/(k.2)				
(44)	LSI-C-L5-17	217/(n.1)							
(45)	LSI-M-L5-11	217/(n.1)							

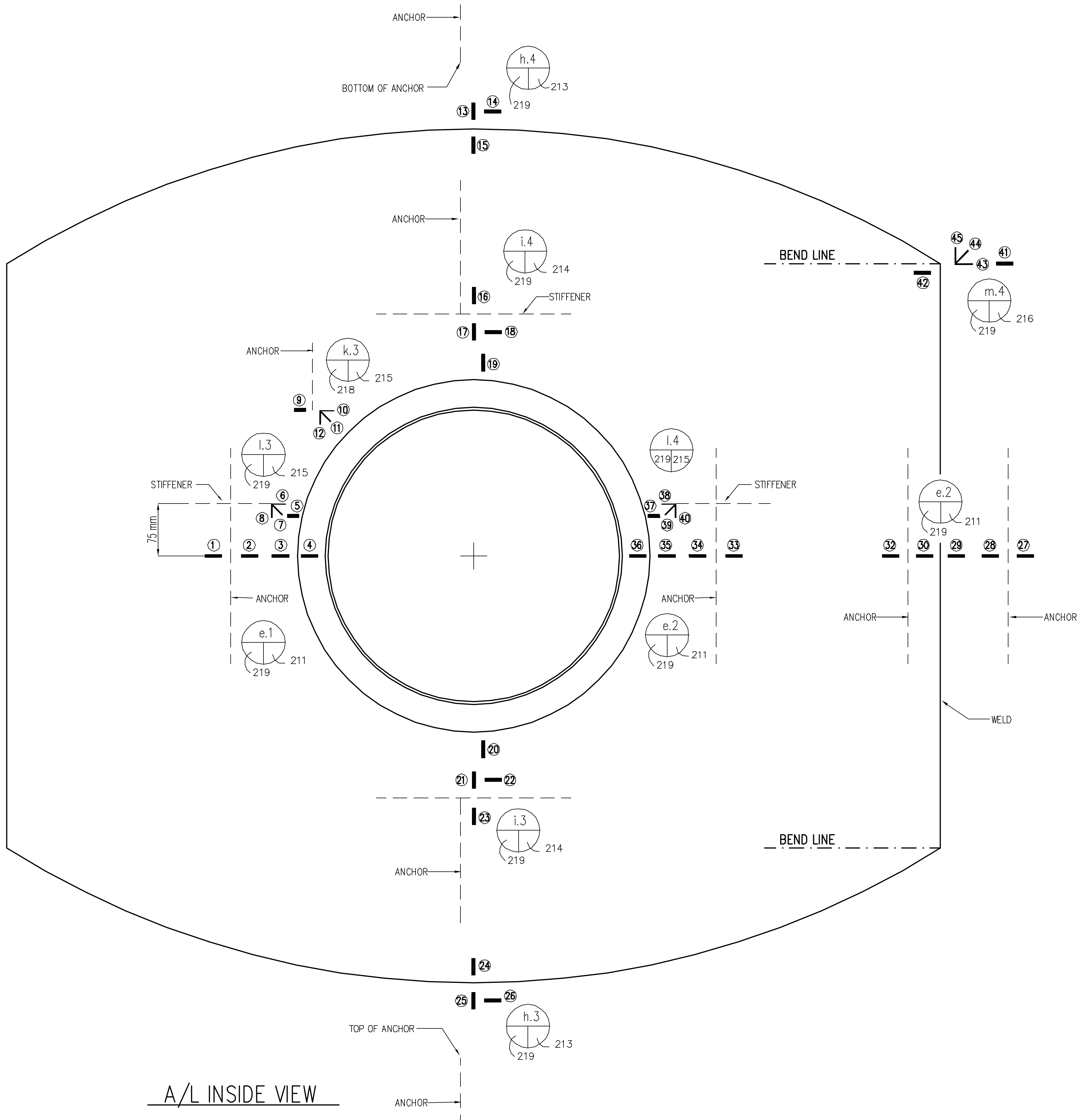
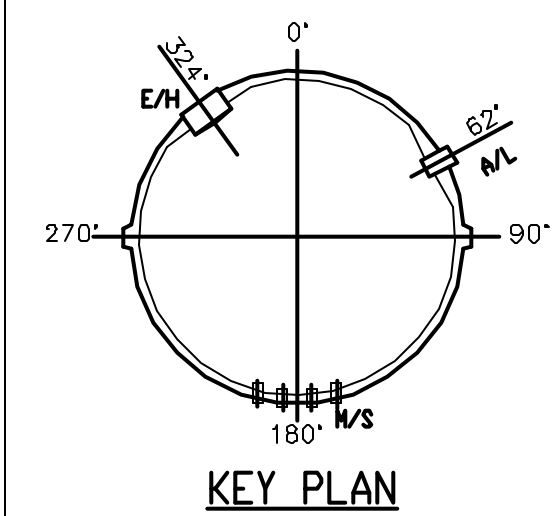


REVISION					
NO.	DATE	DRAWN BY	CHECKED BY	APPROVED BY	NOTES
0	July 20, 1999	J. Tenorio			


NUPEC/NRC PCCV STRUCTURAL BEHAVIOR TEST MODEL					
DRAWING NO. D-SN-P-218		INTERIOR LINER GAGE LAYOUT			SCALE NO SCALE
E/H					

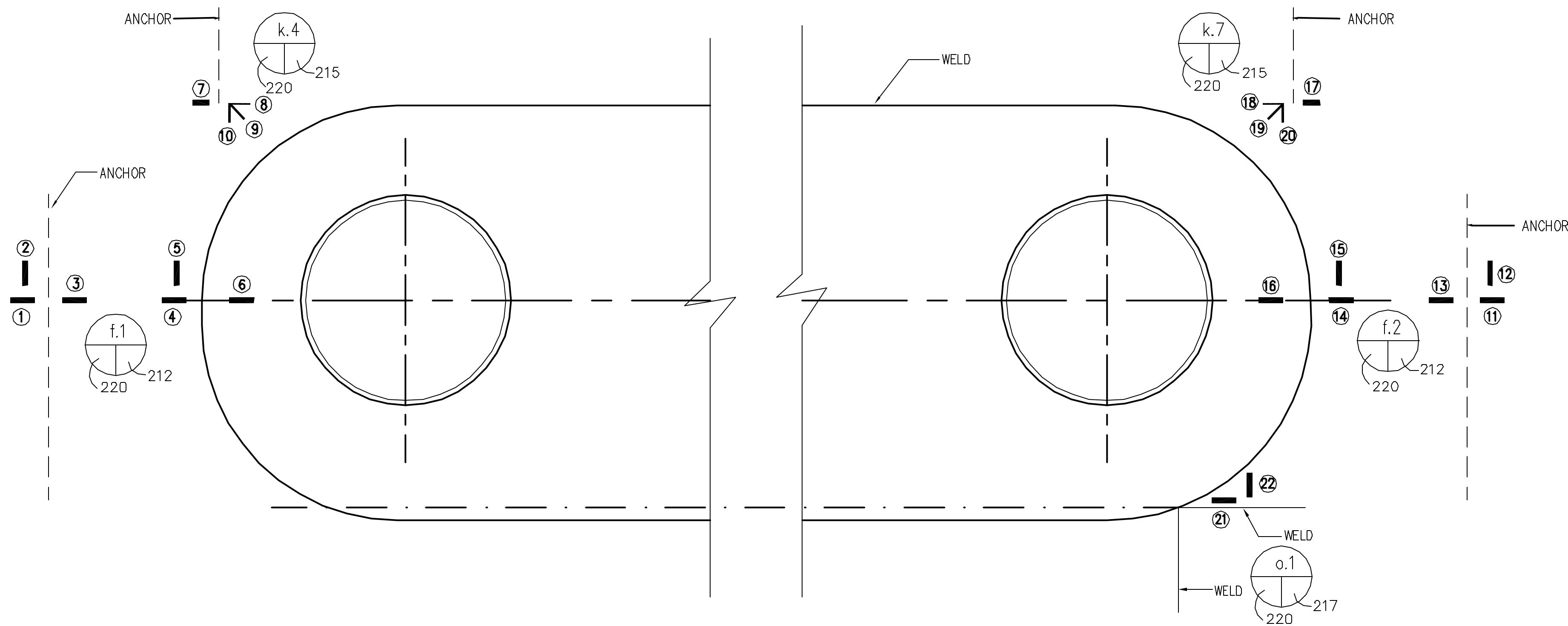
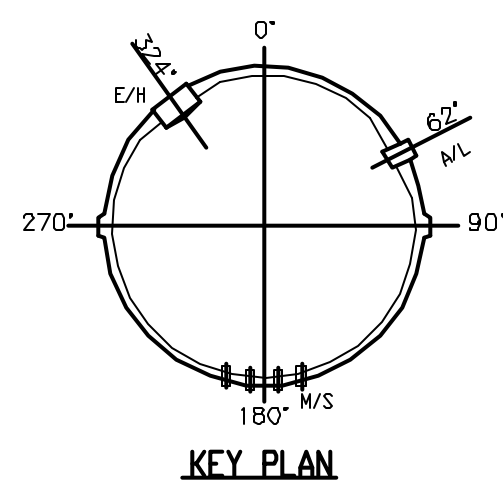
SANDIA NATIONAL LABORATORIES FACILITIES ENGINEERING					
ALBUQUERQUE, NEW MEXICO;		LIVERMORE, CALIFORNIA;		TONOPAH, NEVADA	



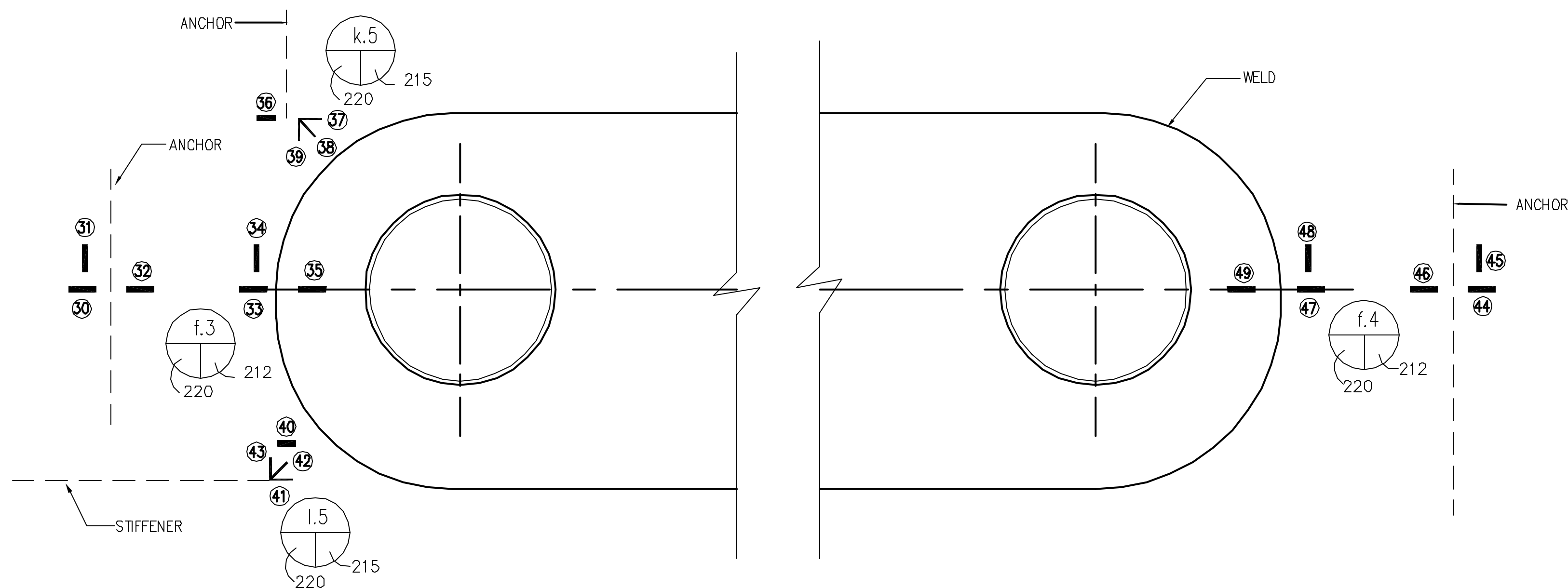


INSTRUMENTATION GAGES					
Instr. #	Labeling	Details	Instr. #	Labeling	Details
	I.D.	Drawing #		I.D.	Drawing #
	(Name)	D-SN-P-		(Name)	D-SN-P-
1	LSI-C-C5-05	211/(e.1)	28	LSI-C-C5-20	211/(e.2)
2	LSI-C-C5-04	211/(e.1)	29	LSI-C-C5-19	211/(e.2)
3	LSI-C-C5-03	211/(e.1)	30	LSI-C-C5-18	211/(e.2)
4	LSI-C-C5-02	211/(e.1)	31	LSI-C-C5-17	211/(e.2)
5	LSI-C-C5-31	215/(i.3)	32	LSI-C-C5-16	211/(e.2)
6	LRI-M-C5-2h	215/(i.3)	33	LSI-C-C5-15	211/(e.2)
7	LRI-M-C5-2d	215/(i.3)	34	LSI-C-C5-14	211/(e.2)
8	LRI-M-C5-2m	215/(i.3)	35	LSI-C-C5-13	211/(e.2)
9	LSI-C-C5-29	215/(k.3)	36	LSI-C-C5-12	211/(e.2)
10	LRI-M-C5-1h	215/(k.3)	37	LSI-C-C5-33	215/(i.4)
11	LRI-M-C5-1d	215/(k.3)	38	LRI-M-C5-3h	215/(i.4)
12	LRI-M-C5-1m	215/(k.3)	39	LRI-M-C5-3d	215/(i.4)
13	LSI-M-C6-04	213/(h.4)	40	LRI-M-C5-3m	215/(i.4)
14	LSI-C-C6-03	213/(h.4)	41	LSI-C-C5-37	216/(m.4)
15	LSI-M-C6-05	213/(h.4)	42	LSI-C-C5-36	216/(m.4)
16	LSI-M-C5-07	214/(i.4)	43	LRI-M-C5-5h	216/(m.4)
17	LSI-M-C5-06	214/(i.4)	44	LRI-M-C5-5d	216/(m.4)
18	LSI-C-C5-26	214/(i.4)	45	LRI-M-C5-5m	216/(m.4)
19	LSI-M-C5-05	214/(i.4)			
20	LSI-M-C5-02	214/(i.3)			
21	LSI-M-C5-03	214/(i.3)			
22	LSI-C-C5-23	214/(i.3)			
23	LSI-M-C5-04	214/(i.3)			
24	LSI-M-C4-05	213/(h.3)			
25	LSI-M-C4-04	213/(h.3)			
26	LSI-C-C4-03	213/(h.3)			
27	LSI-C-C5-21	211/(e.2)			

REVISION					
NO.	DATE	DRAWN BY	CHECKED BY	APPROVED BY	NOTES
0	July 26, 1999	J. Tenorio			
1	Jan. 31, 2001	J. Tenorio			Remove Gage 31
NUPEC/NRC PCCV STRUCTURAL BEHAVIOR TEST MODEL					
DRAWING NO.		INTERIOR LINER GAGE LAYOUT			SCALE
D-SN-P-219		A/L			NO SCALE
SANDIA NATIONAL LABORATORIES FACILITIES ENGINEERING					
ALBUQUERQUE, NEW MEXICO; LIVERMORE, CALIFORNIA; TONOPAH, NEVADA					
					



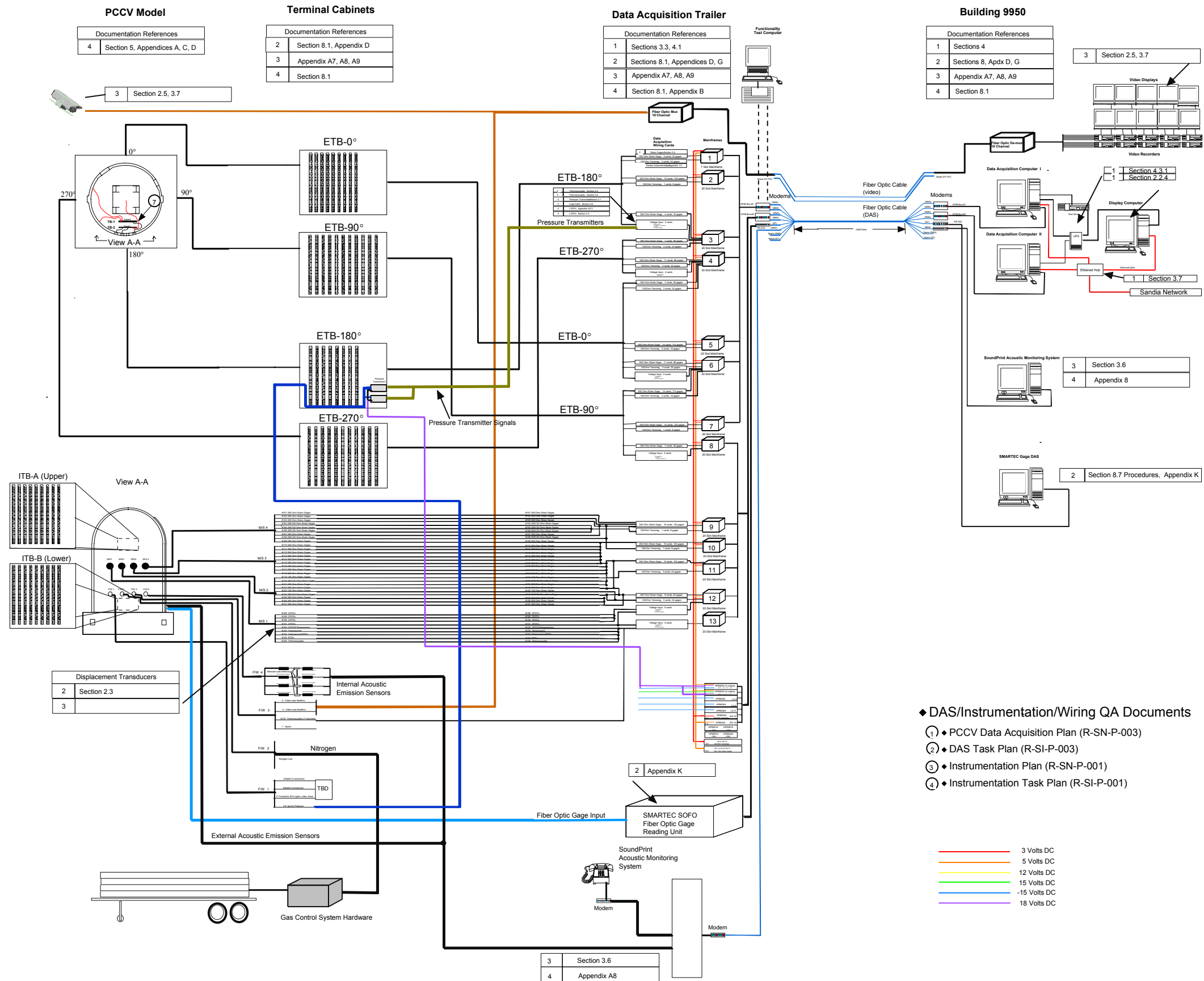
INSTRUMENTATION GAGES		
Instr. #	Labeling	Details
	I.D.	Drawing #
	(Name)	D-SN-P-
1	LSI-C-F5-05	212/(f.1)
2	LSI-M-F5-03	212/(f.1)
3	LSI-C-F5-04	212/(f.1)
4	LSI-C-F5-03	212/(f.1)
5	LSI-M-F5-02	212/(f.1)
6	LSI-C-F5-02	212/(f.1)
7	LSI-C-F5-07	215/(k.4)
8	LRI-M-F5-1h	215/(k.4)
9	LRI-M-F5-1d	215/(k.4)
10	LRI-M-F5-1m	215/(k.4)
11	LSI-C-H5-05	212/(f.2)
12	LSI-M-H5-03	212/(f.2)
13	LSI-C-H5-04	212/(f.2)
14	LSI-C-H5-03	212/(f.2)
15	LSI-M-H5-02	212/(f.2)
16	LSI-C-H5-02	212/(f.2)
17	LSI-C-H5-07	215/(k.7)
18	LRI-M-H5-1h	215/(k.7)
19	LRI-M-H5-1d	215/(k.7)
20	LRI-M-H5-1m	215/(k.7)
21	LSI-C-H5-08	217/(o.1)
22	LSI-M-H5-04	217/(o.1)



INSTRUMENTATION GAGES		
Instr. #	Labeling	Details
	I.D.	Drawing #
	(Name)	D-SN-P-
30	LSI-C-F4-04	212/(f.3)
31	LSI-M-F4-02	212/(f.3)
32	LSI-C-F4-03	212/(f.3)
33	LSI-C-F4-02	212/(f.3)
34	LSI-M-F4-01	212/(f.3)
35	LSI-C-F4-01	212/(f.3)
36	LSI-C-F4-06	215/(k.5)
37	LRI-M-F4-1h	215/(k.5)
38	LRI-M-F4-1d	215/(k.5)
39	LRI-M-F4-1m	215/(k.5)
40	LSI-C-F4-08	215/(l.5)
41	LRI-M-F4-2h	215/(l.5)
42	LRI-M-F4-2d	215/(l.5)
43	LRI-M-F4-2m	215/(l.5)
44	LSI-C-H4-04	212/(f.4)
45	LSI-M-H4-02	212/(f.4)
46	LSI-C-H4-03	212/(f.4)
47	LSI-C-H4-02	212/(f.4)
48	LSI-M-H4-01	212/(f.4)
49	LSI-C-H4-01	212/(f.4)

REVISION					
NO.	DATE	DRAWN BY	CHECKED BY	APPROVED BY	NOTES
0	July 20, 1999	J. Tenorio			
NUPEC/NRC PCCV STRUCTURAL BEHAVIOR TEST MODEL					
DRAWING NO.		INTERIOR LINER GAGE LAYOUT			SCALE
D-SN-P-220		M/S AND F/W			NO SCALE
SANDIA NATIONAL LABORATORIES FACILITIES ENGINEERING					
ALBUQUERQUE, NEW MEXICO;		LIVERMORE, CALIFORNIA;		TONOPAH, NEVADA	

Appendix F: Prestressed Concrete Containment Vessel Data Acquisition System/Instrumentation Schematic



◆ DAS/Instrumentation/Wiring QA Documents

- ① ◆ PCCV Data Acquisition Plan (R-SN-P-003)
- ② ◆ DAS Task Plan (R-SI-P-003)
- ③ ◆ Instrumentation Plan (R-SN-P-001)
- ④ ◆ Instrumentation Task Plan (R-SI-P-001)

Appendix G: Posttest Data Correction

G.1 Data Uncertainty

Before a discussion of gage uncertainty can begin, the terms accuracy, precision, and uncertainty must be defined. As per standard practice, accuracy is defined as the deviation of an instrument's reading from a **known** input. Precision indicates an instrument's ability to reproduce a certain reading with a given accuracy. Uncertainty is defined as the plus or minus deviation range of a reading from the true value. In many experimental situations (certainly in the PCCV experiments), this true value is not known, however, the fairly high confidence exists in the uncertainty range.

Each gage used on the PCCV model had an associated uncertainty. Efforts were made to ensure that the level of uncertainty associated with each gage was appropriate for the magnitude of the expected data. This was done to avoid losing meaningful data because of relatively high inaccuracies of instruments.

G.2 Post Test Data Conversion and Correction

After the high pressure PCCV test was conducted, the data collected by the DAS during this final test was subjected to conversion and correction. The purpose of the conversion was to convert the data from raw form (usually volts) into engineering units. The purpose of the corrections was to correct the data for any offsets or external effects such as temperature. The specific details per instrument type are detailed in the sections below.

G.2.1 Corrections Made to Strain Gage Raw Data

Basic strain data reduction was accomplished through two major steps: 1) firmware reduction from measurements of the bridge-balancing voltages to values of strain and 2) post-test data corrections to compensate for various effects (i.e. temperature effects, transverse strain, etc.).

The first step will not be discussed here except to note that the data acquisition firmware automatically converts the voltages received from the strain gages to strain data. Therefore, for the PCCV test, the raw data from strain gages was in microstrain. The last steps (referred to here as the data corrections) are discussed in the following sections.

The least count requirement for the strain gages used in this test will be ± 0.01 % strain. The data acquisition system used in the PCCV high pressure test recorded seven significant digits for each data point. This is not meant to imply that the data was believed to be accurate to that extent. A study on the uncertainty of the data from the various instruments was performed.

The strain gage raw data obtained during the PCCV High Pressure Test was in the units of microstrain. Three types of data correction were done to the raw strain gage data. These are: corrections for gage specific gage factors, corrections for temperature effects, and corrections for transverse sensitivity.

G.2.1.1 Instrument Specific Gage Factor Correction

The data acquisition system (DAS) used in the PCCV High Pressure Test assumed a single gage factor for all strain gages. This factor (2.089) was determined by taking the average value of the gage factors of the strain gages used in the test. The standard practice in data acquisition is to use the value 2.0 for the gage factor while acquiring data. This value was used in the internal firmware of the DAS hardware to determine the strain values output by the system. However, each strain gage has associated with it a *specific* gage factor that is identified and provided by the manufacturer. The data from each gage was corrected, posttest, to reflect the correct GFAC for that gage.

To output strain gage readings in units of strain, the firmware must convert from the output voltage. The following equations were used.

$$\varepsilon = \frac{-4 V_R}{GFAC(1 + 2V_R)} \quad (G-1)$$

where

$$V_R = \left(\frac{V_{out}}{V_S} \right)_{strained} - \left(\frac{V_{out}}{V_S} \right)_{unstrained}$$

ε = “raw” strain

V_{out} = output voltage of gage bridge

V_S = bridge excitation voltage

As stated above, during the acquisition of the PCCV High Pressure Test data, a single GFAC was input into Equation G-1 for all strain gages.

Post test, the gage specific GFAC for each gage was used to correct the raw data. Equation 2 below was used to accomplish this.

$$\varepsilon' = \varepsilon \left(\frac{GFAC_{general}}{GFAC_{specific}} \right) \quad (G-2)$$

G.2.1.2 Corrections for Wire Length Change in Resistance

Because of the long lead wire lengths required for the instrumentation of the PCCV, consideration was given to correcting for changes in the GFACs due to the slight change in resistance. It was decided that this was not necessary because the strain gages were wired in a three-wire configuration, which effectively reduces lead wire resistance effects by 50% over a two-wire configuration, reducing the error to a very small value.

G.2.1.3 Corrections for Temperature Effects on the Lead Wires

Corrections to account for changes in lead wire resistance due to temperature changes over the test duration were also considered, but rejected for the reason mentioned above.

G.2.1.4 Corrections for Temperature Effects on the Strain Gages

There are two corrections that may be made for temperature effects on strain gages. The first is an adjustment of the strain gage data for apparent strain. Apparent strain is a value of strain that appears in the raw data as an artifact of the temperature at which the data was taken. This strain amount must be removed from the raw data to compensate for this effect. If the strain readings were taken at the temperature at which the strain gages were calibrated, there would be no apparent strain.

Correction for Apparent Strain

For the strain gages to be used in the PCCV test, the equation provided by the manufacturer for calculating apparent strain is a fourth order polynomial, shown below. The constants in this equation vary depending on the lot number of each strain gage.

$$\varepsilon_{apparent} = A_0 + A_1T + A_2T^2 + A_3T^3 + A_4T^4 \quad (G-3)$$

where T = testing temperature at time data point was taken, in Celsius.

This value is then subtracted from the correction 1 value.

$$\varepsilon'' = \varepsilon' - \varepsilon_{\text{apparent}} \quad (\text{G-4})$$

Although the strain of interest in the PCCV High Pressure Test will be that strain caused by pressure induced expansion of the model, no attempt was made to eliminate from the strain data the amount of strain caused by thermal expansion of the model.

Corrections for GFAC Temperature Effects

A correction to adjust the gage specific gage factor (GFAC) for temperature, was not done. The manufacturer provides a GFAC for each gage. This factor is determined at a temperature of 24°C. The GFAC value will change with temperature. For the temperature changes during the PCCV test, this correction affected GFAC values by much less than 1%. Therefore, although the impact of this correction was assessed post-test, this correction was not performed on the data.

G.2.1.5 Corrections for Transverse Strain Sensitivity

The final set of corrections to the strain gage data involved correcting for transverse strain sensitivity. These corrections were performed only on the rosette gage data, the strip gage data and data from any hoop/meridional gage pairs. For the strip gages, data from previously identified cross axis gages (of the type SSGH) were used in these corrections. Transverse sensitivity refers to the response of the gages due to cross axis strain.

The strip gages and hoop/meridional gage pairs were treated as a 90°, two element rosette gage. The equation used to correct for transverse sensitivity for these is:

$$\varepsilon_{\text{corr}} = \frac{(1 - \nu_0 K_t)(\varepsilon'' - K_t \varepsilon''_{\text{cross-axis}})}{1 - K_t^2} \quad (\text{G-5})$$

where ν_0 = Poisson's ratio of the material on which the manufacturer's gage factor was measured, usually 0.285

K_t = transverse sensitivity coefficient which is supplied by the gage manufacturer.

$\varepsilon''_{\text{cross-axis}}$ = the strain reading from the cross-axis gage taken at the same time as ε'' . (This reading must have been corrected with the previously discussed corrections before being used here.)

G.2.1.6 Transverse Sensitivity Corrections for Rosette Gages

For the rosette gages, the following equations were used. Consider a three-gage rectangular rosette with the gage elements numbered consecutively. Elements 1 and 3 correspond to the elements that are 90° apart and element 2 is the center 45° gage.

$$\begin{aligned} \varepsilon_{1\text{corr}} &= \frac{(1 - \nu_0 K_t)(\varepsilon''_1 - K_t \varepsilon''_3)}{1 - K_t^2} \\ \varepsilon_{2\text{corr}} &= \frac{(1 - \nu_0 K_t)(\varepsilon''_2 - K_t(\varepsilon''_1 + \varepsilon''_3 - \varepsilon''_2))}{1 - K_t^2} \end{aligned} \quad (\text{G-6})$$

$$\varepsilon_{3\text{corr}} = \frac{(1 - \nu_o K_t)(\varepsilon_3'' - K_t \varepsilon_1'')}{1 - K_t^2}$$

When these corrections were applied to a selected group of gages in areas of liner strain concentration, it was observed that the difference between the uncorrected and the corrected data was very small, on the order of 1%, for strains of approximately 2%. The difference becomes larger as the strains become smaller and is considerably greater for strains on the order of .05%. Because the difference is very small for the larger strains, the correction was not done.

G.2.1.8 Corrections to Rebar Strain Gages

One final correction was investigated for the strain data from gages installed on rebar. During the gage installation process, a small portion of the rebar must be ground flat to provide a suitable installation surface. This changes the cross-sectional area of the rebar at that location and the strain data should be compensated for this. A correction factor to account for this was considered, but later rejected because of inconsistent and non-reproducible results in lab experiments

G.2.2 Corrections Made to LVDT Raw Data

Linear Variable Displacement Transducers (LVDTs) output raw data that vary linearly with displacement. Data reduction for the LVDTs starts with the conversion of the raw signal (in volts) to displacement (in inches). The following single step reduction will provide the displacement of the device, either positive or negative, from its **null** (not necessarily original) position.

$$D_{\text{null}} = V_{\text{raw}_{\text{time}=t}} \left[\frac{1}{CF_{\text{LVDT}}} \right] \quad (\text{G-7})$$

where D_{null} = displacement from the null position (in),

V_{raw} = raw signal from gage at time t (V),

CF_{LVDT} = LVDT calibration factor (V/in).

Note that the polarity of the output voltage is important for these measurements as the device reads in either direction around the null point that represents zero output voltage. The device will be initially spring loaded.

As shown below, for each LVDT location, the initial displacement reading ($V_{\text{time}=0}$) will be algebraically combined with each subsequent reading. The initial reading will be considered an offset. Thus, for each reading, the determination of the actual displacement of the LVDT with respect to the **initial displacement** is obtained as follows.

$$D = (V_{\text{raw}_{\text{time}=t}} - V_{\text{raw}_{\text{time}=0}}) \left[\frac{1}{CF_{\text{LVDT}}} \right] \quad (\text{G-8})$$

where D = displacement from original position (in),

V_{raw} = raw signal from gage at time indicated (V).

Figure G.1 illustrates the layout.

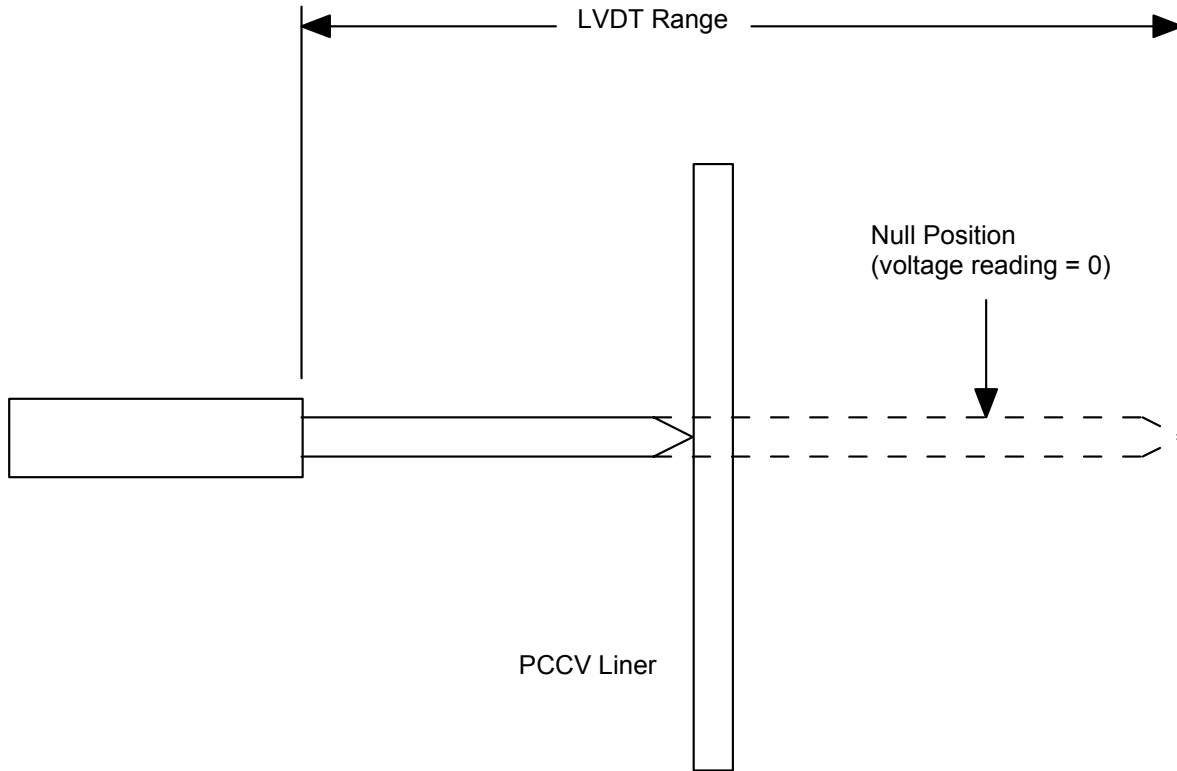


Figure G.1 Geometry for LVDT Measurements

Most of the LVDTs were mounted to the internal framework inside the PCCV model. Because the motion of the internal frame during the tests could affect the measurements, the corrections for motion would be similar to those specified for CPOTs (see G.2.6).

G.2.3 Corrections Made to Inclinometer Raw Data

Conversion of the inclinometer tilt data is accomplished by subtracting the initial raw data point value (in volts) from the current raw data point value (volts) and dividing the result by the calibration factor. This will remove the initial offset angle and provide as final results only the change in angle at any time or pressure.

$$\text{Change in Tilt Angle (}^\circ\text{)} = \frac{\text{Raw Data}_{\text{time} = t} \text{ (V)} - \text{Raw Data}_{\text{time} = 0} \text{ (V)}}{\text{Calibration Factor (volts/}^\circ\text{)}} \quad (\text{G-9})$$

G.2.4 Corrections Made to Thermocouple and RTD Raw Data

All temperature sensor measurements, including both thermocouples and RTDs, are entirely reduced through firmware calculations. Thus, no post-test data reduction is needed. The “raw data” is in the units of °C.

G.2.5 Corrections Made to Pressure Transducer Raw Data

The pressure transducers are voltage type devices and will be factory and SNL calibrated to provide a pressure value (in psia) given a voltage output from the transducers. The following data reduction were used:

$$P(\text{psia}) = [\text{Signal}(\text{V})] \left[\text{CalibrationFactor} \frac{(\text{psia})}{(\text{mV})} \right] \left[1000 \left(\frac{\text{mV}}{\text{V}} \right) \right] \quad (\text{G-10})$$

To convert the pressure readings into psig, the initial pressure gage reading was subtracted from subsequent readings.

$$P(\text{psig}) = [\text{Signal}(\text{V}) - \text{Signal}_{\text{initial}}(\text{V})] \left[\text{CalibrationFactor} \frac{(\text{psia})}{(\text{mV})} \right] \left[1000 \left(\frac{\text{mV}}{\text{V}} \right) \right] \quad (\text{G-11})$$

As the final desired pressure units are MPa, the pressure data in psig was then converted to MPa and reported as gage pressure.

G.2.6 Corrections Made to Cable Potentiometers

G.2.6.1 General Corrections

The cable potentiometers (CPOTs) each have a sensitivity factor. This sensitivity is of the form $mV/(V \cdot \text{in})$. The signal in mV is normalized by the excitation voltage and divided by the sensitivity factor to obtain the CPOT length in inches. It is necessary to monitor the excitation voltage used for each measurement.

The first step in the reduction uses Equation G-12 below.

$$\text{length}(\text{in}) = [\text{Signal}(\text{V})] \left[\frac{1}{\text{Sens.Factor}} \frac{(\text{V} - \text{in})}{(\text{mV})} \right] \left[\frac{1000(\text{mV})}{(\text{V})} \right] \left[\frac{1}{V_{\text{excit.}}(\text{V})} \right] \quad (\text{G-12})$$

For each cable potentiometer location, the **initial length reading** was algebraically combined with each subsequent reading to provide the differential displacement throughout the experiment. This operation is shown in Equation G-13.

$$\text{Displacement}(\text{in}) = [\text{length}]_{\text{current}} - [\text{length}]_{\text{initial}} \quad (\text{G-13})$$

The geometry showing the use of Equation G-13 is shown in Figure G.2. Note that this assumes that the angle between the cable's original horizontal line and its displaced line is small so that the true horizontal and vertical components of the displacement are equal to the indicated displacement.

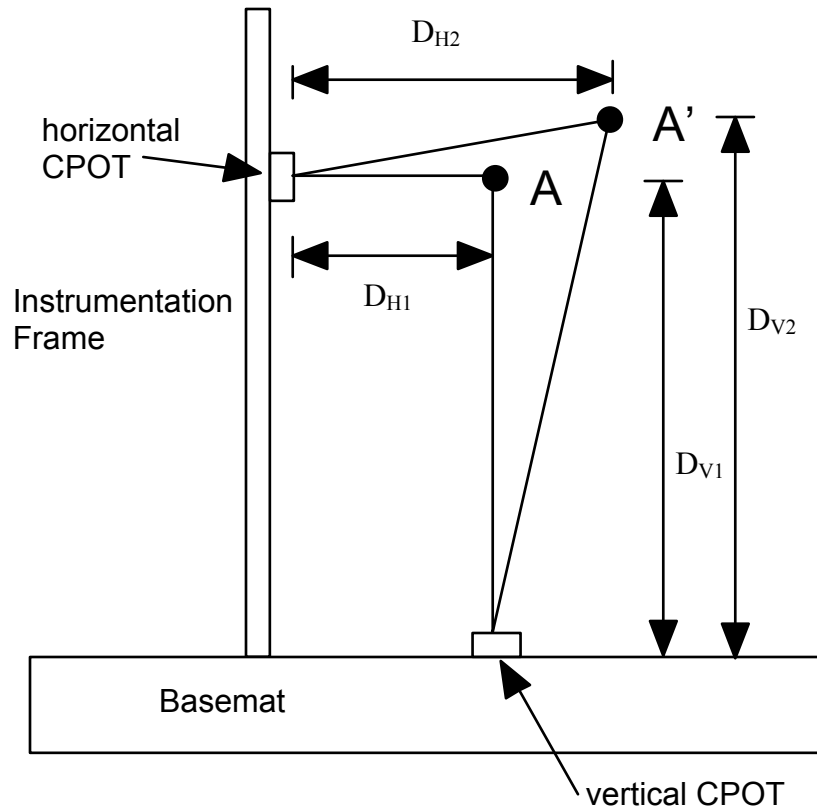


Figure G.2 Displacement Measurements (Showing Offset Subtraction)
horizontal displacement = $D_{H2} - D_{H1}$
vertical displacement = $D_{V2} - D_{V1}$

G.2.6.2 Corrections for Movement of Instrumentation Frame

For the PCCV model tests, there was the possibility of instrumentation frame movement caused by thermal expansion. The PCCV high pressure test duration was more than one day. The effect of thermal cycling from day to night temperature changes was characterized, and it was determined that the movement of the frame affected the measurements by a very small amount and no corrections were performed.

G.2.6.3 Correction in Horizontal Displacement Measurements for Vertical Translations

A sketch of the geometry for this case is shown in Figure G.3. Note that the liner motion imparts a vertical component of elongation of the cable-type displacement transducer. Vertical displacement measurements of the liner attachment point would be required to resolve the purely horizontal movement. Several of the CPOT attachment locations on the PCCV liner had both horizontally and vertically aligned gages. Thus, the true horizontal and vertical motions of those points was resolved.

The vertical displacements were corrected in a similar manner for horizontal translations.

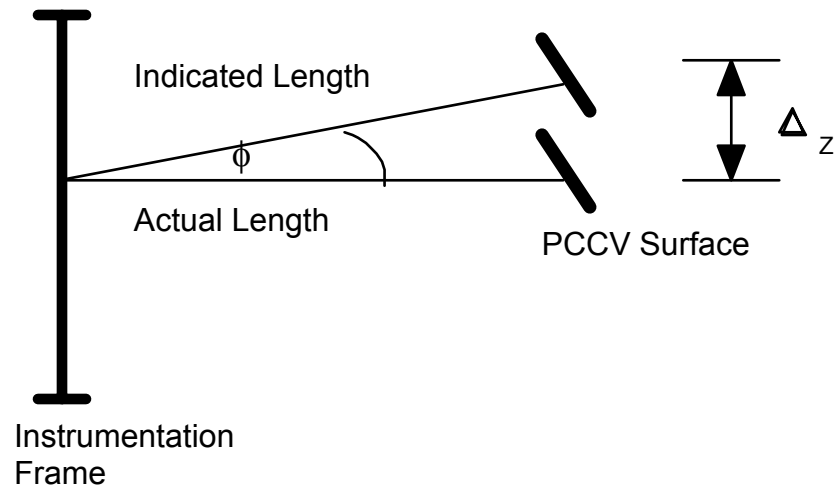


Figure G.3 Geometry for Vertical Movement of Liner at Horizontal Gage Locations

Appendix H: SFMT Instrumentation List

Displacement Instrumentation List

Labeling	Azimuthal	Vertical	Radial	Transducer	Location	Details	Initial	Modified	Comnts	Calibration
I D	Angle	Elevation	Distance	Designation	Drawing #	Drawing #	Offset	Mark #		
(name)	(deg)	(in)	(in)			D-SN-P-				
DL-R-B5-05	30	184.0	211.0		P-131	N/A	-4.5	LVDT-10	Disp	
DL-R-D5-05	90	184.0	211.0		P-131	N/A	-4.5	LVDT-10	Radial	
DL-R-Z2-05	135	10.0	211.0	GCD-121-500	P-131	N/A	-0.3	LVDT-1		
DL-R-Z3-05	135	56.0	211.0	GCD-121-2000-1283	P-131	N/A	-1.5	LVDT-4		
DL-R-Z4-05	135	104.0	211.0	GCD-121-2000-1283	P-131	N/A	-1.5	LVDT-4		
DL-R-Z5-05	135	184.0	211.0		P-131	N/A	-4.5	LVDT-10		
DL-R-Z6-05	135	244.0	211.0		P-131	N/A	-4.5	LVDT-10		
DL-R-Z7-05	135	304.0	211.0		P-131	N/A	-4.5	LVDT-10		
DL-R-Z9-05	135	423.0	211.0	GCD-121-2000-1283	P-131	N/A	-1.5	LVDT-4		
DL-R-G5-05	180	184.0	211.0		P-131	N/A	-4.5	LVDT-10		
DL-R-I5-05	240	184.0	211.0		P-131	N/A	-4.5	LVDT-10		
DL-R-J5-05	270	184.0	211.0		P-131	N/A	-4.5	LVDT-10		
DL-R-L2-05	324	10.0	211.0	GCD-121-500	P-131	N/A	-0.3	LVDT-1		
DL-R-L5-05	334	184.0	200.0		P-131	N/A	-4.5	LVDT-10		
DL-R-L6-05	324	244.0	211.0		P-131	N/A	-4.5	LVDT-10		
DL-R-L7-05	324	304.0	211.0		P-131	N/A	-4.5	LVDT-10		
DL-R-L9-05	324	423.0	211.0	GCD-121-2000-1283	P-131	N/A	-1.5	LVDT-4		
DL-M-Z9-05	135	423.0	211.0	GCD-121-2000-1283	P-131	N/A	-1.5	LVDT-4	Disp.	
DL-M-Z13-05	-	635.0	0.0		P-131	N/A	-2.5	LVDT-6	Vert	
DL-M-L9-05	324	423.0	211.0	GCD-121-2000-1283	P-131	N/A	-1.5	LVDT-4		

PreCal - Calibration was preformed on this instrument prior to model testing only

PostOK - Calibration was performed on this instrument Before and After model testing and remained within tolerance

PostOUT - Calibration was performed on this instrument Before and After model testing and difference was Out-of Tolerance

Rebar Strain Instrumentation List

Labeling	Azimuthal	Vertical	Radial	Transducer	Location	Details	Basic	Modified	Comnts	Calibration
I D	Angle	Elevation	Distance	Designation	Drawing #	Drawing #	Mark #	Mark #		
(name)	(deg)	(in)	(in)			D-SN-P-				
GB-M-A1-04	350	12.3	214.0	EP-08-062AQ-350	124/(A)	124/(1)	-	G15A1A	Gage	NoCal
GB-M-A1-08	350	7.9	217.2	EP-08-062AQ-350	124/(A)	124/(1)	-	G15A1B	Bars	NoCal
GB-M-A1-12	350	3.4	220.4	EP-08-062AQ-350	124/(A)	124/(1)	-	G15A1C		NoCal
GB-M-A1-14	350	12.3	220.4	EP-08-062AQ-350	124/(A)	124/(1)	-	G15A1C		NoCal
GB-M-A1-17	350	3.4	223.6	EP-08-062AQ-350	124/(A)	124/(1)	-	G15A1D		NoCal
GB-M-A1-19	350	12.3	223.6	EP-08-062AQ-350	124/(A)	124/(1)	-	G15A1D		NoCal
GB-M-A1-20	350	16.8	223.6	EP-08-062AQ-350	124/(A)	124/(1)	-	G15A1D		NoCal
GB-M-A1-21	351	-1.0	223.6	EP-08-062AQ-350	TBD	TBD	-	G15A1E	Added	NoCal
GB-M-A1-22	351	3.4	223.6	EP-08-062AQ-350	TBD	TBD	-	G15A1E	Added	NoCal
GB-M-D1-08	90	7.9	220.0	EP-08-062AQ-350	124/(A)	124/(1)	-	G15D1B		NoCal
GB-M-D1-13	90	7.9	226.0	EP-08-062AQ-350	124/(A)	124/(1)	-	G15D1C		NoCal
GB-M-D1-14	90	12.3	226.0	EP-08-062AQ-350	124/(A)	124/(1)	-	G15D1C		NoCal
GB-M-D1-15	90	16.8	226.0	EP-08-062AQ-350	124/(A)	124/(1)	-	G15D1C		NoCal
GB-M-D1-19	90	12.3	232.0	EP-08-062AQ-350	124/(A)	124/(1)	-	G15D1D		NoCal
GB-M-D1-20	90	16.8	232.0	EP-08-062AQ-350	124/(A)	124/(1)	-	G15D1D		NoCal
GB-M-Z1-03	135	7.9	214.0	EP-08-062AQ-350	124/(A)	124/(1)	-	G15Z1A		NoCal
GB-M-Z1-05	135	16.8	214.0	EP-08-062AQ-350	124/(A)	124/(1)	-	G15Z1A		NoCal
GB-M-Z1-09	135	12.3	217.2	EP-08-062AQ-350	124/(A)	124/(1)	-	G15Z1B		NoCal
GB-M-Z1-10	135	16.8	217.2	EP-08-062AQ-350	124/(A)	124/(1)	-	G15Z1B		NoCal
GB-M-Z1-13	135	7.9	220.4	EP-08-062AQ-350	124/(A)	124/(1)	-	G15Z1C		NoCal
GB-M-Z1-14	135	12.3	220.4	EP-08-062AQ-350	124/(A)	124/(1)	-	G15Z1C		NoCal
GB-M-Z1-17	135	3.4	223.6	EP-08-062AQ-350	124/(A)	124/(1)	-	G15Z1D		NoCal
GB-M-Z1-18	135	7.9	223.6	EP-08-062AQ-350	124/(A)	124/(1)	-	G15Z1D		NoCal
GB-M-Z1-19	135	12.3	223.6	EP-08-062AQ-350	124/(A)	124/(1)	-	G15Z1D		NoCal
GB-M-Z1-20	135	16.8	223.6	EP-08-062AQ-350	124/(A)	124/(1)	-	G15Z1D		NoCal
GB-M-Z1-21	136	-1.0	223.6	EP-08-062AQ-350	TBD	TBD	-	G15Z1E	Added	NoCal
GB-M-Z1-22	136	3.4	223.6	EP-08-062AQ-350	TBD	TBD	-	G15Z1E	Added	NoCal
RS-M-A1-01	0	2.0	214.0	EP-08-250BF-350	PCCV-S-2i	102/(5)	S2V002	S2V002A	SOL	NoCal
RS-M-A1-02	0	2.0	221.5	EP-08-250BF-350	PCCV-S-6i	102/(9)	S6V002	S6V002A	&	NoCal
RS-M-A2-01	0	10.0	214.0	EP-08-250BF-350	PCCV-S-2i	102/(5)	S2V002	S2V002A	Vert	NoCal
RS-M-D1-01	90	2.0	214.0	EP-08-250BF-350	PCCV-S-1i	102/(3)	S1VA02	S1VA02A	Wall	NoCal
RS-M-D1-02	89	2.0	230.0	EP-08-250BF-350	PCCV-SB-1i	102/(11)	SB1VA04	SB1VA04A	Base	NoCal
RS-M-D2-01	90	10.0	214.0	EP-08-250BF-350	PCCV-S-1i	102/(3)	S1VA02	S1VA02A		NoCal
RS-M-D2-02	89	10.0	230.0	EP-08-250BF-350	PCCV-SB-1i	102/(11)	SB1VA04	SB1VA04A		NoCal
RS-M-D6-02	89.5	244.0	230.0	EP-08-250BF-350	PCCV-SB-2i	108/(12)	SB2V002	SB2V002A		NoCal
RS-M-Z1-01	135	2.0	214.0	EP-08-250BF-350	PCCV-S-1i	102/(4)	S1VA02	S1VA02B		NoCal
RS-M-Z1-02	135	2.0	221.5	EP-08-250BF-350	PCCV-S-5i	102/(8)	S5VA03	S5VA03A		NoCal
RS-M-Z2-01	135	10.0	214.0	EP-08-250BF-350	PCCV-S-1i	102/(4)	S1VA02	S1VA02B		NoCal
RS-M-Z2-02	135	10.0	221.5	EP-08-250BF-350	PCCV-S-5i	102/(8)	S5VA03	S5VA03A		NoCal
RS-M-Z3-01	135	56.0	214.0	EP-08-250BF-350	PCCV-S-1i	104/(2)	S1VA03	S1VA03A		NoCal
RS-M-Z3-02	135	56.0	221.5	EP-08-250BF-350	PCCV-S-5i	106/(5)	S5VB03	S5VB03A		NoCal
RS-M-Z6-02	135	244.0	221.5	EP-08-250BF-350	PCCV-S-5i	106/(12)	S5VA07	S5VA07A		NoCal
RS-M-Z9-01	135	423.0	214.0	EP-08-250BF-350	PCCV-S-1i	104/(12)	S1V005	S1V005B		NoCal
RS-M-Z9-02	135	423.0	221.5	EP-08-250BF-350	PCCV-S-5i	106/(11)	S5V007	S5V007A		NoCal
RS-M-Z9-03	135	423.0	214.0	EP-08-250BF-350	PCCV-S-1i	104/(12)	S1V005	S1V005B		NoCal
RS-M-Z9-04	135	423.0	221.5	EP-08-250BF-350	PCCV-S-5i	106/(11)	S5V007	S5V007A		NoCal
RS-M-Z11-01	135	573.0	152.0	EP-08-250BF-350	PCCV-D-1i	117/(2)	D1V003	D1V003A		NoCal
RS-M-Z11-02	135	573.0	162.0	EP-08-250BF-350	PCCV-D-4i	117/(11)	D4VA03	D4VA03A		NoCal
RS-M-Z11-03	135	573.0	152.0	EP-08-250BF-350	PCCV-D-1i	117/(2)	D1V003	D1V003A		NoCal
RS-M-Z11-04	135	573.0	162.0	EP-08-250BF-350	PCCV-D-4i	117/(11)	D4VA03	D4VA03A		NoCal
RS-M-J1-01	270	2.0	214.0	EP-08-250BF-350	PCCV-S-2i	102/(6)	S2V002	S2V002B		NoCal
RS-M-J2-01	270	10.0	214.0	EP-08-250BF-350	PCCV-S-2i	102/(6)	S2V002	S2V002B		NoCal
RS-M-J2-02	269	10.0	230.0	EP-08-250BF-350	PCCV-SB-1i	102/(12)	SB1V004	SB1V004B		NoCal
RS-M-L1-01	324	2.0	214.0	EP-08-250BF-350	PCCV-S-2i	102/(7)	S2VA02	S2VA02A		NoCal
RS-M-L1-02	324	2.0	221.5	EP-08-250BF-350	PCCV-S-6i	102/(10)	S6V002	S6V002B		NoCal
RS-M-L2-01	324	10.0	214.0	EP-08-250BF-350	PCCV-S-2i	102/(7)	S2VA02	S2VA02A		NoCal
RS-M-L2-02	324	10.0	221.5	EP-08-250BF-350	PCCV-S-6i	102/(10)	S6V002	S6V002B		NoCal
RS-C-D6-02	90	246.0	223.0	EP-08-250BF-350	PCCV-S-8i	115/(9)	S8H033	S8H033A		NoCal
RS-C-Z6-01	135	246.0	215.0	EP-08-250BF-350	PCCV-S-3i	110/(10)	S3H026	S3H026A		NoCal
RS-C-Z6-02	135	246.0	223.0	EP-08-250BF-350	PCCV-S-7i	113/(2)	S7H031	S7H031A		NoCal
RS-C-Z9-02	135	423.0	223.0	EP-08-250BF-350	PCCV-S-7i	113/(4)	S7H036	S7H036B		NoCal
RS-C-Z11-02	135	573.0	163.0	EP-08-250BF-350	PCCV-D-6i	116/(11)	D6H048	D6H048B		NoCal

Liner Strain Instrumentation List

Labeling	Azimuthal	Vertical	Radial	Transducer	Location	Details	Basic	Modified	Comnts	Calibration
I D	Angle	Elevation	Distance	Designation	Drawing #	Drawing #	Mark #	Mark #		
(name)	(deg)	(in)	(in)			D-SN-P-				
LSO-C-A7-01	1.8	305.3	211.7	EP-08-125AC-350	ZCD1007Ai	209/(a.1)	4-1B	4-1B	Vert.	NoCal
LSO-C-Z5-01	137.5	216.2	211.7	EP-08-125AC-350	ZCD1008Ai	209/(a.2)	3-6B	3-6B	Weld	NoCal
LSO-C-Z6-01	137.5	229.7	211.7	EP-08-125AC-350	ZCD1008Ai	209/(a.3)	3-6B	3-6B		NoCal
LSO-C-D7-01	95.8	305.3	211.7	EP-08-125AC-350	ZCD1009Ai	209/(a.4)	4-3B	4-3B		NoCal
LSO-C-D7-02	95.8	291.5	211.7	EP-08-125AC-350	ZCD1009Ai	209/(a.5)	4-3B	4-3B		NoCal
LSO-M-A1-03	0	0.4	211.7	EP-08-125MW-120	ZCD1002Ai	208/(c.1)	1-12C	1-12C	Wall	NoCal
LSO-M-A1-04	0	0.5	211.7	EP-08-125MW-120	ZCD1002Ai	208/(c.1)	1-12C	1-12C	Base	NoCal
LSO-M-D1-01	89.6	-0.7	211.7	EP-08-125MW-120	ZCD1002Ai	208/(c.2)	1-3C	1-3C		NoCal
LSO-M-D1-02	89.6	-0.2	211.7	EP-08-125MW-120	ZCD1002Ai	208/(c.2)	1-3C	1-3C		NoCal
LSO-M-D1-03	89.6	0.4	211.7	EP-08-125MW-120	ZCD1002Ai	208/(c.2)	1-3C	1-3C		NoCal
LSO-M-D1-05	88.9	-0.7	211.7	EP-08-125MW-120	ZCD1002Ai	207/(c.3)	1-3C	1-3C		NoCal
LSO-M-I1-01	239.4	-0.7	211.7	EP-08-125MW-120	ZCD1002Ai	207/(c.6)	1-8C	1-8C		NoCal
LSO-M-I1-02	239.4	-0.2	211.7	EP-08-125MW-120	ZCD1002Ai	207/(c.6)	1-8C	1-8C		NoCal
LSO-M-L1-03	324.6	0.4	211.7	EP-08-125MW-120	ZCD1002Ai	208/(c.7)	1-11C	1-11C		NoCal
LSO-M-L1-04	324.6	0.5	211.7	EP-08-125MW-120	ZCD1002Ai	208/(c.7)	1-11C	1-11C		NoCal

Tendon Instrumentation List

Labeling	Azimuthal	Vertical	Radial	Transducer	Location	Details	Basic	Modified	Comnts	Calibration
I D	Angle	Elevation	Distance	Designation	Drawing #	Drawing #	Mark #	Mark #		
(name)	(deg)	(in)	(in)			D-SN-P-				
TT-M-Z6-01	135	244.0	218.0	TENSMEG-120	120/(2)	121/(1)	V46	V46-1	Tensmeg	NoCal
TT-M-Z9-01	135	380.0	218.0	TENSMEG-120	120/(2)	121/(1)	V46	V46-1		NoCal
TT-M-E10-01	121	537.0	178.0	TENSMEG-120	120/(2)	121/(1)	V46	V46-1		NoCal
TT-M-D11-01	90	580.0	141.0	TENSMEG-120	120/(2)	121/(1)	V46	V46-1		NoCal
TT-M-I3-01	241	64.0	218.0	TENSMEG-120	120/(1)	121/(2)	V37	V37-1		NoCal
TT-M-I3-02	241	90.0	218.0	TENSMEG-120	120/(1)	121/(2)	V37	V37-2		NoCal
TT-M-I9-01	241	380.0	218.0	TENSMEG-120	120/(1)	121/(2)	V37	V37-1		NoCal
TT-M-I9-02	241	406.0	218.0	TENSMEG-120	120/(1)	121/(2)	V37	V37-2		NoCal
TT-M-I9-03	241	354.0	218.0	TENSMEG-120	120/(1)	121/(2)	V37	V37-3		NoCal
TT-M-G12-01	180	615.0	87.0	TENSMEG-120	120/(1)	121/(1)	V37	V37-1		NoCal
TT-M-L9-03	325	354.0	218.0	TENSMEG-120	120/(3)	122/(6)	V85	V85-3		NoCal
TT-M-J11-01	270	588.0	132.0	TENSMEG-120	120/(3)	121/(1)	V85	V85-1		NoCal
TT-C-D3-01	90	73.0	220.0	TENSMEG-120	119/(1)	121/(1)	H11	H11-1		NoCal
TT-C-G3-01	180	73.0	220.0	TENSMEG-120	119/(1)	121/(1)	H11	H11-1		NoCal
TT-C-A5-01	0	180.0	220.0	TENSMEG-120	119/(2)	122/(6)	H35	H35-1		NoCal
TT-C-A5-02	7	180.0	220.0	TENSMEG-120	119/(2)	122/(6)	H35	H35-2		NoCal
TT-C-G5-01	180	174.0	220.0	TENSMEG-120	119/(2)	121/(1)	H35	H35-1		NoCal
TT-C-K5-03	278	180.0	220.0	TENSMEG-120	119/(2)	122/(6)	H35	H35-3		NoCal
TT-C-D6-01	90	259.0	220.0	TENSMEG-120	119/(3)	121/(2)	H53	H53-1		NoCal
TT-C-D6-03	97	259.0	220.0	TENSMEG-120	119/(3)	121/(2)	H53	H53-3		NoCal
TF-M-Z6-01	135	244.0	218.0	EP-08-062AQ-350	120/(2)	121/(1)	V46	V46-1	WSG	NoCal
TF-M-Z6-02	135	244.0	218.0	EP-08-062AQ-350	120/(2)	121/(1)	V46	V46-1		NoCal
TF-M-Z9-01	135	380.0	218.0	EP-08-062AQ-350	120/(2)	121/(1)	V46	V46-1		NoCal
TF-M-Z9-02	135	380.0	218.0	EP-08-062AQ-350	120/(2)	121/(1)	V46	V46-1		NoCal
TF-M-E10-01	121	537.0	178.0	EP-08-062AQ-350	120/(2)	121/(1)	V46	V46-1		NoCal
TF-M-E10-02	121	537.0	178.0	EP-08-062AQ-350	120/(2)	121/(1)	V46	V46-1		NoCal
TF-M-D11-01	90	580.0	141.0	EP-08-062AQ-350	120/(2)	121/(1)	V46	V46-1		NoCal
TF-M-D11-02	90	580.0	141.0	EP-08-062AQ-350	120/(2)	121/(1)	V46	V46-1		NoCal
TF-M-I3-01	241	64.0	218.0	EP-08-062AQ-350	120/(1)	121/(2)	V37	V37-1		NoCal
TF-M-I3-02	241	64.0	218.0	EP-08-062AQ-350	120/(1)	121/(2)	V37	V37-1		NoCal
TF-M-I3-03	241	90.0	218.0	EP-08-062AQ-350	120/(1)	121/(2)	V37	V37-2		NoCal
TF-M-I3-04	241	90.0	218.0	EP-08-062AQ-350	120/(1)	121/(2)	V37	V37-2		NoCal
TF-M-I3-05	241	38.0	218.0	EP-08-062AQ-350	120/(1)	121/(2)	V37	V37-3		NoCal
TF-M-I9-01	241	380.0	218.0	EP-08-062AQ-350	120/(1)	121/(2)	V37	V37-1		NoCal
TF-M-I9-02	241	380.0	218.0	EP-08-062AQ-350	120/(1)	121/(2)	V37	V37-1		NoCal
TF-M-I9-03	241	406.0	218.0	EP-08-062AQ-350	120/(1)	121/(2)	V37	V37-2		NoCal
TF-M-I9-04	241	406.0	218.0	EP-08-062AQ-350	120/(1)	121/(2)	V37	V37-2		NoCal
TF-M-I9-05	241	354.0	218.0	EP-08-062AQ-350	120/(1)	121/(2)	V37	V37-3		NoCal
TF-M-I9-06	241	354.0	218.0	EP-08-062AQ-350	120/(1)	121/(2)	V37	V37-3		NoCal
TF-M-G12-01	180	615.0	87.0	EP-08-062AQ-350	120/(1)	121/(1)	V37	V37-1		NoCal
TF-M-G12-02	180	615.0	87.0	EP-08-062AQ-350	120/(1)	121/(1)	V37	V37-1		NoCal
TF-M-L9-01	325	380.0	218.0	EP-08-062AQ-350	120/(3)	122/(6)	V85	V85-1		NoCal
TF-M-L9-02	325	380.0	218.0	EP-08-062AQ-350	120/(3)	122/(6)	V85	V85-1		NoCal
TF-M-L9-03	325	380.0	218.0	EP-08-062AQ-350	120/(3)	122/(6)	V85	V85-1		NoCal
TF-M-L9-07	325	354.0	218.0	EP-08-062AQ-350	120/(3)	122/(6)	V85	V85-3		NoCal
TF-M-L9-08	325	354.0	218.0	EP-08-062AQ-350	120/(3)	122/(6)	V85	V85-3		NoCal
TF-M-L9-09	325	354.0	218.0	EP-08-062AQ-350	120/(3)	122/(6)	V85	V85-3		NoCal
TF-M-J11-01	270	588.0	132.0	EP-08-062AQ-350	120/(3)	121/(1)	V85	V85-1		NoCal
TF-M-J11-02	270	588.0	132.0	EP-08-062AQ-350	120/(3)	121/(1)	V85	V85-1		NoCal
TF-C-D3-01	90	73.0	220.0	EP-08-062AQ-350	119/(1)	121/(1)	H11	H11-1		NoCal
TF-C-D3-02	90	73.0	220.0	EP-08-062AQ-350	119/(1)	121/(1)	H11	H11-1		NoCal
TF-C-G3-02	180	73.0	220.0	EP-08-062AQ-350	119/(1)	121/(1)	H11	H11-1		NoCal
TF-C-I3-01	260	73.0	220.0	EP-08-062AQ-350	119/(1)	121/(1)	H11	H11-1		NoCal
TF-C-I3-02	260	73.0	220.0	EP-08-062AQ-350	119/(1)	121/(1)	H11	H11-1		NoCal
TF-C-I3-03	260	73.0	220.0	EP-08-062AQ-350	119/(1)	121/(1)	H11	H11-1		NoCal
TF-C-A5-01	0	180.0	220.0	EP-08-062AQ-350	119/(2)	122/(6)	H35	H35-1		NoCal

Tendon Instrumentation List

Labeling I D	Azimuthal Angle	Vertical Elevation	Radial Distance	Transducer Designation	Location Drawing #	Details Drawing #	Basic Mark #	Modified Mark #	Comnts	Calibration
(name)	(deg)	(in)	(in)			D-SN-P-				
TF-C-A5-02	0	180.0	220.0	EP-08-062AQ-350	119/(2)	122/(6)	H35	H35-1		NoCal
TF-C-A5-03	0	180.0	220.0	EP-08-062AQ-350	119/(2)	122/(6)	H35	H35-1		NoCal
TF-C-A5-04	7	180.0	220.0	EP-08-062AQ-350	119/(2)	122/(6)	H35	H35-2		NoCal
TF-C-A5-05	7	180.0	220.0	EP-08-062AQ-350	119/(2)	122/(6)	H35	H35-2		NoCal
TF-C-A5-06	7	180.0	220.0	EP-08-062AQ-350	119/(2)	122/(6)	H35	H35-2		NoCal
TF-C-G5-01	180	174.0	220.0	EP-08-062AQ-350	119/(2)	121/(1)	H35	H35-1		NoCal
TF-C-G5-02	180	174.0	220.0	EP-08-062AQ-350	119/(2)	121/(1)	H35	H35-1		NoCal
TF-C-K5-07	278	180.0	220.0	EP-08-062AQ-350	119/(2)	122/(6)	H35	H35-3		NoCal
TF-C-K5-08	278	180.0	220.0	EP-08-062AQ-350	119/(2)	122/(6)	H35	H35-3		NoCal
TF-C-K5-09	278	180.0	220.0	EP-08-062AQ-350	119/(2)	122/(6)	H35	H35-3		NoCal
TF-C-D6-01	90	259.0	220.0	EP-08-062AQ-350	119/(3)	121/(2)	H53	H53-1		NoCal
TF-C-D6-02	90	259.0	220.0	EP-08-062AQ-350	119/(3)	121/(2)	H53	H53-1		NoCal
TF-C-D6-05	97	259.0	220.0	EP-08-062AQ-350	119/(3)	121/(2)	H53	H53-3		NoCal
TF-C-D6-06	97	259.0	220.0	EP-08-062AQ-350	119/(3)	121/(2)	H53	H53-3		NoCal
TF-C-K6-03	280	259.0	220.0	EP-08-062AQ-350	119/(3)	122/(5)	H53	H53-1		NoCal
TF-C-A7-01	0	321.0	220.0	EP-08-062AQ-350	119/(4)	121/(3)	H67	H67-1		NoCal
TF-C-A7-02	0	321.0	220.0	EP-08-062AQ-350	119/(4)	121/(3)	H67	H67-1		NoCal
TF-C-A7-03	0	321.0	220.0	EP-08-062AQ-350	119/(4)	121/(3)	H67	H67-1		NoCal
TF-C-D7-01	90	321.0	220.0	EP-08-062AQ-350	119/(4)	121/(3)	H67	H67-1		NoCal
TF-C-D7-02	90	321.0	220.0	EP-08-062AQ-350	119/(4)	121/(3)	H67	H67-1		NoCal
TF-C-D7-03	90	321.0	220.0	EP-08-062AQ-350	119/(4)	121/(3)	H67	H67-1		NoCal
TF-C-Z7-01	135	321.0	220.0	EP-08-062AQ-350	119/(4)	121/(3)	H67	H67-1		NoCal
TF-C-K7-01	280	321.0	220.0	EP-08-062AQ-350	119/(4)	121/(3)	H67	H67-1		NoCal
TF-C-K7-02	280	321.0	220.0	EP-08-062AQ-350	119/(4)	121/(3)	H67	H67-1		NoCal
TF-C-K7-03	280	321.0	220.0	EP-08-062AQ-350	119/(4)	121/(3)	H67	H67-1		NoCal
TF-C-E8-03	105	326.0	220.0	EP-08-062AQ-350	119/(5)	121/(4)	H68	H68-1		NoCal
TF-C-E8-07	98	326.0	220.0	EP-08-062AQ-350	119/(5)	121/(4)	H68	H68-3		NoCal
TF-C-E8-08	98	326.0	220.0	EP-08-062AQ-350	119/(5)	121/(4)	H68	H68-3		NoCal
TF-C-E8-09	98	326.0	220.0	EP-08-062AQ-350	119/(5)	121/(4)	H68	H68-3		NoCal
TF-C-Z8-01	135	326.0	220.0	EP-08-062AQ-350	119/(5)	121/(3)	H68	H68-1		NoCal
TF-C-Z8-03	135	326.0	220.0	EP-08-062AQ-350	119/(5)	121/(3)	H68	H68-1		NoCal
TF-C-G8-02	180	326.0	220.0	EP-08-062AQ-350	119/(5)	121/(3)	H68	H68-1		NoCal
TF-C-G8-03	180	326.0	220.0	EP-08-062AQ-350	119/(5)	121/(3)	H68	H68-1		NoCal
TF-C-J8-01	270	326.0	220.0	EP-08-062AQ-350	119/(5)	121/(4)	H68	H68-1		NoCal
TF-C-J8-02	270	326.0	220.0	EP-08-062AQ-350	119/(5)	121/(4)	H68	H68-1		NoCal
TF-C-J8-03	270	326.0	220.0	EP-08-062AQ-350	119/(5)	121/(4)	H68	H68-1		NoCal
TF-C-J8-07	277	326.0	220.0	EP-08-062AQ-350	119/(5)	121/(4)	H68	H68-3		NoCal
TF-C-J8-08	277	326.0	220.0	EP-08-062AQ-350	119/(5)	121/(4)	H68	H68-3		NoCal
TF-C-J8-09	277	326.0	220.0	EP-08-062AQ-350	119/(5)	121/(4)	H68	H68-3		NoCal
TL-M-A0-03	1	-46.0	218.0	GK-3000-200-2.0	-QCON-06i	N/A	V67	V67	Vert.	PreCal
TL-M-A0-05	13	-46.0	218.0	GK-3000-200-2.0	-QCON-06i	N/A	V61	V61	Load	PreCal
TL-M-B0-02	25	-46.0	218.0	GK-3000-200-2.0	-QCON-06i	N/A	V55	V55	Cells	PreCal
TL-M-B0-04	37	-46.0	218.0	GK-3000-200-2.0	-QCON-06i	N/A	V49	V49		PreCal
TL-M-B0-05	43	-46.0	218.0	GK-3000-200-2.0	-QCON-06i	N/A	V46	V46		PreCal
TL-M-C0-01	45	-46.0	218.0	GK-3000-200-2.0	-QCON-06i	N/A	V1	V1		PreCal
TL-M-C0-03	57	-46.0	218.0	GK-3000-200-2.0	-QCON-06i	N/A	V7	V7		PreCal
TL-M-C0-05	69	-46.0	218.0	GK-3000-200-2.0	-QCON-06i	N/A	V13	V13		PreCal
TL-M-D0-02	81	-46.0	218.0	GK-3000-200-2.0	-QCON-06i	N/A	V19	V19		PreCal
TL-M-D0-04	93	-46.0	218.0	GK-3000-200-2.0	-QCON-05i	N/A	V25	V25		PreCal
TL-M-E0-01	105	-46.0	218.0	GK-3000-200-2.0	-QCON-05i	N/A	V31	V31		PreCal
TL-M-E0-03	117	-46.0	218.0	GK-3000-200-2.0	-QCON-05i	N/A	V37	V37		PreCal
TL-M-Z0-01	129	-46.0	218.0	GK-3000-200-2.0	-QCON-05i	N/A	V43	V43		PreCal
TL-M-Z0-02	135	-46.0	218.0	HBM-C6-100t	-QCON-05i	N/A	V46	V46		PreCal
TL-M-Z0-03	141	-46.0	218.0	GK-3000-200-2.0	-QCON-05i	N/A	V49	V49		PreCal
TL-M-F0-02	153	-46.0	218.0	GK-3000-200-2.0	-QCON-05i	N/A	V55	V55		PreCal
TL-M-G0-01	165	-46.0	218.0	GK-3000-200-2.0	-QCON-05i	N/A	V61	V61		PreCal
TL-M-G0-03	177	-46.0	218.0	GK-3000-200-2.0	-QCON-05i	N/A	V67	V67		PreCal

Tendon Instrumentation List

Labeling I D	Azimuthal Angle	Vertical Elevation	Radial Distance	Transducer Designation	Location Drawing #	Details Drawing #	Basic Mark #	Modified Mark #	Comnts	Calibration
(name)	(deg)	(in)	(in)			D-SN-P-				
TL-M-G0-05	189	-46.0	218.0	GK-3000-200-2.0	-QCON-05i	N/A	V73	V73		PreCal
TL-M-H0-02	201	-46.0	218.0	GK-3000-200-2.0	-QCON-05i	N/A	V79	V79		PreCal
TL-M-H0-04	213	-46.0	218.0	GK-3000-200-2.0	-QCON-05i	N/A	V85	V85		PreCal
TL-M-I0-01	229	-46.0	218.0	GK-3000-200-2.0	-QCON-05i	N/A	V43	V43		PreCal
TL-M-I0-03	241	-46.0	218.0	HBM-C6-100t	-QCON-05i	N/A	V37	V37		PreCal
TL-M-I0-05	253	-46.0	218.0	GK-3000-200-2.0	-QCON-05i	N/A	V31	V31		PreCal
TL-M-J0-02	265	-46.0	218.0	GK-3000-200-2.0	-QCON-05i	N/A	V25	V25		PreCal
TL-M-J0-04	277	-46.0	218.0	GK-3000-200-2.0	-QCON-06i	N/A	V19	V19		PreCal
TL-M-K0-01	289	-46.0	218.0	GK-3000-200-2.0	-QCON-06i	N/A	V13	V13		PreCal
TL-M-K0-03	301	-46.0	218.0	GK-3000-200-2.0	-QCON-06i	N/A	V7	V7		PreCal
TL-M-K0-05	313	-46.0	218.0	GK-3000-200-2.0	-QCON-06i	N/A	V1	V1		PreCal
TL-M-L0-02	325	-46.0	218.0	HBM-C6-100t	-QCON-06i	N/A	V85	V85		PreCal
TL-M-L0-04	337	-46.0	218.0	GK-3000-200-2.0	-QCON-06i	N/A	V79	V79		PreCal
TL-M-A0-01	349	-46.0	218.0	GK-3000-200-2.0	-QCON-06i	N/A	V73	V73		PreCal
TL-C-D3-01	85	44.0	230.0	GK-3000-200-2.0	-QCON-06i	N/A	H4	H4	Hoop	PreCal
TL-C-D3-02	95	41.0	230.0	GK-3000-200-2.0	-QCON-05i	N/A	H4	H4	Load	PreCal
TL-C-D4-01	85	106.0	230.0	GK-3000-200-2.0	-QCON-06i	N/A	H18	H18	Cells	PreCal
TL-C-D4-02	95	103.0	230.0	GK-3000-200-2.0	-QCON-05i	N/A	H18	H18	90 Deg.	PreCal
TL-C-D5-01	85	159.0	230.0	GK-3000-200-2.0	-QCON-06i	N/A	H30	H30		PreCal
TL-C-D5-02	95	156.0	230.0	GK-3000-200-2.0	-QCON-05i	N/A	H30	H30		PreCal
TL-C-D5-03	85	203.0	230.0	GK-3000-200-2.0	-QCON-06i	N/A	H40	H40		PreCal
TL-C-D5-04	95	200.0	230.0	GK-3000-200-2.0	-QCON-05i	N/A	H40	H40		PreCal
TL-C-D6-01	85	230.0	230.0	GK-3000-200-2.0	-QCON-06i	N/A	H46	H46		PreCal
TL-C-D6-02	95	227.0	230.0	GK-3000-200-2.0	-QCON-05i	N/A	H46	H46		PreCal
TL-C-D7-01	85	283.0	230.0	GK-3000-200-2.0	-QCON-06i	N/A	H58	H58		PreCal
TL-C-D7-02	95	280.0	230.0	GK-3000-200-2.0	-QCON-05i	N/A	H58	H58		PreCal
TL-C-D8-01	85	327.0	230.0	HBM-C6-100t	-QCON-06i	N/A	H68	H68		PreCal
TL-C-D8-02	95	324.0	230.0	HBM-C6-100t	-QCON-05i	N/A	H68	H68		PreCal
TL-C-D9-01	85	389.0	230.0	GK-3000-200-2.0	-QCON-06i	N/A	H82	H82		PreCal
TL-C-D9-02	95	386.0	230.0	GK-3000-200-2.0	-QCON-05i	N/A	H82	H82		PreCal
TL-C-D10-01	85	481.0	230.0	GK-3000-200-2.0	-QCON-06i	N/A	H96	H96		PreCal
TL-C-D10-02	95	478.0	230.0	GK-3000-200-2.0	-QCON-05i	N/A	H96	H96		PreCal
TL-C-J3-01	265	75.0	230.0	GK-3000-200-2.0	-QCON-05i	N/A	H11	H11	Hoop	PreCal
TL-C-J3-02	275	72.0	230.0	HBM-C6-100t	-QCON-06i	N/A	H11	H11	Load	PreCal
TL-C-J4-01	265	137.0	230.0	GK-3000-200-2.0	-QCON-05i	N/A	H25	H25	Cells	PreCal
TL-C-J4-02	275	134.0	230.0	GK-3000-200-2.0	-QCON-06i	N/A	H25	H25	270 Deg	PreCal
TL-C-J5-01	265	181.0	230.0	HBM-C6-100t	-QCON-05i	N/A	H35	H35		PreCal
TL-C-J5-02	275	178.0	230.0	HBM-C6-100t	-QCON-06i	N/A	H35	H35		PreCal
TL-C-J6-01	265	261.0	230.0	HBM-C6-100t	-QCON-05i	N/A	H53	H53		PreCal
TL-C-J6-02	275	258.0	230.0	GK-3000-200-2.0	-QCON-06i	N/A	H53	H53		PreCal
TL-C-J7-01	265	305.0	230.0	GK-3000-200-2.0	-QCON-05i	N/A	H63	H63		PreCal
TL-C-J7-02	275	302.0	230.0	GK-3000-200-2.0	-QCON-06i	N/A	H63	H63		PreCal
TL-C-J7-03	265	323.0	230.0	HBM-C6-100t	-QCON-05i	N/A	H67	H67		PreCal
TL-C-J7-04	275	320.0	230.0	HBM-C6-100t	-QCON-06i	N/A	H67	H67		PreCal
TL-C-J8-01	265	358.0	230.0	GK-3000-200-2.0	-QCON-05i	N/A	H75	H75		PreCal
TL-C-J8-02	275	355.0	230.0	GK-3000-200-2.0	-QCON-06i	N/A	H75	H75		PreCal
TL-C-J9-01	265	420.0	230.0	GK-3000-200-2.0	-QCON-05i	N/A	H89	H89		PreCal
TL-C-J9-02	275	417.0	230.0	GK-3000-200-2.0	-QCON-06i	N/A	H89	H89		PreCal
TL-C-J10-01	265	543.0	230.0	GK-3000-200-2.0	-QCON-05i	N/A	H103	H103		PreCal
TL-C-J10-02	275	540.0	230.0	GK-3000-200-2.0	-QCON-06i	N/A	H103	H103		PreCal

NoCal - No calibration was performed on this instrument before or after model testing

PreCal - Calibration was performed on this instrument prior to model testing only

Other Instrumentation List

Labeling I D	Azimuthal Angle	Vertical Elevation	Radial Distance	Transducer Designation	Location Drawing #	Details Drawing #	Basic Mark #	Modified Mark #	Comnts	Calibration
(name)	(deg)	(in)	(in)			D-SN-P-				
TC-R-D0-01	90	-134.0	48.0	K-24-2-505	PCCV-F-1i	N/A	N/A	N/A	(Thermoc.	NoCal
TC-R-D0-02	90	-104.0	48.0	K-24-2-505	PCCV-F-1i	N/A	N/A	N/A	embedded	NoCal
TC-R-D0-03	90	-104.0	200.0	K-24-2-505	PCCV-F-1i	N/A	N/A	N/A	basemat)	NoCal
TC-R-D0-04	90	-6.0	48.0	CASS-116U-240	PCCV-F-8i	N/A	N/A	N/A		NoCal
TC-R-D0-05	90	-36.0	214.0	CASS-116U-240	PCCV-F-5i	N/A	N/A	N/A		NoCal
TC-R-Z0-01	135	-36.0	214.0	CASS-116U-240	PCCV-F-5i	N/A	N/A	N/A		NoCal
TW-R-A2-01	0	10.0	218.0	TQSS-116U-180	PCCV-S-8ii	N/A	N/A	N/A	(Thermoc.	NoCal
TW-R-A4-01	0	104.0	218.0	TQSS-116U-72	PCCV-S-8ii	N/A	N/A	N/A	embedded	NoCal
TW-R-A5-01	0	184.0	218.0	TQSS-116U-72	PCCV-S-8ii	N/A	N/A	N/A	cylinder	NoCal
TW-R-A5-02	349	184.0	218.0	TQSS-116U-72	PCCV-S-8ii	N/A	N/A	N/A	& dome)	NoCal
TW-R-A6-01	0	244.0	218.0	TQSS-116U-72	PCCV-S-8ii	N/A	N/A	N/A		NoCal
TW-R-A7-01	0	304.0	218.0	TQSS-116U-72	PCCV-S-8ii	N/A	N/A	N/A		NoCal
TW-R-A9-01	0	423.0	218.0	TQSS-116U-72	PCCV-S-8ii	N/A	N/A	N/A		NoCal
TW-R-A11-01	0	573.0	158.0	TQSS-116U-240	PCCV-D-6ii	N/A	N/A	N/A		NoCal
TW-R-C5-01	44	184.0	218.0	TQSS-116U-96	PCCV-S-8ii	N/A	N/A	N/A		NoCal
TW-R-C5-02	62	125.0	218.0	TQSS-116U-96	PCCV-S-8ii	N/A	N/A	N/A		NoCal
TW-R-C5-03	62	230.0	218.0	TQSS-116U-96	PCCV-S-8ii	N/A	N/A	N/A		NoCal
TW-R-C5-04	80	184.0	218.0	TQSS-116U-96	PCCV-S-8ii	N/A	N/A	N/A		NoCal
TW-R-D2-01	90	10.0	222.0	TQSS-116U-180	PCCV-S-8ii	N/A	N/A	N/A		NoCal
TW-R-D4-01	90	104.0	222.0	TQSS-116U-96	PCCV-S-8ii	N/A	N/A	N/A		NoCal
TW-R-D5-01	90	184.0	222.0	TQSS-116U-96	PCCV-S-8ii	N/A	N/A	N/A		NoCal
TW-R-D7-01	90	304.0	222.0	TQSS-116U-96	PCCV-S-8ii	N/A	N/A	N/A		NoCal
TW-R-D9-01	90	423.0	222.0	TQSS-116U-72	PCCV-S-8ii	N/A	N/A	N/A		NoCal
TW-R-D11-01	62	180.0	220.0	TQSS-116U-240	PCCV-D-6ii	N/A	N/A	N/A	A/L	NoCal
TW-R-Z2-01	135	10.0	218.0	TQSS-116U-180	PCCV-S-7ii	N/A	N/A	N/A		NoCal
TW-R-Z4-01	135	104.0	218.0	TQSS-116U-72	PCCV-S-7ii	N/A	N/A	N/A		NoCal
TW-R-Z5-01	135	184.0	218.0	TQSS-116U-96	PCCV-S-7ii	N/A	N/A	N/A		NoCal
TW-R-Z6-01	135	244.0	218.0	TQSS-116U-96	PCCV-S-7ii	N/A	N/A	N/A		NoCal
TW-R-Z7-01	135	304.0	218.0	TQSS-116U-96	PCCV-S-7ii	N/A	N/A	N/A		NoCal
TW-R-Z9-01	135	423.0	218.0	TQSS-116U-72	PCCV-S-7ii	N/A	N/A	N/A		NoCal
TW-R-Z11-01	135	573.0	158.0	TQSS-116U-240	PCCV-D-6ii	N/A	N/A	N/A		NoCal
TW-R-Z13-01	-	640.0	0.0	TQSS-116U-480	PCCV-D-6ii	N/A	N/A	N/A		NoCal
TW-R-G5-01	180	184.0	218.0	TQSS-116U-96	PCCV-S-7ii	N/A	N/A	N/A		NoCal
TW-R-I2-01	240	10.0	218.0	TQSS-116U-180	PCCV-S-7ii	N/A	N/A	N/A		NoCal
TW-R-I5-01	240	184.0	218.0	TQSS-116U-96	PCCV-S-7ii	N/A	N/A	N/A		NoCal
TW-R-I9-01	240	423.0	218.0	TQSS-116U-72	PCCV-S-7ii	N/A	N/A	N/A		NoCal
TW-R-I11-01	324	184.0	220.0	TQSS-116U-240	PCCV-D-6ii	N/A	N/A	N/A	E/H	NoCal
TW-R-K5-01	299	184.0	218.0	TQSS-116U-96	PCCV-S-8ii	N/A	N/A	N/A		NoCal
TW-R-L2-01	324	10.0	218.0	TQSS-116U-180	PCCV-S-8ii	N/A	N/A	N/A		NoCal
TW-R-L4-01	324	79.0	218.0	TQSS-116U-96	PCCV-S-8ii	N/A	N/A	N/A		NoCal
TW-R-L7-01	324	289.0	218.0	TQSS-116U-96	PCCV-S-8ii	N/A	N/A	N/A		NoCal
TW-R-L9-01	324	423.0	218.0	TQSS-116U-72	PCCV-S-8ii	N/A	N/A	N/A		NoCal
TW-R-L11-01	324	573.0	158.0	TQSS-116U-240	PCCV-D-6ii	N/A	N/A	N/A		NoCal
RT-M-A3-01	0	40.0	150.0	RTD-805	TBD	N/A	N/A	N/A	(RTD	NoCal
RT-M-A5-01	0	170.0	150.0	RTD-805	TBD	N/A	N/A	N/A	inside	NoCal
RT-M-A7-01	0	290.0	150.0	RTD-805	TBD	N/A	N/A	N/A	air	NoCal
RT-M-A9-01	0	423.0	150.0	RTD-805	TBD	N/A	N/A	N/A	Temp.)	NoCal
RT-M-A10-01	0	533.0	120.0	RTD-805	TBD	N/A	N/A	N/A		NoCal
RT-M-D3-01	90	40.0	150.0	RTD-805	TBD	N/A	N/A	N/A		NoCal
RT-M-D5-01	90	170.0	150.0	RTD-805	TBD	N/A	N/A	N/A		NoCal
RT-M-D7-01	90	290.0	150.0	RTD-805	TBD	N/A	N/A	N/A		NoCal
RT-M-D9-01	90	423.0	150.0	RTD-805	TBD	N/A	N/A	N/A		NoCal

Other Instrumentation List

Labeling I D	Azimuthal Angle	Vertical Elevation	Radial Distance	Transducer Designation	Location Drawing #	Details Drawing #	Basic Mark #	Modified Mark #	Comnts	Calibration
(name)	(deg)	(in)	(in)			D-SN-P-				
RT-M-D10-01	90	533.0	120.0	RTD-805	TBD	N/A	N/A	N/A		NoCal
RT-M-Z12-01	-	608.0	0.0	RTD-805	TBD	N/A	N/A	N/A		NoCal
RT-M-G3-01	180	40.0	150.0	RTD-805	TBD	N/A	N/A	N/A		NoCal
RT-M-G5-01	180	170.0	150.0	RTD-805	TBD	N/A	N/A	N/A		NoCal
RT-M-G7-01	180	290.0	150.0	RTD-805	TBD	N/A	N/A	N/A		NoCal
RT-M-G9-01	180	423.0	150.0	RTD-805	TBD	N/A	N/A	N/A		NoCal
RT-M-G10-01	180	533.0	120.0	RTD-805	TBD	N/A	N/A	N/A		NoCal
RT-M-J3-01	270	40.0	150.0	RTD-805	TBD	N/A	N/A	N/A		NoCal
RT-M-J5-01	270	170.0	150.0	RTD-805	TBD	N/A	N/A	N/A		NoCal
RT-M-J7-01	270	290.0	150.0	RTD-805	TBD	N/A	N/A	N/A		NoCal
RT-M-J9-01	270	423.0	150.0	RTD-805	TBD	N/A	N/A	N/A		NoCal
RT-M-J10-01	270	533.0	120.0	RTD-805	TBD	N/A	N/A	N/A		NoCal
RT-R-G0-01	180	-60.0	400.0	RTD-805	TBD	N/A	N/A	N/A	Outside	NoCal
PG-R-G4-01	180	96.5	230.0	4040	N/A	N/A	N/A	N/A	(pressure	PostOK
PG-R-G4-02	180	96.5	230.0	4040	N/A	N/A	N/A	N/A	gages)	PostOK
PG-R-G2-01	180	5.0	200.0						Hydro	
PG-R-G6-01	180	210.0	200.0						Pressure	
PG-R-G9-01	180	423.0	200.0						Gages	
CE-M-Z2-01	135	10.0	214.0	SOFO-500	TBD	N/A	684	684	(fiber	NoCal
CE-M-Z2-02	135	10.0	221.0	SOFO-500	TBD	N/A	683	683	optic	NoCal
CE-M-A6-01	0	244.0	214.0	SOFO-500	TBD	N/A	682	682	concrete	NoCal
CE-M-A6-02	0	244.0	221.0	SOFO-500	TBD	N/A	738	738	gages)	NoCal
CE-C-Z6-01	135	244.0	214.0	SOFO-500	TBD	N/A	685	685		NoCal
CE-C-Z6-02	135	244.0	221.0	SOFO-500	TBD	N/A	687	687		NoCal
CE-C-Z11-01	135	573.0	157.0	SOFO-500	TBD	N/A	776	776		NoCal
A00	0	423.0	224.0						Acoustic	PreCal
A01	0	304.0	224.0						Sensors	PreCal
A02	0	184.0	224.0						(Ext)	PreCal
A03	0	10.0	224.0							PreCal
A04	0	-79.0	206.0							PreCal
A05	62	423.0	224.0							PreCal
A06	62	304.0	224.0							PreCal
A07	60	10.0	224.0							PreCal
A08	60	-79.0	206.0							PreCal
A09	90	580.0	170.0							PreCal
A10	90	423.0	230.0							PreCal
A11	90	244.0	230.0							PreCal
A12	90	127.0	230.0							PreCal
A13	90	10.0	230.0							PreCal
A14	120	-79.0	206.0							PreCal
A15	150	423.0	224.0							PreCal
A16	150	304.0	224.0							PreCal
A17	150	184.0	224.0							PreCal
A18	150	10.0	224.0							PreCal
A19	180	644.0	0.0							PreCal
A20	180	184.0	224.0							PreCal
A21	180	10.0	224.0							PreCal
A22	180	-79.0	206.0							PreCal
A23	210	423.0	224.0							PreCal
A24	210	304.0	224.0							PreCal
A25	210	184.0	224.0							PreCal
A26	210	10.0	224.0							PreCal
A27	240	-79.0	206.0							PreCal
A28	270	580.0	170.0							PreCal
A29	270	423.0	230.0							PreCal

Other Instrumentation List

Labeling	Azimuthal	Vertical	Radial	Transducer	Location	Details	Basic	Modified	Comnts	Calibration
I D	Angle	Elevation	Distance	Designation	Drawing #	Drawing #	Mark #	Mark #		
(name)	(deg)	(in)	(in)			D-SN-P-				
A30	270	244.0	230.0							PreCal
A31	270	127.0	230.0							PreCal
A32	270	10.0	230.0							PreCal
A33	285	304.0	224.0							PreCal
A34	285	56.0	224.0							PreCal
A35	300	-79.0	206.0							PreCal
A36	318	423.0	224.0							PreCal
A37	324	10.0	224.0							PreCal

NoCal - No calibration was performed on this instrument before or after model testing

PreCal - Calibration was performed on this instrument prior to model testing only

PostOK - Calibration was performed on this instrument Before and After model testing and remained within tolerance

Appendix I: Data File Index

Converted Data

01. BPS (Before Prestressing)

DISP_CVTD_DOR_BPS.xls
DISP_CVTD_DYN_BPS.xls
GBST_CVTD_DOR_BPS.xls
GBST_CVTD_DYN_BPS.xls
LINST_CVTD_DOR_BPS.xls
LINST_CVTD_DYN_BPS.xls
PRES_CVTD_DOR_BPS.xls
PRES_CVTD_DYN_BPS.xls
REBST_CVTD_DOR_BPS.xls
REBST_CVTD_DYN_BPS.xls
TEMP_CVTD_DOR_BPS.xls
TEMP_CVTD_DYN_BPS.xls
TENDON_CVTD_DOR_BPS.xls
TENDON_CVTD_DYN_BPS.xls

02. PS (Prestressing)

DISP_CVTD_DOR_PS.xls
DISP_CVTD_DYN_PS1.xls
DISP_CVTD_DYN_PS2.xls
DISP_CVTD_DYN_PS3.xls
GBST_CVTD_DOR_PS.xls
GBST_CVTD_DYN_PS1.xls
GBST_CVTD_DYN_PS2.xls
GBST_CVTD_DYN_PS3.xls
LINST_CVTD_DOR_PS.xls
LINST_CVTD_DYN_PS1.xls
LINST_CVTD_DYN_PS2.xls
LINST_CVTD_DYN_PS3.xls
PRES_CVTD_DOR_PS.xls
PRES_CVTD_DYN_PS1.xls
PRES_CVTD_DYN_PS2.xls
PRES_CVTD_DYN_PS3.xls
RBST_CVTD_DOR_PS.xls
RBST_CVTD_DYN_PS1.xls
RBST_CVTD_DYN_PS2.xls
RBST_CVTD_DYN_PS3.xls
TEMP_CVTD_DOR_PS.xls
TEMP_CVTD_DYN_PS1.xls
TEMP_CVTD_DYN_PS2.xls
TEMP_CVTD_DYN_PS3.xls
TENDON_CVTD_DOR_PS.xls
TENDON_CVTD_DYN_PS1.xls
TENDON_CVTD_DYN_PS2.xls
TENDON_CVTD_DYN_PS3.xls

03. PPS (Post-Prestressing)

DISP_CVTD_DYN_PPS.xls
GBST_CVTD_DYN_PPS.xls
LINST_CVTD_DYN_PPS.xls
PRES_CVTD_DYN_PPS.xls
REBST_CVTD_DYN_PPS.xls
REBST_CVTD_DYN_PPS.xls
SOFO_CVTD_DYN_PPS.xls
TENDON_CVTD_DYN_PPS.xls

04. SFT (System Functionality Test)

DISP_CVTD_DOR_SFT.xls
DISP_CVTD_DYN_SFT.xls
GBST_CVTD_DOR_SFT.xls
GBST_CVTD_DYN_SFT.xls
LINST_CVTD_DOR_SFT.xls
LINST_CVTD_DYN_SFT.xls
PRES_CVTD_DOR_SFT.xls
PRES_CVTD_DYN_SFT.xls
REBST_CVTD_DOR_SFT.xls
REBST_CVTD_DYN_SFT.xls
TEMP_CVTD_DOR_SFT.xls
TEMP_CVTD_DYN_SFT.xls
TENDON_CVTD_DOR_SFT.xls
TENDON_CVTD_DYN_SFT.xls

05. PSFT (Post-System Functionality Test)

DISP_CVTD_DYN_PSFT.xls
GBST_CVTD_DYN_PSFT.xls
LINST_CVTD_DYN_PSFT.xls
PRES_CVTD_DYN_PSFT.xls
REBST_CVTD_DYN_PSFT.xls
TEMP_CVTD_DYN_PSFT.xls
TENDON_CVTD_DYN_PSFT.xls

06. SITILRT (Structural Integrity Test/Integrated Leak Rate Test)

DISP_CVTD_DOR_SITILRT.xls
DISP_CVTD_DYN_SITILRT.xls
GBST_CVTD_DOR_SITILRT.xls
GBST_CVTD_DYN_SITILRT.xls
LINST_CVTD_DOR_SITILRT.xls
LINST_CVTD_DYN_SITILRT.xls
PRES_CVTD_DOR_SITILRT.xls
PRES_CVTD_DYN_SITILRT.xls
REBST_CVTD_DOR_SITILRT.xls
REBST_CVTD_DYN_SITILRT.xls
TEMP_CVTD_DOR_SITILRT.xls
TEMP_CVTD_DYN_SITILRT.xls
TENDON_CVTD_DOR_SITILRT.xls
TENDON_CVTD_DYN_SITILRT.xls

07. PSITILRT (Post-Structural Integrity Test/Integrated Leak Rate Test)

DISP_CVTD_DYN_PSITILRT.xls
GBST_CVTD_DYN_PSITILRT.xls
LINST_CVTD_DYN_PSITILRT.xls
PRES_CVTD_DYN_PSITILRT.xls
RBST_CVTD_DYN_PSITILRT.xls
TEMP_CVTD_DYN_PSITILRT.xls
TENDON_CVTD_DYN_PSITILRT.xls

08. LST (Limit State Test)

DISP_CVTD_DOR_LST.xls
DISP_CVTD_DYN_LST.xls
GBST_CVTD_DOR_LST.xls
GBST_CVTD_DYN_LST.xls
LINST_CVTD_DOR_LST.xls
LINST_CVTD_DYN_LST.xls
PRES_CVTD_DOR_LST.xls
PRES_CVTD_DYN_LST.xls
REBST_CVTD_DOR_LST.xls
REBST_CVTD_DYN_LST.xls
SOFO_CVTD_DOR_LST.xls
SOFO_CVTD_DYN_LST.xls
TEMP_CVTD_DOR_LST.xls
TEMP_CVTD_DYN_LST.xls
TENDON_CVTD_DOR_LST.xls
TENDON_CVTD_DYN_LST.xls

09. PLST (Post-Limit State Test)

DISP_CVTD_DYN_PLST.xls
GBST_CVTD_DYN_PLST.xls
LINST_CVTD_DYN_PLST.xls
PRES_CVTD_DYN_PLST.xls
REBST_CVTD_DYN_PLST.xls
SOFO_CVTD_DYN_PLST.xls
TEMP_CVTD_DYN_PLST.xls
TENDON_CVTD_DYN_PLST.xls

10. SFMT (Structural Failure Mode Test)

ACOUSTIC_SFMT.xls
DISP_CVTD_DYN_SFMT.xls
GBST_CVTD_DYN_SFMT.xls
LINST_CVTD_DYN_SFMT.xls
PRES_CVTD_DYN_SFMT.xls
REBST_CVTD_DYN_SFMT.xls
SOFO_CVTD_DYN_SFMT.xls
SOL_CVTD_SFMT.xls
TENDON_CVTD_DYN_SFMT.xls

Acoustic Event Times

LST/PLST and SFMT Dynamic Data for
all Standard Output Locations

Corrected Data (LST)

DISP_COR_DOR_LST.xls
DISP_COR_DYN_LST.xls
GBST_COR_DOR_LST.xls
GBST_COR_DYN_LST.xls
LINST_COR_DOR_LST.xls
LINST_COR_DYN_LST.xls
REBST_COR_DOR_LST.xls
REBST_COR_DYN_LST.xls
TENDON_COR_DOR_LST.xls
TENDON_COR_DYN_LST.xls

SFMT Video Files

PCCV_SFMT2.mpg

Appendix J: Data Correction for Ambient Thermal Response

J.1 Overview of Instrumentation

As part of the post-test analysis effort, ANATECH was also tasked with reviewing and standardizing the measurements taken during the Limit State Test (LST). There are a variety of factors that can influence gage read-outs so the goal of this standardization effort was to identify these factors and, to the extent that their influence is significant, adjust the raw data to produce a uniform data set.

Detailed presentation and discussion of the PCCV instrumentation is beyond the scope of this Appendix. The instrumentation measurements that were addressed in the "data correction" effort, and the effects and phenomena that were addressed, are listed in Table J.1.

Table J.1

Measurement	Name Abbreviation	Effects Considered for Correction
Displacement	DISP	Temp., Rigid Body Motion
Strains in Special Gaged Rebars	GBST	Temp., Strain Localization
Strains in Liner	LINST	Temp.
Pressure	PRES	--
Strains in Rebar	REBST	Temp., Strain Localization
Tendon Strains	TENDON	Temp.
Temperatures	TEMP	--

The data acquisition system was installed and activated more than seven months prior to the LST. Gage measurements taken at various time intervals throughout this seven months have provided a vast database of the model's response to changes in temperature. Since the goal of the "data correction" effort is to create a standardized set of data that is free of temperature effects, two sets of this history data were extracted from the data base to calibrate a correction formula for each individual gage. These two datasets are the following: 1) March X - March Y, Before Prestressing (BPS) and 2) August 7-9, Post System Functionality Test, PSFT. The datasets are also designated as "dynamic" data (DYN) and "data of record" (DOR). The dynamic data represents nearly continuous scanning of data, at every frequent intervals, regardless of whether strain and displacement readings have stabilized, and the DOR are scanned only at pressure holds (during the LST) after gage readings have reached a stability criteria. The filenames for the data, therefore, are as listed in Table J.2 below.

Table J-2. Gage Data Filename Matrix

Data Type	DYN_BPS	DYN_PSFT	DYN_LST	DOR_LST
DISP_CVTD	X	X	X	X
GBST_CVTD	X	X	X	X
LINST_CVTD	X	X	X	X
PRES_CVTD			X	X
REBST_CVTD	X	X	X	X
TEDON_CVTD	X	X	X	X
TEMP_CVTD	X	X	X	X

The "DYN_BPS" and DYN_PSFT" data are used to develop the correction algorithms and the "DYN_LST" and "DOR_LST" are the data that are corrected. ANATECH was also tasked with correcting SOL_CVTD_LST_PLST, the standard output location data file.

J.2 Temperature Effects on Measurements

Change in temperature has a direct influence on the strains and displacements of a free-standing structure. Further, temperature changes have secondary effects on the voltage readouts of strain gages. Both of these effects have been considered and quantified in the data correction effort, the former being calibrated by direct observation of the model response during the two calibration periods and the latter being provided by the gage manufacturer. To correct for either phenomena, first requires that the temperature be known at every gage, or in effect, at all possible locations within the PCCV. This information has been obtained by developing a temperature mapping algorithm based on interpolation between the matrix of temperature gages. Development of this algorithm is described below.

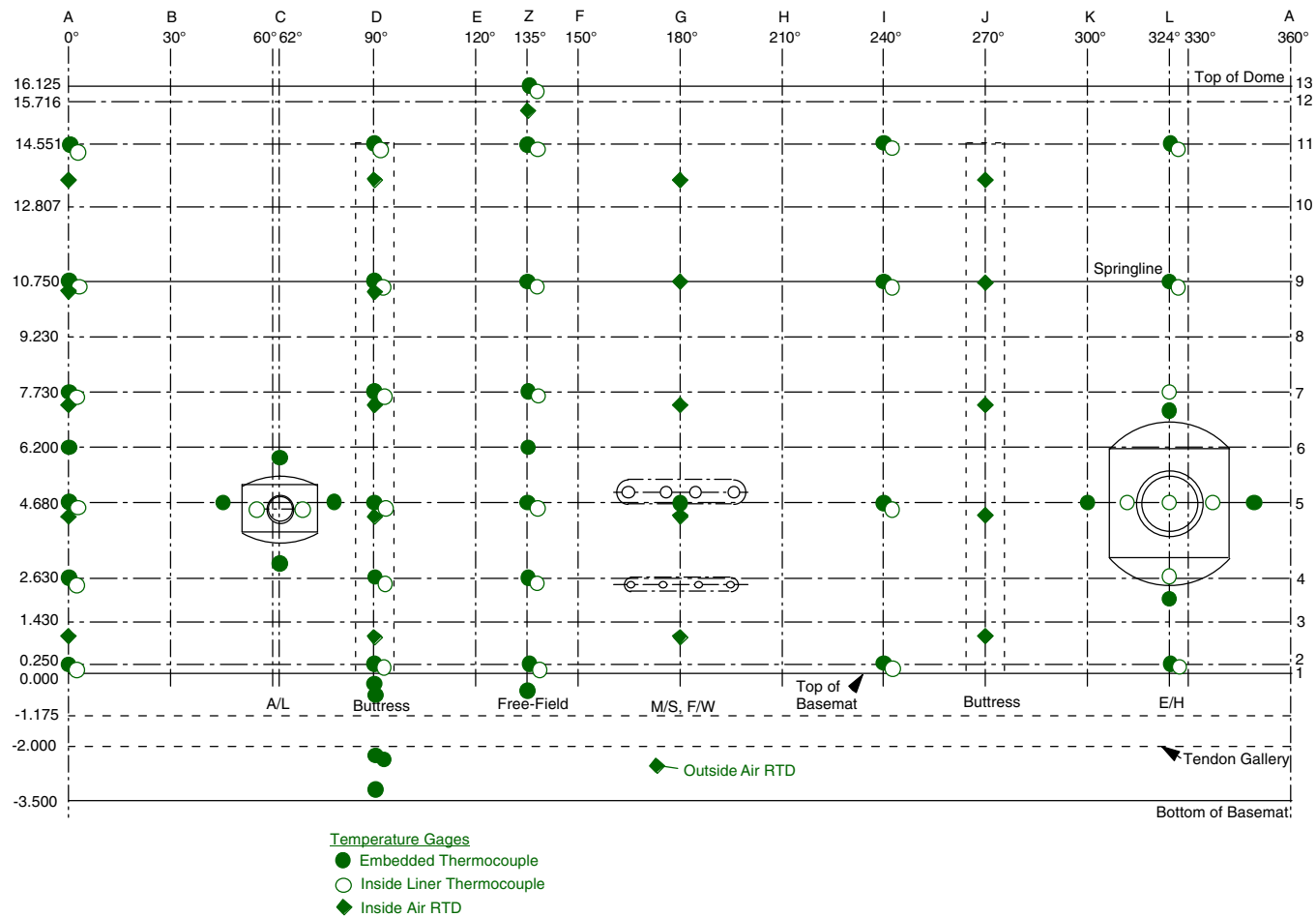
J.2.1 Temperature Measurements

The matrix of temperature measuring gages in the PCCV is shown in Figure J-1. Temperature Gages exist on the inside surface of the liner and at certain locations embedded in the concrete wall. Since the matrix of gages has gaps (no gage) at certain elevations and certain azimuths, the interpolation mapping was done in three steps as follows:

1. Extrapolation of Temperature Readings For Liner Inside Surface
(TI-C-##-##) and the Liner Outside Surface (TW-R-##-##) at Azimuth
Locations (0° 90°, 135°, 240°, 324°).
2. Compute the thermal gradients at the inside of liner wall.
3. Produce a temperature reading at all strain gage locations using the extrapolated temperature readings and thermal gradients.

Procedure Followed:

1. Read in the Temperature Data for the DOR and the Temperature for the Dynamic Record.
2. Data is read into an array
 - a. Gage = G (1D array)
 - b. Azimuth = AZ (1D array)
 - c. Elevation = EL (1D array)
 - d. Radial Distance = RA (1D array)
 - e. Temperature Readings = TEMP (2D array)
3. Output a new array
 - a. Gage = GB (1D array)
 - b. Azimuth = AZN (1D array)
 - c. Elevation = ELN (1D array)



- d. Radial Distance = RAN (1D array)
 - e. Temperature Readings = R(i , j) (2D array)
4. Output the Thermal Gradients of Inside Liner Location
- a. Formula used:

$$1 \quad T_{\text{grad}} = (T_{\text{conc}} - T_{\text{liner}}) / \Delta r$$

where $\Delta r = R_{\text{conc}} - R_{\text{liner}}$

- 5. Data array of strain gage locations read into new program with corresponding temperature readings on the inner liner and middle thickness of wall. The Subprogram Inter produces a temperature corresponding to a given elevation, azimuth, and radial distance.
- 6. Output strain gage readings and temperature readings.

J.2.2 Temperature Interpolation

The FORTRAN program algorithms for this procedure and three illustrative examples are outlined below. These examples show the temperature interpolation at three specific points within the PCCV cylinder. It should be noted that no basemat temperature extrapolation was attempted due to the lack of detailed temperature information within the basemat. Basemat gages were all assumed to be the same as the temperature at the base of the wall.

Temperature Interpolation of the Absent Strain Gages

The following example shows how temperature is extrapolated to a "missing" location.

Gages on Line 0 Degree

Gage 1 - TW-R-A2-01

Gage 2 - TW-R-A3-01

Gage 3 - TW-R-A4-01

Given: Gage 1 - Given by TEMP_CVTD_DOR_LST
Gage 3 - Given by TEMP_CVTD_DOR_LST

Required: Extrapolation of Gage 2

$$X(1) = 1 - \frac{\text{elev.}(TW - R - A3 - 01) - \text{elev.}(TW - R - A2 - 01)}{\text{elev.}(TW - R - A4 - 01) - \text{elev.}(TW - R - A2 - 01)} = 1 - \left(\frac{1430 - 254}{2642 - 254} \right) = 0.50754$$

$$X(2) = 1 + \frac{(\text{elev.}(TW - R - A3 - 01) - \text{elev.}(TW - R - A4 - 01))}{\text{elev.}(TW - R - A4 - 01) - \text{elev.}(TW - R - A2 - 01)} = 1 + \left(\frac{1430 - 2642}{2642 - 254} \right) = 0.4924$$

Temperature TW-R-A3-01 = Temperature (TW-R-A2-01)*X(1) + Temperature (TW-R-A4-01)*X(2)

Temperature TW-R-A3-01 = (13.864)*0.50754 + 16.294901*(0.4924) = 15.0601 @ Time = 03/03/00 11:47

Temperature placed into Data Array at Time "L"

Temperature Interpolation at a Specific Location

Given: Temperature reading on line (2,3,4,5,6,7,8,9,10,11,12,13) and on azimuth (0°, 90°, 135°, 240°, 324°)

Examples: Extrapolation of Temperatures for Following Locations

1. Location1: Elevation =1425 Azimuth 35 degree, Radius 5699.7mm
2. Location2: Elevation =9130 Azimuth 210 degree, Radius 5359.4mm
3. Location3: Elevation =12900 Azimuth 310degree, Radius 5780.95mm

Information entered for subroutine temperature extrapolation

1. Azimuth Data: data az / 0.0, 90.0, 135.0, 240.0, 324.0, 360.0 /
2. Elevation Data: data elev / 254.0, 1430.0, 2642.0, 4674.0, 6200.0, 7722.0, 9230.0, 10744.0, 12807.0, 14554.0, 15716.0, 16125.0 /
3. Radial Data: data ra / 5359.4, 5537.2, 5638.8 /
where, data ra / inner liner radius, middle wall radius (except on line D), middle wall radius on line D /

Example 1.

- (a) Search on Azimuth Location
First Azimuth Location = 0° (a)
Second Azimuth Location = 90° (a+1)
- (b) Search on Elevation Location
First Elevation Location = 250.0 (e)
Second Elevation Location = 1430.0 (e+1)
- (c) Search for Radial location
 1. Since the gage is located at 35 degrees
 - If radius of wall temperature is located at 0° then Radius = 5537.2 mm
 - If radius of wall temperature is located at 90° then Radius = 5638.8 mm
 - 5638.8 mm - 5537.2 mm = 101.6 mm

Therefore, radius of the wall for the example 1 gage location:

Formula: (liner radius + (wall radius on Line D) - (wall radius on Line A)

$$\left(\frac{(Az.(2) - Az.(gage))}{Az.(2) - Az.(1)} \right)$$

Value for Wall Radius:

$$5537.2 \text{ mm (liner radius)} + (5537.2 \text{ mm}) \left(\frac{(90 - 35)}{90 - 0} \right) = 5599.29 \text{ mm}$$

- (d) Temperature is interpolated for Vertical Elevation

$$\text{fact1} = (\text{elev}(e+1) - \text{EL1}(i)) / (\text{elev}(e+1) - \text{elev}(e)) = (1430.0 - 1425) / (1430.0 - 254.0) = 0.00425$$

$$\text{fact2} = (\text{EL1}(i) - \text{elev}(e)) / (\text{elev}(e+1) - \text{elev}(e)) = (1425 - 254) / (1430 - 254) = 0.99575$$

1. LINER Temperature taken as % from 1st loc. + % from 2nd loc. data temperature at 1st elev., 1st az, 1st rad. loc. and 2nd elev., 1st az, 1st rad. loc.

temp(1,ii)=fact1* temp. liner(254mm, 0°, 1-34) + fact2* temp. liner(1430mm, 0°, 1-34)
temp(1,2) = 0.00425*20.1455 + 0.99575 * 19.616 =19.6183

2. LINER Temperature taken as % from 1st loc. + % from 2nd loc.
1st elev., 2nd az, 1st rad. loc.to 2nd elev.,2nd az,1st rad. loc.

temp(2,ii)=fact1* temp. liner(254mm, 90°, 1-34)+fact2* temp. liner(1430mm, 90°, 1-34)
temp(2,2) = 0.00425*20.2373 + 0.99575 * 19.783 =19.7849

3. WALL Temperature taken as % from 1st loc. + % from 2nd loc.
1st elev., 1st az, 2nd rad. loc.to 2nd elev.,1st az,2nd rad. loc.

temp(3,ii)=fact1* temp. wall(254mm, 0°, 1-34)+fact2* temp. wall(1430mm, 0°, 1-34)
temp(3,2) = 0.00425*19.2764 + 0.99575 * 18.519 =18.5222

4. WALL Temperature taken as % from 1st loc. + % from 2nd loc.
1st elev., 2nd az, 2nd rad. loc.to 2nd elev.,2nd az,2nd rad. loc.

temp(4,ii)=fact1* temp. wall(254mm, 90°, 1-34)+fact2* temp. wall(1430mm, 90°, 1-34)
temp(4,2) = 0.00425*19.9335 + 0.99575 * 19.436 =19.4381

2. Interpolation along the azimuth

fact1=(az(a+1)-AZ1(i))/(az(a+1)-az(a)) = (90-35)/(90-0) = 0.611
fact2=(AZ1(i)-az(a))/(az(a+1)-az(a)) = (35-0)/(90-0)=0.3889
tempa(1,ii)=fact1* temp(1,ii)+fact2* temp(2,ii)
tempa(1,2) = 0.611*19.6183+ 0.3889 * 19.7849 =19.6811

tempa(2,ii)=fact1*temp(3,ii)+ fact2*temp(4,ii)
tempa(2,2) = 0.611*18.5222 + 0.3889 * 19.4381 =18.8764

3. Finally the interpolation through the thickness

fact1=(rm-RA1(i))/(rm-ra(1)) = (5599.29 mm -5699.7 mm)/(5599.29 mm-5359.4) = -0.4186
fact2=(RA1(i)-ra(1))/(rm-ra(1)) = (5699.7mm-5359.4)/(5599.29 mm-5359.4) = 1.4186

tempr(i,ii)=fact1*tempa(1,ii)+fact2*tempa(2,ii)
tempr(1,2) = -0.4186*19.6811+1.4186*18.8764 = 18.5396

Example 1 for DOR_LST @ 9/26/00 10:03

Example Pt.	Gage 1	Temp.	Gage 2	Temp.	Gage 3	Temp.	Gage 4	Temp.
Liner	TI – C-A2-01	20.146	TI – C-A3-01	19.62	TI – C-D2-01	20.237	TI – C-D3-01	19.7838
Outside	TW – R-A2-01	19.276	TW – R-A3-01	18.52	TW – R-D2-01	19.9335	TW – R-D3-01	19.4368
Final								18.5396

Example 2.

- (a) Search on Azimuth Location
First Azimuth Location = 135° (a)
Second Azimuth Location = 240° (a+1)
- (b) Search on Elevation Location
First Elevation Location = 7722.0 (e)

Second Elevation Location = 9230 (e+1)

(c) Search for Radial location

Since the gage is located at 200 degrees Radius of wall = 5537.2 mm

- If radius of wall temperature is located at 135° then Radius = 5537.2 mm

- If radius of wall temperature is located at 240° then Radius = 5537.2 mm

$$5537.2 \text{ mm} - 5537.2 \text{ mm} = 0 \text{ mm}$$

(d) Temperature is interpolated for Vertical Elevation

$$\text{fact1} = (\text{elev}(e+1) - \text{EL1}(i)) / (\text{elev}(e+1) - \text{elev}(e)) = (9230 - 9130) / (9230 - 7722.0) = 0.066313$$

$$\text{fact2} = (\text{EL1}(i) - \text{elev}(e)) / (\text{elev}(e+1) - \text{elev}(e)) = (9130 - 7722.0) / (9230 - 7722.0) = 0.933687$$

1. LINER Temperature taken as % from 1st loc. + % from 2nd loc.

data temperature at 1st elev., 1st az, 1st rad. loc. and 2nd elev., 1st az, 1st rad. loc.

$$\text{temp}(1, \text{ii}) = \text{fact1} * \text{temp. liner}(7722 \text{ mm}, 135^\circ, 1-34) + \text{fact2} * \text{temp. liner}(9230 \text{ mm}, 135^\circ, 1-34)$$

$$\text{temp}(1, 2) = 0.066313 * 17.0938 + 0.933687 * 17.065506 = 17.06738$$

2. LINER Temperature taken as % from 1st loc. + % from 2nd loc.

1st elev., 2nd az, 1st rad. loc. to 2nd elev., 2nd az, 1st rad. loc.

$$\text{temp}(2, \text{ii}) = \text{fact1} * \text{temp. liner}(7722 \text{ mm}, 240^\circ, 1-34) + \text{fact2} * \text{temp. liner}(9230 \text{ mm}, 240^\circ, 1-34)$$

$$\text{temp}(2, 2) = 0.066313 * 16.8714 + 0.933687 * 16.794495 = 16.799594$$

3. WALL Temperature taken as % from 1st loc. + % from 2nd loc.

1st elev., 1st az, 2nd rad. loc. to 2nd elev., 1st az, 2nd rad. loc.

$$\text{temp}(3, \text{ii}) = \text{fact1} * \text{temp. wall}(7722 \text{ mm}, 135^\circ, 1-34) + \text{fact2} * \text{temp. wall}(9230 \text{ mm}, 135^\circ, 1-34)$$

$$\text{temp}(3, 2) = 0.066313 * 15.5703 + 0.933687 * 15.857828 = 15.83876$$

4. WALL Temperature taken as % from 1st loc. + % from 2nd loc.

1st elev., 2nd az, 2nd rad. loc. to 2nd elev., 2nd az, 2nd rad. loc.

$$\text{temp}(4, \text{ii}) = \text{fact1} * \text{temp. wall}(7722 \text{ mm}, 240^\circ, 1-34) + \text{fact2} * \text{temp. wall}(9230 \text{ mm}, 240^\circ, 1-34)$$

$$\text{temp}(4, 2) = 0.066313 * 16.368855 + 0.933687 * 14.087605 = 14.2388$$

(e) Interpolation along the azimuth

$$\text{fact1} = (\text{az}(a+1) - \text{AZ1}(i)) / (\text{az}(a+1) - \text{az}(a)) = (240 - 210) / (240 - 135) = 0.2857$$

$$\text{fact2} = (\text{AZ1}(i) - \text{az}(a)) / (\text{az}(a+1) - \text{az}(a)) = (210 - 135) / (240 - 135) = 0.71429$$

$$\text{tempa}(1, \text{ii}) = \text{fact1} * \text{temp.}(1, \text{ii}) + \text{fact2} * \text{temp.}(2, \text{ii})$$

$$\text{tempa}(1, 2) = 0.2857 * 17.06738 + 0.71429 * 16.799594 = 16.87593$$

$$\text{tempa}(2, \text{ii}) = \text{fact1} * \text{temp}(3, \text{ii}) + \text{fact2} * \text{temp}(4, \text{ii})$$

$$\text{tempa}(2, 2) = 0.2857 * 15.83876 + 0.71429 * 14.2388 = 14.69577$$

(f) Finally the interpolation through the thickness

$$\text{fact1} = (\text{rm} - \text{RA1}(i)) / (\text{rm} - \text{ra}(1)) = (5537.2 \text{ mm} - 5359.4 \text{ mm}) / (5537.2 \text{ mm} - 5359.4 \text{ mm}) = 1.0$$

$$\text{fact2} = (\text{RA1}(i) - \text{ra}(1)) / (\text{rm} - \text{ra}(1)) = (5359.4 \text{ mm} - 5359.4) / (5537.2 \text{ mm} - 5359.4 \text{ mm}) = 0.0$$

$$\text{tempr}(i, \text{ii}) = \text{fact1} * \text{tempa}(1, \text{ii}) + \text{fact2} * \text{tempa}(2, \text{ii})$$

$$\text{tempr}(1, 2) = 1.0 * 16.87593 + 1.0 * 14.2388 = 16.87593$$

Example 2 for DOR_LST @ 9/26/00 10:03

Example Pt.	Gage 1	Temp.	Gage 2	Temp.	Gage 3	Temp.	Gage 4	Temp.
Liner	TI – C-Z7-01	17.094	TI – C-Z8-01	17.06551	TI – C-I7-01	16.87147	TI – C-I8-01	16.7945
Outside	TW – R-Z7-01	15.570	TW – R-Z8-01	15.8578	TW – R-I7-01	16.36885	TW – R-I8-01	14.08761
Final								16.87593

Example 3.

- (a) Search on Azimuth Location
First Azimuth Location = 240° (a)
Second Azimuth Location = 324° (a+1)
- (b) Search on Elevation Location
First Elevation Location = 12807.0 (e)
Second Elevation Location = 14554.0 (e+1)
- (c) Search for Radial location

Since the gage is located at 310 degrees Radius of wall = 5537.2 mm
 - If radius of wall temperature is located at 135° then Radius = 5537.2 mm
 - If radius of wall temperature is located at 240° then Radius = 5537.2 mm
 5537.2 mm - 5537.2 mm = 0 mm

- (d) Temperature is interpolated for Vertical Elevation

$$\text{fact1} = (\text{elev}(e+1) - \text{EL1}(i)) / (\text{elev}(e+1) - \text{elev}(e)) = (14554. - 12900) / (14554 - 12807.0) = 0.9468$$

$$\text{fact2} = (\text{EL1}(i) - \text{elev}(e)) / (\text{elev}(e+1) - \text{elev}(e)) = (12900 - 12807.0) / (14554 - 12807.0) = 0.05323$$

1. LINER Temperature taken as % from 1st loc. + % from 2nd loc.
 data temperature at 1st elev., 1st az, 1st rad. loc. and 2nd elev., 1st az, 1st rad. loc.

$$\text{temp}(1,ii) = \text{fact1} * \text{temp. liner}(12807\text{mm}, 240^\circ, 1-34) + \text{fact2} * \text{temp. liner}(14554, 240^\circ, 1-34)$$

$$\text{temp}(1,2) = 0.9468 * 16.584515 + 0.05323 * 15.8984 = 16.5485$$

2. LINER Temperature taken as % from 1st loc. + % from 2nd loc.
 1st elev., 2nd az, 1st rad. loc. to 2nd elev., 2nd az, 1st rad. loc.

$$\text{temp}(2,ii) = \text{fact1} * \text{temp. liner}(12807, 324^\circ, 1-34) + \text{fact2} * \text{temp. liner}(14554, 324^\circ, 1-34)$$

$$\text{temp}(2,2) = 0.9468 * 17.45914 + 0.05323 * 17.5098 = 17.4624$$

3. WALL Temperature taken as % from 1st loc. + % from 2nd loc.
 1st elev., 1st az, 2nd rad. loc. to 2nd elev., 1st az, 2nd rad. loc.

$$\text{temp}(3,ii) = \text{fact1} * \text{temp. wall}(12807, 240^\circ, 1-34) + \text{fact2} * \text{temp. wall}(14554, 240^\circ, 1-34)$$

$$\text{temp}(3,2) = 0.9468 * 15.976255 + 0.05323 * 15.619388 = 15.9577$$

4. WALL Temperature taken as % from 1st loc. + % from 2nd loc.
 1st elev., 2nd az, 2nd rad. loc. to 2nd elev., 2nd az, 2nd rad. loc.

$$\text{temp}(4,ii) = \text{fact1} * \text{temp. wall}(12807, 324^\circ, 1-34) + \text{fact2} * \text{temp. wall}(14554, 324^\circ, 1-34)$$

$$\text{temp}(4,2) = 0.9468 * 18.13707 + 0.05323 * 18.0732 = 18.1342$$

- (e) Interpolation along the azimuth

$$\begin{aligned} \text{fact1} &= (\text{az}(\text{a}+1) - \text{AZ1}(\text{i})) / (\text{az}(\text{a}+1) - \text{az}(\text{a})) = (324 - 310) / (324 - 240) = 0.1667 \\ \text{fact2} &= (\text{AZ1}(\text{i}) - \text{az}(\text{a})) / (\text{az}(\text{a}+1) - \text{az}(\text{a})) = (310 - 240) / (324 - 240) = 0.8333 \\ \text{tempa}(1, \text{ii}) &= \text{fact1} * \text{temp.}(1, \text{ii}) + \text{fact2} * \text{temp.}(2, \text{ii}) \\ \text{tempa}(1, 2) &= 0.1667 * 16.5485 + 0.8333 * 17.4624 = 17.3101 \end{aligned}$$

$$\begin{aligned} \text{tempa}(2, \text{ii}) &= \text{fact1} * \text{temp}(3, \text{ii}) + \text{fact2} * \text{temp}(4, \text{ii}) \\ \text{tempa}(2, 2) &= 0.1667 * 15.9577 + 0.8333 * 18.1342 = 17.7713 \end{aligned}$$

(f) Finally the interpolation through the thickness

$$\begin{aligned} \text{fact1} &= (\text{rm} - \text{RA1}(\text{i})) / (\text{rm} - \text{ra}(1)) = (5537.2\text{mm} - 5780.95\text{mm}) / (5537.2\text{mm} - 5359.4\text{mm}) = -1.371 \\ \text{fact2} &= (\text{RA1}(\text{i}) - \text{ra}(1)) / (\text{rm} - \text{ra}(1)) = (5780.95\text{mm} - 5359.4) / (5537.2\text{mm} - 5359.4\text{mm}) = 2.37 \end{aligned}$$

$$\begin{aligned} \text{tempr}(\text{i}, \text{ii}) &= \text{fact1} * \text{tempa}(1, \text{ii}) + \text{fact2} * \text{tempa}(2, \text{ii}) \\ \text{tempr}(1, 2) &= -1.371 * 17.3101 + 2.371 * 17.7713 = 18.4195 \end{aligned}$$

Example 3 for DOR_LST @ 9/26/00 10:03

Example Pt.	Gage 1	Temp.	Gage 2	Temp.	Gage 3	Temp.	Gage 4	Temp.
Liner	TI – C-I10-01	16.584	TI – C-I11-01	15.8984	TI – C-L10-01	17.459	TI – C-L11-01	17.51
Outside	TW – R-I10-01	15.976	TW – R-I11-01	15.619	TW – R-L10 - 01	18.137	TW – R-L11-01	18.073
Final								18.4195

J.2.3 Direct Temperature Effects on Gages

The basic premise for the gate temperature corrections is to calculate, for each gage, a gage adjustment function that is a function only of the temperature at that gage. This premise accepts the simplification that the correction is only a function of the individual gage temperature, when in reality it may be a function of the complete temperature distribution caused structural interaction effects. Since these interactions are judged to be secondary effects compared to the direct thermal expansion occurring directly at each gage, these secondary effects are being ignored in the data correction. Further, since much of the temperature changes are caused by passage of the sum, it is likely that daytime temperature distributions will at least be similar to each other (i.e. the sun will never be shining on the north side of the model, regardless of the seasonal changes in solar apogee). It is also noted that by using the BPS and the PSFT datasets, temperature corrections at a range of different PCCV stress levels have been evaluated.

J.2.4 Secondary Temperature Effects on Strain Gages(Correction Terms)

These effects are provided directly from the gage manufacturer. The corrections are in the form of Lot Numbers, with corrections given in units of microstrain.

Lot Number R-A12BP25:

$$\Sigma = 4.97 \times 10^1 + 1.12 \times 10^0 T - 2.81 \times 10^{-2} T^2 + 6.18 \times 10^{-5} T^3 - 3.11 \times 10^{-8} T^4 \text{ (deg F)}$$

$$\Sigma = 5.87 \times 10^1 - 8.93 \times 10^{-1} T - 7.24 \times 10^{-2} T^2 + 3.37 \times 10^{-4} T^3 - 3.26 \times 10^{-7} T^4 \text{ (deg C)}$$

Lot Numbers R-A19A595, R-A19AP58, R-A19AP61, R-A19AP75, R-A19AP81, R-A19AP82, R-A19AP83,

R-A19AP95, R-A19AP96, R-A19AP97:

$$\Sigma = -3.81 \times 10^1 + 2.74 \times 10^0 T - 3.52 \times 10^{-2} T^2 + 7.64 \times 10^{-5} T^3 - 4.30 \times 10^{-8} T^4 \text{ (deg F)}$$

$$\Sigma = 1.60 \times 10^1 + 1.29 \times 10^0 T - 9.11 \times 10^{-2} T^2 + 4.13 \times 10^{-4} T^3 - 4.51 \times 10^{-7} T^4 \text{ (deg C)}$$

Lot Number R-A19BP02:

$$\Sigma = -1.39 \times 10^1 + 2.41 \times 10^0 T - 3.51 \times 10^{-2} T^2 + 7.74 \times 10^{-5} T^3 - 4.62 \times 10^{-8} T^4 \text{ (deg F)}$$

$$\Sigma = 2.99 \times 10^1 + 7.17 \times 10^{-1} T - 9.06 \times 10^{-2} T^2 + 4.17 \times 10^{-4} T^3 - 4.85 \times 10^{-7} T^4 \text{ (deg C)}$$

Lot Numbers R-A42AP02, R-A42AP04, R-A42AP08:

$$\Sigma = -1.50 \times 10^2 + 4.44 \times 10^0 T - 3.82 \times 10^{-2} T^2 + 7.93 \times 10^{-5} T^3 - 4.33 \times 10^{-8} T^4 \text{ (deg F)}$$

$$\Sigma = -4.45 \times 10^1 + 4.02 \times 10^0 T - 1.00 \times 10^{-1} T^2 + 4.30 \times 10^{-4} T^3 - 4.54 \times 10^{-7} T^4 \text{ (deg C)}$$

J.3 Standardize Gage Measurements

The development of the algorithm for temperature correction proceeded as follows.

1. Compute a mean linearized temperature correction factor \overline{A}_1 , and standard deviation, σ_{A1} for every gage from Data Set 1 (the BPS data).

Typical calculation

\mathbf{e}_{n_i} is a set of dynamic gage data for gage n and time/temperature $i=1, 2, 3, \dots$

$$\mathbf{e}_{n_i}^t = \mathbf{e}_{n_i} - \Sigma_{n_i} \text{ (where } \Sigma \text{ is a polynomial correction from Section 3.2.4)}$$

$$\mathbf{e}_{n_i}' = f_n(\mathbf{e}_{n_i}^t)$$

Where f_n is a non-temperature correction function defined only for certain gages; in most cases $\mathbf{e}_{n_i}' = \mathbf{e}_{n_i}^t$

$$\Delta \mathbf{e}_{n_i}' = \mathbf{e}_{n_i}' - \mathbf{e}_{n_1}'$$

$$\Delta T_{n_i}^T = T_{n_i} - T_{n_1}$$

$$A_{i_n} = \frac{\Delta \mathbf{e}_{n_i}'}{\Delta T_{n_i}}$$

Calculate a weighted average A_n - weighted average because we want the data correction to be the most heavily influenced by strain-temperature observation data that causes the largest strains:

$$\bar{A}_n = \frac{\frac{1}{\bar{\Delta e}_{n_i}} \sum_{i=1}^I \Delta e_{n_i}' \frac{\Delta e_{n_i}'}{\Delta T_{n_i}}}{I}$$

Where I = number of temperature points and $\bar{\Delta e}_{n_i}'$ is the average of $\Delta e_{n_i}'$

Check s_A (Criteria $s_{A_n} < 0.2\bar{A}_n$)

The assumed basic correction formula is therefore: $e_{n_i}^c = e_{n_i} - \Sigma_{n_i} - \bar{A}_n \Delta T_{n_i}$

This should produce a set of "corrected" gage readings that have less than 20% variation from the reading at time 1 over the entire time period.

2. Repeat same procedure for \bar{A}_2 and s_{A_2} for every gage from Data Set 2 (the PSFT data)

$$\text{Let } a_n = \frac{\bar{A}_{n_1} + \bar{A}_{n_2}}{2} \text{ (or some other combination using other parameters or judgment)}$$

3. Apply the correction to the DYN_LST and DOR_LST data.

The data for comparison to analysis that is free of temperature effects the (DYN_LST and DOR_LST), cannot be simply "zeroed" at the start, because the strains and displacements associated with the prestressing load and dead weight of the structure are important. To make the data free of temperature effects, the temperature corrections must be applied to a certain reference temperature. Since the LST started in the early morning prior to solar heating of the PCCV (and of course, prior to any heating or cooling caused by pumped in nitrogen), the LST DOR point 1 (zero pressure) is used as the reference temperature at each gage. (These temperatures can be different at each gage.) Using this reference temperature, the final correction formula becomes

$$e_{n_i}^c = f_n(e_{n_i} - \Sigma_{n_i}) - a_n(T_{n_i} - T_{n_i}) \quad (J-1)$$

Note that the function f_n could cover other, non-temperature related correction terms and might only be defined for certain gages.

J.3.1 Correction Summaries by Gage Group

Displacements

For the displacement measurements, Equation J-1 is followed without further correction except for some of the vertical displacement measurements. For the vertical displacement, there may have also been some movement of a portion of the instrumentation frame that influenced the gage readings.

Rebar Strains

Equation J-1 is followed with no function f_n .

A typical bar area reduction as a result of the grinding is 1.019. Then it is assumed that for all strain ϵ , there is a unique stress, σ , according to the engineering stress-versus engineering strain data. Using the data for the SD390-D13 bars, averaged, the yield curve is approximately

ϵ	σ
.002	58 ksi
.009	60.9 ksi
.013	62.06 ksi
.015	63.075 ksi
.020	66.7 ksi

For $\mathbf{e}_{n_i}^t, \mathbf{s}_{n_i}^t$ is "looked-up" from the yield function

Then $\mathbf{s}_{n_i}' = \mathbf{s}_{n_i}^t / (\text{Area Ratio})$

\mathbf{e}_{e_i}' is then "looked-up" from the yield function.

Thus, function "f" for rebar strain is a two-step "look-up" function.

Liner Strains

Equation J-1 is followed with no function f_n .

Tendon Strains

Equation J-1 is followed with no function f_n .

Appendix K: Soundprint® Acoustic System Reports

**SoundPrintä Acoustic Monitoring Report
Sandia PCCV**

LST Sept 26-27, 2001

SFMT November 14, 2001

Background

Acoustic monitoring captures acoustic data arriving at sensors distributed over the PCCV model. For the LST and SIT, fifty-four sensors were used, sixteen of which were inside the vessel on the steel liner, and thirty-eight were installed on the outside of the concrete surface. For the SFMT test, no sensors were remaining inside the model, and thirty-eight sensors remained on the outside of the vessel.

The output of the sensors was recorded as acoustic energy arrived. Post-processing of the recorded information was done to estimate the location and the nature of the source of each event. Event classifications used throughout the testing included:

- Concrete cracking
- Wire Breaks
- Other emissions from the tendons
- Nitrogen Flow
- Leaks

Summary of Results

Concrete cracking events were dominant in SIT and the LST, but were largely absent during the SFMT. During the LST, analysis of the signals from the sensors appear to have detected the appearance of leaks in the liner.

The nitrogen flow noise, wire breaks, and other events originating from the area of tendon anchorages were the dominant features of the SFMT. The classification “tendon pings” was used to describe emissions showing resonant peaks in the 4KHz. To 8 KHz band. The classifications “wire break”, “double wire break”, and “multiple wire break”, were used to describe emissions that had other characteristics consistent with the failure of one or more wires in a tendon.

Estimates were made of the amount of energy released by each event relative to a reference impact. These estimates are qualitative only, as increasing amounts of damage to the concrete affected the propagation of acoustic energy from the source to the sensors.

Streaming audio files were available in real time to assist in understanding the developments on the model during each phase of the test.

Detection of Concrete Cracking

Concrete cracking was detected during the stressing phase, during aging of the vessel, and during the pressurization phases. Some of the events recorded were confirmed by visual examination. The cracking was audible during pressurization as continuous Kaiser effect cracking as each new pressure plateau was realized.

Larger cracks affected a sufficient number of sensors that the position of the origin of the cracks could be estimated.

Detection of Leaks during the LST

Analysis of the output of the sensors during the pressurization of the LST was done in an attempt to determine the development of leaks, and to determine the location of the first leaks as they appeared. In observing the FFT of all of the internal sensors, anomalies started to appear at 2.4 Pd in the area around the equipment hatch. This appearance is illustrated below in Figures 1 to 3.

Graph of FFT of Internal Sensors at different pressures during LST

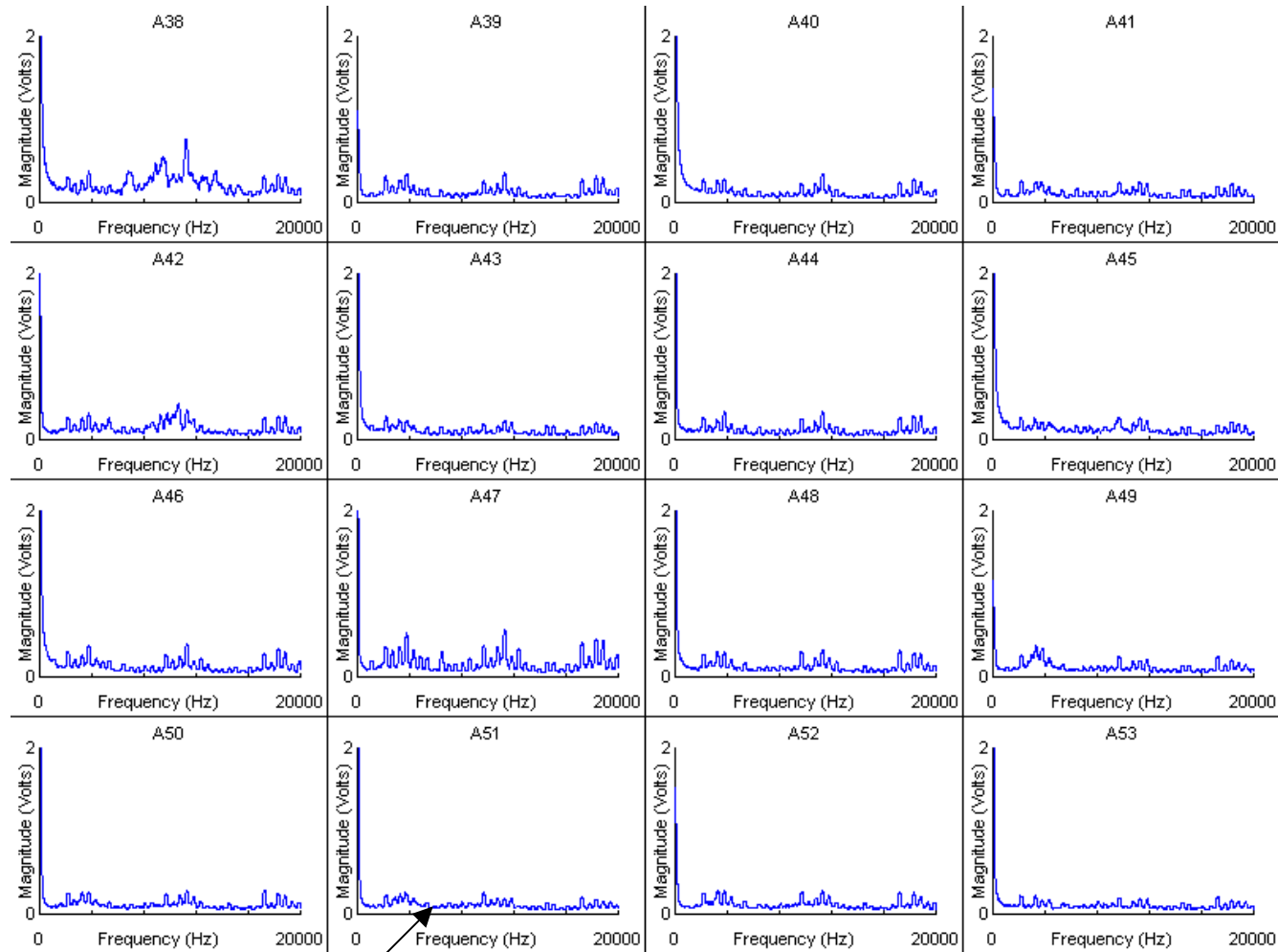


Figure 1: Internal Sensors (FFT) at 2.3 Pd

Normal Background

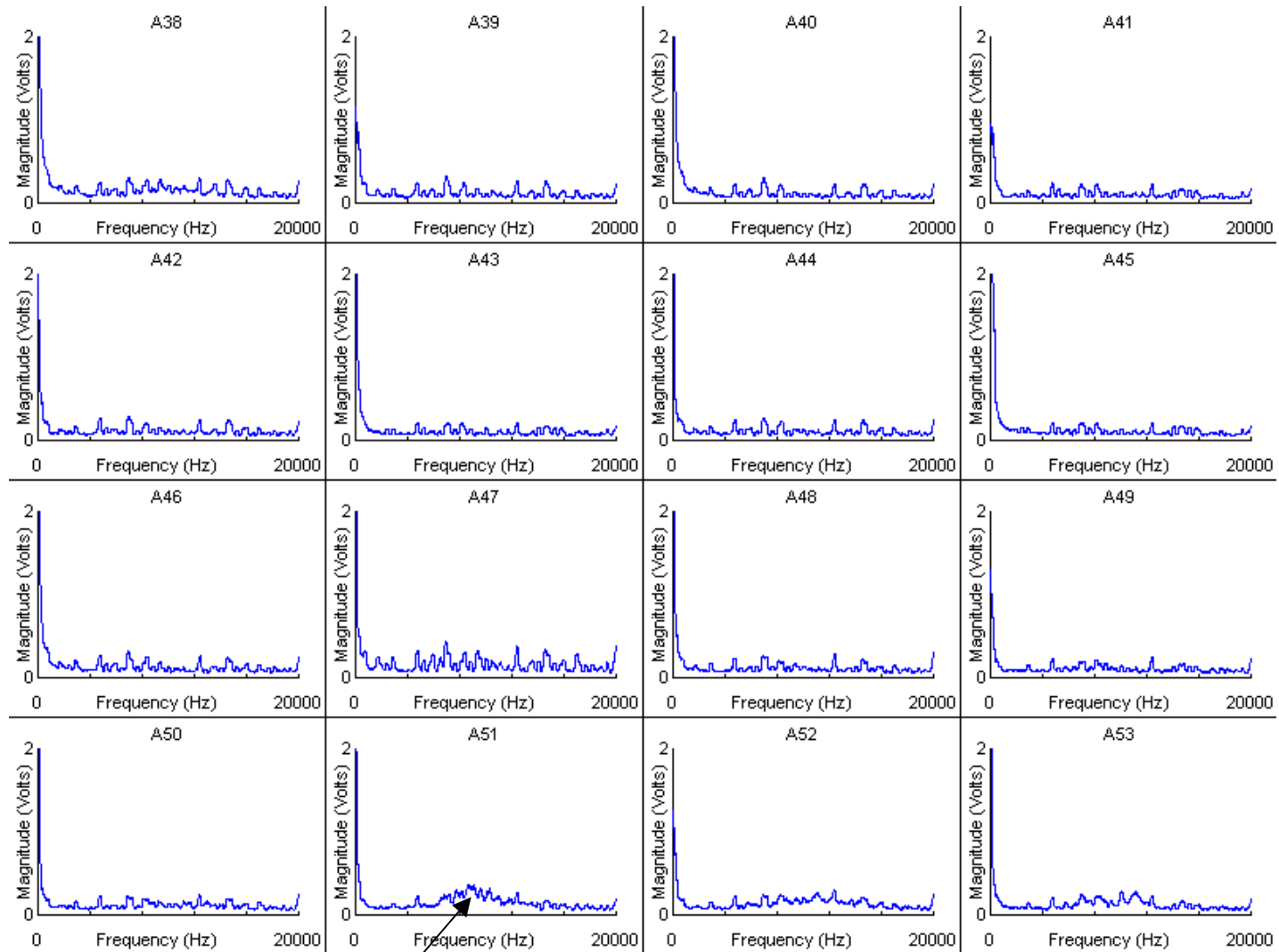
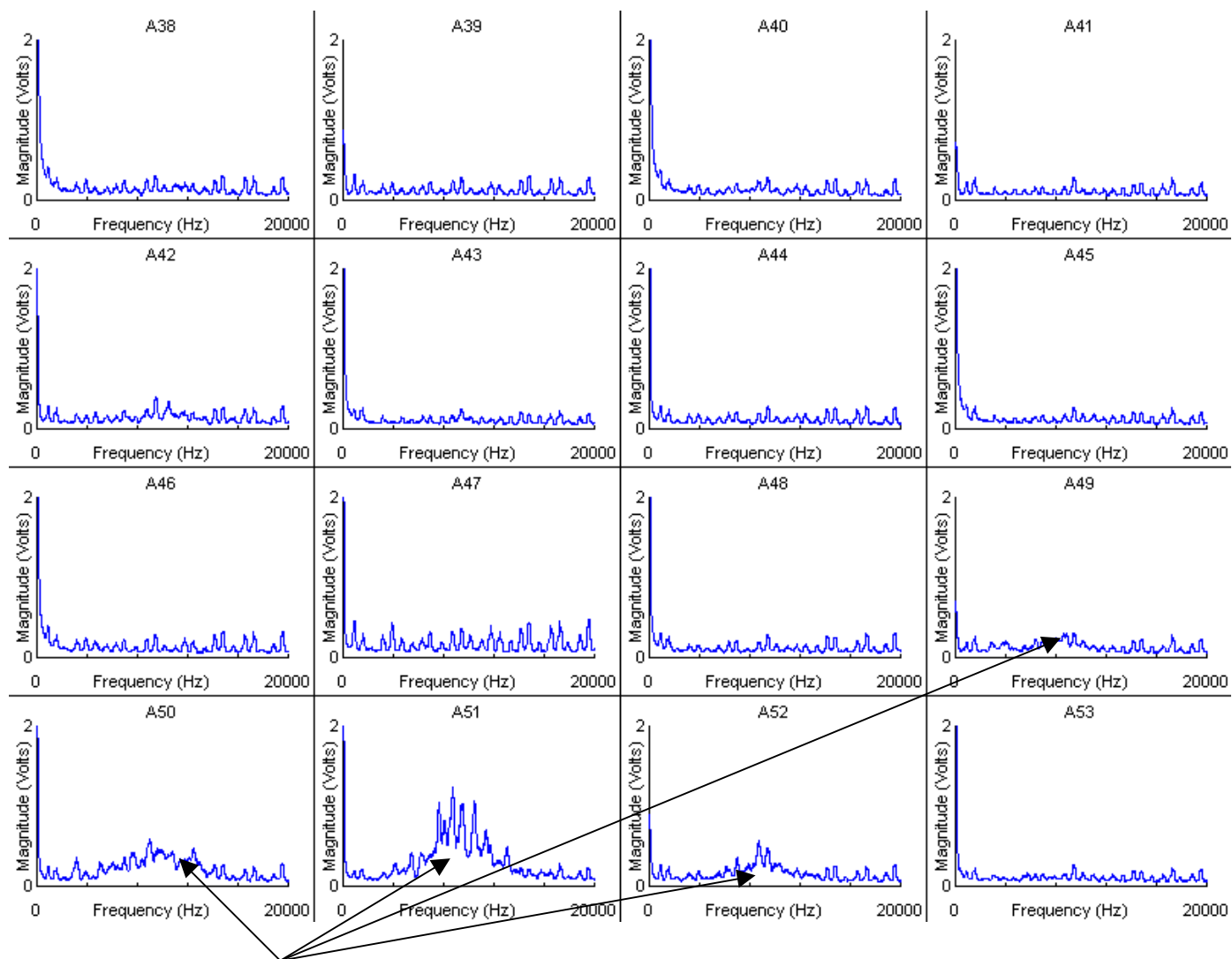


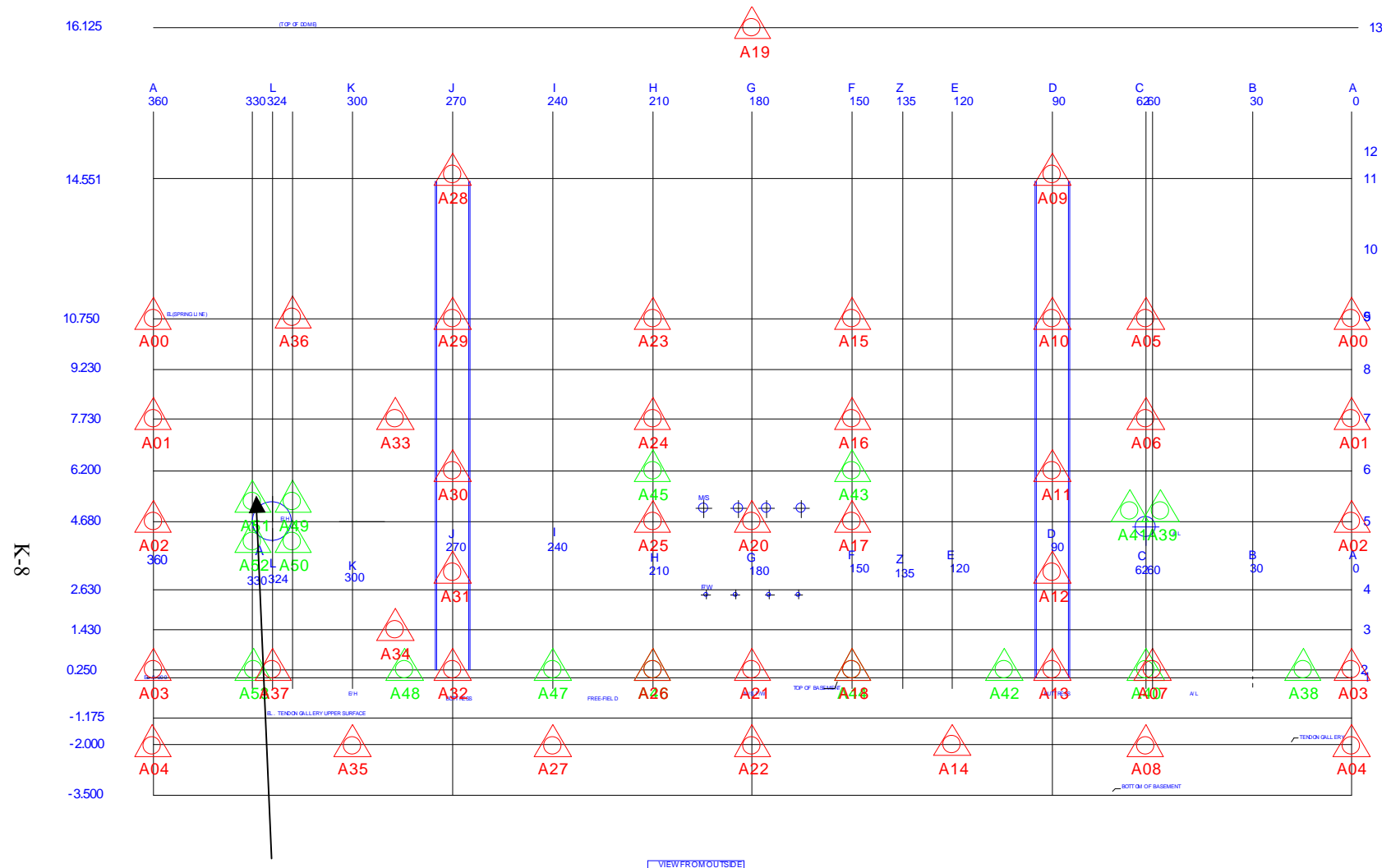
Figure 2: Internal Sensors (FFT) at 2.4 Pd

Elevated White Noise



Elevated Levels on Sensors

Figure 3: Internal Sensors (FFT) at 2.5 Pd



Sensor A51 Showing First Anomaly

Figure 4: Location of Sensor Detecting the first leak during LST

Effect of Schmidt Hammer on PCCV

Use of a Sclerometer or Schmidt hammer allows the estimation of the size of an acoustic event. The Schmidt hammer generates about 1 Joule of energy. Below are two graphs showing the time domain and energy estimate of a Schmidt hammer impact on the PCCV wall.

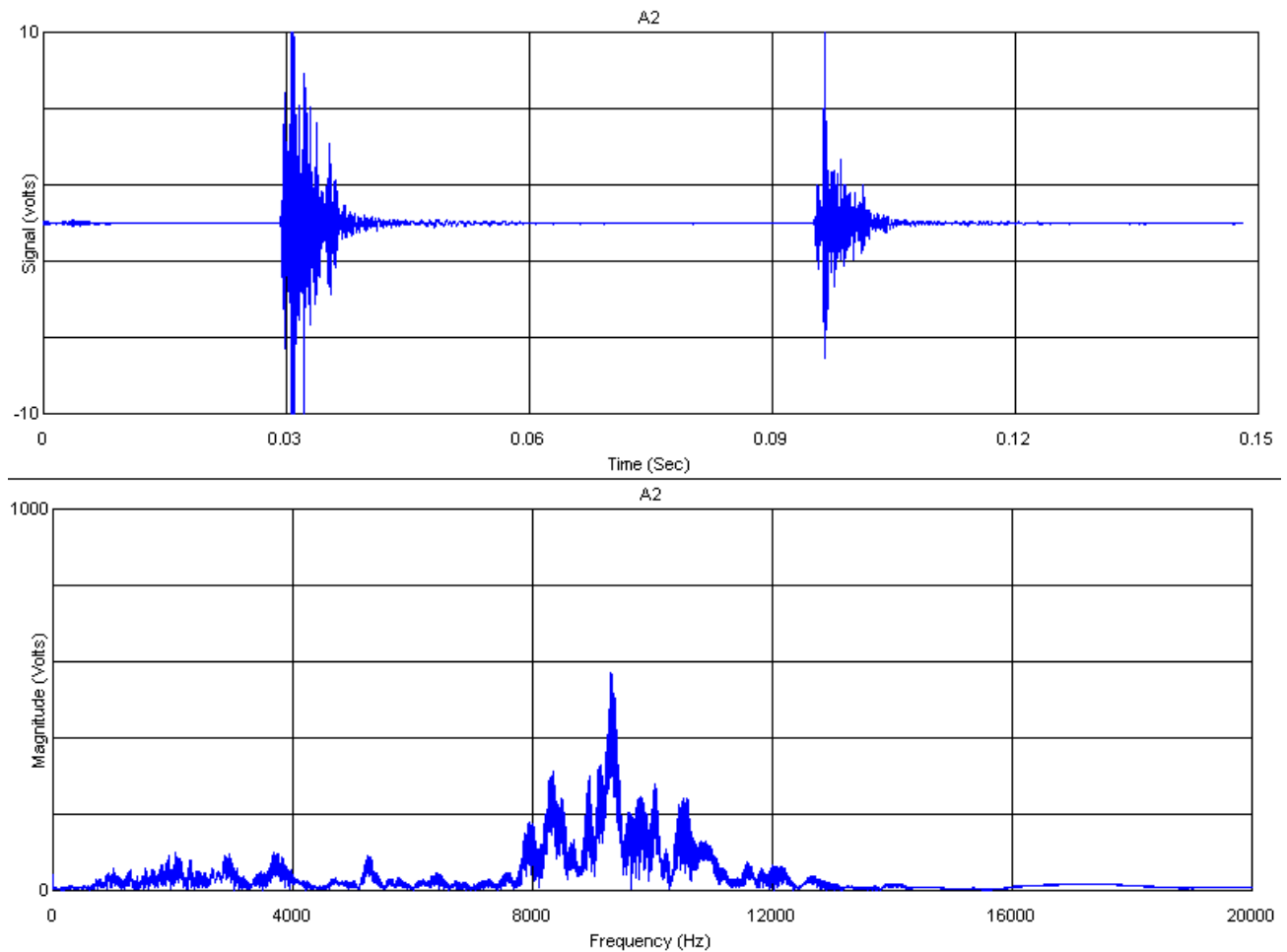


Fig 5: Time Domain and Frequency Domain of Schmidt Hammer Impact

Detection of “Tendon Pings during LST and SFMT

The phenomenon of “tendon pings” appeared during the LST. These emissions are characterized by a modest energy emission and a ringing sound, as if a taut string were plucked. Virtually all of these originated at or near the buttresses. The ringing manifests itself as a sharp peak in the FFT of the event. Below are two graphs showing the Time domain and Frequency domain graphs of a typical “Tendon Ping”. These started occurring at a pressure of 1.7 Pd and continued to a pressure of 2.9 Pd during the LST

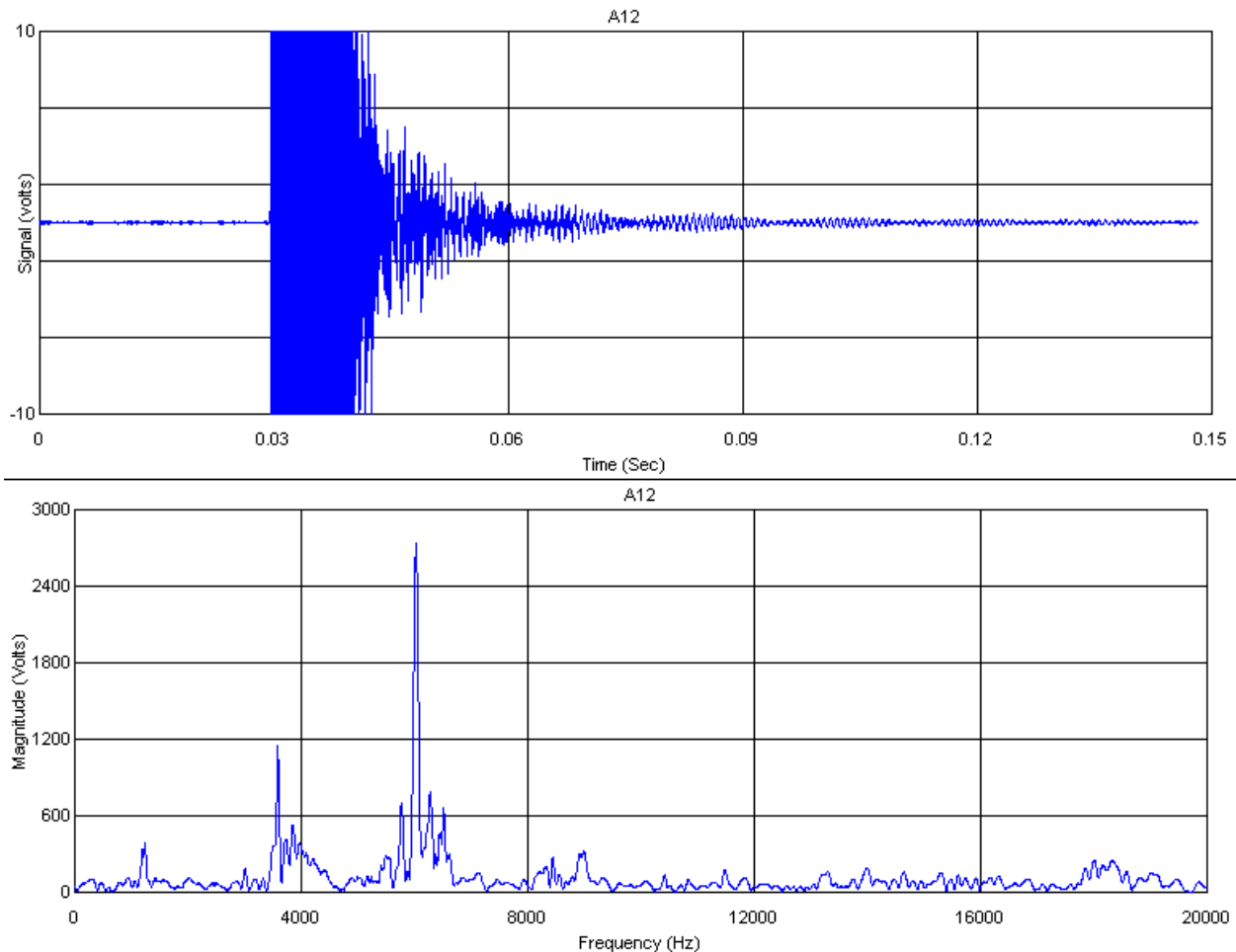


Figure 6: Time and Frequency Domain Plots of a “Tendon Ping”

Detection of Wire Breaks during SFMT

No wire break events were detected during the LST. The first wire break occurred at 10:39:47 Nov 14, during the SFMT. Wire breaks are expected to have at least as much energy as a Schmidt hammer impact, and are expected to show preferential propagation of acoustic energy along the tendon. However, as the concrete of the vessel became increasingly cracked, it became a poorer medium for the transmission of the sound. As a consequence, only the magnitude and frequency content of the output of sensors near each event could be used to assess whether or not a given event was likely the result of a wire break. Fifty-eight events were detected that matched these criteria. Three of these events detected double wire breaks, and Six events detected multiple wire breaks, excluding the final rupture of the vessel.

Most of the wire breaks were located near 20 deg. Azimuth at elevations between 3m and 9 m. The graph below plots an asterisk at the position of the source of each wire break.

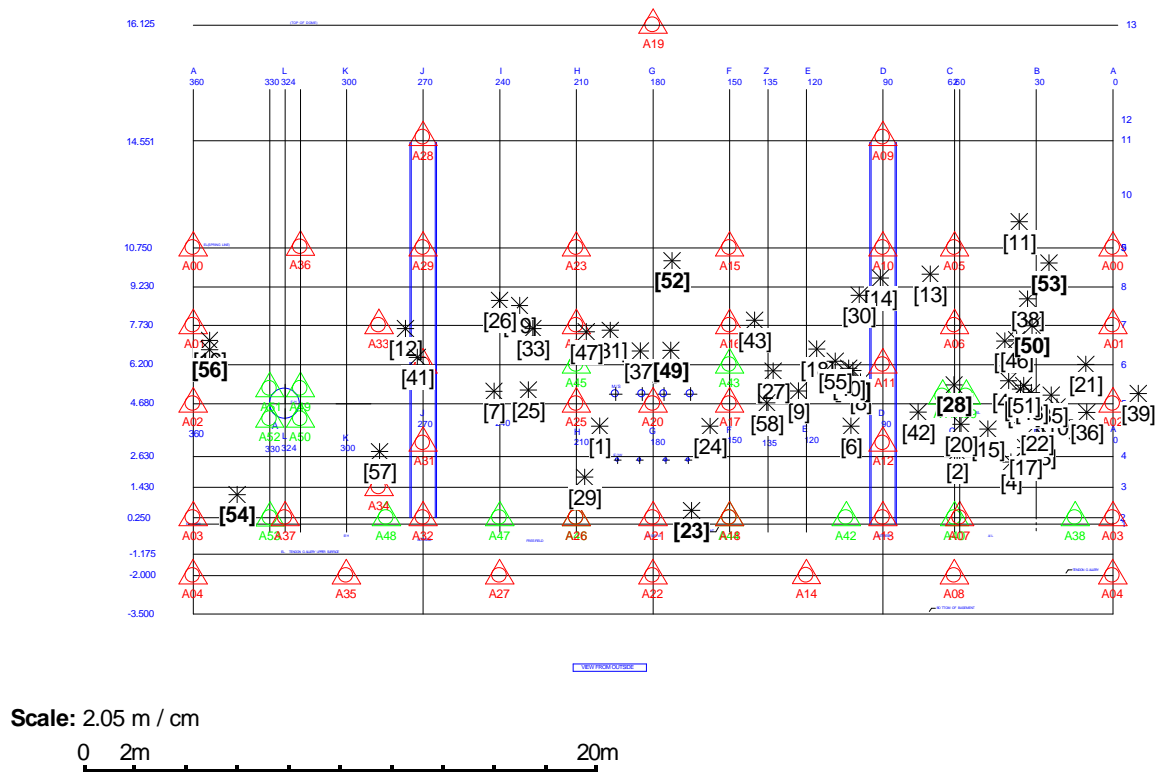


Figure 7: Flattened elevation view (from outside) of location of wire breaks during SFMT

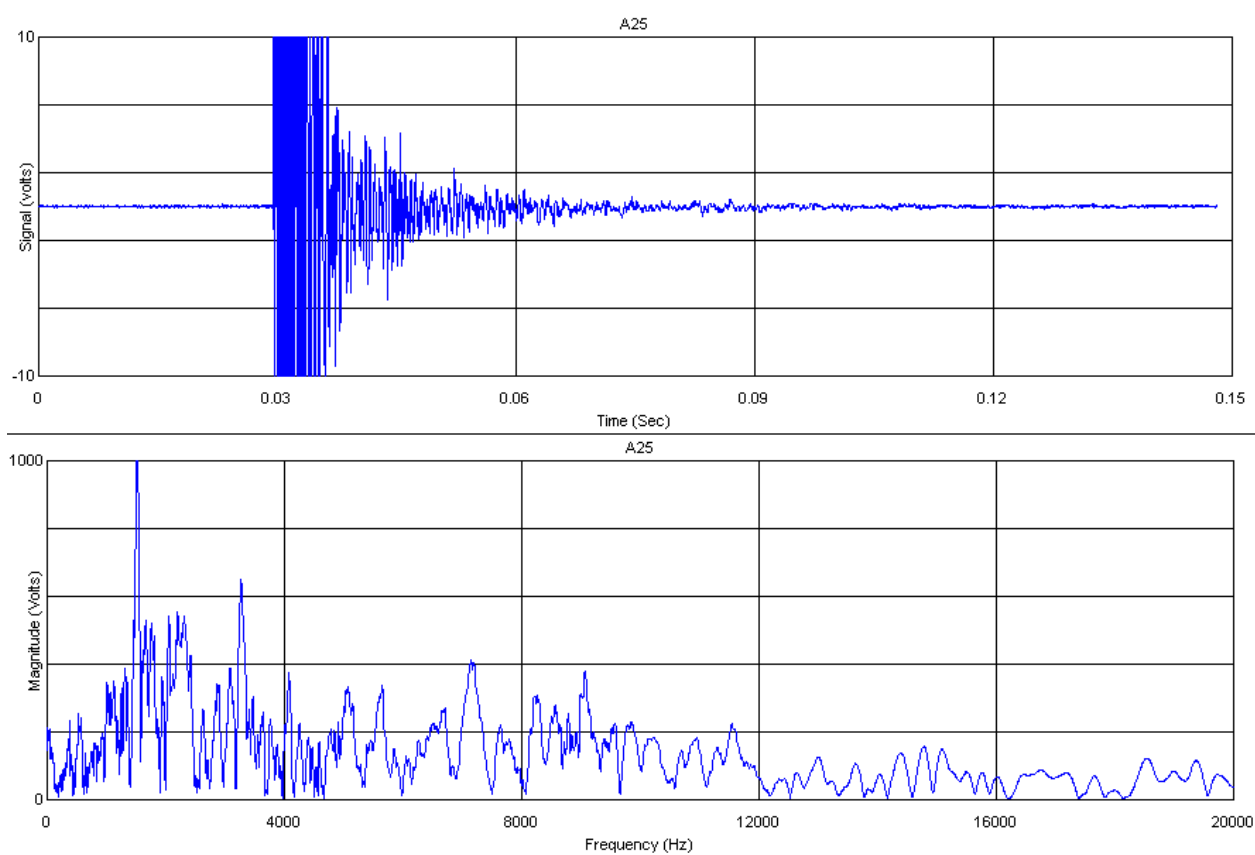


Figure 8: Time Domain and Frequency domain plots of a typical wire break recorded by a nearby sensor

Detection of Events in Basemat during SFMT

During the later stages of the SFMT, events started occurring that originated in the basemat of the PCCV, but which did not have all of the characteristics expected of wire breaks. Sixty-Five events of this type occurred between 10:43:37 and at 10:46:03. The graph below shows the locations of these events.

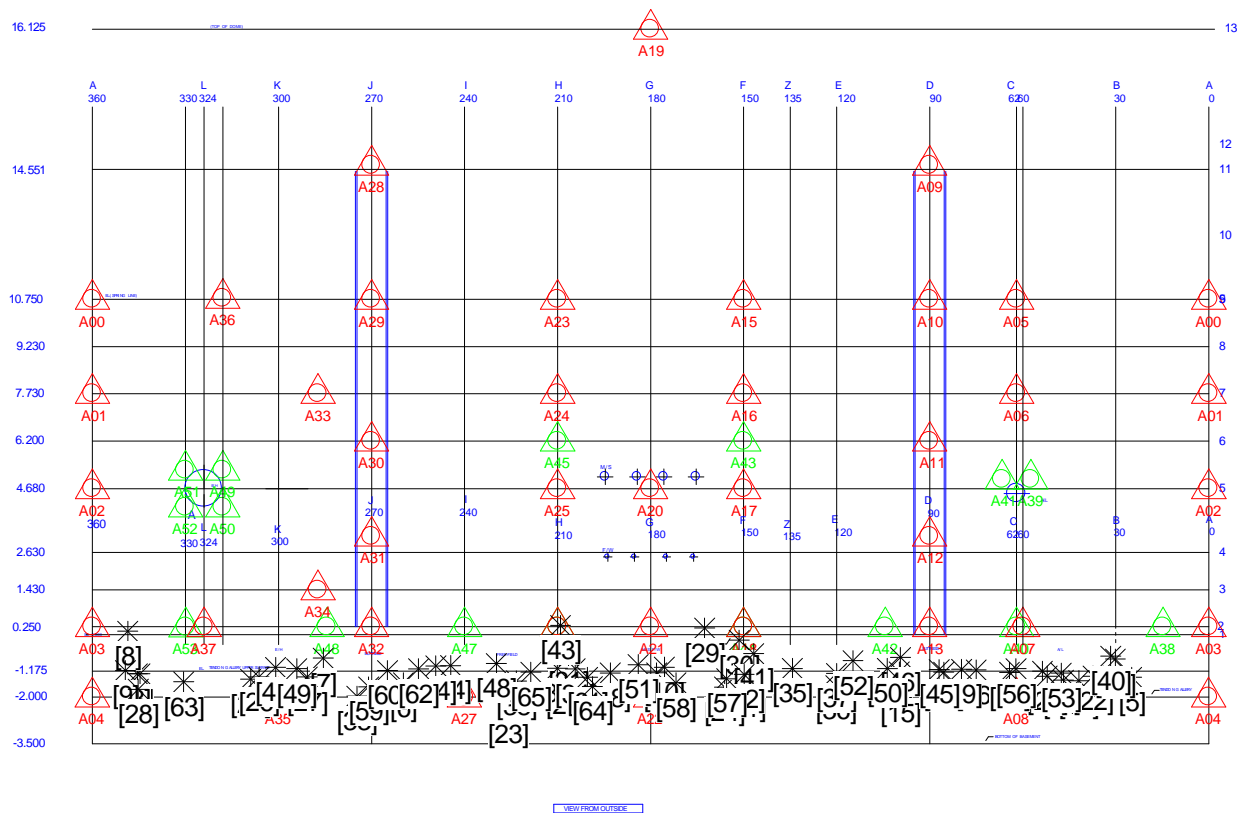


Figure 9: Location of Events in Basemat during SFMT

Detection of Average Energies of Wire Breaks

As the SFMT progressed, successive wire breaks were detected at increasing pressures. An estimate of the relative energy released by these breaks is made below. Note that the last event is the rupture of the vessel.

PCCV : Energy At Nearest Sensor Vs. Elapsed Time Nov 14/01

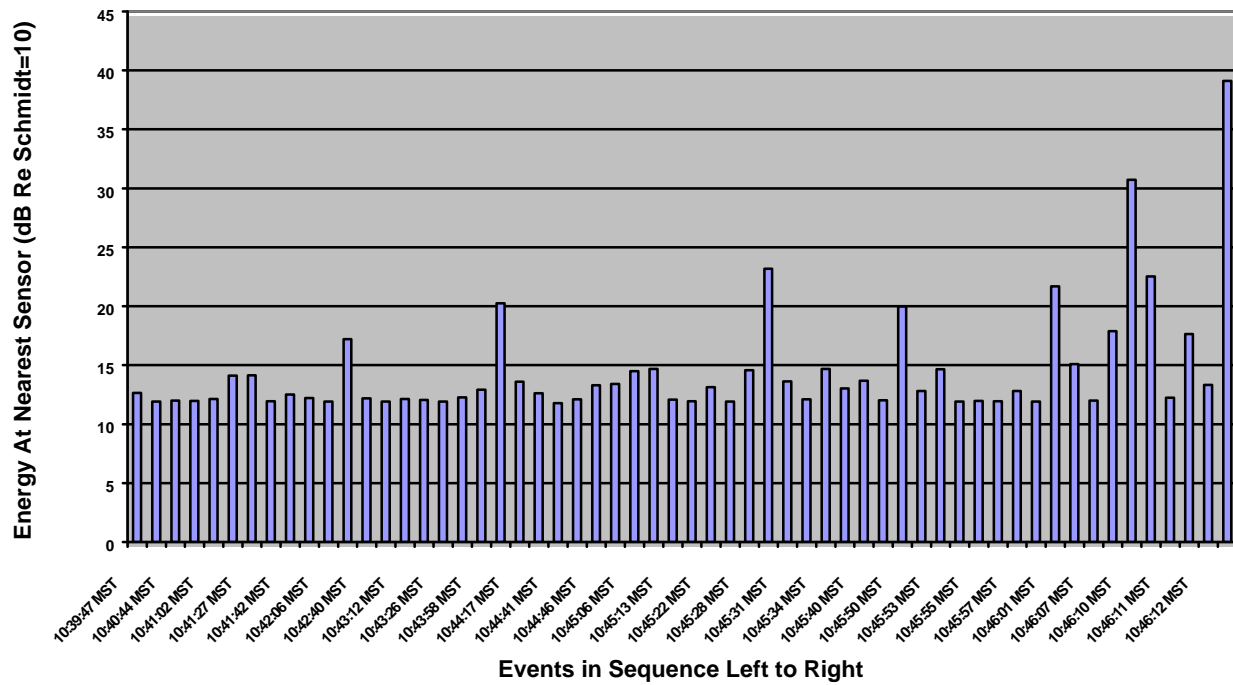


Figure 10 Energy vs Time of wire breaks in SMFT

Detection of Cracking

Throughout the SIT, LST and SFMT, events were detected that had properties consistent with concrete cracking. Most of these events occurred during the LST. Many thousands of these events were heard. Events sufficiently large to be detected at >5dB were located. During the SIT, there were 20 events located, and during the LST, there were 264 events located. Typical cracking behaviour has a time domain graph with multiple events, and a frequency domain that has anomalies from 6 KHz to 12 KHz.

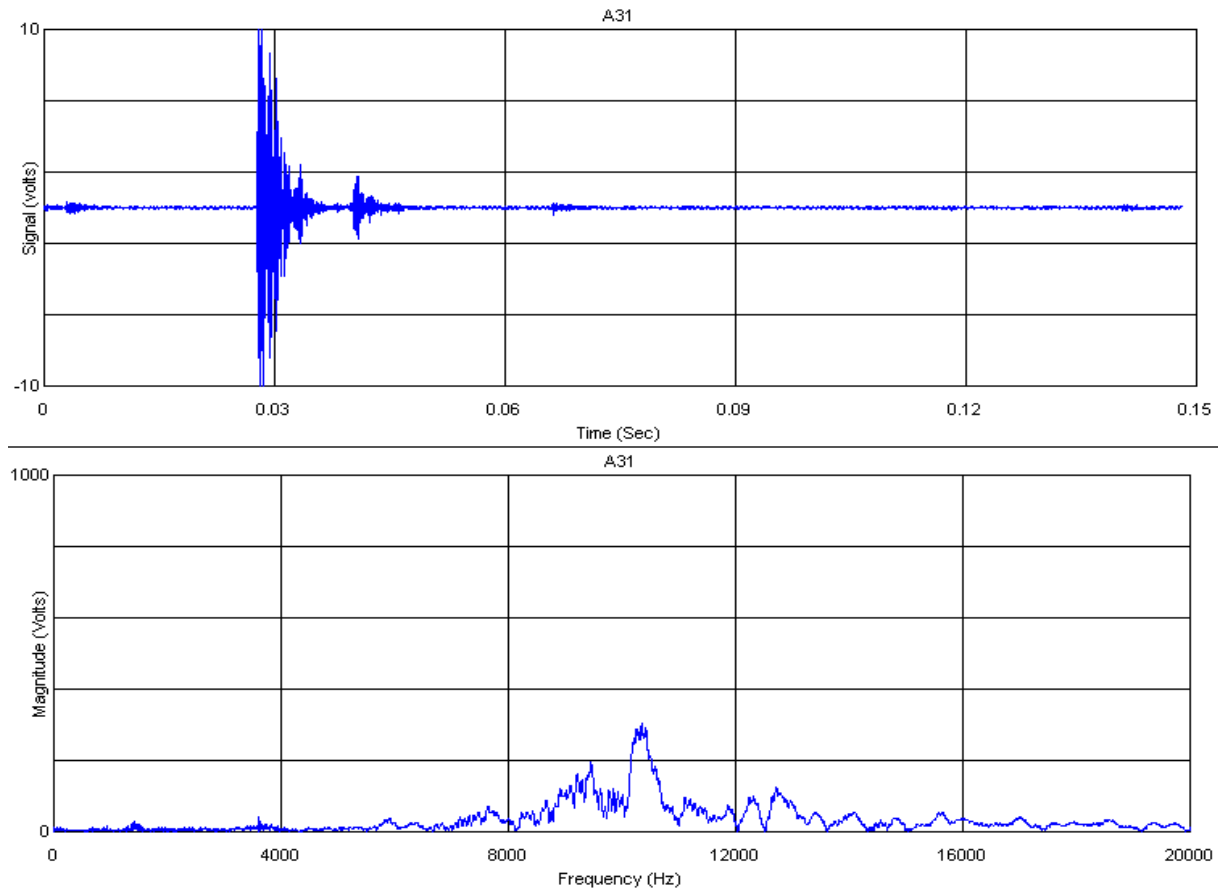


Figure 11 Typical Concrete Cracking Event Large Enough to Locate

Tendon Pings During SFMT

Most of the tendon pings detected during the SFMT occurred in the buttresses with a few originating from the basemat area.

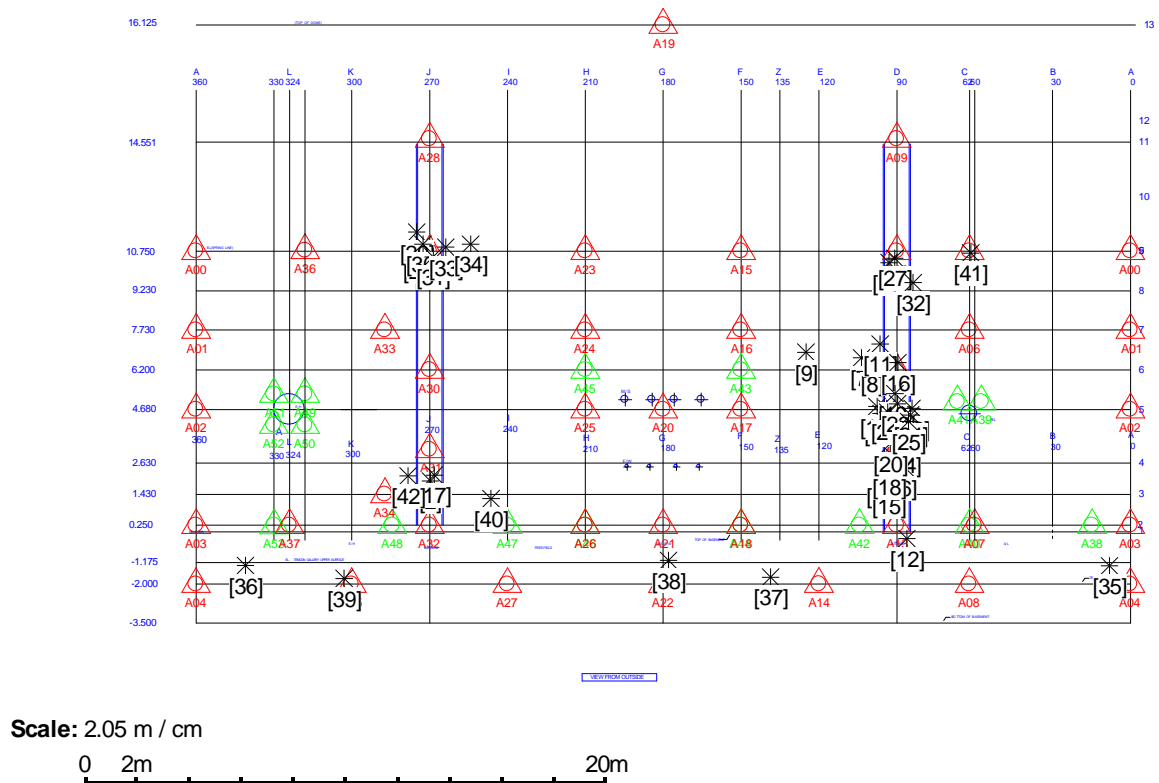


Figure 12: Tendon Pings During SFMT

Summary of Acoustic Monitoring on PCCV

Background

The PCCV vessel was designed to test the failure modes and prediction strategies developed to model the behavior of the vessel as containment pressures exceed the design pressures.

Acoustic monitoring was represented as being able to detect several useful types of information. These included:

1. Failure of Post-Tensioning Strand Wires
2. Concrete Cracking

Although not originally planned, it was hoped that leak development would also be detected.

Throughout the prestressing phase, and the three testing phases, the monitoring system was continuously active. Fifty Four sensors were applied to the vessel, forty eight externally, and sixteen on the liner internally to the vessel.

Summary of Results

Acoustic monitoring of the vessel detected no wire breaks during the prestressing phase, but detected the development of several large cracks during and after the prestressing phase completion. The largest of these were confirmed by visual examination of the external surface of the vessel before pressurization.

During the LST, 136 large events emanating from the buttresses were detected and identified as “tendon pings” meaning a readjustment of position of the tendon near the anchorage, but these were not wire or tendon failures.

A total of 489 cracking events were detected and mapped on the attached drawings. Some views of these data are available with the visual mapping of the cracks overlaying the plots.

Ten events originating near the tendon gallery indicate concrete crushing in that area.

No tendon failures were detected.

One leak was detected at 2.4 Pd near the equipment hatch. Other leaks became apparent as the pressures increased.

Real time audio of the acoustic sensors was made available to the participants in the LST.

Development of Leaks

Tear in the liner allow nitrogen to flow. This process generates acoustic noise that is detectable by nearby sensors. The graphics below are Fourier Transforms of events detected by the sensors mounted internally on the liner. Figure 1 shows the response before any tearing is suspected. Notice that the output of all of the sensors is very low and displays no anomalies.

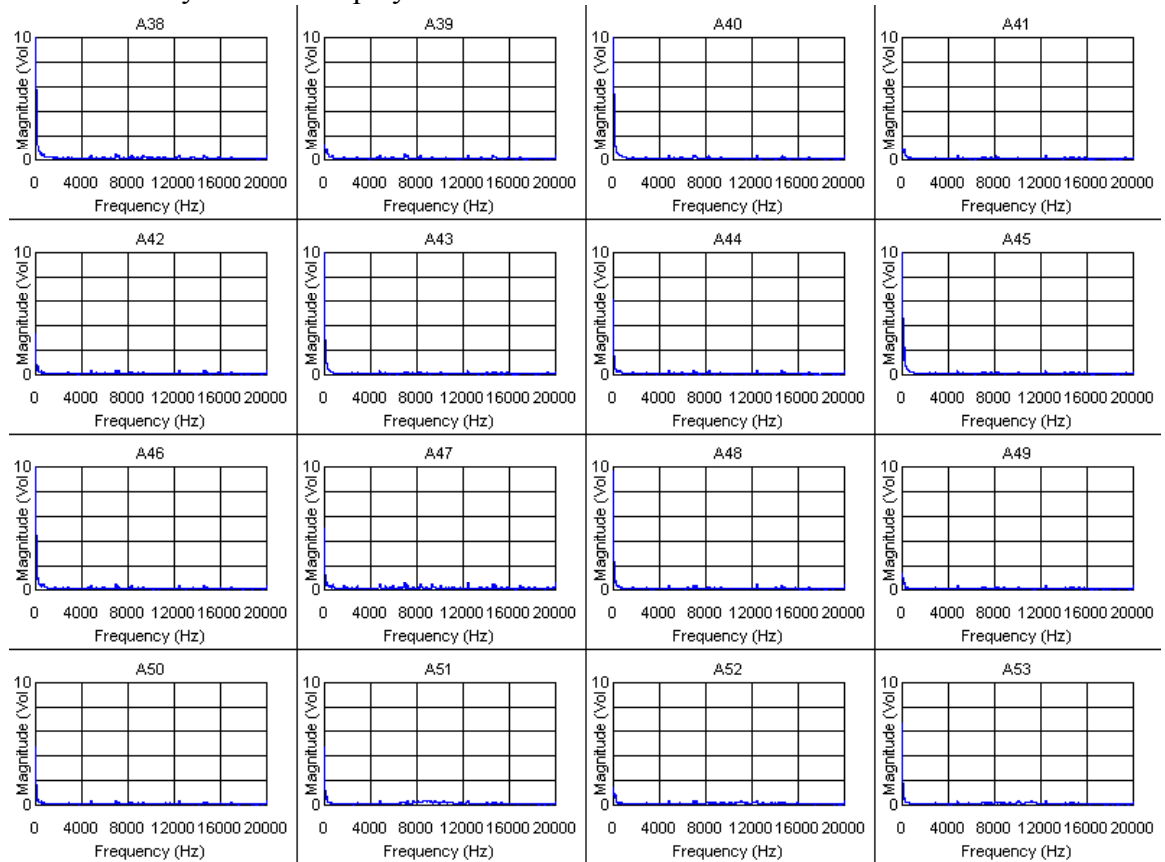


FIG. 1 FFT of internal sensors before liner tearing
Time: 09:27:52 Wed Sept 27, 2000

Figure 2 below shows the development of a suspected tear in the liner near the equipment hatch. Notice that sensors A50, A51, and A52 all show a broadband white noise centered around 8 KHz.

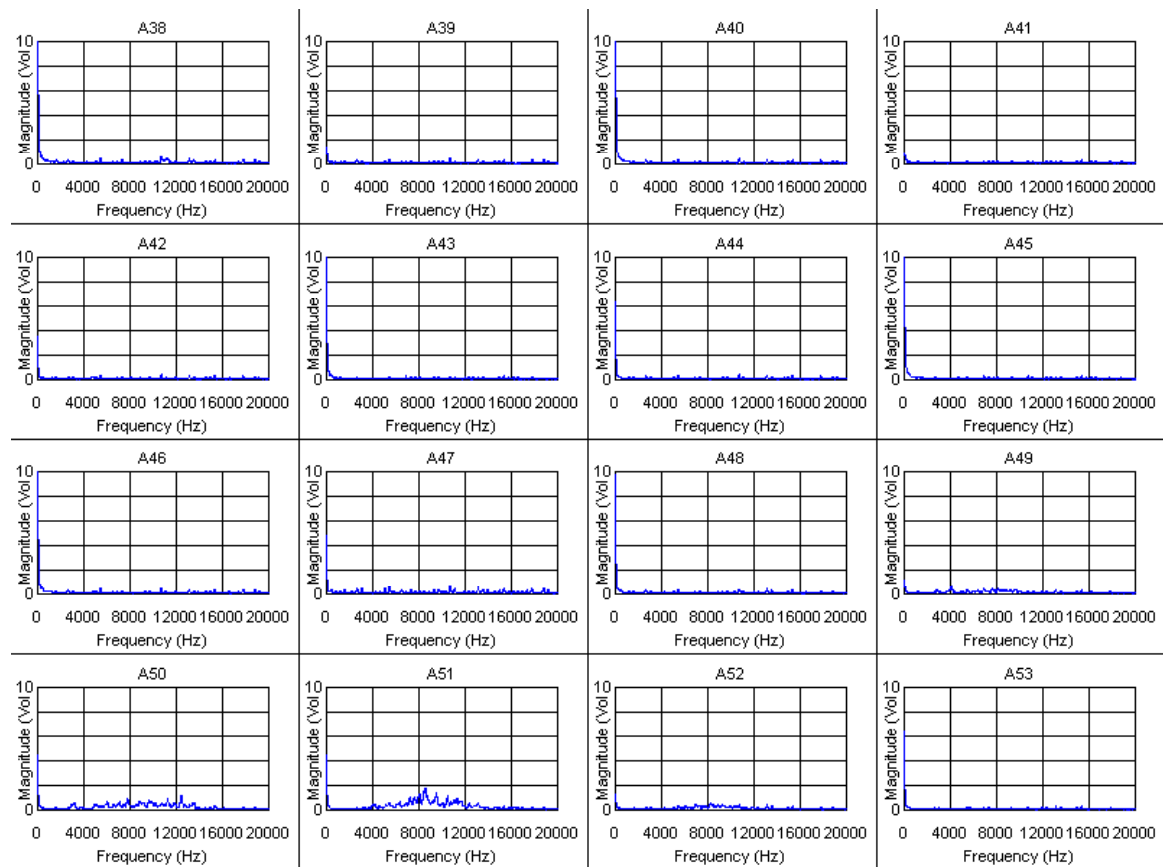


Figure 2. FFT of internal sensors showing noise from liner tear near equipment hatch

Time: 11:18:21 Wed Sept 27, 2000

Figure 3 below shows anomalies that have developed in several places on the liner. Notice that the amplitude of the noise has increased sharply in A50, 51, and 52, indicating that the tears in that area are increasing in size and flow. These anomalies were also detectable on the external sensors.

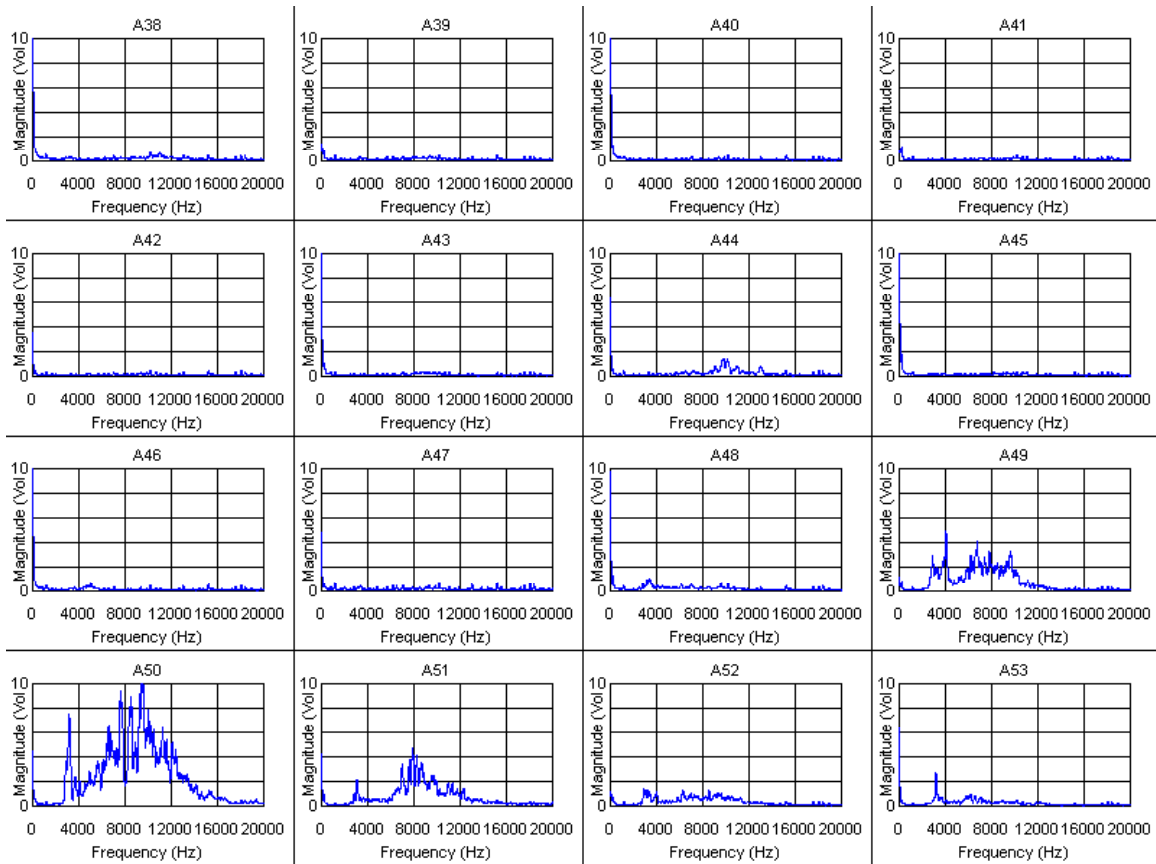


Figure 3. FFT of Internal Sensors showing well developed flow noise from suspected tearing of the liner.

Time 12:12:44 Wed Sept 27, 2000

Figure 4 below also shows increased flow noise in many areas of the liner.

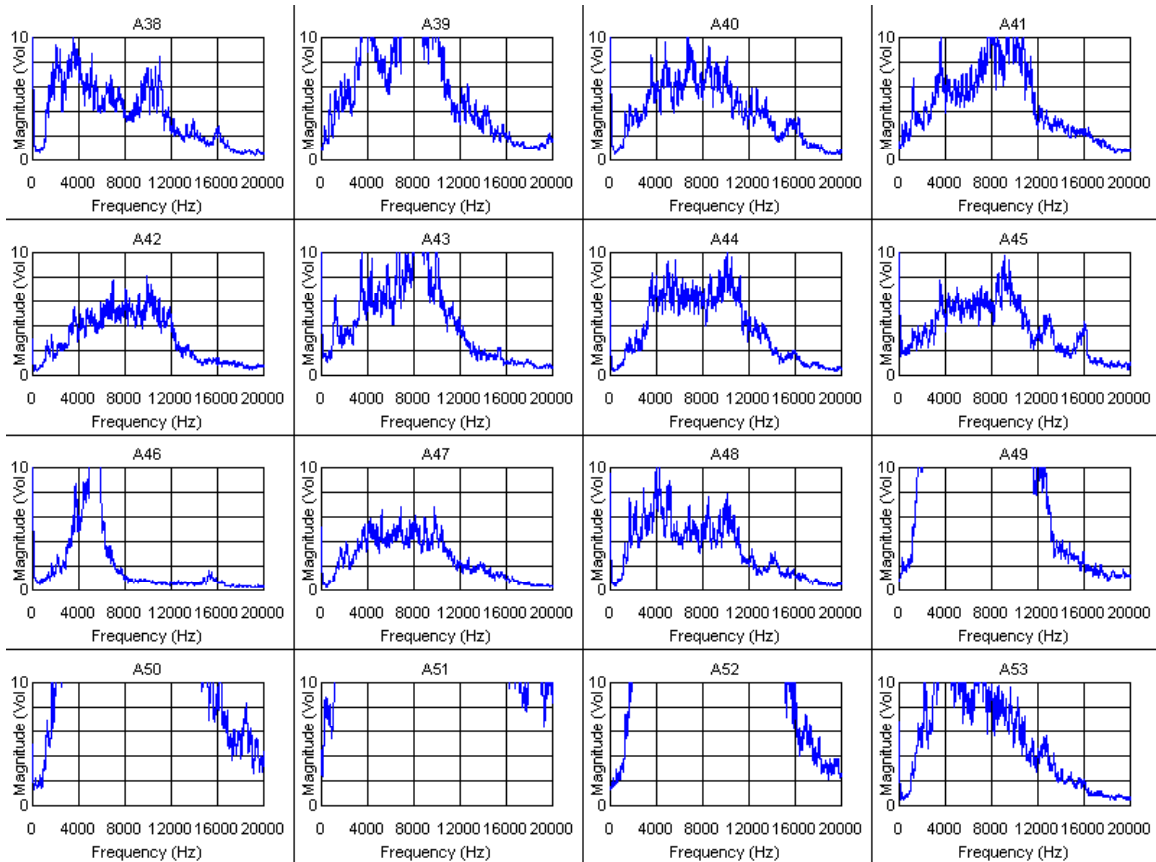


Figure 4. FFT of internal sensors with increased flow
noise from many suspected liner tears
Time: 15:45:49 Wed Sept 27, 2000

Development of concrete cracking

Concrete cracking was detected throughout the construction and testing of the PCCV. Large cracking sounds were located on the elevation view of the vessel. For this summary, only three figures are shown.. Figure 4 shows the position of cracks during the LST. Other views of cracks are available in the attached reports.

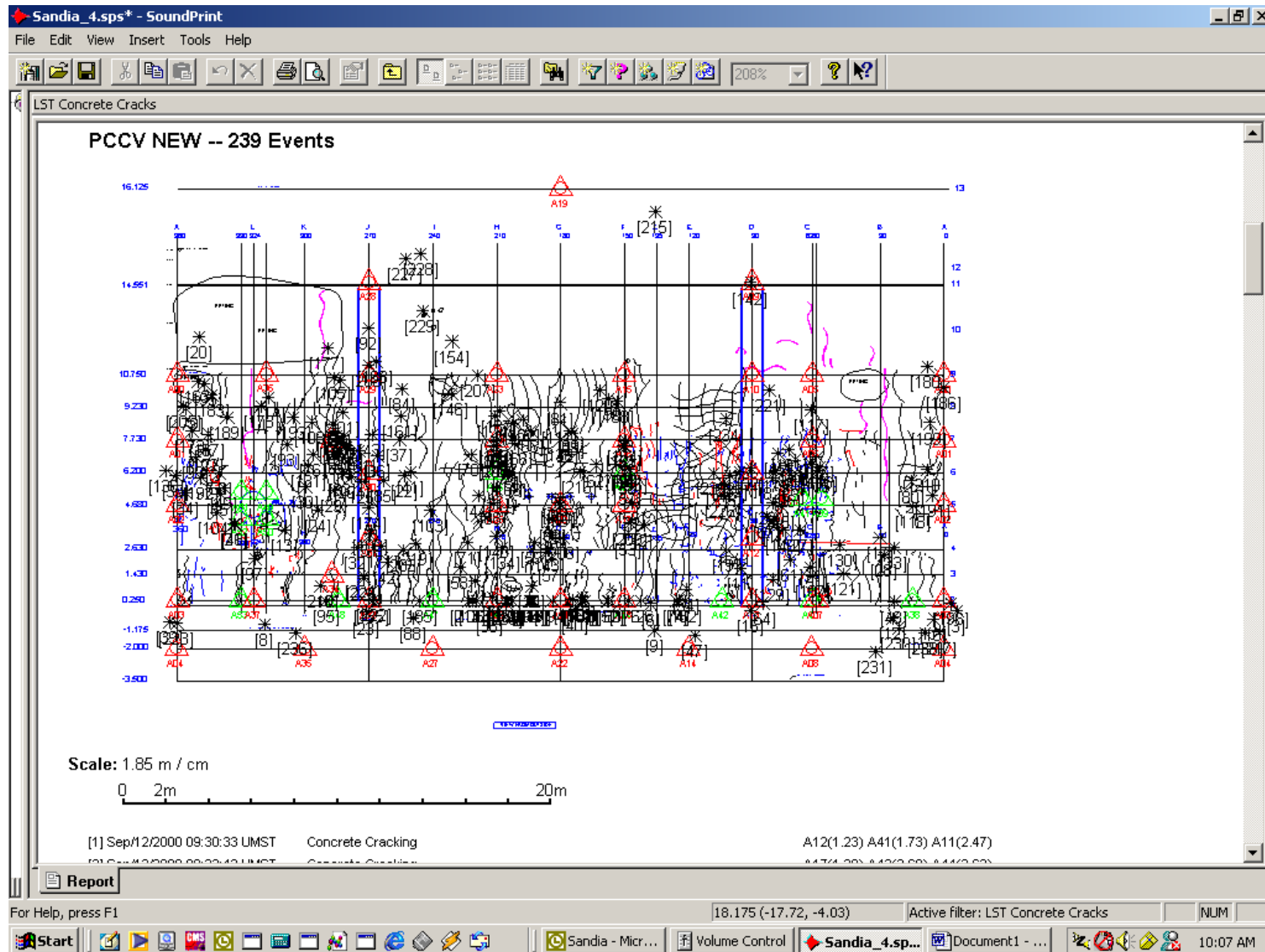


Figure 4 Position of cracking during LST overlay onto map of visual cracking

Events identified as concrete cracking have a sharp time domain signature and a FFT signature with anomalies from 8 KHz to about 12 KHz in the frequency domain. Figure 5 below shows a typical event from cracking of the concrete. The top chart is the time domain representation of the event, while the bottom chart is the frequency domain representation of the same event on the same sensor.

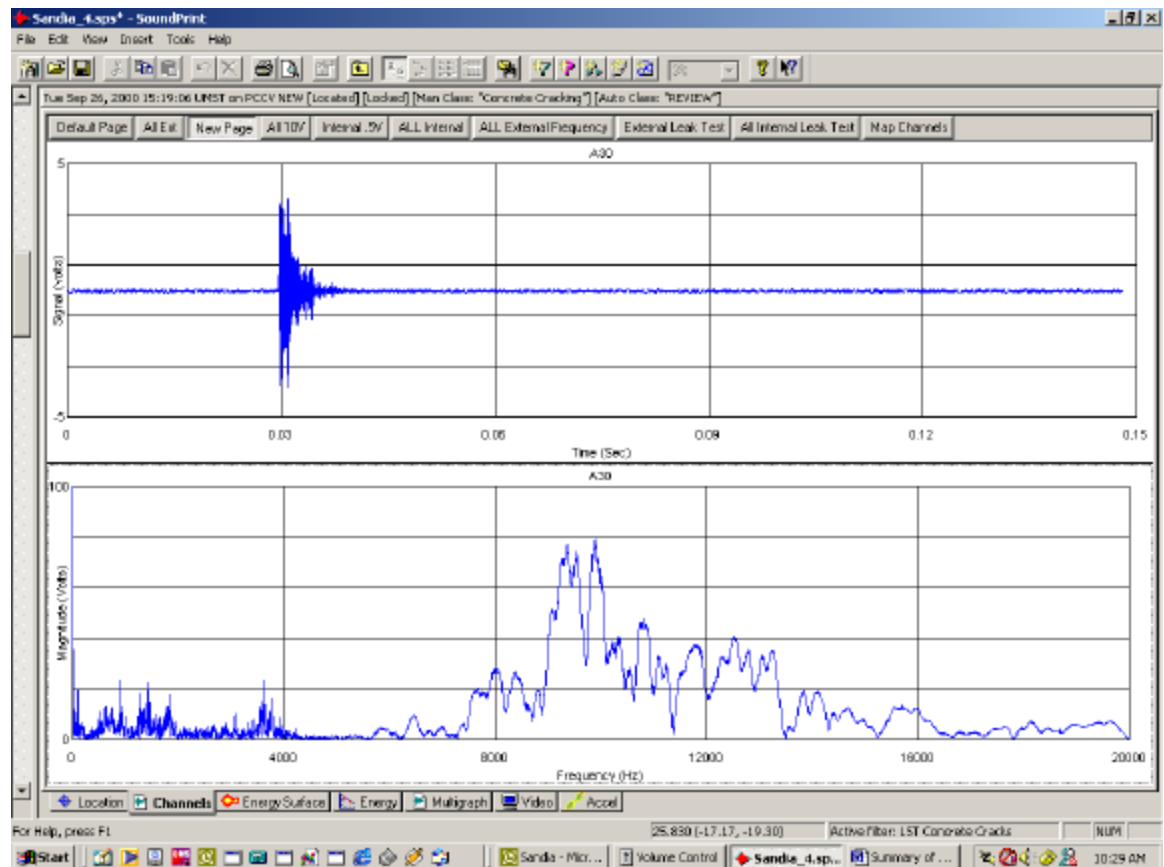


Figure 5 Typical event resulting from concrete cracking during LST

The locations of the “tendon pings” that may have resulted from load distribution is shown below in figure 6.

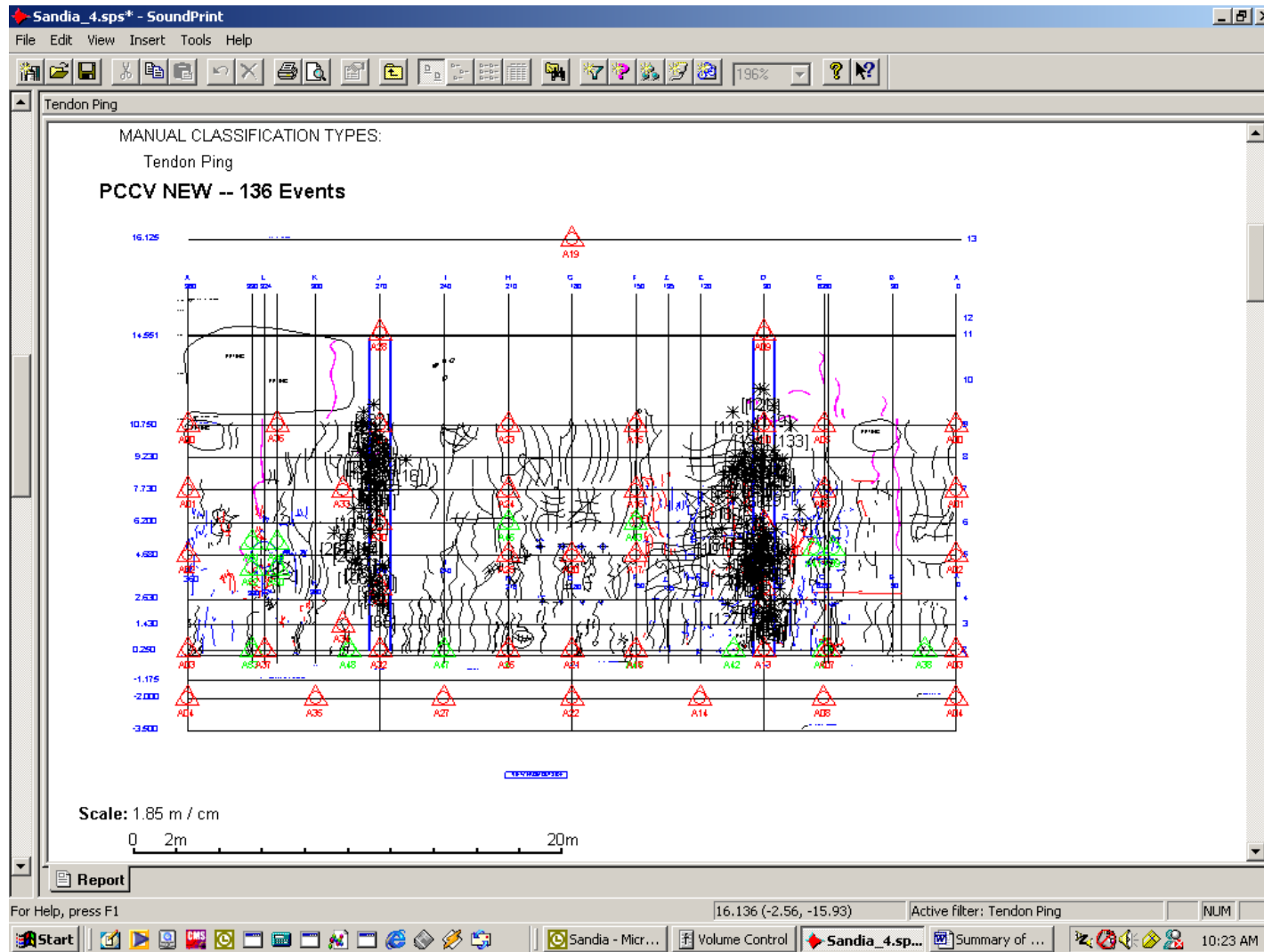


Figure 6 Locations of events identified as tendon pings during the LST

Figure 7 below shows the time and frequency domain plots of a typical tendon ping event.

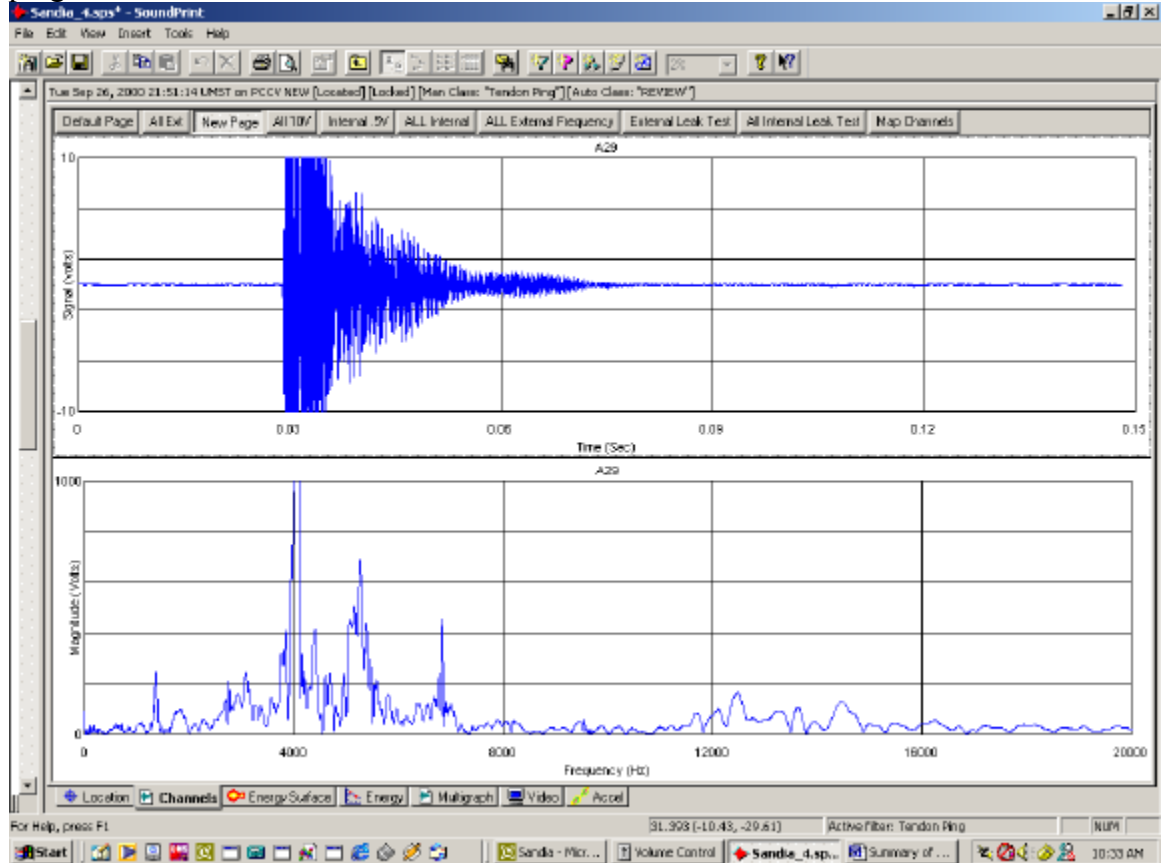


Figure 7 showing Time domain and FFT of a typical tendon ping event.

Conclusion

Acoustic monitoring of the PCCV was able to detect and identify all of the features intended, and some supplementary information was also reported.

- No tendon failures occurred during the construction, the SIT or the LST
- Cracking was widespread and easily detected and mapped
- Other tendon behavior was tracked and reported (tendon pings)
- Localized crushing of the concrete was detected
- Leaks were detected and reported at levels of about 1 mass percent per day

Acoustic monitoring can provide global information about the behavior of a PCCV with widely distributed surface mounted sensors.

SANDIA PCCV
ALBUQUERQUE, NM

SOUNDPRINT® ACOUSTIC MONITORING PROGRAM

REPORT

REPORTING PERIOD: MARCH 13 TO SEPTEMBER 27, 2000

DISCLAIMER

The information provided in this report is not intended to constitute an engineering report and should not be construed as such. The client is advised to retain qualified engineering expertise to interpret the data contained in this report. The information contained in this report is provided “as is” without warranty of any kind, either express or implied. Pure Technologies Ltd. is not liable for any lost profits, lost savings or other incidental, special or consequential damage arising out of the use of the monitoring system or the information contained in this report. Please refer to the terms and conditions attached to Pure’s SoundPrint® System Purchase Agreement and Pure’s Technical Support Agreement for further details.

® Registered Trademark, property of Pure Technologies Ltd.

TABLE OF CONTENTS

<i>Section</i>	<i>Title</i>
1.0	Executive Summary
2.0	SoundPrint [®] Report: ALL Cracks: (03/13/2000)

1.0 EXECUTIVE SUMMARY

The following is a summary of relevant activity recorded by the SoundPrint® monitoring system. The summary includes information for both the latest monitoring period and for the entire monitoring period from the start-up date up to and including the most recent monitoring period.

	Period 03/13/2000– 09/27/2000
Operating Efficiency	88.4%
ALL Cracks	489

Comments

Recommendations

There are no new recommendations at this time.

Prepared by:

Peter Paulson
President & CEO

REPORT PRESENTATION

A computerized drawing of the slab with the sensor layout is included on the following page and contains the following symbols:



Sensor Symbol with individual sensor name beneath



Symbolizes an event location. Event details are listed on the page following the drawing.

A list describing event details is provided for each drawing and lists the event number, shown on the computerized drawing, followed by the date, time, event classification and co-ordinates (in meters) to the origin of the events using the three closes sensors.

Event Report For Sandia PCCV

Albuquerque, NM

System Uptime 175 Days (88.4%)

ALL CRACKS

Period: 03/13/2000 to 09/27/2000

Matched Events: 489



SoundPrint® Acoustic Monitoring Report
Sandia PCCV



A horizontal number line starting at 0 and ending at 20m. There are tick marks at 0, 2m, 4m, 6m, 8m, 10m, 12m, 14m, 16m, 18m, and 20m.

Events

No.	Date/Time	Classification	Location (m)
[1]	Mar/13/2000 23:25:01 UMST	Possible Cracking Sound	A48(0.90)A34(1.30) A32(2.33)
[2]	Mar/18/2000 07:37:50 UMST	Circumferential Event	A28(2.46) A29(3.86) A36(4.07)
[3]	Mar/20/2000 10:04:33 UMST	Circumferential Event	A19(3.44) A15(5.81) A23(7.33)
[4]	Mar/20/2000 11:20:19 UMST	Circumferential Event	A09(1.82) A10(3.03) A05(3.31)
[5]	Mar/21/2000 14:42:51 UMST	Circumferential Event	A05(2.21) A10(3.05) A09(3.08)
[6]	Mar/25/2000 12:35:37 UMST	Possible Cracking Sound	A09(2.54)A05(2.62) A10(2.85)
[7]	Apr/04/2000 13:42:13 UMST	Possible Cracking Sound	A36(1.52) A33(3.56) A49(4.00)
[8]	Apr/04/2000 14:07:13 UMST	Possible Cracking Sound	A30(2.40) A24(3.84) A33(3.90)
[9]	Apr/06/2000 07:07:36 UMST	Possible Cracking Sound	A29(2.18) A36(2.75) A33(3.67)
[10]	Apr/06/2000 08:42:23 UMST	Circumferential Event	A01(2.30) A02(3.49) A06(3.92)
[11]	Apr/06/2000 09:37:58 UMST	Circumferential Event	A29(2.45) A28(3.42) A23(4.28)
[12]	Apr/06/2000 09:51:18 UMST	Circumferential Event	A05(1.32) A10(2.74) A09(3.88)
[13]	Apr/06/2000 09:51:59 UMST	Possible Cracking Sound	A29(2.01)A28(2.52) 36(4.46)
[14]	Apr/06/2000 12:51:40 UMST	Circumferential Event	A28(2.72) A29(3.09) A36(3.69)
[15]	Apr/12/2000 08:25:11 UMST	Circumferential Event	A00(1.30) A01(1.83) A36(3.98)
[16]	Apr/12/2000 11:31:41 UMST	Circumferential Event	A23(1.45) A24(1.64) A45(3.15)
[17]	Apr/12/2000 11:45:43 UMST	Circumferential Event	A16(3.37) A10(3.40) A15(3.76)
[18]	Apr/13/2000 09:30:02 UMST	Possible Cracking Sound	A05(3.49) A00(4.49) A09(5.52)
[19]	Apr/14/2000 12:46:01 UMST	Possible Cracking Sound	A15(3.51) A09(3.91) A10(4.24)
[20]	Apr/19/2000 15:18:44 UMST	Circumferential Event	A36(1.00) A00(3.33) A01(4.18)
[21]	Apr/19/2000 15:26:04 UMST	Possible Cracking Sound	A51(2.46) A49(2.61) A36(3.21)
[22]	Apr/20/2000 06:43:28 UMST	Possible Cracking Sound	A15(3.30) A09(5.55) A16(6.30)
[23]	Apr/21/2000 10:17:03 UMST	Possible Cracking Sound	A00(0.62) A01(3.10) A36(4.79)
[24]	Apr/24/2000 07:47:13 UMST	Possible Cracking Sound	A02(1.21) A01(3.13) A39(4.51)
[25]	May/02/2000 16:50:19 UMST	Circumferential Event	A10(3.30) A16(3.43) A15(3.69)
[26]	May/02/2000 16:50:29 UMST	Circumferential Event	A15(1.90) A16(2.22) A43(3.54)
[27]	Jul/18/2000 08:31:27 UMST	Possible Cracking Sound	A01(3.02) A06(3.15) A39(3.76)
[28]	Jul/18/2000 08:31:35 UMST	Possible Cracking Sound	A22(1.26) A21(2.28) A44(2.61)
[29]	Jul/18/2000 08:31:45 UMST	Possible Cracking Sound	A40(1.57) A07(1.73) A08(1.78)
[30]	Jul/18/2000 08:31:47 UMST	Possible Cracking Sound	Not Located
[31]	Jul/18/2000 08:32:09 UMST	Possible Cracking Sound	Not Located
[32]	Jul/18/2000 08:32:10 UMST	Possible Cracking Sound	A22(2.00) A18(2.47) A44(2.47)
[33]	Jul/18/2000 08:32:23 UMST	Possible Cracking Sound	Not Located
[34]	Jul/18/2000 08:32:44 UMST	Possible Cracking Sound	A22(0.28) A21(2.53) A46(3.91)
[35]	Jul/18/2000 08:32:50 UMST	Possible Cracking Sound	Not Located
[36]	Jul/18/2000 08:32:50 UMST	Possible Cracking Sound	Not Located
[37]	Jul/18/2000 08:32:53 UMST	Possible Cracking Sound	Not Located
[38]	Jul/18/2000 08:33:01 UMST	Possible Cracking Sound	A35(1.16) A48(1.78) A34(2.54)
[39]	Jul/18/2000 08:33:05 UMST	Possible Cracking Sound	A14(1.89) A18(2.03) A44(2.03)
[40]	Jul/18/2000 08:33:07 UMST	Possible Cracking Sound	A23(0.51) A24(3.50) A45(5.03)
[41]	Jul/18/2000 08:33:10 UMST	Possible Cracking Sound	A32(1.93) A48(2.24) A35(2.74)
[42]	Jul/18/2000 08:33:13 UMST	Possible Cracking Sound	A23(0.84) A24(2.51) A45(4.01)
[43]	Jul/18/2000 08:33:15 UMST	Possible Cracking Sound	A22(0.32) A21(2.58) A46(3.93)

[44]	Jul/18/2000 08:33:16 UMST	Possible Cracking Sound	Not Located
[45]	Jul/18/2000 08:33:32 UMST	Possible Cracking Sound	A35(1.82) A48(2.82) A32(3.08)
[46]	Jul/18/2000 08:33:38 UMST	Possible Cracking Sound	Not Located
[47]	Jul/18/2000 08:33:44 UMST	Possible Cracking Sound	Not Located
[48]	Jul/18/2000 08:33:45 UMST	Possible Cracking Sound	A22(1.11) A21(1.15) A26(3.11)
[49]	Jul/18/2000 08:34:27 UMST	Possible Cracking Sound	Not Located
[50]	Jul/18/2000 08:34:34 UMST	Possible Cracking Sound	A22(2.19) A44(2.67) A18(2.67)
[51]	Jul/18/2000 08:34:35 UMST	Possible Cracking Sound	A23(2.00) A24(4.52) A15(4.55)
[52]	Jul/18/2000 08:34:57 UMST	Possible Cracking Sound	Not Located
[53]	Jul/18/2000 08:35:10 UMST	Possible Cracking Sound	A32(2.17) A27(2.65) A48(2.78)
[54]	Jul/18/2000 08:35:11 UMST	Possible Cracking Sound	A13(1.65) A08(1.95) A40(2.05)
[55]	Jul/18/2000 08:35:32 UMST	Possible Cracking Sound	Not Located
[56]	Jul/18/2000 08:36:09 UMST	Possible Cracking Sound	Not Located
[57]	Jul/18/2000 08:36:15 UMST	Possible Cracking Sound	Not Located
[58]	Jul/18/2000 08:37:02 UMST	Possible Cracking Sound	A48(0.84) A32(1.53) A34(2.05)
[59]	Jul/18/2000 08:37:06 UMST	Possible Cracking Sound	Not Located
[60]	Jul/18/2000 08:37:19 UMST	Possible Cracking Sound	Not Located
[61]	Jul/18/2000 08:37:20 UMST	Possible Cracking Sound	A42(1.25) A14(1.77) A13(1.97)
[62]	Jul/18/2000 08:37:23 UMST	Possible Cracking Sound	Not Located
[63]	Jul/18/2000 08:37:31 UMST	Possible Cracking Sound	Not Located
[64]	Jul/18/2000 08:37:48 UMST	Possible Cracking Sound	A42(0.70) A13(1.99) A14(2.04)
[65]	Jul/18/2000 08:38:32 UMST	Possible Cracking Sound	A20(1.47) A17(1.56) A43(2.36)
[66]	Jul/18/2000 08:39:36 UMST	Possible Cracking Sound	Not Located
[67]	Jul/18/2000 08:39:36 UMST	Possible Cracking Sound	A27(0.66) A47(2.85) A32(3.89)
[68]	Jul/18/2000 08:39:42 UMST	Possible Cracking Sound	A22(1.34) A21(3.60) A46(4.67)
[69]	Jul/18/2000 08:40:00 UMST	Possible Cracking Sound	A35(1.78) A48(1.99) A32(2.33)
[70]	Jul/18/2000 08:40:01 UMST	Possible Cracking Sound	A22(0.04) A21(2.30) A46(3.76)
[71]	Jul/18/2000 08:40:22 UMST	Possible Cracking Sound	A44(1.46) A18(1.46) A21(2.25)
[72]	Jul/18/2000 08:40:25 UMST	Possible Cracking Sound	A35(1.18) A48(1.88) A34(2.58)
[73]	Jul/18/2000 08:40:25 UMST	Possible Cracking Sound	A35(1.24) A37(2.06) A53(2.54)
[74]	Jul/18/2000 08:40:50 UMST	Possible Cracking Sound	A14(2.56) A13(2.76) A42(2.88)
[75]	Jul/18/2000 08:41:39 UMST	Possible Cracking Sound	A21(0.07) A22(2.33) A26(2.98)
[76]	Jul/18/2000 08:42:23 UMST	Possible Cracking Sound	Not Located
[77]	Jul/18/2000 08:42:37 UMST	Possible Cracking Sound	A42(0.18) A13(1.33) A14(2.92)
[78]	Jul/18/2000 08:43:10 UMST	Possible Cracking Sound	A47(1.12) A27(1.69) A26(2.31)
[79]	Jul/18/2000 08:43:13 UMST	Possible Cracking Sound	A18(1.95) A44(1.95) A22(2.08)
[80]	Jul/18/2000 08:43:23 UMST	Possible Cracking Sound	A15(2.14) A16(3.70) A23(3.82)
[81]	Jul/18/2000 08:43:24 UMST	Possible Cracking Sound	Not Located
[82]	Jul/18/2000 08:43:32 UMST	Possible Cracking Sound	A46(1.49) A26(1.49) A27(2.98)
[83]	Jul/18/2000 08:43:33 UMST	Possible Cracking Sound	A14(0.91) A42(2.62) A44(2.86)
[84]	Jul/18/2000 08:43:38 UMST	Possible Cracking Sound	A03(2.23) A02(2.47) A52(2.81)
[85]	Jul/18/2000 08:43:40 UMST	Possible Cracking Sound	A38(2.17) A03(2.21) A02(2.49)
[86]	Jul/18/2000 09:36:32 UMST	Possible Cracking Sound	A05(3.11) A06(3.37) A00(3.53)
[87]	Jul/18/2000 09:46:29 UMST	Possible Cracking Sound	A31(1.06) A32(1.93) A34(2.17)
[88]	Jul/18/2000 09:46:50 UMST	Possible Cracking Sound	A03(0.43) A38(1.52) A04(2.68)
[89]	Jul/18/2000 09:47:46 UMST	Possible Cracking Sound	A44(1.07) A18(1.07) A21(1.91)

[90]	Jul/18/2000 09:47:47 UMST	Possible Cracking Sound	A42(1.67) A14(2.25) A44(2.87)
[91]	Jul/18/2000 09:47:48 UMST	Possible Cracking Sound	A09(4.32) A19(5.64) A15(6.61)
[92]	Jul/18/2000 09:48:04 UMST	Possible Cracking Sound	A29(2.24) A36(2.53) A33(3.06)
[93]	Jul/18/2000 09:48:09 UMST	Possible Cracking Sound	A13(0.93) A42(1.93) A40(2.65)
[94]	Jul/18/2000 09:48:11 UMST	Possible Cracking Sound	A21(1.44) A44(1.54) A18(1.54)
[95]	Jul/18/2000 09:48:20 UMST	Possible Cracking Sound	A18(0.04) A44(0.04) A21(3.02)
[96]	Jul/18/2000 09:48:35 UMST	Possible Cracking Sound	A14(1.19) A18(2.64) A44(2.64)
[97]	Jul/18/2000 09:49:02 UMST	Possible Cracking Sound	Not Located
[98]	Jul/18/2000 09:49:20 UMST	Possible Cracking Sound	A21(0.68) A22(2.02) A26(2.41)
[99]	Jul/18/2000 09:49:21 UMST	Possible Cracking Sound	Not Located
[100]	Jul/18/2000 09:49:30 UMST	Possible Cracking Sound	A04(1.31) A38(1.65) A03(1.99)
[101]	Jul/18/2000 09:49:35 UMST	Possible Cracking Sound	A35(1.18) A37(2.17) A48(2.50)
[102]	Jul/18/2000 09:49:36 UMST	Possible Cracking Sound	A22(0.36) A21(2.01) A44(3.38)
[103]	Jul/18/2000 09:50:01 UMST	Possible Cracking Sound	A14(1.18) A18(2.62) A44(2.62)
[104]	Jul/18/2000 09:51:48 UMST	Possible Cracking Sound	A35(0.76) A48(2.09) A37(2.91)
[105]	Jul/18/2000 09:52:28 UMST	Possible Cracking Sound	A44(0.56) A18(0.56) A21(3.31)
[106]	Jul/18/2000 09:52:54 UMST	Possible Cracking Sound	A53(1.60) A37(2.05) A04(2.18)
[107]	Jul/18/2000 09:53:04 UMST	Possible Cracking Sound	A42(0.73) A13(1.39) A14(2.36)
[108]	Jul/18/2000 09:54:10 UMST	Possible Cracking Sound	A26(1.12) A46(1.12) A47(2.79)
[109]	Jul/18/2000 09:55:48 UMST	Possible Cracking Sound	A37(1.56) A53(2.14) A48(2.38)
[110]	Jul/18/2000 09:56:11 UMST	Possible Cracking Sound	A38(1.39) A04(1.63) A03(1.96)
[111]	Jul/18/2000 09:56:41 UMST	Possible Cracking Sound	A13(1.08) A42(2.02) A40(2.68)
[112]	Jul/18/2000 09:56:49 UMST	Possible Cracking Sound	A13(2.88) A08(2.93) A14(2.97)
[113]	Sep/12/2000 09:30:33 UMST	Concrete Cracking	A12(1.23) A41(1.73) A11(2.47)
[114]	Sep/12/2000 09:33:43 UMST	Concrete Cracking	A17(1.29) A43(2.60) A44(3.62)
[115]	Sep/12/2000 09:48:50 UMST	Concrete Cracking	A00(2.08) A01(2.31) A05(4.77)
[116]	Sep/12/2000 12:21:44 UMST	Concrete Cracking	A03(0.76) A04(1.89) A38(2.12)
[117]	Sep/12/2000 12:22:09 UMST	Possible Cracking Sound	A44(1.74) A18(1.74) A14(2.58)
[118]	Sep/12/2000 12:22:52 UMST	Possible Cracking Sound	Not Located
[119]	Sep/12/2000 12:23:53 UMST	Possible Cracking Sound	A43(2.06) A17(2.12) A16(2.94)
[120]	Sep/12/2000 12:24:10 UMST	Possible Cracking Sound	A09(4.81) A19(5.15) A15(6.72)
[121]	Sep/12/2000 12:24:48 UMST	Possible Cracking Sound	A35(1.50) A48(1.84) A32(2.40)
[122]	Sep/12/2000 12:25:23 UMST	Possible Cracking Sound	A19(5.16) A09(5.33) A15(8.28)
[123]	Sep/12/2000 12:26:53 UMST	Possible Cracking Sound	A21(0.89) A22(1.40) A26(2.90)
[124]	Sep/12/2000 12:28:49 UMST	Possible Cracking Sound	A47(1.27) A26(2.20) A46(2.20)
[125]	Sep/12/2000 12:31:04 UMST	Possible Cracking Sound	A37(0.16) A53(0.72) A35(3.25)
[126]	Sep/12/2000 12:31:55 UMST	Possible Cracking Sound	A08(0.82) A40(1.45) A07(1.48)
[127]	Sep/12/2000 13:22:51 UMST	Concrete Cracking	A26(1.37) A46(1.37) A47(2.18)
[128]	Sep/12/2000 13:27:45 UMST	Concrete Cracking	A26(0.26) A46(0.26) A47(2.77)
[129]	Sep/12/2000 13:53:08 UMST	Concrete Cracking	A44(1.25) A18(1.25) A14(2.73)
[130]	Sep/13/2000 13:06:27 UMST	Concrete Cracking	A42(2.01) A14(2.31) A44(2.53)
[131]	Sep/13/2000 14:27:30 UMST	Concrete Cracking	A37(1.22) A53(1.55) A35(2.20)
[132]	Sep/14/2000 15:57:41 UMST	Concrete Cracking	A14(1.81) A44(1.96) A18(1.96)
[133]	Sep/15/2000 06:45:19 UMST	Small Event on Apex Area	A15(2.64) A09(5.49) A16(5.59)
[134]	Sep/26/2000 13:54:31 UMST	Concrete Cracking	A19(4.57) A28(5.43) A23(6.30)
[135]	Sep/26/2000 13:55:42 UMST	Concrete Cracking	A21(1.05) A44(1.96) A18(1.96)

[136]	Sep/26/2000 14:25:54 UMST	Concrete Cracking	A12(1.51) A13(1.59) A42(1.73)
[137]	Sep/26/2000 14:27:18 UMST	Concrete Cracking	A38(1.22) A03(2.52) A04(2.80)
[138]	Sep/26/2000 14:27:20 UMST	Concrete Cracking	A50(1.01) A49(1.93) A52(2.12)
[139]	Sep/26/2000 14:30:04 UMST	Concrete Cracking	A45(0.62) A24(1.63) A25(1.66)
[140]	Sep/26/2000 14:30:22 UMST	Concrete Cracking	A13(0.45) A42(1.44) A40(2.88)
[141]	Sep/26/2000 14:30:32 UMST	Concrete Cracking	A03(0.99) A38(1.28) A04(1.49)
[142]	Sep/26/2000 14:31:58 UMST	Concrete Cracking	A27(1.89) A32(2.31) A47(2.77)
[143]	Sep/26/2000 14:47:36 UMST	Concrete Cracking	A39(3.27) A38(3.29) A02(3.35)
[144]	Sep/26/2000 14:50:18 UMST	Concrete Cracking	A21(1.51) A26(1.79) A46(1.79)
[145]	Sep/26/2000 14:50:47 UMST	Concrete Cracking	A12(1.32) A42(2.36) A13(2.64)
[146]	Sep/26/2000 14:54:19 UMST	Concrete Cracking	A00(2.07) A36(3.61) A01(4.93)
[147]	Sep/26/2000 15:16:32 UMST	Concrete Cracking	A52(0.43) A51(1.50) A50(1.54)
[148]	Sep/26/2000 15:18:38 UMST	Concrete Cracking	A42(0.17) A13(1.59) A14(2.64)
[149]	Sep/26/2000 15:18:51 UMST	Concrete Cracking	A31(1.67) A30(2.40) A34(2.78)
[150]	Sep/26/2000 15:19:06 UMST	Concrete Cracking	A30(1.65) A31(3.36) A33(3.75)
[151]	Sep/26/2000 15:19:19 UMST	Concrete Cracking	A15(2.92) A23(3.19) A16(4.66)
[152]	Sep/26/2000 15:20:32 UMST	Concrete Cracking	A19(4.61) A09(5.36) A15(6.56)
[153]	Sep/26/2000 15:20:55 UMST	Concrete Cracking	A32(0.57) A48(1.42) A34(2.36)
[154]	Sep/26/2000 15:21:38 UMST	Concrete Cracking	A02(1.24) A51(1.82) A52(2.08)
[155]	Sep/26/2000 15:21:47 UMST	Concrete Cracking	A50(2.45) A49(2.56) A31(2.69)
[156]	Sep/26/2000 15:21:50 UMST	Concrete Cracking	A33(1.02) A30(1.59) A49(3.59)
[157]	Sep/26/2000 15:21:51 UMST	Concrete Cracking	A41(1.03) A39(1.92) A12(2.01)
[158]	Sep/26/2000 15:21:59 UMST	Concrete Cracking	A41(0.91) A39(1.69) A11(1.77)
[159]	Sep/26/2000 15:22:18 UMST	Concrete Cracking	A41(1.44) A39(1.75) A12(2.28)
[160]	Sep/26/2000 15:22:27 UMST	Concrete Cracking	A38(2.50) A03(3.51) A02(3.65)
[161]	Sep/26/2000 15:22:45 UMST	Concrete Cracking	A30(1.85) A33(2.38) A31(2.75)
[162]	Sep/26/2000 15:22:54 UMST	Concrete Cracking	A49(1.82) A50(2.31) A33(2.53)
[163]	Sep/26/2000 15:23:02 UMST	Concrete Cracking	A45(0.74) A25(0.78) A24(2.27)
[164]	Sep/26/2000 15:23:03 UMST	Concrete Cracking	A51(1.64) A02(2.14) A01(2.25)
[165]	Sep/26/2000 15:23:21 UMST	Concrete Cracking	A31(2.09) A30(2.31) A34(3.10)
[166]	Sep/26/2000 15:23:23 UMST	Concrete Cracking	A30(0.74) A33(1.61) A31(3.41)
[167]	Sep/26/2000 15:23:40 UMST	Concrete Cracking	A31(0.62) A30(2.43) A34(2.90)
[168]	Sep/26/2000 15:23:58 UMST	Concrete Cracking	A31(1.77) A30(2.59) A34(2.67)
[169]	Sep/26/2000 15:24:00 UMST	Concrete Cracking	A30(0.66) A33(1.63) A31(3.51)
[170]	Sep/26/2000 15:24:01 UMST	Concrete Cracking	A31(0.69) A34(1.74) A32(2.51)
[171]	Sep/26/2000 15:24:02 UMST	Concrete Cracking	A38(2.59) A02(3.05) A03(3.37)
[172]	Sep/26/2000 15:24:06 UMST	Concrete Cracking	A02(0.71) A01(2.48) A51(2.60)
[173]	Sep/26/2000 15:24:08 UMST	Concrete Cracking	A02(1.38) A01(1.68) A51(3.15)
[174]	Sep/26/2000 15:24:09 UMST	Concrete Cracking	A01(1.31) A02(2.45) A51(2.55)
[175]	Sep/26/2000 15:24:41 UMST	Concrete Cracking	A02(1.26) A01(1.79) A51(3.12)
[176]	Sep/26/2000 15:25:22 UMST	Concrete Cracking	A30(0.87) A33(2.23) A29(3.79)
[177]	Sep/26/2000 15:25:24 UMST	Concrete Cracking	A30(2.11) A33(3.16) A29(3.35)
[178]	Sep/26/2000 15:25:29 UMST	Concrete Cracking	A33(1.15) A29(2.36) A30(2.59)
[179]	Sep/26/2000 15:25:32 UMST	Concrete Cracking	A26(0.54) A46(0.54) A47(2.73)
[180]	Sep/26/2000 15:25:33 UMST	Concrete Cracking	A03(1.04) A04(1.32) A53(3.49)
[181]	Sep/26/2000 15:25:37 UMST	Concrete Cracking	A21(0.80) A22(1.94) A18(2.35)

[182]	Sep/26/2000 15:25:38 UMST	Concrete Cracking	A33(0.95) A30(2.38) A29(2.59)
[183]	Sep/26/2000 15:25:41 UMST	Concrete Cracking	A20(1.14) A45(2.42) A25(2.54)
[184]	Sep/26/2000 15:25:53 UMST	Concrete Cracking	A30(1.94) A31(3.66) A33(3.95)
[185]	Sep/26/2000 15:25:59 UMST	Concrete Cracking	A06(1.32) A11(1.86) A41(2.31)
[186]	Sep/26/2000 15:26:00 UMST	Concrete Cracking	A31(1.39) A32(2.00) A34(2.64)
[187]	Sep/26/2000 15:26:01 UMST	Concrete Cracking	A30(1.79) A33(1.87) A29(2.77)
[188]	Sep/26/2000 15:26:33 UMST	Concrete Cracking	A30(1.76) A33(2.60) A29(3.15)
[189]	Sep/26/2000 15:27:21 UMST	Concrete Cracking	A25(0.98) A45(1.35) A24(2.71)
[190]	Sep/26/2000 15:27:22 UMST	Concrete Cracking	A11(1.52) A06(1.69) A41(2.42)
[191]	Sep/26/2000 15:27:43 UMST	Concrete Cracking	A52(0.40) A50(1.49) A51(1.50)
[192]	Sep/26/2000 15:28:18 UMST	Concrete Cracking	A16(2.19) A43(2.97) A15(3.26)
[193]	Sep/26/2000 15:28:58 UMST	Concrete Cracking	A14(0.69) A42(2.05) A13(3.12)
[194]	Sep/26/2000 15:29:51 UMST	Concrete Cracking	A38(0.84) A03(2.31) A04(3.19)
[195]	Sep/26/2000 15:32:46 UMST	Concrete Cracking	A51(0.84) A52(1.63) A49(2.02)
[196]	Sep/26/2000 15:33:46 UMST	Concrete Cracking	A51(1.37) A52(2.32) A49(2.41)
[197]	Sep/26/2000 15:35:01 UMST	Concrete Cracking	A31(0.19) A34(2.59) A30(2.87)
[198]	Sep/26/2000 15:37:31 UMST	Concrete Cracking	A11(0.20) A41(2.77) A06(3.15)
[199]	Sep/26/2000 15:39:04 UMST	Concrete Cracking	A02(2.91) A39(3.08) A38(3.92)
[200]	Sep/26/2000 15:43:25 UMST	Concrete Cracking	A02(2.38) A39(3.35) A01(3.62)
[201]	Sep/26/2000 15:52:30 UMST	Concrete Cracking	A17(1.31) A43(2.83) A18(3.13)
[202]	Sep/26/2000 16:12:23 UMST	Concrete Cracking	A42(1.75) A14(2.79) A44(2.92)
[203]	Sep/26/2000 16:48:11 UMST	Concrete Cracking	A02(2.73) A39(3.20) A38(3.96)
[204]	Sep/26/2000 19:40:55 UMST	Concrete Cracking	A30(1.04) A33(1.67) A29(3.51)
[205]	Sep/26/2000 19:44:44 UMST	Concrete Cracking	A30(1.15) A33(1.68) A31(3.21)
[206]	Sep/26/2000 19:56:32 UMST	Concrete Cracking	A51(0.96) A52(1.48) A02(2.09)
[207]	Sep/26/2000 19:56:33 UMST	Concrete Cracking	A17(0.37) A43(1.46) A16(2.96)
[208]	Sep/26/2000 19:56:57 UMST	Concrete Cracking	A21(1.97) A20(2.55) A46(3.19)
[209]	Sep/26/2000 19:57:02 UMST	Concrete Cracking	A30(1.52) A33(1.94) A29(3.05)
[210]	Sep/26/2000 19:57:03 UMST	Concrete Cracking	A47(1.98) A26(2.30) A46(2.30)
[211]	Sep/26/2000 19:57:05 UMST	Concrete Cracking	A20(2.14) A25(2.47) A21(2.95)
[212]	Sep/26/2000 19:57:09 UMST	Concrete Cracking	A26(0.72) A46(0.72) A21(2.26)
[213]	Sep/26/2000 19:57:11 UMST	Concrete Cracking	A31(1.66) A34(2.35) A30(2.87)
[214]	Sep/26/2000 19:57:19 UMST	Concrete Cracking	A12(2.05) A40(2.15) A07(2.25)
[215]	Sep/26/2000 19:57:30 UMST	Concrete Cracking	A30(0.49) A31(2.57) A33(2.58)
[216]	Sep/26/2000 19:57:32 UMST	Concrete Cracking	A26(0.53) A46(0.53) A21(2.46)
[217]	Sep/26/2000 19:57:37 UMST	Concrete Cracking	A43(1.36) A16(1.76) A17(2.29)
[218]	Sep/26/2000 19:57:45 UMST	Concrete Cracking	A41(1.04) A39(1.68) A11(1.86)
[219]	Sep/26/2000 19:57:50 UMST	Concrete Cracking	A13(0.52) A42(1.95) A40(2.27)
[220]	Sep/26/2000 19:57:55 UMST	Concrete Cracking	A31(1.77) A30(1.95) A34(4.19)
[221]	Sep/26/2000 19:58:08 UMST	Concrete Cracking	A33(0.67) A30(1.72) A49(3.78)
[222]	Sep/26/2000 19:58:09 UMST	Concrete Cracking	A30(1.80) A33(2.45) A31(2.64)
[223]	Sep/26/2000 19:58:15 UMST	Concrete Cracking	A30(0.55) A33(1.75) A31(3.42)
[224]	Sep/26/2000 19:58:20 UMST	Concrete Cracking	A24(1.64) A45(2.50) A23(3.07)
[225]	Sep/26/2000 19:58:31 UMST	Concrete Cracking	A12(1.22) A41(1.85) A11(2.13)
[226]	Sep/26/2000 19:58:40 UMST	Concrete Cracking	A26(0.63) A46(0.63) A21(2.35)
[227]	Sep/26/2000 19:59:04 UMST	Concrete Cracking	A24(2.24) A45(3.08) A23(3.15)

[228]	Sep/26/2000 19:59:07 UMST	Concrete Cracking	A47(2.33) A31(3.22) A25(3.50)
[229]	Sep/26/2000 19:59:13 UMST	Concrete Cracking	A25(0.19) A45(1.38) A24(2.91)
[230]	Sep/26/2000 19:59:25 UMST	Concrete Cracking	A33(0.33) A30(1.98) A29(3.60)
[231]	Sep/26/2000 19:59:26 UMST	Concrete Cracking	A24(1.39) A45(1.48) A25(2.67)
[232]	Sep/26/2000 19:59:27 UMST	Concrete Cracking	A25(2.18) A46(3.03) A26(3.03)
[233]	Sep/26/2000 19:59:39 UMST	Concrete Cracking	A21(0.53) A22(2.78) A26(3.03)
[234]	Sep/26/2000 20:00:00 UMST	Concrete Cracking	A12(1.35) A41(1.61) A11(2.40)
[235]	Sep/26/2000 20:00:04 UMST	Concrete Cracking	A30(0.21) A33(2.10) A31(3.14)
[236]	Sep/26/2000 20:00:15 UMST	Concrete Cracking	A06(1.23) A41(1.83) A11(2.08)
[237]	Sep/26/2000 20:00:16 UMST	Concrete Cracking	A29(2.51) A30(3.08) A33(3.51)
[238]	Sep/26/2000 20:00:18 UMST	Concrete Cracking	A29(0.83) A33(3.81) A30(4.46)
[239]	Sep/26/2000 20:00:20 UMST	Concrete Cracking	A42(2.13) A14(2.32) A44(2.41)
[240]	Sep/26/2000 20:00:25 UMST	Concrete Cracking	A30(2.82) A24(3.39) A45(3.53)
[241]	Sep/26/2000 20:00:27 UMST	Concrete Cracking	A33(1.10) A30(2.73) A49(2.83)
[242]	Sep/26/2000 20:00:27 UMST	Concrete Cracking	A45(0.50) A24(1.34) A25(1.83)
[243]	Sep/26/2000 20:00:46 UMST	Concrete Cracking	A20(1.46) A21(2.97) A25(3.31)
[244]	Sep/26/2000 20:01:11 UMST	Concrete Cracking	A29(1.36) A33(2.82) A36(3.45)
[245]	Sep/26/2000 20:01:19 UMST	Concrete Cracking	A21(0.87) A44(2.11) A18(2.11)
[246]	Sep/26/2000 20:01:20 UMST	Concrete Cracking	A43(0.32) A16(1.21) A17(1.84)
[247]	Sep/26/2000 20:01:31 UMST	Concrete Cracking	A46(0.45) A26(0.45) A21(2.53)
[248]	Sep/26/2000 20:01:33 UMST	Concrete Cracking	A33(1.43) A36(3.12) A49(3.35)
[249]	Sep/26/2000 20:02:17 UMST	Concrete Cracking	A02(0.95) A52(2.25) A51(2.54)
[250]	Sep/26/2000 20:02:29 UMST	Concrete Cracking	A30(0.14) A33(2.17) A31(3.09)
[251]	Sep/26/2000 20:02:41 UMST	Concrete Cracking	A06(1.24) A39(1.62) A41(1.89)
[252]	Sep/26/2000 20:02:45 UMST	Concrete Cracking	A30(3.10) A24(3.48) A29(3.70)
[253]	Sep/26/2000 20:03:01 UMST	Concrete Cracking	A02(1.88) A01(2.44) A39(4.29)
[254]	Sep/26/2000 20:03:35 UMST	Concrete Cracking	A24(2.30) A45(2.94) A20(3.45)
[255]	Sep/26/2000 20:03:36 UMST	Concrete Cracking	A23(3.26) A15(3.26) A24(3.44)
[256]	Sep/26/2000 20:03:43 UMST	Concrete Cracking	A11(1.02) A41(1.66) A39(2.46)
[257]	Sep/26/2000 20:06:01 UMST	Concrete Cracking	A30(1.21) A33(1.71) A31(3.18)
[258]	Sep/26/2000 20:08:46 UMST	Concrete Cracking	A29(1.67) A33(4.04) A30(4.21)
[259]	Sep/26/2000 20:09:33 UMST	Concrete Cracking	A30(0.78) A31(2.80) A33(3.06)
[260]	Sep/26/2000 20:11:46 UMST	Concrete Cracking	A39(2.57) A07(3.10) A41(3.17)
[261]	Sep/26/2000 20:36:14 UMST	Concrete Cracking	A20(1.63) A21(2.80) A25(3.39)
[262]	Sep/26/2000 20:36:38 UMST	Concrete Cracking	A24(0.32) A45(1.24) A25(2.76)
[263]	Sep/26/2000 20:36:47 UMST	Concrete Cracking	A06(1.66) A11(1.67) A41(1.69)
[264]	Sep/26/2000 20:37:09 UMST	Concrete Cracking	A47(1.24) A27(1.70) A32(2.22)
[265]	Sep/26/2000 20:37:13 UMST	Concrete Cracking	A47(1.59) A32(1.98) A31(2.59)
[266]	Sep/26/2000 20:37:14 UMST	Concrete Cracking	A26(0.59) A46(0.59) A47(2.40)
[267]	Sep/26/2000 20:37:17 UMST	Concrete Cracking	A21(1.64) A26(1.69) A46(1.69)
[268]	Sep/26/2000 20:37:25 UMST	Concrete Cracking	A14(1.34) A18(2.47) A44(2.47)
[269]	Sep/26/2000 20:37:39 UMST	Concrete Cracking	A16(2.54) A43(3.17) A24(3.49)
[270]	Sep/26/2000 20:37:52 UMST	Concrete Cracking	A20(0.76) A25(2.71) A17(3.41)
[271]	Sep/26/2000 20:38:00 UMST	Concrete Cracking	A33(0.27) A30(2.25) A29(3.23)
[272]	Sep/26/2000 20:38:04 UMST	Concrete Cracking	A28(2.12) A29(2.18) A36(5.23)
[273]	Sep/26/2000 20:38:27 UMST	Concrete Cracking	A41(0.90) A39(1.25) A12(2.55)

[274]	Sep/26/2000 20:38:28 UMST	Concrete Cracking	A33(2.12) A49(2.41) A51(3.08)
[275]	Sep/26/2000 20:38:44 UMST	Concrete Cracking	A21(1.34) A46(1.64) A26(1.64)
[276]	Sep/26/2000 20:38:57 UMST	Concrete Cracking	A48(0.57) A34(1.22) A32(2.00)
[277]	Sep/26/2000 20:39:01 UMST	Concrete Cracking	A20(0.01) A25(2.98) A17(2.99)
[278]	Sep/26/2000 20:39:13 UMST	Concrete Cracking	A37(1.94) A50(1.98) A52(2.00)
[279]	Sep/26/2000 20:39:21 UMST	Concrete Cracking	A16(2.47) A43(3.07) A20(3.41)
[280]	Sep/26/2000 20:39:24 UMST	Concrete Cracking	A01(1.16) A02(2.44) A51(2.71)
[281]	Sep/26/2000 20:39:28 UMST	Concrete Cracking	A31(0.40) A30(2.66) A34(2.78)
[282]	Sep/26/2000 20:39:42 UMST	Concrete Cracking	A06(1.16) A11(2.03) A41(2.35)
[283]	Sep/26/2000 20:39:45 UMST	Concrete Cracking	A24(1.53) A23(2.41) A45(2.75)
[284]	Sep/26/2000 20:39:48 UMST	Concrete Cracking	A25(3.09) A31(3.17) A30(3.37)
[285]	Sep/26/2000 20:39:50 UMST	Concrete Cracking	A52(1.16) A51(1.48) A02(1.88)
[286]	Sep/26/2000 20:39:54 UMST	Concrete Cracking	A29(1.65) A33(2.89) A36(3.13)
[287]	Sep/26/2000 20:40:20 UMST	Concrete Cracking	A46(1.14) A26(1.14) A47(1.85)
[288]	Sep/26/2000 20:40:29 UMST	Concrete Cracking	A40(1.15) A07(1.16) A13(3.05)
[289]	Sep/26/2000 20:40:31 UMST	Concrete Cracking	A33(1.25) A36(3.07) A29(3.42)
[290]	Sep/26/2000 20:40:32 UMST	Concrete Cracking	A33(0.24) A30(2.16) A29(3.31)
[291]	Sep/26/2000 20:40:33 UMST	Concrete Cracking	A20(0.14) A25(2.90) A17(3.07)
[292]	Sep/26/2000 20:40:47 UMST	Concrete Cracking	A24(3.05) A16(3.13) A23(3.69)
[293]	Sep/26/2000 20:41:04 UMST	Concrete Cracking	A24(1.08) A23(2.37) A45(2.42)
[294]	Sep/26/2000 20:41:10 UMST	Concrete Cracking	A20(0.23) A25(2.99) A17(3.00)
[295]	Sep/26/2000 20:41:12 UMST	Concrete Cracking	A30(1.11) A33(1.19) A31(3.84)
[296]	Sep/26/2000 20:41:16 UMST	Concrete Cracking	A36(1.08) A33(3.58) A00(4.37)
[297]	Sep/26/2000 20:41:21 UMST	Concrete Cracking	A23(2.98) A15(2.99) A24(4.24)
[298]	Sep/26/2000 20:41:27 UMST	Concrete Cracking	A39(1.34) A06(1.45) A41(1.51)
[299]	Sep/26/2000 20:41:28 UMST	Concrete Cracking	A06(1.32) A39(1.48) A41(1.70)
[300]	Sep/26/2000 20:41:36 UMST	Concrete Cracking	A30(0.71) A33(1.62) A31(3.44)
[301]	Sep/26/2000 20:41:37 UMST	Concrete Cracking	A00(1.23) A36(2.96) A01(3.36)
[302]	Sep/26/2000 20:41:39 UMST	Concrete Cracking	A06(1.41) A05(1.61) A10(3.20)
[303]	Sep/26/2000 20:41:53 UMST	Concrete Cracking	A33(1.03) A29(2.47) A30(2.84)
[304]	Sep/26/2000 20:41:55 UMST	Concrete Cracking	A02(2.29) A39(3.55) A38(4.05)
[305]	Sep/26/2000 20:41:57 UMST	Concrete Cracking	A02(1.44) A01(3.41) A39(4.28)
[306]	Sep/26/2000 20:42:03 UMST	Concrete Cracking	A21(1.38) A26(1.60) A46(1.60)
[307]	Sep/26/2000 20:42:19 UMST	Concrete Cracking	A26(0.66) A46(0.66) A21(2.32)
[308]	Sep/26/2000 20:42:20 UMST	Concrete Cracking	A25(1.57) A20(1.85) A45(2.70)
[309]	Sep/26/2000 20:42:28 UMST	Concrete Cracking	A15(1.33) A16(2.59) A43(4.03)
[310]	Sep/26/2000 20:42:29 UMST	Concrete Cracking	A07(1.80) A40(1.95) A38(3.44)
[311]	Sep/26/2000 20:42:33 UMST	Concrete Cracking	A01(1.43) A51(2.58) A02(2.91)
[312]	Sep/26/2000 20:42:49 UMST	Concrete Cracking	A21(1.39) A26(1.59) A46(1.59)
[313]	Sep/26/2000 20:42:50 UMST	Concrete Cracking	A29(0.69) A28(3.61) A33(4.07)
[314]	Sep/26/2000 20:42:51 UMST	Concrete Cracking	A20(1.35) A25(2.76) A21(3.23)
[315]	Sep/26/2000 20:42:53 UMST	Concrete Cracking	A24(1.08) A23(1.94) A45(2.61)
[316]	Sep/26/2000 20:42:57 UMST	Concrete Cracking	A30(0.54) A33(2.40) A31(2.64)
[317]	Sep/26/2000 20:43:00 UMST	Concrete Cracking	A18(0.78) A44(0.78) A14(3.15)
[318]	Sep/26/2000 20:43:02 UMST	Concrete Cracking	A29(1.73) A33(1.90) A30(2.87)
[319]	Sep/26/2000 20:43:21 UMST	Concrete Cracking	A06(0.83) A39(1.96) A41(2.06)

[320]	Sep/26/2000 20:43:30 UMST	Concrete Cracking	A43(0.34) A16(1.19) A17(1.86)
[321]	Sep/26/2000 20:43:38 UMST	Concrete Cracking	A13(1.37) A40(2.09) A12(2.13)
[322]	Sep/26/2000 20:44:11 UMST	Concrete Cracking	A39(2.32) A41(2.79) A07(2.81)
[323]	Sep/26/2000 20:55:32 UMST	Concrete Cracking	A30(1.49) A31(1.61) A33(3.31)
[324]	Sep/26/2000 20:59:54 UMST	Concrete Cracking	A33(1.65) A49(2.30) A30(2.85)
[325]	Sep/26/2000 21:17:59 UMST	Concrete Cracking	A46(0.46) A26(0.46) A47(2.81)
[326]	Sep/26/2000 21:18:32 UMST	Concrete Cracking	A21(1.46) A26(1.53) A46(1.53)
[327]	Sep/26/2000 21:18:34 UMST	Concrete Cracking	A44(1.22) A18(1.22) A14(2.86)
[328]	Sep/26/2000 21:18:38 UMST	Concrete Cracking	A21(0.95) A44(2.03) A18(2.03)
[329]	Sep/26/2000 21:18:46 UMST	Concrete Cracking	A21(1.42) A26(1.56) A46(1.56)
[330]	Sep/26/2000 21:18:49 UMST	Concrete Cracking	A46(1.01) A26(1.01) A47(3.14)
[331]	Sep/26/2000 21:18:51 UMST	Concrete Cracking	A20(0.01) A25(2.98) A17(2.99)
[332]	Sep/26/2000 21:18:52 UMST	Concrete Cracking	A26(0.94) A46(0.94) A47(2.04)
[333]	Sep/26/2000 21:18:55 UMST	Concrete Cracking	A23(3.54) A15(3.55) A24(5.77)
[334]	Sep/26/2000 21:18:59 UMST	Concrete Cracking	A25(2.00) A26(2.47) A46(2.47)
[335]	Sep/26/2000 21:19:01 UMST	Concrete Cracking	A47(1.13) A32(2.16) A27(3.05)
[336]	Sep/26/2000 21:19:06 UMST	Concrete Cracking	A32(0.16) A48(1.59) A34(2.22)
[337]	Sep/26/2000 21:19:06 UMST	Concrete Cracking	A01(1.53) A02(1.68) A51(3.62)
[338]	Sep/26/2000 21:19:12 UMST	Concrete Cracking	A21(1.26) A46(1.72) A26(1.72)
[339]	Sep/26/2000 21:19:15 UMST	Concrete Cracking	A20(1.52) A43(2.49) A17(2.88)
[340]	Sep/26/2000 21:19:17 UMST	Concrete Cracking	A21(1.00) A44(1.98) A18(1.98)
[341]	Sep/26/2000 21:19:18 UMST	Concrete Cracking	A24(2.98) A16(2.99) A20(3.05)
[342]	Sep/26/2000 21:19:19 UMST	Concrete Cracking	A15(0.65) A16(2.37) A43(3.90)
[343]	Sep/26/2000 21:19:22 UMST	Concrete Cracking	A25(1.46) A46(2.97) A26(2.97)
[344]	Sep/26/2000 21:19:35 UMST	Concrete Cracking	A23(2.98) A15(2.99) A24(4.24)
[345]	Sep/26/2000 21:19:38 UMST	Concrete Cracking	A43(0.56) A16(1.18) A17(1.97)
[346]	Sep/26/2000 21:19:39 UMST	Concrete Cracking	A26(1.49) A46(1.49) A21(1.50)
[347]	Sep/26/2000 21:19:42 UMST	Concrete Cracking	A09(0.09) A10(4.29) A05(5.16)
[348]	Sep/26/2000 21:19:50 UMST	Concrete Cracking	A20(2.13) A21(2.46) A25(3.14)
[349]	Sep/26/2000 21:19:52 UMST	Concrete Cracking	A06(1.14) A41(1.67) A39(1.67)
[350]	Sep/26/2000 21:19:54 UMST	Concrete Cracking	A20(1.04) A45(3.02) A43(3.03)
[351]	Sep/26/2000 21:19:57 UMST	Concrete Cracking	A24(0.68) A45(0.85) A25(2.37)
[352]	Sep/26/2000 21:20:17 UMST	Concrete Cracking	A23(2.99) A15(3.02) A24(3.99)
[353]	Sep/26/2000 21:20:37 UMST	Concrete Cracking	A20(1.31) A45(2.15) A25(2.27)
[354]	Sep/26/2000 21:20:42 UMST	Concrete Cracking	A43(0.53) A17(0.99) A16(2.06)
[355]	Sep/26/2000 21:20:47 UMST	Concrete Cracking	A23(2.31) A24(3.01) A29(3.94)
[356]	Sep/26/2000 21:20:51 UMST	Concrete Cracking	A21(1.38) A26(1.60) A46(1.60)
[357]	Sep/26/2000 21:20:56 UMST	Concrete Cracking	A24(2.98) A16(2.99) A20(3.05)
[358]	Sep/26/2000 21:21:00 UMST	Concrete Cracking	A15(2.58) A16(3.44) A23(3.53)
[359]	Sep/26/2000 21:21:03 UMST	Concrete Cracking	A11(1.83) A06(2.68) A10(2.72)
[360]	Sep/26/2000 21:21:07 UMST	Concrete Cracking	A24(2.98) A16(2.99) A20(3.05)
[361]	Sep/26/2000 21:21:09 UMST	Concrete Cracking	A21(0.30) A22(2.27) A44(2.68)
[362]	Sep/26/2000 21:21:12 UMST	Concrete Cracking	A31(1.50) A32(1.53) A34(2.18)
[363]	Sep/26/2000 21:21:14 UMST	Concrete Cracking	A23(3.82) A15(4.28) A19(5.94)
[364]	Sep/26/2000 21:21:15 UMST	Concrete Cracking	A12(1.50) A41(1.69) A39(2.30)
[365]	Sep/26/2000 21:21:24 UMST	Concrete Cracking	A21(0.54) A22(2.37) A44(2.44)

[366]	Sep/26/2000 21:21:29 UMST	Concrete Cracking	A40(1.56) A07(1.58) A12(3.02)
[367]	Sep/26/2000 21:21:32 UMST	Concrete Cracking	A18(0.80) A44(0.80) A21(2.18)
[368]	Sep/26/2000 21:21:38 UMST	Concrete Cracking	A32(1.19) A47(1.79) A48(2.62)
[369]	Sep/26/2000 21:21:43 UMST	Concrete Cracking	A31(0.91) A34(1.82) A32(2.00)
[370]	Sep/26/2000 21:21:51 UMST	Concrete Cracking	A16(0.26) A43(1.27) A17(2.79)
[371]	Sep/26/2000 21:21:55 UMST	Concrete Cracking	A23(2.61) A29(4.20) A28(4.74)
[372]	Sep/26/2000 21:21:57 UMST	Concrete Cracking	A26(1.55) A46(1.55) A21(2.18)
[373]	Sep/26/2000 21:21:59 UMST	Concrete Cracking	A49(0.56) A51(0.63) A50(1.31)
[374]	Sep/26/2000 21:22:00 UMST	Concrete Cracking	A43(0.28) A16(1.41) A17(1.68)
[375]	Sep/26/2000 21:22:05 UMST	Concrete Cracking	A24(0.30) A45(1.23) A25(2.75)
[376]	Sep/26/2000 21:22:07 UMST	Concrete Cracking	A43(0.48) A17(1.04) A16(2.01)
[377]	Sep/26/2000 21:22:08 UMST	Concrete Cracking	A43(0.01) A17(1.52) A16(1.52)
[378]	Sep/26/2000 21:22:11 UMST	Concrete Cracking	A24(0.06) A45(1.47) A25(2.99)
[379]	Sep/26/2000 21:22:19 UMST	Concrete Cracking	A18(0.72) A44(0.72) A21(2.26)
[380]	Sep/26/2000 21:22:25 UMST	Concrete Cracking	A29(2.43) A30(3.01) A33(3.37)
[381]	Sep/26/2000 21:22:32 UMST	Concrete Cracking	A39(2.22) A41(3.02) A02(3.99)
[382]	Sep/26/2000 21:22:38 UMST	Concrete Cracking	A42(1.73) A14(2.26) A44(2.81)
[383]	Sep/26/2000 21:22:43 UMST	Concrete Cracking	A23(0.44) A24(3.05) A45(4.57)
[384]	Sep/26/2000 21:22:46 UMST	Concrete Cracking	A00(1.01) A01(2.91) A36(3.22)
[385]	Sep/26/2000 21:22:51 UMST	Concrete Cracking	A33(1.84) A36(2.55) A49(3.78)
[386]	Sep/26/2000 21:22:52 UMST	Concrete Cracking	A16(0.08) A43(1.46) A17(2.98)
[387]	Sep/26/2000 21:22:53 UMST	Concrete Cracking	A24(2.25) A45(2.67) A25(3.71)
[388]	Sep/26/2000 21:22:55 UMST	Concrete Cracking	A20(0.32) A25(2.99) A17(3.01)
[389]	Sep/26/2000 21:23:06 UMST	Concrete Cracking	A24(0.86) A45(1.63) A25(3.03)
[390]	Sep/26/2000 21:23:08 UMST	Concrete Cracking	A01(1.45) A00(3.10) A51(3.14)
[391]	Sep/26/2000 21:23:11 UMST	Concrete Cracking	A24(2.98) A16(2.99) A20(3.05)
[392]	Sep/26/2000 21:23:27 UMST	Concrete Cracking	A29(0.73) A28(3.67) A33(4.20)
[393]	Sep/26/2000 21:23:32 UMST	Concrete Cracking	A24(0.27) A45(1.26) A25(2.78)
[394]	Sep/26/2000 21:23:36 UMST	Concrete Cracking	A21(1.12) A18(1.86) A44(1.86)
[395]	Sep/26/2000 21:23:38 UMST	Concrete Cracking	A21(1.40) A26(1.59) A46(1.59)
[396]	Sep/26/2000 21:23:43 UMST	Concrete Cracking	A31(0.65) A32(2.61) A34(2.64)
[397]	Sep/26/2000 21:23:45 UMST	Concrete Cracking	A15(2.27) A23(3.70) A16(3.74)
[398]	Sep/26/2000 21:24:34 UMST	Concrete Cracking	A16(0.29) A43(1.24) A17(2.76)
[399]	Sep/26/2000 21:45:39 UMST	Concrete Cracking	A01(0.81) A00(2.71) A02(3.52)
[400]	Sep/26/2000 21:45:40 UMST	Concrete Cracking	A31(1.43) A30(1.62) A33(3.59)
[401]	Sep/26/2000 21:45:54 UMST	Concrete Cracking	A11(1.11) A41(1.81) A06(2.20)
[402]	Sep/26/2000 21:45:55 UMST	Concrete Cracking	A44(0.17) A18(0.17) A21(3.15)
[403]	Sep/26/2000 21:45:59 UMST	Concrete Cracking	A29(2.31) A36(3.10) A28(3.59)
[404]	Sep/26/2000 21:46:00 UMST	Concrete Cracking	A36(1.51) A33(3.64) A49(4.03)
[405]	Sep/26/2000 21:46:17 UMST	Concrete Cracking	A01(1.54) A00(1.59) A36(4.08)
[406]	Sep/26/2000 21:46:23 UMST	Concrete Cracking	A20(0.96) A45(3.03) A43(3.04)
[407]	Sep/26/2000 21:46:51 UMST	Concrete Cracking	A46(0.82) A26(0.82) A47(3.09)
[408]	Sep/26/2000 21:47:11 UMST	Concrete Cracking	A00(0.87) A01(3.51) A05(5.41)
[409]	Sep/26/2000 21:47:15 UMST	Concrete Cracking	A19(3.12) A23(6.08) A15(6.69)
[410]	Sep/26/2000 21:47:56 UMST	Concrete Cracking	A30(1.14) A33(1.32) A29(3.56)
[411]	Sep/26/2000 21:48:15 UMST	Concrete Cracking	A46(0.47) A26(0.47) A21(2.51)

[412]	Sep/26/2000 21:48:21 UMST	Concrete Cracking	A00(1.87) A01(2.66) A36(2.72)
[413]	Sep/26/2000 21:48:22 UMST	Concrete Cracking	A23(2.98) A15(2.99) A24(4.24)
[414]	Sep/26/2000 21:48:23 UMST	Concrete Cracking	A23(2.99) A15(3.00) A24(4.04)
[415]	Sep/26/2000 21:48:24 UMST	Concrete Cracking	A33(0.71) A30(2.79) A29(2.85)
[416]	Sep/26/2000 21:48:32 UMST	Concrete Cracking	A47(0.61) A27(2.33) A32(2.37)
[417]	Sep/26/2000 21:48:40 UMST	Concrete Cracking	A00(2.80) A05(3.38) A01(3.95)
[418]	Sep/26/2000 21:48:55 UMST	Concrete Cracking	A23(2.98) A15(2.99) A24(4.24)
[419]	Sep/26/2000 21:48:59 UMST	Concrete Cracking	A00(0.59) A01(2.43) A02(5.48)
[420]	Sep/26/2000 21:49:03 UMST	Concrete Cracking	A24(1.35) A23(1.68) A45(2.88)
[421]	Sep/26/2000 21:49:06 UMST	Concrete Cracking	A15(1.28) A16(1.83) A43(3.34)
[422]	Sep/26/2000 21:49:33 UMST	Concrete Cracking	A01(2.56) A36(2.72) A00(3.05)
[423]	Sep/26/2000 21:49:34 UMST	Concrete Cracking	A15(1.33) A16(2.04) A43(3.51)
[424]	Sep/26/2000 21:49:38 UMST	Concrete Cracking	A00(0.69) A01(2.45) A02(5.48)
[425]	Sep/26/2000 21:49:52 UMST	Concrete Cracking	A02(0.71) A01(2.65) A03(4.91)
[426]	Sep/26/2000 21:50:19 UMST	Concrete Cracking	A15(4.23) A23(4.26) A19(5.64)
[427]	Sep/26/2000 21:50:20 UMST	Concrete Cracking	A02(1.69) A51(1.98) A01(2.11)
[428]	Sep/26/2000 21:50:22 UMST	Concrete Cracking	A24(3.05) A16(3.06) A45(3.69)
[429]	Sep/26/2000 21:50:32 UMST	Concrete Cracking	A33(2.10) A36(2.35) A49(3.74)
[430]	Sep/26/2000 21:51:07 UMST	Concrete Cracking	A21(0.39) A22(2.29) A26(2.60)
[431]	Sep/26/2000 21:52:40 UMST	Concrete Cracking	A00(1.34) A01(2.90) A36(2.94)
[432]	Sep/26/2000 21:53:16 UMST	Concrete Cracking	A03(0.34) A38(1.80) A04(2.17)
[433]	Sep/26/2000 21:53:27 UMST	Concrete Cracking	A33(0.40) A30(2.48) A29(3.08)
[434]	Sep/26/2000 22:16:26 UMST	Concrete Cracking	A45(0.58) A25(1.57) A24(1.69)
[435]	Sep/26/2000 22:17:08 UMST	Concrete Cracking	A01(1.03) A00(2.33) A02(3.90)
[436]	Sep/26/2000 22:17:15 UMST	Concrete Cracking	A33(0.55) A30(2.07) A29(3.09)
[437]	Sep/26/2000 22:17:38 UMST	Concrete Cracking	A33(1.36) A29(2.14) A30(3.06)
[438]	Sep/26/2000 22:17:46 UMST	Concrete Cracking	A23(2.98) A15(2.99) A24(4.24)
[439]	Sep/26/2000 22:17:49 UMST	Concrete Cracking	A24(0.74) A45(0.79) A25(2.31)
[440]	Sep/26/2000 22:18:01 UMST	Concrete Cracking	A31(1.71) A47(2.74) A32(2.88)
[441]	Sep/26/2000 22:18:21 UMST	Concrete Cracking	A30(0.83) A33(1.95) A31(2.96)
[442]	Sep/26/2000 22:18:36 UMST	Concrete Cracking	A00(1.46) A01(1.61) A36(4.16)
[443]	Sep/26/2000 22:19:09 UMST	Concrete Cracking	A20(1.50) A21(2.94) A17(3.27)
[444]	Sep/26/2000 22:19:24 UMST	Concrete Cracking	A23(3.18) A15(3.19) A24(5.09)
[445]	Sep/26/2000 22:19:27 UMST	Concrete Cracking	A23(0.89) A24(3.15) A45(4.63)
[446]	Sep/26/2000 22:20:24 UMST	Concrete Cracking	A29(0.46) A28(3.84) A33(3.88)
[447]	Sep/26/2000 22:20:29 UMST	Concrete Cracking	A17(0.88) A43(2.37) A20(3.36)
[448]	Sep/26/2000 22:21:12 UMST	Concrete Cracking	A01(1.56) A02(1.86) A00(4.44)
[449]	Sep/26/2000 22:21:36 UMST	Concrete Cracking	A26(0.53) A46(0.53) A47(2.45)
[450]	Sep/26/2000 22:21:57 UMST	Concrete Cracking	A21(1.45) A26(1.53) A46(1.53)
[451]	Sep/26/2000 22:22:36 UMST	Concrete Cracking	A29(1.44) A33(2.04) A30(3.32)
[452]	Sep/26/2000 22:25:01 UMST	Concrete Cracking	A33(0.69) A30(1.67) A29(3.43)
[453]	Sep/26/2000 22:25:09 UMST	Concrete Cracking	A33(0.74) A30(1.58) A29(3.55)
[454]	Sep/26/2000 22:33:24 UMST	Concrete Cracking	A46(1.31) A26(1.31) A47(1.68)
[455]	Sep/26/2000 22:43:32 UMST	Concrete Cracking	A19(4.53) A09(5.63) A15(7.75)
[456]	Sep/27/2000 03:05:13 UMST	Concrete Cracking	A20(1.79) A43(2.07) A16(2.56)
[457]	Sep/27/2000 07:09:31 UMST	Concrete Cracking	A04(0.80) A03(1.50) A38(1.93)

[458]	Sep/27/2000 07:22:25 UMST	Concrete Cracking	A34(0.73) A48(1.08) A32(2.36)
[459]	Sep/27/2000 07:56:41 UMST	Concrete Cracking	A31(2.18) A47(2.77) A32(3.42)
[460]	Sep/27/2000 07:59:36 UMST	Concrete Cracking	A41(1.38) A11(1.70) A12(1.90)
[461]	Sep/27/2000 08:00:09 UMST	Concrete Cracking	A10(1.05) A05(2.11) A06(3.07)
[462]	Sep/27/2000 12:05:41 UMST	Concrete Cracking	A32(0.25) A48(1.68) A34(2.27)
[463]	Sep/27/2000 12:22:49 UMST	Concrete Cracking	A03(1.05) A04(1.20) A53(3.18)
[464]	Sep/27/2000 12:49:41 UMST	Crushing Concrete	A35(1.50) A48(1.58) A34(2.23)
[465]	Sep/27/2000 13:01:32 UMST	Concrete Cracking	A32(1.16) A34(1.46) A48(1.63)
[466]	Sep/27/2000 13:01:32 UMST	Concrete Cracking	A32(1.03) A34(1.49) A48(1.56)
[467]	Sep/27/2000 13:01:56 UMST	Concrete Cracking	A11(1.73) A12(2.39) A41(3.68)
[468]	Sep/27/2000 13:04:28 UMST	Concrete Cracking	A28(2.03) A29(5.65) A23(6.86)
[469]	Sep/27/2000 13:04:29 UMST	Concrete Cracking	A28(2.78) A29(6.15) A23(6.67)
[470]	Sep/27/2000 13:05:35 UMST	Concrete Cracking	A28(2.84) A29(3.89) A23(4.56)
[471]	Sep/27/2000 13:20:04 UMST	Concrete Cracking	A38(1.41) A04(2.34) A03(2.46)
[472]	Sep/27/2000 13:21:07 UMST	Concrete Cracking	A38(2.93) A08(2.96) A04(3.21)
[473]	Sep/27/2000 13:34:56 UMST	Crushing Concrete	A04(1.15) A03(1.92) A53(2.61)
[474]	Sep/27/2000 13:35:58 UMST	Crushing Concrete	A38(0.70) A03(2.09) A04(3.33)
[475]	Sep/27/2000 13:37:28 UMST	Concrete Cracking	A11(1.04) A12(3.10) A41(3.53)
[476]	Sep/27/2000 13:37:46 UMST	Crushing Concrete	A08(0.23) A40(2.02) A07(2.03)
[477]	Sep/27/2000 13:38:01 UMST	Concrete Cracking	A11(1.43) A12(2.82) A41(3.70)
[478]	Sep/27/2000 13:38:03 UMST	Concrete Cracking	A10(2.39) A11(2.77) A06(4.11)
[479]	Sep/27/2000 13:43:18 UMST	Crushing Concrete	A26(0.57) A46(0.57) A21(2.50)
[480]	Sep/27/2000 13:49:57 UMST	Crushing Concrete	A22(1.50) A21(2.24) A46(2.34)
[481]	Sep/27/2000 13:50:01 UMST	Crushing Concrete	A27(0.62) A47(1.90) A32(3.12)
[482]	Sep/27/2000 13:51:37 UMST	Concrete Cracking	A46(0.43) A26(0.43) A21(2.58)
[483]	Sep/27/2000 14:05:10 UMST	Crushing Concrete	A21(0.21) A22(2.26) A26(2.78)
[484]	Sep/27/2000 14:15:21 UMST	Concrete Cracking	A35(0.86) A37(2.46) A48(2.51)
[485]	Sep/27/2000 14:15:22 UMST	Crushing Concrete	A35(1.67) A37(1.72) A53(2.09)
[486]	Sep/27/2000 14:18:42 UMST	Concrete Cracking	A11(0.58) A12(3.11) A41(3.15)
[487]	Sep/27/2000 14:24:44 UMST	Crushing Concrete	A44(1.46) A18(1.46) A22(2.38)
[488]	Sep/27/2000 14:36:18 UMST	Concrete Cracking	A04(1.13) A38(1.64) A03(1.76)
[489]	Sep/27/2000 14:44:02 UMST	Concrete Cracking	A11(1.79) A12(3.54) A43(4.17)

SANDIA PCCV
ALBUQUERQUE, NM

SOUNDPRINT® ACOUSTIC MONITORING PROGRAM

REPORT

REPORTING PERIOD: SEPTEMBER 12 TO SEPTEMBER 27, 2000

DISCLAIMER

The information provided in this report is not intended to constitute an engineering report and should not be construed as such. The client is advised to retain qualified engineering expertise to interpret the data contained in this report. The information contained in this report is provided “as is” without warranty of any kind, either express or implied. Pure Technologies Ltd. is not liable for any lost profits, lost savings or other incidental, special or consequential damage arising out of the use of the monitoring system or the information contained in this report. Please refer to the terms and conditions attached to Pure’s SoundPrint® System Purchase Agreement and Pure’s Technical Support Agreement for further details.

® Registered Trademark, property of Pure Technologies Ltd.

TABLE OF CONTENTS

<i>Section</i>	<i>Title</i>
1.0	Executive Summary
2.0	SoundPrint® Report: LST Concrete Cracks: (09/12/2000)

1.0 EXECUTIVE SUMMARY

The following is a summary of relevant activity recorded by the SoundPrint® monitoring system. The summary includes information for both the latest monitoring period and for the entire monitoring period from the start-up date up to and including the most recent monitoring period.

	Period 09/12/2000– 09/27/2000
Operating Efficiency	100 %
LST Concrete Cracks	239

Comments

Recommendations

There are no new recommendations at this time.

Prepared by:

Peter Paulson
President & CEO

REPORT PRESENTATION

A computerized drawing of the slab with the sensor layout is included on the following page and contains the following symbols:



Sensor Symbol with individual sensor name beneath



Symbolizes an event location. Event details are listed on the page following the drawing.

A list describing event details is provided for each drawing and lists the event number, shown on the computerized drawing, followed by the date, time, event classification and coordinates (in meters) to the origin of the events using the three closest sensors.

Event Report For Sandia PCCV

Albuquerque, NM

System Uptime 15.9 Days (100%)

LST Concrete Cracks

Period: 09/12/2000 to 09/27/2000



Matched Events: 239

SoundPrint® Acoustic Monitoring Report
Sandia PCCV



June 7, 2001
Page 4



Events

No.	Date/Time	Classification	Location (m)
[1]	Sep/12/2000 09:30:33 UMST	Concrete Cracking	A12(1.23) A41(1.73) A11(2.47)
[2]	Sep/12/2000 09:33:43 UMST	Concrete Cracking	A17(1.29) A43(2.60) A44(3.62)
[3]	Sep/12/2000 12:21:44 UMST	Concrete Cracking	A03(0.76) A04(1.89) A38(2.12)
[4]	Sep/12/2000 13:22:51 UMST	Concrete Cracking	A26(1.37) A46(1.37) A47(2.18)
[5]	Sep/12/2000 13:27:45 UMST	Concrete Cracking	A26(0.26) A46(0.26) A47(2.77)
[6]	Sep/12/2000 13:53:08 UMST	Concrete Cracking	A44(1.25) A18(1.25) A14(2.73)
[7]	Sep/13/2000 13:06:27 UMST	Concrete Cracking	A42(2.01) A14(2.31) A44(2.53)
[8]	Sep/13/2000 14:27:30 UMST	Concrete Cracking	A37(1.22) A53(1.55) A35(2.20)
[9]	Sep/14/2000 15:57:41 UMST	Concrete Cracking	A14(1.81) A44(1.96) A18(1.96)
[10]	Sep/26/2000 13:55:42 UMST	Concrete Cracking	A21(1.05) A44(1.96) A18(1.96)
[11]	Sep/26/2000 14:25:54 UMST	Concrete Cracking	A12(1.51) A13(1.59) A42(1.73)
[12]	Sep/26/2000 14:27:18 UMST	Concrete Cracking	A38(1.22) A03(2.52) A04(2.80)
[13]	Sep/26/2000 14:27:20 UMST	Concrete Cracking	A50(1.01) A49(1.93) A52(2.12)
[14]	Sep/26/2000 14:30:04 UMST	Concrete Cracking	A45(0.62) A24(1.63) A25(1.66)
[15]	Sep/26/2000 14:30:22 UMST	Concrete Cracking	A13(0.45) A42(1.44) A40(2.88)
[16]	Sep/26/2000 14:30:32 UMST	Concrete Cracking	A03(0.99) A38(1.28) A04(1.49)
[17]	Sep/26/2000 14:47:36 UMST	Concrete Cracking	A39(3.27) A38(3.29) A02(3.35)
[18]	Sep/26/2000 14:50:18 UMST	Concrete Cracking	A21(1.51) A26(1.79) A46(1.79)
[19]	Sep/26/2000 14:50:47 UMST	Concrete Cracking	A12(1.32) A42(2.36) A13(2.64)
[20]	Sep/26/2000 14:54:19 UMST	Concrete Cracking	A00(2.07) A36(3.61) A01(4.93)
[21]	Sep/26/2000 15:16:32 UMST	Concrete Cracking	A52(0.43) A51(1.50) A50(1.54)
[22]	Sep/26/2000 15:19:06 UMST	Concrete Cracking	A30(1.65) A31(3.36) A33(3.75)
[23]	Sep/26/2000 15:20:55 UMST	Concrete Cracking	A32(0.57) A48(1.42) A34(2.36)
[24]	Sep/26/2000 15:21:47 UMST	Concrete Cracking	A50(2.45) A49(2.56) A31(2.69)
[25]	Sep/26/2000 15:21:51 UMST	Concrete Cracking	A41(1.03) A39(1.92) A12(2.01)
[26]	Sep/26/2000 15:21:59 UMST	Concrete Cracking	A41(0.91) A39(1.69) A11(1.77)
[27]	Sep/26/2000 15:22:18 UMST	Concrete Cracking	A41(1.44) A39(1.75) A12(2.28)
[28]	Sep/26/2000 15:22:27 UMST	Concrete Cracking	A38(2.50) A03(3.51) A02(3.65)
[29]	Sep/26/2000 15:22:45 UMST	Concrete Cracking	A30(1.85) A33(2.38) A31(2.75)
[30]	Sep/26/2000 15:22:54 UMST	Concrete Cracking	A49(1.82) A50(2.31) A33(2.53)
[31]	Sep/26/2000 15:23:02 UMST	Concrete Cracking	A45(0.74) A25(0.78) A24(2.27)
[32]	Sep/26/2000 15:24:01 UMST	Concrete Cracking	A31(0.69) A34(1.74) A32(2.51)
[33]	Sep/26/2000 15:24:02 UMST	Concrete Cracking	A38(2.59) A02(3.05) A03(3.37)
[34]	Sep/26/2000 15:24:06 UMST	Concrete Cracking	A02(0.71) A01(2.48) A51(2.60)
[35]	Sep/26/2000 15:24:08 UMST	Concrete Cracking	A02(1.38) A01(1.68) A51(3.15)
[36]	Sep/26/2000 15:25:22 UMST	Concrete Cracking	A30(0.87) A33(2.23) A29(3.79)
[37]	Sep/26/2000 15:25:24 UMST	Concrete Cracking	A30(2.11) A33(3.16) A29(3.35)
[38]	Sep/26/2000 15:25:32 UMST	Concrete Cracking	A26(0.54) A46(0.54) A47(2.73)
[39]	Sep/26/2000 15:25:33 UMST	Concrete Cracking	A03(1.04) A04(1.32) A53(3.49)
[40]	Sep/26/2000 15:25:37 UMST	Concrete Cracking	A21(0.80) A22(1.94) A18(2.35)
[41]	Sep/26/2000 15:25:53 UMST	Concrete Cracking	A30(1.94) A31(3.66) A33(3.95)
[42]	Sep/26/2000 15:26:00 UMST	Concrete Cracking	A31(1.39) A32(2.00) A34(2.64)
[43]	Sep/26/2000 15:26:01 UMST	Concrete Cracking	A30(1.79) A33(1.87) A29(2.77)

[44]	Sep/26/2000 15:27:21 UMST	Concrete Cracking	A25(0.98) A45(1.35) A24(2.71)
[45]	Sep/26/2000 15:27:22 UMST	Concrete Cracking	A11(1.52) A06(1.69) A41(2.42)
[46]	Sep/26/2000 15:27:43 UMST	Concrete Cracking	A52(0.40) A50(1.49) A51(1.50)
[47]	Sep/26/2000 15:28:58 UMST	Concrete Cracking	A14(0.69) A42(2.05) A13(3.12)
[48]	Sep/26/2000 15:29:51 UMST	Concrete Cracking	A38(0.84) A03(2.31) A04(3.19)
[49]	Sep/26/2000 15:32:46 UMST	Concrete Cracking	A51(0.84) A52(1.63) A49(2.02)
[50]	Sep/26/2000 15:33:46 UMST	Concrete Cracking	A51(1.37) A52(2.32) A49(2.41)
[51]	Sep/26/2000 15:35:01 UMST	Concrete Cracking	A31(0.19) A34(2.59) A30(2.87)
[52]	Sep/26/2000 15:37:31 UMST	Concrete Cracking	A11(0.20) A41(2.77) A06(3.15)
[53]	Sep/26/2000 15:52:30 UMST	Concrete Cracking	A17(1.31) A43(2.83) A18(3.13)
[54]	Sep/26/2000 16:12:23 UMST	Concrete Cracking	A42(1.75) A14(2.79) A44(2.92)
[55]	Sep/26/2000 19:56:32 UMST	Concrete Cracking	A51(0.96) A52(1.48) A02(2.09)
[56]	Sep/26/2000 19:56:33 UMST	Concrete Cracking	A17(0.37) A43(1.46) A16(2.96)
[57]	Sep/26/2000 19:56:57 UMST	Concrete Cracking	A21(1.97) A20(2.55) A46(3.19)
[58]	Sep/26/2000 19:57:03 UMST	Concrete Cracking	A47(1.98) A26(2.30) A46(2.30)
[59]	Sep/26/2000 19:57:05 UMST	Concrete Cracking	A20(2.14) A25(2.47) A21(2.95)
[60]	Sep/26/2000 19:57:09 UMST	Concrete Cracking	A26(0.72) A46(0.72) A21(2.26)
[61]	Sep/26/2000 19:57:19 UMST	Concrete Cracking	A12(2.05) A40(2.15) A07(2.25)
[62]	Sep/26/2000 19:57:37 UMST	Concrete Cracking	A43(1.36) A16(1.76) A17(2.29)
[63]	Sep/26/2000 19:57:45 UMST	Concrete Cracking	A41(1.04) A39(1.68) A11(1.86)
[64]	Sep/26/2000 19:57:50 UMST	Concrete Cracking	A13(0.52) A42(1.95) A40(2.27)
[65]	Sep/26/2000 19:58:08 UMST	Concrete Cracking	A33(0.67) A30(1.72) A49(3.78)
[66]	Sep/26/2000 19:58:20 UMST	Concrete Cracking	A24(1.64) A45(2.50) A23(3.07)
[67]	Sep/26/2000 19:58:31 UMST	Concrete Cracking	A12(1.22) A41(1.85) A11(2.13)
[68]	Sep/26/2000 19:59:13 UMST	Concrete Cracking	A25(0.19) A45(1.38) A24(2.91)
[69]	Sep/26/2000 19:59:25 UMST	Concrete Cracking	A33(0.33) A30(1.98) A29(3.60)
[70]	Sep/26/2000 19:59:26 UMST	Concrete Cracking	A24(1.39) A45(1.48) A25(2.67)
[71]	Sep/26/2000 19:59:27 UMST	Concrete Cracking	A25(2.18) A46(3.03) A26(3.03)
[72]	Sep/26/2000 20:00:00 UMST	Concrete Cracking	A12(1.35) A41(1.61) A11(2.40)
[73]	Sep/26/2000 20:00:15 UMST	Concrete Cracking	A06(1.23) A41(1.83) A11(2.08)
[74]	Sep/26/2000 20:00:20 UMST	Concrete Cracking	A42(2.13) A14(2.32) A44(2.41)
[75]	Sep/26/2000 20:00:27 UMST	Concrete Cracking	A45(0.50) A24(1.34) A25(1.83)
[76]	Sep/26/2000 20:00:27 UMST	Concrete Cracking	A33(1.10) A30(2.73) A49(2.83)
[77]	Sep/26/2000 20:01:11 UMST	Concrete Cracking	A29(1.36) A33(2.82) A36(3.45)
[78]	Sep/26/2000 20:01:20 UMST	Concrete Cracking	A43(0.32) A16(1.21) A17(1.84)
[79]	Sep/26/2000 20:01:31 UMST	Concrete Cracking	A46(0.45) A26(0.45) A21(2.53)
[80]	Sep/26/2000 20:03:01 UMST	Concrete Cracking	A02(1.88) A01(2.44) A39(4.29)
[81]	Sep/26/2000 20:03:36 UMST	Concrete Cracking	A23(3.26) A15(3.26) A24(3.44)
[82]	Sep/26/2000 20:03:43 UMST	Concrete Cracking	A11(1.02) A41(1.66) A39(2.46)
[83]	Sep/26/2000 20:06:01 UMST	Concrete Cracking	A30(1.21) A33(1.71) A31(3.18)
[84]	Sep/26/2000 20:08:46 UMST	Concrete Cracking	A29(1.67) A33(4.04) A30(4.21)
[85]	Sep/26/2000 20:09:33 UMST	Concrete Cracking	A30(0.78) A31(2.80) A33(3.06)
[86]	Sep/26/2000 20:36:38 UMST	Concrete Cracking	A24(0.32) A45(1.24) A25(2.76)
[87]	Sep/26/2000 20:36:47 UMST	Concrete Cracking	A06(1.66) A11(1.67) A41(1.69)
[88]	Sep/26/2000 20:37:09 UMST	Concrete Cracking	A47(1.24) A27(1.70) A32(2.22)
[89]	Sep/26/2000 20:37:39 UMST	Concrete Cracking	A16(2.54) A43(3.17) A24(3.49)

[90]	Sep/26/2000 20:37:52 UMST	Concrete Cracking	A20(0.76) A25(2.71) A17(3.41)
[91]	Sep/26/2000 20:38:00 UMST	Concrete Cracking	A33(0.27) A30(2.25) A29(3.23)
[92]	Sep/26/2000 20:38:04 UMST	Concrete Cracking	A28(2.12) A29(2.18) A36(5.23)
[93]	Sep/26/2000 20:38:28 UMST	Concrete Cracking	A33(2.12) A49(2.41) A51(3.08)
[94]	Sep/26/2000 20:38:44 UMST	Concrete Cracking	A21(1.34) A46(1.64) A26(1.64)
[95]	Sep/26/2000 20:38:57 UMST	Concrete Cracking	A48(0.57) A34(1.22) A32(2.00)
[96]	Sep/26/2000 20:39:01 UMST	Concrete Cracking	A20(0.01) A25(2.98) A17(2.99)
[97]	Sep/26/2000 20:39:13 UMST	Concrete Cracking	A37(1.94) A50(1.98) A52(2.00)
[98]	Sep/26/2000 20:39:21 UMST	Concrete Cracking	A16(2.47) A43(3.07) A20(3.41)
[99]	Sep/26/2000 20:39:24 UMST	Concrete Cracking	A01(1.16) A02(2.44) A51(2.71)
[100]	Sep/26/2000 20:39:28 UMST	Concrete Cracking	A31(0.40) A30(2.66) A34(2.78)
[101]	Sep/26/2000 20:39:42 UMST	Concrete Cracking	A06(1.16) A11(2.03) A41(2.35)
[102]	Sep/26/2000 20:39:45 UMST	Concrete Cracking	A24(1.53) A23(2.41) A45(2.75)
[103]	Sep/26/2000 20:39:48 UMST	Concrete Cracking	A25(3.09) A31(3.17) A30(3.37)
[104]	Sep/26/2000 20:39:50 UMST	Concrete Cracking	A52(1.16) A51(1.48) A02(1.88)
[105]	Sep/26/2000 20:39:54 UMST	Concrete Cracking	A29(1.65) A33(2.89) A36(3.13)
[106]	Sep/26/2000 20:40:20 UMST	Concrete Cracking	A46(1.14) A26(1.14) A47(1.85)
[107]	Sep/26/2000 20:40:29 UMST	Concrete Cracking	A40(1.15) A07(1.16) A13(3.05)
[108]	Sep/26/2000 20:40:31 UMST	Concrete Cracking	A33(1.25) A36(3.07) A29(3.42)
[109]	Sep/26/2000 20:40:32 UMST	Concrete Cracking	A33(0.24) A30(2.16) A29(3.31)
[110]	Sep/26/2000 20:40:33 UMST	Concrete Cracking	A20(0.14) A25(2.90) A17(3.07)
[111]	Sep/26/2000 20:40:47 UMST	Concrete Cracking	A24(3.05) A16(3.13) A23(3.69)
[112]	Sep/26/2000 20:41:04 UMST	Concrete Cracking	A24(1.08) A23(2.37) A45(2.42)
[113]	Sep/26/2000 20:41:12 UMST	Concrete Cracking	A30(1.11) A33(1.19) A31(3.84)
[114]	Sep/26/2000 20:41:16 UMST	Concrete Cracking	A36(1.08) A33(3.58) A00(4.37)
[115]	Sep/26/2000 20:41:27 UMST	Concrete Cracking	A39(1.34) A06(1.45) A41(1.51)
[116]	Sep/26/2000 20:41:28 UMST	Concrete Cracking	A06(1.32) A39(1.48) A41(1.70)
[117]	Sep/26/2000 20:41:39 UMST	Concrete Cracking	A06(1.41) A05(1.61) A10(3.20)
[118]	Sep/26/2000 20:41:57 UMST	Concrete Cracking	A02(1.44) A01(3.41) A39(4.28)
[119]	Sep/26/2000 20:42:03 UMST	Concrete Cracking	A21(1.38) A26(1.60) A46(1.60)
[120]	Sep/26/2000 20:42:28 UMST	Concrete Cracking	A15(1.33) A16(2.59) A43(4.03)
[121]	Sep/26/2000 20:42:29 UMST	Concrete Cracking	A07(1.80) A40(1.95) A38(3.44)
[122]	Sep/26/2000 20:42:33 UMST	Concrete Cracking	A01(1.43) A51(2.58) A02(2.91)
[123]	Sep/26/2000 20:42:51 UMST	Concrete Cracking	A20(1.35) A25(2.76) A21(3.23)
[124]	Sep/26/2000 20:42:53 UMST	Concrete Cracking	A24(1.08) A23(1.94) A45(2.61)
[125]	Sep/26/2000 20:42:57 UMST	Concrete Cracking	A30(0.54) A33(2.40) A31(2.64)
[126]	Sep/26/2000 20:43:00 UMST	Concrete Cracking	A18(0.78) A44(0.78) A14(3.15)
[127]	Sep/26/2000 20:43:21 UMST	Concrete Cracking	A06(0.83) A39(1.96) A41(2.06)
[128]	Sep/26/2000 20:43:30 UMST	Concrete Cracking	A43(0.34) A16(1.19) A17(1.86)
[129]	Sep/26/2000 20:43:38 UMST	Concrete Cracking	A13(1.37) A40(2.09) A12(2.13)
[130]	Sep/26/2000 20:44:11 UMST	Concrete Cracking	A39(2.32) A41(2.79) A07(2.81)
[131]	Sep/26/2000 20:59:54 UMST	Concrete Cracking	A33(1.65) A49(2.30) A30(2.85)
[132]	Sep/26/2000 21:18:38 UMST	Concrete Cracking	A21(0.95) A44(2.03) A18(2.03)
[133]	Sep/26/2000 21:18:52 UMST	Concrete Cracking	A26(0.94) A46(0.94) A47(2.04)
[134]	Sep/26/2000 21:18:59 UMST	Concrete Cracking	A25(2.00) A26(2.47) A46(2.47)
[135]	Sep/26/2000 21:19:06 UMST	Concrete Cracking	A01(1.53) A02(1.68) A51(3.62)

[136]	Sep/26/2000 21:19:06 UMST	Concrete Cracking	A32(0.16) A48(1.59) A34(2.22)
[137]	Sep/26/2000 21:19:12 UMST	Concrete Cracking	A21(1.26) A46(1.72) A26(1.72)
[138]	Sep/26/2000 21:19:17 UMST	Concrete Cracking	A21(1.00) A44(1.98) A18(1.98)
[139]	Sep/26/2000 21:19:18 UMST	Concrete Cracking	A24(2.98) A16(2.99) A20(3.05)
[140]	Sep/26/2000 21:19:22 UMST	Concrete Cracking	A25(1.46) A46(2.97) A26(2.97)
[141]	Sep/26/2000 21:19:38 UMST	Concrete Cracking	A43(0.56) A16(1.18) A17(1.97)
[142]	Sep/26/2000 21:19:42 UMST	Concrete Cracking	A09(0.09) A10(4.29) A05(5.16)
[143]	Sep/26/2000 21:19:50 UMST	Concrete Cracking	A20(2.13) A21(2.46) A25(3.14)
[144]	Sep/26/2000 21:19:52 UMST	Concrete Cracking	A06(1.14) A41(1.67) A39(1.67)
[145]	Sep/26/2000 21:19:57 UMST	Concrete Cracking	A24(0.68) A45(0.85) A25(2.37)
[146]	Sep/26/2000 21:20:47 UMST	Concrete Cracking	A23(2.31) A24(3.01) A29(3.94)
[147]	Sep/26/2000 21:20:51 UMST	Concrete Cracking	A21(1.38) A26(1.60) A46(1.60)
[148]	Sep/26/2000 21:21:07 UMST	Concrete Cracking	A24(2.98) A16(2.99) A20(3.05)
[149]	Sep/26/2000 21:21:15 UMST	Concrete Cracking	A12(1.50) A41(1.69) A39(2.30)
[150]	Sep/26/2000 21:21:24 UMST	Concrete Cracking	A21(0.54) A22(2.37) A44(2.44)
[151]	Sep/26/2000 21:21:29 UMST	Concrete Cracking	A40(1.56) A07(1.58) A12(3.02)
[152]	Sep/26/2000 21:21:32 UMST	Concrete Cracking	A18(0.80) A44(0.80) A21(2.18)
[153]	Sep/26/2000 21:21:51 UMST	Concrete Cracking	A16(0.26) A43(1.27) A17(2.79)
[154]	Sep/26/2000 21:21:55 UMST	Concrete Cracking	A23(2.61) A29(4.20) A28(4.74)
[155]	Sep/26/2000 21:22:00 UMST	Concrete Cracking	A43(0.28) A16(1.41) A17(1.68)
[156]	Sep/26/2000 21:22:05 UMST	Concrete Cracking	A24(0.30) A45(1.23) A25(2.75)
[157]	Sep/26/2000 21:22:07 UMST	Concrete Cracking	A43(0.48) A17(1.04) A16(2.01)
[158]	Sep/26/2000 21:22:08 UMST	Concrete Cracking	A43(0.01) A17(1.52) A16(1.52)
[159]	Sep/26/2000 21:22:11 UMST	Concrete Cracking	A24(0.06) A45(1.47) A25(2.99)
[160]	Sep/26/2000 21:22:19 UMST	Concrete Cracking	A18(0.72) A44(0.72) A21(2.26)
[161]	Sep/26/2000 21:22:25 UMST	Concrete Cracking	A29(2.43) A30(3.01) A33(3.37)
[162]	Sep/26/2000 21:22:38 UMST	Concrete Cracking	A42(1.73) A14(2.26) A44(2.81)
[163]	Sep/26/2000 21:22:46 UMST	Concrete Cracking	A00(1.01) A01(2.91) A36(3.22)
[164]	Sep/26/2000 21:22:52 UMST	Concrete Cracking	A16(0.08) A43(1.46) A17(2.98)
[165]	Sep/26/2000 21:22:55 UMST	Concrete Cracking	A20(0.32) A25(2.99) A17(3.01)
[166]	Sep/26/2000 21:23:06 UMST	Concrete Cracking	A24(0.86) A45(1.63) A25(3.03)
[167]	Sep/26/2000 21:23:08 UMST	Concrete Cracking	A01(1.45) A00(3.10) A51(3.14)
[168]	Sep/26/2000 21:23:27 UMST	Concrete Cracking	A29(0.73) A28(3.67) A33(4.20)
[169]	Sep/26/2000 21:23:32 UMST	Concrete Cracking	A24(0.27) A45(1.26) A25(2.78)
[170]	Sep/26/2000 21:23:36 UMST	Concrete Cracking	A21(1.12) A18(1.86) A44(1.86)
[171]	Sep/26/2000 21:23:43 UMST	Concrete Cracking	A31(0.65) A32(2.61) A34(2.64)
[172]	Sep/26/2000 21:24:34 UMST	Concrete Cracking	A16(0.29) A43(1.24) A17(2.76)
[173]	Sep/26/2000 21:45:39 UMST	Concrete Cracking	A01(0.81) A00(2.71) A02(3.52)
[174]	Sep/26/2000 21:45:40 UMST	Concrete Cracking	A31(1.43) A30(1.62) A33(3.59)
[175]	Sep/26/2000 21:45:54 UMST	Concrete Cracking	A11(1.11) A41(1.81) A06(2.20)
[176]	Sep/26/2000 21:45:55 UMST	Concrete Cracking	A44(0.17) A18(0.17) A21(3.15)
[177]	Sep/26/2000 21:45:59 UMST	Concrete Cracking	A29(2.31) A36(3.10) A28(3.59)
[178]	Sep/26/2000 21:46:00 UMST	Concrete Cracking	A36(1.51) A33(3.64) A49(4.03)
[179]	Sep/26/2000 21:46:17 UMST	Concrete Cracking	A01(1.54) A00(1.59) A36(4.08)
[180]	Sep/26/2000 21:47:11 UMST	Concrete Cracking	A00(0.87) A01(3.51) A05(5.41)
[181]	Sep/26/2000 21:47:56 UMST	Concrete Cracking	A30(1.14) A33(1.32) A29(3.56)

[182]	Sep/26/2000 21:48:15 UMST	Concrete Cracking	A46(0.47) A26(0.47) A21(2.51)
[183]	Sep/26/2000 21:48:21 UMST	Concrete Cracking	A00(1.87) A01(2.66) A36(2.72)
[184]	Sep/26/2000 21:48:24 UMST	Concrete Cracking	A33(0.71) A30(2.79) A29(2.85)
[185]	Sep/26/2000 21:48:32 UMST	Concrete Cracking	A47(0.61) A27(2.33) A32(2.37)
[186]	Sep/26/2000 21:48:59 UMST	Concrete Cracking	A00(0.59) A01(2.43) A02(5.48)
[187]	Sep/26/2000 21:49:03 UMST	Concrete Cracking	A24(1.35) A23(1.68) A45(2.88)
[188]	Sep/26/2000 21:49:06 UMST	Concrete Cracking	A15(1.28) A16(1.83) A43(3.34)
[189]	Sep/26/2000 21:49:33 UMST	Concrete Cracking	A01(2.56) A36(2.72) A00(3.05)
[190]	Sep/26/2000 21:49:34 UMST	Concrete Cracking	A15(1.33) A16(2.04) A43(3.51)
[191]	Sep/26/2000 21:49:52 UMST	Concrete Cracking	A02(0.71) A01(2.65) A03(4.91)
[192]	Sep/26/2000 21:50:20 UMST	Concrete Cracking	A02(1.69) A51(1.98) A01(2.11)
[193]	Sep/26/2000 21:50:32 UMST	Concrete Cracking	A33(2.10) A36(2.35) A49(3.74)
[194]	Sep/26/2000 21:51:07 UMST	Concrete Cracking	A21(0.39) A22(2.29) A26(2.60)
[195]	Sep/26/2000 21:52:40 UMST	Concrete Cracking	A00(1.34) A01(2.90) A36(2.94)
[196]	Sep/26/2000 21:53:16 UMST	Concrete Cracking	A03(0.34) A38(1.80) A04(2.17)
[197]	Sep/26/2000 21:53:27 UMST	Concrete Cracking	A33(0.40) A30(2.48) A29(3.08)
[198]	Sep/26/2000 22:16:26 UMST	Concrete Cracking	A45(0.58) A25(1.57) A24(1.69)
[199]	Sep/26/2000 22:17:08 UMST	Concrete Cracking	A01(1.03) A00(2.33) A02(3.90)
[200]	Sep/26/2000 22:17:15 UMST	Concrete Cracking	A33(0.55) A30(2.07) A29(3.09)
[201]	Sep/26/2000 22:17:38 UMST	Concrete Cracking	A33(1.36) A29(2.14) A30(3.06)
[202]	Sep/26/2000 22:17:49 UMST	Concrete Cracking	A24(0.74) A45(0.79) A25(2.31)
[203]	Sep/26/2000 22:18:01 UMST	Concrete Cracking	A31(1.71) A47(2.74) A32(2.88)
[204]	Sep/26/2000 22:18:21 UMST	Concrete Cracking	A30(0.83) A33(1.95) A31(2.96)
[205]	Sep/26/2000 22:18:36 UMST	Concrete Cracking	A00(1.46) A01(1.61) A36(4.16)
[206]	Sep/26/2000 22:19:09 UMST	Concrete Cracking	A20(1.50) A21(2.94) A17(3.27)
[207]	Sep/26/2000 22:19:27 UMST	Concrete Cracking	A23(0.89) A24(3.15) A45(4.63)
[208]	Sep/26/2000 22:20:24 UMST	Concrete Cracking	A29(0.46) A28(3.84) A33(3.88)
[209]	Sep/26/2000 22:20:29 UMST	Concrete Cracking	A17(0.88) A43(2.37) A20(3.36)
[210]	Sep/26/2000 22:21:12 UMST	Concrete Cracking	A01(1.56) A02(1.86) A00(4.44)
[211]	Sep/26/2000 22:21:57 UMST	Concrete Cracking	A21(1.45) A26(1.53) A46(1.53)
[212]	Sep/26/2000 22:25:01 UMST	Concrete Cracking	A33(0.69) A30(1.67) A29(3.43)
[213]	Sep/26/2000 22:25:09 UMST	Concrete Cracking	A33(0.74) A30(1.58) A29(3.55)
[214]	Sep/26/2000 22:33:24 UMST	Concrete Cracking	A46(1.31) A26(1.31) A47(1.68)
[215]	Sep/26/2000 22:43:32 UMST	Concrete Cracking	A19(4.53) A09(5.63) A15(7.75)
[216]	Sep/27/2000 03:05:13 UMST	Concrete Cracking	A20(1.79) A43(2.07) A16(2.56)
[217]	Sep/27/2000 07:09:31 UMST	Concrete Cracking	A04(0.80) A03(1.50) A38(1.93)
[218]	Sep/27/2000 07:22:25 UMST	Concrete Cracking	A34(0.73) A48(1.08) A32(2.36)
[219]	Sep/27/2000 07:56:41 UMST	Concrete Cracking	A31(2.18) A47(2.77) A32(3.42)
[220]	Sep/27/2000 07:59:36 UMST	Concrete Cracking	A41(1.38) A11(1.70) A12(1.90)
[221]	Sep/27/2000 08:00:09 UMST	Concrete Cracking	A10(1.05) A05(2.11) A06(3.07)
[222]	Sep/27/2000 12:05:41 UMST	Concrete Cracking	A32(0.25) A48(1.68) A34(2.27)
[223]	Sep/27/2000 12:22:49 UMST	Concrete Cracking	A03(1.05) A04(1.20) A53(3.18)
[224]	Sep/27/2000 13:01:32 UMST	Concrete Cracking	A32(1.03) A34(1.49) A48(1.56)
[225]	Sep/27/2000 13:01:32 UMST	Concrete Cracking	A32(1.16) A34(1.46) A48(1.63)
[226]	Sep/27/2000 13:01:56 UMST	Concrete Cracking	A11(1.73) A12(2.39) A41(3.68)

[227]	Sep/27/2000 13:04:28 UMST	Concrete Cracking	A28(2.03) A29(5.65) A23(6.86)
[228]	Sep/27/2000 13:04:29 UMST	Concrete Cracking	A28(2.78) A29(6.15) A23(6.67)
[229]	Sep/27/2000 13:05:35 UMST	Concrete Cracking	A28(2.84) A29(3.89) A23(4.56)
[230]	Sep/27/2000 13:20:04 UMST	Concrete Cracking	A38(1.41) A04(2.34) A03(2.46)
[231]	Sep/27/2000 13:21:07 UMST	Concrete Cracking	A38(2.93) A08(2.96) A04(3.21)
[232]	Sep/27/2000 13:37:28 UMST	Concrete Cracking	A11(1.04) A12(3.10) A41(3.53)
[233]	Sep/27/2000 13:38:01 UMST	Concrete Cracking	A11(1.43) A12(2.82) A41(3.70)
[234]	Sep/27/2000 13:38:03 UMST	Concrete Cracking	A10(2.39) A11(2.77) A06(4.11)
[235]	Sep/27/2000 13:51:37 UMST	Concrete Cracking	A46(0.43) A26(0.43) A21(2.58)
[236]	Sep/27/2000 14:15:21 UMST	Concrete Cracking	A35(0.86) A37(2.46) A48(2.51)
[237]	Sep/27/2000 14:18:42 UMST	Concrete Cracking	A11(0.58) A12(3.11) A41(3.15)
[238]	Sep/27/2000 14:36:18 UMST	Concrete Cracking	A04(1.13) A38(1.64) A03(1.76)
[239]	Sep/27/2000 14:44:02 UMST	Concrete Cracking	A11(1.79) A12(3.54) A43(4.17)

SANDIA PCCV
ALBUQUERQUE, NM

SOUNDPRINT® ACOUSTIC MONITORING PROGRAM

REPORT

REPORTING PERIOD: SEPTEMBER 27 TO SEPTEMBER 27, 2000

DISCLAIMER

The information provided in this report is not intended to constitute an engineering report and should not be construed as such. The client is advised to retain qualified engineering expertise to interpret the data contained in this report. The information contained in this report is provided “as is” without warranty of any kind, either express or implied. Pure Technologies Ltd. is not liable for any lost profits, lost savings or other incidental, special or consequential damage arising out of the use of the monitoring system or the information contained in this report. Please refer to the terms and conditions attached to Pure’s SoundPrint® System Purchase Agreement and Pure’s Technical Support Agreement for further details.

® Registered Trademark, property of Pure Technologies Ltd.

TABLE OF CONTENTS

<i>Section</i>	<i>Title</i>
1.0	Executive Summary
2.0	SoundPrint® Report: Concrete Crashing: (09/27/2000)

1.0 EXECUTIVE SUMMARY

The following is a summary of relevant activity recorded by the SoundPrint® monitoring system. The summary includes information for both the latest monitoring period and for the entire monitoring period from the start-up date up to and including the most recent monitoring period.

	Period 09/27/2000– 09/27/2000
Operating Efficiency	100.0%
Concrete Crushing	10

Comments

Recommendations

There are no new recommendations at this time.

Prepared by:

Peter Paulson
President & CEO

REPORT PRESENTATION

A computerized drawing of the slab with the sensor layout is included on the following page and contains the following symbols:



Sensor Symbol with individual sensor name beneath



Symbolizes an event location. Event details are listed on the page following the drawing.

A list describing event details is provided for each drawing and lists the event number, shown on the computerized drawing, followed by the date, time, event classification and coordinates (in meters) to the origin of the events using the three closest sensors.

Event Report For Sandia PCCV

Albuquerque, NM

System Uptime 0.1 Days (100.0%)

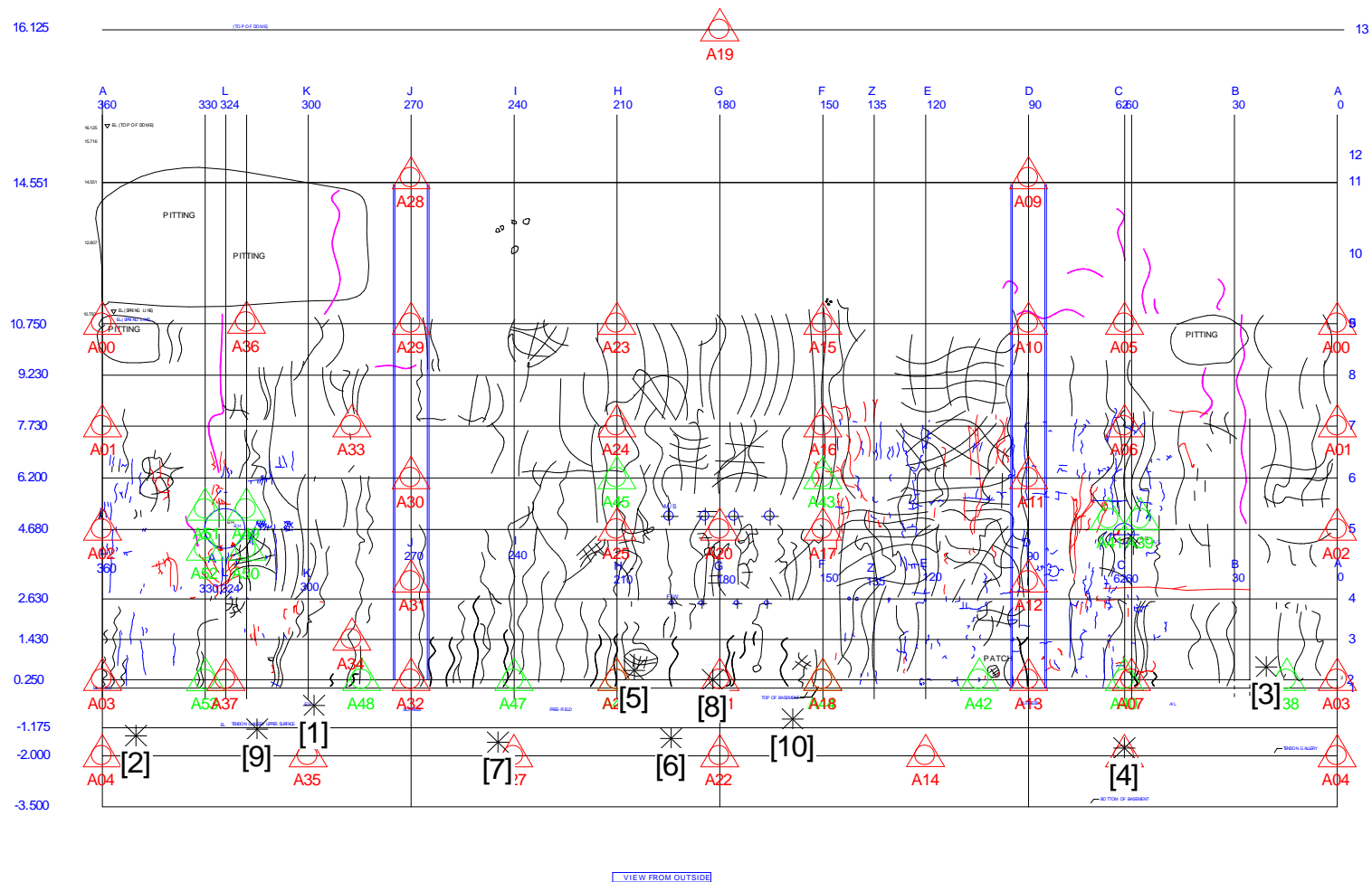
Concrete Crushing

Period: 09/27/2000 to 09/27/2000

Matched Events: 10



PCCV NEW -- 10 EVENTS



Scale: 1.95 m / cm

0 2m 20m

Events

No.	Date/Time	Classification	Location (m)
[1]	Sep/27/2000 12:49:41 UMST	Crushing Concrete	A35(1.50) A48(1.58) A34(2.23)
[2]	Sep/27/2000 13:34:56 UMST	Crushing Concrete	A04(1.15) A03(1.92) A53(2.61)
[3]	Sep/27/2000 13:35:58 UMST	Crushing Concrete	A38(0.70) A03(2.09) A04(3.33)
[4]	Sep/27/2000 13:37:46 UMST	Crushing Concrete	A08(0.23) A40(2.02) A07(2.03)
[5]	Sep/27/2000 13:43:18 UMST	Crushing Concrete	A26(0.57) A46(0.57) A21(2.50)
[6]	Sep/27/2000 13:49:57 UMST	Crushing Concrete	A22(1.50) A21(2.24) A46(2.34)
[7]	Sep/27/2000 13:50:01 UMST	Crushing Concrete	A27(0.62) A47(1.90) A32(3.12)
[8]	Sep/27/2000 14:05:10 UMST	Crushing Concrete	A21(0.21) A22(2.26) A26(2.78)
[9]	Sep/27/2000 14:15:22 UMST	Crushing Concrete	A35(1.67) A37(1.72) A53(2.09)
[10]	Sep/27/2000 14:24:44 UMST	Crushing Concrete	A44(1.46) A18(1.46) A22(2.38)

SANDIA PCCV
ALBUQUERQUE, NM

SOUNDPRINT® ACOUSTIC MONITORING PROGRAM

REPORT

REPORTING PERIOD: SEPTEMBER 26 TO SEPTEMBER 27, 2000

DISCLAIMER

The information provided in this report is not intended to constitute an engineering report and should not be construed as such. The client is advised to retain qualified engineering expertise to interpret the data contained in this report. The information contained in this report is provided “as is” without warranty of any kind, either express or implied. Pure Technologies Ltd. is not liable for any lost profits, lost savings or other incidental, special or consequential damage arising out of the use of the monitoring system or the information contained in this report. Please refer to the terms and conditions attached to Pure’s SoundPrint® System Purchase Agreement and Pure’s Technical Support Agreement for further details.

® Registered Trademark, property of Pure Technologies Ltd.

TABLE OF CONTENTS

<i>Section</i>	<i>Title</i>
1.0	Executive Summary
2.0	SoundPrint [®] Report: Tendon Pings: (09/26/2000)

1.0 EXECUTIVE SUMMARY

The following is a summary of relevant activity recorded by the SoundPrint® monitoring system. The summary includes information for both the latest monitoring period and for the entire monitoring period from the start-up date up to and including the most recent monitoring period.

	Period 09/26/2000– 09/27/2000
Operating Efficiency	100.0%
Tendon Pings	136

Comments

Recommendations

There are no new recommendations at this time.

Prepared by:

Peter Paulson
President & CEO

REPORT PRESENTATION

A computerized drawing of the slab with the sensor layout is included on the following page and contains the following symbols:



Sensor Symbol with individual sensor name beneath



Symbolizes an event location. Event details are listed on the page following the drawing.

A list describing event details is provided for each drawing and lists the event number, shown on the computerized drawing, followed by the date, time, event classification and co-ordinates (in meters) to the origin of the events using the three closes sensors.

Event Report For Sandia PCCV

Albuquerque, NM

System Uptime 1.9 Days (100.0%)

Tendon Pings

Period: 09/26/2000 to 09/27/2000

Matched Events: 136



SoundPrint® Acoustic Monitoring Report
Sandia PCCV



June 7, 2001
Page 4



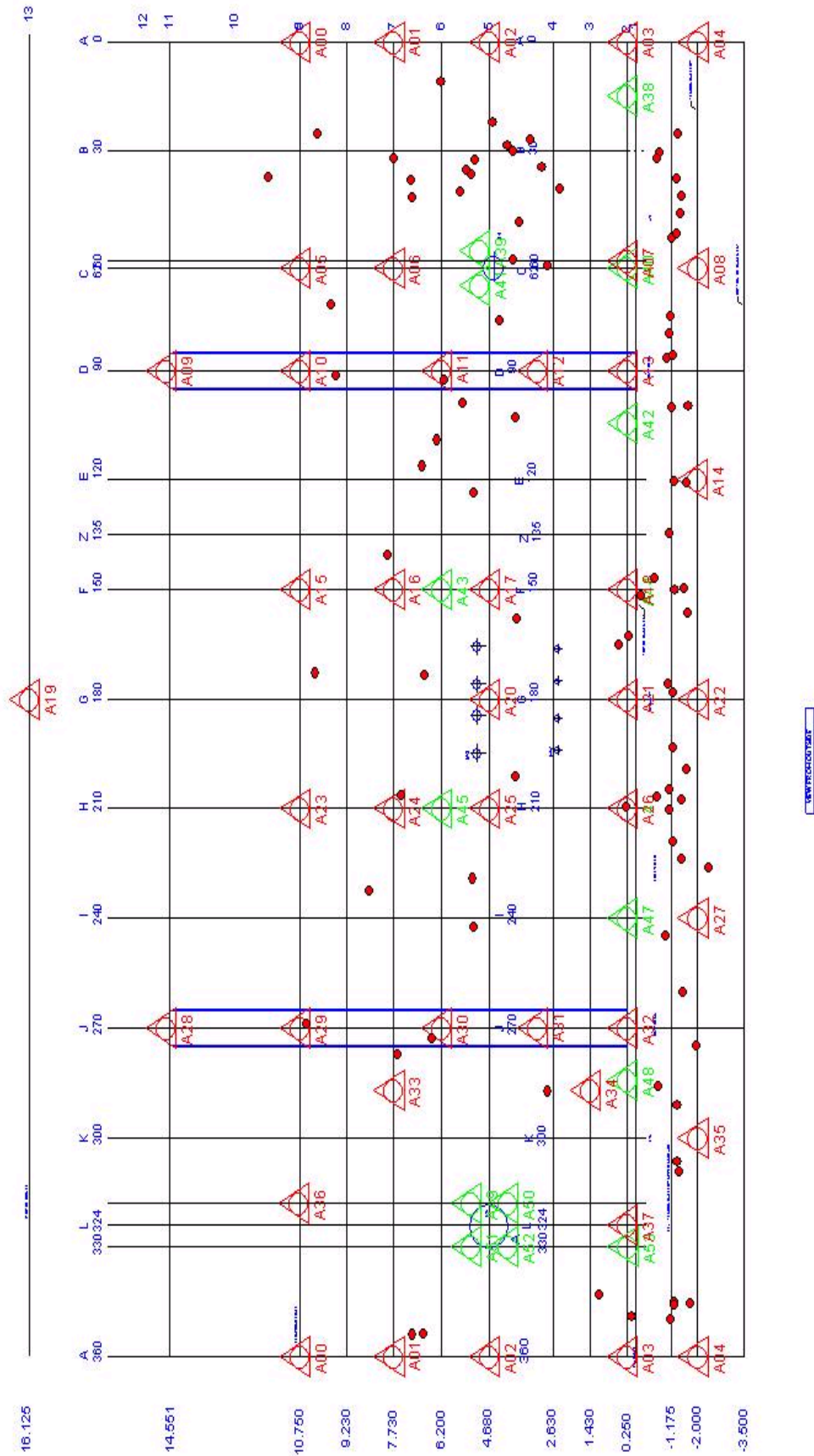
Events

No.	Date/Time	Classification	Location (m)
[1]	Sep/26/2000 20:43:28 UMST	Tendon Ping	A12(1.58) A11(2.00) A41(3.30)
[2]	Sep/26/2000 20:43:36 UMST	Tendon Ping	A41(1.20) A11(1.66) A39(2.11)
[3]	Sep/26/2000 20:43:40 UMST	Tendon Ping	A30(1.63) A31(1.64) A33(3.24)
[4]	Sep/26/2000 20:43:42 UMST	Tendon Ping	A30(1.34) A31(1.88) A33(3.02)
[5]	Sep/26/2000 20:44:18 UMST	Tendon Ping	A11(1.41) A12(1.70) A41(2.64)
[6]	Sep/26/2000 20:44:37 UMST	Tendon Ping	A11(1.28) A12(1.79) A41(2.15)
[7]	Sep/26/2000 20:45:16 UMST	Tendon Ping	A11(1.55) A41(1.56) A12(1.87)
[8]	Sep/26/2000 21:26:04 UMST	Tendon Ping	A33(1.26) A30(1.26) A29(3.44)
[9]	Sep/26/2000 21:26:07 UMST	Tendon Ping	A33(1.26) A30(2.13) A29(2.56)
[10]	Sep/26/2000 21:28:00 UMST	Tendon Ping	A11(0.73) A41(2.24) A12(2.34)
[11]	Sep/26/2000 21:28:36 UMST	Tendon Ping	A29(1.49) A33(2.00) A30(3.26)
[12]	Sep/26/2000 21:28:39 UMST	Tendon Ping	A29(1.72) A33(2.09) A30(2.83)
[13]	Sep/26/2000 21:51:11 UMST	Tendon Ping	A29(0.82) A33(3.26) A36(3.96)
[14]	Sep/26/2000 21:51:14 UMST	Tendon Ping	A29(0.53) A33(3.01) A30(4.02)
[15]	Sep/26/2000 21:51:59 UMST	Tendon Ping	A30(0.59) A33(2.30) A31(2.69)
[16]	Sep/26/2000 21:52:10 UMST	Tendon Ping	A30(0.65) A33(1.80) A31(3.68)
[17]	Sep/26/2000 21:52:18 UMST	Tendon Ping	A33(1.86) A29(1.92) A30(2.65)
[18]	Sep/26/2000 21:52:20 UMST	Tendon Ping	A31(0.51) A34(2.42) A30(2.77)
[19]	Sep/26/2000 21:52:41 UMST	Tendon Ping	A29(0.23) A33(3.26) A30(4.40)
[20]	Sep/26/2000 21:52:43 UMST	Tendon Ping	A29(1.47) A33(2.01) A30(3.43)
[21]	Sep/26/2000 21:52:43 UMST	Tendon Ping	A10(1.58) A11(3.02) A06(3.44)
[22]	Sep/26/2000 21:52:46 UMST	Tendon Ping	A29(1.54) A33(1.96) A30(3.44)
[23]	Sep/26/2000 21:52:53 UMST	Tendon Ping	A29(0.43) A33(3.33) A28(4.27)
[24]	Sep/26/2000 21:53:08 UMST	Tendon Ping	A30(0.65) A33(2.39) A31(2.59)
[25]	Sep/26/2000 21:53:11 UMST	Tendon Ping	A30(1.79) A33(2.38) A31(2.71)
[26]	Sep/26/2000 21:53:11 UMST	Tendon Ping	A33(2.03) A30(2.18) A49(2.68)
[27]	Sep/26/2000 21:53:28 UMST	Tendon Ping	A31(1.71) A30(1.98) A34(3.16)
[28]	Sep/26/2000 21:53:30 UMST	Tendon Ping	A11(0.61) A41(2.02) A12(2.81)
[29]	Sep/26/2000 21:53:39 UMST	Tendon Ping	A11(1.81) A06(2.37) A10(2.82)
[30]	Sep/26/2000 21:54:16 UMST	Tendon Ping	A31(1.09) A30(1.97) A34(3.36)
[31]	Sep/26/2000 21:54:18 UMST	Tendon Ping	A31(0.99) A30(2.09) A34(3.30)
[32]	Sep/26/2000 21:55:21 UMST	Tendon Ping	A33(1.15) A30(2.16) A29(2.59)
[33]	Sep/26/2000 21:55:36 UMST	Tendon Ping	A41(1.49) A11(1.71) A12(1.80)
[34]	Sep/26/2000 22:22:46 UMST	Tendon Ping	A30(1.59) A33(2.06) A31(2.94)
[35]	Sep/26/2000 22:23:22 UMST	Tendon Ping	A12(0.53) A13(2.47) A42(2.71)
[36]	Sep/26/2000 22:23:36 UMST	Tendon Ping	A29(1.25) A33(2.59) A30(3.32)
[37]	Sep/26/2000 22:23:36 UMST	Tendon Ping	A30(1.45) A31(1.94) A33(2.95)
[38]	Sep/26/2000 22:23:38 UMST	Tendon Ping	A29(1.02) A33(2.47) A30(3.62)
[39]	Sep/26/2000 22:23:42 UMST	Tendon Ping	A12(1.18) A11(2.00) A41(2.86)
[40]	Sep/26/2000 22:23:49 UMST	Tendon Ping	A12(1.40) A11(2.20) A41(3.34)
[41]	Sep/26/2000 22:23:50 UMST	Tendon Ping	A33(1.40) A30(1.53) A29(3.07)
[42]	Sep/26/2000 22:24:08 UMST	Tendon Ping	A29(0.89) A33(2.92) A36(3.92)
[43]	Sep/26/2000 22:24:09 UMST	Tendon Ping	A10(1.50) A05(2.66) A06(2.78)

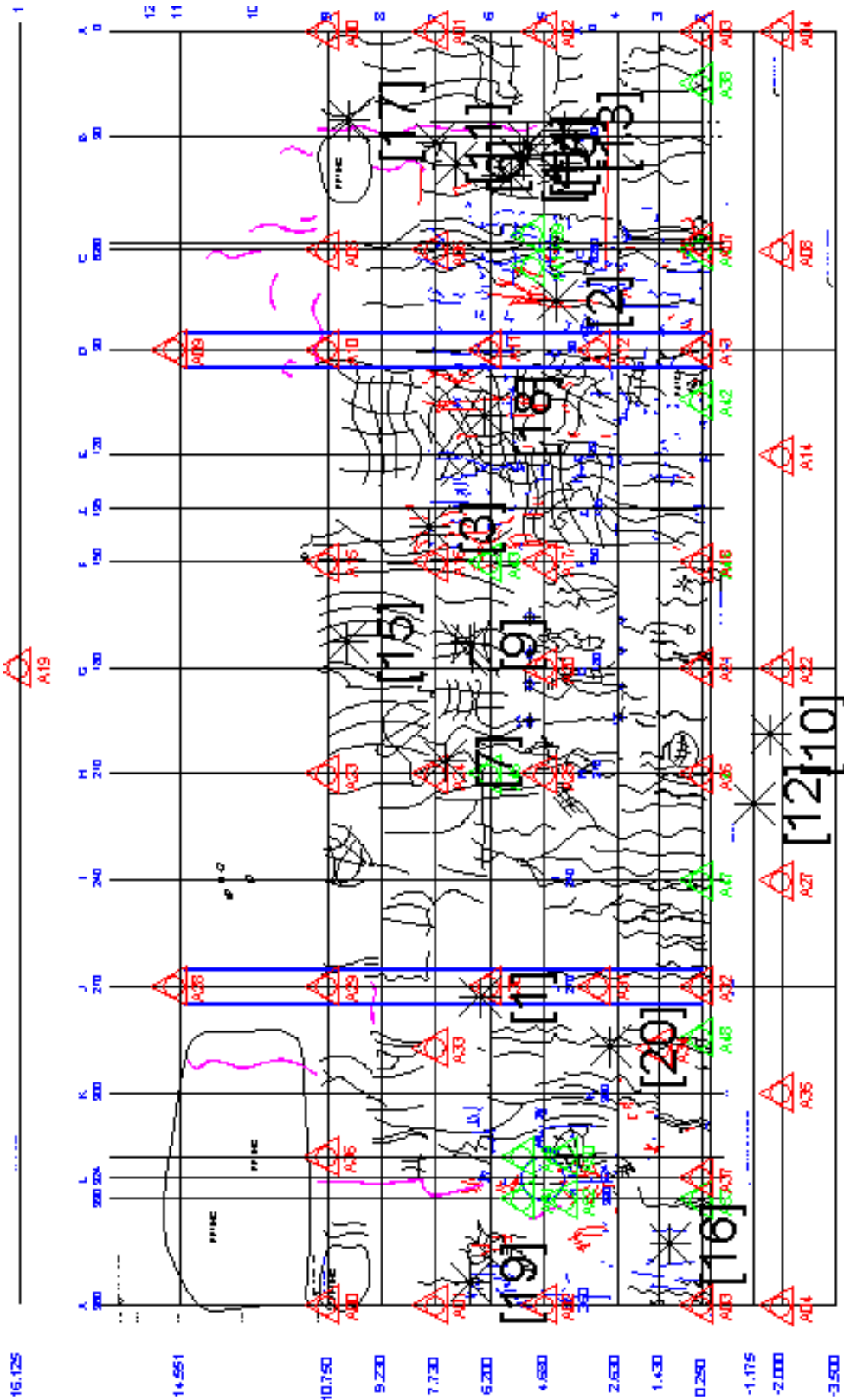
[44]	Sep/26/2000 22:24:10 UMST	Tendon Ping	A10(1.68) A06(2.73) A05(2.86)
[45]	Sep/26/2000 22:24:12 UMST	Tendon Ping	A29(0.88) A33(3.26) A36(3.90)
[46]	Sep/26/2000 22:24:28 UMST	Tendon Ping	A10(2.45) A11(2.92) A06(4.32)
[47]	Sep/26/2000 22:24:29 UMST	Tendon Ping	A11(1.17) A06(3.74) A41(3.77)
[48]	Sep/26/2000 22:24:42 UMST	Tendon Ping	A11(1.04) A12(2.02) A41(2.21)
[49]	Sep/26/2000 22:24:42 UMST	Tendon Ping	A11(1.30) A12(2.04) A41(3.00)
[50]	Sep/26/2000 22:24:58 UMST	Tendon Ping	A33(1.56) A30(1.76) A29(2.80)
[51]	Sep/26/2000 22:24:59 UMST	Tendon Ping	A33(1.64) A29(2.25) A30(2.33)
[52]	Sep/26/2000 22:25:02 UMST	Tendon Ping	A10(0.94) A05(3.36) A11(3.77)
[53]	Sep/26/2000 22:25:03 UMST	Tendon Ping	A30(1.16) A33(1.21) A29(3.64)
[54]	Sep/26/2000 22:25:06 UMST	Tendon Ping	A12(1.38) A11(1.67) A41(2.33)
[55]	Sep/26/2000 22:25:08 UMST	Tendon Ping	A12(1.48) A11(1.58) A41(2.50)
[56]	Sep/26/2000 22:25:08 UMST	Tendon Ping	A12(1.34) A11(1.72) A41(2.30)
[57]	Sep/26/2000 22:25:11 UMST	Tendon Ping	A10(1.61) A11(3.35) A05(3.92)
[58]	Sep/26/2000 22:25:44 UMST	Tendon Ping	A11(0.83) A12(3.16) A41(3.38)
[59]	Sep/26/2000 22:26:01 UMST	Tendon Ping	A12(1.38) A11(1.73) A41(2.07)
[60]	Sep/26/2000 22:26:08 UMST	Tendon Ping	A12(1.35) A11(1.73) A41(2.19)
[61]	Sep/26/2000 22:26:34 UMST	Tendon Ping	A29(0.89) A33(2.91) A30(3.70)
[62]	Sep/26/2000 22:27:04 UMST	Tendon Ping	A11(0.42) A41(2.98) A12(3.03)
[63]	Sep/26/2000 22:30:11 UMST	Tendon Ping	A12(1.23) A13(1.70) A42(2.34)
[64]	Sep/26/2000 22:30:12 UMST	Tendon Ping	A12(1.32) A13(1.74) A42(2.54)
[65]	Sep/27/2000 07:57:00 UMST	Tendon Ping	A31(0.86) A32(2.07) A34(2.08)
[66]	Sep/27/2000 07:57:06 UMST	Tendon Ping	A11(1.74) A10(2.86) A06(3.12)
[67]	Sep/27/2000 07:57:22 UMST	Tendon Ping	A11(1.15) A12(1.97) A41(2.64)
[68]	Sep/27/2000 07:57:23 UMST	Tendon Ping	A11(0.99) A12(2.11) A41(2.57)
[69]	Sep/27/2000 07:57:33 UMST	Tendon Ping	A12(1.34) A11(1.95) A41(3.00)
[70]	Sep/27/2000 07:57:45 UMST	Tendon Ping	A11(0.46) A41(2.34) A12(2.61)
[71]	Sep/27/2000 07:57:49 UMST	Tendon Ping	A12(0.12) A13(2.81) A41(3.08)
[72]	Sep/27/2000 07:57:54 UMST	Tendon Ping	A10(2.00) A11(3.35) A05(4.38)
[73]	Sep/27/2000 07:57:55 UMST	Tendon Ping	A10(2.26) A11(2.37) A06(3.30)
[74]	Sep/27/2000 07:57:56 UMST	Tendon Ping	A10(1.47) A11(3.08) A05(3.24)
[75]	Sep/27/2000 07:57:58 UMST	Tendon Ping	A12(1.06) A11(2.29) A41(3.12)
[76]	Sep/27/2000 07:58:02 UMST	Tendon Ping	A12(0.94) A11(2.60) A41(3.33)
[77]	Sep/27/2000 07:58:03 UMST	Tendon Ping	A12(1.05) A13(2.52) A41(2.78)
[78]	Sep/27/2000 07:58:12 UMST	Tendon Ping	A10(1.78) A06(2.42) A05(2.48)
[79]	Sep/27/2000 07:58:16 UMST	Tendon Ping	A06(1.44) A11(1.78) A41(1.97)
[80]	Sep/27/2000 07:58:18 UMST	Tendon Ping	A11(1.87) A10(3.70) A06(4.27)
[81]	Sep/27/2000 07:58:18 UMST	Tendon Ping	A11(2.46) A16(3.83) A10(3.98)
[82]	Sep/27/2000 07:58:19 UMST	Tendon Ping	A29(2.14) A33(2.27) A30(2.46)
[83]	Sep/27/2000 07:58:20 UMST	Tendon Ping	A11(0.78) A12(2.27) A41(2.46)
[84]	Sep/27/2000 07:58:21 UMST	Tendon Ping	A11(1.99) A12(3.40) A43(4.00)
[85]	Sep/27/2000 07:58:22 UMST	Tendon Ping	A11(1.20) A12(2.17) A41(3.01)
[86]	Sep/27/2000 07:58:23 UMST	Tendon Ping	A29(0.76) A33(2.72) A30(3.87)
[87]	Sep/27/2000 07:58:30 UMST	Tendon Ping	A11(2.19) A10(2.42) A06(3.24)
[88]	Sep/27/2000 07:58:31 UMST	Tendon Ping	A33(1.39) A30(2.00) A29(2.62)
[89]	Sep/27/2000 07:58:33 UMST	Tendon Ping	A11(2.88) A10(2.99) A16(4.16)

[90]	Sep/27/2000 07:58:34 UMST	Tendon Ping	A10(2.23) A11(2.34) A06(3.08)
[91]	Sep/27/2000 07:58:34 UMST	Tendon Ping	A10(2.41) A11(2.82) A06(4.19)
[92]	Sep/27/2000 07:58:35 UMST	Tendon Ping	A31(0.26) A34(2.51) A30(2.82)
[93]	Sep/27/2000 07:58:36 UMST	Tendon Ping	A31(0.70) A30(2.51) A34(2.64)
[94]	Sep/27/2000 07:58:37 UMST	Tendon Ping	A30(1.77) A33(1.89) A29(2.79)
[95]	Sep/27/2000 07:58:37 UMST	Tendon Ping	A29(0.96) A33(3.74) A28(3.77)
[96]	Sep/27/2000 07:58:38 UMST	Tendon Ping	A29(0.54) A33(3.01) A30(4.01)
[97]	Sep/27/2000 07:58:39 UMST	Tendon Ping	A10(1.24) A05(2.62) A06(3.00)
[98]	Sep/27/2000 07:58:40 UMST	Tendon Ping	A10(1.87) A11(3.08) A06(3.99)
[99]	Sep/27/2000 07:58:41 UMST	Tendon Ping	A11(0.64) A12(2.52) A41(2.72)
[100]	Sep/27/2000 07:58:43 UMST	Tendon Ping	A11(0.19) A41(2.59) A12(2.86)
[101]	Sep/27/2000 07:58:53 UMST	Tendon Ping	A11(2.34) A12(3.42) A43(3.72)
[102]	Sep/27/2000 07:58:55 UMST	Tendon Ping	A10(1.71) A11(3.20) A05(3.94)
[103]	Sep/27/2000 07:58:55 UMST	Tendon Ping	A33(0.99) A30(1.40) A49(3.89)
[104]	Sep/27/2000 07:58:57 UMST	Tendon Ping	A10(1.78) A11(2.89) A06(3.54)
[105]	Sep/27/2000 07:58:59 UMST	Tendon Ping	A06(2.19) A11(2.26) A10(2.49)
[106]	Sep/27/2000 07:59:00 UMST	Tendon Ping	A10(2.05) A06(2.37) A11(2.70)
[107]	Sep/27/2000 07:59:01 UMST	Tendon Ping	A12(0.78) A11(2.47) A41(3.05)
[108]	Sep/27/2000 07:59:02 UMST	Tendon Ping	A31(1.64) A30(2.21) A34(2.94)
[109]	Sep/27/2000 07:59:03 UMST	Tendon Ping	A29(1.63) A33(2.16) A30(2.92)
[110]	Sep/27/2000 08:00:05 UMST	Tendon Ping	A31(0.30) A34(2.17) A32(2.62)
[111]	Sep/27/2000 08:00:20 UMST	Tendon Ping	A11(0.29) A41(2.89) A06(3.24)
[112]	Sep/27/2000 08:00:47 UMST	Tendon Ping	A12(1.12) A13(1.81) A42(2.43)
[113]	Sep/27/2000 08:00:48 UMST	Tendon Ping	A12(1.43) A13(1.48) A42(2.01)
[114]	Sep/27/2000 08:01:26 UMST	Tendon Ping	A12(1.28) A13(1.63) A42(2.26)
[115]	Sep/27/2000 08:01:28 UMST	Tendon Ping	A12(1.32) A13(1.63) A42(2.34)
[116]	Sep/27/2000 08:01:38 UMST	Tendon Ping	A29(2.03) A30(3.16) A33(3.24)
[117]	Sep/27/2000 08:01:53 UMST	Tendon Ping	A12(0.69) A13(2.33) A42(2.91)
[118]	Sep/27/2000 08:02:46 UMST	Tendon Ping	A10(1.60) A09(3.96) A05(4.31)
[119]	Sep/27/2000 08:02:53 UMST	Tendon Ping	A10(1.02) A05(2.49) A09(3.42)
[120]	Sep/27/2000 08:04:32 UMST	Tendon Ping	A10(1.67) A09(2.63) A05(3.27)
[121]	Sep/27/2000 08:18:33 UMST	Tendon Ping	A10(1.74) A09(2.58) A05(3.46)
[122]	Sep/27/2000 12:39:29 UMST	Tendon Ping	A29(1.12) A33(2.71) A30(3.45)
[123]	Sep/27/2000 12:43:06 UMST	Tendon Ping	A12(0.95) A13(2.01) A42(2.63)
[124]	Sep/27/2000 12:43:37 UMST	Tendon Ping	A13(1.32) A12(1.60) A42(2.07)
[125]	Sep/27/2000 13:00:14 UMST	Tendon Ping	A12(1.61) A11(1.89) A41(3.21)
[126]	Sep/27/2000 13:00:17 UMST	Tendon Ping	A11(1.54) A12(1.63) A41(2.76)
[127]	Sep/27/2000 13:04:22 UMST	Tendon Ping	A12(1.84) A42(2.21) A13(2.77)
[128]	Sep/27/2000 13:17:59 UMST	Tendon Ping	A12(1.99) A11(2.54) A42(4.02)
[129]	Sep/27/2000 13:58:55 UMST	Tendon Ping	A10(1.35) A11(3.32) A05(3.50)
[130]	Sep/27/2000 13:58:56 UMST	Tendon Ping	A10(1.19) A05(3.15) A11(3.37)
[131]	Sep/27/2000 14:16:51 UMST	Tendon Ping	A33(1.74) A29(1.79) A30(2.94)
[132]	Sep/27/2000 14:18:45 UMST	Tendon Ping	A29(1.04) A28(3.32) A33(4.26)
[133]	Sep/27/2000 14:19:08 UMST	Tendon Ping	A10(1.26) A05(1.52) A06(3.38)
[134]	Sep/27/2000 14:19:09 UMST	Tendon Ping	A10(0.54) A05(3.33) A09(4.33)

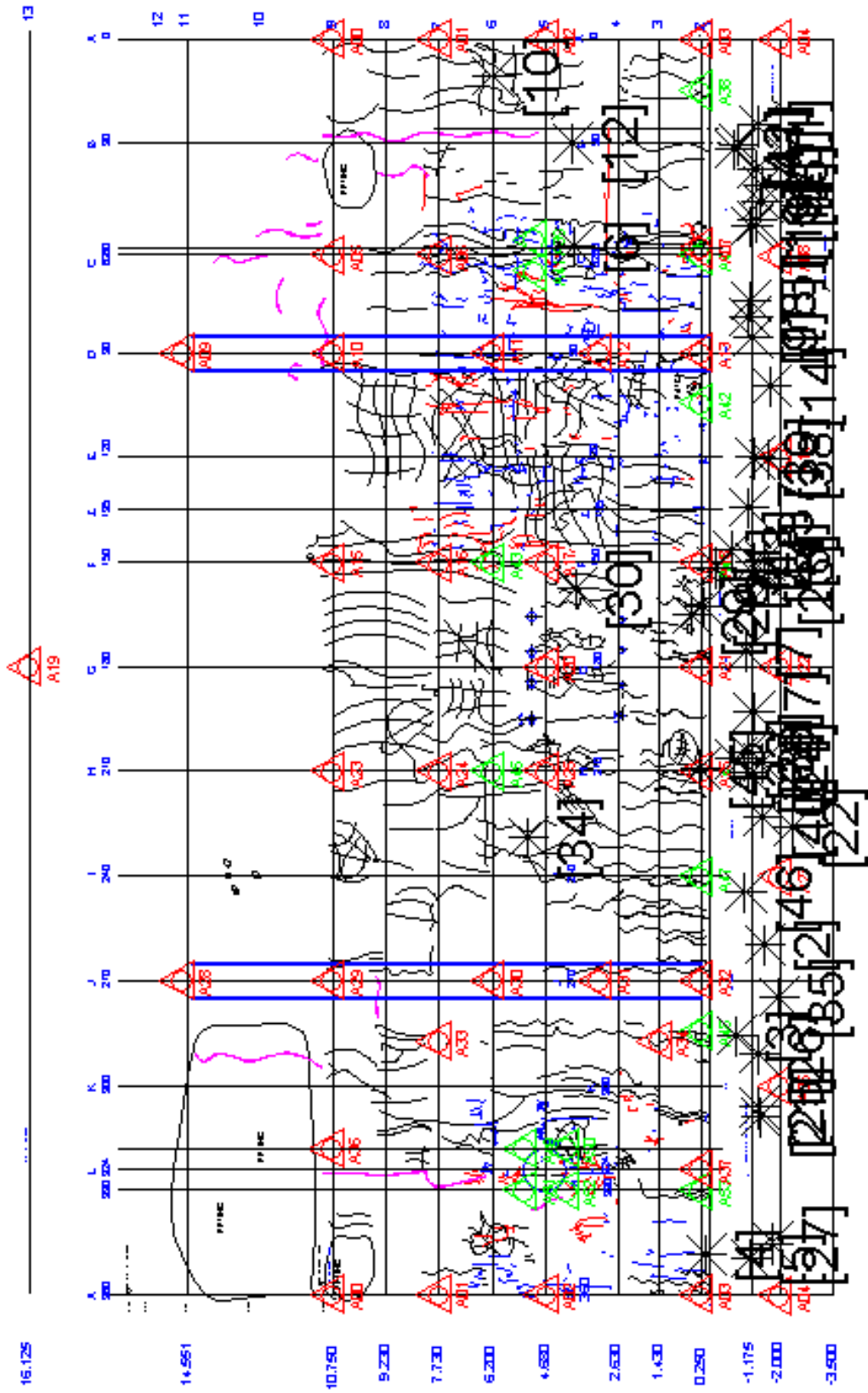
[135]	Sep/27/2000 14:45:59 UMST	Tendon Ping	A12(0.75) A41(2.42) A13(3.00)
[136]	Sep/27/2000 14:46:00 UMST	Tendon Ping	A12(0.39) A13(2.59) A42(2.85)



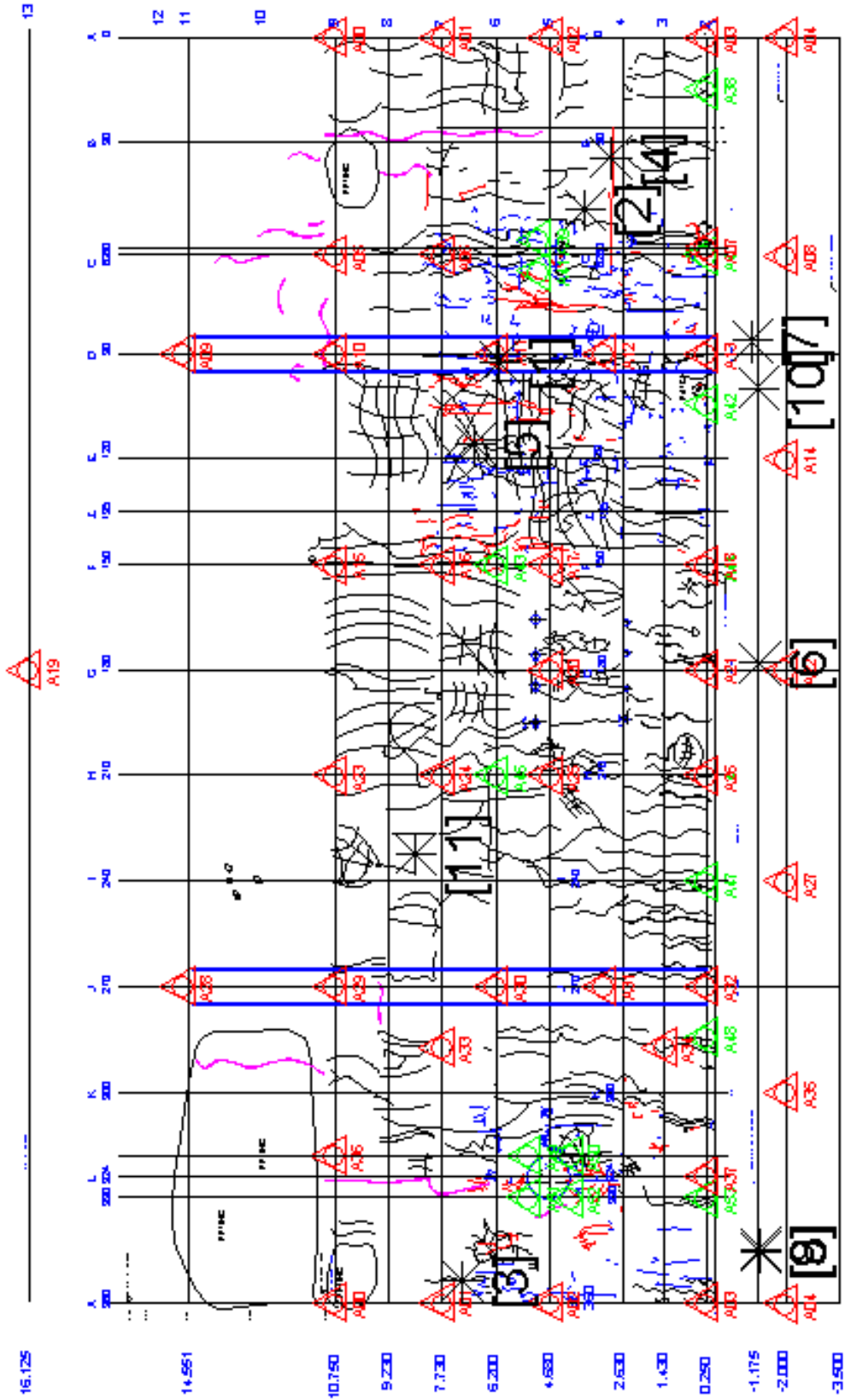
All 92 wire breaks before failure during test Nov. 14, 2001
(Many contain multiple wire failures at one location)



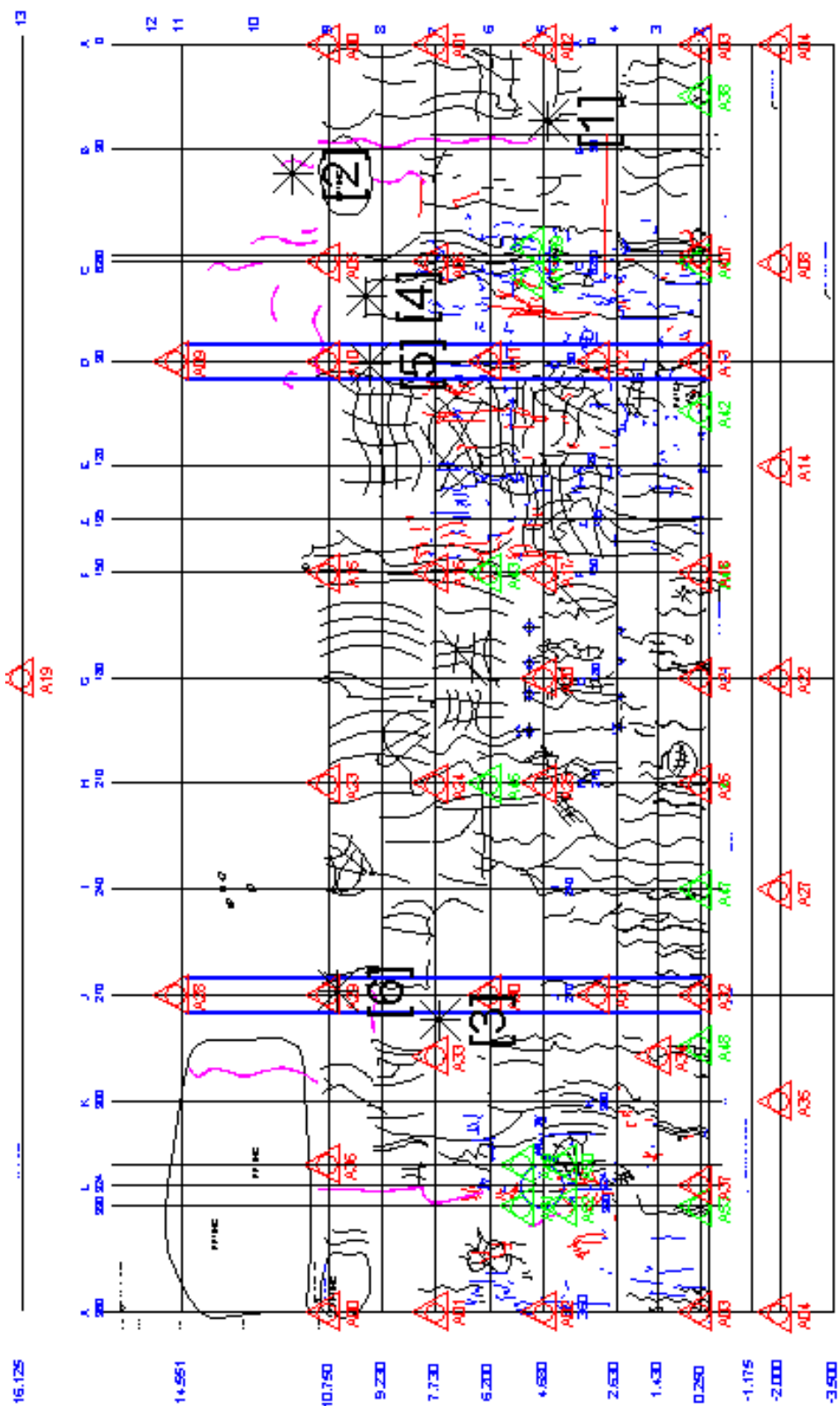
Wire breaks during the period of 10:45 AM to 10:47 AM
End at 10:46:12 (197 psi to 200 psi)



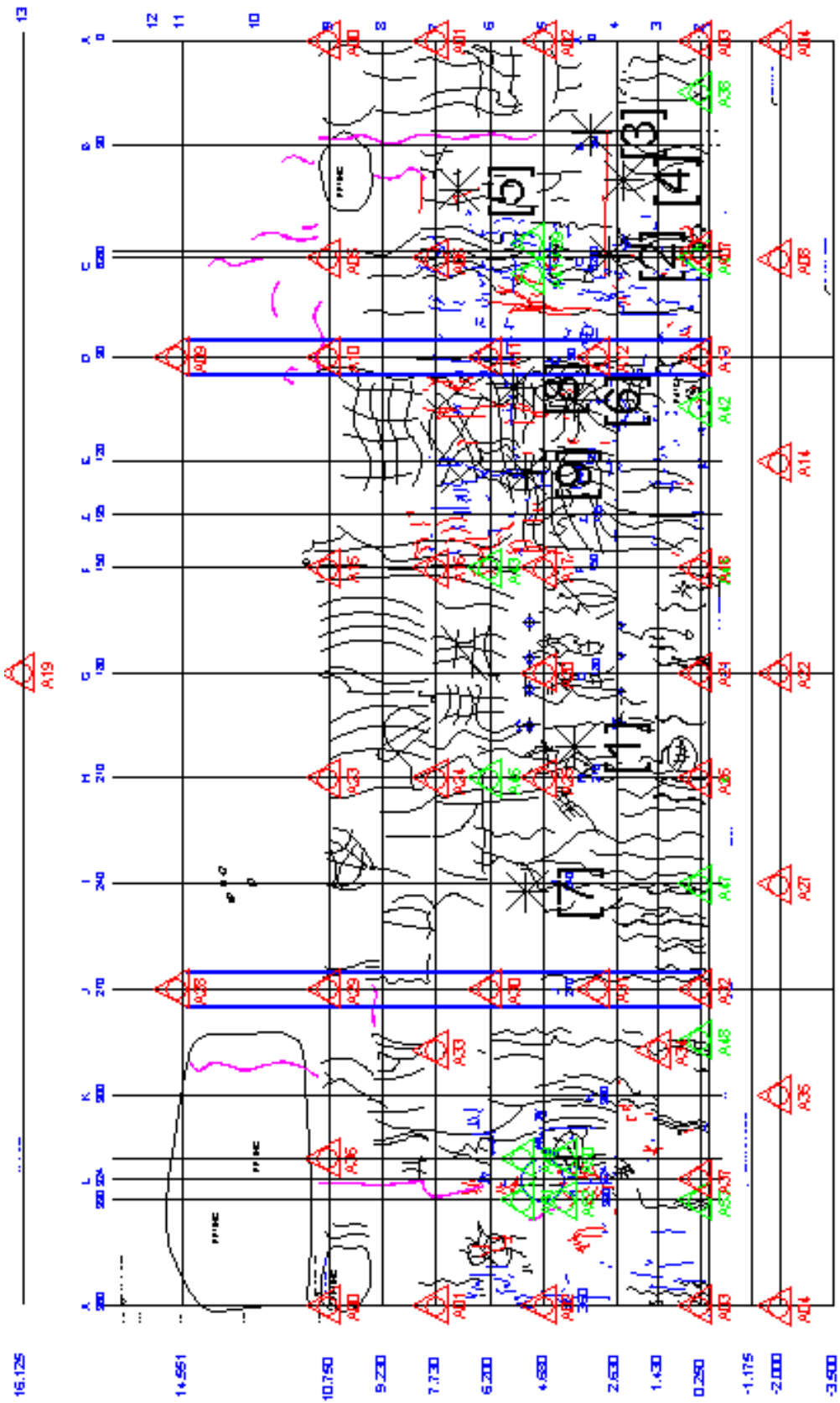
Wire breaks during the minute of 10:44 AM to 10:45 AM
193 psi to 197 psi



Wire breaks during the minute of 10:43 AM to 10:44 AM
192 PSI to 193 PSI



**Wire breaks during the minute of 10:42 AM to 10:43 AM
188 PSI to 192 PSI**



Wire breaks during the period 10:39 AM to 10:42 AM (First Breaks)
Approximately 188 PSI

Appendix L: Metallurgical Analysis of PCCV Liner Tears

Metallurgical Analysis of PCCV Liner Tears

K. H. Eckelmeyer, J. A. VanDenAvyle, A. C. Kilgo, and L. D. Lambert

Executive Summary:

Substantial amounts of grinding done in association with repair welding were observed in conjunction with nearly all of the 26 liner tears. This grinding produced localized thin areas adjacent to a number of the repair welds. Thinning permitted localized plastic deformation culminating in tearing to occur in the more severely ground regions prior to the onset of general plasticity in the bulk of the liner. This appears to have contributed strongly to the observed liner tearing.

Geometric features may also have contributed to formation of some of the tears. Acoustic data suggested that initial tearing occurred in the equipment hatch transition region, despite grinding being less severe here than in some other areas where tearing did not occur until later. Back-up bar irregularities associated with repair welding (missing segments, various sized segments, etc.) may also have contributed to several tears, but appear to have been primarily responsible for only tear #16. Discontinuities in horizontal stiffeners may also have exacerbated strain localization and contributed to the formation of some tears.

While the ¼-scale liner material met most of the mechanical property specifications for full thickness plate, the ratio of yield to ultimate tensile strength was unusually high for hot rolled steel plate, making the model liner particularly sensitive to local variations in thickness. The necessity of rolling the liner plate to ~ 25% of usual thickness may have increased tensile and particularly yield strength, making it more prone to localized plastic deformation and tearing than typical full-thickness liner material.

Portions of the heat affected zones adjacent to the welds were slightly softer than the base metal, possibly because relatively low temperature finish rolling left a small amount of warm work in the base metal. The amount of softening, however, was not sufficient to cause complete plastic strain localization and tearing, as appeared to have occurred in the liner. Consistent with this, tensile tests on welded samples gave similar strengths, but lower elongations, to those of unwelded material. Also consistent with this, lesser but varied degrees of localized plastic deformation were observed adjacent to some liner welds where little or no grinding and/or repair welding had been done, and where tearing had not occurred. In the more severe cases, the onset of necking, which culminates in tearing, may have occurred. Tear #12 may represent a tear that formed in the absence of prior grinding.

There was no indication that deficiencies in the liner material or welds contributed to tearing, other than as described above. The only exception to this was tear #1, which occurred at a lack-of-fusion defect in the region of a repair weld.

Background:

An instrumented quarter-scale model of a nuclear reactor containment structure was constructed and pressure tested to characterize its mechanical response. The design pressure for this structure was 0.39MPa, and analytical predictions were that failure would occur between 2 and 4 times this design pressure. During pressure testing of this structure leaks were detected beginning at 2.5 times design pressure. At 3.3 times design pressure the leak rate exceeded pressurization capacity and the test was terminated prior to structural failure. Approximately 0.4% global hoop strain occurred in the structure. Post-test examination revealed that 26 tears had formed in the interior steel liner, and that these tears were responsible for the leaks.

The locations of these tears are shown in Figure 1. Seven of the tears were associated with structural features, such as feedwater penetrations and the equipment hatch transition boundary. Acoustic signals suggested that the earliest tearing occurred in the equipment hatch area. The remaining nineteen tears occurred in “free-field” areas distant from any gross structural transitions.

A metallurgical study has been conducted to characterize these tears. This report summarizes the findings and conclusions of this study.

Macro Examination of Liner Interior and Exterior:

Initial macroscopic inspection of liner tear regions consisted of visual inspection of the inside surface, inspection of photographs of the outside surface (taken prior to concrete placement), and ultrasonic measurement of liner thickness. (Note that throughout this report the descriptors “inside”, “interior”, and “front side” are used to indicate the surface of the liner facing the inside of the structure, while “outside”, “exterior” and “back side” are used to indicate the liner surface facing the concrete.) Following initial inspection, sections surrounding many of the tears were cut out and removed. This permitted more detailed observation of features such as back-up bars. A number of macroscopic characteristics were found to be common to nearly all of the tears:

- Tears were oriented perpendicular to the circumference of the cylindrical structure, i.e., vertically. This indicated that they formed primarily due to circumferential (hoop) stresses. The only exceptions were tears along the feedwater penetrations – these initiated at the 3 and 9 o’clock positions (vertically), then extended along the semicircular transition boundary.
- Tears occurred in conjunction with vertical field welds. Typically the tears formed parallel to the welds, less than a few millimeters into the plate from the fusion zone boundaries. No cases of failure in the primary fusion zone were observed, except for a few cases where separate tears developed on opposite sides of the weld, then linked together through the fusion zone. Several tears occurred somewhat farther from the vertical field welds, but never more than 3 centimeters.
- Tears occurred in regions in which repair welding and associated grinding (pre-repair and/or post-repair) had been done.

- Substantial localized plastic deformation occurred in the regions of the tears. This suggested that the tears formed by ductile rupture following localized plastic strain, rather than by brittle fracture at abnormally low strain.
- Liner thinning was detected in the vicinities of the tears and the nearby areas where grinding had been done in conjunction with repair welding. It was not apparent, however, whether this thinning was associated with grinding that took place prior to testing of the structure, with plastic deformation which occurred during testing of the structure, or with both.

Summaries of macroscopic observations on the “free-field” and “feature-associated” tears and their surroundings are given in Tables 1 and 2, respectively. The descriptions of “apparent extent of repair welding” and “apparent extent of grinding” are qualitative descriptors based on visual observation only. These were used primarily to aid in the selection of a range of tear samples for more detailed quantitative characterization, which will be described in a later section. Photographs taken during construction helped correlate liner outside features (stiffeners, anchors, weld back-up bars, etc.) with the locations of the tears. Photographs comparing the front side (interior) and back side (exterior prior to concrete placement) features in the vicinities of a number of tears are shown in Figures 2 to 18.

Examination of Table 1 shows no indication that the “free-field” tears occurred preferentially in the proximity of anchors or horizontal welds and the associated stiffeners. Some of these tears, however, may have been exacerbated by abnormalities such as discontinuities in stiffeners and/or back-up bars. This will be discussed in greater detail in a subsequent section.

A number of features were observed in the field welds of the model that would not be characteristic or allowed in full-scale liners. In many cases these were inevitable consequences of the difficulties involved in fabricating a 1/4-scale model. For example, it was clear that fit-up and distortion had been difficult issues during the liner erection and welding process. As a result, there were areas where adjacent plates appeared to be misaligned by more than one-quarter the plate thickness (Ref. 1).

Irregularities were also observed in the back-up bars. It is important to note, however, that while permitted by ASME Code (Ref. 2), MHI does not typically use back-up bars in fabrication of full-sized liners; they were used here because of difficulties associated with fabricating a 1/4-scale model. The irregularities observed included use of varying sizes of back-up bar (ranging from 3 mm thick x 13 mm wide to 6 mm thick x 25 mm wide), areas in which segments of back-up bar were removed and not replaced during repair welding, and the absence of welds between adjacent sections of back-up bar. All of these provide discontinuities that could facilitate strain localization, and would not be allowed in full scale liners (Ref. 2). Subsequent investigation did not suggest that such back-up bar irregularities in the *vertical* welds were primarily responsible for any tears. A missing back-up bar segment in a *horizontal* field weld appeared to be primarily responsible for tear # 16, as will be described in more detail in later sections.

Substantial amounts of grinding were also commonly observed in the vicinities of repair welds. Extensive repair welding had been done, presumably in areas where radiographic examination revealed evidence of porosity in the fusion zones. While the intent of this grinding had been to remove the defected fusion zone volumes, grinding frequently extended out into the adjacent plates, often by one to two centimeters. Heat tinting from subsequent welding confirmed that some of this grinding had been done *prior to* repair welding. However, the absence of heat tinting in other areas indicated that additional grinding had also been done *following* repair welding, apparently for cosmetic purposes. Visual observation indicated that severe grinding had been done in a number of areas, suggesting that grinding depth might have exceeded the 12.5% undercut allowed in full scale liners (Ref. 3), thus promoting plastic strain localization. (This was confirmed by subsequent measurements, as will be described in a later section.)

Thickness measurements were made in the vicinities of many of the tears using an ultrasonic technique. The probe used had a lateral spatial resolution of 2 to 3 mm. Thickness measurements were made alongside and parallel to many of the tears (typically ~4 to 6 mm from the tear), and in some cases both ahead of the tears and at greater lateral distances from the tears. Repeated trials showed these measurements to be reproducible within ~0.05 mm (~3% of initial thickness).

Substantial thinning was detected in the vicinities of most of the tears, as shown in Figures 19 to 36. This thinning was typically confined to ~20 mm on either side of the weld; the nominal thickness of ~1.8 mm was generally found at greater distances from the welds. Adjacent to many of the tears, however, thickness reductions of 25% or greater were frequently observed in one or more measurements. In the most extreme case (tear #17) a thickness reduction of 63% was detected adjacent to the tear. Unfortunately, there was no way to distinguish how much of the measured thinning was caused by grinding (prior to pressurization of the structure) and how much was caused by localized plastic deformation (during pressurization of the structure). Distinguishing the magnitudes of these two contributions to thinning required metallographic cross-sectioning and examination of the torn areas, as will be described in a later section.

Liner buckling was also observed in numerous areas, both areas where tearing occurred and in areas without tears. It was apparent that this compressive buckling occurred during unloading in regions where localized plastic deformation had occurred in tension during testing of the structure. In many cases this buckling occurred adjacent to the welds, indicating that plastic deformation had been locally concentrated there.

The degree of buckling varied with location. The largest amounts of buckling were generally observed in the vicinities of the tears, including along the welds where tearing occurred at higher or lower levels. Relatively large amounts of buckling were also observed in welds associated with structural discontinuities, including the edges of the buttresses. In free-field areas, the degree of buckling seemed relatively high between the equipment hatch transition and the air lock. This may indicate that global strains were higher in this area for some reason. This is also consistent with the observation that a disproportionate number of tears occurred in this region. Considerably less buckling was

observed near the top of the liner, consistent with lower overall stresses expected in this area.

In summary, the most provocative macroscopic observations were that nearly all tears occurred following localized plastic deformation adjacent to weld repairs where grinding may have resulted in localized liner thinning. Some, but not nearly all, of the tears occurred in areas where structural transitions or irregularities in back-up bars may have intensified stress and/or strain localization. Buckling indicated that localized plastic deformation also occurred near some welds where tearing was not observed.

Material and Properties:

The liner material was specified to be SGV 410 per JIS G 3118 (Ref. 4). This is a plain carbon structural steel plate containing 0.21% carbon (maximum), 0.85% to 1.20% manganese, 0.15% to 0.30% silicon, 0.035% phosphorus (maximum), and 0.040% sulfur (maximum). Carbon and manganese are the primary strengtheners in this material, and phosphorus and sulfur are limited to promote weldability. (Excessive P and S promote hot cracking in the weld fusion zones. No evidence of this was observed in the liner welds.) The specified mechanical properties for SGV 410 are:

- Yield Strength: 225 MPa (33 ksi) (minimum)
- Ultimate tensile Strength: 410 to 490 MPa (59 to 71 ksi)
- Elongation: 21% minimum (in 50 mm gauge length of 25 mm wide sample).

SGV 410 plate is not commercially produced in thicknesses below 6.4 mm. MHI was able to obtain 1.8 mm thick material for the liner via a special order. While this material was as close as could be obtained to full scale SGV 410, it is possible that rolling the material to less than 30% of its normal minimum thickness could result in some alteration of mechanical properties, potentially making the model liner material less than perfectly characteristic of full-scale liners.

MHI material qualification tests showed the following average tensile properties (average of six samples, 3 from each orientation; no significant orientation differences were observed):

- Yield Strength: 383 MPa (55 ksi)
- Ultimate Tensile Strength: 498 MPa (72 ksi)
- Elongation: 33%

The observed ultimate tensile strength was slightly higher than the specified upper limit. Otherwise the material conformed to the mechanical properties specified for SGV 410. The yield strength, however, was 70% over the specified minimum, and was quite high for a steel of this composition. Both the high ultimate strength and the high yield strength may have resulted from low finishing temperature, as might be expected when rolling unusually thin material. The 33% elongation to failure dramatically exceeded the ~0.4% global strain at which tearing occurred in the liner.

The ratio of yield strength to ultimate strength provides a measure of the susceptibility of a material to plastic strain localization due to variations in thickness, for example, local thinning resulting from grinding. For the material in question, the yield strength represents 77% of the ultimate tensile strength. This is unusually high for hot rolled plain carbon steel plate, where the YS/UTS ratio is typically in the 0.5 to 0.7 range (Ref. 5). The high YS/UTS ratio of the steel used in the model makes this material unusually susceptible to plastic strain localization and subsequent tearing due to variations in thickness. Based on a simple uniaxial analysis, areas in which grinding resulted in thinning greater than ~23% would exceed the ultimate strength before the yield strength was reached in the surrounding (unthinned) material. This would result in complete localization of plastic deformation culminating in tearing in these thinned regions prior to the onset of general plasticity in the overall structure. Implications based on this simple uniaxial approach may not be quantitatively applicable to the biaxially stressed liner and its geometric complexities. Nonetheless, it appears that the unusually high yield strength of the liner material may have made the liner particularly sensitive to variations in thickness caused by grinding done in conjunction with liner weld repairs.

The microstructures and hardnesses of welded liner material were characterized by Sandia. Samples from two MHI practice weld plates were cross-sectioned, mounted, polished, and etched. Both showed microstructures typical of welded plain carbon structural steel, i.e., a progression from:

- base metal consisting of fine-grained equiaxed ferrite and pearlite (Figure 37), to
- fine-grained heat affected zone (HAZ) consisting of equiaxed ferrite and pearlite (Figure 38), to
- progressively coarser-grained heat affected zone consisting of acicular ferrite and pearlite (Figure 39), to
- fusion zone consisting of coarse columnar grains (formed during solidification) which have transformed on cooling to mixed ferrite and pearlite (Figure 40).

A second weld pass had been made in one of the practice weld panels. The heating from this second pass altered the microstructure of the initial weld metal. Figure 41 shows that the initial weld metal has been re-austenitized and recrystallized, eliminating the prior-columnar solidification structure, then transformed to a finer-grained assemblage of equiaxed ferrite and pearlite. This characteristic microstructural difference was used to distinguish between original and repair welds in metallographic samples taken from the liner tear areas, as will be discussed in a later section.

Microhardness measurements were made to provide an estimate of strength variations across the weld. Twenty-five Vickers hardness measurements were made using a 100 gram load in each of the following areas: the base metal, the fine-grained portion of the heat affected zone adjacent to the base metal, the intermediate-grained portion near the middle of the heat affected zone, the coarse-grained portion of the heat affected zone adjacent to the fusion zone, the as-solidified fusion zone, and the portion of the fusion zone that had been re-austenitized during subsequent weld passes. The results of these measurements are shown in Table 3. It can be seen that the fine and medium grain-sized

portions of the heat affected zone were slightly softer than the base metal. This may reflect annealing out of residual deformation strengthening left in the ¼-scale liner plate due to low finishing temperature. The coarse-grained portion of the heat affected zone was somewhat harder, presumably due to the higher cooling rates in this area (Ref. 6). The fusion zone was considerably harder than either the base metal or any portion of the heat affected zone.

Conversion of these hardness measurements to ultimate tensile strengths (Ref. 7) indicates that the UTS in the outer portions of the HAZ may be ~5% lower than that of the base metal. This may be sufficient to cause some plastic strain localization in the HAZ, but not the dramatic localization that was observed in conjunction with the liner tears. Based on a simple uniaxial analysis, the UTS in the HAZ would have to be ~23% lower than that of the base metal for complete strain localization to occur, i.e., for the HAZ to reach its ultimate strength before the base metal began to plastically deform.

Tensile tests of welded specimens had been previously conducted by MHI (Ref. 8). These tests included plates that had been welded with different root gaps, plates that had been welded with and without back-up bars, and plates that had been repair welded. No significant property variations were detected with any of these welding parameters. Photographs of these samples indicated that the weld beads and back-up bars had been ground off during tensile sample preparation, leaving uniformly thick gauge sections. Yield and ultimate tensile strengths were statistically equivalent to those of the unwelded material. The most obvious effect of welding was a substantial decrease in elongation (33% for unwelded samples vs. an average of 19% for welded samples). None of the 24 samples failed in the fusion zone. Nearly all of them failed adjacent to (within 6 mm of) the weld, either in the weld heat affected zone or in the nearby base metal. The observed decrease in tensile elongation was, at least in part, due to the fact that the harder fusion zones deformed less than the other portions of the samples. The lateral restraint provided by the harder fusion zones may also have increased deformation resistance in the heat affected zones, further decreasing elongation and masking the slight reductions in UTS expected based on the lower hardnesses found in the outer portions of the heat affected zones.

Three sets of tensile bars were also machined from the MHI practice weld panels and tested at Sandia. These samples were geometrically identical to those tested by MHI, i.e., 25 mm wide x 50 mm gauge length. One set consisted of three unwelded base metal samples. The second set consisted of three welded samples, but with the weld beads and back-up bars left in place (in contrast to the MHI tests where these were ground off). The expectation was that the increased lateral constraint might cause failure adjacent to the welds to occur at lower strains more characteristic of the liner. The third set was similar to the second, but represented regions in which there were significant offsets between the two plates (in excess of the 0.25 x thickness limit allowed by the ASME Boiler and Pressure Vessel Code for full-scale liners (Ref. 1)). These tests were intended to simulate locations in the liner where fit-up difficulties resulted in similarly large offsets, as described previously.

The results of these tests are summarized in Table 4 and compared with previous test results in Table 5. It can be seen that the Sandia results are in general agreement with those of MHI. While slightly higher strengths and slightly lower ductilities were obtained by Sandia for similar conditions, these small differences are not believed to be significant. The lower elongations observed in the welded samples were due, at least in part, to the absence of yielding or plastic deformation in the thicker, harder, and highly constrained fusion zones, as well as the increased resistance to deformation in the adjacent HAZ regions due to the lateral restraint provided by the fusion zones. It was clear, however, that substantial plastic deformation occurred in the base metal, even in samples that failed near the weld. This is consistent with expectations based on the hardness measurements, which suggested that the strength of the HAZ was only ~5% lower than that of the base metal, far less than the ~23% difference that would be required to cause complete plastic strain localization in the HAZ.

The location and nature of failure changed with test condition. One of the well-aligned welded samples failed prematurely along the fusion zone boundary due to a lack-of-fusion defect. The other two failed far from the weld. Apparently the additional lateral restraint provided by the weld bead and back-up bar increased resistance to plastic deformation adjacent to the weld enough that it forced deformation to concentrate far away in the region of reduced lateral restraint.

In the three welded samples where the plates were significantly offset, deformation and subsequent failure occurred adjacent to the weld. Apparently the increased bending stresses associated with the offsets caused deformation to concentrate near the weld, despite the high lateral restraint in this area. The yield strength was slightly lower than in the well-aligned weld samples, but ultimate strength and elongation were not reduced by the weld offset.

Scanning electron microscope characterization of the fracture surfaces showed that all of the samples failed by microvoid coalescence, as is typical of ductile failure following extensive plastic deformation (Figures 42 to 44). There may have been some tendency for the microvoids to be less fully developed in samples with substantial weld offsets (compare Figure 44 with 42 and 43), but not a dramatic one. Even in the sample that failed prematurely due to weld lack-of-fusion defects, the adjacent fracture surface (beyond the defect) exhibited typical microvoid coalescence failure.

Combining the Sandia microhardness data with the MHI and Sandia tensile results, the following conclusions can be reached regarding mechanical behavior of welded tensile samples:

- Under conditions of relatively mild lateral restraint (e.g., the MHI tests where the weld bead and back-up bars were ground off), there is a tendency for deformation, tensile instability, and subsequent fracture to concentrate adjacent to the weld. This is consistent with the slightly lower microhardnesses observed in the weld heat affected zones.

- Under conditions of greater lateral restraint (e.g., the Sandia tests where the weld bead and back-up bars were left on), deformation, tensile instability, and subsequent fracture tend to concentrate distant from the weld away from the region of high lateral restraint.
- Substantial weld offsets result in additional bending stresses that cause deformation and subsequent fracture to again concentrate adjacent to the weld, despite high lateral restraint in this area.
- No cases of dramatic strain localization were observed. In the most extreme cases examined plastic deformation was only mildly concentrated near the weld, i.e., plastic strain localization was far less severe than was observed adjacent to many repaired welds in the liner. Consistent with this, no substantial changes in ultimate strength or overall ductility occurred with variations in lateral constraint or weld alignment.

Applying the combined hardness and tensile information to the liner application suggests that, in situations of uniformly high lateral restraint, such as are characteristic of the liner, plastic deformation would be expected to concentrate slightly, but not severely, in the heat affected zones adjacent to the welds. Tearing would typically occur adjacent to the welds, but only after substantial amounts of plastic deformation had occurred throughout the structure (contrary to the observation that liner tearing occurred following only ~0.4% global strain). The presence of offsets in the welds might cause a modest, but not dramatic, increase in the tendency for strain localization adjacent to the welds.

In summary, the mechanical testing results did not suggest that deficiencies in the properties of either the base metal or weld metal, nor excessive softening in the weld heat affected zones could account for the extensive localized plastic deformation culminating in tearing that appeared to have occurred in the liner.

The Sandia tensile tests also provided an opportunity to determine the effects of geometric and stress state variables on reduction of thickness at the point of fracture. Broken tensile bars corresponding to all three sets of conditions were metallographically mounted, ground, and polished, permitting characterization of deformation-induced reduction in thickness at the failure location (as well as a function of distance from the failure). Micrographs of these cross sections are shown in figures 45 to 48. The sample thicknesses at the points of failure were measured using a calibrated scale internal to the metallograph. These are tabulated in Table 4. The reductions in thickness at the point of failure were found to be remarkably constant, regardless of variations such as proximity to the weld, degree of lateral constraint, or extent of weld offset. The average thickness at the point of fracture was 51% of original thickness, with a standard deviation of only 2.6%. The consistent 49% deformation-induced reduction in thickness proved to be very useful in assessing the amounts of grinding that had been done at the tear locations in the liner, as described in the next section.

Measurements were also made of the amounts of thinning that occurred in the offset welded samples on the opposite sides of the weld from the fracture. While necking occurred only on the sides where failure eventually occurred, the opposite sides were presumably approaching the point of incipient necking and tensile instability. These

samples exhibited an average of 12% maximum reduction in thickness in this region. This is in good agreement with the average observed uniform elongation of 12% to 13% (Table 4). It would be expected, then, that weld regions should plastically thin approximately 12% to 13% prior to the onset of non-uniform deformation. Liner regions that have plastically thinned substantially more than this might reasonably be thought to have begun to neck, hence to be approaching the point at which tearing could occur.

Metallographic Examination of Cross-Sections Through Tears:

Sections surrounding a number of the tears were removed from the liner for more detailed examination. These samples were selected to represent a wide range of the macroscopically observed variations, i.e., tear size, proximity to weld fusion line, proximity to structural features, horizontal welds, and anchors; visually apparent extent of repair welding and associated grinding, and nearby back-up bar geometry. The only unique tears that were not removed were numbers 3, 5-1, and 5-2 around the feedwater penetration. These were deemed too difficult to remove, as well as too difficult to repair in the event of a decision to retest the structure.

Metallographic examination was performed on cross-sections of samples from these regions. The cross-sections were taken near the midpoint of each tear, presumably near where each tear initiated. In cases where grinding was visually apparent near the tear midpoint the cross-sections were taken where the grinding appeared to be most severe. The locations where these cross-sections were taken and the surrounding details are shown in Figures 49 to 63. The samples were mounted, polished, and etched with a combination of 2% nital and Vilella's reagent to reveal the microstructure of the fusion zone, the surrounding heat affected zone, and the base metal.

The fracture surfaces of two samples (#12 and #14-2) were also examined by scanning electron microscopy. These fracture surfaces, shown in Figures 64 and 65, exhibited 100% microvoid coalescence, similar to the ductile fracture surfaces observed on the tensile bars, confirming that liner tearing occurred by ductile fracture in association with localized plastic deformation.

The metallographic results are summarized in Tables 6 and 7. Photographs of selected areas surrounding the tears are also shown in Figures 66-83. However, complete metallographic characterization of the tear regions required observation at various magnifications of regions as far as several centimeters on either side of the tear. It was not practical to include all of this information photographically. Hence, Tables 6 and 7 summarize the most important metallographic observations made surrounding each tear.

All of the welds, with the exception of the weld at tear #1, were found to be sound, and the microstructures of the base metal, heat affected zones, and fusion zones were similar to those seen in the weld test panels, as described previously. Localized plastic deformation was observed in conjunction with all of the tears (except the initiation area of tear #1), similar to what was observed in the tensile samples. Tearing was not found to be associated with any *particular* microconstituent, but occurred in various

microstructural regions, including the recrystallized fusion zones of previous welds, the coarse and fine-grained regions of weld heat affected zones, and the base metal.

Estimates of the amounts of grinding associated with each tear were obtained based on the previously described knowledge that $\sim 49\%$ reduction in thickness occurs due to plastic deformation prior to fracture. The method used is illustrated in Figure 84. The liner thickness at each tear location was measured using a calibrated scale internal to the metallograph. This tear thickness was then divided by 0.51 to obtain the local pre-deformation thickness at/near each tear location. This pre-deformation thickness was subtracted from the initial liner thickness to determine the amount of material removed by prior grinding. Finally, the amount of material removed by grinding was divided by initial liner thickness to determine the percentage of grinding-related thickness reduction associated with each tear initiation site. These results are given in Tables 6 and 7. These percentages of original liner thickness removed by grinding are estimated to be accurate to $\pm 5\%$ absolute, i.e., 40% grinding implies 35% to 45%.

Two additional methods were used to confirm these estimates in selected cases, as illustrated in Figure 84. The amounts of grinding deduced from these two additional methods are also included in Tables 6 and 7.

First, in a number of samples where tearing occurred very close to the weld fusion line, the liner thickness immediately next to the thick undeformed weld bead provided a reasonable estimate of the original post-grinding thickness at the (nearby) tear site. Grinding reductions obtained by this method are also estimated to be accurate to $\pm 5\%$ absolute. Consistent with this, no discrepancies greater than 10% were found between the estimates obtained by this method and the primary method, described in the previous paragraph.

Second, in some samples banding (a manifestation of chemical segregation patterns in the original ingot which have been elongated by the plate rolling process) was continuously or semi-continuously apparent from near the tear location back into the unground base metal. These bands are always parallel to the free surfaces of the rolled plates. Hence, locations where the edges of the cross-sectioned samples were at slight angles to these bands represented regions where the liner surfaces had been tapered by grinding. By following the bands from the tear location back into the unground base metal it was possible to estimate the amount of material that had been ground off of each side of the plate. This method was judged to be less accurate than the previous two methods because of the inherent imprecision in following bands over what was frequently a substantial distance from the tear to the unground portion of the plate. As a result, estimates obtained by this method were judged to be accurate to only $\pm 10\%$. Consistent with this, larger discrepancies were found between the estimates obtained by this method and those obtained by the previous two methods. However, with the exception of tear #9, no discrepancies in excess of 15% were observed.

Examination of Tables 6 and 7 reveals that the estimated amounts of grinding obtained by all three methods are in reasonable agreement. Furthermore, it can be seen that, with the

possible exception of tear #12, at least 25% of the original liner thickness had been ground off in all locations where the tears initiated. This provides a strong indication that liner thinning due to grinding predisposed severely ground areas surrounding repair welds to plastic strain localization and tearing during testing of the model.

Descriptions of Specific Free-Field Tears:

Tear #1: Tear #1 was distinct from all other tears in that it initiated at a weld defect. Tear #1 is described in Tables 1 and 6, and pictured in Figures 2, 19, 49, 66 and 67. At its midpoint (presumably the initiation site), the tear was oriented at 90 degrees to the primary tensile stress and there was no microstructural indication of plastic deformation having preceded fracture (Figure 66). Detailed examination of the fracture profile in the initiation region revealed that the surface was covered with a foreign substance, perhaps residue from the primer paint (too dark to be seen in Figure 66) – this indicated that welding had failed to completely melt and join the adjacent pieces in this area. The microstructure on opposite sides of the tear were distinctly different: recrystallized fusion zone from the original weld on the repair weld side, and unaltered heat affected zone from the original weld on the opposite side. No effort was made to remove the surface residue to permit SEM examination of the underlying surface. It seems clear, however, that this represented a weld defect, likely a lack-of-fusion defect similar to the one seen in one of the welded tensile bars. Assuming that no plastic deformation occurred adjacent to this defect, the measured thickness indicated that 22% of the liner thickness had been ground off in this area.

As a check, an additional cross-section was polished ~2 cm down the tear from the initiation site, at a location removed from the weld defect (the opposite edge of the cross-section sample, shown in Figure 49). This cross-section is shown in Figure 67. The tear appeared quite different in this location: a predominantly 45 degree shear failure accompanied by substantial local plastic deformation. This clearly represents a region where the tear had propagated into sound metal after having been initiated at the nearby weld defect. The amount of grinding estimated from the deformation-reduced thickness at the tear in this location was ~20%, in excellent agreement with the 22% measured in the undeformed area adjacent to the weld defect.

Tears #2-1, 2-2, 2-3: These tears are described in Tables 1 and 6, and pictured in Figures 3, 20, 50, 51, 52, 68, 69 and 70. They occurred along a vertical field weld that had undergone numerous overlapping repairs. The repeated repair welding resulted in a band as wide as 3 cm consisting largely of weld metal, much of which had been re-austenitized and recrystallized from the heat associated with subsequent welds. Extensive grinding was visually apparent over a broad area on either side of the tears (Figures 20, 50, 51 and 52). Immediately adjacent to tear #2-1 a small section of plate remained attached to the massive weld bead (Figure 68), permitting direct measurement of the residual thickness after grinding, as illustrated in Figure 84. Sufficiently continuous banding was apparent in #2-2 and #2-3 to permit grinding reduction to be estimated from the tapering of the ground surface with respect to these bands. In all three cases the amounts of grinding inferred by the three different methods were in reasonable agreement with one another,

thus confirming the validity of the primary method based on reduced thickness at the tear location. Grinding had reduced the thickness by 45% or more in the regions where each of these tears occurred, enough to cause complete plastic strain localization culminating in ductile tearing when the structure was tested.

Another distinguishing characteristic of this weld was the large number of short segments of back-up bar resulting from repetitive repair of this joint (Figures 3, 50 and 51). In addition to being short, three different cross-sections of back-up bar were used. These included sections of 3 mm x 13 mm, 3 mm x 19 mm, and 6 mm x 25 mm. Metallographic and hardness measurements on various portions of back-up bar showed ferrite and pearlite microstructures ranging from R_B 62 to R_B 70. It was not clear whether these back-up bar variations contributed significantly to tearing in this area or others.

Tears #4-1 and 4-3: These tears are described in Tables 1 and 6, and pictured in Figures 4, 21, 53, 54, 71 and 72. The joint along which these tears formed was somewhat unusual in that no back-up bar was present (either the weld had been made with no back-up bar, or the back-up bar was later completely ground off). This joint was otherwise similar to #2, i.e., one where numerous overlapping repairs had been made, resulting in a band as wide as 5 cm consisting largely of weld metal, much of which had been re-austenitized and recrystallized. Other than the unusual number of overlapping repair welds, the metallography revealed no distinguishing features associated with the tears. As with tear #2, grinding had reduced the liner thickness by approximately 45% in the regions where each of these tears occurred, enough to cause complete plastic strain localization and ductile tearing when the structure was tested.

In addition, a parallel repair weld approximately 25 mm in from the primary weld near tear #4-3 clearly represented an area in which the liner had been inadvertently breached as repair-associated grinding was being done, and had itself been repair welded. The appearance of this and other similar areas in which liner “grind-through’s” had been repair welded confirmed that grinding done in conjunction with repair welding had, in some areas, removed substantial portions of the adjacent liner, resulting in extensive liner thinning and, in some areas, liner penetration requiring additional repair.

Tear #6-2: This tear was examined as a proxy for four tears, 6-1, 6-2, 11-1, and 11-2, which all occurred along the left-hand side of the same vertical field weld. They are described in Tables 1 and 6, and pictured in Figures 5, 6, 22, 23, 24, 55 and 73. While ultrasonic thickness measurements failed to detect a great deal of thinning adjacent to this tear, far greater thinning was observed below the end of the tear (Figure 23). The metallographic cross-section showed that highly localized grinding had been done on the exterior side adjacent to the edge of the back-up bar. This resulted in a narrow band of thinned material immediately next to the back-up bar, consistent with the ultrasonic measurements. The other distinguishing aspect of these tears was the unusually large number of short back-up bar segments along this weld (Figures 5 and 6). While metallography indicated a single repair weld in sample #6-2, the number of back-up bar segments attests that numerous/repeated repairs had been made at various heights along this joint. It is not clear whether the large number of short back-up bar segments

contributed to tearing. However, approximately 33% of the original liner thickness had been ground off in this region, enough to cause complete plastic strain localization and ductile tearing when the structure was tested.

Tear #8-1: This tear is described in Tables 1 and 6, and pictured in Figures 7, 25, 56 and 78. It represented a tear that occurred in an area where a segment of back-up bar had been left missing during repair welding. This may have exacerbated strain localization in this region, but the estimated 30% grinding reduction of liner thickness observed in this area was, by itself, likely sufficient to cause severe plastic strain localization and subsequent ductile tearing.

Tear #8-2: Tear #8-2 is described in Table 1 and 6, and pictured in Figures 26, 57 and 75. It was unique in that it occurred relatively distant from the weld in an area where macroscopic examination revealed evidence of substantial grinding (Figure 26), but no apparent repair weld. Metallographic examination revealed, however, that at least two repair welds had been made adjacent to the vertical joint, apparently to repair an inadvertent “grind-through” made in association with repairs on the main weld. Following repair of this “grind-through”, the weld bead of this repair had been ground off from both front and back sides, leaving no obvious evidence of this defect having been made or repaired. However, this grinding reduced the wall thickness in the repaired “grind-through” area by approximately 60%, resulting in severe localization of plastic deformation culminating in ductile tearing when the structure was tested.

Tear #9: This tear is described in Tables 1 and 6, and pictured in Figures 8, 27, 58 and 76. It represented a typical repair welded joint far from either anchors or horizontal stiffeners. In other respects it was similar to tear #6-2, one where a narrow band of thinning resulted from heavy grinding adjacent to the back-up bar, and where numerous back-up segments indicated a series of repairs at various heights along a vertical field weld. Metallographic examination revealed no unusual microstructural features. While this sample showed the greatest discrepancy in percent grinding estimated by different methods, all methods indicated that sufficient grinding had been done to cause substantial strain localization and ductile tearing when the structure was tested. Approximately 40 to 45% thinning appears to have been done by grinding based on two of the three estimation methods.

Tear #10: This tear is described in Table 1 and pictured in Figures 9 and 28. No metallographic sample was taken in this region because this tear was similar in most respects to #8-1.

Tears #14-1 and 14-2: These tears are described in Table 1 and pictured in Figures 10 and 29. No metallographic samples were taken in this region because these tears were similar in many respects to #8-1. SEM fractography showed that tearing occurred by microvoid coalescence (Figure 65).

Tear #16: This tear is described in Table 1 and pictured in Figures 11 and 30. It formed distant from the vertical field weld in an area where no grinding or repair of this weld were macroscopically apparent. Back-side photographs, however, showed a missing

segment of back-up bar in a *horizontal* field weld, apparently where a repair had been made in *this* weld (Figure 11). This missing segment of horizontal back-up bar reduced the circumferential stiffness in this area, providing for plastic strain localization and tearing. Comparison of front and back-side photographs (Figure 11) indicated that the tear began at the termination of the horizontal back-up bar, then propagated down through the “rat-hole” in the horizontal stiffener, and along the vertical field weld. The cause of this tear was macroscopically apparent, so no metallography was done on it.

Tear #17: This tear is described in Tables 1 and 6, and pictured in Figures 12, 31, 59, 77 and 78. It represented one that occurred along a relatively isolated single repair weld. As was the case with several vertical welds in the vicinity of the feedwater and main steam penetrations, the original weld appeared to have been made without any back-up bar (or the back-up bar was subsequently ground off). Macroscopic observation suggested that the repair had been made by grinding off the weld bead on the back side, then making a repair weld on the front side (the inside of the liner). The metallographic cross section revealed a much more complex sequence of grinding and repair welding. While the specific order of events could not be deduced, it was clear that multiple side-by-side repair welds had been made in this region. Substantial grinding had been done on both the inside and outside of the liner in association with these repairs. The net result was that the portion of the liner adjacent to the final repair weld was thinned more than 70%. Failure occurred in this thinned region due to plastic strain localization culminating in ductile tearing.

Descriptions of Specific Feature-Associated Tears:

Tears #3 and 5-1: These tears are described in Table 2 and pictured in Figures 13 and 14. They occurred along opposite ends of the feedwater penetration transition weld, i.e., in areas that were mirror images of one another. No metallographic samples were taken from these regions because their locations made removal difficult and because repair would be difficult in the event a decision was made to retest the structure. The fact that tear #3 was substantially larger than tear #5-1 may have resulted from more extensive grinding and weld repair on this end of the transition. On the other hand, it could also have been exacerbated by a difference in horizontal stiffener terminations revealed by the back-side photographs. At #3 the horizontal stiffener ends very close to the transition weld (within 1 cm – see Figure 13), creating a very limited length of low stiffness, hence a region of potentially very high strain localization. At #5-1 the horizontal stiffener ends much farther from the transition weld (~10 cm – see Figure 14), thus providing a longer length of low stiffness over which the local strain could distribute, (i.e., lower strain localization).

Tear #5-2: This tear occurred along a vertical weld slightly above #5-1. No metallographic samples were taken for the same reasons mentioned above. However, the back-side photographs (Figures 13 and 14) revealed a significant difference between the region in which tear #5-2 occurred and the corresponding mirror image region at the opposite end of the feedwater penetration transition. At one end there was a vertical weld in the high strain region between the nearest concrete anchor and the stiff feedwater

transition – tear #5-2 formed along this weld. At the opposite end, no vertical weld was present in the corresponding high strain region and no tearing occurred.

Tears #7 and 15: These tears occurred near the lower and upper corners of the equipment hatch transition joint, respectively. They are described in Tables 2 and 7, and pictured in Figures 15, 16, 32, 33, 60, 61, 79, 80 and 81. Acoustic monitoring suggested that initial tearing occurred in the vicinity of this transition joint. While this transition represented a region where complex stresses and high local strains were expected, liner thinning resulting from grinding done in association with repair welding was also substantial in the areas of these tears: 25% to 30% at tear #7 and ~ 50% at tear #15. This thinning undoubtedly exacerbated plastic strain localization and tearing in these areas, however, it is likely that high strains at this transition also contributed to tearing. No unusual microstructural features were observed in the vicinities of these tears.

Tears #12 and 13: These tears also occurred along the equipment hatch transition joint, but near its midpoint, rather than the corners. They are described in Tables 2 and 7, and pictured in Figures 17, 18, 34, 35, 62, 63, 64, 82 and 83. Both formed near horizontal field welds and the associated “rat-hole” discontinuities in horizontal stiffeners, although back-side photographs indicated that patches were welded in between the adjoining stiffener segments, minimizing strain localization in these regions (unless the welds at the ends of these patches failed). Evidence of ~30% thinning from grinding was found at tear #13.

The extent of thinning from grinding was much less clear in the vicinity of tear #12. Little evidence of grinding or weld repair was macroscopically apparent on either the front or back side. Consistent with this, ultrasonic thickness measurements indicated ~22% thinning approximately 5 mm adjacent to this tear (Figure 34), only slightly greater than the amount expected based on cross-sections of the tensile samples (Figures 45 to 48). Consistent with this, metallographic observation of the portion on the side of the tear where the ultrasonic measurements had been made indicated only a small amount of grinding, ~10%. However, the opposite side (adjacent to the weld fusion zone) showed a different and thinner section at the tear location, suggesting ~27% reduction by grinding. Microstructural observation of the weld failed to unequivocally reveal whether a repair weld had been made in this area. The fusion zone was wider (~8 mm) than most initial welds, suggesting that a repair had been made. But no evidence remained of the previous weld – perhaps the initial fusion zone had been completely ground out prior to repair or the repair weld had completely consumed it – this was observed in several other areas where it was macroscopically apparent that repair welds *had been* made. Tear #12 may be the one most likely to represent a “true structural effect”, i.e., to not have resulted from excessive grinding, backing bar abnormalities, or weld defects. However, there is a substantial degree of uncertainty regarding the amount of thinning from grinding in the vicinity of this tear.

Metallographic Examination of Cross-Sections Through Welds Where Substantial Plastic Deformation But No Tearing Occurred:

In addition to the tear regions, metallographic cross-sections were also taken from several regions where there was evidence of substantial localized plastic deformation, but where no tearing had occurred. Samples 18-1 and 18-2 were across a vertical field weld that exhibited substantial buckling and “orange peel” evidence of localized plasticity. This weld was in the region between the equipment hatch transition and the air lock, where the largest amounts of buckling and tearing were observed. It had been initially made and subsequently repaired from the front side (inside of the liner), but no back-up bar had apparently been used in making either the initial or repair weld. 18-2 contained a single isolated repair weld and a modest amount of associated grinding, while 18-1 was a nearby region with no apparent grinding or repair weld. Samples 24-1 and 24-2 represented a region with no apparent grinding or repair welds, but where the highest liner strains were recorded by strain gauges during the test (~7% strain). This weld was near the edge of a buttress, where substantial buckling was observed. 24-2 was taken near the intersection of horizontal and vertical field welds within a “rat-hole” region in a horizontal stiffener. 24-1 was along the same vertical field weld, but above the horizontal weld and stiffener. The locations where these samples were taken and surrounding details are shown in Figures 85 to 88. Metallographic observations made on these samples are shown in Figures 89 to 92 and summarized in Table 8.

Region #18-1 and 18-2: The observations made in these areas are described in Table 8 and pictured in Figures 36, 85, 86, 89 and 90. The cross-section of #18-1 (Figure 89) showed that a modest amount of localized plastic deformation had occurred adjacent to the weld on both sides of the fusion zone. The greatest amount of deformation thinning occurred in the HAZ near the fusion line (13% on one side, 9% on the other side – note that these amounts of thinning are consistent with the ultrasonic thickness measurements, shown in Figure 36). Approximately 5% thinning was uniformly observed over a ~15 mm wide band in the adjacent base metal. Thinning then tapered out gradually to zero over the next ~15 mm. The amount of thinning in the HAZ is in the vicinity of the 12% to 13% required for the onset of necking, as was determined from analysis of the welded tensile samples. However, considerable additional local deformation would be required before tearing would be expected to occur. Consistent with this, no evidence of void formation or shear banding, which would be indicative of incipient failure, was observed.

The cross-section of #18-2 revealed substantially more thinning, 42% on one side of the weld and 31% on the other side (Figure 90). However, it was clear that a substantial, but not quantifiable, amount of this thinning was due to prior grinding, rather than simply to plastic deformation during testing. While considerably higher levels of localized plastic deformation would be expected in these previously ground areas, no evidence of substantial necking or incipient tearing was apparent. This suggests that, while necking may *begin* after only 12% to 13% local thinning, considerably more localized deformation must be accommodated prior to the onset of tearing.

Regions #24-1 and 24-2: These regions are described in Table 8 and pictured in Figures 87, 88, 91 and 92. Sample #24-2 was taken in the “rat-hole” region immediately between the ends of the bridged horizontal stiffeners. This sample was sharply bent, attesting to the complexity of the stresses in this region. The sample exhibited a maximum of at least 20% thickness reduction on one side of the weld and ~14% thickness reduction on the opposite side of the weld (Figure 91). Presumably, the strain gauge in this area recorded only 7% strain because it was not co-located with the point of peak local strain. Thicknesses change rapidly with position in this region, implying much lower strains within several millimeters of the point of maximum thickness reduction.

Significant depressions were present on both inner and outer surfaces at the point of minimum thickness. It is likely that these represented the early stages of necking; this would be expected based on the fact that thinning clearly exceeded the 12% to 13% required for the onset of necking. Precise measurement of maximum reduction was compromised by a very irregular surface and large non-metallic particles at the base of one of these depressions – this may represent a surface defect in the plate. The maximum reductions in thickness were observed in the weld heat affected zones, then tapered out with increasing distance into the base metal. As in regions 18-1 and 18-2, however, there was no evidence of void formation or shear banding, which would be indicative of incipient tearing. This supports the previous contention that considerably more localized deformation must occur following the onset of necking before localized deformation culminates in tearing.

Sample #24-1, taken some distance away from the horizontal stiffeners, exhibited 6% and 5% maximum thickness reduction of opposite sides of the weld. These maximum reductions occurred in the HAZs, and tapered to zero over approximately 10 mm in the adjacent base metal.

The fact that peak strain in #24-2 was several times that in nearby #24-1 may indicate that much more complex stresses and considerably higher local strains can occur in the “rat-hole” regions associated with horizontal stiffeners. While no general tendency was observed for tears to form in these regions, it is possible that in a limited number of cases, the patches that bridged between stiffeners on opposite sides of the vertical field welds failed. This would most likely occur by failure of one of the welds joining the patch to the adjacent stiffeners. Such failures would dramatically decrease stiffness in the “rat-hole” region, thus causing severe strain localization. It may be possible that this is what occurred in the region of #24-2. It may also be possible that this also occurred near tear #12, which was also in a “rat-hole” region. This may help explain why tear #12 occurred in a region where little or no weld repair or grinding had been done. Unfortunately, the “rat-hole” patches and associated welds were buried in the concrete, so this possibility could neither be confirmed nor refuted.

In summary, it is clear that localized plastic deformation also occurred in the heat affected zones adjacent to some welds that had not been repaired or ground, particularly those in regions of high local or global strain. While these amounts of localized plasticity were considerably lower than those associated with tearing, the necking threshold was

likely exceeded in the most severe cases. No evidence of incipient tearing was observed in these areas, however, and it appears that a substantial amount of additional local deformation must occur following the onset of necking before this culminates in tearing.

Conclusions:

- Nearly all of the tears occurred in areas where the liner thickness had been reduced ~25% or more by grinding done in association with repair welding. Extensive localized plastic deformation culminating in ductile tearing occurred in these thinned areas as the structure was being tested. This appears to have been the most prevalent cause of liner failure.
- Geometric features may also have contributed to the formation of some tears. These include structural transitions, such as those at the feedwater penetration and the equipment hatch transition boundaries, discontinuities in horizontal stiffeners, and discontinuities in weld back-up bars. A missing segment in a horizontal back-up bar appears to have been primarily responsible for one tear (#16).
- Only one tear occurred in association with a material or weld defect: a lack-of fusion weld defect was found at the initiation site of tear #1.
- The specially produced quarter-scale liner material exhibited mechanical properties that may have made it particularly prone to plastic strain localization and tearing. While nearly conforming to the specifications for full-thickness material, the quarter-thickness plate exhibited a yield strength much higher than the specified minimum (383 MPa compared with 225 MPa) and an unusually high yield to ultimate strength ratio (0.77). This high YS/UTS ratio is qualitatively consistent with extensive localized plastic strain culminating in ductile tearing occurring in regions where more than ~25% of the liner thickness had been ground off, as was observed near most of the tears.
- Tensile and hardness tests on welded test samples indicated that modest amounts of plastic strain localization should be expected in the weld heat affected zones, but to a much lesser extent than was observed in association with the liner tears. Consistent with this, smaller but significant amounts of localized plastic strain were observed adjacent to some welds that had not been repaired or ground. These strains were sufficient to initiate necking in the most severely strained regions. However, with the possible exception of tear #12, there was no indication that tearing was imminent in regions other than those where repair welding and substantial grinding had been done.

Acknowledgements: Several others contributed to this effort. We appreciate the assistance of Garry Bryant and Carlos Velasquez with metallography, Tom Crenshaw with tensile testing, and Gary Zender with SEM fractography.

References:

1. 1998 ASME Boiler and Pressure Vessel Code, Code for Concrete Reactor Vessels and Containments, Table CC-4523-1, Maximum Allowable Offsets In Final Welded Joints, p. 103.

2. 1998 ASME Boiler and Pressure Vessel Code, Code for Concrete Reactor Vessels and Containments, Section CC-4542, Specifically CC-4542.2, p. 108.
3. 1998 ASME Boiler and Pressure Vessel Code, Code for Concrete Reactor Vessels and Containments, Section CC-4542.5, Specifically CC-4542.2, p. 116.
4. Japanese Industrial Standard JIS G 3118, Carbon Steel Plates for Pressure Vessels for Intermediate and Moderate Temperature Service, 1987.
5. ASM Handbook, 10th Edition, Volume 1, Properties and Selection of Irons, Steels, and High-Performance Alloys, 1990, p. 230.
6. Metals Handbook, 8th Edition, Volume 1, Properties and selection of Metals, 1961, p. 1235.
7. ASM Metals Handbook Desk Edition, 1998, p. 73.
8. Welded Joint Tensile Test Results of PCCV Liner Welding Re-confirmation Test, MH-K9-43.

Tables

Table 1. Macroscopic Descriptions of Free Field Tears

<u>Tear No.</u>	<u>Tear Length (cm)</u>	<u>Distance From Fusion Line (mm) *</u>	<u>Distance From Horizontal Weld (cm) #</u>	<u>Distance From Concrete Anchor (cm) # **</u>	<u>Visually Apparent Extent of Repair Welding ##</u>	<u>Visually Apparent Extent of Grinding ##</u>	<u>Back-up Bar Description In Repair Area</u>
1	4	0	Midway	8 (46)	Single isolated repair	Moderate	Several long patched segments
2-1	8	*	Midway	37 (46)	Extensive & wide	Extensive	Several patches of various sizes
2-2	8	*	Midway	37 (46)	Extensive & wide	Extensive	Many patches of various sizes
2-3	18	*	6	37 (46)	Extensive & wide	Extensive	Long patched segment
4-1	11	* (both sides, crosses final weld)	Midway	Midway (15)	Extensive & wide	Extensive	No back-up bar on original or repair welds
4-2	4	*	Midway	Midway (15)	Extensive & wide	Extensive	No back-up bar on original or repair welds
4-3	14	*	5	Midway (15)	Extensive & wide (Separate repair to side of main weld – repair of “grind-thru”	Extensive	No back-up bar on original or repair welds

L-23

6-1	10	2 to 3	0 (Crosses shop weld without back-up bar)	38 (46)	Moderate to Extensive	Moderate to Extensive	Several patches of various sizes
6-2	7	2 to 3	Midway	38 (46)	Extensive	Extensive	Numerous short patched segments
8-1	6	0 to 1	Midway	Midway (46)	Moderate	Moderate	Segment missing in tear region
8-2	4	10	Midway	Midway (46)	None apparent	Extensive	Long (apparently original) segment
9	13	0 to 5	Midway	Midway (46)	Extensive	Extensive	Several patches of various sizes
10	1-1/2	0 to 1	Midway	8 (46)	Extensive	Extensive	Segment missing in tear region
11-1	10	2 to 3	8	38 (46)	Extensive	Extensive	Many patches of various sizes
11-2	6	2 to 3	0 (Begins at shop weld without back-up bar)	38 (46)	Extensive	Extensive	Many patches of various sizes
14-1	8	0 to 3	0 (Begins at field weld w/missing segment of back-up bar)	Midway (46)	Extensive	Extensive	Segments in both vertical & horizontal back-up bars missing in tear region
14-2	13	0 to 3	8	Midway (46)	Extensive	Extensive	Segment missing in tear region

16	8	13 to 25	0 (Crosses field weld w/missing segment of back-up bar)	38 (46)	No repair evident in vertical weld, but repair in horizontal weld	Little or none apparent	Weld repair in horizontal weld left ~4 cm segment of back-up bar missing
17	3	0	Midway	Midway (15)	Single isolated front-side repair to original weld made on back-side	Extensive	No back-up bar on original or repair welds

* Tears #2 and #4 occurred where numerous overlapping repair welds had been made, resulting in a wide band of weld metal.

“Midway” implies that tear was distant from horizontal welds and/or anchors, not that centerline of tear was quantitatively equidistant from adjacent features.

** Number in parentheses indicates spacing of anchors in region of tear (in cm)

Qualitative extent of repair welding or grinding based on *visual observation*. Subsequent more detailed examination of metallographic cross-sections showed that these visual estimates were sometimes misleading.

Table 2. Macroscopic Descriptions of Feature-Associated Tears

<u>Tear No.</u>	<u>Tear Description</u>	<u>Apparent Extent of Grinding & Weld Repair *</u>	<u>Structural Features With Potential for Causing Strain Localization</u>
3	>15 cm long tear ~3 mm from fusion line of transition weld of liner to feedwater penetration	Fairly extensive weld repair & grinding in this area	Horizontal stiffener ends very close to transition weld, creating high potential for strain localization in region where tear occurred (compare with less severe mirror image, tear #5-1).
5-1	~4 cm long tear ~6 mm from fusion line of transition weld of liner to feedwater penetration (mirror image of region near tear #3)	Little or no evidence of weld repair or grinding in this area	Similar to, but less severe than situation at tear #3 – horizontal stiffener ends ~10 cm from transition weld, providing a less severe potential for strain localization.
5-2	~8 cm long tear along vertical field weld above tear #5-1	Appears to be front-side repair to original back-side weld in this area (perhaps similar to nearby tear #17)	Vertical field weld between concrete anchor and feedwater transition creates potential for high strain in welded region. No comparable weld is present in the mirror image high strain location, where no tearing occurred.
7	~23 cm long tear along vertical weld near lower corner of equipment hatch transition	Extensive weld repair & grinding in this area	Several horizontal stiffeners end discontinuously in this region, creating high potential for strain localization.
12	~5 cm long tear along vertical weld between liner and equipment hatch transition. Tear crosses horizontal shop weld between “rat-hole” regions in two horizontal stiffeners	Little or no repair welding or grinding apparent in this area	“Rat-hole” region of horizontal stiffeners could cause strain localization if patch-weld failed

13	~9 cm long tear similar to #12, but at near next higher horizontal field weld. Tear midpoint near “rat-hole” region in horizontal stiffener	Extensive grinding and ~10 cm long weld repair in region of tear	“Rat-hole” region of horizontal stiffeners could cause strain localization if patch-weld failed
15	~10 cm long tear along vertical weld near upper corner of equipment hatch transition (similar to #7 at lower corner)	Moderate to extensive grinding and weld repair. Plates appear to have been poorly aligned in this area, creating substantial weld offset.	Two horizontal stiffeners end discontinuously in this area, creating high potential for strain localization.

* *Qualitative* extent of repair welding or grinding based on *visual observation*. Subsequent more detailed examination of metallographic cross-sections showed that these visual estimates were sometimes misleading.

Table 3. Microhardnesses of Zones Surrounding Welds

<u>Zone</u>	<u>Avg. Hardness *</u>	<u>Std. Dev.</u>	<u>UTS (ksi) **</u>	<u>UTS (MPa) **</u>
Base metal	160	6.9	74.5	515
Fine-grained HAZ	151	4.3	71	490
Med-grained HAZ	154	3.4	72	495
Coarse HAZ	164	6.8	76.5	525
Fusion Zone	180	11.4	84	580
Recrystallized fusion zone	173	5.9	80.5	550

* Vickers hardness, 100 gram load

** UTS estimates from Ref. 6. Note that UTS estimates are based on conversion tables for hardness tests made with much heavier loads. As a result, the estimated UTS values should be taken only as approximations; they are useful primarily for comparing the expected *relative* strengths of the various regions, not the *absolute* strengths. For example, the 515 MPa estimated base metal strength is slightly higher than the 498 MPa value measured via tensile tests. The implication regarding the fine and medium grained portions of the HAZ are that their ultimate strengths are expected to be 20 to 25 MPa lower than the base metal. Similarly, the most important implications regarding the ultimate strengths of the virgin and recrystallized fusion zones are that they should be approximately 65 and 35 MPa higher than the base metal, respectively.

Table 4. Results of Tensile Tests Conducted at Sandia

<u>Sample</u>	<u>YS (MPa)</u>	<u>UTS (MPa)</u>	<u>Uniform Elong (%)</u>	<u>Total Elong (%)</u>	<u>Thickness at Fracture (% of original)**</u>
Unwelded					
A1	395	520	15.8	31.3	-
A2	376	512	16.4	30.6	-
A3	418	530	15.7	31.1	48
Welded, No Offset					
B1	409	528	12.2	16.6 *	-
B2	407	497 #	6.2 #	6.6 #	55
B3	403	515	10.6	15.8 *	-
Welded, >25% Offset					
C1	375	520	12.8	16.3	52
C2	350	519	12.7	16.3	50
C3	371	518	12.9	17.2	-

* Failed at or near extensometer knife edge: total elongation reported is artificially low

Failed at apparent weld lack-of-fusion defect

** Average thickness at fracture location for all samples was 51% of original thickness; standard deviation was only 2.6% of original thickness regardless of substantial variations in samples and stress conditions (welded vs. unwelded, amount of lateral constraint, degree of weld offset). The 51% value was later used in conjunction with the thickness measured at each of the liner tears to determine the local liner thicknesses prior to tearing, and from this, the local amounts of liner material that had previously been removed by grinding.

Table 5. Summary of Tensile Properties of Material from Practice Weld Panels

<u>Description</u>	<u>Yield Strength (MPa)</u>	<u>Ultimate Strength (MPa)</u>	<u>Uniform Elongation (%)</u>	<u>Total Elongation (%)</u>
JIS Specification	225 (min)	410 to 490	-	21.0 (min)
Unwelded (MHI)	383	498	-	33.0
Welded (MHI)	379	505	-	18.8
Unwelded (SNL)	396	520	16.0	31.0
Welded – Plates Well Aligned (SNL)	406	521	11.5*	>16.0*
Welded – 36% to 70% Weld Offset (SNL)	365	518	12.8	16.6

* One sample failed prematurely at fusion line due to lack-of-fusion defect – 6.2% uniform elongation, 6.6% total elongation. Other two samples failed at extensometer knife edge distant from weld. Properties represent average of these two samples. Total elongation somewhat greater than measured with extensometer as part of necked regions were outside extensometer.

Table 6. Metallographic Descriptions of Free Field Tears

<u>Tear No.</u>	<u>Weld Description</u>	<u>Tear Description</u>	<u>% Grinding Estimated from Thickness At Tear</u>	<u>% Grinding Estimated from Thickness At Weld</u>	<u>% Grinding Estimated From Banding</u>
1	Single repair weld overlapping original weld	Initiated at lack of fusion defect, no evidence of plastic deformation at initiation site. Shear failure with localized deformation in second sample taken beyond weld defect	20%	22%	
2-1	Multiple overlapping repair welds, 16 mm total width	Shear failure with localized deformation in medium to coarse grained HAZ	61%	57%	
2-2	Multiple overlapping repair welds, 29 mm total width	Shear failure with localized deformation in partially recrystallized fusion zone	46%		45%
2-3	Multiple overlapping repair welds, 21 mm total width	Shear failure with localized deformation in fully recrystallized fusion zone	64%		50%
4-1	Multiple overlapping repair welds, 51 mm total width	Shear & tensile or bending failure with localized deformation in region containing both recrystallized and unrecrystallized fusion zone and coarse grained HAZ	46%		
4-3	Two major welds, one ~25 mm from vertical joint – apparently repair of a “grind-thru” in liner wall	Shear failure with localized deformation in coarse-grained HAZ	44%		

6-2	Single repair weld; original weld ground out prior to repair or completely remelted during repair	Shear failure with localized deformation in medium grained HAZ	33%		
8-1	Single repair weld overlapping original weld	Shear & tensile or bending failure with localized deformation in partially recrystallized HAZ	30%		
8-2	Several welds, including one ~13 mm from vertical joint – apparently repair of a “grind-thru” in liner wall	Shear failure with localized deformation mostly in recrystallized fusion zone	61%		
9	Single repair weld; original weld ground out prior to repair or completely remelted during repair	Shear failure with localized deformation in medium grained HAZ	42%	44%	27%
17	Multiple welds, one ~15 mm from vertical joint – apparently repair of a “grind-thru” in liner wall	Shear failure with localized deformation through recrystallized fusion zone	74%	82%	

Table 7. Metallographic Descriptions of Feature-Associated Tears

<u>Tear No.</u>	<u>Weld Description</u>	<u>Tear Description</u>	<u>% Grinding Estimated from Thickness At Tear</u>	<u>% Grinding Estimated from Thickness At Weld</u>	<u>% Grinding Estimated From Banding</u>
7	Two or more repair welds overlapping original weld	Shear & tensile or bending failure in medium grained HAZ, likely a combination of tensile & bending stresses	30%		25%
12	Possibility of single repair weld; if so, original weld ground out prior to repair or completely remelted during repair. Definite evidence of grinding on both surfaces, but grinding does not appear deep	Shear failure with localized deformation in base metal	10% to 27%*		10%*
13	Single repair weld; original weld ground out prior to repair or completely remelted during repair	Shear failure with localized deformation in medium to coarse grained HAZ	31%		33%
15	Single repair weld overlapping original weld	Shear failure with localized deformation in coarse grained HAZ	54%		50%

* The smaller estimates were based on examination of liner on opposite side of tear from weld. The larger estimate was based on the portion adjacent to the weld where thickness at the point of tearing was smaller.

Table 8. Metallographic Descriptions of Joints with No Tears

<u>Sample Number</u>	<u>Joint Description</u>	<u>Localized Strain / Thinning</u>
18-1	No repair weld, little or no evidence of grinding	13% maximum reduction in thickness. Minimum thickness in coarse-grained HAZ, gradual increase to full thickness over ~30 mm
18-2	Single repair weld; original weld ground out prior to repair or consumed by repair. Some grinding prior to & following repair welding, but extent of grinding appears less than in most joints with tears	Deformation localized in heat affected zones, but cannot be quantified due to unknown amount of prior grinding
24-1	No repair weld or evidence of grinding	6% maximum reduction in thickness. Minimum thickness in HAZ, gradual increase to full thickness over ~15 mm
24-2	No repair weld, little or no evidence of grinding	~ 20% maximum reduction in thickness. Minimum thickness in HAZ*

* Local depressions were observed on both interior and exterior surfaces in the thinnest region. These may represent early stages of necking. Large non-metallic particles and very irregular surface features in one depression likely represent a surface defect in the plate. The ~20% thickness reduction discounts these embedded particles and very local pits on the one surface, but includes the more general depressions.

Figures

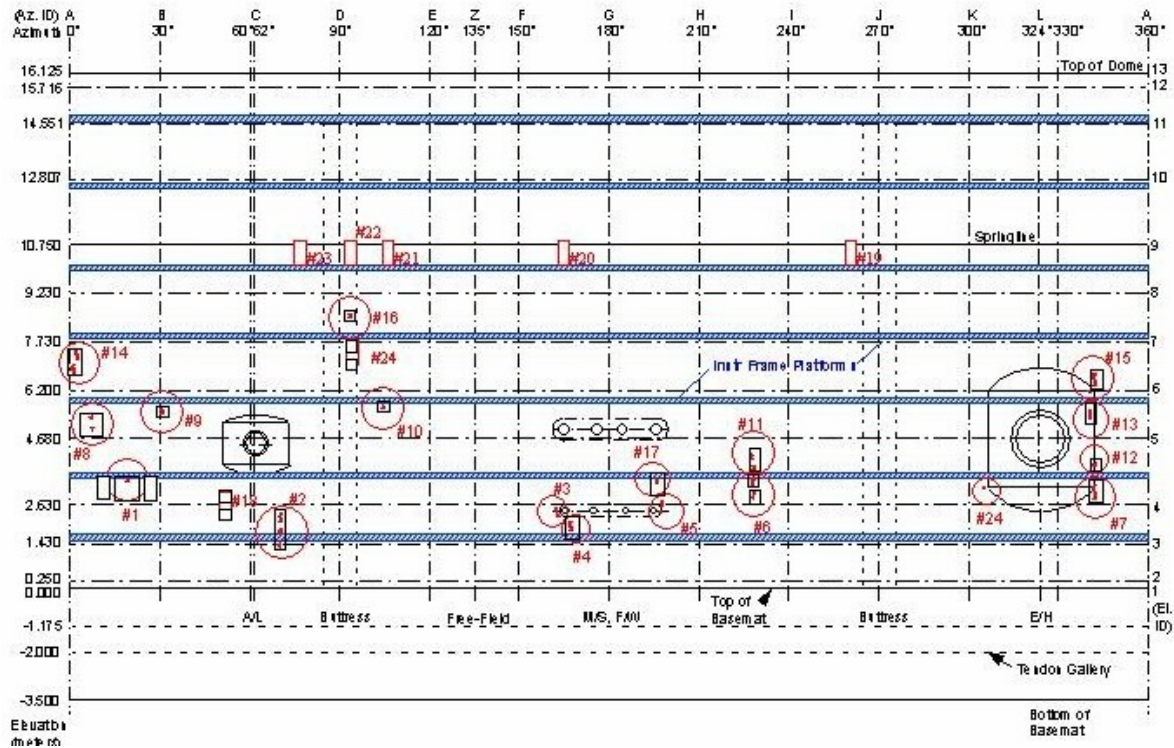


Figure 1. Map showing approximate locations of tears.



Figure 2. Photographs showing region of tear #1 from outside of liner (left) (prior to concrete placement) and inside of liner (right) (prior to removal of paint). The tear occurred under the wide segment of back-up bar near the top of the left-hand photograph, on the side closest to the anchor.

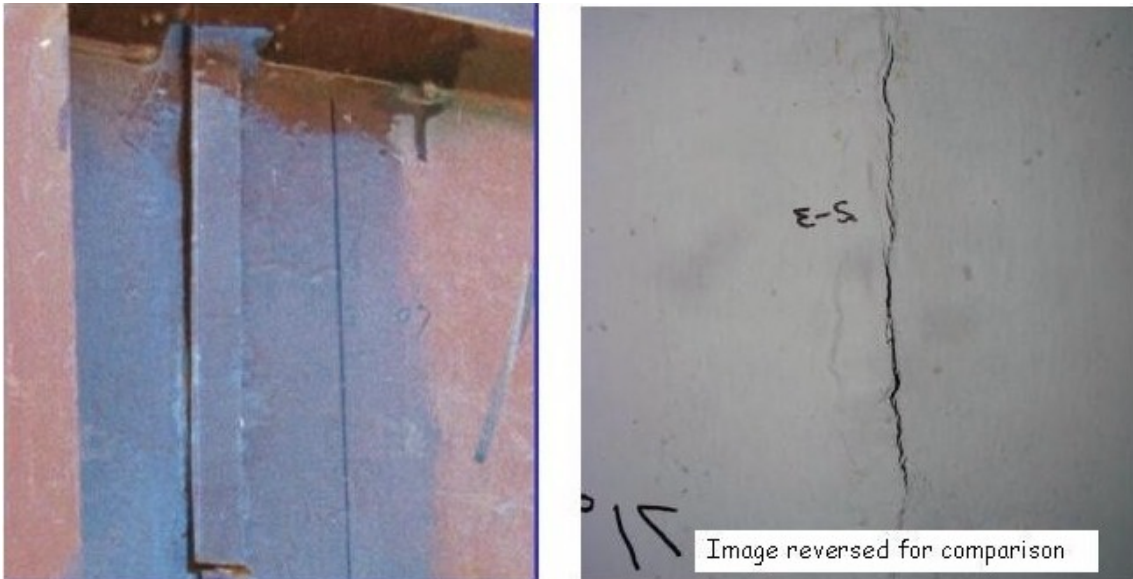


Figure 3. Photographs showing region of tear #2-3 from outside of liner (left) (prior to concrete placement) and inside of liner (right) (prior to removal of paint).



Figure 4. Photographs showing region of tear #4-1 from outside of liner (left) (prior to concrete placement) and inside of liner (right) (prior to removal of paint). Separate tears began of opposite sides of the weld, eventually growing together through the fusion zone.

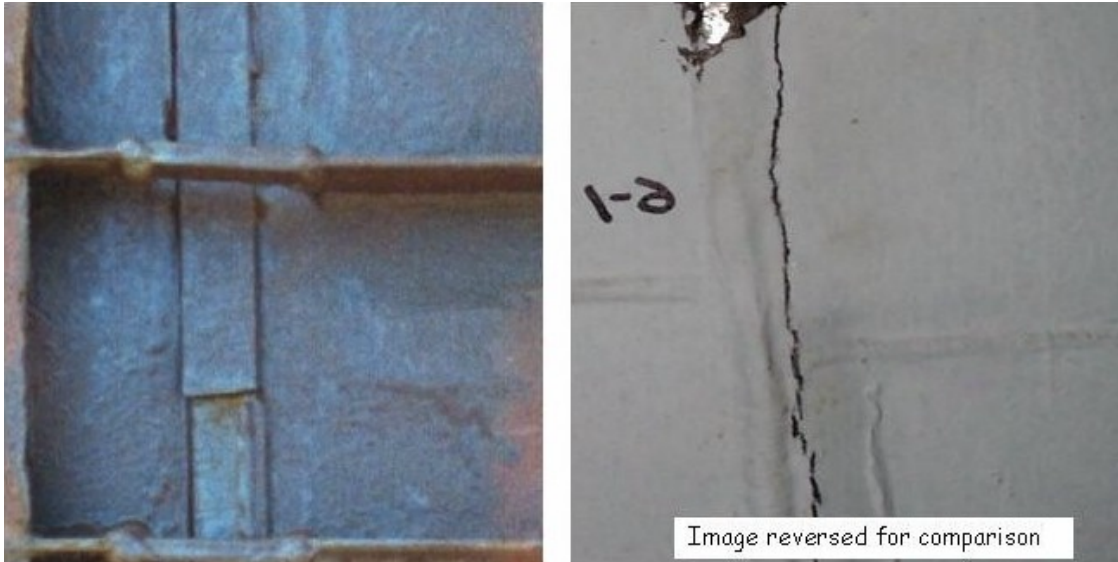


Figure 5. Photographs showing region of tear #6-1 from outside of liner (left) (prior to concrete placement) and inside of liner (right) (prior to removal of paint). Tear #6-2 was along the same vertical weld, but distant from the horizontal weld and associated horizontal stiffeners.

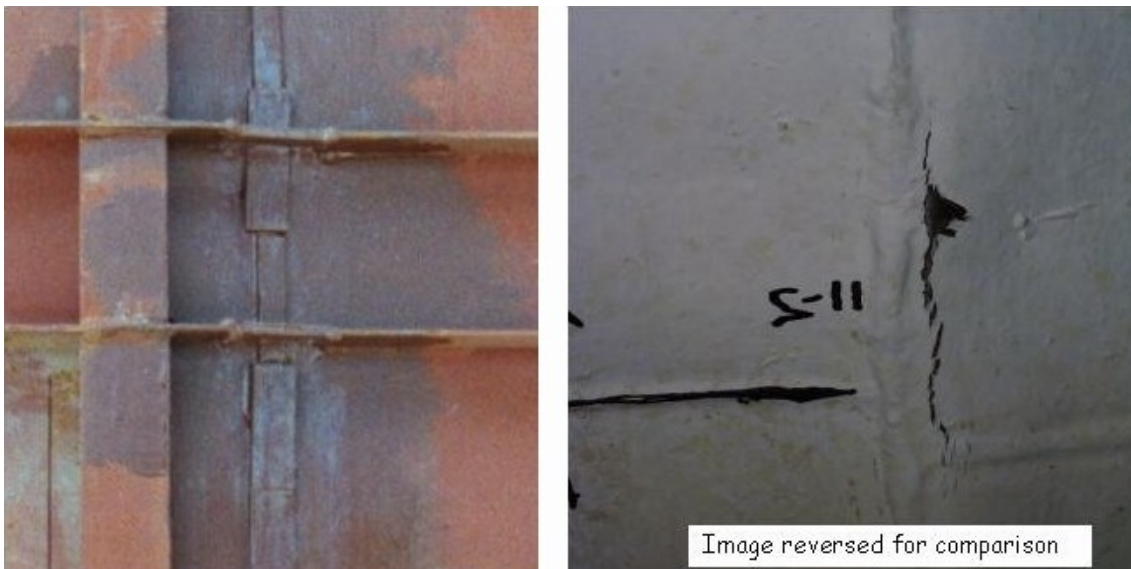


Figure 6. Photographs showing region of tear #11-2 from outside of liner (left) (prior to concrete placement) and inside of liner (right) (prior to removal of paint). Tear #11-1 was along the same vertical weld, but distant from the horizontal weld and associated horizontal stiffeners. Tears #11-1 and 11-2 were along the same vertical weld as tears #6-1 and 6-2.

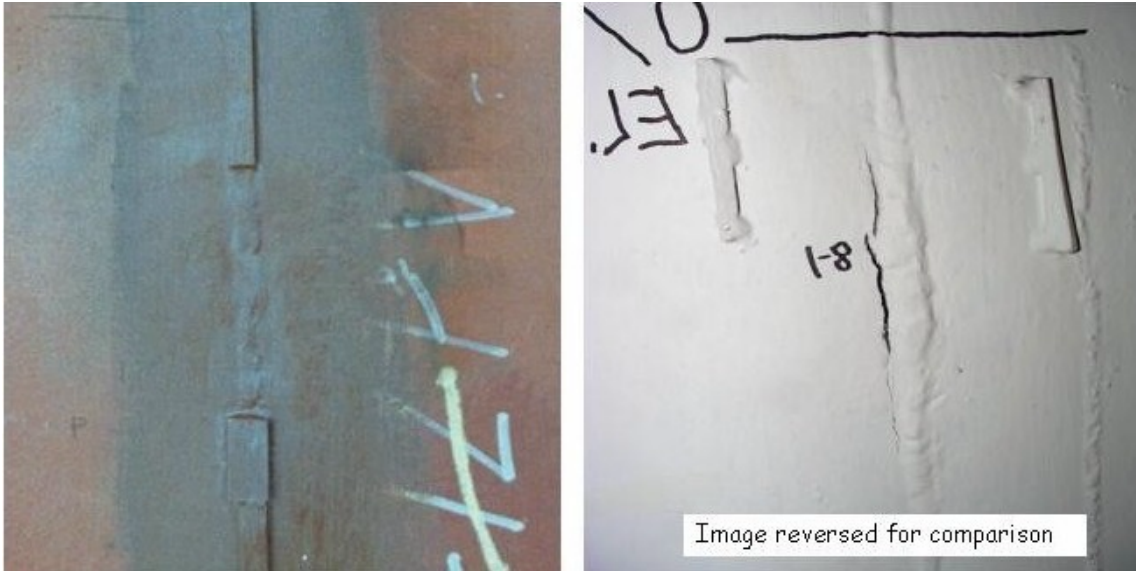


Figure 7. Photographs showing region of tear #8-1 from outside of liner (left) (prior to concrete placement) and inside of liner (right) (prior to removal of paint). Note missing segment of back-up bar in vicinity of repair weld and tear.

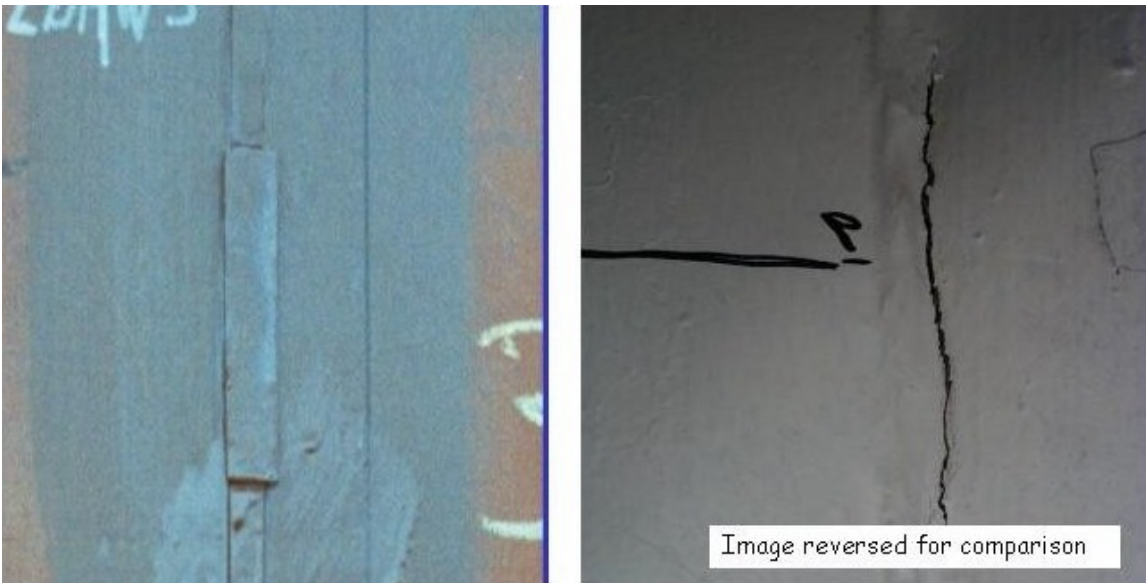


Figure 8. Photographs showing region of tear #9 from outside of liner (left) (prior to concrete placement) and inside of liner (right) (prior to removal of paint).

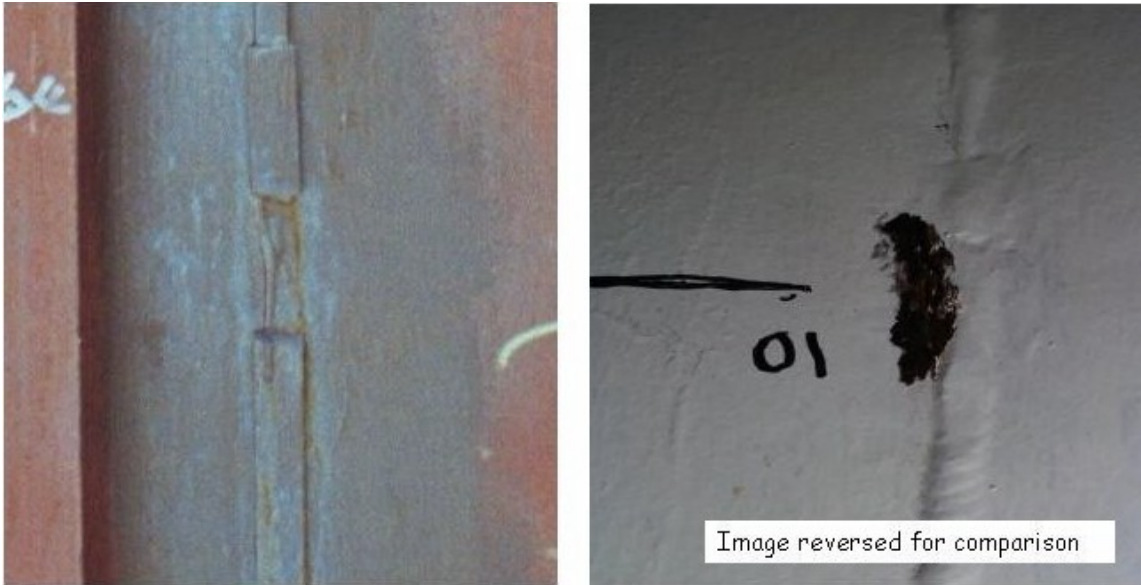


Figure 9. Photographs showing region of tear #10 from outside of liner (left) (prior to concrete placement) and inside of liner (right) (prior to removal of paint). Note missing segment of back-up bar in vicinity of repair weld and tear.



Figure 10. Photographs showing region of tear #14-1 from outside of liner (left) (prior to concrete placement) and inside of liner (right) (prior to removal of paint). Note missing segments of back-up bar in vicinity of repair weld and tear.



Figure 11. Photographs showing region of tear #16 from outside of liner (left) (prior to concrete placement) and inside of liner (right) (prior to removal of paint). Note missing segment of back-up bar on horizontal weld in vicinity tear.



Figure 12. Photographs showing region of tear #17 from outside of liner (left) (prior to concrete placement) and inside of liner (right) (prior to removal of paint). Note how weld bead is ground off on outside surface in vicinity of repair weld (made from inside of liner) and tear.

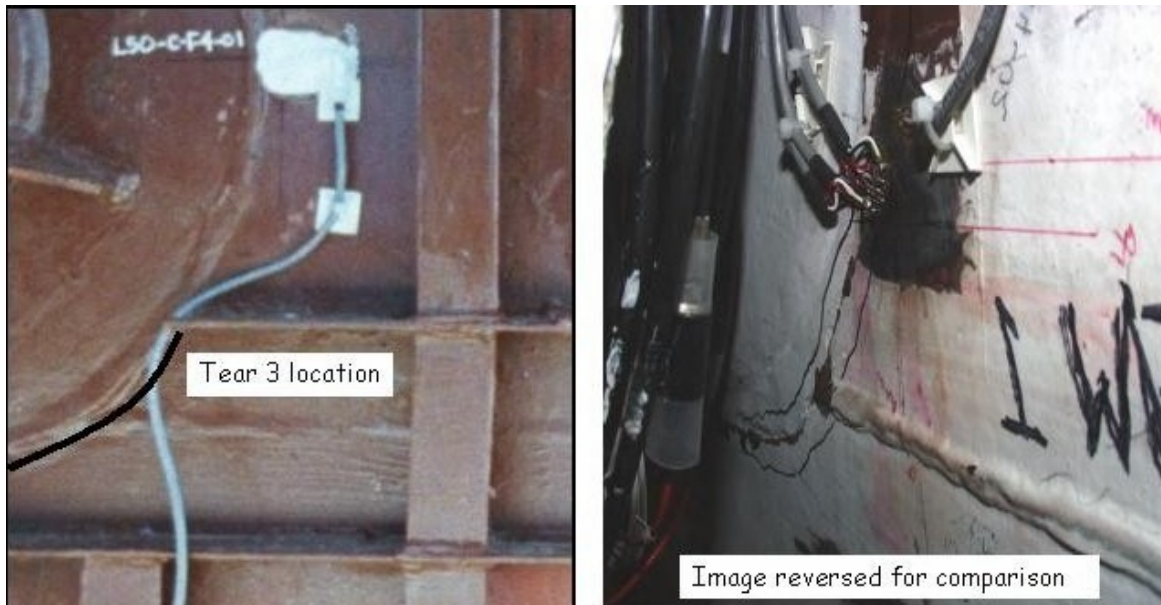


Figure 13. Photographs showing region of tear #3 from outside of liner (left) (prior to concrete placement) and inside of liner (right) (prior to removal of paint).

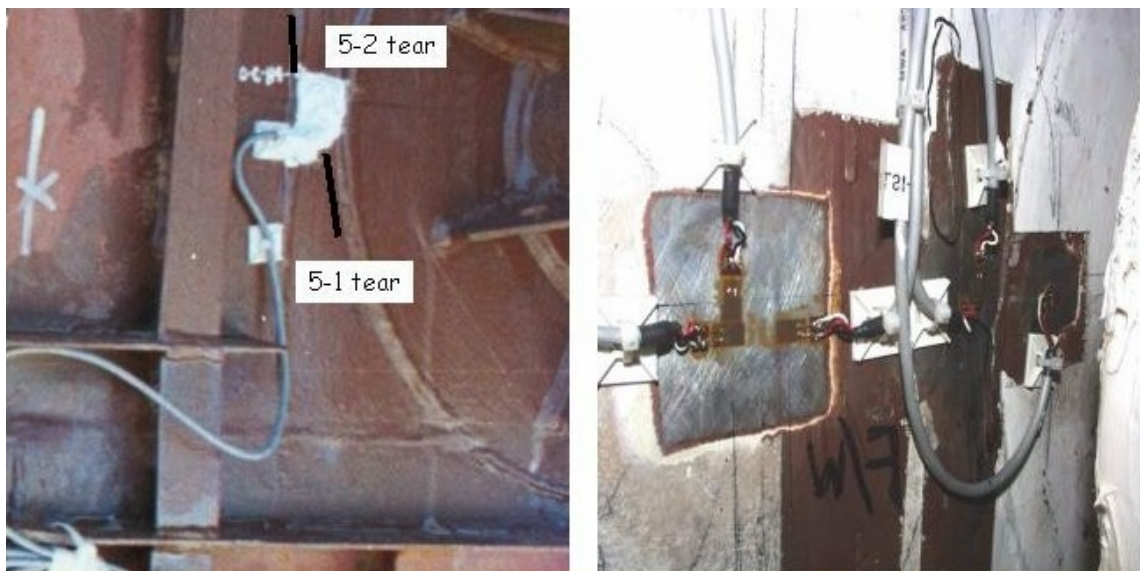


Figure 14. Photographs showing region of tear #5 from outside of liner (left) (prior to concrete placement) and inside of liner (right) (prior to removal of paint).



Figure 15. Photographs showing region of tear #7 from outside of liner (left) (prior to concrete placement) and inside of liner (right) (prior to removal of paint).



Figure 16. Photographs showing region of tear #15 from outside of liner (left) (prior to concrete placement) and inside of liner (right) (prior to removal of paint).



Figure 17. Photographs showing region of tear #12 from outside of liner (left) (prior to concrete placement) and inside of liner (right) (prior to removal of paint).



Figure 18. Photographs showing region of tear #13 from outside of liner (left) (prior to concrete placement) and inside of liner (right) (prior to removal of paint).

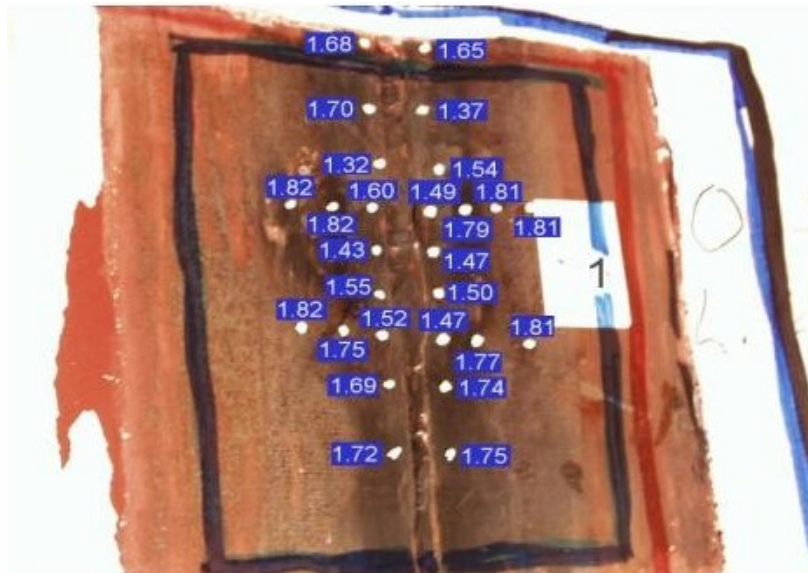


Figure 19. Liner thicknesses (in millimeters) measured ultrasonically in the vicinity of tear #1.



Figure 20. Liner thicknesses (in millimeters) measured ultrasonically in the vicinity of tear #2-2. Note the very wide region of repair welding and grinding. Note also that one measurement is greater than the initial plate thickness due to previous weld repairs.



Figure 21. Liner thicknesses (in millimeters) measured ultrasonically in the vicinity of tear #4 (4-1, 4-2, and 4-3).



Figure 22. Liner thicknesses (in millimeters) measured ultrasonically in the vicinity of tear #6-1.

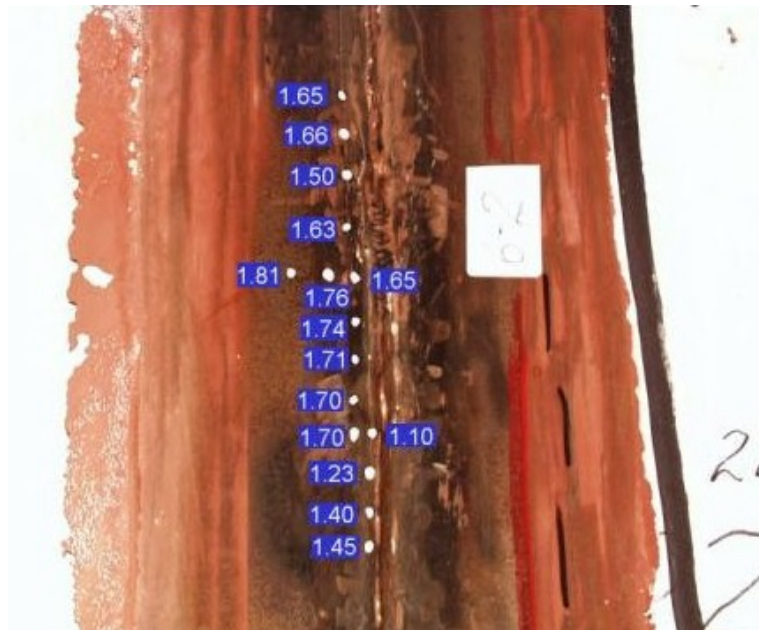


Figure 23. Liner thicknesses (in millimeters) measured ultrasonically in the vicinity of tear #6-2.



Figure 24. Liner thicknesses (in millimeters) measured ultrasonically in the vicinity of tear #11 (11-1 and 11-2).



Figure 25. Liner thicknesses (in millimeters) measured ultrasonically in the vicinity of tear #8-1.

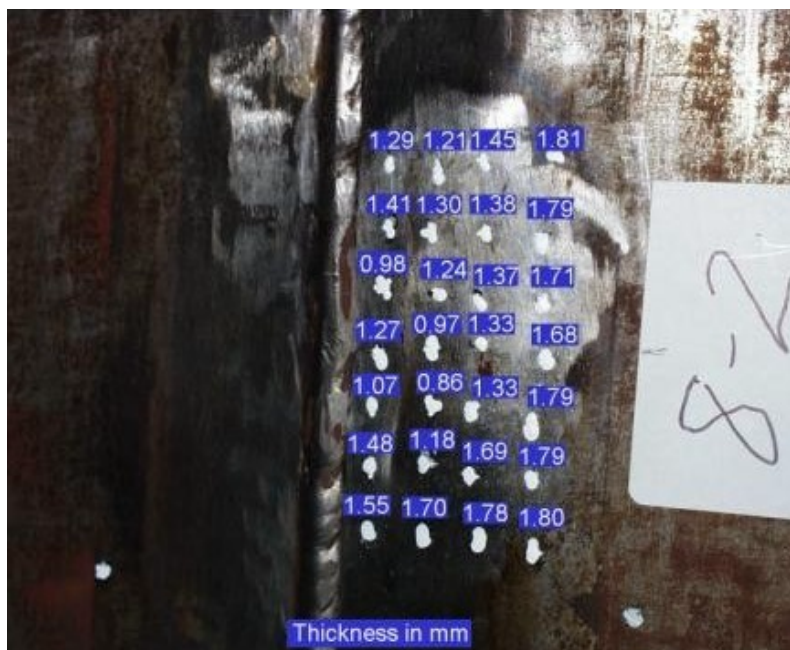


Figure 26. Liner thicknesses (in millimeters) measured ultrasonically in the vicinity of tear #8-2. Note the extensive grinding extending distant from main weld.

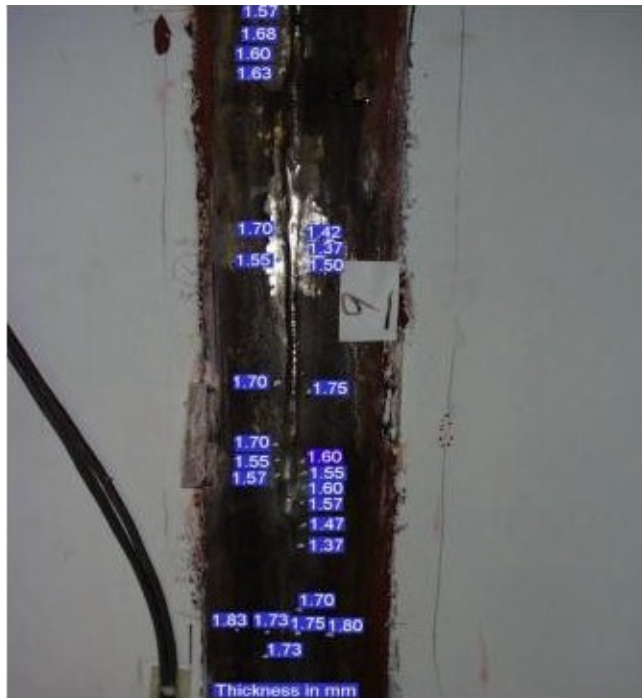


Figure 27. Liner thicknesses (in millimeters) measured ultrasonically in the vicinity of tear #9.



Figure 28. Liner thicknesses (in millimeters) measured ultrasonically in the vicinity of tear #10.



Figure 29. Liner thicknesses (in millimeters) measured ultrasonically in the vicinity of tear #14 (14-1 and 14-2).



Figure 30. Liner thicknesses (in millimeters) measured ultrasonically in the vicinity of tear #16. Note distance of tear from vertical weld and extensive buckling above tear.

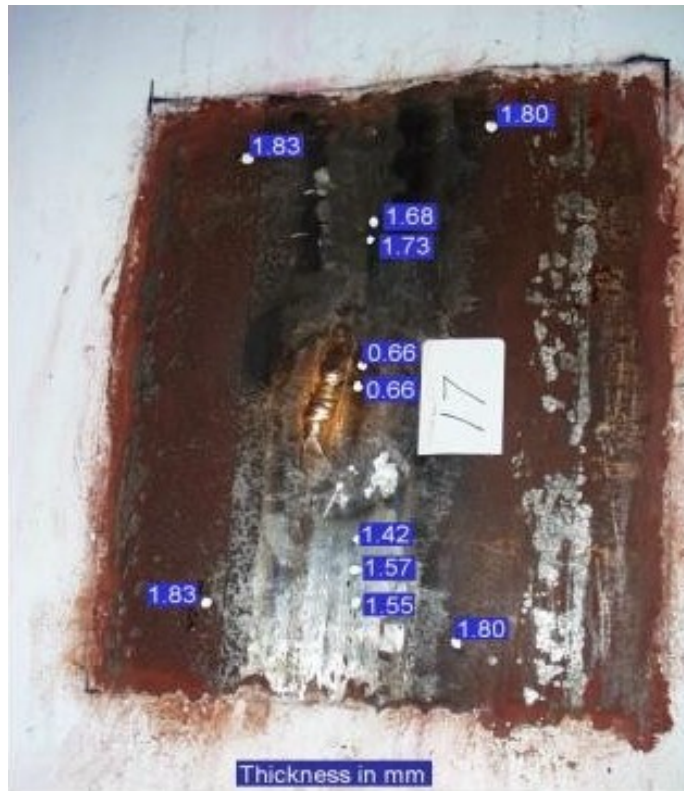


Figure 31. Liner thicknesses (in millimeters) measured ultrasonically in the vicinity of tear #17. Note exceptionally thin areas adjacent to repair weld and tear.

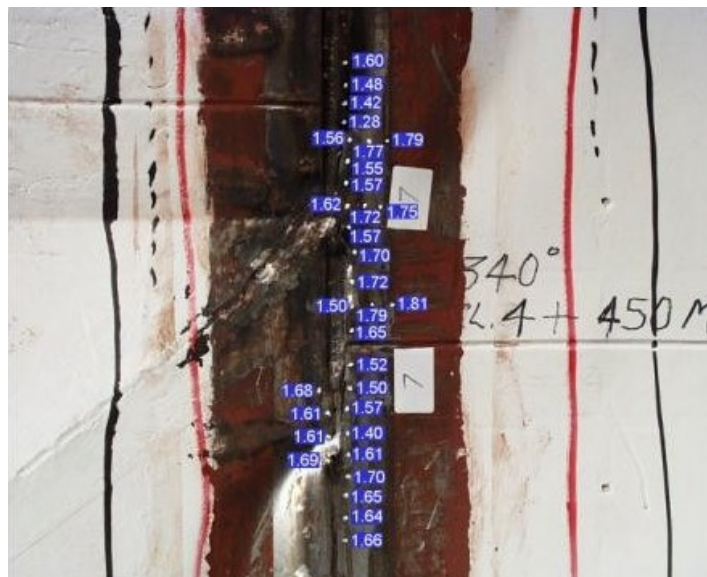


Figure 32. Liner thicknesses (in millimeters) measured ultrasonically in the vicinity of tear #7.



Figure 33. Liner thicknesses (in millimeters) measured ultrasonically in the vicinity of tear #15.



Figure 34. Liner thicknesses (in millimeters) measured ultrasonically in the vicinity of tear #12.

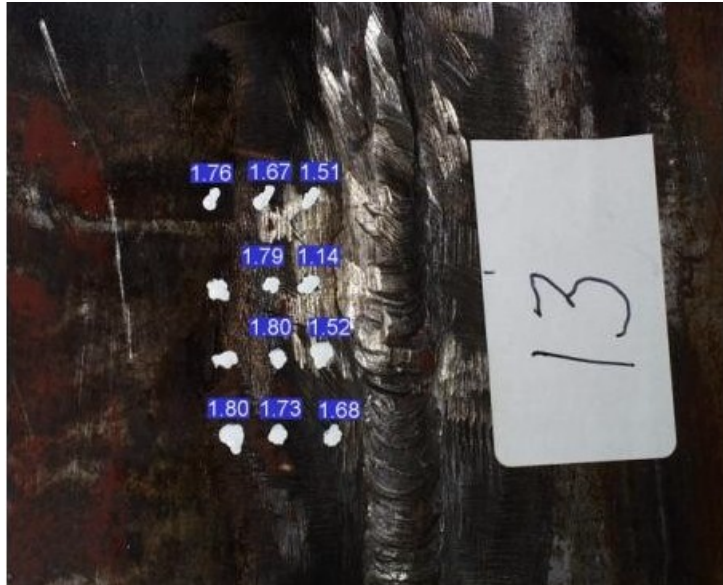


Figure 35. Liner thicknesses (in millimeters) measured ultrasonically in the vicinity of tear #13.



Figure 36. Liner thicknesses (in millimeters) measured ultrasonically in region #18. Buckling and “orange-peel” evidence of substantial plastic deformation, but no tearing, was apparent in this area.

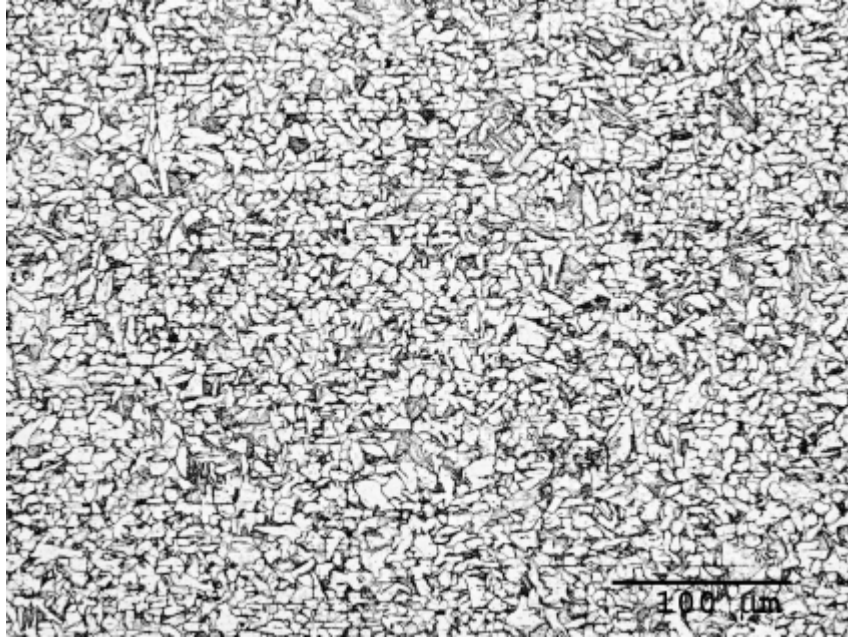


Figure 37. Microstructure of base metal in practice weld panel. Microstructure consists of ferrite (light) and pearlite (dark), typical of hot rolled carbon steel plate. Note the presence of chemical banding parallel to the rolling plane of the plate.

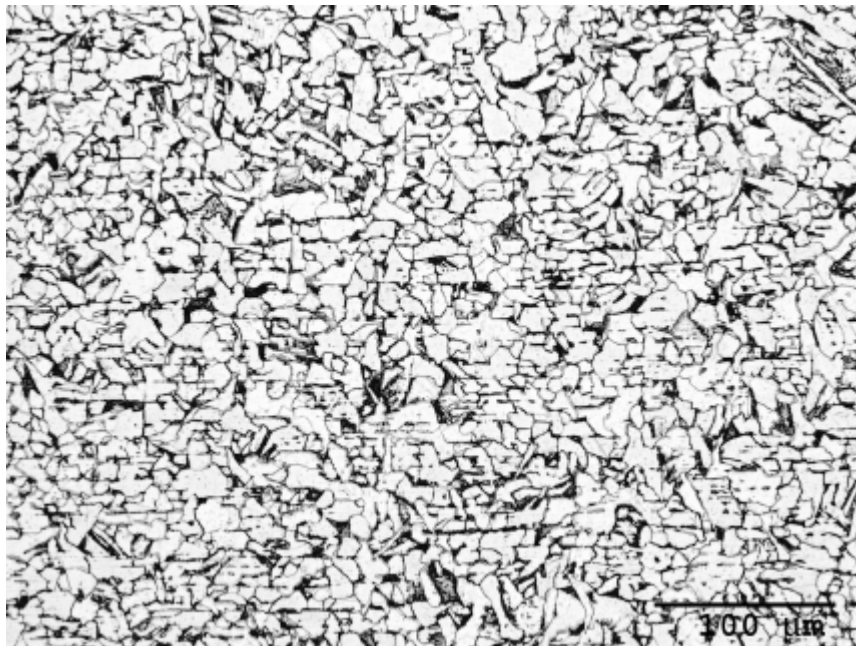


Figure 38. Microstructure of fine-grained portion of heat affected zone (several millimeters from weld) in practice weld panel. Microstructure consists of ferrite (light) and pearlite (dark). Note that the chemical banding persists in this region, indicating that the material, while re-austenitized, had not been heated to a high temperature in the austenite region.

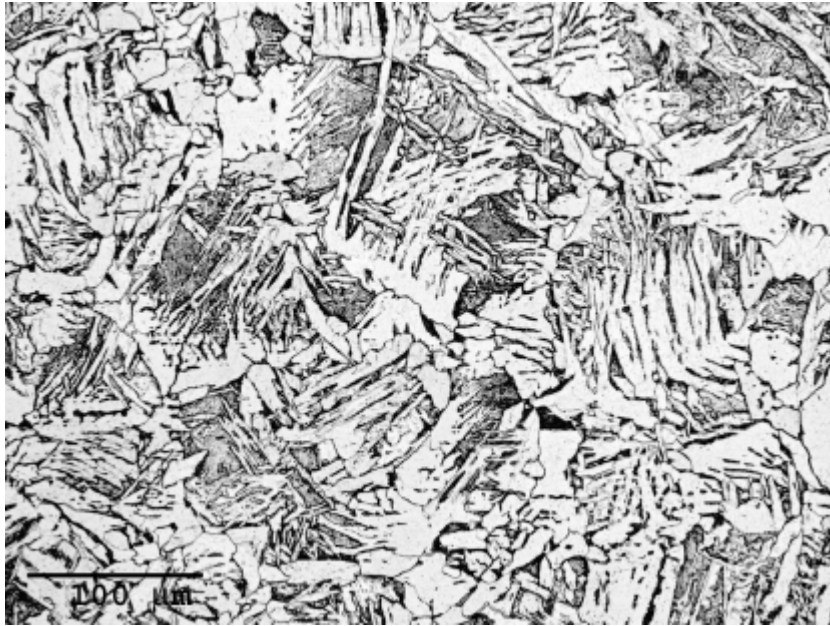


Figure 39. Microstructure of coarse-grained portion of heat affected zone (very close to weld) in practice weld panel. Microstructure consists of acicular ferrite (light) and pearlite (dark), typical of material that had been austenitized at high temperature and cooled fairly rapidly. Note that the chemical banding is no longer present in this region, indicating that the material had been heated to a high temperature in the austenite region.

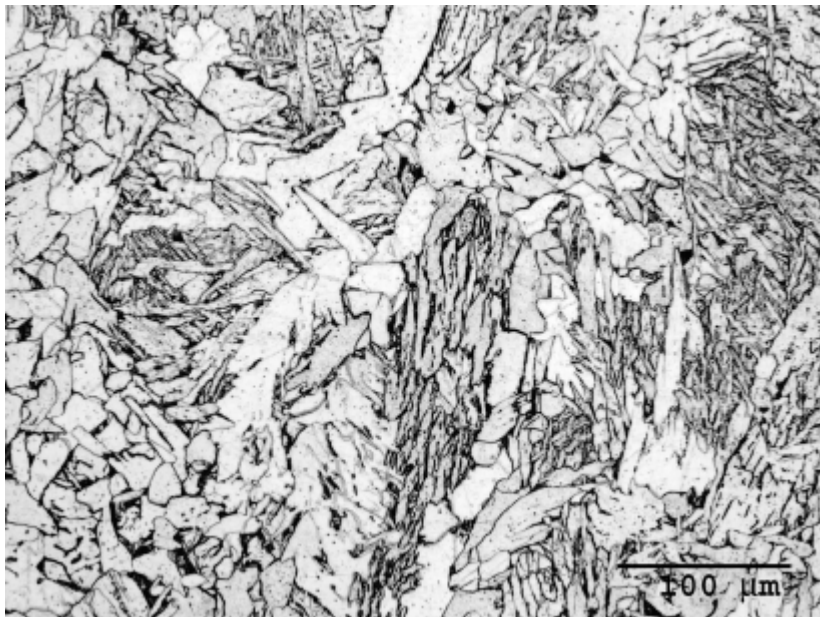


Figure 40. Microstructure of as-solidified fusion zone in practice weld panel. Microstructure consists of columnar prior austenite grains (characteristic of melted and resolidified material) that have transformed on cooling to ferrite and pearlite.

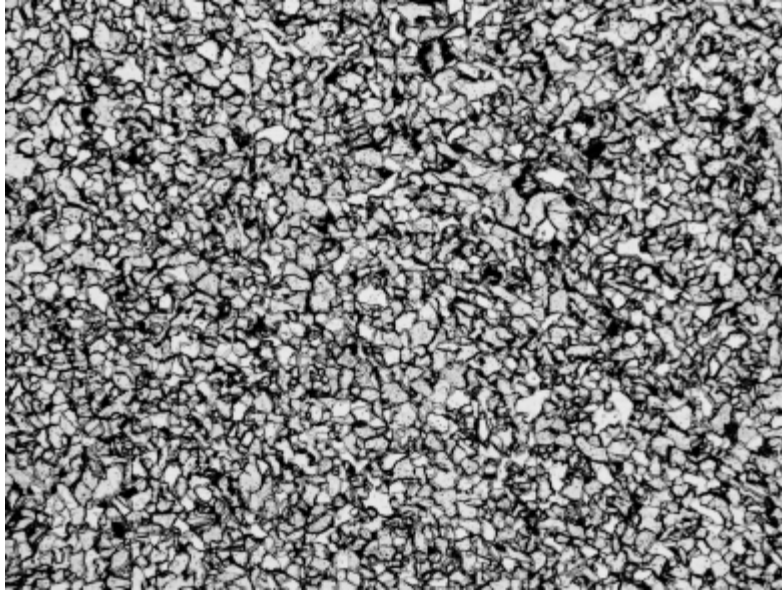


Figure 41. Microstructure of portion of fusion zone that has been re-austenitized during a second weld pass. Note that prior austenite grains have recrystallized, eliminating the columnar appearance, then transformed on cooling to ferrite and pearlite similar in appearance to the fine grained portion of the heat affected zone, but without chemical banding.

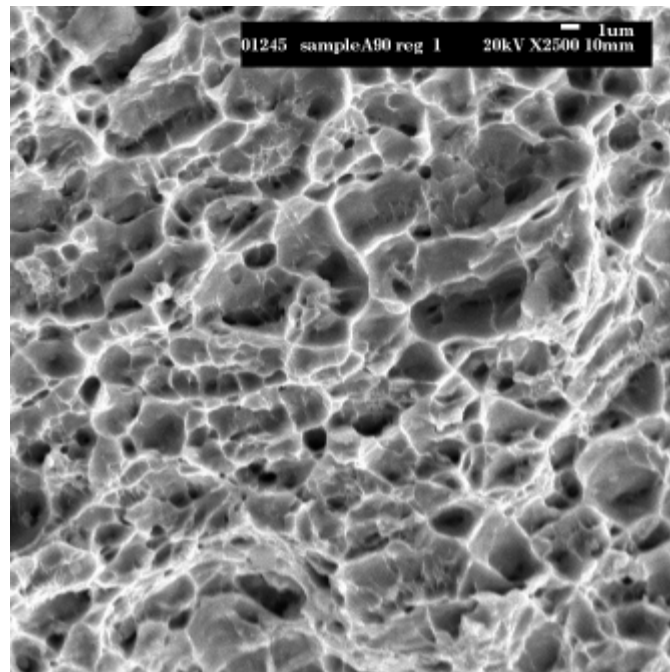


Figure 42. Scanning electron micrograph of fracture surface from tensile sample without any weld. Microvoids indicate that failure occurred by ductile rupture, typical of tearing of mild steel plate following extensive plastic deformation.

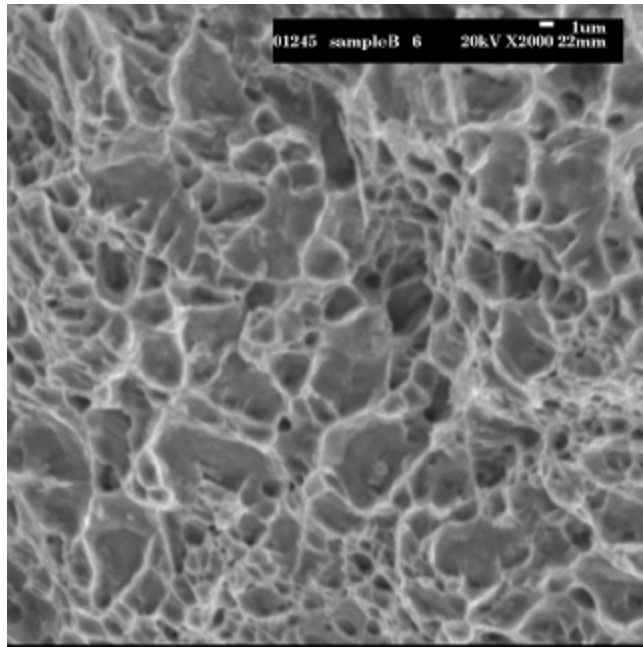


Figure 43. Scanning electron micrograph of fracture surface from welded tensile sample with lack of fusion defect. The location pictured is away from the weld defect, here deformation and fracture occurred in the heat affected zone. Failure here also occurred by ductile rupture.

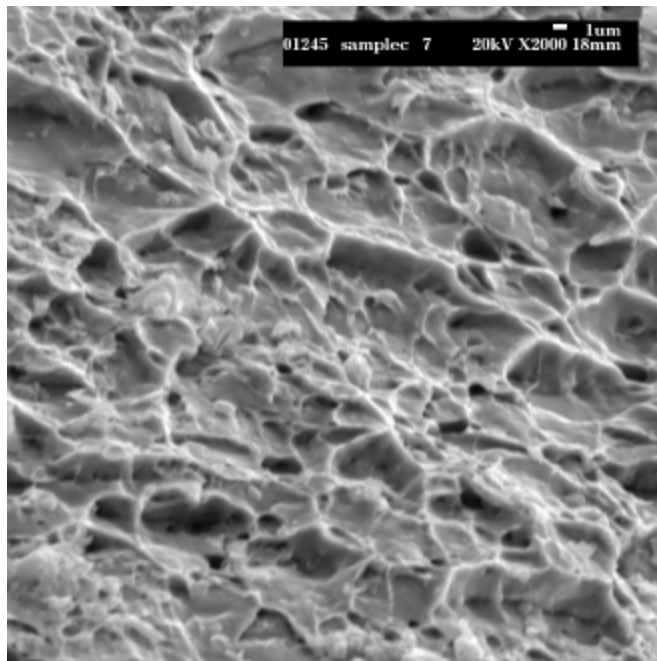


Figure 44. Scanning electron micrograph of fracture surface from welded tensile sample with substantial offset between plates. Failure here also occurred by ductile rupture.

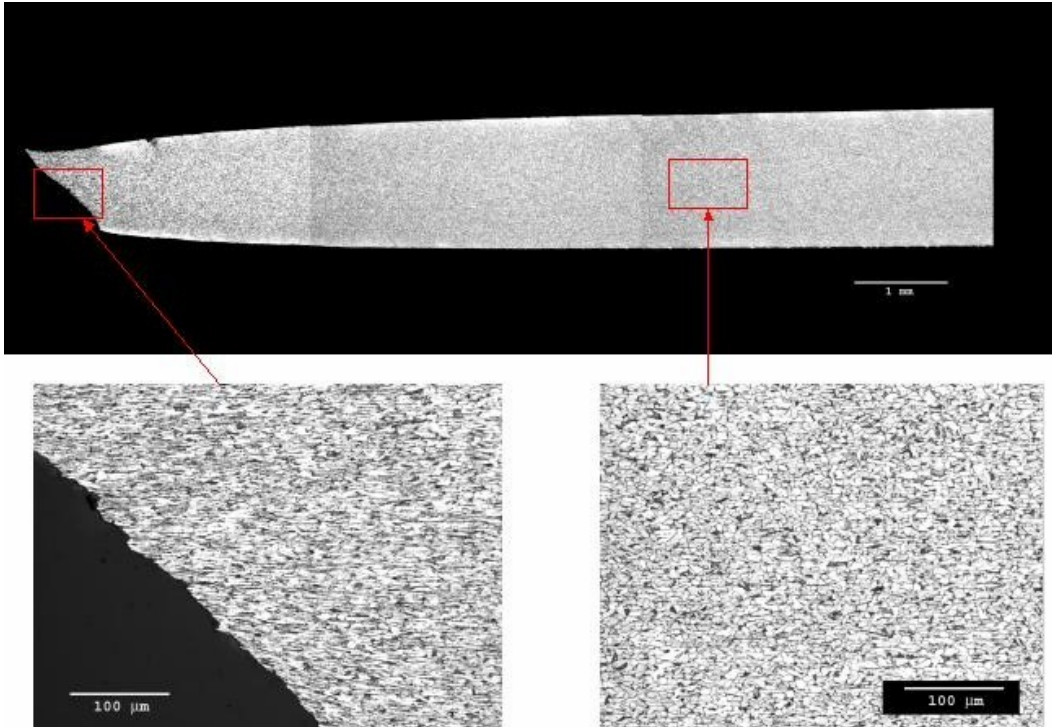


Figure 45. Metallographic cross-section of tensile sample of unwelded base metal (Sample A-3).

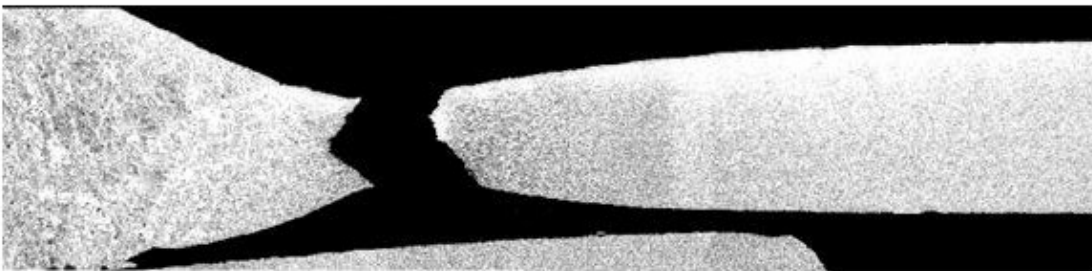


Figure 46. Metallographic cross-section of tensile sample from practice weld panel in area without substantial offset between plates (Sample B-2). This sample broke along the fusion line at an apparent lack of fusion defect. Cross-section is not through defect, but through a sound region adjacent to the defect where ductile tearing occurred.

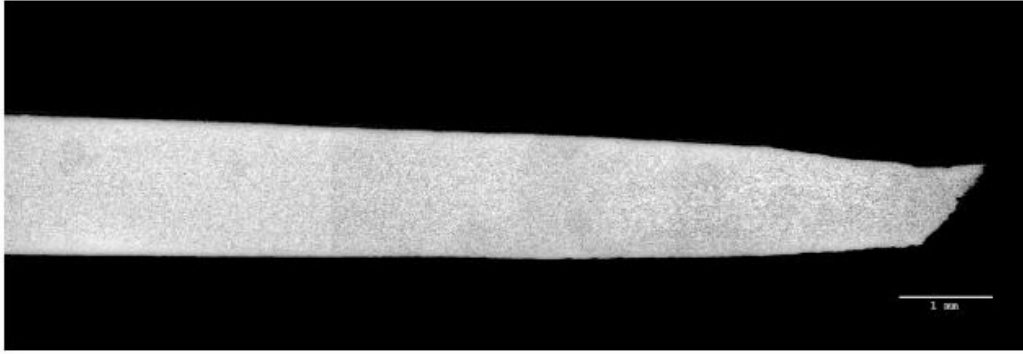


Figure 47. Metallographic cross-section of tensile sample from practice weld panel in area with substantial offset between plates (Sample C-1).

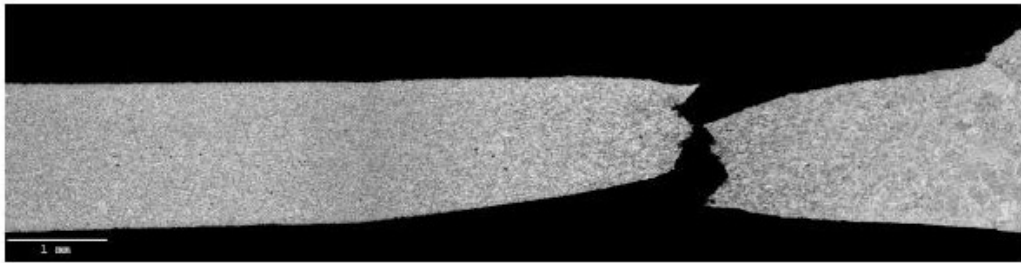


Figure 48. Metallographic cross-section of tensile sample from practice weld panel in area with substantial offset between plates (Sample C-2).



Figure 49. Details of inside (top) and outside (bottom) liner features in region of tear #1 metallographic cross-section (arrows begin at plane of section and indicate view direction).

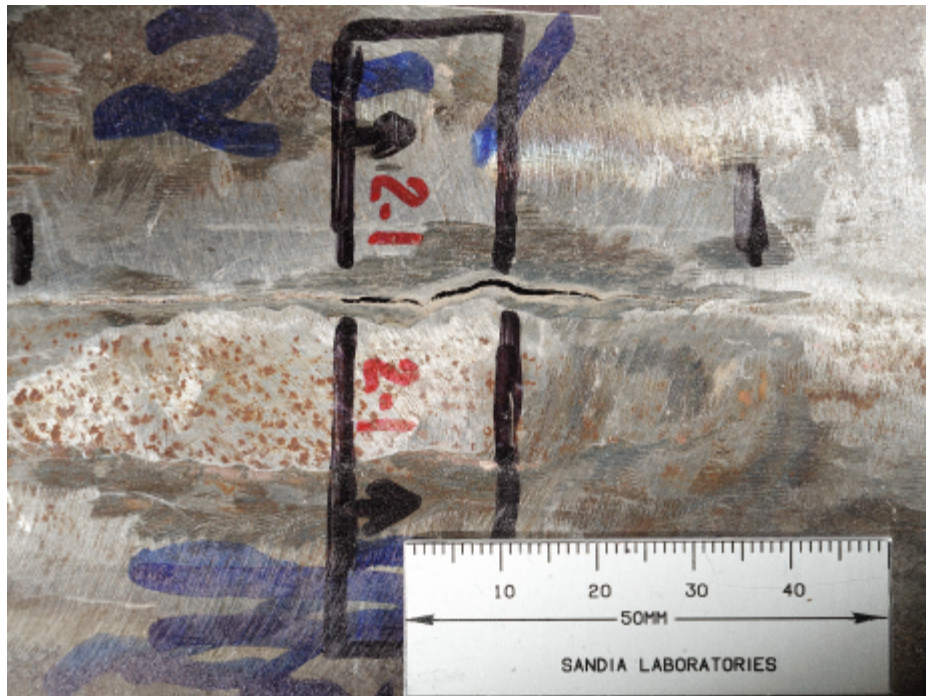


Figure 50. Details of inside (top) and outside (bottom) liner features in region of tear #2-1 metallographic cross-section (arrows begin at plane of section and indicate view direction).

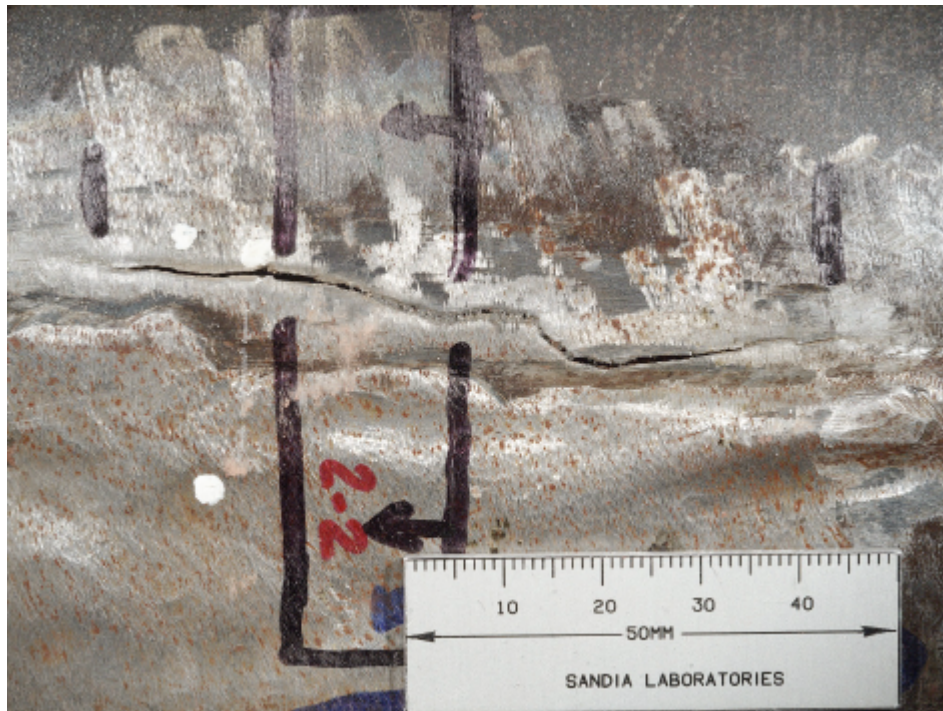


Figure 51. Details of inside (top) and outside (bottom) liner features in region of tear #2-2 metallographic cross-section (arrows begin at plane of section and indicate view direction).



Figure 52. Details of inside (top) and outside (bottom) liner features in region of tear #2-3 metallographic cross-section (arrows begin at plane of section and indicate view direction).



Figure 53. Details of inside (top) and outside (bottom) liner features in region of tear #4-1 metallographic cross-section (arrows begin at plane of section and indicate view direction).



Figure 54. Details of inside (top) and outside (bottom) liner features in region of tear #4-3 metallographic cross-section (arrows begin at plane of section and indicate view direction).



Figure 55. Details of inside (top) and outside (bottom) liner features in region of tear #6-2 metallographic cross-section (arrows begin at plane of section and indicate view direction).

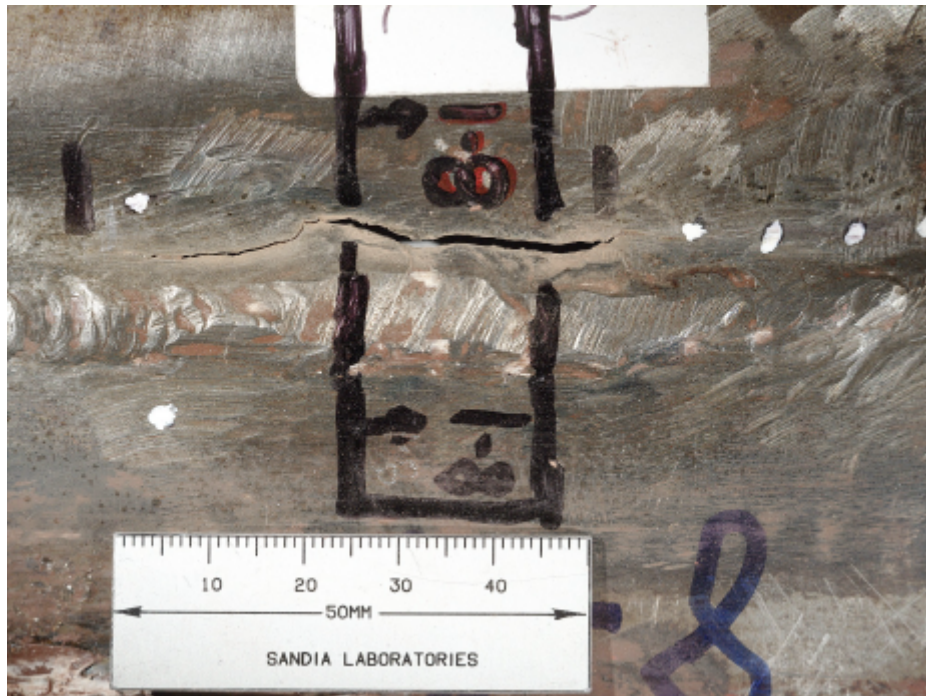


Figure 56. Details of inside (top) and outside (bottom) liner features in region of tear #8-1 metallographic cross-section (arrows begin at plane of section and indicate view direction).

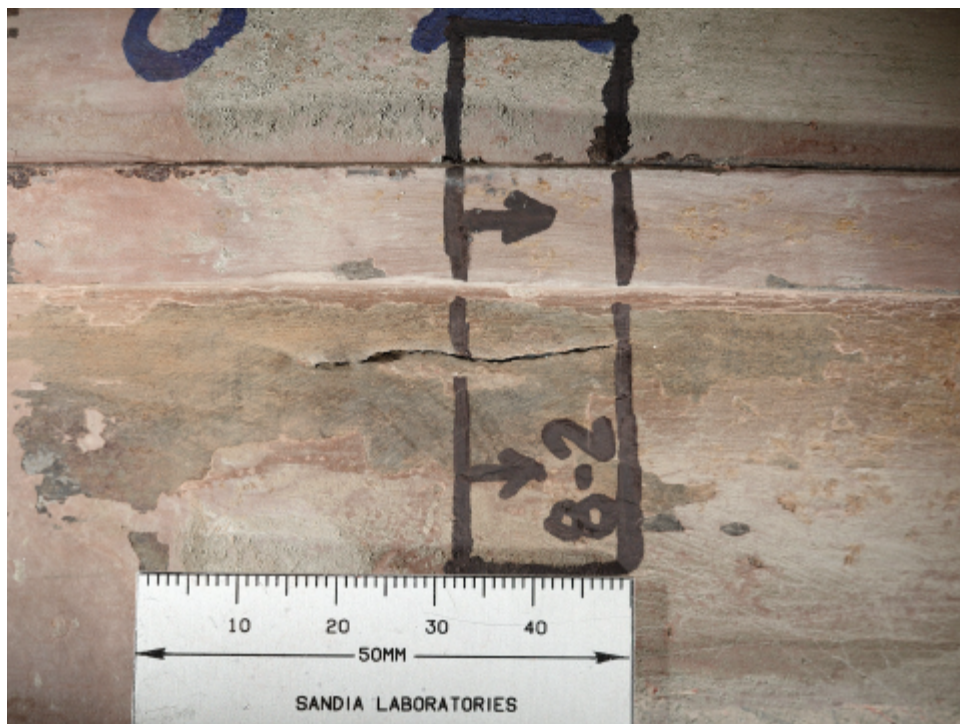


Figure 57. Details of inside (top) and outside (bottom) liner features in region of tear #8-2 metallographic cross-section (arrows begin at plane of section and indicate view direction).

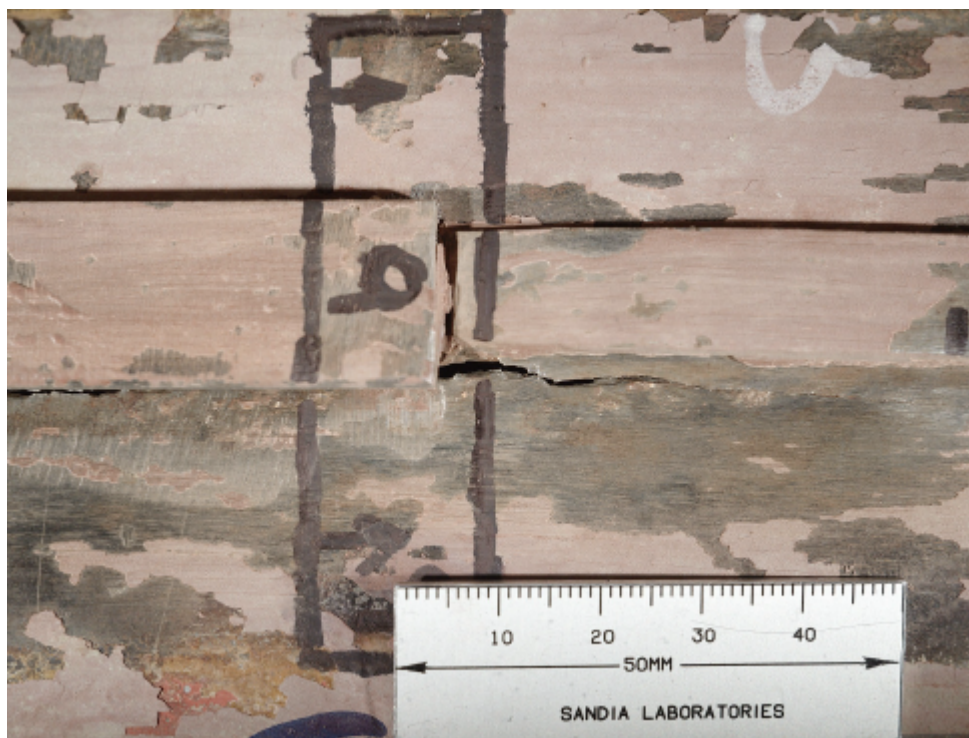
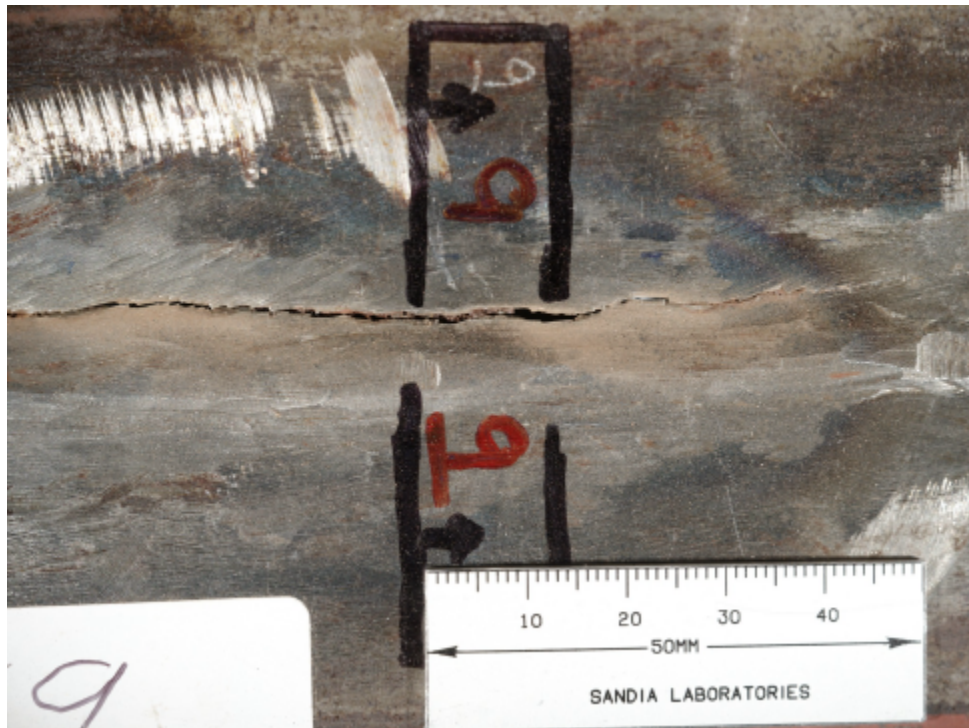


Figure 58. Details of inside (top) and outside (bottom) liner features in region of tear #9 metallographic cross-section (arrows begin at plane of section and indicate view direction).

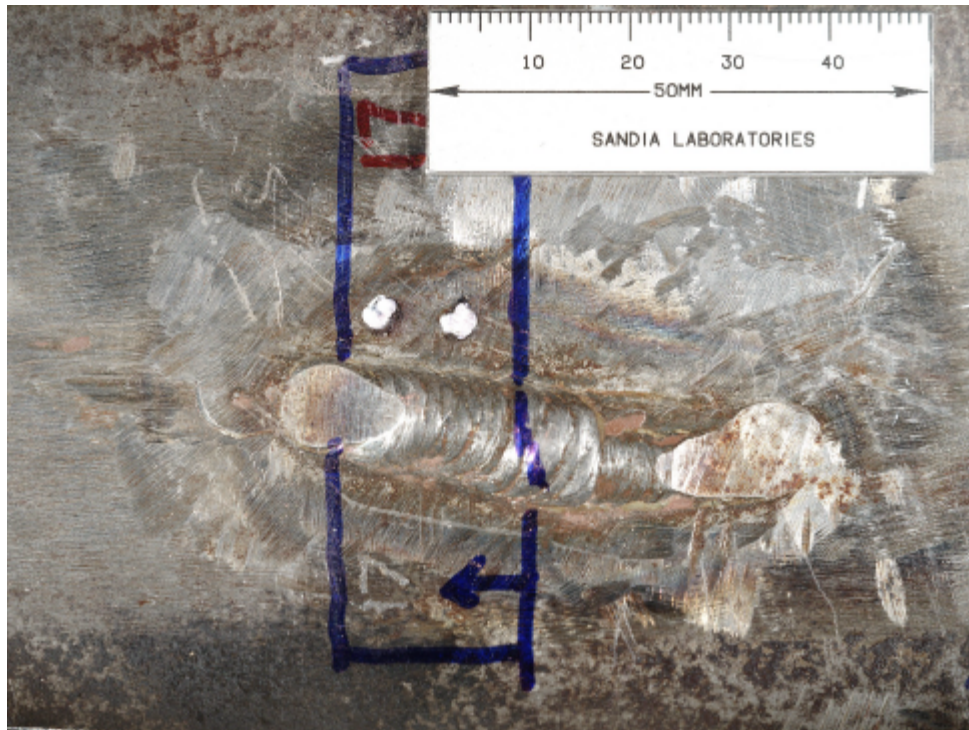


Figure 59. Details of inside (top) and outside (bottom) liner features in region of tear #17 metallographic cross-section (arrows begin at plane of section and indicate view direction).

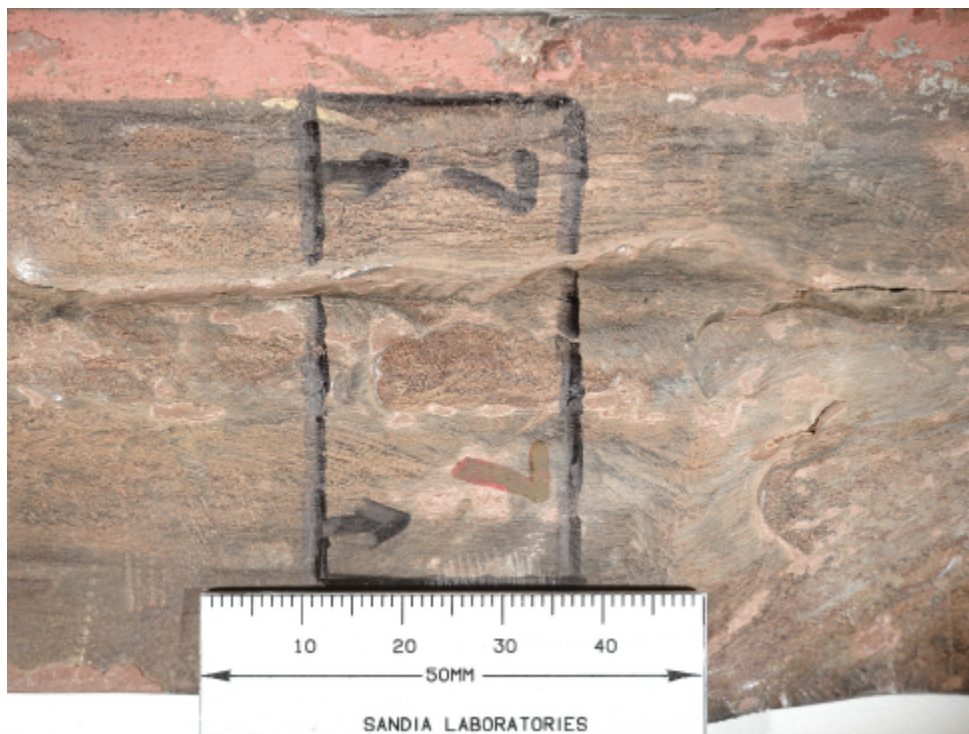
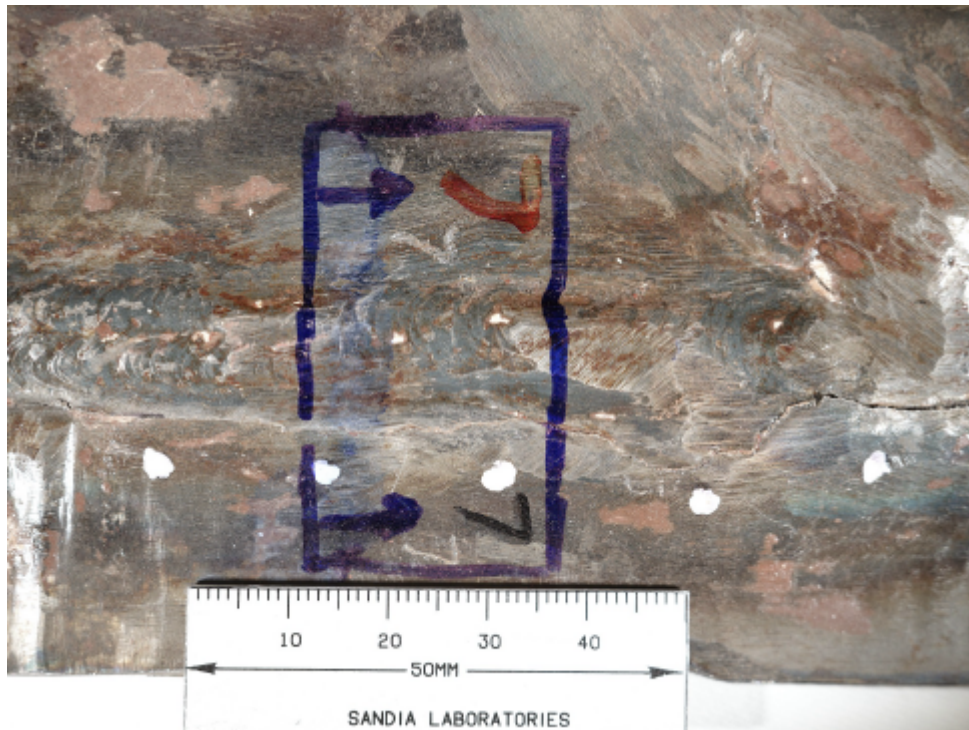


Figure 60. Details of inside (top) and outside (bottom) liner features in region of tear #7 metallographic cross-section (arrows begin at plane of section and indicate view direction).

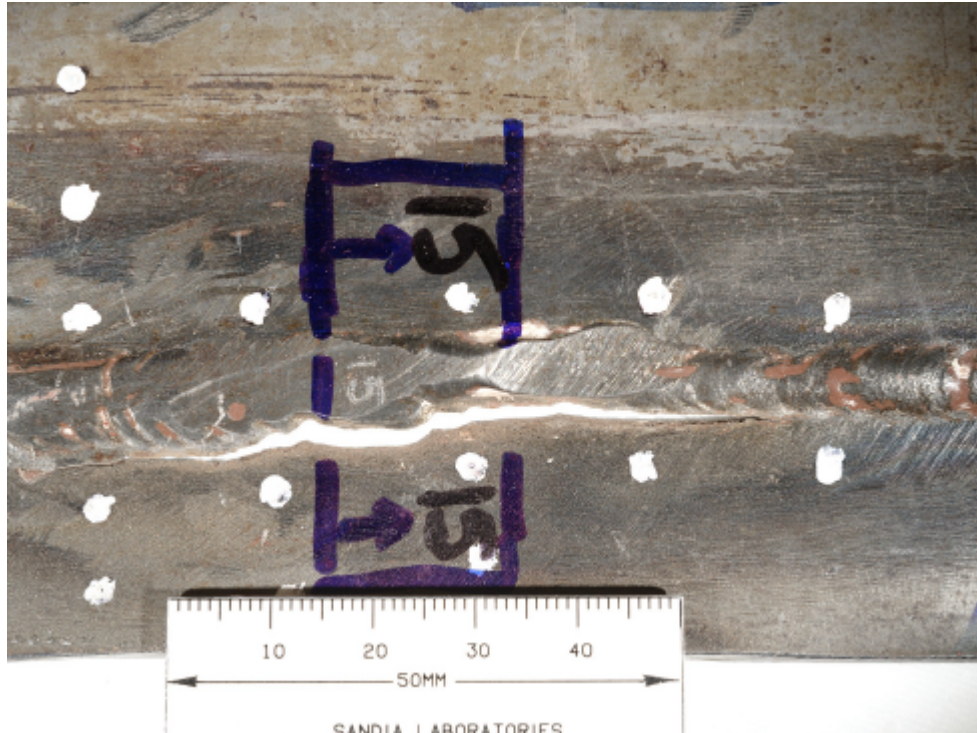


Figure 61. Details of inside (top) and outside (bottom) liner features in region of tear #15 metallographic cross-section (arrows begin at plane of section and indicate view direction).



Figure 62. Details of inside (top) and outside (bottom) liner features in region of tear #12 metallographic cross-section (arrows begin at plane of section and indicate view direction). Location of SEM fractographic sample is also shown.



Figure 63. Details of inside (top) and outside (bottom) liner features in region #18-1 metallographic cross-section (arrows begin at plane of section and indicate view direction).

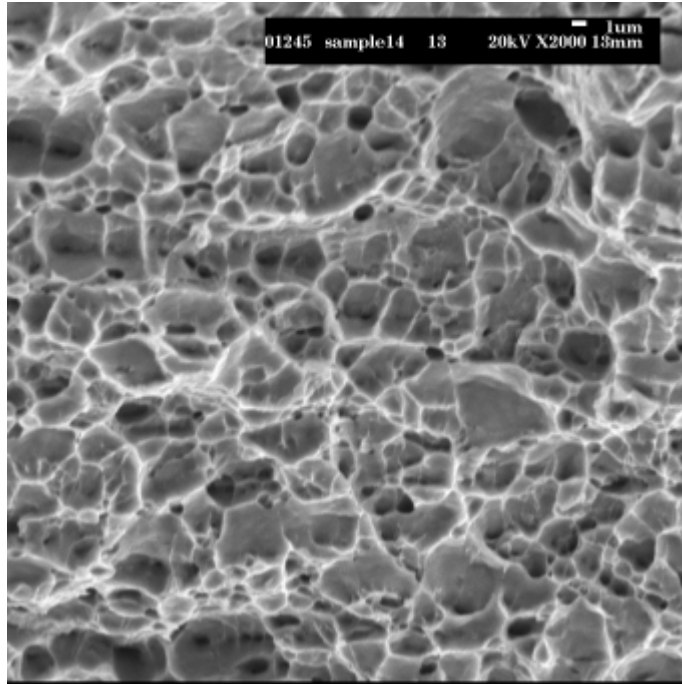


Figure 64. Scanning electron micrograph of fracture surface from tear #14-2. Failure occurred by ductile rupture, as was seen on fracture surfaces from tensile samples shown in Figures 42-44.

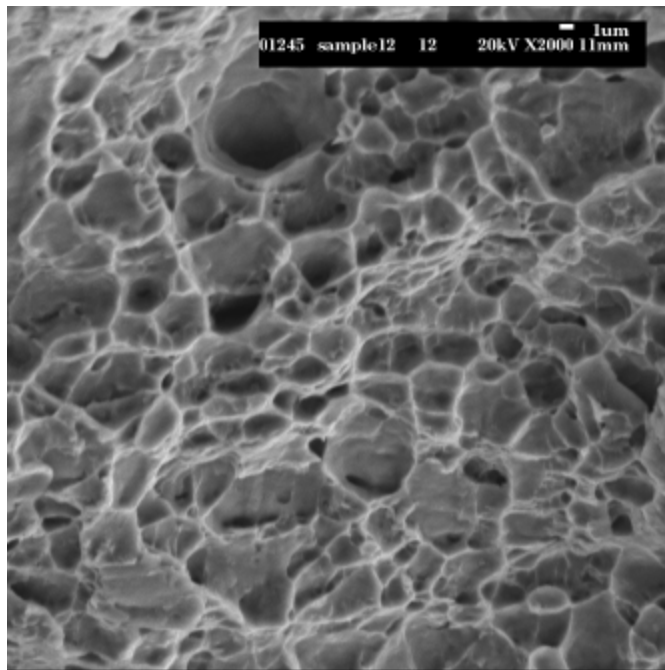


Figure 65. Scanning electron micrograph of fracture surface from tear #12. Failure occurred by ductile rupture, as was seen on fracture surfaces from tensile samples shown in Figures 42-44.

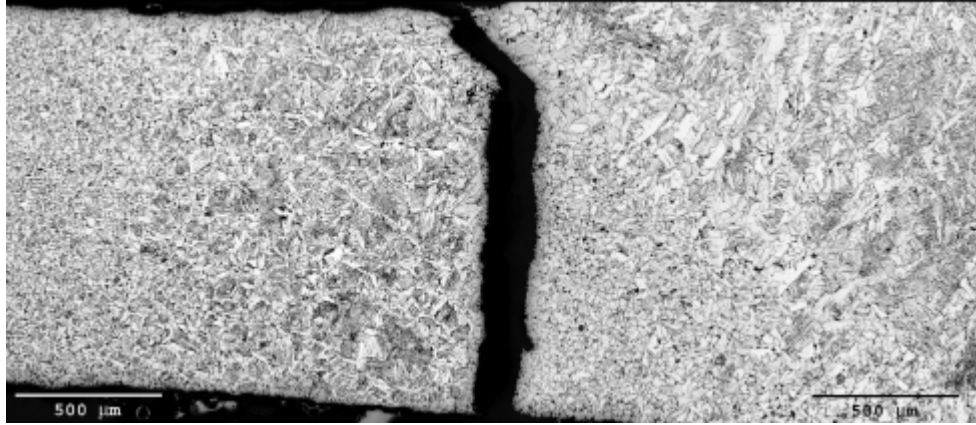


Figure 66. Metallographic cross section of tear #1. This cross section was taken at the location of widest crack opening, corresponding to where the tear apparently initiated. Note that the opening is flat and perpendicular to the liner circumference, and that the microstructure is not continuous across the separation. The “fracture” surfaces were also covered with a layer of foreign material (too dark to be seen here). These features indicate that this area represents a lack of fusion defect, i.e., a region in which the repair weld failed to bridge the gap being welded.

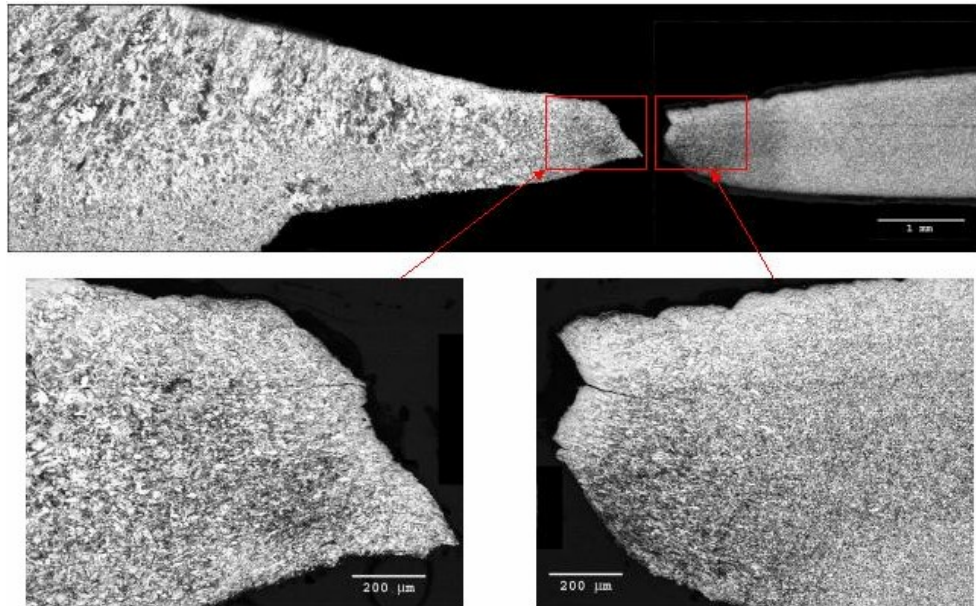


Figure 67. Metallographic cross section of tear #1 approximately 2 cm distant from the cross section shown in Figure 66. Note that failure occurred by more typical shear, and that microstructure shows evidence of substantial localized deformation having occurred prior to final separation. This represents an area removed from the lack of fusion defect where liner tearing occurred as the tear grew in length during testing of the structure. Tearing occurred through the fine grained portion of the heat affected zone.

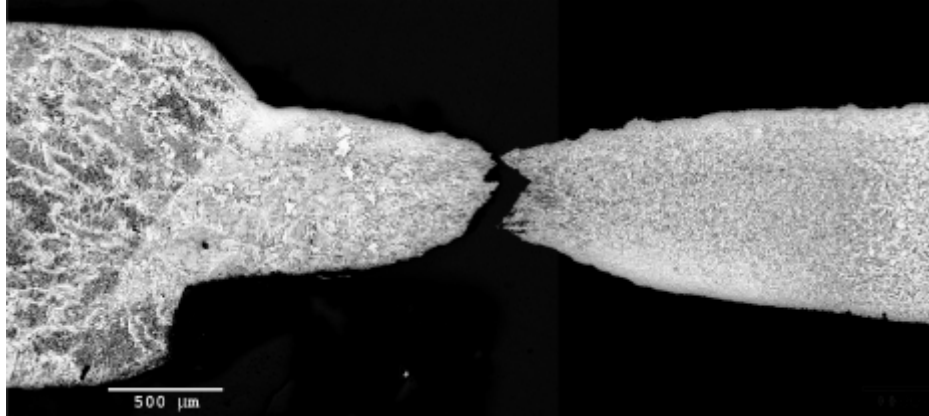


Figure 68. Metallographic cross section of tear #2-1. Tearing occurred in heat affected zone adjacent to repair weld. Note how grinding ends abruptly at edge of fusion zone, providing for measurement of as-ground liner thickness at edge of weld and close to location of tear. Tearing occurred in the adjacent heat affected zone.

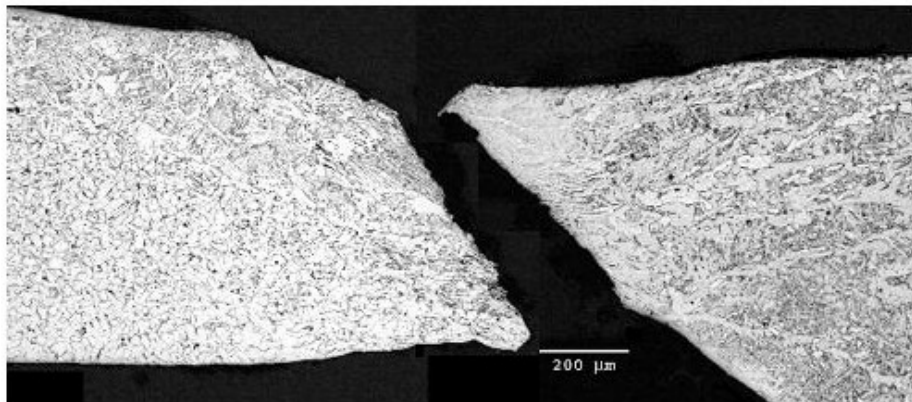


Figure 69. Metallographic cross section of tear #2-2. A very wide region (~29 mm) representing many sequential side-by-side welds was observed in this sample. The fusion zones of many of the early welds had been recrystallized by the heat input from subsequent welds, whereas many of the later welds retained the coarse columnar grain structures characteristic of single pass welds. Tearing occurred in by shear following substantial plastic deformation near the boundary between recrystallized weld metal and a region that could be either unrecrystallized weld metal or coarse grained heat affected zone.

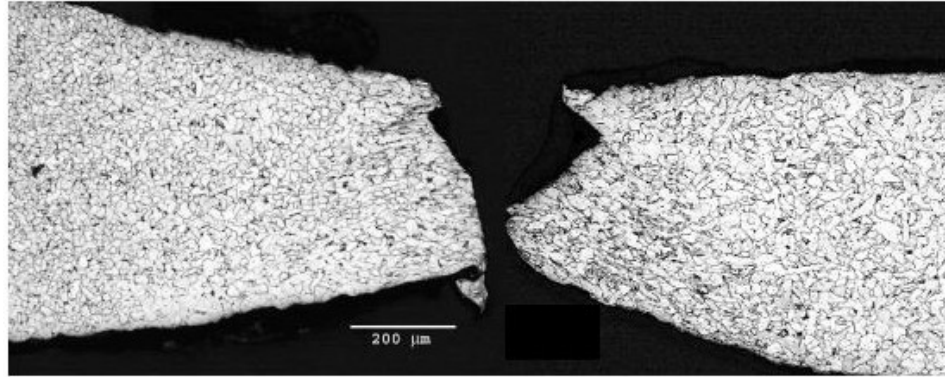


Figure 70. Metallographic cross section of tear #2-3. This sample was similar to #2-2, except that tearing occurred in a completely recrystallized fusion zone of an earlier weld. A portion of the fracture appears to have been mashed flat; this represents an artifact which occurred during unloading or when samples were being removed from the liner.

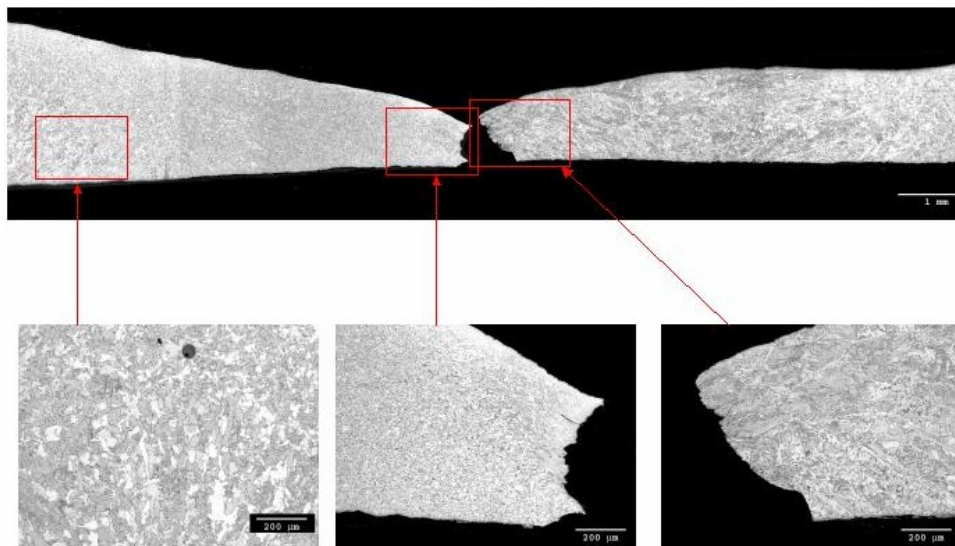


Figure 71. Metallographic cross section of tear #4-1. This sample was similar to #2-2, except that the region of sequential side-by-side welds was even wider, approximately 51 mm. Tearing occurred in an area of mixed recrystallized and unrecrystallized weld metal, and was accompanied by substantial localized plastic deformation.

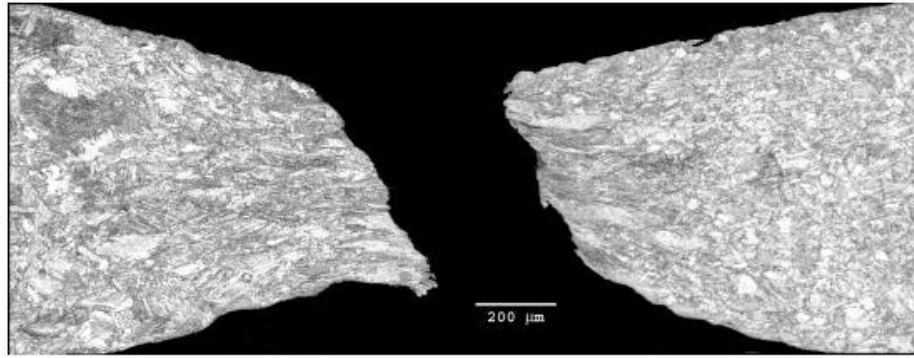


Figure 72. Metallographic cross section of tear #4-3. This sample contained the primary weld and several associated repair welds, plus a second weld approximately 25 mm in from the primary weld. This secondary weld was apparently made to repair the liner where it had been ground through when repairs were being made to the primary weld. Tearing occurred in a coarse grained region of heat affected zone between these two welds, and was preceded by extensive plastic deformation.

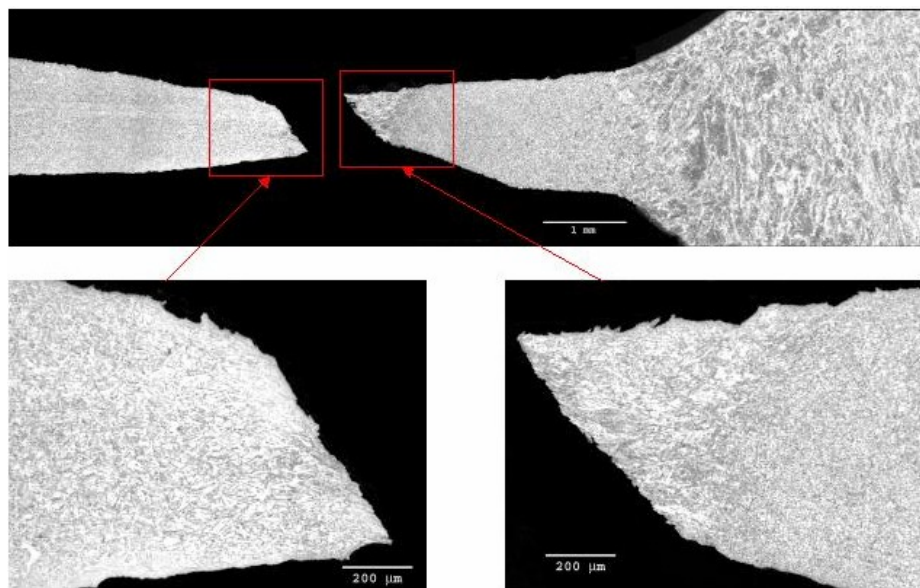


Figure 73. Metallographic cross section of tear #6-2. This sample contained a single repair weld. Grinding on the outside surface ended fairly abruptly at the edge of the back-up bar, resulting in a fairly deep but narrow region of liner thinning. Tearing occurred in the heat affected zone adjacent to the weld, and was accompanied by substantial localized plastic deformation.

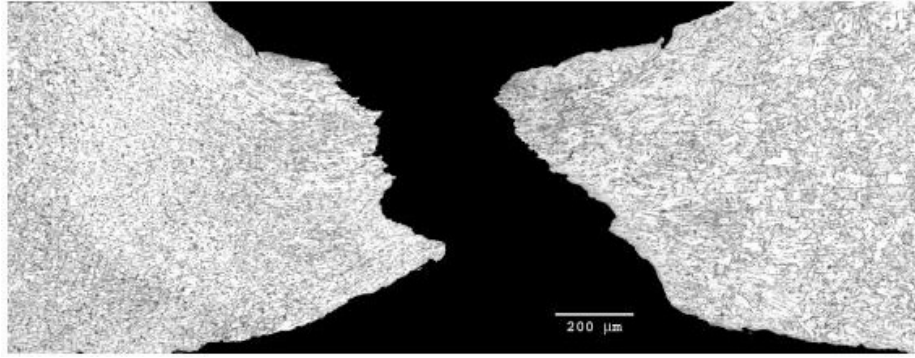


Figure 74. Metallographic cross section of tear #8-1. This sample contained a single repair weld surrounded by a region of recrystallized weld metal representing the original weld. Tearing occurred in either the recrystallized weld metal or the heat affected zone adjacent to the weld, and was accompanied by substantial localized plastic deformation.

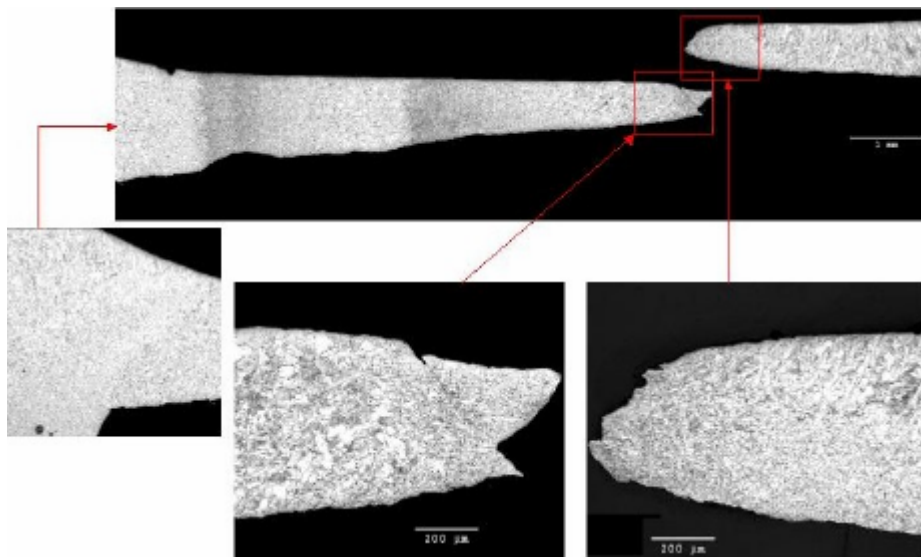


Figure 75. Metallographic cross section of tear #8-2. This sample contained the primary weld, plus a second weld approximately 13 mm in from the primary weld. This secondary weld was apparently made to repair the liner where it had been ground through when repairs were being made to the primary weld, similar to sample #4-3. Tearing occurred adjacent to the secondary weld in what appears to be recrystallized weld metal. Substantial localized plastic deformation accompanied tearing.

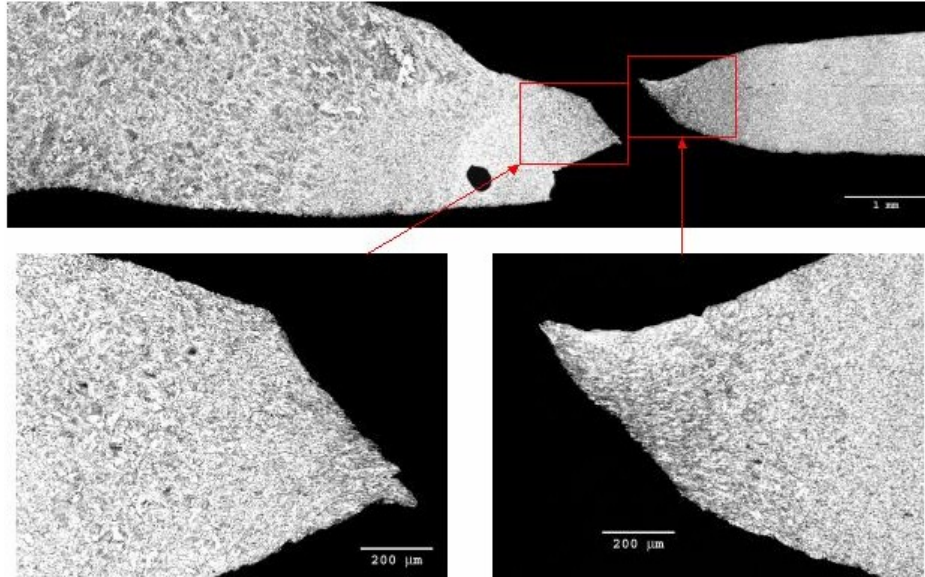


Figure 76. Metallographic cross section of tear #9. This sample contained a single repair weld. Grinding on the outside surface ended abruptly at the edge of the back-up bar, resulting in a deep but narrow region of liner thinning. Tearing occurred in the heat affected zone adjacent to the weld, and was accompanied by substantial localized plastic deformation.

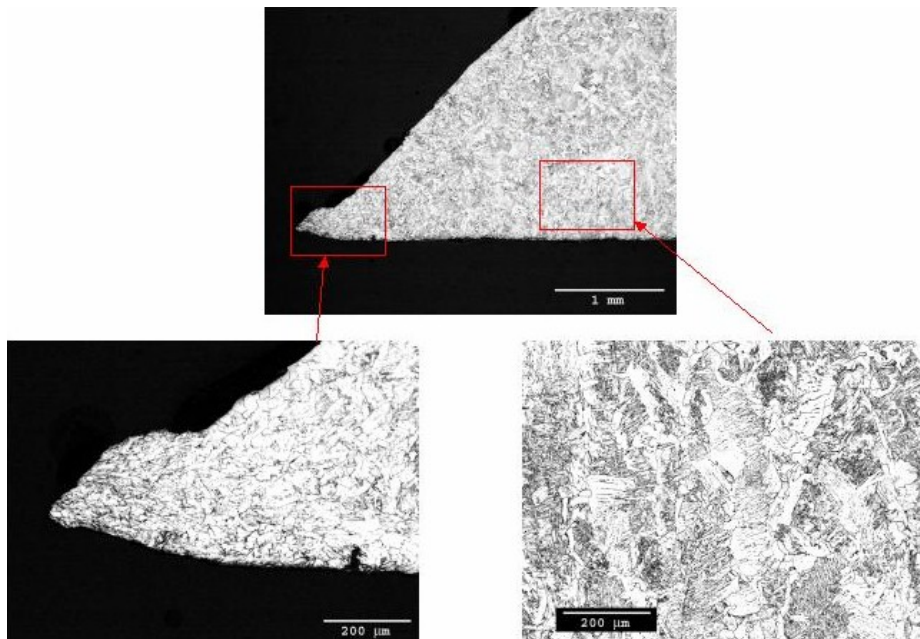


Figure 77. Metallographic cross section of tear #17. This shows the fusion zone of the primary weld, plus the tear adjacent to it. The tear appears to have occurred in a region of recrystallized weld metal from a previous weld. Tearing was accompanied by substantial localized plastic deformation.

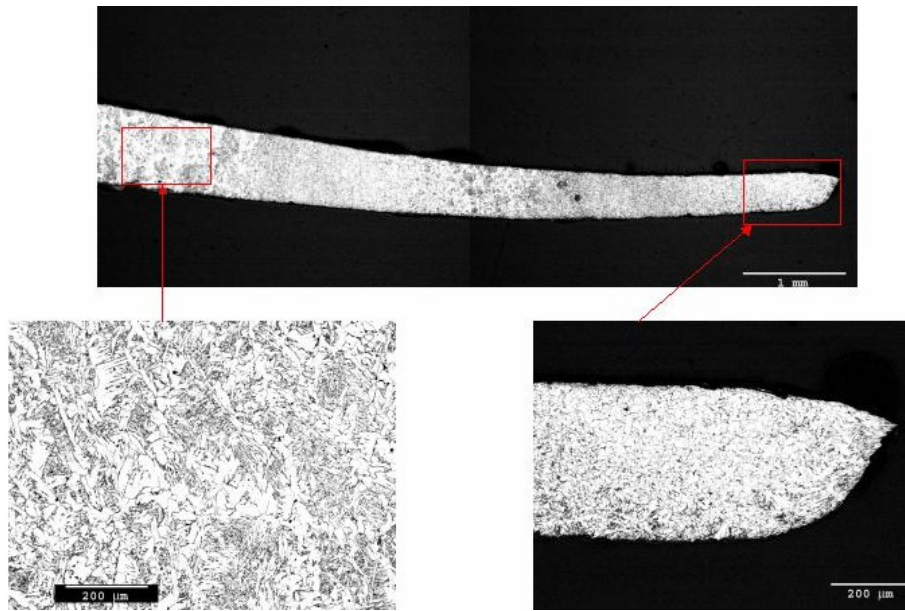


Figure 78. Region of tear #17 adjacent to that shown in Figure 77. Note columnar fusion zone at left; this corresponds to a secondary weld made to repair the liner where it had been ground through when repairs were being made to the primary weld, similar to samples #4-3 and #8-2. Note that the liner thickness was greatly reduced by grinding over the entire region pictured here.

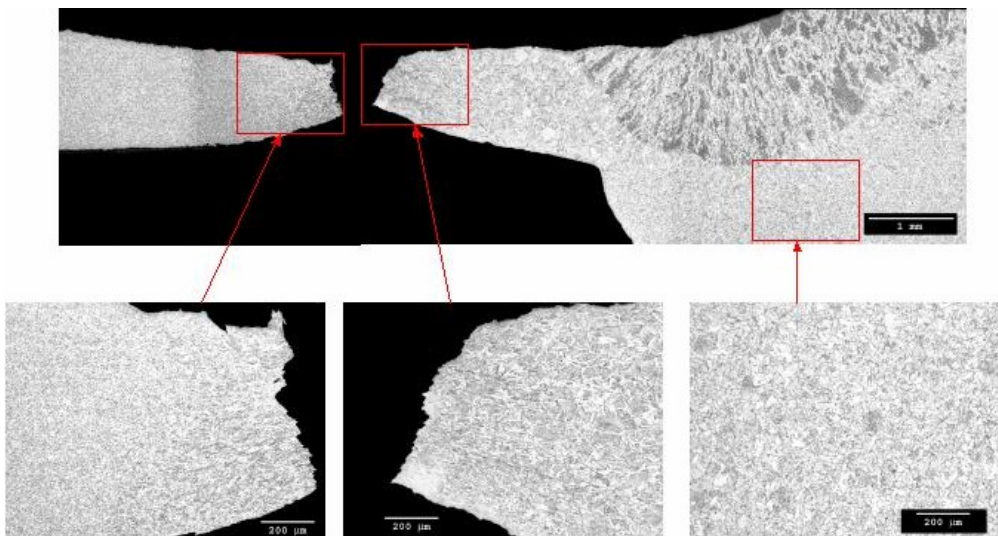


Figure 79. Metallographic cross section of tear #7. Columnar grained region represents repair weld; underlying recrystallized region represents earlier weld. Tearing occurred in heat affected zone adjacent to weld. Less shear and localized deformation appears characteristic of this tear, suggesting that it may have occurred due to more complex stresses.

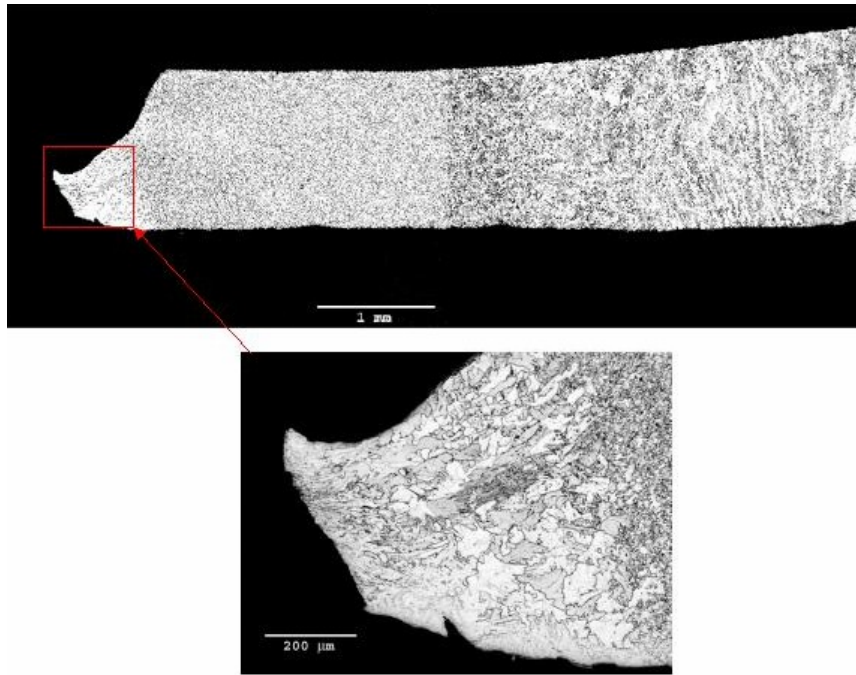


Figure 80. Metallographic cross section of tear #15. Region at right is columnar fusion zone of repair weld. Region at left is recrystallized fusion zone of former weld. Tear (at far left) occurred just left of where recrystallization stopped, either in unrecrystallized weld metal or coarse grained heat affected zone.

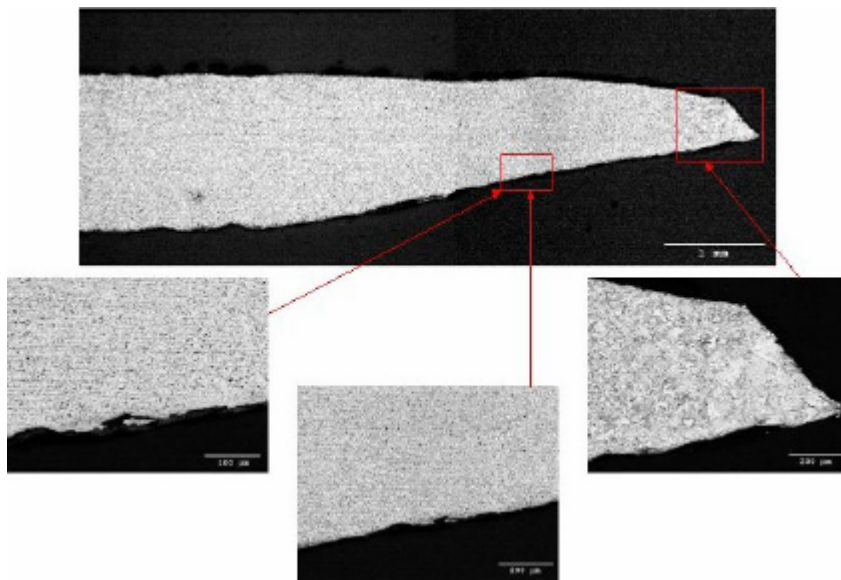


Figure 81. Region of tear #15 adjacent to that shown in Figure 80. Tear (at far right) occurred in coarse grained portion of heat affected zone. Note substantial angle between surface and segregation bands in metal, indicative of grinding in tapered area.

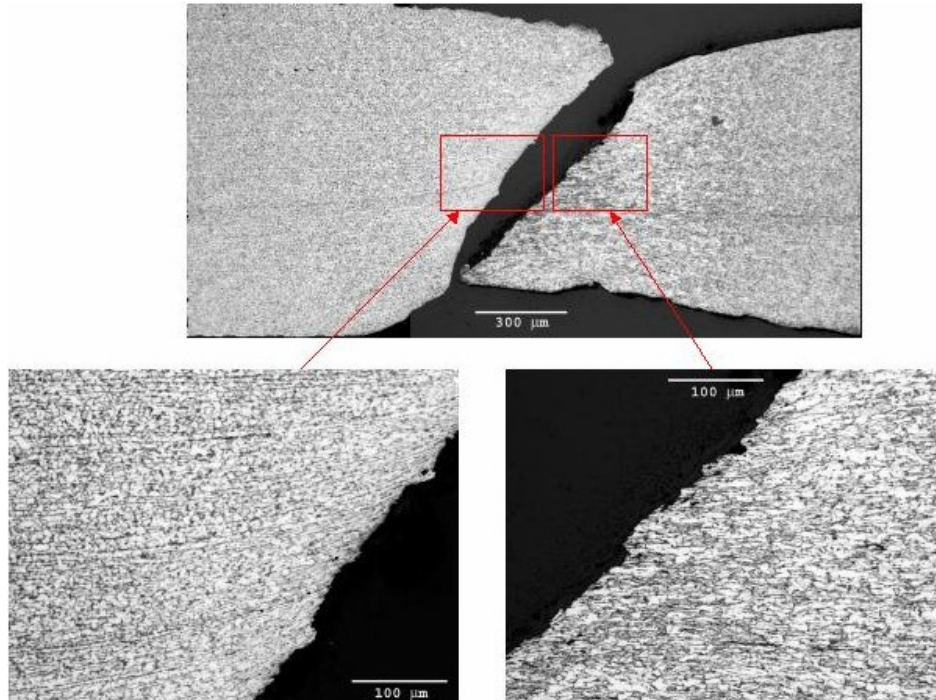


Figure 82. Metallographic cross section of tear #12. Tearing occurred in base metal (or perhaps far out in fine grained portion of heat affected zone). Note that two halves do not match perfectly across tear; this results in uncertainty regarding the amount of grinding done.

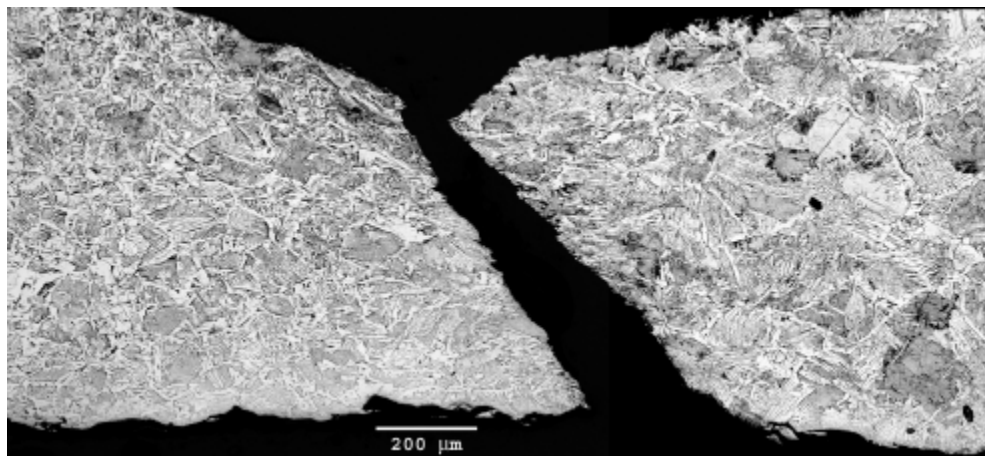
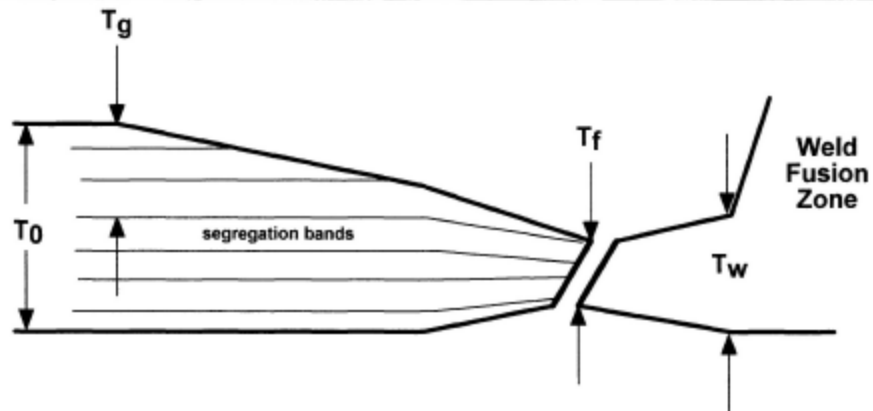


Figure 83. Metallographic cross section of tear #13. Tearing occurred in coarse grained portion of heat affected zone).

Determination of Grinding Reduction



Thickness at Tear: % Grinding = $((T_0 - T_f/0.51) / T_0) \times 100$

Thickness at Weld: % Grinding = $((T_0 - T_w) / T_0) \times 100$

Segregation Bands: % Grinding = $(T_g / T_0) \times 100$

Figure 84. Illustration of three methods used to estimate extent of liner thickness reduction due to grinding from metallographic cross sections.

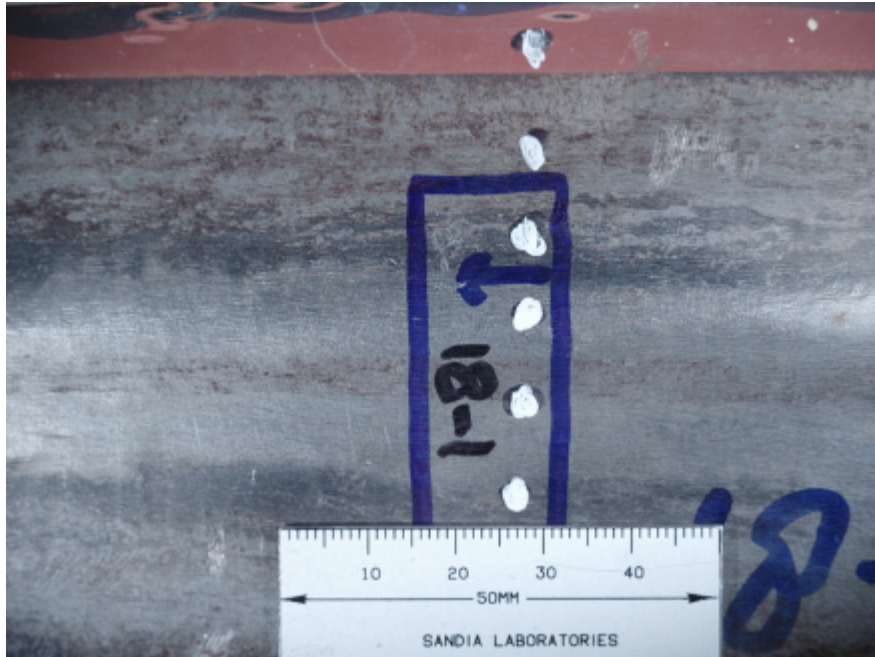


Figure 85. Details of inside (top) and outside (bottom) liner features in region #18-1 metallographic cross-section (arrows begin at plane of section and indicate view direction).

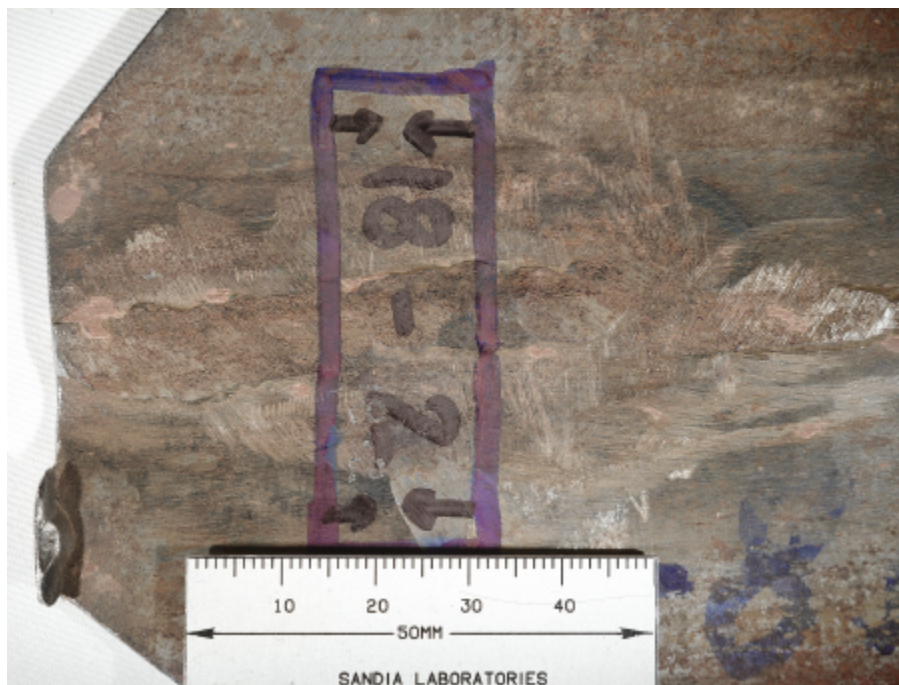
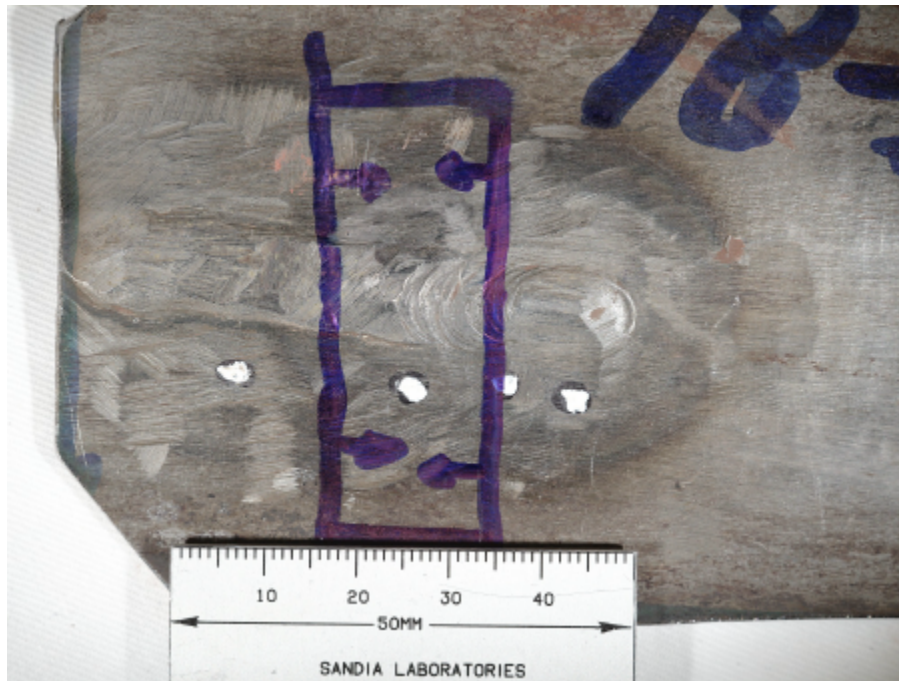


Figure 86. Details of inside (top) and outside (bottom) liner features in region #18-2 metallographic cross-section (arrows begin at plane of section and indicate view direction).

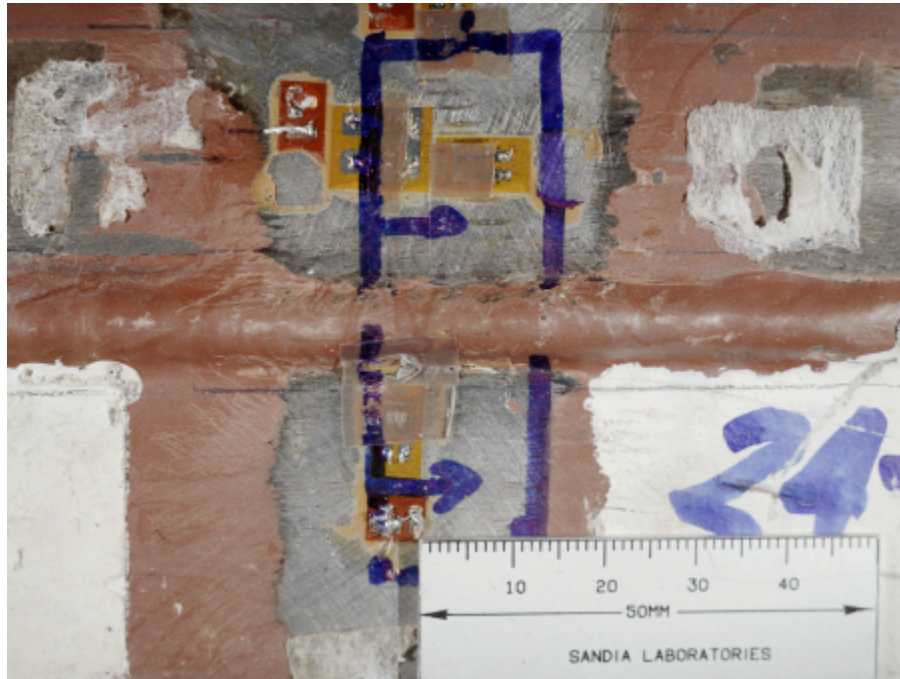


Figure 87. Details of inside (front) and outside (back) liner features in region #24-2 metallographic cross-section (arrows begin at plane of section and indicate view direction).



Figure 88. Details of inside (front) and outside (back) liner features in region #24-1 metallographic cross-section (arrows begin at plane of section and indicate view direction).

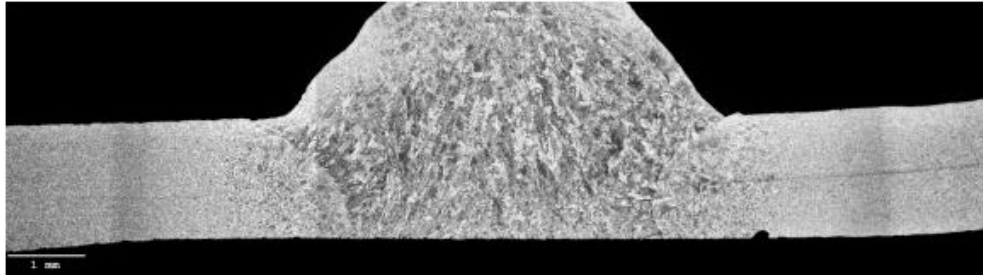


Figure 89. Metallographic cross section of region #18-1. Plastic deformation, but no tearing, occurred in this region. No evidence of repair welding or substantial grinding was found in this area.

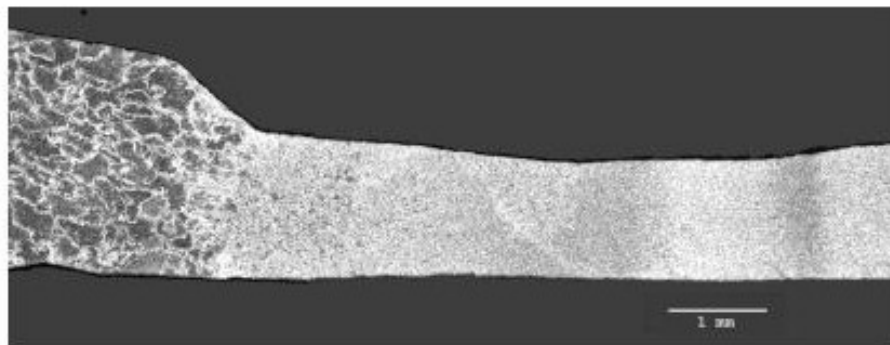
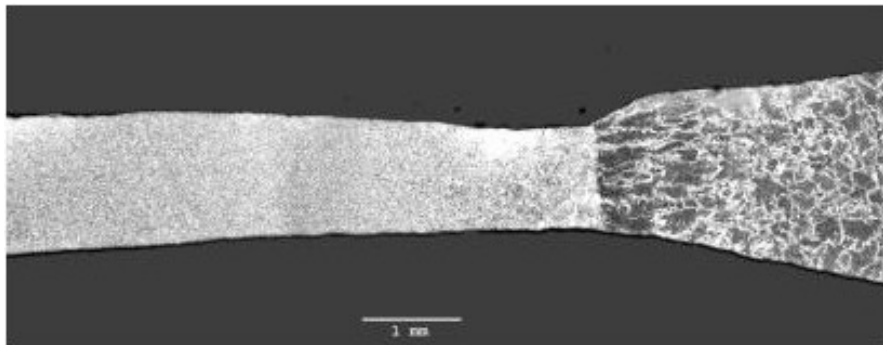


Figure 90. Metallographic cross section of region #18-2. Plastic deformation, but no tearing, occurred in this region. Evidence of repair welding and an undetermined amount of grinding was found in this area.

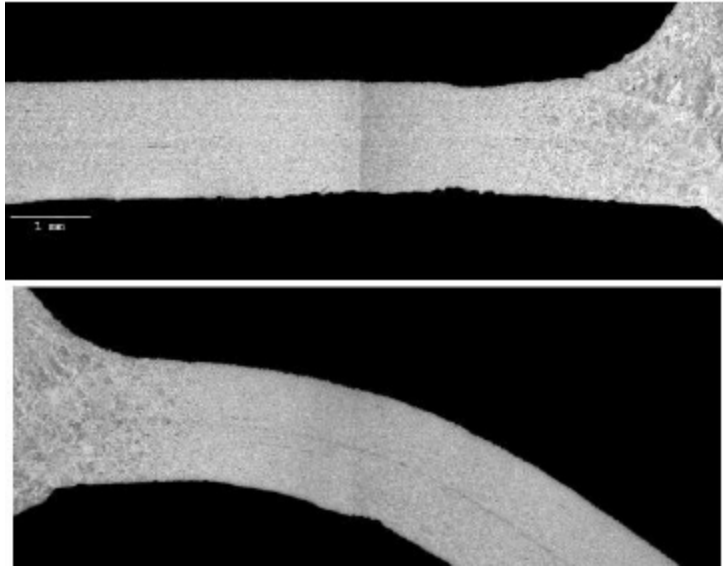


Figure 91. Metallographic cross section of region #24-2, where strain gauges recorded local strain of approximately 7%. No evidence of repair welding or substantial grinding was found in this area. Detailed observation of the surface “depressions” to the left of the weld suggested that they may correspond to surface defects in the plate. In particular, the bottom depression was filled with non-metallic particles, perhaps rolled-in oxide (too dark to be visible on this photo). These depressions may also correspond to the early stages of necking.

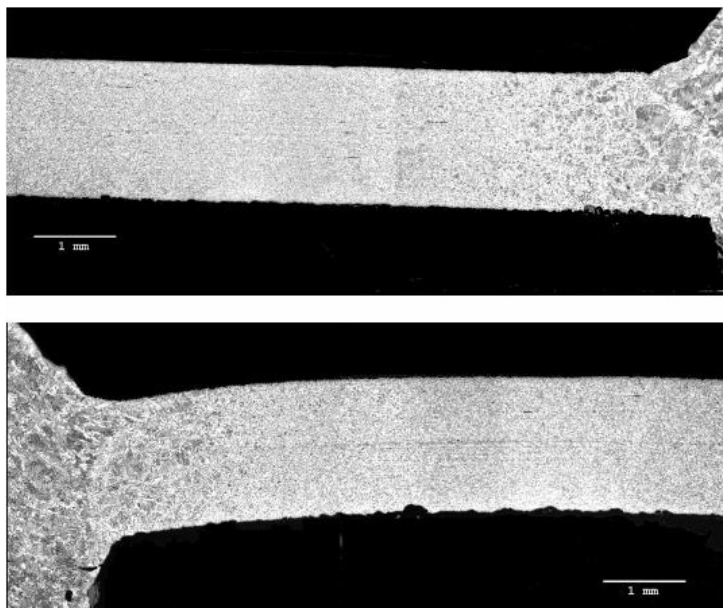
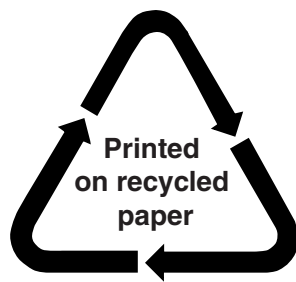


Figure 92. Metallographic cross section of region #24-1. Plastic deformation, but no tearing, occurred in this region. No evidence of repair welding or substantial grinding was found in this area.

NRC FORM 335 (2-89) NRCM 1102, 3201, 3202		U.S. NUCLEAR REGULATORY COMMISSION BIBLIOGRAPHIC DATA SHEET <i>(See instructions on the reverse)</i>		1. REPORT NUMBER (Assigned by NRC, Add Vol., Supp., Rev., and Addendum Numbers, if any) NUREG/CR-6810 SAND2003-0840P			
2. TITLE AND SUBTITLE Overpressurization Test of a 1:4-Scale Prestressed Concrete Containment Vessel Model				3. DATE REPORT PUBLISHED			
				MONTH March	YEAR 2003		
				4. FIN OR GRANT NUMBER Y6131			
5. AUTHOR(S) Hessheimer, M. F., Klamerus, E. W., Lambert, L. D., Rightley, G. S., Dameron, R. A.				6. TYPE OF REPORT Technical			
				7. PERIOD COVERED <i>(inclusive Dates)</i> 6/91 to 6/02			
8. PERFORMING ORGANIZATION – NAME AND ADDRESS <i>(If NRC, provide Division, Office or Region, U.S. Nuclear Regulatory Commission, and mailing address; if contractor, provide name and mailing address.)</i> Sandia National Laboratories, P.O. Box 5800, Albuquerque, NM, 87185-0744							
9. SPONSORING ORGANIZATION – NAME AND ADDRESS <i>(If NRC, type "Same as above", if contractor, provide NRC Division, Office or Region, U.S. Nuclear Regulatory Commission, and mailing address.)</i> <table border="0" style="width: 100%;"> <tr> <td style="width: 50%;"> Nuclear Power Engineering Corporation Systems Safety Department Tokyo 105, Japan under FiA DE-FI04-91-AL73734 </td> <td style="width: 50%;"> Division of Engineering Technology Office of Nuclear Regulatory Research U. S. Nuclear Regulatory Commission Washington, DC 20555-0001 </td> </tr> </table>						Nuclear Power Engineering Corporation Systems Safety Department Tokyo 105, Japan under FiA DE-FI04-91-AL73734	Division of Engineering Technology Office of Nuclear Regulatory Research U. S. Nuclear Regulatory Commission Washington, DC 20555-0001
Nuclear Power Engineering Corporation Systems Safety Department Tokyo 105, Japan under FiA DE-FI04-91-AL73734	Division of Engineering Technology Office of Nuclear Regulatory Research U. S. Nuclear Regulatory Commission Washington, DC 20555-0001						
10. SUPPLEMENTARY NOTES NUPEC Project Manager: S. Shibata NRC Project Manager: J. F. Costello							
11. ABSTRACT <i>(200 words or less)</i> <p>The Nuclear Power Engineering Corporation (NUPEC) of Japan and the U.S. Nuclear Regulatory Commission (NRC), Office of Nuclear Regulatory Research, co-sponsored a Cooperative Containment Research Program. Overpressure tests of a prestressed concrete containment vessel (PCCV) model began in July 2000, culminating in a functional failure mode or Limit State Test (LST) in September 2000 and a Structural Failure Mode Test (SFMT) in November 2001. The PCCV model, uniformly scaled at 1:4, is representative of the containment structure of an actual Pressurized Water Reactor (PWR) plan (OHI-3) in Japan. The objectives of the internal pressurization tests were to obtain measurement data of the structural response of the model to pressure loading beyond design basis accident in order to validate analytical modeling, to find pressure capacity of the model, and to observe its failure mechanisms.</p> <p>This report describes the design, construction, instrumentation and testing of the PCCV model. Detailed results of each test and posttest inspections findings are presented and all model response data is provided on the enclosed Data CD.</p>							
12. KEY WORDS/DESCRIPTORS <i>(List words or phrases that will assist researchers in locating the report.)</i> Containment Severe Accidents Pressure Testing Finite Element Analysis				13. AVAILABILITY STATEMENT Unclassified			
				14. SECURITY CLASSIFICATION <i>(This Page)</i> Unclassified			
				<i>(This Report)</i> Unclassified			
				15. NUMBER OF PAGES 600			
				16. PRICE			



Federal Recycling Program